

Multicomponent synthesis of γ -lactam derivatives and applications as anticancer agents

γ -Laktama-deribatuen osagai anitzeko sintesia eta aplikazioak minbizi-kontrako agente gisa

XABIER DEL CORTE SOLAGUREN-BEASCOA



FACULTY OF PHARMACY
DEPARTMENT OF ORGANIC CHEMISTRY I



Multicomponent synthesis of γ -lactam derivatives and applications as anticancer agents

XABIER DEL CORTE SOLAGUREN-BEASCOA



Vitoria-Gasteiz, 2022

Aita eta Amarentzat.

“Never laugh at live dragons.”

J.R.R. Tolkien

AGRADECIMIENTOS

Me gustaría expresar mi más sincero agradecimiento al Prof. Francisco Palacios, por haberme dado la oportunidad de realizar la tesis doctorar en su grupo de investigación. Patxi, a pesar de que no figuras oficialmente como director, esto no se podría haber llevado a cabo sin ti, muchas gracias por tener la puerta de tu despacho siempre abierta.

A los Drs. Edorta Martínez de Marigorta y Javier Vicario me gustaría agradecerles todo el esfuerzo que han puesto para que este trabajo salga adelante, todo lo que me han enseñado a lo largo de este largo camino y lo mucho que se han preocupado por mí. Edorta, muchas gracias por despertarme el “gusanillo” de la química durante la carrera y acompañarme hasta el final, incluso después de haberte jubilado. Y Javi, gracias por ser como eres, por no mandarme a paseo cuando te saturó con tanto trabajo, por ser positivo cuando yo no lo soy, y por las croquetas.

Siguiendo con otros integrantes del grupo de investigación, Kontxi, gracias por organizar esas actividades fuera del laboratorio, aunque no hayan sido muchas, ¡ayudan a desconectar! A Gloria, que está felizmente jubilada, quiero agradecerle esas charlas en el comedor; y a Ana, le agradezco el haber estado siempre dispuesta a echar un cable cuando lo he necesitado.

Con especial cariño me gustaría dar las gracias a Maria por su felicidad, sus chistes malos y por haberme ayudado cuando se lo he pedido. También, me gustaría dar las gracias a Delos por todas las veces que me ha solucionado problemas, por tranquilizarme, aconsejarme y enseñarme en todo momento. Y qué decir de la pequeña Carme, muuuchas gracias por animarme en los peores momentos y por entenderme tan bien. Y por último Yurre, gracias por tus consejos y contestarme a todas las preguntas, que no son pocas.

Aunque no formen parte del grupo de investigación, también quiero agradecer a Begoña su plena disponibilidad y a Mirari el haberme iniciado en la química orgánica. Gracias a ti tengo la oportunidad de probarme a mí mismo como docente, lo cual estoy disfrutando mucho.

Entre los más jóvenes, primero me gustaría dirigirme a las personas con las que he hecho la mayor parte de la tesis. Aitor, muchas gracias por enseñarme tantísimas cosas, por aclararme dudas, por tus consejos y por tus “xD” y “cosa fina”. A Endika por compartir nuestros éxitos y fracasos, y por cuidarme desde un principio. Asier, muchas gracias por haberme acompañado todo este tiempo; quién nos iba a decir cuando empezamos la carrera que seguiríamos trabajando juntos diez años más tarde. Víctor,

o mejor dicho “pequeño azirino”, gracias por TODO, por hacerme reír, por tus locuras, por aconsejarme y por ser un gran amigo lleno de ira y de ternura. Y, por último, gracias Adrián, “el cabeza”, por ser una persona con la que se puede contar SIEMPRE dentro y fuera del laboratorio.

Entre las incorporaciones más recientes, quiero agradecer a Xabi y Alba el haber hecho del laboratorio un lugar de trabajo más alegre, y en especial a las autobuseras y repartidoras de correcciones a domicilio, Julene y Ángela por sus muchas tonterías, risas y buenos momentos.

No por ello son menos importantes las personas con las que he coincidido menos tiempo, como Zuriñe, Ichrak, Karim, Saverio, Zouhair, Leyre y un largo etcétera. ¡Muchas gracias!

I am really grateful to Prof. Tad Holak for accepting me in his research group for the predoctoral stay and for sharing his office. Also, I want to thank all the lab mates in Krakow (Ewa, Julia, Damian, Asia, Magda, Ismael, Lukasz, ...) for all the received help, support and kind attention. Moreover, I need to express my deepest gratitude to Radek for everything he has taught to me and for taking care of me inside and outside the lab.

A mis padres quiero agradecerles el haber sufrido conmigo, la ayuda prestada en todo momento, el ponerme las cosas fáciles, el haberme aupado en los momentos difíciles y su pensión de cinco estrellas.

También quiero dar las gracias a mi familia y amigos por todo su apoyo y a los predocs por las juergas y los buenos momentos.

Summary

Cancer, the name given to a collection of neoplastic diseases, is the second most important global cause of death. For ages, the treatment of these diseases has been a highly complex process and, although several innovative approaches have been developed and approved for clinical use, today the prevalent general therapies are still a combination of surgery with chemotherapy and/or radiation therapy.

Despite the progress made to date, there is still a serious need to find new chemotherapeutical agents that may be able to bind selective targets at a molecular level. In this context, one promising biochemical target is the interaction between p53 transcription factor, which is mutated or has its function lost in 50% of human cancers, and the MDM2 (Murine Double Minute 2) and MDMX (Murine Double Minute X) proteins.

Among the different families of molecules with the capability to inhibit MDM2/MDMX-p53 protein-protein interaction, those containing a pyrrolidone core (γ -lactam), have a promising inhibitory capacity and have not been studied so far in depth (Figure I).

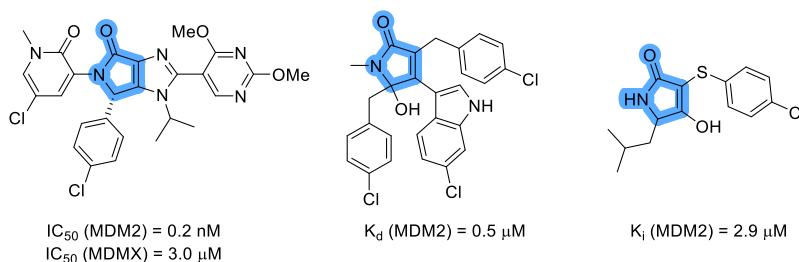


Figure I. MDM2 and MDMX inhibitors with pyrrolidone (blue color) core.

At the heart of the long process for the development of drugs, multicomponent reactions (MCRs) are valuable synthetic processes where three or more reagents react in a 'one-pot' procedure through a sequence of elementary steps. Taking into account the considerations mentioned above, the main objectives of this thesis are the development of efficient organocatalyzed multicomponent processes for the synthesis of γ -lactam derivatives, the exploration of their synthetic applications and the final study of the antiproliferative activity of the substrates against several cancer cell lines, as well as their MDM2/MDMX-p53 protein-protein interaction inhibitory capability (Figure II).

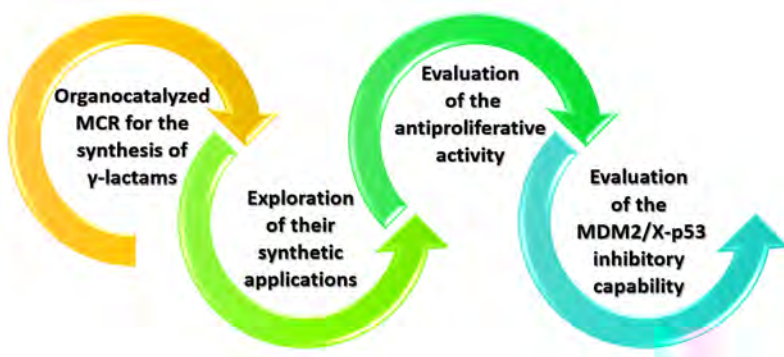
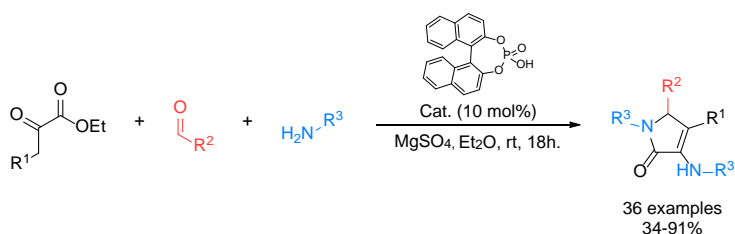


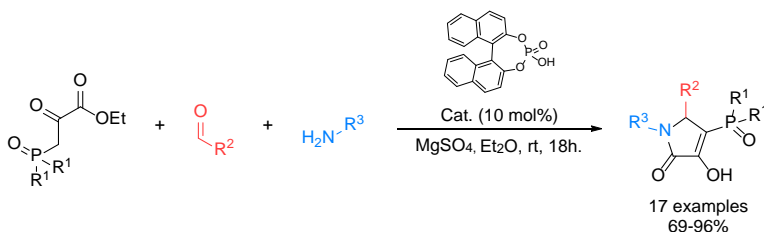
Figure II. General objectives of the thesis.

The first goal of this PhD is the development of a phosphoric acid-catalyzed three-component protocol for the synthesis of 3-amino γ -lactam derivatives using pyruvate derivatives, aldehydes and amines (Scheme I).



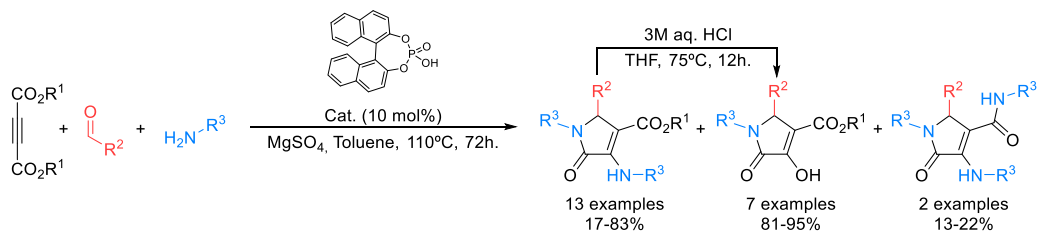
Scheme I. Three-component reaction of pyruvate derivatives, aldehydes and amines.

In addition, due to the relevance of fluorine or phosphorus moieties in bioactive molecules, next, this multicomponent protocol has been extended to the synthesis of phosphorus and fluorine-containing γ -lactam derivatives. Remarkably, the use of phosphorus-substituted pyruvate derivatives leads to the formation of enol-derived γ -lactams (Scheme II).



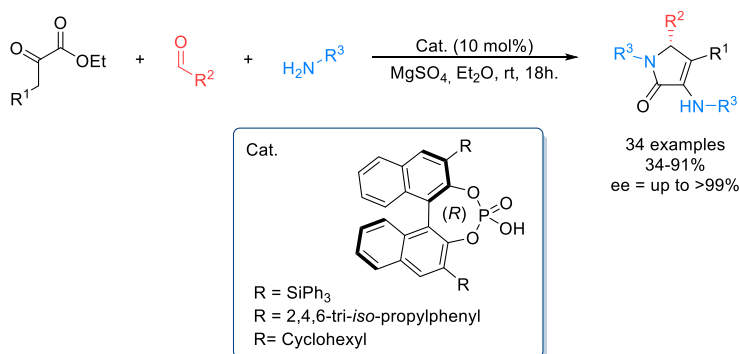
Scheme II. Three-component reaction of phosphorus pyruvate derivatives, aldehydes and amines.

Next, the Brønsted acid-catalyzed multicomponent reaction has been extended to the use of dialkyl acetylenedicarboxylates, as surrogates of pyruvate esters, with amines and aldehydes. As far as we know, this is the first example of such reaction using phosphoric acid species as the catalyst (Scheme III).



Scheme III. Three-component reaction of dialkyl acetylenedicarboxylates, aldehydes and amines.

Nowadays, drug regulatory agencies and pharmaceutical industries have established among their synthetic priorities the preparation of enantiomerically pure molecules. Thus, the development of new methodologies to obtain optically pure chiral molecules is a goal of great interest in organic chemistry. For this reason, and, considering the ability of Brønsted acid catalysts to promote the three-component reaction, we have developed a highly enantioselective version of this reaction for the preparation of enantioenriched γ -lactam derivatives, obtaining excellent yields and enantiomeric excesses (Scheme IV).



Scheme IV. Enantioselective three-component reaction.

The 3-amino-1,5-dihydro-2*H*-pyrrol-2-one substrates obtained from the multicomponent reaction are outstanding tools in chemical synthesis due to the presence of a cyclic α -dehydro α -amino acid, an enone and an enamine moieties in the same molecule (Figure III).

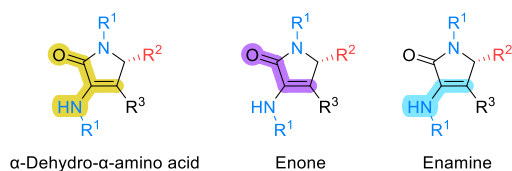
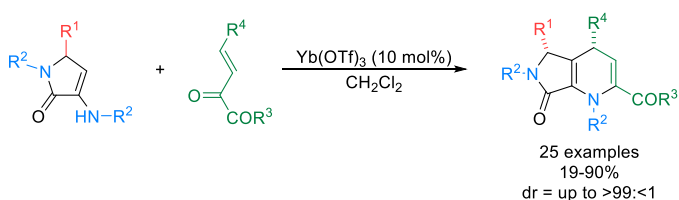


Figure III. The different moieties present in the 3-amino-1,5-dihydro-2H-pyrrol-2-ones.

Therefore, the synthetic potential of the γ -lactam derivatives has been put into manifest through several transformations, such as diastereoselective hydrogenations, alkylation reactions and Horner-Wadsworth-Emmons reactions. In particular, the ytterbium-catalyzed formal [3+3] cycloaddition reaction of γ -lactam derivatives with β,γ -unsaturated α -ketoesters leads to 1,4-dihydropyridines with a high degree of regio- and diastereoselectivity (Scheme V).



Scheme V. Stereoselective formal [3+3] cycloaddition reaction.

In the second part of this PhD the anticancer activity of γ -lactam derivatives has been studied. First, the *in vitro* antiproliferative activity of the synthesized compounds against several human cancer cell lines has been evaluated. In general, γ -lactam derivatives were found to have high activity towards A549 lung cancer cell line and no activity in non-malignant lung MRC5 cell line, with the best IC_{50} value of 0.11 μ M. Some of the most active compounds are shown in Figure IV. In addition, the cell morphology was visualized after exposure, at different times and concentrations, to the most active compound, and some flow cytometry assays determined that these compounds are capable of triggering the apoptosis mechanism.

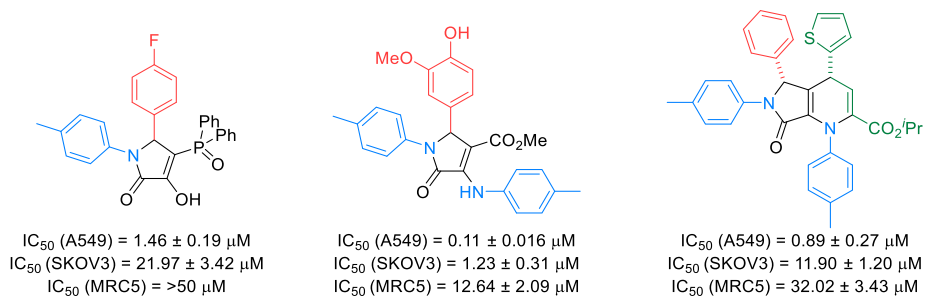


Figure IV. Most active γ -lactam derivatives according to cytotoxicity assays.

Finally, the inhibitory capability of 70 γ -lactam derivatives on the MDM2/MDMX-p53 protein-protein interaction has been evaluated using two different screening techniques, Differential Scanning Fluorimetry (DSF) and Fluorescence Polarization (FP) assays. The best results for each protein are portrayed in Figure V. However, it cannot be surely concluded that the cytotoxic activity of the γ -lactam derivatives is the result of the disruption of the MDM2/MDMX-p53 protein-protein interaction. Nonetheless, the binding mode to MDM2 and MDMX proteins of two γ -lactam derivatives was predicted by molecular modeling simulations.

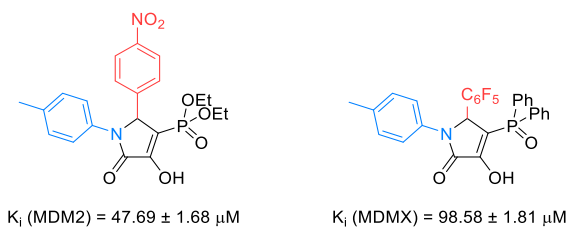


Figure V. Most active γ -lactam derivatives as inhibitors of MDM2/MDMX-p53 protein-protein interaction.

Abbreviations and acronyms

°C	Celsius degrees
1D	One dimension
2D	Two dimensions
3D	Three dimensions
Å	Ångstrom
Ad.	Addition
AIBN	Azobisisobutyronitrile
Alk	Alkyl
APS	Ammonium Persulfate
aq.	Aqueous
Ar	Aromatic
as	Asymmetric
AU	Arbitrary Units
BBBSI	1,1'-Butylenebis(3-sulfo-3 <i>H</i> -imidazol-1-ium)
BINOL	1,1'-Bi-2-naphthol
Bn	Benzyl
Bu	Butyl
Calcd.	Calculated
Cat.	Catalyst
CDK	Cyclin Dependent Kinase
cod	1,5-Cyclooctadiene
Conv.	Conversion
COX2	Cyclooxygenase-2
Cy	Cyclohexyl
Da	Dalton
DABCO	1,4-Diazabicyclo[2.2.2]octane
DCM	Dichloromethane
dec.	Decomposition
DEPT	Distortionless Enhanced Polarization Transfer
DMF	<i>N,N</i> -Dimethylformamide
DMSO	Dimethyl sulfoxide
DNA	Deoxyribonucleic Acid
dr	Diastereomeric ratio
DSF	Differential Scanning Fluorimetry

E	Electrophile
EC₅₀	Half maximal effective concentration
EDTA	Ethylenediamine Tetraacetic Acid
ee	Enantiomeric excess
eq.	Equivalents
ESI	Electrospray ionization
Et	Ethyl
F	Fluorescence
FL	Fluorescence channel in Flow Cytometry
FP	Fluorescence Polarization
<i>g</i>	Relative centrifugal force (<i>g</i> force)
h.	Hours
HDAC	Histone deacetylase
HIV	Human Immunodeficiency Virus
HMQC	Heteronuclear Multiple Quantum Coherence Experiment
HPLC	High-performance liquid chromatography
HRMS	High resolution mass spectrometry
IC₅₀	Half maximal inhibitory concentration
IMAC	Immobilized Metal Affinity Chromatography
^{<i>i</i>}Pr	<i>iso</i> -Propyl
IPTG	<i>iso</i> -propyl β-D-1-thiogalactopyranoside
IR	Infrared spectroscopy
<i>J</i>	Coupling constant
K_d	Dissociation Constant
K_i	Inhibition Constant
LDA	Lithium di- <i>iso</i> -propylamide
Lit.	Literature
M	Molar
<i>m/z</i>	Mass and charge ratio
max	Maximum
MDM2	Murine Double Minute 2
MDMX	Murine Double Minute X
Me	Methyl
min	Minimum
MOMP	Mitochondrial Outer Membrane Permeabilization
Mp	Melting point
MTBE	Methyl <i>tert</i> -butyl ether

MWCO	Molecular Weight Cut Off
n.d.	Not determined
NMR	Nuclear Magnetic Resonance
NOE	Nuclear Overhauser Effect
NOESY	Nuclear Overhauser Enhancement Spectroscopy
Nu	Nucleophile
ORTEP	Oak Ridge Thermal Ellipsoid Plot
PBS	Phosphate-Buffered Saline
PCR	Polymerase Chain Reaction
PDB	Protein Data Bank
PG	Protecting Group
Ph	Phenyl
PIC	Protease Inhibitor Cocktail
Piv	Pivalyl
PMP	<i>p</i> -Methoxyphenyl
PPI	Protein-Protein Interaction
ppm	Parts per million
Pr	Propyl
Prod.	Product
PTSA	<i>p</i> -Toluensulfonic acid
Py	Pyridine
PyBOX	Bis(oxazolin)pyridine
Q-TOF	Quadrupole Time Of Flight
rac	Racemic
ref.	Reference
ROS	Reactive Oxygen Species
rt.	Room temperature
SAR	Structure-Activity Relationship
SD	Standard Deviation
SDS-PAGE	Sodium Dodecyl Sulphate-Polyacrylamide Gel Electrophoresis
SO	Sypro Orange
SOD	Superoxide Dismutases
Solv.	Solvent
st	Tension vibration
sym	Symmetric
T	Temperature
TEMED	Tetramethylethylenediamine

Abbreviations and acronyms

TfO	Triflate
THF	Tetrahydrofuran
TLC	Thin Layer Chromatography
T_m	Melting temperature
TMS	Trimethylsilyl
Tol	Tolyl
TRAIL	TNF-Related Apoptosis-Inducing Ligand
TS	Transition State
UV	Ultraviolet light
VEGF-R	Vascular Endothelial Growth Factors and Receptors
vs.	Versus

Table of contents

Introduction	27
Objectives.....	65
Section I. Multicomponent synthesis and applications of unsaturated γ-lactam derivatives	69
Chapter 1. Multicomponent synthesis of unsaturated γ -lactam derivatives using pyruvates	71
Chapter 2. Multicomponent synthesis of fluorine and phosphorus substituted γ -lactams.....	79
Chapter 3. Multicomponent synthesis of γ -lactam derivatives using activated alkynes	89
Chapter 4. An enantioselective approach for the multicomponent synthesis of γ -lactams.....	97
Chapter 5. Synthetic transformations of γ -lactam derivatives	113
Chapter 6. Stereoselective formal [3+3] reaction of 3-amino γ -lactam derivatives	121
Section II. Anticancer activity of γ-lactam derivatives	137
Chapter 7. Evaluation of the antiproliferative activity and the apoptosis induction capability	149
7.1. Antiproliferative activity of α,β -unsaturated γ -lactam derivatives	149
7.2. Antiproliferative activity of bicyclic 1,4-dihydropyridines.....	165
7.3. Apoptosis detection assays and cell morphology visualization	170
Chapter 8. Evaluation of γ -lactam derivatives as inhibitors of MDM2/MDMX-p53 interaction.....	177
8.1. Expression and purification of MDM2 and MDMX.....	177
8.2. Differential Scanning Fluorimetry (DSF) assay.....	180
8.3. Fluorescence Polarization (FP) assay.....	187
8.4. Molecular modeling simulations	190
Conclusions	193
Experimental Section I. Chemical synthesis.....	197
General methods and materials.....	199
Chapter 1. Multicomponent synthesis of unsaturated γ -lactam derivatives using pyruvates	201
Chapter 2. Multicomponent synthesis of fluorine and phosphorus substituted γ -lactams.....	225
Chapter 3. Multicomponent synthesis of γ -lactam derivatives using activated alkynes	243
Chapter 4. An enantioselective approach for the multicomponent synthesis of γ -lactams.....	259
Chapter 5. Synthetic transformations of γ -lactam derivatives	271
Chapter 6. Stereoselective formal [3+3] reaction of 3-amino γ -lactam derivatives	281
Experimental Section II. Biological assays	321
Chapter 7. Evaluation of the antiproliferative activity and the apoptosis induction capability	323
Compound purity analysis	323

Cytotoxicity assays.....	323
Flow cytometry assays.....	326
Visualization of cell growth and morphology	326
Chapter 8. Evaluation of the MDM2/MDMX-p53 protein-protein interaction inhibitory capacity	327
SDS-PAGE electrophoresis	327
Protein expression and purification buffers	328
Expression and purification of MDM2 (18 - 125).....	330
Expression and purification of MDMX (1 - 134)	333
Differential Scanning Fluorimetry (DSF)	335
Fluorescence Polarization (FP)	336
Molecular modeling simulations	338

The background of the slide is a complex, abstract network diagram. It consists of numerous nodes of varying sizes and shades of gray, connected by thin lines. The nodes are distributed across the entire page, with a higher density in the upper and lower portions. A large, light gray, semi-transparent shape is positioned behind the text, resembling a stylized letter 'A' or a similar geometric form. The overall aesthetic is clean, modern, and technical.

Introduction

Cancer, the second most important global cause of death, is the name given to a group of neoplastic diseases in which an abnormal cell-growth occurs, leading to the formation of a mass called tumor. The whole process is defined as a neoplasm. However, not all tumors can be considered as cancerous. They can be divided into benign, those who are confined in a particular location, not spreading to other body locations, and they are not transformed into cancer, and those that are coined as cancer, which can be divided into malignant, the neoplasms that invade surrounding tissues and metastasize, and potentially malignant ones, those that are still localized but on the way of becoming malignant.¹

Carcinogenesis is the conversion of normal cells with a proper homeostatic feedback mechanism function into cells with an autonomous growth and invasion capability. Initiation, promotion, progression and malignant conversion are the four stages of this process (Figure 1).

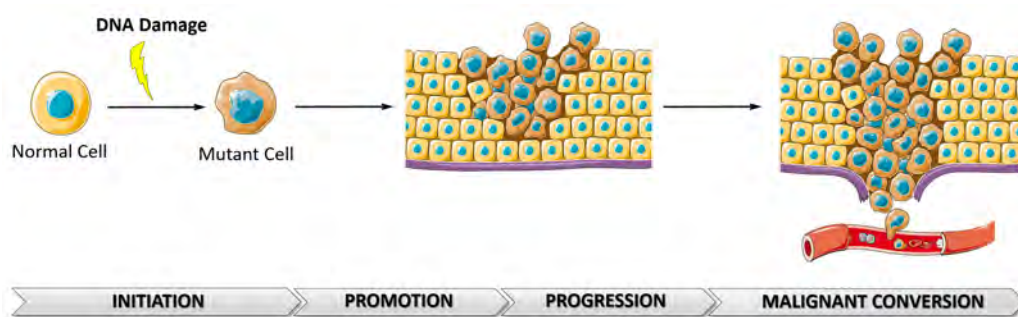


Figure 1. The carcinogenesis process.

The sequential interaction of cells with cancer-causing agents leads to DNA damage. This damage can be either an endogenous process (errors in the replication of DNA, intrinsic chemical instability of certain DNA bases or attack by free radicals generated during metabolism) or a result of the interactions with exogenous chemical, physical or viral agents. If it is not repaired, DNA damage can produce mutations. Most of these alterations are irrelevant from a point of view of cancer risk and do not alter the proper functions of the cell. Nevertheless, some mutations can damage crucial genes for cell survival, becoming lethal for that particular cell. Only occasionally, these mutations give some advantages to the cell, such as the increasing proliferation capability, activating proto-oncogenes and

¹ Roy, M.; Datta, A. Cancer: Types and Hallmarks. In *Cancer, Genetics and Therapeutics*; Springer, 2019; pp 1-26.

inactivating tumor suppressor genes. At this point, the cell enters the initiation step of the carcinogenesis process. Then, promotion or clonal expansion begins, resulting in the formation of pre-neoplastic cells. Here promoters take part, that is, substances that influence the efficiency of carcinogenesis. The promoters are normally non-mutagenic and non-carcinogenic and cause their biological effect without metabolic activation. Progression is the name given to the time interval between the promotion and the formation of a malignant tumor. In this step, cells divide and increase their population until it leads to the last stage, the so-called malignant conversion.²

During this multistage process, only a limited number of cells will progress from one stage to the next one, finally leading to the formation of a malignant tumor. This is due to the natural anticancer defense mechanisms participating at each stage of the carcinogenesis process, which decrease cancer risk.³

Therefore, at this point, a better knowledge of the dissimilarities between ‘normal’ and cancer cells is necessary to better understand the disease. Hanahan and Weinberg defined ten hallmarks involved in the pathogenesis of, possibly, all cancers (Figure 2). These hallmarks consist of distinctive and complementary capabilities that enable tumor growth and metastatic dissemination.⁴

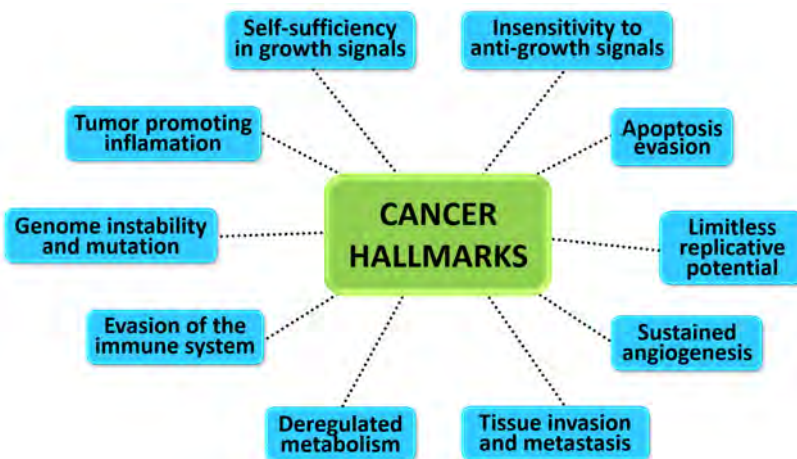


Figure 2. Hallmarks of cancer.

- I. Self-sufficiency in growth signals. While normal cells need extracellular growth factors or signals, to develop and divide, cancer cells do not need external signals to multiply and this leads to an uncontrollable proliferation.¹

² Bertram, J. S. *Mol. Aspects Med.* **2001**, *21*, 167-223.

³ Jakóbsiak, M.; Lasek, W.; Gołab, J. *Immunol. Lett.* **2003**, *90*, 103-122.

⁴ (a) Hanahan, D.; Weinberg, R. A. *Cell* **2011**, *144*, 646-674. (b) Hanahan, D.; Weinberg, R. A. *Cell* **2000**, *100*, 57-70.

- II. Insensitivity to anti-growth signals. In a normal cell, multiple signals operate in order to maintain homeostasis. However, cancer tissues are resistant to those growth-preventing signals.
- III. Apoptosis evasion. Apoptosis is the mechanism used by damaged cells to program their own death. It is triggered by diverse signals that unfold a series of events, ending in the disruption of the cell membrane, the rupture of the cytoplasmic and nuclear skeleton, the degradation of the chromosomes and the fragmentation of the nucleus. However, cancer cells have the ability to bypass this mechanism.
- IV. Limitless replicative potential. As described by Hayflick in 1997 cells have a finite replicative potential.⁵ Once cells have reached a certain limited number of doublings, they stop growing (senescence). Cancer cells are capable of exceeding this limit, having infinite division and growth capability.
- V. Sustained angiogenesis. The supply of nutrients and oxygen and the vascular system is crucial for cell function and survival. The growth of new blood vessels, called angiogenesis, is transitory and carefully regulated. At some point in the carcinogenesis process, tumors appear to activate and increase the angiogenic capability, changing the balance in this process.
- VI. Tissue invasion and metastasis. During the development of most types of human cancer, primary tumor cells move out and invade contiguous tissues, forming new colonies in the body. These new formed metastases are amalgams of healthy and cancer cells. This concept is the main difference between a benignant and a malignant one.
- VII. Deregulated metabolism. Cancer cells are capable of reprogramming their glucose metabolism in order to fuel cell growth and division.
- VIII. Evading the immune system. The immune system is constantly monitoring cells and tissues, and recognizes and eliminates the majority of normal cells that turn malignant.⁶ If cancer develops, it implies that cancer cells have managed to escape the detection of the immune system and have avoided eradication.
- IX. Genome instability and mutations. Some of the hallmarks described before, in great measure, depend on successive genomic alterations of neoplastic cells. Some genome mutations give

⁵ Hayflick, L. *Biochemistry* **1997**, *62*, 1180-1190.

⁶ Nakajima, K.; Nangia-Makker, P.; Hogan, V.; Raz, A. *Cancer Res.* **2017**, *77*, 5441-5444.

advantages to subcloned cells, allowing them to outgrow and develop dominance in the local tissue.

- X. Tumor promoting inflammation. As pathologists agree, every neoplastic lesion contains immune cells infiltrated, ranging from subtle infiltrations to gross inflammations.⁷ The inflammatory response helps emerging neoplasias to acquire hallmark capabilities by supplying bioactive molecules (growth factors, survival factors and proangiogenic factors) to the microenvironment of the tumor.⁸

Non-immune protection mechanisms against carcinogenesis.

The cell itself has some natural immune and non-immune protection or defense mechanisms that prevent recently mutated cells from continuing the path to being converted into malignant cells. Hereunder the non-immune protection mechanisms are detailed.

I. Inactivation and removal of reactive oxygen species.

Some external factors, such as chemicals, UV light and ionizing radiations or other physiological ones, such as cellular respiration in mitochondria or some metabolic pathways can form reactive oxygen species (ROS) like O_2^- , H_2O_2 and $\cdot OH$, that could produce DNA damage. Some enzymes are able to remove those carcinogenic compounds. For instance, superoxide dismutases (SOD) convert superoxide radicals (O_2^-) in H_2O_2 , which is next eliminated by catalases and peroxidases. Glutathione S-transferases conjugate toxic electrophilic molecules (including polycyclic aromatic hydrocarbons present in tobacco) with glutathione, favoring their elimination, and P450 enzymes are responsible for the metabolism of endogenous and exogenous chemicals. On the other hand, some proteins present in the cell membrane, such as P-glycoproteins, are in charge of the excretion of some toxic or potentially toxic molecules. Unfortunately, these transport proteins, which are supposed to protect us from carcinogens, in some cancers are overexpressed and act protecting tumor cells from destruction by excreting the chemotherapeutic agents out of the cell.⁹

II. DNA damage repair.

DNA molecules are exposed continuously to the damaging activity of numerous exogenous and internal genotoxicants. Fortunately, there are different repair pathways such as O6-methylguanine-

⁷ Pages, F.; Galon, J.; Dieu-Nosjean, M.C.; Tartour, E.; Sautes-Fridman, C.; Fridman, W.H. *Oncogene* **2010**, *29*, 1093-1102.

⁸ (a) DeNardo, D.G.; Andreu, P.; Coussens, L.M. *Cancer Metastasis Rev.* **2010**, *29*, 309-316. (b) Grivennikov, S.I.; Greten, F.R.; Karin, M. *Cell* **2010**, *140*, 883-899. (c) Qian, B.Z.; Pollard, J.W. *Cell* **2010**, *141*, 39-51.

⁹ Jakóbsiaki, M.; Lasek, W.; Gołab, J. *Immunol. Lett.* **2003**, *90*, 103-122.

DNA methyltransferase (MGMT), base or nucleotide-excision repair pathways and homologous or non-homologous end-joining recombination pathways for each form of damage.¹⁰

III. Tumor suppressor genes.³

As mentioned above, DNA damage is repaired efficiently in most cases. However, if these alterations are not solved, mutations can be induced and, if these mutations occur in critical genes, healthy cells could be transformed into cancer cells. These genes, which favor carcinogenesis when mutated, are divided in two categories: proto-oncogenes and tumor suppressor genes (anti-oncogenes).

Proto-oncogenes act as positive regulators of many functions, such as cell proliferation, differentiation and programmed cell death. When a mutation takes place in a proto-oncogene, it turns into, what is denominated, an oncogene, being permanently active (when it is not supposed to be). Therefore, the cell grows out of control, intervening in the neoplastic transformation.

Tumor suppressor genes are often identified by their inherited mutations that predispose some humans to inherit certain forms of cancer. The inactivation of these genes, due to mutations that lead to the loss of their functions, contributes to the development of cancer. Some examples of tumor suppressor genes and their functions are summarized in Table 1:

Table 1. Examples of tumor suppressor genes.^{3,11}

Gene	Function
TP53	Cell cycle regulator, induction of growth arrest and apoptosis.
RB1	Cell cycle regulator.
P19ARF	Stabilizes p53.
p16(INK4a)	Cell cycle regulation.
KLF6	Transcriptional regulation.
Wt1	Transcriptional regulation.
BRCA1/2	Transcriptional regulation and DNA repair.
MSH2/ 6	DNA repair.
MLH1	DNA repair.
TGF R I/II	Growth inhibition.
TSC2	Cell cycle regulator.
PMS1/ 2	DNA repair.
Maspin	Tumor metastasis and tumor-induced angiogenesis inhibition.

¹⁰ Kiwerska, K.; Szyfter, K. *J. Appl. Genet.* **2019**, *60*, 329-334.

¹¹ Wang, L. H.; Wu, C. F.; Rajasekaran, N.; Shin, Y. K. *Cell. Physiol. Biochem.* **2019**, *51*, 2647-2693.

One of the most important tumor suppressor genes is the TP53 which encodes p53 protein. Some humans have a mutant allele of this gene, causing the Li-Fraumeni syndrome, which is characterized by an elevated risk of a variety of cancers.¹² In about the 50% of all human cancers this gene is deleted, mutated or compromised, limiting the effectiveness of the p53 pathway.

Other important genes are, for example, the RB1 gene that encodes pRB protein, which main role is to stop the uncontrolled division of cells,¹³ and BRCA1/2 genes, which code proteins involved in the detection and reparation of damaged DNA. These genes are used as screening tests for the early detection of ovarian and breast cancer.¹⁴

M. Cellular senescence.

The cell cycle (Figure 3) is a four-stage process that leads eukaryote cells to their division and replication. In G1 phase diverse metabolic changes take place, preparing the cell for division. Then, the cell moves to the S phase (synthesis phase), where DNA is synthesized. Thereafter, the cell starts preparing for mitosis, growing, duplicating its DNA and accumulating nutrients. This step is commonly denominated as interphase or G2 phase. Once the cell is prepared, it enters into the M phase (Mitosis), which is sub-divided into two tightly coupled processes: the mitosis itself, where the cell splits itself into two identical cells, replicating the chromosomes and the cytokinesis, where the cytoplasm divides in half, forming two daughter cells. Finally, the G0 or resting phase is the stage in which cells exist in a quiescent state, having their division temporary stopped.¹⁵

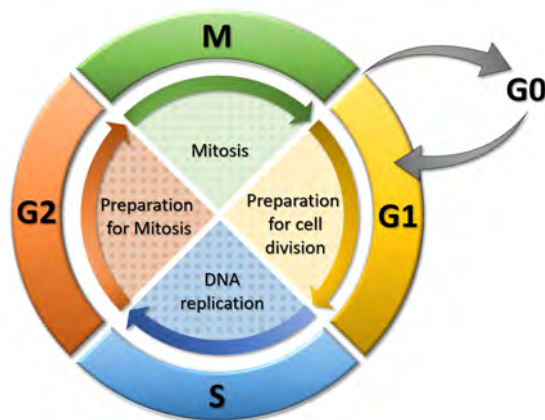


Figure 3. Cell cycle.

¹² Harris, C. C.; Hollstein, M.; *N. Engl. J. Med.* **1993**, 329, 1318-1327.

¹³ Dyson, N. J. *Genes Dev.* **2016**, 30, 1492-1502.

¹⁴ Haffty, B. G; Euhus, D. M. Pierce, L. J. *Int. J. Clin. Oncol.* **2020**, 38, 2220-2229.

¹⁵ Malumbres, M.; Barbacid, M. *Nat. Rev. Cancer* **2001**, 1, 222-231.

Cellular senescence is defined as “a state of permanent cell cycle arrest”, which differs from quiescence in its reversibility. Senescence occurs as a response to DNA damage or degradation that would make the cell’s progeny nonviable. It is also triggered as a mechanism of protection, limiting the cell growth and restricting the proliferation capacity after a certain number of divisions. This capability of growth inhibition after a defined number of mitoses is an important mechanism for the protection against the immortalization of cells and the further development of cancer disease.⁹

V. Apoptosis.

Apoptosis is the mechanism of regulated cell death and, not only occurs as a result of cell damage or external stress, but it is also triggered in normal cell development. This mechanism is modulated by different regulatory molecules and is characterized by chromatin material condensation, DNA fragmentation, cell shrinkage, membrane blebbing and the loss of adhesion to extracellular matrices. This kind of cell death is distinguished from necrosis, which represents the opposite way, unordered cell death in response to severe trauma.¹⁶

The defects in the induction of the apoptosis pathways can lead to the multiplication of neoplastic cells. Apoptosis can be induced in cancer cells through intrinsic and extrinsic pathways:

Intrinsic pathway. The main requirements to trigger this pathway are mitochondrial outer membrane permeabilization (MOMP) and the subsequent release of Cytochrome C into the cytoplasm. The release of Cytochrome C is stimulated by pro-apoptotic members of the BCL-2 protein family (BIM, BID, PUMA and NOXA) and inhibited by the anti-apoptotic members of the same family (BCL-2 and BCL-XL). Pro-apoptotic proteins activate BAX and BAK1, the central effectors of apoptosis, which form a pore in the mitochondrial membrane causing MOMP. Then, Cytochrome C is released, leading to the formation of the apoptosome. Finally, after the sequential activation of various caspase proteins, apoptosis is effected (Figure 4A).¹⁷

Extrinsic pathway: This pathway is initiated by death receptors (cell membrane proteins) such as Fas and TRAIL (TNF-related apoptosis-inducing ligand) that, after ligand binding, trimerize and aggregate. This process is followed by the activation of caspases 8 and 10 that activate effector caspases, triggering apoptosis. In addition, caspases 8 and 10 activate BID pro-apoptotic protein, which is translocated to the mitochondria, contributing to the release of Cytochrome C. BID protein is the link between the extrinsic and intrinsic pathways of the apoptosis (Figure 4B).¹⁷

¹⁶ Jan, R.; Chaudhry, G-S. *Adv Pharm Bull* **2019**, *9*, 205-218.

¹⁷ Carneiro, B. A.; El-Deiry, W. S. *Nat. Rev. Clin. Oncol.* **2020**, *17*, 395-417.

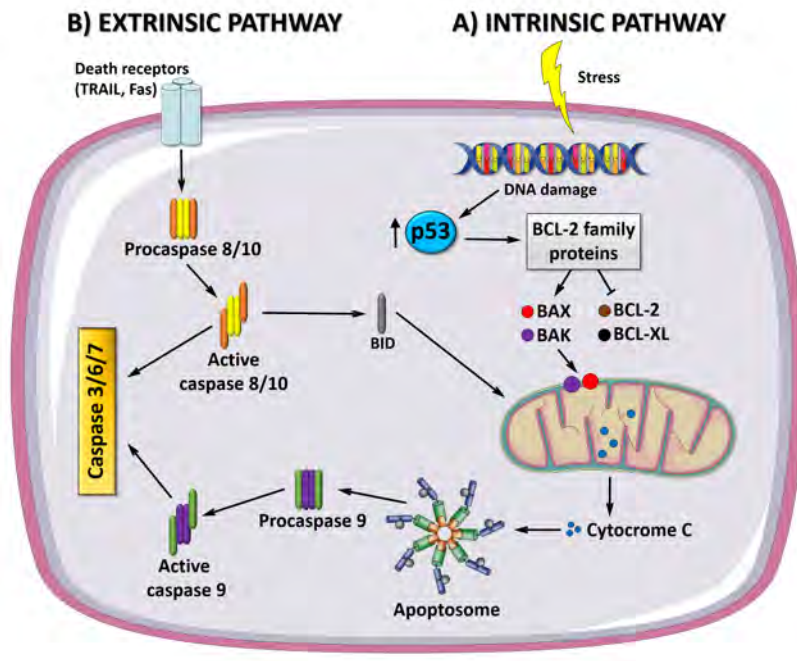


Figure 4. Apoptosis pathways (adapted from Jan *et al.*, 2019).¹⁶

VI. Inhibition of angiogenesis.

As described above, when the tumor grows, it needs to develop a blood supply in order to support its metabolic requirements. These new blood vessels can also be used as an escape route to metastasize. Angiogenesis can be stimulated by various angiogenic factors (fibroblast growth factors, angiogenin and vascular endothelial growth factors) and inhibited by angiostatic molecules (angiostatin, interleukins and interferons α , β and γ). Tumor angiogenesis and uncontrolled metastasis starts when the balance between angiogenic and angiostatic molecules is broken.⁹

Drug therapies against cancer.

For ages, the treatment of cancer diseases has been a highly complex process and, although several innovative approaches have been developed and approved for clinical use, such as stem cell therapy, gene therapy, targeted drug therapy¹⁸ and immunotherapy (i.e. monoclonal antibodies and antibody-

¹⁸ Debela, D. T.; Muzazu, S. G.; Heraro, K. D.; Ndalama, M. T.; Mesele, B. W.; Haile, D. C.; Kitui, S. K.; Manyazewal, T. *SAGE Open Med.* **2021**, *9*, 1-10.

drug conjugates),¹⁹ today the prevalent general therapies are still a combination of surgery with chemotherapy and/or radiation therapy (Figure 5).

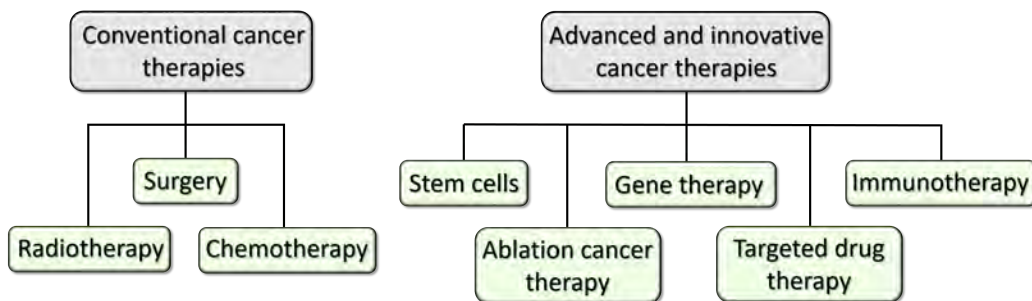


Figure 5. Conventional and advanced and innovative cancer therapy strategies.

One of the most common strategies for cancer treatment includes the surgical resection of the tumors followed by radiation therapy, comprising the use of ionizing radiation to target the cancerous tumor and all surrounding cells of the tumor microenvironment. As a supplement or alternative to radiation, chemotherapy implies the use of natural or synthetic low molecular weight molecules, which are able to kill all rapidly dividing cells and can be used to treat the entire body.²⁰

Radiotherapy and chemotherapy used in conjunction are very effective in order to attack cancer by multiple approaches and can help to prevent cancer cells from becoming resistant to the treatment. It can be conducted in different modes, depending on the treatment type:²¹

- **Neoadjuvant therapy** involves chemotherapy followed by radiation therapy before surgery. It is used to reduce the size of the tumor and scale down the amount of surgery that is necessary
- **Adjuvant therapy** is applied after surgery, in the case some cancer cells may still be present in the patient's organism. Not only chemotherapy and radiotherapy can be used as adjuvant therapy tools, but also hormone therapy, immunotherapy and targeted therapy.
- **Concomitant therapy** is the use of chemotherapy and radiation therapy without surgical intervention.

¹⁹ Chau, C. H.; Steeg, P. S.; Figg, W. D. *Lancet* **2019**, *394*, 793-804.

²⁰ Arruebo, M.; Vilaboa, N.; Sáez-Gutierrez, B.; Lambea, J.; Tres, A.; Valladares, M.; González-Fernández, Á. *Cancers* **2011**, *3*, 3279-3330.

²¹ Baudino, T. *Curr. Drug Discov. Technol.* **2015**, *12*, 3-20.

Chemotherapy comprehends drugs with many different mechanisms of action and chemical structures: alkylating agents (i.e. cyclophosphamide and oxaliplatin),²² anti-metabolites or analogs of nucleic acids (i.e. mercaptopurine, 5-fluorouracil and methotrexate),²³ topoisomerase inhibitors (i.e. camptothecin and topotecan),²⁴ anthracyclines (i.e. daunorubicin and doxorubicin)²⁵ and plant alkaloids (i.e. vinblastine and vincristine)²⁶ (Figure 6).

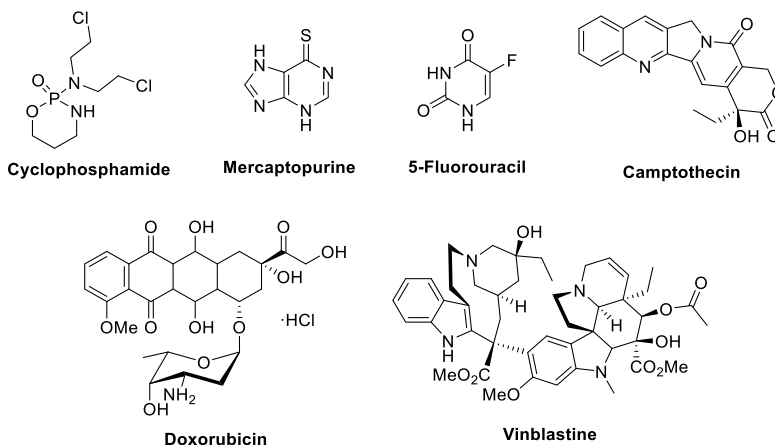


Figure 6. Structures of some chemotherapeutic agents.

This drug therapy shows several limitations, such as dosage selection difficulty, rapid drug metabolism and the development of many harmful side effects.²⁷ These adverse effects are mainly caused in the patients due to the lack of specificity toward malignant cells. Chemotherapeutic agents attack rapidly dividing and growing cells, and since cancerous cells are not the only type of cells with these characteristics in our body, other rapidly dividing and growing cell types are also affected during the treatment, including bone marrow, digestive tract and hair follicle cells.²⁰ Another major disadvantages is the drug resistance, which happens when cancer cells develop resistance to the anti-cancer drug.²⁸

²² Puyo, S.; Montaudon, D.; Pourquier, P. *Crit. Rev. Oncol. Hematol.* **2014**, *89*, 43-61.

²³ Peters, G. J.; Van Der Wilt, C. L.; Van Moorsel, C. J. A.; Kroep, J. R.; Bergman, A. M.; Ackland, S. P. *Pharmacol. Ther.* **2000**, *87*, 227-253.

²⁴ Liang, X.; Wu, Q.; Luan, S.; Yin, Z.; He, C.; Yin, L.; Zou, Y.; Yuan, Z.; Li, L.; Song, X.; He, M.; Lv, C.; Zhang, W. *Eur. J. Med. Chem.* **2019**, *171*, 129-168.

²⁵ Baka, S.; Califano, R.; Ferraldeschi, R.; Aschroft, L.; Thatcher, N.; Taylor, P.; Favre-Finn, C.; Blackhall, F.; Lorigan, P. *Br. J. Cancer* **2008**, *99*, 442-447.

²⁶ Mondal, A.; Gandhi, A.; Fimognari, C.; Atanasov, A. G.; Bishayee, A. *Eur. J. Pharmacol.* **2019**, *858*, 172472.

²⁷ Debela, D. T.; Muzazu, S. G.; Heraro, K. D.; Ndalama, M. T.; Mesele, B. W.; Haile, D. C.; Kitui, S. K.; Manyazewal, T. *SAGE Open Med.* **2021**, *9*, 1-10.

²⁸ Shapira, A.; Livney, Y. D.; Broxterman, H. J.; Assaraf, Y. G. *Drug Resist. Updat.* **2011**, *14*, 150-163.

Taking into account these considerations, it is clear that there is still a serious need to develop new chemotherapeutic agents that may be able to bind selective targets at a molecular level. For instance, during the last decade, our research group has developed new Topoisomerase I inhibitors and tested their anticancer potential against different types of cancer and other infectious diseases.²⁹ In this context, one promising biochemical target is the interaction between p53 transcription factor (encoded by the TP53 tumor suppressor gene) and the MDM2 (Murine Double Minute 2) and MDMX (Murine Double Minute X) proteins.

Indeed, in many cancers, it is common to observe mutations in p53 protein, but also tumors frequently possess WTp53 (Wild Type p53) exhibiting damaged p53 signaling pathways due to mutated or dysregulated protein partners.³⁰ Due to the increased or overexpressed MDM2 and MDMX activity, in many tumors the inactivation and degradation of p53 is favored, thus limiting p53 activity against cancer cell proliferation.³¹ In fact, MDM2 and MDMX mutations and overexpression are observed in human cancers such as sarcoma,³² neuroblastoma,³³ glioblastoma,³⁴ breast,³⁵ prostate,³⁶ ovarian,³⁷ colon³⁸ and lung.³⁹ Other examples and their specific alterations are depicted in Figure 7.

²⁹ (a) Selas, A.; Fuertes, M.; Melcón-Fernández, E.; Pérez-Pertejo, Y.; Reguera, R. M.; Balaña-Fouce, R.; Knudsen, B. R.; Palacios, F.; Alonso, C. *Pharmaceuticals* **2021**, *14*, 784. (b) Rizo-Liendo, A.; Arberas-Jiménez, I.; Martín-Encinas, E.; Sifaoui, I.; Reyes-Battle, M.; Chao-Pellicer, J.; Alonso, C.; Palacios, F.; Piñero, J. E.; Lorenzo-Morales, J. *Pharmaceuticals* **2021**, *14*, 1013. (c) Carramiñana, V.; Ochoa de Retana, A. M.; Palacios, F.; de los Santos, J. M. *Molecules* **2021**, *26*, 4265. (d) Tejería, A.; Pérez-Pertejo, Y.; Reguera, R. M.; Carbajo-Andrés, R.; Balaña-Fouce, R.; Alonso, C.; Martín-Encinas, E.; Selas, A.; Rubiales, G.; Palacios, F. *Eur. J. Med. Chem.* **2019**, *162*, 18-31.

³⁰ Miller, J. J.; Gaiddon, C.; Storr, T. *Chem. Soc. Rev.* **2020**, *49*, 6995-7014.

³¹ Momand, J.; Jung, D.; Wilczynski, S.; Niland, J. *Nucleic Acids Res.* **1998**, *26*, 3453-3459.

³² Flørenes, V. A.; Mælandsmo, G. M.; Forus, A.; Andreassen, Å.; Myklebost, O.; Fodstad, Ø. *J. Natl. Cancer Inst.* **1994**, *86*, 1297-1302.

³³ (a) Zafar, A.; Wang, W.; Liu, G.; Xian, W.; McKeon, F.; Zhou, J.; Zhang, R. *Cancer Lett.* **2021**, *496*, 16-29. (b) Corvi, R.; Savelyeva, L.; Breit, S.; Wenzel, A.; Handgretinger, R.; Barak, J.; Oren, M.; Amler, L.; Schwab, M. *Oncogene* **1995**, *10*, 1081-1086.

³⁴ (a) He, J.; Reifemberger, G.; Liu, L.; Collins, V. P.; James, C. D. *Genes Chromosom. Cancer* **1994**, *11*, 91-96. (b) Reifemberger, G.; Liu, L.; Ichimura, K.; Schmidt, E. E.; Collins, V.P. *Cancer Res.* **1993**, *53*, 2736-2739.

³⁵ (a) Loo, L. W. M.; Gao, C.; Shvetsov, Y. B.; Okoro, D. R.; Hernandez, B. Y.; Bargonetti, J. *Breast Cancer Res. Treat.* **2019**, *174*, 257-269. (b) Turbin, D. A.; Cheang, M. C. U.; Bajdik, C. D.; Gelmon, K. A.; Yorida, E.; De Luca, A.; Nielsen, T. O.; Huntsman, D. G.; Gilks, C. B. *Mod. Pathol.* **2006**, *19*, 69-74.

³⁶ Wang, H.; Yu, D.; Agrawal, S.; Zhang, R. *Prostate* **2003**, *54*, 194-205.

³⁷ (a) Palazzo, J. P.; Monzon, F.; Burke, M.; Hyslop, T.; Duntton, C.; Barusevicius, A.; Capuzzi, D.; Kovatich, A. *J. Hum. Pathol.* **2000**, *31*, 698-704. (b) Skomedal, H.; Kristensen, G. B.; Abeler, V. M.; Børresen-Dale, A. L.; Tropé, C.; Holm, R. *J. Pathol.* **1997**, *181*, 158-165.

³⁸ (a) Barcherini, V.; Almeida, J.; Lopes, E. A.; Wang, M.; Magalhães e Silva, D.; Mori, M.; Wang, S.; Saraiva, L.; Santos, M. M. *ChemMedChem* **2021**, *16*, 250-258. (b) Zhang, R.; Wang, H.; Agrawal, S. *Curr. Cancer Drug Targets* **2005**, *5*, 43-49.

³⁹ Eymin, B.; Gazzeri, S.; Brambilla, C.; Brambilla, E. *Oncogene* **2002**, *21*, 2750-2761.

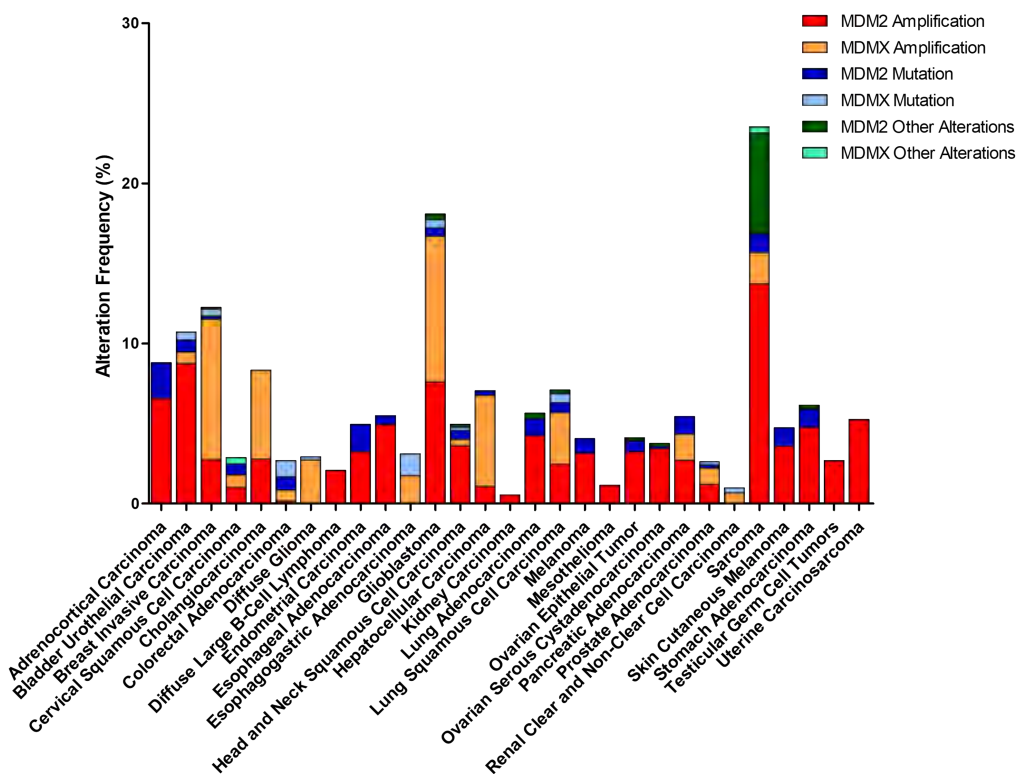


Figure 7. Schematic genetic aberrations of MDM2 and MDMX genes in clinical human cancer samples. Data from TCGA PanCancer Atlas from cBioPortal.⁴⁰

Normal (healthy or non-malignant) cells are less prone to die in response to p53 than the cancer cells are, so specific p53-MDM2/MDMX complex inhibitors are very interesting tools for restoring normal p53 activity and act selectively on malignant cells, thus considering them a promising and confirmed approach to cancer therapy.⁴¹

Although many peptide-type inhibitors with very high affinity towards MDM2 and MDMX have been developed,⁴² they usually suffer from low cell permeability and are proteolytically unstable.⁴³ As a promising field of current research, an alternative to this is the use of small molecules to pursue inhibition of p53/MDM2-MDMX. In the following lines, some of the most representative families and compounds are described. During this section, the inhibitory activity is given as the IC₅₀ value, which is

⁴⁰ cBioPortal Home Page. <https://www.cbioportal.org/> (accessed 2022-01-12).

⁴¹ Khoury, K.; Popowicz, G. M.; Holak, T. A.; Dömling, A. *Med. Chem. Comm.* **2011**, *2*, 246-260.

⁴² (a) Wang, X.; Ni, D.; Liu, Y.; Lu, S. *Front. Chem.* **2021**, *9*, 682-675. (b) Giustiniano, M.; Daniele, S.; Pelliccia, S.; La Pietra, V.; Pietrobono, D.; Brancaccio, D.; Cosconati, S.; Messere, A.; Giuntini, S.; Cerofolini, L.; Fragai, M.; Luchinat, C.; Taliani, S.; La Regina, G.; Da Settimo, F.; Silvestri, R.; Martini, C.; Novellino, E.; Marinelli, L. *J. Med. Chem.* **2017**, *60*, 8115-8130.

⁴³ Baek, S.; Kutchukian, P. S.; Verdine, G. L.; Huber, R.; Holak, T. A.; Lee, K. W.; Popowicz, G. M. *J. Am. Chem. Soc.* **2012**, *134*, 103-106.

the quantitative measure to indicate how much drug is needed to inhibit a biological process or biological component by 50% (usually obtained from cell viability assays), as K_d parameter, that refers to the affinity constant, and is obtained from experiments such as Microscale Thermophoresis (MST), Surface Plasmon Resonance (SPR) and NMR or as K_i value, that is, inhibition constant, measured through experiments such as Fluorescence Polarization (FP) and Homogeneous time-resolved fluorescence (HTRF).

p53-MDM2 and MDMX inhibitors.

Chalcone-like compounds were the first class of small p53-MDM2 inhibitors reported (Figure 8). In 2001 Holak and coworkers proposed a binding model for lead chalcone **1** where the extended π -system of the compound is rigid and planar in the binding pocket, with the *p*-chlorophenyl group occupying Trp23 binding site.⁴⁴ However, it showed low selectivity for cancer cells over non-malignant ones and, after treatment with **1**, the released p53 was unable to bind DNA again.

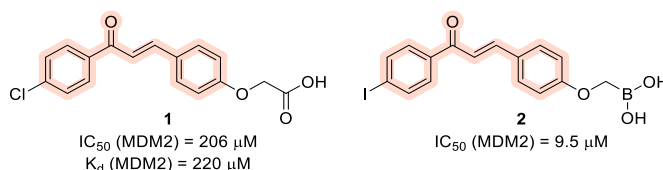


Figure 8. Chalcone (blush color) based analogues, the first described MDM2 inhibitors.

Some years later, Khan and coworkers described boronic acid chalcones **2**, with better results in terms of IC_{50} values.⁴⁵ Due to the general low selectivity toward the protein, the interest in chalcone-based analogues as p53-MDM2 inhibitors has been limited, but this approach has opened the door to a long road, leading to the synthesis of different inhibitors. Below, the most representative families of MDM2 and MDMX antagonists are discussed.

I. Nutlin-type compounds.

In 2004, Vassilev and coworkers identified Nutlins bearing a 1,2,4,5-tetrasubstituted-4,5-*cis*-imidazoline mother nucleus as potent MDM2 inhibitors (Figure 9).⁴⁶ The co-crystal structure of **Nutlin-2** bounded to MDM2 shows that the two halogen-substituted phenyl rings occupy the Trp23 and Leu26

⁴⁴ Stoll, R.; Renner, C.; Hansen, S.; Palme, S.; Klein, C.; Belling, A.; Zeslawski, W.; Kamionka, M.; Rehm, T.; Mühlhahn, P.; Schumacher, R.; Hesse, F.; Kaluza, B.; Voelter, W.; Engh, R. A.; Holak, T. A. *Biochemistry* **2001**, *40*, 336-344.

⁴⁵ Kumar, S. K.; Hager, E.; Pettit, C.; Gurulingappa, H.; Davidson, N. E.; Khan, S. R. *J. Med. Chem.* **2003**, *46*, 2813-2815.

⁴⁶ Vassilev, L. T.; Vu, B. T.; Graves, B.; Carvajal, D.; Podlaski, F.; Filipovic, Z.; Kong, N.; Kammlott, U.; Lukacs, C.; Klein, C.; Fotouhi, N.; Liu, E. A. *Science* **2004**, *303*, 844-848.

pockets, while the ethyl group is inserted in the Phe19 pocket, thereby inducing accumulation and stabilization of p53 and upregulation of p21. This causes cell cycle arrest at the G1 phase and apoptosis in various cell lines and xenograft models.⁴⁷ The most potent member of this family, **Nutlin-3a** is capable of efficiently and selectively blocking MDM2-p53 protein-protein interaction. After optimizing **Nutlin-3a** by structural modification, analogue compound **RG-7112**, obtained by scientists from Roche, ended phase I clinical trials in 2012, displaying better cell activity, good pharmacokinetic properties for oral administration, chemical stability and showing four times more inhibitory potency.⁴⁸

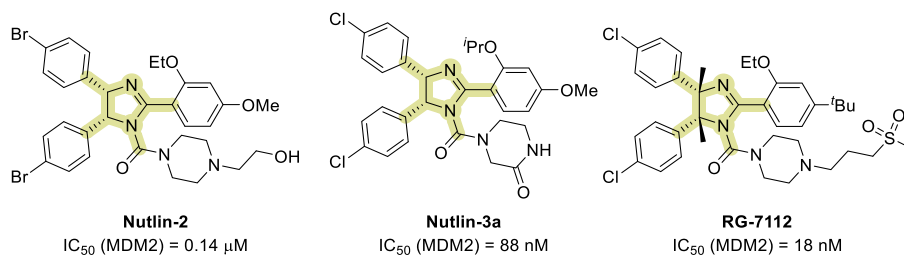


Figure 9. Nutlin (yellow color) type MDM2 inhibitors.

II. Imidazoles and Imidazothiazoles.

Some other imidazole derivatives have also been described as MDM2 inhibitors. Actually, this family of compounds should be considered as dual inhibitors, due to their concurrent ability to inhibit not only MDM2 but also MDMX protein (Figure 10).

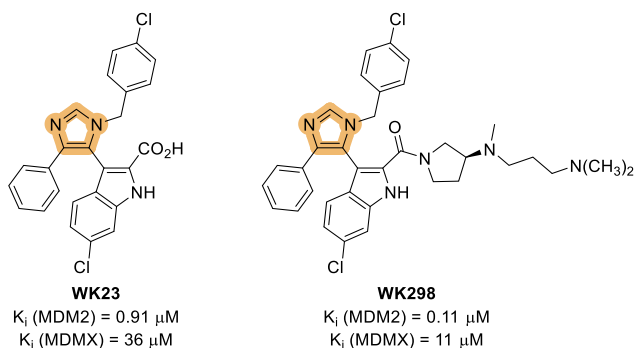


Figure 10. Imidazole (orange color) dual MDM2 and MDMX inhibitors.

⁴⁷ Tovar, C.; Rosinski, J.; Filipovic, Z.; Higgins, B.; Kolinsky, K.; Hilton, H.; Zhao, X.; Vu, B.T.; Qing, W.; Packman, K.; Myklebost, O.; Heimbrook, D. C.; Vassilev, L. T. *Proc. Natl. Acad. Sci. U.S.A.* **2006**, *103*, 1888-1893.

⁴⁸ Vu, B.; Wovkulich, P.; Pizzolato, G.; Lovey, A.; Ding, Q.; Jiang, N.; Liu, J.-J.; Zhao, C.; Glenn, K.; Wen, Y.; Tovar, C.; Packman, K.; Vassilev, L.; Graves, B. *ACS Med. Chem. Lett.* **2013**, *4*, 466-469.

The crystallization of complexes of **WK23** with MDM2, and **WK298** with MDMX, both small molecules, developed by Holak and coworkers, allowed the study of the differences in the binding sites of both proteins (Figure 10). Despite their ability to inhibit the two proteins, the affinity is superior for MDM2, due to the surrounding amino acids at Leu26, that make MDMX binding region more accessible to solvent, thus decreasing its affinity towards imidazoles.⁴⁹

In addition, imidazothiazol-like antagonists have also been described (Figure 11). For example, Uoto *et al.* synthesized bicyclic dihydroimidazothiazole **3**, where the imidazole ring is replaced by a dihydroimidazothiazole scaffold, obtaining an IC₅₀ value of 1.2 nM in MDM2.⁵⁰ In 2013, Miyazaki and coworkers designed a series of inhibitors containing this bicyclic core,⁵¹ such as compound **4**, which is ten times more active than **Nutlin-3a**. Some years later, these authors also synthesized compound **DS-5272**, a derivative of dihydroimidazothiazole **3** that shows good antitumor activity in SJSA-1 tumor xenograft model with high safety and good pharmacokinetic properties.⁵²

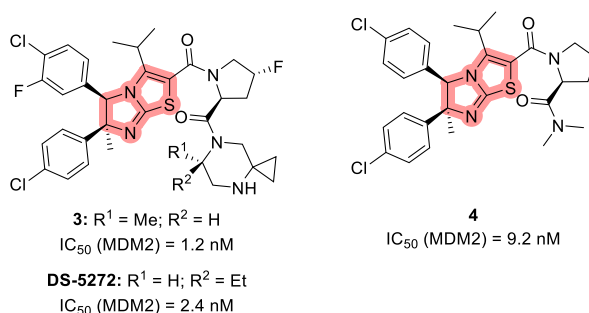


Figure 11. Imidazothiazol-like (red color) MDM2 inhibitors.

III. Benzodiazepines.

Another class of small-molecule inhibitors, 1,4-benzodiazepine-2,5-diones, was reported for the first time in 2005 (Figure 12).⁵³ The authors were able to isolate a crystal structure of MDM2 complexed

⁴⁹ Popowicz, G. M.; Czarna, A.; Wolf, S.; Wang, K.; Wang, W.; Dömling, A.; Holak, T. A. *Cell Cycle* **2010**, *9*, 1104–1111.

⁵⁰ Uoto, K.; Kawato, H.; Sugimoto, Y.; Naito, H.; Miyazaki, M.; Taniguchi, T.; Aonuma, M. Patent Application WO 2009/151069 A1, 2009.

⁵¹ (a) Miyazaki, M.; Naito, H.; Sugimoto, Y.; Yoshida, K.; Kawato, H.; Okayama, T.; Shimizu, H.; Miyazaki, M.; Kitagawa, M.; Seki, T.; Fukutake, S.; Shiose, Y.; Aonuma, M.; Soga, T. *Bioorg. Med. Chem.* **2013**, *21*, 4319–4331. (b) Miyazaki, M.; Naito, H.; Sugimoto, Y.; Kawato, H.; Okayama, T.; Shimizu, H.; Miyazaki, M.; Kitagawa, M.; Seki, T.; Fukutake, S.; Aonuma, M.; Soga, T. *Bioorg. Med. Chem. Lett.* **2013**, *23*, 728–732.

⁵² Miyazaki, M.; Uoto, K.; Sugimoto, Y.; Naito, H.; Yoshida, K.; Okayama, T.; Kawato, H.; Miyazaki, M.; Kitagawa, M.; Seki, T.; Fukutake, S.; Aonuma, M.; Soga, T. *Bioorg. Med. Chem.* **2015**, *23*, 2360–2367.

⁵³ (a) Parks, D. J.; LaFrance, L. V.; Calvo, R. R.; Milkiewicz, K. L.; Gupta, V.; Lattanze, J.; Ramchandren, K.; Carver, T. E.; Petrella, E. C.; Cummings, M. D.; Maguire, D.; Grasberger, B. L.; Lu, T. *Bioorg. Med. Chem. Lett.* **2005**, *15*, 765–770. (b) Raboisson, P.; Marugán, J. J.; Schubert, C.; Koblisch, H. K.; Lu, T.; Zhao, S.; Player, M. R.; Maroney, A. C.; Reed, R. L.; Huebert, N. D.; Lattanze, J.; Parks, D. J.; Cummings, M. D. *Bioorg. Med. Chem. Lett.* **2005**, *15*, 1857–1861.

with compound **5** but, despite the promising result, this molecule was not very active towards cancer cells, putting into manifest the need of improving their cell permeability.⁵⁴ Further optimization, with the introduction of a piperazine group in compound **6**, showed enhanced activity in MCF7 breast cancer cell-based experiments.⁵⁵ In addition, thiobenzodiazepines **7** and **8**, exhibit excellent binding affinities to MDM2 and better biological activity than Nutlin-3a in wild-type p53 osteosarcoma cells.⁵⁶

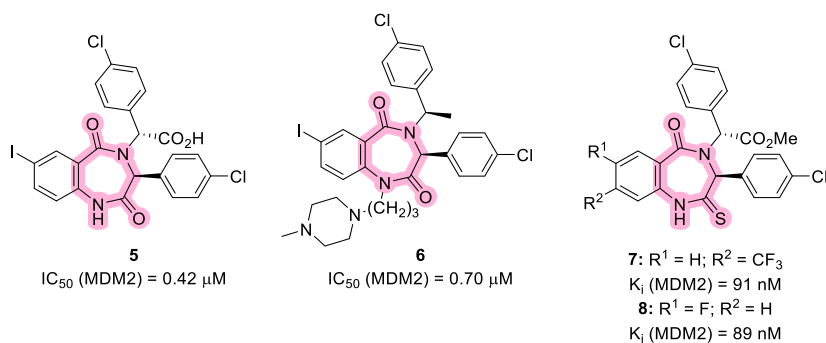


Figure 12. Benzodiazepines and thiobenzodiazepines (pink color) as MDM2 inhibitors.

IV. Spirooxindoles, indoles and indoyl hydantoines.

After an extensive analysis of the crystal structure of the p53-MDM2 complex and noticing that the indole ring of Trp23 is the key motif in this interaction, Wang and coworkers synthesized compound **9** as the first spirooxindole antagonist to mimic this binding engagement (Figure 13).⁵⁷ Since then, over the past decade, spirooxindoles have been extensively studied as MDM2 antagonists and modified, leading to the development of several potent analogues that have undergone preclinical and clinical studies.⁵⁸ For example, two of the most potent analogues are **SAR405838** and **APG-115**, which have

⁵⁴ (a) Parks, D. J.; LaFrance, L. V.; Calvo, R. R.; Milkiewicz, K. L.; José Marugán, J.; Raboisson, P.; Schubert, C.; Koblisch, H. K.; Zhao, S.; Franks, C. F.; Lattanze, J.; Carver, T. E.; Cummings, M. D.; Maguire, D.; Grasberger, B. L.; Maroney, A. C.; Lu, T. *Bioorg. Med. Chem. Lett.* **2006**, *16*, 3310-3314. (b) Grasberger, B. L.; Lu, T.; Schubert, C.; Parks, D. J.; Carver, T. E.; Koblisch, H. K.; Cummings, M. D.; LaFrance, L. V.; Milkiewicz, K. L.; Calvo, R. R.; Maguire, D.; Lattanze, J.; Franks, C. F.; Zhao, S.; Ramachandren, K.; Bylebyl, G. R.; Zhang, M.; Manthey, C. L.; Petrella, E. C.; Pantoliano, M. W.; Deckman, I. C.; Spurlino, J. C.; Maroney, A. C.; Tomczuk, B. E.; Molloy, C. J.; Bone, R. F. *J. Med. Chem.* **2005**, *48*, 909-912.

⁵⁵ Koblisch, H. K.; Zhao, S.; Franks, C. F.; Donatelli, R. R.; Tominovich, R. M.; LaFrance, L. V.; Leonard, K. A.; Gushue, J. M.; Parks, D. J.; Calvo, R. R.; Milkiewicz, K. L.; Marugán, J. J.; Raboisson, P.; Cummings, M. D.; Grasberger, B. L.; Johnson, D. L.; Lu, T.; Molloy, C. J.; Maroney, A. C. *Mol. Cancer Ther.* **2006**, *5*, 160-169.

⁵⁶ Guo, Z.; Zhuang, C.; Zhu, L.; Zhang, Y.; Yao, J.; Dong, G.; Wang, S.; Liu, Y.; Chen, H.; Sheng, C.; Miao, Z.; Zhang, W. *Eur. J. Med. Chem.* **2012**, *56*, 10-16.

⁵⁷ Ding, K.; Lu, Y.; Nikolovska-Coleska, Z.; Qiu, S.; Ding, Y.; Gao, W.; Stuckey, J.; Krajewski, K.; Roller, P. P.; Tomita, Y.; Parrish, D. A.; Deschamps, J. R.; Wang, S. *J. Am. Chem. Soc.* **2005**, *127*, 10130-10131.

⁵⁸ Gupta, A. K.; Bharadwaj, M.; Kumar, A.; Mehrotra, R. *Top. Curr. Chem.* **2017**, *375*, 1-25.

shown sub-nanomolar binding affinity to MDM2, demonstrating their capability of activating p53 in cancer cells and xenograft models and showing promising results in phase I clinical studies.⁵⁹

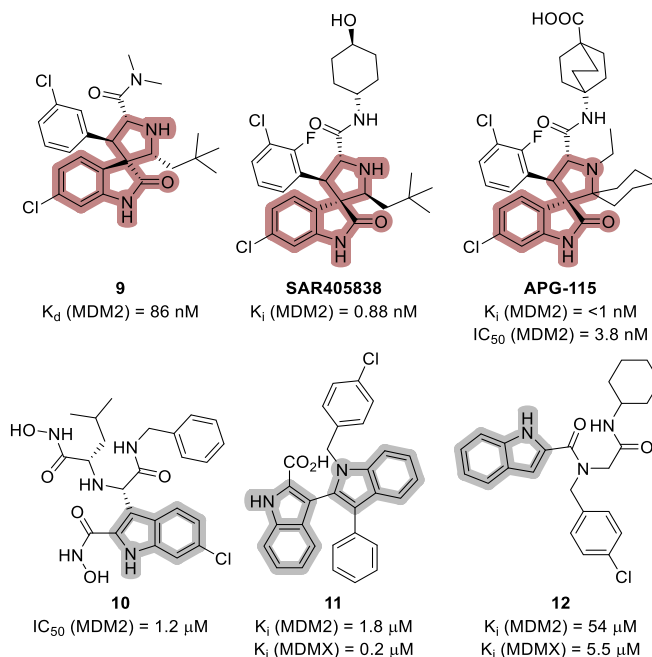


Figure 13. Spirooxindole (brown color) and indol (grey color) type MDM2/X inhibitors.

Moreover, some 3-substituted indole derivatives, such as compound **10**, have also been described as MDM2 inhibitors by Holak and Dömling.⁶⁰ These compounds are also capable to mimic the binding mode of the three amino acid residues of p53 to MDM2. There are some additional examples of inhibitors holding an indole core showing higher affinity to MDMX, like bis-indole **11**⁶¹ and substituted indole **12**.⁶²

Other indole derivatives of this sort, including indolyl hydatoins, have emerged as potent dual inhibitors (Figure 14). For example, despite **RO-2443** shows nanomolar activity against both of the

⁵⁹ (a) Aguilar, A.; Lu, J.; Liu, L.; Du, D.; Bernard, D.; McEachern, D.; Przybranowski, S.; Li, X.; Luo, R.; Wen, B.; Sun, D.; Wang, H.; Wen, J.; Wang, G.; Zhai, Y.; Guo, M.; Yang, D.; Wang, S. *J. Med. Chem.* **2017**, *60*, 2819-2839. (b) Wang, S.; Sun, W.; Zhao, Y.; McEachern, D.; Meaux, I.; Barrière, C.; Stuckey, J. A.; Meagher, J. L.; Bai, L.; Liu, L.; Hoffman-Luca, C. G.; Lu, J.; Shangary, S.; Yu, S.; Bernard, D.; Aguilar, A.; Dos-Santos, O.; Besret, L.; Guerif, S.; Pannier, P.; Gorge-Bernat, D.; Debussche, L. *Cancer Res.* **2014**, *74*, 5855-5865.

⁶⁰ (a) Huang, Y.; Wolf, S.; Beck, B.; Köhler, L. M.; Khoury, K.; Popowicz, G. M.; Goda, S. K.; Subklewe, M.; Twarda, A.; Holak, T. A.; Dömling, A. *ACS Chem. Biol.* **2014**, *9*, 802-811. (b) Bista, M.; Wolf, S.; Khoury, K.; Kowalska, K.; Huang, Y.; Wrona, E.; Arciniega, M.; Popowicz, G. M.; Holak, T. A.; Dömling, A. *Structure* **2013**, *21*, 2143-2151.

⁶¹ Neochoritis, C. G.; Wang, K.; Estrada-Ortiz, N.; Herdtweck, E.; Kubica, K.; Twarda, A.; Zak, K. M.; Holak, T. A.; Dömling, A. *Bioorg Med. Chem. Lett.* **2015**, *25*, 5661-5666.

⁶² Boltjes, A.; Huang, Y.; Van De Velde, R.; Rijke, L.; Wolf, S.; Gaugler, J.; Lesniak, K.; Guzik, K.; Holak, T. A.; Dömling, A. *ACS Comb. Sci.* **2014**, *16*, 393-396.

proteins, its poor water solubility affects cell tests, forcing to perform some chemical optimizations, leading to compound **RO-5963** with improved affinity and solubility.⁶³

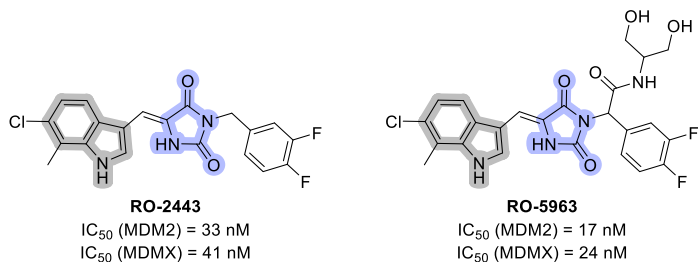


Figure 14. Indolyl (grey color)-hydantoin (light purple color) compounds as dual MDM2 and MDMX inhibitors.

V. Piperidinones and isoquinolines.

Over the last decade, extensive efforts have been made in order to optimize an MDM2 inhibitor bearing a piperidinone core, obtaining excellent results in some cases (Figure 15).

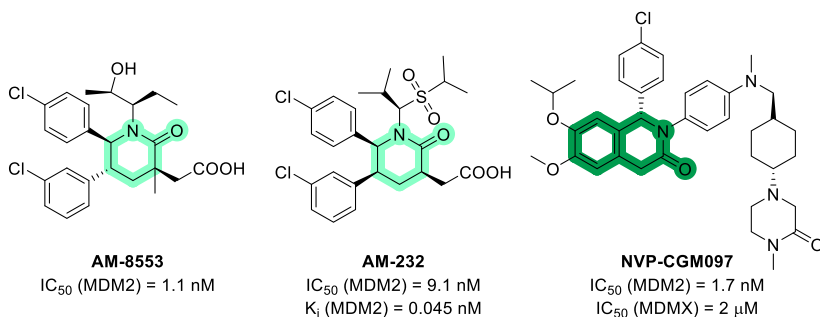


Figure 15. Piperidinones (light green color) and isoquinolines (dark green color) type MDM2/X antagonists.

The most remarkable outcomes were reported by Sun and coworkers. After several rounds of structural optimizations driven by X-ray crystal structure analysis substrate **AM-8553** was devised (Figure 15).⁶⁴ Then, further structural modifications resulted in the development of compound **AM-232**,⁶⁵ which induces significant upregulation of p53, and demonstrates clinically suitable

⁶³ Graves, B.; Thompson, T.; Xia, M.; Janson, C.; Lukacs, C.; Deo, D.; Di Lello, P.; Fry, D.; Garvie, C.; Huang, K. Sen; Gao, L.; Tovar, C.; Lovey, A.; Wanner, J.; Vassilev, L. T. *Proc. Natl. Acad. Sci. U. S. A.* **2012**, *109*, 11788-11793.

⁶⁴ Rew, Y.; Sun, D.; Gonzalez-Lopez De Turiso, F.; Bartberger, M. D.; Beck, H. P.; Canon, J.; Chen, A.; Chow, D.; Deignan, J.; Fox, B. M.; Gustin, D.; Huang, X.; Jiang, M.; Jiao, X.; Jin, L.; Kayser, F.; Kopecky, D. J.; Li, Y.; Lo, M. C.; Long, A. M.; Michelsen, K.; Oliner, J. D.; Osgood, T.; Ragains, M.; Saiki, A. Y.; Schneider, S.; Toteva, M.; Yakowec, P.; Yan, X.; Ye, Q.; Yu, D.; Zhao, X.; Zhou, J.; Medina, J. C.; Olson, S. H. *J. Med. Chem.* **2012**, *55*, 4936-4954.

⁶⁵ Rew, Y.; Sun, D. *J. Med. Chem.* **2014**, *57*, 6332-6341.

pharmacokinetic properties with *in vivo* antitumor activity in xenograft models and is currently on Phase I clinical studies.⁶⁶

Based on a similar core scaffold, Holzer's group developed **NVP-CGM097** (Figure 17) with nanomolar binding affinity for MDM2 and less activity against MDMX.⁶⁷ Indeed, biological studies performed with this molecule, suggested a high selectivity towards MDM2 over other protein targets and exceptional toxicity and pharmacological profiles. This compound has completed phase I clinical trials in 2020.⁶⁸

Other nitrogen-containing heterocycles have also been described, such as pyrrolopyrimidine **13**, which has demonstrated the same inhibitory capability for both proteins,⁶⁹ and acridine derivative **CTX1**, with a selective MDMX affinity. Some cell-based experiments confirmed that **CTX1** is able to increase the level of p53 and arrest cell cycle progression at G2-M phase, inducing apoptosis in p53 wild-type cancer cells as MCF7, HCT116, and A549 lines (Figure 16).⁷⁰

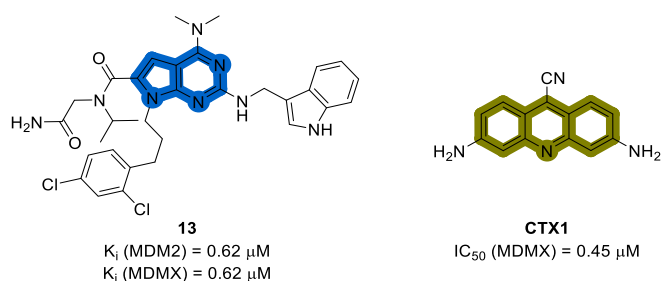


Figure 16. Pyrrolopyrimidine (dark blue color) and acridine (olive color) like inhibitors.

VI. Pyrrolidines and pyrrolidones.

After detecting serious adverse effects in clinical trials for nutlin derivative **RG-7112** and, taking this structure as starting point, Graves and coworkers (Hoffmann-La Roche) reported the discovery of pyrrolidine derivative **RG-7388** (also known as Idasanutlin), as an MDM2 inhibitor with superior

⁶⁶ (a) Her, N. G.; Oh, J. W.; Oh, Y. J.; Han, S.; Cho, H. J.; Lee, Y.; Ryu, G. H.; Nam, D. H. *Cell Death Dis.* **2018**, *9*, 1-12. (b) Canon, J.; Osgood, T.; Olson, S. H.; Saiki, A. Y.; Robertson, R.; Yu, D.; Eksterowicz, J.; Ye, Q.; Jin, L.; Chen, A.; Zhou, J.; Cordover, D.; Kaufman, S.; Kendall, R.; Oliner, J. D.; Coxon, A.; Radinsky, R. *Mol. Cancer Ther.* **2015**, *14*, 649-658.

⁶⁷ Holzer, P.; Masuya, K.; Furet, P.; Kallen, J.; Valat-Stachyra, T.; Ferretti, S.; Berghausen, J.; Bouisset-Leonard, M.; Pissot-Soldermann, C.; Rynn, C.; Ruetz, S.; Stutz, S.; Chène, P.; Jeay, S.; Gessier, F. *J. Med. Chem.* **2015**, *58*, 6348-6358.

⁶⁸ Weisberg, E.; Halilovic, E.; Cooke, V. G.; Nonami, A.; Ren, T.; Sanda, T.; Simkin, I.; Yuan, J.; Antonakos, B.; Barys, L.; Ito, M.; Stone, R.; Galinsky, I.; Cowens, K.; Nelson, E.; Sattler, M.; Jeay, S.; Wuerthner, J. U.; McDonough, S. M.; Wiesmann, M.; Griffin, J. D. *Mol. Cancer Ther.* **2015**, *14*, 2249-2259.

⁶⁹ Lee, J. H.; Zhang, Q.; Jo, S.; Chai, S. C.; Oh, M.; Im, W.; Lu, H.; Lim, H.-S. *J. Am. Chem. Soc.* **2011**, *133*, 676-679.

⁷⁰ Karan, G.; Wang, H.; Chakrabarti, A.; Karan, S.; Liu, Z.; Xia, Z.; Gundluru, M.; Moreton, S.; Sauntharajah, Y.; Jackson, M. W.; Agarwal, M. K.; Wald, D. N. *Mol. Cancer Ther.* **2016**, *15*, 574-582.

potency and selectivity (Figure 17).⁷¹ This compound activates efficiently the p53 pathway, leading to cell cycle arrest or apoptosis in cell lines expressing wild-type p53. In addition, this compound showed the ability to inhibit tumor proliferation in mice osteosarcoma xenograft assays and ended phase III clinical studies for acute myeloid leukemia in 2020. Other active pyrrolidine-derived inhibitors have been also described, such as substituted pyrrolidine-2-carboxamide **14** and cyanohydroxymethylphenyl pyrrolidine **15** (although the authors do not report IC₅₀ values).⁷² In addition, Furet and Kallen described indole and pyrrole-containing compound **16**, with thirteen times higher affinity to MDMX than to MDM2.⁷³

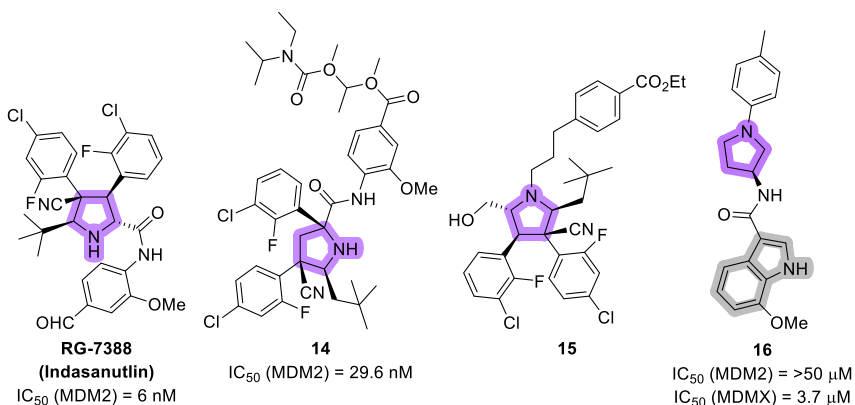


Figure 17. Pyrrolidine-like (dark purple color) MDM2 and MDMX inhibitors.

Not only pyrrolidine but also their carbonyl-containing derivatives, such as pyrrolidones, have proved their ability to inhibit both MDM2 and MDMX proteins (Figure 18). There are several examples of active substrates bearing the pyrrolidone scaffold fused with other heteroaromatic systems such as pyrrolo-pyrrolidone **17**,⁷⁴ pyrazolo-pyrrolidone **18**⁷⁵ and dihydropyrrol-imidazol derivative **HDM201**. For instance, the latter one, designed by Novartis Ag, ended phase I clinical trials in 2019, alone or in combination with other drugs (B-Raf inhibitors).⁷⁶ Additionally, there are other bi-specific MDM2/MDMX inhibitors, containing a pyrrolidone moiety without a fused ring structure. For example,

⁷¹ Ding, Q.; Zhang, Z.; Liu, J. J.; Jiang, N.; Zhang, J.; Ross, T. M.; Chu, X. J.; Bartkovitz, D.; Podlaski, F.; Janson, C.; Tovar, C.; Filipovic, Z. M.; Higgins, B.; Glenn, K.; Packman, K.; Vassilev, L. T.; Graves, B. *J. Med. Chem.* **2013**, *56*, 5979-5983.

⁷² (a) Bartkovitz, D.J.; Chu, X. J.; Vu, B.T.; Zhao, C.; Fishlock, D. Patent Application US 2013/0244958 A1, 2013. (b) Liu, J. J.; Ross, T. M. Patent Application US 2012/0149660 A1, 2012.

⁷³ Kallen, J.; Izaac, A.; Chau, S.; Wirth, E.; Schoepfer, J.; Mah, R.; Schlapbach, A.; Stutz, S.; Vaupel, A.; Guagnano, V.; Masuya, K.; Stachyra, T. M.; Salem, B.; Chene, P.; Gessier, F.; Holzer, P.; Furet, P. *ChemMedChem* **2019**, *14*, 1305-1314.

⁷⁴ Cotesta, S.; Furet, P.; Guagnano, V.; Holzer, P.; Kallen, J.; Mah, R.; Masuya, K.; Schlapbach, A.; Stutz, S.; Vaupel, A. Patent Application US 2013/317024 A1, 2013.

⁷⁵ (a) Kallen, J.; Izaac, A.; Chau, S.; Wirth, E.; Schoepfer, J.; Mah, R.; Schlapbach, A.; Stutz, S.; Vaupel, A.; Guagnano, V.; Masuya, K.; Stachyra, T. M.; Salem, B.; Holzer, P.; Furet, P. *ChemMedChem* **2019**, *14*, 1305-1314. (b) Furet, P.; Guagnano, V.; Holzer, P.; Mah, R.; Masuya, K.; Schlapbach, A.; Stutz, S.; Vaupel, A. Patent Application WO 2013/080141 A1, 2013

⁷⁶ Skalniak, L.; Surmiak, E.; Holak, T. A. *Expert Opin. Ther. Pat.* **2019**, *29*, 151-170.

in 2012, Zhang and coworkers reported a series of novel pyrrolidone inhibitors of p53-MDM2 protein-protein interaction. In particular, compound **20** showed affinity for both proteins, but one of the most active molecules (**19**) exhibited affinity only for MDM2, with higher *in vitro* antitumor potency than **Nutlin-3a** and good selectivity against tumor cells with deleted p53. Remarkably, compound **19** was found also to be orally active in the A549 xenograft model.⁷⁷ Some similar compounds, like 3-pyrrolin-2-one **21**, with the ability to dimerize the protein, were reported by Holak and Dubin in 2016.⁷⁸ A few years later, the same authors reported analog molecular entities, such as tetramic acid derivative **22**, although in this case displaying lower affinities against MDM2.⁷⁹

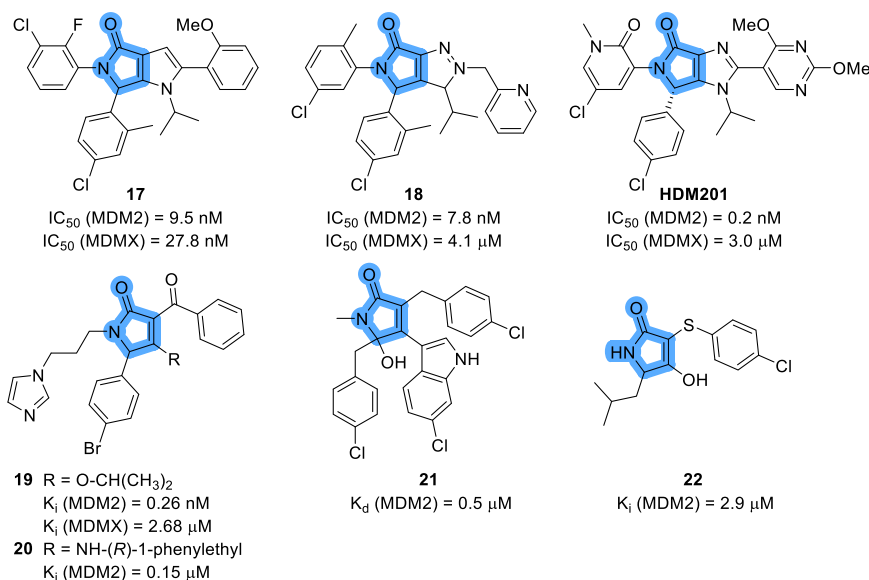


Figure 18. MDM2 and MDMX inhibitors with pyrrolidone (blue color) core.

Due to the promising inhibitory capacity shown by these compounds containing a pyrrolidone core (γ -lactam), in the following section the synthetic methods available for their preparation by means of multicomponent reactions will be explored.

⁷⁷ Zhuang, C.; Miao, Z.; Zhu, L.; Dong, G.; Guo, Z.; Wang, S.; Zhang, Y.; Wu, Y.; Yao, J.; Sheng, C.; Zhang, W. *J. Med. Chem.* **2012**, *55*, 9630-9642.

⁷⁸ Surmiak, E.; Twarda-Clapa, A.; Zak, K. M.; Musielak, B.; Tomala, M. D.; Kubica, K.; Grudnik, P.; Madej, M.; Jablonski, M.; Potempa, J.; Kalinowska-Tluscik, J.; Dömling, A.; Dubin, G.; Holak, T. A. *ACS Chem. Biol.* **2016**, *11*, 3310-3318.

⁷⁹ Muszak, D.; Łabuzek, B.; Brela, M. Z.; Twarda-Clapa, A.; Czub, M.; Musielak, B.; Surmiak, E.; Holak, T. A. *J. Mol. Struct.* **2019**, *1189*, 161-174.

Multicomponent Reactions (MCRs) for the synthesis of α,β -unsaturated γ -lactams.

The γ -lactam scaffold is the fundamental part of the structure of a vast number of natural and non-natural compounds covering an extensive spectrum of biological activities. Historically, the interest in this scaffold started with the increasing bacterial resistance against traditional β -lactam antibiotics,⁸⁰ turning the attention to γ -lactam derivatives and their analogues, thus becoming of primary interest in medicinal chemistry. Within this family of compounds, α,β -unsaturated γ -lactams or 1,5-dihydro-2*H*-pyrrol-2-ones are an exceptional class of compounds, which structure can be found in many pharmaceutically active natural and synthetic products.⁸¹

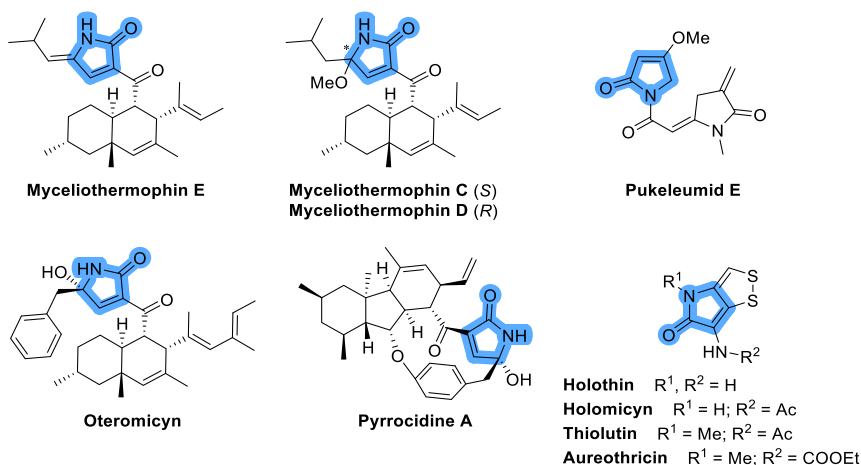


Figure 19. Bioactive natural 1,5-dihydro-2*H*-pyrrol-2-ones.

For example, the α,β -unsaturated γ -lactam core is present in cytotoxic polyketides Myceliothermophins E, C, and D,⁸² cytotoxic Pukeleumid E present in *Lyngbya majuscula* algae,⁸³ HIV-integrase inhibitor Oteromicyn⁸⁴ and antibiotic Pyrrocidine A,⁸⁵ both of them isolated from different

⁸⁰ (a) Allen, N. E.; Boyd, D. B.; Campbell, J. B.; Deeter, J. B.; Elzey, T. K.; Foster, B. J.; Hatfield, L. D.; Hobbs, J. N.; Homback, N. J.; Hunden, D. C.; Jones, N. D.; Kinnick, M. D.; Morin, J. M.; Munroe, J. E.; Swartzendruber, J. K.; Vogt, D. G. *Tetrahedron*, **1989**, *45*, 1905-1928. (b) Baldwin, J. E.; Lowe, C.; Schofield, C. J.; Lee, E. *Tetrahedron Lett.* **1986**, *27*, 3461-3464. (c) Boyd, D. B.; Elzey, T. K.; Hatfield, L. D.; Kinnick, M. D.; Morin, J. M. *Tetrahedron Lett.* **1986**, *27*, 3453-3456.

⁸¹ Caruano, J.; Muccioli, G. G.; Robiette, R. *Org. Biomol. Chem.* **2016**, *14*, 10134-10156.

⁸² Yang, Y.; Lu, C.; Chen, M.; Chen, K.; Wu, Y.; Wu, S. *Chem. Eur. J.* **2007**, *13*, 6985-6991.

⁸³ Janecka, A.; Wyre, A.; Gach, K.; Fichna, J.; Janecki, T. *Drug Discov. Today* **2012**, *17*, 561-572.

⁸⁴ (a) Hazuda, D.; Blau, C. U.; Felock, P.; Hastings, J.; Pramanik, B.; Wolfe, A.; Bushman, F.; Farnet, C.; Goetz, M.; Williams, M.; Silverman, K.; Lingham, R.; Singh, S. *Antivir. Chem. Chemother.* **1999**, *10*, 63-70. (b) Singh, S. B.; Goetz, M. A.; Jones, E. T.; Bills, G. F.; Giacobbe, R. A.; Herranz, L.; Stevens-Miles, S.; Williams, D. L. *J. Org. Chem.* **1995**, *60*, 7040-7042.

⁸⁵ He, H.; Yang, H. Y.; Bigelis, R.; Solum, E. H.; Greenstein, M.; Carter, G. T. *Tetrahedron Lett.* **2002**, *43*, 1633-1636.

fungus, as well as in the basic structure of 1,2-dithiole group antibiotics (Holothin, Holomycin, Thiolutin and Aureothricin)⁸⁶ (Figure 19).

On the other hand, in the literature, there are several examples of human-made drug candidates with diverse pharmacological activities where the dihydro-2H-pyrrol-2-one structure is present. In addition to the MDM2 and MDMX inhibitors described above in Figure 18, unsaturated γ -lactam derivatives show assorted activities as HIV integrase inhibitors,⁸⁷ antimalarial drugs,⁸⁸ anti-biofilm,⁸⁹ P2X3 receptor antagonists (analgesic),⁹⁰ HDAC inhibitors with anticancer activity,⁹¹ anticancer VEGF-R inhibitors⁹² or COX2 inhibitors such as Imrecoxib⁹³ (Figure 20).

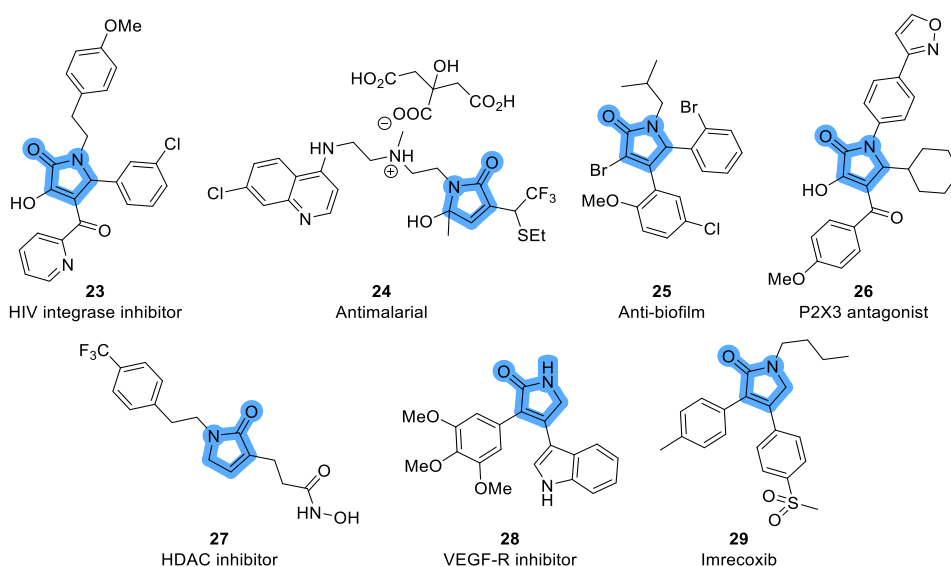


Figure 20. Non-natural 1,5-dihydro-2H-pyrrol-2-ones with pharmacological interest.

⁸⁶ Li, B.; Wever, W. J.; Walsh, C. T.; Bowers, A. A. *Nat. Prod. Rep.* **2014**, *31*, 905-923.

⁸⁷ Ma, K.; Wang, P.; Fu, W.; Wan, X.; Zhou, L.; Chu, Y.; Ye, D. *Bioorg. Med. Chem. Lett.* **2011**, *21*, 6724-6727.

⁸⁸ (a) Kanishchev, O. S.; Lavoignat, A.; Picot, S.; Médebielle, M.; Bouillon, J. P. *Bioorg. Med. Chem. Lett.* **2013**, *23*, 6167-6171. (b) Cornut, D.; Lemoine, H.; Kanishchev, O.; Okada, E.; Albrieux, F.; Beavogui, A. H.; Bienvenu, A.-L.; Picot, S.; Bouillon, J.-P.; Médebielle, M. *J. Med. Chem.* **2012**, *56*, 73-83.

⁸⁹ (a) Sordi, M. B.; Moreira, T. A.; Montero, J. F. D.; Barbosa, L. C.; Benfatti, C. A. M.; Magini, R. de S.; Pimenta, A. de L.; Souza, J. C. M. de. *J. Appl. Oral Sci.* **2018**, *26*, 1-8. (b) Pereira, U. A.; Barbosa, L. C. A.; Maltha, C. R. A.; Demuner, A. J.; Masood, M. A.; Pimenta, A. L. *Eur. J. Med. Chem.* **2014**, *82*, 127-138.

⁹⁰ Tobinaga, H.; Kameyama, T.; Oohara, M.; Kobayashi, N.; Ohdan, M.; Ishizuka, N.; Kume, M.; Tomari, M.; Tanaka, Y.; Takahashi, F.; Kinoshita, H.; Shimada, S.; Shinohara, S.; Kai, H. *Bioorg. Med. Chem. Lett.* **2018**, *28*, 2338-2342.

⁹¹ (a) Lee, C.; Choi, E.; Cho, M.; Lee, B.; Oh, S. J.; Park, S. K.; Lee, K.; Kim, H. M.; Han, G. *Bioorg. Med. Chem. Lett.* **2012**, *22*, 4189-4192. (b) Choi, E.; Lee, C.; Cho, M.; Seo, J. J.; Yang, J. S.; Oh, S. J.; Lee, K.; Park, S. K.; Kim, H. M.; Kwon, H. J.; Han, G. *J. Med. Chem.* **2012**, *55*, 10766-10770.

⁹² Peifer, C.; Selig, R.; Kinkel, K.; Ott, D.; Totzke, F.; Scha, C.; Heidenreich, R.; Schollmeyer, D.; Laufer, S. *J. Med. Chem.* **2008**, *51*, 3814-3824.

⁹³ (a) Feng, Z.; Chu, F.; Guo, Z.; Sun, P. *Bioorg. Med. Chem. Lett.* **2009**, *19*, 2270-2272. (b) Xu, H.; Zhang, Y.; Sun, Y.; Zhang, P.; Chu, F.; Guo, Z.; Zhang, H.; Zhong, D.; Zhang, Y.; Sun, Y.; Zhang, P.; Chu, F.; Guo, Z.; Zhang, H.; Zhong, D. *Xenobiotica* **2006**, *36*, 441-455.

From a synthetic point of view, an ideal reaction protocol should lead to the target product in good yield, using as few steps as possible as well as environmentally friendly reagents and solvents. The variables that need to be optimized are the costs with readily available starting materials, time, overall yield, the difficulty of performance, environmental acceptability, safety and, by today's standards, regio-, chemo- and stereo-selectivity. In multistep syntheses, the time and complexity factors increase proportionally with the number of steps. As an alternative, complex molecules can also be obtained *via* multicomponent reactions (MCRs), where three or more reagents react in a 'one pot' procedure to form a new molecule, which contains significant structural portions of all the participating reagents (Figure 21). It must be pointed out that, in these synthetic protocols, the starting materials do not have to react all together simultaneously in one step, but in a sequence of elementary stages (intermediate reactions), so that those reactions with irreversible steps drive the equilibrium to the formation of the final products (Figure 21).⁹⁴

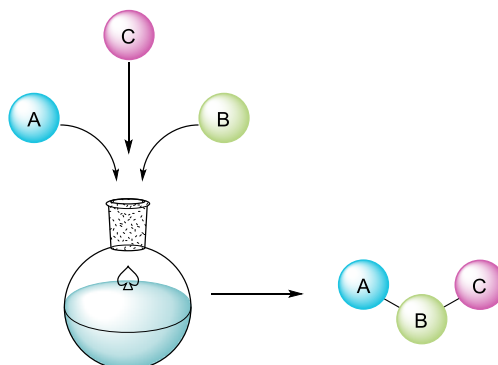


Figure 21. Scheme of a Multicomponent Reaction (MCR).

MCRs have some advantages with respect to ordinary sequential syntheses such as a high level of atom efficiency, the absence of isolation protocols for the intermediates, the optimization of waste production and the reduction of time consumption. Therefore, MCRs come quite close to the idea of an "ideal synthesis".⁹⁵

Since the XIX century, many MCRs have been developed for the construction of complex organic structures, such as Strecker reaction, for α -amino acid synthesis (1850),⁹⁶ Hantzsch reaction, for the synthesis of dihydropyridines (1882),⁹⁷ Biginelli reaction, for the preparation of dihydropyrimidines

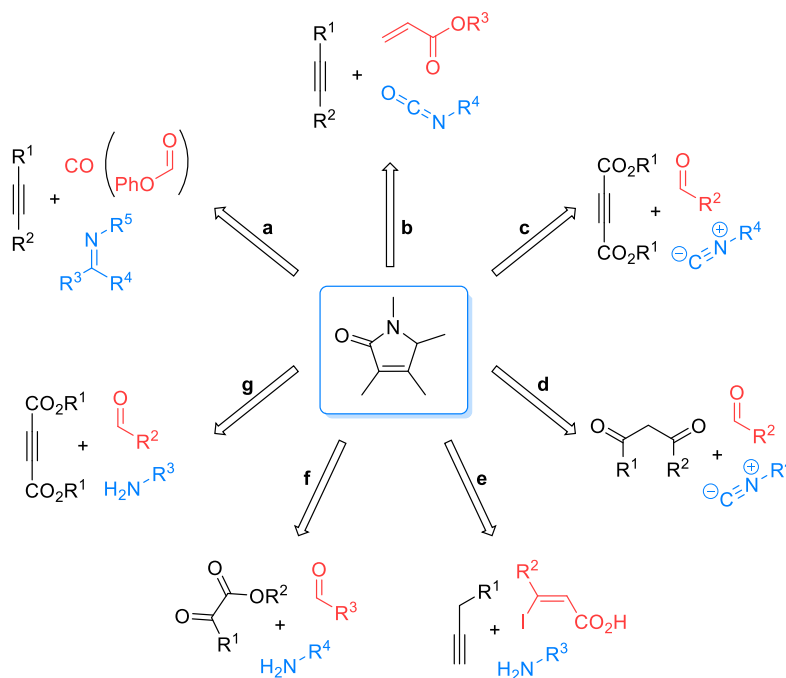
⁹⁴ (a) Török, B.; Schäfer, C.; Kokel, A. *Cancer: Multicomponent reactions*. In *Heterogeneous Catalysis in Sustainable Synthesis*; ScienceDirect, 2022; pp 443-489. (b) Dömling, A.; Ugi, I. *Angew. Chem. Int. Ed.* **2000**, *39*, 3168-3210.

⁹⁵ Orru, R. V. A.; Greef, M. *Synthesis* **2003**, 1471-1499.

⁹⁶ Strecker, A. *Justus Liebigs Ann Chem.* **1850**, *75*, 27-45.

⁹⁷ Hantzsch, A. *Justus Liebigs Ann. Chem.* **1882**, *215*, 1-82.

(1891),⁹⁸ the Mannich reaction (1912)⁹⁹ or the isocyanide-based Passerini (1921)¹⁰⁰ and Ugi reactions (1959).¹⁰¹ These reactions have an incredible potential in organic synthesis and have become an essential tool in the field of medicinal chemistry, where the demand of large collection of compounds or libraries of poly-functional substrates for biological screenings in drug discovery has increased in the last decades.¹⁰²



Scheme 1. Multicomponent synthetic strategies for the synthesis of α,β -unsaturated γ -lactam derivatives.

MCRs have also been applied to the preparation of unsaturated γ -lactam derivatives (Scheme 1).¹⁰³ In summary, some annulation reactions are reported such as [2+2+1] cycloaddition reactions between alkynes, carbon monoxide (or phenyl formate) and imines (Scheme 1, a), or using alkynes, acrylates and isocyanates (Scheme 1, b). Furthermore, [3+2] cycloaddition reactions between acetylenedicarboxylates, aldehydes and isocyanides are also described (Scheme 1, c). γ -Lactam substrates are also obtained from isocyanides using 1,3-dicarbonyl compounds and aldehydes (Scheme 1, d). In addition, α,β -unsaturated γ -lactam derivatives can be prepared *via* Sonogashira-type coupling

⁹⁸ Biginelli, P. *Ber.* **1891**, *24*, 1317-1319.

⁹⁹ Mannich, C.; Krosche, W. *Arch. Pharm.* **1912**, *250*, 647-667.

¹⁰⁰ Passerini, M. *Gazz. Chim. Ital.*, **1921**, *51*, 126-129.

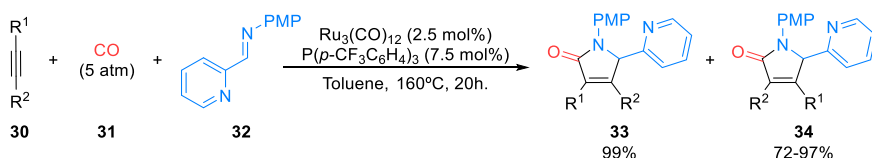
¹⁰¹ Ugi, I. *Angew. Chem., Int. Ed.* **1959**, *71*, 386-386.

¹⁰² Zhu, J.; Bienaymé, H. *Multicomponent Reactions*; Wiley-VCH, 2005.

¹⁰³ (a) Martínez de Marigorta, E.; de Los Santos, J. M.; Ochoa de Retana, A.; Vicario, J.; Palacios, F. *Beilstein J. Org. Chem.* **2019**, *15*, 1065-1085. (b) Martínez de Marigorta, E.; de Los Santos, J. M.; Ochoa de Retana, A.; Vicario, J.; Palacios, F. *Synthesis* **2018**, *50*, 4539-4554.

of terminal alkynes, (*Z*)- β -iodo- α,β -unsaturated acids and aliphatic amines (Scheme 1, e). Finally, the use of pyruvate derivatives or other pyruvate surrogates, such as activated acetylene species, in combination with aldehydes and amines is also plausible for the synthesis of dihydro-2*H*-pyrrol-2-ones (Scheme 1, f-g).

The [2+2+1] cycloaddition reaction is one of the most straightforward multicomponent approaches for the construction of 5-membered heterocycles (Scheme 1, a). For example, in 2000, Murai and coworkers reported the synthesis of 1,5-dihydro-2*H*-pyrrol-2-ones **33** using diphenylacetylene (**30**, R¹, R² = Ph) as a two carbon π -system, carbon monoxide (**31**) and imine **32** in a ruthenium-catalyzed Pauson-Khand type reaction (Scheme 2).¹⁰⁴ Additionally, the use of non-symmetrical alkynes **30** (R¹ = TMS; R² = Me, Ph) in the reaction provides γ -lactam derivatives **33** and **34**, after a spontaneous desilylation, as a mixture of regioisomers (15:85-92:8) in good to excellent yields.

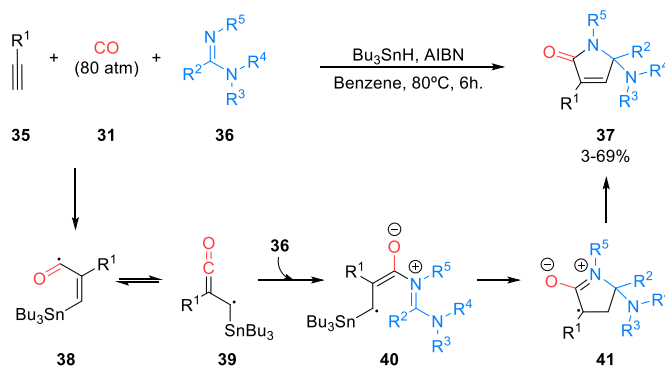


Scheme 2. Ruthenium-catalyzed Pauson-Khand reaction.

This reaction was extended by Ryu and coworkers, through the treatment of terminal alkynes **35** (R¹ = Alk) under carbon monoxide (**31**) atmosphere at high pressure using amidines **36** (R², R³, R⁴, R⁵ = Alk), to provide γ -lactam derivatives **37** by means of a free radical-mediated [2+2+1] cycloaddition reaction triggered by tributylstannane (Scheme 3).¹⁰⁵ The reaction starts with the formation of α,β -unsaturated acyl radical **38** from alkynes **35**, tributyltin radical and carbon monoxide (**31**). Radical species **38** is in equilibrium with α -ketenyl radical isomer **39**, which after the reaction with amidine **36**, leads to intermediate **40**. An *endo*-type cyclization provides cyclic radical **41** and a final β -fission would produce α,β -unsaturated γ -lactams **37** in poor to good yields.

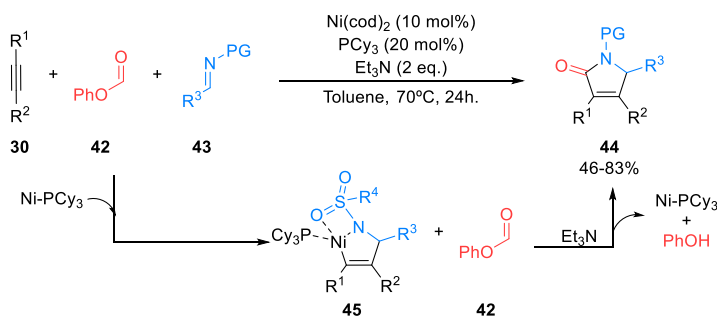
¹⁰⁴ Chatani, N.; Tobisu, M.; Asaumi, T.; Murai, S. *Synthesis* **2000**, 7, 925-928.

¹⁰⁵ Fukuyama, T.; Nakashima, N.; Okada, T.; Ryu, I. *J. Am. Chem. Soc.* **2013**, 135, 1006-1008.



Scheme 3. Free-radical mediated [2+2+1] cycloaddition reaction.

A similar [2+2+1] nickel-catalyzed carbonylative cycloaddition for the preparation of 1,5-dihydro-2*H*-pyrrol-2-ones **44** was described by Ogoshi in 2014 (Scheme 4). In this case, the authors used alkynes **30** ($R^1, R^2 = \text{Ar, Alk, TMS}$), *N*-tosylimines or *N*-(diphenylphosphinyl)imines (DPP) **43**, and phenyl formate (**42**) as a surrogate of carbon monoxide. This method provides better results when aromatic substituents are used at the acetylene substrates.¹⁰⁶



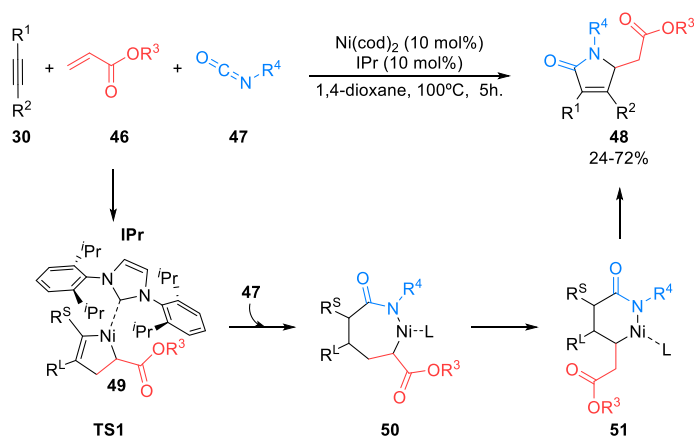
Scheme 4. Nickel-catalyzed [2+2+1] cycloaddition reaction.

Although the authors did not study the mechanism of this reaction in detail, it is known that the mixture of equimolar amounts of nickel (0), alkynes **30**, and sulfonylimines **43** (PG = Ts) leads to the formation of heteronickelacycles **45** that, after treatment with phenyl formate (**42**), produces γ -lactams **44**.¹⁰⁷ Thus, the catalytic version of this reaction is proposed to occur in a similar way. Interestingly the use of phenyl formate (**42**) as the carbon monoxide source in the presence of triethylamine, avoids the formation of catalytically unreactive nickel-tricarbonyl complexes.

¹⁰⁶ Hoshimoto, Y.; Ohata, T.; Sasaoka, Y.; Ohashi, M.; Ogoshi, S. *J. Am. Chem. Soc.* **2014**, *136*, 15877-15880.

¹⁰⁷ Ogoshi, S.; Ikeda, H.; Kurosawa, H. *Angew. Chem. Int. Ed.* **2007**, *46*, 4930-4932.

Other related multicomponent [2+2+1] cycloaddition reaction leading to the formation of γ -lactam derivatives was reported by Kurahashi and Matsubara in 2010. For this particular case, unsaturated γ -lactams **48** are obtained starting from dialkyl substituted alkynes **30** ($R^1, R^2 = \text{Alk}$), acrylates **46** ($R^3 = \text{Alk}$), and isocyanates **47** ($R^4 = \text{Ar, Alk}$) in the presence of a catalytic amount of nickel (Scheme 5).¹⁰⁸ A high degree of regioselectivity is observed for the final substrate bearing the largest substituent from alkyne **30** at the position 4 of the γ -lactam ring.



Scheme 5. Nickel-catalyzed three-component [2+2+1] cycloaddition.

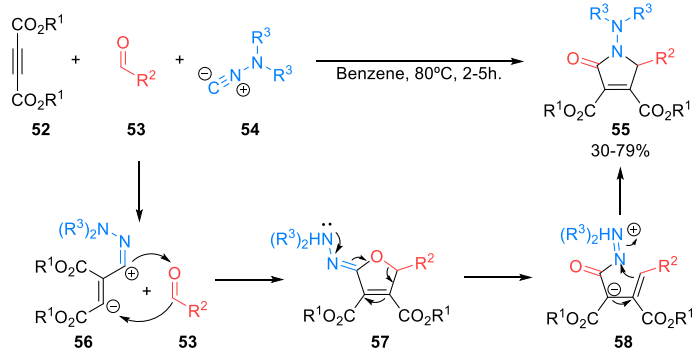
The catalytic cycle for this reaction starts with the oxidative cyclization of nickel-IPr complex with alkynes **30** and acrylates **46** to provide an intermediate nickel complex **49**, preferably with the bulkiest substituent (R^1) at the furthest position from the ligand, in order to minimize the steric hindrance (**TS1**). Next, isocyanate **47** is inserted, giving cyclic nickel(II) intermediate **50** and, after a β -hydride elimination followed by a further insertion of the nickel atom, species **51** is generated. Finally, a reductive elimination releases the active nickel complex and 1,5-dihydro-2H-pyrrol-2-ones **48**.

The use of isocyanide species in MCRs for the preparation of α,β -unsaturated γ -lactams has also been studied. In particular, a mixture of dimethyl acetylenedicarboxylate (**52**, $R^1 = \text{Me}$), benzaldehydes **53** ($R^2 = \text{Ar}$) and *iso*-propyl isocyanide (**54**, $R^3 = \text{Pr}$), in refluxing benzene affords 1-amino-2-oxo-2,5-dihydro-1H-pyrrole-3,4-dicarboxylates **55** in moderate to good yields (Scheme 6).¹⁰⁹ The reaction mechanism may consist of an initial nucleophilic addition of isocyanide **54** to activated acetylenedicarboxylate **52**, resulting in the formation of 1,3-dipole **56** that reacts in a [3+2]

¹⁰⁸ Ozawa, T.; Horie, H.; Kurahashi, T.; Matsubara, S. *Chem. Commun.* **2010**, 46, 8055-8057.

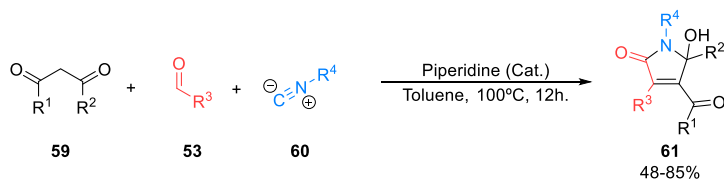
¹⁰⁹ (a) Nair, V.; Mathen, J. S.; Viji, S.; Srinivas, R.; Nandakumar, M. V.; Varma, L. *Tetrahedron* **2002**, 58, 8113-8118. (b) Nair, V.; Mathen, J. S.; Vinod, A. U.; Varma, R. L. *Chem. Lett.* **2001**, 3, 738-739.

cycloaddition process with aldehydes **53** to provide intermediate **57**. Then, γ -lactams **55** arise from a Dimroth-type rearrangement of furanone hydrazone **57** in the unstable open intermediate **58**. The use of acyl chlorides instead of aldehydes has been reported in a similar reaction.¹¹⁰



Scheme 6. Three-component reaction of acetylenedicarboxylates **52**, aldehydes **53** and isocyanide **54**.

In addition, Liang and coworkers described the use of 1,3-dicarbonyl compounds **59** instead of alkynes, in the presence of aldehydes **53** ($R^3 = \text{Ar}$), cyclohexyl isocyanide (**60**, $R^4 = \text{Cy}$) and piperidine as the catalyst to afford 5-hydroxy-1,5-dihydro-2H-pyrrol-2-ones **61** in fair to very good yields (Scheme 7).¹¹¹



Scheme 7. Three-component reaction for the synthesis of 5-hydroxy-1,5-dihydro-2H-pyrrol-2-ones **61**.

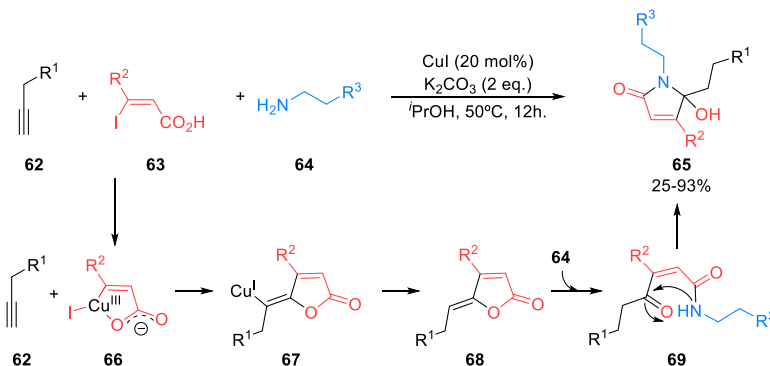
Commeiras and Parrain reported a particular case of a copper-catalyzed three-component reaction using terminal alkynes **62** ($R^1 = \text{Ar}$, Alk), (*Z*)- β -iodo- α,β -unsaturated acids **63** ($R^2 = \text{Ar}$, Alk) and aliphatic amines **64** ($R^3 = \text{Ar}$, Alk), obtaining 5-hydroxy-1H-pyrrol-2(5H)-ones **65** in poor to excellent yields (Scheme 8).¹¹² The authors propose a Sonogashira-type coupling that starts with an oxidative addition of copper(I) into the C-I bond of iodoalkene **63** to obtain copper(III) cyclic intermediate **66**. Then, the copper atom coordinates to the triple bond of alkyne **62** to form intermediate **67** and lactone **68** via a

¹¹⁰ Yavari, I.; Mokhtarporoyani-Sanandaj, A.; Moradi, L.; Mirzaei, A. *Tetrahedron* **2008**, *64*, 5221-5225.

¹¹¹ Fan, M. J.; Qian, B.; Zhao, L. B.; Liang, Y. M. *Tetrahedron* **2007**, *63*, 8987-8992.

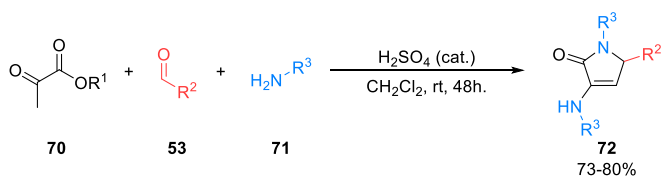
¹¹² (a) Mardjan, M. I. D.; Mayooufi, A.; Parrain, J. L.; Thibonnet, J.; Commeiras, L. *Org. Process Res. Dev.* **2020**, *24*, 606-614. (b) Mardjan, M. I. D.; Perie, S.; Parrain, J. L.; Commeiras, L. *Org. Biomol. Chem.* **2017**, *15*, 3304-3309. (c) Mardjan, M. I. D.; Parrain, J.; Commeiras, L. *Adv. Synth. Catal.* **2016**, *358*, 543-548.

subsequent protodemetalation process. Finally, the aliphatic amine **64** reacts with lactone **68** to yield α,β -unsaturated γ -lactams **65** through the open intermediate **69**.



Scheme 8. Copper-mediated MCR for the synthesis of γ -hydroxybutyrolactams **65**.

Following with the interest in the multicomponent synthesis of γ -lactam derivatives, one of the simplest methods for the construction of the γ -lactam core consists of the Brønsted acid-catalyzed reaction of pyruvates, aldehydes and amines, to give 3-hydroxy or 3-amino substituted α,β -unsaturated γ -lactams. In this context, our research group described in 2006, an efficient three-component reaction of ethyl pyruvate (**70**, $R^1 = \text{Et}$), aldehydes **53** ($R^2 = \text{Ar, Alk, CO}_2\text{Et}$), and aromatic amines **71** in the presence of catalytic amounts of sulfuric acid, affording 3-amino-1,5-dihydro-2H-pyrrol-2-ones **72** in very good yields (Scheme 9).¹¹³



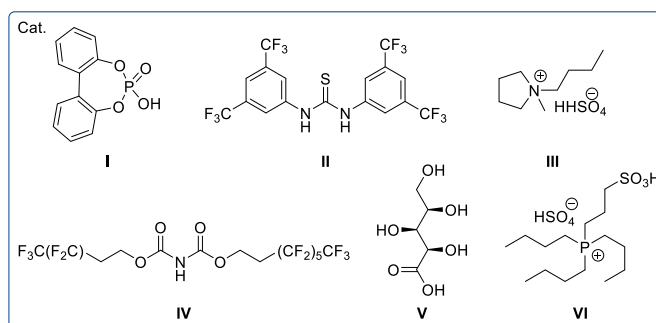
Scheme 9. Brønsted acid-catalyzed three-component reaction of ethyl pyruvate **70**, aldehydes **53**, and amines **71**.

As a continuation of this work, in the following years, several Brønsted acid catalysts demonstrated to be efficient in the same reaction. Some of the most relevant catalysts and conditions are summarized in Table 2 and Figure 22.

¹¹³ Palacios, F.; Vicario, J.; Aparicio, D. *Eur. J. Org. Chem.* **2006**, 2843-2850.

Table 2. Different methodologies for the preparation of 1,5-dihydro-2H-pyrrol-2-ones **72**.

Entry	Catalyst	Reaction conditions	Yield (%)
1	I or II (10 mol%)	Toluene, Na ₂ SO ₄ , rt.	51-89 ¹¹⁴
2	[Et ₃ NH][HSO ₄] (1 eq.)	ⁿ Hexane, rt.	45-93 ¹¹⁵
3	SiO ₂ -FeCl ₃	No Solvent, rt to 100 °C	60-74 ¹¹⁶
4	III (1 equiv.)	Ethanol, rt.	69-93 ¹¹⁷
5	Yb(OTf) ₃ (20 mol%)	No Solvent, rt.	57-84 ¹¹⁸
6	IV (5 mol%)	MeCN, Na ₂ SO ₄ , rt.	41-93 ¹¹⁹
7	V (12 mol%)	No Solvent, rt.	78 ¹²⁰
8	VI (10 mol%)	No Solvent, 60 °C	78-83 ¹²¹
9	-	ⁿ Hexane, 70 °C	60-97 ¹²²
10	-	No Solvent, 80 °C	45-95 ¹²³

**Figure 22.** Some of the catalysts reported for the preparation of 3-amino-1,5-dihydro-2H-pyrrol-2-ones **72**.

Remarkably, as a particular case of this reaction, Gein and coworkers described in 2002 the use of propanediamines to afford dimeric α,β -unsaturated γ -lactams in moderate to good yields.¹²⁴

An extension of this reaction was studied by Kawasuji and coworkers. In this case, the authors described a catalyst-free three-component reaction using heteroaromatic substituted acylpyruvates

¹¹⁴ Li, X.; Deng, H.; Luo, S.; Cheng, J. P. *Eur. J. Org. Chem.* **2008**, 4350-4356.

¹¹⁵ Reza, M.; Shafiee, M.; Najafabadi, B. H.; Ghashang, M. *J. Chem. Res.* **2011**, 35, 634-636.

¹¹⁶ Ghashang, M.; Shaterian, H. R. *Chin. J. Chem* **2011**, 29, 1851-1855.

¹¹⁷ Ghashang, M. *Res. Chem. Intermed.* **2013**, 39, 2187-2195.

¹¹⁸ Nagarajan, A. S.; Reddy, B. S. R. *Synth. Commun.* **2013**, 43, 1229-1236.

¹¹⁹ Qian, J. L.; Yi, W. Bin; Cai, C. *Tetrahedron Lett.* **2013**, 54, 7100-7102.

¹²⁰ Ma, J.; Zhong, L.; Peng, X.; Sun, R. *Green Chem.* **2016**, 18, 1738-1750.

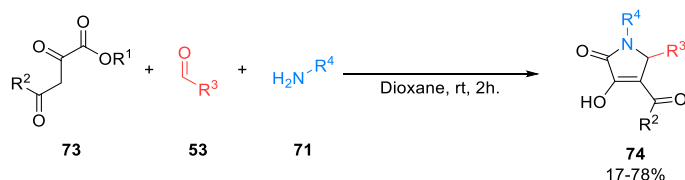
¹²¹ Yarie, M.; Zolfigol, M. A.; Saeidi-Rad, M. *J. Mol. Liq.* **2018**, 249, 144-152.

¹²² Shaterian, H. R.; Ranjbar, M. *Res. Chem. Intermed.* **2014**, 40, 2059-2074.

¹²³ (a) Bavadi, M.; Niknam, K.; Gharibi, M. *Monatsh. Chem.* **2017**, 148, 1025-1034. (b) Niknam, K.; Mojikhalifeh, S. *Mol. Divers.* **2014**, 18, 111-117.

¹²⁴ (a) Gein, V. L.; Kasimova, N. N.; Aliev, Z. G.; Vakhrin, M. I. *Russ. J. Org. Chem.* **2010**, 46, 875-883. (b) Gein, V. L.; Kasimova, N. N.; Potemkin, K. D. *Russ. J. Gen. Chem.* **2002**, 72, 1229-1230.

73, formaldehyde (**53**, $R^3 = H$) and aliphatic amines **71** ($R^4 = Alk$) to obtain C-4 substituted 3-hydroxy-1,5-dihydro-2*H*-pyrrol-2-ones **74** in yields ranging from poor to good (Scheme 10).¹²⁵ In addition, the use of (*E*)-cinnamyl substituted pyruvate derivative **73** ($R^1 = Me$; $R^2 = (E)\text{-CH=CHPh}$) in refluxing acetic acid provided the corresponding γ -lactams **74** in moderate yields (42-45%).¹²⁶ The use of acetic acid is crucial to extend the scope to different acylpyruvates, such as methyl benzoyl pyruvate (**73**, $R^1 = Me$; $R^2 = Ph$)¹²⁷ or heteroaromatic substituted pyruvate derivatives **73** ($R^1 = Me$; $R^2 = 2\text{-furyl, 2-thienyl}$).^{127,128} Other related examples of this reaction were also reported by Dehaen,¹²⁹ Hamzah,¹³⁰ and Komiotis.¹³¹



Scheme 10. Three-component reaction of acylpyruvates **73**, aldehydes **53** and amines **71**.

During the last decades, the relevance of this synthetic protocol in organic and medicinal chemistry has been evidenced by Gein and coworkers. Making use of the MCR of amines, aldehydes and pyruvate derivatives, the synthesis of several polyfunctional γ -lactam derivatives has been achieved and their biological activity has been evaluated, showing interesting properties as HIV integrase inhibitors, chemokine receptor modulators, anti-inflammatories, analgesics or antimicrobials.¹³²

Additionally, acetylenedicarboxylates **52** can be equally used instead of pyruvates, with slight variations in the procedure, for the preparation of γ -lactam derivatives. In this case, an enamine intermediate is preformed from amines **71** and acetylene dicarboxylates **52**, adding subsequently the two remaining reactants (aldehyde **53** and a second equivalent of amine **71**). This methodology is in

¹²⁵ Kawasuji, T.; Fuji, M.; Yoshinaga, T.; Sato, A.; Fujiwara, T.; Kiyama, R. *Bioorg. Med. Chem.* **2007**, *15*, 5487-5492.

¹²⁶ Vydzhak, R. N.; Panchishin, S. Y. *Russ. J. Gen. Chem.* **2008**, *78*, 1641-1642.

¹²⁷ Gein, V. L.; Tsypliyakova, E. P.; Stashina, G. A.; Bakulev, V. A. *Russ. J. Org. Chem.* **2008**, *44*, 478-480.

¹²⁸ Gein, V. L.; Mar'Yasov, M. A. *Russ. J. Org. Chem.* **2015**, *51*, 110-115.

¹²⁹ Metten, B.; Kostermans, M.; Van Baelen, G.; Smet, M.; Dehaen, W. *Tetrahedron* **2006**, *62*, 6018-6028.

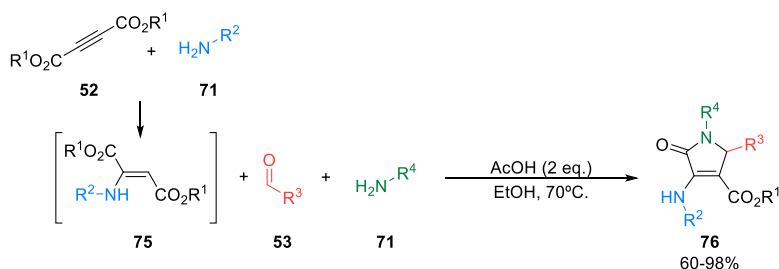
¹³⁰ Mohammat, M. F.; Shaameri, Z.; Hamzah, A. S. *Molecules* **2009**, *14*, 250-256.

¹³¹ Manta, S.; Tzioumaki, N.; Kollatos, N.; Andrea, P.; Margaritoulis, M.; Panagioutopoulou, A.; Papanastasiou, I.; Tsoinidis, A.; Schols, D.; Komiotis, D. *Curr. Microw. Chem.* **2018**, *5*, 23-31.

¹³² (a) Gein, V. L.; Rubtsova, D. D.; Bobyleva, A. A.; Ryabova, O. V.; Novikova, V. V.; Kasimova, N. N.; Yankin, A. N. *Russ. J. Gen. Chem.* **2020**, *90*, 1222-1228. (b) Ortiz Zacarías, N. V.; Van Veldhoven, J. P. D.; Portner, L.; Van Spronsen, E.; Ullo, S.; Veenhuizen, M.; Van Der Velden, W. J. C.; Zweemer, A. J. M.; Kreekel, R. M.; Oenema, K.; Lenselink, E. B.; Heitman, L. H.; Ijzerman, A. P. *J. Med. Chem.* **2018**, *61*, 9146-9161. (c) Gein, V. L.; Odegova, T. F.; Rogachev, S. N.; Bobyleva, A. A.; Gein, L. F. *Pharm. Chem. J.* **2015**, *49*, 175-177. (d) Ma, K.; Wang, P.; Fu, W.; Wan, X.; Zhou, L.; Chu, Y.; Ye, D. *Bioorg. Med. Chem. Lett.* **2011**, *21*, 6724-6727. (e) Gein, V. L.; Vychezhzanina, V. N.; Levandovskaya, E. B.; Syropyatov, B. Y.; Vakhnin, M. I.; Voronina, E. V.; Danilova, N. V. *Pharm. Chem. J.* **2010**, *44*, 370-373.

the midway between an original MCR and a one-pot procedure. The major advantage of this protocol is the possibility to obtain compounds **76** holding two different amine substituents (Scheme 11).

Using this approach, Jiang and coworkers obtained 5-amino substituted γ -lactam derivatives from acetylenedicarboxylates **52** ($R^1 = \text{Me, Et}$), aldehydes **53** ($R^3 = \text{H, Ph, Me}$), and aromatic and aliphatic amines **71** ($R^4 = \text{Ar, Alk}$), in the presence of acetic acid, yielding the corresponding 3-amino-1,5-dihydro-2H-pyrrol-2-ones **76** in fair to excellent yields (Scheme 11).¹³³



Scheme 11. Three-component reaction of dialkyl acetylenedicarboxylates **52**, aldehydes **53**, and amines **71** for the synthesis of 3-amino-1,5-dihydro-2H-pyrrol-2-ones **76**.

This reaction has been extensively studied by different authors during the last decades, and the most relevant experimental conditions are summarized in Table 3.

Table 3. Other procedures for the preparation of 3-amino-1,5-dihydro-2H-pyrrol-2-ones **76**.

Entry	Catalyst	Reaction conditions	Yield (%)
1	I ₂ (10 mol%)	Methanol, rt.	76-83 ¹³⁴
2	Benzoic Acid (20 mol%)	Ethanol, rt.	47-72 ¹³⁵
3	No catalyst or DABCO (25 mol%)	Ethanol	10-72 ¹³⁶
4	(CuOAc)·H ₂ O (40 mol%) + Salicylic Acid (30 mol%)	Methanol, rt.	40-93 ¹³⁷
5	Lemon Juice	110 °C	74-86 ¹³⁸

Besides, a large number of procedures can be found in the literature making use of heterogeneous catalytic systems to perform the above described synthesis. Some of these catalysts are TiO₂

¹³³ (a) Zhu, Q.; Gao, L.; Chen, Z.; Zheng, S.; Shu, H.; Li, J.; Jiang, H.; Liu, S. *Eur. J. Med. Chem.* **2012**, *54*, 232-238. (b) Zhu, Q.; Jiang, H.; Li, J.; Liu, S.; Xia, C.; Zhang, M. *J. Comb. Chem.* **2009**, *11*, 685-696.

¹³⁴ Khan, A. T.; Ghosh, A.; Musawwer Khan, M. *Tetrahedron Lett.* **2012**, *53*, 2622-2626.

¹³⁵ Gao, H.; Sun, J.; Yan, C. G. *Tetrahedron* **2013**, *69*, 589-594.

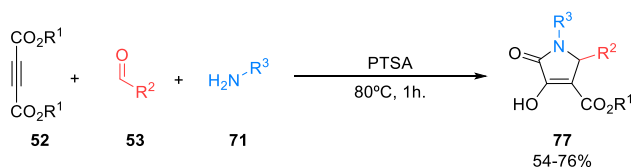
¹³⁶ Gao, H.; Sun, J.; Yan, C. G. *Beilstein J. Org. Chem.* **2013**, *9*, 2934-2939.

¹³⁷ Lv, L.; Zheng, S.; Cai, X.; Chen, Z.; Zhu, Q.; Liu, S. *ACS Comb. Sci.* **2013**, *15*, 183-192.

¹³⁸ Khan, M. M.; Khan, S.; Saigal; Sahoo, S. C. *ChemistrySelect* **2018**, *3*, 1371-1380.

nanopowder,¹³⁹ BF₃/nano-sawdust,¹⁴⁰ bio-based nano-cellulose coated Fe₃O₄,¹⁴¹ L-arginine coated Fe₃O₄ nanoparticles¹⁴² and graphene oxide nanosheets.¹⁴³

In a similar way, 3-hydroxy-1,5-dihydro-2*H*-pyrrol-2-ones **77** can be obtained if only one equivalent of amine **71** is used. Yan and coworkers described this multicomponent methodology for the first time in 2011 using *p*-toluenesulfonic acid as the catalyst, obtaining γ -lactams **77** in good yields (54-76%) (Scheme 12).¹⁴⁴ In addition, the protocol can be extended to the use of lactic acid or acetic acid as catalysts, affording also enol-derived γ -lactams **77** in comparable yields (52-83%).¹⁴⁵ Similarly, the use of oxalyl chloride instead of aldehydes **53** leads to the formation of the corresponding γ -lactams in excellent yields.¹⁴⁶



Scheme 12. Three-component reaction of dialkyl acetylenedicarboxylates **52**, aldehydes **53**, and amines **71** for the synthesis of 3-hydroxy-1,5-dihydro-2*H*-pyrrol-2-ones **77**.

In 2019 1,1'-butylenebis(3-sulfo-3*H*-imidazol-1-ium) hydrogen sulfate ([BBSI][HSO₄]) **VII** (1 mol%) (Figure 25) was used as the catalyst to obtain products **77**, under solvent-free conditions, providing excellent yields (82-92%).¹⁴⁷ Some years later, Nongkhlaw and coworkers described the metal-free photoredox catalysis under irradiation with blue LEDs (450 nm) and the use of Rose Bengal **VIII** as photoredox catalyst (15 mol%) (Figure 25), obtaining a wide scope of γ -lactams in good to excellent yields (77-94% yield) in short reaction times (0.5 hours).¹⁴⁸

¹³⁹ Rana, S.; Brown, M.; Dutta, A.; Bhaumik, A.; Mukhopadhyay, C. *Tetrahedron Lett.* **2013**, *54*, 1371-1379.

¹⁴⁰ Mirjalili, B. B. F.; Zare Reshquiyea, R. *RSC Adv.* **2015**, *5*, 15566-15571.

¹⁴¹ Salehi, N.; Fatameh Mirjalili, B. B. *RSC Adv.* **2017**, *7*, 30303-30309.

¹⁴² Ghasemzadeh, M. A.; Abdollahi-Basir, M. H.; Elyasi, Z. *Curr. Organocatalysis* **2018**, *6*, 61-68.

¹⁴³ Saha, M.; Das, A. R. *ChemistrySelect* **2017**, *2*, 10249-10260.

¹⁴⁴ Sun, J.; Wu, Q.; Xia, E. Y.; Yan, C. G. *Eur. J. Org. Chem.* **2011**, 2981-2986.

¹⁴⁵ Yang, J.; Tan, J. N.; Gu, Y. *Green Chem.* **2012**, *14*, 3304-3317.

¹⁴⁶ Yavari, I.; Souri, S. *Synlett* **2008**, *8*, 1208-1210.

¹⁴⁷ Khaligh, N. G.; Mihankhah, T.; Johan, M. R. *Synth. Commun.* **2019**, *49*, 1334-1342.

¹⁴⁸ Dutta, A.; Rohman, M. A.; Nongrum, R.; Thongni, A.; Mitra, S.; Nongkhaw, R. *New J. Chem.* **2021**, *45*, 8136-8148.

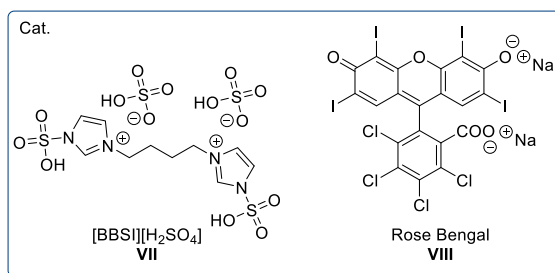


Figure 25. Structures of [BBSI][HSO₄] **VII** and Rose Bengal **VIII** catalyst.

In addition, there are multiple examples where heterogeneous catalysts are used with dialkyl acetylenedicarboxylates **52** ($R^1 = \text{Alk}$), aldehydes **53**, and one equivalent of amines **71** to obtain 3-hydroxy-1,5-dihydro-2*H*-pyrrol-2-ones **77**. Some of the most relevant are, TiO₂ or ZrO₂ nanoparticles,¹⁴⁹ graphene oxide nanosheets¹⁴³ and magnetic CoFe₂O₄ nanoparticles functionalized with citric acid or with SO₂-sulfuric acid.¹⁵⁰

¹⁴⁹ (a) Saha, A.; Payra, S.; Banerjee, S. *RSC Adv.* **2016**, *6*, 101953-101959. (b) Sarkar, R.; Mukhopadhyay, C. *Tetrahedron Lett.* **2013**, *54*, 3706-3711.

¹⁵⁰ (a) Ahankar, H.; Ramazani, A.; Ślepokura, K.; Lis, T.; Kinzhybalov, V. *Res. Chem. Intermed.* **2019**, *45*, 5007-5025. (b) Hosseinzadeh, Z.; Ramazani, A.; Ahankar, H.; Ślepokura, K.; Lis, T. *Silicon* **2019**, *11*, 2933-2943.



Objectives

Taking into account the considerations mentioned above, the general objective of this thesis is the development of efficient organocatalyzed multicomponent processes for the synthesis of γ -lactam derivatives, the exploration of their synthetic applications and the final study of the antiproliferative activity of the substrates against several cancer cell lines, including the MDM2/MDMX-p53 protein-protein interaction inhibitory capability (Figure 26).

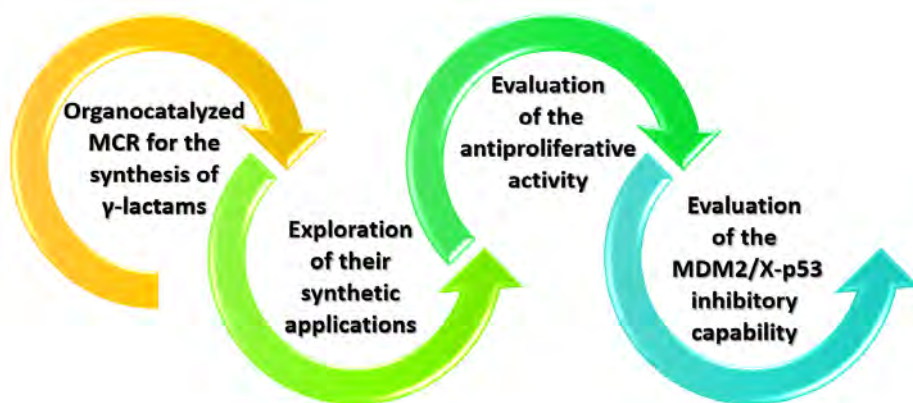
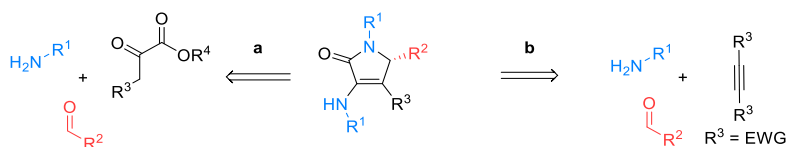


Figure 26. General objectives.

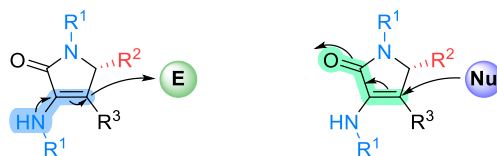
From a synthetic point of view, the main objective is the development of an efficient synthetic methodology for the preparation of 1,5-dihydro-2*H*-pyrrol-2-ones, using multicomponent protocols. Based on the previously described multicomponent reaction of amines, aldehydes and pyruvate derivatives,¹¹³ our first goal is the extension of this synthetic protocol to the use of organocatalysts, to prepare a wide family of highly functionalized chiral unsaturated γ -lactam derivatives (Scheme 13, a). Next, other pyruvate surrogates, such as activated acetylene species, will be tested in the reaction in order to extend further the structural diversity at the γ -lactam core (Scheme 13, b). Due to the unique biological properties of fluorine and phosphorus (V)-containing structures, a special effort will be made in the applications of such reaction in the preparation of γ -lactam substrates holding those moieties, using fluorine and/or phosphorus substituted aldehydes and pyruvates.



Scheme 13. Retrosynthesis of 3-amino-1,5-dihydro-2H-pyrrol-2-ones.

Once the multicomponent protocol has been optimized to proceed efficiently under organocatalysis, the next step will be the development of an enantioselective methodology to provide the enantiomerically enriched substrates, using chiral Brønsted acid catalysts.

In addition, taking the advantage of the unique structural features of 3-amino-1,5-dihydro-2H-pyrrol-2-one skeleton, mainly the enamine moiety and the enone structure, some synthetic transformations of those substrates will be performed. This would allow, not only to justify the synthetic potential of the molecules but also to extend further the structural diversity at the γ -lactam ring. Due to the presence of a chiral carbon at the 5-membered ring, a special focus will be pointed to diastereoselective reactions (Scheme 14).



Scheme 14. Functionalization of the 3-amino-1,5-dihydro-2H-pyrrol-2-one skeleton.

As it has been pointed in the introduction, γ -lactams have demonstrated to have great value in the field of medicinal chemistry with a plethora of compounds, from natural and non-natural sources, showing very interesting and promising biological activities, which include anticancer properties. Within the frame of a global objective of improving the therapeutical effectiveness while reducing the side effects and overcount resistance in the drug therapy against cancer, we propose, as another main goal of this research, the evaluation of the *in vitro* cytotoxic activity of the synthesized compounds in different cancer cell lines, in order to elaborate structure-activity profiles and to identify the most promising molecules.

Finally, the mechanism for the *in vitro* cytotoxicity eventually found, will be explored, in particular, trying to demonstrate their ability to induce apoptosis or to identify some specific interaction at a molecular level with proteins such as MDM2/MDMX-p53 as a possible target for these γ -lactams.

The background of the page is a complex, abstract network of interconnected nodes and lines, resembling a molecular structure or a data network. The nodes are represented by small circles in various shades of gray and blue, connected by thin, light gray lines. The overall effect is a dense, interconnected web of points and lines, with some nodes appearing larger or more prominent than others. The background is light gray and white, with the network pattern overlaid on it.

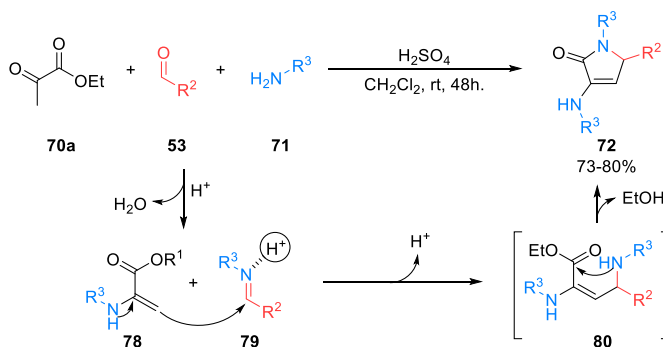
Section I

*Multicomponent synthesis and applications
of unsaturated γ -lactam derivatives*

Chapter 1

Multicomponent synthesis of unsaturated γ -lactam derivatives using pyruvates

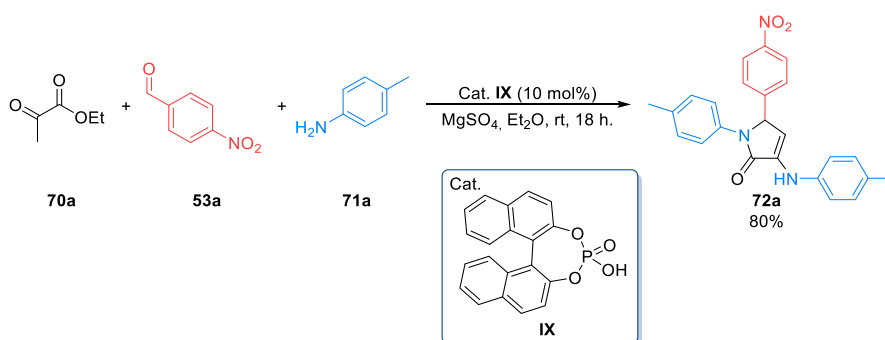
Our research group described in 2006 a three-component acid-catalyzed reaction of ethyl pyruvate (**70a**), aldehydes **53**, and aromatic amines **71** to afford 3-amino-1,5-dihydro-2*H*-pyrrol-2-ones **72** (Scheme 15).¹¹³ The mechanism of this reaction was assumed to consist of two initial simultaneous condensation reactions of amines **71**, with ethyl pyruvate (**70a**) and aldehydes **53**, resulting in the formation of enamine and imine species **78** and **79**. The activation of aldimines **79** by the Brønsted acid facilitates a subsequent Mannich reaction with enamines **78**, affording enamine intermediate **80**. Finally, species **80** undergoes a spontaneous intramolecular nucleophilic attack of the amine to the carboxylic group, resulting in the ring closure, leading to cyclic α -dehydroamino acids **72**.



Scheme 15. Brønsted acid-catalyzed three-component reaction of ethyl pyruvate **70a**, aldehydes **53**, and amines **71**.

Building upon these precedents, our first synthetic goal was the extension of the MCR protocol to the use of phosphoric acid species as organocatalysts. For this propose, first, we explored the multicomponent reaction of ethyl pyruvate (**70a**), *p*-nitrobenzaldehyde (**53a**) and *p*-toluidine (**71a**) under different conditions. Although the stoichiometry of the reaction is indeed 2:1:1

(amine/aldehyde/pyruvate), three equivalents of pyruvate derivative are required to achieve good yields in reasonable reaction times. Diethyl ether was chosen as the optimal reaction media since the reaction in chlorinated solvents, toluene or MeCN afforded γ -lactam derivatives in lower yields and higher reaction times. In addition, the presence of MgSO_4 is necessary in order to remove the water generated in the process. Although the reaction proceeds with similar efficiency using other acidic sources (H_2SO_4 , H_3PO_4 , $\text{Mg}(\text{HSO}_4)_2$), the use of BINOL-derived phosphoric acid **IX** as the catalyst is very convenient since it facilitates the purification process and has no interaction with the drying agent. Accordingly, the model reaction using 3 equivalents of ethyl pyruvate (**70a**), 1 equivalent of *p*-nitrobenzaldehyde (**53a**) and 2 equivalents of *p*-toluidine (**71a**), in the presence of MgSO_4 and 10 mol% of racemic BINOL-derived phosphoric acid **IX** as Brønsted acid catalyst provided γ -lactam derivative **72a** in very good yield after 18 hours (Scheme 16).



Scheme 16. Three-component reaction for the racemic synthesis of **72a**.

γ -Lactam derivative **72a** was fully characterized on the basis of its NMR and IR spectra and HRMS. The most relevant signals of α,β -unsaturated γ -lactam **72a** in the ^1H NMR spectrum are the two doublets assigned to the two protons at the γ -lactam ring, at $\delta_{\text{H}} = 5.75$ and 5.96 ppm ($^3J_{\text{HH}} = 2.7$ Hz), corresponding to the aliphatic CH at the chiral stereocenter and the olefinic =CH, respectively (Figure 28). The broad singlet at $\delta_{\text{H}} = 6.61$ ppm interchanges with D_2O , which suggests that belongs to the enamine NH group, implying that only the enamine form is present. Finally, the two intense singlets at $\delta_{\text{H}} = 2.30$ and 2.27 ppm and the presence of 12 aromatic protons at the aromatic region, indicates that two equivalents of *p*-toluidine have participated in the reaction, allowing to discard the formation of an enol derivative (Figure 28).

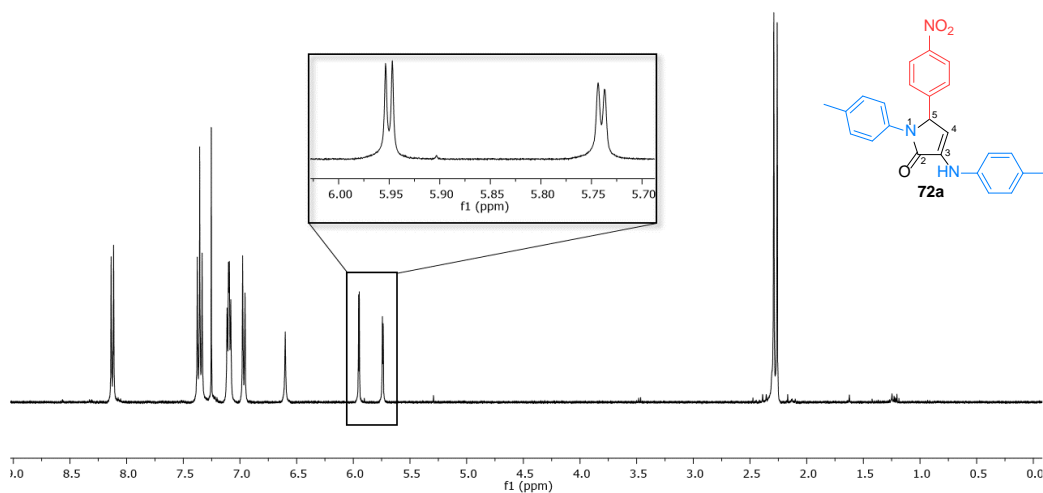


Figure 28. ^1H NMR spectrum of compound **72a** in CDCl_3 .

In addition, the most representative signals in the ^{13}C NMR spectrum of compound **72a** correspond to the four carbons of the γ -lactam ring (Figure 29). The presence of the endocyclic enamine moiety is evident by the chemical shift of its two carbon atoms at $\delta_{\text{C}} = 138.5$ (C-N) and 105.3 (CH) ppm. The carbonyl group appears within the typical range for conjugated cyclic amides at $\delta_{\text{C}} = 167.0$ ppm, and the signal of the aliphatic stereogenic carbon is present at $\delta_{\text{C}} = 63.6$ ppm. In consonance with the ^1H NMR spectrum, the two signals at $\delta_{\text{C}} = 21.0$ and 20.8 ppm belong to the two methyl substituents of the *p*-toluidine groups. Finally, the six intense signals at the aromatic region correspond to the 12 aromatic CH moieties (DEPT) of the three *para*-substituted aromatic rings, and the 6 additional signals of the quaternary aromatic carbons appear at lower field, in the interval $\delta_{\text{C}} = 130$ -140 ppm.

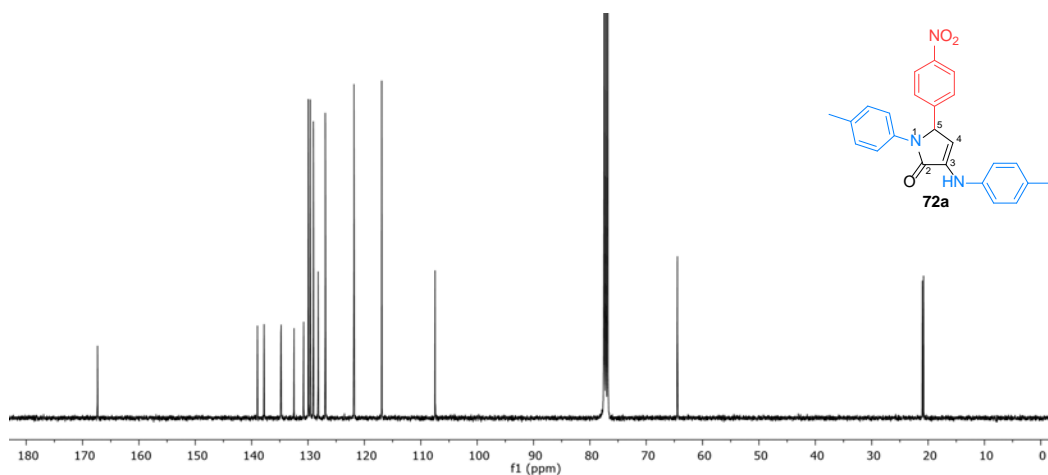


Figure 29. ^{13}C NMR spectrum of compound **72a** in CDCl_3 .

Taking into account the modular character of this MCR, the use of a wide scope of each reagent would allow the preparation of a great number of structures containing the γ -lactam moiety with a plethora of distinct substituents around the heterocycle. Therefore, in order to demonstrate the synthetic potential of the reaction, we extended the scope of the reaction to several functionalized γ -lactam derivatives (Chart 1).

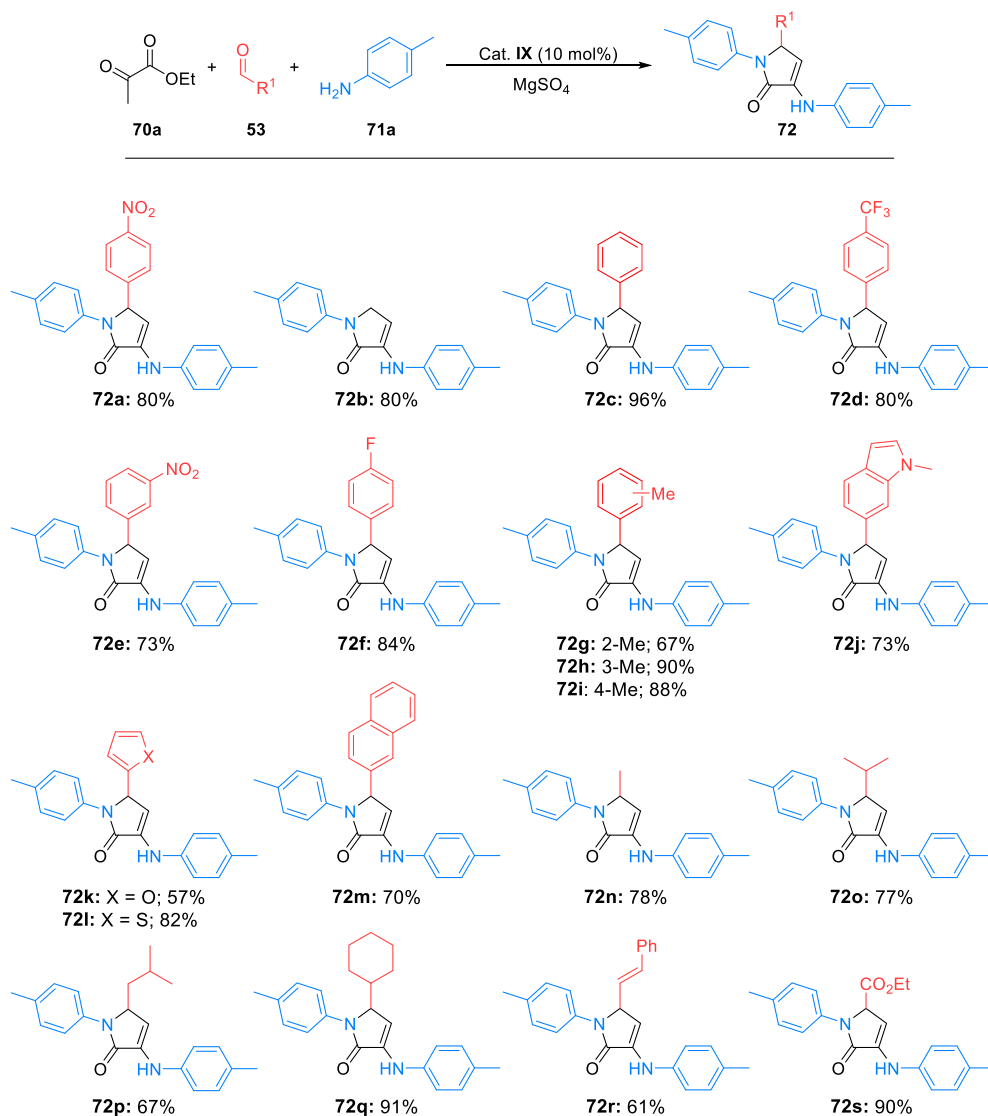


Chart 1. 3-*p*-Tolyl 1,5-dihydro-2*H*-pyrrol-2-ones **72a-s** obtained.

First, several γ -lactams **72** were synthesized using weakly activated *p*-toluidine (**71a**) as the amine substrate, in combination with ethyl pyruvate (**70a**) and different aldehydes. Accordingly, the reaction proceeds successfully using simple formaldehyde (**53b**, R¹ = H) or benzaldehyde (**53c**, R¹ = Ph) under

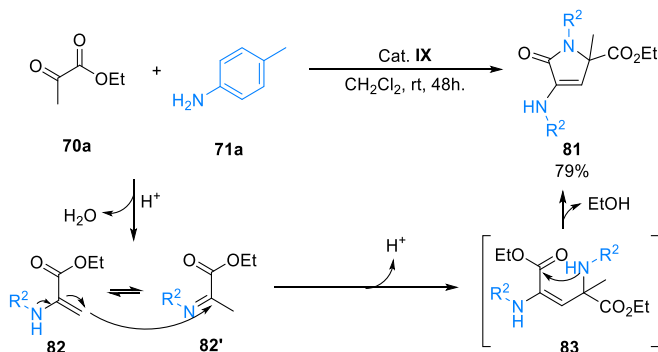
the standard reaction conditions, affording the corresponding dihydro-2*H*-pyrrol-2-ones **72b-c** in very good to excellent yields (Chart 1). The use of electron-poor aromatic aldehydes (**53d-e**, $R^1 = 4\text{-CF}_3\text{C}_6\text{H}_4$ and $3\text{-NO}_2\text{C}_6\text{H}_4$) was also appropriate for this reaction. However, while a very good yield was obtained for *p*-trifluoromethylbenzaldehyde derivative **72d**, the use of *m*-nitrobenzaldehyde provided γ -lactam derivative **72e** with a slightly lower yield (Chart 1). In addition, even though an increase in the reaction time was observed when *p*-fluorobenzaldehyde (**53f**, $R^1 = 4\text{-FC}_6\text{H}_4$) was used, fluorinated γ -lactam **72f** was also obtained in very good yield (Chart 1).

However, the multicomponent protocol using aromatic aldehydes bearing soft electron-donating alkyl groups (**53g-i**, $R^1 = 2\text{-MeC}_6\text{H}_4$, $3\text{-MeC}_6\text{H}_4$ and $4\text{-MeC}_6\text{H}_4$) provided the target γ -lactams in lower yields and longer reaction times. This behavior was attributed to a lower electrophilic character of the imine species **79** involved in the reaction and, accordingly, methyl *tert*-butylether (MTBE) was used instead of diethyl ether due to its higher boiling point. Under those conditions, γ -lactams **72g-i** were obtained in good to excellent yields (Chart 1) in reasonable reaction times (18-72 hours).

Next, the three-component reaction was successfully extended to the use of heteroaromatic aldehydes **53j-l** ($R^1 = 6\text{-}(N\text{-Me-indolyl})$, 2-furyl and 2-thienyl), providing lactams **72j-l** in fair to very good yields (Chart 1). Moreover, despite the high steric crowding expected in the target γ -lactam substrate **72m**, 2-naphthaldehyde (**53m**, $R^1 = 2\text{-naphtyl}$) was proved to be also a suitable substrate in this reaction (Chart 1). In addition, the scope of the reaction was successfully extended to the use of aliphatic aldehydes **53n-q** ($R^1 = \text{Me}$, ^iPr , ^tBu and Cy), affording the corresponding alkyl-substituted γ -lactam derivatives **72n-q** in good to excellent yields (Chart 1). Remarkably, the reaction is also applicable to the use of other polyfunctional aldehydes, since cinnamaldehyde (**53r**, $R^1 = \text{CH=CHPh}$) or ethyl glyoxalate (**53s**, $R^1 = \text{CO}_2\text{Et}$), provided cinnamyl and ester-substituted γ -lactams **72r-s** in good to excellent yields (Chart 1).

Besides, several efforts were made in order to extend the three-component reaction to the use of ketones instead of aldehydes in the MCR procedure willing to obtain 3-amino-1,5-dihydro-2*H*-pyrrol-2-ones holding a tetra-substituted stereocenter. However, all our attempts were unsuccessful, and despite of using different non-symmetrical ketones such as 2-butanone, acetophenone and methyl 3,3,3-trifluoropyruvate, in all cases, only dimeric substrate **81** was obtained as a result of the higher reactivity of the intermediate pyruvate enamine species **82**, which reacts with itself rather than with the imines generated from the second ketone reagent (Scheme 17). According to the accepted pathway for this process, the mechanisms of this reaction may consist of the condensation of the amine **71a** with ethyl pyruvate **70a** to afford a mixture of the enamine and imine tautomers **82** and **82'**, which

are in equilibrium. Then, enamine **82** attacks its imine tautomer **82'** to afford intermediate **83**, which after an intramolecular condensation provides γ -lactam **81**.



Scheme 17. Formation of α,β -unsaturated γ -lactam **81**.

In the next stage of this research, the scope of the reaction was extended to the use of different amine substrates (Chart 2), using ethyl pyruvate (**70a**). For instance, the multicomponent reaction using electron-rich *p*-anisidine (**71b**, $R^2 = 4\text{-MeOC}_6\text{H}_4$) and *p*-nitrobenzaldehyde (**53a**) or benzaldehyde (**53c**) afforded the corresponding γ -lactam derivatives **84a-b** in very good yields (Chart 2). Remarkably, higher reaction times were required in the case of compound **84a**, which may be due to a higher deactivation of the intermediate imine electrophile **79** with respect to the expected activation in the enamine nucleophile **78**, as a consequence of the use of an electron-rich aromatic aldehyde (Scheme 15, *vide supra*). Additionally, several different *ortho*, *meta* and *para*-halogen-substituted anilines **71c-f** ($R^2 = 4\text{-BrC}_6\text{H}_4$, $4\text{-ClC}_6\text{H}_4$, $3\text{-ClC}_6\text{H}_4$ and $2\text{-FC}_6\text{H}_4$;) were successfully used in combination with *p*-nitrobenzaldehyde (**53a**, $R^1 = 4\text{-NO}_2\text{C}_6\text{H}_4$), benzaldehyde (**53c**, $R^1 = \text{Ph}$) or *p*-trifluoromethyl benzaldehyde (**53d**, $R^1 = 4\text{-CF}_3\text{C}_6\text{H}_4$). In all cases, halogen-containing γ -lactams **84c-i** were obtained in very good to excellent yields (Chart 2). However, the utilization of *p*-chloroaniline (**71d**, $R^2 = 4\text{-ClC}_6\text{H}_4$) required heating in refluxing MTBE (55 °C), while higher reaction times were needed when *m*-chloroaniline (**71e**, $R^2 = 3\text{-ClC}_6\text{H}_4$) was used as starting substrate (72 hours). Although a strong deactivation of the enamine nucleophile is expected from the use of deactivated aromatic amines, the reaction using *m*-trifluoromethylaniline (**71g**, $R^2 = 3\text{-CF}_3\text{C}_6\text{H}_4$) provided in fair to good yields trifluoromethyl-containing substrates **84j-l** using formaldehyde (**53b**, $R^1 = \text{H}$), *p*-nitrobenzaldehyde (**53a**, $R^1 = 4\text{-NO}_2\text{C}_6\text{H}_4$.) or benzaldehyde (**53c**, $R^1 = \text{Ph}$) (Chart 2). While, as expected, a lower reactivity was observed in this case, γ -lactams **84j-l** were efficiently obtained by increasing the reaction times to 72 hours. Finally, the use of a quinoline-derived heteroaromatic amine **71h** ($R^2 = 2\text{-quinolinyl}$) led to the target γ -lactam **84m** in poor yield, which may be possibly due to the high steric crowding present in the final structure.

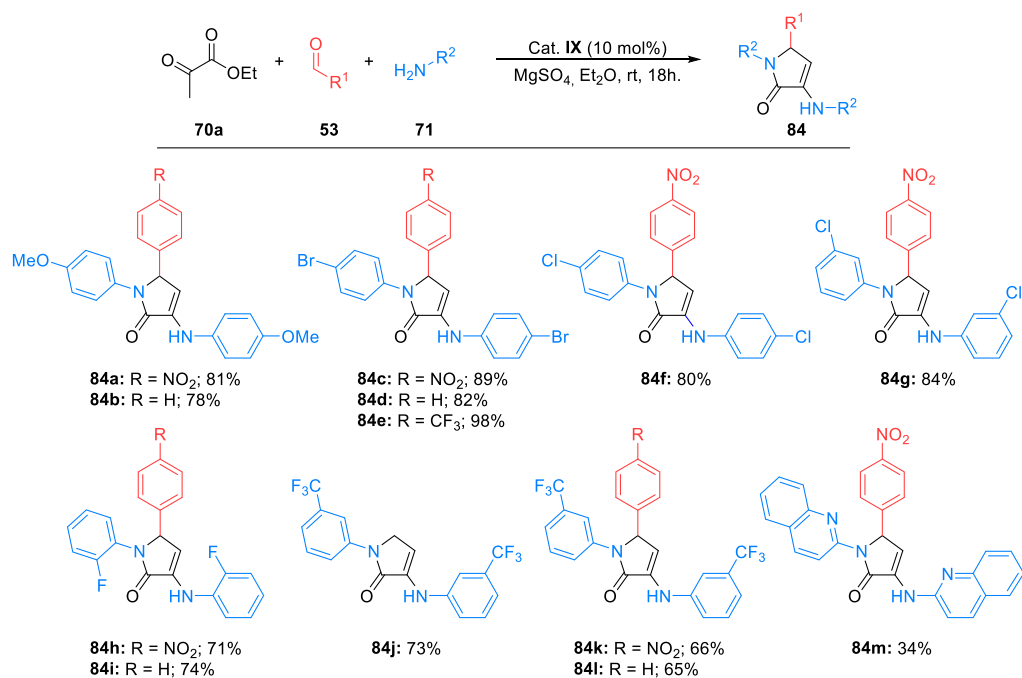


Chart 2. 3-Amino-1,5-dihydro-2H-pyrrol-2-ones **84** obtained.

Even though many other aliphatic and (hetero)aromatic amines were tested in the reaction, such as benzylamine, tritylamine, *p*-nitroaniline, *o*- and *m*-anisidine or 2, 3 or 4-aminopyridine, no significant formation of the γ -lactam substrates was observed in any case, which was mainly attributed to the critical balance between the reactivity of the enamine and imine species. The use of aliphatic amines or electron-rich anilines may provide a highly reactive enamine nucleophile, but an imine intermediate with decreased electrophilic character. On the contrary, the lack of reactivity in the case of electron-deficient amines may reside in a higher deactivation of the enamine nucleophile relative to the activation of the imine species. Additional steric effects may be implicated in the low reactivity observed in *ortho*-substituted anilines.

To end with the scope of the reaction, the effect of the substitution at the pyruvate derivative was explored. Using weakly activated *p*-toluidine (**71a**), substituted pyruvate derivatives **85a-c** ($R^1 = \text{Me}$, Bn and CO_2Me) reacted with *p*-nitrobenzaldehyde (**53a**, $R^2 = 4\text{-NO}_2\text{C}_6\text{H}_4$) or benzaldehyde (**53c**, $R^2 = \text{Ph}$) to afford 4-substituted γ -lactam derivatives **86** in good yields (Chart 3). In this case, the higher steric hindrance present in the pyruvate derivative results in a decreased reactivity of the enamine intermediate and the reaction requires heating using MTBE as a solvent.

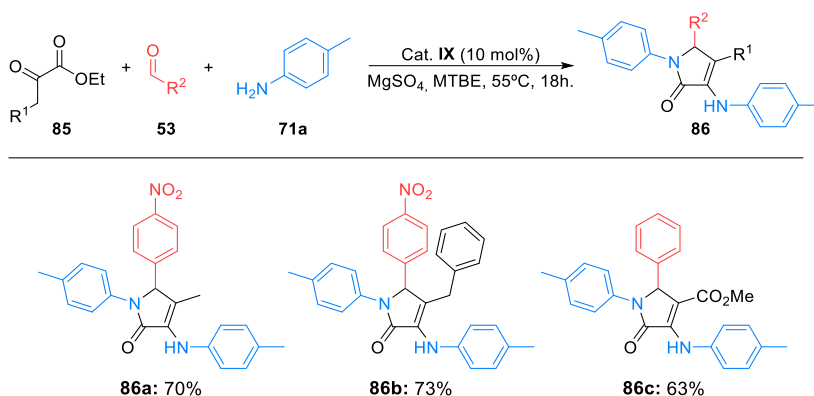


Chart 3. 4-Substituted 3-amino-1,5-dihydro-2H-pyrrol-2-ones **86** obtained.

In summary, a very efficient three-component reaction of pyruvate derivatives, amines and aldehydes is described in this chapter, leading effectively to 3-amino- α,β -unsaturated γ -lactams. The reaction can be applied to several aromatic amines, aromatic and aliphatic aldehydes and some substituted pyruvate derivatives, allowing a straightforward synthesis of highly functionalized γ -lactam derivatives from cheap commercially available starting materials.

Chapter 2

Multicomponent synthesis of fluorine and phosphorus substituted γ -lactams

It is well-known that the introduction of fluorine or phosphorus substituents into bioactive molecules very often leads to increased or new activities. On the one hand, phosphonate derivatives show multiple biological activities due to their chemical similitude to natural phosphate metabolites and, for this reason, they have found several applications in medicine and agrochemistry.¹⁵¹ On the other hand, although the effect of the introduction of fluorine atoms in the structure of organic compounds is rather difficult to predict, very often it leads to increased activities as a consequence of the enhancement of the lipophilic character of the molecules, improving their capability to penetrate across the cell membrane.¹⁵² In addition, other key properties that make fluorine-containing compounds attractive in chemical biology include the small atomic radius and a high electronegativity of the fluorine atom and low polarizability of the C-F bond. In addition, the fact that the only natural isotope of ¹⁹F atom has a nuclear spin of ½ makes it ideal for monitoring studies by NMR.

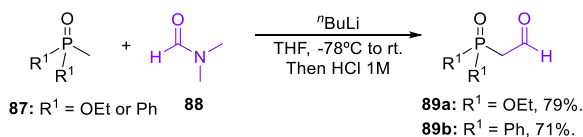
Considering the facts mentioned above, and in view of the efficient methodology described in the previous chapter for the preparation of highly functionalized γ -lactams, next we considered the extension of the multicomponent reaction to the synthesis of phosphorus and fluorine containing γ -lactam derivatives using fluorinated and phosphorylated aldehydes and pyruvates.

Accordingly, first we extended the scope of the multicomponent reaction to the use of phosphorus and fluorine-containing aldehydes. Trifluoroacetaldehyde and perfluorobenzaldehyde were purchased from commercial sources. However β -phosphorated aldehydes **89** derived from phosphonate ($R^1 =$

¹⁵¹ (a) Horsman, G. P.; Zechel, D. L. *Chem. Rev.* **2017**, *117*, 5704-5783. (b) Mucha, A.; Kafarski, P.; Berlicki, L. *J. Med. Chem.* **2011**, *54*, 5955-5980. (c) Karl, D. M. *Nature* **2000**, *406*, 31-33. (d) Engel, R. *Handbook of Organophosphorus Chemistry*; M. Dekker, 1992. (e) Kafarski, P.; Lejczak, B. *Phosphorus, Sulfur Silicon Relat. Elem.* **1991**, *63*, 193-215.

¹⁵² (a) Müller, K.; Faeh, C.; Diederich, F. *Science* **2007**, *317*, 1881-1886. (b) Shah, P.; Westwell, A. D. *J. Enzyme Inhib. Med. Chem.* **2007**, *22*, 527-540. (c) Bégué, J. P.; Bonnet-Delpon, D. *Bioorganic and Medicinal Chemistry of Fluorine*; Wiley, 2007.

$\text{CH}_2\text{P}(\text{O})(\text{OEt})_2$ or phosphine oxide ($\text{R}^1 = \text{CH}_2\text{P}(\text{O})\text{Ph}_2$) for the three-component reaction were synthesized from methylphosphonates or methylphosphine oxides and *N,N*-dimethylformamide (DMF) following Savignac's method (Scheme 18).¹⁵³



Scheme 18. Savignac's synthesis of β -phosphorylated aldehydes **89a-b**.

Initially, the multicomponent reaction was tested using ethyl pyruvate (**70a**), aromatic amines **71** and aldehydes **89** holding fluorinated or phosphorated substituents, in the presence of a catalytic amount of BINOL-derived phosphoric acid **IX**. Following this procedure, several γ -lactam derivatives **90** bearing fluorinated or phosphorated substituents at the position 5 of the ring were obtained in good to very good yields (Chart 4).

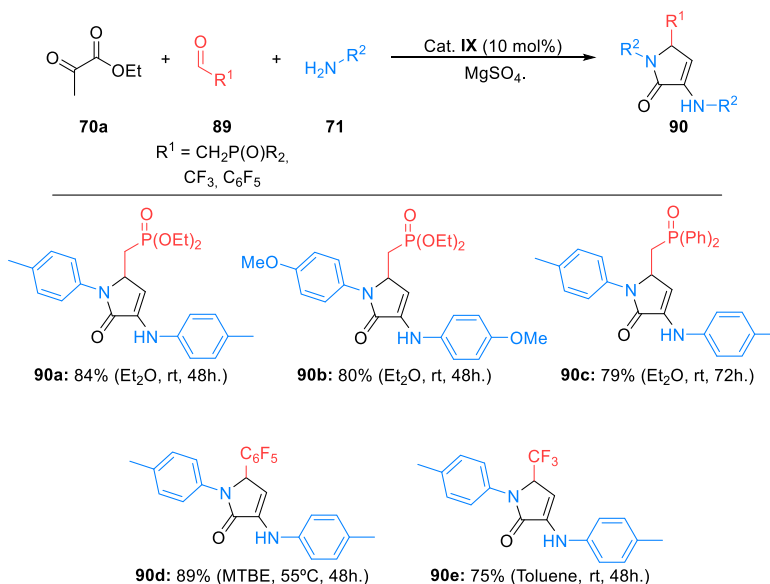


Chart 4. Multicomponent synthesis of phosphorus and fluorine containing γ -lactams **90**.

The reaction of aldehyde **89a** ($\text{R}^1 = \text{CH}_2\text{P}(\text{O})(\text{OEt})_2$), derived from phosphonate, with ethyl pyruvate (**70a**) and *p*-toluidine (**71a**, $\text{R}^2 = 4\text{-MeC}_6\text{H}_4$) or *p*-anisidine (**71b**, $\text{R}^2 = 4\text{-MeOC}_6\text{H}_4$) at room temperature using Et_2O as solvent, smoothly led to the formation of the corresponding phosphorylated γ -lactams **90a-b** (Chart 4). However, the use of aldehyde **89b** ($\text{R}^1 = \text{CH}_2\text{P}(\text{O})\text{Ph}_2$) derived from phosphine oxide,

¹⁵³ Aboujaoude, E. E.; Collignon, N.; Savignac, P. *Synthesis* **1983**, 634-636.

required longer reaction times to achieve the analogous product **90c**. This different reactivity may be attributed to the higher steric hindrance present in the diphenylphosphinoyl moiety with respect to the diethylphosphonate functionality. On the other hand, under the same conditions, commercially available perfluorobenzaldehyde (**89c**, $R^1 = C_6F_5$) did not show any reactivity. In order to overcome this problem MTBE was used as solvent under reflux, affording perfluorophenyl-substituted γ -lactam **90d** in very good yield (Chart 4).

For the particular case of the use of trifluoroacetaldehyde (**89d**, $R^1 = CF_3$), the direct use of the neat aldehyde substrate is unfeasible due to its low boiling point ($-20^\circ C$). However it is well known that the aldehyde species can be generated *in situ* from its commercially available hydrate precursor. For this reason, the corresponding trifluoromethylimine intermediate was preformed from an aqueous solution of trifluoroacetaldehyde hydrate and an excess of *p*-toluidine (**71a**, $R^2 = 4-MeC_6H_4$), using refluxing toluene and a Dean-Stark to remove all the water. Next, one equivalent of ethyl pyruvate and 10 mol% of phosphoric acid catalyst **IX** were added and the reaction was stirred for 72 hours. Using this modified procedure trifluoromethyl substituted γ -lactam **90e** was obtained in good yield (Chart 4).

Fluorinated and phosphorated γ -lactams **90** were fully characterized by NMR, IR and HRMS. Substrate **90c** is selected as a model and the most characteristic signals are discussed below (Figures 30 and 31).

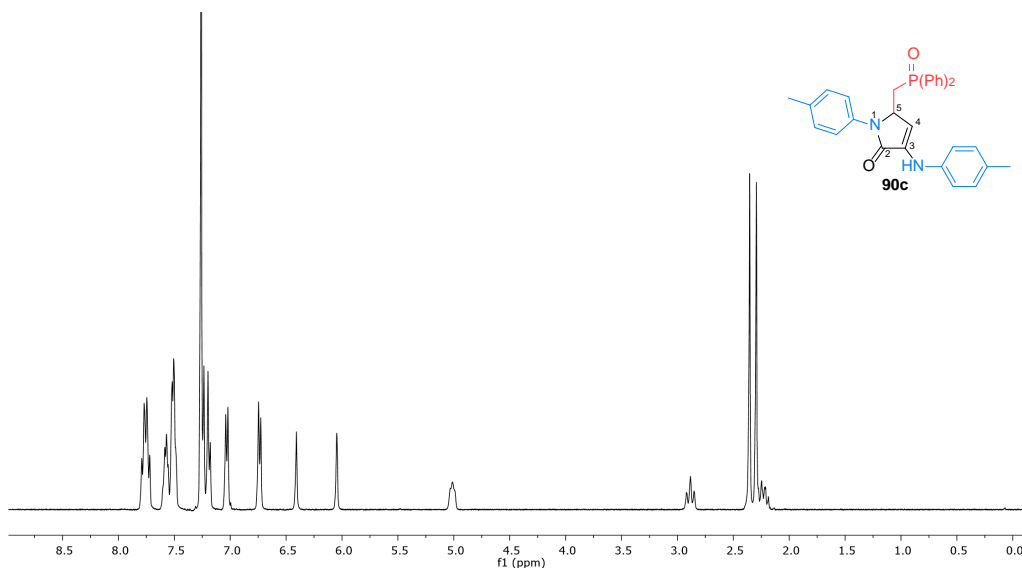


Figure 30. 1H NMR spectrum of compound **90c** in $CDCl_3$.

The presence of the endocyclic enamine group is evidenced in the 1H NMR spectrum from the broad singlet observed at $\delta_H = 6.41$ ppm and the doublet at $\delta_H = 6.05$ ppm ($^3J_{HH} = 2.6$ Hz), that correspond to

the enamine NH group and the olefinic =CH group respectively (Figure 30). The signal of the proton at the chiral stereocenter appears as a multiplet due to the coupling with the olefinic proton, the methylene group and the phosphorus atom. Additionally, the two multiplets at $\delta_{\text{H}} = 2.89$ and 2.22 ppm, correspond to the CH_2 group, where each proton shows coupling between them as well as with the CH group and the phosphorus atom. The fact that these signals appear as two independent multiplets, instead of one, make evident the presence of a chiral stereocenter in the structure due to the diastereotopic character of the protons at this position. Finally, the two intense singlets at $\delta_{\text{H}} = 2.35$ and 2.29 ppm and the presence of 18 protons at the aromatic region, suggest that two molecules of *p*-toluidine and the diphenyl phosphine oxide group are present in the structure.

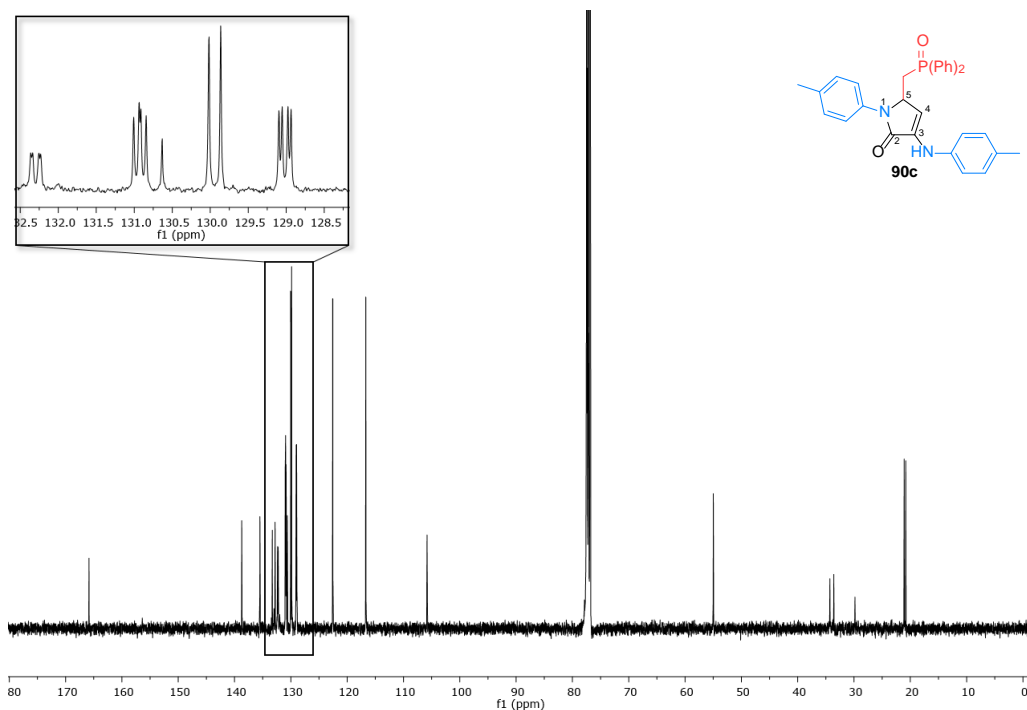
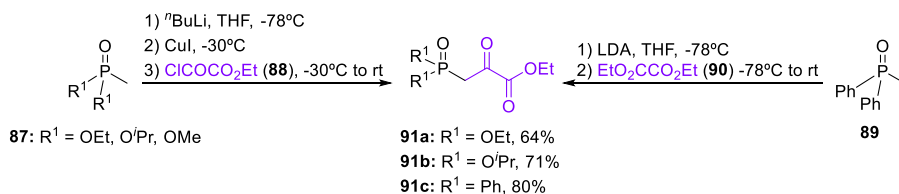


Figure 31. ^{13}C NMR spectrum of compound **90c** in CDCl_3 .

Moreover, the ^{13}C NMR spectrum of compound **90c** shows four characteristic signals for the four carbons of the γ -lactam ring (Figure 31). The peaks at $\delta_{\text{C}} = 130.6$ and 105.8 ppm belong to the two carbons atoms of the enamine moiety, the carbonyl group appears at $\delta_{\text{C}} = 165.9$ ppm, and the signal at $\delta_{\text{C}} = 55.0$ ppm is assigned to the aliphatic stereogenic carbon. In addition, the doublet at $\delta_{\text{C}} = 33.9$ ppm corresponds to the methylene group and shows a characteristic coupling constant with the phosphorus atom of $^1J_{\text{PC}} = 69.8$ Hz. The two signals at $\delta_{\text{C}} = 21.1$ and 20.8 ppm accompanied with four intense signals at the aromatic region indicate the presence of two *p*-toluidine aromatic rings. Due to the presence of the two *p*-tolyl moieties and the diphenylphosphine group, where the phenyl group

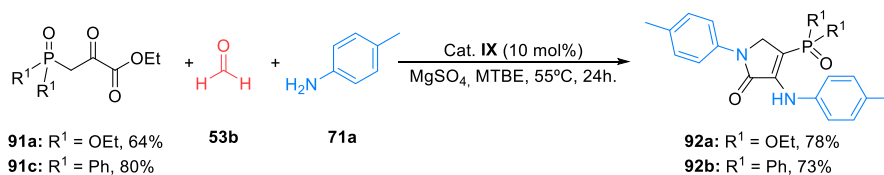
shows additional coupling with the dipolar nucleus of ^{31}P , a complex pattern is observed in the aromatic region in the ^{13}C NMR spectrum.

Following with our interest in phosphorated γ -lactam derivatives and, in order to further expand the scope of the three-component reaction, the utilization of phosphorus-substituted pyruvate derivatives in the MCR reaction was next explored. In a similar manner to β -phosphorated aldehydes **89**, pyruvates **91a-c** containing phosphonate ($\text{R}^1 = \text{O}^i\text{Pr}$, OEt , OMe) or phosphine oxide ($\text{R}^1 = \text{Ph}$) moieties can be easily obtained by a prior metalation of methylphosphonate esters **87** or methyldiphenylphosphine oxide (**89**), followed by the addition of ethyl oxalyl chloride (**88**) or diethyl oxalate (**90**) respectively (Scheme 19).¹⁵⁴



Scheme 19. Synthesis of phosphorated pyruvates **91**.

Initially, the multicomponent reaction of phosphorylated pyruvates **91a,c** ($\text{R}^1 = \text{OEt}$, Ph), derived from phosphonate and phosphine oxide, with simple formaldehyde (**53b**) and *p*-toluidine (**71a**) in the presence of BINOL-derived phosphoric acid catalyst **IX**, using refluxing MTBE as solvent and anhydrous magnesium sulfate to capture the released water, led to the formation of 3-amino-1,5-dihydro-2*H*-pyrrol-2-ones **92** in good yields (Scheme 20).



Scheme 20. Synthesis of C-5 unsubstituted 3-amino-1,5-dihydro-2*H*-pyrrol-2-ones **92**.

However, under identical reaction conditions, the use of benzaldehyde with phosphonate-substituted pyruvate **91a** ($\text{R}^1 = \text{OEt}$) and *p*-toluidine (**71a**) provided enol-derived γ -lactam **93a** in very good yield, instead of the expected enamine derivative (Chart 5). Taking into account the importance of the obtained substrates in this reaction, holding an *iso*-tetronic acid core, next we explored the use

¹⁵⁴ (a) Palacios, F.; Vicario, J.; Aparicio, D. *J. Org. Chem.* **2006**, *71*, 7690-7696. (b) Varlte, J.-M.; Colliguon, N.; Savignac, P. *Can. J. Chem.* **1979**, *57*, 3216-3220.

of other amines **71**, phosphorated pyruvates **91** and aromatic or aliphatic aldehydes **53** ($R^2 = \text{Ar, Alk}$) in the same reaction (Chart 5).

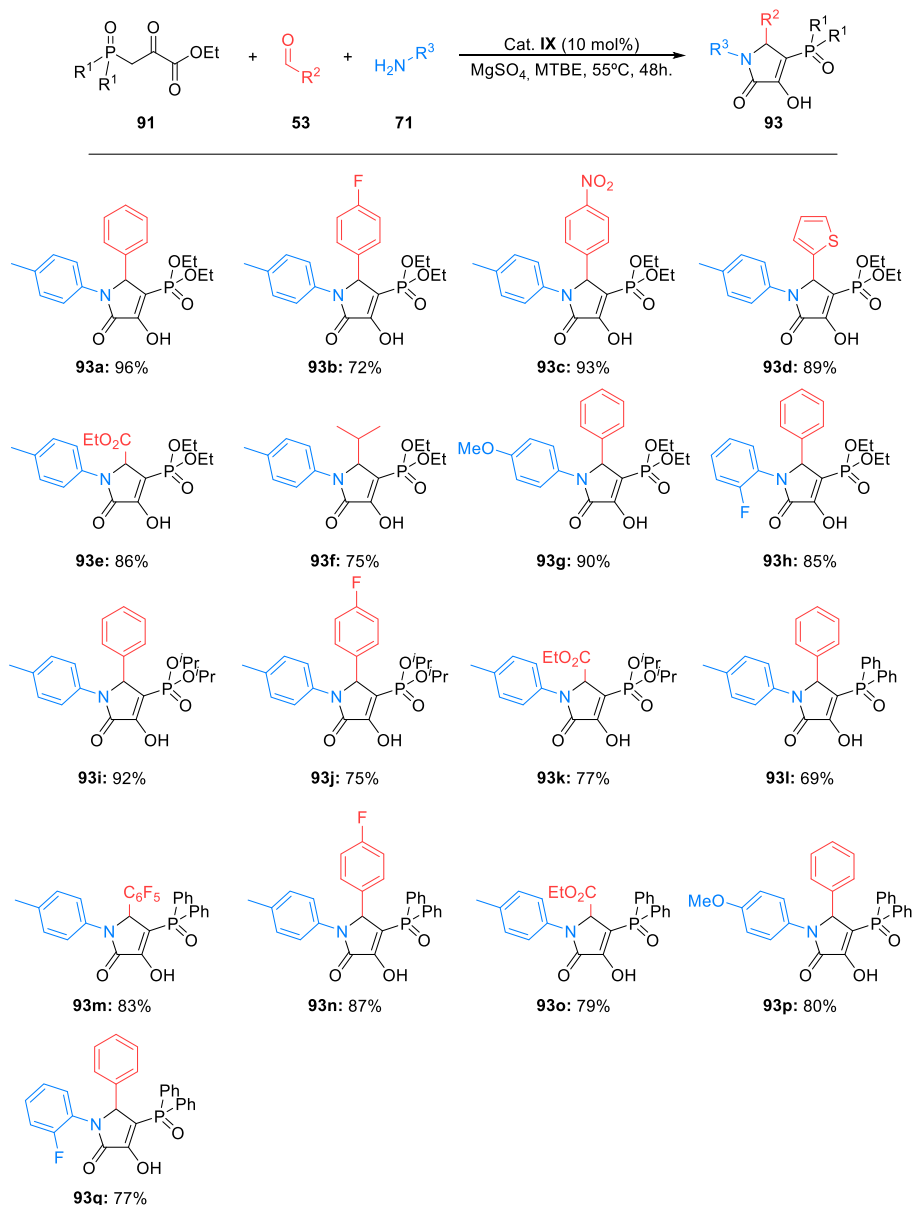


Chart 5. Scope of the three-component reaction for the synthesis of phosphorus-containing 3-hydroxy-1,5-dihydro-2H-pyrrol-2-ones **93**.

The scope of the multicomponent reaction concerning the substituents of the three substrates proved to be very wide. Regarding the structure of the pyruvate reagent, γ -lactams **93** derived from different phosphonate or phosphine oxide groups can be obtained in very good yields (Chart 5).

Aromatic amines bearing weakly or strong electron donating groups can be used in the three-component reaction, such as *p*-toluidine (**71a**, $R^3 = 4\text{-MeC}_6\text{H}_4$), *p*-anisidine (**71b**, $R^3 = 4\text{-MeOC}_6\text{H}_4$) and even *o*-fluoroaniline (**71f**, $R^3 = 2\text{-FC}_6\text{H}_4$). Unfortunately, the use of aliphatic amines or electron poor anilines proved to be ineffective in this multicomponent reaction, and no formation of γ -lactam substrates was observed in those cases.

In relation to the aldehyde substrates **53** used in the multicomponent protocol, besides the use of benzaldehyde (**53c**) as the imine precursor, the reaction proceeds efficiently with other aromatic aldehydes such as *p*-fluorobenzaldehyde (**53h**), for the synthesis of fluorine containing γ -lactams **93b,j,n** in good to very good yields, or *p*-nitrobenzaldehyde (**53a**), for the preparation of γ -lactam **93c**, holding an electron withdrawing aromatic substituent at C-5. The reaction is equally effective when 2-thiophenecarboxaldehyde (**53l**) is used, obtaining 3-hydroxy-1,5-dihydro-2*H*-pyrrol-2-one **93d** in excellent yield. Moreover, ethyl glyoxalate (**53s**) is also a good substrate for this reaction, leading to the formation of α -aminoacid-derived γ -lactams **93e,k,o** also in good yields. Finally, using this methodology, *iso*-propyl substituted substrate **93f** derived from aliphatic isobutyraldehyde (**53o**) is also obtained in good yield (Chart 5).

As usual, γ -lactams **92** and **93** were fully characterized by NMR and IR spectroscopy and HRMS. In particular, 3-hydroxy γ -lactam **93j** shows a very clear and characteristic pattern in NMR (Figures 32 and 33).

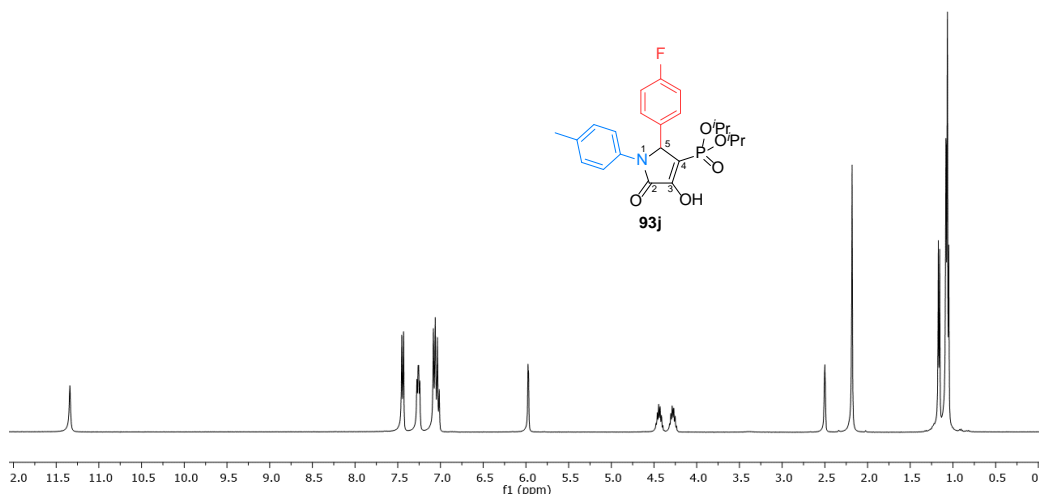


Figure 32. ^1H NMR spectrum of compound **93j** in $\text{DMSO-}d_6$.

The most significant signals of the ^1H NMR spectrum of this compound are the broad singlet at $\delta_{\text{H}} = 11.34$ ppm typical for the enolic OH, which appears at very high field, possibly due to the presence

of an intramolecular hydrogen bond, and the doublet at $\delta_{\text{H}} = 5.97$ ppm corresponding to the proton at the chiral stereocenter that shows a vicinal coupling with the phosphorus atom (${}^3J_{\text{PH}} = 2.8$ Hz). As expected from the presence of a chiral center at the structure, the peaks corresponding to the CH protons of the two diastereotopic *iso*-propyl groups appear as two independent multiplets at $\delta_{\text{H}} = 4.44$ and 4.27 ppm, and the signals corresponding to the CH_3 protons appear as four overlapped doublets between $\delta_{\text{H}} = 1.20$ and 1.00 ppm. Finally, the singlet at $\delta_{\text{H}} = 2.18$ ppm, assigned to the methyl group, and the presence of eight protons at the aromatic region, suggest that a single unit of *p*-toluidine is present in the final structure (Figure 32).

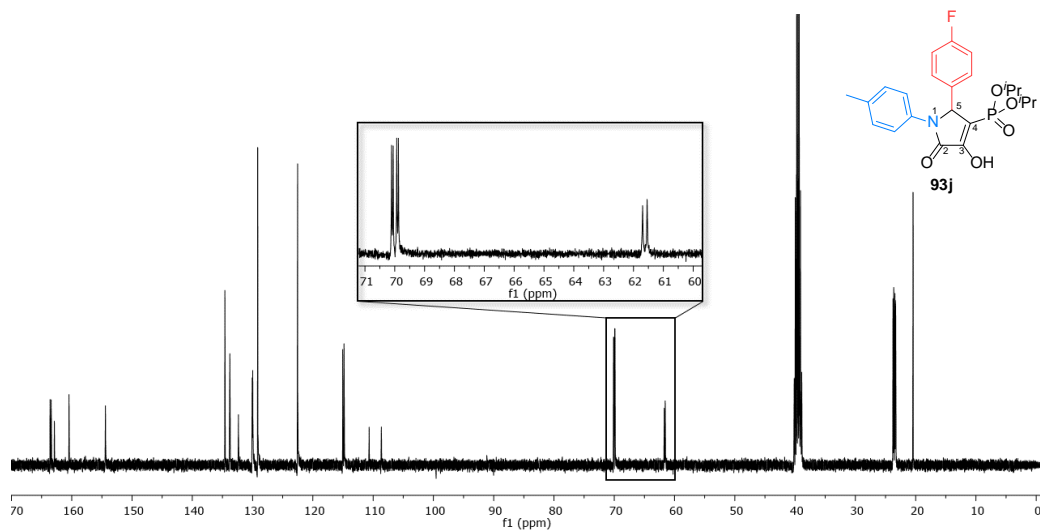


Figure 33. ${}^{13}\text{C}$ NMR spectrum of compound **93j** in $\text{DMSO-}d_6$.

Likewise, the ${}^{13}\text{C}$ NMR spectrum of compound **93j** shows, as expected, the four characteristic signals for the four carbon atoms of the five-membered ring (Figure 33). The most deshielded doublet at $\delta_{\text{C}} = 154.4$ ppm (${}^3J_{\text{PC}} = 4.2$ Hz) belongs to the carbonyl group, and the presence of the enol moiety is evident from the two additional doublets present at $\delta_{\text{C}} = 163.5$ and 109.6 ppm with two typical geminal and *ipso* coupling constants of ${}^2J_{\text{PC}} = 18.4$ Hz and ${}^1J_{\text{PC}} = 203.6$ Hz, respectively. The aliphatic stereogenic carbon appears as a doublet at $\delta_{\text{C}} = 61.6$ ppm, also coupled with the phosphorus atom (${}^2J_{\text{PC}} = 15.3$ Hz). The *iso*-propyl phosphonate group is shown as two doublets at $\delta_{\text{C}} = 70.1$ (${}^2J_{\text{PC}} = 5.4$ Hz) and 69.9 (${}^2J_{\text{PC}} = 5.7$ Hz) ppm belonging to the two diastereotopic CH carbons, and four additional doublets in the interval $\delta_{\text{C}} = 23.7 - 23.3$ (${}^3J_{\text{PC}} \approx 4\text{-}5$ Hz) ppm for the four diastereotopic CH_3 groups. Finally, the *p*-toluidine aromatic ring is deduced by a signal at $\delta_{\text{C}} = 20.4$ ppm for the methyl group, along with two intense signals at the aromatic region. In the same area, the *p*-fluorophenyl group appears as four doublets, with different coupling constants with the fluorine atom.

In view of the resemblance of the structure of 3-hydroxy γ -lactam and 3-amino γ -lactone skeleton, which indeed have an identical molecular formula, a single crystal of enol substrate **93j** was obtained from a mixture of dichloromethane/hexane, and its X-ray diffraction structure was elucidated in order to unambiguously confirm the identity of the obtained substrates (Figure 34).

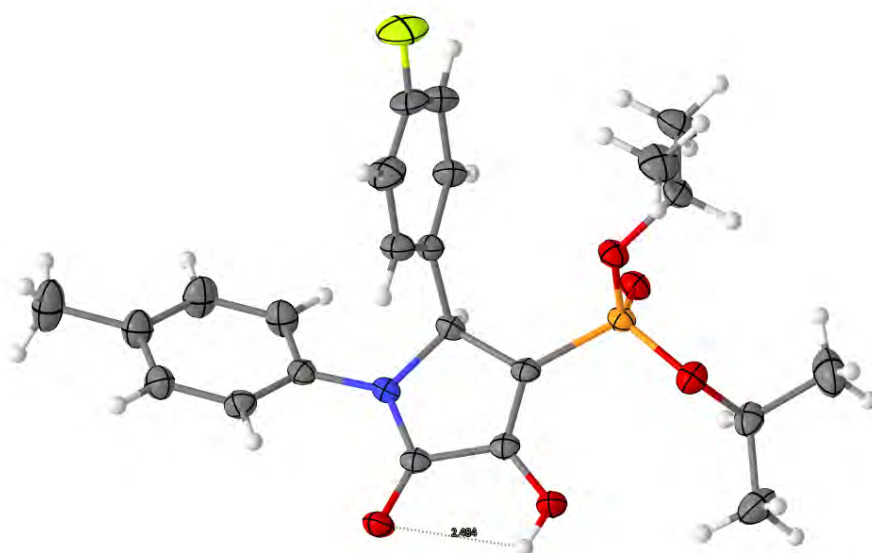
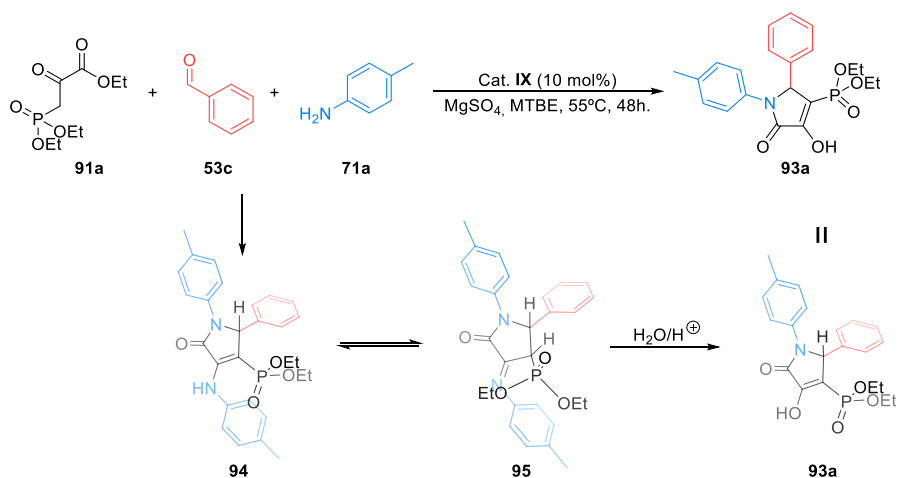


Figure 34. Thermal ellipsoid plot/ORTEP for compound **93j**.

Key features of the crystal structure of **93j** are the almost planar shape of the γ -lactam core, forced by the presence of an endocyclic α,β -unsaturated amide group, and the presence of an intramolecular hydrogen bond between the enol hydrogen and the carbonyl group of the amide moiety in a *pseudo* five-membered ring conformation.

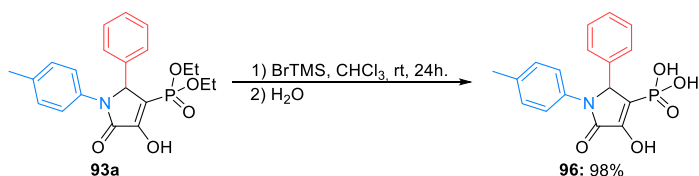
The exclusive formation of the enol substrate instead of the enamines in this case may be explained in view of the high steric hindrance imposed by the bulky phosphoryl group in C-4 at the γ -lactam core inducing a significant strain at the 5-membered ring. The heterocyclic structure is nearly flat due the presence of the carbonyl group and the endocyclic conjugated C=C double bond, thus favoring the spontaneous hydrolysis of the enamine after the initial formation of the imine intermediate **95**. Therefore, the formation of the enol OH group is forced, showing less steric interaction with the phosphorus substituent, providing a thermodynamically more stable structure than in enamine **94** (Scheme 21).



Scheme 21. Proposed pathway for the synthesis 3-hydroxy-1,5-dihydro-2H-pyrrol-2-one **93a**.

Additional experiments were performed with the aim of confirming the proposed mechanism. Accordingly, the use of only one equivalent of the amine substrate also affords enol-like products **93**, although in lower yield. In addition, the same result is obtained when preformed imine and enamine species are used as starting materials. According to this, the initial formation of enamine-derived γ -lactam **94** is essential to obtain the final products **93**.

In order to prepare the phosphonic acid derivatives of γ -lactams **93**, and after unsuccessful attempts of acidic or basic treatments, the hydrolysis of the phosphonate-substituted α,β -unsaturated γ -lactam **93a** to its phosphonic acid derivative **96** could be performed in almost quantitative yield using trimethylsilyl bromide at room temperature, followed by an aqueous workup (Scheme 22).



Scheme 22. Hydrolysis of phosphonate **93a**.

In conclusion, a Brønsted acid catalyzed multicomponent methodology for the synthesis of fluorine and/or phosphorus containing γ -lactam derivatives is described in this chapter. The products are obtained in the form of 3-hydroxy 1,5-dihydro-2H-pyrrol-2-one or their enamine derivatives depending on the substitution at the 5-membered ring heterocycle.

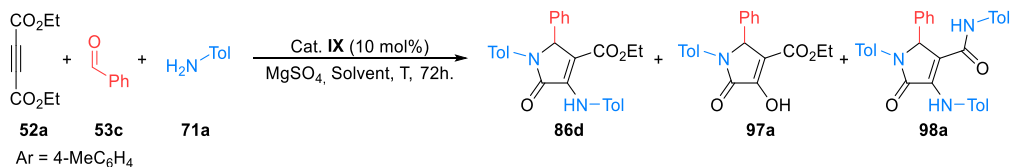
Chapter 3

Multicomponent synthesis of γ -lactam derivatives using activated alkynes

As it has been addressed above, there are some examples in the literature regarding MCRs using activated alkynes, aldehydes and amines for the synthesis of γ -lactam derivatives. However, to the best of our knowledge there are not precedents described of such reaction making use of phosphoric acid organocatalysis. For this reason, given the demonstrated ability of catalyst **IX** to promote the nucleophilic addition of pyruvate-derived enamines **78** to imines **79** (Scheme 15, *vide supra*), next the Brønsted acid-catalyzed MCR was extended to the use of dialkyl acetylenedicarboxylates, which could be considered as surrogates of pyruvate esters. Accordingly, first we performed an optimization of the reaction conditions, using as the model substrates diethyl acetylenedicarboxylate (**52a**), benzaldehyde (**53c**) and *p*-toluidine (**71a**) in the presence of BINOL-derived phosphoric acid catalyst **IX**, as shown in Table 4.

Initially, the three-component reaction was performed in the presence of BINOL-derived phosphoric acid catalyst **IX**, using refluxing dichloromethane as solvent (Table 4, Entry 1). However, the ^1H NMR spectrum of the crude reaction showed only the formation of the imine and enamine intermediates, expected from the reaction of *p*-toluidine (**71a**) with benzaldehyde (**53c**) and alkyne **52a**, and a lack of reactivity between both species. Considering the expected steric hindrance in the target highly substituted γ -lactams, along with the additional deactivation present in the enamine intermediate when acetylenedicarboxylate **52a** is used instead of pyruvate derivatives, next, we performed the reaction at higher temperatures. Even though, a similar result was obtained when tetrahydrofuran (THF) or dimethoxyethane (DME) were used as solvents (Table 4, Entries 2-3), to our delight, a full conversion was observed in refluxing methyl *tert*-butylether (MTBE), affording a mixture of enamine-derived γ -lactam **86d** along with enol derivative **97a** in a 40:60 ratio (Table 4, Entry 4).

Table 4. Optimization of the reaction conditions for the multicomponent reaction of acetylenedicarboxylate **52a**, benzaldehyde (**53c**) and *p*-toluidine (**71a**).



Entry	Ratio 52a:53c:71a	Solvent	T (°C)	Yield (%) ^a	Ratio 86d:97a:98a ^b
1	1:1:2	CH ₂ Cl ₂	40	0	n.d.
2	1:1:2	THF	65	0	n.d.
3	1:1:2	DME	85	0	n.d.
4	1:1:2	MTBE	55	72	40:60:0
5	3:1:2	MTBE	55	0	n.d.
6	1:1:1	MTBE	55	0	n.d.
7	1:1:2	Dioxane	101	81	80:0:20
8	1:1:2	Toluene	110	77	95:0:5
9	1:1:4	Toluene	110	82	92:0:8

^aIsolated total yield. ^bDetermined by ¹H NMR.

In the MCR with ethyl pyruvate, the use of an excess of the ketoester substrate proved to be efficient in reducing the reaction times and temperatures. However, in this case, when three equivalents of acetylene dicarboxylate **52a** were used, no formation of α,β -unsaturated γ -lactam derivatives **86d** or **97a** was detected, since amine **71a** was completely consumed by the excess of diethyl acetylenedicarboxylate (**52a**) (Table 4, Entry 5). For the same reason, the use of only one equivalent of *p*-toluidine (**71a**) proved also to be ineffective (Table 4, Entry 6).

A higher selectivity to afford enamine-derived γ -lactam **86d**, was obtained when the reaction was performed in dioxane at 101 °C. However, in this case, substrate **86d** was obtained together with a significant amount of amide derivative **98a** (Table 4, Entry 7). In addition, the selectivity of the reaction was further improved using refluxing toluene as the reaction solvent, providing enamine-derived γ -lactam **86d** with only a small quantity of amide derivative **98a** (5%) (Table 4, Entry 8). Interestingly, the use of four equivalents of *p*-toluidine (**71a**) did not result in the formation of amide derivative **98a** as the major product (Table 4, Entry 9).

The three substrates obtained in the reaction were isolated and fully characterized by NMR and IR spectroscopy and HRMS. The ¹H NMR spectra of the products are shown piled up in Figure 35, showing some differences between them. The most representative signals of enamine-type γ -lactam **86d** are the chemical shift corresponding to the proton at the asymmetric carbon, that appears as a singlet at $\delta_{\text{H}} = 5.76$ ppm, the enamine NH proton at $\delta_{\text{H}} = 8.17$ ppm, that interchanges with D₂O, and the two

intense singlets at $\delta_{\text{H}} = 2.33$ and 2.22 ppm, that correspond to the two methyl groups of both *p*-tolyl moieties. However, the proton at the asymmetric carbon of the enol-derived γ -lactam **97a** appears at higher field ($\delta_{\text{H}} = 5.69$ ppm) if compared to enamine-derived γ -lactam **86d**. In addition, the broad singlet at $\delta_{\text{H}} = 9.12$ ppm corresponds to the OH group and only one signal of the *p*-tolyl group is present in the spectrum of **97a** at $\delta_{\text{H}} = 2.21$ ppm. Both substrates, **86d** and **97a**, show the characteristic signals of an A_2X_3 system, typical for an ethoxy group. With respect to the spectrum corresponding to amide derivative **98a**, the signal of the proton at the asymmetric carbon appears as a singlet at lower field that in the other two parent compounds ($\delta_{\text{H}} = 5.85$ ppm). In addition, the two NH protons are observed as broad singlets at $\delta_{\text{H}} = 8.33$ and 6.63 ppm, both showing interchange with D_2O . The absence of the signals corresponding to the ethoxy moiety and the existence of three intense singlets at $\delta_{\text{H}} = 2.28$, 2.24 and 2.23 ppm, make evident the addition of a third molecule of *p*-toluidine (Figure 35).

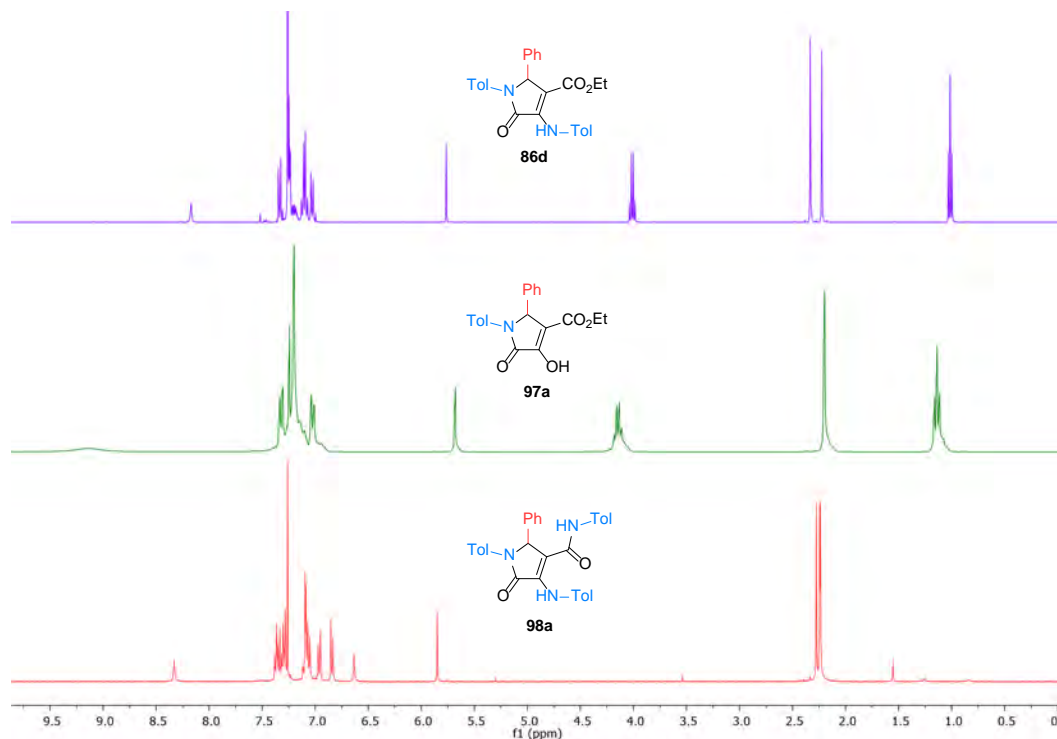


Figure 35. Comparison of the ^1H NMR spectra of compounds **86d**, **97a** and **98a**.

Due to the structural resemblance between all the γ -lactam derivatives obtained and, in order to unambiguously determine structure of the minor product of the reaction, a single crystal of enol **97a** was prepared, and its X-ray diffraction structure was obtained (Figure 36).

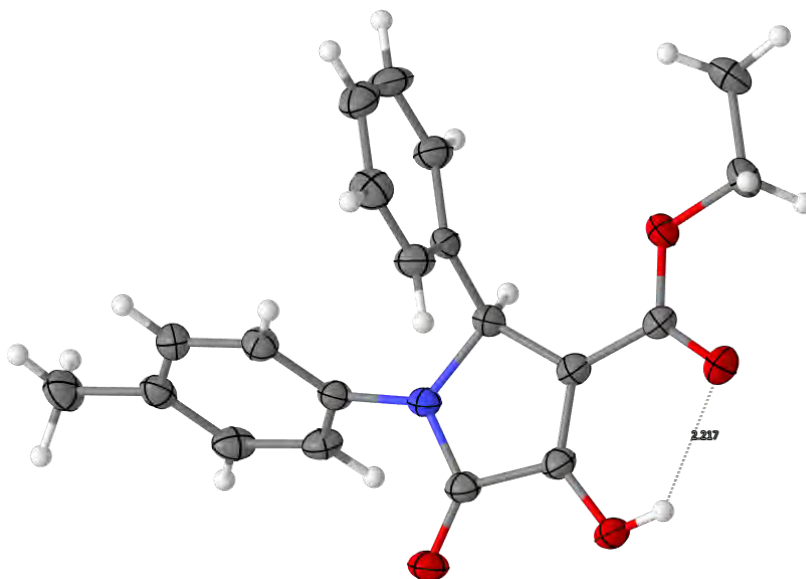
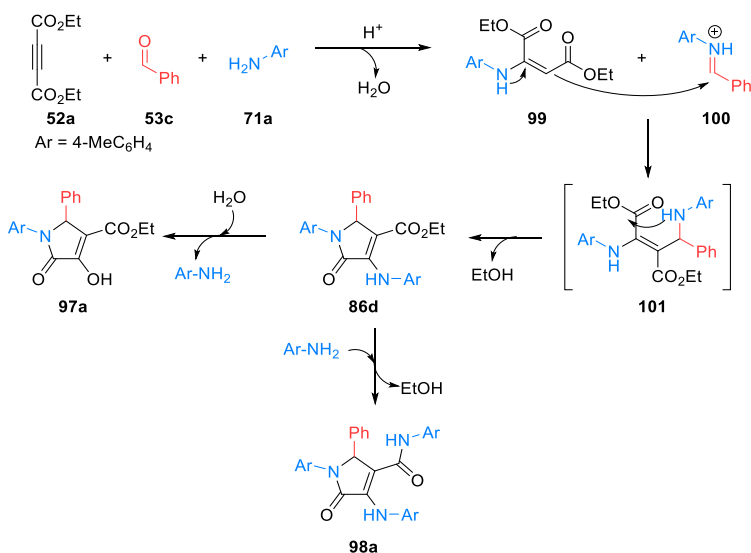


Figure 36. X-ray structure of **97a**.

Key features of the crystal structure of enol-derived γ -lactam **97a** are the almost planar shape of the five-membered ring and the presence of an intramolecular hydrogen bond between the enol hydrogen and the carboxylate group in a *pseudo* six-membered ring conformation, rather than with the amide carbonyl, which observed in the X-ray diffraction structure of compound **93j** (Figure 34, *vide supra*).

Similarly to the reaction using pyruvates, the reaction mechanism may start with an initial simultaneous addition of *p*-toluidine (**71a**) to diethyl acetylenedicarboxylate (**52a**) and benzaldehyde (**53c**) to afford enamine **99** and aldimine **100**, respectively, followed by the formation of adduct **101** *via* a Mannich reaction (Scheme 23). Then, intermediate **101** undergoes an intramolecular cyclization process, between the amine and carboxylate moieties, affording enamine-type γ -lactam **86d**. Moreover, the presence of water in the reaction media would make possible the hydrolysis of the enamine moiety of γ -lactam **86d** to afford enol-type lactam **97a**. On the other hand, if some remaining amine is still present in the mixture, the displacement of ethanol by *p*-toluidine (**71a**) would occur to provide amide derivative **98a**. This proposal is supported by the fact that, using high-boiling point solvents, no enol derivative **97a** is obtained because of the instantaneous evaporation of water, which would prevent the hydrolysis of the enamine group.



Scheme 23. Proposed pathway for the three-component reaction of acetylenedicarboxylate **52a**, benzaldehyde (**53c**) and *p*-toluidine (**71a**).

Once the optimal conditions of the MCR were established, the reaction was extended to the preparation of a family of diverse α,β -unsaturated γ -lactams. The scope is summarized in Chart 6.

First, the reaction was applied to the use of several amines **71**, using benzaldehyde (**53c**, $\text{R}^2 = \text{Ph}$) and diethyl acetylenedicarboxylate (**52a**, $\text{R}^1 = \text{Et}$). The use of an electron rich aniline or aliphatic amines such as *p*-anisidine (**71b**, $\text{R}^3 = 4\text{-CH}_3\text{OC}_6\text{H}_4$) or benzylamine (**71i**, $\text{R}^1 = \text{Bn}$) led to compounds **86e** and **86f**, with a slight decrease in the yield, in comparison to the model reaction giving rise to substrate **86d** (Chart 6). Remarkably, when electron deficient aromatic amines such as *p*-nitroaniline or *p*-trifluoromethylaniline were used as substrates, the formation of the intermediate imine **100** and enamine **99** species was initially observed by NMR but, in these cases, the reaction failed to provide the γ -lactam substrates.

It should be noted that, in view of the mechanism proposed for this reaction (Scheme 23, *vide supra*), the electronic character of the amine substrate might be a crucial factor in the reactivity of the key step of the multicomponent process. Accordingly, while the use of electron rich amines may benefit the nucleophilic character of enamine species **99**, this would result in a decreased electrophilic character of imine species **100**. By contrast, the use of deactivated amines would result in an activation of imine electrophile **100** and a collateral deactivation of enamine nucleophile **99**. Therefore, this behaviour would explain, the lower yield obtained using *p*-anisidine (**71b**) if compared to *p*-toluidine (**71a**) and, additionally, the formation of higher amounts of amide side product **98b** (ratio **86e**:**98b** 70:30) would also reduce the yield of the ethyl carboxylate derivative **86e**.

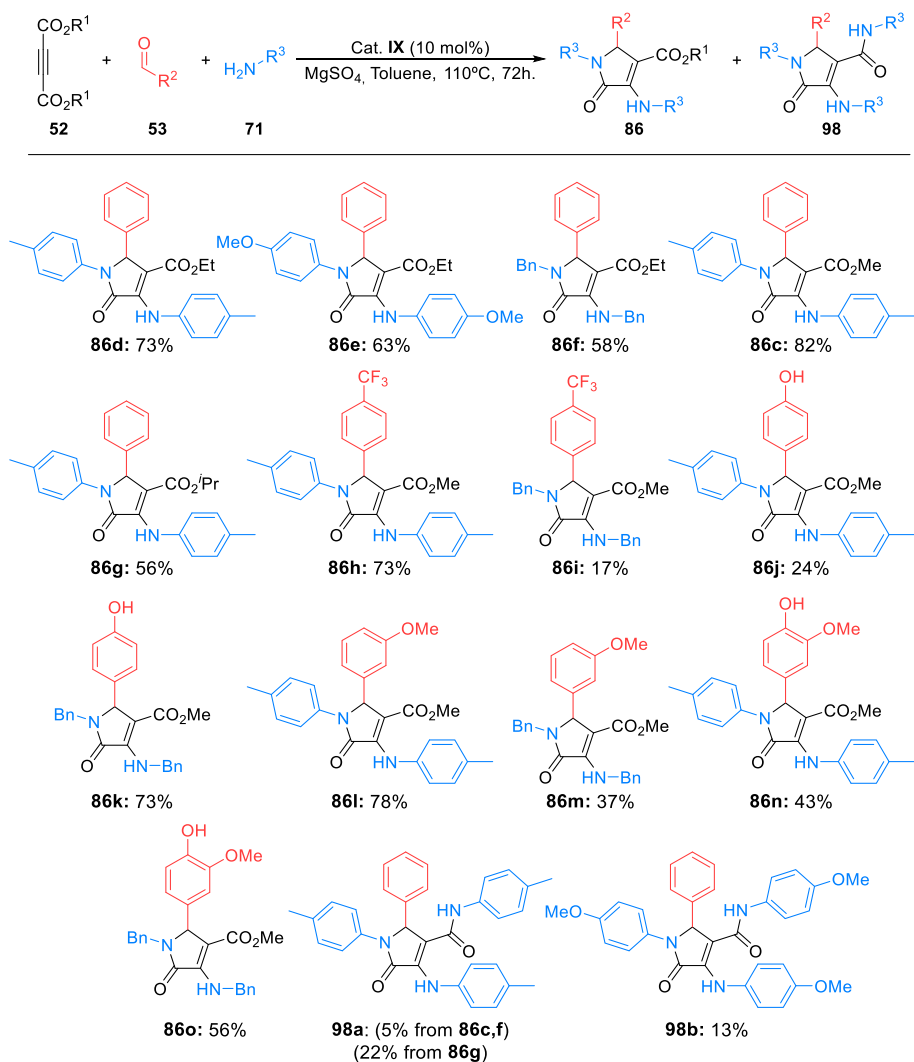


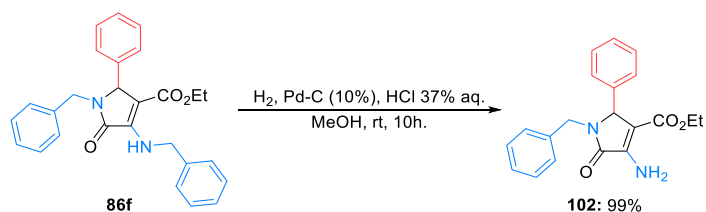
Chart 6. Three-component reaction of dialkyl acetylenedicarboxylates **52**, aldehydes **53** and amines **71**.

Next, the use of different acetylenedicarboxylates **52** as electrophile substrates in the multicomponent reaction was explored in the MCR, with *p*-toluidine (**71a**) and benzaldehyde (**53a**) as the reaction partners. The use of dimethyl acetylenedicarboxylate (**52b**, R¹ = Me) led to the formation of γ -lactam **86c** in very good yield, together with a small amount of amide-derived γ -lactam **98a** (5%), similarly to what is observed for the use of diethyl acetylenedicarboxylate (**52a**, R¹ = Et) (Chart 6). However, when bulkier di-*iso*-propyl acetylenedicarboxylate (**52c**, R¹ = *i*Pr) is used, longer reaction times are required (72 hours), which also facilitates the formation of amide side product **98a** (ratio **86g**:**98a** 70:30), as a result of the longer coexistence of *p*-toluidine (**71a**) and γ -lactam substrate **86g**.

Finally, the scope of the reaction was extended to the use of different aldehydes **53**, utilizing dimethyl acetylenedicarboxylate (**52b**, $R^1 = \text{Me}$) as the electrophile, and *p*-toluidine (**71a**) or benzylamine (**71i**) as amine substrates. The use of electron deficient *p*-trifluoromethyl benzaldehyde (**53i**, $R^2 = 4\text{-CF}_3\text{C}_6\text{H}_4$) in the multicomponent reaction provides a more electrophilic imine species **100**, favoring the reactivity in the Mannich intermediate process. Indeed, using *p*-toluidine (**71a**) as the reaction partner, a very good yield of γ -lactam **86h** was obtained with no presence of the amide side-product, as expected from the less nucleophilic character of the amine. However, although the reaction with benzylamine (**71i**) leads to the formation of a more nucleophilic enamine intermediate **99** in the Mannich reaction, for this particular case, γ -lactam **86i** is obtained only in poor yield, which may be due to the lower electrophilic character of the *N*-benzylimine intermediate **100**. On the contrary, it is expected that the intermediate Mannich reaction would be disfavored by the use of an aldehyde holding a strong electron donating substituent, which generates in this case a less electrophilic imine species **100**. Accordingly, the use of *p*-hydroxybenzaldehyde (**53t**, $R^2 = 4\text{-HOC}_6\text{H}_4$) and *p*-toluidine (**71a**) in the multicomponent reaction leads to the formation of γ -lactam **86j** in modest yield, which may be due to the poorer electrophilic character expected in *N*-arylimine intermediate **100**. Nevertheless, the same reaction using benzylamine (**71i**) yields γ -lactam derivative **86k** in good yield, since an increase in the nucleophilic character of the enamine intermediate seems to drive the Mannich reaction forward and overcome the decreased nucleophilicity expected for *N*-benzylimine species **100**.

In accordance with the trends observed in the reactivity, *m*-anisaldehyde (**71u**, $R^2 = 3\text{-MeOC}_6\text{H}_4$) provided similar results as benzaldehyde (**53a**), with a good yield for *p*-toluidine-derived γ -lactam **86l** and slightly lower reactivity for benzylamine-derived γ -lactam **86m**. Finally, the scope of the reaction was completed using a disubstituted benzaldehyde such as vainillin (**53v**, $R^2 = 3\text{-MeO-4-HO-C}_6\text{H}_3$), and γ -lactams **86n-o** were obtained in poor to fair yields (Chart 6).

A simple derivatization of benzylamine-derived substrates is the cleavage of the benzyl groups located at the nitrogen atoms. According to this, the benzyl group at the enamine moiety in **86f** was selectively removed by hydrogenolysis through the treatment in MeOH under H_2 atmosphere at 80 psi in the presence of 10 mol% of palladium on carbon, leading to γ -lactam derivative **102** in quantitative yield (Scheme 24). Remarkably, under those conditions, only one of the two benzyl groups is removed while the carbon-carbon double bond remains intact.



Scheme 24. Deprotection of benzylamine derivative **86f**.

Other simple transformation of γ -lactams **86** that would contribute to expand the molecular diversity consists of the hydrolysis of the enamine moiety. Accordingly, enol-derived γ -lactams were synthesized upon treatment of substrates **86** with aqueous HCl, affording cyclic enols **97** in very good to excellent yields (Chart 7).

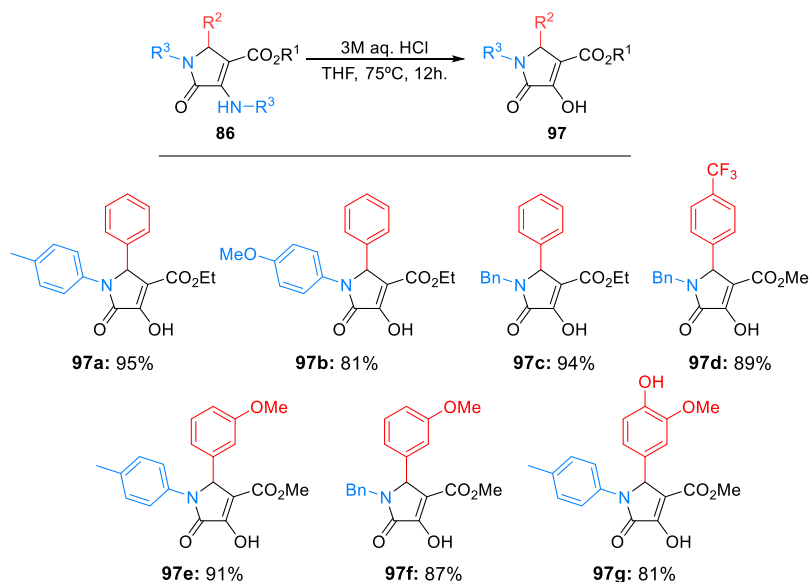


Chart 7. Hydrolysis of 3-amino-1,5-dihydro-2H-pyrrol-2-ones **86**.

As a summary of this chapter, a Brønsted acid catalyzed multicomponent procedure for the preparation of 3-amino-1,5-dihydro-2H-pyrrol-2-ones is described in this chapter, where dialkyl acetylenedicarboxylate, amines and aromatic aldehydes are used as substrates. This is the first example of such reaction using phosphoric acids as catalyst. As far as we are concerned, the hydrolysis process of 1,5-dihydro-2H-pyrrol-2-ones from enamine substrates **86** to the enol derivatives **97** has not been described so far.

Chapter 4

An enantioselective approach for the multicomponent synthesis of γ -lactams

Since the thalidomide tragedy,¹⁵⁵ in order to avoid similar disasters, most of the drug regulatory agencies and pharmaceutical industries have established among their synthetic priorities the preparation of chiral active molecules in an enantiopure form. According to this, the development of new synthetic methodologies to obtain optically pure chiral molecules is a goal of great interest in organic chemistry.

The conventional protocols for the synthesis of chiral substrates normally lead to racemic mixtures. However, during the last decades, the increasing demand for methodologies to synthesize enantioenriched compounds, not only at a laboratory scale, but also at industrial scale,¹⁵⁶ has increased the interest into the development of strategies leading to enantiomerically pure molecules (Figure 37).

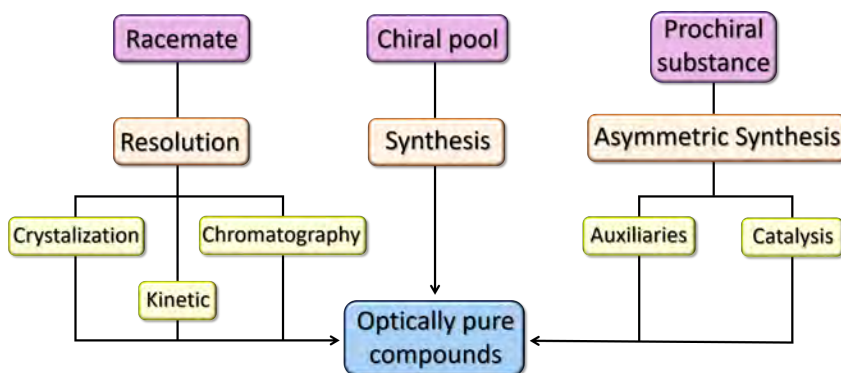


Figure 37. Methods for the synthesis of optically pure compounds.

¹⁵⁵ Therapontos, C.; Erskine, L.; Gardner, E. R.; Figg, W. D.; Vargesson, N. *Proc. Natl. Acad. Sci.* **2009**, *106*, 8573-8578.

¹⁵⁶ (a) Núñez, M. C.; García-Rubiño, M. E.; Conejo-García, A.; Cruz-López, O.; Gallo, M. A.; Espinosa, A.; Campos, J. M. *Curr. Med. Chem.* **2009**, *16*, 2064-2074. (b) Collins, A. N.; Shel Drake, G. N.; Crosby, J. *Chirality in industry: The commercial manufacture and applications of optically active compounds*; John Wiley & Sons, 1992.

In this concern, the most classic method, and one of the most used on an industrial scale, is the resolution of racemates, which consists of the separation of two enantiomers from a racemic mixture. The main methods are the resolution by crystallization, separation by chiral chromatography, kinetic resolution and dynamic kinetic resolution.¹⁵⁷ Obviously, the maximum yield of the global process that can be obtained using such techniques is 50%, except for the dynamic kinetic resolution where, in some cases, it is possible to obtain a single enantiomer in a quantitative yield.¹⁵⁸

The chiral pool strategy is an alternative methodology leading to optically pure compounds. This methodology implies the use of cheap optically pure natural compounds, such as amino acids, terpenes, sugars or alkaloids, as starting materials in order to synthesize the target chiral product as a single enantiomer. Although this is a very effective technique for high scale synthesis of simple bioactive compounds, the chiral pool strategy has some disadvantages over other approaches: The requirement of designing a specific route for each compound, the dependence on the availability of the starting reagents and the risk of racemization of the stereogenic carbon under certain reaction conditions. Despite these handicaps, it is still a very useful strategy for the synthesis of compounds with biological interest like Taxol® or ingenol.¹⁵⁹

Asymmetric synthesis constitutes a third strategy for the synthesis of enantiomerically pure compounds,¹⁶⁰ where stereocontrolled reactions are used to directly obtain enantioenriched products. Here, two approaches can be considered:

- **The use of chiral auxiliaries (diastereoselective methods).** Although this technique often allows to effectively controlling the stereoselectivity of the reaction, two additional steps are needed in the synthetic route; one for the introduction of the chiral auxiliary in the starting material and another one for its removal. In addition, stoichiometric amounts of the chiral auxiliary are required and, besides, the ideal chiral auxiliary must be able to be recovered and recycled.

¹⁵⁷ Reviews about racemate resolution: (a) Faigl, F.; Fogassy, E.; Nógrádi, M.; Pálovics, E.; Schindler, J. *Tetrahedron Asymmetry* **2008**, *19*, 519-536. (b) Anderson, N. G.; Solutions, P.; Lane, G.; Jackson, V. *Org. Process Res. Dev.* **2005**, *9*, 800-813. (c) Vedejs, E.; Jure, M. *Angew. Chem. Int. Ed.* **2005**, *44*, 3974-4001.

¹⁵⁸ Pellissier, H. *Tetrahedron* **2008**, *64*, 1563-1601.

¹⁵⁹ Brill, Z. G.; Condakes, M. L.; Ting, C. P.; Maimone, T. J. *Chem. Rev.* **2017**, *117*, 11753-11795.

¹⁶⁰ (a) Hughes, D. L. Introduction to industrial applications of asymmetric synthesis. In *Comprehensive Chirality*; Elsevier Science, 2012, pp 1-26. (b) Farina, V.; Reeves, J. T.; Senanayake, C. H.; Song, J. J. *Chem. Rev.* **2006**, *106*, 2734-2793.

- **Asymmetric catalytic methods.** These methods involve bio-catalysis,¹⁶¹ metal-catalysis¹⁶² and organocatalysis,¹⁶³ where a substoichiometric amount of a chiral inductor is used as catalyst to directly provide enantioenriched substrates. The use of these methodologies has some evident advantages, such as the reduction of the environmental impact of manufacturing processes by decreasing the number of synthetic steps, minimization of the physical amounts of the required reagents, and reduction of waste volumes.¹⁶³

Due to the obvious advantages of enantioselective methodologies over others, strong efforts have been made during the last decades in order to develop new enantioselective protocols for the preparation of enantioenriched γ -lactam derivatives. However, the vast majority of the described protocols consist of stepwise reactions, and the reports concerning enantioselective multicomponent reactions are still scarce.¹⁶⁴

Only two examples with modest enantiomeric excesses have been described for the synthesis of γ -lactam derivatives through the three-component reaction studied during this dissertation. In 2008 Cheng and Luo reported the enantioselective preparation of 3-amino-1,5-dihydro-2*H*-pyrrol-2-ones **84** using chiral BINOL-derived phosphoric acid catalyst **X** (10 mol%) (Figure 38). In particular, these authors described the three-component reaction, using ethyl pyruvate (**70a**), benzaldehyde (**53c**) and *p*-anisidine (**71b**) in a 3:1:2 ratio, in toluene at room temperature, affording unsaturated γ -lactam **84b** in 77% yield and 44% enantiomeric excess.¹⁶⁵ Later in 2013, Huang and Luo reported another example on this topic, using catalyst **XI** (5 mol%), methyl pyruvate (**70b**), *tert*-butyl glyoxalate (**53t**) and *p*-anisidine (**71b**) in a 1:1:2 ratio, in toluene at room temperature, to yield the corresponding γ -lactam derivative **84n** in 90% yield and 72% ee (Figure 38).¹⁶⁶

¹⁶¹ Wells, A. Industrial applications of biocatalysis: An overview. In *Comprehensive Chirality*; Elsevier Science, 2012, pp 253-287.

¹⁶² For more information see: (a) Ager, D. J.; de Vries, J. G. Industrial applications of asymmetric reduction of C=C Bonds. In *Comprehensive Chirality*; Elsevier Science, 2012, pp 73-82. (b) Komiyama, S.; Shimizu, H.; Nagasaki, I. Industrial application of the asymmetric reduction of C=O and C=N bonds, including enamides and enamines. In *Comprehensive Chirality*; Elsevier Science, 2012, pp 83-103. (c) Wu, G. G.; Chen, F. X.; Yong, K. Industrial applications of metal-promoted C-C, C-N, and C-O asymmetric bond formations. In *Comprehensive Chirality*; Elsevier Science, 2012, pp 147-208.

¹⁶³ Bulger, P. G. Industrial applications of organocatalysis. In *Comprehensive Chirality*; Elsevier Science, 2012, pp 228-252.

¹⁶⁴ del Corte, X.; Maestro, A.; Martinez de Marigorta, E.; Palacios, F.; Vicario, J. In *Targets in Heterocyclic Systems 22*; Società Chimica Italiana, 2022, pp 22-52.

¹⁶⁵ Li, X.; Deng, H.; Luo, S.; Cheng, J. P. *Eur. J. Org. Chem.* **2008**, 4350-4356.

¹⁶⁶ Luo, C.; Huang, Y. *J. Am. Chem. Soc.* **2013**, *135*, 8193-8196.

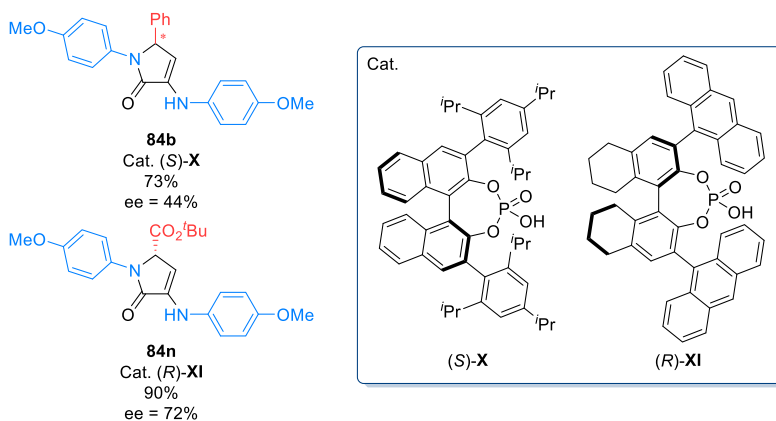
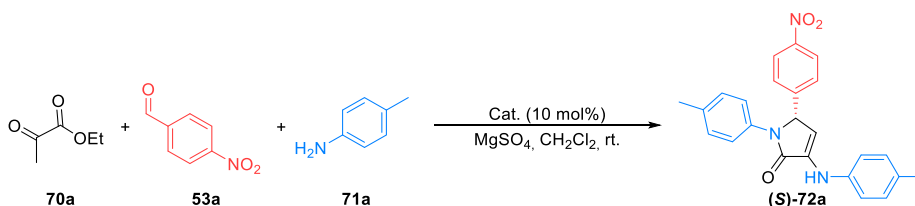


Figure 38. Enantioenriched 3-amino-1,5-dihydro-2H-pyrrol-2-ones **84** obtained.

Building upon these precedents and, considering the demonstrated ability of Brønsted acid catalysts to promote the three-component reaction of pyruvates, aldehydes and amines, the efforts were focused in this case on the development of a highly enantioselective version of this reaction for the preparation of enantioenriched γ -lactam derivatives. Accordingly, the three-component process for the synthesis of γ -lactam derivatives in the presence of chiral catalysts was explored, using ethyl pyruvate (**70a**), benzaldehyde (**53c**) and *p*-toluidine (**71a**), in dichloromethane, as the model reaction (Scheme 25).



Scheme 25. Model reaction for the optimization of the enantioselective multicomponent protocol.

In the first stage of this research, the studies on this reaction were started using several families of organocatalysts (Figure 39). First, the reaction was performed using a 10 mol% of aminophosphine **XII** as the catalyst, only providing mixtures of the enamine and imine intermediates, with no formation of the target γ -lactam **72a** (Table 5, Entry 1). The reaction was also unsuccessful when aminoalcohols **XIII** and **XIV** were used as catalysts (Table 5, Entries 2-3). Additionally, the use of tiourea-catalyst **XV-XIX** was evaluated (Table 7, Entries 4-8), showing in this case a moderate conversion, although some enantiomeric excesses were observed with species **XVIII** and **XIX** (Table 7, Entries 7-8). Moreover, the multicomponent reaction proceeded in very low conversion when phosphoramidite-urea **XX** catalysts

was used (Table 5, Entry 9), and no reaction was also observed with phosphinamide-urea **XXI** (Table 5, Entry 10).

Table 5. Aminophosphine, aminoalcohol, tiourea, phosphoramidite-urea and phosphinamide-urea like catalysts used in the model reaction.

Entry	Catalyst	Conversion (%) ^a	ee (%)	Entry	Catalyst	Conversion (%) ^a	ee (%)
1	XII	No reac.	-	6	XVII	No reac.	-
2	XIII	No reac.	-	7	XVIII	82	3
3	XIV	No reac.	-	8	XIX	80	14
4	XV	No reac.	-	9	XX	12	1
5	XVI	No reac.	-	10	XXI	No reac.	-

^aDetermined by ¹H NMR.

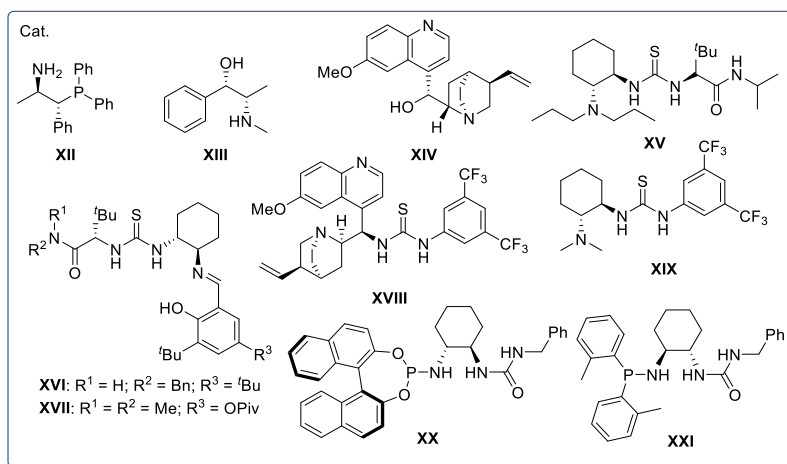
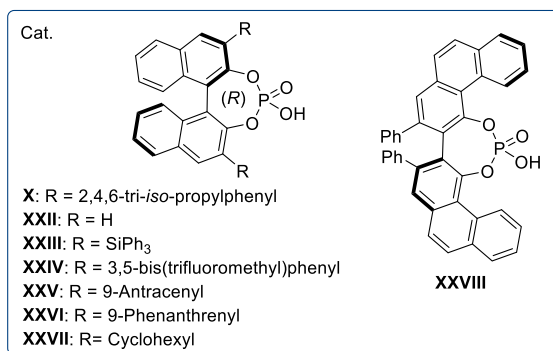


Figure 39. Structure of catalysts **XII-XXI**.

Once discarded catalysts **XII-XXI**, the use of more promising chiral BINOL-derived phosphoric acids was explored (Figure 40). As expected, simple non-substituted BINOL catalyst **XXII** showed to be efficient in catalyzing the reaction, but no appreciable enantiomeric excess was measured (Table 6, Entry 1). On the contrary, triphenylsilyl and 2,4,6-tri-*iso*-propylphenyl substituted species **XXIII** and **X** proved to be equally effective, providing good enantioselectivities (67% and 61%, respectively) (Table 6, Entries 2-3). The three component reaction proceeded also successfully with other BINOL-derived phosphoric acids **XXIV-XXVI**, holding 3,5-bis(trifluoromethyl)phenyl, 9-antracenyl and 9-phenanthrenyl substituents. However, the observed enantiocontrol was very poor in those cases (3-11%) (Table 6, Entries 4-6). Although the use of cyclohexyl-derived BINOL catalyst **XXVII** provided moderate enantiomeric excess, catalysts **XXII** and **X** still proved to be superior (Table 6, Entry 7 vs. Entries 2-3). Finally, the use of VAPOL-derived catalyst **XXVIII** also showed an excellent conversion, but no enantiocontrol was observed (Table 6, Entry 8).

Table 6. BINOL and VAPOL-derived phosphoric acids used in the model reaction.

Entry	Catalyst	Conv. (%) ^a	ee (%)	Entry	Catalyst	Conv. (%) ^a	ee (%)
1	XXII	100	1	5	XXV	100	3
2	XXIII	100	67	6	XXVI	100	11
3	X	100	61	7	XXVII	100	45
4	XXIV	100	5	8	XXVIII	100	2

^aDetermined by ¹H NMR.**Figure 40.** Structure of BINOL and VAPOL-derived catalysts **X**, **XXII-XXVIII**.

Having identified the most appropriate catalysts for the enantioselective multicomponent reaction, next the influence of the solvent in the enantioselectivity of the reaction was studied. In this case, the most promising phosphoric acid catalyst **XXIII** was used and the observed enantioselectivities with the model three-component reaction are summarized in Table 7. The normalized molar electronic translation energies (E_T^N)¹⁶⁷ are used as an indicator of the polarity of the solvent.

Table 7. Optimization of the solvent for the model three-component reaction.

Entry	Solvent	E_T^N	Conv. (%) ^a	ee (%)	Entry	Solvent	E_T^N	Conv. (%) ^a	ee (%)
1	CCl ₄	0.052	90	68	8	CHCl ₃	0.259	100	35
2	Toluene	0.099	100	82	9	CH ₂ Cl ₂	0.309	100	67
3	<i>i</i> Pr ₂ O	0.105	100	78	10	Cl(CH ₂) ₂ Cl	0.327	100	52
4	Et ₂ O	0.117	100	96	11	DMF ^b	0.386	0	-
5	MTBE	0.124	100	85	12	MeCN	0.460	100	89
6	THF	0.207	100	58	13	MeOH ^b	0.762	0	-
7	DME	0.231	100	66	14	CH ₂ Cl ₂ :Et ₂ O (10:1)	-	100	90

^aDetermined by ¹H NMR. ^bReaction stirred for 24 hours.¹⁶⁷ Reichardt, C. *Chem. Rev.* **1994**, *94*, 2319-2358.

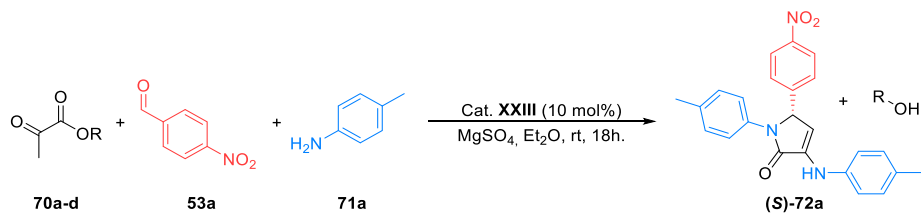
With respect to non-coordinating solvents, in comparison with the original reaction in dichloromethane (Table 7, Entry 9), low polar solvents such as carbon tetrachloride or toluene showed a slight improvement in the enantioselectivity (Table 9, Entries 1-2) while, if the reaction is performed in more polar chloroform or dichloroethane, a drop in the enantiomeric excess is observed (Table 7, Entries 8, 10). Surprisingly, if the reaction is run in diethyl ether, a dramatic increase in the enantioselectivity is measured (Table 7, Entry 4).

In view of this last result, several ethers were tested as solvents in the multicomponent reaction but disparate results were observed and lower enantiomeric excesses were obtained using di-*iso*-propylether, methyl *tert*-butylether, tetrahydrofuran or dimethoxyethane (Table 7, Entries 3, 5-7). In addition, the reaction performed in acetonitrile showed also a good enantioselectivity (Table 7, Entry 12). Moreover, the reaction did not proceed at all in strong polar solvents as dimethylformamide or methanol (Table 7, Entries 11, 13), which may be due to a quenching of the catalyst activity, attributable to a strong coordination capability of the solvents.

Although the effect of the use of ether solvents into the stereoselectivity is normally attributed to a dependence of the energy of activation of ionic transition states with the polarity of the solvent, in our case, the increase in the stereocontrol of the reaction could be explained by the participation of the solvent in the transition state.¹⁶⁸ This idea is supported by the fact that similar enantiomeric excess is obtained when the reaction is performed in a mixture dichloromethane:diethyl ether 10:1 (Table 7, Entry 14). This result suggests a participation of the ether molecule in the transition state, assisting the nucleophilic addition of the enamine to the imine intermediate through a coordination of the heteroatom with the organocatalyst.

In the following step of the optimization process, the influence of the carboxylate group at the pyruvate substrate into the enantioselectivity was studied. The substituent of the ester is released during the final cyclization step of the reaction, without affecting the final structure of the γ -lactam substrate but it may influence the enantiomeric excess of the process, due to steric issues. Therefore, this study aims to determine if the use of different pyruvates could affect to the stereocontrol of the reaction (Table 8).

¹⁶⁸ Some examples: (a) Fukaya, H.; Morokuma, K. *J. Org. Chem.* **2003**, *68*, 8170-8178. (b) Gajewski, J. J. *J. Am. Chem. Soc.* **2001**, *123*, 10877-10883.

Table 8. Effect of the use of different pyruvate esters in the model three-component reaction.

Entry	R	Conv. (%) ^a	ee (%)	Entry	R	Conv. (%) ^a	ee (%)
1	Me	100	89	3	ⁱ Pr	7	43
2	Et	100	96	4	Ph	5	99

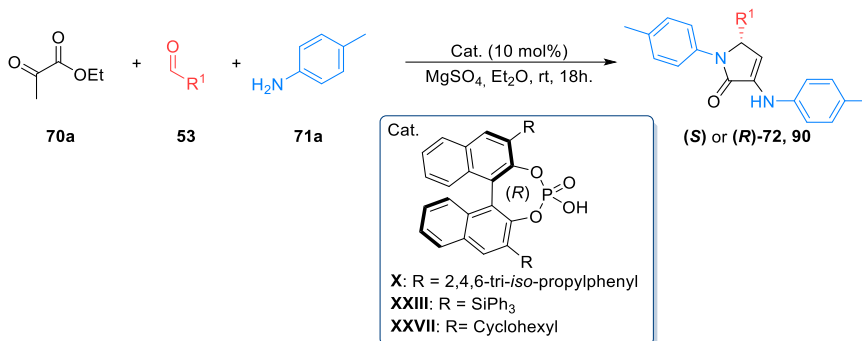
^aDetermined by ¹H NMR.

Accordingly, when phenyl pyruvate (**70d**) is used, 1,5-dihydro-2H-pyrrol-2-one (**(S)-72a**) is obtained with excellent enantiomeric excess but in very low conversion (Table 8, Entry 4). On the other hand, even worse results in terms of conversion and stereoselectivity are obtained with bulkier ⁱPr derivative **70c**. The use of less sterically demanding substrates, such as methyl and ethyl pyruvates (**70a,b**), resulted in a full conversion (Table 8, Entries 1-2), with the best enantioselectivity still corresponding to ethyl pyruvate (**70a**).

In order to further optimize the multicomponent process, and with the aim to check if the Mg²⁺ cation from the drying agent had any influence on the stereocontrol of the reaction, two experiments were conducted, replacing MgSO₄ by Na₂SO₄ or 4Å molecular sieves. We concluded that Mg does not play any role in the catalytic system, since no significant changes were observed in the reactivity or enantioselectivity.

Finally, the reaction was performed with different catalyst loading. However, the same enantioselectivity was observed when the catalyst rate was increased to 20 mol% with respect to the aldehyde, and a substantial drop of the enantiomeric excess was measured when the loading was reduced to 5 mol% (76% ee).

Once the optimal conditions for the enantioselective three-component reaction were established, the extension of the synthetic protocol to the use of differently substituted starting materials was studied. First, the scope using different aldehydes **53** using ethyl pyruvate (**70a**) and *p*-toluidine (**71a**) was explored with the most effective substituted BINOL-derived phosphoric acids **X**, **XXIII** and **XXVII**. The results regarding the scope of the aldehyde substrate are shown in Table 9.

Table 9. Enantioselective MCR using different aldehydes **53**.

Entry	Prod.	R ¹	Yield (%) ^a	ee (%)		
				Cat. X	Cat. XXIII	Cat. XXVII
1	(S)-72a	4-NO ₂ C ₆ H ₄	73	95	96	10
2	(S)-72c	Ph	90	83	87	13
3	(S)-72d	4-CF ₃ C ₆ H ₄	86	82	79	9
4	(S)-72e	3-NO ₂ C ₆ H ₄	73	28	80	15
5	(S)-72f^b	4-FC ₆ H ₄	81	18	52	4
6	(S)-72g^{c,d}	2-MeC ₆ H ₄	65	n.d.	36	26
7	(S)-72h^d	3-MeC ₆ H ₄	83	4	42	70
8	(S)-72i^{c,d}	4-MeC ₆ H ₄	81	9	33	8
9	(S)-72j	6-(<i>N</i> -Me-indolyl)	45	8	0	0
10	(S)-72k	2-Furyl	51	8	16	10
11	(S)-72l^d	2-Thienyl	86	0	67	n.d.
12	(S)-72m	2-Naphtyl	70	0	0	0
13	(R)-72n	Me	54	0	6	36
14	(R)-72o	ⁱ Pr	77	28	82	20
15	(R)-72p	ⁱ Bu	60	7	73	19
16	(R)-72q	Cy	85	72	79	70
17	(R)-72r	CH=CH-Ph	59	32	>99	n.d.
18	(S)-72s	CO ₂ Et	95	41	70	97
20	(S)-90a^b	CH ₂ P(O)(OEt) ₂	80	n.d.	90	n.d.
21	(S)-90c^c	CH ₂ P(O)(Ph) ₂	70	n.d.	91	n.d.
22	(S)-90d^{b,d}	C ₆ F ₅	77	n.d.	60	n.d.
23	(S)-90e^{b,e}	CF ₃	71	n.d.	5	n.d.

^aIsolated yield calculated for the best result. ^bReaction time 48 hours. ^cReaction time 72 hours. ^dReaction in MTBE at 55 °C. ^eReaction in Toluene at room temperature.

Accordingly, the reaction can be performed under the optimized conditions and with good enantioselectivities using less electrophilic benzaldehyde instead of *p*-nitrobenzaldehyde (Table 9, Entry 2 vs. Entry 1). However, the use of *o*-tolualdehyde requires heating and long reaction times (72 hours) to afford only low enantiomeric excesses, which may be due to steric issues and the decreased

electrophilic character of the imine intermediate (Table 9, Entry 6). In a similar way, the use of *p*-tolualdehyde requires high temperatures and the measured stereocontrol is also low (Table 9, Entry 8). Here, the steric issues may be discarded, hence, the low reactivity is only attributed to the electronic character of the aldehyde. In addition, the use of *meta*-substituted aromatic aldehydes in the three-component reaction led to the formation of γ -lactams (**S**-72e,h) in good to very good yields (Table 9, Entries 4 and 7). In these cases, while a good enantioselectivity is observed when *m*-nitrobenzaldehyde is used as substrate (Table 9, Entry 4), the use of less electrophilic *m*-tolualdehyde requires heating of the reaction, which results in a drop in the enantiomeric excess (Table 9, Entry 7).

Good reactivity and enantioselectivity are also obtained using other electron-poor aromatic aldehydes such as *p*-trifluoromethylbenzaldehyde (Table 9, Entry 3). However, a substantial drop in the enantiomeric excess together with an increase in the reaction time is observed when *p*-fluorobenzaldehyde is used as substrate (Table 9, Entry 5).

The reaction can be also extended to the use of aldehydes with heteroaromatic substituents, such as 6-(*N*-Me-indolyl), 2-furyl, 2-thienyl, and 2-naphthyl. However, in this case, γ -lactams (**S**-72j-m) are obtained with low enantiomeric excesses (Table 9, Entries 9-12).

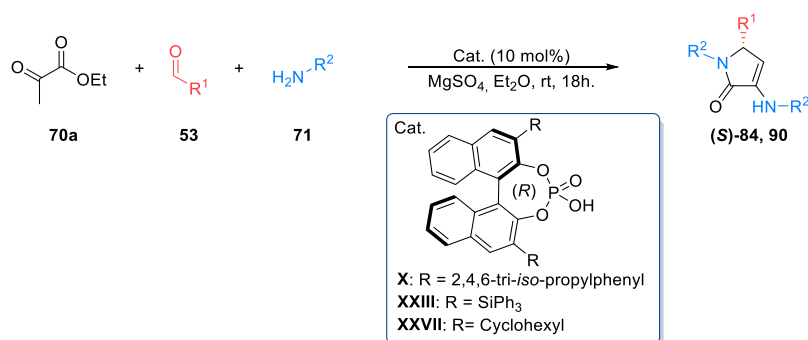
Furthermore, when aliphatic enolizable aldehydes were used as substrates in the three-component reaction, such as *iso*-butyraldehyde, *iso*-valeraldehyde or cyclohexanecarboxaldehyde acceptable enantioselectivities were obtained (Table 9, Entries 14-16). Moreover, other aldehydes such as cinnamaldehyde or ethyl glyoxalate afforded the corresponding γ -lactams (**R**-72r and **S**-72s) with excellent enantiocontrol (Table 9, Entries 17-18). However, the use of acetaldehyde led to a substantial drop in the stereoselectivity, probably due to the small size of the substituent at the aldehyde substrate (Table 9, Entry 13).

In addition, the organocatalyzed asymmetric three-component reaction was extended to the use of β -phosphorated and perfluorinated aldehydes **89** leading to 3-amino-1,5-dihydro-2*H*-pyrrol-2-ones (**S**-90). The use of electron-rich *p*-toluidine with diethylphosphonate substituted aldehyde **89a**, provided the corresponding 1,5-dihydro-2*H*-pyrrol-2-one (**S**-90a) in good yield and enantiomeric excess (Table 9, Entry 20). On the other hand, despite diphenylphosphine oxides usually show a low solubility in organic solvents, especially in ethers, the three-component reaction using phosphine oxide-derived aldehyde **89b** proceeded in suspension, requiring a longer reaction time to afford corresponding γ -lactam (**S**-90c) with good enantioselectivity (Table 9, Entry 21). On the contrary, when perfluorobenzaldehyde was used as substrate, the reaction required refluxing in MTBE to afford γ -lactam (**S**-90d), in this case in good yield, but moderate enantiomeric excesses (Table 9, Entry 22). Nevertheless, the use of trifluoroacetaldehyde, as an aqueous solution of its hydrate, only provided

the racemic mixture of lactam (**S**)-**90e** (Table 9, Entry 23). The lack of enantiocontrol in this reaction may be explained due to the small size of trifluoromethyl substituent (as proposed for acetaldehyde) or because of a possible racemization process through an aromatic pyrrole intermediate, originated as a result of the presence of the strong electron-withdrawing trifluoromethyl group at the stereogenic carbon which makes the proton at that position very acidic.

Continuing with the study of the scope of the reaction, the use of different amine substrates **71** was next explored. In this regard, very good enantiomeric excesses are obtained when, instead of *p*-toluidine, strongly activated aromatic *p*-anisidine is used (Table 10, Entries 1-3), observing however a slower reaction for *p*-nitrobenzaldehyde, which may be due to a higher deactivation of the imine electrophile with respect to the activation of enamine nucleophile.

Table 10. Scope of the enantioselective MCR using different amines **71**.



Entry	Prod.	R ¹	R ²	Yield (%) ^a	ee (%)	ee (%)	ee (%)
					Cat. X	Cat. XXIII	Cat. XXVII
1	(S)- 84a ^b	4-NO ₂ C ₆ H ₄	4-MeOC ₆ H ₄	81	0	90	n.d.
2	(S)- 84b	Ph	4-MeOC ₆ H ₄	74	90	90	5
3	(S)- 90b	CH ₂ P(O)(OEt) ₂	4-MeOC ₆ H ₄	83	n.d.	83	n.d.
4	(S)- 84c	4-NO ₂ C ₆ H ₄	4-BrC ₆ H ₄	89	>99	92	n.d.
5	(S)- 84e	4-CF ₃ C ₆ H ₄	4-BrC ₆ H ₄	89	68	80	n.d.
6	(S)- 84h	4-NO ₂ C ₆ H ₄	2-FC ₆ H ₄	75	86	95	n.d.
7	(S)- 84f ^d	4-NO ₂ C ₆ H ₄	4-ClC ₆ H ₄	74	30	32	42
8	(S)- 84g ^c	4-NO ₂ C ₆ H ₄	3-ClC ₆ H ₄	63	97	85	40
9	(S)- 84k ^{c,d}	4-NO ₂ C ₆ H ₄	3-CF ₃ C ₆ H ₄	63	35	34	62

^aIsolated yield calculated for the best result. ^bReaction time 48 hours. ^cReaction time 72 hours. ^dReaction in MTBE at 55 °C.

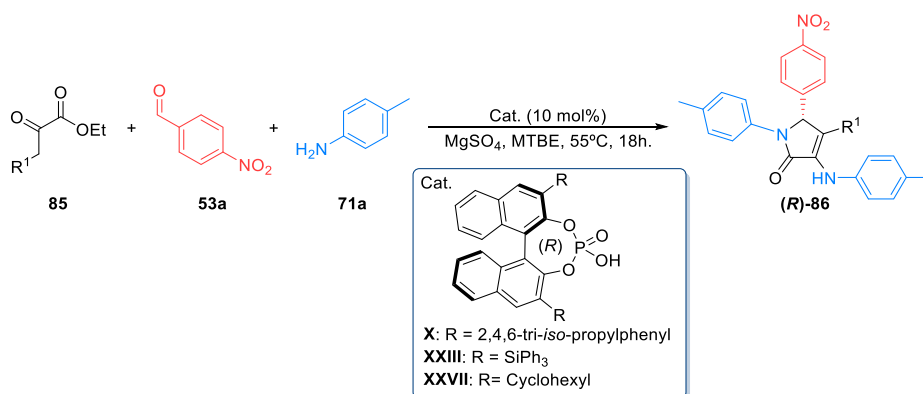
The use of weakly deactivating *p*-bromoaniline or *o*-fluoroaniline in the three-component reaction also afforded the corresponding γ -lactams (**S**)-**84c,e** and (**S**)-**84h** with very good stereocontrol (Table 10, Entries 4-6). Likewise, the use of *p*-chloroaniline required higher temperatures and low enantioselectivity was observed (Table 10, Entry 7) and, besides the use of *m*-chloroaniline, afforded

the corresponding γ -lactam (**S**)-**84g** with excellent enantiocontrol, required longer reaction times (Table 10, Entry 8). Finally, a substantial drop in the enantioselectivity is observed for anilines with strong electron-withdrawing groups, such as *m*-trifluoromethylaniline (Table 10, Entry 9).

Despite the fact that in most of the cases the best enantioselectivities are obtained using triphenylsilyl-substituted BINOL-derived chiral phosphoric acid **XXIII** as the catalyst, for some particular substrates better results are measured if tri-*iso*-propylphenyl or cyclohexyl-substituted chiral catalysts **X** or **XXVII** are used. However, there is no apparent pattern to predict the stereoselectivity of the reaction by the comparison of the structure of the used catalysts and the starting reagents.

To conclude this comprehensive research, the scope of the organocatalyzed asymmetric protocol for the preparation of enantioenriched γ -lactam derivatives was extended to the use of two different substituted pyruvates **85**, as shown in Table 11.

Table 11. Enantioselective MCR using substituted pyruvate derivatives **85**.



Entry	Prod.	R ¹	Yield (%) ^a	ee (%) Cat. X	ee (%) Cat. XXIII	ee (%) Cat. XXVII
1	(R)-86a	Me	70	54	43	33
2	(R)-86b	Bn	71	68	62	10

^a Isolated yield calculated for the best result.

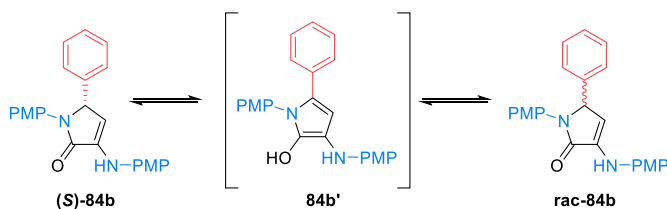
In both cases, the reaction needed to be stirred in MTBE under reflux, to obtain the corresponding products in good yields, but moderate enantioselectivities (Table 11, Entries 1-2), observing a slightly better stereocontrol of the reaction for the benzyl group in comparison with the methyl-substituted pyruvate.

The next obvious stage in the development of the enantioselective multicomponent methodology is its extension to the use of pyruvates **91** containing phosphonate or phosphine oxide moieties but,

despite our efforts, the synthesis of substrates **93** holding phosphorated groups at the position 4 of the γ -lactam ring, with good enantiocontrol, was unsuccessful.

In all these cases, the presence of the enol moiety results in a strong polar character in γ -lactam substrates, which made the separation of both enantiomers *via* HPLC a very difficult task. Acceptable separation conditions were finally found using chiral HPLC but only for di-*iso*-propyl phosphonate substituted γ -lactam **93k** (Chart 5, *vide supra*). However, the reaction only proceeds in reasonable yields at high temperatures and, probably for this reason, an almost racemic mixture of phosphonate-substituted lactam **93k** was obtained with the most effective BINOL-derived phosphoric acid-catalysts **XXIII**, using refluxing MTBE as solvent. Besides, the *in situ* treatment of the reaction with TMS-CHN₂ to generate the less polar enol ether, provided a proper baseline separation of both enantiomers of γ -lactam **93a** (Chart 5, *vide supra*). Unfortunately, as in the case of γ -lactam **93k**, very poor enantiomeric excess (3% ee) was observed. Similarly, also due to the fact that high temperatures are required for the multicomponent reaction using acetylenedicarboxylates **52**, the attempts to extend the enantioselective protocol to the multicomponent synthesis of 4-carboxylate-derived γ -lactams **86** (Chart 6, *vide supra*) were unsuccessful.

Next, in order to determine the absolute configuration of the major enantiomer obtained in the synthesis of 3-amino-1,5-dihydro-2H-pyrrol-2-ones, pure crystalline samples of enantioenriched substrates (**S**)-**72a** and (**S**)-**84b** were prepared. Surprisingly, after several crystallization attempts, only racemic crystals could be obtained. In view of these results, we hypothesized a slow racemization process of the unsaturated γ -lactam ring through an intermediate aromatic pyrrole species (Scheme 26).



Scheme 26. Proposed racemization process of compound **84b**.

We rationalized that this racemization could be promoted by the stabilization of the intermediate pyrrole species, due to the presence of an aromatic ring at position 5 of the γ -lactam ring, thus favoring a highly conjugated system. According to this theory, the use of 5-alkyl substituted γ -lactams would complicate the racemization process, due to the presence of a less acidic proton at C-5. Indeed, the use of an enantioenriched mixture of alkylphosphonate substituted γ -lactam (**S**)-**90a**, allowed the obtaining of optically pure monocrystals and the X-ray diffraction analysis provided unequivocally the

crystal structure, showing an *S* absolute configuration for the stereogenic carbon (Figure 41). As in the previous structures discussed above, an almost planar structure of the γ -lactam core, motivated by the presence of the endocyclic α,β -unsaturated carbonylic moiety, and the intramolecular hydrogen bond is established, in this case, between the enamine hydrogen and the carbonyl oxygen of the amide moiety in a *pseudo*-five-membered ring configuration.

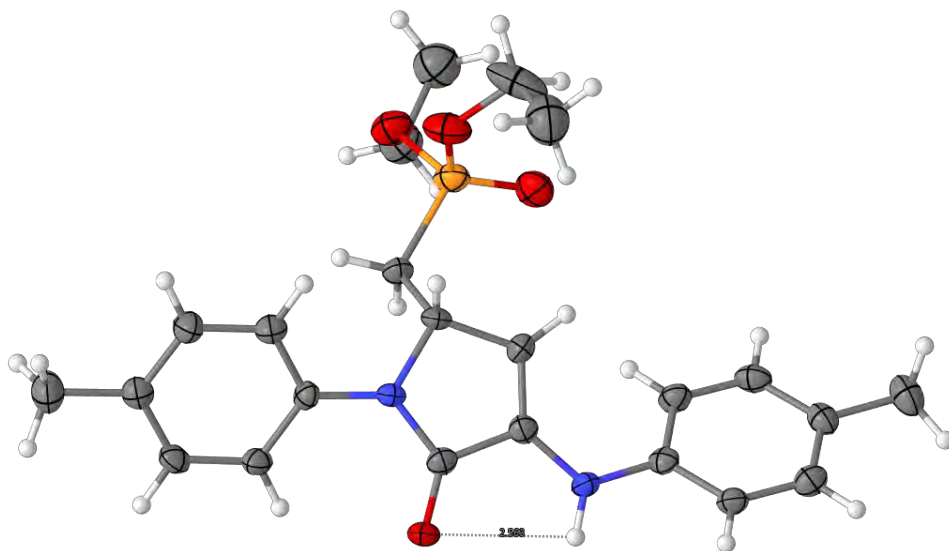
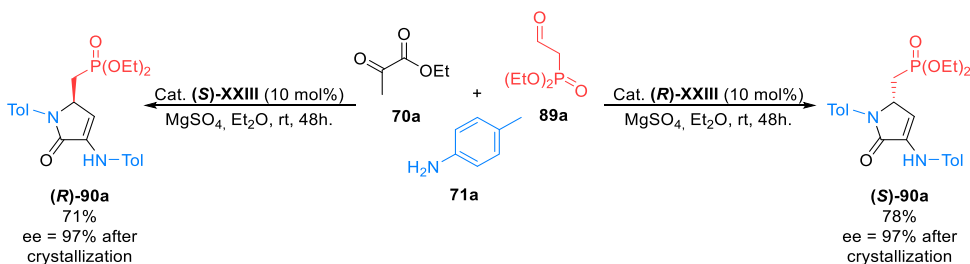


Figure 41. X-ray diffraction structure of α,β -unsaturated γ -lactam (**S**)-**90a**.

Finally, the isolation of both enantiomers of γ -lactam **90a** was accomplished by using both isomers of substituted BINOL phosphoric acid catalyst **XXIII** in the multicomponent reaction (Scheme 27). In both cases, 3-amino-1,5-dihydro-2*H*-pyrrol-2-ones (**R**)-**90a** or (**S**)-**90a** are obtained with 97% enantiomeric excess after subsequent crystallizations.



Scheme 27. Synthesis of both enantiomers of γ -lactam **90a**.

In conclusion, the first highly enantioselective three-component reaction of pyruvate derivatives, amines and aldehydes for the synthesis of 3-amino-1,5-dihydro-2*H*-pyrrol-2-ones has been described in this chapter. The reaction has been generalized to several aromatic amines, aromatic and aliphatic aldehydes and some substituted pyruvate derivatives, allowing the asymmetric synthesis of highly functionalized γ -lactam derivatives.

Chapter 5

Synthetic transformations of γ -lactam derivatives

The structure of 3-amino-1,5-dihydro-2*H*-pyrrol-2-one substrates, is a quite interesting scaffold in medicinal chemistry and may be an outstanding tool in chemical synthesis due to the presence of a cyclic α -dehydro α -amino acid, an enone and an enamine moiety (Figure 42).¹⁶⁹ Considering the easy multicomponent protocol developed for the preparation of α,β -unsaturated γ -lactam derivatives, next, in order to put into manifest the synthetic potential of the 3-amino-1,5-dihydro-2*H*-pyrrol-2-ones described above, several synthetic transformations of the substrates are explored in this chapter.

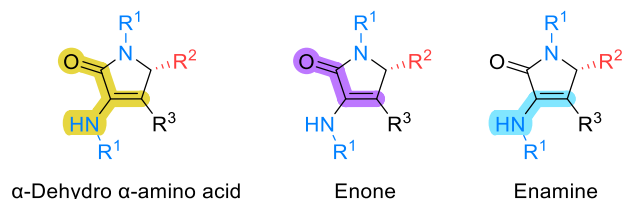
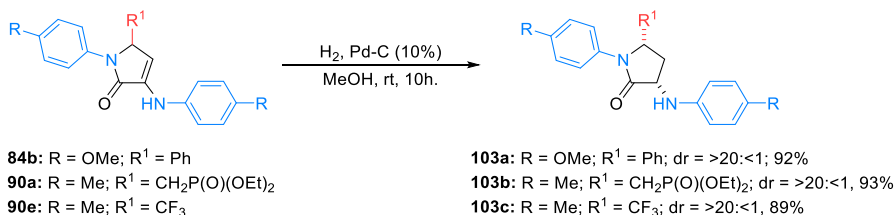


Figure 42. Cyclic α -dehydro α -amino acid (yellow color), conjugated enone (purple color) and enamine (blue color) structures present in 3-amino-1,5-dihydro-2*H*-pyrrol-2-ones.

First, the preparation of saturated γ -lactams was proposed through the simple reduction of the enamine C=C bond of 3-amino-1,5-dihydro-2*H*-pyrrol-2-ones. Accordingly, the treatment of unsaturated γ -lactam **84b** under hydrogen pressure (80 psi) and in the presence of palladium as the catalyst, led to the formation of saturated γ -lactam **103a** in excellent yield and diastereoselectivity (Scheme 28). In addition, compound (**3S,5S**)-**103a** can be prepared in a one-pot procedure through the organocatalyzed enantioselective three-component reaction with catalyst **XXIII**, followed by the hydrogenation reaction, without isolating the intermediate γ -lactam (**S**)-**84b**, avoiding the racemization and thus preserving the initial enantiomeric excess (95% yield, 90% ee).

¹⁶⁹ Harmata, M. The Chemistry of Enols and Enamines. *In Organic Mechanisms: Reactions, Stereochemistry and Synthesis*. Springer, 2010, pp 487.-517.

This protocol can be extended to phosphorylated and trifluoromethyl-substituted γ -lactams **90a** and **90e**, affording the corresponding saturated substrates **103b-c** also in excellent yields and diastereoselectivities.



Scheme 28. Diastereoselective hydrogenation of lactams **84b** and **90a,e**.

The 3*S*, 5*S* absolute configuration of the stereocenters in γ -lactam **103a** was determined by nuclear Overhauser effect (NOE) experiments. The NMR experiments showed NOE effects between the protons at both chiral centers in C-3 and C-5 with the same proton of the diastereotopic CH₂ group, indicating that these three atoms are oriented in the same direction (Figure 43). According to this, the classical *syn* addition of molecular hydrogen, that approaches the C=C double bond from the face opposite to the phenyl substituent is proposed.

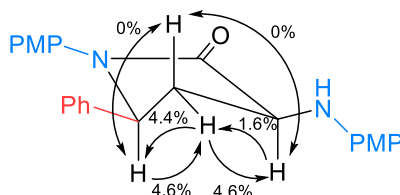
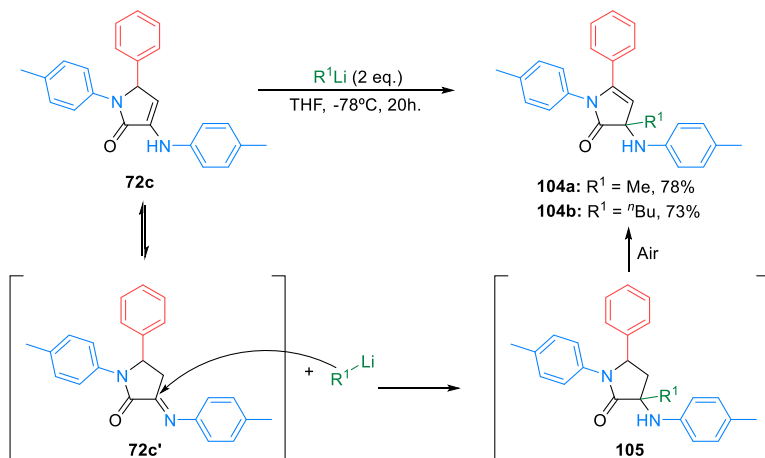


Figure 43. NOE effects observed in saturated γ -lactam **103a**.

Then, taking the advantage of the presence of the enone moiety, and the possibility of an *in situ* tautomerization of the enamine to an imine group, the unsaturated cyclic γ -lactam derivatives were evaluated as electrophiles. For this purpose, initially, α,β -unsaturated γ -lactam **72c** was treated with organolithium reagents in THF at low temperature, affording γ -lactam derivatives **104a-b** holding a tetrasubstituted chiral carbon, in good yields (Scheme 35).

The pathway of this reaction may proceed through an initial nucleophilic addition of the organometallic reagent to the imine tautomer **72c'**, followed by a spontaneous oxidation of the 5-membered lactam ring under exposure to air (Scheme 29). In order to prove this hypothesis, the hydrogenation reaction of the alkene bond was performed in the presence of a catalytic amount of Pd on carbon. After a quick filtration of the reaction, the ¹H NMR spectrum of the crude reaction showed the presence of the characteristic signals corresponding to the diastereotopic protons of the CH₂ group

of intermediate **105** that rapidly disappeared to show again the spectrum corresponding to **104a**, thus making unable its isolation.



Scheme 29. Nucleophilic addition of organolithium reagents to γ -lactam **72c**.

The structure of substrate **104a** was unambiguously confirmed by Heteronuclear Multiple Quantum Coherence (HMQC) experiments (Figure 44).

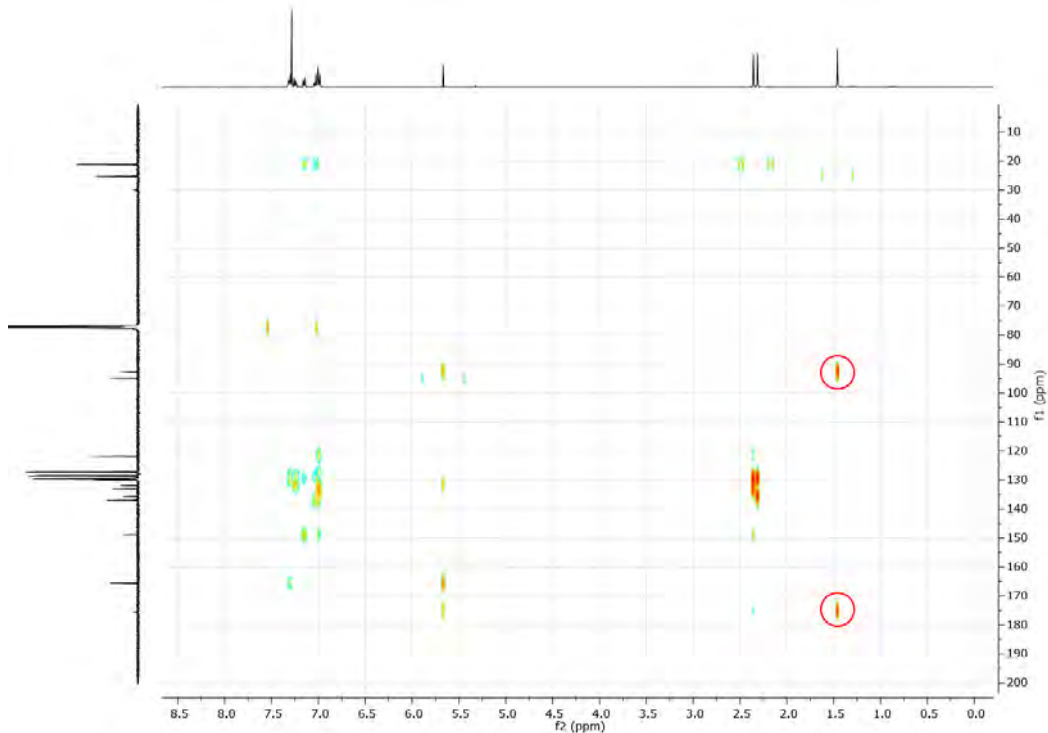
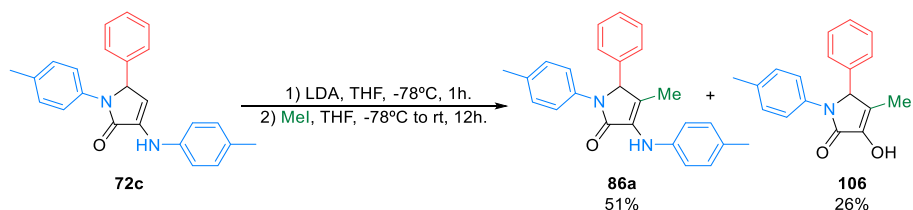


Figure 44. HMQC spectrum of compound **104a**.

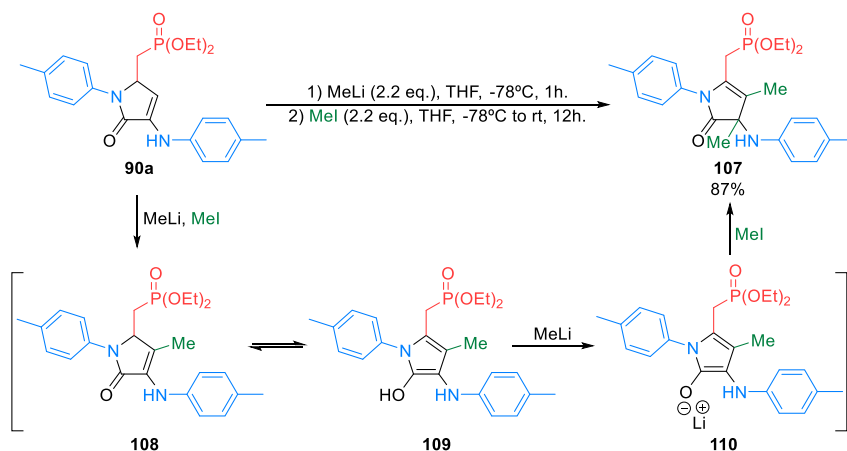
HMQC experiment showed a correlation between the singlet in the ^1H NMR spectrum, corresponding to the methyl group at $\delta_{\text{H}} = 1.45$ ppm, and the signals of the alkene CH and the amide carbonyl groups in the ^{13}C NMR spectrum at $\delta_{\text{C}} = 94.8$ and 175.4 ppm, respectively. In addition, no correlation was observed between any carbon or hydrogen of the methyl and phenyl substituents (Figure 44). These observations imply an unequivocal evidence of the substitution at C-3 of the γ -lactam ring.

Moreover, in view of the potential nucleophilic character of the enamine moiety present in α,β -unsaturated γ -lactam derivatives **72**, a simple alkylation reaction was performed in order to demonstrate that the enamine moiety can be functionalized with electrophiles. The initial treatment of γ -lactam **72c** with LDA at low temperature, followed by the addition of methyl iodide, afforded the expected alkylated substrate **86a** in fair yield (51%), together with hydrolyzed enol-derived γ -lactam **106** (26%) (Scheme 30).

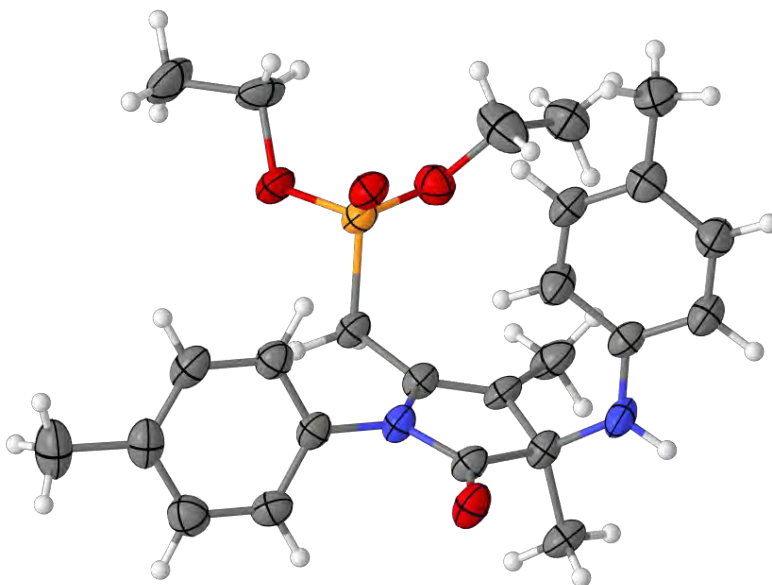


Scheme 30. Enamine alkylation reaction of γ -lactam **72c**.

Our following attempts to extend this protocol to phosphorylated γ -lactam **90a** were unsuccessful using conventional bases such as LDA, tertiary amines, hydrides, or alkoxides. In addition, the use of a strong base such as lithium di-*iso*-propylamide provided unaltered starting materials. However, the use of methyl lithium as a base with methyl iodide as the electrophile afforded dialkylated γ -lactam **107**. The formation of the doubly functionalized substrate may be explained by an initial alkylation of the enamine moiety leading to mono-methylated γ -lactam **108**, which *via* tautomerization would be in equilibrium with hydroxypyrrole **109**. At this stage, the enol moiety present in species **109** is deprotonated to provide enolate **110** which undergoes a subsequent alkylation process, leading to dimethylated γ -lactam derivative **107** (Scheme 31).

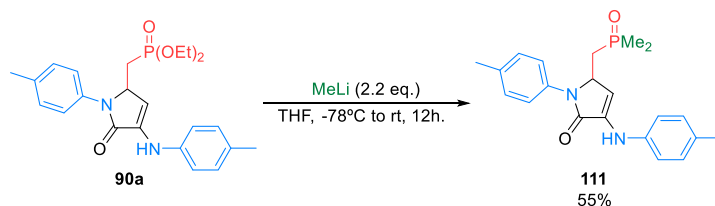
Scheme 31. Dialkylation of γ -lactam **90a**.

Due to the complex substitution pattern obtained in this reaction, the structure of compound **107** was unambiguously determined by X-ray diffraction experiments (Figure 45). Key features of the crystal structure of γ -lactam **107** are the typical almost planar shape of the five-membered ring, with the methyl substituent at C-4 aligned in the same plane with the substituent at C-5, due to the presence of a C=C double bond. In this case, the methyl group at C-3 prevents the formation of the H-bond between the NH of the enamine and the carbonyl group, which is shown in other crystal structures of other similar substrates (Figure 41, *vide supra*).

Figure 45. X-ray diffraction structure of α,β -unsaturated γ -lactam **107**.

Even though several efforts were made to balance the ratio between methyl lithium and methyl iodide in order to obtain selectively the mono-alkylated compound, in all cases dimethylated γ -lactam **107** was obtained.

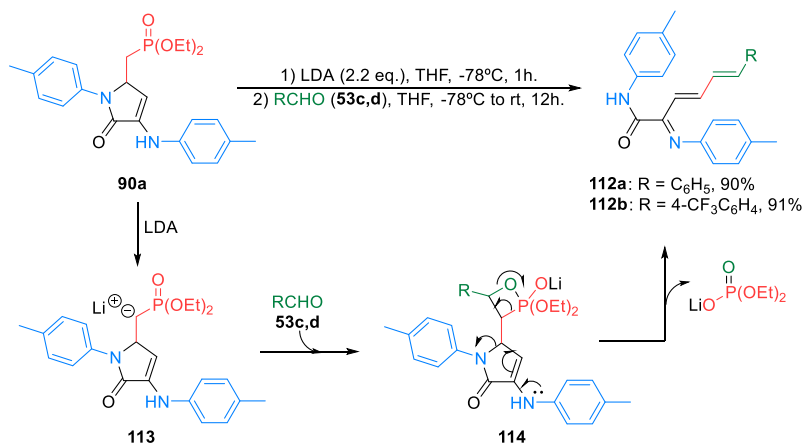
In view that it is clear that the skeleton of the 3-amino-1,5-dihydro-2H-pyrrol-2-ones could also behave as a Michael acceptor, due to the presence of an α,β -unsaturated carbonyl moiety, other key question to be addressed is if both methyl groups come from methyl iodide or if any of them arises from, either a nucleophilic addition to the imine tautomer (as shown in Scheme 29) or a Michael addition of the organometallic reagent to the conjugated double bond. In order to unravel this doubt, γ -lactam **90a** was treated with an excess of methyl lithium, in this case without the presence of any electrophile. To our surprise, we observed as the main reaction the displacement of the ethoxy groups at the phosphonate moiety by the strong nucleophile methyl lithium, transforming the phosphonate into a phosphine oxide group in γ -lactam **111** (Scheme 32).



Scheme 32. Synthesis of phosphine-containing γ -lactam **111**.

Following with our interest in the synthetic potential of the γ -lactam derivatives, the reactivity of the phosphorus substituent in the phosphorated substrates was next explored. In this regard, the Horner-Wadsworth-Emmons reaction consists of the use of stabilized phosphonate carbanions and aldehydes to efficiently afford olefins.¹⁷⁰ In this context, when phosphonate-derived lactam **90a** was treated with LDA at low temperature, followed by the addition of aldehydes **53** (R = Ph or 4-CF₃C₆H₄), surprisingly, conjugated aza-trienes **112** were formed, where a ring-opening of the γ -lactam core occurred. One plausible explanation for the mechanism of this reaction could be an initial formation of anionic species **113** by the presence of a strong base (LDA), followed by the nucleophilic attack to the aldehyde **53** to afford four-membered oxaphosphetane **114**, the accepted intermediate in the Horner-Wadsworth-Emmons reaction. Next, the elimination of the nitrogen of the amide moiety and the phosphorus species would lead to the formation of aza-trienes **112**, which are obtained in excellent yields (Scheme 33).

¹⁷⁰ (a) Wadsworth, W. S.; Emmons, W. D. *J. Am. Chem. Soc.* **1961**, *83*, 1733-1738. (b) Horner, L.; Hoffmann, H.; Wippel, H. *G. Chem. Ber.* **1958**, *91*, 61-63.



Scheme 33. Horner-Wadsworth-Emmons reaction of γ -lactam **90a**.

Being aware that an alternative mechanism for this reaction could imply an olefination process followed by a ring-opening, 3-amino-1,5-dihydro-2*H*-pyrrol-2-ones **72r** (Chart 1, *vide supra*), which is indeed the γ -lactam substrate expected as the product of the olefination reaction of **90a** with benzaldehyde (**53c**), was set under strong basic conditions and/or strong heating. However, the starting material was recovered unaltered, suggesting that the ring-opening step arises from intermediate **114**, as proposed in the mechanism.

Due to the complex signal patterns observed in the NMR spectra, a monocystal of aza-triene **112a** was isolated and its structure was unquestionably established by X-ray diffraction (Figure 46). Key features of the structure of compound **112a** are the long conjugated system formed by the carbonyl group of the amide, the imine and the two alkene groups along with the phenyl and *p*-tolyl aromatic substituents. As shown in Figure 46, the carbonyl group and the imine are disposed in an *anti* configuration, due to the intramolecular H-bond formed between the amide NH and the imine nitrogen atoms.

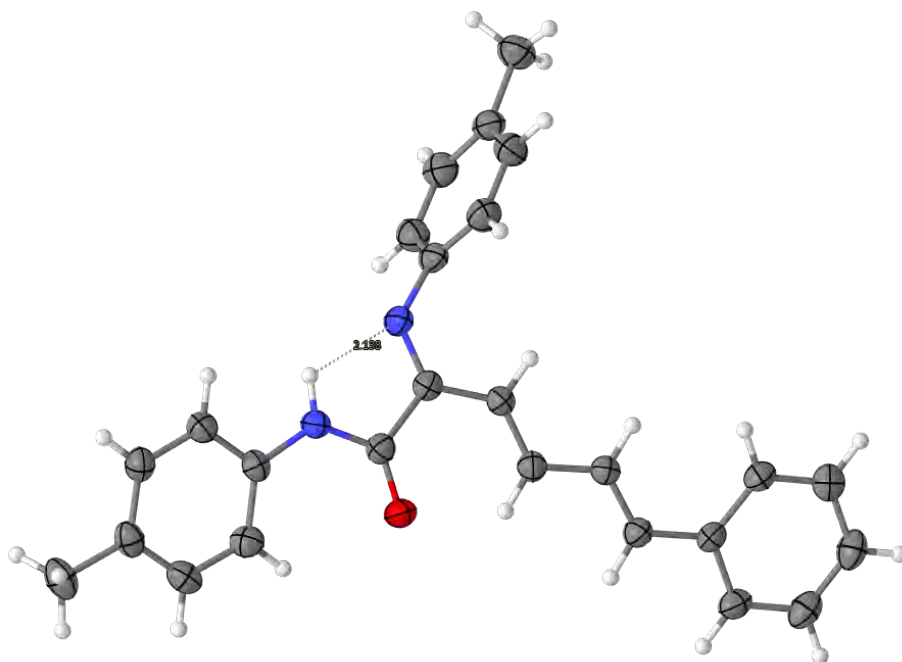


Figure 46. X-ray diffraction structure of aza-triene **112a**.

As a summary of this chapter, the presence of an endocyclic α,β -unsaturated amide moiety and an enamine functionality in γ -lactam substrates, obtained from a multicomponent reaction, makes them very convenient starting materials for the synthesis of polyfunctional γ -lactam substrates. Taking the advantage of the chiral stereocenter, highly diastereoselective hydrogenation reactions are described. Moreover, the selective functionalization at C-4 is feasible making use of enamine chemistry, while the addition of organometallic species allows functionalization at C-3. In addition, phosphonate-derived substrates can be used as starting materials in olefination reactions.

Chapter 6

Stereoselective formal [3+3] reaction of 3-amino γ -lactam derivatives

The 1,4-dihydropyridine skeleton is a privileged scaffold in medicinal chemistry, present in numerous pharmacologically active substances with a wide range of biological activities,¹⁷¹ including currently marketed dihydropyridine-family calcium-channel blockers (i.e. Amlodipine, Nifedipine),¹⁷² antidiabetics,¹⁷³ anticoagulants,¹⁷⁴ antioxidants¹⁷⁵, antidyslipidemics¹⁷⁵ and efficient antiproliferative agents¹⁷⁶ (Figure 47).

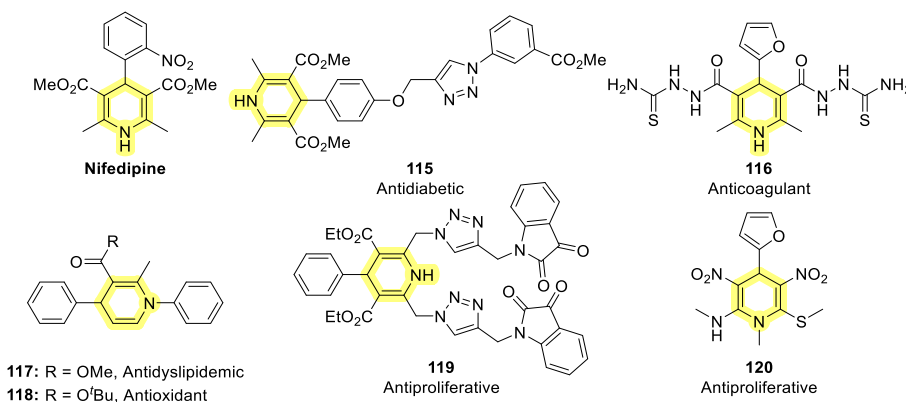
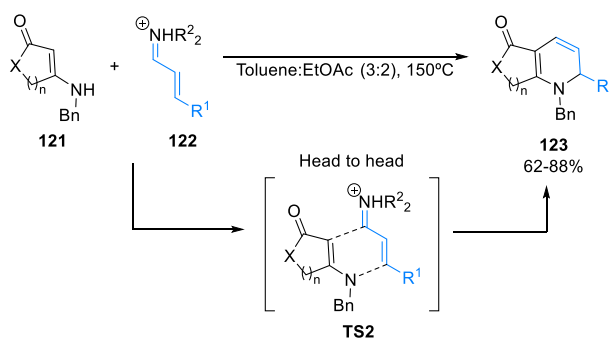


Figure 47. Pharmacologically active molecules based in 1,4-dihydropyridine skeleton.

- ¹⁷¹ Reviews: (a) Swarnalatha, G.; Prasanthi, G.; Sirisha, N.; Madhusudhana Chetty, C. *Int. J. ChemTech Res.* **2011**, *3*, 75-89. (b) Edraki, N.; Mehdi-pour, A. R.; Khoshneviszadeh, M.; Miri, R. *Drug Discov. Today* **2009**, *14*, 1058-1066.
- ¹⁷² (a) Siddiq, A.; Mukhtar, I.; Baig, S. G. *World. J. Pharm. Pharm. Sci.* **2019**, *8*, 1674-1687. (b) Elliott, W. J.; Ram, C. V. S. *J. Clin. Hypertens.* **2011**, *13*, 687-689. (c) Elmslie, K. S. *J. Neurosci. Res.* **2004**, *75*, 733-741.
- ¹⁷³ Praveenkumar, E.; Gurrapu, N.; Kumar Kolluri, P.; Reddy Kunduru, B.; Subhashini, N. J. P. *Bioorg. Chem.* **2019**, *90*, 1-9.
- ¹⁷⁴ Kumar, R. S.; Idhayadhulla, A.; Abdul Nasser, A. J.; Selvin, J. *Eur. J. Med. Chem.* **2011**, *46*, 804-810.
- ¹⁷⁵ Kumar, A.; Maurya, R. A.; Sharma, S.; Kumar, M.; Bhatia, G. *Eur. J. Med. Chem.* **2010**, *45*, 501-509.
- ¹⁷⁶ (a) Deswal, N.; Shrivastava, A.; Summon Hossain, M.; Gahlyan, P.; Bawa, R.; Gupta, R. D.; Kumar, R. *ChemistrySelect* **2021**, *6*, 717-725. (b) Anaikutti, P.; Makam, P. *Bioorg. Chem.* **2020**, *105*, 104379. (c) Abbas, H. A. S.; El Sayed, W. A.; Fathy, N. M. *Eur. J. Med. Chem.* **2010**, *45*, 973-982.

From a synthetic point of view, annulation reactions using α,β -unsaturated carbonyl compounds and enamines have proven to be powerful and rapid methodologies for the preparation of nitrogenated heterocycles.¹⁷⁷ These stepwise processes between two bidentate fragments with complementary reactivity lead to the formation of a pyridine derivative and, due to their non-concerted mechanism, they are usually referred as ‘formal [3+3] cycloadditions’.

In this context, in 1999 Hsung developed a formal aza-[3+3] annulation of cyclic enamines **121** and vinyliminium ions **122**, for the construction of piperidinylderived heterocycles **123**.¹⁷⁸ This reaction consists of a ‘head to head’ tandem sequence (**TS2**), starting with a Knoevenagel reaction of the enamine **121** to iminium species **122**, followed by a pericyclic ring closure (Scheme 34).



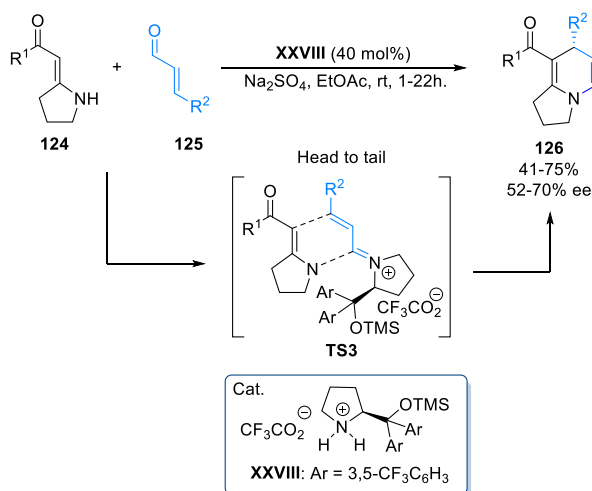
Scheme 34. Formal [3+3] cycloaddition reaction with a ‘head to head’ regioselectivity.

A few years later, the same authors reported an unexpected reversal of the regiochemistry in a similar reaction, where pyrrolidine-based exocyclic enamines **124** and α,β -unsaturated aldehydes **125**, in the presence of substoichiometric amounts of chiral amine salt **XXVIII**, react in a ‘head to tail’ formal [3+3] cycloaddition reaction (**TS3**), providing 1,4-dihydropyridines **126** in fair to good yields and enantioselectivities (Scheme 35). In addition, the use of chiral enamines in such reactions also leads to a high degree of stereocontrol. The reaction proceeds by means of an initial conjugate addition of enamine **124** to the conjugated olefin **125**, followed by a subsequent ring closure through the internal nucleophilic attack of the enamine nitrogen to the iminium moiety (Scheme 35).¹⁷⁹

¹⁷⁷ Reviews: (a) Xu, X.; Doyle, M. P. *Acc. Chem. Res.* **2014**, *47*, 1396-1405. (b) Buchanan, G. S.; Feltenberger, J. B.; Hsung, R. P. *Curr. Org. Chem.* **2010**, *7*, 363-401. (c) Harrity, J. P. A.; Provoost, O. *Org. Biomol. Chem.* **2005**, *3*, 1349-1358. (d) Hsung, R. P.; Kurdyumov, A. V.; Sydorenko, N. *Eur. J. Org. Chem.* **2005**, 23-44.

¹⁷⁸ Hsung, R. P.; Wei, L. L.; Sklenicka, H. M.; Douglas, C. J.; McLaughlin, M. J.; Mulder, J. A.; Yao, L. J. *Org. Lett.* **1999**, *1*, 509-512.

¹⁷⁹ (a) Buchanan, G. S.; Dai, H.; Hsung, R. P.; Gerasyuto, A. I.; Scheinebeck, C. M. *Org. Lett.* **2011**, *13*, 4402-4405. (b) Sklenicka, H. M.; Hsung, R. P.; McLaughlin, M. J.; Wei, L. L.; Gerasyuto, A. I.; Brennessel, W. B. *J. Am. Chem. Soc.* **2002**, *124*, 10435-10442.



Scheme 35. Formal [3+3] cycloaddition reaction with a 'head to tail' regioselectivity.

Typical substrates in formal [3+3] cycloaddition reactions are cyclic β -enaminones, where the reactivity of the enamine functionality is enhanced due to the presence of the β -carbonyl group. In this regard, 3-amino-1,5-dihydro-2*H*-pyrrol-2-ones could be very appropriate substrates for annulation reactions for several reasons (Figure 48). Those molecules have already shown to behave as enamines and, additionally, if C-5 substituted chiral substrates are used in the reaction, the presence of a stereogenic center embedded in a restricted five-membered heterocycle may work as an excellent chiral director, thus inducing a high degree of stereoselectivity in the process.

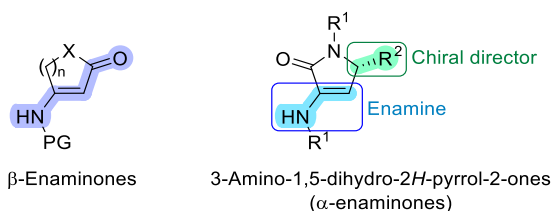
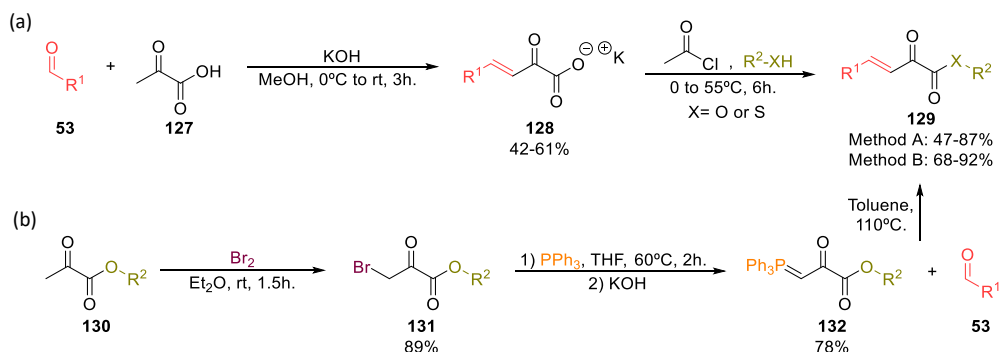


Figure 48. Structure of β -enaminones and 3-amino-1,5-dihydro-2*H*-pyrrol-2-ones.

Taking into account the considerations mentioned below, in this chapter, the applications of 3-amino-1,5-dihydro-2*H*-pyrrol-2-ones as enamine substrates in formal [3+3] cycloaddition reactions are explored for the synthesis of pyridine derivatives. As the partners of the reaction, β,γ -unsaturated α -ketoesters are chosen as substrates, due to the additional electronic activation of the conjugated system by the presence of the carboxylic group.

The required β,γ -unsaturated α -ketoesters were prepared using described procedures. The aldol condensation reaction between aldehydes **53** and pyruvic acid (**127**), in the presence of potassium

hydroxide, is an efficient method leading to intermediate potassium carboxylates **128**, in moderate yields, as the precursors of β,γ -unsaturated α -ketoesters **129** by simple esterification (Scheme 36, a).¹⁸⁰ As an alternative, the halogenation of pyruvates derivatives **130**, provides access in very good yields to α -bromo pyruvates **131**, which are suitable starting materials for the preparation of phosphorus ylides **132** in the presence of triphenylphosphine (78% yield). Then a classical Wittig olefination reaction between ylides **132** and aldehydes **53** furnishes the corresponding ketoesters **129** in good to excellent yields (Scheme 36, b).¹⁸¹



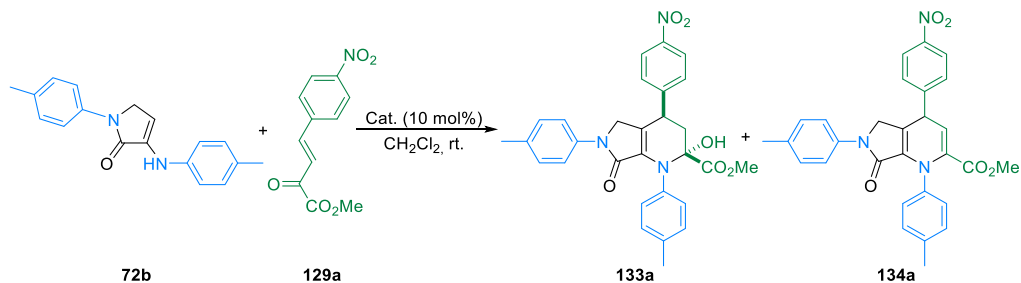
Scheme 36. Complementary methodologies for the preparation of β,γ -unsaturated α -ketoesters **129**.

With the required starting materials in hands, then, the reaction conditions were optimized for the annulation reaction, initially using unsubstituted 3-amino α,β -unsaturated γ -lactam **72b** and β,γ -unsaturated α -ketoester **129a** in the presence of a catalytic amount of several Lewis acids. The results are summarized in Table 12.

Although the reaction did not proceed at all using a Cu (II) salt (Table 12, Entry 1), full conversion was observed after 140 hours in the presence of a Cu (I) species, selectively obtaining bicyclic tetrahydropyridine **133a** in very good yield (Table 12, Entry 2). In agreement with other described similar reactions, tetrahydropyridine **133a** could be formed through a ‘head to tail’ formal [3+3] cyclization process, consisting of an initial conjugate addition of the enamine moiety to β,γ -unsaturated α -ketoester **129a**, followed by the intramolecular nucleophilic attack of the nitrogen of the enamine to the ketone of **129a**. The same reaction in the presence of ZnCl_2 provided similar results although in lower conversions after 140 hours (Table 12, Entry 3). To our surprise, using $\text{Ag}(\text{OTf})$ as the catalyst, a 30:70 mixture of tetrahydropyridine **133a** and 1,4-dihydropyridine substrate **134a** is obtained (Table 14, Entry 4). Certainly, compound **134a** is originated by the dehydration of tetrahydropyridine **133a**.

¹⁸⁰ Tang, Q.; Fu, K.; Ruan, P.; Dong, S.; Su, Z.; Liu, X.; Feng, X. *Angew. Chem. Int. Ed.* **2019**, *131*, 11972-11977.

¹⁸¹ Albrecht, Ł.; Dickmeiss, G.; Weise, C. F.; Rodríguez Escrich, C.; Jørgensen, K. A. *Angew. Chem. Int. Ed.* **2012**, *51*, 13109-13113.

Table 12. Optimization of the catalyst for the formal [3+3] cycloaddition reaction.

Entry	Catalyst	Time (h)	Conv. (%)	Ratio 133a:134a ^a	Yield (%) ^b
1	Cu(OTf) ₂	140	0	-	n.d.
2	Cu(CH ₃ CN) ₄ PF ₆	140	100	>99:<1	88
3	ZnCl ₂	140	40	>99:<1	n.d.
4	Ag(OTf)	120	100	30:70	n.d.
5	NiCl ₂ (PPh ₃) ₂	24	100	<1:>99	n.d.
6	Sml ₂	24	100	<1:>99	n.d.
7	In(OTf) ₃	24	100	<1:>99	n.d.
8	TiCl ₄	24	100	<1:>99	n.d.
9	Sc(OTf) ₃	24	100	<1:>99	n.d.
10	YbCl ₃	24	30	8:92	n.d.
11	Yb(OTf) ₃	1	100	50:50	n.d.
12	Yb(OTf) ₃	7	100	<1:>99	84

^aDetermined by ¹H NMR. ^bIsolated yield.

Following with our pursuit for the most efficient catalyst for the annulation reaction, next, other Lewis acids were tested as catalyst. To our delight, a full conversion to the formal [3+3] cycloaddition product **134a** was observed after 24 hours using NiCl₂(PPh₃)₂, Sml₂, In(OTf)₃, TiCl₄ or Sc(OTf)₃ (Table 12, Entries 5-9). The reaction in the presence of YbCl₃ provided a mixture 8:92 of **133a** and **134a** but in very low conversion after 24 hours (Table 12, Entry 10). Due to the low solubility of YbCl₃, next, we tested Yb(OTf)₃ as the catalyst in the annulation reaction and a very fast disappearance of the starting materials was observed in this case, obtaining a mixture 50:50 of **133a** and **134a** after 1 hour (Table 12, Entry 11). However, Yb(OTf)₃ was found to be the optimal catalyst for the reaction in dichloromethane at room temperature for 7 hours, and bicyclic 1,4-dihydropyridine **134a** was isolated as a single product in very good yield (Table 12, Entry 12).

Substrates **133a** and **134a** were isolated and fully characterized by NMR and IR spectroscopy and HRMS. The ¹H NMR spectra of the two products of the reaction are shown piled up in Figure 49. Some of the most representative signals of bicyclic tetrahydropyridine **133a** are the broad singlet at $\delta_{\text{H}} = 4.33$ ppm, that interchanges with D₂O and corresponds to the OH group, which appears overlapped with

the double doublet at $\delta_{\text{H}} = 4.32$ ppm, assigned to the CH proton of the asymmetric carbon, with two different coupling constants with the vicinal diastereotopic CH_2 group of $^3J_{\text{HH}} = 1.4$ and 5.2 Hz. The two double doublets at $\delta_{\text{H}} = 4.13$ and 3.86 ppm correspond to the two diastereotopic protons of the CH_2 at the γ -lactam core, showing a reciprocal geminal coupling of $^2J_{\text{HH}} = 17.8$ Hz. Similarly, the other two diastereotopic protons of the CH_2 at the tetrahydropyridine ring appear as two double doublets at $\delta_{\text{H}} = 2.64$ and 2.35 ppm, both showing a typical geminal coupling constant of $^2J_{\text{HH}} = 12.8$ Hz and an additional coupling with the CH group at the chiral center of $^3J_{\text{HH}} = 1.4$ and 5.2 Hz, respectively.

On the contrary, the ^1H NMR spectrum of 1,4-dihydropyridine **134a** shows two doublets at lower field than **133a**, assigned to the two CH protons at the dihydropyridine ring, at $\delta_{\text{H}} = 5.75$ and 4.93 ppm with a coupling constant of $^3J_{\text{HH}} = 3.8$ Hz as well as two doublets for the two diastereotopic protons of the CH_2 group at the γ -lactam ring at $\delta_{\text{H}} = 4.09$ and 3.85 ppm with a typical strong geminal coupling of $^2J_{\text{HH}} = 18.0$ Hz. In addition, both compounds show one intense singlet in the interval $\delta_{\text{H}} = 3.50 - 3.80$ ppm corresponding to the methoxy group, and two additional intense singlets around $\delta_{\text{H}} = 2.20$ and 2.40 ppm which, together with the presence of 12 aromatic protons at the aromatic region, suggest that two *p*-toluidine groups and one *p*-nitrophenyl groups are present in each structure (Figure 49).

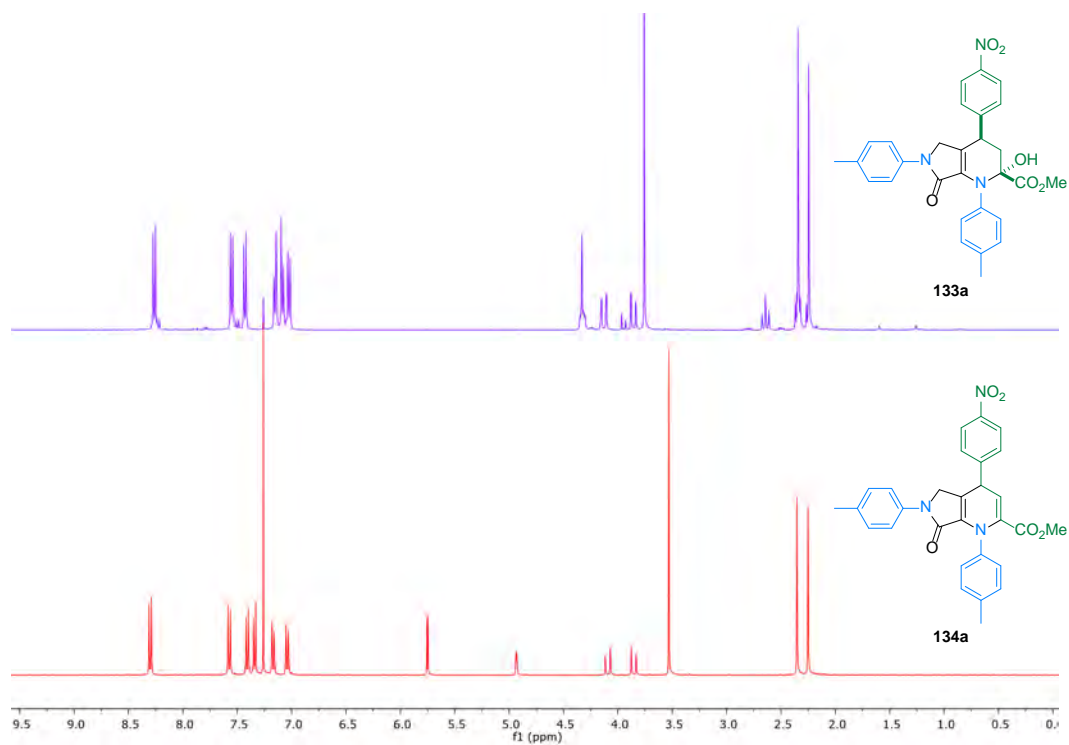
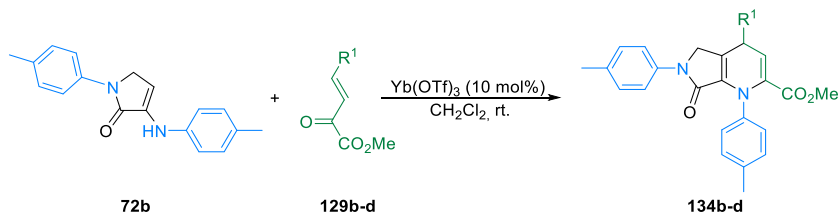


Figure 49. Comparison of the ^1H NMR spectra of compounds **133a** and **134a**.

The optimal reaction conditions for the formal [3+3] cycloaddition reaction were next extended to the use of other β,γ -unsaturated α -ketoesters **129b-d**, with unsubstituted 3-amino- α,β -unsaturated γ -lactam **72b** as the reaction partner (Table 13).

Table 13. Application of the optimal reaction conditions with C-5 substituted γ -lactam **72b** and different unsaturated keto esters **129**.



Entry	Product	R ¹	Time (h)	Yield (%) ^a
1	134b	4-CF ₃ C ₆ H ₄	7	78
2	134c	Ph	14	76
3	134d	4-MeC ₆ H ₄	14	72

^aIsolated yield.

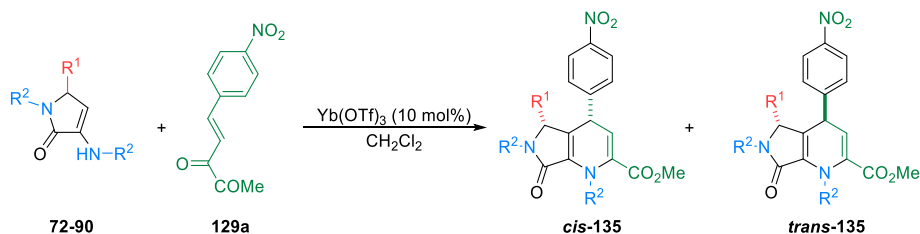
α -Ketoester **129b**, bearing a trifluoromethyl substituted deactivated aromatic ring, reacted in the same conditions to afford 1,4-dihydropyridine **134b** in good yield (Table 13, Entry 1). However, the presence of a simple phenyl substituent in **129c** or an activated aromatic ring in **129d** required higher reaction times, although 1,4-dihydropyridines **134c,d** were obtained in good yields overnight (Table 13, Entries 2-3).

With these results in hands, we focused our next objective on the study of the stereoselective formal [3+3] reaction using chiral substrates. First, the use of several chiral cyclic enamines **72-90** was explored, using β,γ -unsaturated α -ketoester **129a** as the model substrate, leading to the formation of bicyclic dihydropyridines **135**, holding two stereogenic centers. The results are summarized in Table 14.

Phenyl substituted cyclic enamine **72c** (R¹ = Ph, R² = 4-MeC₆H₄) reacted in full conversion overnight with β,γ -unsaturated α -ketoester **129a** in the presence of a catalytic amount of Yb(OTf)₃ to afford, in very good yields, exclusively the *cis* isomer of bicyclic 1,4-dihydropyridine **135a** (Table 14, Entry 1). The reaction was also extended to different aromatic-substituted cyclic enamines with a very high degree of diastereoselectivity, using substrates derived from aromatic rings bearing electron-withdrawing groups (**72d**, R¹ = 4-CF₃C₆H₄, R² = 4-MeC₆H₄), fluorine (**72f**, R¹ = 4-FC₆H₄, R² = 4-MeC₆H₄), as well as perfluorophenyl substituted γ -lactam **90d** (R¹ = C₆F₅, R² = 4-MeC₆H₄) or even heteroaromatic-substituted substrate **72l** (R¹ = 2-thiophene, R² = 4-MeC₆H₄), affording in all cases the corresponding

bicyclic 1,4-dihydropyridines **135b-e** in good to excellent yields as single *cis* diastereoisomers (Table 14, Entries 2-5).

Table 14. Stereoselective formal [3+3] cycloaddition reaction. Scope of C-5 substituted γ -lactams **72-90**.



Entry	Prod.	R ¹	R ²	Time (h)	Temp. (°C)	Cis/Trans ^a	Yield (%) ^b
1	135a	Ph	4-MeC ₆ H ₄	14	rt	>99:<1	82
2	135b	4-CF ₃ C ₆ H ₄	4-MeC ₆ H ₄	14	rt	>99:<1	90
3	135c	<i>p</i> -FC ₆ H ₄	4-MeC ₆ H ₄	14	rt	>99:<1	79
4	135d	C ₆ F ₅	4-MeC ₆ H ₄	14	rt	>99:<1	65
5	135e	2-Thiophenyl	4-MeC ₆ H ₄	14	rt	>99:<1	66
6	135f	Cy	4-MeC ₆ H ₄	24	40	<1:>99	19
7	135g	CH ₂ P(O)(OEt) ₂	4-MeC ₆ H ₄	14	rt	<1:>99	87
8	135h	CF ₃	4-MeC ₆ H ₄	14	40	70:30	72 ^c
9	135i	Ph	4-MeOC ₆ H ₄	14	rt	>99:<1	76
10	135j	Ph	2-FC ₆ H ₄	14	rt	>99:<1	84
11	135k	Ph	4-BrC ₆ H ₄	14	40	70:30	91 ^c
12	135l	Ph	3-CF ₃ C ₆ H ₄	56	40	65:35	94 ^c

^aDetermined by ¹H NMR. ^bIsolated yield. ^cCombined yield for both isomers.

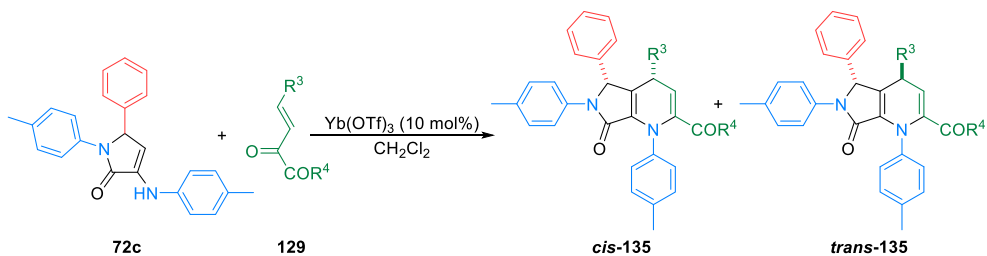
Interestingly, when aliphatic-substituted cyclic enamines were used as the nucleophilic partners, such as cyclohexyl or phosphorylmethyl enamines **72q** (R¹ = Cy, R² = 4-MeC₆H₄) and **90a** (R¹ = CH₂P(O)(OEt)₂, R² = 4-MeC₆H₄), the exclusive formation of the *trans* isomer was observed (Table 14, Entries 6-7). However, the reaction performed with trifluoromethyl substituted substrate **90e** (R¹ = CF₃, R² = 4-MeC₆H₄) afforded a 70:30 mixture of *cis* and *trans* isomers in good yield (Table 14, Entry 8).

Next, the effect of the substituents at both nitrogen atoms of the γ -lactam substrates was explored, using 5-phenyl substituted cyclic enamines and β,γ -unsaturated α -ketoester **129a** again as the electrophilic partner. *p*-Anisidine-derived enamine **84b** (R¹ = Ph, R² = 4-MeOC₆H₄) showed very good reactivity and bicyclic 1,4-dihydropyridine **135i** was obtained in good yield as a single *cis* isomer (Table 14, Entry 9). A similar result was obtained for *o*-fluoroaniline derivative **84i** (R¹ = Ph, R² = 2-FC₆H₄) with a very good yield and diastereoselectivity (Table 14, Entry 10). Nevertheless, enamines **84d** (R¹ = Ph, R² = 4-BrC₆H₄) and **84l** (R¹ = Ph, R² = 3-CF₃C₆H₄), derived from *p*-bromoaniline and *m*-trifluoromethylaniline, respectively, required higher reaction temperatures to afford the *cis* isomer

as the major product in excellent yields, together with a significant amount of the *trans* isomer (Table 14, Entries 11-12).

Then, the scope of the reaction was further explored using different substituted β,γ -unsaturated α -keto(thio)esters **129** as bidentate electrophilic substrates as shown in Table 15.

Table 15. Stereoselective formal [3+3] cycloaddition. Scope of β,γ -unsaturated α -keto(thio)esters **129**.



Entry	Prod.	R ³	R ⁴	Time (h)	Temp. (°C)	Cis:Trans ^a	Yield (%) ^b
1	135m	4-NO ₂ C ₆ H ₄	OBn	14	rt	>99:<1	68
2	135n	4-NO ₂ C ₆ H ₄	OEt	14	rt	>99:<1	79
3	135o	4-NO ₂ C ₆ H ₄	O ⁱ Pr	14	rt	>99:<1	76
4	135p	4-NO ₂ C ₆ H ₄	SEt	24	40	88:12	85 ^c
5	135q	4-CF ₃ C ₆ H ₄	O ⁱ Pr	14	rt	>99:<1	89
6	135r	Ph	O ⁱ Pr	14	rt	>99:<1	84
7	135s	4-MeC ₆ H ₄	OMe	14	rt	>99:<1	63
8	135t	4-MeC ₆ H ₄	O ⁱ Pr	14	rt	>99:<1	76
9	135u	2-Thiophenyl	O ⁱ Pr	14	rt	>99:<1	67
10	135v	CO ₂ Et	O ⁱ Pr	14	rt	>99:<1	86
11	135w	CF ₃	O ⁱ Pr	14	rt	>99:<1	84
12	135x	CH ₃	O ⁱ Pr	24	rt	85:15	65 ^c

^aDetermined by ¹H NMR. ^bIsolated yield. ^cCombined yield for both isomers.

First, the influence of the carboxylate group (R⁴) on the reactivity and the diastereoselectivity of the reaction was explored. As in the case of methyl carboxylate substituted bicyclic 1,4-dihydropyridine **135a**, similar substrates derived from benzyl, ethyl or *iso*-propyl carboxylates (**135m-o** (R³ = 4-NO₂C₆H₄; R⁴ = OBn, OEt, OⁱPr) were obtained at room temperature in good yields and as single *cis* diastereoisomers (Table 15, Entries 1-3). However, the replacement of the ester by a thioester group in β,γ -unsaturated α -ketothioester **129h** (R³ = 4-NO₂C₆H₄; R⁴ = SEt) had a strong influence into the reaction, requiring 24 hours in refluxing dichloromethane to obtain bicyclic **135p** in very good yield. (Table 15, Entry 4). Nevertheless, an 88:12 mixture of *cis* and *trans* isomers was isolated in this case. We hypothesized that the lower diastereoselectivity and reactivity observed in this case, could be attributed to a lower affinity of thiocarbonyl group to the Lewis acid catalyst, due to its less basicity,

and to the higher steric crowding present in thioester than in the ester group, in view of the higher Van der Waals radius of sulfur atom versus the oxygen (180 pm vs. 152 pm).

Finally, the last point that remains to be addressed in the annulation process is the evaluation of the influence of the substitution pattern in the conjugated double bond of β,γ -unsaturated α -ketoesters **129**. As expected, the presence of other electron-poor aromatic substituents at the electrophile, such as *p*-trifluoromethylphenyl, yielded bicyclic 1,4-dihydropyridine **135q** ($R^3 = 4\text{-CF}_3\text{C}_6\text{H}_4$; $R^4 = \text{O}^i\text{Pr}$) in very good yield and complete distereoselectivity (Table 15, Entry 5). The reaction also tolerates the presence of a simple phenyl ($R^3 = \text{Ph}$), an electron-rich aromatic ring ($R^3 = 4\text{-MeC}_6\text{H}_4$) and even a heteroaromatic substituent ($R^3 = 2\text{-thiophene}$), providing good yields for substrates **135r-u**, that were obtained as a single *cis* isomer (Table 15, Entries 6-9).

In addition, other non-aromatic electron-withdrawing substituents, such as ethylcarbonyl or trifluoromethyl groups were successfully used in β,γ -unsaturated α -ketoesters **129m** ($R^3 = \text{CO}_2\text{Me}$; $R^4 = \text{O}^i\text{Pr}$) and **129n** ($R^3 = \text{CF}_3$; $R^4 = \text{O}^i\text{Pr}$), leading to the formation of substrates **135v,w** exclusively in a *cis* configuration (Table 15, Entries 10-11). To end with the scope of the annulation reaction, aliphatic substituted bicyclic 1,4-dihydropyridine **135x** ($R^3 = \text{Me}$; $R^4 = \text{O}^i\text{Pr}$) was obtained in fair yield as *cis:trans* mixture in a 85:15 rate (Table 15, Entry 12).

Both diastereoisomers of **135h** were isolated by chromatography and fully characterized by FTIR and NMR spectroscopy and HRMS. In order to determine the regiochemistry of the reaction and the relative configuration of the two stereocenters in bicyclic dihydropyridines **135**, nuclear Overhauser effect spectroscopy (NOESY) experiments were performed with both isomers of **135h**. The protons in *ortho* position of the nitro-aromatic ring of both compounds showed a 0.9% NOE with the olefinic proton at C-3 and about 5% NOE with the proton the at C-4 of the dihydropyridine ring. However, the C-H proton at the 5-membered γ -lactam ring of the major diastereoisomer of **135h** showed 1.5% NOE with the proton at C-4 of dihydropyridine ring and no NOE was observed with the closest hydrogen atoms at the aromatic ring, suggesting a *cis* relative configuration of both protons (Figure 50).

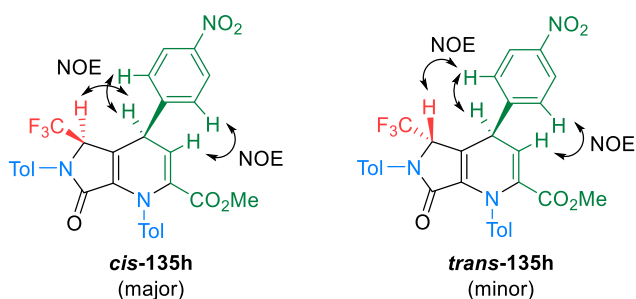


Figure 50. Comparison of the NOE effect observed in *cis-135h* and *trans-135h* 1,4-dihydropyridines.

On the other hand, the C-H proton at the 5-membered γ -lactam ring of the minor diastereoisomer of **135h** showed 1.1% NOE effect with the *ortho* protons at the nitrophenyl group and no interaction at all with the proton at C-4 of the dihydropyridine ring, suggesting a *trans* relative configuration between both substituents (Figure 50).

The relative configuration of the other bicyclic 1,4-dihydropyridines **135** was established by analogy of their NOESY spectra with those described for *cis*-**135h** and *trans*-**135h** (Figure 50). The observed NOE effects in the isolated isomers of compounds **135** were, in all cases, comparable to either *cis*-**135h** or *trans*-**135h**. However, in order to reliably corroborate the matching of the observed NOE effects with the real structure of both isomers of **135**, the absolute configuration of *cis*-**135i** and *trans*-**135g** was unambiguously determined by X-ray diffraction (Figure 51).

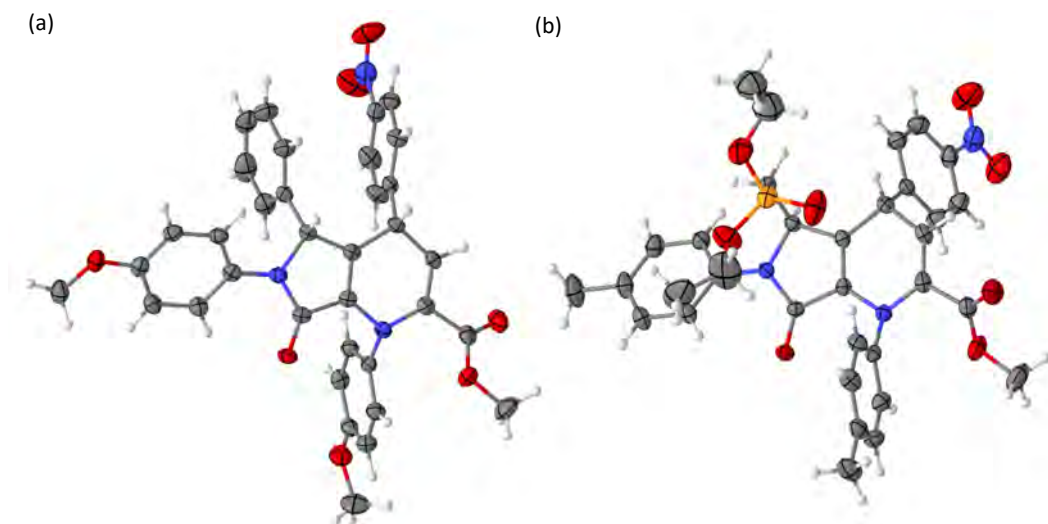
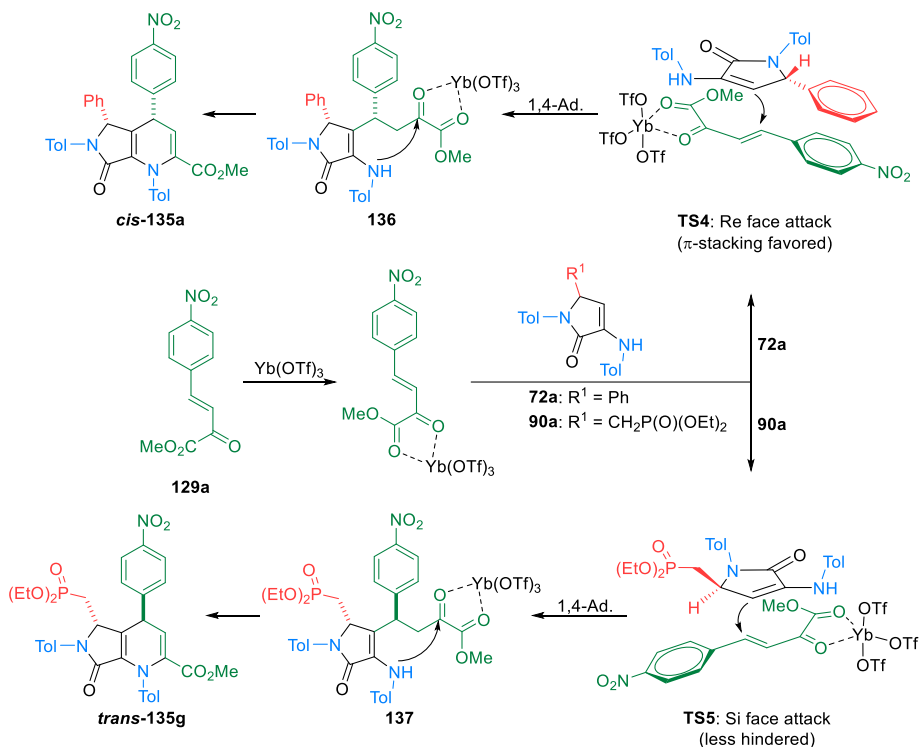


Figure 51. X-ray diffraction structure of 1,4-dihydropyridines *cis*-**135i** (a) and *trans*-**135g** (b).

Based on the observed results a plausible pathway for the reaction is proposed. The mechanism is supposed to be triggered by the initial activation of ketoester **129a** by ytterbium triflate catalyst, followed by the addition of cyclic enamine **72** to the activated conjugated ketoester (Scheme 37). At this point, the selective formation of the *cis* diastereoisomer is explained by a π -stacking effect between the aromatic group at the stereocenter of in cyclic enamine substrate **72c** and the aromatic substituent present in β,γ -unsaturated α -ketoester **129a** (**TS4**), that would push both substituents to the same orientation. On the contrary, in the absence of an aromatic ring at the stereogenic carbon of cyclic enamines, the diastereoselectivity of the reaction is driven by the steric repulsion between the tetrahedral aliphatic groups of cyclic enamines **90a** and the aromatic substituent in β,γ -unsaturated α -ketoester **129a**, that pushes both substituents to opposite orientations, obtaining exclusively the

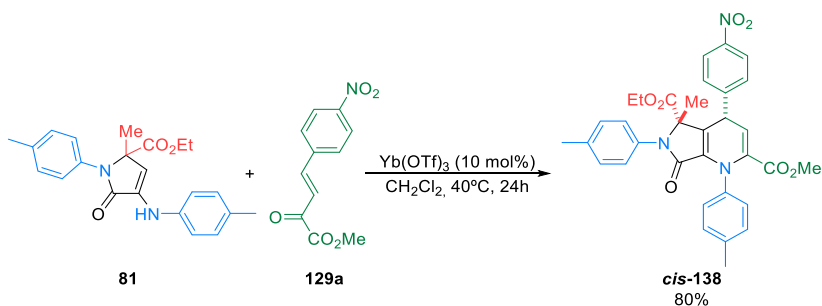
trans diastereoisomer (**TS5**). The mechanism of the reaction ends with the ring closure through the nucleophilic attack of the enamine nitrogen to the ketone group (Scheme 37).



Scheme 37. Proposed mechanism for the formation of both isomers of bicyclic 1,4-dihydropyridines **135**.

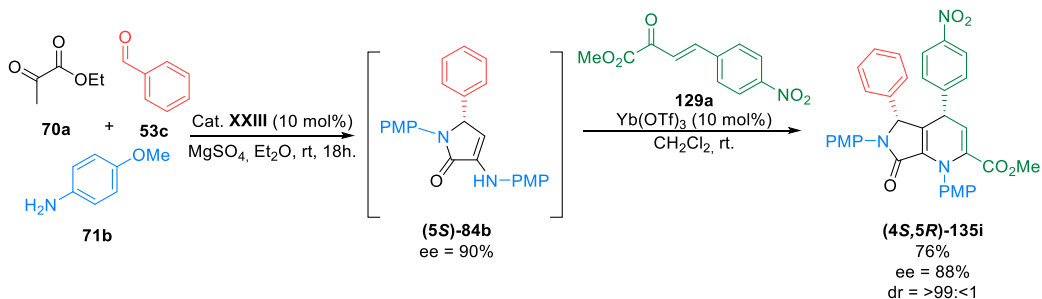
It should be pointed out that, a thermodynamic equilibrium between the two diastereoisomers is discarded since both pure isomers of **135h** were separately heated, neat or in the presence of a base, an acid or $\text{Yb}(\text{OTf})_3$ without detecting any trace of the opposite diastereoisomer.

In addition, the formal [3+3] cycloaddition reaction can also be performed using cyclic enamine **81** holding a quaternary stereocenter, with ketoester **129a** and $\text{Yb}(\text{OTf})_3$ to yield exclusively bicyclic dihydropyridine *cis*-**138**. The fact that, in this case, a *cis* relative orientation is observed between the carboxyl and the aromatic substituent may be also explained by the prevalence of the π -stacking effect over the steric interaction, thus giving support to our proposed mechanism (Scheme 38).



Scheme 38. Stereoselective formal [3+3] cycloaddition of cyclic enamine **81**.

In addition, a combination of the enantioselective multicomponent protocol for the synthesis of γ -lactam substrates with the formal [3+3] cycloaddition reaction was proposed for the preparation of enantiopure bicyclic dihydropyridines. Thus, in order to overcome the slow racemization process observed in 3-amino-1,5-dihydro-2*H*-pyrrol-2-ones, freshly prepared γ -lactam (**S**)-**84b** (90% ee) was reacted with β,γ -unsaturated α -ketoesters **129a** in the presence of ytterbium triflate in a 'one pot' procedure to afford bicyclic 1,4-dihydropyridine (**4S,5R**)-**135i** in 88% ee, that was isolated in very good yield as a single enantiomer after crystallization (Scheme 39).



Scheme 39. Synthesis of enantioenriched 1,4-dihydropyridine (**4S,5R**)-**135i**.

The obtention of enantioenriched substrate (**4S,5R**)-**135i** was verified by chiral HPLC and, after crystallization, optically pure monocrystals of the major enantiomer of bicycle **cis-135i** were obtained, determining a 4*S*, 5*R* absolute configuration of the stereocenters *via* X-ray diffraction experiments (Figure 52). Key features of the crystal structure of compound (**4S,5R**)-**135i** are the almost planar structures of the γ -lactam and the 1,4-dihydropyridine cores and the parallel alignment of the phenyl and *p*-nitrophenyl groups, possibly due to a π - π stacking effect.

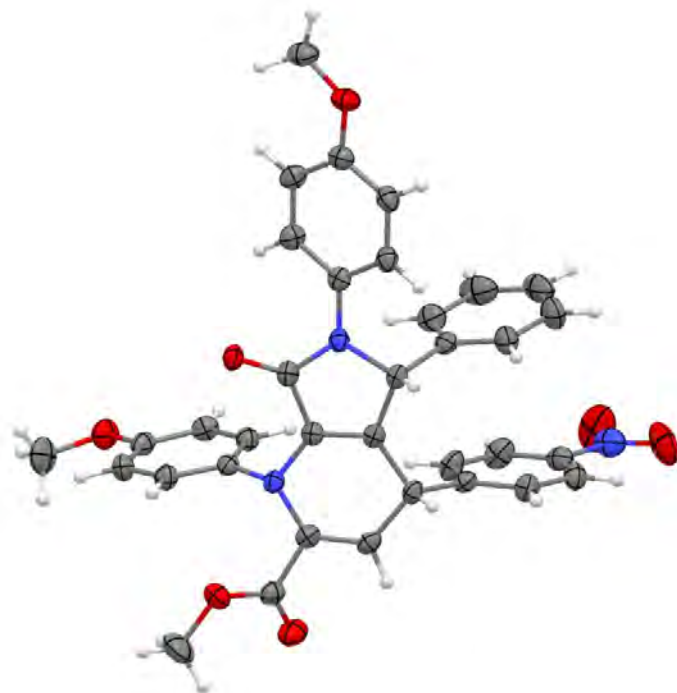
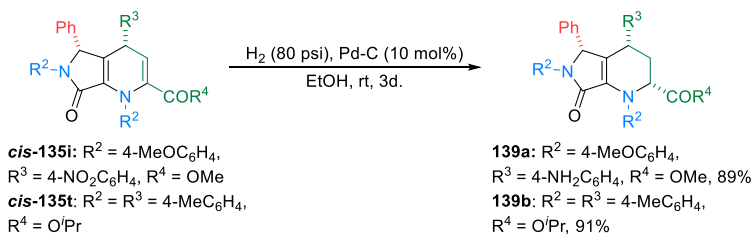


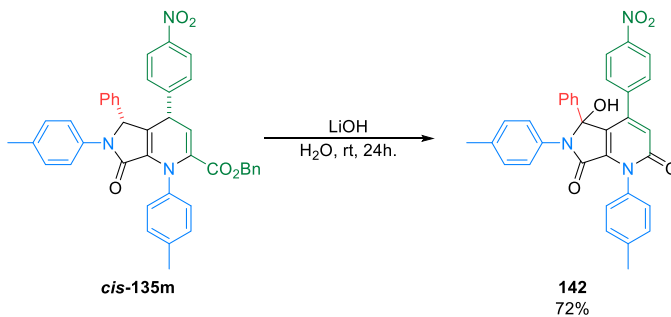
Figure 52. X-ray diffraction structure of 1,4-dihydropyridine (**4S,5R**)-*cis*-**135i**.

Furthermore, in order to put into manifest the usefulness of bicyclic 1,4-dihydropyridines **135**, some synthetic transformations of the substrates were proposed. First, the reduction of the 1,4-dihydropyridine ring was performed through the treatment of substrates *cis*-**135i** and *cis*-**135t** under hydrogen pressure at 80 psi in the presence of a catalytic amount of palladium on carbon, obtaining tetrahydropyridines **139a-b** with an all-*cis* relative configuration. NOESY experiments revealed a relative *cis* configuration of the new stereocenter with respect to the other two chiral carbons, which is in agreement with a *syn* addition mechanism of molecular hydrogen approaching to the olefinic bond from the opposite face to the substituent at both stereogenic carbons. The use of these reaction conditions on *p*-nitrophenyl substituted dihydropyridine *cis*-**135i**, also led to the reduction of the nitro to an amine group (Scheme 40).



Scheme 40. Diastereoselective hydrogenation of the 1,4-dihydropyridine ring.

In addition, the attempts to perform the hydrolysis of the ester substituent in the 1,4-dihydropyridine ring for the synthesis of the carboxylic acid derivative were unsuccessful under conventional conditions using basic or acidic hydrolyses. The hydrogenolysis of benzylic esters also proved to be unfeasible but, curiously, the treatment of benzyloxy ester with lithium hydroxide afforded bicyclic 2-pyridone derivative **142**. Compound **142** could arise from the hydrolysis of the benzyloxy ester group, followed by a decarboxylation and the subsequent oxidation and hydroxylation of the γ -lactam ring (Scheme 41).



Scheme 41. Synthesis of bicyclic 2-pyridone derivative **142**.

In conclusion, a highly stereoselective formal [3+3] cycloaddition of cyclic enamines and conjugated α -ketoesters catalyzed by ytterbium triflate to afford bicyclic 1,4-dihydropyridines is described. The generality of the reaction has been put into manifest with a scope comprising 27 substrates. As a result of the detection of the intermediate in the stepwise process, prior to the final dehydration step, it was possible to determine the reaction mechanism. The results obtained suggest a relation between steric and π -stacking effects into the final determination of the stereoselectivity of the reaction. Some synthetic transformations are also reported, including a catalytic hydrogenation that generates a third stereogenic center in a diastereoselective fashion.

The background of the page is a complex, abstract network of interconnected nodes and lines, resembling a molecular structure or a data network. The nodes are represented by small circles in various shades of gray and blue, connected by thin, light gray lines. The overall effect is a dense, interconnected web of points and lines, with some nodes appearing larger or more prominent than others. The network is distributed across the entire page, with a slight concentration in the upper and lower portions.

Section II

Anticancer activity of γ -lactam derivatives

The p53 is a nuclear transcription factor, encoded by TP53 tumor suppressor gene, also known as “the guardian of the genome” since it is mutated or has its function lost in 50% of human cancers.¹⁸² It was discovered in 1979 by several research groups, complexed with Simian Virus (SV40), a large T-antigen.¹⁸³ In the first studies, it was thought to be an oncogene and, although several investigations were made in the eighties that revealed that p53 was somehow inactivated in tumor cells,¹⁸⁴ it was not until 1989 that p53 was identified to be, not an oncogene but rather the opposite, a tumor suppressor.¹⁸⁵ Since then, functions, regulation mechanisms and medical applications involving this protein have been described, being one of the most extensively studied ones.¹⁸⁶

The p53 is a 393 amino acid long protein, which in its functional state is a homo-tetramer, each monomer possessing different regions or domains (Figure 53).¹⁸⁷ First, it holds an N-terminal transactivation domain or TAD (residues 1-42), which is a binding site for a multitude of transcriptional co-activators or co-repressors. Then, a proline-rich region or PRR is found (residues 61-94), with multiple copies of PXXP sequence, that play a crucial role in the p53-mediated induction of apoptosis.¹⁸⁸ The central domain or the DNA binding core domain (residues 102-292) is where DNA binds and also accommodates a Zn²⁺ ion that gives structural stability to the protein. Finally, in the C-terminal domain (residues 301-393) several post-translational modifications take place that are known to play an important role in the activity and stability. This terminal region contains the tetramerization domain (TD) (residues 324-355) that enables the formation of an active p53 tetramer.¹⁸⁷

¹⁸² (a) Alvi, M. S.; Rizvi, I. F.; Siddiqui, M. H.; Farooqui, A. **2016**, *8*, 112-118. (b) Ozaki, T.; Nakagawara, A. **Cancers** **2011**, *3*, 994-1013.

¹⁸³ (a) Lane, D. P.; Crawford, L. V. **Nature** **1979**, *278*, 261-263. (b) Linzer, D. I.; Levine, A. J. **Cell** **1979**, *17*, 43-52. (c) Kress, M.; May, E.; Cassingena, R.; May, P. J. **Virology** **1979**, *31*, 472-483. (d) Melero, J. A.; Stitt, D. T.; Mangel, W. F.; Carroll, R. B. **Virology** **1979**, *93*, 466-480. (e) Smith, A. E.; Smith, R.; Paucha, E. **Cell** **1979**, *18*, 335-346. (f) DeLeo, A. B.; Jay, G.; Apella, E.; Dubois, G. C.; Law, L. W.; Old, L. J. **Proc. Natl. Acad. Sci. USA** **1979**, *76*, 2420-2424.

¹⁸⁴ (a) Ben David, Y.; Prideaux, V. R.; Chow, V. **Oncogene** **1988**, *3*, 179-185. (b) Mowat, M.; Cheng, A.; Kimura, N.; Bernstein, A. **Nature** **1985**, *314*, 633-636. (c) Wolf, D.; Rotter, V. **Proc. Natl. Acad. Sci. USA** **1985**, *82*, 790-794. (d) Wolf, D.; Rotter, V. **Mol. Cell. Biol.** **1984**, *4*, 1402-1410.

¹⁸⁵ (a) Baker, S. J.; Fearon, E. R.; Nigro, J. M.; Hamilton, A. C.; Preisinger, A. C.; Jessup, J. M.; Van Tuinen, P.; Ledbetter, D. H.; Barker, D. F.; Nakamura, Y.; White, R.; Vogelstein, B. **Science** **1989**, *244*, 217-221. (b) Eliyahu, D.; Michalovitz, D.; Eliyahu, S.; Pinhasi-Kimhi, O.; Oren, M. **Proc. Natl. Acad. Sci. USA** **1989**, *86*, 8763-8767. (c) Finlay, C. A.; Hinds, P. W.; Levine, A. J. **Cell** **1989**, *57*, 1083-1093.

¹⁸⁶ Levine, A. J.; Oren, M. **Nat. Rev. Cancer** **2009**, *9*, 749-758.

¹⁸⁷ (a) Saha, T.; Kar, R. K.; Sa, G. **Prog. Biophys. Mol. Biol.** **2015**, *117*, 250-263. (b) Joerger, A. C.; Fersht, A. R. **Annu. Rev. Biochem.** **2008**, *77*, 557-582.

¹⁸⁸ Sakamuro, D.; Sabbatini, P.; White, E.; Prendergast, G. C. **Oncogene** **1997**, *15*, 887-898.

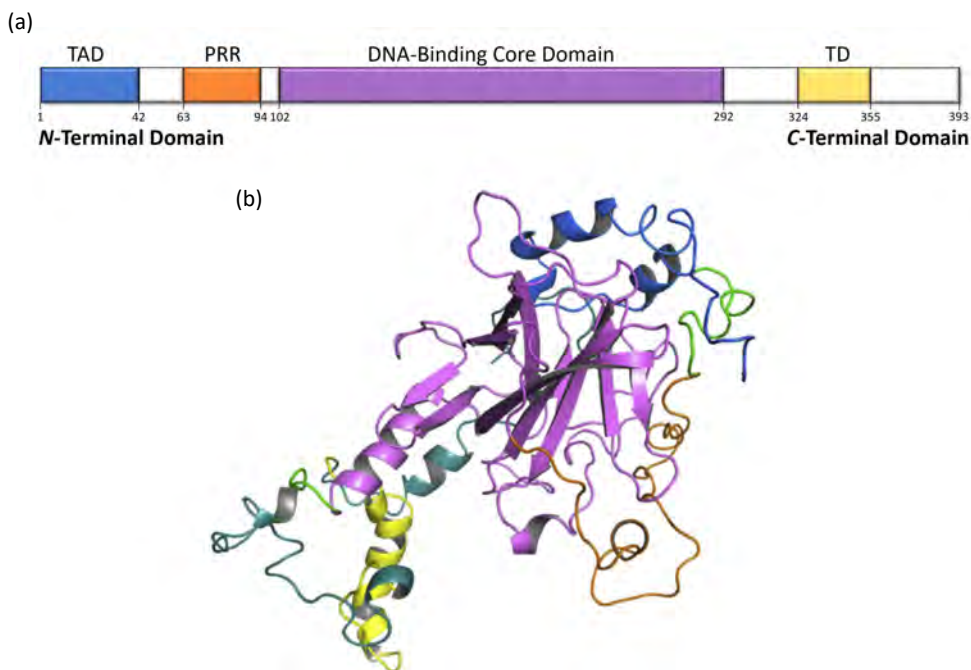


Figure 53. (a) Schematic structure of p53. (b) Full-length structure of p53 prepared with homology modeling and molecular dynamics simulation (Saha *et al.*, 2015).¹⁸⁷

The activation of p53 is boosted *via* multiple acetylation/phosphorylation events of its *N*-terminal transactivation domain and other post-translational modifications,¹⁸⁹ triggered by a wide variety of cellular stress signals such as DNA damage, hypoxia, genotoxic damage, oncogene activation or the loss of normal cell contacts. As a result, it has its translation increased, accumulates and forms tetramers with other p53 subunits, conducting their functions as transcriptional factors. The key function of p53 protein is to organize the cell defense by synchronizing the signal transduction network.¹⁹⁰ Protein p53 mainly promotes cell cycle arrest, senescence or DNA repair, in case of a low/repairable stress, and apoptosis, in case of an abnormally wide or irreparable damage (Figure 54).¹⁹¹ Other studies also have revealed that p53 is able to exert additional functions, such as the regulation of energy metabolism, anti-angiogenesis effect and antioxidant defense.^{191,192}

¹⁸⁹ (a) Bulavin, D. V.; Saito, S.; Hollander, M. C.; Sakaguchi, K.; Anderson, C. W.; Appella, E.; Fornace, A. J. *EMBO J.* **1999**, *18*, 6845-6854. (b) Canman, C. E.; Lim, D. S.; Cimprich, K. A.; Taya, Y.; Tamai, K.; Sakaguchi, K.; Appella, E.; Kastan, M. B.; Siliciano, J. D. *Science* **1998**, *281*, 1677-1679. (c) Milne, D. M.; Campbell, L. E.; Campbell, D. G.; Meek, D. W. *J. Biol. Chem.* **1995**, *270*, 5511-5518.

¹⁹⁰ Harris, S. L.; Levine, A. J. *Oncogene* **2005**, *24*, 2899-2908.

¹⁹¹ Perri, F.; Pisconti, S.; Vittoria Scarpati, G. Della. *Ann. Transl. Med.* **2016**, *4*, 2-5.

¹⁹² Lahalle, A.; Lacroix, M.; De Blasio, C.; Ciss, M. Y.; Linares, L. K.; Le Cam, L. *Cancers* **2021**, *13*, 133-150.

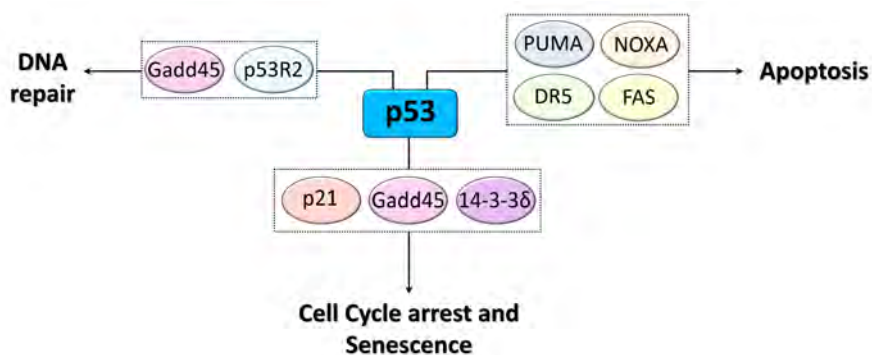


Figure 54. Main tumor-suppressive functions of p53.

As explained above, there are some stages at the cell cycle (G1, S, G2 and M) and the progression through the stages is controlled by Cyclins and Cyclin Dependent Kinase (CDK) complexes (Figure 55). The p53 mediated cell-cycle arrest is mainly promoted by the transcriptional activation of p21 which has the ability to bind cyclin E/CDK2 and cyclin D/CDK4 complexes to cause G1-S arrest in the cell cycle, thus favoring the cell entrance in the G0 phase (Figure 55). In addition, G2-M transition can be blocked by other p53 target genes, such as 14-3-3 δ and Gadd45.¹⁹³ Furthermore, while the cell-cycle is arrested, p53 can promote DNA repair in response to low stress conditions, activating Gadd45 and p53R2 genes. As a result of this activation, DNA damage can be repaired, avoiding the accumulation of mutations and their transference to descendent cells.¹⁹¹

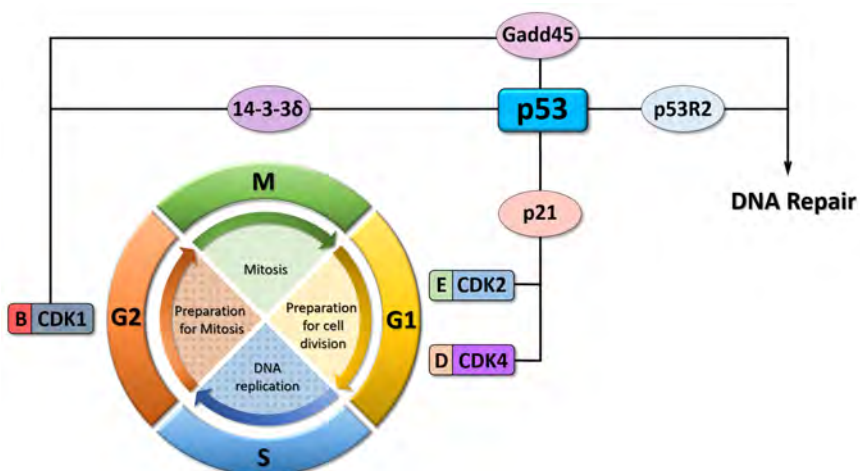


Figure 55. Checkpoints controlled by p53 in the cell cycle.

¹⁹³ (a) Chen, J. *Cold Spring Harb. Perspect. Biol.* **2016**, 1-16. (b) Chi, S. W. *BMB Rep.* **2014**, *47*, 167-172. (c) Vousden, K. H.; Prives, C. *Cell* **2009**, *137*, 413-431.

In response to irreparable or oncogenic stress, causing irreversible DNA damage, p53 induces apoptosis *via* intrinsic and extrinsic pathways. In the nucleus, p53 acts as a transcriptional factor and activates the expression of various genes involved in diverse steps of execution of this mechanism, such as pro-apoptotic proteins members of BCL-2 family (PUMA, NOXA), activating the intrinsic pathway of apoptosis. On the other hand, p53 also induces the expression of transmembrane death receptors, such as FAS and DR5, triggering the extrinsic pathway.¹⁹³

In normal cells and under physiological conditions, steady-state levels of p53 are maintained very low by means of its negative regulators.¹⁹⁴ Tetrameric p53 is activated by acetylation at C-terminal. This means that its deacetylation would play an important role in down-regulating or negatively regulating p53.¹⁹⁵ Some examples of mammalian histone deacetylases (HDAC) that can deacetylate p53 at C-terminal lysines, thus repressing its functions, are HDAC1 and SIRT1.¹⁹⁶ At this point, the excessive loss of acetylation enables the ubiquitylation of p53. This process is an enzymatic post-translational modification in which an ubiquitin protein is attached to the target protein, labelling it for destruction. In p53 this task is made by ARF-BP1 (ARF binding protein 1), Pirh2 (p53-induced protein with a RING-H2 domain), E4F1 (E4F transcription factor 1) or MDM2 (Murine Double Minute 2).¹⁹⁷ This last protein is one of the major negative regulators of p53, in collaboration with its homologous protein MDMX (Murine Double Minute X), also known as MDM4.

MDM2 and MDMX proteins.

MDM2 gene was first identified in 1987 in Donna George's laboratory while studying amplified DNA sequences on extra-chromosomal elements, known as double-minute (DM) chromosomes.¹⁹⁸ MDM1 and MDM3 genes were also identified. Some experiments performed in mice, where these genes were overexpressed, showed that only those where MDM2 gene was overexpressed developed tumors,¹⁹⁹ being the first evidence to describe the MDM2 gene as an oncogene. This gene encodes MDM2 protein, which, as demonstrated by Levine's group in 1992, acts as a negative regulator of p53, moving it to the epicenter of cancer research.²⁰⁰ In the same year, Vogelstein's laboratory achieved the goal of cloning

¹⁹⁴ Ribeiro, C. J. A.; Rodrigues, C. M. P.; Moreira, R.; Santos, M. M. M. *Pharmaceuticals* **2016**, *9*, 1-33.

¹⁹⁵ Reed, S. M.; Quelle, D. E. *Cancers* **2014**, *7*, 30-69.

¹⁹⁶ (a) Luo, J. Y.; Nikolaev, A. Y.; Imai, S.; Chen, D. L.; Su, F.; Shiloh, A.; Guarente, L.; Gu, W. *Cell* **2001**, *107*, 137-148. (b) Vaziri, H.; Dessain, S. K.; Eagon, E. N.; Imai, S. I.; Frye, R. A.; Pandita, T. K.; Guarente, L.; Weinberg, R. A. *Cell* **2001**, *107*, 149-159. (c) Luo, J. Y.; Su, F.; Chen, D. L.; Shiloh, A.; Gu, W. *Nature* **2000**, *408*, 377-381.

¹⁹⁷ (a) Lee, S. W.; Seong, M. W.; Jeon, Y. J.; Chung, C. H. *Anim. Cells Syst.* **2012**, *16*, 173-182. (b) Lee, J. T.; Gu, W. *Cell Death Differ.* **2010**, *17*, 86-92.

¹⁹⁸ Cahilly-Snyder, L.; Yang-Feng, T.; Francke, U.; George, D. L. *Somat. Cell Mol. Genet.* **1987**, *13*, 235-244.

¹⁹⁹ Fakharzadeh, S. S.; Trusko, S. P.; George, D. L. *EMBO J.* **1991**, *10*, 1565-1569.

²⁰⁰ Momand, J.; Zambetti, G. P.; Olson, D. C.; George, D.; Levine, A. J. *Cell* **1992**, *69*, 1237-1245.

human MDM2 gene and described that both, gene and protein, are involved in one third of 47 human sarcomas,²⁰¹ demonstrating the relevance of the overexpression of this protein in cancer development.

Human MDM2 protein consists of a 491 amino acid sequence with different functional domains (Figure 56). The *N*-terminal begins with a p53 binding region (residues 18-101). Three amino acids of the transactivation domain of p53 (Phe19, Trp23 and Leu26) are inserted into a deep hydrophobic cleft in MDM2's p53 binding domain, thus inhibiting its transcriptional activity.²⁰² This region is also involved in the binding to other proteins. Furthermore, MDM2 possesses nuclear localization (NLS) and nuclear export (NES) sequences (residues 178-192) which gives it the ability to move in and out of the nucleus.²⁰³ The central acidic domain (residues 237-288) is the responsible of the interaction between MDM2 and ribosomal proteins and the efficient degradation of p53. The zinc finger domain is a small region between amino acids 289 and 331.²⁰⁴ Finally, in the *C*-terminus, there is the RING Finger domain (residues 436-482), which gives the E3 ligase activity to MDM2, labeling p53 with ubiquitin for further destruction.²⁰⁵

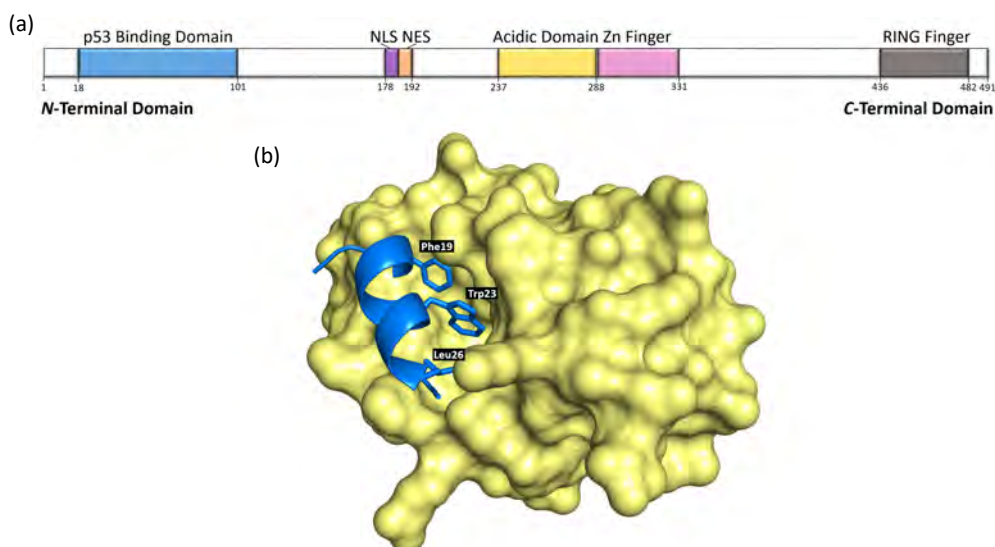


Figure 56. (a) Schematic structure of MDM2 (ref. 206). (b) Crystal structure of MDM2-p53 peptide complex (PDB code 4HFZ).

²⁰¹ Oliner, J. D.; Kinzler, K. W.; Meltzer, P. S.; George, D. L.; Vogelstein, B. *Nature* **1992**, *358*, 80-83.

²⁰² Kussie, P. H.; Gorina, S.; Marechal, V.; Elenbaas, B.; Moreau, J.; Levine, A. J.; Pavletich, N. P. *Science* **1996**, *274*, 948-953.

²⁰³ Roth, J.; Dobbstein, M.; Freedman, D. A.; Shenk, T.; Levine, A. J. *EMBO J.* **1998**, *17*, 554-564.

²⁰⁴ Hou, H.; Sun, D.; Zhang, X. *Cancer Cell Int.* **2019**, *19*, 1-8.

²⁰⁵ Lai, Z.; Ferry, K. V.; Diamond, M. A.; Wee, K. E.; Kim, Y. B.; Ma, J.; Yang, T.; Benfield, P. A.; Copeland, R. A.; Auger, K. R. *J. Biol. Chem.* **2001**, *276*, 31357-31367.

²⁰⁶ Wade, M.; Wang, Y. V.; Wahl, G. M. *Trends Cell Biol.* **2010**, *20*, 299-309.

While using radioactive p53 protein to screen a mouse embryonic fibroblast expression library Jochemsen and coworkers discovered in 1996 a novel p53-binding protein with homology to MDM2.²⁰⁷ Originally, it was named as MDMX, however, after some mice knockout studies it was renamed as MDM4. In literature both nomenclatures are accepted, but it is important to note that MDMX has no relation with murine double minute genes and it was named like this just based on its homology to MDM2.²⁰⁸

MDMX has also an *N*-terminal p53 binding domain (residues 19-102), central acidic and zinc finger domains (residues 215-255 and 290-332 respectively) and the *C*-terminal RING Finger domain (residues 437-483).²⁰⁶ However, the main difference in comparison to MDM2 is the lack of NLS or NES motifs in MDMX, restricting the presence of this protein to the cytoplasm (Figure 57).

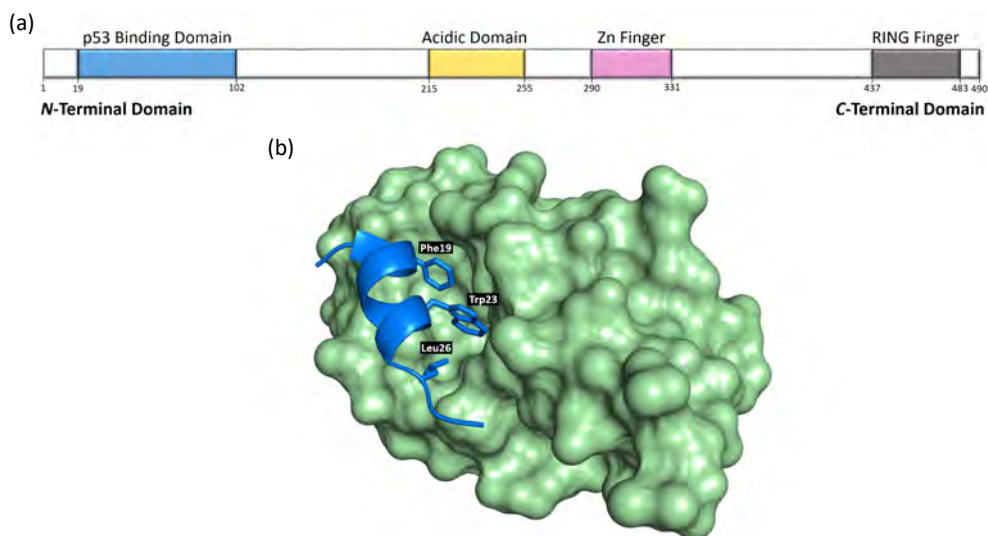


Figure 57. (a) Schematic structure of MDMX (ref. 206). (b) Crystal structure of MDMX-p53 peptide complex (PDB code 3DAB).

While both proteins have the ability to form homodimers, by the association of their RING Finger domains, only MDM2 has E3 ligase activity in its RING Finger domain. Thus, MDMX alone cannot degrade p53.²⁰⁹ In addition, both proteins can form heterodimers by the association of their RING Finger domains, therefore decreasing or increasing MDM2's E3 ligase activity towards p53. From the

²⁰⁷ Shvarts, A.; Steegenga, W. T.; Riteco, N.; Van Laar, T.; Dekker, P.; Bazuine, M.; Van Ham, R. C. A.; Van Der Houven Van Oordt, W.; Hateboer, G.; Van Der Eb, A. J.; Jochemsen, A. G. *EMBO J.* **1996**, *15*, 5349-5357.

²⁰⁸ Berberich, S. J. MDM2 and MDMX involvement in human cancer. In *Mutant p53 and MDM2 in cancer*; Springer, 2014; pp 263-280

²⁰⁹ Jackson, M. W.; Berberich, S. J.; *Mol Cell Biol.* **2000**, *20*, 1001-1007.

point of view of stability, MDMX is a very stable protein, with a half-life of over 24 hours, compared to the less stable MDM2 with a half-life of 30 minutes.

MDM2/MDMX-p53 loop.

As described before, C-terminal lysines of p53 are competitively targeted for acetylation, leading to its activation or ubiquitylation, thus marking p53 ready for further degradation.²¹⁰ Ubiquitin ligases not only degrade p53 by ubiquitylating it, but they are also capable of negatively regulate the acetylation of p53 by ubiquitylating acetyltransferases for their degradation at the proteasome, thereby reducing their expression and ability to acetylate and activate p53.²¹¹

The main E3 ubiquitin ligase and negative regulator of p53, MDM2, is itself a transcriptional target of p53. At high levels of MDM2, p53 suffers polyubiquitylation and further proteasome degradation. In this process, MDMX (or MDM4) also takes part, which has the function to bind p53 promoting its nuclear export to the cytoplasm.²¹² Additionally, MDMX can inhibit the activity of p53 as a transcription factor but does not have E3 ubiquitin ligase activity as MDM2 does (Figure 58, Black arrows).²¹³

Under stress conditions MDM2 degrades itself and MDMX, resulting in the activation, accumulation and tetramer formation of p53 (Figure 58, Red arrows). The increased levels of activated p53 in the nucleus turn on the transcription p53 target genes, including MDM2/X transcription genes. This results in increased levels of MDM2 and MDMX (Figure 58, Blue arrows). Increased MDM2 degrades itself and MDMX more efficiently, repeating the loop and enabling full activation of p53.

Following the stress relief, MDM2 targets p53 again with the collaboration of MDMX, leading to p53 inactivation (Figure 58, Black arrows). Finally, due to the presence of small amounts of p53, the concentration of MDM2 protein will decrease, thus increasing p53 protein to physiological levels, and completing the loop.^{195,214} The mechanism in which MDM2 preferentially targets p53 for degradation in unstressed cells, but targets itself and MDMX after stress, still requires full elucidation.

²¹⁰ (a) Ito, A.; Kawaguchi, Y.; Lai, C. H.; Kovacs, J. J.; Higashimoto, Y.; Appella, E.; Yao, T. P. *EMBO J.* **2002**, *21*, 6236-6245. (b) Nakamura, S.; Roth, J.A.; Mukhopadhyay, T. *Mol. Cell. Biol.* **2000**, *20*, 9391-9398. (c) Rodriguez, M. S.; Desterro, J. M. P.; Lain, S.; Lane, D. P.; Hay, R. T. *Mol. Cell. Biol.* **2000**, *20*, 8458-8467. (d) Gu, W.; Roeder, R. G. *Cell* **1997**, *90*, 595-606.

²¹¹ (a) Jin, Y. T.; Zeng, S. X.; Dai, M. S.; Yang, X. J.; Lu, H. J. *Biol. Chem.* **2002**, *277*, 30838-30843. (b) Kobet, E.; Zeng, X. Y.; Zhu, Y.; Keller, D.; Lu, H. *Proc. Natl. Acad. Sci. USA* **2000**, *97*, 12547-12552. (c) Wadgaonkar, R.; Collins, T. J. *Biol. Chem.* **1999**, *274*, 13760-13767. (d) Grossman, S. R.; Perez, M.; Kung, A. L.; Joseph, M.; Mansur, C.; Ziao, Z. X.; Kumar, S.; Howley, P. M.; Livingston, D. M. *Mol. Cell* **1998**, *2*, 405-415.

²¹² (a) Brooks, C. L.; Li, M.; Gu, W. *J. Biol. Chem.* **2007**, *282*, 22804-22815. (b) Li, M. Y.; Brooks, C. L.; Wu-Baer, F.; Chen, D. L.; Baer, R.; Gu, W. *Science* **2003**, *302*, 1972-1975. (c) Lohrum, M. A. E.; Woods, D. B.; Ludwig, R. L.; Balint, E.; Vousden, K. H. *Mol. Cell. Biol.* **2001**, *21*, 8521-8532.

²¹³ Marine, J. C.; Jochemsen, A. G. *Biochem. Biophys. Res. Comm.* **2005**, *331*, 750-760.

²¹⁴ Khoury, K.; Popowicz, G. M.; Holak, T. A.; Dömling, A. *Med. Chem. Comm.* **2011**, *2*, 246-260.

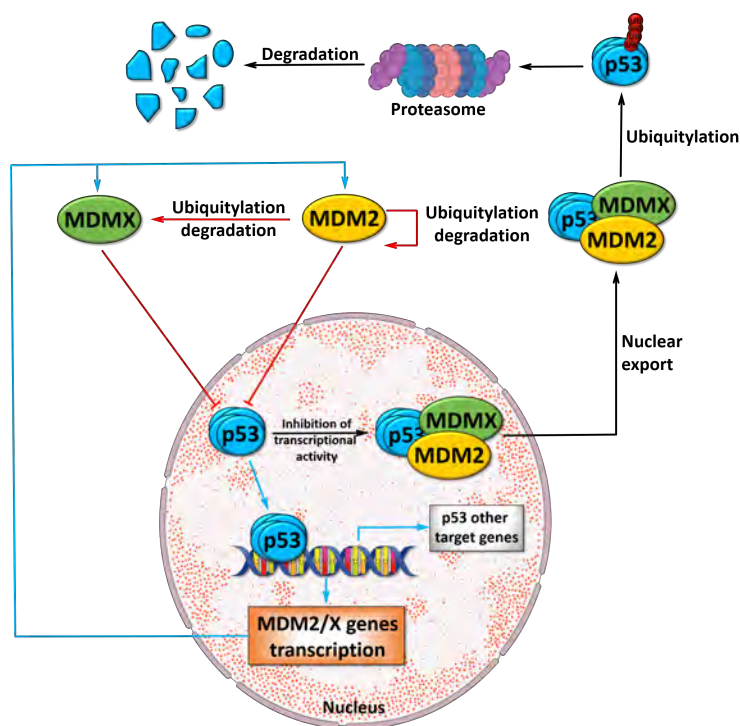


Figure 58. Schematic representation of p53-MDM2/MDMX loop. (Adapted from Khoury *et al.*, 2011).²¹⁴

Targeting p53-MDM2/MDMX for cancer treatment.

The bonding between p53 and MDM2 or MDMX is defined as a protein-protein interaction (PPI). The PPI inhibition is usually a challenging task in drug discovery due to the large area (between 600 and 1300 Å²) in the interface between both proteins, involving interactions from as many as 30 side chains from each protein.²¹⁵ However, it has been shown that, despite the interaction surface is big, there is generally a small pocket of a few amino acids, called “hot spot”, that makes up for the majority of the binding energy, so that it can be used as a target for small molecule inhibitors.²¹⁶

The “hot spot” in p53-MDM2/X complex has a “three-finger pharmacophore” made up of Trp23, Leu26, and Phe19 aminoacids of p53. These three hydrophobic amino acids fit into three shape and electrostatic complementary hydrophobic pockets, in addition to the formation of an hydrogen bond between the indole nitrogen of Trp23 in p53 and Leu54 of MDM2 (Met53 in MDMX).²¹⁴ Therefore, a

²¹⁵ Sperandio, O.; Reynes, C. H.; Camproux, A. C.; Villoutreix, B. O. *Drug Discov. Today* **2010**, *15*, 220-229.

²¹⁶ Clackson, T.; Wells, J. A. *Science* **1995**, *267*, 383-386.

requirement for high-affinity MDM2/X antagonists should be the ability of that molecules to mimic the “hot spot triad” (Trp23, Leu26, and Phe19) in p53.

Taking into account the considerations mentioned below and, considering that some α,β -unsaturated γ -lactam derivatives have proved their ability to inhibit MDM2 and MDMX proteins (Figure 18, vide supra), in the following chapters, the evaluation of the cytotoxic activity of the synthesized compounds against different cancer cell lines and the ability of those compounds to inhibit the MDM2/MDMX-p53 protein-protein interaction is presented.

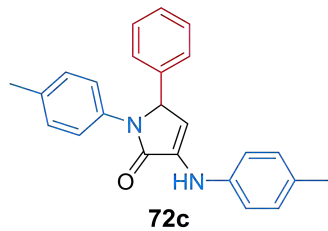
Chapter 7

Evaluation of the antiproliferative activity and the apoptosis induction capability

In this chapter, the elaboration of structure-activity profiles of the synthesized γ -lactam derivatives is envisaged. For this purpose, the *in vitro* cytotoxic activity of the diverse substrates was evaluated by testing their antiproliferative activities against several human cancer cell lines. Cell counting kit (CCK-8) colorimetric assay is used for the evaluation of the growth inhibition activity. Moreover, non-malignant MRC5 lung fibroblasts are tested for studying selective toxicity, using chemotherapeutic doxorubicin as the reference value.

7.1. Antiproliferative activity of α,β -unsaturated γ -lactam derivatives.

In a preliminary study, the cytotoxicity of γ -lactam **72c** was tested as lead compound towards seven human cancer cell lines: HEK293 (human embryonic kidney), MCF7 (human breast adenocarcinoma), HTB81 (human prostate carcinoma), HeLa (human epithelioid cervix carcinoma), RKO (human colon epithelial carcinoma), SKOV3 (human ovarian carcinoma) and A549 (carcinomic human alveolar basal epithelial cell). The cell proliferation inhibitory activity of γ -lactam **72c** is shown as IC_{50} values (Figure 59).



The chemical structure of γ -lactam **72c** is shown. It features a five-membered lactam ring with a carbonyl group at the 2-position. The nitrogen atom is substituted with a 4-methylphenyl group. The 3-position of the ring is substituted with a phenyl group. The 4-position of the ring is substituted with an NH group, which is further substituted with a 4-methylphenyl group.

Cell line	IC_{50} (μM)
HEK293 (Kidney)	>50
MCF7 (Breast)	>50
HTB81 (Prostate)	27.93 ± 2.73
HeLa (Cervix)	30.23 ± 3.75
RKO (Colon)	22.07 ± 2.98
SKOV3 (Ovarian)	9.62 ± 1.18
A549 (Lung)	2.34 ± 0.28
MRC5 (Lung)	>50

Figure 59. Antiproliferative activity of γ -lactam **72c** in multiple cell lines.

Although no growth-inhibition activity was detected against HEK293 and MCF7 cell lines, moderate cytotoxicity was observed in the case of HTB81, HeLa, and RKO cell lines. Remarkably, promising IC₅₀ values of γ -lactam **72c** against SKOV3 and A549 cell lines and, interestingly, no activity was measured towards MRC5 non-malignant cell line, suggesting a very good selectivity for malignant cell lines (Figure 59).

With these results in hand, the study of the cell proliferation inhibitory activities was extended to other γ -lactam derivatives, using RKO, SKOV3, and A549 cell lines. First, in order to evaluate the effect of the substituent at C-5 of the heterocycle (R¹), the IC₅₀ values of *p*-toluidine-derived 3-amino-1,5-dihydro-2*H*-pyrrol-2-ones **72** and **90** were measured (Table 16).

The simplest member of this family is substrate **72b**, which is obtained from formaldehyde and holds no substituent at the position 5 of the ring, did not show *in vitro* activity against SKOV3 cell line, but a slight activity was observed for A549 cell line, with a modest IC₅₀ values of 38.25 ± 3.35 μ M (Table 16, Entry 1). The cytotoxicity of γ -lactams **72** was found to be strongly dependent on the substituent at C-5 of the ring, since phenyl substituted lactam **72c** showed improved IC₅₀ values of = 9.62 ± 1.18 and 2.34 ± 0.28 μ M against SKOV3 and A549, respectively, and still good selectivity with respect to non-malignant lung fibroblasts (Table 16, Entry 2).

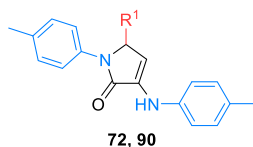
The introduction of methyl groups into a bioactive structure commonly results in a more lipophilic character, often leading to molecules with an improved ability to cross cell membranes.²¹⁷ However, in this case, *ortho*, *meta* or *para* methyl-substituted phenyl groups at the position 5 of the ring resulted in a drop in the cytotoxic activity against the A549 cell line, with IC₅₀ values around 20-40 μ M, and a complete loss of the activity in SKOV3 cell line, with IC₅₀ values over 50 μ M (Table 16, Entries-3-5).

Although the effect of the introduction of fluorine atoms in the structure of organic compounds is rather difficult to predict, very often it leads to increased activities.²¹⁸ For this reason, next, the *in vitro* cytotoxicity of fluorine-containing γ -lactams **72d,f** was tested against SKOV3 and A549 cell lines. The introduction of a *p*-fluorophenyl substituent into the 5-membered ring did not result in an improved activity, obtaining IC₅₀ values of 23.52 ± 0.75 and 10.72 ± 1.21 μ M in SKOV3 and A549 cell lines, respectively, for compound **72f** (Table 16, Entry 7). Similarly, *p*-trifluoromethylphenyl substituted γ -lactam **72d** showed IC₅₀ values over 50 μ M for both cancer cell lines (Table 16, Entry 6).

²¹⁷ (a) Schönherr, H.; Cernak, T. *Angew. Chem. Int. Ed.* **2013**, *52*, 12256-12267. (b) Barreiro, E. J.; Kümmerle, A. E.; Fraga, C. A. M. *Chem. Rev.* **2011**, *111*, 5215-5246

²¹⁸ (a) Müller, K.; Faeh, C.; Diederich, F. *Science* **2007**, *317*, 1881-1886. (b) Shah, P.; Westwell, A. D. *J. Enzym. Inhib. Med. Chem.* **2007**, *22*, 527-540.

Table 16. Evaluation of the influence of the substitution at C-5 of 3-amino-1,5-dihydro-2*H*-pyrrol-2-ones **72** and **90** into their antiproliferative activity



Entry	Prod.	R ¹	IC ₅₀ (μM)			
			A549	SKOV3	RKO	MRC5
1	72b	H	38.25 ± 3.35	>50	n.d.	>50
2	72c	Ph	2.34 ± 0.28	9.62 ± 1.18	22.07 ± 2.98	>50
3	72g	2-MeC ₆ H ₄	41.28 ± 1.29	>50	n.d.	>50
4	72i	3-MeC ₆ H ₄	31.16 ± 1.04	>50	n.d.	>50
5	72h	4-MeC ₆ H ₄	21.02 ± 1.64	>50	n.d.	>50
6	72d	4-CF ₃ C ₆ H ₄	>50	>50	>50	n.d.
7	72f	4-FC ₆ H ₄	10.72 ± 1.21	23.52 ± 0.75	n.d.	>50
8	72a	4-NO ₂ C ₆ H ₄	17.08 ± 1.58	22.87 ± 0.63	23.84 ± 2.53	26.55 ± 2.89
9	72e	3-NO ₂ C ₆ H ₄	7.33 ± 0.57	27.65 ± 1.32	n.d.	27.23 ± 1.24
10	72j	6-(<i>N</i> -Me-indolyl)	19.34 ± 0.7	>50	n.d.	>50
11	72k	2-Furyl	11.52 ± 0.85	>50	n.d.	>50
12	72l	2-Thienyl	12.71 ± 1.07	12.65 ± 1.83	n.d.	>50
13	72m	2-Naphthyl	12.1 ± 0.74	30.52 ± 1.34	n.d.	21.29 ± 0.74
14	72n	Me	15.68 ± 0.92	29.16 ± 1.00	n.d.	>50
15	72o	ⁱ Pr	11.08 ± 0.71	>50	n.d.	>50
16	72p	^t Bu	20.08 ± 2.00	>50	n.d.	24.05 ± 1.64
17	72q	Cy	10.99 ± 0.90	>50	23.79 ± 1.32	>50
18	72r	CH=CH-Ph	10.26 ± 0.8	9.59 ± 0.82	n.d.	18.24 ± 0.81
19	72s	CO ₂ Et	>50	>50	n.d.	n.d.
20	90d	C ₆ F ₅	33.50 ± 1.68	>50	>50	>50
21	90e	CF ₃	>50	>50	>50	n.d.
22	90a	CH ₂ P(O)(OEt) ₂	11.29 ± 1.80	>50	>50	>50
23	90c	CH ₂ P(O)(Ph) ₂	5.67 ± 0.9	10.76 ± 0.88	28.14 ± 1.47	30.10 ± 0.49
24	Doxorubicin		<0.1	0.13 ± 0.098	<0.1	>50

In addition, γ -lactam substrates bearing other electron-poor aromatic rings, such as *p*-nitrophenyl substituted compound **72a** showed IC₅₀ values of 22.87 ± 0.63 and 17.08 ± 1.58 μM in SKOV3 and A549 cell lines, respectively (Table 16, Entry 8). Moreover, IC₅₀ values of 27.65 ± 1.32 and 7.33 ± 0.57 μM were obtained in the case of *m*-nitrophenyl substituted γ -lactam **72e** in the same cell lines (Table 16, Entry 9). Remarkably, compound **72a** did show some cytotoxicity against RKO cell line with an IC₅₀ value

of $23.84 \pm 2.53 \mu\text{M}$, although a little toxicity in non-malignant MRC5 cells was also observed in this case (Table 16, Entry 8).

Moreover, switching the aromatic substituent at C-5 by a heteroaromatic or a naphthyl group did not have any positive effect on the cytotoxicity against SKOV3 and A549 cell lines, since *N*-methyl-indolyl, furyl, thiophene, or naphthyl substituted γ -lactam derivatives **72j-m** presented higher IC_{50} values if compared with the parent phenyl substituted substrate **72c** (Table 16, Entries 10-13 vs. Entry 2).

In the same context, next, the influence of the introduction of aliphatic substituents of the γ -lactam ring was investigated. Accordingly, methyl-substituted γ -lactam **72n** presented a slightly lower cytotoxic effect if compared with phenyl substituted lactam **72c**, with IC_{50} values of 29.16 ± 1.00 and $15.68 \pm 0.92 \mu\text{M}$ in SKOV3 and A549 cell lines, respectively (Table 16, Entry 14 vs. Entry 2). Substitution with larger aliphatic substituents, such as *iso*-propyl, *iso*-butyl, or cyclohexyl groups, resulted in a complete loss of the cytotoxic activity of substrates **72o-q** against SKOV3 cell line and nearly the same IC_{50} values or slightly better against A549 cell line. However, cyclohexyl substituted substrate **72q** displayed an IC_{50} value of $23.79 \pm 1.32 \mu\text{M}$ against RKO cell line (Table 16, Entries 15-17). Besides, cinnamyl substituted γ -lactam **72r** showed modest IC_{50} values of about $10 \mu\text{M}$ for SKOV3 and A549 cell lines, but not much selectivity with respect to non-malignant cells, and, in addition, ethoxycarbonyl substituted γ -lactam **72s** did not exhibit any cytotoxic activity (Table 16, Entries 18-19).

Continuing with the interest in fluorine-containing substrates, next, the study of the effect of the presence of perfluorinated substituents at the γ -lactam heterocycle into their antiproliferative activity was contemplated. Nevertheless, perfluorophenyl and trifluoromethyl substituted γ -lactams **90d,e** showed lower cytotoxic activity than their parent non-fluorinated derivatives **72c** and **72n** (Table 16, Entries 20, 21 vs. Entries 2, 14).

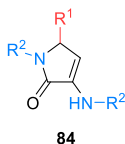
Likewise, it is well known that structural modifications of active molecules involving the introduction of phosphorus-containing functional groups, very often result in enhanced or even new activities.²¹⁹ For this reason, next, we studied the cell proliferation inhibitory activities of phosphonate and phosphine oxide-derived substrates **90a,c**. Phosphonate derivative **90a** showed some cytotoxic activity only against A549 cell line, with an IC_{50} value of $11.29 \pm 1.80 \mu\text{M}$ (Table 16, Entry 22) and, although phosphine oxide derivative **90c** presented cytotoxic properties against the three studied

²¹⁹ (a) Karl, D. M. *Nature* **2000**, *406*, 31-33. (b) Engel, R. *Handbook of Organophosphorus Chemistry*; Dekker M. Inc, 1992. (c) Kafarski, P.; Lejczak, B. *Phosphorus Sulfur Silicon Relat. Elem.* **1991**, *63*, 193-215.

cancer cell lines, it was found to be also toxic towards non-malignant lung fibroblasts (Table 16, Entry 23).

Once the influence of the substituents at the chiral center of the γ -lactam ring into the cell proliferation inhibitory activities has been described, the next point to be addressed in the SAR study is the impact of the amine substituent at the heterocyclic structure into the activity (Table 17).

Table 17. Antiproliferative activity of 3-amino-1,5-dihydro-2*H*-pyrrol-2-ones **84**. Effect of the amine substituent.



Entry	Prod.	R ¹	R ²	IC ₅₀ (μM)			
				A549	SKOV3	RKO	MRC5
1	84b	Ph	4-MeOC ₆ H ₄	12.02 ± 1.96	6.84 ± 0.59	n.d.	>50
2	84a	4-NO ₂ C ₆ H ₄	4-MeOC ₆ H ₄	31.48 ± 1.37	>50	>50	>50
3	90b	CH ₂ P(O)(OEt) ₂	4-MeOC ₆ H ₄	6.84 ± 0.22	>50	n.d.	>50
4	84f	4-NO ₂ C ₆ H ₄	4-ClC ₆ H ₄	17.16 ± 2.10	>50	n.d.	>50
5	84g	4-NO ₂ C ₆ H ₄	3-ClC ₆ H ₄	8.37 ± 1.27	16.13 ± 0.81	n.d.	23.81 ± 1.70
6	84c	4-NO ₂ C ₆ H ₄	4-BrC ₆ H ₄	>50	>50	n.d.	n.d.
7	84d	4-CF ₃ C ₆ H ₄	4-BrC ₆ H ₄	>50	>50	>50	n.d.
8	84h	4-NO ₂ C ₆ H ₄	2-FC ₆ H ₄	4.36 ± 0.51	5.55 ± 0.62	n.d.	>50
9	84j	H	3-CF ₃ C ₆ H ₄	22.94 ± 1.13	>50	n.d.	>50
10	84k	4-NO ₂ C ₆ H ₄	3-CF ₃ C ₆ H ₄	2.00 ± 0.78	8.50 ± 0.54	n.d.	44.50 ± 1.16
11	84m	4-NO ₂ C ₆ H ₄	2-Quinoliny	9.25 ± 1.49	>50	n.d.	>50
12	Doxorubicin			<0.1	0.13 ± 0.098	<0.1	>50

In this regard, the methoxy group is a strong electron-donating substituent in aromatic rings, which is known to be a widespread motif in drugs and natural products. The introduction of this moiety in potential anticancer agents very often leads to increased and more selective activities,²²⁰ which is attributed, in part, to its weak to medium antimitotic activity. For this reason, *p*-anisidine-derived γ -lactams **84a-b** and **90b** were next evaluated as antiproliferative agents. In this case, γ -lactam **84b**, bearing a simple phenyl group at C-5, showed improved cytotoxicity against SKOV3 cell line but slightly worse against A549 cell line than its parent *p*-toluidine derivative **72c** with IC₅₀ values of 6.84 ± 0.59

²²⁰ (a) Metwally, K., Khalil, A., Sallam, A.; Pratsinis, H.; Kletas, D.; El Sayed, K. *Med. Chem. Res.* **2013**, *22*, 4481-4491. (b) Patani, G. A.; Lavoie, E. J. *Chem. Rev.* **1996**, *96*, 3147-3176.

and $12.02 \pm 1.96 \mu\text{M}$, showing still selectivity in non-malignant cells (Table 17, Entry 1 vs. Table 16, Entry 2). On the contrary, no improvement in the toxicity was observed in C-5 *p*-nitrophenyl substituted substrate **84a** with respect to its parent derivative **72a** (Table 17, Entry 2 vs. Table 16, Entry 8). However, despite phosphonate derivative **90b** was not active in SKOV3 cell line, an IC_{50} value of $6.84 \pm 0.22 \mu\text{M}$, against A549 cells was measured, improving the values obtained for its parent substrate **90a**, (Table 17, Entry 3 vs. Table 16, Entry 22).

Following with the study of the influence of the amine substituent at the γ -lactam ring into the antiproliferative activity, the effect of the introduction of halogen atoms in the structure of the aniline moiety in substrates **84c-g** was next explored. No significant changes were observed in the cytotoxic effect of *p*-chloroaniline derivative **84f**, holding a *p*-nitrophenyl at the position 5 of the ring, if compared to its *p*-toluidine or *p*-anisidine derivatives **72a** or **84a** (Table 17, Entry 4 vs. Table 17, Entry 2 vs. Table 16, Entry 8). Switching the chlorine atom from *para* to the *meta* position in the aromatic ring of the aniline moiety resulted in an improvement in the cytotoxic activity in both cell lines for γ -lactam **84g**, although in this case, the selectivity towards non-malignant cells decayed (Table 17, Entry 5). Moreover, *p*-bromoaniline derivatives **84c,d** did not show any growth inhibition activity in any of the cell lines (Table 17, Entries 6, 7). However, very good results, were obtained for *o*-fluoroaniline-derived γ -lactam **84h** in terms of cytotoxicity and selectivity, with IC_{50} values of 5.55 ± 0.62 and $4.36 \pm 0.51 \mu\text{M}$ in SKOV3 and A549 cell lines, respectively, substantially improving the values observed for its non-fluorinated derivative **72a** (Table 17, Entry 8 vs. Table 16, Entry 8). The use of *m*-trifluoromethyl substituted aniline substrates resulted also in an improvement of the growth inhibition power of compounds **84j,k**. Unsubstituted formaldehyde derivative **84j** displayed slightly better IC_{50} values than the model derivative **72b** (Table 17, Entry 9 vs. Table 16, Entry 1), but substrate **84k**, holding a *p*-nitrophenyl substituent at C-5, showed very good IC_{50} values of 8.50 ± 0.54 and $2.00 \pm 0.78 \mu\text{M}$ in SKOV3 and A549 cell lines, respectively, significantly lower than the values observed for the parent *p*-toluidine-derived substrate **72a** (Table 17, Entry 10 vs. Table 16, Entry 8).

The effect of a heteroaromatic amine moiety at the γ -lactam structure was also studied. For this purpose, the quinoline scaffold was selected, due to the important role that has demonstrated to play in drug development.²²¹ Indeed, many quinoline derivatives have shown a huge potential as anticancer agents.²²² However, although an improvement in the cytotoxic activity and selectivity in A549 cell line was observed in 2-quinolinylamine substituted γ -lactam **84m** in comparison to *p*-toluidine, *p*-anisidine,

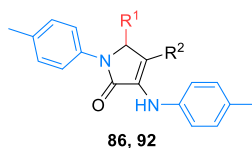
²²¹ (a) Shang, X.-F.; Morris-Natschke, S. L.; Liu, Y.-Q.; Guo, X.; Xu, X.-S.; Goto, M.; Li, J.-C.; Yang, G.-Z.; Lee, K.-H. *Med. Res. Rev.* **2018**, *38*, 775-828. (b) Diaz, G.; Miranda, I. L.; Diaz, M. A. N. Quinolines, Isoquinolines, Angustureine, and Congeneric Alkaloids-Occurrence, Chemistry, and Biological Activity. In *Phytochemicals-Isolation, Characterisation and Role in Human Health*; InTech, 2015; pp 141-162.

²²² Afzal, O.; Kumar, S.; Haider, R.; Ali, R.; Kumar, R.; Jaggi, M.; Bawa, S. *Eur. J. Med. Chem.* **2015**, *97*, 871-910.

p-chloroaniline, and *p*-bromoaniline parent derivatives **72a**, **84a**, **84f**, and **84c** (Table 17, Entry 11 vs. Table 16, Entry 8 and Table 17, Entries 2, 4 and 6), no activity against SKOV3 cell line is observed.

After the examination of the effect of the substitution at C-5 and the amines in the γ -lactam core into the antiproliferative activity of 1,5-dihydro-2*H*-pyrrol-2-ones **72**, **84** and **90**, the next step was the study of the effect of the substitution pattern at the C-4 of enamine-derived γ -lactams **86** and **92** (Table 18).

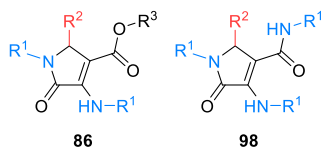
Table 18. Evaluation of the effect of the substitution at C-4 in the antiproliferative activity.



Entry	Prod.	R ¹	R ²	IC ₅₀ (μM)			
				A549	SKOV3	RKO	MRC5
1	86a	4-NO ₂ C ₆ H ₄	Me	2.05 ± 0.23	>50	n.d.	>50
2	86b	4-NO ₂ C ₆ H ₄	Bn	9.92 ± 1.15	>50	n.d.	47.56 ± 1.67
3	86c	Ph	CO ₂ Me	1.67 ± 0.49	>50	n.d.	>50
4	92a	H	P(O)(OEt) ₂	>50	>50	>50	>50
5	92b	H	P(O)(Ph) ₂	n.d.	n.d.	n.d.	n.d.
6	Doxorubicin			<0.1	0.13 ± 0.098	<0.1	>50

Although none of those substrates showed activity against SKOV3 cell line, some interesting results were obtained in A549 cell line. 4-Methyl and 4-benzyl substituted γ -lactams **86a,b** exhibited improved IC₅₀ values of 2.05 ± 0.23 and 9.92 ± 1.15 μM in comparison with the parent unsubstituted derivative **72a** (Table 18, Entries 1, 2 vs. Table 16, Entry 8). Remarkably, γ -lactam **86c** holding a methyl carboxylate substituent at C-4 gave a very good IC₅₀ value of 1.67 ± 0.49 μM in A549 cell line, with very good selectivity if compared with SKOV3 or non-malignant cells (Table 18, Entry 3). Moreover, the introduction of a phosphonate substituent at the 4 position results in a dramatic decrease in the antiproliferative activity of γ -lactam **92a** in all cell lines, by comparison with the IC₅₀ value observed in its unsubstituted derivative **72b** (Table 18, Entry 4 vs. Table 16, Entry 1). Unfortunately, the activity of diphenylphosphine oxide-derived compound **92b** could not be tested due to its low solubility in the solvents that are compatible with the tests for *in vitro* assays (Table 18, Entry 5).

In view of the improved cytotoxic activity detected when carboxylate substituents are introduced at C-4 in γ -lactam derivative **86c**, the *in vitro* antiproliferative activity of 3-amino-4-carboxylate-derived 1,5-dihydro-2*H*-pyrrol-2-ones **86** was next studied in detail (Table 19).

Table 19. Antiproliferative activity of 3-amino-4-carboxylate-derived γ -lactams **86** and **98**.

Entry	Prod.	R ¹	R ²	R ³	IC ₅₀ (μM)			
					A549	SKOV3	RKO	MRC5
1	86d	4-MeC ₆ H ₄	Ph	Et	11.70 ± 1.02	>50	>50	>50
2	86e	4-MeOC ₆ H ₄	Ph	Et	14.26 ± 1.80	>50	>50	>50
3	86f	Bn	Ph	Et	2.42 ± 0.15	>50	>50	>50
4	86g	4-MeC ₆ H ₄	Ph	<i>i</i> Pr	3.34 ± 0.29	48.45 ± 2.90	n.d.	>50
5	86c	4-MeC ₆ H ₄	Ph	Me	1.67 ± 0.49	>50	n.d.	>50
6	86h	4-MeC ₆ H ₄	4-CF ₃ C ₆ H ₄	Me	42.58 ± 2.55	30.27 ± 1.03	n.d.	>50
7	86i	Bn	4-CF ₃ C ₆ H ₄	Me	7.64 ± 0.17	>50	n.d.	>50
8	86j	4-MeC ₆ H ₄	4-HOC ₆ H ₄	Me	1.98 ± 0.18	10.37 ± 1.41	n.d.	10.01 ± 1.79
9	86k	Bn	4-HOC ₆ H ₄	Me	10.71 ± 1.35	21.91 ± 1.53	n.d.	17.37 ± 1.68
10	86l	4-MeC ₆ H ₄	3-MeOC ₆ H ₄	Me	13.03 ± 1.48	43.93 ± 1.66	n.d.	30.93 ± 6.16
11	86m	Bn	3-MeOC ₆ H ₄	Me	11.39 ± 1.49	>50	>50	>50
12	86n	4-MeC ₆ H ₄	4-HO,3-Me OC ₆ H ₄	Me	0.11 ± 0.016	1.23 ± 0.31	10.92 ± 1.18	12.64 ± 2.09
13	86o	Bn	4-HO,3-Me OC ₆ H ₄	Me	6.02 ± 1.01	>50	n.d.	>50
14	98a	4-MeC ₆ H ₄	Ph	-	2.97 ± 0.29	6.95 ± 0.59	>50	>50
15	98b	4-MeOC ₆ H ₄	Ph	-	32.38 ± 1.58	16.62 ± 0.19	n.d.	21.42 ± 2.71
16	Doxorubicin				<0.1	0.13 ± 0.098	<0.1	>50

First, the effect of the amine substituent at the γ -lactam skeleton was evaluated. Accordingly, *p*-toluidine derivative **86d**, showed modest IC₅₀ values of 11.70 ± 1.02 μM against A549 cell line (Table 19, Entry 1). Analogous γ -lactams **86e,f**, derived from *p*-anisidine or benzylamine, presented IC₅₀ values of 14.26 ± 1.80 and 2.42 ± 0.15 μM, respectively, in the same cancer cell line (Table 19, Entries 2-3). Remarkably, substrates **86d-f** did not display a significant cytotoxicity against SKOV3, RKO and non-malignant MRC5 cell lines (Table 19, Entries 1-3). Besides, *N*-unprotected γ -lactam **102**, obtained from the exocyclic *N*-debenzylation of substrate **86f** presented very low cytotoxic activity and similar substrates were not considered for a further studies.

Next, the influence of the ester substituent into the cytotoxic activity was studied. Accordingly, switching from an ethyl ester to an *iso*-propylester group resulted in improved toxicities towards A549 and SKOV3 cell lines, with IC₅₀ values of 3.34 ± 0.29 and 48.45 ± 2.90 μM, respectively, in substrate **86g**, and still no activity was observed in MRC5 cell line (Table 19, Entry 4). Remarkably, the presence of a

methyl ester substituent in **86c** provided a notable improvement in the cell growth inhibition activity in A549 cell line with a very good IC₅₀ value of 1.67 ± 0.49 μM and a very good selectivity if compared to SKOV3 and MRC5 cell lines (Table 19, Entry 5).

In view that the best toxicity values were obtained for methyl ester derivative **86c**, next, we extended the structure-activity relationship study to the evaluation of the influence of the substituent at the chiral center of the γ-lactam ring using methyl carboxylate derivatives. Accordingly, the introduction of a *p*-trifluorophenyl substituent at the 5-membered ring did not result an improved activity and IC₅₀ values of 42.58 ± 2.55 and 7.64 ± 0.17 μM were obtained in A549 cell line, for compounds **86h,i**, respectively. However, compound **86h** did show a moderate toxicity against SKOV3 cell line, and, remarkably, both compounds exhibited very high selectivity towards malignant lung cells, since IC₅₀ values higher than 50 μM were measured in MRC5 cell line (Table 19, Entries 6-7).

The antioxidant properties of phenols is known to be associated with the antitumor activities of a plethora of compounds bearing this moiety.²²³ According to this, the antiproliferative activity of phenol substituted γ-lactams **86j,k** was tested. An excellent IC₅₀ value of 1.98 ± 0.18 μM was found in A549 cell line for *p*-toluidine-derived γ-lactam **86j**, and although it was found to present some toxicity against non-malignant cells, the activity resulted to be five times lower if compared to malignant cells. Likewise, in this case, the toxicity towards ovarian carcinoma was comparable to the one observed in MRC5 cell line (Table 19, Entry 8). In addition, benzylamine-derived γ-lactam **86k** presented IC₅₀ values of 10.71 ± 1.35 and 21.91 ± 1.53 μM in A549 and SKOV3 cell lines, respectively, although a similar toxicity was measured in non-malignant lung cells (Table 19, Entry 9). Regarding the cytotoxicity of *m*-methoxyphenyl-substituted 3-amino-1,5-dihydro-2*H*-pyrrol-2-ones, *p*-toluidine-derived γ-lactam **86l** showed some cytotoxicity against A549 and SKOV3 cell lines with IC₅₀ values of 13.03 ± 1.48 and 43.93 ± 1.66 μM, respectively, although no much selectivity was obtained if compared with non-malignant cells (Table 19, Entry 10). Moreover, switching from a *p*-toluidine to a benzylamine group in **86m** did not have a positive effect into the cytotoxicity against A549 cell line, measuring a similar IC₅₀ value in both compounds (Table 19, Entry 11 vs. Entry 1). However, compound **86m** was found to be very selective in A549 cells if compared to SKOV3, RKO or MRC5 cell lines (Table 19, Entry 11). Curiously, the combination of phenol and methoxy moieties in γ-lactams **86n,o** provided excellent IC₅₀ values of 0.11 ± 0.016 and 6.02 ± 1.01 μM in A549 cell line for *p*-toluidine and benzylamine-derived substrates, respectively, with also a high selectivity if compared to non-malignant cells. Noticeably, *p*-toluidine

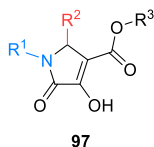
²²³ Elford H. L., Van't Riet, B. Phenols and Polyphenols as Antioxidants and Anticancer Agents. In *Eicosanoids and Other Bioactive Lipids in Cancer and Radiation Injury. Developments in Oncology*; Springer, 1991; pp 201-204.

derivative **86n** delivered a very good IC₅₀ value of $1.23 \pm 0.31 \mu\text{M}$ and 10.92 ± 1.18 against SKOV3 and RKO cells respectively (Table 19, Entries 12-13).

In addition, the effect of the replacement of the methyl ester by an amide group in γ -lactam derivatives was also studied, which had disparate effects into the antiproliferative activity of γ -lactam substrates. While a very good IC₅₀ value of $2.97 \pm 0.29 \mu\text{M}$ was obtained in A549 cell line for *p*-toluidine derivative **98a**, an IC₅₀ value ten times higher was observed in *p*-anisidine-derived substrate **98b**. Even more, both compounds showed also toxicity in SKOV3 cell line with IC₅₀ values of 6.95 ± 0.59 and $16.62 \pm 0.19 \mu\text{M}$, respectively. In addition, compound **98a** was found to be very selective towards malignant lung cells when compared to MRC5 cell line, although substrate **98b** presented also toxicity in non-malignant cell line (Table 19, Entries 14-15).

In order to further extend the structure-activity study of the γ -lactam derivatives presented in this thesis, next, the antiproliferative activity of enol-derived γ -lactam derivatives **97**, obtained from the hydrolysis of their parent enamine derivatives **86** was evaluated (Table 20).

Table 20. Antiproliferative activity of 3-hydroxy-4-carboxylate-derived γ -lactams **97**.



Entry	Prod.	R ¹	R ²	R ³	IC ₅₀ (μM)			
					A549	SKOV3	RKO	MRC5
1	97a	4-MeC ₆ H ₄	Ph	Et	15.73 ± 1.27	>50	>50	>50
2	97b	4-MeOC ₆ H ₄	Ph	Et	13.05 ± 0.56	>50	>50	>50
3	97c	Bn	Ph	Et	4.50 ± 0.18	>50	>50	>50
4	97d	Bn	4-CF ₃ C ₆ H ₄	Me	19.13 ± 3.00	>50	n.d.	>50
5	97e	4-MeC ₆ H ₄	3-MeOC ₆ H ₄	Me	17.64 ± 3.76	>50	n.d.	>50
6	97f	Bn	3-MeOC ₆ H ₄	Me	15.96 ± 1.97	>50	n.d.	>50
7	97g	4-MeC ₆ H ₄	4-HO,3-MeOC ₆ H ₄	Me	13.30 ± 2.19	10.36 ± 0.35	n.d.	>50
8	Doxorubicin				<0.1	0.13 ± 0.098	<0.1	>50

The replacement of the enamine by an enol moiety in ethyl ester substituted structures **86d-f** resulted in similar cytotoxic activity against A549 cell line in 5-phenyl-substituted compounds **97a-c** (Table 20, Entries 1-3 vs. Table 19, Entries 1-3). Moreover, these compounds did not present significant toxicity in SKOV3, RKO and MRC5 cell lines. Similarly, methyl ester substituted 3-hydroxy γ -lactam **97d**, holding a *p*-trifluoromethyl substituent at the chiral carbon of the γ -lactam ring, exhibited lower

toxicity against A549 cell line if compared with the parent enamine substrate **86i**, with an IC_{50} value of $19.13 \pm 3.00 \mu\text{M}$ and no toxicity towards SKOV3 and MRC5 cell lines (Table 20, Entry 4 vs. Table 19, Entry 7). The same drop into the antiproliferative activity in A549 cell line was observed for *m*-anisyl derivatives **97e-f** and vanillin derivative **97g** relative to their enamine precursors **86l-n**, with IC_{50} values of 17.64 ± 3.76 , 15.96 ± 1.97 and $13.30 \pm 2.19 \mu\text{M}$, respectively (Table 20, Entries 5-7 vs. Table 19, Entries 10-12). Although none of compounds **97e-f** showed any toxicity in SKOV3 or MRC5 cell lines, when an additional hydroxyl moiety is introduced at the aromatic ring in compound **97g**, it results in some activity in ovarian cancer cell line (Table 20, Entry 7).

As it has been addressed above, bioisosterism represents one approach that is widely used for the rational modification of lead compounds into safer and more clinically effective therapeutic agents.²²⁴ Accordingly, it is well known that the substitution of a carboxylate by a phosphonate group in active substrates may result in new or increased activities.^{151, 219} For this reason, next we extended our SAR study to the evaluation of the antiproliferative activity of C-4 phosphorus-substituted γ -lactam derivatives **93** (Table 21). A comparison of the cytotoxicity of phosphorus-substituted γ -lactams **93** with the already measured for the parent carboxylate-substituted substrates **97** would provide some information about the convenience of the replacement of an ester by a phosphorated-substituent.

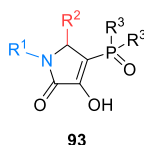
Indeed, the replacement of ethyl carboxylate by a diethyl phosphonate group in *p*-toluidine and *p*-anisidine-derived γ -lactams **97a,b**, resulted in an increase in the cytotoxic activity towards A549 cell line in **93a,g** with IC_{50} values of 3.11 ± 0.31 and $4.56 \pm 0.44 \mu\text{M}$, respectively, and a higher selectivity if compared with SKOV3 and MCR5 cell lines (Table 21, Entries 1-2 vs. Table 20, Entries 1-2). However, phosphorated γ -lactam **93h**, derived from *o*-fluoroaniline, presented a decreased activity in A549 cell, with an IC_{50} value of $16.03 \pm 1.49 \mu\text{M}$ (Table 21, Entry 3 vs. Entries 1-2).

Next, the effect of the substituent at the chiral carbon of the five-membered ring in phosphorus substituted 3-hydroxy dihydropyrrol-2-ones **93b-f** was studied, using the most active substrate **93a**, derived from *p*-toluidine and diethyl phosphonate, as the model compound. *p*-Fluorophenyl substituted γ -lactam **93b** provided a slightly worse IC_{50} value of $6.6 \pm 0.58 \mu\text{M}$ in A549 cell line, relative to the parent compound **93a** (Table 20, Entry 4 vs. Entry 1). The introduction of a stronger electron-withdrawing *p*-nitrophenyl group at the stereogenic carbon of the γ -lactam ring had a very negative effect into the cytotoxicity and IC_{50} values higher than $50 \mu\text{M}$ were found for compound **93c** in both A549 and SKOV3 cell lines (Table 21, Entry 5).

²²⁴ Patani, G. A.; Lavoie, E. J. *Chem. Rev.* **1996**, *96*, 3147-3176.

The substitution by other heteroaromatic, ester or aliphatic substituents at C-5 had also a negative effect into the toxicity of substrates **93**, observing a drop into the antiproliferative activity towards A549 cells for 2-thienyl, ethoxycarbonyl and *iso*-propyl substituted γ -lactams **93d-f**, with IC₅₀ values of 23.29 ± 2.4, 8.27 ± 0.91 and 24.20 ± 0.81 μ M. However, these compounds presented a high selectivity if compared with SKOV3 cell line and non-malignant cells (Table 21, Entries 6-8).

Table 21. Antiproliferative activity of phosphorus substituted 3-hydroxy γ -lactam derivatives **93**.



Entry	Prod.	R ¹	R ²	R ³	IC ₅₀ (μ M)			
					A549	SKOV3	RKO	MRC5
1	93a	4-MeC ₆ H ₄	Ph	OEt	3.11 ± 0.31	>50	n.d.	>50
2	93g	4-MeOC ₆ H ₄	Ph	OEt	4.56 ± 0.44	>50	>50	>50
3	93h	2-FC ₆ H ₄	Ph	OEt	16.03 ± 1.49	>50	n.d.	>50
4	93b	4-MeC ₆ H ₄	4-FC ₆ H ₄	OEt	6.60 ± 0.58	>50	n.d.	>50
5	93c	4-MeC ₆ H ₄	4-NO ₂ C ₆ H ₄	OEt	>50	>50	>50	n.d.
6	93d	4-MeC ₆ H ₄	2-Thienyl	OEt	23.29 ± 2.40	>50	>50	>50
7	93e	4-MeC ₆ H ₄	CO ₂ Et	OEt	8.27 ± 0.91	>50	n.d.	>50
8	93f	4-MeC ₆ H ₄	<i>i</i> Pr	OEt	24.20 ± 0.81	>50	n.d.	>50
9	93i	4-MeC ₆ H ₄	Ph	O ^{<i>i</i>} Pr	5.36 ± 0.28	11.56 ± 3.36	33.62 ± 0.41	>50
10	93j	4-MeC ₆ H ₄	4-FC ₆ H ₄	O ^{<i>p</i>} Pr	5.91 ± 0.69	15.55 ± 1.60	n.d.	>50
11	93k	4-MeC ₆ H ₄	CO ₂ Et	O ^{<i>p</i>} Pr	>50	>50	n.d.	n.d.
12	93l	4-MeC ₆ H ₄	Ph	Ph	11.86 ± 1.35	>50	>50	>50
13	93p	4-MeOC ₆ H ₄	Ph	Ph	3.72 ± 0.32	>50	>50	>50
14	93q	2-FC ₆ H ₄	Ph	Ph	5.50 ± 1.35	>50	n.d.	>50
15	93n	4-MeC ₆ H ₄	4-FC ₆ H ₄	Ph	1.46 ± 0.19	21.97 ± 3.42	n.d.	>50
16	93m	4-MeC ₆ H ₄	C ₆ F ₅	Ph	20.34 ± 0.79	>50	>50	>50
17	Doxorubicin				<0.1	0.13 ± 0.098	<0.1	>50

Continuing with the interest in phosphorus-containing heterocycles, next the cell growth inhibition activity of bulkier di-*iso*-propyl phosphonates **93i-k** was tested. Although slightly higher IC₅₀ values of 5.36 ± 0.28 and 5.91 ± 0.69 μ M were found in A549 cell line for phenyl and *p*-fluorophenyl C-5 substituted γ -lactams **93i,j**, with respect to their parent diethyl phosphonate derivatives **93a,b**, those substrates also presented activity in SKOV3 cells with IC₅₀ values of 11.56 ± 3.36 and 15.55 ± 1.60 μ M, and no cytotoxic effect into non-malignant cells (Table 21, Entries 9-10 vs. Entries 1-4). Moreover, the

presence of a carboxylate group at C-5 in di-*iso*-propyl phosphonate substituted γ -lactam **93f** led to a complete loss of the cytotoxicity in all cancer cell lines (Table 21, Entry 11).

Although the appearance of phosphine oxides in drug discovery is rare if compared with their counterpart phosphates, phosphonates or phosphoramidates, a few of those derivatives have proven to be excellent drug candidates such as anticancer drugs ridaforolimus²²⁵ or brigatinib.²²⁶ For this reason, the structure-activity study was extended to substrates **93l-q**, holding a phosphine oxide substituent at C-4. Accordingly, first, the antiproliferative activity of 5-phenyl-substituted γ -lactam substrates holding a diphenylphosphine oxide moiety at C-4 was studied. In this case, *p*-toluidine-derived substrate **93l** presented lower cytotoxicity than its phosphonate analogs **93a,i**, with an IC₅₀ value of 11.86 ± 1.35 μ M in A549 cell line (Table 21, Entry 12 vs. Entries 1, 9). However, the presence of a diphenylphosphine oxide moiety in *p*-anisidine and *o*-fluoroaniline derivatives **93p,q**, resulted in an improvement in their cytotoxicity towards A549 cell line if compared with the parent diethyl phosphonate substrates **93g,h**, showing IC₅₀ values of 3.72 ± 0.32 and 5.5 ± 1.35 μ M, respectively (Table 21, Entries 13-14 vs. Entries 2-3). Likewise, the presence of a *p*-fluorophenyl substituent at the chiral center in phosphine oxide derivative **93n**, provided a very active substrate with IC₅₀ values of 1.46 ± 0.19 and 21.97 ± 3.42 μ M in A549 and SKOV3 cell lines, respectively (Table 21, Entry 15). Nevertheless, the parent perfluorophenyl derivative **93m** displayed lower activity with a modest IC₅₀ value of 20.34 ± 0.79 μ M against A549 cell line and no cytotoxicity in SKOV3 cell line (Table 21, Entry 16). It should be remarked that all active phosphorylated 3-hydroxy γ -lactams **93** presented an excellent selectivity towards malignant cells with IC₅₀ values higher than 50 μ M in non-malignant cells in all the cases. Moreover, these compounds did not show a significant activity in RKO cell line.

Finally, in order to study the real activity of the individual enantiomers of the chiral substrates, the antiproliferative activity of both enantiomers of γ -lactam **90a**, with a 97% optical purity was evaluated (Figure 60). However, no significant differences were observed for (*R*)-**90a** or (*S*)-**90a** enantiomers if compared with the racemic sample (Table 16, Entry 22), with IC₅₀ values of 9.23 ± 1.68 and 10.53 ± 0.80 μ M, respectively.

²²⁵ (a) Rivera, V. M.; Squillace, R. M.; Miller, D.; Berk, L.; Wardwell, S. D.; Ning, Y.; Pollock, R.; Narasimhan, N. I.; Iulucci, J. D.; Wang, F.; Clackson, T. *Mol. Cancer Ther.* **2011**, *10*, 1059-1071. (b) Ridaforolimus. *Drugs R D* **2010**, *10*, 165-178.

²²⁶ (a) Markham, A. *Drugs* **2017**, *77*, 1131-1135. (b) Huang, W. S.; Liu, S.; Zou, D.; Thomas, M.; Wang, Y.; Zhou, T.; Romero, J.; Kohlmann, A.; Li, F.; Qi, J.; Cai, L.; Dwight, T. A.; Xu, Y.; Xu, R.; Dodd, R.; Toms, A.; Parillon, L.; Lu, X.; Anjum, R.; Zhang, S.; Wang, F.; Keats, J.; Wardwell, S. D.; Ning, Y.; Xu, Q.; Moran, L. E.; Mohemmad, Q. K.; Jang, H. G.; Clackson, T.; Rivera, V. M.; Zhu, X.; Dalgarno, D.; Shakespeare, W. C. *J. Med. Chem.* **2016**, *59*, 4948-4964.

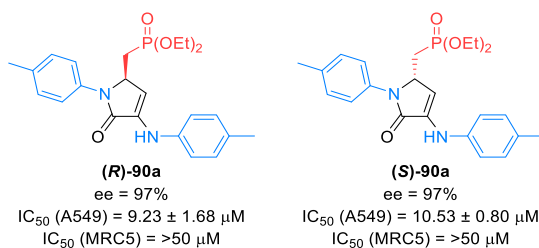


Figure 60. Antiproliferative activity of each enantiomer of γ -lactam **90a**.

In the following lines, a summary of the most remarkable effects found in the SAR study is presented for the most active substrates. The most effective C-4 unsubstituted γ -lactam derivatives in A549 cell line are substrates **72c** and **84k** with 2.34 ± 0.28 and $2.00 \pm 0.78 \mu\text{M}$ IC_{50} values respectively. However, substrate **84k** also shows some activity in non-malignant lung cell line. With respect to SKOV3 cell line, the best cytotoxic activity, with IC_{50} values of $5.55 \pm 0.62 \mu\text{M}$, is measured for compound **84h** (Figure 61).

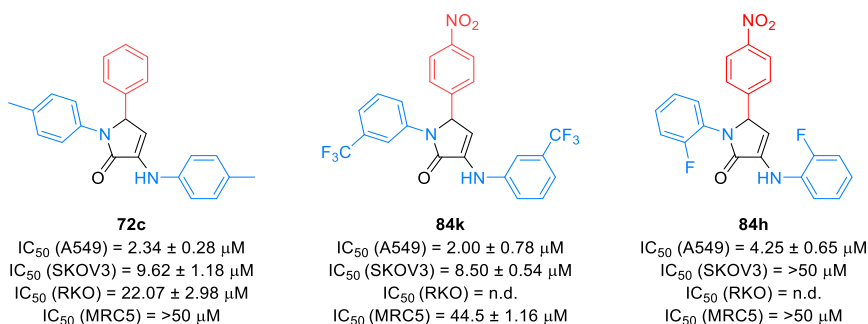


Figure 61. Most active C-4 unsubstituted enamine-derived γ -lactams.

The introduction of a substituent at the position 4 of the γ -lactam ring proved to influence positively the cytotoxic activity. Among the enamine-derived C-4 substituted γ -lactams, substrates **86a** and **86c** showed excellent activity in A549 cell line, with IC_{50} values of 2.05 ± 0.23 and $1.67 \pm 0.49 \mu\text{M}$ respectively, and good selectivity if compared to MRC5 cell line (Figure 62). In addition, for this set of compounds, it is observed that the substitution of the enamine moiety by an enol does not significantly affect the antiproliferative activity. In the case of enol-derived γ -lactams, the presence of a phosphorus substituent at C-4 seems to be a better option than the carboxylate group. The most active phosphorus substituted 3-hydroxy γ -lactams are compounds **93a** and **93n**, with IC_{50} values of 3.11 ± 0.31 and $1.46 \pm 0.19 \mu\text{M}$ in A549 cell line. Moreover, it must be pointed out that, for this series of compounds, no improvement was observed in the antiproliferative activity against SKOV3 and RKO cell lines (Figure 62).

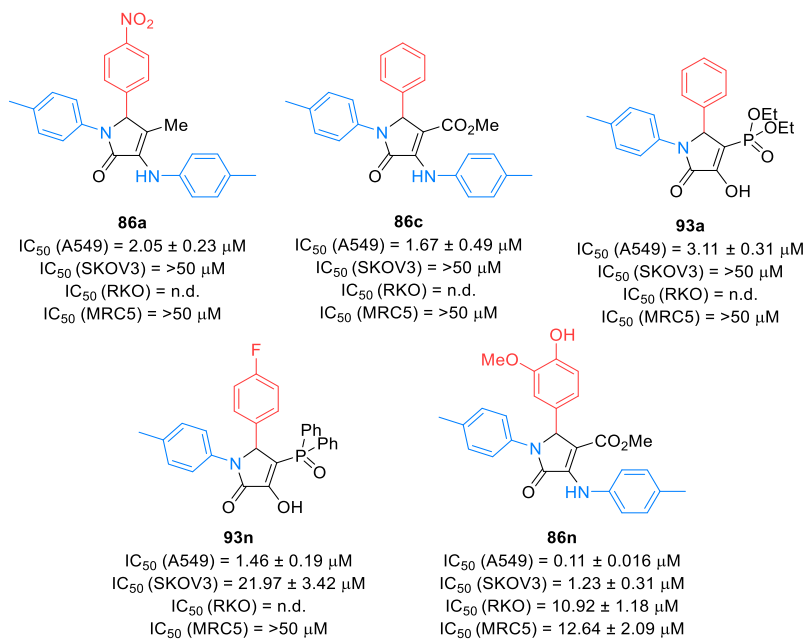


Figure 62. Some active C-4 substituted γ -lactams.

Finally, the most active compound among all the synthesized γ -lactam derivatives was found to be substrate **86n**, with IC_{50} values of 0.11 ± 0.016 , 1.23 ± 0.31 and $10.92 \pm 1.18 \mu\text{M}$ in A549, SKOV3 and RKO cell lines respectively. Additionally, compound **86n** shows 115-fold higher IC_{50} value in non-malignant lung cell line, making clear its selectivity towards lung malignant cells (Figure 62).

In order to further extend the SAR study, other substrates obtained by the diverse modifications of the γ -lactam derivatives were also evaluated as antiproliferative agents. First, the cell proliferation inhibitory activity of γ -lactam derivative **81**, obtained by the dimerization reaction of two pyruvate enamine/imine intermediates, was evaluated, showing a modest IC_{50} value of $13.97 \pm 1.05 \mu\text{M}$ in A549 cell line, with high selectivity if compared with SKOV3, RKO, or MRC5 cell lines (Figure 63).

Moreover, the effect of the hydrogenation of the endocyclic enamine moiety was studied in *p*-anisidine γ -lactam derivatives **103a-c**. In the case of saturated γ -lactam **103a**, with a phenyl substituent at C-5, a slightly worse IC_{50} value of $19.45 \pm 0.34 \mu\text{M}$ was found in A549 cell line if compared with its parent unsaturated derivative **84b** (Figure 63 vs. Table 17, Entry 1). However, phosphonomethyl and trifluoromethyl substituted substrates **103b** and **103c**, showed a clear improvement into the cytotoxic activity in A549 cell line with respect to their parent unsaturated γ -lactams **90a** and **90e**, showing IC_{50} values of 3.27 ± 0.65 and $4.25 \pm 0.65 \mu\text{M}$ in lung cancer cell line respectively (Figure 63 vs. Table 16, Entries 21-22). Remarkably, saturated γ -lactam substrates **103** did

not show any activity in SKOV3 and MRC5 cell lines. These results suggest that the presence of the conjugated double bond at the γ -lactam ring is crucial in order to obtain a good anticancer activity.

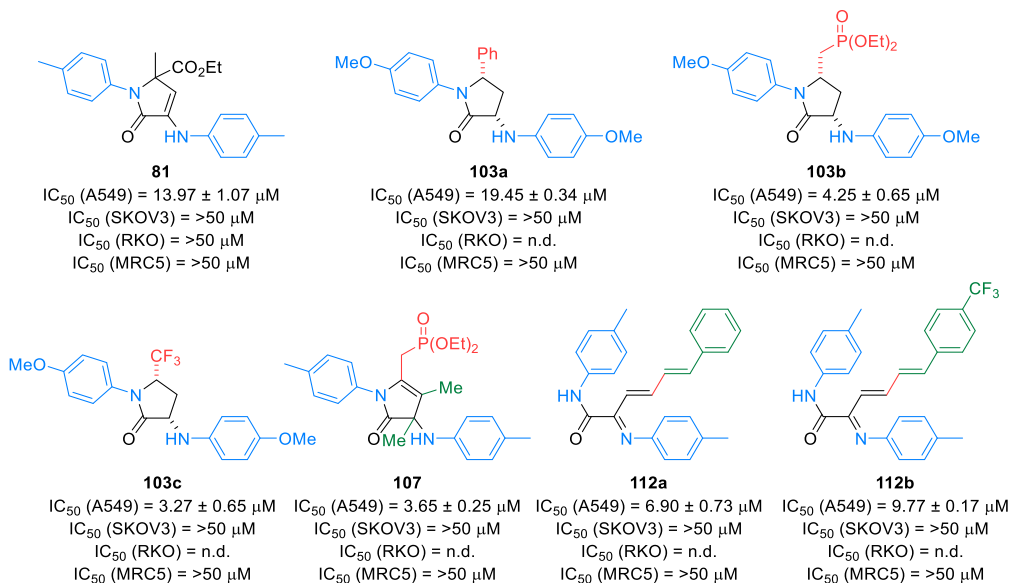


Figure 63. Antiproliferative activity of other γ -lactam derivatives.

Due to the known lipophilic character of aliphatic groups, the functionalization of bioactive molecules with methyl moieties often results in stronger activities than the parent structures.²²⁷ For this reason, the evaluation of the cytotoxicity of γ -lactam derivative **107**, holding four methyl groups into its structure was performed. Indeed an improved IC_{50} value of $3.65 \pm 0.25 \mu\text{M}$ against A549 cell line was obtained for functionalized compound **107** if compared to the parent γ -lactam **90a** (Figure 63 vs. Table 16, Entry 22). In addition, a high selectivity was observed for this compound since it did not show any toxicity against SKOV3, RKO and MRC5 cell lines.

Finally, the evaluation of the antiproliferative activity of highly conjugated compounds **112a,b**, obtained after the ring-opening of γ -lactam **90a**, was performed. Accordingly, both compounds presented good cytotoxicity against A549 cell line, showing IC_{50} values of 6.90 ± 0.73 and $9.77 \pm 0.17 \mu\text{M}$, respectively, and no activity in SKOV3 and non-malignant lung cells (Figure 63).

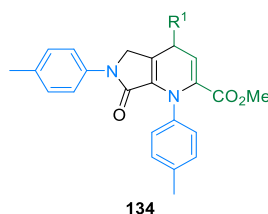
²²⁷ Schönherr, H.; Cernak, T. *Angew. Chem. Int. Ed.* **2013**, *52*, 12256-12267.

7.2. Antiproliferative activity of bicyclic 1,4-dihydropyridines.

Following with the study of the anticancer properties of the substrates obtained in this research, next, the efforts were focused towards the evaluation of the antiproliferative activity of bicyclic substrates obtained from the formal [3+3] cycloaddition reaction of γ -lactams with β,γ -unsaturated α -ketoesters. In this regard, 1,4-dihydropyridines are well known as calcium channel modulating agents, very adequate for the treatment of hypertension.¹⁷² Remarkably, many calcium channel blockers have demonstrated their efficacy as anticancer agents, and several 1,4-dihydropyridines have been reported as efficient antiproliferative agents in several studies.¹⁷⁶ Considering this, and the fact that the substrates obtained from the formal [3+3] cycloaddition reaction contain a 1,4-dihydropyridine ring fused with a γ -lactam scaffold, a study of the growth inhibition activity of these hybrid substrates might be of high interest in the field.

Accordingly, in the first part of this study, the cytotoxic activity of the most simple 1,4-dihydropyridines **134**, prepared from C-5 unsubstituted γ -lactams, was evaluated (Table 22). However, to our surprise, only substrate **134a**, bearing a *p*-nitrophenyl substituent at the 6-membered ring, showed some activity against A549 cell line, with a modest IC₅₀ value of 44.83 \pm 2.57 μ M. In addition, this substrate proved to have no effect in non-malignant lung cell line (Table 22, Entry 1).

Table 22. Antiproliferative activity of 1,4-dihydropyridines **134**.

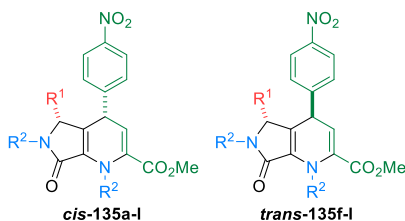


Entry	Prod.	R ¹	IC ₅₀ (μ M)		
			A549	SKOV3	MRC5
1	134a	4-NO ₂ C ₆ H ₄	44.83 \pm 2.57	>50	>50
2	134b	4-CF ₃ C ₆ H ₄	>50	>50	n.d.
3	134c	Ph	>50	>50	n.d.
4	134d	4-MeC ₆ H ₄	>50	>50	n.d.
5	Doxorubicin		<0.1	0.13 \pm 0.098	>50

Due to the high structural diversity obtained in the formal [3+3] annulation reaction a study of the influence of the diverse substituents into the antiproliferative activity of bicyclic 1,4-dihydropyridines was conducted. Considering the results obtained in our preliminary study, unsubstituted compound

134a was next used as a template, in order to assess the effect of the introduction of a variety of substituents at the γ -lactam core into the biological activity of our substrates. The obtained results are summarized in Table 23.

Table 23. Effect of the substituents at the γ -lactam core in the antiproliferative activity of compounds **135a-l**.



Entry	Product	R ¹	R ²	IC ₅₀ (μM)		
				A549	SKOV3	MRC5
1	<i>cis</i> -135a	Ph	4-MeC ₆ H ₄	>50	>50	n.d.
2	<i>cis</i> -135b	4-CF ₃ C ₆ H ₄	4-MeC ₆ H ₄	>50	>50	n.d.
3	<i>cis</i> -135c	4-FC ₆ H ₄	4-MeC ₆ H ₄	>50	>50	n.d.
4	<i>cis</i> -135d	C ₆ F ₅	4-MeC ₆ H ₄	2.04 ± 0.68	9.05 ± 1.39	20.16 ± 0.71
5	<i>cis</i> -135e	2-Thiophenyl	4-MeC ₆ H ₄	>50	>50	n.d.
6	<i>trans</i> -135f	Cy	4-MeC ₆ H ₄	>50	>50	n.d.
7	<i>trans</i> -135g	CH ₂ P(O)(OEt) ₂	4-MeC ₆ H ₄	>50	>50	n.d.
8	<i>cis</i> -135h	CF ₃	4-MeC ₆ H ₄	>50	>50	n.d.
9	<i>trans</i> -135h	CF ₃	4-MeC ₆ H ₄	>50	>50	n.d.
10	<i>cis</i> -135i	Ph	4-MeOC ₆ H ₄	>50	>50	n.d.
11	<i>cis</i> -135j	Ph	2-FC ₆ H ₄	>50	>50	n.d.
12	<i>cis</i> -135k	Ph	4-BrC ₆ H ₄	36.51 ± 5.14	>50	>50
13	<i>trans</i> -135k	Ph	4-BrC ₆ H ₄	>50	>50	>50
14	<i>cis</i> -135l	Ph	3-CF ₃ C ₆ H ₄	7.79 ± 1.59	>50	>50
15	<i>trans</i> -135l	Ph	3-CF ₃ C ₆ H ₄	7.33 ± 0.37	>50	>50
16	Doxorubicin			<0.1	0.13 ± 0.098	>50

In the first part of the SAR study, the influence of the substituent at the stereocenter of the γ -lactam scaffold was evaluated. Accordingly, bicyclic 1,4-dihydropyridines *cis*-135a-c bearing different aromatic substituents at the γ -lactam unit showed IC₅₀ values over 50 μM (Table 23, Entries 1-3). However, the introduction of a perfluorophenyl group at the γ -lactam ring in substrate *cis*-135d resulted in good IC₅₀ values of 2.04 ± 0.68 and 9.05 ± 1.39 μM towards A549 and SKOV3 cell lines, respectively, although some toxicity in non-malignant cells was also observed (Table 23, Entry 4). Besides, heteroaromatic-substituted derivative *cis*-135e did not present any toxicity against both cell lines (Table 23, Entry 5)

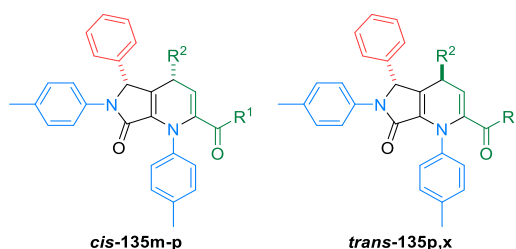
and no activity was observed for bicyclic 1,4-dihydropyridines bearing aliphatic substituents, such as cyclohexyl, diethyl phosphorylmethyl or trifluoromethyl groups in compounds **135f-h** (Table 23, Entries 6-9).

Next, the impact of using different amine substituents at the γ -lactam unit into the antiproliferative activity of bicyclic 1,4-dihydropyridines was studied. Although no improvement was observed using *p*-anisidine or *o*-fluoroaniline derivatives **cis-135i,j** (Table 23, Entries 10-11), *p*-bromophenyl substituted substrate **cis-135k** showed an IC_{50} value of $36.51 \pm 5.14 \mu\text{M}$ towards A549 cell line and no toxicity in SKOV3 or MRC5 cell lines (Table 23, Entry 12). Curiously, the isomer with the opposite configuration, **trans-135k**, did not show any activity (Table 23, Entry 13). Interestingly, both isomers of *m*-trifluorophenyl substituted substrate **cis-135l** and **trans-135l** showed good toxicity and selectivity in A549 cell line with IC_{50} values of 7.79 ± 1.59 and $7.33 \pm 0.37 \mu\text{M}$, respectively (Table 23, Entries 14-15).

Following with the SAR study, the next objective was moved to the evaluation of the influence of the substituents at the 1,4-dihydropyridine unit into the activity of bicyclic substrates. In this part of the study, first, the influence of the ester group was evaluated (Table 24).

For the assessment of the effect of the carboxylate group in the antiproliferative activity, compound **cis-135a** was used as a template. The replacement of the methyl ester by a benzyl or ethyl ester did not result in any antiproliferative activity in substrates **cis-135m,n** (Table 24, Entries 1-2). However, to our delight, *iso*-propyl ester substituted **cis-135o** proved to be far superior than the other derivatives, measuring IC_{50} values of 10.12 ± 1.03 and $10.71 \pm 0.87 \mu\text{M}$ against A549 and SKOV3 cell lines, respectively, with no activity in non-malignant lung cell lines (Table 24, Entry 3). Likewise, thioester derivatives **cis-135p** and **trans-135p** did not provide any cytotoxicity (Table 24, Entries 4-5).

Finally, the SAR study was completed with the evaluation of the influence of the substitution at the chiral carbon of the 1,4-dihydropyridine ring, into the antiproliferative activity of bicyclic substrates **135**. In this case, the most active *iso*-propyl ester **cis-135o** was chosen as the headliner and its activity was compared with differently substituted bicyclic 1,4-dihydropyridines. Accordingly, switching from *p*-nitrophenyl substituent to a *p*-trifluoromethylphenyl group had a slightly positive effect into the activity against A549 cell line and compound **cis-135q** presented an IC_{50} value of $8.44 \pm 0.79 \mu\text{M}$ (Table 24, Entry 6). However, the presence of such substituent led to a complete loss of its toxicity against SKOV3 cell line and proved to be also very selective against A549 cell line, since an IC_{50} value over 50 μM was observed in MRC5 cells (Table 24, Entry 6).

Table 24. Effect of the substituents at the 1,4-dihydropyridine core in the antiproliferative activity.

Entry	Product	R ¹	R ²	IC ₅₀ (μM)		
				A549	SKOV3	MRC5
1	<i>cis</i> -135m	OBn	Ph	>50	>50	n.d.
2	<i>cis</i> -135n	OEt	Ph	>50	>50	n.d.
3	<i>cis</i> -135o	O ⁱ Pr	Ph	10.12 ± 1.03	10.71 ± 0.87	>50
4	<i>cis</i> -135p	SEt	Ph	>50	>50	n.d.
5	<i>trans</i> -135p	SEt	Ph	>50	>50	n.d.
6	<i>cis</i> -135q	O ⁱ Pr	4-CF ₃ C ₆ H ₄	8.44 ± 0.79	>50	>50
7	<i>cis</i> -135r	O ⁱ Pr	Ph	30.69 ± 1.38	>50	>50
8	<i>cis</i> -135t	O ⁱ Pr	4-MeC ₆ H ₄	>50	>50	n.d.
9	<i>cis</i> -135u	O ⁱ Pr	2-Thiophene	0.89 ± 0.27	11.90 ± 1.20	32.02 ± 3.43
10	<i>cis</i> -135v	O ⁱ Pr	CO ₂ Et	>50	>50	n.d.
11	<i>cis</i> -135w	O ⁱ Pr	CF ₃	5.07 ± 0.74	6.69 ± 0.13	15.97 ± 1.11
12	<i>cis</i> -135x	O ⁱ Pr	CH ₃	>50	>50	n.d.
13	<i>trans</i> -135x	O ⁱ Pr	CH ₃	>50	>50	n.d.
14	Doxorubicin			<0.1	0.13 ± 0.098	>50

Other aromatic substituents at the stereocenter of the 1,4-dihydropyridine core, such as simple phenyl or *p*-tolyl, in *cis*-135r and *cis*-135t did not prove to be superior to *p*-trifluoromethylphenyl group (Table 24, Entries 7-8 vs. Entry 6). Likewise, thiophene derivative *cis*-135u showed a strong antiproliferative activity against A549 cell line and moderate activity in SKOV3 cell line, with IC₅₀ values of 0.89 ± 0.27 and 11.90 ± 1.20 μM, respectively (Table 24, Entry 9). Although substrate *cis*-135u presented some toxicity against non-malignant cells, with an IC₅₀ value of 32.02 ± 3.43 μM, its selectivity was demonstrated to be far superior against SKOV3 cell line and, particularly, against A549 cell line (Table 24, Entry 9). Besides, the replacement of the aromatic substituent by a carboxylate group at the 1,4-dihydropyridine ring had a negative effect and compound *cis*-135v presented IC₅₀ values higher than 50 μM (Table 24, Entry 10). Despite the fact that the introduction of a trifluoromethyl group resulted in a good cytotoxic activity in *cis*-135w, with IC₅₀ values of 5.07 ± 0.74 and 6.69 ± 0.13 μM in A549 and SKOV3 cell lines, respectively, this substrate showed moderate toxicity

in MRC5 cell line (Table 24, Entry 11). Finally, a simple methyl group in the 1,4-dihydropyridine structure led to an absolute loss of the cytotoxicity for both isomers of **135x** (Table 24, Entries 12-13).

In summary, 1,4-dihydropyridines have shown disparate cytotoxic activities. Some of the most active compounds are **cis-135d**, with IC_{50} values of 2.04 ± 0.68 and 9.05 ± 1.39 μM in A549 and SKOV3 cell lines, with low selectivity if compared to non-malignant lung cell line, and both diastereoisomers of **135l**, with IC_{50} values around 7 μM in lung cancer cell line, but measuring no activity in SKOV3 and MRC5 cell lines. Both compounds contain fluorinated substituents, which seems to be fundamental for the antiproliferative activity of bicyclic 1,4-dihydropyridines. Furthermore, the *iso*-propyl group at the ester moiety increases the antiproliferative activity, measuring IC_{50} values of 10.12 ± 1.03 and 10.71 ± 0.87 μM for compound **cis-135o** in A549 and SKOV3 cell lines, respectively, and no activity in non-malignant lung cell line. The most active compound was **cis-135u** with 0.89 ± 0.27 and 11.90 ± 1.20 μM IC_{50} values in A549 and SKOV3 cell lines, and with thirty-six-fold worst activity in the parent non-malignant cell line, which is a clear proof of selectivity towards lung cancer cells.

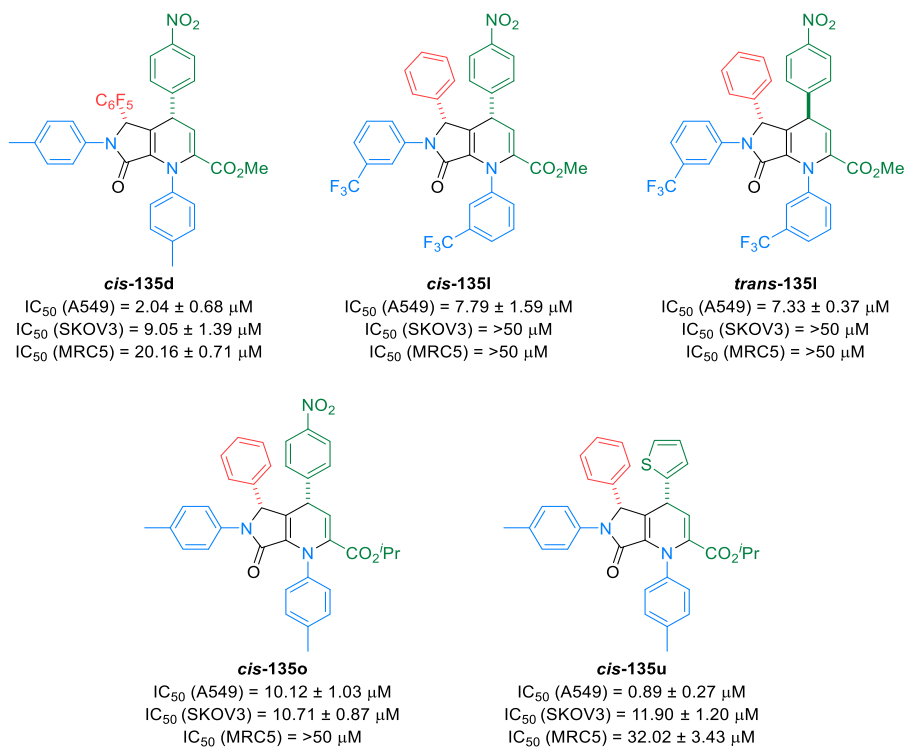


Figure 64. Some active 1,4-dihydropyridines.

7.3. Apoptosis detection assays and cell morphology visualization.

In order to shed some light into the mechanism by which our γ -lactam derivatives are able to inhibit the cell growth of cancer cells, some additional experiments were conducted using some of the most active substrates. First, flow cytometry assays were performed in order to determine whether these γ -lactam derivatives are capable of triggering the apoptosis mechanism by means of Annexin V-FITC apoptosis detection commercial kit. This assay allows to distinguish four separate cell populations after the cells are treated with the selected compound: live cells, early apoptotic live cells, late apoptotic dead cells (and non-apoptotic (necrotic) dead cells).

First, the apoptosis activation capability of the most active compound of C-4 unsubstituted substrates **72c** was evaluated in A549 cells at 12, 24, and 48 hours post-exposure and at 5 μ M concentration (Figure 65).

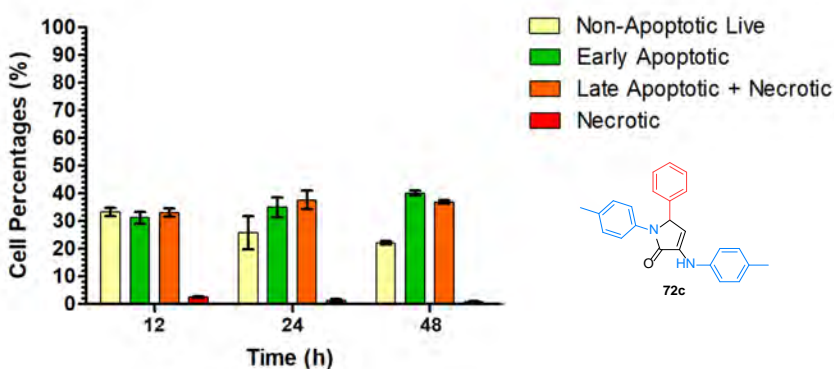


Figure 65. Percentages of non-apoptotic (yellow bars), early apoptotic (green bars), necrotic and late apoptotic (orange bars), and necrotic (red bars) A549 cells at 12, 24, and 48 hours after exposure to **72c**.

Each value represents the mean \pm SD of 3 measurements.

Early apoptotic cells were FL-1 positive and FL-3 negative, meaning that they had initialized the apoptotic process but were still alive at the time of the measurement. Percentages of these early-apoptotic cells after 12, 24, and 48 hours were, respectively, 31.17 ± 2.04 %, 34.97 ± 3.62 % and 40.13 ± 0.81 %. On the other hand, late apoptotic and necrotic cells were both FL-1 and FL-3 positive, meaning that they are able to activate the apoptotic machinery and were dead at the time of the measurement. Percentages of late-apoptotic and necrotic cells after 12, 24 and 48 hours were, respectively, 33.03 ± 1.43 %, 37.60 ± 3.37 % and 36.90 ± 0.70 % (Figure 65). Taken together, these results suggest that one of the main mechanisms by which **72c** induces cytotoxicity is based on the activation of intracellular apoptotic mechanisms. In fact, among all the dead cells detected, which were FL-1 positive, almost all

were simultaneously positive for the FL-3 channel too, while only a small percentage (2% or lower) of dead cells were exclusively FL-1 positive. Therefore, the majority of dead cells detected in this study were apoptotic cells. In addition, the total percentages of FL-3 positive cells, which comprised early and late apoptotic cells, were over 60%, and the percentage increased over time.

Next, the apoptosis triggering capability of the most active C-4 substituted γ -lactam **86n** was studied. However, since there was no much difference between the apoptosis percentage detected at different exposure times, this experiment was only conducted after 24 hours post-exposure in A549 cell line at 1 μ M concentration (Figure 66).

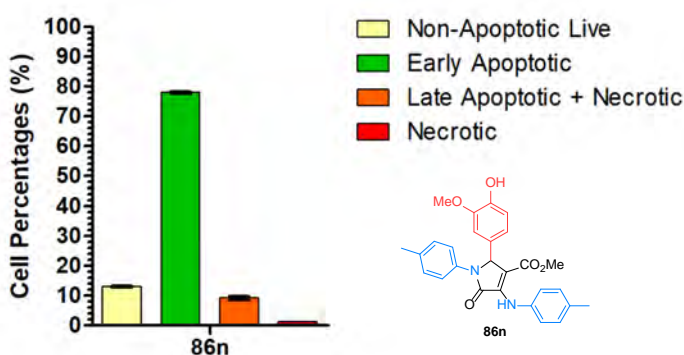


Figure 66. Percentages of non-apoptotic (yellow bars), early apoptotic (green bars), necrotic and late apoptotic (orange bars), and necrotic (red bars) A549 cells at 24 hours after exposure to the compounds **86n**. Each value represents the mean \pm SD of 3 measurements.

At the time of the measurement, around 80% of cells exposed to compound **86n** showed positive FL-1 signal and negative FL-3 signal, indicating an early apoptotic cell population. At this point, late apoptotic and necrotic cells were both FL-1 and FL-3 positive, with still low percentages below 10%. These results indicate that, within 24 hours after exposure to compound **86n**, 90% of cells had activated the apoptotic mechanisms. Necrotic cells that were non-apoptotic represented less than 1% of the whole cell population with both compounds, suggesting that the majority of dead cells detected in this study were apoptotic cells. Finally, non-apoptotic live cells represented around 12% of the whole cell population. These measurements revealed a higher capacity to induce apoptosis for C-4 substituted γ -lactam **86n** if compared to **72c**, even at lower concentrations.

Lastly, the same experiment was conducted using the most active bicyclic 1,4-dihydropyridine *cis*-**135u** in A549 cells after 24 hours post-exposure at 5 μ M concentration (Figure 67).

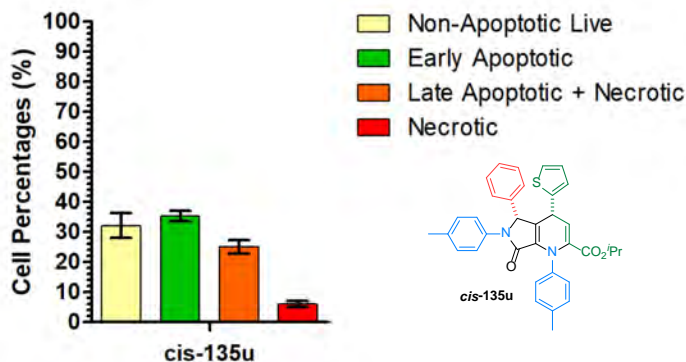


Figure 67. Percentages of non-apoptotic (yellow bars), early apoptotic (green bars), necrotic and late apoptotic (orange bars), and necrotic (red bars) A549 cells at 24 hours after exposure to the compounds *cis-135u*. Each value represents the mean \pm SD of 3 measurements.

In this case, the percentage of the living cells (FL-1 and FL-3 negative) represented more than 30% of the total population, and only around 35% of cells exposed to compound *cis-135u* showed positive FL-1 signal and negative FL-3 signal, indicating an early apoptotic cell population. With respect to late apoptotic and necrotic cells (FL-1 and FL-3 positive), the obtained percentage was around 26%. Additionally, non-apoptotic necrotic cells (FL-1 negative, FL-3 positive), represented almost 6% of the total population. The obtained results indicate that, after 24 hours of exposure to 1,4-dihydropyridine *cis-135u* at 5 μ M concentration, around 60% of cells had activated the apoptotic mechanisms. This result is far away from that measured for compound **86n** (Figure 66) even if the experiment is performed at higher concentrations. Furthermore, these values are similar to the results obtained at 24 hours after exposure to γ -lactam **72c**, which is used as starting material for the preparation of *cis-135u*, at the same concentration, even if *cis-135u* has a 2.6 times more potent cytotoxic activity.

Next, the morphologic changes in A549 cell line were analyzed at different exposure times after the addition of the most cytotoxic γ -lactam **86n** at three different concentrations, in order to visualize the cellular changes during the treatment (Figure 68 in Pages 172-173).

The first studied concentration was 1.1 μ M, which is a ten-fold higher concentration of the IC_{50} of γ -lactam **86n**. At that high concentration, a disruption of the cellular growth was noticed, especially after 6 hours of exposure, and the suspension of cellular growth was gradually more pronounced over the time (Figure 68, a). Then, the IC_{50} concentration of **86n** was used (0.11 μ M) for this experiment, and the peak of cellular death was observed at 24 or 48 hours after the addition of the cytotoxic substrate, then live cells started growing again, witnessing higher cellular confluence after 72 hours (Figure 68, b). On the contrary, upon the addition of **86n** at 0.02 μ M, a five-fold lower concentration

than the measured IC_{50} , showed cells with a healthy, uniform morphology and cellular growth was recognizable over time, suggesting that this concentration was well tolerated (Figure 68, c).

In conclusion, the cytotoxic activity of the compounds synthesized in this thesis has been evaluated against several cancer cell lines. In general terms, the obtained γ -lactam derivatives showed *in vitro* cytotoxicity, especially towards A549 (carcinomic human alveolar basal epithelial cell) cell line, while SKOV3 (human ovarian carcinoma) and RKO (human colon epithelial carcinoma) cell lines were found to be more resistant. In addition, low activity toward MRC5 non-malignant lung fibroblasts is typically observed. This study also showed that the substituent at the C-5 of the γ -lactam ring is essential for the cytotoxic activity. Furthermore, the most active C-4 non-substituted γ -lactam derivative was compound **72c**, showing an IC_{50} value of 2.34 μ M in A549 cell line, and a very high selectivity if compared with MRC5 cell line. With respect to C-4 substituted γ -lactam derivatives, better antiproliferative activities are obtained when an ester group is present at C-4 of the 5-membered heterocycle, in contrast to tetrahedral phosphonate or phosphine oxide moiety. The most active compound, **86n**, provides excellent IC_{50} values of 0.11 and 1.23 μ M in A549 and SKOV3 cell lines, with a high selectivity towards non-malignant cells. Even more, the two enantiomers of γ -lactam **90a** have been evaluated separately and no difference was observed between them separately and the racemic substrate. In addition, the activity of bicyclic 1,4-dihydropyridines **135** was also evaluated, measuring the best result for *cis*-**135u**, which has IC_{50} values of 0.89 and 11.90 μ M in A549 and SKOV3 cell lines. Finally, it has also been evidenced that the main mechanism by which γ -lactams derivatives induce cytotoxicity towards cancer cells is based on the activation of intracellular apoptotic mechanisms.

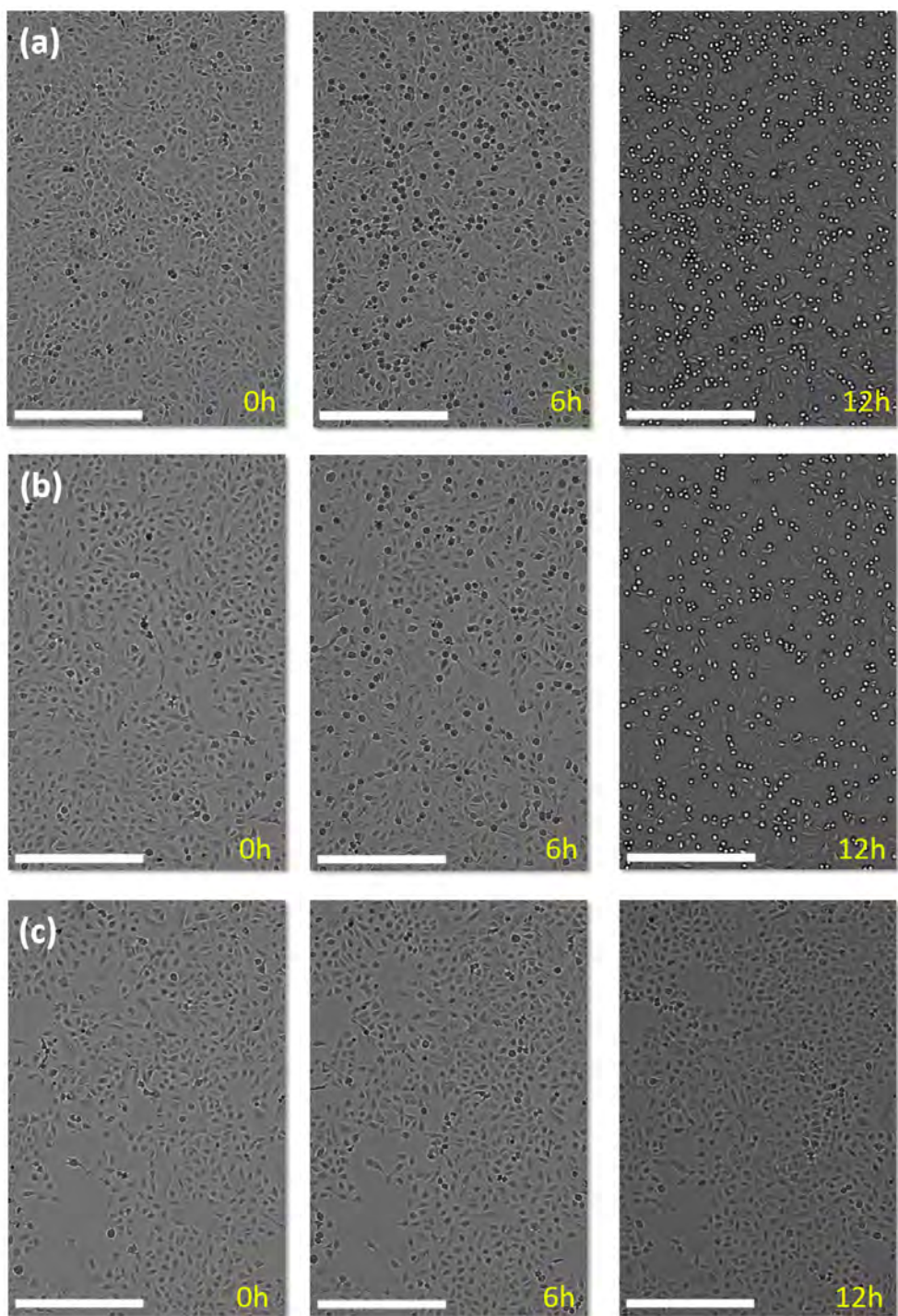
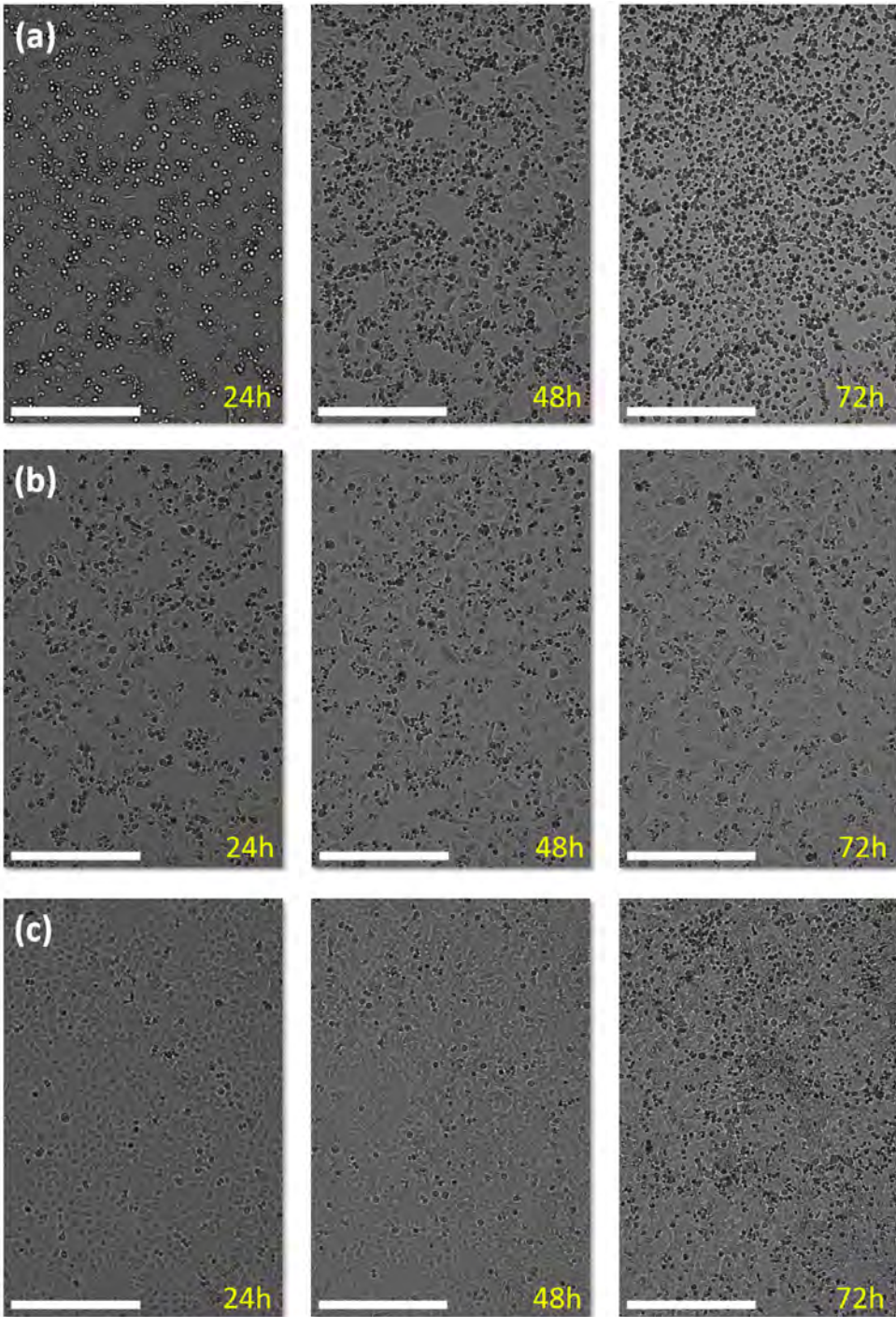


Figure 68. Cell morphology visualization with X4 lens at 0, 6, 12, 24, 48 and 72 hours after exposure to compound **86n**. Scale bar: 300 μm . (a) A549 cells treated with 1.1 μM of **86n**. (b) A549 cells treated with 0.11 μM of **86n**. (c) A549 cells treated with 0.02 μM of **86n**.



Chapter 8

Evaluation of γ -lactam derivatives as inhibitors of MDM2/MDMX-p53 interaction

In the last part of this thesis, the goal will be to determine the mechanism of the biological action of the synthesized γ -lactam derivatives at a molecular level, in order to try to establish more evidence on the relation between the antiproliferative activity and the apoptosis induction mechanisms. For this purpose, the ability of these γ -lactams to inhibit the MDM2/MDMX-p53 protein-protein interaction was studied, considering that there are multiple examples in the literature of similar substrates with this capability (Figure 18, *vide supra*).

8.1. Expression and purification of MDM2 and MDMX.

Recombinant human proteins were expressed in *Escherichia coli* (*E. coli*) since it is the simplest and most employed expression system, which offers several advantages, such as fast growth, low costs and straightforward procedures with high yield.²²⁸ The target proteins were expressed either in a soluble form, in the case of MDMX (1-134 amino acid residues), or as inclusion bodies (non-soluble form) in the case of MDM2 (18-125 amino acid residues), and purified in native or denatured conditions followed by the refolding. A modified procedure of the one described by Stoll²²⁹ and Popowicz²³⁰ was followed in order to achieve the expression and purification of the p53 binding domains of MDM2 and MDMX proteins. The protocols are described in detail in Experimental Section II.

The final step of the purification process for both, MDM2 and MDMX protein constructs, consisted of a gel filtration on HiLoad 16/600 S75 pg (120 mL volume) connected to ÄKTA Pure system using *Assay Buffer*. In addition, the purity of the protein was monitored at each step by SDS-PAGE. The

²²⁸ (a) Rosano, G. L.; Morales, E. S.; Ceccarelli, E. A. *Protein Sci.* **2019**, *28*, 1412-1422. (b) Rosano, G. L.; Ceccarelli, E. A. *Front. Microbiol.* **2014**, *5*, 1-17.

²²⁹ Stoll, R.; Renner, C.; Hansen, S.; Palme, S.; Klein, C.; Belling, A.; Zeslawski, W.; Kamionka, M.; Rehm, T.; Mühlhahn, P.; Schumacher, R.; Hesse, F.; Kaluza, B.; Voelter, W.; Engh, R. A.; Holak, T. A. *Biochemistry* **2001**, *40*, 336-344.

²³⁰ Popowicz, G. M.; Czarna, A.; Rothweiler, U.; Szwagierczak, A.; Krajewski, M.; Weber, L.; Holak, T. A. *Cell Cycle* **2007**, *6*, 2386-2392.

obtained chromatograms and the results of SDS-PAGE for MDM2 and MDMX proteins are presented below (Figure 69).

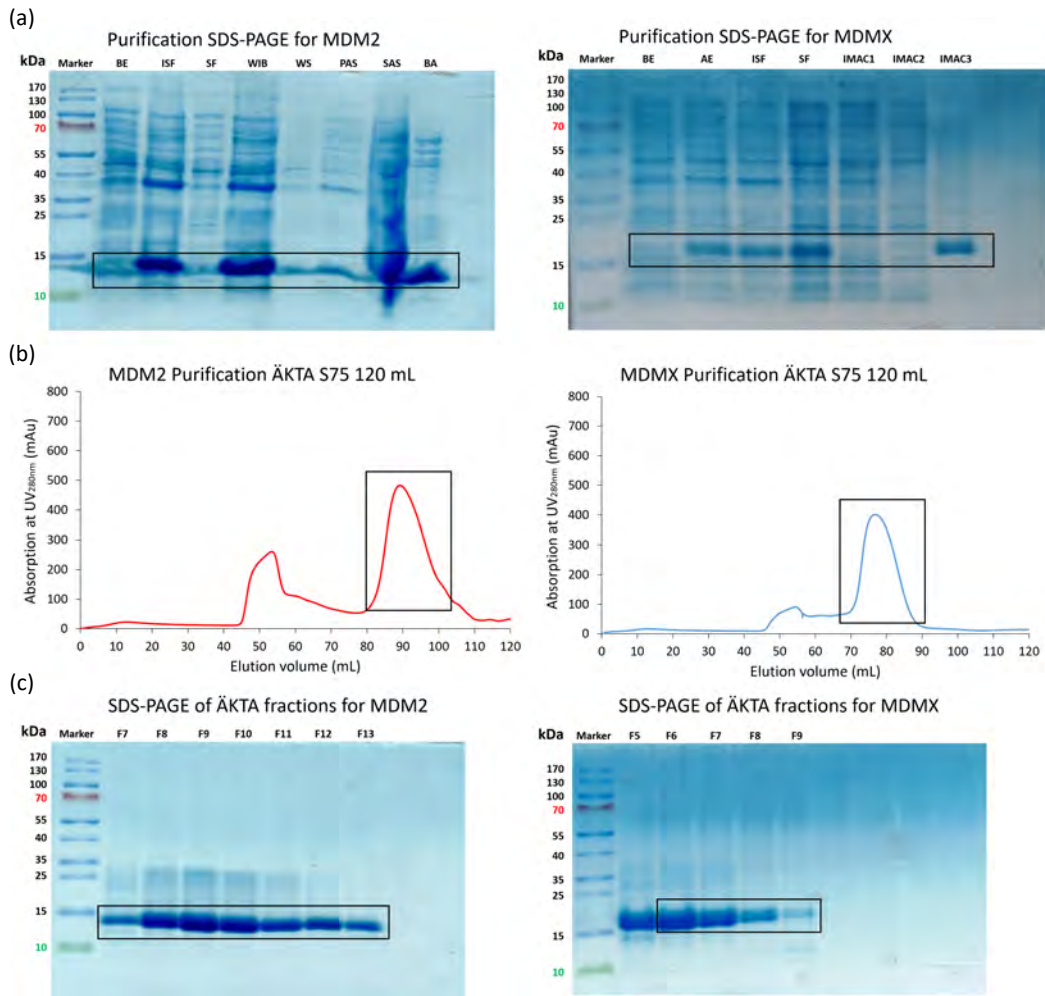


Figure 69. (a) SDS-PAGE of the different purification steps. Samples collected: Before Expression (BE), After Expression (AE), Insoluble Fraction (ISF) and Soluble Fraction (SF) obtained after sonication, Washed Inclusion Bodies (WIB) and Washed Supernatant (WS) with Triton X-100, Pellet After Solubilisation (PAS), Supernatant After Solubilisation (SAS) with Guanidine Hydrochloride, and Before ÄKTA (BA) fraction with the refolded protein and after hydrophobic interaction chromatography (HIC, butyl sepharose), IMAC1-3 which are different fractions of MDMX after Immobilized Metal Affinity Chromatography (IMAC).

(b) Chromatograms of MDM2 and MDMX after gel filtration in *Assay Buffer* at HiLoad 16/600 S75 pg column (MDM2 peak around 90 ml and MDMX peak around 77 ml). (c) SDS-PAGE of the different fractions collected in ÄKTA.

Finally, in order to estimate the proper folding of both proteins, one-dimensional ^1H NMR spectra were recorded (Figure 70). The manifestation of a large signal dispersion at the aliphatic region of the spectrum (between $\delta_{\text{H}} = 1.0$ and -1.0 ppm) *versus* a steep flank of the dominant peaks at approximately $\delta_{\text{H}} = 1$ ppm differentiates a structured protein from a disordered one.²³¹ Indeed, the signals are dispersed due to the different chemical environments, causing the distribution of the chemical shifts of single protons over a wider range of frequencies when the protein is folded.

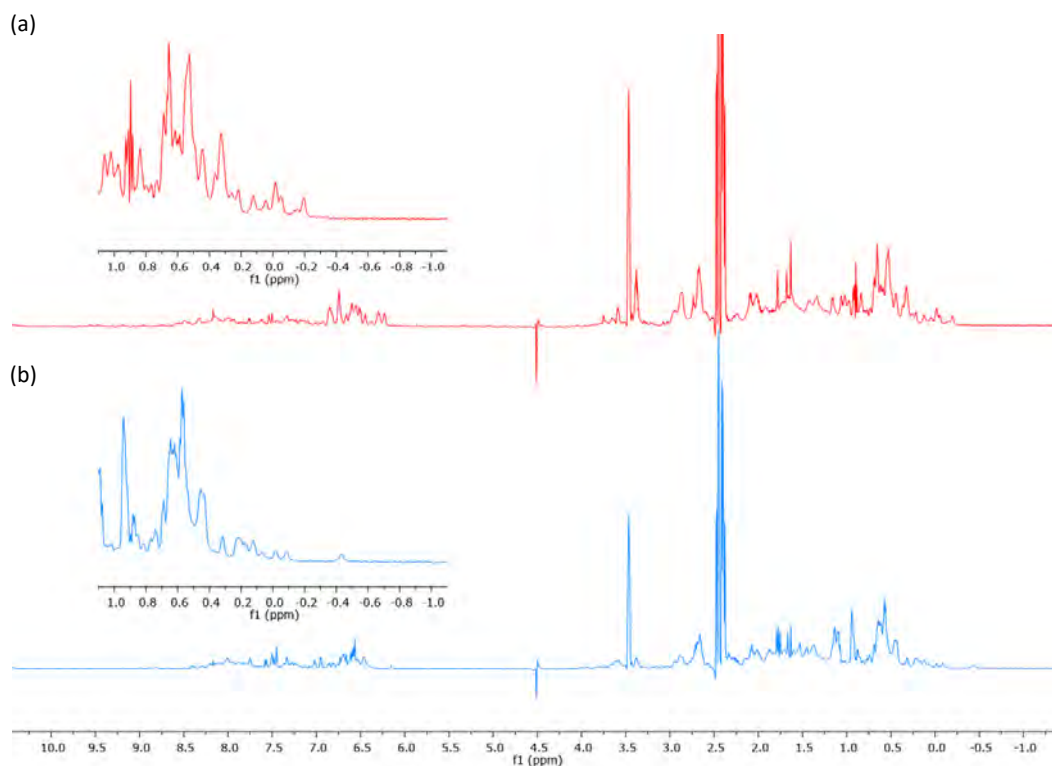


Figure 70. (a) ^1H NMR spectrum of MDM2 (18-125). (b) 1D ^1H NMR spectrum of MDMX (1-134).

Taking into account the aforementioned and, observing the ^1H NMR spectra of MDM2 and MDMX proteins (Figure 70), it can be concluded that it is confirmed the presence of the properly folded protein in solution.

In order to provide solid evidences of the MDM2/MDMX-p53 PPI inhibition capability of the γ -lactam derivatives, a multistep methodology was followed, first with Differential Scanning Fluorimetry (DSF) and then using Fluorescence Polarization (FP) assays.

²³¹ Rehm, T.; Huber, R.; Holak, T. A. *Structure* **2002**, *10*, 1613-1618.

8.2. Differential Scanning Fluorimetry (DSF) assay.

DSF is an inexpensive and rapid screening method which allows to identify low-molecular-weight ligands that bind and stabilize (or destabilize) purified proteins. This assay is best performed using a conventional real-time PCR thermal cycler, where ligand solutions are added into the wells of a PCR plate containing a solution of protein and fluorescent dye, in order to determine the thermal unfolding of proteins as the temperature is gradually increased.²³² This experiment can be applied to a wide range of proteins²³³ including MDM2 and MDMX.²³⁴

The used fluorescent dyes, like *SYPRO orange* (SO), are highly fluorescent in a non-polar environment, if compared to aqueous solutions, where the fluorescence is quenched. The temperature at which the protein unfolds (melting temperature, T_m) is measured by an increase in the fluorescence of the dye, which has a high affinity for the hydrophobic parts of the protein, which are exposed when the protein unfolds (Figure 71, a). Regarding the intensity of the peak, once the protein is completely unfolded, a gradual decrease should be observed, due to the elimination of the protein from the solution owing to precipitation and aggregation. So, in DSF, the fluorescence intensity is plotted as a function of temperature, plotting a sigmoidal curve.

The inflection point of the transition curve (T_m) is calculated using the Boltzmann equation (Figure 71, c), where F_{min} and F_{max} are the values of minimum and maximum intensities, respectively. However, the simplest method for the calculation of T_m value is the determination of the maximum of the first derivative of the curve of the fluorescence *versus* temperature (Figure 71, b).

Several factors can influence the stability of the protein, such as generic ingredients (buffers, salts and detergents) with non-specific interactions, or also ligands, which bind to the protein at a specific site. In addition, protein-ligand interactions can also affect the protein unfolding temperature (T_m). Thus this assay can be of high value for identifying allosteric effectors, which is the starting point in the development drug candidates.

²³² (a) Gao, K.; Oerlemans, R.; Groves, M. R. *Biophys. Rev.* **2020**, *12*, 85-104. (b) Niesen, F. H.; Berglund, H.; Vedadi, M. *Nat. Protoc.* **2007**, *2*, 2212-2221.

²³³ Ericsson, U. B.; Hallberg, B. M.; DeTitta, G. T.; Dekker, N.; Nordlund, P. *Anal. Biochem.* **2006**, *357*, 289-298.

²³⁴ (a) Anil, B.; Riedinger, C.; Endicott, J. A.; Noble, M. E. M. *Acta Crystallogr. Sect. D Biol. Crystallogr.* **2013**, *69*, 1358-1366. (b) Kallen, J.; Goepfert, A.; Blechschmidt, A.; Izaac, A.; Geiser, M.; Tavares, G.; Ramage, P.; Furet, P.; Masuya, K.; Lisztwan, J. *J. Biol. Chem.* **2009**, *284*, 8812-8821.

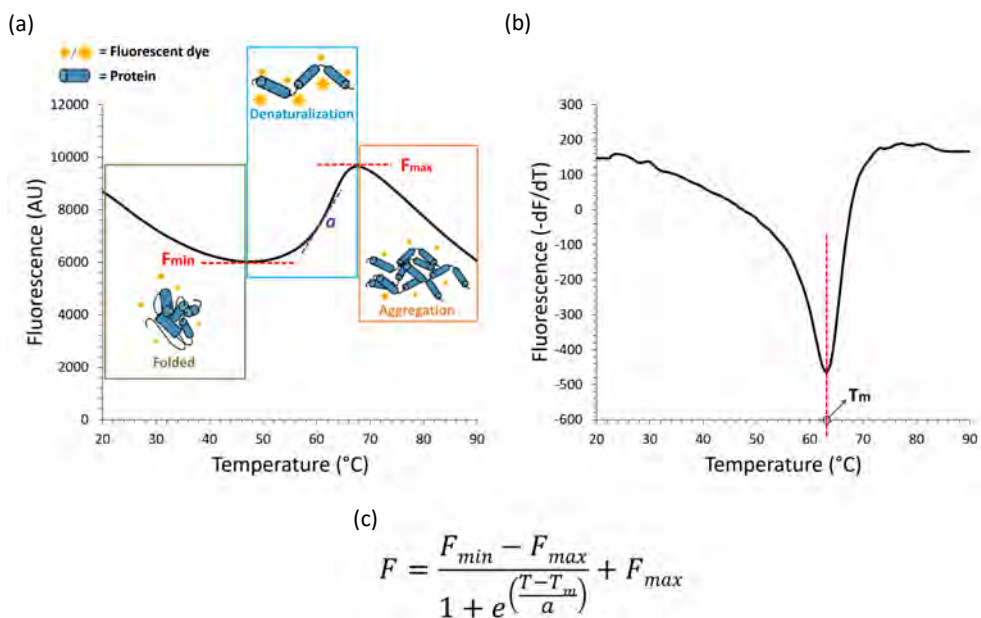


Figure 71. (a) Typical recording of the process and of the fluorescence intensity vs. temperature for the unfolding of protein in the presence of SYPRO orange. (b) Boltzmann equation. (c) Curve with the first derivative of the fluorescence vs. temperature.

The stability of a protein is related to its Gibbs free energy of unfolding (ΔG_u), which is temperature-dependent. When the temperature increases, the ΔG_u decreases and it will become zero at the equilibrium, where the concentrations of folded and unfolded protein are equal, considering this temperature as the melting temperature (T_m).²³⁵ If a ligand binds to a protein, the free energy contribution of ligand binding affects the ΔG_u value, which may result in an increment in the T_m if the compound stabilizes the protein, or in a drop in the melting temperature if the compound destabilizes the protein.

It has been reported that the stabilizing effect is proportional to the affinity of the ligands to the protein. However, interpretations regarding thermodynamics need to be conducted with caution and confirmed by other methods.²³²

In order to evaluate whether the γ -lactam derivatives described in this thesis are able to alter the T_m of the MDM2 and MDMX proteins, first, the ideal concentrations of the protein and *Sypro Orange* required to obtain the best fluorescent signal and the T_m value of the protein without compound, need to be identified. For this reason, DSF experiments were accomplished using sixteen combinations with different concentrations of protein (MDM2 or MDMX) and *Sypro Orange* (Figures 72 and 73).

²³⁵ Schellman, J. A. *Biophys. J.* **1997**, *73*, 2960-2964.

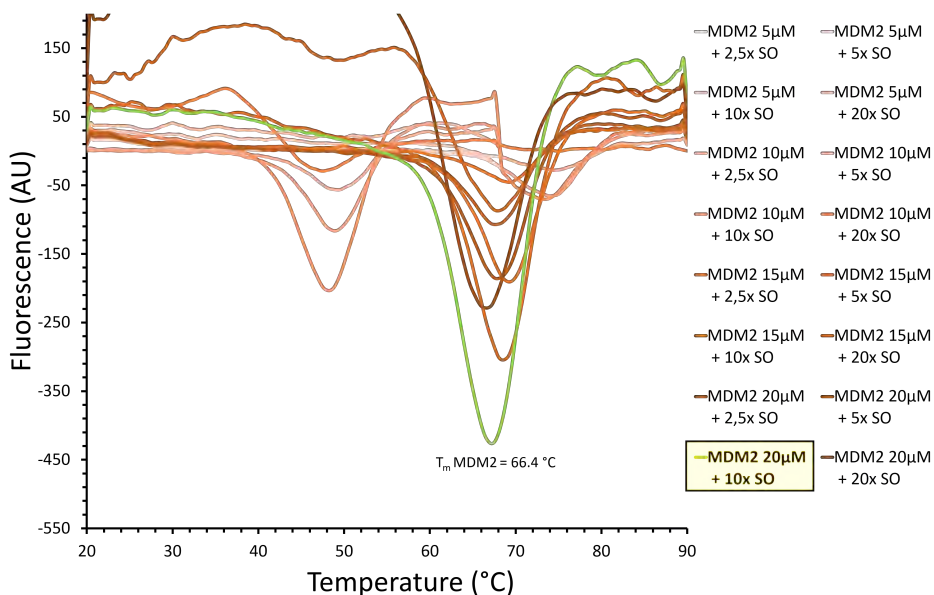


Figure 72. Melting curve of MDM2 with different combinations of concentration of protein and SO.

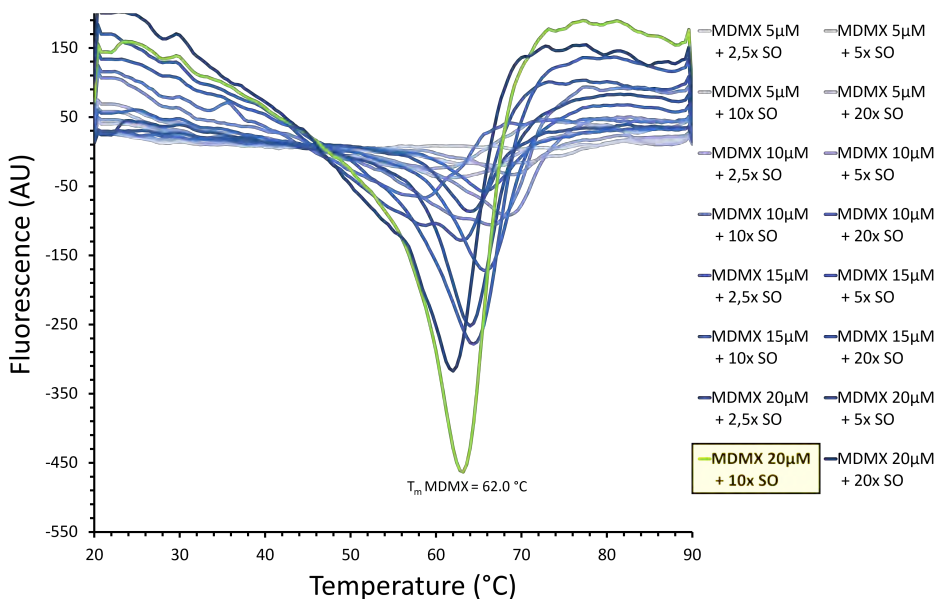


Figure 73. Melting curve of MDMX with different combinations of concentration of protein and SO.

As shown in Figures 72 and 73, the optimal concentration of the protein and fluorescent dye needed to obtain the best fluorescent signal are the same, which is 20 μM of the corresponding protein and 10x of SYPRO Orange. In addition, the measured melting temperature for MDM2 ($T_{m \text{ MDM2}}$) was 66.4 $^{\circ}\text{C}$, and 62.0 $^{\circ}\text{C}$ for MDMX ($T_{m \text{ MDMX}}$).

With the optimized conditions for the DSF assay in hands, next, the screening of 70 γ -lactam derivatives was carried out. The compounds were tested as singletons at 100 μ M final concentration, and, since the tested compounds are dissolved in DMSO, protein with the same concentration of DMSO (0.2% v/v) was used as control. The melting point of MDM2 was only slightly affected by the presence of DMSO ($T_{m, \text{MDM2+DMSO}} = 66.2$ °C) and the melting point of MDMX was not altered ($T_{m, \text{MDMX+DMSO}} = 62.0$ °C).

DSF positive hits were defined as compounds that increase or decrease the melting point of MDM2 or MDMX by at least 1 °C. The ΔT_m value of each compound is calculated by subtracting the T_m value of the protein to the T_m value of the compound ($\Delta T_m = T_m - T_{m, \text{Prot.+DMSO}}$). For this experiment, Nutlin-3a was used as positive control, which stabilizes MDM2 protein. The results are summarized in Figures 74 and 75.

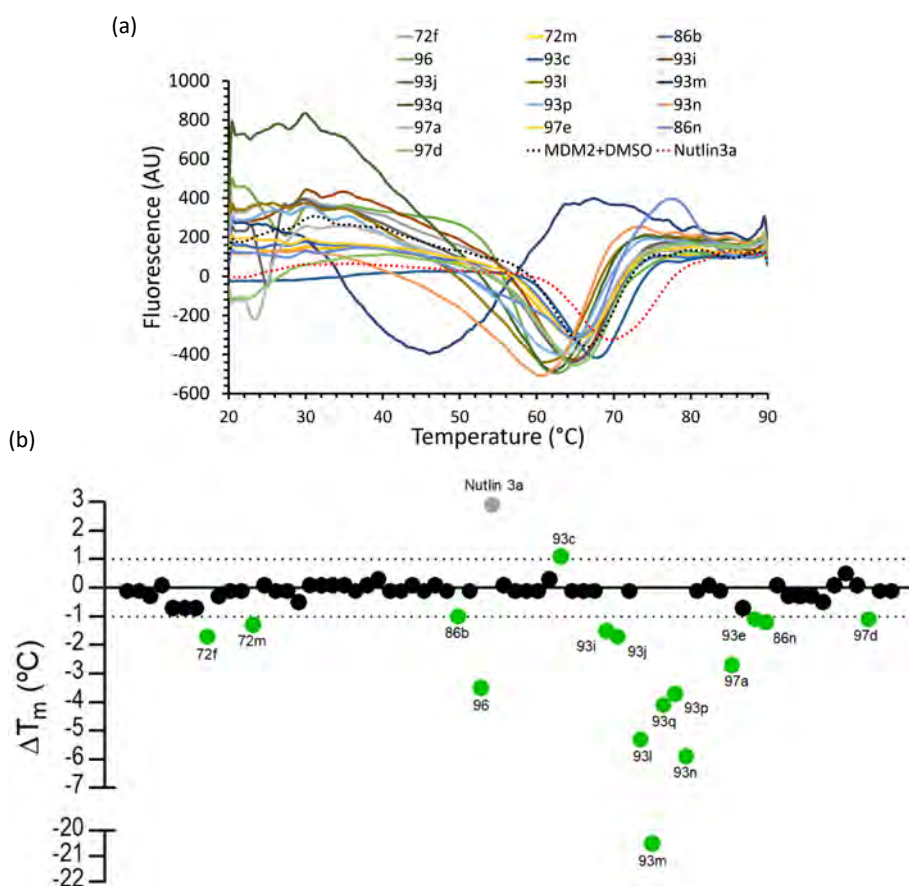


Figure 74. DSF results for MDM2. (a) Melting curves of MDM2. Only the positive hits ($\Delta T_m = \pm 1$ °C) are shown. (b) Hit identification. Schematic representation of the ΔT_m values of the tested compounds with MDM2 protein.

As shown in Figure 74 and in Table 25, sixteen γ -lactams were identified as positive hits against MDM2. Among C-4 unsubstituted 3-amino-1,5-dihydro-2H-pyrrol-2-ones **72**, **84**, **86** and **90**, only two hits were identified, **72f** and **72m**, with ΔT_m values of -1.7 ± 0.3 and -1.3 ± 0.1 °C respectively, both of them destabilizing the protein (Table 25, Entries 1-2). C-4 Benzyl or methyl carboxylate substituted enamines **86b** and **86n** also showed to be destabilizing compounds, with ΔT_m -1.0 ± 0.0 and -1.2 ± 0.2 °C (Table 25, Entries 3-4). However, the majority of the hits, twelve, were 3-hydroxy substituted derivatives **93**, **96** and **97** (Table 25, Entries 5-16). Within this group of compounds, **93m** appeared to be the strongest destabilizing compound with a ΔT_m value of -20.5 ± 1.5 °C (Table 25, Entry 9). Unfortunately, there was only a single compound that stabilizes the protein, γ -lactam **93c**, with a positive ΔT_m of 1.1 ± 0.1 °C (Table 25, Entry 5).

Table 25. ΔT_m values of the hits obtained in DSF assay with MDM2.



72-97

Entry	Prod.	X	R ¹	R ²	R ³	ΔT_m (°C)
1	72f	NH-4-MeC ₆ H ₄	4-MeC ₆ H ₄	4-FC ₆ H ₄	H	-1.7 ± 0.3
2	72m	NH-4-MeC ₆ H ₄	4-MeC ₆ H ₄	2-Naphtyl	H	-1.3 ± 0.1
3	86b	NH-4-MeC ₆ H ₄	4-MeC ₆ H ₄	4-NO ₂ C ₆ H ₄	Bn	-1.0 ± 0.0
4	86n	NH-4-MeC ₆ H ₄	4-MeC ₆ H ₄	4-OH-3-MeOC ₆ H ₄	CO ₂ Me	-1.2 ± 0.2
5	93c	OH	4-MeC ₆ H ₄	4-NO ₂ C ₆ H ₄	P(O)(OEt) ₂	$+1.1 \pm 0.1$
6	93i	OH	4-MeC ₆ H ₄	Ph	P(O)(<i>i</i> Pr) ₂	-1.5 ± 0.3
7	93j	OH	4-MeC ₆ H ₄	4-FC ₆ H ₄	P(O)(<i>i</i> Pr) ₂	-1.7 ± 0.1
8	93l	OH	4-MeC ₆ H ₄	Ph	P(O)(Ph) ₂	-5.3 ± 0.1
9	93m	OH	4-MeC ₆ H ₄	C ₆ F ₅	P(O)(Ph) ₂	-20.5 ± 1.5
10	93n	OH	4-MeC ₆ H ₄	4-FC ₆ H ₄	P(O)(Ph) ₂	-5.9 ± 0.7
11	93p	OH	4-MeOC ₆ H ₄	Ph	P(O)(Ph) ₂	-3.7 ± 0.7
12	93q	OH	4-MeC ₆ H ₄	Ph	P(O)(Ph) ₂	-4.1 ± 0.5
13	96	OH	4-MeC ₆ H ₄	Ph	P(O)(OH) ₂	-3.5 ± 0.1
14	97a	OH	4-MeC ₆ H ₄	Ph	CO ₂ Me	-2.7 ± 0.3
15	97d	OH	Bn	4-CF ₃ C ₆ H ₄	CO ₂ Me	-1.1 ± 0.1
16	97e	OH	4-MeC ₆ H ₄	3-MeOC ₆ H ₄	CO ₂ Me	-1.1 ± 0.1

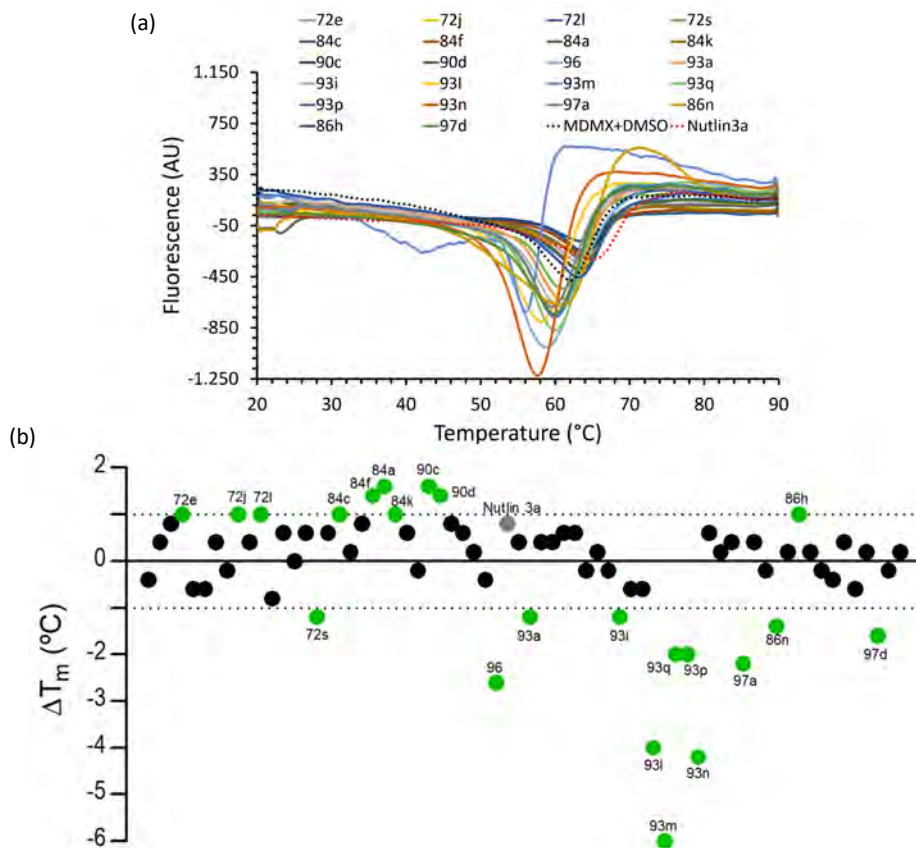
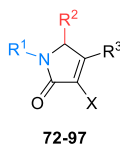


Figure 75. DSF results for MDMX. (a) Melting curves of MDMX. Only the positive hits ($\Delta T_m = \pm 1$ °C) are shown. (b) Hit identification. Schematic representation of the ΔT_m values of the tested compounds with MDMX protein.

In the case of MDMX, (Figure 75 and Table 26) twenty-two positive hits were identified. Almost half of those hits were obtained among the C-4 unsubstituted 3-amino-1,5-dihydro-2H-pyrrol-2-ones **72**, **84**, **86** and **90** (Table 26, Entries 1-10). All of these compounds, except γ -lactam **72s**, with a ΔT_m value of -1.2 ± 0.2 °C (Table 26, Entry 4), stabilized the protein, and compounds **84a** and **90c** appeared to be the strongest stabilizing molecules with ΔT_m values of 1.6 ± 0.0 and 1.6 ± 0.2 °C (Table 26, Entries 5 and 9). Amidst C-4 substituted enamine derivatives, γ -lactams **86n** and **86h** were detected as a hits, with a ΔT_m value of -1.4 ± 0.2 and $+1.0 \pm 0.0$ °C respectively (Table 26, Entries 11-12). Enol-derived γ -lactams **93**, **96** and **97**, gave also some positive hits. However, most of those compounds showed to be destabilizers of MDMX protein (Table 26, Entries 13-22), being **93m** the strongest destabilizing substrate with a ΔT_m value of -6.0 ± 0.4 °C (Table 26, Entry 16).

Table 26. ΔT_m values of the hits obtained in DSF assay with MDMX.

Entry	Prod.	X	R ¹	R ²	R ³	ΔT_m (°C)
1	72e	NH-4-MeC ₆ H ₄	4-MeC ₆ H ₄	3-NO ₂ C ₆ H ₄	H	+1.0 ± 0.2
2	72j	NH-4-MeC ₆ H ₄	4-MeC ₆ H ₄	6-(N-Me-indolyl)	H	+1.0 ± 0.2
3	72l	NH-4-MeC ₆ H ₄	4-MeC ₆ H ₄	2-Thienyl	H	+1.0 ± 0.0
4	72s	NH-4-MeC ₆ H ₄	4-MeC ₆ H ₄	CO ₂ Et	H	-1.2 ± 0.2
5	84a	NH-4-MeOC ₆ H ₄	4-MeOC ₆ H ₄	4-NO ₂ C ₆ H ₄	H	+1.6 ± 0.0
6	84c	NH-4-BrC ₆ H ₄	4-BrC ₆ H ₄	4-NO ₂ C ₆ H ₄	H	+1.0 ± 0.4
7	84f	NH-4-ClC ₆ H ₄	4-ClC ₆ H ₄	4-NO ₂ C ₆ H ₄	H	+1.4 ± 0.2
8	84k	NH-3-CF ₃ C ₆ H ₄	3-CF ₃ C ₆ H ₄	4-NO ₂ C ₆ H ₄	H	+1.0 ± 0.2
9	90c	NH-4-MeC ₆ H ₄	4-MeC ₆ H ₄	CH ₂ P(O)(Ph) ₂	H	+1.6 ± 0.2
10	90d	NH-4-MeC ₆ H ₄	4-MeC ₆ H ₄	C ₆ F ₅	H	+1.4 ± 0.4
11	86n	NH-4-MeC ₆ H ₄	4-MeC ₆ H ₄	4-OH-3-MeOC ₆ H ₄	CO ₂ Me	-1.4 ± 0.2
12	86h	NH-4-MeC ₆ H ₄	4-MeC ₆ H ₄	4-CF ₃ C ₆ H ₄	CO ₂ Me	+1.0 ± 0.0
13	93a	OH	4-MeC ₆ H ₄	Ph	P(O)(Et) ₂	-1.2 ± 0.4
14	93i	OH	4-MeC ₆ H ₄	Ph	P(O)(<i>i</i> Pr) ₂	-1.2 ± 0.2
15	93l	OH	4-MeC ₆ H ₄	Ph	P(O)(Ph) ₂	-4.0 ± 0.6
16	93m	OH	4-MeC ₆ H ₄	C ₆ F ₅	P(O)(Ph) ₂	-6.0 ± 0.4
17	93n	OH	4-MeC ₆ H ₄	4-FC ₆ H ₄	P(O)(Ph) ₂	-4.2 ± 0.4
18	93p	OH	4-MeOC ₆ H ₄	Ph	P(O)(Ph) ₂	-2.0 ± 0.2
19	93q	OH	2-FC ₆ H ₄	Ph	P(O)(Ph) ₂	-2.0 ± 0.4
20	96	OH	4-MeC ₆ H ₄	Ph	P(O)(OH) ₂	-2.6 ± 0.4
21	97a	OH	4-MeC ₆ H ₄	Ph	CO ₂ Me	-2.2 ± 0.2
22	97d	OH	Bn	4-CF ₃ C ₆ H ₄	CO ₂ Me	-1.6 ± 0.0

In summary, more hits were obtained for MDMX protein than for MDM2 (Table 25 vs. Table 26). In addition and, taking into account that the ideal compounds are those that are able to stabilize the protein, there are also more stabilizing compounds for MDMX than for MDM2. Both, enol and enamine-derived γ -lactams proved to be able to modify the T_m of both proteins. However, it must be pointed that, in general, there are more hits for γ -lactams with phosphoryl moiety than for those holding a carboxyl group at C-4. Indeed, with respect to phosphorylated moieties, surprisingly, phosphine oxide seems to be a better option than phosphonate. Finally, compounds **86n**, **93i**, **93l**, **93m**, **93n**, **93p**, **93q**, **96**, **97a**, and **97d** where all considered as positive hits for both proteins.

Once the screening was performed and the compounds, which cause no effect in the ΔT_m value of MDM2 and MDMX proteins, were discarded, the positive hits were subjected to Fluorescence Polarization (FP) assays in order to determine the inhibition constant (K_i) towards MDM2 and MDMX proteins.

8.3. Fluorescence Polarization (FP) assay.

The fluorescence Polarization (FP) assay technique is based on the property whereby, when a fluorescently labeled molecule is excited by polarized light, it emits light with a degree of polarization that is inversely proportional to the rate of molecular rotation. This can be used to measure the interaction of a small labeled ligand with a larger protein and provides a basis for direct and competition binding assays, which is particularly valuable in screening for inhibitors of protein-protein interactions.²³⁶ The principle of fluorescence polarization is depicted in Figure 76.

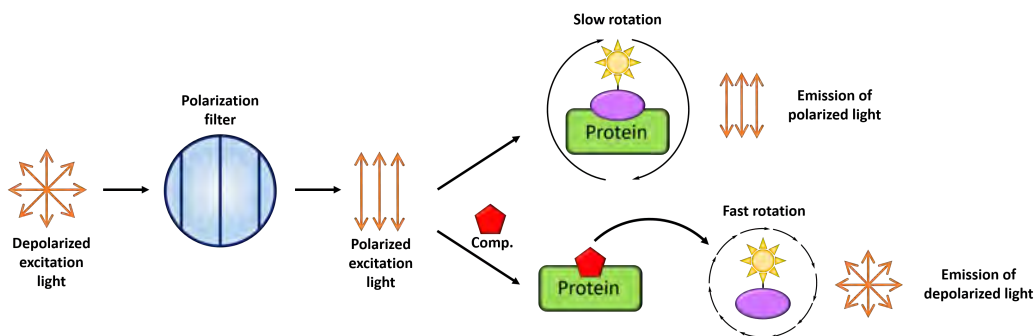


Figure 76. The basic principle of fluorescence polarization.

When a small ligand, such as a peptide with an attached fluorophore, is excited by polarized light, the emitted light will be largely depolarized due to the rapid molecular rotation of the labeled species. However, if the labeled ligand is bonded to a high-molecular-weight protein (>10 kDa), the emitted light will be still polarized to a significant degree, due to the significantly reduced rotational speed of the complex. Thus, this assay is used to measure the binding capability of potential ligands, since the measured polarized light in a mixture of a labeled ligand and a receptor is proportional to the fraction of bonded ligand. So, it is straightforward to establish a competition binding assay, where a drop in the signal of the polarized light is detected if an inhibitor is added to the mixture of labeled ligand and binds to the receptor.²³⁷

²³⁶ Moerke, N. J. *Curr. Protoc. Chem. Biol.* **2009**, *1*, 1-15.

²³⁷ (a) Jameson, D.; Croney, J. *Comb. Chem. High Throughput Screen.* **2003**, *6*, 167-176. (b) Jameson, D. M.; Seifried, S. E. *Methods A Companion to Methods Enzymol.* **1999**, *19*, 222-233.

First, the K_d values of the high-affinity p53-derived peptide FAM-P2 (sequence LTFEHWQAQLTS), labeled with carboxyfluorescein, towards MDM2 and MDMX proteins were determined in the presence of 5% DMSO. For this purpose, 10 nM solutions of the FAM-P2 peptide were treated with serial dilutions of each protein (ranging from 750 to 0.012 nM for MDM2 and from 3750 to 0.10 nM for MDMX). Fluorescence polarization was established *via* binding equation for 1:1 complex formation (Figure 77, a), where FP is the determined value of fluorescence polarization, FP_{min} is the fluorescence polarization value for ligand only, FP_{max} is the fluorescence polarization at protein concentration saturating the ligand, and c the protein concentration. The calculated K_d value for MDM2 was 5.47 ± 0.67 nM (Figure 77, b) and for MDMX was 13.89 ± 1.59 nM (Figure 77, c). The obtained results were in agreement with the literature data.²³⁸

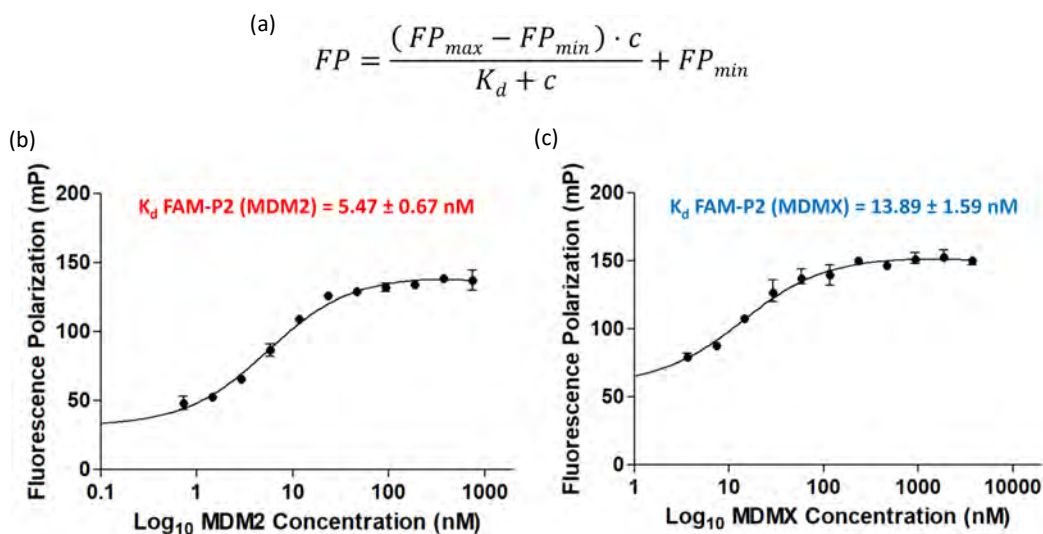


Figure 77. (a) Binding equation to determine fluorescence polarization. (b) FP binding curve of FAM-P2 for MDM2. (c) FP binding curve of FAM-P2 for MDMX.

Then, the optimal concentrations of the protein to perform the FP assays were selected according to Huang and coworkers, choosing the concentration of protein at FP = 80%.²³⁹

Once the binding affinity values for the fluorescent peptide towards MDM2 and MDMX and the optimal concentrations of protein were determined, competitive binding assays were performed with the obtained positive hits in DSF, that is, sixteen for MDM2 and twenty-two for MDMX, at a concentration ranging from 2 mM to 2 μ M and using Nutlin-3a as the positive control. The inhibition constant (K_i) values of the γ -lactam derivatives were elaborated using the equations shown in Figure

²³⁸ Czarna, A.; Popowicz, G. M.; Pecak, A.; Wolf, S.; Dubin, G.; Holak, T. A. *Cell Cycle* **2009**, *8*, 1176-1184.

²³⁹ Huang, X. J. *Biomol. Screen.* **2003**, *8*, 34-38.

78a, where x and y are the values of each axis at 50% of the binding, FP_{max} and FP_{min} belonging to the values of the upper and down plateaus, c is the concentration of the used affinity peptide (10 nM) and K_d is the binding affinity of the FAM-P2 peptide with the protein (5.5 nM for MDM2 and 13.9 nM for MDMX calculated above).

$$(a) \quad \log EC_{50} = \log\left(10^{\log K_i} \cdot \left(\frac{1+c}{K_d}\right)\right)$$

$$y = FP_{min} + \frac{FP_{max} - FP_{min}}{1 + 10^{(x - \log EC_{50})}}$$

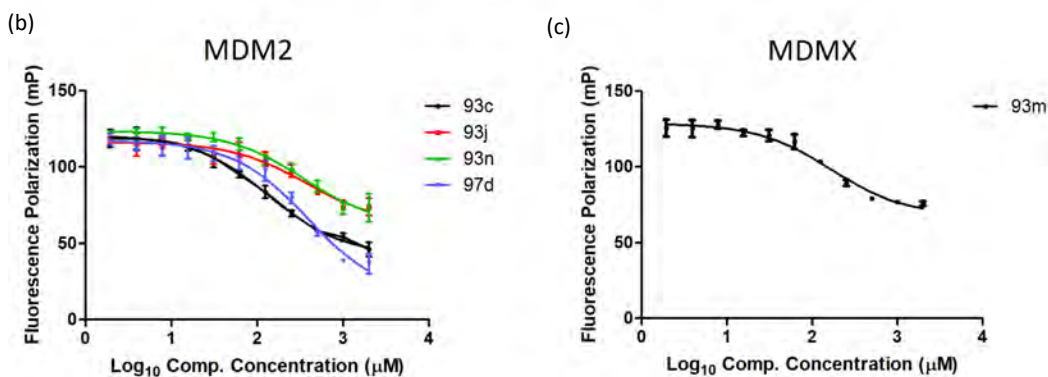


Figure 78. (a) Equations for the calculation of K_i . (b) FP binding curves of MDM2 titrated with different γ -lactams. (c) FP binding curve of MDMX titrated with **93m**.

Unfortunately, in the case of MDM2, only four compounds gave measurable results (Figure 78, b), since other γ -lactam derivatives did not show any affinity for the protein at the measured concentrations. Therefore C-4 phosphorus substituted 3-hydroxy-1,5-dihydro-2H-pyrrol-2-ones **93c**, **93j** and **93n** showed inhibition constant (K_i) values of 47.69 ± 1.68 , 131.30 ± 13.2 and 122.2 ± 2.4 μ M respectively. Furthermore, C-4 methyl carboxylate substituted enol-derived γ -lactam **97d** showed a weaker K_i value of 138.1 ± 3.3 μ M (Figure 79).

In the case of MDMX protein, only one measurable result was obtained (Figure 78, c). Interestingly, the active compound, **93m**, is also an enol derivative, in this case with a diphenyl phosphine oxide functionality at C-4 and a perfluorophenyl group at C-5 (Figure 79).

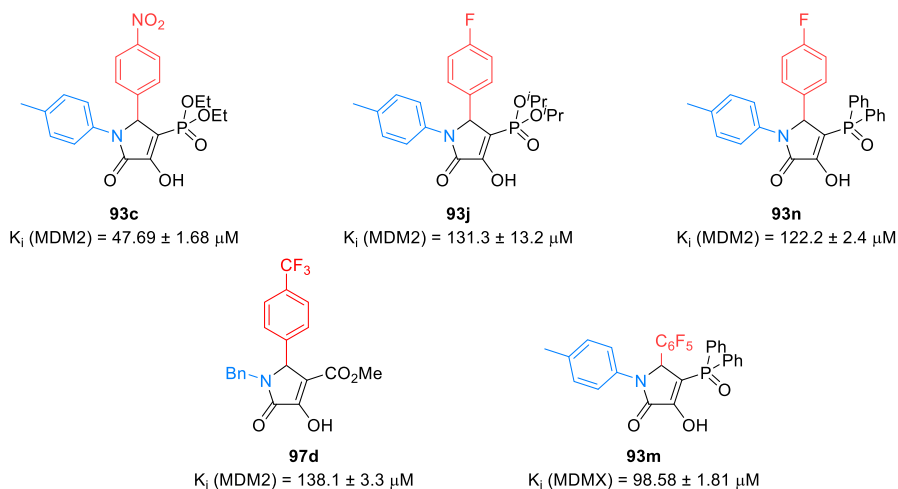


Figure 79. Inhibition constant values of the γ -lactam derivatives towards MDM2 and MDMX proteins.

In brief, the most potent inhibitor for MDM2 protein was compound **93c** with a K_i value of 47.69 μ M. On the other hand, the best inhibitory constant value for MDMX protein was obtained with compound **93m**, with a value of 98.58 μ M.

8.4. Molecular modeling simulations.

Despite the measured modest affinities, in order to predict the binding mode for these compounds, molecular modeling simulations were performed on the most active γ -lactam substrates for each protein.

In the case of compound **93c** towards MDM2, the binding mode prediction made with Autodock VINA indicates that the *p*-toluidine group occupies the hydrophobic Trp23 binding site of p53, while OH and P=O groups establish a H-bond with the Ser17 residue of MDM2. In addition, the phosphoryl and ethoxy groups of the ethyl phosphonate moiety can generate a polar interaction with the Gly16 backbone. Regarding the substituent at the position 5 of the γ -lactam ring, the nitro group at the aromatic ring is supposed to interact with Gln59 while a π -amide stacking interaction is formed with Gly58 (Figure 80).

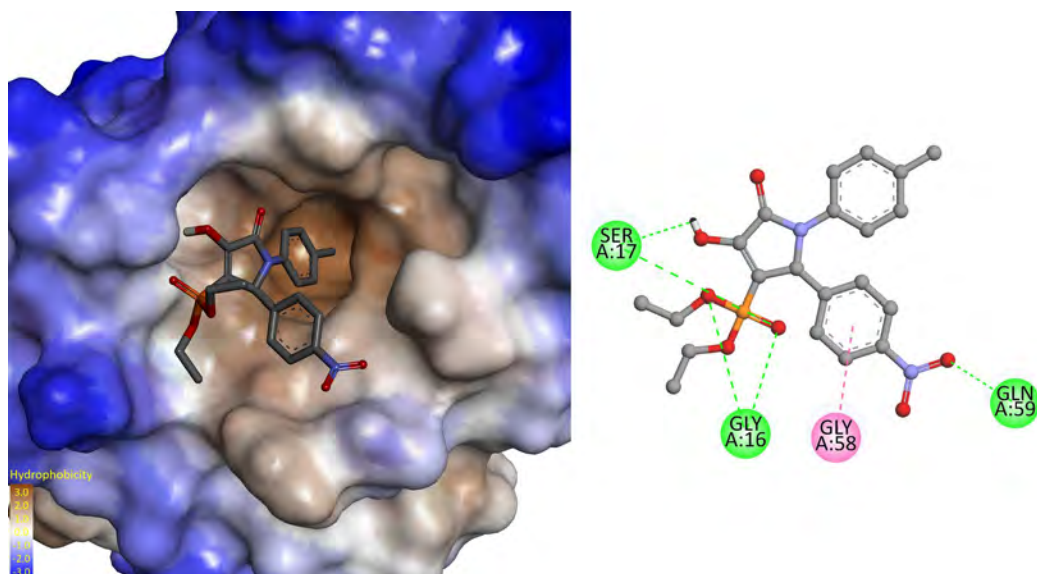


Figure 80. 3D and 2D binding mode prediction of **93c** to MDM2 (PDB code 1T4E).

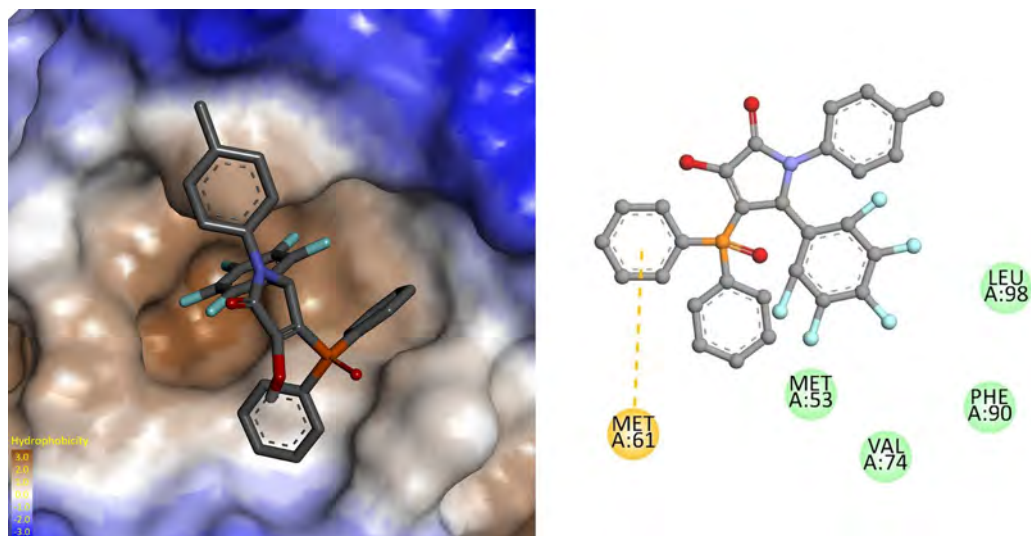


Figure 81. 3D and 2D binding mode prediction of **93m** to MDMX (PDB code 3DAB).

On the other hand, in view of the binding mode proposed between γ -lactam **93m** and MDMX (Figure 81), the lower K_i value observed may be explained due to the lack of H-bonds in the interaction model. In this case, the perfluorophenyl group at C-5 of the heterocycle is inserted in the Trp23 binding site of p53 by means of a Van der Waals interaction with the side chains of Met53, Val74, Phe90 and Leu98 residues. However, due to the narrower shape of the MDMX binding pocket, compared to

Leu98 residues. However, due to the narrower shape of the MDMX binding pocket, compared to MDM2, the *p*-tolyl and the phosphine oxide group is positioned in such a manner that it prevents the perfluorophenyl ring go deeper inside the pocket. In addition, a π -sulfur interaction is observed between MDMX Met61 and one of the aromatic rings of the diphenyl phosphine oxide group at the γ -lactam ring.

In conclusion, the inhibitory capability of the γ -lactam derivatives towards the MDM2/MDMX-p53 protein-protein interaction has been evaluated using two different screening techniques. First, by means of Differential Scanning Fluorimetry assays, a large number of compounds were tested, taking the advantage of the simplicity of this method. Then, the obtained positive hits were subjected to a Fluorescence Polarization assay in order to determine their inhibition constants. Taking into account the obtained low values, it can be assumed that the inhibition of the MDM2/MDMX-p53 protein-protein interaction is only partially responsible for the observed cytotoxic activity of the γ -lactam derivatives. The primary mechanism of action of these compounds requires further investigation.

The background features a complex network of interconnected nodes and lines, resembling a molecular or data structure. The nodes are represented by circles of varying sizes and shades of gray, connected by thin lines. A large, white, irregular shape is positioned in the center, partially overlapping the network. The overall aesthetic is clean and modern, with a focus on geometric and network-based patterns.

Conclusions

A wide range of 3-amino- α,β -unsaturated γ -lactams can be prepared by a very efficient Brønsted acid-catalyzed three-component reaction of pyruvate derivatives, amines and aldehydes. This reaction can be applied to several aromatic amines, aromatic and aliphatic aldehydes and some substituted pyruvate derivatives, enabling a straightforward synthesis of highly functionalized γ -lactam derivatives. In addition, the multicomponent methodology is applicable to the synthesis of fluorine and/or phosphorus-containing γ -lactam derivatives, obtaining the final products in the form of 3-hydroxy-1,5-dihydro-2*H*-pyrrol-2-ones or their enamine derivatives, depending on the substitution at the 5-membered ring heterocycle.

Dialkyl acetylenedicarboxylates have also demonstrated to be useful starting reagents for the multicomponent synthesis of 3-amino-1,5-dihydro-2*H*-pyrrol-2-ones as surrogates of pyruvates, being this one the first example of such reaction using phosphoric acids as the catalyst. Furthermore, the hydrolysis of the enamine moiety on 1,5-dihydro-2*H*-pyrrol-2-ones to the enol functionality has been successfully performed, which has not been described so far.

Taking the advantage of the ability of phosphoric acids to catalyze the multicomponent process, a highly enantioselective organocatalytic version of the three-component reaction of pyruvate derivatives, amines and aldehydes has been developed, allowing the preparation of highly enantioenriched 3-amino-1,5-dihydro-2*H*-pyrrol-2-ones.

The synthetic potential of the γ -lactam substrates obtained from the multicomponent reaction has been evaluated, using these products as starting materials for the synthesis of polyfunctional γ -lactam derivatives. Taking the advantage of the chiral stereocenter, highly diastereoselective hydrogenation reactions are described. Moreover, selective functionalization at C-4 is feasible making use of enamine chemistry, while the addition of organometallic species allows the functionalization at C-3. In addition, phosphonate-derived substrates can be used as starting materials in olefination reactions.

A highly stereoselective formal [3+3] cycloaddition of cyclic enamines and conjugated α -ketoesters catalyzed by ytterbium triflate to afford bicyclic 1,4-dihydropyridines has been described, putting into manifest the generality of the reaction with a wide scope comprising twenty-seven substrates. The detection of the reaction intermediate allowed the determination of the reaction mechanism. In view of the obtained results, a relationship between steric and π -stacking effects into the stereoselectivity of the reaction is proposed. Furthermore, some synthetic transformations of these bicyclic compounds

are also reported, including a catalytic hydrogenation that generates a third stereogenic center in a diastereoselective fashion.

The antiproliferative activity of the synthesized compounds has been evaluated against several cancer cell lines. In general terms, the obtained γ -lactam derivatives showed *in vitro* cytotoxicity, especially towards A549 (carcinomic human alveolar basal epithelial cell) cell line, while SKOV3 (human ovarian carcinoma) and RKO (human colon epithelial carcinoma) cell lines were found to be more resistant. In addition, low activity toward MRC5 non-malignant lung fibroblasts is generally observed. The most active compound provides excellent IC_{50} values of 0.11 and 1.23 μ M in A549 and SKOV3 cell lines, with a high selectivity towards non-malignant cells. It has also been evidenced that the main mechanisms by which γ -lactams derivatives induce cytotoxicity towards cancer cells is based on the activation of intracellular apoptotic mechanisms.

The MDM2/MDMX-p53 protein-protein interaction inhibitory capability of the γ -lactam derivatives has been evaluated, using two different screening techniques. First, Differential Scanning Fluorimetry assay have been performed, and then, the obtained positive hits were subjected to a Fluorescence Polarization assay in order to determine their inhibition constant values. However, taking into account the low inhibitory values determined, it cannot be surely concluded that the cytotoxic activity of the γ -lactam derivatives is the result of the disruption of the MDM2/MDMX-p53 protein-protein interaction.



Experimental Section I

Chemical synthesis

General methods and materials.

^1H , ^{13}C , ^{31}P and ^{19}F NMR spectra were recorded on a Varian Unity Plus spectrometer (at 300 MHz, 75 MHz, 120 MHz and 282 MHz respectively) or on a Bruker Avance 400 spectrometer (at 400 MHz for ^1H , 101 MHz for ^{13}C and 162 MHz for ^{31}P).

Chemical shifts are reported in parts per million (ppm) with the internal chloroform signal at 7.26 ppm, the internal DMSO signal at 2.50 ppm or the internal methanol signal at 3.31 ppm as standard for ^1H NMR. Chemical shifts are reported in parts per million (ppm) with the internal chloroform signal at 77.16 ppm, the internal DMSO signal at 39.52 ppm or the internal methanol signal at 49.00 ppm as standard for ^{13}C NMR. External references of phosphoric acid (50%) ($\delta_{\text{P}} = 0.0$ ppm) and of CFCl_3 ($\delta_{\text{F}} = 0.0$ ppm) are used for ^{31}P NMR and ^{19}F NMR spectra respectively. All coupling constants (J) are reported in Hertz (Hz). ^{13}C NMR spectra were recorded in a broad band decoupled mode, and peak assignments were supported by Distortionless Enhanced Polarization Transfer (DEPT). Relative stereochemistry was assigned based on 1D-NOE experiments. The data is reported as follows: chemical shift (multiplicity, coupling constant, integration). Multiplicity abbreviations are as follows: s = singlet, bs = broad singlet, d = doublet, dd = double doublet, dt = double triplet, dq = double quartet, ddd = double double doublet, t = triplet, q = quartet, hept = heptuplet, m = multiplet).

The infrared spectra (IR) were registered using a Nicolet iS10 spectrophotometer (Thermo Scientific), using Smart iTR accessory and reporting the value of the peaks in cm^{-1} . IR spectra were taken as neat solids or oils.

High resolution mass spectra (HRMS) spectra were obtained by positive-ion electrospray ionization (ESI) using a LC-QTOF method. Data are reported in the form m/z (intensity relative to base = 100).

Melting points (Mp) were determined in digital measurement devices Büchi MPB-540 in opened capillary tubes.

Solvents for extraction, chromatography and crystallization were technical grade. All solvents used in reactions were treated with dry molecular sieves as specified in the literature.²⁴⁰ All other reagents were recrystallized or distilled as necessary.

Chromatographic purification was performed by flash chromatography using commercial grades of silica gel finer than 230 mesh with pressure.

Analytical thin layer chromatography (TLC) was performed with silica gel 60 F₂₅₄ TLC aluminum plates. Visualization was accomplished by UV light or permanganate stain. Permanganate solution was prepared with potassium permanganate (3 g), potassium carbonate (20 g) and 5% sodium hydroxide aqueous solution (5 mL) in 300 mL of water.

In order to determine the enantiomeric excesses, HPLC Agilent 1100/1200 Series system was used, with Chiracel® IA, Chiracel® IB and Chiracel® IC columns as stationary phases.

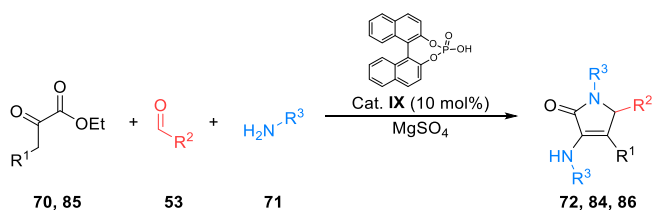
The X-ray diffraction analysis experiments were conducted using diffractometers for monocrystals.

β -Phosphorated aldehydes **89** and pyruvates **91** containing phosphonate or phosphine oxide moieties were synthesized according to literature procedures.^{153,154}

²⁴⁰ Williams, D. B. G.; Lawton, M. *J. Org. Chem.* **2010**, *75*, 8351-8354.

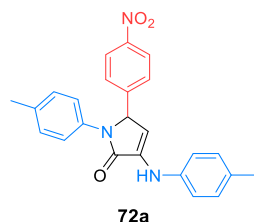
Chapter 1. Multicomponent synthesis of unsaturated γ -lactam derivatives using pyruvates.

General procedure for the synthesis of 3-amino-1,5-dihydro-2H-pyrrol-2-ones **72, **84** and **86** using pyruvates.**



A solution of amine **71** (4 mmol), aldehyde **53** (2 mmol), ethyl pyruvate derivative **70** or **85** (6 mmol), and BINOL-derived phosphoric acid **IX** (70 mg, 0.2 mmol) in diethyl ether (10 mL) at room temperature or in MTBE (10 mL) at 55 °C was stirred for 18-72 hours in the presence of anhydrous MgSO_4 (500 mg). Next, the reaction was filtered, the volatiles were distilled off at reduced pressure and the crude residue was purified by crystallization from diethyl ether or flash column chromatography (Hexanes/AcOEt) to afford pure γ -lactams **72**, **84** or **86**.

5-(4-Nitrophenyl)-1-(*p*-tolyl)-3-(*p*-tolylamino)-1,5-dihydro-2H-pyrrol-2-one (**72a**).



The general procedure was followed in diethyl ether at room temperature for 18 hours, using *p*-toluidine (429 mg, 4 mmol), *p*-nitrobenzaldehyde (302 mg, 2 mmol) and ethyl pyruvate (670 μL , 6 mmol). The crude residue was purified by crystallization from diethyl ether, affording 637 mg (80%) of **72a** as a yellow solid.

Mp (Et_2O): 142 - 145 °C. Lit. 142 - 145 °C.¹¹³

¹H NMR (400 MHz, CDCl_3) δ 8.13 (d, $^3J_{\text{HH}} = 8.7$ Hz, 2H, 2 $\times\text{CH}_{\text{Ar}}$), 7.37 (d, $^3J_{\text{HH}} = 8.4$ Hz, 2H, 2 $\times\text{CH}_{\text{Ar}}$), 7.35 (d, $^3J_{\text{HH}} = 8.4$ Hz, 2H, 2 $\times\text{CH}_{\text{Ar}}$), 7.11 (d, $^3J_{\text{HH}} = 8.1$ Hz, 2H, 2 $\times\text{CH}_{\text{Ar}}$), 7.10 (d, $^3J_{\text{HH}} = 8.1$ Hz, 2H, 2 $\times\text{CH}_{\text{Ar}}$),

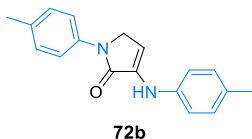
6.97 (d, $^3J_{\text{HH}} = 8.4$ Hz, 2H, 2xCH_{Ar}), 6.61 (bs, 1H, NH), 5.96 (d, $^3J_{\text{HH}} = 2.7$ Hz, 1H, =CH), 5.75 (d, $^3J_{\text{HH}} = 2.7$ Hz, 1H, CHN), 2.30 (s, 3H, CH₃), 2.27 (s, 3H, CH₃) ppm.

^{13}C { ^1H } NMR (101 MHz, CDCl₃) δ 167.0 (C=O), 147.8 (C_{quat}), 145.6 (C_{quat}), 138.5 (C_{quat}), 135.4 (C_{quat}), 134.2 (C_{quat}), 133.3 (C_{quat}), 131.4 (C_{quat}), 130.1 (2xCH_{Ar}), 129.9 (2xCH_{Ar}), 127.8 (2xCH_{Ar}), 124.4 (2xCH_{Ar}), 121.7 (2xCH_{Ar}), 117.2 (2xCH_{Ar}), 105.3 (=CH), 63.6 (CHN), 21.0 (CH₃), 20.8 (CH₃) ppm.

FTIR ν_{max} 3309 (N-H_{st}), 3037 (=C-H_{st}), 1682 (C=O_{st}), 1664 (C=CH_{st}), 1508 (NO_{2 st as}), 1342 (NO_{2 st sym}) cm⁻¹.

HRMS (ESI-TOF) m/z calcd. for C₂₄H₂₂N₃O₃ [M+H]⁺ 400.1661, found 400.1655.

1-(*p*-Tolyl)-3-(*p*-tolylamino)-1,5-dihydro-2H-pyrrol-2-one (72b).



The general procedure was followed in diethyl ether at room temperature for 18 hours, using *p*-toluidine (429 mg, 4 mmol), a 37% aqueous solution of formaldehyde (150 μL , 2 mmol) and ethyl pyruvate (670 μL , 6 mmol). The crude residue was purified by flash column chromatography (Hexanes/AcOEt 90:10), affording 433 mg (78%) of **72b** as an orange solid.

Mp (Et₂O): 178 - 180 °C.

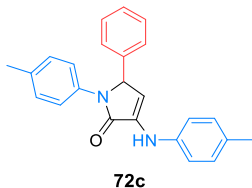
^1H NMR (400 MHz, CDCl₃) δ 7.64 (d, $^3J_{\text{HH}} = 8.5$ Hz, 2xCH_{Ar}), 7.20 (d, $^3J_{\text{HH}} = 8.2$ Hz, 2xCH_{Ar}), 7.13 (d, $^3J_{\text{HH}} = 8.2$ Hz, 2xCH_{Ar}), 7.1 (d, $^3J_{\text{HH}} = 8.5$ Hz, 2xCH_{Ar}), 6.53 (s, 1H, NH), 5.97 (t, $^3J_{\text{HH}} = 2.6$ Hz, 1H, =CH), 4.37 (d, $^3J_{\text{HH}} = 2.6$ Hz, 2H, CH₂), 2.34 (s, 3H, CH₃), 2.32 (s, 3H, CH₃) ppm.

^{13}C { ^1H } NMR (101 MHz, CDCl₃) δ 166.5 (C=O), 139.2 (C_{quat}), 136.8 (C_{quat}), 134.5 (C_{quat}), 134.3 (C_{quat}), 130.7 (=C_{quat}), 130.0 (2xCH_{Ar}), 129.8 (2xCH_{Ar}), 119.0 (2xCH_{Ar}), 116.8 (2xCH_{Ar}), 99.8 (=CH), 49.8 (CH₂), 21.0 (CH₃), 20.8 (CH₃) ppm.

FTIR ν_{max} 3325 (N-H_{st}), 3073 (=CH_{st}), 1671 (C=O_{st}), 1644 (C=CH_{st}) cm⁻¹.

HRMS (ESI-TOF) m/z calcd. for C₁₈H₁₈N₂O [M+H]⁺ 279.1497, found 279.1501.

5-Phenyl-1-(*p*-tolyl)-3-(*p*-tolylamino)-1,5-dihydro-2H-pyrrol-2-one (72c).



The general procedure was followed in diethyl ether at room temperature for 18 hours, using *p*-toluidine (429 mg, 4 mmol), benzaldehyde (204 μL , 2 mmol) and ethyl pyruvate (670 μL , 6 mmol). The crude residue was purified by crystallization from diethyl ether, affording 680 mg (96%) of **72c** as a white solid.

M.p. (Et₂O): 214 - 215 °C. Lit. 215 - 217 °C.²⁴¹

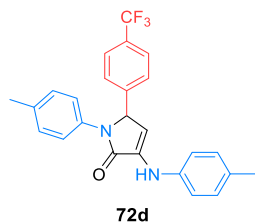
¹H NMR (400 MHz, CDCl₃) δ 7.40 (d, ³J_{HH} = 8.5 Hz, 2H, 2xCH_{Ar}), 7.32 - 7.17 (m, 5H, 5xCH_{Ar}), 7.10 (d, ³J_{HH} = 8.0 Hz, 2H, 2xCH_{Ar}), 7.09 (d, ³J_{HH} = 8.0 Hz, 2H, 2xCH_{Ar}), 6.98 (d, ³J_{HH} = 8.5 Hz, 2H, 2xCH_{Ar}), 6.58 (s, 1H, NH), 6.01 (d, ³J_{HH} = 2.6 Hz, 1H, =CH), 5.63 (d, ³J_{HH} = 2.6 Hz, 1H, CHN), 2.29 (s, 3H, CH₃), 2.26 (s, 3H, CH₃) ppm.

¹³C {¹H} NMR (101 MHz, CDCl₃) δ 167.0 (C=O), 138.8 (C_{quat}), 137.6 (C_{quat}), 134.8 (C_{quat}), 134.8 (C_{quat}), 132.0 (C_{quat}), 130.5 (C_{quat}), 129.9 (2xCH_{Ar}), 129.6 (2xCH_{Ar}), 129.0 (2xCH_{Ar}), 128.2 (CH_{Ar}), 126.9 (2xCH_{Ar}), 121.6 (2xCH_{Ar}), 116.8 (2xCH_{Ar}), 107.2 (=CH), 64.3 (CHN), 21.0 (CH₃), 20.8 (CH₃) ppm.

FTIR ν_{max} 3306 (N-H_{st}), 1684 (C=O_{st}), 1665 (C=CH_{st}) cm⁻¹.

HRMS (ESI-TOF) *m/z* calcd. for C₂₄H₂₃N₂O [M+H]⁺ 355.1810, found 355.1805.

1-(*p*-Tolyl)-3-(*p*-tolylamino)-5-(4-(trifluoromethyl)phenyl)-1,5-dihydro-2H-pyrrol-2-one (72d).



The general procedure was followed in diethyl ether at room temperature for 18 hours, using *p*-toluidine (429 mg, 4 mmol), *p*-(trifluoromethyl) benzaldehyde (273 μL, 2 mmol) and ethyl pyruvate (670 μL, 6 mmol). The crude residue was purified by crystallization from diethyl ether, affording 675 mg (80%) of **72d** as a white solid.

M.p. (Et₂O): 197 - 199 °C (dec.).

¹H NMR (400 MHz, CDCl₃) δ 7.53 (d, ³J_{HH} = 8.1 Hz, 2H, 2xCH_{Ar}), 7.37 (d, ³J_{HH} = 8.5 Hz, 2H, 2xCH_{Ar}), 7.32 (d, ³J_{HH} = 8.2 Hz, 2H, 2xCH_{Ar}), 7.10 (d, ³J_{HH} = 8.2 Hz, 4H, 4xCH_{Ar}), 6.97 (d, ³J_{HH} = 8.5 Hz, 2H, 2xCH_{Ar}), 6.58 (bs, 1H, NH), 5.96 (d, ³J_{HH} = 2.7 Hz, 1H, =CH), 5.69 (d, ³J_{HH} = 2.4 Hz, 1H, CHN), 2.29 (s, 3H, CH₃), 2.27 (s, 3H, CH₃) ppm.

¹³C {¹H} NMR (101 MHz, CDCl₃) δ 167.2 (C=O), 142.2 (C_{quat}), 138.7 (C_{quat}), 135.2 (C_{quat}), 134.4 (C_{quat}), 133.0 (C_{quat}), 131.2 (C_{quat}), 130.4 (q, ²J_{FC} = 32.3 Hz, C_{CF₃}), 130.0 (2xCH_{Ar}), 129.8 (2xCH_{Ar}), 127.2 (2xCH_{Ar}), 126.1 (q, ³J_{FC} = 3.8 Hz, 2xCH_{Ar}), 124.0 (q, ¹J_{FC} = 272.2 Hz, CF₃), 121.7 (2xCH_{Ar}), 117.1 (2xCH_{Ar}), 106.3 (=CH), 63.9 (CHN), 21.1 (CH₃), 20.9 (CH₃) ppm.

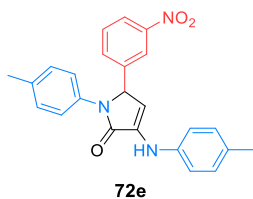
¹⁹F NMR (282 MHz, CDCl₃) δ -63.0 ppm.

FTIR ν_{max} 3328 (N-H_{st}), 1666 (C=O_{st}), 1651 (C=CH_{st}), 1324 (C-F_{st}) cm⁻¹.

HRMS (ESI-TOF) *m/z* calcd. for C₂₅H₂₂F₃N₂O [M+H]⁺ 423.1684, found 423.1681.

²⁴¹ Wu, Y. C.; Liu, L.; Wang, D.; Chen, Y. J. *J. Heterocycl. Chem.* **2006**, *43*, 949–955.

5-(3-Nitrophenyl)-1-(*p*-tolyl)-3-(*p*-tolylamino)-1,5-dihydro-2*H*-pyrrol-2-one (72e).



The general procedure was followed in diethyl ether at room temperature for 18 hours, using *p*-toluidine (429 mg, 4 mmol), *m*-nitrobenzaldehyde (302 mg, 2 mmol) and ethyl pyruvate (670 μ L, 6 mmol). The crude residue was crystallized from diethyl ether, affording 580 mg (73%) of **72e** as a yellow solid.

Mp (Et₂O): 194 - 196 °C (dec.).

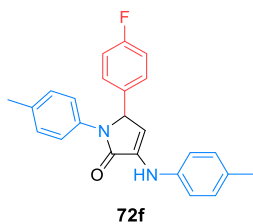
¹H NMR (400 MHz, CDCl₃) δ 8.11 - 8.06 (m, 2H, 2xCH_{Ar}), 7.50 (d, ³J_{HH} = 7.8 Hz, 1H, CH_{Ar}), 7.44 (d, ³J_{HH} = 7.8 Hz, 2H, 2xCH_{Ar}), 7.35 (d, ³J_{HH} = 8.5 Hz, 2H, 2xCH_{Ar}), 7.11 (d, ³J_{HH} = 8.1 Hz, 2H, 2xCH_{Ar}), 7.10 (d, ³J_{HH} = 8.1 Hz, 2H, 2xCH_{Ar}), 6.98 (d, ³J_{HH} = 8.5 Hz, 2H, 2xCH_{Ar}), 6.63 (bs, 1H, NH), 5.98 (d, ³J_{HH} = 2.6 Hz, 1H, =CH), 5.75 (d, ³J_{HH} = 2.6 Hz, 1H, CHN), 2.30 (s, 3H, CH₃), 2.26 (s, 3H, CH₃) ppm.

¹³C {¹H} NMR (101 MHz, CDCl₃) δ 167.0 (C=O), 148.7 (C_{quat}), 140.5 (C_{quat}), 138.6 (C_{quat}), 135.4 (C_{quat}), 134.1 (C_{quat}), 133.3 (C_{quat}), 132.8 (CH_{Ar}), 131.3 (C_{quat}), 130.2 (CH_{Ar}), 130.0 (2xCH_{Ar}), 129.9 (CH_{Ar}), 123.4 (2xCH_{Ar}), 122.2 (CH_{Ar}), 122.0 (CH_{Ar}), 117.2 (CH_{Ar}), 105.6 (=CH), 63.6 (CHN), 21.0 (CH₃), 20.8 (CH₃) ppm.

FTIR ν_{\max} 3316 (N-H_{st}), 3021 (=C-H_{st}), 1682 (C=O_{st}), 1665 (C=CH_{st}), 1533 (NO_{2 st as}), 1346 (NO_{2 st sym}) cm⁻¹.

HRMS (ESI-TOF) *m/z* calcd. for C₂₄H₂₂N₃O₃ [M+H]⁺ 400.1661, found 400.1659.

5-(4-Fluorophenyl)-1-(*p*-tolyl)-3-(*p*-tolylamino)-1,5-dihydro-2*H*-pyrrol-2-one (72f).



The general procedure was followed in diethyl ether at room temperature for 48 hours, using *p*-toluidine (429 mg, 4 mmol), *p*-fluoroaldehyde (214 μ L, 2 mmol) and ethyl pyruvate (670 μ L, 6 mmol). The crude residue was purified by crystallization from diethyl ether, affording 623 mg (84%) of **72f** as a white solid.

Mp (Et₂O): 185 - 187 °C (dec.).

¹H NMR (400 MHz, CDCl₃) δ 7.34 (d, ³J_{HH} = 8.5 Hz, 2H, 2xCH_{Ar}), 7.17 (dd, ³J_{HH} = 8.7 Hz, ³J_{FH} = 5.2 Hz, 2H, 2xCH_{Ar}), 7.10 (d, ³J_{HH} = 8.0 Hz, 2H, 2xCH_{Ar}), 7.09 (d, ³J_{HH} = 8.0 Hz, 2H, 2xCH_{Ar}), 7.03 - 6.92 (m, 2H, 2xCH_{Ar}), 6.95 (d, ³J_{HH} = 8.7 Hz, 2H, 2xCH_{Ar}), 6.57 (bs, 1H, NH), 5.98 (d, ³J_{HH} = 2.6 Hz, 1H, =CH), 5.62 (d, ³J_{HH} = 2.6 Hz, 1H, CHN), 2.30 (s, 3H, CH₃), 2.27 (s, 3H, CH₃) ppm.

¹³C {¹H} NMR (101 MHz, CDCl₃) δ 167.2 (C=O), 162.6 (d, ¹J_{FC} = 249 Hz, CF), 138.9 (C_{quat}), 135.1 (C_{quat}), 134.5 (C_{quat}), 133.5 (d, ⁴J_{FC} = 3.3 Hz, C_{quat}), 132.7 (C_{quat}), 131.0 (C_{quat}), 130.0 (2xCH_{Ar}), 129.7 (2xCH_{Ar}),

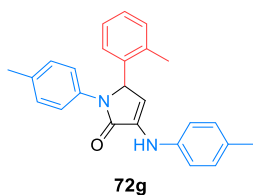
128.7 (d, $^3J_{FC} = 8.2$ Hz, 2xCH_{Ar}), 122.1 (2xCH_{Ar}), 117.0 (2xCH_{Ar}), 116.0 (d, $^2J_{FC} = 21.7$ Hz, 2xCH_{Ar}), 107.0 (=CH), 63.8 (CHN), 21.0 (CH₃), 20.8 (CH₃) ppm.

^{19}F NMR (282 MHz, CDCl₃) δ -114.2 ppm.

FTIR ν_{max} 3304 (N-H_{st}), 1669 (C=O_{st}), 1668 (C=CH_{st}), 1195 (C-F_{st}) cm⁻¹.

HRMS (ESI-TOF) m/z calcd. for C₂₄H₂₂FN₂O [M+H]⁺ 373.1716, found 373.1710.

5-(*o*-Tolyl)-1-(*p*-tolyl)-3-(*p*-tolylamino)-1,5-dihydro-2H-pyrrol-2-one (72g).



The general procedure was followed in MTBE at 55 °C (heating plate) for 72 hours, using *p*-toluidine (429 mg, 4 mmol), *o*-tolualdehyde (231 μL , 2 mmol) and ethyl pyruvate (670 μL , 6 mmol). The crude residue was purified by crystallization from diethyl ether, affording 491 mg (67%) of **72g** as an orange solid.

Mp (Et₂O): 198 - 200 °C (dec.).

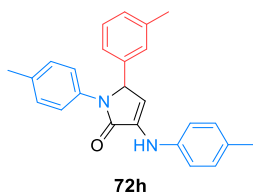
^1H NMR (400 MHz, CDCl₃) δ 7.39 (d, $^3J_{\text{HH}} = 8.5$ Hz, 2H, 2xCH_{Ar}), 7.14 - 7.11 (m, 2H, 2xCH_{Ar}), 7.11 - 7.07 (m, 5H, 5xCH_{Ar}), 7.01 (m, 1H, CH_{Ar}), 6.97 (d, $^3J_{\text{HH}} = 8.5$ Hz, 2H, 2xCH_{Ar}), 6.57 (bs, 1H, NH), 5.99 (d, $^3J_{\text{HH}} = 2.6$ Hz, 1H, =CH), 5.89 (d, $^3J_{\text{HH}} = 2.6$ Hz, 1H, CHN), 2.45 (s, 3H, CH₃), 2.29 (s, 3H, CH₃), 2.26 (s, 3H, CH₃) ppm.

$^{13}\text{C}\{^1\text{H}\}$ NMR (101 MHz, CDCl₃) δ 167.5 (C=O), 139.0 (C_{quat}), 135.4 (2xC_{quat}), 135.1 (C_{quat}), 134.6 (C_{quat}), 132.8 (C_{quat}), 131.1 (C_{quat}), 130.8 (CH_{Ar}), 129.9 (2xCH_{Ar}), 129.6 (2xCH_{Ar}), 127.8 (CH_{Ar}), 127.0 (CH_{Ar}), 121.2 (2xCH_{Ar}), 116.9 (2xCH_{Ar}), 106.1 (=CH), 61.4 (CHN), 21.0 (CH₃), 20.8 (CH₃), 19.3 (CH₃) ppm.

FTIR ν_{max} 3310 (N-H_{st}), 1687 (C=O_{st}), 1645 (C=CH_{st}) cm⁻¹.

HRMS (ESI-TOF) m/z calcd. for C₂₅H₂₅N₂O [M+H]⁺ 369.1967, found 369.1953.

5-(*m*-Tolyl)-1-(*p*-tolyl)-3-(*p*-tolylamino)-1,5-dihydro-2H-pyrrol-2-one (72h).



The general procedure was followed in MTBE at 55 °C (heating plate) for 72 hours, using *p*-toluidine (429 mg, 4 mmol), *m*-tolualdehyde (235 μL , 2 mmol) and ethyl pyruvate (670 μL , 6 mmol). The crude residue was purified by crystallization from diethyl ether, affording 661 mg (90%) of **72h** as a white solid.

Mp (Et₂O): 186 - 188 °C (dec.).

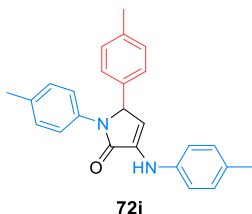
¹H NMR (400 MHz, CDCl₃) δ 7.42 (d, ³J_{HH} = 8.5 Hz, 2H, 2xCH_{Ar}), 7.16 (t, ³J_{HH} = 7.8 Hz, 1H, CH_{Ar}), 7.10 (d, ³J_{HH} = 8.1 Hz, 2H, 2xCH_{Ar}), 7.09 (d, ³J_{HH} = 8.1 Hz, 2H, 2xCH_{Ar}), 7.05 - 6.99 (m, 3H, 3xCH_{Ar}), 6.98 (d, ³J_{HH} = 8.5 Hz, 2H, 2xCH_{Ar}), 6.58 (bs, 1H, NH), 6.00 (d, ³J_{HH} = 2.6 Hz, 1H, =CH), 5.59 (d, ³J_{HH} = 2.6 Hz, 1H, CHN), 2.29 (s, 3H, CH₃), 2.28 (s, 3H, CH₃), 2.27 (s, 3H, CH₃) ppm.

¹³C {¹H} NMR (101 MHz, CDCl₃) δ 167.4 (C=O), 139.0 (C_{quat}), 138.8 (C_{quat}), 137.7 (C_{quat}), 134.9 (C_{quat}), 134.7 (C_{quat}), 132.3 (C_{quat}), 130.7 (C_{quat}), 129.9 (2xCH_{Ar}), 129.6 (2xCH_{Ar}), 129.0 (CH_{Ar}), 128.9 (CH_{Ar}), 127.4 (CH_{Ar}), 124.0 (CH_{Ar}), 121.7 (2xCH_{Ar}), 116.9 (2xCH_{Ar}), 107.7 (=CH), 64.4 (CHN), 21.5 (CH₃), 21.0 (CH₃), 20.8 (CH₃) ppm.

FTIR ν_{max} 3312 (N-H_{st}), 1669 (C=O_{st}), 1663 (C=CH_{st}) cm⁻¹.

HRMS (ESI-TOF) *m/z* calcd. for C₂₅H₂₅N₂O [M+H]⁺ 369.1967, found 369.1952.

1,5-Di-*p*-tolyl-3-(*p*-tolylamino)-1,5-dihydro-2*H*-pyrrol-2-one (72i).



The general procedure was followed in MTBE at 55 °C (heating plate) for 18 hours, using *p*-toluidine (429 mg, 4 mmol), *p*-tolualdehyde (236 μL, 2 mmol) and ethyl pyruvate (670 μL, 6 mmol). The crude residue was purified by crystallization from diethyl ether, affording 648 mg (88%) of **72i** as an orange solid.

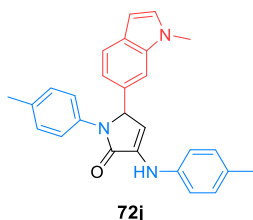
Mp (Et₂O): 210 - 212 °C. Lit. 250 - 252 °C.¹¹⁵

¹H NMR (400 MHz, CDCl₃) δ 7.39 (d, ³J_{HH} = 8.5 Hz, 2H, 2xCH_{Ar}), 7.11 - 7.06 (m, 8H, 8xCH_{Ar}), 6.97 (d, ³J_{HH} = 8.4 Hz, 2H, 2xCH_{Ar}), 6.56 (bs, 1H, NH), 5.99 (d, ³J_{HH} = 2.5 Hz, 1H, =CH), 5.60 (d, ³J_{HH} = 2.5 Hz, 1H, CHN), 2.29 (s, 3H, CH₃), 2.28 (s, 3H, CH₃), 2.26 (s, 3H, CH₃) ppm.

¹³C {¹H} NMR (101 MHz, CDCl₃) δ 167.3 (C=O), 139.0 (C_{quat}), 138.0 (C_{quat}), 134.8 (C_{quat}), 134.7 (C_{quat}), 134.6 (C_{quat}), 132.4 (C_{quat}), 130.7 (C_{quat}), 129.9 (2xCH_{Ar}), 129.7 (2xCH_{Ar}), 129.6 (2xCH_{Ar}), 126.9 (2xCH_{Ar}), 121.9 (2xCH_{Ar}), 116.9 (2xCH_{Ar}), 107.7 (=CH), 64.2 (CHN), 21.3 (CH₃), 21.0 (CH₃), 20.8 (CH₃) ppm.

FTIR ν_{max} 3316 (N-H_{st}), 1666 (C=O_{st}), 1648 (C=CH_{st}) cm⁻¹.

HRMS (ESI-TOF) *m/z* calcd. for C₂₅H₂₅N₂O [M+H]⁺ 369.1967, found 369.1952.

5-(1-Methyl-1H-indol-6-yl)-1-(*p*-tolyl)-3-(*p*-tolylamino)-1,5-dihydro-2H-pyrrol-2-one (72j).

The general procedure was followed in diethyl ether at room temperature for 18 hours, using *p*-toluidine (429 mg, 4 mmol), 1-methyl-1H-indole-6-carboxaldehyde (318 mg, 2 mmol) and ethyl pyruvate (670 μ L, 6 mmol). The crude residue was purified by flash column chromatography (Hexanes/AcOEt 90:10), affording 588 mg (73%) of **72j** as an orange solid.

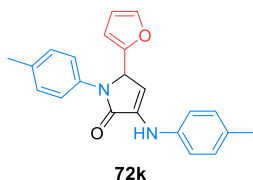
Mp (Et₂O): 185 - 187 °C (dec.).

¹H NMR (300 MHz, CDCl₃) δ 7.52 (d, ³J_{HH} = 8.1 Hz, 1H, CH_{Ar}), 7.44 (d, ³J_{HH} = 8.5 Hz, 2H, 2xCH_{Ar}), 7.14 - 6.95 (m, 9H, 9xCH_{Ar}), 6.58 (bs, 1H, NH), 6.41 (d, ³J_{HH} = 2.8 Hz, 1H, CH_{Ar}), 6.07 (d, ³J_{HH} = 2.6 Hz, 1H, =CH), 5.75 (d, ³J_{HH} = 2.6 Hz, 1H, CHN), 3.72 (s, 3H, NCH₃), 2.28 (s, 3H, CH₃), 2.23 (s, 3H, CH₃) ppm.

¹³C {¹H} NMR (75 MHz, CDCl₃) δ 167.6 (C=O), 139.2 (C_{quat}), 137.1 (C_{quat}), 135.2 (C_{quat}), 134.7 (C_{quat}), 132.1 (C_{quat}), 131.1 (C_{quat}), 130.70 (C_{quat}), 130.0 (2xCH_{Ar}), 129.6 (2xCH_{Ar}), 128.6 (C_{quat}), 127.3 (CH_{Ar}), 122.0 (2xCH_{Ar}), 121.5 (CH_{Ar}), 118.5 (CH_{Ar}), 116.9 (2xCH_{Ar}), 108.8 (CH_{Ar}), 107.7 (=CH), 101.0 (CH_{Ar}), 65.4 (CHN), 33.2 (NCH₃), 21.1 (CH₃), 20.9 (CH₃) ppm.

FTIR ν_{\max} 3301 (N-H_{st}), 1672 (C=O_{st}), 1651 (C=CH_{st}) cm⁻¹.

HRMS (ESI-TOF) *m/z* calcd. for C₂₇H₂₆N₃O [M+H]⁺ 408.2076, found 408.2071.

5-(Furan-2-yl)-1-(*p*-tolyl)-3-(*p*-tolylamino)-1,5-dihydro-2H-pyrrol-2-one (72k).

The general procedure was followed in diethyl ether at room temperature for 18 hours, using *p*-toluidine (429 mg, 4 mmol), 2-furfural (166 μ L, 2 mmol) and ethyl pyruvate (670 μ L, 6 mmol). The crude residue was purified by flash column chromatography (Hexanes/AcOEt 90:10), affording 392 mg (57%) of **72k** as a white solid.

Mp (Et₂O): 151 - 153 °C. Lit. 151 - 152 °C.¹¹³

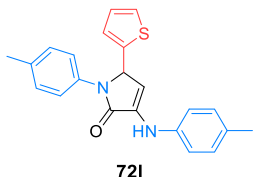
¹H NMR (300 MHz, CDCl₃) δ 7.36 (d, ³J_{HH}=8.5 Hz, 2H, 2xCH_{Ar}), 7.33 (d, ³J_{HH} = 1.8 Hz, 1H, CH furyl), 7.17 (d, ³J_{HH} = 8.1 Hz, 2H, 2xCH_{Ar}), 7.14 (d, ³J_{HH} = 8.1 Hz, 2H, 2xCH_{Ar}), 7.03 (d, ³J_{HH} = 8.5 Hz, 2H, 2xCH_{Ar}), 6.61 (bs, 1H, NH), 6.28 (dd, ³J_{HH} = 1.8, ³J_{HH} = 3.1 Hz, 1H, CH furyl), 6.19 (d, ³J_{HH} = 3.1 Hz, 1H, CH furyl), 6.03 (d, ³J_{HH} = 2.6 Hz, 1H, =CH), 5.76 (d, ³J_{HH} = 2.6 Hz, 1H, CHN), 2.34 (s, 6H, 2xCH₃) ppm.

¹³C {¹H} NMR (75 MHz, CDCl₃) δ 166.6 (C=O), 150.1 (C_{quat}), 142.5 (CH furyl), 138.8 (C_{quat}), 135.3 (C_{quat}), 134.4 (C_{quat}), 133.5 (C_{quat}), 130.7 (C_{quat}), 129.8 (2xCH_{Ar}), 129.4 (2xCH_{Ar}), 122.5 (2xCH_{Ar}), 116.9 (2xCH_{Ar}), 110.4 (CH furyl), 108.3 (CH furyl), 102.8 (=CH), 58.8 (CHN), 20.9 (CH₃), 20.6 (CH₃) ppm.

FTIR ν_{\max} 3309 (N-H_{st}), 1675 (C=O_{st}), 1658 (C=CH_{st}) cm^{-1} .

HRMS (ESI-TOF) m/z calcd. for $\text{C}_{22}\text{H}_{21}\text{N}_2\text{O}_2$ $[\text{M}+\text{H}]^+$ 345.1600, found 345.1599.

5-(Thiophen-2-yl)-1-(*p*-tolyl)-3-(*p*-tolylamino)-1,5-dihydro-2*H*-pyrrol-2-one (72l).



The general procedure was followed in MTBE at 55 °C (heating plate) for 18 hours, using *p*-toluidine (429 mg, 4 mmol), 2-thiophenecarboxaldehyde (187 μL , 2 mmol) and ethyl pyruvate (670 μL , 6 mmol). The crude residue was purified by crystallization from diethyl ether, affording 587 mg (82%) of

72l as a yellow solid.

Mp (Et_2O): 204 - 206 °C.

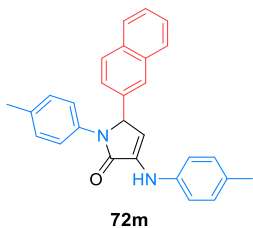
^1H NMR (300 MHz, CDCl_3) δ 7.31 (d, $^3J_{\text{HH}} = 8.3$ Hz, 2H, $2\times\text{CH}_{\text{Ar}}$), 7.18 (d, $^3J_{\text{HH}} = 5.1$ Hz, 1H, CH thienyl), 7.16 - 7.10 (m, 4H, $4\times\text{CH}_{\text{Ar}}$), 7.02 (d, $^3J_{\text{HH}} = 8.3$ Hz, 2H, $2\times\text{CH}_{\text{Ar}}$), 6.98 (d, $^3J_{\text{HH}} = 3.6$ Hz, 1H, CH thienyl), 6.86 (dd, $^3J_{\text{HH}} = 5.1, 3.6$ Hz, 1H, CH thienyl), 6.58 (bs, 1H, NH), 6.08 (d, $^3J_{\text{HH}} = 2.5$ Hz, 1H, =CH), 5.94 (d, $^3J_{\text{HH}} = 2.5$ Hz, 1H, CHN), 2.31 (s, 3H, CH_3), 2.30 (s, 3H, CH_3) ppm.

^{13}C { ^1H } NMR (75 MHz, CDCl_3) δ 166.6 (C=O), 141.7 (C_{quat}), 138.9 (C_{quat}), 135.7 (C_{quat}), 134.3 (C_{quat}), 133.1 (C_{quat}), 131.1 (C_{quat}), 130.1 ($2\times\text{CH}_{\text{Ar}}$), 129.8 ($2\times\text{CH}_{\text{Ar}}$), 126.8 (CH thienyl), 126.8 (CH thienyl), 125.9 (CH thienyl), 123.3 ($2\times\text{CH}_{\text{Ar}}$), 117.1 ($2\times\text{CH}_{\text{Ar}}$), 106.4 (=CH), 60.1 (CHN), 21.2 (CH_3), 20.9 (CH_3) ppm.

FTIR ν_{\max} 3313 (N-H_{st}), 3015 (=C-H_{st}), 1669 (C=O_{st}), 1648 (C=CH_{st}) cm^{-1} .

HRMS (ESI-TOF) m/z calcd. for $\text{C}_{22}\text{H}_{21}\text{N}_2\text{OS}$ $[\text{M}+\text{H}]^+$ 361.1296, found 361.1360.

5-(Naphthalen-2-yl)-1-(*p*-tolyl)-3-(*p*-tolylamino)-1,5-dihydro-2*H*-pyrrol-2-one (72m).



The general procedure was followed in diethyl ether at room temperature for 18 hours, using *p*-toluidine (429 mg, 4 mmol), 2-naphthaldehyde (312 mg, 2 mmol) and ethyl pyruvate (670 μL , 6 mmol). The crude residue was purified by flash column chromatography (Hexanes/ AcOEt 90:10), affording 561 mg (70%) of **72m** as an orange solid.

Mp (Et_2O): 189 - 190 °C (dec.).

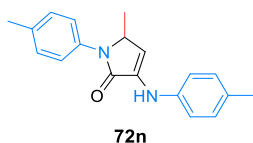
^1H NMR (400 MHz, CDCl_3) δ 7.79 - 7.72 (m, 4H, $4\times\text{CH}_{\text{Ar}}$), 7.47 - 7.41 (m, 4H, $4\times\text{CH}_{\text{Ar}}$), 7.22 (dd, $^3J_{\text{HH}} = 8.5$ Hz, $^3J_{\text{HH}} = 1.5$ Hz, 1H, CH_{Ar}), 7.09 (d, $^3J_{\text{HH}} = 8.3$ Hz, 2H, $2\times\text{CH}_{\text{Ar}}$), 7.05 (d, $^3J_{\text{HH}} = 8.3$ Hz, 2H, $2\times\text{CH}_{\text{Ar}}$), 6.99 (d, $^3J_{\text{HH}} = 8.5$ Hz, 2H, $2\times\text{CH}_{\text{Ar}}$), 6.63 (bs, 1H, NH), 6.05 (d, $^3J_{\text{HH}} = 2.6$ Hz, 1H, =CH), 5.79 (d, $^3J_{\text{HH}} = 2.6$ Hz, 1H, CHN), 2.28 (s, 3H, CH_3), 2.22 (s, 3H, CH_3) ppm.

^{13}C { ^1H } NMR (101 MHz, CDCl_3) δ 167.4 (C=O), 138.9 (C_{quat}), 135.3 (C_{quat}), 134.9 (C_{quat}), 134.8 (C_{quat}), 133.5 (C_{quat}), 133.3 (C_{quat}), 132.7 (C_{quat}), 130.8 (C_{quat}), 130.0 ($2\times\text{CH}_{\text{Ar}}$), 129.6 ($2\times\text{CH}_{\text{Ar}}$), 129.1 (CH_{Ar}), 127.9 (CH_{Ar}), 127.8 (CH_{Ar}), 126.7 (CH_{Ar}), 126.3 (CH_{Ar}), 123.9 (CH_{Ar}), 122.0 ($2\times\text{CH}_{\text{Ar}}$), 116.9 ($2\times\text{CH}_{\text{Ar}}$), 107.3 (=CH), 64.7 (CHN), 21.0 (CH_3), 20.8 (CH_3) ppm.

FTIR ν_{max} 3316 (N-H_{st}), 1663 (C=O_{st}), 1658 (C=CH_{st}) cm^{-1} .

HRMS (ESI-TOF) m/z calcd. for $\text{C}_{28}\text{H}_{25}\text{N}_2\text{O}$ $[\text{M}+\text{H}]^+$ 405.1967, found 405.1949.

5-Methyl-1-(*p*-tolyl)-3-(*p*-tolylamino)-1,5-dihydro-2*H*-pyrrol-2-one (**72n**).



The general procedure was followed in diethyl ether at room temperature for 18 hours, using *p*-toluidine (429 mg, 4 mmol), acetaldehyde (112 μL , 2 mmol) and ethyl pyruvate (670 μL , 6 mmol). The crude residue was purified by flash column chromatography (Hexanes/AcOEt 90:10), affording 445 mg (78%) of **72n** as a white solid.

Mp (Et_2O): 121 - 122 °C. Lit. 121 - 122 °C.¹¹³

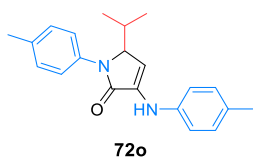
^1H NMR (300 MHz, CDCl_3) δ 7.40 (d, $^3J_{\text{HH}} = 7.8$ Hz, 2H, $2\times\text{CH}_{\text{Ar}}$), 7.23 (d, $^3J_{\text{HH}} = 8.2$ Hz, 2H, $2\times\text{CH}_{\text{Ar}}$), 7.13 (d, $^3J_{\text{HH}} = 8.2$ Hz, 2H, $2\times\text{CH}_{\text{Ar}}$), 7.00 (d, $^3J_{\text{HH}} = 7.8$ Hz, 2H, $2\times\text{CH}_{\text{Ar}}$), 6.49 (bs, 1H, NH), 6.00 (d, $^3J_{\text{HH}} = 2.5$ Hz, 1H, =CH), 4.73 (dq, $^3J_{\text{HH}} = 2.4$ Hz, $^3J_{\text{HH}} = 6.6$ Hz, 1H, CHN), 2.37 (s, 3H, CH_3 TolyI), 2.31 (s, 3H, CH_3 TolyI), 1.27 (d, $^3J_{\text{HH}} = 6.6$ Hz, 3H, CH_3) ppm.

^{13}C { ^1H } NMR (75 MHz, CDCl_3) δ 166.0 (C=O), 139.1 (C_{quat}), 134.9 (C_{quat}), 134.1 (C_{quat}), 132.9 (C_{quat}), 130.3 (C_{quat}), 129.8 ($2\times\text{CH}_{\text{Ar}}$), 129.6 ($2\times\text{CH}_{\text{Ar}}$), 122.5 ($2\times\text{CH}_{\text{Ar}}$), 116.6 ($2\times\text{CH}_{\text{Ar}}$), 107.34 (=CH), 55.6 (CHN), 20.8 (CH_3), 20.6 (CH_3), 18.7 (CH_3) ppm.

FTIR ν_{max} 3312 (N-H_{st}), 1676 (C=O_{st}), 1661 (C=CH_{st}) cm^{-1} .

HRMS (ESI-TOF) m/z calcd. for $\text{C}_{19}\text{H}_{21}\text{N}_2\text{O}$ $[\text{M}+\text{H}]^+$ 293.1653, found 293.1665.

5-*Iso*-propyl-1-(*p*-tolyl)-3-(*p*-tolylamino)-1,5-dihydro-2*H*-pyrrol-2-one (**72o**).



The general procedure was followed in diethyl ether at room temperature for 18 hours, using *p*-toluidine (429 mg, 4 mmol), isobutyraldehyde (114 μL , 2 mmol) and ethyl pyruvate (670 μL , 6 mmol). The crude residue was purified by flash column chromatography (Hexanes/AcOEt 85:15), affording 492 mg (77%) of **72o** as a white solid.

Mp (Et_2O): 201 - 203 °C.

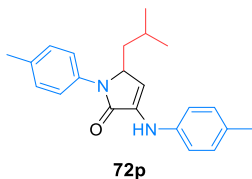
¹H NMR (300 MHz, CDCl₃) δ 7.35 (d, ³J_{HH} = 8.4 Hz, 2H, 2xCH_{Ar}), 7.23 (d, ³J_{HH} = 8.0 Hz, 2H, 2xCH_{Ar}), 7.14 (d, ³J_{HH} = 8.1 Hz, 2H, 2xCH_{Ar}), 7.01 (d, ³J_{HH} = 8.5 Hz, 2H, 2xCH_{Ar}), 6.54 (bs, 1H, NH), 5.93 (d, ³J_{HH} = 2.5 Hz, 1H, =CH), 4.68 (dd, ³J_{HH} = 3.7 Hz, ³J_{HH} = 2.5 Hz, 1H, CHN), 2.36 (s, 3H, CH₃ tolyl), 2.32 (s, 3H, CH₃ tolyl), 2.15 - 2.04 (m, 1H, CH ⁱPr), 1.09 (d, ³J_{HH} = 7.0 Hz, 3H, CH₃ ⁱPr), 0.56 (d, ³J_{HH} = 6.7 Hz, 3H, CH₃ ⁱPr) ppm.

¹³C {¹H} NMR (75 MHz, CDCl₃) δ 166.5 (C=O), 139.3 (C_{quat}), 135.4 (C_{quat}), 134.3 (C_{quat}), 134.2 (C_{quat}), 130.6 (C_{quat}), 130.0 (2xCH_{Ar}), 129.8 (2xCH_{Ar}), 123.3 (2xCH_{Ar}), 116.8 (2xCH_{Ar}), 101.8 (=CH), 65.0 (CHN), 28.4 (CH ⁱPr), 21.1 (CH₃ tolyl), 20.8 (CH₃ tolyl), 19.6 (CH₃ ⁱPr), 14.3 (CH₃ ⁱPr) ppm.

FTIR ν_{max} 3309 (N-H_{st}), 3021 (=C-H_{st}), 1666 (C=O_{st}), 1644 (C=CH_{st}) cm⁻¹.

HRMS (ESI-TOF) *m/z* calcd. for C₂₁H₂₅N₂O [M+H]⁺ 321.1967, found 321.1960.

5-Isobutyl-1-(*p*-tolyl)-3-(*p*-tolylamino)-1,5-dihydro-2H-pyrrol-2-one (72p).



The general procedure was followed in diethyl ether at room temperature for 18 hours, using *p*-toluidine (429 mg, 4 mmol), isovaleraldehyde (214 μL, 2 mmol) and ethyl pyruvate (670 μL, 6 mmol). The crude residue was purified by flash column chromatography (Hexanes/AcOEt 90:10), affording 449 mg (67%) of **72p** as a yellow solid.

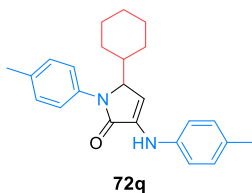
Mp (Et₂O): 178 - 179 °C.

¹H NMR (400 MHz, CDCl₃) δ 7.36 (d, ³J_{HH} = 8.4 Hz, 2H, 2xCH_{Ar}), 7.23 (d, ³J_{HH} = 8.4 Hz, 2H, 2xCH_{Ar}), 7.13 (d, ³J_{HH} = 8.4 Hz, 2H, 2xCH_{Ar}), 7.00 (d, ³J_{HH} = 8.4 Hz, 2H, 2xCH_{Ar}), 6.49 (bs, 1H, NH), 6.10 (d, ³J_{HH} = 2.5 Hz, 1H, =CH), 4.76 (m, 1H, CHN), 2.37 (s, 3H, CH₃ tolyl), 2.31 (s, 3H, CH₃ tolyl), 1.78 (m, 1H, CH ⁱBu), 1.24 (m, 2H, CH₂), 1.00 (d, ³J_{HH} = 6.5 Hz, 3H, CH₃ ⁱBu), 0.86 (d, ³J_{HH} = 6.5 Hz, 3H, CH₃ ⁱBu) ppm.

¹³C {¹H} NMR (101 MHz, CDCl₃) δ 166.2 (C=O), 139.3 (C_{quat}), 135.2 (C_{quat}), 134.3 (C_{quat}), 133.5 (C_{quat}), 130.6 (C_{quat}), 130.0 (2xCH_{Ar}), 129.8 (2xCH_{Ar}), 123.0 (2xCH_{Ar}), 116.8 (2xCH_{Ar}), 105.6 (=CH), 58.7 (CHN), 41.8 (CH₂), 25.3 (CH ⁱBu), 24.1 (CH₃ ⁱBu), 22.2 (CH₃ ⁱBu), 21.1 (CH₃ tolyl), 20.8 (CH₃ tolyl) ppm.

FTIR ν_{max} 3300 (N-H_{st}), 1675 (C=O_{st}), 1662 (C=CH_{st}) cm⁻¹.

HRMS (ESI-TOF) *m/z* calcd. for C₂₂H₂₇N₂O [M+H]⁺ 335.2123, found 335.2124.

5-Cyclohexyl-1-(*p*-tolyl)-3-(*p*-tolylamino)-1,5-dihydro-2*H*-pyrrol-2-one (72q).

The general procedure was followed in diethyl ether at room temperature for 18 hours, using *p*-toluidine (429 mg, 4 mmol), cyclohexanecarboxaldehyde (242 μ L, 2 mmol) and ethyl pyruvate (670 μ L, 6 mmol). The crude residue was purified by crystallization from diethyl ether, affording 655 mg (91%) of **72q** as a white solid.

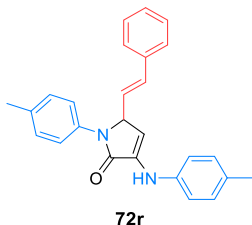
Mp (Et₂O): 212 - 214 °C.

¹H NMR (300 MHz, CDCl₃) δ 7.33 (d, ³J_{HH} = 8.4 Hz, 2H, 2xCH_{Ar}), 7.23 (d, ³J_{HH} = 8.4 Hz, 2H, 2xCH_{Ar}), 7.13 (d, ³J_{HH} = 8.4 Hz, 2H, 2xCH_{Ar}), 7.00 (d, ³J_{HH} = 8.4 Hz, 2H, 2xCH_{Ar}), 6.50 (bs, 1H, NH), 5.96 (d, ³J_{HH} = 2.5 Hz, 1H, =CH), 4.64 (d, ³J_{HH} = 2.5 Hz, 1H, CHN), 2.37 (s, 3H, CH₃), 2.32 (s, 3H, CH₃), 1.82 - 1.72 (m, 3H, Cy), 1.62 - 1.54 (m, 2H, Cy), 1.34 - 1.18 (m, 4H, Cy), 0.97 - 0.81 (m, 2H, Cy) ppm.

¹³C {¹H} NMR (75 MHz, CDCl₃) δ 166.6 (C=O), 139.3 (C_{quat}), 135.3 (C_{quat}), 134.3 (C_{quat}), 133.8 (C_{quat}), 130.5 (C_{quat}), 130.0 (2xCH_{Ar}), 129.8 (2xCH_{Ar}), 123.4 (2xCH_{Ar}), 116.8 (2xCH_{Ar}), 103.2 (=CH), 64.7 (CHN), 38.7 (CH Cy), 30.4 (CH₂ Cy), 26.7 (CH₂ Cy), 26.6 (CH₂ Cy), 25.6 (CH₂ Cy), 25.2 (CH₂ Cy), 21.2 (CH₃), 20.8 (CH₃) ppm.

FTIR ν_{\max} 3310 (N-H_{st}), 3017(=C-H_{st}), 1663 (C=O_{st}), 1648 (C=CH_{st}) cm⁻¹.

HRMS (ESI-TOF) *m/z* calcd. for C₂₄H₂₉N₂O [M+H]⁺ 361.2280, found 361.2266.

(*E*)-5-Styryl-1-(*p*-tolyl)-3-(*p*-tolylamino)-1,5-dihydro-2*H*-pyrrol-2-one (72r).

The general procedure was followed in diethyl ether at room temperature for 18 hours, using *p*-toluidine (429 mg, 4 mmol), cinnamaldehyde (252 μ L, 2 mmol) and ethyl pyruvate (670 μ L, 6 mmol). The crude residue was purified by flash column chromatography (Hexanes/AcOEt 80:20), affording 462 mg (61%) of **72r** as a white solid.

Mp (Et₂O): 180 - 182 °C (dec.).

¹H NMR (300 MHz, CDCl₃) δ 7.39 (d, ³J_{HH} = 7.9 Hz, 2H, 2xCH_{Ar}), 7.31 - 7.17 (m, 7H, 5xCH_{Ar} + 2xCH vinyl), 7.10 (d, ³J_{HH} = 7.5 Hz, 2H, 2xCH_{Ar}), 7.08 (d, ³J_{HH} = 7.5 Hz, 2H, 2xCH_{Ar}), 6.98 (d, ³J_{HH} = 7.7 Hz, 2H, 2xCH_{Ar}), 6.56 (bs, 1H, NH), 6.01 (m, 1H, =CH), 5.64 (m, 1H, CHN), 2.29 (s, 3H, CH₃), 2.26 (s, 3H, CH₃) ppm.

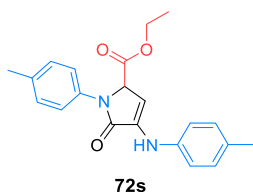
¹³C {¹H} NMR (75 MHz, CDCl₃) δ 167.4 (C=O), 139.1 (C_{quat}), 137.9 (C_{quat}), 134.9 (C_{quat}), 134.9 (C_{quat}), 132.6 (C_{quat}), 130.9 (C_{quat}), 130.1 (2xCH_{Ar}), 129.7 (2xCH_{Ar}), 129.2 (2xCH_{Ar}), 128.3 (CH_{Ar}), 127.0 (2xCH_{Ar}),

121.9 (2xCH_{Ar}), 120.5 (=CH), 117.0 (2xCH_{Ar}), 108.2 (=CH), 107.5 (=CH), 64.6 (CHN), 21.1 (CH₃), 20.9 (CH₃) ppm.

FTIR ν_{\max} 3303 (N-H_{st}), 3022 (=C-H_{st}), 1669 (C=O_{st}), 1657 (C=CH_{st}) cm⁻¹.

HRMS (ESI-TOF) m/z calcd. for C₂₆H₂₅N₂O [M+H]⁺ 381.1967, found 381.1960.

Ethyl 5-oxo-1-(*p*-tolyl)-4-(*p*-tolylamino)-2,5-dihydro-1*H*-pyrrole-2-carboxylate (72s).



The general procedure was followed in diethyl ether at room temperature for 18 hours, using *p*-toluidine (429 mg, 4 mmol), a 50% solution of ethyl glyoxalate in toluene (407 μ L, 2 mmol) and ethyl pyruvate (670 μ L, 6 mmol). The crude residue crystallized from diethyl ether, affording 633 mg (90%) of **72s** as a white solid.

Mp (Et₂O): 159 - 160 °C. Lit.159 - 160 °C.¹¹³

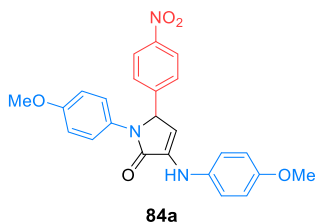
¹H NMR (400 MHz, CDCl₃) δ 7.48 (d, ³J_{HH} = 8.5 Hz, 2H, 2xCH_{Ar}), 7.20 (d, ³J_{HH} = 8.5 Hz, 2H, 2xCH_{Ar}), 7.14 (d, ³J_{HH} = 8.2 Hz, 2H, 2xCH_{Ar}), 6.99 (d, ³J_{HH} = 8.4 Hz, 2H, 2xCH_{Ar}), 6.59 (bs, 1H, NH), 5.91 (d, ³J_{HH} = 2.9 Hz, 1H, =CH), 5.26 (d, ³J_{HH} = 2.8 Hz, 1H, CHN), 4.13 (m, 2H, CH₂), 2.34 (s, 3H, CH₃ tolyl), 2.32 (s, 3H, CH₃ tolyl), 1.16 (t, ³J_{HH} = 7.1 Hz, 3H, CH₃) ppm.

¹³C {¹H} NMR (101 MHz, CDCl₃) δ 169.0 (C=O ester), 166.7 (C=O amide), 138.5 (C_{quat}), 135.3 (C_{quat}), 135.2 (C_{quat}), 135.2 (C_{quat}), 131.4 (C_{quat}), 130.0 (2xCH_{Ar}), 129.9 (2xCH_{Ar}), 120.7 (2xCH_{Ar}), 117.2 (2xCH_{Ar}), 98.2 (=CH), 62.9 (CHN), 62.1 (CH₂), 21.1 (CH₃ tolyl), 20.8 (CH₃ tolyl), 14.1 (CH₃) ppm.

FTIR ν_{\max} 3312 (N-H_{st}), 1750 (C=O_{st} ester), 1670 (C=O_{st} amide), 1650 (C=CH_{st}), 1175 (C-O_{st}) cm⁻¹.

HRMS (ESI-TOF) m/z calcd. for C₂₁H₂₃N₂O₃ [M+H]⁺ 351.1708, found 351.1701.

1-(4-Methoxyphenyl)-3-((4-methoxyphenyl)amino)-5-(4-nitrophenyl)-1,5-dihydro-2*H*-pyrrol-2-one (84a).



The general procedure was followed in diethyl ether at room temperature for 24 hours, using *p*-anisidine (492 mg, 4 mmol), *p*-nitrobenzaldehyde (302 mg, 2 mmol) and ethyl pyruvate (670 μ L, 6 mmol). The crude residue was purified by flash column chromatography (Hexanes/AcOEt 80:20), affording 698 mg (81%) of **84a** as a yellow solid.

Mp (Et₂O): 207 - 209 °C. Lit. 214 - 216 °C.¹¹⁵

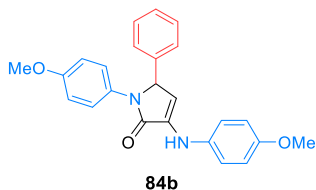
$^1\text{H NMR}$ (400 MHz, CDCl_3) δ 8.13 (d, $^3J_{\text{HH}} = 6.9$ Hz, 2H, 2xCH_{Ar}), 7.38 (d, $^3J_{\text{HH}} = 7.0$ Hz, 2H, 2xCH_{Ar}), 7.35 (d, $^3J_{\text{HH}} = 7.1$ Hz, 2H, 2xCH_{Ar}), 7.04 (d, $^3J_{\text{HH}} = 7.0$ Hz, 2H, 2xCH_{Ar}), 6.97 - 6.79 (m, 4H, 4xCH_{Ar}), 6.53 (s, 1H, NH), 5.88 (d, $^3J_{\text{HH}} = 2.6$ Hz, 1H, =CH), 5.68 (d, $^3J_{\text{HH}} = 2.6$ Hz, 1H, CHN), 3.78 (s, 3H, CH₃O), 3.74 (s, 3H, CH₃O) ppm.

$^{13}\text{C}\{^1\text{H}\}$ NMR (101 MHz, CDCl_3) δ 167.0 (C=O), 157.4 (C_{quat}), 154.9 (C_{quat}), 147.8 (C_{quat}), 145.7 (C_{quat}), 134.4 (C_{quat}), 134.0 (C_{quat}), 129.7 (C_{quat}), 127.9 (2xCH_{Ar}), 124.4 (2xCH_{Ar}), 123.8 (2xCH_{Ar}), 118.9 (2xCH_{Ar}), 114.9 (2xCH_{Ar}), 114.5 (2xCH_{Ar}), 104.2 (=CH), 64.0 (CHN), 55.7 (CH₃O), 55.5 (CH₃O) ppm.

FTIR ν_{max} 3303 (N-H_{st}), 1685 (C=O_{st}), 1653 (C=CH_{st}), 1511 (NO_{2st}as), 1340 (NO_{2st}sym), 1220 (C-O_{st}), 1248 (C-O_{st}) cm^{-1} .

HRMS (ESI-TOF) m/z calcd. for C₂₄H₂₂N₃O₅ [M+H]⁺ 432.1559, found 432.1553.

1-(4-Methoxyphenyl)-3-((4-methoxyphenyl)amino)-5-phenyl-1,5-dihydro-2H-pyrrol-2-one (84b).



The general procedure was followed in diethyl ether at room temperature for 18 hours, using *p*-anisidine (492 mg, 4 mmol), benzaldehyde (204 μL , 2 mmol) and ethyl pyruvate (670 μL , 6 mmol).

The crude residue was purified by flash column chromatography (Hexanes/AcOEt 80:20), affording 600 mg (78%) of **84b** as a white solid.

Mp (Et₂O): 198 - 200 °C. Lit. 197 - 199 °C.²⁴¹

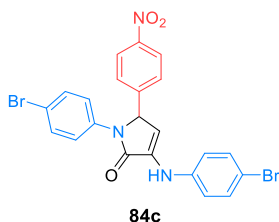
$^1\text{H NMR}$ (300 MHz, CDCl_3) δ 7.36 (d, $^3J_{\text{HH}} = 9.1$ Hz, 2H, 2xCH_{Ar}), 7.30 - 7.16 (m, 5H, 5xCH_{Ar}), 7.03 (d, $^3J_{\text{HH}} = 8.9$ Hz, 2H, 2xCH_{Ar}), 6.86 (d, $^3J_{\text{HH}} = 8.9$ Hz, 2H, 2xCH_{Ar}), 6.81 (d, $^3J_{\text{HH}} = 9.1$ Hz, 2H, 2xCH_{Ar}), 6.46 (bs, 1H, NH), 5.94 (d, $^3J_{\text{HH}} = 2.5$ Hz, 1H, =CH), 5.57 (d, $^3J_{\text{HH}} = 2.5$ Hz, 1H, CHN), 3.78 (s, 3H, CH₃), 3.74 (s, 3H, CH₃) ppm.

$^{13}\text{C}\{^1\text{H}\}$ NMR (75 MHz, CDCl_3) δ 167.3 (C=O), 157.1 (C_{quat}), 154.5 (C_{quat}), 137.8 (C_{quat}), 135.0 (C_{quat}), 133.1 (C_{quat}), 130.4 (C_{quat}), 129.0 (2xCH_{Ar}), 128.2 (2xCH_{Ar}), 127.1 (2xCH_{Ar}), 123.9 (2xCH_{Ar}), 118.6 (2xCH_{Ar}), 114.8 (2xCH_{Ar}), 114.3 (2xCH_{Ar}), 106.3 (=CH), 64.9 (CHN), 55.7 (CH₃), 55.5 (CH₃) ppm.

FTIR ν_{max} 3304 (N-H_{st}), 3017 (=C-H_{st}), 1669 (C=O_{st}), 1659 (C=CH_{st}), 1250 (C-O_{st}), 1032 (C-O_{st}) cm^{-1} .

HRMS (ESI-TOF) m/z calcd. for C₂₄H₂₃N₂O₃ [M+H]⁺ 387.1708, found 387.1702.

1-(4-Bromophenyl)-3-((4-bromophenyl)amino)-5-(4-nitrophenyl)-1,5-dihydro-2H-pyrrol-2-one (84c).



The general procedure was followed in diethyl ether at room temperature for 18 hours, using *p*-bromoaniline (688 mg, 4 mmol), *p*-nitrobenzaldehyde (302 mg, 2 mmol) and ethyl pyruvate (670 μ L, 6 mmol). The crude residue was purified by flash column chromatography (Hexanes/AcOEt 80:20), affording 938 mg (89%) of **84c** as a yellow solid.

Mp (Et₂O): 119 - 220 °C.

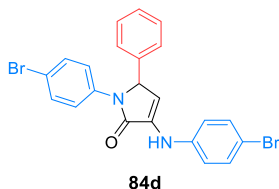
¹H NMR (300 MHz, DMSO-*d*₆) δ 8.49 (bs, 1H, NH), 8.15 (d, 2H, 2xCH_{Ar}), 7.70 - 7.20 (m, 10H, 10xCH_{Ar}), 6.43 (bs, 1H, =CH), 6.27 (bs, 1H, CHN) ppm.

¹³C {¹H} NMR (75 MHz, DMSO-*d*₆) δ 166.2 (C=O), 147.1 (C_{quat}), 145.5 (C_{quat}), 141.2 (C_{quat}), 136.1 (C_{quat}), 132.1 (C_{quat}), 131.7 (2xCH_{Ar}), 131.6 (2xCH_{Ar}), 128.2 (2xCH_{Ar}), 124.1 (2xCH_{Ar}), 123.2 (2xCH_{Ar}), 118.9 (2xCH_{Ar}), 117.0 (C_{quat}), 111.7 (C_{quat}), 109.6 (=CH), 61.5 (CHN) ppm.

FTIR ν_{\max} 3317 (N-H_{st}), 3116 (=C-H_{st}), 1679 (C=O_{st}), 1661 (C=CH_{st}), 1519 (NO_{2st}as), 1348 (NO_{2st}sym), 1077 (C-Br_{st}), 824 (C-Br_{st}) cm⁻¹.

HRMS (ESI-TOF) *m/z* calcd. for C₂₂H₁₆Br₂N₃O₃ [M+H]⁺ 527.9558, found 527.9597.

1-(4-Bromophenyl)-3-((4-bromophenyl)amino)-5-phenyl-1,5-dihydro-2H-pyrrol-2-one (84d).



The general procedure was followed in diethyl ether at room temperature for 24 hours, using *p*-bromoaniline (688 mg, 4 mmol), benzaldehyde (204 μ L, 2 mmol) and ethyl pyruvate (670 μ L, 6 mmol). The crude residue was purified by flash column chromatography (Hexanes/AcOEt 80:20), affording 792 mg (82%) of **84d** as a white solid.

Mp (Et₂O): 225 - 226 °C. Lit. 226 - 228 °C.^{123b}

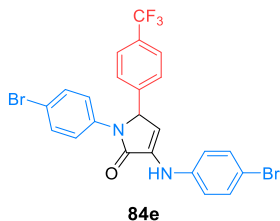
¹H NMR (400 MHz, CDCl₃) δ 7.45 (d, ³J_{HH} = 9.0 Hz, 2H, 2xCH_{Ar}), 7.39 (d, ³J_{HH} = 9.2 Hz, 2H, 2xCH_{Ar}), 7.38 (d, ³J_{HH} = 8.9 Hz, 2H, 2xCH_{Ar}), 7.32 - 7.24 (m, 3H, 3xCH_{Ar}), 7.18 (d, ³J_{HH} = 8.3 Hz, 2H, 2xCH_{Ar}), 6.94 (d, ³J_{HH} = 8.9 Hz, 2H, 2xCH_{Ar}), 6.66 (s, 1H, NH), 6.05 (d, ³J_{HH} = 2.6 Hz, 1H, =CH), 5.63 (d, ³J_{HH} = 2.6 Hz, 1H, CHN) ppm.

¹³C {¹H} NMR (101 MHz, CDCl₃) δ 167.1 (C=O), 140.3 (C_{quat}), 136.9 (C_{quat}), 136.4 (C_{quat}), 132.4 (2xCH_{Ar}), 132.1 (2xCH_{Ar}), 131.8 (C_{quat}), 129.3 (2xCH_{Ar}), 128.6 (CH_{Ar}), 126.7 (2xCH_{Ar}), 122.9 (2xCH_{Ar}), 118.4 (2xCH_{Ar}), 118.1 (C_{quat}), 113.6 (C_{quat}), 108.9 (=CH), 64.3 (CHN) ppm.

FTIR ν_{\max} 3327 (N-H_{st}), 1672 (C=O_{st}), 1642 (C=CH_{st}), 1073 (C-Br_{st}), 820 (C-Br_{st}) cm⁻¹.

HRMS (ESI-TOF) m/z calcd. for $C_{22}H_{17}Br_2N_2O$ $[M+H]^+$ 482.9707, found 482.9715.

1-(4-Bromophenyl)-3-((4-bromophenyl)amino)-5-(4-(trifluoromethyl)phenyl)-1,5-dihydro-2H-pyrrol-2-one (84e).



The general procedure was followed in diethyl ether at room temperature for 18 hours, using *p*-bromoaniline (688 mg, 4 mmol), *p*-(trifluoromethyl)benzaldehyde (273 μ L, 2 mmol) and ethyl pyruvate (670 μ L, 6 mmol). The crude residue was purified by crystallization from diethyl ether, affording 1.077 g of **84e** (98%) as a white solid.

Mp (Et₂O): 240 - 242 °C (dec.).

¹H NMR (400 MHz, CDCl₃) δ 7.57 (d, ³*J*_{HH} = 8.2 Hz, 2H, 2xCH_{Ar}), 7.44 - 7.41 (m, 4H, 4xCH_{Ar}), 7.40 (d, ³*J*_{HH} = 8.9 Hz, 2H, 2xCH_{Ar}), 7.31 (d, ³*J*_{HH} = 7.9 Hz, 2H, 2xCH_{Ar}), 6.94 (d, ³*J*_{HH} = 8.9 Hz, 2H, 2xCH_{Ar}), 6.65 (bs, 1H, NH), 6.01 (d, ³*J*_{HH} = 2.6 Hz, 1H, =CH), 5.70 (d, ³*J*_{HH} = 2.6 Hz, 1H, CHN) ppm.

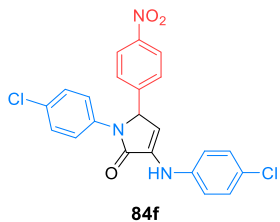
¹³C {¹H} NMR (101 MHz, CDCl₃) δ 166.9 (C=O), 141.2 (C_{quat}), 140.0 (C_{quat}), 136.0 (C_{quat}), 132.5 (2xCH_{Ar}), 132.3 (2xCH_{Ar}), 132.2 (C_{quat}), 130.9 (q, ²*J*_{FC} = 32.7 Hz, C_{quat}), 127.1 (2xCH_{Ar}), 126.4 (q, ³*J*_{FC} = 3.7 Hz, 2xCH_{Ar}), 123.9 (q, ¹*J*_{FC} = 272.2 Hz, CF₃), 122.7 (2xCH_{Ar}), 118.5 (2xCH_{Ar}), 118.5 (C_{quat}), 114.0 (C_{quat}), 107.7 (=CH), 63.6 (CHN) ppm.

¹⁹F NMR (282 MHz, CDCl₃) δ -63.1 ppm.

FTIR ν_{max} 3444 (N-H_{st}), 1678 (C=O_{st}), 1664 (C=CH_{st}), 1162 (C-F_{st}) 1071 (C-Br_{st}) cm⁻¹.

HRMS (ESI-TOF) m/z calcd. for $C_{23}H_{16}Br_2F_3N_2O$ $[M+H]^+$ 550.9581, found 550.9603.

1-(4-Chlorophenyl)-3-((4-chlorophenyl)amino)-5-(4-nitrophenyl)-1,5-dihydro-2H-pyrrol-2-one (84f).



The general procedure was followed in MTBE at 55 °C (heating plate) for 18 hours, using *p*-chloroaniline (510 mg, 4 mmol), *p*-nitrobenzaldehyde (302 mg, 2 mmol) and ethyl pyruvate (670 μ L, 6 mmol). The crude residue was purified by flash column chromatography (Hexanes/AcOEt 90:10), affording 692 mg (80%) of **84f** as a yellow solid.

Mp (Et₂O): 151 - 153 °C.

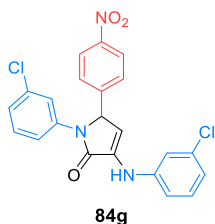
¹H NMR (400 MHz, DMSO-*d*₆) δ 8.49 (bs, 1H, NH), 8.15 (d, ³*J*_{HH} = 8.8 Hz, 2H, 2xCH_{Ar}), 7.67 (d, ³*J*_{HH} = 8.9 Hz, 2H, 2xCH_{Ar}), 7.56 (d, ³*J*_{HH} = 8.7 Hz, 2H, 2xCH_{Ar}), 7.40 (d, ³*J*_{HH} = 8.9 Hz, 2H, 2xCH_{Ar}), 7.32 (d, ³*J*_{HH} = 9.1 Hz, 2H, 2xCH_{Ar}), 7.27 (d, ³*J*_{HH} = 8.8 Hz, 2H, 2xCH_{Ar}), 6.43 (d, ³*J*_{HH} = 2.7 Hz, 1H, =CH), 6.28 (d, ³*J*_{HH} = 2.7 Hz, 1H, CHN) ppm.

¹³C {¹H} NMR (101 MHz, DMSO-*d*₆) δ 166.3 (C=O), 147.1 (C_{quat}), 145.5 (C_{quat}), 140.8 (C_{quat}), 135.7 (C_{quat}), 132.2 (C_{quat}), 128.9 (2xCH_{Ar}), 128.8 (2xCH_{Ar}), 128.2 (2xCH_{Ar}), 124.1 (2xCH_{Ar}), 124.0 (C_{quat}), 122.9 (2xCH_{Ar}), 118.5 (2xCH_{Ar}), 109.4 (=CH), 61.6 (CHN) ppm.

FTIR ν_{max} 3310 (N-H_{st}), 1679 (C=O_{st}), 1657 (C=CH_{st}), 1516 (NO₂_{st as}), 1347 (NO₂_{st sym}), 1110 (C-Cl_{st}) cm⁻¹.

HRMS (ESI-TOF) *m/z* calcd. for C₂₂H₁₆Cl₂N₃O₃ [M+H]⁺ 440.0568, found 440.0551.

1-(3-Chlorophenyl)-3-((3-chlorophenyl)amino)-5-(4-nitrophenyl)-1,5-dihydro-2H-pyrrol-2-one (84g).



The general procedure was followed in diethyl ether at room temperature for 72 hours, using *m*-chloroaniline (423 μL, 4 mmol), *p*-nitrobenzaldehyde (302 mg, 2 mmol) and ethyl pyruvate (670 μL, 6 mmol). The crude residue was purified by crystallization from diethyl ether, affording 737 mg (84%) of **84g** as a yellow solid.

Mp (Et₂O): 149 - 151 °C.

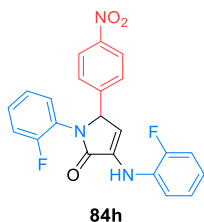
¹H NMR (400 MHz, CDCl₃) δ 8.18 (d, ³J_{HH} = 8.7 Hz, 2H, 2xCH_{Ar}), 7.66 (t, ⁴J_{HH} = 1.9 Hz, 1H, CH_{Ar}), 7.39 (d, ³J_{HH} = 8.7 Hz, 2H, 2xCH_{Ar}), 7.34 (d, ³J_{HH} = 8.2 Hz, 1H, CH_{Ar}), 7.23 (dt, ³J_{HH} = 8.1 Hz, ⁴J_{HH} = 3.0 Hz, 2H, 2xCH_{Ar}), 7.10 (d, ³J_{HH} = 8.0 Hz, 1H, CH_{Ar}), 7.06 (s, 1H, CH_{Ar}), 6.98 - 6.91 (m, 2H, 2xCH_{Ar}), 6.72 (bs, 1H, NH), 6.06 (d, ³J_{HH} = 2.7 Hz, 1H, =CH), 5.78 (d, ³J_{HH} = 2.7 Hz, 1H, CHN) ppm.

¹³C {¹H} NMR (101 MHz, CDCl₃) δ 166.7 (C=O), 148.1 (C_{quat}), 144.5 (C_{quat}), 141.9 (C_{quat}), 137.8 (C_{quat}), 135.4 (C_{quat}), 135.1 (C_{quat}), 132.2 (C_{quat}), 130.7 (CH_{Ar}), 130.3 (CH_{Ar}), 127.6 (2xCH_{Ar}), 125.7 (CH_{Ar}), 124.8 (2xCH_{Ar}), 122.1 (CH_{Ar}), 121.4 (CH_{Ar}), 119.0 (CH_{Ar}), 116.8 (CH_{Ar}), 115.4 (CH_{Ar}), 107.5 (=CH), 63.3 (CHN) ppm.

FTIR ν_{max} 3307 (N-H_{st}), 1675 (C=O_{st}), 1648 (C=CH_{st}), 1516 (NO₂_{st as}), 1348 (NO₂_{st sym}), 1109 (C-Cl_{st}) cm⁻¹.

HRMS (ESI-TOF) *m/z* calcd. for C₂₂H₁₆Cl₂N₃O₃ [M+H]⁺ 440.0568, found 440.0541.

1-(2-Fluorophenyl)-3-((2-fluorophenyl)amino)-5-(4-nitrophenyl)-1,5-dihydro-2H-pyrrol-2-one (84h).



The general procedure was followed in diethyl ether at room temperature for 18 hours, using *o*-fluoroaniline (386 μL, 4 mmol), *p*-nitrobenzaldehyde (302 mg, 2 mmol) and ethyl pyruvate (670 μL, 6 mmol). The crude residue was purified by flash column chromatography (Hexanes/AcOEt 80:20), affording 577 mg (71%) of **84h** as a yellow solid.

Mp (Et₂O): 164 - 166 °C.

¹H NMR (300 MHz, CDCl₃) δ 8.13 (d, ³J_{HH} = 8.0 Hz, 2H, 2xCH_{Ar}), 7.41 (d, ³J_{HH} = 8.0 Hz, 2H, 2xCH_{Ar}), 7.38 - 7.04 (m, 7H, 7xCH_{Ar}), 6.96 (m, 1H, CH_{Ar}), 6.89 (bs, 1H, NH), 6.17 (d, ³J_{HH} = 2.6 Hz, 1H, =CH), 5.86 (d, ³J_{HH} = 2.6 Hz, 1H, CHN) ppm.

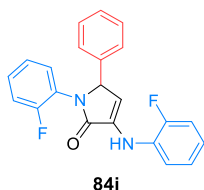
¹³C {¹H} NMR (75 MHz, CDCl₃) δ 166.7 (C=O), 157.1 (d, ¹J_{FC} = 250.2 Hz, C_{quat}), 152.6 (d, ¹J_{FC} = 244.0 Hz, C_{quat}), 148.1 (C_{quat}), 144.3 (C_{quat}), 132.8 (C_{quat}), 129.6 (d, ²J_{FC} = 10.9 Hz, C_{quat}), 129.1 (d, ³J_{FC} = 8.0 Hz, CH_{Ar}), 128.4 (2xCH_{Ar}), 128.2 (d, ⁴J_{FC} = 1.1 Hz, CH_{Ar}), 124.9 (d, ³J_{FC} = 3.6 Hz, CH_{Ar}), 124.7 (d, ³J_{FC} = 3.8 Hz, CH_{Ar}), 124.3 (2xCH_{Ar}), 123.6 (d, ²J_{FC} = 11.4 Hz, C_{quat}), 122.0 (d, ³J_{FC} = 7.3 Hz, CH_{Ar}), 117.0 (d, ⁴J_{FC} = 1.1 Hz, CH_{Ar}), 116.9 (d, ²J_{FC} = 20.0 Hz, CH_{Ar}), 115.7 (d, ²J_{FC} = 19.0 Hz, CH_{Ar}), 107.9 (=CH), 64.4 (d, ⁴J_{FC} = 4.8 Hz, CHN) ppm.

¹⁹F NMR (282 MHz, CDCl₃) δ -120.7, -131.5 ppm.

FTIR ν_{max} 3354 (N-H_{st}), 1717 (C=O_{st}), 1691 (C=CH_{st}), 1489 (NO₂_{st as}), 1346 (NO₂_{st sym}), 1220 (C-F_{st}), 1096 (C-F_{st}) cm⁻¹.

HRMS (ESI-TOF) *m/z* calcd. for C₂₂H₁₆F₂N₃O₃ [M+H]⁺ 408.1159, found 408.1152.

1-(2-Fluorophenyl)-3-((2-fluorophenyl)amino)-5-phenyl-1,5-dihydro-2H-pyrrol-2-one (84i).



The general procedure was followed in diethyl ether at room temperature for 24 hours, using *o*-fluoroaniline (386 μL, 4 mmol), benzaldehyde (204 μL, 2 mmol) and ethyl pyruvate (670 μL, 6 mmol). The crude residue crystallized from diethyl ether, affording 533 mg (74%) of **84i** as a white solid.

Mp (Et₂O): 176 - 178 °C.

¹H NMR (400 MHz, CDCl₃) δ 7.33 - 7.19 (m, 6H, 6xCH_{Ar}), 7.17 - 7.03 (m, 5H, 5xCH_{Ar}), 6.94 - 6.84 (m, 2H, 2xCH_{Ar}), 6.21 (d, ³J_{HH} = 2.6 Hz, 1H, =CH), 5.73 (d, ³J_{HH} = 2.6 Hz, 1H, CHN) ppm.

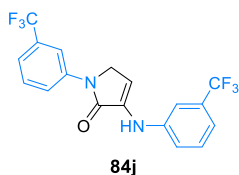
¹³C {¹H} NMR (101 MHz, CDCl₃) δ 167.0 (C=O), 157.4 (d, ¹J_{FC} = 250.3 Hz, C_{quat}), 152.5 (d, ¹J_{FC} = 243.6 Hz, C_{quat}), 136.6 (C_{quat}), 132.1 (C_{quat}), 130.1 (d, ²J_{FC} = 10.9 Hz, C_{quat}), 128.9 (2xCH_{Ar}), 128.7 (CH_{Ar}), 128.6 (d, ³J_{FC} = 8.0 Hz, CH_{Ar}), 128.5 (d, ⁴J_{FC} = 1.6 Hz, CH_{Ar}), 127.5 (2xCH_{Ar}), 124.6 (d, ³J_{FC} = 6.6 Hz, CH_{Ar}), 124.5 (d, ³J_{FC} = 6.6 Hz, CH_{Ar}), 124.1 (d, ²J_{FC} = 11.6 Hz, C_{quat}), 121.4 (d, ³J_{FC} = 7.2 Hz, CH_{Ar}), 116.7 (d, ⁴J_{FC} = 1.7 Hz, CH_{Ar}), 116.6 (d, ²J_{FC} = 20.3 Hz, CH_{Ar}), 115.5 (d, ²J_{FC} = 18.7 Hz, CH_{Ar}), 109.8 (=CH), 65.41 (d, ⁴J_{FC} = 4.3 Hz, CHN) ppm.

¹⁹F NMR (282 MHz, CDCl₃) δ -120.6, -132.1 ppm.

FTIR ν_{max} 3323 (N-H_{st}), 1693 (C=O_{st}), 1657 (C=CH_{st}), 1112 (C-F_{st}) cm⁻¹.

HRMS (ESI-TOF) m/z calcd. for $C_{22}H_{17}F_2N_2O$ $[M+H]^+$ 363.1309, found 363.1303.

1-(3-(Trifluoromethyl)phenyl)-3-((3-(trifluoromethyl)phenyl)amino)-1,5-dihydro-2H-pyrrol-2-one (84j).



The general procedure was followed in diethyl ether at room temperature for 72 hours, using *m*-(trifluoromethyl)aniline (499 mg, 4 mmol), 37% aqueous solution of formaldehyde (150 μ L, 2 mmol) and ethyl pyruvate (670 μ L, 6 mmol). The crude residue was purified by flash column chromatography (Hexanes/AcOEt 90:10), affording 562 mg (73%) of **84j** as an orange solid.

Mp (Et₂O): 160 - 162 °C.

¹H NMR (300 MHz, CDCl₃) δ 8.08 - 8.03 (m, 2H, 2xCH_{Ar}), 7.58 - 7.23 (m, 6H, 6xCH_{Ar}), 6.76 (s, 1H, NH), 6.17 (t, ³J_{HH} = 2.6 Hz, 1H, =CH), 4.50 (d, ³J_{HH} = 2.6 Hz, 2H, CH₂) ppm.

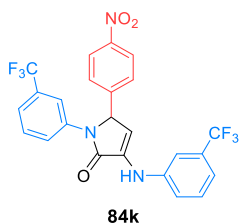
¹³C {¹H} NMR (75 MHz, CDCl₃) δ 166.5 (C=O), 141.9 (C_{quat}), 139.6 (C_{quat}), 133.7 (C_{quat}), 132.1 (q, ²J_{FC} = 32.4 Hz, C_{quat}), 131.9 (q, ²J_{FC} = 32.4 Hz, C_{quat}), 130.2 (CH_{Ar}), 130.1 (CH_{Ar}), 124.1 (q, ¹J_{FC} = 272.5 Hz, CF₃), 124.0 (q, ¹J_{FC} = 272.4 Hz, CF₃), 121.8 (CH_{Ar}), 121.3 (q, ³J_{FC} = 3.7 Hz, CH_{Ar}), 120.0 (CH_{Ar}), 118.1 (q, ³J_{CF} = 3.9 Hz, CH_{Ar}), 115.3 (q, ³J_{CF} = 3.9 Hz, CH_{Ar}), 112.9 (q, ³J_{CF} = 3.8 Hz, CH_{Ar}), 102.4 (=CH), 49.7 (CH₂) ppm.

¹⁹F NMR (282 MHz, CDCl₃) δ -63.2, -63.3 ppm.

FTIR ν_{max} 3342 (N-H_{st}), 3092 (=C-H_{st}), 1685 (C=O_{st}), 1654 (C=C_{st}) cm⁻¹.

HRMS (ESI-TOF) m/z calcd. for $C_{18}H_{13}F_6N_2O$ $[M+H]^+$ 387.0932, found 387.0934.

5-(4-Nitrophenyl)-1-(3-(trifluoromethyl)phenyl)-3-((3-(trifluoromethyl)phenyl)amino)-1,5-dihydro-2H-pyrrol-2-one (84k).



The general procedure was followed in diethyl ether at room temperature for 72 hours, using *m*-(trifluoromethyl)aniline (499 mg, 4 mmol), *p*-nitrobenzaldehyde (302 mg, 2 mmol) and ethyl pyruvate (670 μ L, 6 mmol). The crude residue was purified by flash column chromatography (Hexanes/AcOEt 80:20), affording 667 mg (66%) of **84k** as a yellow solid.

Mp (Et₂O): 122 - 124 °C.

¹H NMR (400 MHz, CDCl₃) δ 8.19 (d, ³J_{HH} = 8.7 Hz, 2H, 2xCH_{Ar}), 7.90 (bs, 1H, CH_{Ar}), 7.68 (d, ³J_{HH} = 7.9 Hz, 1H, CH_{Ar}), 7.48 - 7.34 (m, 5H, 5xCH_{Ar}), 7.30 (s, 1H, CH_{Ar}), 7.26 - 7.21 (m, 2H, 2xCH_{Ar}), 6.88 (bs, 1H, NH), 5.55 (d, ³J_{HH} = 3.9 Hz, 1H, =CH), 5.18 (d, ³J_{HH} = 3.9 Hz, 1H, CHN) ppm.

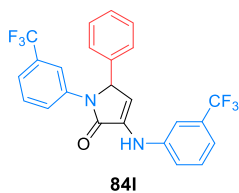
^{13}C { ^1H } NMR (101 MHz, CDCl_3) δ 166.8 (C=O), 148.2 (C_{quat}), 144.1 (C_{quat}), 141.2 (C_{quat}), 137.2 (C_{quat}), 132.4 (C_{quat}), 132.1 (q, $^2J_{\text{FC}}=32.5$ Hz, C_{quat}), 131.8 (q, $^2J_{\text{FC}}=32.6$ Hz, C_{quat}), 130.2 (CH_{Ar}), 130.0 (CH_{Ar}), 127.7 (2x CH_{Ar}), 124.8 (2x CH_{Ar}), 124.0 (CH_{Ar}), 123.9 (q, $^1J_{\text{FC}}=273.0$ Hz, CF_3), 123.7 (q, $^1J_{\text{FC}}=273.0$ Hz, CF_3), 122.2 (q, $^3J_{\text{FC}}=3.7$ Hz, CH_{Ar}), 120.2 (CH_{Ar}), 118.6 (q, $^3J_{\text{FC}}=3.8$ Hz, CH_{Ar}), 117.8 (q, $^3J_{\text{FC}}=3.9$ Hz, CH_{Ar}), 113.3 (q, $^3J_{\text{FC}}=3.9$ Hz, CH_{Ar}), 107.7 (=CH), 63.3 (CHN) ppm.

^{19}F NMR (282 MHz, CDCl_3) δ -63.3, -63.2 ppm.

FTIR ν_{max} 3312 (N-H_{st}), 3038 (=C-H_{st}), 1676 (C=O_{st}), 1650 (C=CH_{st}), 1527 (NO_{2st as}), 1330 (NO_{2st sym}), 1254 (C-F_{st}) cm^{-1} .

HRMS (ESI-TOF) m/z calcd. for $\text{C}_{24}\text{H}_{16}\text{F}_6\text{N}_3\text{O}_3$ [M+H]⁺ 508.1096, found 508.1091.

5-Phenyl-1-(3-(trifluoromethyl)phenyl)-3-((3-(trifluoromethyl)phenyl)amino)-1,5-dihydro-2H-pyrrol-2-one (84I).



The general procedure was followed in diethyl ether at room temperature for 72 hours, using *m*-(trifluoromethyl)aniline (499 mg, 4 mmol), benzaldehyde (204 μL , 2 mmol) and ethyl pyruvate (670 μL , 6 mmol). The crude residue was purified by flash column chromatography (Hexanes/AcOEt 80:20), affording 602 mg (65%) of **84I** as a white solid.

Mp (Et_2O): 126 - 128 °C.

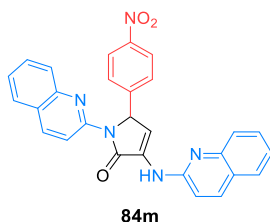
^1H NMR (400 MHz, CDCl_3) δ 7.93 (s, 1H, CH_{Ar}), 7.72 (d, $^3J_{\text{HH}}=8.3$ Hz, 1H, CH_{Ar}), 7.44 - 7.37 (m, 2H, 2x CH_{Ar}), 7.35 - 7.27 (m, 5H, 5x CH_{Ar}), 7.24 (d, $^3J_{\text{HH}}=1.8$ Hz, 2H, 2x CH_{Ar}), 7.23 - 7.19 (m, 2H, 2x CH_{Ar}), 6.85 (s, 1H, NH), 6.15 (d, $^3J_{\text{HH}}=2.6$ Hz, 1H, =CH), 5.73 (d, $^3J_{\text{HH}}=2.6$ Hz, 1H, CHN) ppm.

^{13}C { ^1H } NMR (101 MHz, CDCl_3) δ 167.2 (C=O), 141.7 (C_{quat}), 137.8 (C_{quat}), 136.4 (C_{quat}), 132.0 (q, $^2J_{\text{FC}}=32.4$ Hz, C_{quat}), 131.6 (C_{quat}), 131.5 (q, $^2J_{\text{FC}}=32.4$ Hz, C_{quat}), 130.1 (CH_{Ar}), 129.6 (CH_{Ar}), 129.4 (2x CH_{Ar}), 128.8 (CH_{Ar}), 126.8 (2x CH_{Ar}), 124.2 (CH_{Ar}), 124.0 (q, $^1J_{\text{FC}}=272.4$ Hz, CF_3), 123.9 (q, $^1J_{\text{FC}}=272.5$ Hz, CF_3), 121.61 (q, $^3J_{\text{FC}}=3.8$ Hz, CH_{Ar}), 119.9 (CH_{Ar}), 118.1 (q, $^3J_{\text{FC}}=3.8$ Hz, CH_{Ar}), 118.0 q, $^3J_{\text{FC}}=4.0$ Hz, CH_{Ar}), 113.1 (q, $^3J_{\text{FC}}=3.9$ Hz, CH_{Ar}), 109.7 (=CH), 64.3 (CHN) ppm.

^{19}F NMR (282 MHz, CDCl_3) δ -63.3, -63.2 ppm.

FTIR ν_{max} 3323 (N-H_{st}), 1675 (C=O_{st}), 1663 (C=CH_{st}), 1513 (NO_{2st as}), 1321 (NO_{2st sym}), 1201 (C-F_{st}) cm^{-1} .

HRMS (ESI-TOF) m/z calcd. for $\text{C}_{24}\text{H}_{17}\text{F}_6\text{N}_2\text{O}$ [M+H]⁺ 463.1245, found 463.1247.

5-(4-Nitrophenyl)-1-(quinolin-2-yl)-3-(quinolin-2-ylamino)-1,5-dihydro-2H-pyrrol-2-one (84m).

The general procedure was followed in MTBE at 55 °C (heating plate) for 72 hours, using 2-aminoquinoline (576 mg, 4 mmol), *p*-nitrobenzaldehyde (302 mg, 2 mmol) and ethyl pyruvate (670 μ L, 6 mmol). The crude residue was purified by flash column chromatography (Hexanes/AcOEt 80:20), affording 321 mg (34%) of **84m** as a yellow solid.

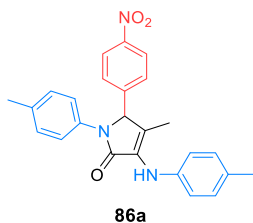
Mp (Et₂O): 201 - 203 °C (dec.).

¹H NMR (300 MHz, CDCl₃) δ 9.04 (d, ⁴J_{HH} = 1.5 Hz, 1H, CH_{Ar}), 8.79 (d, ⁴J_{HH} = 1.7 Hz, 1H, CH_{Ar}), 8.46 (d, ⁴J_{HH} = 2.6 Hz, 1H, CH_{Ar}), 8.17 (d, ³J_{HH} = 7.4 Hz, 2H, 2xCH_{Ar}), 8.03 (t, ³J_{HH} = 8.4 Hz, 2H, 2xCH_{Ar}), 7.83 - 7.52 (m, 7H, 7xCH_{Ar}), 7.50 (d, ³J_{HH} = 8.8 Hz, 2H, 2xCH_{Ar}), 7.04 (s, 1H, NH), 6.32 (d, ³J_{HH} = 1.5 Hz, 1H, =CH), 6.05 (d, ³J_{HH} = 1.7 Hz, 1H, CHN) ppm.

¹³C {¹H} NMR (75 MHz, CDCl₃) δ 166.9 (C=O), 148.2 (C_{quat}), 145.74 (C_{quat}), 144.1 (CH_{Ar}), 144.0 (CH_{Ar}), 143.9 (C_{quat}), 134.3 (C_{quat}), 132.5 (C_{quat}), 130.3 (C_{quat}), 129.5 (CH_{Ar}), 129.4 (CH_{Ar}), 129.3 (CH_{Ar}), 128.4 (C_{quat}), 127.9 (2xCH_{Ar} + CH_{Ar}), 127.8 (C_{quat}), 127.8 (CH_{Ar}), 127.7 (CH_{Ar}), 127.6 (CH_{Ar}), 126.8 (CH_{Ar}), 126.6 (CH_{Ar}), 124.9 (2xCH_{Ar}), 120.5 (C_{quat}), 117.8 (CH_{Ar}), 108.4 (=CH), 63.4 (CHN) ppm.

FTIR ν_{\max} 3305 (N-H_{st}), 3051 (=C-H_{st}), 1679 (C=O_{st}), 1640 (C=CH_{st}), 1508 (NO_{2 st as}), 1338 (NO_{2 st sym}) cm⁻¹.

HRMS (ESI-TOF) *m/z* calcd. for C₂₈H₂₀N₅O₃ [M+H]⁺ 474.1566, found 474.1561.

4-Methyl-5-(4-nitrophenyl)-1-(*p*-tolyl)-3-(*p*-tolylamino)-1,5-dihydro-2H-pyrrol-2-one (86a).

The general procedure was followed in MTBE at 55 °C (heating plate) for 18 hours, using *p*-toluidine (429 mg, 4 mmol), *p*-nitrobenzaldehyde (302 mg, 2 mmol) and methyl 2-oxobutanoate (704 μ L, 6 mmol). The crude residue was purified by crystallization from diethyl ether, affording 578 mg (70%) of **86a** as a yellow solid.

Mp (Et₂O): 215 - 217 °C.

¹H NMR (400 MHz, CDCl₃) δ 8.17 (d, ³J_{HH} = 8.8 Hz, 2H, 2xCH_{Ar}), 7.40 (d, ³J_{HH} = 8.7 Hz, 2H, 2xCH_{Ar}), 7.34 (d, ³J_{HH} = 8.5 Hz, 2H, 2xCH_{Ar}), 7.07 (d, ³J_{HH} = 8.1 Hz, 2H, 2xCH_{Ar}), 7.06 (d, ³J_{HH} = 7.9 Hz, 2H, 2xCH_{Ar}), 6.78 (d, ³J_{HH} = 8.3 Hz, 2H, 2xCH_{Ar}), 5.99 (bs, 1H, NH), 5.44 (s, 1H, CHN), 2.28 (s, 3H, CH₃ tolyl), 2.25 (s, 3H, CH₃ tolyl), 1.58 (d, ⁴J_{HH} = 1.03 Hz, 3H, CH₃) ppm.

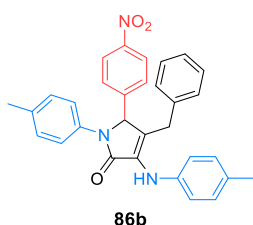
¹³C {¹H} NMR (75 MHz, CDCl₃) δ 167.8 (C=O), 148.0 (C_{quat}), 145.2 (C_{quat}), 138.9 (C_{quat}), 135.0 (C_{quat}), 134.5 (C_{quat}), 131.7 (C_{quat}), 130.5 (C_{quat}), 129.8 (2xCH_{Ar}), 129.7 (2xCH_{Ar}), 128.1 (2xCH_{Ar}), 124.5 (2xCH_{Ar}),

121.3 (2xCH_{Ar}), 119.5 (2xCH_{Ar}), 108.1 (C_{quat}-CH₃), 66.8 (CHN), 21.0 (CH₃ tolyl), 20.8 (CH₃ tolyl), 13.5 (CH₃) ppm.

FTIR ν_{\max} 3310 (N-H_{st}), 1672 (C=O_{st}), 1650 (C=C_{st}), 1513 (NO_{2st as}), 1348 (NO_{2st sym}) cm⁻¹.

HRMS (ESI-TOF) m/z calcd. for C₂₅H₂₄N₃O₃ [M+H]⁺ 414.1817, found 414.1813.

4-Benzyl-5-(4-nitrophenyl)-1-(*p*-tolyl)-3-(*p*-tolylamino)-1,5-dihydro-2H-pyrrol-2-one (86b).



The general procedure was followed in in MTBE at 55 °C (heating plate) for 18 hours, using *p*-toluidine (429 mg, 4 mmol), *p*-nitrobenzaldehyde (302 mg, 2 mmol) and ethyl 2-oxo-4-phenylbutanoate (1.13 ml, 6 mmol). The crude residue was purified by crystallization from diethyl ether, affording 712 mg (73%) of **86b** as a yellow solid.

Mp (Et₂O): 219 - 220 °C.

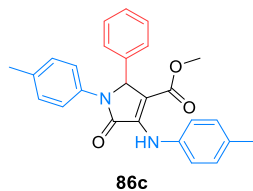
¹H NMR (300 MHz, CDCl₃) δ 8.12 (d, ³J_{HH} = 8.7 Hz, 2H, 2xCH_{Ar}), 7.34 - 7.14 (m, 7H, 7xCH_{Ar}), 7.04 (d, ³J_{HH} = 7.7 Hz, 2H, 2xCH_{Ar}), 7.02 (d, ³J_{HH} = 7.7 Hz, 2H, 2xCH_{Ar}), 6.94 (d, ³J_{HH} = 6.9 Hz, 2H, 2xCH_{Ar}), 6.88 (d, ³J_{HH} = 8.3 Hz, 2H, 2xCH_{Ar}), 6.10 (bs, 1H, NH), 5.37 (s, 1H, CHN), 3.67 (d, ²J_{HH} = 16.0 Hz, 1H, CH_aH_b), 2.86 (d, ²J_{HH} = 16.0 Hz, 1H, CH_aH_b), 2.27 (s, 3H, CH₃), 2.22 (s, 3H, CH₃) ppm.

¹³C {¹H} NMR (75 MHz, CDCl₃) δ 167.6 (C=O), 147.9 (C_{quat}), 145.1 (C_{quat}), 138.5 (C_{quat}), 138.3 (C_{quat}), 135.0 (C_{quat}), 134.4 (C_{quat}), 132.5 (C_{quat}), 131.2 (C_{quat}), 129.8 (2xCH_{Ar}), 129.8 (2xCH_{Ar}), 128.9 (4xCH_{Ar}), 128.3 (2xCH_{Ar}), 126.8 (CH_{Ar}), 124.4 (2xCH_{Ar}), 121.3 (2xCH_{Ar}), 120.5 (2xCH_{Ar}), 120.5 (C_{quat}-Bn), 64.6 (CHN), 33.1 (CH₂), 21.1 (CH₃), 21.0 (CH₃) ppm.

FTIR ν_{\max} 3306 (N-H_{st}), 1675 (C=O_{st}), 1649 (C=C_{st}), 1513 (NO_{2st as}), 1345 (NO_{2st sym}) cm⁻¹.

HRMS (ESI-TOF) m/z calcd. for C₃₁H₂₈N₃O₃ [M+H]⁺ 490.2130, found 490.2126.

Methyl 5-oxo-2-phenyl-1-(*p*-tolyl)-4-(*p*-tolylamino)-2,5-dihydro-1H-pyrrole-3-carboxylate (86c).



The general procedure was followed in in MTBE at 55 °C (heating plate) for 18 hours, using *p*-toluidine (429 mg, 4 mmol), *p*-nitrobenzaldehyde (302 mg, 2 mmol) and dimethyl 2-oxosuccinate (636 mg, 6 mmol). The crude residue was purified by flash column chromatography (Hexanes/AcOEt 90:10), affording 519 mg (63%) of **86c** as a white solid.

Mp (Et₂O): 179 - 181 °C. Lit. 184 - 185 °C.¹³⁷

¹H NMR (400 MHz, CDCl₃) δ 8.14 (s, 1H, NH), 7.33 (d, ³J_{HH} = 8.5 Hz, 2H, 2xCH_{Ar}), 7.25 (m, 4H, 4xCH_{Ar}), 7.20 (m, 1H, CH_{Ar}), 7.13 (d, ³J_{HH} = 8.3 Hz, 2H, 2xCH_{Ar}), 7.09 (d, ³J_{HH} = 8.5 Hz, 2H, 2xCH_{Ar}), 7.03 (d, ³J_{HH} =

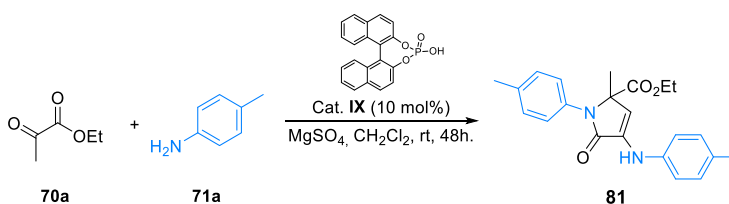
8.3 Hz, 2H, 2xCH_{Ar}), 5.77 (s, 1H, CHN), 3.54 (s, 3H, OCH₃), 2.34 (s, 3H, CH₃ tolyl), 2.23 (s, 3H, CH₃ tolyl) ppm.

¹³C {¹H} NMR (101 MHz, CDCl₃) δ 164.9 (C=O), 163.9 (C=O), 142.8 (C_{quat}), 137.2 (C_{quat}), 136.0 (C_{quat}), 135.5 (C_{quat}), 134.7 (C_{quat}), 134.1 (C_{quat}), 129.5 (2xCH_{Ar}), 129.1 (2xCH_{Ar}), 128.5 (2xCH_{Ar}), 128.1 (CH_{Ar}), 127.7 (2xCH_{Ar}), 123.3 (2xCH_{Ar}), 122.8 (2xCH_{Ar}), 108.9 (C_{quat}), 63.2 (CHN), 51.2 (OCH₃), 21.1 (CH₃ tolyl), 21.0 (CH₃ tolyl) ppm.

FTIR ν_{max} 3386 (N-H_{st}), 1715 (C=O_{st} ester), 1677 (C=O_{st} amide), 1652 (C=C_{st}) cm⁻¹.

HRMS (ESI-TOF) *m/z* calcd. for C₂₆H₂₅N₂O₃ [M+H]⁺ 413.1865, found 413.1863.

Synthesis of ethyl 2-methyl-5-oxo-1-(*p*-tolyl)-4-(*p*-tolylamino)-2,5-dihydro-1*H*-pyrrole-2-carboxylate (**81**).



A solution of ethyl pyruvate (**70a**) (446 μ L, 4 mmol), *p*-toluidine (**71a**) (429 mg, 4 mmol) and BINOL-derived phosphoric acid catalyst **IX** (35 mg, 0.1 mmol) was stirred in dichloromethane (10 mL) at room temperature for 48 hours in the presence of anhydrous MgSO₄ (500 mg). The reaction was filtered, the volatiles were distilled off at reduced pressure and the crude residue was purified by flash column chromatography (Hexanes/AcOEt 80:20) affording 496 mg (79%) of **81** as a white solid.

Mp (Et₂O): 188 - 190 °C. Lit. 190 - 191 °C.^{123b}

¹H NMR (300 MHz, CDCl₃) δ 7.26 - 7.19 (m, 4H, 4xCH_{Ar}), 7.15 (d, ³J_{HH} = 8.2 Hz, 2H, 2xCH_{Ar}), 6.99 (d, ³J_{HH} = 8.3 Hz, 2H, 2xCH_{Ar}), 6.59 (s, 1H, NH), 5.92 (s, 1H, =CH), 4.31 - 4.06 (m, 2H, CH₂), 2.37 (s, 3H, CH₃ tolyl), 2.33 (s, 3H, CH₃ tolyl), 1.64 (s, 3H, CCH₃), 1.25 (t, ³J_{HH} = 7.1 Hz, 3H, CH₃ ester) ppm.

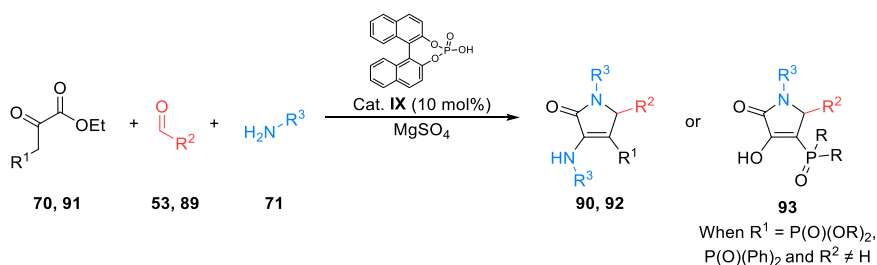
¹³C {¹H} NMR (75 MHz, CDCl₃) δ 171.9 (C=O), 167.8 (C=O), 138.8 (C_{quat}), 137.0, (C_{quat}), 134.2, (C_{quat}), 133.5, (C_{quat}), 131.3, (C_{quat}), 130.1, (2xCH_{Ar}), 130.0 (2xCH_{Ar}), 126.0 (2xCH_{Ar}), 117.3 (2xCH_{Ar}), 107.0 (=CH), 68.9 (CN), 62.3 (CH₂), 21.5 (CH₃), 21.3 (CH₃), 20.9 (CH₃), 14.3 (CH₃) ppm.

FTIR ν_{\max} 3305 (N-H_{st}), 1705 (C=O_{st} ester), 1679 (C=O_{st} amide), 1680 (C=CH_{st}) cm⁻¹.

HRMS (ESI-TOF) *m/z* calcd. for C₂₂H₂₅N₂O₃ [M+H]⁺ 365.1865, found 365.1860.

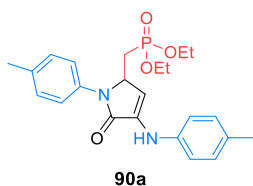
Chapter 2. Multicomponent synthesis of fluorine and phosphorus substituted γ -lactams.

General procedure for the synthesis of fluorine and phosphorus substituted γ -lactams **90**, **92** and **93**.



A solution of amine **71** (4 mmol), aldehyde **53** or **89** (2 mmol), ethyl pyruvate derivative **70** or **91** (6 mmol) and BINOL-derived phosphoric acid **IX** (70 mg, 0.2 mmol) in diethyl ether (10 mL) at room temperature or in MTBE (10 mL) at 55 °C was stirred in the presence of anhydrous MgSO_4 , for 24 - 72 hours. The reaction was filtered and the volatiles were distilled off at reduced pressure. The crude residue was purified by crystallization from diethyl ether or by flash column chromatography (Hexanes/AcOEt) to afford pure enamine-derived γ -lactams **90** and **92**, or enol-derived γ -lactams **93**.

Diethyl ((5-oxo-1-(*p*-tolyl)-4-(*p*-tolylamino)-2,5-dihydro-1*H*-pyrrol-2-yl)methyl)phosphonate (**90a**).



The general procedure was followed in diethyl ether at room temperature for 48 hours, using *p*-toluidine (429 mg, 4 mmol), diethyl (2-oxoethyl)phosphonate (360 mg, 2 mmol) and ethyl pyruvate (670 μL , 6 mmol). The crude residue was purified by flash column chromatography (Hexanes/AcOEt 90:10), affording 726 mg (84%) of **90a** as a yellow solid.

Mp (Et_2O): 119 - 121 °C.

$^1\text{H NMR}$ (300 MHz, CDCl_3) δ 7.37 (d, $^3J_{\text{HH}} = 8.4$ Hz, 2H, $2\times\text{CH}_{\text{Ar}}$), 7.24 (d, $^3J_{\text{HH}} = 8.4$ Hz, 2H, $2\times\text{CH}_{\text{Ar}}$), 7.12 (d, $^3J_{\text{HH}} = 8.4$ Hz, 2H, $2\times\text{CH}_{\text{Ar}}$), 7.02 (d, $^3J_{\text{HH}} = 8.4$ Hz, 2H, $2\times\text{CH}_{\text{Ar}}$), 6.49 (bs, 1H, NH), 6.34 (d, $^3J_{\text{HH}} = 2.5$

Hz, 1H, =CH), 4.93 (m, 1H, CHN), 4.20 - 4.05 (m, 4H, 2xCH₂ phosphonate), 2.37 (s, 3H, CH₃ tolyl), 2.31 (s, 3H, CH₃ tolyl), 1.65 (m, 2H, CH₂P), 1.35 (t, ³J_{HH} = 7.1 Hz, 6H, 2xCH₃ phosphonate) ppm.

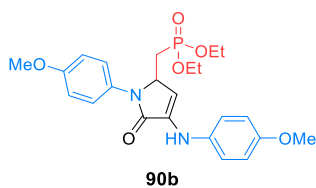
¹³C {¹H} NMR (75 MHz, CDCl₃) δ 165.9 (C=O), 138.9 (C_{quat}), 135.7 (C_{quat}), 133.4 (C_{quat}), 130.9 (C_{quat}), 130.1 (2xCH_{Ar}), 130.0 (2xCH_{Ar}), 122.7 (2xCH_{Ar}), 120.5 (C_{quat}), 116.9 (2xCH_{Ar}), 105.3 (=CH), 62.2 (d, ²J_{PC} = 4.0 Hz, CH₂ phosphonate), 62.1 (d, ²J_{PC} = 3.9 Hz, CH₂ phosphonate), 55.3 (CHN), 29.9 (d, ¹J_{PC} = 140.3 Hz, CH₂P), 21.1 (CH₃ tolyl), 20.8 (CH₃ tolyl), 16.7 (CH₃ phosphonate), 16.6 (CH₃ phosphonate) ppm.

³¹P NMR (121 MHz, CDCl₃) δ 27.6 ppm.

FTIR ν_{max} 3411 (N-H_{st}), 1682 (C=O_{st}), 1650 (C=CH_{st}), 1292 (P=O_{st}), 1028 (P-O-C_{st}) cm⁻¹.

HRMS (ESI-TOF) *m/z* calcd. for C₂₃H₃₀N₂O₄P [M+H]⁺ 429.1943, found 429.1936.

Diethyl ((1-(4-methoxyphenyl)-4-((4-methoxyphenyl)amino)-5-oxo-2,5-dihydro-1H-pyrrol-2-yl)methyl)phosphonate (90b).



The general procedure was followed in diethyl ether at room temperature for 48 hours, using *p*-anisidine (492 mg, 4 mmol), diethyl (2-oxoethyl)phosphonate (360 mg, 2 mmol) and ethyl pyruvate (670 μL, 6 mmol). The crude residue was purified by flash column chromatography (Hexanes/AcOEt 90:10), affording 737 mg (80%) of

90b as a white solid.

Mp (Et₂O): 119 - 121 °C.

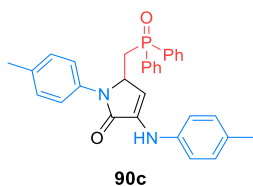
¹H NMR (300 MHz, CDCl₃) δ 7.37 (d, ³J_{HH} = 8.8 Hz, 2H, 2xCH_{Ar}), 7.07 (d, ³J_{HH} = 8.9 Hz, 2H, 2xCH_{Ar}), 6.97 (d, ³J_{HH} = 8.9 Hz, 2H, 2xCH_{Ar}), 6.88 (d, ³J_{HH} = 8.8 Hz, 2H, 2xCH_{Ar}), 6.37 (bs, 1H, NH), 6.26 (d, ³J_{HH} = 2.2 Hz, 1H, =CH), 4.86 (m, 1H, CHN), 4.19 - 4.05 (m, 4H, 2xCH₂ phosphonate), 3.83 (s, 3H, OCH₃), 3.80 (s, 3H, OCH₃), 2.35 (m, 1H, CH_AH_BP), 1.63 (m, 1H, CH_AH_BP), 1.34 (t, ³J_{HH} = 6.7 Hz, 6H, 2xCH₃ phosphonate) ppm.

¹³C {¹H} NMR (75 MHz, CDCl₃) δ 166.0 (C=O), 157.7 (C_{quat}), 154.6 (C_{quat}), 134.9 (C_{quat}), 134.0 (C_{quat}), 128.9 (C_{quat}), 124.7 (2xCH_{Ar}), 118.6 (2xCH_{Ar}), 114.9 (2xCH_{Ar}), 114.8 (2xCH_{Ar}), 104.3 (=CH), 62.1 (d, ²J_{PC} = 6.5 Hz, CH₂ phosphonate), 62.1 (d, ²J_{PC} = 6.5 Hz, CH₂ phosphonate), 55.8 (OCH₃), 55.7 (OCH₃), 55.6 (CHN), 30.0 (d, ¹J_{PC} = 140.5 Hz, CH₂P), 16.7 (CH₃ phosphonate), 16.6 (CH₃ phosphonate) ppm.

³¹P NMR (121 MHz, CDCl₃) δ 26.9 ppm.

FTIR ν_{max} 3309 (N-H_{st}), 1685 (C=O_{st}), 1650 (C=CH_{st}), 1251 (P=O_{st}), 1030 (P-O-C_{st}) cm⁻¹.

HRMS (ESI-TOF) *m/z* calcd. for C₂₃H₃₀N₂O₆P [M+H]⁺ 461.1841, found 461.1834.

5-((Diphenylphosphoryl)methyl)-1-(*p*-tolyl)-3-(*p*-tolylamino)-1,5-dihydro-2H-pyrrol-2-one (90c).

The general procedure was followed in diethyl ether at room temperature for 72 hours, using *p*-toluidine (429 mg, 4 mmol), 2-(diphenylphosphoryl)acetaldehyde (488 mg, 2 mmol) and ethyl pyruvate (670 μ L, 6 mmol). The crude residue was purified by flash column chromatography (Hexanes/AcOEt 90:10), affording 778 mg (79%) of **90c** as

a white solid.

Mp (Et₂O): 215 - 216 °C.

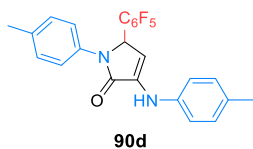
¹H NMR (400 MHz, CDCl₃) δ 7.78 (d, ³J_{HH} = 8.5 Hz, 2H, 2xCH_{Ar}), 7.73 (d, ³J_{HH} = 8.5 Hz, 2H, 2xCH_{Ar}), 7.62 - 7.46 (m, 6H, 6xCH_{Ar}), 7.25 (m, 2H, 2xCH_{Ar}), 7.19 (d, ³J_{HH} = 7.9 Hz, 2H, 2xCH_{Ar}), 7.03 (d, ³J_{HH} = 8.0 Hz, 2H, 2xCH_{Ar}), 6.74 (d, ³J_{HH} = 8.0 Hz, 2H, 2xCH_{Ar}), 6.41 (s, 1H, NH), 6.05 (s, 1H, =CH), 5.01 (m, 1H, CHN), 2.89 (m, 1H, CH_AH_BP), 2.35 (s, 3H, CH₃), 2.29 (s, 3H, CH₃), 2.22 (m, 1H, CH_AH_BP) ppm.

¹³C {¹H} NMR (101 MHz, CDCl₃) δ 165.9 (C=O), 138.7 (C_{quat}), 135.5 (C_{quat}), 133.3 (C_{quat}), 132.9 (d, ¹J_{PC} = 102.3 Hz, C_{Ar}P), 132.8 (C_{quat}), 132.5 (d, ¹J_{PC} = 101.2 Hz, C_{Ar}P), 132.4 (d, ⁴J_{PC} = 2.6 Hz, CH_{Ar}), 132.3 (d, ⁴J_{PC} = 2.6 Hz, CH_{Ar}), 131.0 (d, ²J_{PC} = 9.4 Hz, 2xCH_{Ar}), 130.9 (d, ²J_{PC} = 9.3 Hz, 2xCH_{Ar}), 130.6 (C_{quat}), 130.0 (2xCH_{Ar}), 129.9 (2xCH_{Ar}), 129.1 (d, ³J_{PC} = 11.9 Hz, 2xCH_{Ar}), 129.0 (d, ³J_{PC} = 11.8 Hz, 2xCH_{Ar}), 122.6 (2xCH_{Ar}), 116.7 (2xCH_{Ar}), 105.8 (=CH), 55.0 (CHN), 33.9 (d, ¹J_{PC} = 69.8 Hz, CH₂P), 21.1 (CH₃), 20.8 (CH₃) ppm.

³¹P NMR (121 MHz, CDCl₃) δ 28.3 ppm.

FTIR ν_{\max} 3397 (N-H_{st}), 1682 (C=O_{st}), 1666 (C=CH_{st}), 1191 (P=O_{st}) cm⁻¹.

HRMS (ESI-TOF) *m/z* calcd. for C₃₁H₃₀N₂O₂P [M+H]⁺ 493.2045, found 493.2042.

5-(Perfluorophenyl)-1-(*p*-tolyl)-3-(*p*-tolylamino)-1,5-dihydro-2H-pyrrol-2-one (90d).

The general procedure was followed in MTBE at 55 °C (heating plate) for 48 hours, using *p*-toluidine (429 mg, 4 mmol), perfluorobenzaldehyde (247 μ L, 2 mmol) and ethyl pyruvate (670 μ L, 6 mmol). The crude residue was purified by flash column chromatography (Hexanes/AcOEt 90:10), affording

793 mg (89%) of **90d** as a white solid.

Mp (Et₂O): 224 - 226 °C (dec.).

¹H NMR (400 MHz, CDCl₃) δ 7.37 (d, ³J_{HH} = 8.4 Hz, 2H, 2xCH_{Ar}), 7.16 (d, ³J_{HH} = 8.4 Hz, 2xCH_{Ar}), 7.13 (d, ³J_{HH} = 8.4 Hz, 2xCH_{Ar}), 7.00 (d, ³J_{HH} = 8.4 Hz, 2xCH_{Ar}), 6.66 (bs, 1H, NH), 6.13 (d, ³J_{HH} = 2.5 Hz, 1H, =CH), 5.92 (d, ³J_{HH} = 2.5 Hz, 1H, CHN), 2.31 (CH₃), 2.30 (CH₃) ppm.

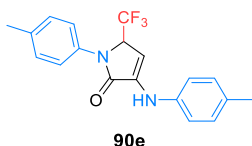
^{13}C { ^1H } NMR (101 MHz, CDCl_3) δ 166.4 (C=O), 147.1 (m, $\text{C}_{\text{quat-F}}$), 143.8 (m, $\text{C}_{\text{quat-F}}$), 142.8 (m, $\text{C}_{\text{quat-F}}$), 139.4 (m, $\text{C}_{\text{quat-F}}$), 138.5 (C_{quat}), 136.1 (m, $\text{C}_{\text{quat-F}}$), 135.8 (C_{quat}), 134.7 (C_{quat}), 133.8 (C_{quat}), 131.5 (C_{quat}), 130.1 ($4\times\text{CH}_{\text{Ar}}$), 121.6 ($2\times\text{CH}_{\text{Ar}}$), 117.3 ($2\times\text{CH}_{\text{Ar}}$), 111.3 (m, $\text{C}_{\text{quat-CHN}}$), 100.8 (=CH), 54.4 (CHN), 21.1 (CH_3), 20.8 (CH_3) ppm.

^{19}F NMR (282 MHz, CDCl_3) δ -145.3 (bd, $^3J_{\text{FF}} = 18.3$ Hz, $2\times\text{F}_{\text{orto}}$), -153.8 (t, $^3J_{\text{FF}} = 20.8$ Hz, $1\times\text{F}_{\text{para}}$), -161.4 (dt, $^3J_{\text{FF}} = 20.9$ Hz, $^4J_{\text{FF}} = 7.6$ Hz, $2\times\text{F}_{\text{meta}}$) ppm.

FTIR ν_{max} 3322 (N-H_{st}), 1693 (C=O_{st}), 1669 (C=CH_{st}) cm^{-1} .

HRMS (ESI-TOF) m/z calcd. for $\text{C}_{24}\text{H}_{18}\text{F}_5\text{N}_2\text{O}$ [$\text{M}+\text{H}$]⁺ 445.1339, found 445.1339.

1-(*p*-Tolyl)-3-(*p*-tolylamino)-5-(trifluoromethyl)-1,5-dihydro-2H-pyrrol-2-one (90e).



A modified procedure was followed: To a solution of *p*-toluidine (214 mg, 2 mmol) in toluene (10 mL) a 75% aqueous solution of trifluoroacetaldehyde hydrate (107 μL , 1 mmol) was added. The mixture was heated at 110 °C using a Dean-Stark on a heating plate until water was fully removed. Once the imine intermediate was formed (monitored by ^{19}F NMR: 2,2,2-trifluoroethane-1,1-diol: -85.5 ppm; imine: -79.0 ppm), ethyl pyruvate (670 μL , 6 mmol) and **IX** phosphoric acid catalyst (70 mg, 0.2 mmol) were added, and the reaction was stirred at room temperature for 48 hours. The reaction was filtered, the volatiles were distilled off at reduced pressure and the crude residue was purified by flash column chromatography (Hexanes/AcOEt 90:10) to afford 520 mg (75%) of **90e** as a white solid.

Mp (Et_2O): 205 - 206 °C.

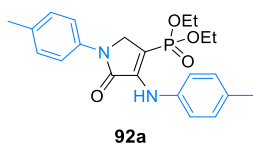
^1H NMR (400 MHz, CDCl_3) δ 7.16 (d, $^3J_{\text{HH}} = 8.5$ Hz, 2H, $2\times\text{CH}_{\text{Ar}}$), 7.02 (d, $^3J_{\text{HH}} = 8.4$ Hz, 2H, $2\times\text{CH}_{\text{Ar}}$), 6.62 (s, 1H, NH), 5.86 (d, $^3J_{\text{HH}} = 2.7$ Hz, 1H, =CH), 5.12 (dq, $^3J_{\text{FH}} = 5.3$, $^3J_{\text{HH}} = 2.7$ Hz, 1H, CHN), 2.39 (s, 3H, CH_3), 2.33 (s, 3H, CH_3) ppm.

^{13}C { ^1H } NMR (101 MHz, CDCl_3) δ 167.3 (C=O), 138.1 (C_{quat}), 137.3 (C_{quat}), 136.3 (C_{quat}), 133.6 (C_{quat}), 131.9 (C_{quat}), 130.1 ($2\times\text{CH}_{\text{Ar}}$), 130.0 ($2\times\text{CH}_{\text{Ar}}$), 125.0 ($2\times\text{CH}_{\text{Ar}}$), 124.0 (q, $^1J_{\text{FC}} = 282.6$ Hz, CF_3), 117.6 ($2\times\text{CH}_{\text{Ar}}$), 94.7 (d, $^3J_{\text{FC}} = 2.3$ Hz, =CH), 61.7 (q, $^2J_{\text{FC}} = 32.3$ Hz, CHN), 21.2 (CH_3), 20.9 (CH_3) ppm.

^{19}F NMR (282 MHz, CDCl_3) δ -73.2 ppm.

FTIR ν_{max} 3314 (N-H_{st}), 1693 (C=O_{st}), 1657 (C=CH_{st}), 1382 (C-F_{st}) cm^{-1} .

HRMS (ESI-TOF) m/z calcd. for $\text{C}_{19}\text{H}_{18}\text{F}_3\text{N}_2\text{O}$ [$\text{M}+\text{H}$]⁺ 347.1371, found 347.1370.

Diethyl (5-oxo-1-(*p*-tolyl)-4-(*p*-tolylamino)-2,5-dihydro-1*H*-pyrrol-3-yl) phosphonate (92a).

The general procedure was followed in MTBE at 55 °C (heating plate) for 24 hours, using *p*-toluidine (429 mg, 4 mmol), a 37% aqueous solution of formaldehyde (150 μ L, 2 mmol) and ethyl 3-(diethoxyphosphoryl)-2-oxopropanoate (1.513 g, 6 mmol). The crude residue was purified by flash column chromatography (Hexanes/AcOEt 90:10), affording 629 mg (76%) of **92a** as an orange solid.

Mp (Et₂O): 120 - 122 °C (dec.).

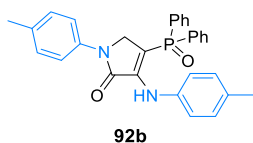
¹H NMR (300 MHz, CDCl₃) δ 7.79 (d, ³*J*_{HH} = 8.5 Hz, 2H, 2xCH_{Ar}), 7.56 (bs, 1H, NH), 7.34 (d, ³*J*_{HH} = 8.5 Hz, 2H, 2xCH_{Ar}), 7.29 - 7.21 (m, 4H, 4xCH_{Ar}), 4.61 (d, ³*J*_{PH} = 3.2 Hz, 2H, CH₂N), 7.28 - 7.06 (m, 4H, 2xCH₂ phosphonate), 2.49 (s, 3H, CH₃ tolyl), 2.48 (s, 3H, CH₃ tolyl), 1.42 (t, ³*J*_{HH} = 7.0 Hz, 6H, 2xCH₃ phosphonate) ppm.

¹³C {¹H} NMR (75 MHz, CDCl₃) δ 164.1 (d, ²*J*_{PC} = 20.5 Hz, C_{quat}-CO), 145.2 (d, ³*J*_{PC} = 7.4 Hz, C=O), 137.0 (C_{quat}), 136.2 (C_{quat}), 135.0 (C_{quat}), 134.3 (C_{quat}), 129.8 (2xCH_{Ar}), 129.2 (2xCH_{Ar}), 123.1 (2xCH_{Ar}), 119.2 (2xCH_{Ar}), 96.2 (d, ¹*J*_{PC} = 212.8 Hz, CP), 62.0 (d, ²*J*_{PC} = 5.5 Hz, 2xCH₂ phosphonate), 50.4 (d, ²*J*_{PC} = 16.0 Hz, CH₂N), 21.1 (CH₃ tolyl), 21.0 (CH₃ tolyl), 16.4 (d, ³*J*_{PC} = 6.9 Hz, 2xCH₃ phosphonate) ppm.

³¹P NMR (121 MHz, CDCl₃) δ 14.7 ppm.

FTIR ν_{\max} 3281 (N-H_{st}), 1693 (C=O_{st}), 1652 (C=C_{st}), 1267 (P=O_{st}), 1018 (P-O-C_{st}) cm⁻¹.

HRMS (ESI-TOF) *m/z* calcd. for C₂₂H₂₈N₂O₄P [M+H]⁺ 415.1787, found 415.1789.

4-(Diphenylphosphoryl)-1-(*p*-tolyl)-3-(*p*-tolylamino)-1,5-dihydro-2*H*-pyrrol-2-one (92b).

The general procedure was followed in MTBE at 55 °C (heating plate) for 24 hours, using *p*-toluidine (429 mg, 4 mmol), a 37% aqueous solution of formaldehyde (150 μ L, 2 mmol) and ethyl 3-(diphenylphosphoryl)-2-oxopropanoate (1.897 g, 6 mmol). The crude residue was purified by flash column chromatography (Hexanes/AcOEt 90:10), affording 698 mg (73%) of **92b** as an orange solid.

Mp (Et₂O): 188 - 189 °C (dec.).

¹H NMR (300 MHz, CDCl₃) δ 7.70 - 7.62 (m, 5H, 4xCH_{Ar} + NH), 7.56 - 7.41 (m, 9H, 9xCH_{Ar}), 7.13 (d, ³*J*_{HH} = 8.2 Hz, 2H, 2xCH_{Ar}), 6.92 (bs, 3H, 3xCH_{Ar}), 4.15 (d, ³*J*_{PH} = 2.6 Hz, 2H, CH₂), 2.31 (s, 3H, CH₃), 2.25 (s, 3H, CH₃) ppm.

¹³C {¹H} NMR (75 MHz, CDCl₃) δ 164.2 (d, ³*J*_{PC} = 14.0 Hz, C=O), 146.9 (d, ²*J*_{PC} = 2.8 Hz, C_{quat}-CO), 136.8 (C_{quat}), 136.1 (C_{quat}), 135.0 (C_{quat}), 134.1 (C_{quat}), 132.3 (d, ¹*J*_{PC} = 108.3 Hz, CP), 132.1 (d, ⁴*J*_{PC} = 2.8 Hz, 2xCH_{Ar}), 131.3 (d, ²*J*_{PC} = 10.1 Hz, 4xCH_{Ar}), 129.7 (2xCH_{Ar}), 129.3 (2xCH_{Ar}), 128.8 (d, ³*J*_{PC} = 12.3 Hz, 4xCH_{Ar}),

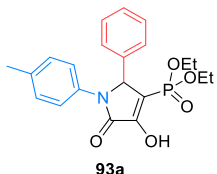
123.5 (2xCH_{Ar}), 119.4 (2xCH_{Ar}), 99.2 (d, ¹J_{PC} = 115.1 Hz, CP), 51.0 (d, ²J_{PC} = 15.5 Hz, CH₂), 21.0 (2xCH₃) ppm.

³¹P NMR (121 MHz, CDCl₃) δ 21.8 ppm.

FTIR ν_{max} 3245 (N-H_{st}), 3091 (=C-H_{st}), 1689 (C=O_{st}), 1651 (C=C_{st}), 1185 (P=O_{st}) cm⁻¹.

HRMS (ESI-TOF) *m/z* calcd. for C₃₀H₂₈N₂O₂P [M+H]⁺ 479.1888, found 479.1888.

Diethyl (4-hydroxy-5-oxo-2-phenyl-1-(*p*-tolyl)-2,5-dihydro-1*H*-pyrrol-3-yl) phosphonate (93a).



The general procedure was followed in MTBE at 55 °C (heating plate) for 48 hours, using *p*-toluidine (429 mg, 4 mmol), benzaldehyde (204 μL, 2 mmol) and ethyl 3-(diethoxyphosphoryl)-2-oxopropanoate (1.513 g, 6 mmol). The crude residue was purified by flash column chromatography (Hexanes/AcOEt 30:70), affording 770 mg (96%) of **93a** as a white solid.

Mp (Et₂O): 145 - 147 °C.

¹H NMR (300 MHz, CDCl₃) δ 9.75 (bs, 1H, OH), 7.36 (d, ³J_{HH} = 8.5 Hz, 2H, 2xCH_{Ar}), 7.26 - 7.13 (m, 5H, 5xCH_{Ar}), 7.05 (d, ³J_{HH} = 8.3 Hz, 2H, 2xCH_{Ar}), 5.58 (d, ³J_{PH} = 2.8 Hz, 1H, CHN), 4.15 (m, 2H, CH₂), 3.70 (m, 1H, CH_ACH_B), 3.16 (m, 1H, CH_ACH_B), 2.23 (s, 3H, CH₃ tolyl), 1.39 (t, ³J_{HH} = 7.1 Hz, 3H, CH₃ phosphonate), 0.80 (t, ³J_{HH} = 7.1 Hz, 3H, CH₃ phosphonate) ppm.

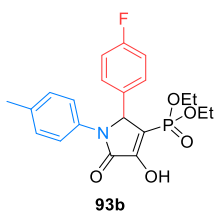
¹³C {¹H} NMR (75 MHz, CDCl₃) δ 163.0 (d, ²J_{PC} = 19.8 Hz, COH), 160.0 (d, ³J_{PC} = 6.5 Hz, C=O), 135.7 (C_{quat}), 135.5 (C_{quat}), 134.1 (C_{quat}), 129.7 (2xCH_{Ar}), 129.1 (2xCH_{Ar}), 128.7 (CH_{Ar}), 127.1 (2xCH_{Ar}), 121.9 (2xCH_{Ar}), 106.6 (d, ¹J_{PC} = 200.8 Hz, CP), 62.98 (d, ²J_{PC} = 5.4 Hz, CH₂), 62.71 (CHN), 62.56 (d, ²J_{PC} = 4.5 Hz, CH₂), 21.01 (CH₃ tolyl), 16.54 (d, ³J_{PC} = 6.4 Hz, CH₃ phosphonate), 15.63 (d, ³J_{PC} = 7.5 Hz, CH₃ phosphonate) ppm.

³¹P NMR (121 MHz, CDCl₃) δ 15.4 ppm.

FTIR ν_{max} 3390 (O-H_{st}), 1692 (C=O_{st}), 1663 (C=C_{st}), 1265 (P=O_{st}), 1021 (P-O-C_{st}) cm⁻¹.

HRMS (ESI-TOF) *m/z* calcd. for C₂₁H₂₅NO₅P [M+H]⁺ 402.1470, found 402.14688.

Diethyl (2-(4-fluorophenyl)-4-hydroxy-5-oxo-1-(*p*-tolyl)-2,5-dihydro-1*H*-pyrrol-3-yl) phosphonate (93b).



The general procedure was followed in MTBE at 55 °C (heating plate) for 48 hours, using *p*-toluidine (429 mg, 4 mmol), *p*-fluorobenzaldehyde (214 μL, 2 mmol) and ethyl 3-(diethoxyphosphoryl)-2-oxopropanoate (1.513 g, 6 mmol).

The crude residue was purified by flash column chromatography (Hexanes/AcOEt 30:70), affording 604 mg (72%) of **93b** as a pale yellow solid.

Mp (Et₂O): 141 - 142 °C.

¹H NMR (400 MHz, DMSO-*d*₆, 70 °C) δ 10.99 (bs, 1H, OH), 7.39 (d, ³*J*_{HH} = 8.4 Hz, 2H, 2xCH_{Ar}), 7.26 (dd, ⁴*J*_{FH} = 5,4, ³*J*_{HH} = 8.8 Hz, 2H, 2xCH_{Ar}), 7.08 (d, ³*J*_{HH} = 8.4 Hz, 2H, 2xCH_{Ar}), 7.03 (t, ³*J*_{HH} and ³*J*_{FH} = 8.9 Hz, 2H, 2xCH_{Ar}), 5.90 (d, ³*J*_{PH} = 2.9 Hz, 1H, CHN), 3.97 - 3.67 (m, 4H, 2xCH₂), 2.21 (s, 3H, CH₃ tolyl), 1.10 (t, ³*J*_{HH} = 7.0, 3H, CH₃ phosphonate), 1.09 (t, ³*J*_{HH} = 7.0, 3H, CH₃ phosphonate) ppm.

¹³C {¹H} NMR (101 MHz, DMSO-*d*₆, 70 °C) δ 163.4 (d, ²*J*_{PC} = 18.3 Hz, COH), 161.7 (d, ¹*J*_{FC} = 244.0 Hz, CF), 154.9 (d, ³*J*_{PC} = 4.1 Hz, C=O), 134.7 (C_{quat}), 133.71 (C_{quat}), 132.3 (d, ⁴*J*_{FC} = 2.8 Hz, C_{quat}), 129.9 (d, ³*J*_{FC} = 8.4 Hz, 2xCH_{Ar}), 129.2 (2xCH_{Ar}), 122.6 (2xCH_{Ar}), 115.1 (d, ²*J*_{FC} = 21.6 Hz, 2xCH_{Ar}), 108.2 (d, ¹*J*_{PC} = 201.6 Hz, CP), 61.5 (s, CHN), 61.3 (d, ²*J*_{PC} = 5.3 Hz, CH₂), 61.2 (d, ²*J*_{PC} = 5.0 Hz, CH₂), 20.4 (CH₃ tolyl), 16.0 (d, ³*J*_{PC} = 3.4 Hz CH₃ phosphonate), 15.9 (d, ³*J*_{PC} = 3.4 Hz CH₃ phosphonate) ppm.

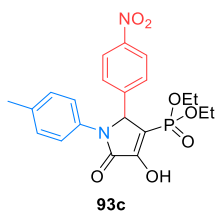
¹⁹F NMR (282 MHz, DMSO-*d*₆) δ -110.0 ppm.

³¹P NMR (162 MHz, DMSO-*d*₆) δ 11.4 ppm.

FTIR ν_{max} 3422 (O-H_{st}), 1704 (C=O_{st}), 1651 (C=C_{st}), 1266 (P=O_{st}), 1157 (C-F_{st}), 1020 (P-O-C_{st}) cm⁻¹.

HRMS (ESI-TOF) *m/z* calcd. for C₂₁H₂₄FNO₅P [M+H]⁺ 420.1376, found 420.1372.

Diethyl (4-hydroxy-2-(4-nitrophenyl)-5-oxo-1-(*p*-tolyl)-2,5-dihydro-1*H*-pyrrol-3-yl) phosphonate (93c).



The general procedure was followed in MTBE at 55 °C (heating plate) for 48 hours, using *p*-toluidine (429 mg, 4 mmol), *p*-nitrobenzaldehyde (302 mg, 2 mmol) and ethyl 3-(diethoxyphosphoryl)-2-oxopropanoate (1.513 g, 6 mmol). The crude residue was purified by flash column chromatography (Hexanes/AcOEt 30:70), affording 829 mg (93%) of **93c** as a pale orange solid.

Mp (Et₂O): 188 - 190 °C (dec.).

¹H NMR (400 MHz, DMSO-*d*₆, 70 °C) δ 8.05 (d, ³*J*_{HH} = 8.2 Hz, 2H, 2xCH_{Ar}), 7.45 (d, ³*J*_{HH} = 7.6 Hz, 4H, 4xCH_{Ar}), 7.05 (d, ³*J*_{HH} = 8.0 Hz, 2H, 2xCH_{Ar}), 5.84 (s, 1H, CHN), 4.06 (m, 2H, CH₂), 3.73 (m, 1H, CH_ACH_B), 3.27 (m, 1H, CH_ACH_B), 2.19 (s, 3H, CH₃ tolyl), 1.26 (t, ³*J*_{HH} = 7.0 Hz, 3H, CH₃ phosphonate), 0.74 (t, ³*J*_{HH} = 7.0 Hz, 3H, CH₃ phosphonate) ppm.

¹³C {¹H} NMR (101 MHz, DMSO-*d*₆, 70 °C) δ 169.2 (COH), 167.7 (C=O), 148.3 (C_{quat}), 146.7 (C_{quat}), 134.7 (C_{quat}), 133.9 (C_{quat}), 129.1 (2xCH_{Ar}), 128.4 (2xCH_{Ar}), 123.4 (2xCH_{Ar}), 121.7 (2xCH_{Ar}), 113.7 (CP),

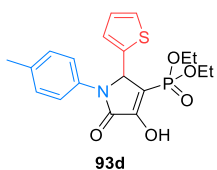
61.1 (CH₂), 60.3 (CH₂), 55.1 (CHN), 20.4 (CH₃ tolyl), 16.3 (d, ³J_{PC} = 6.5 Hz, CH₃ phosphonate), 15.5 (d, ³J_{PC} = 6.5 Hz, CH₃ phosphonate) ppm.

³¹P NMR (162 MHz, DMSO-*d*₆, 60 °C) δ 22.3 ppm.

FTIR ν_{max} 3419 (O-H_{st}), 1679 (C=O_{st}), 1596 (C=C_{st}), 1511 (NO₂_{st as}), 1346 (NO₂_{st sym}), 1294 (P=O_{st}), 1052 (P-O-C_{st}) cm⁻¹.

HRMS (ESI-TOF) *m/z* calcd. for C₂₁H₂₄N₂O₇P [M+H]⁺ 447.1321, found 447.1319.

Diethyl (4-hydroxy-5-oxo-2-(thiophen-2-yl)-1-(*p*-tolyl)-2,5-dihydro-1*H*-pyrrol-3-yl) phosphonate (93d).



The general procedure was followed in MTBE at 55 °C (heating plate) for 48 hours, using *p*-toluidine (429 mg, 4 mmol), 2-thiophenecarboxaldehyde (187 μL, 2 mmol) and ethyl 3-(diethoxyphosphoryl)-2-oxopropanoate (1.513 g, 6 mmol).

The crude residue was purified by flash column chromatography (Hexanes/AcOEt 30:70), affording 724 mg (89%) of **93d** as a white solid.

Mp (Et₂O): 143 - 144 °C.

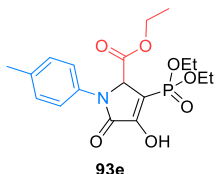
¹H NMR (400 MHz, CDCl₃) δ 9.82 (bs, 1H, OH), 7.31 (d, ³J_{HH} = 8.3. Hz, 2H, 2xCH_{Ar}), 7.16 (d, ³J_{HH} = 5.0 Hz, 1H, CH thienyl), 7.07 (d, ³J_{HH} = 8.3. Hz, 2H, 2xCH_{Ar}), 7.02 (d, ³J_{HH} = 3.4 Hz, 1H, CH thienyl), 6.83 (dd, ³J_{HH} = 5.0, ³J_{HH} 3.4 Hz, 1H, CH thienyl), 5.92 (d, ⁴J_{HH} = 2.8 Hz, 1H, CHN), 4.12 (m, 2H, CH₂), 3.88 (m, 1H, CH_ACH_B), 3.49 (m, 1H, CH_ACH_B), 2.24 (s, 3H, CH₃ tolyl), 1.35 (t, ³J_{HH} = 7.1 Hz, 3H, CH₃ phosphonate), 0.98 (t, ³J_{HH} = 7.1 Hz, 3H, CH₃ phosphonate) ppm.

¹³C {¹H} NMR (101 MHz, CDCl₃) δ 162.4 (d, ²J_{PC} = 19.5 Hz, COH), 159.4 (d, ³J_{PC} = 6.3 Hz, C=O), 139.2 (d, ³J_{PC} = 1.2 Hz, C_{quat}), 135.9 (C_{quat}), 133.4 (C_{quat}), 129.6 (2xCH_{Ar}), 127.5 (CH thienyl), 126.7 (CH thienyl), 126.1 (CH thienyl), 122.6 (2xCH_{Ar}), 106.4 (d, ¹J_{PC} = 202.6 Hz, CP), 62.9 (d, ²J_{PC} = 5.6 Hz, CH₂), 62.8 (d, ²J_{PC} = 5.3 Hz, CH₂), 58.4 (d, ²J_{PC} = 13.0 Hz, CHN), 21.0 (CH₃ tolyl), 16.4 (d, ³J_{PC} = 6.4 Hz, CH₃ phosphonate), 15.8 (d, ³J_{PC} = 7.5 Hz, CH₃ phosphonate) ppm.

³¹P NMR (162 MHz, DMSO-*d*₆) δ 14.6 ppm.

FTIR ν_{max} 3490 (O-H_{st}), 1701 (C=O_{st}), 1653 (C=C_{st}), 1232 (P=O_{st}), 1017 (P-O-C_{st}) cm⁻¹.

HRMS (ESI-TOF) *m/z* calcd. for C₁₉H₂₃NO₅PS [M+H]⁺ 408.1035, found 408.1033.

Ethyl 3-(diethoxyphosphoryl)-4-hydroxy-5-oxo-1-(*p*-tolyl)-2,5-dihydro-1H-pyrrole-2-carboxylate (93e).

The general procedure was followed in MTBE at 55 °C (heating plate) for 48 hours, using *p*-toluidine (429 mg, 4 mmol), a 50% solution of ethyl glyoxalate in toluene (396 μ L, 2 mmol) and ethyl 3-(diethoxyphosphoryl)-2-oxopropanoate (1.513 g, 6 mmol). The crude residue was purified by flash column chromatography (Hexanes/AcOEt 20:80), affording 682 mg (86%) of **93e** as a pale orange solid.

Mp (Et₂O): 123 - 124 °C.

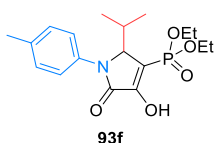
¹H NMR (400 MHz, DMSO-*d*₆, 60 °C) δ 7.47 (d, ³*J*_{HH} = 8.1 Hz, 2H, 2xCH_{Ar}), 7.23 (d, ³*J*_{HH} = 8.1 Hz, 2H, 2xCH_{Ar}), 5.42 (d, ³*J*_{PH} = 2.9 Hz, 1H, CHN), 4.13 - 3.99 (m, 6H, 3xCH₂), 2.31 (s, 3H, CH₃ tolyl), 1.34 - 1.23 (m, 6H, 2xCH₃ phosphonate), 1.07 (t, ³*J*_{HH} = 7.0 Hz, 3H, CH₃ ester) ppm.

¹³C {¹H} NMR (101 MHz, DMSO-*d*₆, 60 °C) δ 167.8 (C=O), 163.6 (d, ²*J*_{PC} = 18.0 Hz, COH), 156.6 (C=O), 135.4 (C_{quat}), 134.11 (C_{quat}), 129.5 (2xCH_{Ar}), 121.4 (2xCH_{Ar}), 102.5 (d, ¹*J*_{PC} = 203.6 Hz, CP), 61.8 (d, ²*J*_{PC} = 5.3 Hz, 2xCH₂ phosphonate), 61.6 (CH₂ ester), 61.4 (d, ²*J*_{PC} = 15.4 Hz, CHN), 20.5 (CH₃ tolyl), 16.1 (d, ³*J*_{PC} = 6.4 Hz, 2xCH₃ phosphonate), 13.7 (CH₃ ester) ppm.

³¹P NMR (162 MHz, DMSO-*d*₆) δ 10.2 ppm.

FTIR ν_{\max} 3478 (O-H_{st}), 1748 (C=O_{st} ester), 1710 (C=O_{st} amide), 1654 (C=C_{st}), 1182 (P=O_{st}), 1027 (P-O-C_{st}) cm⁻¹.

HRMS (ESI-TOF) *m/z* calcd. for C₁₈H₂₅NO₇P [M+H]⁺ 398.1369, found 398.1374.

Diethyl (4-hydroxy-2-*iso*-propyl-5-oxo-1-(*p*-tolyl)-2,5-dihydro-1H-pyrrol-3-yl) phosphonate (93f).

The general procedure was followed in MTBE at 55 °C (heating plate) for 48 hours, using *p*-toluidine (429 mg, 4 mmol), isobutyraldehyde (182 μ L, 2 mmol) and ethyl 3-(diethoxyphosphoryl)-2-oxopropanoate (1.513 g, 6 mmol). The crude residue was purified by flash column chromatography (Hexanes/AcOEt 20:80), affording 550 mg (75%) of **93f** as a white solid.

Mp (Et₂O): 79 - 81 °C.

¹H NMR (400 MHz, CDCl₃) δ 10.01 (s, 1H, OH), 7.23 (d, ³*J*_{HH} = 8.5 Hz, 2H, 2xCH_{Ar}), 7.18 (d, ³*J*_{HH} = 8.5 Hz, 2H, 2xCH_{Ar}), 4.64 (t, ³*J*_{HH} and ³*J*_{PH} = 2.6 Hz, 1H, CHN), 4.16 (m, 4H, m, 4H, 2xCH₂), 2.32 (s, 3H, CH₃ tolyl), 2.10 (m, 1H, CHⁱPr), 1.40 - 1.30 (m, 6H, 2xCH₃ phosphonate), 0.96 (d, ³*J*_{HH} = 7.1 Hz, 3H, CH₃ⁱPr), 0.59 (d, ³*J*_{HH} = 6.9 Hz, 3H, CH₃ⁱPr) ppm.

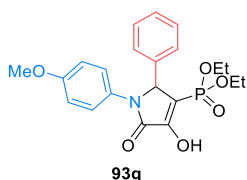
^{13}C { ^1H } NMR (101 MHz, CDCl_3) δ 162.7 (d, $^2J_{\text{PC}} = 19.9$ Hz, COH), 161.2 (d, $^3J_{\text{PC}} = 5.9$ Hz, C=O) 136.5 (C_{quat}), 133.9 (C_{quat}), 129.8 ($2\times\text{CH}_{\text{Ar}}$), 124.3 ($2\times\text{CH}_{\text{Ar}}$), 103.2 (d, $^1J_{\text{PC}} = 200.6$ Hz, CP), 64.8 (d, $^2J_{\text{PC}} = 14.0$ Hz, CHN), 62.9 (t, $^2J_{\text{PC}} = 5.3$ Hz, $2\times\text{CH}_2$), 29.4 (CH ^iPr), 21.1 (CH_3 tolyl), 16.9 (CH_3 ^iPr), 16.3 (CH_3 ^iPr), 16.3 (d, $^3J_{\text{PC}} = 6.4$ Hz, CH_3 phosphonate), 16.2 (d, $^3J_{\text{PC}} = 6.7$ Hz, $2\times\text{CH}_3$ phosphonate) ppm.

^{31}P NMR (162 MHz, CDCl_3) δ 17.1 ppm.

FTIR ν_{max} 3428 (O-H $_{\text{st}}$), 1696 (C=O $_{\text{st}}$), 1657 (C=C $_{\text{st}}$), 1242 (P=O $_{\text{st}}$), 1030 (P-O-C $_{\text{st}}$) cm^{-1} .

HRMS (ESI-TOF) m/z calcd. for $\text{C}_{18}\text{H}_{27}\text{NO}_5\text{P}$ $[\text{M}+\text{H}]^+$ 368.1627, found 368.1603.

Diethyl (4-hydroxy-1-(4-methoxyphenyl)-5-oxo-2-phenyl-2,5-dihydro-1H-pyrrol-3-yl) phosphonate (93g).



The general procedure was followed in MTBE at 55 °C (heating plate) for 48 hours, using *p*-anisidine (492 mg, 4 mmol), benzaldehyde (204 μL , 2 mmol) and ethyl 3-(diethoxyphosphoryl)-2-oxopropanoate (1.513 g, 6 mmol). The crude residue was purified by flash column chromatography (Hexanes/AcOEt 30:70), affording 751 mg (90%) of **93g** as a yellow solid.

M.p. (Et_2O):132 - 133 °C.

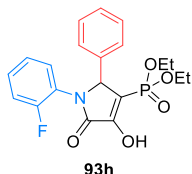
^1H NMR (400 MHz, CDCl_3) δ 9.81 (s, 1H, OH), 7.34 (d, $^3J_{\text{HH}} = 9.0$ Hz, 2H, $2\times\text{CH}_{\text{Ar}}$), 7.27-7.28 (m, 3H, $3\times\text{CH}_{\text{Ar}}$), 7.15 (d, $^3J_{\text{HH}} = 8.1$ Hz, 2H, $2\times\text{CH}_{\text{Ar}}$), 6.75 (d, $^3J_{\text{HH}} = 9.1$ Hz, 2H, $2\times\text{CH}_{\text{Ar}}$), 5.54 (d, $^3J_{\text{PH}} = 2.8$, 1H, CHN), 4.16-4.05 (m, 2H, CH_2), 3.71 (m, 1H, CH_2), 3.67 (s, 3H, OCH_3), 3.18 (m, 1H, CH_2), 1.35 (t, $^3J_{\text{HH}} = 7.1$ Hz, 3H, CH_3 phosphonate), 0.79 (t, $^3J_{\text{HH}} = 7.1$ Hz, 3H, CH_3 phosphonate) ppm.

^{13}C { ^1H } NMR (101 MHz, CDCl_3) δ 162.9 (d, $^2J_{\text{PC}} = 20.4$ Hz, COH), 159.8 (d, $^3J_{\text{PC}} = 6.12$ Hz, C=O), 157.3 (C_{quat}), 135.48 (C_{quat}), 129.5 (C_{quat}), 128.9 ($2\times\text{CH}_{\text{Ar}}$), 128.6 (CH_{Ar}), 127.1 ($2\times\text{CH}_{\text{Ar}}$), 123.8 ($2\times\text{CH}_{\text{Ar}}$), 114.2 ($2\times\text{CH}_{\text{Ar}}$), 106.5 (d, $^1J_{\text{PC}} = 201.1$ Hz, CP), 62.9 (d, $^2J_{\text{PC}} = 13.8$ Hz, CHN), 62.8 (d, $^2J_{\text{PC}} = 5.1$ Hz, CH_2), 62.4 (d, $^2J_{\text{PC}} = 4.8$ Hz, CH_2), 55.3 (OCH_3) 16.4 (d, $^3J_{\text{PC}} = 6.4$ Hz, CH_3 phosphonate), 15.5 (d, $^3J_{\text{PC}} = 7.5$, Hz CH_3 phosphonate) ppm.

^{31}P NMR (162 MHz, CDCl_3) δ 15.2 ppm.

FTIR ν_{max} 3482 (O-H $_{\text{st}}$), 1698 (C=O $_{\text{st}}$), 1657 (C=C $_{\text{st}}$), 1248 (P=O $_{\text{st}}$), 1023 (P-O-C $_{\text{st}}$) cm^{-1} .

HRMS (ESI-TOF) m/z calcd. for $\text{C}_{21}\text{H}_{25}\text{NO}_6\text{P}$ $[\text{M}+\text{H}]^+$ 418.1419, found 418.1424.

Diethyl (1-(2-fluorophenyl)-4-hydroxy-5-oxo-2-phenyl-2,5-dihydro-1H-pyrrol-3-yl) phosphonate (93h).

The general procedure was followed in MTBE at 55 °C (heating plate) for 48 hours, using *o*-fluoroaniline (386 μ L, 4 mmol), benzaldehyde (204 μ L, 2 mmol) and ethyl 3-(diethoxyphosphoryl)-2-oxopropanoate (1.513 g, 6 mmol). The crude residue was purified by flash column chromatography (Hexanes/AcOEt 30:70), affording 687 mg (85%) of **93h** as a pale orange solid.

Mp (Et₂O): 143 - 144 °C.

¹H NMR (400 MHz, CDCl₃) δ 9.79 (s, 1H, OH), 7.32 (t, ³J_{HH} = 8.1 Hz, 1H, CH_{Ar}), 7.25 - 7.21 (m, 3H, 3xCH_{Ar}), 7.20 - 7.12 (m, 3H, 3xCH_{Ar}), 7.09 - 6.99 (m, 2H, 2xCH_{Ar}), 5.64 (d, ³J_{PH} = 2.9, 1H, CHN), 4.17 (dq, ³J_{HH} = 7.1, ³J_{PH} = 9.8 Hz, 2H, CH₂), 3.73 (dq, ³J_{HH} = 6.9, ³J_{PH} = 9.7 Hz, 1H, CH_ACH_B), 3.28 (dq, ³J_{HH} = 7.2, ³J_{PH} = 9.8 Hz, 1H, CH_ACH_B), 1.40 (t, ³J_{HH} = 7.0, 3H, CH₃), 0.80 (t, ³J_{HH} = 6.9, 3H, CH₃) ppm.

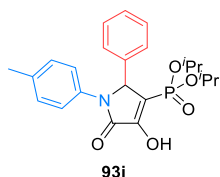
¹³C {¹H} NMR (101 MHz, CDCl₃) δ 163.1 (d, ²J_{PC} = 19.7 Hz, COH), 160.0 (d, ³J_{PC} = 6.7 Hz, C=O), 157.1 (d, ¹J_{FC} = 250.6 Hz, CF), 134.8 (C_{quat}), 129.1 (d, ³J_{FC} = 8.0 Hz, CH_{Ar}), 129.0 (CH_{Ar}), 128.9 (2xCH_{Ar}), 128.4 (d, ⁴J_{FC} = 1.6 Hz, CH_{Ar}), 127.4 (2xCH_{Ar}), 124.6 (d, ³J_{FC} = 3.7 Hz, CH_{Ar}), 123.5 (d, ²J_{FC} = 11.5 Hz, C_{quat}), 116.7 (d, ²J_{FC} = 20.1 Hz, CH_{Ar}), 107.8, (d, ¹J_{PC} = 200.0 Hz, CP), 63.58 (dd, ²J_{PC} = 13.5, ⁴J_{FC} = 5.1 Hz, CHN), 63.1 (d, ²J_{PC} = 5.4 Hz, CH₂), 62.7 (d, ²J_{PC} = 4.5 Hz, CH₂), 16.5 (d, ³J_{PC} = 6.3 Hz, CH₃), 15.6 (d, ³J_{PC} = 7.5 Hz, CH₃) ppm.

¹⁹F NMR (282 MHz, CDCl₃) δ -120.6 ppm.

³¹P NMR (162 MHz, CDCl₃) δ 15.2 ppm.

FTIR ν_{\max} 3490 (O-H_{st}), 1707 (C=O_{st}), 1659 (C=C_{st}), 1223 (P=O_{st}), 1185 (C-F_{st}), 1045 (P-O-C_{st}) cm⁻¹.

HRMS (ESI-TOF) *m/z* calcd. for C₂₀H₂₂FNO₅P [M+H]⁺ 406.1220, found 406.1222.

Di *iso*-propyl (4-hydroxy-5-oxo-2-phenyl-1-(*p*-tolyl)-2,5-dihydro-1H-pyrrol-3-yl) phosphonate (93i).

The general procedure was followed in MTBE at 55 °C (heating plate) for 48 hours, using *p*-toluidine (429 mg, 4 mmol), benzaldehyde (204 μ L, 2 mmol) and ethyl 3-(di-*iso*-propoxyphosphoryl)-2-oxopropanoate (1.681 g, 6 mmol). The crude residue was purified by flash column chromatography (Hexanes/AcOEt 30:70), affording 788 mg (92%) of **93i** as a white solid.

Mp (Et₂O): 171 - 172 °C.

¹H NMR (400 MHz, CDCl₃) δ 9.88 (s, 1H, OH), 7.35 (d, ³J_{HH} = 8.5 Hz, 2H, 2xCH_{Ar}), 7.28 - 7.18 (m, 3H, 3xCH_{Ar}), 7.17 - 7.11 (m, 2H, 2xCH_{Ar}), 7.03 (d, ³J_{HH} = 8.5 Hz, 2H, 2xCH_{Ar}), 5.57 (d, ³J_{PH} = 3.0, 1H, CHN), 4.68

(m, 1H, CH ⁱPr), 4.26 (m, 1H, CH ⁱPr), 2.21 (s, 3H, CH₃ tolyl), 1.38 (d, ³J_{HH} = 6.2 Hz, 6H, 2xCH₃ ⁱPr), 1.02 (d, ³J_{HH} = 6.1 Hz, 3H, CH₃ ⁱPr), 0.63 (d, ³J_{HH} = 6.1 Hz, 3H, CH₃ ⁱPr) ppm.

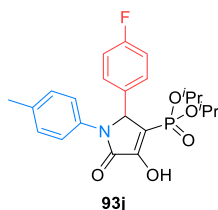
¹³C {¹H} NMR (101 MHz, CDCl₃) δ 163.1 (d, ²J_{PC} = 19.9 Hz, COH), 158.9 (d, ³J_{PC} = 6.6 Hz, C=O), 135.7 (d, ³J_{PC} = 1.0 Hz, C_{quat}), 135.3 (C_{quat}), 134.1 (C_{quat}), 129.5 (2xCH_{Ar}), 128.9 (2xCH_{Ar}), 128.5 (CH_{Ar}), 127.2 (2xCH_{Ar}), 121.8 (2xCH_{Ar}), 108.2 (d, ¹J_{PC} = 203.9 Hz, CP), 72.3 (d, ²J_{PC} = 5.8 Hz, CH ⁱPr), 72.0 (d, ²J_{PC} = 5.8 Hz, CH ⁱPr), 62.7 (d, ²J_{PC} = 13.2 Hz, CHN), 24.2 (d, ³J_{PC} = 4.7 Hz, CH₃ ⁱPr), 24.1 (d, ³J_{PC} = 4.3 Hz, CH₃ ⁱPr), 23.7 (d, ³J_{PC} = 4.2 Hz, CH₃ ⁱPr), 22.9 (d, ³J_{PC} = 5.6 Hz, CH₃ ⁱPr), 20.9 (CH₃ tolyl) ppm.

³¹P NMR (162 MHz, CDCl₃) δ 13.0 ppm.

FTIR ν_{max} 3412 (O-H_{st}), 1691 (C=O_{st}), 1663 (C=C_{st}), 1288 (P=O_{st}), 1102 (P-O-C_{st}) cm⁻¹.

HRMS (ESI-TOF) *m/z* calcd. for C₂₃H₂₉NO₅P [M+H]⁺ 430.1784, found 430.1789.

Di iso-propyl (2-(4-fluorophenyl)-4-hydroxy-5-oxo-1-(*p*-tolyl)-2,5-dihydro-1*H*-pyrrol-3-yl) phosphonate (93j).



The general procedure was followed in MTBE at 55 °C (heating plate) for 48 hours, using *p*-toluidine (429 mg, 4 mmol), *p*-fluorobenzaldehyde (214 μL, 2 mmol) and ethyl 3-(di-*iso*-propoxyphosphoryl)-2-oxopropanoate (1.681 g, 6 mmol). The crude residue was purified by flash column chromatography (Hexanes/AcOEt 30:70), affording 670 mg (75%) of **93j** as a white solid.

Mp (Et₂O): 107 - 108 °C.

¹H NMR (400 MHz, DMSO-*d*₆) δ 11.34 (s, 1H, OH), 7.44 (d, ³J_{HH} = 8.5 Hz, 2H, 2xCH_{Ar}), 7.26 (dd, ³J_{HH} = 8.5, ³J_{FH} = 5.4 Hz, 2H, 2xCH_{Ar}), 7.07 (d, ³J_{HH} = 8.5 Hz, 3H, 2xCH_{Ar}), 7.03 (d, ³J_{HH} = 8.5 Hz, 1H, 2xCH_{Ar}), 5.97 (d, ³J_{HH} = 2.8 Hz, 1H, CHN), 4.44 (hept, ³J_{HH} = 6.1 Hz, 1H, CH ⁱPr), 4.27 (m, 1H, CH ⁱPr), 2.18 (s, 3H, CH₃ tolyl), 1.16 (d, ³J_{HH} = 6.1 Hz, 3H, CH₃ ⁱPr), 1.12 - 1.02 (m, 9H, 3xCH₃ ⁱPr) ppm.

¹³C {¹H} NMR (101 MHz, CDCl₃) δ 163.5 (d, ²J_{PC} = 18.4 Hz, COH), 161.7 (d, ¹J_{FC} = 244.0 Hz, CF), 154.4 (d, ³J_{PC} = 4.2 Hz, C=O), 134.6 (C_{quat}), 133.77 (C_{quat}), 132.4 (d, ⁴J_{FC} = 3.1 Hz, C_{quat}), 130.0 (d, ³J_{FC} = 8.4 Hz, 2xCH_{Ar}), 129.1 (2xCH_{Ar}), 122.5 (2xCH_{Ar}), 114.9 (d, ²J_{FC} = 21.6 Hz, 2xCH_{Ar}), 109.6 (d, ¹J_{PC} = 203.6 Hz, CP), 70.1 (d, ²J_{PC} = 5.4 Hz, CH ⁱPr), 69.9 (d, ²J_{PC} = 5.7 Hz, CH ⁱPr), 61.6 (d, ²J_{PC} = 15.3 Hz, CHN), 23.7 (d, ³J_{PC} = 3.8 Hz, CH₃ ⁱPr), 23.6 (d, ³J_{PC} = 3.9 Hz, CH₃ ⁱPr), 23.5 (d, ³J_{PC} = 5.1 Hz, CH₃ ⁱPr), 23.3 (d, ³J_{PC} = 5.4 Hz, CH₃ ⁱPr), 20.4 (CH₃ tolyl) ppm.

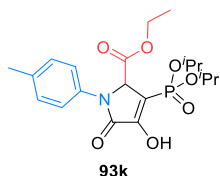
¹⁹F NMR (282 MHz, CDCl₃) δ -110.1 ppm.

³¹P NMR (162 MHz, CDCl₃) δ 8.9 ppm.

FTIR ν_{\max} 3501 (O-H_{st}), 1704 (C=O_{st}), 1663 (C=C_{st}), 1226 (P=O_{st}), 1185 (C-F_{st}), 1011 (P-O-C_{st}) cm^{-1} .

HRMS (ESI-TOF) m/z calcd. for $\text{C}_{23}\text{H}_{28}\text{FNO}_5\text{P}$ $[\text{M}+\text{H}]^+$ 448.1689, found 448.1677.

Ethyl 3-(di iso-propoxyphosphoryl)-4-hydroxy-5-oxo-1-(*p*-tolyl)-2,5-dihydro-1H-pyrrole-2-carboxylate (93k).



The general procedure was followed in MTBE at 55 °C (heating plate) for 48 hours, using *p*-toluidine (429 mg, 4 mmol), a 50% solution of ethyl glyoxalate in toluene (396 μL , 2 mmol) and ethyl 3-(di-*iso*-propoxyphosphoryl)-2-oxopropanoate (1.681 g, 6 mmol). The crude residue was purified by flash column chromatography (Hexanes/AcOEt 2:8), affording 654 mg (77%) of **93k** as a white solid.

Mp (Et_2O): 131 - 132 °C.

^1H NMR (400 MHz, CDCl_3) δ 10.00 (s, 1H, OH), 7.43 (d, $^3J_{\text{HH}} = 8.4$ Hz, 2H, $2\times\text{CH}_{\text{Ar}}$), 7.16 (d, $^3J_{\text{HH}} = 8.4$ Hz, 2H, $2\times\text{CH}_{\text{Ar}}$), 5.15 (d, $^3J_{\text{PH}} = 3.0$, 1H, CHN), 4.81 - 4.64 (m, 2H, $2\times\text{CH}^i\text{Pr}$), 4.15 - 4.02 (m, 2H, CH_2), 2.31 (s, 3H, CH_3 tolyl), 1.40 (d, $^3J_{\text{HH}} = 6.2$ Hz, 3H, CH_3^iPr), 1.37 (d, $^3J_{\text{HH}} = 6.2$ Hz, 3H, CH_3^iPr), 1.34 (d, $^3J_{\text{HH}} = 6.2$ Hz, 3H, CH_3^iPr), 1.24 (d, $^3J_{\text{HH}} = 6.2$ Hz, 3H, CH_3^iPr), 1.14 (t, $^3J_{\text{HH}} = 7.1$ Hz, 3H, CH_3 ester) ppm.

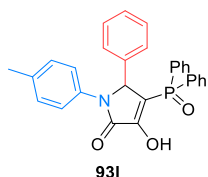
^{13}C $\{^1\text{H}\}$ NMR (101 MHz, CDCl_3) δ 167.3 (d, $^3J_{\text{PC}} = 1.1$ Hz, C=O), 162.7 (d, $^2J_{\text{PC}} = 19.6$ Hz, COH), 161.1 (d, $^3J_{\text{PC}} = 6.5$ Hz, C=O), 136.0 (C_{quat}), 134.5 (C_{quat}), 129.9 ($2\times\text{CH}_{\text{Ar}}$), 120.9 ($2\times\text{CH}_{\text{Ar}}$), 101.8 (d, $^1J_{\text{PC}} = 206.6$ Hz, CP), 73.1 (d, $^2J_{\text{PC}} = 5.9$ Hz, CH^iPr), 72.7 (d, $^2J_{\text{PC}} = 6.1$ Hz, CH^iPr), 62.2 (CH_2), 61.1 (d, $^2J_{\text{PC}} = 13.0$ Hz, CHN), 24.2 (d, $^3J_{\text{PC}} = 4.5$ Hz, CH_3^iPr), 24.1 (d, $^3J_{\text{PC}} = 4.9$ Hz, CH_3^iPr), 24.0 (d, $^3J_{\text{PC}} = 4.9$ Hz, CH_3^iPr), 23.7 (d, $^3J_{\text{PC}} = 4.6$ Hz, CH_3^iPr), 21.1 (CH_3 tolyl), 14.0 (CH_3 ester) ppm.

^{31}P NMR (162 MHz, CDCl_3) δ 12.0 ppm.

FTIR ν_{\max} 3425 (O-H_{st}), 1742 (C=O_{st} ester), 1715 (C=O_{st} amide), 1658 (C=C_{st}), 1269 (P=O_{st}), 1106 (P-O-C_{st}) cm^{-1} .

HRMS (ESI-TOF) m/z calcd. for $\text{C}_{20}\text{H}_{29}\text{NO}_7\text{P}$ $[\text{M}+\text{H}]^+$ 426.1682, found 426.1688.

4-(Diphenylphosphoryl)-3-hydroxy-5-phenyl-1-(*p*-tolyl)-1,5-dihydro-2H-pyrrol-2-one (93l).



The general procedure was followed in MTBE at 55 °C (heating plate) for 48 hours, using *p*-toluidine (429 mg, 4 mmol), benzaldehyde (204 μL , 2 mmol) and ethyl 3-(diphenylphosphoryl)-2-oxopropanoate (1.897 g, 6 mmol). The crude residue was purified by flash column chromatography (Hexanes/AcOEt 30:70), affording 642 mg (69%) of **93l** as a pale yellow solid.

Mp (Et_2O): 121 - 122 °C.

¹H NMR (400 MHz, CDCl₃) δ 10.59 (bs, 1H, OH), 7.71 (m, 2H, 2xCH_{Ar}), 7.63 (m, 1H, CH_{Ar}), 7.54 (m, 2H, 2xCH_{Ar}), 7.35 (m, 1H, CH_{Ar}), 7.25 - 7.12 (m, 6H, 6xCH_{Ar}), 7.03 - 6.98 (m, 3H, 3xCH_{Ar}), 6.94 (d, ³J_{HH} = 6.9 Hz, 2H, 2xCH_{Ar}), 6.88 (d, ³J_{HH} = 6.8 Hz, 2H, 2xCH_{Ar}), 5.58 (d, ³J_{PH} = 2.1 Hz, 1H, CHN), 2.20 (s, 3H, CH₃) ppm.

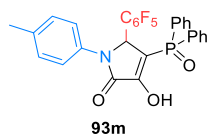
¹³C {¹H} NMR (101 MHz, CDCl₃) δ 163.4 (d, ²J_{PC} = 13.3 Hz, COH), 159.3 (C=O), 135.7 (C_{quat}), 134.8 (C_{quat}), 133.8 (C_{quat}), 132.9 (d, ⁴J_{PC} = 2.8 Hz, CH_{Ar}), 132.2 (d, ⁴J_{PC} = 2.8 Hz, CH_{Ar}), 131.5 (d, ²J_{PC} = 10.8 Hz, 2xCH_{Ar}), 131.4 (d, ²J_{PC} = 11.2 Hz, 2xCH_{Ar}), 130.4 (d, ¹J_{PC} = 108.3 Hz, C_{Ar}P), 130.1 (d, ¹J_{PC} = 108.4 Hz, C_{Ar}P), 129.6 (2xCH_{Ar}), 129.0 (d, ³J_{PC} = 12.7 Hz, 2xCH_{Ar}), 128.8 (2xCH_{Ar}), 128.6 (CH_{Ar}), 128.3 (d, ³J_{PC} = 13.0 Hz, 2xCH_{Ar}), 127.7 (2xCH_{Ar}), 122.6 (2xCH_{Ar}), 109.3 (d, ¹J_{PC} = 110.1 Hz, =CP), 64.1 (d, ²J_{PC} = 11.8 Hz, CHN), 21.0 (CH₃) ppm.

³¹P NMR (121 MHz, CDCl₃) δ 29.8 ppm.

FTIR ν_{max} 3478 (O-H_{st}), 1690 (C=O_{st}), 1654 (C=C_{st}), 1147 (P=O_{st}) cm⁻¹.

HRMS (ESI-TOF) *m/z* calcd. for C₂₉H₂₅NO₃P [M+H]⁺ 466.1572, found 466.1572.

4-(Diphenylphosphoryl)-3-hydroxy-5-(perfluorophenyl)-1-(*p*-tolyl)-1,5-dihydro-2H-pyrrol-2-one (93m).



The general procedure was followed in MTBE at 55 °C (heating plate) for 48 hours, using *p*-toluidine (429 mg, 4 mmol), 2,3,4,5,6-pentafluorobenzaldehyde (247 μL, 2 mmol) and ethyl 3-(diphenylphosphoryl)-2-oxopropanoate (1.90 g, 6 mmol). The crude residue was purified by flash column chromatography (Hexanes/AcOEt 30:70), affording 920 mg (83%) of **93m** as a white solid.

Mp (Et₂O): 202 - 204 °C (dec.).

¹H NMR (400 MHz, Methanol-*d*₄) δ 7.74 - 7.43 (m, 10H, 10xCH_{Ar}), 7.23 (d, ³J_{HH} = 8.1 Hz, 2H, 2xCH_{Ar}), 7.03 (d, ³J_{HH} = 8.1 Hz, 2H, 2xCH_{Ar}), 6.39 (bs, 1H, CHN), 2.13 (s, 3H, CH₃) ppm.

¹³C {¹H} NMR (101 MHz, Methanol-*d*₄) δ 164.9 (m, COH), 157.3 (m, C=O), 146.7 (m, C_{quat}), 144.7 (m, C_{quat}), 144.0 (m, C_{quat}), 142.3 (m, C_{quat}), 138.4 (m, C_{quat}), 137.9 (C_{quat}), 134.4 (C_{quat}), 133.7 (2xCH_{Ar}), 132.6 (d, ²J_{PC} = 11.4 Hz, 2xCH_{Ar}), 132.0 (d, ²J_{PC} = 10.4 Hz, 2xCH_{Ar}), 130.9 (d, ¹J_{PC} = 111.6 Hz, C_{Ar}P), 130.8 (2xCH_{Ar}), 130.6 (d, ¹J_{PC} = 124.7 Hz, C_{Ar}P), 129.7 (d, ³J_{PC} = 4.9 Hz, 2xCH_{Ar}), 129.6 (d, ³J_{PC} = 4.9 Hz, 2xCH_{Ar}), 123.4 (2xCH_{Ar}), 111.4 (m, =CP), 55.2 (CHN), 20.9 (CH₃) ppm.

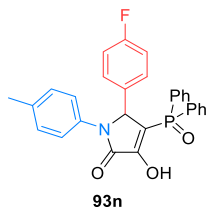
¹⁹F NMR (282 MHz, CDCl₃) δ -144.1 (dd, ³J_{FF} = 142.3, 21.9 Hz), -152.8 (t, ³J_{FF} = 20.9 Hz), -161.1 (td, ³J_{FF} = 21.4, 7.7 Hz), -161.5 (td, ³J_{FF} = 21.9, 8.3 Hz) ppm.

³¹P NMR (162 MHz, CDCl₃) δ 27.2 ppm.

FTIR ν_{\max} 3414 (O-H_{st}), 1691 (C=O_{st}), 1659 (C=C_{st}), 1151 (P=O_{st}) cm^{-1} .

HRMS (ESI-TOF) m/z calcd. for $\text{C}_{29}\text{H}_{20}\text{F}_5\text{NO}_3\text{P}$ $[\text{M}+\text{H}]^+$ 556.1101, found 556.1109.

4-(Diphenylphosphoryl)-5-(4-fluorophenyl)-3-hydroxy-1-(*p*-tolyl)-1,5-dihydro-2H-pyrrol-2-one (93n).



The general procedure was followed in MTBE at 55 °C (heating plate) for 48 hours, using *p*-toluidine (429 mg, 4 mmol), *p*-fluorobenzaldehyde (214 μL , 2 mmol) and ethyl 3-(diphenylphosphoryl)-2-oxopropanoate (1.897 g, 6 mmol). The crude residue was purified by flash column chromatography (Hexanes/AcOEt 30:70), affording 830 mg (87%) of **93n** as a white solid.

Mp (Et₂O): 208 - 210 °C (dec.).

¹H NMR (400 MHz, CDCl₃) δ 10.49, (s, 1H, OH), 7.75 - 7.55 (m, 4H, 4xCH_{Ar}), 7.53 - 7.44 (2H, 2xCH_{Ar}), 7.44-7.38 (m, 2H, 2xCH_{Ar}), 7.32 (dd, ³J_{FH} = 12.9, ³J_{HH} = 7.7 Hz, 2H, 2xCH_{Ar}), 7.21 (d, ³J_{HH} = 8.5 Hz, 2H, 2xCH_{Ar}), 7.03 (d, ³J_{HH} = 8.0 Hz, 2H, 2xCH_{Ar}), 6.86 (dd, *J* = 8.4, 5.3 Hz, 2H, 2xCH_{Ar}), 6.60 (t, ³J_{HH} = 8.6 Hz, 2H, 2xCH_{Ar}), 5.69 (bs, 1H, CHN), 2.22 (s, 3H, CH₃) ppm.

¹³C {¹H} NMR (101 MHz, CDCl₃) δ 163.7 (C=O), 163.5 (d, ²J_{PC} = 13.1 Hz, COH), 159.3 (d, ¹J_{FC} = 258.8 Hz, CF), 135.8 (C_{quat}), 133.5 (C_{quat}), 132.6 (d, ⁴J_{PC} = 2.9 Hz, CH_{Ar}), 132.2 (d, ⁴J_{PC} = 2.5 Hz, CH_{Ar}), 131.6 (d, ²J_{PC} = 11.1 Hz, 2xCH_{Ar}), 131.4 (d, ²J_{PC} = 10.1 Hz, 2xCH_{Ar}), 130.6 (d, ¹J_{PC} = 110.1 Hz, C_{Ar}P), 130.5 (d, ⁴J_{FC} = 4.0 Hz, C_{quat}), 130.4 (d, ¹J_{PC} = 110.1 Hz, C_{Ar}P), 129.7 (2xCH_{Ar}), 129.5 (d, ³J_{FC} = 9.1 Hz, 2xCH_{Ar}), 128.8 (d, ³J_{PC} = 12.1 Hz, 2xCH_{Ar}), 128.3 (d, ³J_{PC} = 13.1 Hz, 2xCH_{Ar}), 122.5 (2xCH_{Ar}), 115.5 (d, ²J_{FC} = 22.0 Hz, 2xCH_{Ar}), 110.3 (d, ¹J_{PC} = 111.1 Hz, =CP), 63.3 (d, ²J_{PC} = 11.0 Hz, CHN), 21.0 (CH₃) ppm.

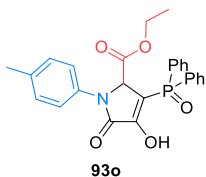
¹⁹F NMR (282 MHz, CDCl₃) δ -113.5 ppm.

³¹P NMR (162 MHz, CDCl₃) δ 29.4 ppm.

FTIR ν_{\max} 3422 (O-H_{st}), 1696 (C=O_{st}), 1656 (C=C_{st}), 1226 (P=O_{st}), 1153 (C-F_{st}) cm^{-1} .

HRMS (ESI-TOF) m/z calcd. for $\text{C}_{29}\text{H}_{24}\text{FNO}_3\text{P}$ $[\text{M}+\text{H}]^+$ 484.1478, found 484.1473.

Ethyl 3-(diphenylphosphoryl)-4-hydroxy-5-oxo-1-(*p*-tolyl)-2,5-dihydro-1H-pyrrole-2-carboxylate (93o).



The general procedure was followed in MTBE at 55 °C (heating plate) for 48 hours, using *p*-toluidine (429 mg, 4 mmol), a 50% solution of ethyl glyoxalate in toluene (396 μL , 2 mmol) and ethyl 3-(diphenylphosphoryl)-2-oxopropanoate (1.897 g, 6 mmol). The crude residue was purified by flash column chromatography (Hexanes/AcOEt 30:70), affording 729 mg (79%) of **93o** as a white solid.

Mp (Et₂O): 107 - 108 °C.

¹H NMR (400 MHz, CDCl₃) δ 11.47 (s, 1H, OH), 8.06 (dd, ³J_{HH} = 7.0, ³J_{PH} = 12.8 Hz, 2H, 2xCH_{Ar}), 7.75 - 7.64 (m, 3H, 3xCH_{Ar}), 7.64 - 7.55 (m, 3H, 3xCH_{Ar}), 7.51 - 7.45 (m, 2H, 2xCH_{Ar}), 7.38 (d, ³J_{HH} = 8.3 Hz, 2H, 2xCH_{Ar}), 7.14 (d, ³J_{HH} = 8.1 Hz, 2H, 2xCH_{Ar}), 5.08 (d, ³J_{PH} = 2.2 Hz, 1H, CHN), 3.52 (m, 1H, CH_AH_B), 3.33 (m, 1H, CH_AH_B), 2.30 (s, 3H, CH₃ tolyl), 0.83 (t, ³J_{HH} = 7.1 Hz, 3H, CH₃ ester) ppm.

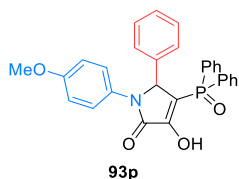
¹³C {¹H} NMR (101 MHz, CDCl₃) δ 167.3 (C=O), 163.2 (C=O), 162.8 (d, ²J_{PC} = 13.0 Hz, COH), 136.0 (C_{quat}), 134.5 (C_{quat}), 133.3 - 133.2 (m, 2xCH_{Ar}), 131.8 (d, ²J_{PC} = 10.5 Hz, 2xCH_{Ar}), 131.6 (d, ²J_{PC} = 11.8 Hz, 2xCH_{Ar}), 130.2 (d, ¹J_{PC} = 106.7 Hz, C_{Ar}P), 129.9 (2xCH_{Ar}), 129.3 (d, ²J_{PC} = 13.0 Hz, 2xCH_{Ar}), 128.9 (d, ²J_{PC} = 12.8 Hz, 2xCH_{Ar}), 128.1 (d, ¹J_{PC} = 110.7 Hz, C_{Ar}P), 120.9 (2xCH_{Ar}), 101.3 (d, ¹J_{PC} = 110.1 Hz, =CP), 62.2 (CH₂), 61.8 (d, ²J_{PC} = 12.0, CHN), 21.1 (CH₃ tolyl), 13.6 (CH₃ ester) ppm.

³¹P NMR (121 MHz, CDCl₃) δ 32.1 ppm.

FTIR ν_{max} 3467 (O-H_{st}), 1737 (C=O_{st} ester), 1697 (C=O_{st} amide), 1650 (C=C_{st}), 1182 (P=O_{st}) cm⁻¹.

HRMS (ESI-TOF) *m/z* calcd. for C₂₆H₂₅NO₅P [M+H]⁺ 462.1470, found 462.1475.

4-(Diphenylphosphoryl)-3-hydroxy-1-(4-methoxyphenyl)-5-phenyl-1,5-dihydro-2H-pyrrol-2-one (93p).



The general procedure was followed in MTBE at 55 °C (heating plate) for 48 hours, using *p*-anisidine (492 mg, 4 mmol), benzaldehyde (204 μL, 2 mmol) and ethyl 3-(diphenylphosphoryl)-2-oxopropanoate (1.897 g, 6 mmol). The crude residue was purified by flash column chromatography

(Hexanes/AcOEt 30:70), affording 770 mg (80%) of **93p** as a white solid.

Mp (Et₂O): 175 - 177 °C (dec.).

¹H NMR (300 MHz, CDCl₃) δ 10.74 (s, 1H, OH), 7.87 (m, 1H, CH_{Ar}), 7.74 - 7.56 (m, 4H, 4xCH_{Ar}), 7.58 - 7.48 (m, 2H, 2xCH_{Ar}), 7.42 - 7.29 (m, 2H, 2xCH_{Ar}), 7.25 - 7.11 (m, 4H, 4xCH_{Ar}), 7.02 - 6.90 (m, 2H, 2xCH_{Ar}), 6.85 (d, ³J_{HH} = 7.7 Hz, 2H, 2xCH_{Ar}), 6.72 (d, ³J_{HH} = 7.2 Hz, 2H, 2xCH_{Ar}), 5.52 (s, 1H, CHN), 3.68 (s, 3H, OCH₃) ppm.

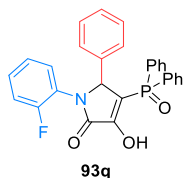
¹³C {¹H} NMR (75 MHz, CDCl₃) δ 163.3 (d, ²J_{PC} = 12.5 Hz, COH), 159.6 (C=O), 157.5 (C_{quat}), 134.7 (C_{quat}), 132.9 (d, ⁴J_{PC} = 2.9 Hz, CH_{Ar}), 132.2 (d, ⁴J_{PC} = 3.1 Hz, CH_{Ar}), 131.6 (d, ²J_{PC} = 10.8 Hz, 2xCH_{Ar}), 131.5 (d, ²J_{PC} = 11.2 Hz, 2xCH_{Ar}), 130.4 (d, ¹J_{PC} = 108.6 Hz, C_{Ar}P), 130.1 (d, ¹J_{PC} = 110.2 Hz, C_{Ar}P), 129.0 (d, ³J_{PC} = 12.7 Hz, 2xCH_{Ar}), 128.7 (2xCH_{Ar}), 128.6 (CH_{Ar}), 128.3 (d, ³J_{PC} = 13.0 Hz, 2xCH_{Ar}), 127.8 (2xCH_{Ar}), 124.6 (2xCH_{Ar}), 120.5 (C_{quat}), 114.2 (2xCH_{Ar}), 109.0 (d, ¹J_{PC} = 109.9 Hz, =CP), 64.6 (d, ²J_{PC} = 11.7 Hz, CHN), 55.4 (OCH₃) ppm.

^{31}P NMR (121 MHz, CDCl_3) δ 30.2 ppm.

FTIR ν_{max} 3490 (O-H_{st}), 1690 (C=O_{st}), 1694 (C=C_{st}), 1156 (P=O_{st}) cm^{-1} .

HRMS (ESI-TOF) m/z calcd. for $\text{C}_{29}\text{H}_{25}\text{NO}_4\text{P}$ $[\text{M}+\text{H}]^+$ 482.1521, found 482.1524.

4-(Diphenylphosphoryl)-1-(2-fluorophenyl)-3-hydroxy-5-phenyl-1,5-dihydro-2H-pyrrol-2-one (93q).



The general procedure was followed in MTBE at 55 °C (heating plate) for 48 hours, using *o*-fluoroaniline (386 μL , 4 mmol), benzaldehyde (**2a**) (204 μL , 2 mmol) and ethyl 3-(diphenylphosphoryl)-2-oxopropanoate (1.897 g, 6 mmol). The crude residue was purified by flash column chromatography (Hexanes/AcOEt 30:70),

affording 722 mg (77%) of **93q** as a pale yellow solid.

Mp (Et_2O): 218 - 219 °C (dec.).

^1H NMR (400 MHz, CDCl_3) δ 11.17 (s, 1H, OH), 7.79 - 7.70 (m, 2H, 2xCH_{Ar}), 7.69 - 7.63 (m, 1H, CH_{Ar}), 7.61 - 7.54 (m, 2H, 2xCH_{Ar}), 7.36 - 7.29 (m, 1H, CH_{Ar}), 7.24 - 7.17 (m, 2H, 2xCH_{Ar}), 7.17 - 7.07 (m, 4H, 4xCH_{Ar}), 7.02 - 6.94 (m, 3H, 3xCH_{Ar}), 6.93 - 6.86 (m, 2H, 2xCH_{Ar}), 6.84 - 6.77 (m, 2H, 2xCH_{Ar}), 5.63 (d, $^3J_{\text{PH}} = 2.0$ Hz, 1H, CHN) ppm.

^{13}C { ^1H } NMR (101 MHz, CDCl_3) δ 163.3 (d, $^2J_{\text{PC}} = 20.4$ Hz, COH), 160.6 (C=O), 157.1 (d, $^1J_{\text{FC}} = 250.0$ Hz, CF), 134.0 (C_{quat}), 133.1 (d, $^4J_{\text{PC}} = 2.9$ Hz, CH_{Ar}), 132.2 (d, $^4J_{\text{PC}} = 3.0$ Hz, CH_{Ar}), 131.6 (d, $^2J_{\text{PC}} = 10.9$ Hz, 2xCH_{Ar}), 131.5 (d, $^2J_{\text{PC}} = 11.0$ Hz, 2xCH_{Ar}), 130.3 (d, $^1J_{\text{PC}} = 107.0$ Hz, C_{Ar}P), 129.8 (d, $^1J_{\text{PC}} = 107.8$ Hz, C_{Ar}P), 129.4 - 127.7 (m, 11xCH_{Ar}), 124.5 (d, $^4J_{\text{PC}} = 3.7$ Hz, CH_{Ar}), 123.3 (d, $^2J_{\text{FC}} = 11.5$ Hz, C_{quat}), 116.5 (d, $^2J_{\text{FC}} = 20.1$ Hz, CH_{Ar}), 109.3 (d, $^1J_{\text{PC}} = 110.1$ Hz, =CP), 64.8 (dd, $^2J_{\text{PC}} = 11.9$, $^4J_{\text{FC}} = 4.9$ Hz, CHN) ppm.

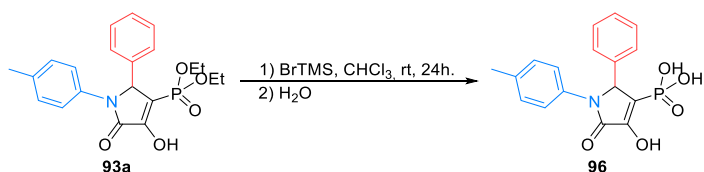
^{19}F NMR (282 MHz, CDCl_3) δ -120.3 ppm.

^{31}P NMR (121 MHz, CDCl_3) δ 31.4 ppm.

FTIR ν_{max} 3482 (O-H_{st}), 1701 (C=O_{st}), 1653 (C=C_{st}), 1153 (P=O_{st}), 1118 (C-F_{st}) cm^{-1} .

HRMS (ESI-TOF) m/z calcd. for $\text{C}_{28}\text{H}_{22}\text{FNO}_3\text{P}$ $[\text{M}+\text{H}]^+$ 470.1321, found 470.1302.

Synthesis of 4-hydroxy-5-oxo-2-phenyl-1-(*p*-tolyl)-2,5-dihydro-1*H*-pyrrol-3-yl phosphonic acid (**96**).



A solution of γ -lactam **93a** (0.402 g, 1 mmol) and bromotrimethylsilane (0.765 g, 5 mmol) was stirred at room temperature in dry chloroform (5 mL). The reaction was monitored by ^{31}P NMR until the disappearance of the starting material (24 hours). Then, water was added (5 mL), and the volatiles were distilled off at reduced pressure. The crude residue was purified by crystallization from a mixture dichloromethane/methanol (95:5), affording 338 mg (98%) of **96** as a white solid.

Mp ($\text{CH}_2\text{Cl}_2/\text{MeOH}$): 183 - 185 °C (dec.).

^1H NMR (400 MHz, $\text{DMSO}-d_6$) δ 10.81 (s, 3H), 7.39 (d, $^3J_{\text{HH}} = 8.3$ Hz, 2H, $2\times\text{CH}_{\text{Ar}}$), 7.27 - 7.10 (m, 5H, $5\times\text{CH}_{\text{Ar}}$), 7.06 (d, $^3J_{\text{HH}} = 8.3$ Hz, 2H, $2\times\text{CH}_{\text{Ar}}$), 5.86 (d, $^3J_{\text{PH}} = 3.0$ Hz, 1H, CHN), 2.18 (s, 3H, CH_3) ppm.

^{13}C $\{^1\text{H}\}$ NMR (101 MHz, $\text{DMSO}-d_6$) δ 163.6 (d, $^2J_{\text{PC}} = 18.1$ Hz, COH), 154.0 (d, $^3J_{\text{PC}} = 5.3$ Hz, C=O), 136.4 (C_{quat}), 134.3 (C_{quat}), 134.0 (C_{quat}), 129.1 ($2\times\text{CH}_{\text{Ar}}$), 128.2 ($2\times\text{CH}_{\text{Ar}}$), 127.8 (CH_{Ar}), 127.7 ($2\times\text{CH}_{\text{Ar}}$), 122.5 ($2\times\text{CH}_{\text{Ar}}$), 113.6 (d, $^1J_{\text{PC}} = 194.0$ Hz, CP), 62.1 (d, $^2J_{\text{PC}} = 14.2$ Hz, CHN), 20.5 (CH_3) ppm.

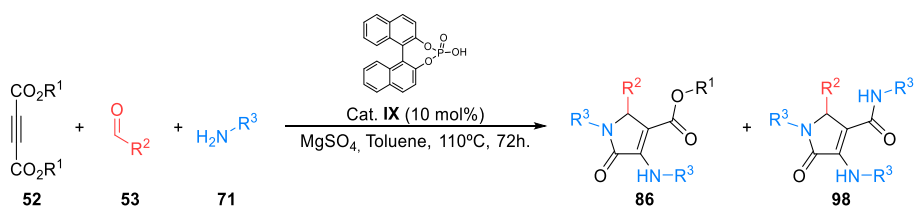
^{31}P NMR (121 MHz, $\text{DMSO}-d_6$) δ -1.9 ppm.

FTIR ν_{max} 3464 (O-H_{st}), 1688 (C=O_{st}), 1669 (C=C_{st}), 1264 (P=O_{st}), 992 (P-O-H_{st}) cm^{-1} .

HRMS (ESI-TOF) m/z calcd. for $\text{C}_{17}\text{H}_{17}\text{NO}_5\text{P}$ $[\text{M}+\text{H}]^+$ 346.0844, found 346.0848.

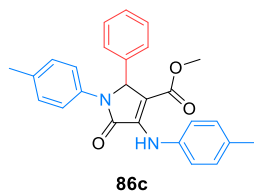
Chapter 3. Multicomponent synthesis of γ -lactam derivatives using activated alkynes.

General procedure for the synthesis of 3-amino-1,5-dihydro-2H-pyrrol-2-ones **86** and **98** using activated alkynes.



A solution of amine **71** (4 mmol), aldehyde **53** (2 mmol), acetylene dicarboxylate derivative **52** (2 mmol) and BINOL-derived phosphoric acid **IX** (70 mg, 0.2 mmol) was stirred in toluene (10 mL) at 110°C (heating plate) in the presence of anhydrous MgSO_4 for 72 hours. Then, the reaction was filtered, the volatiles were distilled off at reduced pressure and the crude residue was purified by flash column chromatography (Hexanes/ AcOEt) to afford pure γ -lactams **86** and **98**.

Methyl 5-oxo-2-phenyl-1-(*p*-tolyl)-4-(*p*-tolylamino)-2,5-dihydro-1H-pyrrole-3-carboxylate (**86c**).



The general procedure was followed using *p*-toluidine (429 mg, 4 mmol), benzaldehyde (204 μL , 2 mmol) and dimethyl acetylenedicarboxylate (246 μL , 2 mmol). The crude residue was purified by flash column chromatography (Hexanes/ AcOEt 90:10), affording 675 mg (82%) of **86c** as a white solid.

Mp (Et_2O): $179 - 181^\circ\text{C}$. Lit. $184 - 185^\circ\text{C}$.¹³⁷

$^1\text{H NMR}$ (400 MHz, CDCl_3) δ 8.14 (s, 1H, NH), 7.33 (d, $^3J_{\text{HH}} = 8.5\text{ Hz}$, 2H, $2\times\text{CH}_{\text{Ar}}$), 7.25 (m, 4H), 7.20 (m, 1H, CH_{Ar}), 7.13 (d, $^3J_{\text{HH}} = 8.3\text{ Hz}$, 2H, $2\times\text{CH}_{\text{Ar}}$), 7.09 (d, $^3J_{\text{HH}} = 8.5\text{ Hz}$, 2H, $2\times\text{CH}_{\text{Ar}}$), 7.03 (d, $^3J_{\text{HH}} = 8.3\text{ Hz}$, 2H, $2\times\text{CH}_{\text{Ar}}$), 5.77 (s, 1H, CHN), 3.54 (s, 3H, OCH_3), 2.34 (s, 3H, CH_3 tolyl), 2.23 (s, 3H, CH_3 tolyl) ppm.

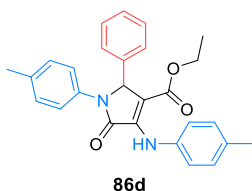
$^{13}\text{C}\{^1\text{H}\}$ NMR (101 MHz, CDCl_3) δ 164.9 (C=O), 163.9 (C=O), 142.8 (C_{quat}), 137.2 (C_{quat}), 136.0 (C_{quat}), 135.5 (C_{quat}), 134.7 (C_{quat}), 134.1 (C_{quat}), 129.5 ($2\times\text{CH}_{\text{Ar}}$), 129.1 ($2\times\text{CH}_{\text{Ar}}$), 128.5 ($2\times\text{CH}_{\text{Ar}}$), 128.1 (CH_{Ar}),

127.7 (2xCH_{Ar}), 123.3 (2xCH_{Ar}), 122.8 (2xCH_{Ar}), 108.9 (=C), 63.2 (CHN), 51.2 (OCH₃), 21.1 (CH₃ tolyl), 21.0 (CH₃ tolyl) ppm.

FTIR ν_{\max} 3286 (N-H_{st}), 1705 (C=O_{st} ester), 1705 (C=O_{st} amide), 1677 (C=C_{st}) cm⁻¹.

HRMS (ESI-TOF) m/z calcd. for C₂₆H₂₅N₂O₃ [M+H]⁺ 413.1865, found 413.1863.

Ethyl 5-oxo-2-phenyl-1-(*p*-tolyl)-4-(*p*-tolylamino)-2,5-dihydro-1*H*-pyrrole-3-carboxylate (86d).



The general procedure was followed using *p*-toluidine (429 mg, 4 mmol), benzaldehyde (204 μ L, 2 mmol) and diethyl acetylenedicarboxylate (320 μ L, 2 mmol). The crude residue was purified by flash column chromatography (Hexanes/AcOEt 90:10), affording 656 mg (77%) of **86d** as a white solid.

Mp (Et₂O): 154 - 155 °C. Lit. 156 - 158 °C.^{133b}

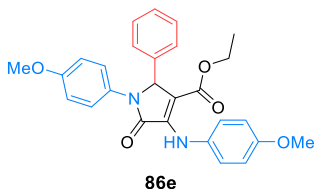
¹H NMR (400 MHz, CDCl₃) δ 8.17 (bs, 1H, NH), 7.34 (d, ³ J_{HH} = 8.5 Hz, 2H, 2xCH_{Ar}), 7.26 - 7.21 (m, 5H, 5xCH_{Ar}), 7.12 (d, ³ J_{HH} = 8.3 Hz, 2H, 2xCH_{Ar}), 7.08 (d, ³ J_{HH} = 8.5 Hz, 2H, 2xCH_{Ar}), 7.03 (d, ³ J_{HH} = 8.3 Hz, 2H, 2xCH_{Ar}), 5.77 (s, 1H, CHN), 4.01 (q, ³ J_{HH} = 7.1 Hz, 2H, CH₂), 2.33 (s, 3H, CH₃ tolyl), 2.23 (s, 3H, CH₃ tolyl), 1.01 (t, ³ J_{HH} = 7.1 Hz, 3H, CH₃ ester) ppm.

¹³C {¹H} NMR (101 MHz, CDCl₃) δ 164.7 (C=O), 164.1 (C=O), 142.72 (C_{quat}), 137.2 (C_{quat}), 136.1 (C_{quat}), 135.5 (C_{quat}), 134.6 (C_{quat}), 134.2 (C_{quat}), 129.5 (2xCH_{Ar}), 129.1 (2xCH_{Ar}), 128.4 (2xCH_{Ar}), 128.1 (CH_{Ar}), 127.8 (2xCH_{Ar}), 123.2 (2xCH_{Ar}), 122.8 (2xCH_{Ar}), 108.9 (=C), 63.3 (CHN), 60.2 (CH₂), 21.1 (CH₃ tolyl), 21.0 (CH₃ tolyl), 14.0 (CH₃ ester) ppm.

FTIR ν_{\max} 3389 (N-H_{st}), 1741 (C=O_{st} ester), 1700 (C=O_{st} amide), 1679 (C=C_{st}) cm⁻¹.

HRMS (ESI-TOF) m/z calcd. for C₂₇H₂₇N₂O₃ [M+H]⁺ 427.2021, found 427.2020.

Ethyl 1-(4-methoxyphenyl)-4-((4-methoxyphenyl)amino)-5-oxo-2-phenyl-2,5-dihydro-1*H*-pyrrole-3-carboxylate (86e).



The general procedure was followed using *p*-anisidine (492 mg, 4 mmol), benzaldehyde (204 μ L, 2 mmol) and diethyl acetylenedicarboxylate (320 μ L, 2 mmol). The crude residue was purified by flash column chromatography (Hexanes/AcOEt 80:20), affording 695 mg (76%) of **86e** as a yellow solid.

Mp (Et₂O): 116 - 117 °C.

¹H NMR (300 MHz, CDCl₃) δ 8.20 (bs, 1H, NH), 7.29 (d, ³ J_{HH} = 9.1, 2H, 2xCH_{Ar}), 7.24 - 7.18 (m, 5H, 5xCH_{Ar}), 7.15 (d, ³ J_{HH} = 8.9 Hz, 2H, 2xCH_{Ar}), 6.85 (d, ³ J_{HH} = 8.9 Hz, 2H, 2xCH_{Ar}), 6.74 (d, ³ J_{HH} = 9.1, 2H,

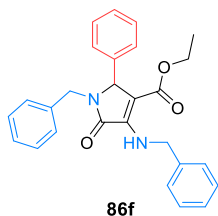
$2\times\text{CH}_{\text{Ar}}$, 5.69 (bs, 1H, CHN), 4.01 (q, $^3J_{\text{HH}} = 7.1$, 2H, CH_2), 3.80 (s, 3H, OCH_3), 3.71 (s, 3H, OCH_3), 1.02 (t, $^3J_{\text{HH}} = 7.1$, 3H, CH_3) ppm.

^{13}C { ^1H } NMR (75 MHz, CDCl_3) δ 164.9 (C=O), 163.9 (C=O), 157.5 (C_{quat}), 157.3 (C_{quat}), 143.4 (C_{quat}), 137.3 (C_{quat}), 131.6 (C_{quat}), 129.7 (C_{quat}), 128.4 ($2\times\text{CH}_{\text{Ar}}$), 128.1 (CH_{Ar}), 127.9 ($2\times\text{CH}_{\text{Ar}}$), 125.1 ($2\times\text{CH}_{\text{Ar}}$), 124.8 ($2\times\text{CH}_{\text{Ar}}$), 114.1 ($2\times\text{CH}_{\text{Ar}}$), 113.8 ($2\times\text{CH}_{\text{Ar}}$), 107.86 (=C), 63.6 (CHN), 60.1 (CH_2), 55.6 (OCH_3), 55.5 (OCH_3), 14.1 (CH_3) ppm.

FTIR ν_{max} 3436 (N-H_{st}), 1714 (C=O_{st} ester), 1705 (C=O_{st} amide), 1672 (C=C_{st}) cm^{-1} .

HRMS (ESI-TOF) m/z calcd. for $\text{C}_{27}\text{H}_{27}\text{N}_2\text{O}_5$ [M+H]⁺ 459.1920, found 459.1918.

Ethyl 1-benzyl-4-(benzylamino)-5-oxo-2-phenyl-2,5-dihydro-1H-pyrrole-3-carboxylate (**86f**).



The general procedure was followed using benzylamine (437 μL , 4 mmol), benzaldehyde (204 μL , 2 mmol) and diethyl acetylenedicarboxylate (320 μL , 2 mmol). The crude residue was purified by flash column chromatography (Hexanes/AcOEt 90:10), affording 494 mg (58%) of **86f** as a white solid.

Mp (Et_2O): 106 - 108 °C. Lit. 104 - 106 °C.^{133b}

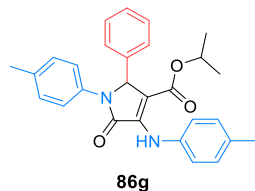
^1H NMR (400 MHz, $\text{DMSO}-d_6$, 60 °C) δ 7.39 - 7.36 (m, 4H, $4\times\text{CH}_{\text{Ar}}$), 7.34 - 7.21 (m, 8H, $7\times\text{CH}_{\text{Ar}}$ + NH), 7.14 - 7.08 (m, 4H, $4\times\text{CH}_{\text{Ar}}$), 5.09 (d, $^3J_{\text{HH}} = 6.8$ Hz, 2H, CH_2 Bn), 4.95 (s, 1H, CHN), 4.86 (d, $^2J_{\text{HH}} = 15.1$ Hz, 1H, CH_AH_B Bn), 3.96 - 3.81 (m, 2H, CH_2 ester), 3.65 (d, $^2J_{\text{HH}} = 15.1$ Hz, 1H, CH_AH_B Bn), 0.91 (t, $^3J_{\text{HH}} = 7.1$ Hz, 3H, CH_3) ppm.

^{13}C { ^1H } NMR (101 MHz, $\text{DMSO}-d_6$, 60 °C) δ 164.6 (C=O), 163.5 (C=O), 145.3 (C_{quat}), 139.8 (C_{quat}), 137.0 (C_{quat}), 136.2 (C_{quat}), 128.0 ($2\times\text{CH}_{\text{Ar}}$), 127.9 ($2\times\text{CH}_{\text{Ar}}$), 127.8 ($2\times\text{CH}_{\text{Ar}}$), 127.5 (CH_{Ar}), 127.3 ($2\times\text{CH}_{\text{Ar}}$), 127.1 ($2\times\text{CH}_{\text{Ar}}$), 126.8 (CH_{Ar}), 126.7, ($2\times\text{CH}_{\text{Ar}}$), 126.4 (CH_{Ar}), 103.4 (=C), 60.8 (CHN), 58.4 (CH_2 ester), 45.3 (CH_2 Bn), 43.4 (CH_2 Bn), 13.3 (CH_3) ppm.

FTIR ν_{max} 3430 (N-H_{st}), 1721 (C=O_{st} ester), 1703 (C=O_{st} amide), 1665 (C=C_{st}) cm^{-1} .

HRMS (ESI-TOF) m/z calcd. for $\text{C}_{27}\text{H}_{27}\text{N}_2\text{O}_3$ [M+H]⁺ 427.2021, found 427.2014.

Iso-propyl 5-oxo-2-phenyl-1-(*p*-tolyl)-4-(*p*-tolylamino)-2,5-dihydro-1H-pyrrole-3-carboxylate (**86g**).



The general procedure was followed using *p*-toluidine (429 mg, 4 mmol), benzaldehyde (204 μL , 2 mmol) and di-*iso*-propyl acetylenedicarboxylate (396 mg, 2 mmol). The crude residue was purified by flash column chromatography (Hexanes/AcOEt 90:10), affording 493 mg (56%) of **86g** as a white solid.

Mp (Et₂O): 156 - 157 °C.

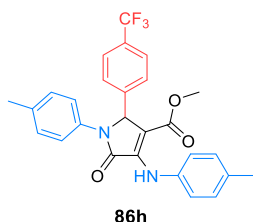
¹H NMR (400 MHz, CDCl₃) δ 8.26 (s, 1H, NH), 7.35 (d, ³J_{HH} = 8.6 Hz, 2H, 2xCH_{Ar}), 7.24-7.21 (m, 3H, 3xCH_{Ar}), 7.20 - 7.17 (m, 2H, 2xCH_{Ar}), 7.11 (d, ³J_{HH} = 8.5 Hz, 2H, 2xCH_{Ar}), 7.09 (d, ³J_{HH} = 8.5 Hz, 2H, 2xCH_{Ar}), 7.02 (d, ³J_{HH} = 8.6 Hz, 2H, 2xCH_{Ar}), 5.74 (s, 1H, CHN), 4.90 (hept, ³J_{HH} = 6.3 Hz, 1H, CHⁱPr), 2.33 (s, 3H, CH₃ tolyl), 2.22 (s, 3H, CH₃ tolyl), 1.18 (d, ³J_{HH} = 6.3 Hz, 3H, CH₃ⁱPr), 0.86 (d, ³J_{HH} = 6.2 Hz, 3H, CH₃ⁱPr) ppm.

¹³C {¹H} NMR (101 MHz, CDCl₃) δ 164.4 (C=O), 164.0 (C=O), 143.0 (C_{quat}), 137.3 (C_{quat}), 136.1 (C_{quat}), 135.5 (C_{quat}), 134.5 (C_{quat}), 134.2 (C_{quat}), 129.5 (2xCH_{Ar}), 129.2 (2xCH_{Ar}), 128.4 (2xCH_{Ar}), 128.1 (CH_{Ar}), 128.0 (2xCH_{Ar}), 123.2 (2xCH_{Ar}), 122.9 (2xCH_{Ar}), 109.4 (=C), 67.8 (CHⁱPr) 63.2 (CHN), 22.1 (CH₃), 21.5 (CH₃), 21.1 (CH₃), 21.0 (CH₃) ppm.

FTIR ν_{max} 3312 (N-H_{st}), 1721 (C=O_{st} ester), 1703 (C=O_{st} amide), 1679 (C=C_{st}) cm⁻¹.

HRMS (ESI-TOF) *m/z* calcd. for C₂₈H₂₉N₂O₃ [M+H]⁺ 441.5508, found 441.5506.

Methyl 5-oxo-1-(*p*-tolyl)-4-(*p*-tolylamino)-2-(4-(trifluoromethyl)phenyl)-2,5-dihydro-1*H*-pyrrole-3-carboxylate (86h).



The general procedure was followed using *p*-toluidine (429 mg, 4 mmol), *p*-(trifluoromethyl)benzaldehyde (273 μL, 2 mmol) and dimethyl acetylenedicarboxylate (246 μL, 2 mmol). The crude residue was purified by flash column chromatography (Hexanes/AcOEt 90:10), affording 701 mg (73%) of **86h** as a white solid.

Mp (Et₂O): 207 - 208 °C.

¹H NMR (400 MHz, CDCl₃) δ 8.16 (bs, 1H, NH), 7.50 (d, ³J_{HH} = 7.9 Hz, 2H, 2xCH_{Ar}), 7.36 (d, ³J_{HH} = 7.9 Hz, 2H, 2xCH_{Ar}), 7.31 (d, ³J_{HH} = 8.5 Hz, 2H, 2xCH_{Ar}), 7.13 (d, ³J_{HH} = 8.4 Hz, 2H, 2xCH_{Ar}), 7.08 (d, ³J_{HH} = 8.4 Hz, 2H, 2xCH_{Ar}), 7.08 - 7.01 (m, 2H, 2xCH_{Ar}), 5.82 (s, 1H, CHN), 3.55 (s, 3H, OCH₃), 2.34 (s, 3H, CH₃ tolyl), 2.24 (s, 3H, CH₃ tolyl) ppm.

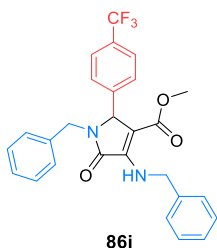
¹³C {¹H} NMR (101 MHz, CDCl₃) δ 164.7 (C=O), 163.8 (C=O), 143.0 (C_{quat}), 141.5 (d, ⁵J_{FC} = 1.6 Hz, C_{quat}), 135.8 (C_{quat}), 135.7 (C_{quat}), 135.0 (C_{quat}), 133.7 (C_{quat}), 130.2 (q, ²J_{FC} = 32.4 Hz, C_{quat}), 129.6 (2xCH_{Ar}), 129.1 (2xCH_{Ar}), 128.0 (2xCH_{Ar}), 125.5 (q, ³J_{FC} = 3.7 Hz, 2xCH_{Ar}), 124.0 (q, ¹J_{FC} = 273.4 Hz, CF₃), 123.5 (2xCH_{Ar}), 122.6 (2xCH_{Ar}), 107.3 (=C), 62.5 (CHN), 51.2 (OCH₃), 21.1 (CH₃ tolyl), 21.0 (CH₃ tolyl) ppm.

¹⁹F NMR (282 MHz, CDCl₃) δ -63.0 ppm.

FTIR ν_{max} 3345 (N-H_{st}), 1714 (C=O_{st} ester), 1701 (C=O_{st} amide), 1685 (C=C_{st}), 1330 (C-F_{st}) cm⁻¹.

HRMS (ESI-TOF) *m/z* calcd. for C₂₇H₂₃F₃N₂O₃ [M+H]⁺ 481.1739, found 481.1756.

Methyl 1-benzyl-4-(benzylamino)-5-oxo-2-(4-(trifluoromethyl)phenyl)-2,5-dihydro-1H-pyrrole-3-carboxylate (86i).



The general procedure was followed using benzylamine (437 μL , 4 mmol), *p*-(trifluoromethyl)benzaldehyde (273 μL , 2 mmol) and dimethyl acetylenedicarboxylate (246 μL , 2 mmol). The crude residue was purified by flash column chromatography (Hexanes/AcOEt 90:10), affording 134 mg (17%) of **86i** as a white solid.

Mp (Et₂O): 128 - 129 °C.

¹H NMR (400 MHz, DMSO-*d*₆, 60 °C) δ 7.62 (d, ³*J*_{HH} = 8.1 Hz, 2H, 2xCH_{Ar}), 7.40 - 7.34 (m, 5H, 5xCH_{Ar}), 7.29 (d, ³*J*_{HH} = 8.1 Hz, 3H, 3xCH_{Ar}), 7.25 (d, ³*J*_{HH} = 7.5 Hz, 2H, 2xCH_{Ar}), 7.05 (dd, ³*J*_{HH} = 7.5, ³*J*_{FH} = 1.8 Hz, 2H, 2xCH_{Ar}), 5.09 (d, ³*J*_{HH} = 6.9 Hz, 2H, CH₂ Bn), 5.08 (s, 1H, CHN), 4.80 (d, ²*J*_{HH} = 15.2 Hz, 1H, CH_ACH_B Bn), 3.79 (d, ²*J*_{HH} = 15.2 Hz, 1H, CH_ACH_B Bn), 3.44 (s, 1H, OCH₃) ppm.

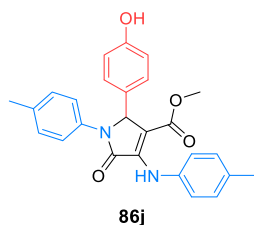
¹³C {¹H} NMR (101 MHz, DMSO-*d*₆, 60 °C) δ 164.6 (C=O), 163.6 (C=O), 145.4 (C_{quat}), 142.0 (C_{quat}), 139.7 (C_{quat}), 136.0 (C_{quat}), 128.35 (d, ²*J*_{FH} = 31.5 Hz, C_{quat}), 128.0 (4xCH_{Ar}), 127.9 (2xCH_{Ar}), 127.3 (2xCH_{Ar}), 126.8 (CH_{Ar}), 126.7 (2xCH_{Ar}), 126.4 (CH_{Ar}), 124.8 (q, ³*J*_{FH} = 3.9 Hz, 2xCH_{Ar}), 123.7 (q, ¹*J*_{FH} = 272.1 Hz, CF₃), 102.5 (=C), 60.3 (CHN), 49.9 (OCH₃), 45.3 (CH₂), 43.8 (CH₂) ppm.

¹⁹F NMR (282 MHz, CDCl₃) δ -63.0 ppm.

FTIR ν_{max} 3331 (N-H_{st}), 1713 (C=O_{st} ester), 1698 (C=O_{st} amide), 1682 (C=C_{st}), 1321 (C-F_{st}) cm⁻¹.

HRMS (ESI-TOF) *m/z* calcd. for C₂₇H₂₃F₃N₂O₃ [M+H]⁺ 481.1739, found 481.1714.

Methyl 2-(4-hydroxyphenyl)-5-oxo-1-(*p*-tolyl)-4-(*p*-tolylamino)-2,5-dihydro-1H-pyrrole-3-carboxylate (86j).



The general procedure was followed using *p*-toluidine (429 mg, 4 mmol), *p*-hydroxybenzaldehyde (244 mg, 2 mmol) and dimethyl acetylenedicarboxylate (246 μL , 2 mmol). The crude residue was purified by flash column chromatography (Hexanes/AcOEt 1:1), affording 205 mg (24%) of **86j** as a yellow solid.

Mp (MeOH): 253 - 255 °C (dec.).

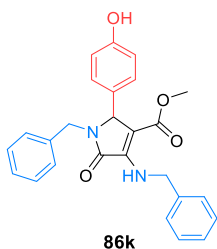
¹H NMR (400 MHz, CDCl₃) δ 8.08 (bs, 1H, NH), 7.29 (d, ³*J*_{HH} = 8.4 Hz, 2H, 2xCH_{Ar}), 7.13 - 7.01 (m, 8H, 8xCH_{Ar}), 6.67 (d, ³*J*_{HH} = 8.4 Hz, 2H, 2xCH_{Ar}), 5.70 (s, 1H, CHN), 4.77 (s, 1H, OH), 3.54 (s, 3H, OCH₃), 2.33 (s, 3H, CH₃ tolyl), 2.23 (s, 3H, CH₃ tolyl) ppm.

^{13}C { ^1H } NMR (101 MHz, CDCl_3) δ 165.0 (C=O), 163.9 (C=O), 155.3 (C_{quat}), 142.6 (C_{quat}), 136.1 (C_{quat}), 135.6 (C_{quat}), 134.7 (C_{quat}), 134.0 (C_{quat}), 129.5 ($2\times\text{CH}_{\text{Ar}}$), 129.2 (C_{quat}), 129.2 ($2\times\text{CH}_{\text{Ar}}$), 129.1 ($2\times\text{CH}_{\text{Ar}}$), 123.3 ($2\times\text{CH}_{\text{Ar}}$), 123.0 ($2\times\text{CH}_{\text{Ar}}$), 115.50 ($2\times\text{CH}_{\text{Ar}}$), 108.5 (=C), 62.8 (CHN), 51.2 (OCH_3), 21.1 (CH_3 tolyl), 21.1 (CH_3 tolyl) ppm.

FTIR ν_{max} 3407 (O-H_{st}), 3259 (N-H_{st}), 1718 (C=O_{st} ester), 1698 (C=O_{st} amide), 1672 (C=C_{st}) cm^{-1} .

HRMS (ESI-TOF) m/z calcd. for $\text{C}_{26}\text{H}_{25}\text{N}_2\text{O}_4$ $[\text{M}+\text{H}]^+$ 429.1806, found 429.1833.

Methyl 1-benzyl-4-(benzylamino)-2-(4-hydroxyphenyl)-5-oxo-2,5-dihydro-1H-pyrrole-3-carboxylate (86k).



The general procedure was followed using benzylamine (437 μL , 4 mmol), *p*-hydroxybenzaldehyde (244 mg, 2 mmol) and dimethyl acetylenedicarboxylate (246 μL , 2 mmol). The crude residue was purified by flash column chromatography (Hexanes/AcOEt 1:1), affording 625 mg (73%) of **86k** as a white solid.

Mp (MeOH): 216 - 217 $^{\circ}\text{C}$.

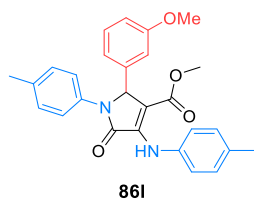
^1H NMR (400 MHz, $\text{DMSO}-d_6$, 60 $^{\circ}\text{C}$) δ 9.13 (s, 1H, NH), 7.35 - 7.32 (m, 4H), 7.31 - 7.21 (m, 4H, $4\times\text{CH}_{\text{Ar}}$), 7.06 (d, $^3J_{\text{HH}} = 6.5$ Hz, 2H, $2\times\text{CH}_{\text{Ar}}$), 6.85 (d, $^3J_{\text{HH}} = 8.6$ Hz, 2H, $2\times\text{CH}_{\text{Ar}}$), 6.71 (d, $^3J_{\text{HH}} = 8.6$ Hz, 2H, $2\times\text{CH}_{\text{Ar}}$), 5.05 (d, $^3J_{\text{HH}} = 6.8$ Hz, 2H, CH_2 Bn), 4.83 (bs, 1H, OH), 4.81 (d, $^2J_{\text{HH}} = 15.2$ Hz, 1H, CH_ACH_B Bn), 3.61 (d, $^2J_{\text{HH}} = 15.2$ Hz, 1H, CH_ACH_B Bn), 3.43 (s, 3H, OCH_3) ppm.

^{13}C { ^1H } NMR (101 MHz, $\text{DMSO}-d_6$, 60 $^{\circ}\text{C}$) δ 164.4 (C=O), 164.0 (C=O), 156.8 (C_{quat}), 145.2 (C_{quat}), 139.8 (C_{quat}), 136.4 (C_{quat}), 128.1 ($4\times\text{CH}_{\text{Ar}}$), 127.9 ($2\times\text{CH}_{\text{Ar}}$), 127.2 ($2\times\text{CH}_{\text{Ar}}$), 126.8 (CH_{Ar}), 126.8 (C_{quat}), 126.7 ($2\times\text{CH}_{\text{Ar}}$), 126.4 (CH_{Ar}), 115.0 ($2\times\text{CH}_{\text{Ar}}$), 103.4 (=C), 60.2 (CHN), 49.9 (OCH_3), 45.3 (CH_2), 43.2 (CH_2) ppm.

FTIR ν_{max} 3430 (O-H_{st}), 3284 (N-H_{st}), 1715 (C=O_{st} ester), 1698 (C=O_{st} amide), 1669 (C=C_{st}) cm^{-1} .

HRMS (ESI-TOF) m/z calcd. for $\text{C}_{26}\text{H}_{25}\text{N}_2\text{O}_4$ $[\text{M}+\text{H}]^+$ 429.1814, found 429.1833.

Methyl 2-(3-methoxyphenyl)-5-oxo-1-(*p*-tolyl)-4-(*p*-tolylamino)-2,5-dihydro-1H-pyrrole-3-carboxylate (86l).



The general procedure was followed using *p*-toluidine (429 mg, 4 mmol), *m*-anisaldehyde (243 μL , 2 mmol) and dimethyl acetylenedicarboxylate (246 μL , 2 mmol). The crude residue was purified by flash column

chromatography (Hexanes/AcOEt 80:20), affording 688 mg (78%) of **86l** as a yellow solid.

Mp (MeOH): 171 - 172 °C.

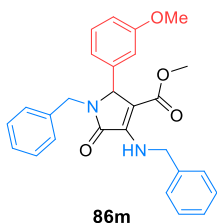
$^1\text{H NMR}$ (400 MHz, CDCl_3) δ 8.15 (bs, 1H, NH), 7.33 (d, $^3J_{\text{HH}} = 8.5$ Hz, 2H, $2\times\text{CH}_{\text{Ar}}$), 7.19 - 7.01 (m, 7H, $7\times\text{CH}_{\text{Ar}}$), 6.85 (m, 1H, CH_{Ar}), 6.76 (t, $^3J_{\text{HH}} = 2.1$ Hz, 1H, CH_{Ar}), 6.72 (m, 1H, CH_{Ar}), 5.73 (s, 1H, CHN), 3.73 (s, 3H, OCH_3), 3.56 (s, 3H, OCH_3), 2.33 (s, 3H, CH_3 tolyl), 2.23 (s, 3H, CH_3 tolyl) ppm.

$^{13}\text{C}\{^1\text{H}\}$ NMR (101 MHz, CDCl_3) δ 164.8 (C=O), 164.0 (C=O), 159.6 (C_{quat}), 138.7 (C_{quat}), 135.9 (C_{quat}), 135.4 (C_{quat}), 134.6 (C_{quat}), 134.0 (C_{quat}), 129.4 ($2\times\text{CH}_{\text{Ar}}$), 129.3 (CH_{Ar}), 129.0 ($2\times\text{CH}_{\text{Ar}}$), 123.2 ($2\times\text{CH}_{\text{Ar}}$), 122.7 ($2\times\text{CH}_{\text{Ar}}$), 120.1 (CH_{Ar}), 113.4 (CH_{Ar}), 113.3 (CH_{Ar}), 113.2 (=C), 108.2 (C_{quat}), 63.0 (CHN), 55.2 (OCH_3), 51.1 (OCH_3), 21.0 (CH_3 tolyl), 20.9 (CH_3 tolyl) ppm.

FTIR ν_{max} 3382 (N-H_{st}), 1714 (C=O_{st} ester), 1694 (C=O_{st} amide), 1655 (C=C_{st}) cm^{-1} .

HRMS (ESI-TOF) m/z calcd. for $\text{C}_{27}\text{H}_{27}\text{N}_2\text{O}_4$ $[\text{M}+\text{H}]^+$ 443.1971, found 443.1981.

Methyl 1-benzyl-4-(benzylamino)-2-(3-methoxyphenyl)-5-oxo-2,5-dihydro-1H-pyrrole-3-carboxylate (86m).



The general procedure was followed using benzylamine (437 μL , 4 mmol), *m*-anisaldehyde (243 μL , 2 mmol) and dimethyl acetylenedicarboxylate (246 μL , 2 mmol). The crude residue was purified by flash column chromatography (Hexanes/AcOEt 90:10), affording 327 mg (37%) of **83m** as a white solid.

Mp (MeOH): 111 - 112 °C.

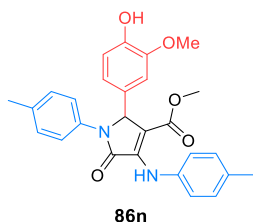
$^1\text{H NMR}$ (400 MHz, $\text{DMSO}-d_6$, 60 °C) δ 7.38 - 7.34 (m, 4H, $4\times\text{CH}_{\text{Ar}}$), 7.36 - 7.19 (m, 6H, $5\times\text{CH}_{\text{Ar}}$ + NH), 7.10 - 7.06 (m, 2H, $2\times\text{CH}_{\text{Ar}}$), 6.86 (ddd, $^3J_{\text{HH}} = 8.2$ Hz, $^4J_{\text{HH}} = 2.5$, 0.9 Hz, 1H, CH_{Ar}), 6.66 (dt, $^3J_{\text{HH}} = 7.7$, $^4J_{\text{HH}} = 1.2$ Hz, 1H, CH_{Ar}), 6.60 (t, $^4J_{\text{HH}} = 2.0$ Hz, 1H, CH_{Ar}), 5.11 (dd, $^2J_{\text{HH}} = 15.0$, $^3J_{\text{HH}} = 6.8$ Hz, 1H, CH_AH_B Bn), 5.07 (dd, $^2J_{\text{HH}} = 15.0$, $^3J_{\text{HH}} = 6.8$ Hz, 1H, CH_AH_B Bn), 4.94 (s, 1H, CHN), 4.83 (d, $^2J_{\text{HH}} = 15.1$ Hz, 1H, CH_ACH_B Bn), 3.72 (s, 3H, OCH_3 Ar), 3.69 (d, $^2J_{\text{HH}} = 15.1$ Hz, 1H, CH_ACH_B Bn), 3.45 (s, 3H, OCH_3 ester) ppm.

$^{13}\text{C}\{^1\text{H}\}$ NMR (101 MHz, $\text{DMSO}-d_6$, 60 °C) δ 164.5 (C=O), 163.9 (C=O), 159.1 (C_{quat}), 145.3 (C_{quat}), 139.8 (C_{quat}), 138.6 (C_{quat}), 136.2 (C_{quat}), 129.1 (CH_{Ar}), 128.0 ($2\times\text{CH}_{\text{Ar}}$), 127.9 ($2\times\text{CH}_{\text{Ar}}$), 127.3 ($2\times\text{CH}_{\text{Ar}}$), 126.8 (CH_{Ar}), 126.7 ($2\times\text{CH}_{\text{Ar}}$), 126.4 (CH_{Ar}), 119.2 (CH_{Ar}), 113.2 (CH_{Ar}), 112.9 (CH_{Ar}), 103.0 (=C), 60.7 (CHN), 54.7 (OCH_3 Ar), 49.9 (OCH_3 ester), 45.2 (CH_2), 43.5 (CH_2) ppm.

FTIR ν_{max} 3338 (N-H_{st}), 1745 (C=O_{st} ester), 1701 (C=O_{st} amide), 1672 (C=C_{st}) cm^{-1} .

HRMS (ESI-TOF) m/z calcd. for $\text{C}_{27}\text{H}_{27}\text{N}_2\text{O}_4$ $[\text{M}+\text{H}]^+$ 443.1971, found 443.1942.

Methyl 2-(4-hydroxy-3-methoxyphenyl)-5-oxo-1-(*p*-tolyl)-4-(*p*-tolylamino)-2,5-dihydro-1*H*-pyrrole-3-carboxylate (86n**).**



The general procedure was followed using *p*-toluidine (429 mg, 4 mmol), vanillin (304 mg, 2 mmol) and dimethyl acetylenedicarboxylate (246 μ L, 2 mmol). The crude residue was purified by flash column chromatography (Hexanes/AcOEt 1:1), affording 394 mg (43%) of **86n** as a yellow solid.

Mp (MeOH): 160 - 162 $^{\circ}$ C.

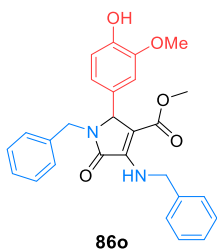
$^1\text{H NMR}$ (400 MHz, CDCl_3) δ 8.14 (bs, 1H, NH), 7.32 (d, $^3J_{\text{HH}} = 8.4$ Hz, 2H, $2\times\text{CH}_{\text{Ar}}$), 7.12 (d, $^3J_{\text{HH}} = 8.5$ Hz, 2H, $2\times\text{CH}_{\text{Ar}}$), 7.08 (d, $^3J_{\text{HH}} = 8.5$ Hz, 2H, $2\times\text{CH}_{\text{Ar}}$), 7.05 (d, $^3J_{\text{HH}} = 8.4$ Hz, 2H, $2\times\text{CH}_{\text{Ar}}$), 6.81 (dd, $^3J_{\text{HH}} = 8.2$ Hz, $^4J_{\text{HH}} = 1.9$ Hz, 1H, CH_{Ar}), 6.77 (d, $^3J_{\text{HH}} = 8.2$ Hz, 1H, CH_{Ar}), 6.62 (d, $^4J_{\text{HH}} = 1.9$ Hz, 1H, CH_{Ar}), 5.71 (s, 1H, CHN), 5.61 (s, 1H, OH), 3.77 (s, 3H, OCH_3 Ar), 3.56 (s, 3H, OCH_3 ester), 2.34 (s, 3H, CH_3 tolyl), 2.24 (s, 3H, CH_3 tolyl) ppm.

$^{13}\text{C}\{^1\text{H}\}$ NMR (101 MHz, CDCl_3) δ 165.0 (C=O), 163.9 (C=O), 146.6 (C_{quat}), 145.4 (C_{quat}), 142.5 (C_{quat}), 136.0 (C_{quat}), 135.6 (C_{quat}), 134.6 (C_{quat}), 134.0 (C_{quat}), 129.5 ($2\times\text{CH}_{\text{Ar}}$), 129.1 ($2\times\text{CH}_{\text{Ar}}$), 128.6 (C_{quat}), 123.1 ($2\times\text{CH}_{\text{Ar}}$), 123.0 ($2\times\text{CH}_{\text{Ar}}$), 121.5 (CH_{Ar}), 114.2 (CH_{Ar}), 109.3 (CH_{Ar}), 108.5 (=C), 63.2 (CHN), 56.0 (OCH_3 Ar), 51.2 (OCH_3 ester), 21.1 (CH_3 tolyl), 21.0 (CH_3 tolyl) ppm.

FTIR ν_{max} 3404 (O-H_{st}), 3281 (N-H_{st}), 1733 (C=O_{st} ester), 1694 (C=O_{st} amide), 1637 (C=C_{st}) cm^{-1} .

HRMS (ESI-TOF) m/z calcd. for $\text{C}_{27}\text{H}_{27}\text{N}_2\text{O}_5$ $[\text{M}+\text{H}]^+$ 459.1920, found 459.1930.

Methyl 1-benzyl-4-(benzylamino)-2-(4-hydroxy-3-methoxyphenyl)-5-oxo-2,5-dihydro-1*H*-pyrrole-3-carboxylate (86o**).**



The general procedure was followed using benzylamine (437 μ L, 4 mmol), vanillin (304 mg, 2 mmol) and dimethyl acetylenedicarboxylate (246 μ L, 2 mmol). The crude residue was purified by flash column chromatography (Hexanes/AcOEt 1:1), affording 513 mg (56%) of **86o** as a white solid.

Mp (MeOH): 154 - 156 $^{\circ}$ C.

$^1\text{H NMR}$ (400 MHz, $\text{DMSO}-d_6$, 60 $^{\circ}$ C) δ 8.64 (s, 1H, NH), 7.40 - 7.19 (m, 10H, $10\times\text{CH}_{\text{Ar}}$), 7.09 (d, $^3J_{\text{HH}} = 7.5$ Hz, 1H, CH_{Ar}), 6.76 (d, $^3J_{\text{HH}} = 7.5$ Hz, 1H, CH_{Ar}), 6.54 (s, 1H, CH_{Ar}), 6.52 (bs, 1H, OH), 5.09 (m, 2H, CH_2 Bn), 4.88 (s, 1H, CHN), 4.83 (d, $^2J_{\text{HH}} = 15.1$ Hz, 1H, CH_ACH_B Bn), 3.74 (d, $^2J_{\text{HH}} = 15.1$ Hz, 1H, CH_ACH_B Bn), 3.69 (s, 3H, OCH_3 Ar), 3.46 (s, 3H, OCH_3 ester) ppm.

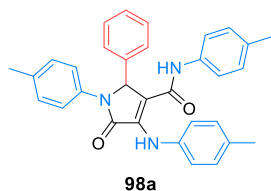
$^{13}\text{C}\{^1\text{H}\}$ NMR (101 MHz, $\text{DMSO}-d_6$, 60 $^{\circ}$ C) δ 164.3 (C=O), 163.9 (C=O), 147.2 (C_{quat}), 146.2 (C_{quat}), 145.1 (C_{quat}), 139.8 (C_{quat}), 136.3 (C_{quat}), 127.9 ($2\times\text{CH}_{\text{Ar}}$), 127.8 ($2\times\text{CH}_{\text{Ar}}$), 127.4 (C_{quat}), 127.2 ($2\times\text{CH}_{\text{Ar}}$),

126.6 (CH_{Ar}), 126.5 (2xCH_{Ar}), 126.3 (CH_{Ar}), 119.9 (CH_{Ar}), 115.2 (CH_{Ar}), 111.5 (CH_{Ar}), 103.2 (=C), 60.5 (CHN), 55.5 (OCH₃ Ar), 49.7 (OCH₃ ester), 45.1 (CH₂ Bn), 43.2 (CH₂ Bn) ppm.

FTIR ν_{\max} 3512 (O-H_{st}), 3347 (N-H_{st}), 1721 (C=O_{st} ester), 1688 (C=O_{st} amide), 1672 (C=C_{st}) cm⁻¹.

HRMS (ESI-TOF) m/z calcd. for C₂₇H₂₆N₂O₅ [M+H]⁺ 458.1842, found 458.1857.

5-Oxo-2-phenyl-N,1-di-*p*-tolyl-4-(*p*-tolylamino)-2,5-dihydro-1*H*-pyrrole-3-carboxamide (**98a**).



affording 214 mg (22%) of **98a** as a white solid.

The general procedure was followed using *p*-toluidine (429 mg, 4 mmol), benzaldehyde (204 μ L, 2 mmol) and di-*iso*-propyl acetylenedicarboxylate (396 mg, 2 mmol). The crude residue was purified by flash column chromatography (Hexanes/AcOEt 80:20), affording 214

Mp (Et₂O): 226 - 228 °C (dec.).

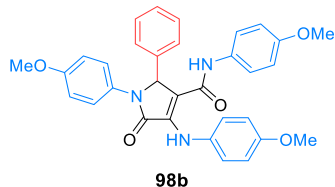
¹H NMR (300 MHz, CDCl₃) δ 8.31 (bs, 1H, NH), 7.38 - 7.28 (m, 6H, 6xCH_{Ar}), 7.11 - 7.04 (m, 7H, 7xCH_{Ar}), 6.96 (d, ³J_{HH} = 8.5 Hz, 2H, 2xCH_{Ar}), 6.84 (d, ³J_{HH} = 8.5 Hz, 2H, 2xCH_{Ar}), 6.63 (bs, 1H, NH), 5.85 (s, 1H, CHN), 2.28 (s, 3H, CH₃), 2.25 (s, 3H, CH₃), 2.24 (s, 3H, CH₃) ppm.

¹³C {¹H} NMR (75 MHz, CDCl₃) δ 164.7 (C=O), 162.1 (C=O), 139.1 (C_{quat}), 136.6 (C_{quat}), 136.1 (C_{quat}), 135.8 (C_{quat}), 134.8 (C_{quat}), 134.6 (C_{quat}), 133.9 (C_{quat}), 133.8 (C_{quat}), 129.7 (4xCH_{Ar}), 129.5 (2xCH_{Ar}), 129.3 (2xCH_{Ar}), 129.2 (CH_{Ar}), 128.0 (2xCH_{Ar}), 123.3 (2xCH_{Ar}), 122.5 (2xCH_{Ar}), 119.8 (2xCH_{Ar}), 112.4 (=C), 63.8 (CHN), 21.1 (CH₃), 21.0 (CH₃), 20.9 (CH₃) ppm.

FTIR ν_{\max} 3309 (N-H_{st}), 3251 (N-H_{st}), 1685 (C=O_{st}), 1632 (C=C_{st}) cm⁻¹.

HRMS (ESI-TOF) m/z calcd. for C₃₂H₃₀N₃O₂ [M+H]⁺ 488.2337, found 488.2327.

N,1-bis(4-methoxyphenyl)-4-((4-methoxyphenyl)amino)-5-oxo-2-phenyl-2,5-dihydro-1*H*-pyrrole-3-carboxamide (**98b**).



affording 139 mg (13%) of **98b** as a white solid.

The general procedure was followed using *p*-anisidine (492 mg, 4 mmol), benzaldehyde (204 μ L, 2 mmol) and di-*iso*-propyl acetylenedicarboxylate (396 mg, 2 mmol). The crude residue was purified by flash column chromatography (Hexanes /AcOEt 70:30),

Mp (Et₂O): 228 - 229 °C.

¹H NMR (400 MHz, CDCl₃) δ 8.46 (bs, 1H, NH), 7.37 - 7.28 (m, 5H, 5xCH_{Ar}), 7.26 - 7.22 (m, 2H, 2xCH_{Ar}), 7.17 (d, ³J_{HH} = 8.9 Hz, 2H, 2xCH_{Ar}), 6.90 (d, ³J_{HH} = 9.1 Hz, 2H, 2xCH_{Ar}), 6.82 (d, ³J_{HH} = 8.9 Hz, 2H, 2xCH_{Ar}),

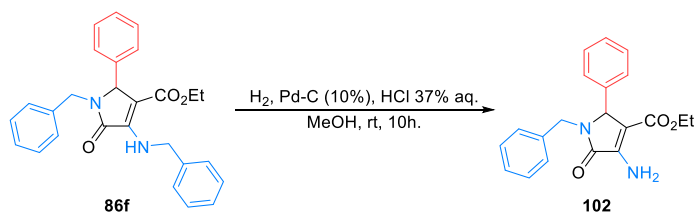
6.78 (d, $^3J_{HH} = 9.1$ Hz, 2H, 2xCH_{Ar}), 6.71 (d, $^3J_{HH} = 9.1$ Hz, 2H, 2xCH_{Ar}), 6.56 (bs, 1H, NH), 5.76 (s, 1H, CHN), 3.74 (s, 3H, OCH₃), 3.73 (s, 3H, OCH₃), 3.72 (s, 3H, OCH₃) ppm.

¹³C {¹H} NMR (101 MHz, CDCl₃) δ 164.6 (C=O), 162.4 (C=O), 157.8 (C_{quat}), 157.2 (C_{quat}), 156.5 (C_{quat}), 140.2 (C_{quat}), 136.6 (C_{quat}), 131.6 (C_{quat}), 130.5 (C_{quat}), 129.5 (2xCH_{Ar}), 129.3 (CH_{Ar}), 129.3 (C_{quat}), 128.0 (2xCH_{Ar}), 125.4 (2xCH_{Ar}), 124.5 (2xCH_{Ar}), 121.5 (2xCH_{Ar}), 114.3 (2xCH_{Ar}), 114.2 (2xCH_{Ar}), 114.1 (2xCH_{Ar}), 110.9 (=C), 64.1 (CHN), 55.6 (OCH₃), 55.6 (OCH₃), 55.5 (OCH₃) ppm.

FTIR ν_{\max} 3344 (N-H_{st}), 3286 (N-H_{st}), 1682 (C=O_{st}), 1662 (C=O_{st}), 1634 (C=C_{st}) cm⁻¹.

HRMS (ESI-TOF) m/z calcd. for C₃₂H₃₀N₃O₅ [M+H]⁺ 536.2185, found 536.2177.

Debenzylation of γ -lactam **86f**. Synthesis of ethyl 4-amino-1-benzyl-5-oxo-2-phenyl-2,5-dihydro-1*H*-pyrrole-3-carboxylate **102**.



A mixture of γ -lactam **86f** (21.3 mg, 0.5 mmol), 10% palladium on carbon (53.2 mg, 0.05 mmol), and 37% HCl (0.05 mL, 0.5 mmol) was stirred in methanol (30 mL) at room temperature for 10 hours under hydrogen pressure (80 psi). The reaction mixture was filtered, and the mother liquor was neutralized with an aqueous saturated solution of NaHCO_3 and extracted with dichloromethane (3 \times 15 mL). The combined organic layers were dried over anhydrous MgSO_4 , filtered and concentrated under reduced pressure. The crude residue was purified by crystallization from a mixture of Et_2O /pentane (1:2) to afford 163 mg (99%) of **102** as a white solid.

Mp (Et_2O): 139 - 142 $^\circ\text{C}$.

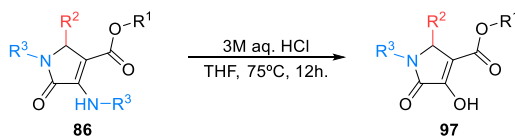
^1H NMR (300 MHz, CDCl_3) δ 7.37 - 7.27 (m, 6H, 6 $\times\text{CH}_{\text{Ar}}$), 7.18 - 7.05 (m, 4H, 4 $\times\text{CH}_{\text{Ar}}$), 5.74 (bs, 2H, NH_2), 5.13 (d, $^2J_{\text{HH}} = 14.8$ Hz, 1H, $\text{CH}_{\text{A}}\text{H}_{\text{B}}$ Bn), 4.89 (s, 1H, CHN), 4.10 - 3.87 (m, 2H, CH_2 ester), 3.57 (d, $^2J_{\text{HH}} = 14.8$ Hz, 1H, $\text{CH}_{\text{A}}\text{H}_{\text{B}}$ Bn), 1.05 (t, $^3J_{\text{HH}} = 6.9$ Hz, 3H, CH_3) ppm.

^{13}C $\{^1\text{H}\}$ NMR (75 MHz, CDCl_3) δ 165.5 (C=O), 165.0 (C=O), 145.9 (C_{quat}), 136.6 (C_{quat}), 136.57 (C_{quat}), 128.9 (2 $\times\text{CH}_{\text{Ar}}$), 128.7 (2 $\times\text{CH}_{\text{Ar}}$), 128.5 (2 $\times\text{CH}_{\text{Ar}}$), 128.4 (2 $\times\text{CH}_{\text{Ar}}$), 128.0 (CH_{Ar}), 127.9 (CH_{Ar}), 104.8 (=C), 61.5 (CHN), 59.8 (CH_2 ester), 44.2 (CH_2 Bn), 14.2 (CH_3) ppm.

FTIR ν_{max} 3450 and 3319 (N-H_{st}), 1715 (C=O_{st} ester), 1695 (C=O_{st} amide), 1654 (C=C_{st}) cm^{-1} .

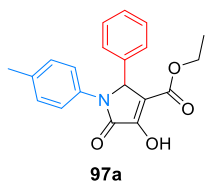
HRMS (ESI-TOF) m/z calcd. for $\text{C}_{20}\text{H}_{21}\text{N}_2\text{O}_3$ $[\text{M}+\text{H}]^+$ 337.1552, found 337.1547.

General procedure for the hydrolysis of the enamine moiety. Synthesis of 3-hydroxy-1,5-dihydro-2H-pyrrol-2-ones **97**.



To a 1:1 mixture of an aqueous solution of HCl 3M and THF (10 mL), γ -lactam **86** (0.5 mmol) was added. The mixture was stirred at 75 °C (heating plate) and monitored by TLC until the disappearance of the starting material (12 hours). The mixture was then concentrated under reduced pressure and the crude residue was diluted with AcOEt (10 mL), washed with a 3 M aqueous solution of NaOH (2×5 mL) and H₂O (2×5 mL). The organic layer was dried over anhydrous MgSO₄, and concentrated under reduced pressure. The crude residue was purified by crystallization from a mixture of Et₂O/pentane (1:2) to afford pure enol-derived γ -lactams **97**.

Ethyl 4-hydroxy-5-oxo-2-phenyl-1-(*p*-tolyl)-2,5-dihydro-1H-pyrrole-3-carboxylate (**97a**).



The general procedure was followed using enamine-derived γ -lactam **86d** to afford 160 mg (95%) of **98a** as a white solid.

Mp (Et₂O/pentane): 170 - 172 °C.

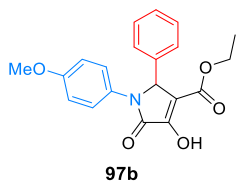
¹H NMR (300 MHz, CDCl₃) δ 9.19 (bs, 1H, OH), 7.38 (d, ³J_{HH} = 8.2 Hz, 2H, 2xCH_{Ar}), 7.32-7.25 (m, 5H, 5xCH_{Ar}), 7.09 (d, ³J_{HH} = 8.2 Hz, 2H, 2xCH_{Ar}), 5.74 (s, 1H, CHN), 4.20 (q, ³J_{HH} = 7.1 Hz, 2H, CH₂), 2.26 (s, 3H, CH₃ tolyl), 1.20 (t, ³J_{HH} = 7.1 Hz, 3H, CH₃ ester) ppm.

¹³C {¹H} NMR (75 MHz, CDCl₃) δ 165.0 (C=O), 162.9 (C=O), 156.4 (C_{quat}), 135.7 (C_{quat}), 135.3 (C_{quat}), 133.7 (C_{quat}), 129.6 (2xCH_{Ar}), 128.6 (2xCH_{Ar}), 128.5 (CH_{Ar}), 127.6 (2xCH_{Ar}), 122.4 (2xCH_{Ar}), 113.1 (=C), 61.8 (CHN), 61.2 (CH₂), 20.9 (CH₃ tolyl), 14.0 (CH₃) ppm.

FTIR ν_{\max} 3425 (O-H_{st}), 1704 (C=O_{st} ester), 1675 (C=O_{st} amide), 1643 (C=C_{st}) cm⁻¹.

HRMS (ESI-TOF) m/z calcd. for C₂₀H₂₀NO₄ [M+H]⁺ 338.1392, found 338.1393.

Ethyl 4-hydroxy-1-(4-methoxyphenyl)-5-oxo-2-phenyl-2,5-dihydro-1H-pyrrole-3-carboxylate (**97b**).



The general procedure was followed using enamine-derived γ -lactam **86e** to afford 143 mg (81%) of **97b** as a white solid.

Mp (Et₂O/pentane): 182 - 184 °C (dec.).

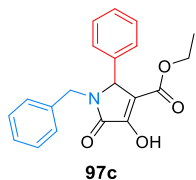
¹H NMR (300 MHz, CDCl₃) δ 9.05 (bs, 1H, OH), 7.30 (d, ³J_{HH} = 8.9 Hz, 2H, 2xCH_{Ar}), 7.24 - 7.16 (m, 5H, 5xCH_{Ar}), 6.79 (d, ³J_{HH} = 8.8 Hz, 2H, 2xCH_{Ar}), 5.63 (s, 1H, CHN), 4.17 (q, ³J_{HH} = 7.1 Hz, 2H, CH₂), 3.72 (s, 3H, OCH₃), 1.16 (t, ³J_{HH} = 7.1 Hz, 3H, CH₃ ester) ppm.

¹³C {¹H} NMR (75 MHz, CDCl₃) δ 165.4 (C=O), 162.8 (C=O), 157.7 (C_{quat}), 157.1 (C_{quat}), 135.3 (C_{quat}), 129.3 (C_{quat}), 128.7 (2xCH_{Ar}), 127.7 (2xCH_{Ar}), 124.5 (2xCH_{Ar}), 120.5 (CH_{Ar}), 114.4 (2xCH_{Ar}), 113.0 (=C), 62.2 (CHN), 61.3 (CH₂), 55.5 (OCH₃), 14.1 (CH₃ ester) ppm.

FTIR ν_{max} 3431 (O-H_{st}), 1711 (C=O_{st} ester), 1697 (C=O_{st} amide), 1677 (C=C_{st}) cm⁻¹.

HRMS (ESI-TOF) *m/z* calcd. for C₂₀H₂₀NO₅ [M+H]⁺ 354.1346, found 354.1338.

Ethyl 1-benzyl-4-hydroxy-5-oxo-2-phenyl-2,5-dihydro-1H-pyrrole-3-carboxylate (**97c**).



The general procedure was followed using enamine-derived γ-lactam **86f** to afford 157 mg (94%) of **97c** as a white solid.

Mp (Et₂O/pentane): 178 - 179 °C (dec.). Lit. 190 - 192 °C.²⁴²

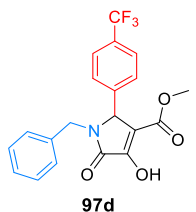
¹H NMR (300 MHz, CDCl₃) δ 9.11 (bs, 1H, OH), 7.39 - 7.33 (m, 3H, 3xCH_{Ar}), 7.32 - 7.27 (m, 3H, 3xCH_{Ar}), 7.15 - 7.08 (m, 4H, 4xCH_{Ar}), 5.20 (d, ²J_{HH} = 14.8 Hz, 1H, CH_ACH_B Bn), 4.88 (s, 1H, CHN), 4.08 (q, ³J_{HH} = 7.2, 2H, CH₂ ester), 3.55 (d, ²J_{HH} = 14.8 Hz, 1H, CH_ACH_B Bn), 1.06 (t, ³J_{HH} = 7.2 Hz, 3H, CH₃ ester) ppm.

¹³C {¹H} NMR (75 MHz, CDCl₃) δ 165.6 (C=O), 163.6 (C=O), 157.9 (C_{quat}), 136.4 (C_{quat}), 134.7 (C_{quat}), 129.0 (4xCH_{Ar}), 128.7 (2xCH_{Ar}), 128.0 (2xCH_{Ar}), 128.0 (2xCH_{Ar}), 113.4 (=C), 61.1 (CH₂ Ester), 59.7 (CHN), 44.1 (CH₂ Bn), 14.0 (CH₃) ppm.

FTIR ν_{max} 3450 (O-H_{st}), 1735 (C=O_{st} ester), 1704 (C=O_{st} amide), 1675 (C=C_{st}) cm⁻¹.

HRMS (ESI-TOF) *m/z* calcd. for C₂₀H₂₀NO₄ [M+H]⁺ 338.1392, found 338.1406.

Methyl 1-benzyl-4-hydroxy-5-oxo-2-(4-(trifluoromethyl) phenyl) -2,5-dihydro-1H-pyrrole-3-carboxylate (**97d**).



The general procedure was followed using enamine-derived γ-lactam **86i** to afford 174 mg (89%) of **97d** as a white solid.

Mp (Et₂O/pentane): 207 - 208 °C (dec.).

¹H NMR (400 MHz, CDCl₃) δ 9.07 (bs, 1H, OH), 7.62 (d, ³J_{HH} = 8.6 Hz, 2H, 2xCH_{Ar}), 7.34 - 7.27 (m, 3H, 3xCH_{Ar}), 7.23 (d, ³J_{HH} = 7.4 Hz, 2H, 2xCH_{Ar}), 7.13 - 7.03 (m, 2H, 2xCH_{Ar}), 5.19 (d, ²J_{HH} =

²⁴² Castellano, T. G.; Neo, A. G.; Marcaccini, S.; Marcos, C. F. *Org. Lett.* **2012**, *14*, 6218-6221.

15.0 Hz, 1H, CH_ACH_B Bn), 4.94 (s, 1H, CHN), 3.64 (s, 3H, OCH_3), 3.56 (d, $^2J_{HH} = 15.0$ Hz, 1H, CH_ACH_B Bn) ppm.

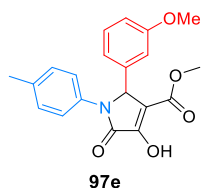
^{13}C { ^1H } NMR (101 MHz, CDCl_3) δ 165.3 (C=O), 163.6 (C=O), 157.6 (C_{quat}), 139.0 (C_{quat}), 135.9 (C_{quat}), 131.3 (q, $^2J_{FH} = 31.5$ Hz, C_{quat}), 129.1 (2x CH_{Ar}), 128.6 (2x CH_{Ar}), 128.4 (2x CH_{Ar}), 128.2 (CH_{Ar}), 126.1 (q, $^3J_{FH} = 3.9$ Hz, 2x CH_{Ar}), 123.9 (d, $^1J_{FH} = 272.4$ Hz, CF_3), 112.6 (=C), 59.3 (CHN), 52.2 (OCH_3), 44.4 (CH_2) ppm.

^{19}F NMR (282 MHz, CDCl_3) δ -63.1 ppm.

FTIR ν_{max} 3407 (O-H_{st}), 1712 (C=O_{st} ester), 1685 (C=O_{st} amide), 1672 (C=C_{st}), 1326 (C-F_{st}) cm^{-1} .

HRMS (ESI-TOF) m/z calcd. for $\text{C}_{20}\text{H}_{17}\text{F}_3\text{NO}_4$ [$\text{M}+\text{H}$]⁺ 392.1101, found 392.1119.

Methyl 4-hydroxy-2-(3-methoxyphenyl)-5-oxo-1-(*p*-tolyl)-2,5-dihydro-1*H*-pyrrole-3-carboxylate (97e).



The general procedure was followed using enamine-derived γ -lactam **86l** to afford 161 mg (91%) of **97e** as a white solid.

Mp (Et_2O /pentane): 170 - 172 °C (dec.).

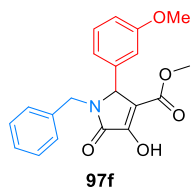
^1H NMR (400 MHz, CDCl_3) δ 8.93 (bs, 1H, OH), 7.32 (d, $^3J_{HH} = 8.5$ Hz, 2H, 2x CH_{Ar}), 7.17 (t, $^3J_{HH} = 7.9$ Hz, 1H, CH_{Ar}), 7.07 (d, $^3J_{HH} = 8.5$ Hz, 2H, 2x CH_{Ar}), 6.83 (m, 1H, CH_{Ar}), 6.75 (ddd, $^3J_{HH} = 8.2$ Hz, $^4J_{HH} = 2.6$, 0.9 Hz, 1H, CH_{Ar}), 6.71 (m, 1H, CH_{Ar}), 5.66 (s, 1H, CHN), 3.75 (s, 3H, OCH_3 Ar), 3.72 (s, 3H, OCH_3 ester), 2.25 (s, 3H, CH_3 tolyl) ppm.

^{13}C { ^1H } NMR (101 MHz, CDCl_3) δ 165.5 (C=O), 162.8 (C=O), 159.4 (C_{quat}), 156.2 (C_{quat}), 136.8 (C_{quat}), 136.0 (C_{quat}), 133.7 (C_{quat}), 129.8 (CH_{Ar}), 129.7 (2x CH_{Ar}), 122.6 (2x CH_{Ar}), 120.2 (CH_{Ar}), 113.9 (CH_{Ar}), 113.2 (CH_{Ar}), 112.7 (=C), 61.8 (CHN), 55.4 (OCH_3 Ar), 52.2 (OCH_3 ester), 21.1 (CH_3 tolyl) ppm.

FTIR ν_{max} 3453 (O-H_{st}), 1715 (C=O_{st} ester), 1685 (C=O_{st} amide), 1674 (C=C_{st}) cm^{-1} .

HRMS (ESI-TOF) m/z calcd. for $\text{C}_{20}\text{H}_{20}\text{NO}_5$ [$\text{M}+\text{H}$]⁺ 354.1333, found 354.1348.

Methyl 1-benzyl-4-hydroxy-2-(3-methoxyphenyl)-5-oxo-2,5-dihydro-1*H*-pyrrole-3-carboxylate (97f).



The general procedure was followed using enamine-derived γ -lactam **86m** to afford 154 mg (87%) of **97f** as a white solid.

Mp (Et_2O /pentane): 189 - 190 °C.

^1H NMR (400 MHz, CDCl_3) δ 9.09 (bs, 1H, OH), 7.36 - 7.27 (m, 4H, 4x CH_{Ar}), 7.12 (d, $^3J_{HH} = 7.8$, 1.8 Hz, 1H, CH_{Ar}), 7.11 (d, $^3J_{HH} = 6.9$ Hz, 1H, CH_{Ar}), 6.89 (ddd, $^3J_{HH} = 8.2$ Hz, $^4J_{HH} = 2.6$ Hz, 1H, CH_{Ar}), 6.72 (dt, $^3J_{HH} = 7.6$, $^4J_{HH} = 1.2$ Hz, 1H, CH_{Ar}), 6.60 (t, $^4J_{HH} = 2.1$ Hz, 1H, CH_{Ar}), 5.18 (d, $^2J_{HH} = 14.8$ Hz,

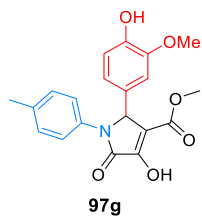
1H, CH_ACH_B Bn), 4.86 (s, 1H, CHN), 3.78 (s, 3H, OCH_3 Ar), 3.64 (s, 3H, OCH_3 ester), 3.57 (d, $^2J_{HH} = 14.8$ Hz, 1H, CH_ACH_B Bn) ppm.

^{13}C { ^1H } NMR (101 MHz, CDCl_3) δ 165.7 (C=O), 163.5 (C=O), 160.1 (C_{quat}), 157.6 (C_{quat}), 136.4 (C_{quat}), 136.1 (C_{quat}), 130.1 (CH_{Ar}), 129.0 (CH_{Ar}), 128.7 (2x CH_{Ar}), 128.0 (2x CH_{Ar}), 120.4 (CH_{Ar}), 114.4 (CH_{Ar}), 113.2 (CH_{Ar}), 112.9 (=C), 59.8 (CHN), 55.5 (OCH_3 Ar), 52.0 (OCH_3 ester), 44.2 (CH_2) ppm.

FTIR ν_{max} 3226 (O-H_{st}), 1688 (C=O_{st} ester), 1669 (C=O_{st} amide), 1640 (C=C_{st}) cm^{-1} .

HRMS (ESI-TOF) m/z calcd. for $\text{C}_{20}\text{H}_{20}\text{NO}_5$ [M+H]⁺ 354.1333, found 354.1347.

Methyl 4-hydroxy-2-(4-hydroxy-3-methoxyphenyl)-5-oxo-1-(*p*-tolyl)-2,5-dihydro-1H-pyrrole-3-carboxylate (97g).



The general procedure was followed using enamine-derived γ -lactam **86n** to afford 150 mg (81%) of **97g** as a white solid.

Mp (Et_2O /pentane): 158 - 160 °C (dec.).

^1H NMR (400 MHz, CDCl_3) δ 9.04 (bs, 1H, OH Enol), 7.29 (d, $^3J_{HH} = 8.1$ Hz, 2H, 2x CH_{Ar}), 7.07 (d, $^3J_{HH} = 8.1$ Hz, 2H, 2x CH_{Ar}), 6.79 (bs, 2H, 2x CH_{Ar}), 6.54 (s, 1H, CH_{Ar}), 5.63 (s, 1H, CHN), 5.58 (bs, 1H, OH Phenol), 3.78 (s, 3H, OCH_3 Ar), 3.75 (s, 3H, OCH_3 ester), 2.26 (s, 3H, CH_3 tolyl) ppm.

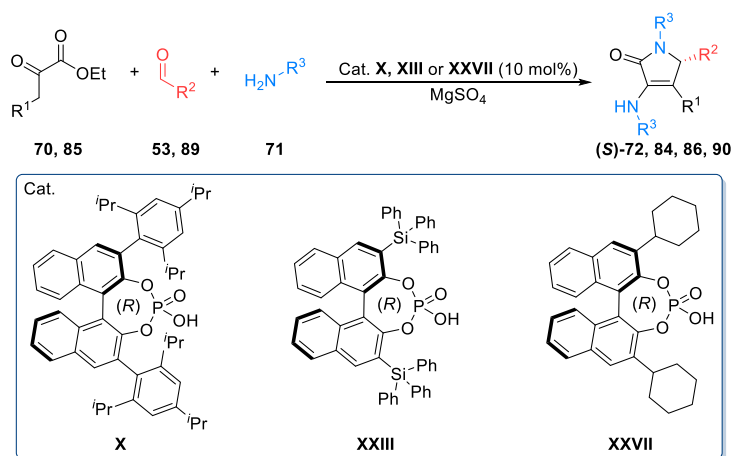
^{13}C { ^1H } NMR (101 MHz, CDCl_3) δ 165.6 (C=O), 162.8 (C=O), 156.4 (C_{quat}), 146.9 (C_{quat}), 145.9 (C_{quat}), 136.1 (C_{quat}), 133.7 (C_{quat}), 129.7 (2x CH_{Ar}), 126.7 (C_{quat}), 122.8 (2x CH_{Ar}), 121.8 (CH_{Ar}), 114.4 (CH_{Ar}), 112.8 (=C), 108.8 (CH_{Ar}), 61.9 (CHN), 56.1 (OCH_3 Ar), 52.2 (OCH_3 ester), 21.1 (CH_3 tolyl) ppm.

FTIR ν_{max} 3420 (O-H_{st}), 1721 (C=O_{st} ester), 1697 (C=O_{st} amide), 1657 (C=C_{st}) cm^{-1} .

HRMS (ESI-TOF) m/z calcd. for $\text{C}_{20}\text{H}_{20}\text{NO}_6$ [M+H]⁺ 370.1282, found 370.1292.

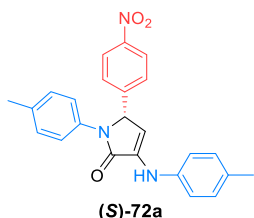
Chapter 4. An enantioselective approach for the multicomponent synthesis of γ -lactams.

General procedure for the organocatalyzed enantioselective multicomponent synthesis of 3-amino-1,5-dihydro-2*H*-pyrrol-2-ones **72, **84**, **86** and **90**.**



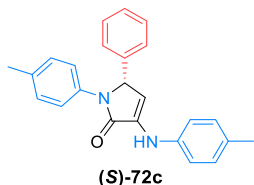
A solution of amine **71** (200 μmol), aldehyde **53** or **89** (100 μmol), ethyl pyruvate derivative **70**, **85** or **91** (300 μmol) and BINOL-derived chiral phosphoric acid (**R**)-**X**, **XXIII** or **XXVII** (10 μmol) was stirred in diethyl ether at room temperature or in MTBE at 55 $^\circ\text{C}$ (2 mL) in the presence of anhydrous MgSO_4 for 18 - 72 hours. The resulting solution was filtered and the mother liquor was concentrated at reduced pressure. The crude residue was purified by crystallization from diethyl ether or by flash column chromatography (Hexanes/AcOEt) to afford pure enantioenriched enamine-derived γ -lactams **72**, **84**, **86** or **90**.

(S)-5-(4-Nitrophenyl)-1-(p-tolyl)-3-(p-tolylamino)-1,5-dihydro-2H-pyrrol-2-one ((S)-72a).



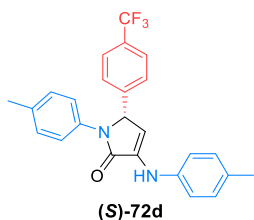
The general procedure was followed in diethyl ether at room temperature for 18 hours, using *p*-toluidine (21 mg, 200 μ mol), *p*-nitrobenzaldehyde (15 mg, 100 μ mol), ethyl pyruvate (34 μ L, 300 μ mol) and BINOL-derived chiral phosphoric acid (**R**)-XXIII (9 mg, 10 μ mol). The crude residue was purified by crystallization from diethyl ether, affording 29 mg (73%) of (**S**)-72a as a yellow solid. Ee (96%) was determined by HPLC analysis (Chiracel-IC, Heptane/DCM/AcOEt 50:47:3, 1 mL/min). Retention time (min): 17.8 (major) and 21.1 (minor). Spectroscopic data are in agreement with the data described for the racemic mixture (See Chapter 1).

(S)-5-Phenyl-1-(p-tolyl)-3-(p-tolylamino)-1,5-dihydro-2H-pyrrol-2-one ((S)-72c).



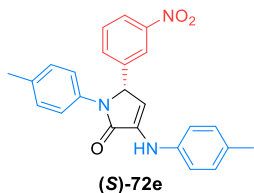
The general procedure was followed in diethyl ether at room temperature for 18 hours, using *p*-toluidine (21 mg, 200 μ mol), benzaldehyde (10 μ L, 100 μ mol), ethyl pyruvate (34 μ L, 300 μ mol) and BINOL-derived chiral phosphoric acid (**R**)-XXIII (9 mg, 10 μ mol). The crude residue was purified by crystallization from diethyl ether, affording 32 mg (90%) of (**S**)-72c as a white solid. Ee (87%) was determined by HPLC analysis (Chiracel-IC, Heptane/DCM/AcOEt 50:47:3, 1 mL/min). Retention time (min): 10.9 (major) and 13.7 (minor). Spectroscopic data are in agreement with the data described for the racemic mixture (See Chapter 1).

(S)-1-(p-Tolyl)-3-(p-tolylamino)-5-(4-(trifluoromethyl)phenyl)-1,5-dihydro-2H-pyrrol-2-one ((S)-72d).



The general procedure was followed in diethyl ether at room temperature for 18 hours, using *p*-toluidine (21 mg, 200 μ mol), *p*-(trifluoromethyl) benzaldehyde (14 μ L, 100 μ mol), ethyl pyruvate (34 μ L, 300 μ mol) and BINOL-derived chiral phosphoric acid (**R**)-X (8 mg, 10 μ mol). The crude residue was purified by crystallization from diethyl ether, affording 36 mg (86%) of (**S**)-72d as a white solid. Ee (82%) was determined by HPLC analysis (Chiracel-IC, Heptane/EtOH 99:1, 1 mL/min). Retention time (min): 10.7 (minor) and 12.8 (major). Spectroscopic data are in agreement with the data described for the racemic mixture (See Chapter 1).

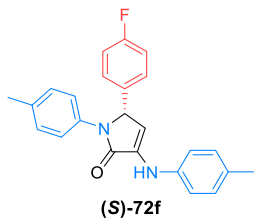
(S)-5-(3-Nitrophenyl)-1-(p-tolyl)-3-(p-tolylamino)-1,5-dihydro-2H-pyrrol-2-one ((S)-72e).



The general procedure was followed in diethyl ether at room temperature for 18 hours, using *p*-toluidine (21 mg, 200 μ mol), *m*-nitrobenzaldehyde (15 mg, 100 μ mol), ethyl pyruvate (34 μ L, 300 μ mol) and BINOL-derived chiral phosphoric acid (**R**)-XXIII (9 mg, 10 μ mol). The crude residue was purified by crystallization from diethyl ether, affording 29 mg (73%) of (**S**)-72e as a

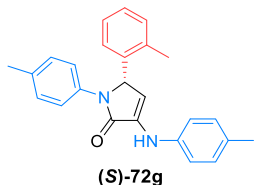
yellow solid. Ee (80%) was determined by HPLC analysis (Chiracel-IC, Heptane/DCM/AcOEt 60:30:10, 1 mL/min). Retention time (min): 15.8 (major) and 20.38 (minor). Spectroscopic data are in agreement with the data described for the racemic mixture (See Chapter 1).

(S)-5-(4-Fluorophenyl)-1-(*p*-tolyl)-3-(*p*-tolylamino)-1,5-dihydro-2H-pyrrol-2-one ((S)-72f).



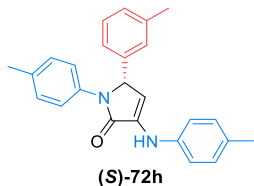
The general procedure was followed in diethyl ether at room temperature for 48 hours, using *p*-toluidine (21 mg, 200 μ mol), *p*-fluorobenzaldehyde (11 μ L, 100 μ mol), ethyl pyruvate (34 μ L, 300 μ mol) and BINOL-derived chiral phosphoric acid (**R**)-**XXIII** (9 mg, 10 μ mol). The crude residue was purified by crystallization from diethyl ether, affording 30 mg (81%) of (**S**)-**72f** as a white solid. Ee (52%) was determined by HPLC analysis (Chiracel-IC, Heptane/DCM/AcOEt 65:30:5, 1 mL/min). Retention time (min): 11.5 (minor) and 20.38 (major). Spectroscopic data are in agreement with the data described for the racemic mixture (See Chapter 1).

(S)-5-(*o*-Tolyl)-1-(*p*-tolyl)-3-(*p*-tolylamino)-1,5-dihydro-2H-pyrrol-2-one ((S)-72g).



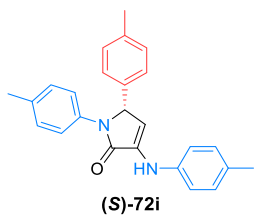
The general procedure was followed in MTBE at 55 $^{\circ}$ C (heating plate) for 72 hours, using *p*-toluidine (21 mg, 200 μ mol), *o*-tolualdehyde (16 μ L, 100 μ mol), ethyl pyruvate (34 μ L, 300 μ mol) and BINOL-derived chiral phosphoric acid (**R**)-**XXIII** (9 mg, 10 μ mol). The crude residue was purified by crystallization from diethyl ether, affording 24 mg (65%) of (**S**)-**72g** as an orange solid. Ee (36%) was determined by HPLC analysis (Chiracel-IC, Heptane/DCM/EtOH 90:9:1, 1 mL/min). Retention time (min): 9.8 (minor) and 14.0 (major). Spectroscopic data are in agreement with the data described for the racemic mixture (See Chapter 1).

(S)-5-(*m*-Tolyl)-1-(*p*-tolyl)-3-(*p*-tolylamino)-1,5-dihydro-2H-pyrrol-2-one ((S)-72h).



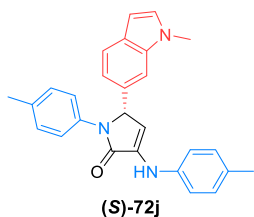
The general procedure was followed in MTBE at 55 $^{\circ}$ C (heating plate) for 72 hours, using *p*-toluidine (21 mg, 200 μ mol), *m*-tolualdehyde (12 μ L, 100 μ mol), ethyl pyruvate (34 μ L, 300 μ mol) and BINOL-derived chiral phosphoric acid (**R**)-**XXVII** (6 mg, 10 μ mol). The crude residue was purified by crystallization from diethyl ether, affording 31 mg (83%) of (**S**)-**72h** as a white solid. Ee (70%) was determined by HPLC analysis (Chiracel-IC, Heptane/DCM/AcOEt 50:47:3, 1 mL/min). Retention time (min): 11.0 (major) and 14.0 (minor). Spectroscopic data are in agreement with the data described for the racemic mixture (See Chapter 1).

(S)-1,5-Di-*p*-tolyl-3-(*p*-tolylamino)-1,5-dihydro-2*H*-pyrrol-2-one ((S)-72i).



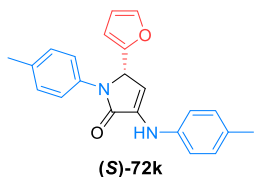
The general procedure was followed in MTBE at 55 °C (heating plate) for 18 hours, using *p*-toluidine (21 mg, 200 μmol), *p*-tolualdehyde (19 μL, 100 μmol), ethyl pyruvate (34 μL, 300 μmol) and BINOL-derived chiral phosphoric acid **(R)-XXIII** (9 mg, 10 μmol). The crude residue was purified by crystallization from diethyl ether, affording 30 mg (81%) of **(S)-72i** as an orange solid. Ee (33%) was determined by HPLC analysis (Chiracel-IC, Heptane/DCM/AcOEt 50:47:3, 1 mL/min). Retention time (min): 9.7 (minor) and 11.3 (major). Spectroscopic data are in agreement with the data described for the racemic mixture (See Chapter 1).

(S)-5-(1-Methyl-1*H*-indol-6-yl)-1-(*p*-tolyl)-3-(*p*-tolylamino)-1,5-dihydro-2*H*-pyrrol-2-one ((S)-72j).



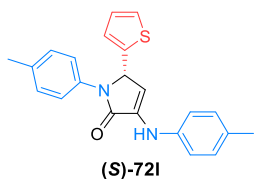
The general procedure was followed in diethyl ether at room temperature for 18 hours, using *p*-toluidine (21 mg, 200 μmol), 1-methyl-1*H*-indole-6-carboxaldehyde (16 mg, 100 μmol), ethyl pyruvate (34 μL, 300 μmol) and BINOL-derived chiral phosphoric acid **(R)-X** (8 mg, 10 μmol). The crude residue was purified by flash column chromatography (Hexanes/AcOEt 90:10), affording 19 mg (45%) of **(S)-72j** as an orange solid. Ee (8%) was determined by HPLC analysis (Chiracel-IC, Heptane/DCM/EtOH 90:9:1, 1 mL/min). Retention time (min): 12.6 (minor) and 15.3 (major). Spectroscopic data are in agreement with the data described for the racemic mixture (See Chapter 1).

(S)-5-(Furan-2-yl)-1-(*p*-tolyl)-3-(*p*-tolylamino)-1,5-dihydro-2*H*-pyrrol-2-one one ((S)-72k).



The general procedure was followed in diethyl ether at room temperature for 18 hours, using *p*-toluidine (21 mg, 200 μmol), 2-furaldehyde (9 μL, 100 μmol), ethyl pyruvate (34 μL, 300 μmol) and BINOL-derived chiral phosphoric acid **(R)-XXIII** (9 mg, 10 μmol). The crude residue was purified by flash column chromatography (Hexanes/AcOEt 90:10), affording 18 mg (51%) of **(S)-72k** as a white solid. Ee (16%) was determined by HPLC analysis (Chiracel-IC, Heptane/DCM/EtOH 65:35:5, 1 mL/min). Retention time (min): 17.2 (minor) and 21.5 (major). Spectroscopic data are in agreement with the data described for the racemic mixture (See Chapter 1).

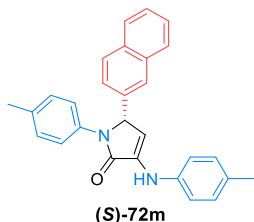
(S)-5-(Thiophen-2-yl)-1-(*p*-tolyl)-3-(*p*-tolylamino)-1,5-dihydro-2*H*-pyrrol-2-one ((S)-72l).



The general procedure was followed in MTBE at 55 °C (heating plate) for 18 hours, using *p*-toluidine (21 mg, 200 μmol), 2-thiophenecarboxaldehyde (10 μL, 100 μmol), ethyl pyruvate (34 μL, 300 μmol) and BINOL-derived chiral phosphoric acid **(R)-XXIII** (8.65 mg, 10 μmol).

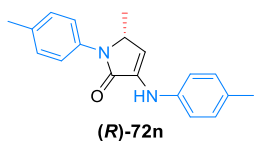
μmol). The crude residue was purified by crystallization from diethyl ether, affording 31 mg (86%) of **(S)-72l** as a yellow solid. Ee (67%) was determined by HPLC analysis (Chiracel-IC, Heptane/DCM/EtOH 90:9:1, 1 mL/min). Retention time (min): 12.5 (major) and 14.3 (minor). Spectroscopic data are in agreement with the data described for the racemic mixture (See Chapter 1).

(S)-5-(Naphthalen-2-yl)-1-(*p*-tolyl)-3-(*p*-tolylamino)-1,5-dihydro-2H-pyrrol-2-one ((S)-72m**).**



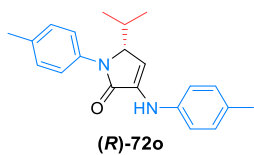
The general procedure was followed in diethyl ether at room temperature for 18 hours, using *p*-toluidine (21 mg, 200 μmol), 2-naphthaldehyde (16 mg, 100 μmol), ethyl pyruvate (34 μL , 300 μmol) and BINOL-derived chiral phosphoric acid **(R)-XXIII** (9 mg, 10 μmol). The crude residue was purified by flash column chromatography (Hexanes/AcOEt 90:10), affording 29 mg (70%) of **(S)-72m** as an orange solid. Ee (0%) was determined by HPLC analysis (Chiracel-IC, Heptane/DCM/EtOH 90:9:1, 1 mL/min). Retention time (min): 20.2 and 29.1. Spectroscopic data are in agreement with the data described for the racemic mixture (See Chapter 1).

(R)-5-Methyl-1-(*p*-tolyl)-3-(*p*-tolylamino)-1,5-dihydro-2H-pyrrol-2-one ((R)-72n**).**



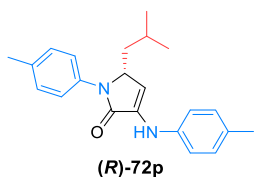
The general procedure was followed in diethyl ether at room temperature for 18 hours, using *p*-toluidine (21 mg, 200 μmol), acetaldehyde (6 μL , 100 μmol), ethyl pyruvate (34 μL , 300 μmol) and BINOL-derived chiral phosphoric acid **(R)-XXVII** (6 mg, 10 μmol). The crude residue was purified by flash column chromatography (Hexanes/AcOEt 90:10), affording 16 mg (54%) of **(R)-72n** as a white solid. Ee (36%) was determined by HPLC analysis (Chiracel-IC, Heptane/DCM/AcOEt 60:30:10, 1 mL/min). Retention time (min): 8.0 (minor) and 11.3 (major). Spectroscopic data are in agreement with the data described for the racemic mixture (See Chapter 1).

(R)-5-Iso-propyl-1-(*p*-tolyl)-3-(*p*-tolylamino)-1,5-dihydro-2H-pyrrol-2-one ((R)-72o**).**



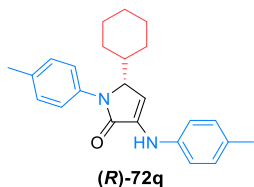
The general procedure was followed in diethyl ether at room temperature for 18 hours, using *p*-toluidine (21 mg, 200 μmol), isobutyraldehyde (6 μL , 100 μmol), ethyl pyruvate (34 μL , 300 μmol) and BINOL-derived chiral phosphoric acid **(R)-XXIII** (9 mg, 10 μmol). The crude residue was purified by flash column chromatography (Hexanes/AcOEt 85:15), affording 27 mg (77%) of **(R)-72o** as a white solid. Ee (82%) was determined by HPLC analysis (Chiracel-IC, Heptane/DCM/AcOEt 65:30:5, 1 mL/min). Retention time (min): 14.8 (major) and 16.0 (minor). Spectroscopic data are in agreement with the data described for the racemic mixture (See Chapter 1).

(R)-5-Iso-butyl-1-(p-tolyl)-3-(p-tolylamino)-1,5-dihydro-2H-pyrrol-2-one ((R)-72p).



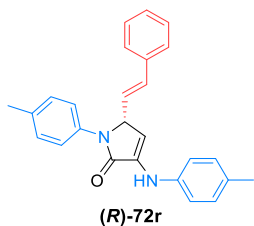
The general procedure was followed in diethyl ether at room temperature for 18 hours, using *p*-toluidine (21 mg, 200 μ mol), *iso*-valeraldehyde (11 μ L, 100 μ mol), ethyl pyruvate (34 μ L, 300 μ mol) and BINOL-derived chiral phosphoric acid **(R)-XXIII** (9 mg, 10 μ mol). The crude residue was purified by flash column chromatography (Hexanes/AcOEt 90:10), affording 20 mg (60%) of **(R)-72p** as a yellow solid. Ee (73%) was determined by HPLC analysis (Chiracel-IC, Heptane/DCM/AcOEt 60:30:10, 1 mL/min). Retention time (min): 9.4 (major) and 10.4 (minor). Spectroscopic data are in agreement with the data described for the racemic mixture (See Chapter 1).

(R)-5-Cyclohexyl-1-(p-tolyl)-3-(p-tolylamino)-1,5-dihydro-2H-pyrrol-2-one ((S)-72q).



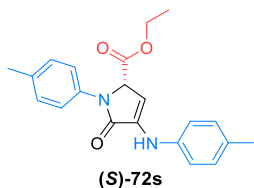
The general procedure was followed in diethyl ether at room temperature for 18 hours, using *p*-toluidine (21 mg, 200 μ mol), cyclohexane carboxaldehyde (12 μ L, 100 μ mol), ethyl pyruvate (34 μ L, 300 μ mol) and BINOL-derived chiral phosphoric acid **(R)-XXIII** (9 mg, 10 μ mol). The crude residue was purified by crystallization from diethyl ether, affording 31 mg (85%) of **(R)-72q** as a white solid. Ee (79%) was determined by HPLC analysis (Chiracel-IC, Heptane/DCM/AcOEt 60:30:10, 1 mL/min). Retention time (min): 10.9 (major) and 11.8 (minor). Spectroscopic data are in agreement with the data described for the racemic mixture (See Chapter 1).

(R,E)-5-styryl-1-(p-tolyl)-3-(p-tolylamino)-1,5-dihydro-2H-pyrrol-2-one ((R)-72r).



The general procedure was followed in diethyl ether at room temperature for 18 hours, using *p*-toluidine (21 mg, 200 μ mol), cinnamaldehyde (13 μ L, 100 μ mol), ethyl pyruvate (34 μ L, 300 μ mol) and BINOL-derived chiral phosphoric acid **(R)-XXIII** (9 mg, 10 μ mol). The crude residue was purified by flash column chromatography (Hexanes/AcOEt 80:20), affording 23 mg (59%) of **(R)-72r** as a white solid. Ee (>99%) was determined by HPLC analysis (Chiracel-IC, Heptane/EtOH 98:2, 1 mL/min). Retention time (min): 13.5 (minor) and 16.2 (major). Spectroscopic data are in agreement with the data described for the racemic mixture (See Chapter 1).

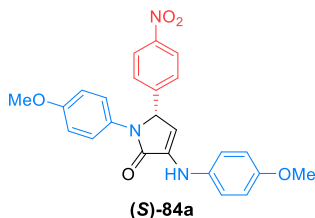
Ethyl (S)-5-oxo-1-(p-tolyl)-4-(p-tolylamino)-2,5-dihydro-1H-pyrrole-2-carboxylate ((S)-72s).



The general procedure was followed in diethyl ether at room temperature for 18 hours, using *p*-toluidine (21 mg, 200 μ mol), a 50% solution of ethyl glyoxalate in toluene (20 μ L, 100 μ mol), ethyl pyruvate (34 μ L, 300 μ mol) and BINOL-derived chiral phosphoric acid **(R)-XXVII** (6 mg, 10 μ mol). The crude residue was purified by crystallization from diethyl ether, affording 34 mg (95%) of

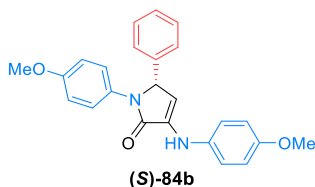
(S)-72s as a white solid. Ee (97%) was determined by HPLC analysis (Chiracel-IC, Heptane/DCM/EtOH 90:9:1, 1 mL/min). Retention time (min): 12.4 (major) and 15.3 (minor). Spectroscopic data are in agreement with the data described for the racemic mixture (See Chapter 1).

(S)-1-(4-Methoxyphenyl)-3-((4-methoxyphenyl)amino)-5-(4-nitrophenyl)-1,5-dihydro-2H-pyrrol-2-one ((S)-84a).



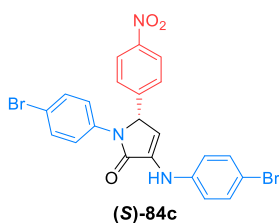
The general procedure was followed in diethyl ether at room temperature for 24 hours, using *p*-anisidine (25 mg, 200 μ mol), *p*-nitrobenzaldehyde (15 mg, 100 μ mol), ethyl pyruvate (34 μ L, 300 μ mol) and BINOL-derived chiral phosphoric acid **(R)-XXIII** (9 mg, 10 μ mol). The crude residue was purified by flash column chromatography (Hexanes/AcOEt 80:20), affording 35 mg (81%) of **(S)-84a** as a yellow solid. Ee (90%) was determined by HPLC analysis (Chiracel-IC, Heptane/DCM/EtOH 60:39:1, 1 mL/min). Retention time (min): 20.1 (major) and 21.2 (minor). Spectroscopic data are in agreement with the data described for the racemic mixture (See Chapter 1).

(S)-1-(4-Methoxyphenyl)-3-((4-methoxyphenyl)amino)-5-phenyl-1,5-dihydro-2H-pyrrol-2-one ((S)-84b).



The general procedure was followed in diethyl ether at room temperature for 18 hours, using *p*-anisidine (25 mg, 200 μ mol), benzaldehyde (10 μ L, 100 μ mol), ethyl pyruvate (34 μ L, 300 μ mol) and BINOL-derived chiral phosphoric acid **(R)-XXIII** (9 mg, 10 μ mol). The crude residue was purified by flash column chromatography (Hexanes/AcOEt 80:20), affording 29 mg (74%) of **(S)-84b** as a white solid. Ee (90%) was determined by HPLC analysis (Chiracel-IC, Heptane/DCM/AcOEt 60:30:10, 1 mL/min). Retention time (min): 18.0 (major) and 22.3 (minor). Spectroscopic data are in agreement with the data described for the racemic mixture (See Chapter 1).

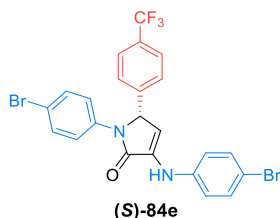
(S)-1-(4-Bromophenyl)-3-((4-bromophenyl)amino)-5-(4-nitrophenyl)-1,5-dihydro-2H-pyrrol-2-one ((S)-84c).



The general procedure was followed in diethyl ether at room temperature for 18 hours, using *p*-bromoaniline (35 mg, 200 μ mol), *p*-nitrobenzaldehyde (15 mg, 100 μ mol), ethyl pyruvate (34 μ L, 300 μ mol) and BINOL-derived chiral phosphoric acid **(R)-X** (8 mg, 10 μ mol). The crude residue was purified by flash column chromatography (Hexanes/AcOEt 80:20), affording 47 mg (89%) of **(S)-84c** as a yellow solid. Ee (>99%) was determined by HPLC analysis (Chiracel-IC, Heptane/DCM/AcOEt 90:9:1, 1 mL/min). Retention time (min): 33.8

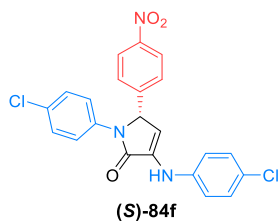
(minor) and 35.5 (major). Spectroscopic data are in agreement with the data described for the racemic mixture (See Chapter 1).

(S)-1-(4-Bromophenyl)-3-((4-bromophenyl)amino)-5-(4-(trifluoromethyl)phenyl)-1,5-dihydro-2H-pyrrol-2-one ((S)-84e).



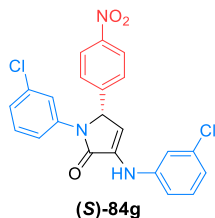
The general procedure was followed in diethyl ether at room temperature for 18 hours, using *p*-bromoaniline (35 mg, 200 μ mol), *p*-(trifluoromethyl)benzaldehyde (14 μ L, 100 μ mol), ethyl pyruvate (34 μ L, 300 μ mol) and BINOL-derived chiral phosphoric acid (**R**)-**XXIII** (9 mg, 10 μ mol). The crude residue was crystallized from diethyl ether, affording 49 mg (89%) of (**S**)-**84e** as a white solid. Ee (80%) was determined by HPLC analysis (Chiracel-IC, Heptane/DCM/EtOH 90:9:1, 1 mL/min). Retention time (min): 8.5 (minor) and 9.2 (major). Spectroscopic data are in agreement with the data described for the racemic mixture (See Chapter 1).

(S)-1-(4-Chlorophenyl)-3-((4-chlorophenyl)amino)-5-(4-nitrophenyl)-1,5-dihydro-2H-pyrrol-2-one ((S)-84f).



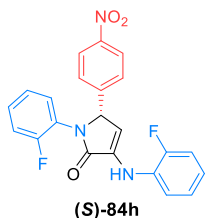
The general procedure was followed in MTBE at 55 $^{\circ}$ C (heating plate) for 18 hours, using *p*-chloroaniline (26 mg, 200 μ mol), *p*-nitrobenzaldehyde (15 mg, 100 μ mol), ethyl pyruvate (34 μ L, 300 μ mol) and BINOL-derived chiral phosphoric acid (**R**)-**XXVII** (6 mg, 10 μ mol). The crude residue was purified by flash column chromatography (Hexanes/AcOEt 90:10), affording 33 mg (74%) of (**S**)-**84f** as a white solid. Ee (42%) was determined by HPLC analysis (Chiracel-IC, Heptane/DCM/AcOEt 60:30:10, 1 mL/min). Retention time (min): 9.3 (minor) and 10.9 (major). Spectroscopic data are in agreement with the data described for the racemic mixture (See Chapter 1).

(S)-1-(3-Chlorophenyl)-3-((3-chlorophenyl)amino)-5-(4-nitrophenyl)-1,5-dihydro-2H-pyrrol-2-one ((S)-84g).



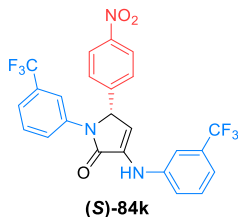
The general procedure was followed in diethyl ether at room temperature for 72 hours, using *m*-chloroaniline (22 μ L, 200 μ mol), *p*-nitrobenzaldehyde (15 mg, 100 μ mol), ethyl pyruvate (34 μ L, 300 μ mol) and BINOL-derived chiral phosphoric acid (**R**)-**X** (8 mg, 10 μ mol). The crude residue was purified by crystallization from diethyl ether, affording 28 mg (63%) of (**S**)-**84g** as a yellow solid. Ee (97%) was determined by HPLC analysis (Chiracel-IC, Heptane/DCM/AcOEt 60:30:10, 1 mL/min). Retention time (min): 9.8 (minor) and 11.1 (major). Spectroscopic data are in agreement with the data described for the racemic mixture (See Chapter 1).

(S)-1-(2-Fluorophenyl)-3-((2-fluorophenyl)amino)-5-(4-nitrophenyl)-1,5-dihydro-2H-pyrrol-2-one ((S)-84h).



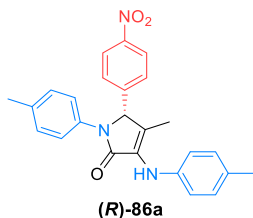
The general procedure was followed in diethyl ether at room temperature for 18 hours, using *o*-fluoroaniline (19 μ L, 200 μ mol), *p*-nitrobenzaldehyde (15 mg, 100 μ mol), ethyl pyruvate (34 μ L, 300 μ mol) and BINOL-derived chiral phosphoric acid **(R)-XXIII** (9 mg, 10 μ mol). The crude residue was purified by flash column chromatography (Hexanes/AcOEt 80:20), affording 31 mg (75%) of **(S)-84h** as a yellow solid. Ee (95%) was determined by HPLC analysis (Chiracel-IC, Heptane/DCM/AcOEt 50:48:2, 1 mL/min). Retention time (min): 15.9 (major) and 17.9 (minor). Spectroscopic data are in agreement with the data described for the racemic mixture (See Chapter 1).

(S)-5-(4-Nitrophenyl)-1-(3-(trifluoromethyl)phenyl)-3-((3-(trifluoromethyl)phenyl)amino)-1,5-dihydro-2H-pyrrol-2-one ((S)-84k).



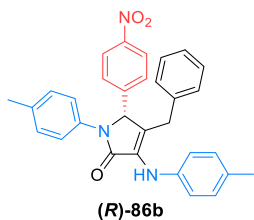
The general procedure was followed in MTBE at 55 $^{\circ}$ C (heating plate) for 72 hours, using *m*-(trifluoromethyl)aniline (25 mg, 200 μ mol), *p*-nitrobenzaldehyde (15 mg, 100 μ mol), ethyl pyruvate (34 μ L, 300 μ mol) and BINOL-derived chiral phosphoric acid **(R)-XXVII** (6 mg, 10 μ mol). The crude residue was purified by flash column chromatography (Hexanes/AcOEt 80:20), affording 32 mg (63%) of **(S)-84k** as a yellow solid. Ee (62%) was determined by HPLC analysis (Chiracel-IC, Heptane/DCM/EtOH 90:9:1, 1 mL/min). Retention time (min): 11.2 (minor) and 13.9 (major). Spectroscopic data are in agreement with the data described for the racemic mixture (See Chapter 1).

(R)-4-Methyl-5-(4-nitrophenyl)-1-(*p*-tolyl)-3-(*p*-tolylamino)-1,5-dihydro-2H-pyrrol-2-one ((R)-86a).



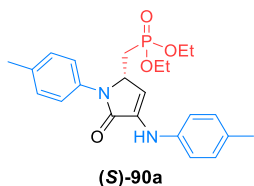
The general procedure was followed in MTBE at 55 $^{\circ}$ C (heating plate) for 18 hours, using *p*-toluidine (21 mg, 200 μ mol), *p*-nitrobenzaldehyde (15 mg, 100 μ mol), methyl 2-oxobutanoate (36 μ L, 6 mmol) and BINOL-derived chiral phosphoric acid **(R)-X** (8 mg, 10 μ mol). The crude residue was purified by crystallization from diethyl ether, affording 29 mg (70%) of **(R)-86a** as a yellow solid. Ee (54%) was determined by HPLC analysis (Chiracel-IC, Heptane/DCM/EtOH 80:19:1, 1 mL/min). Retention time (min): 27.1 (major) and 31.7 (minor). Spectroscopic data are in agreement with the data described for the racemic mixture (See Chapter 1).

(R)-4-Benzyl-5-(4-nitrophenyl)-1-(p-tolyl)-3-(p-tolylamino)-1,5-dihydro-2H-pyrrol-2-one ((R)-86b).



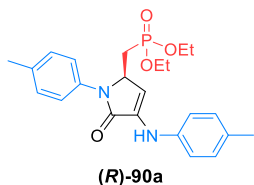
The general procedure was followed in MTBE at 55 °C (heating plate) for 18 hours, using *p*-toluidine (21 mg, 200 μmol), *p*-nitrobenzaldehyde (15 mg, 100 μmol), ethyl 2-oxo-4-phenylbutanoate (57 μL, 6 mmol) and BINOL-derived chiral phosphoric acid **(R)-X** (8 mg, 10 μmol). The crude residue was purified by crystallization from diethyl ether, affording 44 mg (71%) of **(R)-86b** as a yellow solid. Ee (68%) was determined by HPLC analysis (Chiracel-IC, Heptane/DCM/EtOH 80:19:1, 1 mL/min). Retention time (min): 18.3 (major) and 19.9 (minor). Spectroscopic data are in agreement with the data described for the racemic mixture (See Chapter 1).

Diethyl (S) ((5-oxo-1-(p-tolyl)-4-(p-tolylamino)-2,5-dihydro-1H-pyrrol-2-yl)methyl)phosphonate ((S)-90a).



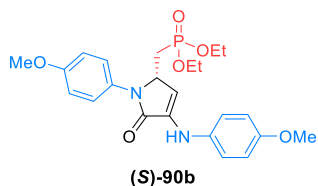
The general procedure was followed in diethyl ether at room temperature for 48 hours, using *p*-toluidine (21 mg, 200 μmol), diethyl (2-oxoethyl)phosphonate (18 mg, 200 μmol), ethyl pyruvate (34 μL, 300 μmol) and BINOL-derived chiral phosphoric acid **(R)-XXIII** (9 mg, 10 μmol). The crude residue was purified by flash column chromatography (Hexanes/AcOEt 90:10), affording 35 mg (80%) of **(S)-90a** as a yellow solid. Ee (90% or 97% after crystallization in Et₂O) was determined by HPLC analysis (Chiracel-IC, Heptane/DCM/EtOH 50:47:3, 1 mL/min). Retention time (min): 13.6 (minor) and 14.7 (major). Spectroscopic data are in agreement with the data described for the racemic mixture (See Chapter 2).

Diethyl (R) ((5-oxo-1-(p-tolyl)-4-(p-tolylamino)-2,5-dihydro-1H-pyrrol-2-yl)methyl)phosphonate ((R)-90a).



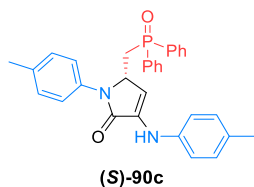
The general procedure was followed in diethyl ether at room temperature for 48 hours, using *p*-toluidine (21 mg, 200 μmol), diethyl (2-oxoethyl)phosphonate (18 mg, 200 μmol), ethyl pyruvate (34 μL, 300 μmol) and BINOL-derived chiral phosphoric acid **(S)-XXIII** (9 mg, 10 μmol). The crude residue was purified by flash column chromatography (Hexanes/AcOEt 90:10), affording 31 mg (71%) of **(R)-90a** as a yellow solid. Ee (84% or 97% after crystallization in Et₂O) was determined by HPLC analysis (Chiracel-IC, Heptane/DCM/EtOH 50:47:3, 1 mL/min). Retention time (min): 13.6 (minor) and 14.7 (major). Spectroscopic data are in agreement with the data described for the racemic mixture (See Chapter 2).

Diethyl (S) ((1-(4-methoxyphenyl)-4-((4-methoxyphenyl)amino)-5-oxo-2,5-dihydro-1H-pyrrol-2-yl)methyl)phosphonate ((S)-90b).



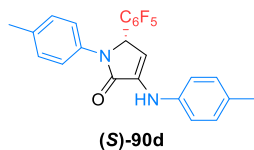
The general procedure was followed in diethyl ether at room temperature for 48 hours, using *p*-anisidine (25 mg, 200 μ mol), diethyl (2-oxoethyl)phosphonate (18 mg, 200 μ mol), ethyl pyruvate (34 μ L, 300 μ mol) and BINOL-derived chiral phosphoric acid (**R**)-**XXIII** (9 mg, 10 μ mol). The crude residue was purified by flash column chromatography (Hexanes/AcOEt 90:10), affording 38 mg (83%) of (**S**)-**90b** as a white solid. Ee (83%) was determined by HPLC analysis (Chiracel-IC, Heptane/DCM/EtOH 50:40:10, 1 mL/min). Retention time (min): 8.3 (minor) and 9.2 (major). Spectroscopic data are in agreement with the data described for the racemic mixture (See Chapter 2).

(S)-5-((Diphenylphosphoryl)methyl)-1-(*p*-tolyl)-3-(*p*-tolylamino)-1,5-dihydro-2H-pyrrol-2-one ((S)-90c).



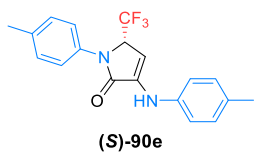
The general procedure was followed in diethyl ether at room temperature for 72 hours, using *p*-toluidine (21 mg, 200 μ mol), 2-(diphenylphosphoryl)acetaldehyde (25 mg, 200 μ mol), ethyl pyruvate (34 μ L, 300 μ mol) and BINOL-derived chiral phosphoric acid (**R**)-**XXIII** (9 mg, 10 μ mol). The crude residue was purified by flash column chromatography (Hexanes/AcOEt 90:10), affording 35 mg (70%) of (**S**)-**90c** as a white solid. Ee (91%) was determined by HPLC analysis (Chiracel-IB, Heptane/EtOH 95:5, 1 mL/min). Retention time (min): 26.2 (major) and 40.8 (minor). Spectroscopic data are in agreement with the data described for the racemic mixture (See Chapter 2).

(S)-5-(Perfluorophenyl)-1-(*p*-tolyl)-3-(*p*-tolylamino)-1,5-dihydro-2H-pyrrol-2-one ((S)-90d).



The general procedure was followed in MTBE at 55 $^{\circ}$ C (heating plate) for 48 hours, using *p*-toluidine (21 mg, 200 μ mol), perfluorobenzaldehyde (13 μ L, 200 μ mol), ethyl pyruvate (34 μ L, 300 μ mol) and BINOL-derived chiral phosphoric acid (**R**)-**XXIII** (9 mg, 10 μ mol). The crude residue was purified by flash column chromatography (Hexanes/AcOEt 90:10), affording 34 mg (77%) of (**S**)-**90d** as a white solid. Ee (60%) was determined by HPLC analysis (Chiracel-IB, Heptane/EtOH 98:2, 1 mL/min). Retention time (min): 9.5 (minor) and 11.1 (major). Spectroscopic data are in agreement with the data described for the racemic mixture (See Chapter 2).

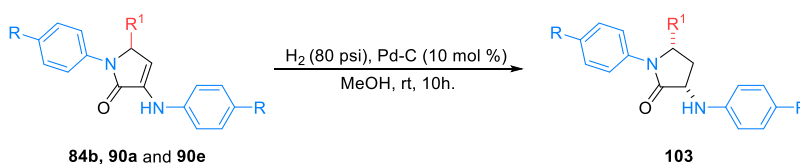
(S)-1-(*p*-Tolyl)-3-(*p*-tolylamino)-5-(trifluoromethyl)-1,5-dihydro-2*H*-pyrrol-2-one ((S)-90e).



A modified procedure was followed: To a solution of *p*-toluidine (21 mg, 200 μmol) in toluene (1 mL) a 75% aqueous solution of trifluoroacetaldehyde hydrate (6 μL , 100 μmol) was added. The mixture was heated at 110 $^{\circ}\text{C}$ on a heating plate using a Dean-Stark on a heating plate until water was fully removed. Once the imine intermediate was formed (monitored by ^{19}F NMR: 2,2,2-trifluoroethane-1,1-diol: -85.5 ppm; imine: -79.0 ppm), ethyl pyruvate (34 μL , 300 μmol) and BINOL-derived chiral phosphoric acid (**R**)-**XXIII** (9 mg, 10 μmol) were added, and the reaction was stirred at room temperature for 48 hours. The reaction was filtered, the volatiles were distilled off at reduced pressure and the crude residue was purified by flash column chromatography (Hexanes/AcOEt 90:10) to afford 25 mg (71%) of (**S**)-**90e** as a white solid. Ee (5%) was determined by HPLC analysis (Chiracel-IB, Heptane/EtOH 98:2, 1 mL/min). Retention time (min): 12.1 (major) and 16.2 (minor). Spectroscopic data are in agreement with the data described for the racemic mixture (See Chapter 2).

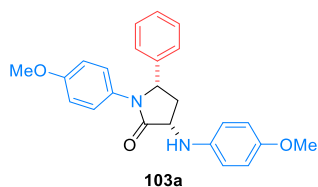
Chapter 5. Synthetic transformations of γ -lactam derivatives.

General procedure for the diastereoselective hydrogenation of γ -lactams. Synthesis of saturated 3-amino-2*H*-pyrrolidin-2-ones **103**.



A mixture of the corresponding γ -lactam (0.5 mmol) and 53 mg of 10% palladium on carbon (0.05 mmol Pd) in methanol (30 mL) was stirred under hydrogen pressure (80 psi) at room temperature for 10 hours. The reaction mixture was filtered, and the retained solid was extracted with dichloromethane (2×10 mL). The resulting solution was concentrated under reduced pressure and the crude residue was purified by crystallization from methanol to afford pure γ -lactams **103** as single diastereoisomers.

(3*S**,5*S**)-1-(4-Methoxyphenyl)-3-((4-methoxyphenyl)amino)-5-phenylpyrrolidin-2-one (**103a**).



The general procedure was followed, using γ -lactam **84b** (194 mg, 0.5 mmol) to afford 178 mg (92%) of **103a** as a white solid.

Mp (MeOH): 199 - 201 °C.

¹H NMR (400 MHz, CDCl₃) δ 7.28 - 7.17 (m, 7H, 7xCH_{Ar}), 6.81 (d, ³J_{HH} = 9.0 Hz, 2H, 2xCH_{Ar}), 6.76 (d, ³J_{HH} = 9.1 Hz, 2H, 2xCH_{Ar}), 7.36 (d, ³J_{HH} = 9.0 Hz, 2H, 2xCH_{Ar}), 5.15 (dd, ³J_{HH} = 9.2 Hz, ³J_{HH} = 6.4 Hz, 1H, CHN), 4.51 (bs, 1H, NH), 4.14 (dd, ³J_{HH} = 10.4 Hz, ³J_{HH} = 8.0 Hz, 1H, CHCO), 3.75 (s, 3H, OCH₃), 3.71 (s, 3H, OCH₃), 3.22 (ddd, ²J_{HH} = 12.8 Hz, ³J_{HH} = 8.0 Hz, ³J_{HH} = 6.4 Hz, 1H, CH_AH_B), 1.98 (ddd, ²J_{HH} = 12.8 Hz, ³J_{HH} = 10.4 Hz, ³J_{HH} = 9.2 Hz, 1H, CH_AH_B) ppm.

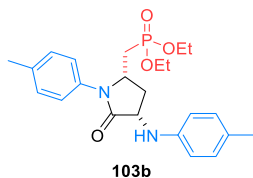
¹³C {¹H} NMR (101 MHz, CDCl₃) δ 173.3 (C=O), 157.3 (C_{quat}), 153.1 (C_{quat}), 141.56 (C_{quat}), 140.0 (C_{quat}), 130.2 (C_{quat}), 128.9 (2xCH_{Ar}), 128.1 (CH_{Ar}), 127.1 (2xCH_{Ar}), 125.1 (2xCH_{Ar}), 115.4 (2xCH_{Ar}), 115.0 (2xCH_{Ar}), 114.0 (2xCH_{Ar}), 61.4 (CHCO), 56.7 (CHN), 55.9 (OCH₃), 55.4 (OCH₃), 40.8 (CH₂) ppm.

FTIR ν_{max} 3307 (N-H_{st}), 1704 (C=O_{st}) cm⁻¹.

HRMS (ESI-TOF) m/z calcd. for $C_{24}H_{25}N_2O_3$ $[M+H]^+$ 389.1865, found 389.1861.

Additionally, the synthesis of an enantioenriched sample of compound **(3S,5S)-103a** was carried out in a one-pot process starting from *p*-anisidine (25 mg, 200 μ mol), benzaldehyde (10 μ L, 100 μ mol), ethyl pyruvate (34 μ L, 300 μ mol) and BINOL-derived chiral phosphoric acid **(R)-XXIII** (9 mg, 10 μ mol). The mixture was stirred in diethyl ether (2 mL) at room temperature for 18 hours, and the reaction was monitored by 1H NMR until the disappearance of the starting materials. Once γ -lactam **(S)-84a** was formed, 10 mL of methanol and 11 mg of 10% palladium on carbon (10 μ mol Pd) were added, and the reaction was stirred for 10 hours under hydrogen pressure (80 psi) at room temperature. The reaction mixture was filtered, and the retained solid was extracted with dichloromethane (2 \times 5 mL). The resulting solution was concentrated under reduced pressure and the crude residue was purified by crystallization from methanol to afford 37 mg (95%) of pure **(3S,5S)-103a** as a single diastereoisomer. Ee (90%) was determined by HPLC analysis (Chiracel-IC, Heptane/DCM/AcOEt 60:30:10, 1 mL/min). Retention time (min): 15.8 (major) and 20.5 (minor). Physical and spectroscopy data described above.

Diethyl (((2S*,4S*)-5-oxo-1-(*p*-tolyl)-4-(*p*-tolylamino)pyrrolidin-2-yl)methyl) phosphonate (103b).



The general procedure was followed, using γ -lactam **90a** (214 mg, 0.5 mmol) to afford 199 mg (93%) of **103b** as a white solid.

Mp (MeOH): 119 - 120 $^{\circ}C$.

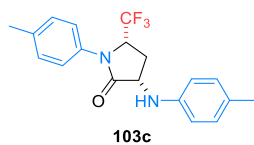
1H NMR (400 MHz, $CDCl_3$) δ 7.24 (d, $^3J_{HH} = 8.5$ Hz, 2H, $2xCH_{Ar}$), 7.19 (d, $^3J_{HH} = 8.5$ Hz, 2H, $2xCH_{Ar}$), 7.03 (d, $^3J_{HH} = 8.3$ Hz, 2H, $2xCH_{Ar}$), 6.64 (d, $^3J_{HH} = 8.3$ Hz, 2H, $2xCH_{Ar}$), 4.50 (m, 1H, CHN), 4.17 - 4.02 (m, 5H, $2xCH_2$ phosphonate+CHCO), 3.25 (ddd, $^2J_{HH} = 13.6$ Hz, $^3J_{HH} = 7.8, 6.4$ Hz, 1H, CH_AH_B lactam), 2.34 (m, 1H, CH_AH_B lactam), 2.36 (s, 3H, CH_3 tolyl), 2.26 (s, 3H, CH_3 tolyl), 1.84 (m, 1H, CH_ACH_BP), 1.66 (m, 1H, CH_ACH_BP), 1.31 (t, $^4J_{PH} = 7.1$ Hz, 3H, CH_3 phosphonate), 1.30 (t, $^4J_{PH} = 7.1$ Hz, 3H, CH_3 phosphonate) ppm.

^{13}C $\{^1H\}$ NMR (101 MHz, $CDCl_3$) δ 172.6 (d, $^4J_{PC} = 1.1$ Hz, C=O), 145.2 (C_{quat}), 136.9 (d, $^4J_{PC} = 1.2$ Hz, C_{quat}), 133.5 (C_{quat}), 130.1 ($2xCH_{Ar}$), 129.9 ($2xCH_{Ar}$), 127.9 (C_{quat}), 124.7 ($2xCH_{Ar}$), 114.0 ($2xCH_{Ar}$), 62.1 (d, $^2J_{PC} = 6.4$ Hz, CH_2 phosphonate), 62.0 (d, $^2J_{PC} = 6.7$ Hz, CH_2 phosphonate), 55.8 ($CHCO$), 52.3 (d, $^2J_{PC} = 2.4$ Hz, CHN), 37.4 (CH_2 lactam), 31.3 (d, $^1J_{PC} = 139.3$ Hz, CH_2P), 21.2 (CH_3 tolyl), 20.5 (CH_3 tolyl), 16.6 (CH_3 phosphonate), 16.5 (CH_3 phosphonate) ppm.

^{31}P NMR (162 MHz, $CDCl_3$) δ 26.7 ppm.

FTIR ν_{max} 3357 (N-H_{st}), 1701 (C=O_{st}), 1269 (P=O_{st}), 1055 (P-O-C_{st}). cm^{-1} .

HRMS (ESI-TOF) m/z calcd. for $C_{23}H_{32}N_2O_4P$ $[M+H]^+$ 431.2100, found 431.2101.

(3*S,5*S**)-1-(*p*-Tolyl)-3-(*p*-tolylamino)-5-(trifluoromethyl) pyrrolidin-2-one (103c).**

The general procedure was followed, using γ -lactam **90e** (173 mg, 0.5 mmol) to afford 154 mg (89%) of **103c** as a white solid.

Mp (MeOH): 183 - 184 °C.

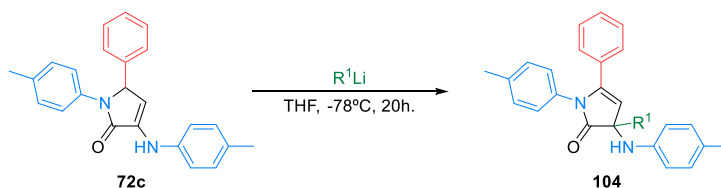
¹H NMR (400 MHz, CDCl₃) δ 7.25 (d, ³*J*_{HH} = 8.5 Hz, 2H, 2xCH_{Ar}), 7.19 (d, ³*J*_{HH} = 8.5 Hz, 2H, 2xCH_{Ar}), 7.04 (d, ³*J*_{HH} = 8.5 Hz, 2H, 2xCH_{Ar}), 6.61 (d, ³*J*_{HH} = 8.5 Hz, 2H, 2xCH_{Ar}), 4.62 (m, 1H, CHN), 4.16 (t, ³*J*_{HH} = 8.5 Hz, 1H, CHCO), 3.05 (ddd, ²*J*_{HH} = 13.6 Hz, ³*J*_{HH} = 8.8, 7.9 Hz, 1H, CH_ACH_B), 2.37 (s, 3H, CH₃ tolyl), 2.27 (s, 3H, CH₃ tolyl), 2.13 (ddd, ³*J*_{HH} = 13.6 Hz, ³*J*_{HH} = 8.3, 7.4 Hz, 1H, CH_ACH_B) ppm.

¹³C {¹H} NMR (101 MHz, CDCl₃) δ 173.3 (C=O), 144.57 (C_{quat}), 138.2 (C_{quat}), 133.7 (C_{quat}), 130.1 (2xCH_{Ar}), 130.0 (2xCH_{Ar}), 128.4 (C_{quat}), 125.9 (2xCH_{Ar}), 124.0 (q, ¹*J*_{FC} = 197.1 Hz, CF₃), 114.0 (2xCH_{Ar}), 58.8 (q, ²*J*_{FC} = 32.3 Hz, CHN), 54.1 (CHCO), 29.1 (CH₂), 21.3 (CH₃ tolyl), 20.6 (CH₃ tolyl) ppm.

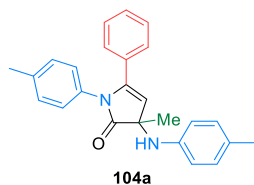
¹⁹F NMR (282 MHz, CDCl₃) δ -74.3 ppm.

FTIR ν_{max} 3309 (N-H_{st}), 1704 (C=O_{st}), 1140 (C-F_{st}) cm⁻¹.

HRMS (ESI-TOF) *m/z* calcd. for C₁₉H₂₀F₃N₂O [M+H]⁺ 349.1527, found 349.1532.

General procedure for the nucleophilic addition of organolithium reagents to γ -lactam72c. Synthesis of γ -lactam derivatives 104.

A 1.6 M solution of the corresponding organolithium reagent in hexanes (2 mmol) was added dropwise to a solution of γ -lactam **72c** (354 mg, 1 mmol) in dry THF (5 ml) at -78°C under N_2 atmosphere. The reaction was warmed to room temperature overnight, quenched with a 0.5 M aqueous solution of HCl (5 mL), and extracted with dichloromethane (3×10 mL). The combined organic layers were dried over anhydrous MgSO_4 and concentrated under reduced pressure. The crude residue was purified by flash column chromatography (Hexanes/AcOEt) to afford pure γ -lactams **104**.

3-Methyl-5-phenyl-1-(*p*-tolyl)-3-(*p*-tolylamino)-1,3-dihydro-2H-pyrrol-2-one (**104a**).

The general procedure was followed using a 1.6 M solution of methyllithium in hexanes (1.25 ml, 2 mmol). The crude residue was purified by flash column chromatography (Hexanes/AcOEt 80:20), affording 288 mg (78%) of **104a** as a yellow solid.

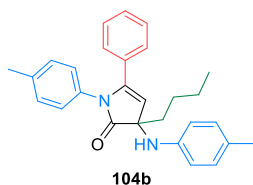
Mp (Et_2O): $183 - 185^\circ\text{C}$.

$^1\text{H NMR}$ (400 MHz, CDCl_3) δ 7.31 - 7.25 (m, 4H, $4 \times \text{CH}_{\text{Ar}}$), 7.24 - 7.20 (m, 2H, $2 \times \text{CH}_{\text{Ar}}$), 7.11 (d, $^3J_{\text{HH}} = 8.1$ Hz, 2H, $2 \times \text{CH}_{\text{Ar}}$), 7.03 - 6.95 (m, 6H, $5 \times \text{CH}_{\text{Ar}} + \text{NH}$), 5.63 (s, 1H, =CH), 2.33 (s, 3H, CH_3 tolyl), 2.28 (s, 3H, CH_3 tolyl), 1.45 (s, 3H, CH_3) ppm.

$^{13}\text{C } \{^1\text{H}\}$ NMR (101 MHz, CDCl_3) δ 175.4 (C_{quat}), 165.6 ($\text{C}=\text{O}$), 148.9 (C_{quat}), 137.1 (C_{quat}), 135.6 (C_{quat}), 133.1 (C_{quat}), 131.9 (C_{quat}), 130.0 (CH_{Ar}), 129.6 ($2 \times \text{CH}_{\text{Ar}}$), 129.4 ($2 \times \text{CH}_{\text{Ar}}$), 128.6 ($2 \times \text{CH}_{\text{Ar}}$), 128.3 ($2 \times \text{CH}_{\text{Ar}}$), 127.3 ($2 \times \text{CH}_{\text{Ar}}$), 121.8 ($2 \times \text{CH}_{\text{Ar}}$), 94.8 (=CH), 92.8 (C_{quat}), 25.3 (CH_3), 21.1 (CH_3 tolyl), 21.1 (CH_3 tolyl) ppm.

FTIR ν_{max} 3403 (N-H_{st}), 3053 (=C-H_{st}), 1703 ($\text{C}=\text{O}$ _{st}), 1674 ($\text{C}=\text{CH}$ _{st}) cm^{-1} .

HRMS (ESI-TOF) m/z calcd. for $\text{C}_{25}\text{H}_{25}\text{N}_2\text{O}$ $[\text{M}+\text{H}]^+$ 369.1967, found 369.1972.

3-Butyl-5-phenyl-1-(*p*-tolyl)-3-(*p*-tolylamino)-1,3-dihydro-2*H*-pyrrol-2-one (104b).

The general procedure was followed using a 1.6 M solution of *n*-butyllithium in hexanes (1.25 ml, 2 mmol). The crude residue was purified by flash column chromatography (Hexanes/AcOEt 80:20), affording 300 mg (73%) of **104b** as an orange oil.

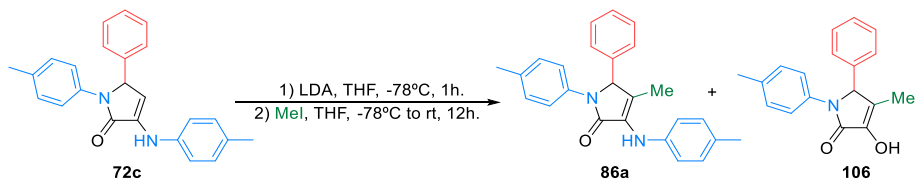
¹H NMR (400 MHz, CDCl₃) δ 7.34 - 7.16 (m, 6H, 6xCH_{Ar}), 7.11 (d, ³J_{HH} = 8.3 Hz, 2H, 2xCH_{Ar}), 7.05 - 6.95 (m, 6H, 5xCH_{Ar} + NH), 5.61 (s, 1H, =CH), 2.33 (s, 3H, CH₃ tolyl), 2.29 (s, 3H, CH₃ tolyl), 2.12 (m, 1H, CH_AH_B Bu), 1.85 (m, 1H, CH_AH_B Bu), 1.36 - 1.00 (m, 4H, 2xCH₂), 0.76 (t, ³J_{HH} = 6.9 Hz, 3H, CH₃ Bu) ppm.

¹³C {¹H} NMR (101 MHz, CDCl₃) δ 175.0 (C_{quat}), 166.6 (C=O), 148.6 (C_{quat}), 136.2 (C_{quat}), 135.2 (C_{quat}), 133.0 (C_{quat}), 131.9 (C_{quat}), 129.9 (CH_{Ar}), 129.5 (2xCH_{Ar}), 129.2 (2xCH_{Ar}), 128.6 (2xCH_{Ar}), 128.2 (2xCH_{Ar}), 127.0 (2xCH_{Ar}), 121.9 (2xCH_{Ar}), 95.5 (=CH), 95.0 (C_{quat}), 38.0 (CH₂), 25.0 (CH₂), 22.6 (CH₂), 21.1 (CH₃ tolyl), 21.0 (CH₃ tolyl), 14.1 (CH₃ Bu) ppm.

FTIR ν_{max} 3391 (N-H_{st}), 3047 (=C-H_{st}), 1693 (C=O_{st}), 1670 (C=CH_{st}) cm⁻¹.

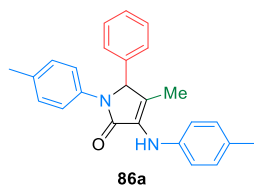
HRMS (ESI-TOF) *m/z* calcd. for C₂₈H₃₁N₂O [M+H]⁺ 411.2436, found 411.2442.

General procedure for the functionalization of γ -lactam **72c** with methyl iodide.



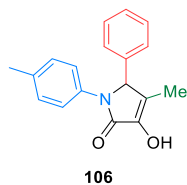
A solution of γ -lactam **72c** (354 mg, 1 mmol) in THF (3 mL) was added dropwise to a solution of freshly prepared LDA (1.2 mmol) in THF (2 mL) at -78°C under N_2 atmosphere. After 1 hour, an excess of methyl iodide (93 μl , 1.5 mmol) was added dropwise and the solution was stirred overnight at -78°C . The reaction was then quenched with a 0.5 M aqueous solution of HCl (10 mL) and the mixture was extracted with dichloromethane (3×10 mL). The combined organic layers were washed with water (2×10 mL), dried over MgSO_4 and concentrated under vacuum. The crude residue was purified by flash column chromatography (Hexanes/ AcOEt 80:20) to afford a mixture of γ -lactams **86a** and **106**.

4-Methyl-5-phenyl-1-(*p*-tolyl)-3-(*p*-tolylamino)-1,5-dihydro-2H-pyrrol-2-one (**86a**).



According to the procedure 188 mg (51%) of **86a** were obtained as a white solid. Physical and spectroscopic data are in agreement with the data described above (See Chapter 1).

3-Hydroxy-4-methyl-5-phenyl-1-(*p*-tolyl)-1,5-dihydro-2H-pyrrol-2-one (**106**).



oil.

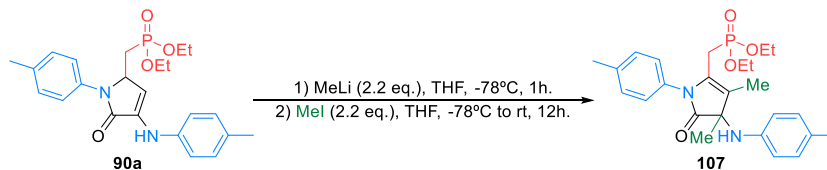
$^1\text{H NMR}$ (400 MHz, CDCl_3) δ 7.34 (d, $^3J_{\text{HH}} = 8.5$ Hz, 2H, $2 \times \text{CH}_{\text{Ar}}$), 7.33 - 7.24 (m, 3H, $3 \times \text{CH}_{\text{Ar}}$), 7.16 (d, $^3J_{\text{HH}} = 8.3$ Hz, 2H, $2 \times \text{CH}_{\text{Ar}}$), 7.04 (d, $^3J_{\text{HH}} = 8.5$ Hz, 2H, $2 \times \text{CH}_{\text{Ar}}$), 6.15 (s, 1H, OH), 5.26 (s, 1H, CHN), 2.23 (s, 3H, CH_3 tolyl), 1.73 (s, 3H, CH_3) ppm.

$^{13}\text{C}\{^1\text{H}\}$ NMR (101 MHz, CDCl_3) δ 166.9 (C=O), 140.7 (C_{quat}), 136.2 (C_{quat}), 134.8 (C_{quat}), 134.6 (C_{quat}), 129.6 ($2 \times \text{CH}_{\text{Ar}}$), 129.1 ($2 \times \text{CH}_{\text{Ar}}$), 128.5 (CH_{Ar}), 127.3 ($2 \times \text{CH}_{\text{Ar}}$), 122.1 (C_{quat}), 121.3 ($2 \times \text{CH}_{\text{Ar}}$), 66.0 (CHN), 21.0 (CH_3 tolyl), 9.5 (CH_3) ppm.

FTIR ν_{max} 3501 (O-H_{st}), 1701 (C=O_{st}), 1681 (C=C_{st}) cm^{-1} .

HRMS (ESI-TOF) m/z calcd. for $\text{C}_{18}\text{H}_{18}\text{N}_2\text{O}$ $[\text{M}+\text{H}]^+$ 280.1338, found 280.1343.

Synthesis of diethyl ((3,4-dimethyl-5-oxo-1-(*p*-tolyl)-4-(*p*-tolylamino)-4,5-dihydro-1*H*-pyrrol-2-yl)methyl) phosphonate **107**.



A 1.6 M solution of methyllithium in hexanes (700 μ L, 1.1 mmol) was added dropwise to a solution of γ -lactam **90a** (214 mg, 0.5 mmol) in THF (3 mL) at -78 $^{\circ}$ C under N_2 atmosphere. After 1 hour at -78 $^{\circ}$ C a solution of methyl iodide (70 μ L, 1.1 mmol) in THF (1 mL) was slowly added and the reaction was warmed to room temperature overnight. Water (5mL) was then added and the resulting mixture was extracted with AcOEt (3 \times 10mL). The combined organic layers were dried over anhydrous $MgSO_4$ and concentrated under reduced pressure. The crude residue was purified by flash column chromatography (Hexanes/AcOEt 70:30), affording 196 mg (87%) of **107** as a yellow solid.

Mp (Et_2O): 144 - 145 $^{\circ}$ C.

1H NMR (400 MHz, $CDCl_3$) δ 7.21 (d, $^3J_{HH} = 8.2$ Hz, 2H, $2 \times CH_{Ar}$), 7.09 (d, $^3J_{HH} = 8.2$ Hz, 2H, $2 \times CH_{Ar}$), 6.92 (d, $^3J_{HH} = 8.5$ Hz, 2H, $2 \times CH_{Ar}$), 6.52 (d, $^3J_{HH} = 8.5$ Hz, 2H, $2 \times CH_{Ar}$), 4.09 - 3.92 (m, 4H, $2 \times CH_2$ phosphonate), 3.92 - 3.81 (m, 2H, CH_2P), 2.36 (s, 3H, CH_3 tolyl), 2.20 (s, 3H, CH_3 tolyl), 1.80 (d, $^5J_{PH} = 6.1$ Hz, 3H, $=CCH_3$), 1.50 (s, 3H, CH_3), 1.24 (t, $^3J_{HH} = 7.1$ Hz, 2H, CH_3 phosphonate), 1.21 (t, $^3J_{HH} = 7.1$ Hz, 3H, CH_3 phosphonate) ppm.

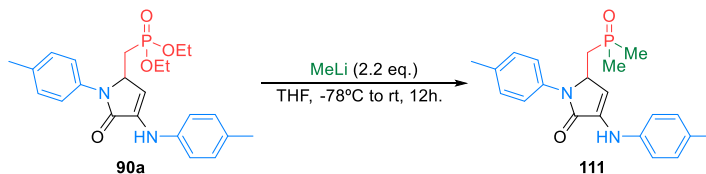
$^{13}C \{^1H\}$ NMR (101 MHz, $CDCl_3$) δ 179.8 (C=O), 143.8 (C_{quat}), 138.0 (C_{quat}), 132.2 (C_{quat}), 129.9 ($2 \times CH_{Ar}$), 129.7 ($2 \times CH_{Ar}$), 128.3 ($2 \times CH_{Ar}$), 128.2 (C_{quat}), 127.6 (d, $^2J_{PC} = 13.6$ Hz, $C=CN$), 120.5 (d, $^3J_{PC} = 12.4$ Hz, $C=CN$), 115.0 ($2 \times CH_{Ar}$), 64.1 (d, $^4J_{PC} = 3.4$ Hz, CNH), 62.2 (d, $^2J_{PC} = 6.7$ Hz, CH_2 phosphonate), 62.0 (d, $^2J_{PC} = 6.7$ Hz, CH_2 phosphonate), 25.1 (d, $^5J_{PC} = 5.0$, CH_3), 23.6 (d, $^1J_{PC} = 143.1$ Hz, CH_2P), 21.6 (CH_3 tolyl), 20.6 (CH_3 tolyl), 16.6 (t, $^3J_{PC} = 7.4$ Hz, CH_3 phosphonate), 16.5 (t, $^3J_{PC} = 7.7$ Hz, CH_3 phosphonate), 8.9 (d, $^4J_{PC} = 3.6$ Hz, CH_3) ppm.

^{31}P NMR (162 MHz, $CDCl_3$) δ 23.7 ppm.

FTIR ν_{max} 3411 (N-H $_{st}$), 1723 (C=O $_{st}$), 1672 (C=C $_{st}$), 1254 (P=O $_{st}$), 963 (P-O-C $_{st}$) cm^{-1} .

HRMS (ESI-TOF) m/z calcd. for $C_{25}H_{33}KN_2O_4P$ $[M+K]^+$ 495.1815, found 495.1817.

Synthesis of 5-((dimethylphosphoryl)methyl)-1-(*p*-tolyl)-3-(*p*-tolylamino)-1,5-dihydro-2*H*-pyrrol-2-one **111**.



A 1.6 M solution of methyllithium in hexanes (700 μL , 1.1 mmol) was added dropwise to a solution of γ -lactam **90a** (214 mg, 0.5 mmol) in THF (3 mL) at -78°C under N_2 atmosphere. The reaction was warmed to room temperature overnight. Water (5 mL) was then added and the resulting mixture was extracted with AcOEt ($3 \times 10\text{mL}$). The combined organic layers were dried over anhydrous MgSO_4 and concentrated under reduced pressure. The crude residue was purified by flash column chromatography (Hexanes/AcOEt 70:30), affording 280 mg (55%) of **111** as a white solid.

Mp (Et_2O): $185 - 187^\circ\text{C}$ (dec.).

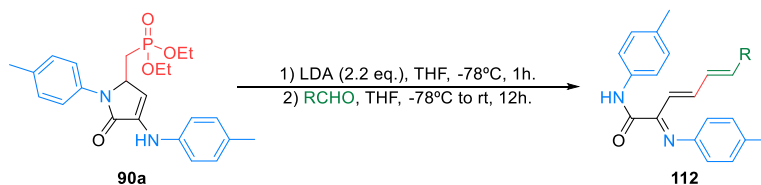
^1H NMR (400 MHz, CDCl_3) δ 7.36 (d, $^3J_{\text{HH}} = 8.4$ Hz, 2H, $2 \times \text{CH}_{\text{Ar}}$), 7.26 (m, 2H, $2 \times \text{CH}_{\text{Ar}}$), 7.12 (d, $^3J_{\text{HH}} = 8.4$ Hz, 2H, $2 \times \text{CH}_{\text{Ar}}$), 7.01 (d, $^3J_{\text{HH}} = 8.4$ Hz, 2H, $2 \times \text{CH}_{\text{Ar}}$), 6.52 (s, 1H, NH), 6.40 (d, $^3J_{\text{HH}} = 2.6$ Hz, 1H, =CH), 5.07 (m, 1H, CHN), 2.37 (s, 3H, CH_3 tolyl), 2.30 (s, 3H, CH_3 tolyl), 1.69 (m, 1H, CH_AH_B), 1.56 (d, $^2J_{\text{PH}} = 4.0$ Hz, 3H, PCH_3), 1.53 (d, $^2J_{\text{PH}} = 4.0$ Hz, 3H, PCH_3), 1.48 (m, 1H, CH_AH_B) ppm.

^{13}C { ^1H } NMR (101 MHz, CDCl_3) δ 165.9 (C=O), 138.8 (C_{quat}), 135.9 (C_{quat}), 133.5 (C_{quat}), 133.4 (C_{quat}), 131.0 (C_{quat}), 130.2 ($2 \times \text{CH}_{\text{Ar}}$), 130.1 ($2 \times \text{CH}_{\text{Ar}}$), 122.9 ($2 \times \text{CH}_{\text{Ar}}$), 117.0 ($2 \times \text{CH}_{\text{Ar}}$), 105.5 (=CH), 55.3 (CHN), 35.4 (d, $^1J_{\text{PC}} = 67.0$ Hz, CH_2P), 21.1 (CH_3 tolyl), 20.8 (CH_3 tolyl), 18.5 (d, $^1J_{\text{PC}} = 69.4$ Hz, PCH_3), 17.6 (d, $^1J_{\text{PC}} = 69.2$ Hz, PCH_3) ppm.

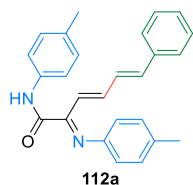
^{31}P NMR (162 MHz, CDCl_3) δ 39.1 ppm.

FTIR ν_{max} 3445 (N-H_{st}), 1725 (C=O_{st}), 1666 (C=CH_{st}), 1159 (P=O_{st}) cm^{-1} .

HRMS (ESI-TOF) m/z calcd. for $\text{C}_{21}\text{H}_{26}\text{N}_2\text{O}_2\text{P}$ [$\text{M}+\text{H}$]⁺ 369.1732, found 369.1728.

General procedure for the Horner-Wadsworth-Emmons reaction of γ -lactam **90a**.

A solution of γ -lactam **90a** (214 mg, 0.5 mmol) in THF (2 mL) was added dropwise to a solution of freshly prepared LDA (1.2 mmol) in THF (2 ml) at -78°C under N_2 atmosphere. The mixture was stirred for 1 hour at -78°C and, then, the corresponding aldehyde (0.75 mmol) was added. The reaction was warmed to room temperature overnight and was then quenched with water (10 mL) and extracted with dichloromethane (3×10 mL). The combined organic layers were dried over anhydrous MgSO_4 and concentrated under reduced pressure. The crude residue was purified by flash column chromatography (Hexanes /AcOEt 90:10) to afford pure substrates **112**.

(2E,3E,5E)-6-phenyl-N-(p-tolyl)-2-(p-tolylimino)hexa-3,5-dienamide (112a).

The general procedure was followed using benzaldehyde (76 μL , 0.75 mmol) to afford 172 mg (90%) of **112a** as a yellow solid.

Mp (Et_2O): $158 - 159^\circ\text{C}$.

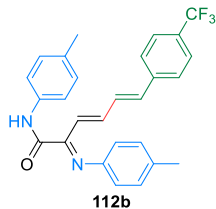
$^1\text{H NMR}$ (400 MHz, CDCl_3) δ 9.47 (s, 1H, NH), 8.02 (dd, $^3J_{\text{HH}} = 15.5, 10.7$ Hz, 1H, Ph-CH=CH), 7.61 (d, $^3J_{\text{HH}} = 8.0$ Hz, 2H, $2 \times \text{CH}_{\text{Ar}}$), 7.42 (d, $^3J_{\text{HH}} = 7.4$ Hz, 2H, $2 \times \text{CH}_{\text{Ar}}$), 7.37 - 7.27 (m, 3H, $3 \times \text{CH}_{\text{Ar}}$), 7.23 (d, $^3J_{\text{HH}} = 7.8$ Hz, 2H, $2 \times \text{CH}_{\text{Ar}}$), 7.19 (d, $^3J_{\text{HH}} = 8.0$ Hz, 2H, $2 \times \text{CH}_{\text{Ar}}$), 6.84 (d, $^3J_{\text{HH}} = 7.8$ Hz, 2H, $2 \times \text{CH}_{\text{Ar}}$), 6.94 - 6.69 (m, 2H, $2 \times \text{CH}=\text{CH}$), 6.29 (d, $^3J_{\text{HH}} = 15.5$ Hz, 1H, Ph-CH=CH), 2.40 (s, 3H, CH_3 tolyl), 2.36 (s, 3H, CH_3 tolyl) ppm.

^{13}C { ^1H } NMR (101 MHz, CDCl_3) δ 161.8 (C=O), 157.7 (C=N), 146.0 (C_{quat}), 144.6 (=CH), 139.6 (=CH), 136.5 (C_{quat}), 135.1 (C_{quat}), 134.9 (C_{quat}), 134.0 (C_{quat}), 129.8 ($2 \times \text{CH}_{\text{Ar}}$), 129.6 ($2 \times \text{CH}_{\text{Ar}}$), 129.0 (=CH), 128.8 ($3 \times \text{CH}_{\text{Ar}}$), 127.1 ($2 \times \text{CH}_{\text{Ar}}$), 120.7 (=CH), 120.4 ($2 \times \text{CH}_{\text{Ar}}$), 119.8 ($2 \times \text{CH}_{\text{Ar}}$), 21.08 (CH_3 tolyl), 21.0 (CH_3 tolyl) ppm.

FTIR ν_{max} 3411 (N-H_{st}), 1688 (C=O/C=N_{st}), 1600 (C=CH_{st}), 1590 (C=CH_{st}), 1517 (C=CH_{st}) cm^{-1} .

HRMS (ESI-TOF) m/z calcd. for $\text{C}_{26}\text{H}_{25}\text{N}_2\text{O}$ [M+H]⁺ 381.1967, found 381.1972.

(2*E*,3*E*,5*E*)-*N*-(*p*-tolyl)-2-(*p*-tolylimino)-6-(4-(trifluoromethyl)phenyl)hexa-3,5-dienamide (112b**).**



The general procedure was followed using *p*-(trifluoromethyl) benzaldehyde (102 μ L, 0.75 mmol) to afford 204 mg (91%) of **112b** as an orange solid.

Mp (Et₂O): 114 - 115 °C.

¹H NMR (400 MHz, CDCl₃) δ 9.48 (s, 1H, NH), 8.02 (dd, ³*J*_{HH} = 15.6, 10.0 Hz, 1H, Ar-CH=CH), 7.61 (d, ³*J*_{HH} = 8.2 Hz, 2H, 2xCH_{Ar}), 7.57 (d, ³*J*_{HH} = 8.4 Hz, 2H, 2xCH_{Ar}), 7.49 (d, ³*J*_{HH} = 8.4 Hz, 2H, 2xCH_{Ar}), 7.24 (d, ³*J*_{HH} = 8.0 Hz, 2H, 2xCH_{Ar}), 7.20 (d, ³*J*_{HH} = 8.0 Hz, 2H, 2xCH_{Ar}), 6.85 (d, ³*J*_{HH} = 8.2 Hz, 2H, 2xCH_{Ar}), 6.83 (m, 2H, 2x=CH), 6.34 (d, ³*J*_{HH} = 15.6 Hz, 1H, Ar-CH=CH), 2.41 (s, 3H, CH₃ tolyl), 2.36 (s, 3H, CH₃ tolyl) ppm.

¹³C {¹H} NMR (101 MHz, CDCl₃) δ 161.7 (C=O), 157.4 (C=N), 145.9 (C_{quat}), 143.7 (=CH), 139.9 (d, ⁵*J*_{FC} = 1.6 Hz, C_{quat}), 137.5 (=CH), 135.2 (C_{quat}), 135.1 (C_{quat}), 134.2 (C_{quat}), 131.4 (=CH), 130.3 (q, ²*J*_{FC} = 32.4 Hz, C_{quat}), 129.9 (2xCH_{Ar}), 129.7 (2xCH_{Ar}), 127.2 (2xCH_{Ar}), 125.8 (q, ³*J*_{FC} = 3.8 Hz, 2xCH_{Ar}), 124.2 (q, ¹*J*_{FC} = 271.9 Hz, CF₃), 122.2 (=CH), 120.5 (2xCH_{Ar}), 119.9 (2xCH_{Ar}), 21.1 (CH₃ tolyl), 21.0 (CH₃ tolyl) ppm.

¹⁹F NMR (282 MHz, CDCl₃) δ -63.1 ppm.

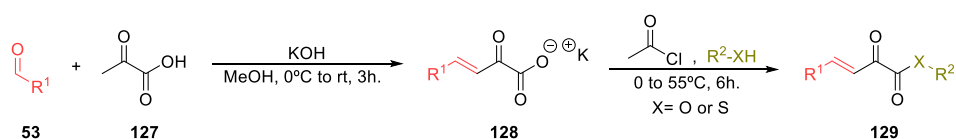
FTIR ν_{max} 3335 (N-H_{st}), 1732 (C=O_{st} ester), 1688 (C=O_{st} amide), 1612 (C=CH_{st}), 1587 (C=CH_{st}), 1524 (C=CH_{st}), 1151 (C-F_{st}) cm⁻¹.

HRMS (ESI-TOF) *m/z* calcd. for C₂₇H₂₄F₃N₂O [M+H]⁺ 449.1841, found 449.1848.

Chapter 6. Stereoselective formal [3+3] reaction of 3-amino γ -lactam derivatives.

General procedure for the preparation of β,γ -unsaturated α -ketoesters **129**.

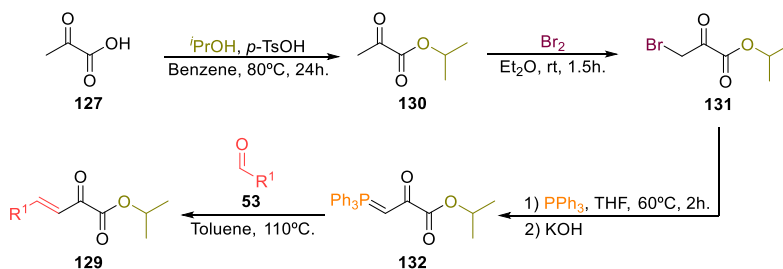
Method A. Aldol Condensation.²⁴³



Step 1. Aldol condensation. To a solution of corresponding the aldehyde **53** (60 mmol) in methanol (15 mL), pyruvic acid **127** (4.2 mL, 60 mmol) was added, and the mixture was cooled to 0°C. A solution of KOH (5.05 g, 90 mmol) in methanol (15 mL) was added dropwise at 0°C and, after the addition of two thirds of potassium hydroxide solution, the reaction was warmed to room temperature. Then, the remaining base was added. The reaction mixture was stirred at room temperature for 3 hours, and the precipitate was filtered and washed with chilled methanol (50 mL) and diethyl ether (75 mL) to afford the corresponding potassium salt **128** as a solid.

Step 2. Esterification. To the corresponding alcohol (30 mL) at 0°C, acetyl chloride (7 mL) was added dropwise until the generation of HCl stopped. Then, 10 mmol of the corresponding potassium salt **128** was added at 0°C. The reaction mixture was warmed to room temperature, stirred for 2 hours and then refluxed (heating plate) for 6 additional hours. The volatiles were removed under reduced pressure and the crude residue was dissolved in water (20 mL) and extracted with dichloromethane (2×20 mL). The combined organic layers were washed with an aqueous saturated solution of NaHCO₃ (2×15 mL) and water (20 mL). The organic layer was dried over anhydrous MgSO₄, and distilled off at reduced pressure. The crude residue was crystallized from the corresponding alcohol (at -5°C) or purified by column chromatography (Hexanes/AcOEt) to provide the corresponding pure β,γ -unsaturated α -ketoesters **129**.

²⁴³ Liu, W. B.; Okamoto, N.; Alexy, E. J.; Hong, A. Y.; Tran, K.; Stoltz, B. M. *J. Am. Chem. Soc.* **2016**, *138*, 5234-5237.

Method B. Wittig olefination.

Step 1. Synthesis of *iso*-propyl-3-bromo-2-oxopropanoate 131. Following a modified literature procedure,²⁴⁴ in a 250 mL flask, fitted with a reflux condenser and a Dean-Stark apparatus, pyruvic acid (10.5 ml, 150 mmol), 2-propanol (70 ml), *p*-toluenesulfonic acid (2.85 g, 15 mmol), and benzene (100 mL) were mixed and refluxed on a heating plate for 24 hours. Upon cooling, the reaction mixture was quenched with a 10% aqueous solution of Na₂CO₃ until neutral. The organic layer was separated and washed with a 10% aqueous solution of Na₂CO₃ (20 mL) and brine (20 mL). The organic layer was dried over anhydrous MgSO₄, concentrated under reduced pressure and the resulting crude oil was distilled under reduced pressure using an oil pump (1 mmHg) at 30 °C to provide 16.98 g (87%) of *iso*-propyl-2-oxopropanoate **130** as a clear colorless liquid.

iso-propyl-2-oxopropanoate **130** (15.62 g, 120 mmol) was dissolved in diethyl ether (100 mL). Bromine (6.20 mL, 120 mmol) was then added dropwise at room temperature through a septum with a syringe. The reaction was stirred for 1.5 hours and monitored by ¹H NMR [(*iso*-propyl pyruvate: 2.42 ppm (CH₃); *iso*-propyl-3-bromo-2-oxopropanoate **131**: 4.30 ppm (CH₂-Br); *iso*-propyl-3,3-dibromo-2-oxopropanoate: 6.71 ppm (CH-Br₂). If bromine is not slowly added or the temperature of the flask increases during the procedure, a higher amount of the dihalogenated product is formed]. Once the reaction is finished, the volatiles were distilled off under reduced pressure, and the crude residue was purified by distillation using an oil pump (1 mmHg) at 50 °C to provide 22.21 g (89%) of *iso*-propyl-3-bromo-2-oxopropanoate **131** as a clear colorless oil.

¹H NMR (400 MHz, CDCl₃) δ 5.16 (hept, ³J_{HH} = 6.3 Hz, 1H, CH ^{*i*}Pr), 4.30 (s, 2H, CH₂), 1.34 (d, ³J_{HH} = 6.3 Hz, 6H, CH₃ ^{*i*}Pr) ppm.

¹³C {¹H} NMR (101 MHz, CDCl₃) δ 185.1 (C=O), 159.0 (C=O), 71.8 (CH ^{*i*}Pr), 31.0 (CH₂), 21.6 (2xCH₃ ^{*i*}Pr) ppm.

FTIR ν_{max} 1750 (C=O_{st}), 1725 (C=O_{st}), 1048 (C-Br_{st}). cm⁻¹.

HRMS (ESI-TOF) *m/z* calcd. for C₆H₉BrO₃ [M+H]⁺ 209.0390, found 209.0393.

²⁴⁴ Zhao, B.; Loh, T. P. *Org. Lett.* **2013**, *15*, 2914-2917.

Step 2. Preparation of phosphorus ylide **132.**²⁴⁵ *iso*-propyl-3-bromo-2-oxopropanoate **131** (20.91 g, 100 mmol) was dissolved in THF (120 ml) and PPh₃ (26.30 g, 100 mmol) was added at room temperature. The reaction mixture was heated at 60 °C (heating plate) for 2 hours, and the solvent was removed under reduced pressure. The crude residue was dissolved in dichloromethane (120 mL) and water (180 mL) and a 2 M aqueous solution of KOH (50 mL, 110 mmol) were then added. After stirring vigorously for 30 min at room temperature, the organic layer was collected. The aqueous layer was extracted with dichloromethane (3×40 mL) and the combined organic extracts were washed with brine (40 mL), dried over anhydrous MgSO₄, and concentrated under vacuum to provide a thick oil. Upon addition of Et₂O (150 mL), followed by vigorous stirring, a precipitate was formed. The solid was collected by filtration and washed with Et₂O to provide 30.45 g (78%) of phosphorus ylide **132** as a yellow solid.

Mp (MeOH): 163 - 165 °C (dec.).

¹H NMR (400 MHz, CDCl₃) δ 7.71 - 7.62 (m, 6H, 6xCH_{Ar}), 7.60 - 7.54 (m, 3H, 3xCH_{Ar}), 7.51 - 7.44 (m, 6H, 6xCH_{Ar}), 5.09 (hept, ³J_{HH} = 6.2 Hz, 1H, CH ⁱPr), 4.81 (d, ¹J_{PH} = 23.5 Hz, 1H, PCH), 1.32 (d, ³J_{HH} = 6.2 Hz, 6H, 2xCH₃ ⁱPr) ppm.

¹³C {¹H} NMR (101 MHz, CDCl₃) δ 174.7 (d, ²J_{PC} = 5.0 Hz, C=O), 165.5 (d, ³J_{PC} = 20.6 Hz, C=O), 133.3 (d, ²J_{PC} = 10.4 Hz, 6xCH_{Ar}), 132.6 (d, ⁴J_{PC} = 2.1 Hz, 3xCH_{Ar}), 129.2 (d, ³J_{PC} = 12.5 Hz, 6xCH_{Ar}), 125.6 (d, ¹J_{PC} = 91.7 Hz, 3xCH_{quat}), 68.9 (CH ⁱPr), 56.3 (d, ¹J_{PC} = 108.0 Hz, PCH), 21.9 (2xCH₃ ⁱPr) ppm.

³¹P NMR (162 MHz, CDCl₃) δ 17.0 ppm.

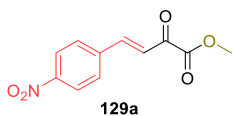
FTIR ν_{max} 1704 (C=O_{st}), 1701 (C=O_{st}), 1239 (C-O-C_{st as}), 1096 (P=O_{st}) cm⁻¹.

HRMS (ESI-TOF) *m/z* calcd. for C₂₄H₂₃O₃P [M+H]⁺ 391.1463, found 391.1449.

Step 3: Olefination reaction. The phosphorus ylide **132** (3.90 g, 10 mmol) and the corresponding aldehyde (15 mmol) were stirred in toluene (20 mL) at room temperature or at 110 °C (heating plate). The reaction was monitored by ³¹P NMR until ylide species **132** was completely consumed (phosphorus ylide: 17.0 ppm). The reaction was then concentrated under reduced pressure, and the crude residue was purified by crystallization or by flash column chromatography (Hexanes/AcOEt), affording pure β,γ-unsaturated α-ketoesters **129**.

²⁴⁵ Albrecht, Ł.; Dickmeiss, G.; Weise, C. F.; Rodríguez-Eschrich, C.; Jørgensen, K. A. *Angew. Chem. Int. Ed.* **2012**, *51*, 13109-13113.

Methyl (*E*)-4-(4-nitrophenyl)-2-oxobut-3-enoate (129a**).**



Method A was followed, using potassium (*E*)-4-(4-nitrophenyl)-2-oxobut-3-enoate (2.59 g, 10 mmol) and methanol (30 mL). The crude residue was purified by crystallization from methanol, affording 1.46 g (62%) of **129a** as a yellow solid.

Mp (MeOH): 183 - 184 °C. Lit. 180 - 182 °C.²⁴⁶

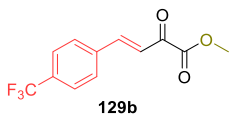
¹H NMR (400 MHz, CDCl₃) δ 8.29 (d, ³J_{HH} = 8.8 Hz, 2H, 2xCH_{Ar}), 7.89 (d, ³J_{HH} = 16.2 Hz, 1H, Ar-CH=CH), 7.80 (d, ³J_{HH} = 8.7 Hz, 2H, 2xCH_{Ar}), 7.50 (d, ³J_{HH} = 16.2 Hz, 1H, Ar-CH=CH), 3.97 (s, 3H, OCH₃) ppm.

¹³C {¹H} NMR (101 MHz, CDCl₃) δ 181.7 (C=O), 161.9 (C=O), 149.2 (C_{quat}), 145.0 (Ar-CH=CH), 139.9 (C_{quat}), 129.6 (2xCH_{Ar}), 124.3 (2xCH_{Ar}), 123.8 (Ar-CH=CH), 53.4 (OCH₃) ppm.

FTIR ν_{max} 1727 (C=O_{st}), 1696 (C=O_{st}), 1679 (CH=CH_{st}), 1520 (NO_{2st as}), 1343 (NO_{2st sym}) cm⁻¹.

HRMS (ESI-TOF) *m/z* calcd. for C₁₁H₁₀NO₅ [M+H]⁺ 236.0559, found 236.0564.

Methyl (*E*)-2-oxo-4-(4-(trifluoromethyl)phenyl)but-3-enoate (129b**).**



Method A was followed, using (*E*)-2-oxo-4-(4-(trifluoromethyl)phenyl)but-3-enoate (2.82 g, 10 mmol) and methanol (30 mL). The crude residue was purified by crystallization from methanol, affording 1.73 g (67%) of **129b** as a yellow solid.

Mp (MeOH): 120 - 122 °C. Lit. 122 - 123 °C.²⁴⁷

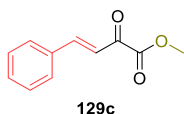
¹H NMR (400 MHz, CDCl₃) δ 7.85 (d, ³J_{HH} = 16.2 Hz, 1H, Ar-CH=CH), 7.76 - 7.63 (m, 4H, 4xCH_{Ar}), 7.43 (d, ³J_{HH} = 16.2 Hz, 1H, Ar-CH=CH), 3.93 (s, 3H, OCH₃) ppm.

¹³C {¹H} NMR (101 MHz, CDCl₃) δ 182.2 (C=O), 162.2 (C=O), 146.4 (Ar-CH=CH), 137.3 (d, ⁵J_{FC} = 1.1 Hz, C_{quat}), 133.1 (q, ²J_{FC} = 32.7 Hz, C_{quat}CF₃), 129.2 (2xCH_{Ar}), 126.1 (q, ³J_{FC} = 4.1 Hz, 2xCH_{Ar}), 122.6 (Ar-CH=CH), 53.3 (OCH₃) ppm.

¹⁹F NMR (282 MHz, CDCl₃) δ -63.1 ppm.

²⁴⁶ Hua, Y. Z.; Liu, M. M.; Huang, P. J.; Song, X.; Wang, M. C.; Chang, J. B. *Chem. Eur. J.* **2015**, *21*, 11994–11998.

²⁴⁷ Tang, X. Z.; Tong, L.; Liang, H. J.; Liang, J.; Zou, Y.; Zhang, X. J.; Yan, M.; Chan, A. S. C. *Org. Biomol. Chem.* **2018**, *16*, 3560–3563.

Methyl (*E*)-2-oxo-4-phenylbut-3-enoate (129c).

Method A was followed, using potassium (*E*)-2-oxo-4-phenylbut-3-enoate (2.14 g, 10 mmol) and methanol (30 mL). The crude residue was purified by crystallization in methanol, affording 1.12 g (59%) of **129c** as an orange solid.

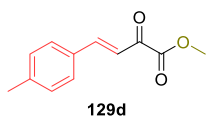
Mp (MeOH): 68 - 69 °C. Lit. 70 - 72 °C.²⁴⁶

¹H NMR (400 MHz, CDCl₃) δ 7.89 (d, ³J_{HH} = 16.1 Hz, 1H, Ar-CH=CH), 7.69 - 7.61 (m, 2H, 2xCH_{Ar}), 7.48 - 7.42 (m, 3H, 3xCH_{Ar}), 7.39 (d, ³J_{HH} = 16.1 Hz, 1H, Ar-CH=CH), 3.94 (s, 3H, OCH₃) ppm.

¹³C {¹H} NMR (101 MHz, CDCl₃) δ 182.4 (C=O), 162.6 (C=O), 148.7 (Ar-CH=CH), 134.0 (C_{quat}), 131.8 (CH_{Ar}), 129.1 (2xCH_{Ar}), 129.0 (2xCH_{Ar}), 120.5 (Ar-CH=CH), 53.1 (OCH₃) ppm.

FTIR ν_{max} 1726 (C=O_{st}), 1691 (C=O_{st}), 1607 (CH=CH_{st}) cm⁻¹.

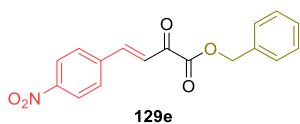
HRMS (ESI-TOF) *m/z* calcd. for C₁₁H₁₁O₃ [M+H]⁺ 191.0703, found 191.0701.

Methyl (*E*)-2-oxo-4-(*p*-tolyl)but-3-enoate (129d).

Method A was followed, using potassium (*E*)-2-oxo-4-(*p*-tolyl)but-3-enoate (2.28 g, 10 mmol) and methanol (30 mL). The crude residue was purified by flash column chromatography (Hexanes/AcOEt 95:5), affording 0.96 g (47%) of **129d** as a white solid.

Mp (MeOH): 66 - 68 °C. Lit. 70 - 72 °C.²⁴⁶

¹H NMR (400 MHz, CDCl₃) δ 7.86 (d, ³J_{HH} = 16.1 Hz, 1H, Ar-CH=CH), 7.54 (d, ³J_{HH} = 8.1 Hz, 2H, 2xCH_{Ar}), 7.33 (d, ³J_{HH} = 16.1 Hz, 1H, Ar-CH=CH), 7.23 (d, ³J_{HH} = 8.1 Hz, 2H, 2xCH_{Ar}), 3.93 (s, 3H, OCH₃), 2.40 (s, 3H, CH₃ tolyl) ppm.

Benzyl (*E*)-4-(4-nitrophenyl)-2-oxobut-3-enoate (129e).

Method A was followed, using potassium (*E*)-4-(4-nitrophenyl)-2-oxobut-3-enoate (2.59 g, 10 mmol) and benzyl alcohol (15 mL). The crude residue was purified by crystallization from diethyl ether, affording 1.59 g (51%) of **129e** as a yellow solid

Mp (MeOH): 158 - 159 °C.

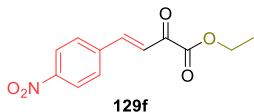
¹H NMR (400 MHz, CDCl₃) δ 8.27 (d, ³J_{HH} = 8.6 Hz, 2H, 2xCH_{Ar}), 7.84 (d, ³J_{HH} = 16.2 Hz, 1H, Ar-CH=CH), 7.76 (d, ³J_{HH} = 8.6 Hz, 2H, 2xCH_{Ar}), 7.47 (d, ³J_{HH} = 16.2 Hz, 1H, Ar-CH=CH), 7.47 - 7.35 (m, 5H, 5xCH_{Ar}), 5.37 (s, 2H, CH₂) ppm.

^{13}C { ^1H } NMR (101 MHz, CDCl_3) δ 182.0 (C=O), 161.5 (C=O), 149.2 (C_{quat}), 145.0 (Ar- $\text{CH}=\text{CH}$), 140.0 (C_{quat}), 134.5 (C_{quat}), 129.6 (2 $\times\text{CH}_{\text{Ar}}$), 129.1 (CH_{Ar}), 128.9 (2 $\times\text{CH}_{\text{Ar}}$), 128.8 (2 $\times\text{CH}_{\text{Ar}}$), 124.4 (2 $\times\text{CH}_{\text{Ar}}$), 124.1 (Ar- $\text{CH}=\text{CH}$), 68.5 (CH_2) ppm.

FTIR ν_{max} 1729 (C=O_{st}), 1691 (C=O_{st}), 1679 (CH=CH_{st}), 1524 (NO_{2st as}), 1343 (NO_{2st sym}) cm^{-1} .

HRMS (ESI-TOF) m/z calcd. for $\text{C}_{17}\text{H}_{14}\text{NO}_5$ [$\text{M}+\text{H}$]⁺ 312.0872, found 312.0879.

Ethyl (*E*)-4-(4-nitrophenyl)-2-oxobut-3-enoate (129f**).**



Method A was followed, using potassium (*E*)-4-(4-nitrophenyl)-2-oxobut-3-enoate (2.59 g, 10 mmol) and ethanol (30 mL). The crude residue was purified by crystallization from ethanol, affording 1.62 g (65%) of **129f** as a yellow solid.

Mp (EtOH): 108 - 109 °C. Lit. 108 - 109 °C.²⁴⁸

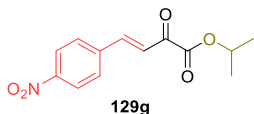
^1H NMR (400 MHz, CDCl_3) δ 8.27 (d, $^3J_{\text{HH}} = 8.8$ Hz, 2H, 2 $\times\text{CH}_{\text{Ar}}$), 7.87 (d, $^3J_{\text{HH}} = 16.2$ Hz, 1H, Ar- $\text{CH}=\text{CH}$), 7.79 (d, $^3J_{\text{HH}} = 8.8$ Hz, 2H, 2 $\times\text{CH}_{\text{Ar}}$), 7.49 (d, $^3J_{\text{HH}} = 16.2$ Hz, 1H, Ar- $\text{CH}=\text{CH}$), 4.41 (q, $^3J_{\text{HH}} = 7.1$ Hz, 2H, CH_2), 1.42 (t, $^3J_{\text{HH}} = 7.2$ Hz, 3H, CH_3) ppm.

^{13}C { ^1H } NMR (101 MHz, CDCl_3) δ 182.2 (C=O), 161.6 (C=O), 149.1 (C_{quat}), 144.7 (Ar- $\text{CH}=\text{CH}$), 140.0 (C_{quat}), 129.5 (2 $\times\text{CH}_{\text{Ar}}$), 124.3 (2 $\times\text{CH}_{\text{Ar}}$), 124.0 (Ar- $\text{CH}=\text{CH}$), 62.9 (CH_2), 14.0 (CH_3) ppm.

FTIR ν_{max} 1724 (C=O_{st}), 1699 (C=O_{st}), 1672 (CH=CH_{st}), 1522 (NO_{2st as}), 1339 (NO_{2st sym}) cm^{-1} .

HRMS (ESI-TOF) m/z calcd. for $\text{C}_{11}\text{H}_{10}\text{NO}_5$ [$\text{M}+\text{H}$]⁺ 250.0715, found 250.0709.

Iso-propyl (*E*)-4-(4-nitrophenyl)-2-oxobut-3-enoate (129g**).**



Method A was followed, using potassium (*E*)-4-(4-nitrophenyl)-2-oxobut-3-enoate (2.59 g, 10 mmol) and propan-2-ol (30 mL). The crude residue was purified by crystallization from 2-propanol, affording 1.55 g (59%) of **129g** as an orange solid.

Mp (^{*i*}PrOH): 110 - 111 °C.

^1H NMR (400 MHz, CDCl_3) δ 8.27 (d, $^3J_{\text{HH}} = 8.6$ Hz, 2H, 2 $\times\text{CH}_{\text{Ar}}$), 7.84 (d, $^3J_{\text{HH}} = 16.2$ Hz, 1H, Ar- $\text{CH}=\text{CH}$), 7.78 (d, $^3J_{\text{HH}} = 8.6$ Hz, 2H, 2 $\times\text{CH}_{\text{Ar}}$), 7.47 (d, $^3J_{\text{HH}} = 16.2$ Hz, 1H, Ar- $\text{CH}=\text{CH}$), 5.22 (hept, $^3J_{\text{HH}} = 6.3$ Hz, 1H, CH ^{*i*}Pr), 1.39 (d, $^3J_{\text{HH}} = 6.3$ Hz, 6H, 2 $\times\text{CH}_3$ ^{*i*}Pr) ppm.

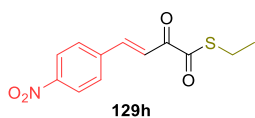
²⁴⁸ Belmessieri, D.; Morrill, L. C.; Simal, C.; Slawin, A. M. Z.; Smith, A. D. *J. Am. Chem. Soc.* **2011**, *133*, 2714-2720.

^{13}C $\{^1\text{H}\}$ NMR (101 MHz, CDCl_3) δ 182.6 (C=O), 161.2 (C=O), 149.1 (C_{quat}), 144.5 (Ar- $\underline{\text{C}}\text{H}=\text{CH}$), 140.0 (C_{quat}), 129.5 (2x CH_{Ar}), 124.3 (2x CH_{Ar}), 124.2 (Ar- $\text{CH}=\underline{\text{C}}\text{H}$), 71.2 (CH^iPr), 21.7 (2x CH_3^iPr) ppm.

FTIR ν_{max} 1710 (C=O_{st}), 1698 (C=O_{st}), 1688 (CH=CH_{st}), 1517 (NO_{2st as}), 1340 (NO_{2st sym}) cm^{-1} .

HRMS (ESI-TOF) m/z calcd. for $\text{C}_{13}\text{H}_{14}\text{NO}_5$ $[\text{M}+\text{H}]^+$ 264.0872, found 264.0870.

S-Ethyl (*E*)-4-(4-nitrophenyl)-2-oxobut-3-enethioate (**129h**).



Method A was followed, using potassium (*E*)-4-(4-nitrophenyl)-2-oxobut-3-enoate (2.59 g, 10 mmol) and ethanethiol (10 mL). The crude residue was purified by flash column chromatography (Hexanes/AcOEt 95:5), affording 1.59 g (60%) of **129h** as a yellow solid.

Mp (Et_2O): 130 - 131 °C.

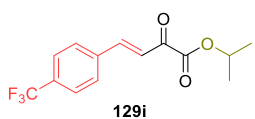
^1H NMR (400 MHz, CDCl_3) δ 8.28 (d, $^3J_{\text{HH}} = 8.7$ Hz, 2H, 2x CH_{Ar}), 7.95 (d, $^3J_{\text{HH}} = 16.2$ Hz, 1H, Ar- $\underline{\text{C}}\text{H}=\text{CH}$), 7.80 (d, $^3J_{\text{HH}} = 8.7$ Hz, 2H, 2x CH_{Ar}), 7.54 (d, $^3J_{\text{HH}} = 16.2$ Hz, 1H, Ar- $\text{CH}=\underline{\text{C}}\text{H}$), 3.01 (q, $^3J_{\text{HH}} = 7.5$ Hz, 2H, CH_2), 1.34 (t, $^3J_{\text{HH}} = 7.5$ Hz, 3H, CH_3) ppm.

^{13}C $\{^1\text{H}\}$ NMR (101 MHz, CDCl_3) δ 192.4 (C=O), 182.8 (C=O), 149.3 (C_{quat}), 145.2 (Ar- $\underline{\text{C}}\text{H}=\text{CH}$), 140.2 (C_{quat}), 129.7 (2x CH_{Ar}), 124.4 (2x CH_{Ar}), 121.5 (Ar- $\text{CH}=\underline{\text{C}}\text{H}$), 23.4 (CH_2), 14.3 (CH_3) ppm.

FTIR ν_{max} 1682 (C=O_{st}), 1677 (C=O_{st}), 1666 (CH=CH_{st}), 1609 (NO_{2st as}), 1346 (NO_{2st sym}) cm^{-1} .

HRMS (ESI-TOF) m/z calcd. for $\text{C}_{12}\text{H}_{12}\text{NO}_4\text{S}$ $[\text{M}+\text{H}]^+$ 266.0487, found 266.0488.

Iso-propyl (*E*)-2-oxo-4-(4-(trifluoromethyl)phenyl)but-3-enoate (**129i**).



Method A was followed, using potassium (*E*)-2-oxo-4-(4-(trifluoromethyl)phenyl)but-3-enoate (2.82 g, 10 mmol) and propan-2-ol (30 mL). The crude residue was purified by flash column chromatography (Hexanes/AcOEt 95:5), affording 2.49 g (87%) of **129i** as a white solid.

Mp (Et_2O): 58 - 59 °C.

^1H NMR (400 MHz, CDCl_3) δ 7.84 (d, $^3J_{\text{HH}} = 16.2$ Hz, 1H, Ar- $\underline{\text{C}}\text{H}=\text{CH}$), 7.73 (d, $^3J_{\text{HH}} = 8.6$ Hz, 2H, 2x CH_{Ar}), 7.67 (d, $^3J_{\text{HH}} = 8.6$ Hz, 2H, 2x CH_{Ar}), 7.42 (d, $^3J_{\text{HH}} = 16.2$ Hz, 1H, Ar- $\text{CH}=\underline{\text{C}}\text{H}$), 5.23 (hept, $^3J_{\text{HH}} = 6.2$ Hz, 1H, $\underline{\text{C}}\text{H}$ (CH_3)₂), 1.39 (d, $^3J_{\text{HH}} = 6.2$ Hz, 6H, 2x CH_3) ppm.

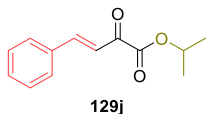
^{13}C $\{^1\text{H}\}$ NMR (101 MHz, CDCl_3) δ 182.9 (C=O), 161.6 (C=O), 146.0 (Ar- $\underline{\text{C}}\text{H}=\text{CH}$), 137.5 (d, $^5J_{\text{FC}} = 1.7$ Hz, C_{quat}), 132.9 (q, $^2J_{\text{FC}} = 32.8$ Hz, $\text{C}_{\text{quat}}\text{CF}_3$), 129.1 (2x CH_{Ar}), 126.1 (q, $^3J_{\text{FC}} = 3.8$ Hz, 2x CH_{Ar}), 123.8 (q, $^1J_{\text{FC}} = 272.4$ Hz, CF_3), 122.9 (Ar- $\text{CH}=\underline{\text{C}}\text{H}$), 71.1 ($\underline{\text{C}}\text{H}$ (CH_3)₂), 21.8 (2x CH_3) ppm.

^{19}F NMR (282 MHz, CDCl_3) δ -63.5 ppm.

FTIR ν_{max} 1736 ($\text{C}=\text{O}_{\text{st}}$), 1679 ($\text{C}=\text{O}_{\text{st}}$), 1660 ($\text{CH}=\text{CH}_{\text{st}}$), 1153 ($\text{C}-\text{F}_{\text{st}}$) cm^{-1} .

HRMS (ESI-TOF) m/z calcd. for $\text{C}_{14}\text{H}_{13}\text{F}_3\text{O}_3$ $[\text{M}+\text{H}]^+$ 287.0896, found 287.0895.

***Iso*-propyl (*E*)-2-oxo-4-phenylbut-3-enoate (**129j**).**



Method B was followed, using phosphorus ylide (3.90 g, 10 mmol) and benzaldehyde (1.59 g, 15 mmol) in toluene (20 mL) at 110°C (heating plate) for 12 hours. The crude residue was purified by flash column chromatography (Hexanes/ AcOEt 70:30), affording 1.96 g (90%) of **129j** as a yellow oil.

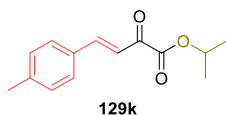
^1H NMR (400 MHz, CDCl_3) δ 7.84 (d, $^3J_{\text{HH}} = 16.2$ Hz, 1H, $\text{Ar}-\underline{\text{C}}\text{H}=\text{CH}$), 7.67 - 7.61 (m, 2H, $2\times\text{CH}_{\text{Ar}}$), 7.47 - 7.39 (m, 3H, $3\times\text{CH}_{\text{Ar}}$), 7.35 (d, $^3J_{\text{HH}} = 16.2$ Hz, 1H, $\text{Ar}-\text{CH}=\underline{\text{C}}\text{H}$), 5.23 (hept, $^3J_{\text{HH}} = 6.3$ Hz, 1H, CH^iPr), 1.40 (d, $^3J_{\text{HH}} = 6.3$ Hz, 6H, $2\times\text{CH}_3^i\text{Pr}$) ppm.

^{13}C $\{^1\text{H}\}$ NMR (101 MHz, CDCl_3) δ 183.3 ($\text{C}=\text{O}$), 161.9 ($\text{C}=\text{O}$), 148.3 ($\text{Ar}-\underline{\text{C}}\text{H}=\text{CH}$), 134.1 (C_{quat}), 131.6 (CH_{Ar}), 129.1 ($2\times\text{CH}_{\text{Ar}}$), 129.0 ($2\times\text{CH}_{\text{Ar}}$), 120.8 ($\text{Ar}-\text{CH}=\underline{\text{C}}\text{H}$), 70.7 (CH^iPr), 21.7 ($2\times\text{CH}_3^i\text{Pr}$) ppm.

FTIR ν_{max} 1736 ($\text{C}=\text{O}_{\text{st}}$), 1694 ($\text{C}=\text{O}_{\text{st}}$), 1660 ($\text{CH}=\text{CH}_{\text{st}}$) cm^{-1} .

HRMS (ESI-TOF) m/z calcd. for $\text{C}_{13}\text{H}_{15}\text{O}_3$ $[\text{M}+\text{H}]^+$ 219.1021, found 219.1025.

***Iso*-propyl (*E*)-2-oxo-4-(*p*-tolyl)but-3-enoate (**129k**).**



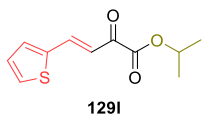
Method A was followed, using potassium (*E*)-2-oxo-4-(*p*-tolyl)but-3-enoate (2.28 g, 10 mmol) and propan-2-ol (30 mL). The crude residue was purified by flash column chromatography (Hexanes/ AcOEt 70:30), affording 1.88 g (81%) of **129k** as a yellow oil.

^1H NMR (400 MHz, CDCl_3) δ 7.82 (d, $^3J_{\text{HH}} = 16.1$ Hz, 1H, $\text{Ar}-\underline{\text{C}}\text{H}=\text{CH}$), 7.53 (d, $^3J_{\text{HH}} = 8.0$ Hz, 2H, $2\times\text{CH}_{\text{Ar}}$), 7.29 (d, $^3J_{\text{HH}} = 16.1$ Hz, 1H, $\text{Ar}-\text{CH}=\underline{\text{C}}\text{H}$), 7.23 (d, $^3J_{\text{HH}} = 8.0$ Hz, 2H, $2\times\text{CH}_{\text{Ar}}$), 5.22 (hept, $^3J_{\text{HH}} = 6.3$ Hz, 1H, CH^iPr), 2.40 (s, 3H, CH_3 tolyl), 1.39 (d, $^3J_{\text{HH}} = 6.3$ Hz, 6H, $2\times\text{CH}_3^i\text{Pr}$) ppm.

^{13}C $\{^1\text{H}\}$ NMR (101 MHz, CDCl_3) δ 183.4 ($\text{C}=\text{O}$), 162.1 ($\text{C}=\text{O}$), 148.4 ($\text{Ar}-\underline{\text{C}}\text{H}=\text{CH}$), 142.4 (C_{quat}), 131.5 (C_{quat}), 129.9 ($2\times\text{CH}_{\text{Ar}}$), 129.1 ($2\times\text{CH}_{\text{Ar}}$), 119.8 ($\text{Ar}-\text{CH}=\underline{\text{C}}\text{H}$), 70.6 (CH^iPr), 21.7 ($2\times\text{CH}_3^i\text{Pr}$), 21.6 (CH_3 tolyl) ppm.

FTIR ν_{max} 1723 ($\text{C}=\text{O}_{\text{st}}$), 1688 ($\text{C}=\text{O}_{\text{st}}$), 1660 ($\text{CH}=\text{CH}_{\text{st}}$) cm^{-1} .

HRMS (ESI-TOF) m/z calcd. for $\text{C}_{14}\text{H}_{17}\text{O}_3$ $[\text{M}+\text{H}]^+$ 233.1177, found 233.1174.

Iso-propyl (*E*)-2-oxo-4-(thiophen-2-yl)but-3-enoate (129l**).**

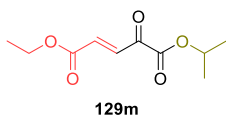
Method A was followed, using potassium (*E*)-2-oxo-4-(thiophen-2-yl)but-3-enoate (2.20 g, 10 mmol) and propan-2-ol (30 mL). The crude residue was purified by flash column chromatography (Hexanes/AcOEt 70:30), affording 1.84 g (82%) of **129l** as a yellow oil.

¹H NMR (400 MHz, CDCl₃) δ 7.97 (d, ³J_{HH} = 15.6 Hz, 1H, Ar-CH=CH), 7.50 (d, ³J_{HH} = 5.1 Hz, 1H, CH_{Ar}), 7.41 (d, ³J_{HH} = 3.7 Hz, 1H, CH_{Ar}), 7.14 (d, ³J_{HH} = 15.6 Hz, 1H, Ar-CH=CH), 7.11 (dd, ³J_{HH} = 5.1, 3.7 Hz, 1H, CH_{Ar}), 5.20 (hept, ³J_{HH} = 6.3 Hz, 1H, CH ⁱPr), 1.38 (d, ³J_{HH} = 6.3 Hz, 6H, 2xCH₃ ⁱPr) ppm.

¹³C {¹H} NMR (101 MHz, CDCl₃) δ 182.7 (C=O), 161.9 (C=O), 140.4 (Ar-CH=CH), 139.9 (C_{quat}), 133.7 (CH_{Ar}), 130.9 (CH_{Ar}), 128.8 (CH_{Ar}), 119.5 (Ar-CH=CH), 70.8 (CH ⁱPr), 21.8 (2xCH₃ ⁱPr) ppm.

FTIR ν_{max} 1726 (C=O_{st}), 1688 (C=O_{st}), 1660 (CH=CH_{st}) cm⁻¹.

HRMS (ESI-TOF) *m/z* calcd. for C₁₁H₁₃O₃S [M+H]⁺ 225.0585, found 225.0585.

1-Ethyl 5-iso-propyl (*E*)-4-oxopent-2-enedioate (129m**).**

Method B was followed, using phosphorus ylide (3.90 g, 10 mmol) and a 50% solution of ethyl glyoxalate in toluene (3.06 g, 3.0 ml, 15 mmol) in toluene (20 mL) at room temperature for 3 hours. The crude residue was purified by flash column chromatography (Hexanes/AcOEt 970:30), affording 1.97 g (92%) of **129m** as a yellow oil.

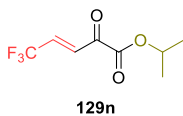
Mp (MeOH): 183 - 184 °C. Lit. 180 - 182 °C.

¹H NMR (400 MHz, CDCl₃) δ 7.52 (d, ³J_{HH} = 16.0 Hz, 1H, EtO₂C-CH=CH), 6.87 (d, ³J_{HH} = 16.0 Hz, 1H, EtO₂C-CH=CH), 5.14 (hept, ³J_{HH} = 6.3 Hz, 1H, CH ⁱPr), 4.23 (q, ³J_{HH} = 7.1 Hz, 2H, CH₂), 1.32 (d, ³J_{HH} = 6.3 Hz, 6H, 2xCH₃ ⁱPr), 1.28 (t, ³J_{HH} = 7.1 Hz, 3H, CH₂CH₃) ppm.

¹³C {¹H} NMR (101 MHz, CDCl₃) δ 183.0 (C=O), 164.7 (C=O), 160.3 (C=O), 135.6 (EtO₂C-CH=CH), 134.1 (EtO₂C-CH=CH), 71.4 (CH ⁱPr), 61.7 (CH₂), 21.6 (2xCH₃ ⁱPr), 14.1 (CH₂CH₃) ppm.

FTIR ν_{max} 1739 (C=O_{st}), 1732 (C=O_{st}), 1710 (C=O_{st}), 1691 (CH=CH_{st}) cm⁻¹.

HRMS (ESI-TOF) *m/z* calcd. for C₁₀H₁₅O₅ [M+H]⁺ 215.0919, found 215.0918.

Iso-propyl (*E*)-5,5,5-trifluoro-2-oxopent-3-enoate (129n**).**

Method B was followed, using a 75% aqueous solution of 2,2,2-trifluoroethane-1,1-diol (2.32 g, 1.65 ml, 15 mmol). In order to remove the water present in the reactant, first toluene (20 mL), 2,2,2-trifluoroethane-1,1-diol and MgSO₄ were stirred for 5 minutes, then phosphorus ylide (3.90 g, 10 mmol) was added. The reaction

was stirred for 3 hours at room temperature and the crude residue was purified by flash column chromatography (Hexanes/AcOEt 970:30), affording 1.74 g (83%) of **129n** as a yellow oil.

¹H NMR (400 MHz, CDCl₃) δ 7.34 (dq, ³J_{HH} = 16.0 Hz, ⁴J_{FH} = 1.9 Hz, 1H, CF₃-CH=CH), 6.90 (dq, ³J_{HH} = 16.0 Hz, ³J_{FH} = 6.5 Hz, 1H, CF₃-CH=CH), 5.21 (hept, ³J_{HH} = 6.2 Hz, 1H, CH ⁱPr), 1.38 (d, ³J_{HH} = 6.2 Hz, 6H, 2xCH₃ ⁱPr) ppm.

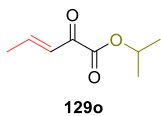
¹³C {¹H} NMR (101 MHz, CDCl₃) δ 181.5 (C=O), 159.9 (C=O), 133.2 (q, ²J_{FC} = 35.9 Hz, CF₃-CH=CH), 129.6 (q, ³J_{FC} = 5.8 Hz, CF₃-CH=CH), 122.1 (q, ¹J_{FC} = 270.7 Hz, CF₃), 71.9 (CH ⁱPr), 21.7 (2xCH₃ ⁱPr) ppm.

¹⁹F NMR (282 MHz, CDCl₃) δ -66.1 ppm.

FTIR ν_{max} 1755 (C=O_{st}), 1742 (C=O_{st}), 1707 (CH=CH_{st}), 1191 (C-F_{st}) cm⁻¹.

HRMS (ESI-TOF) *m/z* calcd. for C₈H₁₀F₃O₃ [M+H]⁺ 211.0582, found 211.0579.

Iso-propyl (E)-2-oxopent-3-enoate(129o).



Method B was followed, using phosphorus ylide (3.90 g, 10 mmol) and acetaldehyde (1.32 g, 1.70 ml, 30 mmol) in toluene (20 mL) at room temperature for 18 hours. The crude residue was purified by flash column chromatography (Hexanes/AcOEt 970:30), affording 1.06 g (68%) of **129o** as a yellow oil.

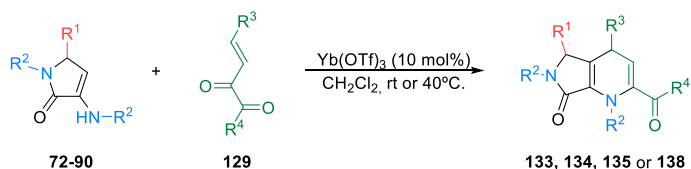
¹H NMR (400 MHz, CDCl₃) δ 7.16 (dq, ³J_{HH} = 15.8 Hz, ³J_{HH} = 6.9 Hz, 1H, CH₃-CH=CH), 6.63 (dq, ³J_{HH} = 15.8 Hz, ⁴J_{HH} = 1.7 Hz, 1H, CH₃-CH=CH), 5.17 (hept, ³J_{HH} = 6.2 Hz, 1H, CH ⁱPr), 2.00 (dd, ³J_{HH} = 6.9 Hz, ³J_{HH} = 1.7 Hz, 3H, CH₃-CH=CH), 1.35 (d, ³J_{HH} = 6.3 Hz, 6H, 2xCH₃ ⁱPr) ppm.

¹³C {¹H} NMR (101 MHz, CDCl₃) δ 183.9 (C=O), 162.2 (C=O), 150.1 (CH₃-CH=CH), 127.1 (CH₃-CH=CH), 70.5 (CH ⁱPr), 21.7 (2xCH₃ ⁱPr), 19.1 (CH₃-CH=CH) ppm.

FTIR ν_{max} 1721 (C=O_{st}), 1683 (C=O_{st}), 1673 (CH=CH_{st}) cm⁻¹.

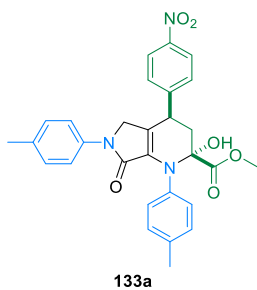
HRMS (ESI-TOF) *m/z* calcd. for C₈H₁₃O₃ [M+H]⁺ 157.0864, found 157.0870.

General procedure for the formal [3+3] cycloaddition reaction of γ -lactams **72-90** with β,γ -unsaturated α -ketoesters **129**.



Neat Yb(OTf)_3 (62.0 mg, 0.1 mmol) and α,β -unsaturated ketoester **129** (1.1 mmol) were added to a solution of γ -lactam (1 mmol) in dichloromethane (10 mL) and the reaction mixture was stirred at 40 °C or at room temperature for 7 - 72 hours. The resulting mixture was washed with a saturated solution of NaHCO_3 (2×5 mL) and H_2O (2×5 mL) and the combined organic layers were dried over anhydrous MgSO_4 and concentrated under reduced pressure. The crude residue was purified by flash column chromatography (Hexanes/AcOEt) to afford pure bicyclic dihydropyridines **133-135** or **138**.

Methyl (**2R***, **4R***)-2-hydroxy-4-(4-nitrophenyl)-7-oxo-1,6-di-*p*-tolyl-2,3,4,5,6,7-hexahydro-1*H*-pyrrolo[3,4-*b*]pyridine-2-carboxylate (**133a**).



The general procedure was followed at room temperature for 72 hours using 1-(*p*-tolyl)-3-(*p*-tolylamino)-1,5-dihydro-2*H*-pyrrol-2-one **72b** (278 mg, 1 mmol), methyl (*E*)-2-oxo-4-(4-nitrophenyl)but-3-enoate **129a** (259 mg, 1.1 mmol) and $\text{Cu}(\text{CH}_3\text{CN})_4\text{PF}_6$ (37.3 mg, 0.1 mmol) instead of Yb(OTf)_3 . The crude residue was purified by flash column chromatography (Hexanes/AcOEt 90:10) followed by crystallization (Dichloromethane/Hexanes 1:3), affording 452 mg (88%) of **133a** as a pale yellow solid.

Mp ($\text{CH}_2\text{Cl}_2/\text{Hex.}$): 165 - 166 °C.

$^1\text{H NMR}$ (400 MHz, CDCl_3) δ 8.26 (d, $^3J_{\text{HH}} = 8.7$ Hz, 2H, $2\times\text{CH}_{\text{Ar}}$), 7.55 (d, $^3J_{\text{HH}} = 8.7$ Hz, 2H, $2\times\text{CH}_{\text{Ar}}$), 7.43 (d, $^3J_{\text{HH}} = 8.5$ Hz, 2H, $2\times\text{CH}_{\text{Ar}}$), 7.15 (d, $^3J_{\text{HH}} = 8.1$ Hz, 2H, $2\times\text{CH}_{\text{Ar}}$), 7.08 (d, $^3J_{\text{HH}} = 8.5$ Hz, 2H, $2\times\text{CH}_{\text{Ar}}$), 7.02 (d, $^3J_{\text{HH}} = 8.1$ Hz, 2H, $2\times\text{CH}_{\text{Ar}}$), 4.33 (bs, 1H, OH), 4.32 (dd, $^4J_{\text{HH}} = 1.4$ Hz, $^3J_{\text{HH}} = 5.2$ Hz, 1H, CH-Ar), 4.13 (dd, $^2J_{\text{HH}} = 17.8$ Hz, 1H, CH_ACH_B), 3.86 (dd, $^2J_{\text{HH}} = 17.8$ Hz, 1H, CH_ACH_B), 3.76 (s, 3H, OCH_3), 2.64 (dd, $^4J_{\text{HH}} = 1.4$ Hz, $^2J_{\text{HH}} = 12.8$ Hz, 1H, CH_ACH_B), 2.35 (dd, $^3J_{\text{HH}} = 5.2$ Hz, $^2J_{\text{HH}} = 12.8$ Hz, 1H, CH_ACH_B), 2.34 (s, 3H, CH_3 tolyl), 2.24 (s, 3H, CH_3 tolyl) ppm.

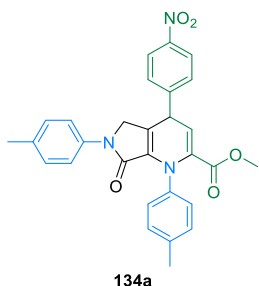
$^{13}\text{C} \{^1\text{H}\}$ NMR (101 MHz, CDCl_3) δ 171.9 (C=O), 163.9 (C=O), 148.9 (C_{quat}), 147.5 (C_{quat}), 137.6 (C_{quat}), 137.3 (C_{quat}), 136.0 (C_{quat}), 133.6 (C_{quat}), 129.7 ($2\times\text{CH}_{\text{Ar}}$), 129.5 ($2\times\text{CH}_{\text{Ar}}$), 129.3 ($2\times\text{CH}_{\text{Ar}}$), 128.8 ($2\times\text{CH}_{\text{Ar}}$),

124.5 (2xCH_{Ar}), 121.4 (C_{quat}), 118.6 (2xCH_{Ar}), 86.1 (C_{quat}), 53.6 (OCH₃), 49.0 (CH₂), 40.6 (CH₂), 36.8 (CH-Ar), 21.4 (CH₃ tolyl), 20.9 (CH₃ tolyl) ppm.

FTIR ν_{\max} 3506 (O-H_{st}), 1742 (C=O_{st} ester), 1698 (C=O_{st} amide), 1666 (C=C_{st}), 1514 (NO₂_{st} as), 1267 (NO₂_{st} sym) cm⁻¹.

HRMS (ESI-TOF) m/z calcd. for C₂₉H₂₈N₃O₆ [M+H]⁺ 514.1978, found 514.1972.

Methyl 4-(4-nitrophenyl)-7-oxo-1,6-di-*p*-tolyl-4,5,6,7-tetrahydro-1*H*-pyrrolo[3,4-*b*]pyridine-2-carboxylate (134a).



The general procedure was followed using 1-(*p*-tolyl)-3-(*p*-tolylamino)-1,5-dihydro-2*H*-pyrrol-2-one **72b** (278 mg, 1 mmol) and methyl (*E*)-4-(4-nitrophenyl)-2-oxobut-3-enoate **129a** (259 mg, 1.1 mmol) at room temperature for 7 hours to afford, after flash column chromatography (Hexanes/AcOEt 90:10), 415 mg (84%) of **134a** as an orange solid.

Mp (Et₂O): 171 - 173 °C (dec.).

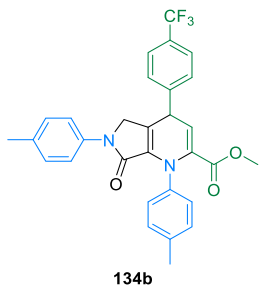
¹H NMR (400 MHz, CDCl₃) δ 8.30 (d, ³J_{HH} = 8.7 Hz, 2H, 2xCH_{Ar}), 7.57 (d, ³J_{HH} = 8.7 Hz, 2H, 2xCH_{Ar}), 7.41 (d, ³J_{HH} = 8.7 Hz, 2H, 2xCH_{Ar}), 7.34 (d, ³J_{HH} = 8.3 Hz, 2H, 2xCH_{Ar}), 7.17 (d, ³J_{HH} = 8.3 Hz, 2H, 2xCH_{Ar}), 7.04 (d, ³J_{HH} = 8.7 Hz, 2H, 2xCH_{Ar}), 5.75 (d, ³J_{HH} = 3.8 Hz, 1H, =CH), 4.93 (d, ³J_{HH} = 3.8 Hz, 1H, CH-Ar), 4.09 (d, ²J_{HH} = 18.0, 1H, CH_AH_B), 3.85 (d, ¹J_{HH} = 18.0, 1H, CH_AH_B), 3.53 (s, 3H, OCH₃), 2.35 (s, 3H, CH₃ tolyl), 2.25 (s, 3H, CH₃ tolyl) ppm.

¹³C {¹H} NMR (101 MHz, CDCl₃) δ 164.0 (C=O), 163.1 (C=O), 150.1 (C_{quat}), 147.6 (C_{quat}), 138.9 (C_{quat}), 137.8 (C_{quat}), 137.3 (C_{quat}), 136.5 (C_{quat}), 134.7 (C_{quat}), 134.0 (C_{quat}), 129.5 (2xCH_{Ar}), 129.1 (2xCH_{Ar}), 129.0 (2xCH_{Ar}), 128.8 (2xCH_{Ar}), 124.6 (2xCH_{Ar}), 122.5 (C_{quat}), 118.9 (2xCH_{Ar}), 112.0 (=CH), 52.3 (OCH₃), 48.7 (CH₂), 41.2 (CH-Ar), 21.4 (CH₃ tolyl), 20.9 (CH₃ tolyl) ppm.

FTIR ν_{\max} 1742 (C=O_{st} ester), 1712 (C=O_{st} amide), 1694 (C=C_{st}), 1691 (C=C_{st}), 1517 (NO₂_{st} as), 1232 (NO₂_{st} sym) cm⁻¹.

HRMS (ESI-TOF) m/z calcd. for C₂₉H₂₅N₃O₅ [M+H]⁺ 496.1872, found 496.1864.

Methyl 7-oxo-1,6-di-*p*-tolyl-4-(4-(trifluoromethyl)phenyl)-4,5,6,7-tetrahydro-1*H*-pyrrolo-[3,4-*b*]pyridine-2-carboxylate (134b).



The general procedure was followed using 1-(*p*-tolyl)-3-(*p*-tolylamino)-1,5-dihydro-2*H*-pyrrol-2-one **72b** (278 mg, 1 mmol) and (*E*)-2-oxo-4-(4-(trifluoromethyl)phenyl)but-3-enoate **129b** (284 mg, 1.1 mmol) at room temperature for 7 hours to afford, after crystallization (CH₂Cl₂/Hexanes 1:3), 404 mg (78%) of **134b** as an orange solid.

Mp (CH₂Cl₂/Hex.): 99 - 100 °C.

¹H NMR (400 MHz, CDCl₃) δ 7.70 (d, ³J_{HH} = 8.3 Hz, 2H, 2xCH_{Ar}), 7.52 (d, ³J_{HH} = 8.3 Hz, 2H, 2xCH_{Ar}), 7.43 (d, ³J_{HH} = 8.4 Hz, 2H, 2xCH_{Ar}), 7.38 (d, ³J_{HH} = 8.4 Hz, 2H, 2xCH_{Ar}), 7.18 (d, ³J_{HH} = 8.8 Hz, 2H, 2xCH_{Ar}), 7.04 (d, ³J_{HH} = 8.8 Hz, 2H, 2xCH_{Ar}), 5.81 (d, ³J_{HH} = 3.8 Hz, 1H, =CH), 4.86 (d, ³J_{HH} = 3.8 Hz, 1H, CH-Ar), 4.07 (dd, ²J_{HH} = 18.0 Hz, ⁴J_{HH} = 1.5 Hz, 1H, CH_ACH_B), 3.87 (dd, ²J_{HH} = 18.0 Hz, ⁴J_{HH} = 0.9 Hz, 1H, CH_ACH_B), 3.54 (s, 3H, OCH₃), 2.36 (s, 3H, CH₃ tolyl), 2.25 (s, 3H, CH₃ tolyl) ppm.

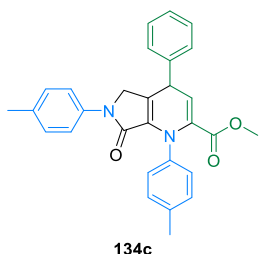
¹³C {¹H} NMR (101 MHz, CDCl₃) δ 164.1 (C=O), 163.3 (C=O), 147.0 (C_{quat}), 139.3 (C_{quat}), 137.6 (C_{quat}), 137.0 (C_{quat}), 136.6 (C_{quat}), 134.6 (C_{quat}), 133.8 (C_{quat}), 130.1 (q, ²J_{FC} = 32.5 Hz, C_{quat}), 129.5 (2xCH_{Ar}), 129.1 (2xCH_{Ar}), 128.8 (2xCH_{Ar}), 128.5 (2xCH_{Ar}), 126.3 (q, ³J_{FC} = 3.7 Hz, 2xCH_{Ar}), 124.2 (q, ¹J_{FC} = 272.2 Hz, CF₃), 123.6 (C_{quat}), 118.8 (2xCH_{Ar}), 113.3 (=CH), 52.2 (OCH₃), 48.7 (CH₂), 41.1 (CH-Ar), 21.4 (CH₃ tolyl), 20.9 (CH₃ tolyl) ppm.

¹⁹F NMR (282 MHz, CDCl₃) δ -62.9 ppm.

FTIR ν_{max} 1735 (C=O_{st} ester), 1695 (C=O_{st} amide), 1680 (C=C_{st}), 1671 (C=C_{st}), 1147 (C-F_{st}) cm⁻¹.

HRMS (ESI-TOF) *m/z* calcd. for C₃₀H₂₆F₃N₂O₃ [M+H]⁺ 519.1896, found 519.1896.

Methyl 7-oxo-4-phenyl-1,6-di-*p*-tolyl-4,5,6,7-tetrahydro-1*H*-pyrrolo[3,4-*b*]pyridine-2-carboxylate (134c).



The general procedure was followed using 1-(*p*-tolyl)-3-(*p*-tolylamino)-1,5-dihydro-2*H*-pyrrol-2-one **72b** (278 mg, 1 mmol) and methyl (*E*)-2-oxo-4-phenylbut-3-enoate **129c** (209 mg, 1.1 mmol) at room temperature for 14 hours to afford, after crystallization (CH₂Cl₂/Hexanes 1:3), 343 mg (76%) of **134c** as a yellowish solid.

Mp (CH₂Cl₂/Hex.): 96 - 98 °C.

¹H NMR (400 MHz, CDCl₃) δ 7.48 - 7.37 (m, 8H, 8xCH_{Ar}), 7.33 (m, 1H, 1xCH_{Ar}), 7.18 (d, ³J_{HH} = 8.0 Hz, 2H, 2xCH_{Ar}), 7.04 (d, ³J_{HH} = 8.0 Hz, 2H, 2xCH_{Ar}), 5.89 (d, ³J_{HH} = 3.8 Hz, 1H, =CH), 4.78 (d, ³J_{HH} = 3.8 Hz, 1H,

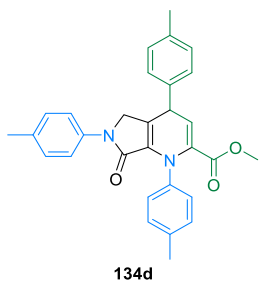
CH-Ar), 4.07 (dd, $^2J_{\text{HH}} = 18.0$ Hz, $^4J_{\text{HH}} = 1.5$ Hz, 1H, CH_ACH_B), 3.90 (dd, $^2J_{\text{HH}} = 18.0$ Hz, $^4J_{\text{HH}} = 1.1$ Hz, 1H, CH_ACH_B), 3.54 (s, 3H, OCH_3), 2.36 (s, 3H, CH_3 tolyl), 2.26 (s, 3H, CH_3 tolyl) ppm.

^{13}C { ^1H } NMR (101 MHz, CDCl_3) δ 164.3 (C=O), 163.6 (C=O), 143.1 (C_{quat}), 139.7 (C_{quat}), 137.3 (C_{quat}), 136.8 (C_{quat}), 136.5 (C_{quat}), 134.3 (C_{quat}), 133.5 (C_{quat}), 129.4 ($2\times\text{CH}_{\text{Ar}}$), 129.3 ($2\times\text{CH}_{\text{Ar}}$), 129.0 ($2\times\text{CH}_{\text{Ar}}$), 128.8 ($2\times\text{CH}_{\text{Ar}}$), 128.1 ($2\times\text{CH}_{\text{Ar}}$), 127.7 (CH_{Ar}), 125.0 (C_{quat}), 118.7 ($2\times\text{CH}_{\text{Ar}}$), 114.8 (=CH), 52.1 (OCH_3), 48.8 (CH_2), 41.2 (CH-Ar), 21.4 (CH_3 tolyl), 20.8 (CH_3 tolyl) ppm.

FTIR ν_{max} 1733 (C=O_{st} ester), 1698 (C=O_{st} amide), 1694 (C=C_{st}), 1691 (C=C_{st}) cm^{-1} .

HRMS (ESI-TOF) m/z calcd. for $\text{C}_{29}\text{H}_{27}\text{N}_2\text{O}_3$ [$\text{M}+\text{H}$] $^+$ 451.2022, found 451.2020.

Methyl 7-oxo-1,4,6-tri-*p*-tolyl-4,5,6,7-tetrahydro-1*H*-pyrrolo[3,4-*b*]pyridine-2-carboxylate (134d).



The general procedure was followed using 1-(*p*-tolyl)-3-(*p*-tolylamino)-1,5-dihydro-2*H*-pyrrol-2-one **72b** (278 mg, 1 mmol) and methyl (*E*)-2-oxo-4-(*p*-tolyl)but-3-enoate **129d** (224 mg, 1.1 mmol) at room temperature for 14 hours to afford, after crystallization ($\text{CH}_2\text{Cl}_2/\text{Hexanes}$ 1:3), 334 mg (72%) of **134d** as a yellow solid.

Mp ($\text{CH}_2\text{Cl}_2/\text{Hex.}$): 99 - 101 °C.

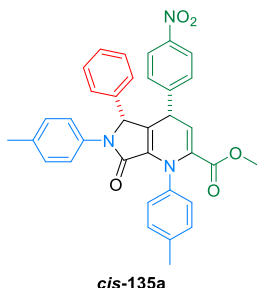
^1H NMR (400 MHz, CDCl_3) δ 7.51 - 7.40 (m, 4H, $4\times\text{CH}_{\text{Ar}}$), 7.35 - 7.22 (m, 4H, $4\times\text{CH}_{\text{Ar}}$), 7.20 (d, $^3J_{\text{HH}} = 7.8$ Hz, 2H, $2\times\text{CH}_{\text{Ar}}$), 7.05 (d, $^3J_{\text{HH}} = 7.8$ Hz, 2H, $2\times\text{CH}_{\text{Ar}}$), 5.91 (d, $^3J_{\text{HH}} = 4.0$ Hz, 1H, =CH), 4.75 (d, $^3J_{\text{HH}} = 4.0$ Hz, 1H, CH-Ar), 4.06 (dd, $^2J_{\text{HH}} = 18.0$ Hz, $^4J_{\text{HH}} = 1.5$ Hz, 1H, CH_ACH_B), 3.92 (dd, $^2J_{\text{HH}} = 18.0$ Hz, $^4J_{\text{HH}} = 1.1$ Hz, 1H, CH_ACH_B), 3.55 (s, 3H, OCH_3), 2.40 (s, 3H, CH_3 tolyl), 2.38 (s, 3H, CH_3 tolyl), 2.27 (s, 3H, CH_3 tolyl) ppm.

^{13}C { ^1H } NMR (101 MHz, CDCl_3) δ 164.3 (C=O), 163.8 (C=O), 140.3 (C_{quat}), 139.9 (C_{quat}), 137.5 (C_{quat}), 137.3 (C_{quat}), 136.9 (C_{quat}), 136.4 (C_{quat}), 134.3 (C_{quat}), 133.5 (C_{quat}), 130.0 ($2\times\text{CH}_{\text{Ar}}$), 129.5 ($2\times\text{CH}_{\text{Ar}}$), 129.0 ($2\times\text{CH}_{\text{Ar}}$), 128.9 ($2\times\text{CH}_{\text{Ar}}$), 128.0 ($2\times\text{CH}_{\text{Ar}}$), 125.5 (C_{quat}), 118.7 ($2\times\text{CH}_{\text{Ar}}$), 115.4 (=CH), 52.1 (OCH_3), 48.8 (CH_2), 40.8 (CH-Ar), 21.5 (CH_3 tolyl), 21.3 (CH_3 tolyl), 20.9 (CH_3 tolyl) ppm.

FTIR ν_{max} 1732 (C=O_{st} ester), 1698 (C=O_{st} amide), 1697 (C=C_{st}), 1681 (C=C_{st}) cm^{-1} .

HRMS (ESI-TOF) m/z calcd. for $\text{C}_{30}\text{H}_{29}\text{N}_2\text{O}_3$ [$\text{M}+\text{H}$] $^+$ 465.2168, found 465.2174.

Methyl (4*S,5*R**)-4-(4-nitrophenyl)-7-oxo-5-phenyl-1,6-di-*p*-tolyl-4,5,6,7-tetrahydro-1*H*-pyrrolo[3,4-*b*]pyridine-2-carboxylate (*cis*-135a).**



The general procedure was followed using 5-phenyl-1-(*p*-tolyl)-3-(*p*-tolylamino)-1,5-dihydro-2*H*-pyrrol-2-one **72c** (354 mg, 1 mmol) and methyl (*E*)-4-(4-nitrophenyl)-2-oxobut-3-enoate **129a** (259 mg, 1.1 mmol) at room temperature for 14 hours to afford, after flash column chromatography (Hexanes/AcOEt 80:20), 469 mg (82%) of *cis*-**135a** as a single diastereoisomer (a yellow solid).

Mp (Et₂O): 171 - 173 °C (dec.).

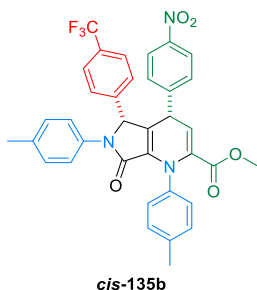
¹H NMR (400 MHz, CDCl₃) δ 7.79 (d, ³J_{HH} = 8.7 Hz, 2H, 2xCH_{Ar}), 7.43 (d, ³J_{HH} = 8.1 Hz, 2H, 2xCH_{Ar}), 7.21 (d, ³J_{HH} = 8.1 Hz, 2H, 2xCH_{Ar}), 7.20 (d, ³J_{HH} = 8.7 Hz, 2H, 2xCH_{Ar}), 7.07 (d, ³J_{HH} = 8.7 Hz, 2H, 2xCH_{Ar}), 6.93 (d, ³J_{HH} = 8.7 Hz, 2H, 2xCH_{Ar}), 6.88 - 6.75 (m, 5H, 5xCH_{Ar}), 5.73 (d, ³J_{HH} = 4.6 Hz, 1H, =CH-CH), 5.39 (d, ⁴J_{HH} = 1.2 Hz, 1H, CHN), 4.80 (dd, ³J_{HH} = 4.6 Hz, ⁴J_{HH} = 1.2 Hz, 1H, =CH-CH), 3.51 (s, 3H, OCH₃), 2.38 (s, 3H, CH₃ tolyl), 2.15 (s, 3H, CH₃ tolyl) ppm.

¹³C {¹H} NMR (101 MHz, CDCl₃) δ 163.9 (C=O), 163.6 (C=O), 149.8 (C_{quat}), 146.4 (C_{quat}), 138.9 (C_{quat}), 137.7 (C_{quat}), 136.3 (C_{quat}), 136.1 (C_{quat}), 134.6 (C_{quat}), 134.2 (C_{quat}), 133.8 (C_{quat}), 129.3 (2xCH_{Ar}), 129.2 (2xCH_{Ar}), 128.9 (2xCH_{Ar}), 128.6 (2xCH_{Ar}), 128.6 (2xCH_{Ar}), 128.2 (2xCH_{Ar}), 127.6 (C_{quat}), 127.5 (CH_{Ar}), 123.4 (2xCH_{Ar}), 122.1 (2xCH_{Ar}), 113.6 (=CH-CH), 64.8 (CHN), 52.3 (OCH₃), 41.5 (=CH-CH), 21.4 (CH₃ tolyl), 20.9 (CH₃ tolyl) ppm.

FTIR ν_{max} 1736 (C=O_{st} ester), 1701 (C=O_{st} amide), 1679 (C=C_{st}), 1666 (C=C_{st}), 1511 (NO₂_{st} as), 1353 (NO₂_{st} sym) cm⁻¹.

HRMS (ESI-TOF) *m/z* calcd. for C₃₅H₃₀N₃O₅ [M+H]⁺ 572.2185, found 572.2195.

Methyl (4*S,5*R**)-7-oxo-1,4,6-tri-*p*-tolyl-5-(4-(trifluoromethyl)phenyl)-4,5,6,7-tetrahydro-1*H*-pyrrolo[3,4-*b*]pyridine-2-carboxylate (*cis*-135b).**



The general procedure was followed using 1-(*p*-tolyl)-3-(*p*-tolylamino)-5-(4-(trifluoromethyl)phenyl)-1,5-dihydro-2*H*-pyrrol-2-one **72d** (422 mg, 1 mmol) and methyl (*E*)-4-(4-nitrophenyl)-2-oxobut-3-enoate **129a** (259 mg, 1.1 mmol) at room temperature for 14 hours to afford, after flash column chromatography (Hexanes/AcOEt 80:20), 0.576 g (90%) of *cis*-**135b** as a single diastereoisomer (an orange solid).

Mp (Et₂O): 189 - 190 °C.

¹H NMR (400 MHz, CDCl₃) δ 7.82 (d, ³J_{HH} = 8.7 Hz, 2H, 2xCH_{Ar}), 7.41 (d, ³J_{HH} = 8.3 Hz, 2H, 2xCH_{Ar}), 7.22 (d, ³J_{HH} = 8.7 Hz, 2H, 2xCH_{Ar}), 7.18 (d, ³J_{HH} = 8.7 Hz, 2H, 2xCH_{Ar}), 7.11 - 7.02 (m, 4H, 4xCH_{Ar}), 6.99 - 6.91 (m, 4H, 4xCH_{Ar}), 5.71 (d, ³J_{HH} = 4.5 Hz, 1H, =CH-CH), 5.47 (d, ⁴J_{HH} = 1.2 Hz, 1H, CHN), 4.81 (dd, ³J_{HH} = 4.5, ⁴J_{HH} = 1.2 Hz, 1H, =CH-CH), 3.51 (s, 3H, OCH₃), 2.38 (s, 3H, CH₃ tolyl), 2.17 (s, 3H, CH₃ tolyl) ppm.

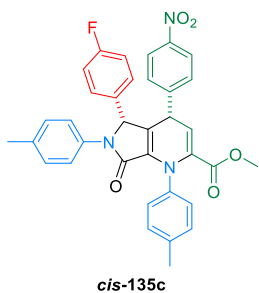
¹³C {¹H} NMR (101 MHz, CDCl₃) δ 163.7 (C=O), 163.4 (C=O), 149.5 (C_{quat}), 146.7 (C_{quat}), 140.7 (C_{quat}), 138.6 (C_{quat}), 137.9 (C_{quat}), 136.4 (C_{quat}), 135.1 (C_{quat}), 134.1 (C_{quat}), 133.9 (C_{quat}), 130.6 (q, ²J_{FC} = 32.5 Hz, C_{quat}), 129.6 (2xCH_{Ar}), 129.3 (2xCH_{Ar}), 129.0 (2xCH_{Ar}), 128.6 (2xCH_{Ar}), 127.9 (2xCH_{Ar}), 126.6 (C_{quat}), 125.5 (q, ³J_{FC} = 3.7 Hz, 2xCH_{Ar}), 123.5 (q, ¹J_{FC} = 272.2 Hz, CF₃), 123.5 (2xCH_{Ar}), 122.1 (2xCH_{Ar}), 113.2 (=CH-CH), 64.2 (CHN), 52.4 (OCH₃), 41.5 (=CH-CH), 21.4 (CH₃ tolyl), 20.9 (CH₃ tolyl) ppm.

¹⁹F NMR (282 MHz, CDCl₃) δ -63.6 ppm.

FTIR ν_{max} 1736 (C=O_{st} ester), 1704 (C=O_{st} amide), 1691 (C=C_{st}), 1666 (C=C_{st}), 1524 (NO₂_{st} as), 1353 (NO₂_{st} sym), 1145 (C-F_{st}) cm⁻¹.

HRMS (ESI-TOF) *m/z* calcd. for C₃₆H₂₉F₃N₃O₅ [M+H]⁺ 640.1981, found 640.2060.

Methyl (4S*,5R*)-5-(4-fluorophenyl)-4-(4-nitrophenyl)-7-oxo-1,6-di-*p*-tolyl-4,5,6,7-tetrahydro-1*H*-pyrrolo[3,4-*b*]pyridine-2-carboxylate (*cis*-135c).



The general procedure was followed using 5-(4-fluorophenyl)-1-(*p*-tolyl)-3-(*p*-tolylamino)-1,5-dihydro-2*H*-pyrrol-2-one **72f** (372 mg, 1 mmol) and methyl (*E*)-4-(4-nitrophenyl)-2-oxobut-3-enoate **129a** (259 mg, 1.1 mmol) at room temperature for 14 hours to afford, after flash column chromatography (Hexanes/AcOEt 80:20), 465 mg (79%) of *cis*-135c as a single diastereoisomer (a greenish solid).

Mp (Et₂O): 175 - 177 °C (dec.).

¹H NMR (400 MHz, CDCl₃) δ 7.87 (d, ³J_{HH} = 8.6 Hz, 2H, 2xCH_{Ar}), 7.41 (d, ³J_{HH} = 8.4 Hz, 2H, 2xCH_{Ar}), 7.21 (d, ³J_{HH} = 7.9 Hz, 2H, 2xCH_{Ar}), 7.15 (d, ³J_{HH} = 8.4 Hz, 2H, 2xCH_{Ar}), 7.10 (d, ³J_{HH} = 8.6 Hz, 2H, 2xCH_{Ar}), 6.94 (d, ³J_{HH} = 7.9 Hz, 2H, 2xCH_{Ar}), 6.78 (bs, 2H, 2xCH_{Ar}), 6.52 (t, ³J_{HH} and ³J_{FH} = 8.6 Hz, 2H, 2xCH_{Ar}), 5.72 (d, ³J_{HH} = 4.6 Hz, 1H, =CH-CH), 5.39 (s, 1H, CHN), 4.78 (d, ³J_{HH} = 4.6 Hz, =CH-CH), 3.51 (s, 3H, OCH₃), 2.38 (s, 3H, CH₃ tolyl), 2.17 (s, 3H, CH₃ tolyl) ppm.

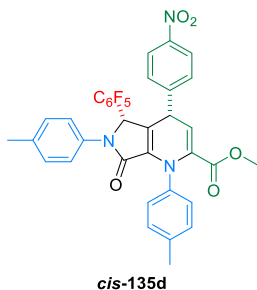
¹³C {¹H} NMR (101 MHz, CDCl₃) δ 163.8 (C=O), 163.4 (C=O), 162.4 (d, ¹J_{FC} = 248.6 Hz, CF), 149.9 (C_{quat}), 146.6 (C_{quat}), 138.7 (C_{quat}), 137.8 (C_{quat}), 136.4 (C_{quat}), 134.9 (C_{quat}), 133.9 (d, ³J_{FC} = 10.6 Hz, 2xCH_{Ar}), 131.9 (d, ⁴J_{FC} = 3.2 Hz, C_{quat}), 129.4 (2xCH_{Ar}), 129.2 (2xCH_{Ar}), 129.0 (2xCH_{Ar}), 128.6 (2xCH_{Ar}), 127.3 (C_{quat}), 123.5 (2xCH_{Ar}), 122.3 (2xCH_{Ar}), 115.5 (d, ²J_{FC} = 21.7 Hz, 2xCH_{Ar}), 113.4 (=CH-CH), 64.1 (CHN), 52.3 (OCH₃), 41.5 (=CH-CH), 21.4 (CH₃ tolyl), 20.9 (CH₃ tolyl) ppm.

¹⁹F NMR (282 MHz, CDCl₃) δ -113.2 ppm.

FTIR ν_{max} 1739 (C=O_{st} ester), 1701 (C=O_{st} amide), 1694 (C=C_{st}), 1666 (C=C_{st}), 1514 (NO_{2st} as), 1346 (NO_{2st} sym) cm⁻¹.

HRMS (ESI-TOF) *m/z* calcd. for C₃₅H₂₉FN₃O₅ [M+H]⁺ 590.2091, found 590.2085.

Methyl (4*S,5*S**)-4-(4-nitrophenyl)-7-oxo-5-(perfluorophenyl)-1,6-di-*p*-tolyl-4,5,6,7-tetrahydro-1*H*-pyrrolo[3,4-*b*]pyridine-2-carboxylate (*cis*-135d).**



The general procedure was followed using 5-(perfluorophenyl)-1-(*p*-tolyl)-3-(*p*-tolylamino)-1,5-dihydro-2*H*-pyrrol-2-one **90d** (444 mg, 1 mmol) and methyl (*E*)-4-(4-nitrophenyl)-2-oxobut-3-enoate **129a** (259 mg, 1.1 mmol) at room temperature for 14 hours to afford, after flash column chromatography (Hexanes/AcOEt 90:10), 429 mg (65%) of *cis*-**135d** as a single diastereoisomer (a yellow solid).

Mp (Et₂O): 185 - 186 °C (dec.).

¹H NMR (400 MHz, CDCl₃) δ 8.04 (d, ³J_{HH} = 8.7 Hz, 2H, 2xCH_{Ar}), 7.42 - 7.33 (m, 4H, 4xCH_{Ar}), 7.20 (d, ³J_{HH} = 8.0 Hz, 2H, 2xCH_{Ar}), 7.14 (d, ³J_{HH} = 8.5 Hz, 2H, 2xCH_{Ar}), 7.00 (d, ³J_{HH} = 8.0 Hz, 2H, 2xCH_{Ar}), 5.86 (s, 1H, CHN), 5.67 (d, ³J_{HH} = 4.1 Hz, 1H, =CH-CH), 4.90 (dd, ³J_{HH} = 4.1, ⁴J_{HH} = 1.3 Hz, 1H, =CH-CH), 3.53 (s, 3H, OCH₃), 2.37 (s, 3H, CH₃ tolyl), 2.20 (s, 3H, CH₃ tolyl) ppm.

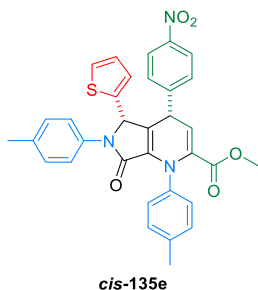
¹³C {¹H} NMR (101 MHz, CDCl₃) δ 163.7 (C=O), 162.4 (C=O), 149.5 (C_{quat}), 147.4 (C_{quat}), 146.1 (m, C_{quat}-F), 143.8 (m, C_{quat}-F), 142.3 (m, C_{quat}-F), 139.7 (m, C_{quat}-F), 138.3 (C_{quat}), 138.1 (C_{quat}), 137.1 (C_{quat}), 135.7 (C_{quat}), 135.2 (C_{quat}), 133.3 (C_{quat}), 129.8 (2xCH_{Ar}), 129.3 (2xCH_{Ar}), 128.8 (2xCH_{Ar}), 128.7 (2xCH_{Ar}), 123.5 (2xCH_{Ar}), 122.0 (2xCH_{Ar}), 121.3 (C_{quat}), 111.7 (=CH-CH), 110.9 (m, C_{quat}-F), 54.3 (d, ³J_{FC} = 4.6 Hz, CHN), 52.3 (OCH₃), 41.6 (=CH-CH), 21.4 (CH₃ tolyl), 20.9 (CH₃ tolyl) ppm.

¹⁹F NMR (282 MHz, CDCl₃) δ -142.8 (d, ³J_{FF} = 21.6 Hz), -145.3 (d, ³J_{FF} = 22.8 Hz), -152.6 (t, ³J_{FF} = 20.1 Hz), -161.0 (dt, ³J_{FF} = 21.1 Hz, ⁴J_{FF} = 7.9 Hz), -161.6 (dt, ³J_{FF} = 21.6 Hz, ⁴J_{FF} = 8.7 Hz) ppm.

FTIR ν_{max} 1736 (C=O_{st} ester), 1688 (C=O_{st} amide), 1667 (C=C_{st}), 1637 (C=C_{st}), 1505 (NO_{2st} as), 1340 (NO_{2st} sym) cm⁻¹.

HRMS (ESI-TOF) *m/z* calcd. for C₃₅H₂₅F₅N₃O₅ [M+H]⁺ 662.1714, found 662.1716.

Methyl (4S*,5S*)-4-(4-nitrophenyl)-7-oxo-5-(thiophen-2-yl)-1,6-di-*p*-tolyl-4,5,6,7-tetra-hydro-1*H*-pyrrolo[3,4-*b*]pyridine-2-carboxylate (*cis*-135e).



The general procedure was followed using 5-(thiophen-2-yl)-1-(*p*-tolyl)-3-(*p*-tolylamino)-1,5-dihydro-2*H*-pyrrol-2-one **72i** (360 mg, 1 mmol) and methyl (*E*)-4-(4-nitrophenyl)-2-oxobut-3-enoate **129a** (259 mg, 1.1 mmol) at room temperature for 14 hours to afford, after flash column chromatography (Hexanes/AcOEt 90:10), 380 mg (66%) of *cis*-135e as a single diastereoisomer (an orange solid).

Mp (Et₂O): 193- 194 °C.

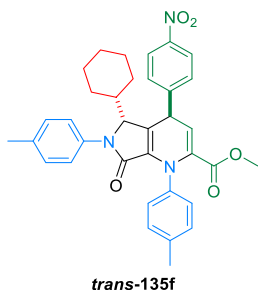
¹H NMR (400 MHz, CDCl₃) δ 7.92 (d, ³J_{HH} = 8.7 Hz, 2H, 2xCH_{Ar}), 7.41 (d, ³J_{HH} = 8.2 Hz, 2H, 2xCH_{Ar}), 7.25 - 7.15 (m, 6H, 6xCH_{Ar}), 6.98 (d, ³J_{HH} = 8.2 Hz, 2H, 2xCH_{Ar}), 6.79 (dd, ³J_{HH} = 5.1, ⁴J_{HH} = 1.2 Hz, 1H, CH_{Ar}), 6.60 (dd, ³J_{HH} = 3.5, ⁴J_{HH} = 1.2 Hz, 1H, CH_{Ar}), 6.39 (dd, ³J_{HH} = 5.1, ³J_{HH} = 3.5 Hz, 1H, CH_{Ar}), 5.75 (d, ³J_{HH} = 4.6 Hz, 1H, =CH-CH), 5.73 (s, 1H, CHN), 4.82 (dd, ³J_{HH} = 4.6, ⁴J_{HH} = 1.3 Hz, 1H, =CH-CH), 3.51 (s, 3H, OCH₃), 2.37 (s, 3H, CH₃ tolyl), 2.19 (s, 3H, CH₃ tolyl) ppm.

¹³C {¹H} NMR (101 MHz, CDCl₃) δ 163.8 (C=O), 163.1 (C=O), 149.9 (C_{quat}), 146.6 (C_{quat}), 140.1 (C_{quat}), 138.7 (C_{quat}), 137.8 (C_{quat}), 136.4 (C_{quat}), 135.1 (C_{quat}), 133.8 (C_{quat}), 133.7 (C_{quat}), 129.4 (2xCH_{Ar}), 129.2 (2xCH_{Ar}), 128.8 (2xCH_{Ar}), 128.6 (2xCH_{Ar}), 127.4 (CH_{Ar}), 126.8 (C_{quat}), 126.5 (CH_{Ar}), 126.4 (CH_{Ar}), 123.5 (2xCH_{Ar}), 122.7 (2xCH_{Ar}), 113.5 (=CH-CH), 60.4 (CHN), 52.3 (OCH₃), 41.5 (=CH-CH), 21.4 (CH₃ tolyl), 21.0 (CH₃ tolyl) ppm.

FTIR ν_{max} 1732 (C=O_{st} ester), 1717 (C=O_{st} amide), 1685 (C=C_{st}), 1679 (C=C_{st}), 1511 (NO_{2st} as), 1337 (NO_{2st} sym) cm⁻¹.

HRMS (ESI-TOF) *m/z* calcd. for C₃₃H₂₈N₃O₅S [M+H]⁺ 578.1749, found 578.1746.

Methyl (4R*,5R*)-5-cyclohexyl-4-(4-nitrophenyl)-7-oxo-1,6-di-*p*-tolyl-4,5,6,7-tetrahydro-1*H*-pyrrolo[3,4-*b*]pyridine-2-carboxylate (*trans*-135f).



The general procedure was followed using 5-cyclohexyl-1-(*p*-tolyl)-3-(*p*-tolylamino)-1,5-dihydro-2*H*-pyrrol-2-one **72q** (360 mg, 1 mmol) and methyl (*E*)-4-(4-nitrophenyl)-2-oxobut-3-enoate **129a** (259 mg, 1.1 mmol) at 40 °C (heating plate) for 24 hours to afford, after flash column chromatography (Hexanes/AcOEt 85:15), 109 mg (19%) of *trans*-135f as an orange-red solid.

Mp (Et₂O): 173 - 175 °C (dec.).

¹H NMR (400 MHz, CDCl₃) δ 8.28 (d, ³J_{HH} = 8.7 Hz, 2H, 2xCH_{Ar}), 7.62 (d, ³J_{HH} = 8.7 Hz, 2H, 2xCH_{Ar}), 7.39 (d, ³J_{HH} = 8.3 Hz, 2H, 2xCH_{Ar}), 7.15 (d, ³J_{HH} = 8.6 Hz, 2H, 2xCH_{Ar}), 7.15 - 7.05 (m, 4H, 4xCH_{Ar}), 5.80 (d,

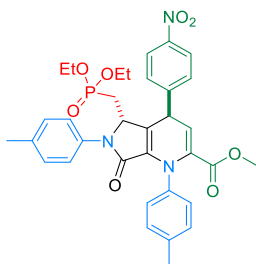
$^3J_{HH} = 5.1$ Hz, 1H, =CH-CH), 4.73 (d, $^3J_{HH} = 5.1$ Hz, =CH-CH), 4.46 (bs, 1H, CHN), 3.49 (s, 3H, OCH₃), 2.34 (CH₃ tolyl), 2.30 (CH₃ tolyl), 1.54 (bs, 1H, CH Cy), 1.41 - 1.19 (m, 5H, 5xCH Cy), 1.04 (t, $^3J_{HH} = 12.5$ Hz, 2H, CH₂ Cy), 0.76 - 0.41 (m, 2H, 2xCH Cy), 0.02 (m, 1H, CH Cy) ppm.

$^{13}\text{C} \{^1\text{H}\}$ NMR (101 MHz, CDCl₃) δ 164.1 (C=O), 164.0 (C=O), 150.8 (C_{quat}), 147.5 (C_{quat}), 138.9 (C_{quat}), 137.4 (C_{quat}), 136.1 (2xC_{quat}), 135.3 (C_{quat}), 135.0 (C_{quat}), 129.5 (2xCH_{Ar}), 129.4 (2xCH_{Ar}), 129.2 (2xCH_{Ar}), 128.2 (2xCH_{Ar}), 125.9 (C_{quat}), 125.4 (2xCH_{Ar}), 124.3 (2xCH_{Ar}), 113.8 (=CH-CH), 66.3 (CHN), 52.3 (OCH₃), 42.1 (CH Cy), 41.3(=CH-CH), 31.5 (CH₂ Cy), 27.1 (CH₂ Cy), 25.9 (CH₂ Cy), 25.8 (CH₂ Cy), 25.5 (CH₂ Cy), 21.4 (CH₃ tolyl), 21.2 (CH₃ tolyl) ppm.

FTIR ν_{max} 1736 (C=O_{st} ester), 1698 (C=O_{st} amide), 1691 (C=C_{st}), 1666 (C=C_{st}), 1505 (NO₂_{st} as), 1340 (NO₂_{st} sym) cm⁻¹.

HRMS (ESI-TOF) m/z calcd. for C₃₅H₃₆N₃O₅ [M+H]⁺ 578.2655, found 578.2654.

Methyl (4R*,5S*)-5-((diethoxyphosphoryl)methyl)-4-(4-nitrophenyl)-7-oxo-1,6-di-*p*-tolyl-4,5,6,7-tetrahydro-1*H*-pyrrolo[3,4-*b*]pyridine-2-carboxylate (*trans*-135g).



trans-135g

The general procedure was followed using diethyl ((5-oxo-1-(*p*-tolyl)-4-(*p*-tolylamino)-2,5-dihydro-1*H*-pyrrol-2-yl)methyl)phosphonate **90a** (428 mg, 1 mmol) and methyl (*E*)-4-(4-nitrophenyl)-2-oxobut-3-enoate **129a** (259 mg, 1.1 mmol) at room temperature for 14 hours to afford, after flash column chromatography (Hexanes/AcOEt 75:25), 561 mg (87%) of *trans*-**135g** as a single diastereoisomer (an orange solid).

Mp (Et₂O): 117 - 119 °C (dec.).

^1H NMR (400 MHz, CDCl₃) δ 8.30 (d, $^3J_{HH} = 8.7$ Hz, 2H, 2xCH_{Ar}), 7.65 (d, $^3J_{HH} = 8.7$ Hz, 2H, 2xCH_{Ar}), 7.37 (d, $^3J_{HH} = 8.2$ Hz, 2H, 2xCH_{Ar}), 7.17 (d, $^3J_{HH} = 8.6$ Hz, 2H, 2xCH_{Ar}), 7.14 (d, $^3J_{HH} = 8.6$ Hz, 2H, 2xCH_{Ar}), 7.07 (d, $^3J_{HH} = 8.2$ Hz, 2H, 2xCH_{Ar}), 5.84 (d, $^3J_{HH} = 4.3$ Hz, 1H, =CH-CH), 5.37 (m, 1H, =CH-CH), 4.42 (dt, $^3J_{HH} = 4.8$, $^3J_{PH} = 28.6$, Hz, 1H, CHN), 4.02 (m, 2H, CH₂ phosphonate), 3.90 (m, 2H, CH₂ phosphonate), 3.52 (s, 3H, OCH₃), 2.33 (s, 3H, CH₃ tolyl), 2.27 (s, 3H, CH₃ tolyl), 2.13 (m, 2H, CH₂P), 1.25 (t, $^3J_{HH} = 7.1$ Hz, 3H, CH₃ phosphonate), 1.18 (t, $^3J_{HH} = 7.0$ Hz, 3H, CH₃ phosphonate) ppm.

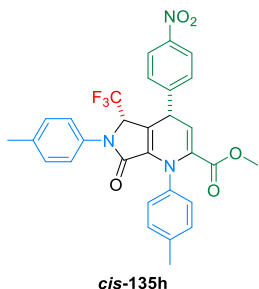
$^{13}\text{C} \{^1\text{H}\}$ NMR (101 MHz, CDCl₃) δ 163.8 (C=O), 162.61 (C=O), 150.6 (C_{quat}), 147.5 (C_{quat}), 139.1 (C_{quat}), 137.6 (C_{quat}), 136.3 (C_{quat}), 135.1 (C_{quat}), 134.8 (C_{quat}), 133.3 (C_{quat}), 129.6 (2xCH_{Ar}), 129.4 (2xCH_{Ar}), 129.0 (2xCH_{Ar}), 128.9 (2xCH_{Ar}), 126.5 (d, $^3J_{PC} = 2.9$ Hz, C_{quat}), 124.6 (2xCH_{Ar}), 122.5 (2xCH_{Ar}), 114.1 (=CH-CH), 62.2 (d, $^2J_{PC} = 6.8$ Hz, CH₂ phosphonate), 62.0 (d, $^2J_{PC} = 6.6$ Hz, CH₂ phosphonate), 53.1 (d, $^2J_{PC} = 4.1$ Hz, CHN), 52.2 (OCH₃), 39.9 (=CH-CH), 26.4 (d, $^1J_{PC} = 143.2$ Hz, CH₂P), 21.4 (CH₃ tolyl), 21.0 (CH₃ tolyl), 16.5 (d, $^3J_{PC} = 6.2$ Hz, CH₃ phosphonate), 16.4 (d, $^3J_{PC} = 5.9$ Hz, CH₂ phosphonate) ppm.

^{31}P NMR (162 MHz, CDCl_3) δ 25.4 ppm.

FTIR ν_{max} 1732 ($\text{C}=\text{O}_{\text{st}}$ ester), 1704 ($\text{C}=\text{O}_{\text{st}}$ amide), 1612 ($\text{C}=\text{C}_{\text{st}}$), 1666 ($\text{C}=\text{C}_{\text{st}}$), 1511 ($\text{NO}_2_{\text{st as}}$), 1353 ($\text{NO}_2_{\text{st sym}}$), 1275 ($\text{P}=\text{O}_{\text{st}}$), 1159 ($\text{P}-\text{O}-\text{C}_{\text{st}}$) cm^{-1} .

HRMS (ESI-TOF) m/z calcd. for $\text{C}_{34}\text{H}_{37}\text{N}_3\text{O}_8\text{P}$ $[\text{M}+\text{H}]^+$ 646.2318, found 646.2325.

Methyl (4S*,5S*)-4-(4-nitrophenyl)-7-oxo-1,6-di-*p*-tolyl-5-(trifluoromethyl)-4,5,6,7-tetra-hydro-1*H*-pyrrolo[3,4-*b*]pyridine-2-carboxylate (*cis*-135h).



The general procedure was followed using 1-(*p*-tolyl)-3-(*p*-tolylamino)-5-(trifluoromethyl)-1,5-dihydro-2*H*-pyrrol-2-one **90e** (346 mg, 1 mmol) and methyl (*E*)-4-(4-nitrophenyl)-2-oxobut-3-enoate **129a** (259 mg, 1.1 mmol) at 40 °C (heating plate) for 14 hours, affording a 70:30 mixture of *cis*-**135h** and *trans*-**135h** diastereoisomers. After flash column chromatography (Hexanes/AcOEt 80:20), 281 mg (50%) of *cis*-**135h** isomer were isolated as a yellow solid.

Mp (Et_2O): 192 - 194 °C (dec.).

^1H NMR (400 MHz, CDCl_3) δ 8.27 (d, $^3J_{\text{HH}} = 8.7$ Hz, 2H, $2\times\text{CH}_{\text{Ar}}$), 7.51 (d, $^3J_{\text{HH}} = 8.7$ Hz, 2H, $2\times\text{CH}_{\text{Ar}}$), 7.34 (d, $^3J_{\text{HH}} = 8.4$ Hz, 2H, $2\times\text{CH}_{\text{Ar}}$), 7.17 (d, $^3J_{\text{HH}} = 8.0$ Hz, 2H, $2\times\text{CH}_{\text{Ar}}$), 7.16 (d, $^3J_{\text{HH}} = 8.0$ Hz, 2H, $2\times\text{CH}_{\text{Ar}}$), 7.10 (d, $^3J_{\text{HH}} = 8.4$ Hz, 2H, $2\times\text{CH}_{\text{Ar}}$), 5.90 (d, $^3J_{\text{HH}} = 5.6$ Hz, 1H, $=\text{CH}-\text{CH}$), 4.90 (q, $^3J_{\text{FH}} = 5.8$ Hz, 1H, CHN), 4.76 (d, $^3J_{\text{HH}} = 5.6$ Hz, 1H, $=\text{CH}-\text{CH}$), 3.49 (s, 3H, OCH_3), 2.36 (s, 3H, CH_3 tolyl), 2.32 (s, 3H, CH_3 tolyl) ppm.

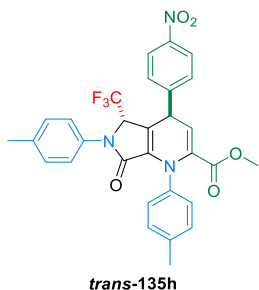
^{13}C $\{^1\text{H}\}$ NMR (101 MHz, CDCl_3) δ 164.0 ($\text{C}=\text{O}$), 163.3 ($\text{C}=\text{O}$), 150.08 (C_{quat}), 147.4 (C_{quat}), 138.0 (C_{quat}), 137.9 (C_{quat}), 137.6 (C_{quat}), 137.4 (C_{quat}), 134.7 (C_{quat}), 133.4 (C_{quat}), 129.8 ($2\times\text{CH}_{\text{Ar}}$), 129.3 ($2\times\text{CH}_{\text{Ar}}$), 128.5 ($2\times\text{CH}_{\text{Ar}}$), 128.3 ($2\times\text{CH}_{\text{Ar}}$), 125.5 ($2\times\text{CH}_{\text{Ar}}$), 124.4 ($2\times\text{CH}_{\text{Ar}}$), 122.9 (q, $^1J_{\text{FC}} = 283.5$ Hz, CF_3), 117.7 (C_{quat}), 114.5 ($=\text{CH}-\text{CH}$), 61.6 (q, $^2J_{\text{FC}} = 32.8$ Hz, CHN), 52.4 (OCH_3), 41.2 ($=\text{CH}-\text{CH}$), 21.4 (CH_3 tolyl), 21.2 (CH_3 tolyl) ppm.

^{19}F NMR (282 MHz, CDCl_3) δ -70.6 ppm.

FTIR ν_{max} 1729 ($\text{C}=\text{O}_{\text{st}}$ ester), 1672 ($\text{C}=\text{O}_{\text{st}}$ amide), 1615 ($\text{C}=\text{C}_{\text{st}}$), 1514 ($\text{NO}_2_{\text{st as}}$), 1346 ($\text{NO}_2_{\text{st sym}}$), 1145 ($\text{C}-\text{F}_{\text{st}}$) cm^{-1} .

HRMS (ESI-TOF) m/z calcd. for $\text{C}_{30}\text{H}_{25}\text{F}_3\text{N}_3\text{O}_5$ $[\text{M}+\text{H}]^+$ 564.1746, found 564.1752.

Methyl (4*R,5*S**)-4-(4-nitrophenyl)-7-oxo-1,6-di-*p*-tolyl-5-(trifluoromethyl)-4,5,6,7-tetra-hydro-1*H*-pyrrolo[3,4-*b*]pyridine-2-carboxylate (*trans*-135h).**



as a pale yellow solid.

The general procedure was followed using 1-(*p*-tolyl)-3-(*p*-tolylamino)-5-(trifluoromethyl)-1,5-dihydro-2*H*-pyrrol-2-one **90e** (346 mg, 1 mmol) and methyl (*E*)-4-(4-nitrophenyl)-2-oxobut-3-enoate **129a** (259 mg, 1.1 mmol) at 40 °C (heating plate) for 14 hours, affording a 70:30 mixture of *cis*-**135h** and *trans*-**135h** diastereoisomers. After flash column chromatography (Hexanes/AcOEt 85:15), 123 mg (22%) of *trans*-**135h** isomer were obtained

Mp (Et₂O): 195 - 197 °C (dec.).

¹H NMR (400 MHz, CDCl₃) δ 8.34 (d, ³J_{HH} = 8.7 Hz, 2H, 2xCH_{Ar}), 7.62 (d, ³J_{HH} = 8.7 Hz, 2H, 2xCH_{Ar}), 7.31 (d, ³J_{HH} = 8.3 Hz, 2H, 2xCH_{Ar}), 7.16 (d, ³J_{HH} = 8.0 Hz, 2H, 2xCH_{Ar}), 7.08 (d, ³J_{HH} = 8.0 Hz, 2H, 2xCH_{Ar}), 7.02 (d, ³J_{HH} = 8.3 Hz, 2H, 2xCH_{Ar}), 5.74 (d, ³J_{HH} = 4.1 Hz, 1H, =CH-CH), 5.00 (d, ³J_{HH} = 4.1 Hz, 1H, =CH-CH), 4.60 (q, ³J_{FH} = 5.6 Hz, 1H, CHN), 3.53 (s, 3H, OCH₃), 2.34 (s, 3H, CH₃ tolyl), 2.28 (s, 3H, CH₃ tolyl) ppm.

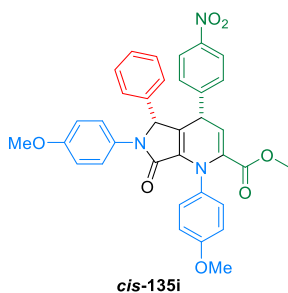
¹³C {¹H} NMR (101 MHz, CDCl₃) δ 163.5 (C=O), 163.27 (C=O), 149.8 (C_{quat}), 147.8 (C_{quat}), 138.2 (C_{quat}), 137.9 (C_{quat}), 137.1 (C_{quat}), 136.6 (C_{quat}), 136.3 (C_{quat}), 133.2 (C_{quat}), 129.6 (2xCH_{Ar}), 129.4 (2xCH_{Ar}), 129.2 (2xCH_{Ar}), 128.7 (2xCH_{Ar}), 124.9 (2xCH_{Ar}), 124.8 (2xCH_{Ar}), 123.6 (q, ¹J_{FC} = 284.9 Hz, CF₃), 117.6 (C_{quat}), 112.7 (=CH-CH), 59.6 (q, ²J_{FC} = 31.4 Hz, CHN), 52.4 (OCH₃), 40.5 (=CH-CH), 21.4 (CH₃ tolyl), 21.1 (CH₃ tolyl) ppm.

¹⁹F NMR (282 MHz, CDCl₃) δ -71.0 ppm.

FTIR ν_{max} 1739 (C=O_{st ester}), 1669 (C=O_{st amide}), 1631 (C=C_{st}), 1520 (NO₂_{st as}), 1346 (NO₂_{st sym}), 1142 (C-F_{st}) cm⁻¹.

HRMS (ESI-TOF) *m/z* calcd. for C₃₀H₂₅F₃N₃O₅ [M+H]⁺ 564.1746, found 564.1753.

Methyl (4*S,5*R**)-1,6-bis(4-methoxyphenyl)-4-(4-nitrophenyl)-7-oxo-5-phenyl-4,5,6,7-tetrahydro-1*H*-pyrrolo[3,4-*b*]pyridine-2-carboxylate (*cis*-135i).**



The general procedure was followed using 1-(4-methoxyphenyl)-3-((4-methoxyphenyl)amino)-5-phenyl-1,5-dihydro-2*H*-pyrrol-2-one **84b** (386 mg, 1 mmol) and methyl (*E*)-4-(4-nitrophenyl)-2-oxobut-3-enoate **129a** (259 mg, 1.1 mmol) at room temperature for 14 hours to afford, after flash column chromatography (Hexanes/AcOEt 85:15), 458 mg (76%) of *cis*-**135i** as a single diastereoisomer (an orange solid).

Mp (Et₂O): 186 - 188 °C (dec.).

$^1\text{H NMR}$ (300 MHz, CDCl_3) δ 7.79 (d, $^3J_{\text{HH}} = 8.8$ Hz, 2H, 2xCH_{Ar}), 7.44 (d, $^3J_{\text{HH}} = 9.0$ Hz, 2H, 2xCH_{Ar}), 7.17 (d, $^3J_{\text{HH}} = 9.2$ Hz, 2H, 2xCH_{Ar}), 7.06 (d, $^3J_{\text{HH}} = 8.8$ Hz, 2H, 2xCH_{Ar}), 6.91 (d, $^3J_{\text{HH}} = 9.0$ Hz, 2H, 2xCH_{Ar}), 6.88 - 6.73 (m, 5H, 5xCH_{Ar}), 6.66 (d, $^3J_{\text{HH}} = 9.2$ Hz, 2H, 2xCH_{Ar}), 5.69 (d, $^3J_{\text{HH}} = 4.5$ Hz, 1H, =CH-CH), 5.34 (d, $^4J_{\text{HH}} = 0.9$ Hz, 1H, CHN), 4.79 (d, $^3J_{\text{HH}} = 4.5$ Hz, 1H, =CH-CH), 3.82 (s, 3H, OCH₃), 3.64 (s, 3H, OCH₃), 3.52 (s, 3H, OCH₃) ppm.

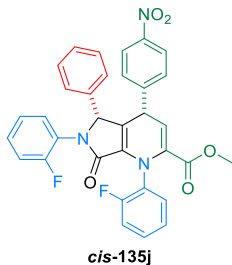
$^{13}\text{C}\{^1\text{H}\}$ NMR (75 MHz, CDCl_3) δ 163.9 (C=O), 163.69 (C=O), 158.9 (C_{quat}), 156.9 (C_{quat}), 149.8 (C_{quat}), 146.4 (C_{quat}), 136.5 (C_{quat}), 136.0 (C_{quat}), 134.1 (C_{quat}), 133.8 (C_{quat}), 130.0 (2xCH_{Ar}), 129.7 (C_{quat}), 128.9 (2xCH_{Ar}), 128.6 (2xCH_{Ar}), 128.2 (CH_{Ar}), 127.5 (2xCH_{Ar}), 127.2 (C_{quat}), 124.2 (2xCH_{Ar}), 123.4 (2xCH_{Ar}), 114.0 (2xCH_{Ar}), 113.6 (2xCH_{Ar}), 113.2 (=CH-CH), 65.3 (CHN), 55.5 (OCH₃), 55.4 (OCH₃), 52.3 (OCH₃), 41.5 (=CH-CH) ppm.

FTIR ν_{max} 1669 (2xC=O_{st}), 1666 (C=C_{st}), 1510 (NO_{2st as}), 1354 (NO_{2st sym}) cm^{-1} .

HRMS (ESI-TOF) m/z calcd. for C₃₅H₃₀N₃O₇ [M+H]⁺ 604.2084, found 604.2075.

Additionally, the synthesis of enantioenriched compound **(4S,5R)-135i** was carried out in a one-pot procedure starting from *p*-anisidine (25 mg, 200 μmol), benzaldehyde (10 μL , 100 μmol), ethyl pyruvate (34 μL , 300 μmol) and BINOL-derived chiral phosphoric acid **(R)-XXIII** (9 mg, 10 μmol). The mixture was stirred in diethyl ether (2 mL) at room temperature for 18 hours, and the reaction was monitored by $^1\text{H NMR}$ until the disappearance of the starting materials. Once γ -lactam **(S)-84a** was completely formed, the reaction was diluted in dichloromethane (5 mL), and YbTf₃ (7 mg, 10 μmol) and methyl (*E*)-4-(4-nitrophenyl)-2-oxobut-3-enoate **129a** (24 mg, 100 μmol) were added. The reaction was stirred at room temperature for 15 hours. The resulting mixture was washed with a saturated solution of NaHCO₃ (2 \times 5 mL) and H₂O (2 \times 5 mL) and the combined organic layers were dried over anhydrous MgSO₄ and concentrated under reduced pressure. The crude residue was purified by flash column chromatography (Hexanes/AcOEt) to afford 46 mg (76%) of pure bicyclic dihydropyridine **(4S,5R)-135i** as an orange solid. Ee (90%) was determined by HPLC analysis (Chiracel-IC, Heptane/DCM/AcOEt 60:30:10, 1 mL/min). Retention time (min): 10.8 (minor) and 19.8 (major). Spectroscopic data are in agreement with the data described above for the racemic mixture.

Methyl (4S*, 5R*)-1,6-bis(2-fluorophenyl)-4-(4-nitrophenyl)-7-oxo-5-phenyl-4,5,6,7-tetrahydro-1H-pyrrolo[3,4-b]pyridine-2-carboxylate (*cis*-135j).



The general procedure was followed using 1-(2-fluorophenyl)-3-((2-fluorophenyl)amino)-5-phenyl-1,5-dihydro-2H-pyrrol-2-one **84i** (362 mg, 1 mmol) and methyl (*E*)-4-(4-nitrophenyl)-2-oxobut-3-enoate **129a** (259 mg, 1.1 mmol) at room temperature for 14 hours to afford, after flash column chromatography (Hexanes/AcOEt 80:20), 485 mg (84%) of *cis*-135j as a single diastereoisomer (a yellow solid).

Mp (Et₂O): 199 - 200 °C.

¹H NMR (400 MHz, CDCl₃) δ 7.79 (d, ³J_{HH} = 8.7 Hz, 2xCH_{Ar}), 7.56 (td, ³J_{HH} = ³J_{FH} = 8.0, ⁴J_{FH} = 1.8 Hz, 1H, CH_{Ar}), 7.35 (m, 1H, CH_{Ar}), 7.21 - 7.15 (m, 2H, 2xCH_{Ar}), 7.14 - 7.09 (m, 3H, 3xCH_{Ar}), 7.02 (m, 1H, CH_{Ar}), 6.96 - 6.84 (m, 3H, 3xCH_{Ar}), 6.83 - 6.73 (m, 4H, 4xCH_{Ar}), 5.79 (d, ³J_{HH} = 4.4 Hz, 1H, =CH-CH), 5.48 (d, ⁴J_{HH} = 1.3 Hz, 1H, CHN), 4.83 (dd, ³J_{HH} = 4.4, ⁴J_{HH} = 1.3 Hz, 1H, =CH-CH), 3.56 (s, 3H, OCH₃) ppm.

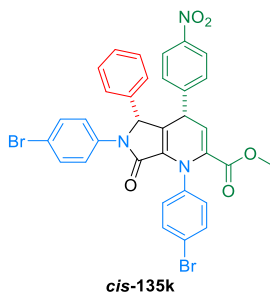
¹³C {¹H} NMR (101 MHz, CDCl₃) δ 163.3 (C=O), 163.2 (C=O), 160.4 (d, ¹J_{FC} = 249.3 Hz, C_{quat}), 157.2 (d, ¹J_{FC} = 249.3 Hz, C_{quat}), 149.7 (C_{quat}), 146.6 (C_{quat}), 135.2 (d, ²J_{FC} = 11.5 Hz, 2xC_{quat}), 132.3 (C_{quat}), 132.1 (CH_{Ar}), 130.1 (d, ³J_{FC} = 7.9 Hz, 2xCH_{Ar}), 129.2 (2xCH_{Ar}), 128.9 (CH_{Ar}), 128.4 (4xCH_{Ar}), 128.3 (C_{quat}), 128.1 (C_{quat}), 127.8 (2xCH_{Ar}), 124.3 (CH_{Ar}), 123.7 (CH_{Ar}), 123.6 (C_{quat}), 123.3 (2xCH_{Ar}), 116.34 (d, ²J_{FC} = 20.4 Hz, CH_{Ar}), 115.83 (d, ²J_{FC} = 20.4 Hz, CH_{Ar}), 112.9 (=CH-CH), 65.85 (d, ⁴J_{FC} = 5.0 Hz, CHN), 52.4 (OCH₃), 41.6 (=CH-CH) ppm.

¹⁹F NMR (282 MHz, CDCl₃) δ -121.2, -121.5 ppm.

FTIR ν_{max} 1726 (C=O_{st} ester), 1698 (C=O_{st} amide), 1691 (C=C_{st}), 1672 (C=C_{st}), 1495 (NO_{2st}as), 1343 (NO_{2st}sym) cm⁻¹.

HRMS (ESI-TOF) *m/z* calcd. for C₃₃H₂₄F₂N₃O₅ [M+H]⁺ 580.1684, found 580.1682.

Methyl (4S*,5R*)-4-(4-nitrophenyl)-7-oxo-1,6-di-*p*-tolyl-5-(trifluoromethyl)-4,5,6,7-tetrahydro-1*H*-pyrrolo[3,4-*b*]pyridine-2-carboxylate (*cis*-135k).



The general procedure was followed using 1-(4-bromophenyl)-3-((4-bromophenyl)amino)-5-phenyl-1,5-dihydro-2*H*-pyrrol-2-one **84d** (484 mg, 1 mmol) and methyl (*E*)-4-(4-nitrophenyl)-2-oxobut-3-enoate **129a** (259 mg, 1.1 mmol) at 40 °C (heating plate) for 14 hours, affording a 75:25 mixture of *cis*-**135k** and *trans*-**135k** diastereoisomers. After flash column chromatography (Hexanes/ACOEt 80:20), 485 mg (69%) of *cis*-**135k** isomer were isolated as a yellow solid.

Mp (Et₂O): 177 - 179 °C (dec.).

¹H NMR (400 MHz, CDCl₃) δ 7.80 (d, ³J_{HH} = 8.7 Hz, 2H, 2xCH_{Ar}), 7.54 (d, ³J_{HH} = 8.7 Hz, 2H, 2xCH_{Ar}), 7.41 (d, ³J_{HH} = 8.7 Hz, 2H, 2xCH_{Ar}), 7.30 - 7.18 (m, 4H, 4xCH_{Ar}), 7.04 (d, ³J_{HH} = 8.7 Hz, 2H, 2xCH_{Ar}), 6.92 - 6.76 (m, 5H, 5xCH_{Ar}), 5.81 (d, ³J_{HH} = 4.6 Hz, 1H, =CH-CH), 5.39 (d, ⁴J_{HH} = 1.2 Hz, 1H, CHN), 4.80 (dd, ³J_{HH} = 4.6, ⁴J_{HH} = 1.2 Hz, 1H, =CH-CH), 3.53 (s, 3H, OCH₃) ppm.

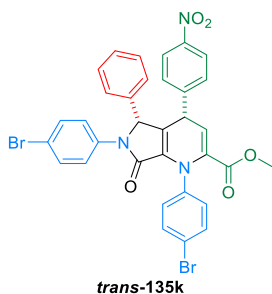
¹³C {¹H} NMR (101 MHz, CDCl₃) δ 163.4 (2xC=O), 149.1 (C_{quat}), 146.6 (C_{quat}), 140.6 (C_{quat}), 135.8 (C_{quat}), 135.7 (C_{quat}), 135.4 (C_{quat}), 133.4 (C_{quat}), 131.9 (2xCH_{Ar}), 131.8 (2xCH_{Ar}), 130.6 (2xCH_{Ar}), 128.9 (2xCH_{Ar}),

128.8 (2xCH_{Ar}), 128.6 (2xCH_{Ar}), 128.4 (C_{quat}), 127.3 (CH_{Ar}), 123.5 (2xCH_{Ar}), 123.3 (2xCH_{Ar}), 122.0 (C_{quat}), 118.1 (C_{quat}), 114.7 (=CH-CH), 64.7 (CHN), 52.5 (OCH₃), 41.4 (=CH-CH) ppm.

FTIR ν_{\max} 1729 (C=O_{st ester}), 1698 (C=O_{st amide}), 1691 (C=C_{st}), 1663 (C=C_{st}), 1489 (NO_{2st as}), 1340 (NO_{2st sym}) cm⁻¹.

HRMS (ESI-TOF) m/z calcd. for C₃₃H₂₄Br₂N₃O₅ [M+H]⁺ 702.0062, found 702.0050.

Methyl (4R*,5R*)-1,6-bis(4-bromophenyl)-4-(4-nitrophenyl)-7-oxo-5-phenyl-4,5,6,7-tetra-hydro-1H-pyrrolo[3,4-b]pyridine-2-carboxylate (*trans*-135k).



The general procedure was followed using 1-(4-bromophenyl)-3-((4-bromophenyl)amino)-5-phenyl-1,5-dihydro-2H-pyrrol-2-one **84d** (484 mg, 1 mmol) and methyl (*E*)-4-(4-nitrophenyl)-2-oxobut-3-enoate **129a** (259 mg, 1.1 mmol) at 40 °C (heating plate) for 14 hours, affording a 75:25 mixture of *cis*-**135k** and *trans*-**135k** diastereoisomers. After flash column chromatography (Hexanes/AcOEt 85:15), 154 mg (22%) of *trans*-**135k** isomer were isolated as a white solid.

Mp (Et₂O): 196 - 198 °C (dec.).

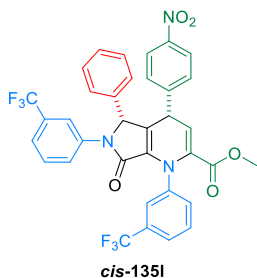
¹H NMR (400 MHz, CDCl₃) δ 8.33 (d, ³J_{HH} = 8.7 Hz, 2H, 2xCH_{Ar}), 7.54 (d, ³J_{HH} = 8.7 Hz, 2H, 2xCH_{Ar}), 7.46 (d, ³J_{HH} = 8.6 Hz, 2H, 2xCH_{Ar}), 7.40 (d, ³J_{HH} = 8.6 Hz, 2H, 2xCH_{Ar}), 7.38 - 7.32 (m, 3H, 3xCH_{Ar}), 7.27 - 7.16 (m, 4H, 4xCH_{Ar}), 7.06 - 6.99 (m, 2H, 2xCH_{Ar}), 5.74 (d, ³J_{HH} = 4.0 Hz, 1H, =CH-CH), 5.01 (s, 1H, CHN), 4.35 (d, ³J_{HH} = 4.0 Hz, 1H, =CH-CH), 3.54 (s, 3H, OCH₃) ppm.

¹³C {¹H} NMR (101 MHz, CDCl₃) δ 163.4 (2xC=O), 149.6 (C_{quat}), 147.8 (C_{quat}), 145.1 (C_{quat}), 140.7 (C_{quat}), 136.1 (C_{quat}), 133.7 (C_{quat}), 132.7 (C_{quat}), 131.9 (2xCH_{Ar}), 131.8 (2xCH_{Ar}), 130.7 (2xCH_{Ar}), 129.7 (2xCH_{Ar}), 129.5 (2xCH_{Ar}), 129.4 (CH_{Ar}), 128.7 (C_{quat}), 127.2 (2xCH_{Ar}), 124.7 (2xCH_{Ar}), 122.1 (C_{quat}), 118.0 (C_{quat}), 122.8 (2xCH_{Ar}), 114.1 (=CH-CH), 62.8 (CHN), 52.5 (OCH₃), 39.8 (=CH-CH) ppm.

FTIR ν_{\max} 1732 (C=O_{st ester}), 1707 (C=O_{st amide}), 1687 (C=C_{st}), 1659 (C=C_{st}), 1495 (NO_{2st as}), 1346 (NO_{2st sym}) cm⁻¹.

HRMS (ESI-TOF) m/z calcd. for C₃₃H₂₄Br₂N₃O₅ [M+H]⁺ 702.0062, found 702.0059.

Methyl (4*S,5*R**)-4-(4-nitrophenyl)-7-oxo-5-phenyl-1,6-bis(3-(trifluoromethyl)phenyl)-4,5,6,7-tetrahydro-1*H*-pyrrolo[3,4-*b*]pyridine-2-carboxylate (*cis*-135I).**



The general procedure was followed using 5-phenyl-1-(3-(trifluoromethyl)phenyl)-3-((3-(trifluoromethyl)phenyl)amino)-1,5-dihydro-2*H*-pyrrol-2-one **84I** (462 mg, 1 mmol) and methyl (*E*)-4-(4-nitrophenyl)-2-oxobut-3-enoate **129a** (259 mg, 1.1 mmol) at 40 °C (heating plate) for 56 hours, affording a 65:35 mixture of *cis*-**135I** and *trans*-**135I** diastereoisomers. After flash column chromatography (Hexanes/AcOEt 80:20), 414 mg (61%) of *cis*-**135I** isomer were isolated as a yellow solid.

Mp (Et₂O): 159 - 160 °C (dec.).

¹H NMR (400 MHz, CDCl₃) δ 7.81 (d, ³J_{HH} = 8.7 Hz, 3H, 3xCH_{Ar}), 7.73 (bs, 1H, CH_{Ar}), 7.68 - 7.50 (m, 4H, 4xCH_{Ar}), 7.31 - 7.18 (m, 2H, 2xCH_{Ar}), 7.07 (d, ³J_{HH} = 8.7 Hz, 2H, 2xCH_{Ar}), 6.93 - 6.77 (m, 5H, 5xCH_{Ar}), 5.88 (d, ³J_{HH} = 4.5 Hz, 1H, =CH-CH), 5.48 (d, ⁴J_{HH} = 1.3 Hz, 1H, CHN), 4.85 (dd, ³J_{HH} = 4.5, ⁵J_{HH} = 1.3 Hz, 1H, =CH-CH), 3.52 (s, 3H, OCH₃) ppm.

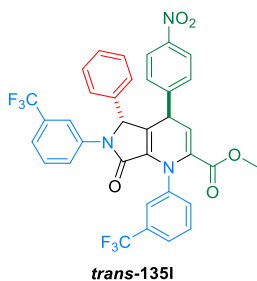
¹³C {¹H} NMR (101 MHz, CDCl₃) δ 163.4 (C=O), 163.2 (C=O), 148.9 (C_{quat}), 146.7 (C_{quat}), 142.1 (C_{quat}), 137.2 (C_{quat}), 135.6 (C_{quat}), 135.1 (C_{quat}), 133.1 (C_{quat}), 133.0 (CH_{Ar}), 131.26 (q, ²J_{FC} = 32.5 Hz, C_{quat}), 131.1 (q, ²J_{FC} = 32.5 Hz, C_{quat}), 129.4 (CH_{Ar}), 129.1 (CH_{Ar}), 129.0 (2xCH_{Ar}), 128.9 (2xCH_{Ar}), 128.7 (C_{quat}), 128.6 (CH_{Ar}), 127.4 (CH_{Ar}), 125.4 (q, ³J_{FC} = 3.7 Hz, CH_{Ar}), 125.0 (2xCH_{Ar}), 123.8 (q, ¹J_{FC} = 272.6 Hz, CF₃), 123.7 (q, ¹J_{FC} = 272.7 Hz, CF₃), 123.5 (2xCH_{Ar}), 121.6 (q, ³J_{FC} = 3.7 Hz, CH_{Ar}), 118.4 (q, ³J_{FC} = 4.0 Hz, CH_{Ar}), 115.1 (=CH-CH), 68.4 (CHN), 52.5 (OCH₃), 41.4 (=CH-CH) ppm.

¹⁹F NMR (282 MHz, CDCl₃) δ -62.9, -63.3 ppm.

FTIR ν_{max} 1736 (C=O_{st} ester), 1710 (C=O_{st} amide), 1676 (C=C_{st}), 1676 (C=C_{st}), 1530 (NO_{2st} as), 1267 (NO_{2st} sym), 1127 (C-F_{st}) cm⁻¹.

HRMS (ESI-TOF) *m/z* calcd. for C₃₅H₂₃F₆N₃O₅ [M+H]⁺ 680.1620, found 680.1620.

Methyl (4*R,5*R**)-4-(4-nitrophenyl)-7-oxo-5-phenyl-1,6-bis(3-(trifluoromethyl)phenyl)-4,5,6,7-tetrahydro-1*H*-pyrrolo[3,4-*b*]pyridine-2-carboxylate (*trans*-135I).**



The general procedure was followed using 5-phenyl-1-(3-(trifluoromethyl)phenyl)-3-((3-(trifluoromethyl)phenyl)amino)-1,5-dihydro-2*H*-pyrrol-2-one **84I** (462 mg, 1 mmol) and methyl (*E*)-4-(4-nitrophenyl)-2-oxobut-3-enoate **129a** (259 mg, 1.1 mmol) at 40 °C (heating plate) for 56 hours, affording a 65:35 mixture of *cis*-**135I** and *trans*-**135I**

diastereoisomers. After flash column chromatography (Hexanes/AcOEt 85:15), 223 mg (33%) of **trans-135l** isomer were isolated as a yellow solid.

Mp (Et₂O): 190 - 192 °C (dec.).

¹H NMR (400 MHz, CDCl₃) δ 8.35 (d, ³J_{HH} = 8.7 Hz, 2H, 2xCH_{Ar}), 7.80 (m, 1H, CH_{Ar}), 7.71 (bs, 1H, CH_{Ar}), 7.68 - 7.48 (m, 4H, 4xCH_{Ar}), 7.47 (d, ³J_{HH} = 8.7 Hz, 2H, 2xCH_{Ar}), 7.43 - 7.32 (m, 3H, 3xCH_{Ar}), 7.28 - 7.19 (m, 2H, 2xCH_{Ar}), 7.11 - 7.02 (m, 2H, 2xCH_{Ar}), 5.81 (d, ³J_{HH} = 4.0 Hz, 1H, =CH-CH), 5.08 (d, ⁴J_{HH} = 1.0 Hz, 1H, CHN), 4.39 (dd, ³J_{HH} = 4.0, ⁵J_{HH} = 1.0 Hz, 1H, =CH-CH), 3.53 (s, 3H, OCH₃) ppm.

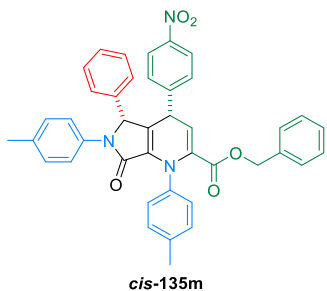
¹³C {¹H} NMR (101 MHz, CDCl₃) δ 163.4 (C=O), 163.2 (C=O), 149.4 (C_{quat}), 147.9 (C_{quat}), 142.1 (C_{quat}), 137.6 (C_{quat}), 135.9 (C_{quat}), 133.4 (C_{quat}), 133.2 (C_{quat}), 132.5 (CH_{Ar}), 131.3 (q, ²J_{FC} = 32.3 Hz, C_{quat}), 131.1 (q, ²J_{FC} = 33.0 Hz, C_{quat}), 129.7 (2xCH_{Ar}), 129.6 (CH_{Ar}), 129.5 (2xCH_{Ar}), 129.4 (2xCH_{Ar}), 129.1 (C_{quat}), 129.0 (CH_{Ar}), 127.2 (CH_{Ar}), 125.4 (q, ³J_{FC} = 3.7 Hz, CH_{Ar}), 125.1 (q, ³J_{FC} = 3.7 Hz, CH_{Ar}), 124.8 (2xCH_{Ar}), 124.5 (CH_{Ar}), 123.9 (q, ¹J_{FC} = 272.6 Hz, CF₃), 123.8 (q, ¹J_{FC} = 272.5 Hz, CF₃), 121.5 (q, ³J_{FC} = 3.5 Hz, CH_{Ar}), 117.9 (q, ³J_{FC} = 3.7 Hz, CH_{Ar}), 114.5 (=CH-CH), 62.9 (CHN), 52.5 (OCH₃), 38.9 (=CH-CH) ppm.

¹⁹F NMR (282 MHz, CDCl₃) δ -62.9, -63.3 ppm.

FTIR ν_{max} 1736 (C=O_{st} ester), 1707 (C=O_{st} amide), 1694 (C=C_{st}), 1672 (C=C_{st}), 1517 (NO_{2st}as), 1330 (NO_{2st}sym), 1134 (C-F_{st}) cm⁻¹.

HRMS (ESI-TOF) *m/z* calcd. for C₃₅H₂₃F₆N₃O₅ [M+H]⁺ 680.1620, found 680.1614.

Benzyl (4S*,5R*)-4-(4-nitrophenyl)-7-oxo-5-phenyl-1,6-di-*p*-tolyl-4,5,6,7-tetrahydro-1*H*-pyrrolo[3,4-*b*]pyridine-2-carboxylate (*cis*-135m).



The general procedure was followed using 5-phenyl-1-(*p*-tolyl)-3-(*p*-tolylamino)-1,5-dihydro-2*H*-pyrrol-2-one **72c** (354 mg, 1 mmol) and benzyl (*E*)-4-(4-nitrophenyl)-2-oxobut-3-enoate **129e** (342 mg, 1.1 mmol) at room temperature for 14 hours to afford, after flash column chromatography (Hexanes/AcOEt 80:20), 440 mg (68%) of **cis-135m** as a single diastereoisomer (a yellow solid).

Mp (Et₂O): 190 - 191 °C.

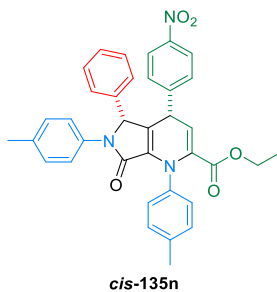
¹H NMR (400 MHz, CDCl₃) δ 7.78 (d, ³J_{HH} = 8.7 Hz, 2xCH_{Ar}), 7.40 (d, ³J_{HH} = 8.2 Hz, 2xCH_{Ar}), 7.28 - 7.26 (m, 2xCH_{Ar}), 7.18 (d, ³J_{HH} = 8.4 Hz, 2xCH_{Ar}), 7.14 (d, ³J_{HH} = 8.0 Hz, 2xCH_{Ar}), 7.10 - 7.02 (m, 5H, 5xCH_{Ar}), 6.93 (d, ³J_{HH} = 8.4 Hz, 2H, 2xCH_{Ar}), 6.87 - 6.73 (m, 5H, 2xCH_{Ar}), 5.75 (d, ³J_{HH} = 4.6 Hz, 1H, =CH-CH), 5.37 (d, ⁴J_{HH} = 1.2 Hz, 1H, CHN), 4.97 (d, ²J_{HH} = 12.2 Hz, 1H, CH_ACH_B Bn), 4.89 (d, ²J_{HH} = 12.2 Hz, 1H, CH_ACH_B Bn), 4.78 (dd, ³J_{HH} = 4.6 Hz, ⁴J_{HH} = 1.2 Hz, 1H, =CH-CH), 2.37 (s, 3H, CH₃), 2.15 (s, 3H, CH₃) ppm.

^{13}C { ^1H } NMR (101 MHz, CDCl_3) δ 163.6 (C=O), 163.5 (C=O), 149.7 (C_{quat}), 146.5 (C_{quat}), 138.8 (C_{quat}), 137.7 (C_{quat}), 136.5 (C_{quat}), 136.1 (C_{quat}), 135.1 (C_{quat}), 134.6 (C_{quat}), 134.2 (C_{quat}), 133.8 (C_{quat}), 129.3 ($2\times\text{CH}_{\text{Ar}}$), 129.2 ($2\times\text{CH}_{\text{Ar}}$), 128.9 ($2\times\text{CH}_{\text{Ar}}$), 128.6 ($5\times\text{CH}_{\text{Ar}}$), 128.5 ($2\times\text{CH}_{\text{Ar}}$), 128.4 ($2\times\text{CH}_{\text{Ar}}$), 128.2 ($2\times\text{CH}_{\text{Ar}}$), 127.8 (C_{quat}), 127.5 (CH_{Ar}), 123.4 ($2\times\text{CH}_{\text{Ar}}$), 122.2 ($2\times\text{CH}_{\text{Ar}}$), 113.9 ($=\text{CH}-\text{CH}$), 67.3 (CH_2 Bn), 64.8 (CHN), 41.5 ($=\text{CH}-\text{CH}$), 21.4 (CH_3), 20.9 (CH_3) ppm.

FTIR ν_{max} 1732 (C=O_{st} ester), 1717 (C=O_{st} amide), 1688 (C=C_{st}), 1669 (C=C_{st}), 1514 (NO_{2st} as), 1356 (NO_{2st} sym) cm^{-1} .

HRMS (ESI-TOF) m/z calcd. for $\text{C}_{41}\text{H}_{34}\text{N}_3\text{O}_5$ [$\text{M}+\text{H}$]⁺ 648.2498, found 648.2500.

Ethyl (4*S,5*R**)-4-(4-nitrophenyl)-7-oxo-5-phenyl-1,6-di-*p*-tolyl-4,5,6,7-tetrahydro-1*H*-pyrrolo[3,4-*b*]pyridine-2-carboxylate (*cis*-135n).**



The general procedure was followed using 5-phenyl-1-(*p*-tolyl)-3-(*p*-tolylamino)-1,5-dihydro-2*H*-pyrrol-2-one **72c** (354 mg, 1 mmol) and ethyl (*E*)-4-(4-nitrophenyl)-2-oxobut-3-enoate **129f** (274 mg, 1.1 mmol) at room temperature for 14 hours to afford, after flash column chromatography (Hexanes/AcOEt 80:20), 463 mg (79%) of *cis*-**135n** as a single diastereoisomer (a white solid).

Mp (Et_2O): 189 - 190 °C.

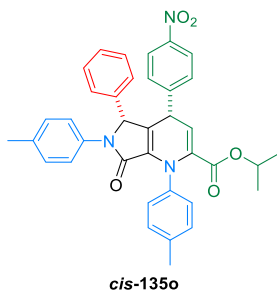
^1H NMR (400 MHz, CDCl_3) δ 7.79 (d, $^3J_{\text{HH}} = 8.7$ Hz, 2H, $2\times\text{CH}_{\text{Ar}}$), 7.44 (d, $^3J_{\text{HH}} = 8.2$ Hz, 2H, $2\times\text{CH}_{\text{Ar}}$), 7.24 - 7.16 (m, 4H, $4\times\text{CH}_{\text{Ar}}$), 7.07 (d, $^3J_{\text{HH}} = 8.7$ Hz, 2H, $2\times\text{CH}_{\text{Ar}}$), 6.93 (d, $^3J_{\text{HH}} = 8.2$ Hz, 2H, $2\times\text{CH}_{\text{Ar}}$), 6.87 - 6.74 (m, 5H, $5\times\text{CH}_{\text{Ar}}$), 5.71 (d, $^3J_{\text{HH}} = 4.6$ Hz, 1H, $=\text{CH}-\text{CH}$), 5.38 (d, $^4J_{\text{HH}} = 1.2$ Hz, 1H, CHN), 4.79 (dd, $^3J_{\text{HH}} = 4.6$ Hz, $^4J_{\text{HH}} = 1.2$ Hz, 1H, $=\text{CH}-\text{CH}$), 4.03 - 3.88 (m, 2H, CH_2), 2.38 (s, 3H, CH_3 tolyl), 2.15 (s, 3H, CH_3 tolyl), 0.98 (t, $^3J_{\text{HH}} = 7.1$ Hz, 3H, CH_2CH_3) ppm.

^{13}C { ^1H } NMR (101 MHz, CDCl_3) δ 163.6 (C=O), 163.5 (C=O), 149.9 (C_{quat}), 146.4 (C_{quat}), 138.9 (C_{quat}), 137.6 (C_{quat}), 136.7 (C_{quat}), 136.1 (C_{quat}), 134.6 (C_{quat}), 134.2 (C_{quat}), 133.6 (C_{quat}), 129.3 ($2\times\text{CH}_{\text{Ar}}$), 129.1 ($2\times\text{CH}_{\text{Ar}}$), 128.9 ($2\times\text{CH}_{\text{Ar}}$), 128.7 ($2\times\text{CH}_{\text{Ar}}$), 128.5 ($2\times\text{CH}_{\text{Ar}}$), 128.1 ($2\times\text{CH}_{\text{Ar}}$), 127.6 (C_{quat}), 127.4 (CH_{Ar}), 123.4 ($2\times\text{CH}_{\text{Ar}}$), 122.1 ($2\times\text{CH}_{\text{Ar}}$), 113.3 ($=\text{CH}-\text{CH}$), 64.8 (CHN), 61.5 (CH_2), 41.5 ($=\text{CH}-\text{CH}$), 21.38 (CH_3 tolyl), 20.9 (CH_3 tolyl), 13.8 (CH_2CH_3) ppm.

FTIR ν_{max} 1732 (C=O_{st} ester), 1716 (C=O_{st} amide), 1688 (C=C_{st}), 1666 (C=C_{st}), 1508 (NO_{2st} as), 1340 (NO_{2st} sym) cm^{-1} .

HRMS (ESI-TOF) m/z calcd. for $\text{C}_{36}\text{H}_{32}\text{N}_3\text{O}_5$ [$\text{M}+\text{H}$]⁺ 586.2343, found 586.2355.

Iso-propyl (4*S,5*R**)-4-(4-nitrophenyl)-7-oxo-5-phenyl-1,6-di-*p*-tolyl-4,5,6,7-tetrahydro-1*H*-pyrrolo[3,4-*b*]pyridine-2-carboxylate (*cis*-135o).**



The general procedure was followed using 5-phenyl-1-(*p*-tolyl)-3-(*p*-tolylamino)-1,5-dihydro-2*H*-pyrrol-2-one **72c** (354 mg, 1 mmol) and iso-propyl (*E*)-4-(4-nitrophenyl)-2-oxobut-3-enoate **129g** (289 mg, 1.1 mmol) at room temperature for 14 hours to afford, after flash column chromatography (Hexanes/AcOEt 80:20), 456 mg (76%) of *cis*-**135o** as a single diastereoisomer (a white solid).

Mp (Et₂O): 187 - 188 °C.

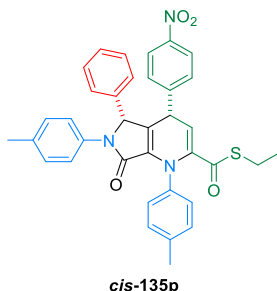
¹H NMR (400 MHz, CDCl₃) δ 7.79 (d, ³J_{HH} = 8.7 Hz, 2H, 2xCH_{Ar}), 7.44 (d, ³J_{HH} = 8.2 Hz, 2H, 2xCH_{Ar}), 7.22 - 7.16 (m, 4H, 4xCH_{Ar}), 7.07 (d, ³J_{HH} = 8.7 Hz, 2H, 2xCH_{Ar}), 6.93 (d, ³J_{HH} = 8.2 Hz, 2H, 2xCH_{Ar}), 6.87 - 6.75 (m, 5H, 5xCH_{Ar}), 5.69 (d, ³J_{HH} = 4.6 Hz, 1H, =CH-CH), 5.37 (d, ⁴J_{HH} = 1.2 Hz, 1H, CHN), 4.87 - 4.68 (m, 2H, CH ⁱPr + =CH-CH), 2.37 (s, 3H, CH₃ tolyl), 2.15 (s, 3H, CH₃ tolyl), 0.99 (d, ³J_{HH} = 6.2 Hz, 3H, CH₃ ⁱPr), 0.90 (d, ³J_{HH} = 6.2 Hz, 3H, CH₃ ⁱPr) ppm.

¹³C {¹H} NMR (101 MHz, CDCl₃) δ 163.7 (C=O), 163.3 (C=O), 149.9 (C_{quat}), 146.4 (C_{quat}), 139.0 (C_{quat}), 137.6 (C_{quat}), 137.0 (C_{quat}), 136.1 (C_{quat}), 134.6 (C_{quat}), 134.2 (C_{quat}), 133.6 (C_{quat}), 129.3 (2xCH_{Ar}), 129.0 (2xCH_{Ar}), 128.9 (2xCH_{Ar}), 128.8 (2xCH_{Ar}), 128.6 (2xCH_{Ar}), 128.2 (2xCH_{Ar}), 127.7 (C_{quat}), 127.0 (CH_{Ar}), 123.4 (2xCH_{Ar}), 122.2 (2xCH_{Ar}), 113.1 (=CH-CH), 69.4 (CH ⁱPr), 64.8 (CHN), 41.5 (=CH-CH), 21.4 (CH₃), 21.3 (CH₃), 21.2 (CH₃), 20.9 (CH₃) ppm.

FTIR ν_{max} 1723 (C=O_{st} ester), 1704 (C=O_{st} amide), 1675 (C=C_{st}), 1669 (C=C_{st}), 1514 (NO_{2st} as), 1346 (NO_{2st} sym) cm⁻¹.

HRMS (ESI-TOF) *m/z* calcd. for C₃₇H₃₄N₃O₅ [M+H]⁺ 600.2517, found 600.2512.

Ethyl (4*S,5*R**)-4-(4-nitrophenyl)-7-oxo-5-phenyl-1,6-di-*p*-tolyl-4,5,6,7-tetrahydro-1*H*-pyrrolo[3,4-*b*]pyridine-2-carbothioate (*cis*-135p).**



as a yellow solid.

The general procedure was followed using 5-phenyl-1-(*p*-tolyl)-3-(*p*-tolylamino)-1,5-dihydro-2*H*-pyrrol-2-one **72c** (354 mg, 1 mmol) and ethyl (*E*)-4-(4-nitrophenyl)-2-oxobut-3-enethioate **129h** (292 mg, 1.1 mmol) at 40 °C (heating plate) for 24 hours, affording a 88:12 mixture of *cis*-**135p** and *trans*-**135p** diastereoisomers. After flash column chromatography (Hexanes/AcOEt 80:20), 475 mg (79%) of *cis*-**135p** isomer were isolated

Mp (Et₂O): 184 - 186 °C (dec.).

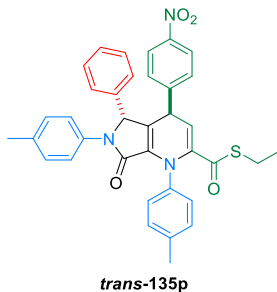
¹H NMR (400 MHz, CDCl₃) δ 7.80 (d, ³J_{HH} = 8.6 Hz, 2H, 2xCH_{Ar}), 7.40 (d, ³J_{HH} = 8.2 Hz, 2H, 2xCH_{Ar}), 7.19 (d, ³J_{HH} = 8.2 Hz, 2H, 2xCH_{Ar}), 7.18 (d, ³J_{HH} = 8.5 Hz, 2H, 2xCH_{Ar}), 7.06 (d, ³J_{HH} = 8.6 Hz, 2H, 2xCH_{Ar}), 6.93 (d, ³J_{HH} = 8.5 Hz, 2H, 2xCH_{Ar}), 6.88 - 6.73 (m, 5H, 5xCH_{Ar}), 5.62 (d, ³J_{HH} = 4.6 Hz, 1H, =CH-CH), 5.38 (d, ⁴J_{HH} = 1.2 Hz, 1H, CHN), 4.78 (d, ³J_{HH} = 4.6 Hz, 1H, =CH-CH), 2.72 (q, ³J_{HH} = 7.4 Hz, 2H, CH₂), 2.37 (s, 3H, CH₃ tolyl), 2.15 (s, 3H, CH₃ tolyl), 1.05 (t, ³J_{HH} = 7.4 Hz, 3H, CH₂CH₃) ppm.

¹³C {¹H} NMR (101 MHz, CDCl₃) δ 189.5 (C=O), 163.5 (C=O), 150.1 (C_{quat}), 146.5 (C_{quat}), 142.9 (C_{quat}), 137.8 (C_{quat}), 137.8 (C_{quat}), 136.1 (C_{quat}), 134.6 (C_{quat}), 134.2 (C_{quat}), 133.3 (C_{quat}), 129.3 (2xCH_{Ar}), 129.2 (2xCH_{Ar}), 128.9 (2xCH_{Ar}), 128.8 (2xCH_{Ar}), 128.6 (2xCH_{Ar}), 128.2 (2xCH_{Ar}), 127.7 (C_{quat}), 127.5 (CH_{Ar}) 123.4 (2xCH_{Ar}), 122.2 (2xCH_{Ar}), 110.8 (=CH-CH), 64.9 (CHN), 41.5 (=CH-CH), 23.9 (CH₂), 21.5 (CH₃ tolyl), 20.9 (CH₃ tolyl), 14.3 (CH₂CH₃) ppm.

FTIR ν_{max} 1698 (C=O_{st} Tioester), 1682 (C=O_{st} amide), 1675 (C=C_{st}), 1663 (C=C_{st}), 1511 (NO₂_{st} as), 1349 (NO₂_{st} sym) cm⁻¹.

HRMS (ESI-TOF) *m/z* calcd. for C₃₆H₃₂N₃O₄S [M+H]⁺ 602.2113, found 602.2117.

Ethyl (4*R,5*R**)-4-(4-nitrophenyl)-7-oxo-5-phenyl-1,6-di-*p*-tolyl-4,5,6,7-tetrahydro-1*H*-pyrrolo[3,4-*b*]pyridine-2-carbothioate (*trans*-135*p*).**



as a yellow solid.

The general procedure was followed using 5-phenyl-1-(*p*-tolyl)-3-(*p*-tolylamino)-1,5-dihydro-2*H*-pyrrol-2-one **72c** (354 mg, 1 mmol) and ethyl (*E*)-4-(4-nitrophenyl)-2-oxobut-3-enethioate **129h** (292 mg, 1.1 mmol) at 40 °C (heating plate) for 24 hours, affording a 88:12 mixture of *cis*-**135p** and *trans*-**135p** diastereoisomers. After flash column chromatography (Hexanes/AcOEt 81:15), 36.1 mg (6%) of *trans*-**135p** isomer were isolated

Mp (Et₂O): 187 - 189 °C (dec.).

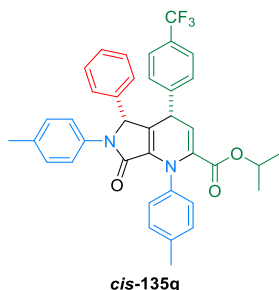
¹H NMR (400 MHz, CDCl₃) δ 7.80 (d, ³J_{HH} = 8.6 Hz, 2H, 2xCH_{Ar}), 7.40 (d, ³J_{HH} = 8.2 Hz, 2H, 2xCH_{Ar}), 7.19 (d, ³J_{HH} = 8.2 Hz, 2H, 2xCH_{Ar}), 7.18 (d, ³J_{HH} = 8.5 Hz, 2H, 2xCH_{Ar}), 7.06 (d, ³J_{HH} = 8.6 Hz, 2H, 2xCH_{Ar}), 6.93 (d, ³J_{HH} = 8.5 Hz, 2H, 2xCH_{Ar}), 6.88 - 6.73 (m, 5H, 5xCH_{Ar}), 5.62 (d, ³J_{HH} = 4.6 Hz, 1H, =CH-CH), 5.38 (d, ⁴J_{HH} = 1.2 Hz, 1H, CHN), 4.78 (d, ³J_{HH} = 4.6 Hz, 1H, =CH-CH), 2.72 (q, ³J_{HH} = 7.4 Hz, 2H, CH₂), 2.37 (s, 3H, CH₃ tolyl), 2.15 (s, 3H, CH₃ tolyl), 1.05 (t, ³J_{HH} = 7.4 Hz, 3H, CH₂CH₃) ppm.

¹³C {¹H} NMR (101 MHz, CDCl₃) δ 189.5 (C=O), 163.5 (C=O), 150.1 (C_{quat}), 146.5 (C_{quat}), 142.9 (C_{quat}), 137.8 (C_{quat}), 137.8 (C_{quat}), 136.1 (C_{quat}), 134.6 (C_{quat}), 134.2 (C_{quat}), 133.3 (C_{quat}), 129.3 (2xCH_{Ar}), 129.2 (2xCH_{Ar}), 128.9 (2xCH_{Ar}), 128.8 (2xCH_{Ar}), 128.6 (2xCH_{Ar}), 128.2 (2xCH_{Ar}), 127.7 (C_{quat}), 127.5 (CH_{Ar}) 123.4 (2xCH_{Ar}), 122.2 (2xCH_{Ar}), 110.8 (=CH-CH), 64.9 (CHN), 41.5 (=CH-CH), 23.9 (CH₂), 21.5 (CH₃ tolyl), 20.9 (CH₃ tolyl), 14.3 (CH₂CH₃) ppm.

FTIR ν_{\max} 1698 (C=O_{st} Tioster), 1682 (C=O_{st} amide), 1672 (C=C_{st}), 1653 (C=C_{st}), 1514 (NO₂_{st as}), 1365 (NO₂_{st sym}) cm⁻¹.

HRMS (ESI-TOF) m/z calcd. for C₃₆H₃₂N₃O₄S [M+H]⁺ 602.2113, found 602.2117.

Iso-propyl (4S*,5R*)-7-oxo-5-phenyl-1,6-di-*p*-tolyl-4-(4-(trifluoromethyl)phenyl)-4,5,6,7-tetrahydro-1*H*-pyrrolo[3,4-*b*]pyridine-2-carboxylate (*cis*-135q).



The general procedure was followed using 5-phenyl-1-(*p*-tolyl)-3-(*p*-tolylamino)-1,5-dihydro-2*H*-pyrrol-2-one **72c** (354 mg, 1 mmol) and *iso*-propyl (*E*)-2-oxo-4-(4-(trifluoromethyl)phenyl)but-3-enoate **129i** (314 mg, 1.1 mmol) at room temperature for 14 hours to afford, after flash column chromatography (Hexanes/AcOEt 80:20), 554 mg (89%) of *cis*-**135q** as a single diastereoisomer (a white solid).

Mp (Et₂O): 192 °C.

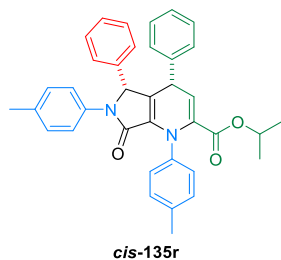
¹H NMR (400 MHz, CDCl₃) δ 7.46 (d, ³J_{HH} = 8.2 Hz, 2H, 2xCH_{Ar}), 7.23 - 7.14 (m, 6H, 6xCH_{Ar}), 7.02 (d, ³J_{HH} = 7.7 Hz, 2H, 2xCH_{Ar}), 6.93 (d, ³J_{HH} = 8.2 Hz, 2H, 2xCH_{Ar}), 6.88 - 6.70 (m, 5H, 5xCH_{Ar}), 5.74 (d, ³J_{HH} = 4.5 Hz, 1H, =CH-CH), 5.36 (d, ³J_{HH} = 1.2 Hz, 1H, CHN), 4.80 (hept, ³J_{HH} = 6.2 Hz, 1H, CHⁱPr), 4.72 (dd, ³J_{HH} = 4.5, ³J_{HH} = 1.2 Hz, 1H, =CH-CH), 2.37 (s, 3H, CH₃ tolyl), 2.15 (s, 3H, CH₃ tolyl), 1.00 (d, ³J_{HH} = 6.2 Hz, 3H, CH₃ⁱPr), 0.91 (d, ³J_{HH} = 6.2 Hz, 3H, CH₃ⁱPr) ppm.

¹³C {¹H} NMR (101 MHz, CDCl₃) δ 163.9 (C=O), 163.4 (C=O), 146.5 (C_{quat}), 139.4 (C_{quat}), 137.4 (C_{quat}), 136.7 (C_{quat}), 136.1 (C_{quat}), 134.4 (C_{quat}), 134.3 (C_{quat}), 133.4 (C_{quat}), 129.3 (2xCH_{Ar}), 129.0 (2xCH_{Ar}), 128.8 (2xCH_{Ar}), 128.5 (2xCH_{Ar}), 128.4 (2xCH_{Ar}), 128.1 (CH_{Ar}), 127.5 (2xCH_{Ar}), 125.1 (2xCH_{Ar}), 122.2 (2xCH_{Ar}), 124.10 (q, ¹J_{FC} = 271.7 Hz, CF₃) 114.1 (=CH-CH), 69.2 (CHⁱPr), 64.9 (CHN), 41.5 (=CH-CH), 21.4 (CH₃), 21.3 (CH₃), 21.2 (CH₃), 20.9 (CH₃) ppm.

¹⁹F NMR (282 MHz, CDCl₃) δ -63.2 ppm.

FTIR ν_{\max} 1723 (C=O_{st} ester), 1701 (C=O_{st} amide), 1669 (2xC=C_{st}), 1195 (C-F_{st}) cm⁻¹.

HRMS (ESI-TOF) m/z calcd. for C₃₈H₃₄F₃N₂O₃ [M+H]⁺ 623.2521, found 623.2505.

Iso-propyl (4S*,5R*)-7-oxo-4,5-diphenyl-1,6-di-*p*-tolyl-4,5,6,7-tetrahydro-1H-pyrrolo[3,4-b]pyridine-2-carboxylate (*cis*-135r).

The general procedure was followed using 5-phenyl-1-(*p*-tolyl)-3-(*p*-tolylamino)-1,5-dihydro-2*H*-pyrrol-2-one **72c** (354 mg, 1 mmol) and *iso*-propyl (*E*)-2-oxo-4-phenylbut-3-enoate **129j** (240 mg, 1.1 mmol) at room temperature for 14 hours to afford, after flash column chromatography (Hexanes/AcOEt 90:10), 464 mg (84%) of *cis*-135r as a single diastereoisomer (a white solid).

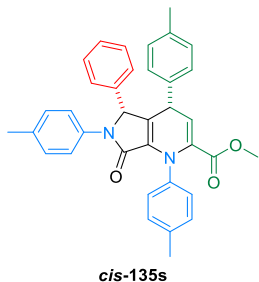
Mp (Et₂O): 196 - 197 °C.

¹H NMR (400 MHz, CDCl₃) δ 7.49 (d, ³*J*_{HH} = 8.2 Hz, 2H, 2xCH_{Ar}), 7.20 (d, ³*J*_{HH} = 8.5 Hz, 2H, 2xCH_{Ar}), 7.19 (d, ³*J*_{HH} = 8.0 Hz, 2H, 2xCH_{Ar}), 6.97 - 6.87 (m, 7H, 7xCH_{Ar}), 6.79 (s, 5H, 5xCH_{Ar}), 5.83 (d, ³*J*_{HH} = 4.8 Hz, 1H, =CH-CH), 5.36 (d, ⁴*J*_{HH} = 1.2 Hz, 1H, CHN), 4.79 (hept, ³*J*_{HH} = 6.2 Hz, 1H, CH ^{*i*}Pr), 4.62 (dd, ³*J*_{HH} = 4.8, ³*J*_{HH} = 1.2 Hz, 1H, =CH-CH), 2.37 (s, 3H, CH₃ tolyl), 2.15 (s, 3H, CH₃ tolyl), 1.00 (d, ³*J*_{HH} = 6.2 Hz, 3H, CH₃ ^{*i*}Pr), 0.89 (d, ³*J*_{HH} = 6.2 Hz, 3H, CH₃ ^{*i*}Pr) ppm.

¹³C {¹H} NMR (101 MHz, CDCl₃) δ 164.3 (C=O), 163.6 (C=O), 142.5 (C_{quat}), 139.8 (C_{quat}), 137.1 (C_{quat}), 136.2 (C_{quat}), 136.0 (C_{quat}), 134.5 (C_{quat}), 134.3 (C_{quat}), 133.4 (C_{quat}), 129.8 (C_{quat}), 129.2 (2xCH_{Ar}), 128.9 (2xCH_{Ar}), 128.8 (2xCH_{Ar}), 128.2 (4xCH_{Ar}), 128.1 (2xCH_{Ar}), 127.8 (CH_{Ar}), 127.5 (2xCH_{Ar}), 126.5 (CH_{Ar}), 122.2 (2xCH_{Ar}), 116.0 (=CH-CH), 69.0 (CH ^{*i*}Pr), 65.1 (CHN), 41.7 (=CH-CH), 21.5 (CH₃), 21.3 (CH₃), 21.2 (CH₃), 20.9 (CH₃) ppm.

FTIR ν_{max} 1723 (C=O_{st} ester), 1704 (C=O_{st} amide), 1698 (C=C_{st}), 1666 (C=C_{st}) cm⁻¹.

HRMS (ESI-TOF) *m/z* calcd. for C₃₇H₃₅N₂O₃ [M+H]⁺ 555.2647, found 555.2632.

Methyl (4S*,5R*)-7-oxo-5-phenyl-1,4,6-tri-*p*-tolyl-4,5,6,7-tetrahydro-1H-pyrrolo[3,4-b]pyridine-2-carboxylate (*cis*-135s).

The general procedure was followed using 5-phenyl-1-(*p*-tolyl)-3-(*p*-tolylamino)-1,5-dihydro-2*H*-pyrrol-2-one **72c** (354 mg, 1 mmol) and methyl (*E*)-2-oxo-4-(*p*-tolyl)but-3-enoate **129d** (224 mg, 1.1 mmol) at room temperature for 14 hours to afford, after flash column chromatography (Hexanes/AcOEt 90:10), 341 mg (63%) of *cis*-135s as a single diastereoisomer (a white solid).

Mp (Et₂O): 203 - 205 °C (dec.).

¹H NMR (400 MHz, CDCl₃) δ 7.48 (d, ³*J*_{HH} = 8.3 Hz, 2H, 2xCH_{Ar}), 7.20 (d, ³*J*_{HH} = 8.6 Hz, 2H, 2xCH_{Ar}), 7.19 (d, ³*J*_{HH} = 8.1 Hz, 2H, 2xCH_{Ar}), 6.92 (d, ³*J*_{HH} = 7.9 Hz, 2H, 2xCH_{Ar}), 6.86 - 6.74 (m, 7H, 7xCH_{Ar}), 6.72 (d,

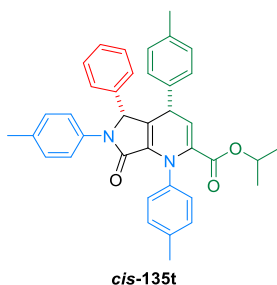
$^3J_{\text{HH}} = 7.9$ Hz, 2H, 2xCH_{Ar}), 5.87 (d, $^3J_{\text{HH}} = 4.6$ Hz, 1H, =CH-CH), 5.36 (d, $^4J_{\text{HH}} = 1.2$ Hz, 1H, CHN), 4.60 (dd, $^3J_{\text{HH}} = 4.6$ Hz, $^4J_{\text{HH}} = 1.2$ Hz, 1H, =CH-CH), 3.50 (s, 3H, OCH₃), 2.37 (s, 3H, CH₃ tolyl), 2.15 (s, 6H, 2xCH₃ tolyl) ppm.

^{13}C { ^1H } NMR (101 MHz, CDCl₃) δ 164.2 (C=O), 164.2 (C=O), 139.8 (C_{quat}), 139.5 (C_{quat}), 137.2 (C_{quat}), 136.4 (C_{quat}), 136.1 (C_{quat}), 135.3 (C_{quat}), 134.5 (C_{quat}), 134.2 (C_{quat}), 133.5 (C_{quat}), 130.0 (C_{quat}), 129.2 (2xCH_{Ar}), 129.1 (2xCH_{Ar}), 128.9 (2xCH_{Ar}), 128.7 (2xCH_{Ar}), 128.2 (2xCH_{Ar}), 128.1 (2xCH_{Ar}), 127.6 (CH_{Ar}), 127.4 (2xCH_{Ar}), 122.1 (2xCH_{Ar}), 116.8 (=CH-CH), 65.1 (CHN), 52.1 (OCH₃), 41.2 (=CH-CH), 21.4 (CH₃ tolyl), 21.0 (CH₃ tolyl), 20.9 (CH₃ tolyl) ppm.

FTIR ν_{max} 1732 (C=O_{st} ester), 1698 (C=O_{st} amide), 1691 (C=C_{st}), 1660 (C=C_{st}) cm⁻¹.

HRMS (ESI-TOF) m/z calcd. for C₃₆H₃₃N₂O₃ [M+H]⁺ 541.2491, found 541.2500.

Iso-propyl (4S*,5R*)-7-oxo-5-phenyl-1,4,6-tri-*p*-tolyl-4,5,6,7-tetrahydro-1H-pyrrolo[3,4-b]pyridine-2-carboxylate (*cis*-135t).



The general procedure was followed using 5-phenyl-1-(*p*-tolyl)-3-(*p*-tolylamino)-1,5-dihydro-2H-pyrrol-2-one **72c** (354 mg, 1 mmol) and iso-propyl (*E*)-2-oxo-4-(*p*-tolyl)but-3-enoate **129k** (255 mg, 1.1 mmol) at room temperature for 14 hours to afford, after flash column chromatography (Hexanes/AcOEt 80:20), 430 mg (76%) of *cis*-135t as a single diastereoisomer (a yellow solid).

Mp (Et₂O): 100 -101 °C.

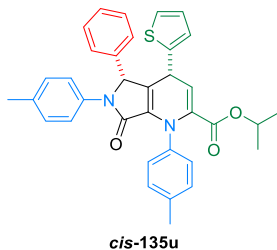
^1H NMR (400 MHz, CDCl₃) δ 7.49 (d, $^3J_{\text{HH}} = 8.2$ Hz, 2H, 2xCH_{Ar}), 7.23 - 7.16 (m, 4H, 4xCH_{Ar}), 6.93 (d, $^3J_{\text{HH}} = 8.2$ Hz, 2H, 2xCH_{Ar}), 6.87 - 6.75 (m, 7H, 7xCH_{Ar}), 6.72 (d, $^3J_{\text{HH}} = 7.9$ Hz, 2H, 2xCH_{Ar}), 5.83 (d, $^3J_{\text{HH}} = 4.7$ Hz, 1H, =CH-CH), 5.35 (d, $^4J_{\text{HH}} = 1.2$ Hz, 1H, CHN), 4.80 (hept, $^3J_{\text{HH}} = 6.3$ Hz, 1H, CH^{*i*}Pr), 4.59 (dd, $^3J_{\text{HH}} = 4.7$, $^4J_{\text{HH}} = 1.2$ Hz, 1H, =CH-CH), 2.37 (s, 3H, CH₃ tolyl), 2.15 (s, 6H, 2xCH₃ tolyl), 1.00 (d, $^3J_{\text{HH}} = 6.3$ Hz, 3H, CH₃^{*i*}Pr), 0.91 (d, $^3J_{\text{HH}} = 6.3$ Hz, 3H, CH₃^{*i*}Pr) ppm.

^{13}C { ^1H } NMR (101 MHz, CDCl₃) δ 164.3 (C=O), 163.6 (C=O), 139.9 (C_{quat}), 139.6 (C_{quat}), 137.1 (C_{quat}), 136.4 (C_{quat}), 136.0 (C_{quat}), 136.0 (C_{quat}), 134.5 (C_{quat}), 134.2 (C_{quat}), 133.3 (C_{quat}), 130.1 (C_{quat}), 129.2 (2xCH_{Ar}), 128.9 (2xCH_{Ar}), 128.8 (2xCH_{Ar}), 128.8 (2xCH_{Ar}), 128.1 (4xCH_{Ar}), 127.6 (2xCH_{Ar}), 127.3 (CH_{Ar}), 122.2 (2xCH_{Ar}), 116.7 (=CH-CH), 68.9 (CH^{*i*}Pr), 65.1 (CHN), 41.2 (=CH-CH), 21.5 (CH₃), 21.3 (CH₃), 21.2 (CH₃), 21.0 (CH₃), 20.9 (CH₃) ppm.

FTIR ν_{max} 1726 (C=O_{st} ester), 1704 (C=O_{st} amide), 1691 (C=C_{st}), 1672 (C=C_{st}) cm⁻¹.

HRMS (ESI-TOF) m/z calcd. for C₃₈H₃₆N₂O₃ [M+H]⁺ 569.2804, found 569.2806.

Iso-propyl (4R*,5R*)-7-oxo-5-phenyl-4-(thiophen-2-yl)-1,6-di-*p*-tolyl-4,5,6,7-tetrahydro-1H-pyrrolo[3,4-b]pyridine-2-carboxylate (*cis*-135u).



The general procedure was followed using 5-phenyl-1-(*p*-tolyl)-3-(*p*-tolylamino)-1,5-dihydro-2H-pyrrol-2-one **72c** (354 mg, 1 mmol) and *iso*-propyl (*E*)-2-oxo-4-(thiophen-2-yl)but-3-enoate **129l** (247 mg, 1.1 mmol) at room temperature for 14 hours to afford, after flash column chromatography (Hexanes/AcOEt 85:15), 376 mg (67%) of *cis*-135u as a single diastereoisomer (a yellow solid).

Mp (Et₂O): 146 - 148 °C (dec.).

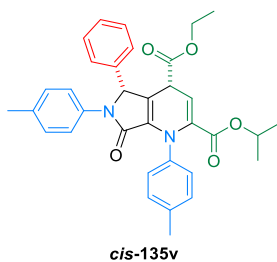
¹H NMR (400 MHz, CDCl₃) δ 7.53 (d, ³J_{HH} = 8.2 Hz, 2H, 2xCH_{Ar}), 7.19 (d, ³J_{HH} = 7.9 Hz, 2H, 2xCH_{Ar}), 7.18 (d, ³J_{HH} = 8.5 Hz, 2H, 2xCH_{Ar}), 6.97 - 6.86 (m, 8H, 8xCH_{Ar}), 6.47 (dd, ³J_{HH} = 5.1 Hz, ³J_{HH} = 3.5 Hz, 1H, CH thienyl), 6.28 (dd, ³J_{HH} = 3.5 Hz, ⁴J_{HH} = 1.2 Hz, 1H, CH thienyl), 5.91 (d, ³J_{HH} = 5.0 Hz, 1H, =CH-CH), 5.38 (d, ⁴J_{HH} = 1.2 Hz, 1H, CHN), 4.91 (dd, ³J_{HH} = 5.0 Hz, ⁴J_{HH} = 1.2 Hz, 1H, =CH-CH), 4.82 (hept, ³J_{HH} = 6.2 Hz, 1H, CH ⁱPr), 2.37 (s, 3H, CH₃ tolyl), 2.16 (s, 3H, CH₃ tolyl), 1.04 (d, ³J_{HH} = 6.2 Hz, 3H, CH₃ ⁱPr), 0.88 (d, ³J_{HH} = 6.2 Hz, 3H, CH₃ ⁱPr) ppm.

¹³C {¹H} NMR (101 MHz, CDCl₃) δ 164.2 (C=O), 163.4 (C=O), 147.5 (C_{quat}), 139.4 (C_{quat}), 137.3 (C_{quat}), 136.3 (C_{quat}), 135.9 (C_{quat}), 134.4 (2xC_{quat}), 132.9 (C_{quat}), 129.5 (C_{quat}), 129.2 (2xCH_{Ar}), 129.1 (2xCH_{Ar}), 128.9 (2xCH_{Ar}), 128.3 (2xCH_{Ar}), 127.8 (CH_{Ar}), 127.6 (2xCH_{Ar}), 126.5 (CH_{Ar}), 124.9 (2xCH_{Ar}), 122.5 (2xCH_{Ar}), 115.1 (=CH-CH), 69.1 (CH ⁱPr), 65.1 (CHN), 35.9 (=CH-CH), 21.5 (CH₃), 21.4 (CH₃), 21.2 (CH₃), 20.9 (CH₃) ppm.

FTIR ν_{max} 1726 (C=O_{st} ester), 1713 (C=O_{st} amide), 1694 (C=C_{st}), 1669 (C=C_{st}) cm⁻¹.

HRMS (ESI-TOF) *m/z* calcd. for C₃₅H₃₃N₂O₃S [M+H]⁺ 561.2212, found 561.2192.

4-Ethyl 2-*iso*-propyl (4R*,5R*)-7-oxo-5-phenyl-1,6-di-*p*-tolyl-4,5,6,7-tetrahydro-1H-pyrrolo[3,4-b]pyridine-2,4-dicarboxylate (*cis*-135v).



The general procedure was followed using 5-phenyl-1-(*p*-tolyl)-3-(*p*-tolylamino)-1,5-dihydro-2H-pyrrol-2-one **72c** (354 mg, 1 mmol) and 1-ethyl 5-*iso*-propyl (*E*)-4-oxopent-2-enedioate **129m** (235 mg, 1.1 mmol) at room temperature for 14 hours to afford, after flash column chromatography (Hexanes/AcOEt 90:10), 473 mg (86%) of *cis*-135v as a single diastereoisomer (yellow oil).

¹H NMR (400 MHz, CDCl₃) δ 7.34 (d, ³J_{HH} = 8.1 Hz, 2H, 2xCH_{Ar}), 7.34 - 7.22 (m, 5H, 5xCH_{Ar}), 7.20 (d, ³J_{HH} = 8.1 Hz, 2H, 2xCH_{Ar}), 7.14 (d, ³J_{HH} = 8.1 Hz, 2H, 2xCH_{Ar}), 6.96 (d, ³J_{HH} = 8.1 Hz, 2H, 2xCH_{Ar}), 5.77 (m,

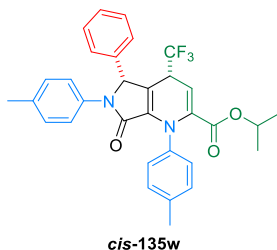
2H, =CH-CH and CHN), 4.81 (hept, $^3J_{\text{HH}} = 6.2$ Hz, 1H, CH i Pr), 4.30 (m, 2H, CH₂), 3.87 (m, 1H, =CH-CH), 2.33 (s, 3H, CH₃ tolyl), 2.19 (s, 3H, CH₃ tolyl), 1.38 (t, $^3J_{\text{HH}} = 7.1$ Hz, 3H, CH₂CH₃), 0.99 (d, $^3J_{\text{HH}} = 6.2$ Hz, 3H, CH₃ i Pr), 0.95 (d, $^3J_{\text{HH}} = 6.2$ Hz, 3H, CH₃ i Pr) ppm.

^{13}C { ^1H } NMR (101 MHz, CDCl₃) δ 170.4 (C=O), 163.7 (C=O), 163.3 (C=O), 139.0 (C_{quat}), 138.3 (C_{quat}), 137.5 (C_{quat}), 134.9 (C_{quat}), 134.9 (C_{quat}), 134.3 (C_{quat}), 133.7 (C_{quat}), 129.3 (2xCH_{Ar}), 129.2 (2xCH_{Ar}), 129.0 (2xCH_{Ar}), 128.9 (2xCH_{Ar}), 128.6 (CH_{Ar}), 127.1 (2xCH_{Ar}), 124.8 (C_{quat}), 121.7 (2xCH_{Ar}), 108.1 (=CH-CH), 69.3 (CH i Pr), 63.4 (CHN), 61.9 (CH₂), 39.8 (=CH-CH-), 21.3 (2xCH₃), 21.2 (CH₃), 20.9 (CH₃), 14.4 (CH₃) ppm.

FTIR ν_{max} 1732 (C=O_{st} ester), 1720 (C=O_{st} ester), 1698 (C=O_{st} amide), 1694 (C=C_{st}), 1669 (C=C_{st}) cm⁻¹.

HRMS (ESI-TOF) m/z calcd. for C₃₄H₃₅N₂O₅ [M+H]⁺ 551.2546, found 551.2543.

Iso-propyl (4*R,5*R**)-7-oxo-5-phenyl-1,6-di-*p*-tolyl-4-(trifluoromethyl)-4,5,6,7-tetrahydro-1*H*-pyrrolo[3,4-*b*]pyridine-2-carboxylate (*cis*-135*w*).**



The general procedure was followed using 5-phenyl-1-(*p*-tolyl)-3-(*p*-tolylamino)-1,5-dihydro-2*H*-pyrrol-2-one **72c** (354 mg, 1 mmol) and iso-propyl (*E*)-5,5,5-trifluoro-2-oxopent-3-enoate **129n** (231 mg, 1.1 mmol) at room temperature for 14 hours to afford, after flash column chromatography (Hexane/AcOEt 80:20), 459 mg (84%) of *cis*-135*w* as a single diastereoisomer (a yellow solid).

Mp (Et₂O): 90 - 91 °C (dec.).

^1H NMR (400 MHz, CDCl₃) δ 7.41 (d, $^3J_{\text{HH}} = 8.3$ Hz, 2H, 2xCH_{Ar}), 7.28 - 7.14 (m, 7H, 7xCH_{Ar}), 7.15 (d, $^3J_{\text{HH}} = 8.5$ Hz, 2H, 2xCH_{Ar}), 6.96 (d, $^3J_{\text{HH}} = 8.3$ Hz, 2H, 2xCH_{Ar}), 5.70 (d, $^3J_{\text{HH}} = 5.2$ Hz, 1H, =CH-CH), 5.35 (d, $^4J_{\text{HH}} = 1.0$ Hz, 1H, CHN), 4.84 (hept, $^3J_{\text{HH}} = 6.3$ Hz, 1H, CH i Pr), 4.23 - 4.08 (m, 1H, =CH-CH), 2.36 (s, CH₃ tolyl), 2.18 (s, CH₃ tolyl), 1.05 (d, $^3J_{\text{HH}} = 6.3$ Hz, 3H, CH₃ i Pr), 0.93 (d, $^3J_{\text{HH}} = 6.3$ Hz, 3H, CH₃ i Pr) ppm.

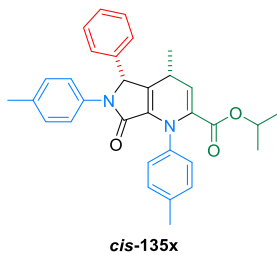
^{13}C { ^1H } NMR (101 MHz, CDCl₃) δ 163.1 (C=O), 162.6 (C=O), 140.3 (C_{quat}), 137.9 (C_{quat}), 137.8 (C_{quat}), 137.2 (C_{quat}), 135.1 (C_{quat}), 135.0 (C_{quat}), 133.8 (C_{quat}), 129.9 (2xCH_{Ar}), 129.3 (2xCH_{Ar}), 129.1 (2xCH_{Ar}), 129.0 (2xCH_{Ar}), 128.7 (CH_{Ar}), 128.2 (2xCH_{Ar}), 123.6 (q, $^1J_{\text{FC}} = 282.3$ Hz, CF₃), 123.2 (2xCH_{Ar}), 120.8 (C_{quat}), 104.2 (d, $^3J_{\text{FC}} = 3.7$ Hz, =CH-CH), 69.6 (CH i Pr), 65.2 (CHN), 40.5 (q, $^2J_{\text{FC}} = 31.6$ Hz, =CH-CH), 21.4 (CH₃), 21.3 (CH₃), 21.2 (CH₃), 21.0 (CH₃) ppm.

^{19}F NMR (282 MHz, CDCl₃) δ -70.7 ppm.

FTIR ν_{max} 1726 (C=O_{st} ester), 1726 (C=O_{st} amide), 1701 (C=O_{st}), 1688 (C=C_{st}), 1663 (C=C_{st}) cm⁻¹.

HRMS (ESI-TOF) m/z calcd. for C₃₂H₃₀F₃N₂O₃ [M+H]⁺ 547.2208, found 547.2201.

Iso-propyl (4*R,5*R**)-4-methyl-7-oxo-5-phenyl-1,6-di-*p*-tolyl-4,5,6,7-tetrahydro-1*H*-pyrrolo[3,4-*b*]pyridine-2-carboxylate (*cis*-135*x*).**



as a pale violet solid.

Mp (Et₂O): 93 - 95 °C.

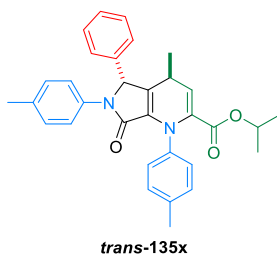
¹H NMR (400 MHz, CDCl₃) δ 7.42 (d, ³J_{HH} = 8.2 Hz, 2H, 2xCH_{Ar}), 7.29 - 7.16 (m, 7H, 7xCH_{Ar}), 7.14 (d, ³J_{HH} = 8.6 Hz, 2H, 2xCH_{Ar}), 6.96 (d, ³J_{HH} = 8.6 Hz, 2H, 2xCH_{Ar}), 5.84 (d, ³J_{HH} = 4.8 Hz, 1H, =CH-CH), 5.32 (d, ⁴J_{HH} = 1.2 Hz, 1H, CHN), 4.81 (hept, ³J_{HH} = 6.3 Hz, 1H, CH ⁱPr), 3.48 (qdd, ³J_{HH} = 6.8 Hz, ³J_{HH} = 4.8 Hz, ⁴J_{HH} = 1.2 Hz, 1H, =CH-CH), 2.34 (s, CH₃ tolyl), 2.18 (s, CH₃ tolyl), 1.03 (d, ³J_{HH} = 6.3 Hz, 3H, CH₃ ⁱPr), 0.90 (d, ³J_{HH} = 6.3 Hz, 3H, CH₃ ⁱPr), 0.62 (d, ³J_{HH} = 6.8 Hz, 3H, CH-CH₃) ppm.

¹³C {¹H} NMR (101 MHz, CDCl₃) δ 164.6 (C=O), 163.8 (C=O), 140.4 (C_{quat}), 137.6 (C_{quat}), 136.9 (C_{quat}), 136.7 (C_{quat}), 134.6 (C_{quat}), 134.2 (C_{quat}), 133.8 (C_{quat}), 133.36 (C_{quat}), 129.3 (2xCH_{Ar}), 129.1 (4xCH_{Ar}), 128.9 (2xCH_{Ar}), 128.8 (2xCH_{Ar}), 128.7 (CH_{Ar}), 122.2 (2xCH_{Ar}), 119.3 (=CH-CH), 68.9 (CH ⁱPr), 64.9 (CHN), 29.7 (=CH-CH), 23.7 (CH₃), 21.5 (CH₃), 21.3 (CH₃), 21.2 (CH₃), 20.9 (CH₃) ppm.

FTIR ν_{max} 1729 (C=O_{st} ester), 1694 (C=O_{st} amide), 1682 (C=C_{st}), 1669 (C=C_{st}) cm⁻¹.

HRMS (ESI-TOF) *m/z* calcd. for C₃₂H₃₃N₂O₃ [M+H]⁺ 493.2491, found 493.2486.

Iso-propyl (4*S,5*R**)-4-methyl-7-oxo-5-phenyl-1,6-di-*p*-tolyl-4,5,6,7-tetrahydro-1*H*-pyrrolo[3,4-*b*]pyridine-2-carboxylate (*trans*-135*x*).**



as a pale violet solid.

Mp (Et₂O): 93 - 95 °C.

The general procedure was followed using 5-phenyl-1-(*p*-tolyl)-3-(*p*-tolylamino)-1,5-dihydro-2*H*-pyrrol-2-one **72c** (354 mg, 1 mmol) and *iso*-propyl (*E*)-2-oxopent-3-enoate **129o** (172 mg, 1.1 mmol) at room temperature for 24 hours, affording a 85:15 mixture of *cis*-135*x* and *trans*-135*x* diastereoisomers. After flash column chromatography (Hexanes/AcOEt 80:20), 281 mg (57%) of *cis*-135*x* isomer were isolated

The general procedure was followed using 5-phenyl-1-(*p*-tolyl)-3-(*p*-tolylamino)-1,5-dihydro-2*H*-pyrrol-2-one **72c** (354 mg, 1 mmol) and *iso*-propyl (*E*)-2-oxopent-3-enoate **129o** (172 mg, 1.1 mmol) at room temperature for 24 hours, affording a 85:15 mixture of *cis*-135*x* and *trans*-135*x* diastereoisomers. After flash column chromatography (Hexanes/AcOEt 80:20), 49 mg (8%) of *trans*-135*x* isomer were isolated

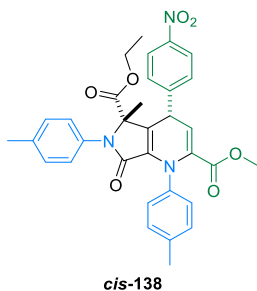
¹H NMR (400 MHz, CDCl₃) δ 7.39 (d, ³J_{HH} = 8.2 Hz, 2H, 2xCH_{Ar}), 7.35 - 7.19 (m, 7H, 7xCH_{Ar}), 7.14 (d, ³J_{HH} = 8.5 Hz, 2H, 2xCH_{Ar}), 6.96 (d, ³J_{HH} = 8.8 Hz, 2H, 2xCH_{Ar}), 5.71 (d, ³J_{HH} = 4.0 Hz, 1H, =CH-CH), 5.43 (d, ⁴J_{HH} = 0.9 Hz, 1H, CHN), 4.81 (hept, ³J_{HH} = 6.2 Hz, 1H, CH ⁱPr), 3.09 (qdd, ³J_{HH} = 6.9 Hz, ³J_{HH} = 4.0 Hz, ⁴J_{HH} = 0.9 Hz, 1H, =CH-CH), 2.33 (s, CH₃ tolyl), 2.18 (s, CH₃ tolyl), 1.39 (d, ³J_{HH} = 6.9 Hz, 3H, CH-CH₃), 0.99 (d, ³J_{HH} = 6.2 Hz, 3H, CH₃ ⁱPr), 0.95 (d, ³J_{HH} = 6.2 Hz, 3H, CH₃ ⁱPr) ppm.

¹³C {¹H} NMR (101 MHz, CDCl₃) δ 164.4 (C=O), 163.8 (C=O), 140.3 (C_{quat}), 137.0 (C_{quat}), 137.0 (C_{quat}), 135.0 (C_{quat}), 135.0 (C_{quat}), 134.2 (C_{quat}), 133.0 (C_{quat}), 132.6 (C_{quat}), 129.2 (2xCH_{Ar}), 129.1 (2xCH_{Ar}), 128.9 (2xCH_{Ar}), 128.8 (2xCH_{Ar}), 128.6 (CH_{Ar}), 127.2 (2xCH_{Ar}), 121.8 (2xCH_{Ar}), 117.8 (=CH-CH), 68.9 (CH ⁱPr), 62.9 (CHN), 27.9 (=CH-CH), 23.0 (CH₃), 21.4 (CH₃), 21.3 (CH₃), 21.2 (CH₃), 20.9 (CH₃) ppm.

FTIR ν_{max} 1726 (C=O_{st} ester), 1698 (C=O_{st} amide), 1684 (C=C_{st}), 1662 (C=C_{st}) cm⁻¹.

HRMS (ESI-TOF) *m/z* calcd. for C₃₂H₃₃N₂O₃ [M+H]⁺ 493.2491, found 493.2467.

5-Ethyl 2-methyl (4*S,5*S**)-5-methyl-4-(4-nitrophenyl)-7-oxo-1,6-di-*p*-tolyl-4,5,6,7-tetrahydro-1*H*-pyrrolo[3,4-*b*]pyridine-2,5-dicarboxylate (*cis*-138).**



The general procedure was followed using ethyl 2-methyl-5-oxo-1-(*p*-tolyl)-4-(*p*-tolylamino)-2,5-dihydro-1*H*-pyrrole-2-carboxylate **81** (364 mg, 1 mmol) and methyl (*E*)-4-(4-nitrophenyl)-2-oxobut-3-enoate **129a** (259 mg, 1.1 mmol) at room temperature for 24 hours to afford, after flash column chromatography (Hexane/AcOEt 90:10), 465 mg (80%) of *cis*-**138** as a single diastereoisomer (an orange solid).

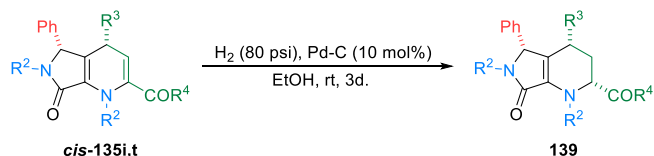
Mp (Et₂O): 179 - 181 °C (dec.).

¹H NMR (400 MHz, CDCl₃) δ 78.24 (d, ³J_{HH} = 8.7 Hz, 2H, 2xCH_{Ar}), 7.54 (d, ³J_{HH} = 8.7 Hz, 2H, 2xCH_{Ar}), 7.36 (d, ³J_{HH} = 8.3 Hz, 2H, 2xCH_{Ar}), 7.16 (d, ³J_{HH} = 8.3 Hz, 2H, 2xCH_{Ar}), 7.08 (d, ³J_{HH} = 8.4 Hz, 2H, 2xCH_{Ar}), 7.00 (d, ³J_{HH} = 8.4 Hz, 2H, 2xCH_{Ar}), 5.74 (d, ³J_{HH} = 4.6 Hz, 1H, =CH-CH), 4.84 (d, ³J_{HH} = 4.6 Hz, 1H, =CH-CH), 3.52 (s, 3H, OCH₃), 3.40 (dq, ²J_{HH} = 10.8, ³J_{HH} = 7.2 Hz, 1H, CH_AH_B), 3.18 (dq, ²J_{HH} = 10.8, ³J_{HH} = 7.2 Hz, 1H, CH_AH_B), 2.34 (s, 3H, CH₃ tolyl), 2.27 (s, 3H, CH₃ tolyl), 1.64 (s, 3H, CCH₃), 0.96 (t, ³J_{HH} = 7.2 Hz, 3H, CH₂CH₃) ppm.

¹³C {¹H} NMR (101 MHz, CDCl₃) δ 170.1 (C=O), 164.1 (C=O), 163.8 (C=O), 149.3 (C_{quat}), 147.5 (C_{quat}), 138.3 (C_{quat}), 137.8 (C_{quat}), 137.5 (C_{quat}), 136.2 (C_{quat}), 134.7 (C_{quat}), 132.7 (C_{quat}), 129.8 (2xCH_{Ar}), 129.6 (2xCH_{Ar}), 129.1 (2xCH_{Ar}), 128.5 (2xCH_{Ar}), 127.1 (2xCH_{Ar}), 126.0 (C_{quat}), 124.0 (2xCH_{Ar}), 113.1 (=CH-CH), 67.8 (CN), 62.0 (CH₂), 52.4 (OCH₃), 39.8 (=CH-CH), 21.4 (CH₃ tolyl), 21.1 (CH₃ tolyl), 18.8 (CH₂CH₃), 13.8 (CCH₃) ppm.

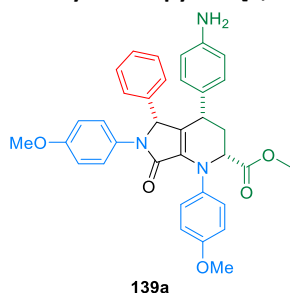
FTIR ν_{\max} 1736 (C=O_{st} ester), 1710 (C=O_{st} ester), 1707 (C=O_{st} amide), 1672 (C=C_{st}), 1514 (NO_{2st} as), 1356 (NO_{2st} sym) cm⁻¹.

HRMS (ESI-TOF) m/z calcd. for C₃₃H₃₂N₃O₇ [M+H]⁺ 582.2240, found 582.2239.

General procedure for the diastereoselective hydrogenation of compounds *cis*-135i,t.

A mixture of the bicyclic 1,4-dihydropyridines *cis*-135 (0.5 mmol) and 53.2 mg of 10% palladium on carbon (0.05 mmol Pd) in ethanol (100 mL) was stirred for 3 days under hydrogen at 80 psi. The reaction mixture was filtered, and the filter washed with dichloromethane (2×20 mL). The combined organic fractions were distilled off at reduced pressure and the crude residue was purified by flash column chromatography (Hexanes/AcOEt) to afford pure products **139**.

Methyl (2*R,4*S**,5*R**)-4-(4-aminophenyl)-1,6-bis(4-methoxyphenyl)-7-oxo-5-phenyl-2,3,4,5,6,7-hexahydro-1*H*-pyrrolo[3,4-*b*]pyridine-2-carboxylate (**139a**).**



The general procedure was followed using bicyclic 1,4-dihydropyridine *cis*-135i (302 mg, 0.5 mmol) to afford, after flash column chromatography (Hexanes/AcOEt 85:15), 256 mg (89%) of **139a** as a white solid.

Mp (Et₂O): 199 - 201 °C.

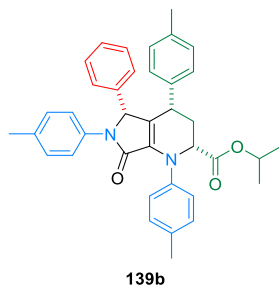
¹H NMR (400 MHz, CDCl₃) δ 7.36 (d, ³J_{HH} = 9.0 Hz, 2H, 2xCH_{Ar}), 7.21 (d, ³J_{HH} = 8.8 Hz, 2H, 2xCH_{Ar}), 6.93 (s, 5H, 5xCH_{Ar}), 6.85 (d, ³J_{HH} = 8.8 Hz, 2H, 2xCH_{Ar}), 6.68 (d, ³J_{HH} = 9.0 Hz, 2H, 2xCH_{Ar}), 6.49 (d, ³J_{HH} = 8.2 Hz, 2H, 2xCH_{Ar}), 6.31 (d, ³J_{HH} = 8.2 Hz, 2H, 2xCH_{Ar}), 5.41 (d, ⁴J_{HH} = 1.2 Hz, 1H, CHN), 4.89 (bs, 2H, NH₂), 4.25 (t, ³J_{HH} = 4.7 Hz, 1H, CH-CO₂Me), 3.94 (m, 1H, CH-Ar), 3.78 (s, 3H, OCH₃), 3.66 (s, 3H, OCH₃), 3.16 (s, 3H, OCH₃), 2.58 (dt, ²J_{HH} = 13.4, ³J_{HH} = 3.8 Hz, 1H, CH_ACH_B), 2.40 (dt, ²J_{HH} = 13.4, ³J_{HH} = 5.6 Hz, 1H, CH_ACH_B) ppm.

¹³C {¹H} NMR (101 MHz, CDCl₃) δ 171.8 (C=O), 164.8 (C=O), 157.4 (C_{quat}), 156.2 (C_{quat}), 138.6 (C_{quat}), 137.5 (C_{quat}), 134.7 (C_{quat}), 130.9 (C_{quat}), 129.3 (2xCH_{Ar}), 128.4 (2xCH_{Ar}), 127.4 (4xCH_{Ar}), 127.4 (C_{quat}), 127.0 (CH_{Ar}), 124.1 (C_{quat}), 123.3 (4xCH_{Ar}), 113.9 (4xCH_{Ar}), 66.0 (CHN), 62.8 (CH-CO₂Me), 55.5 (OCH₃), 55.4 (OCH₃), 51.8 (OCH₃), 37.8 (CH-Ar), 33.5 (CH₂) ppm.

FTIR ν_{max} 3461 and 3376 (N-H₂ st), 1755 (C=O_{st} ester), 1698 (C=O_{st} amide), 1647 (C=C_{st}) cm⁻¹.

HRMS (ESI-TOF) *m/z* calcd. for C₃₅H₃₃N₃O₅ [M+H]⁺ 576.2498, found 576.2492.

Iso-propyl (2*R,4*S**,5*R**)-7-oxo-5-phenyl-1,4,6-tri-*p*-tolyl-2,3,4,5,6,7-hexahydro-1*H*-pyrrolo[3,4-*b*]pyridine-2-carboxylate (139b).**



The general procedure was followed using bicyclic 1,4-dihydropyridine *cis*-**135t** (185 mg, 0.5 mmol) to afford, after flash column chromatography (Hexanes/AcOEt 90:10), 259 mg (96%) of **139b** as a white solid.

Mp (Et₂O): 84 - 86 °C (dec.).

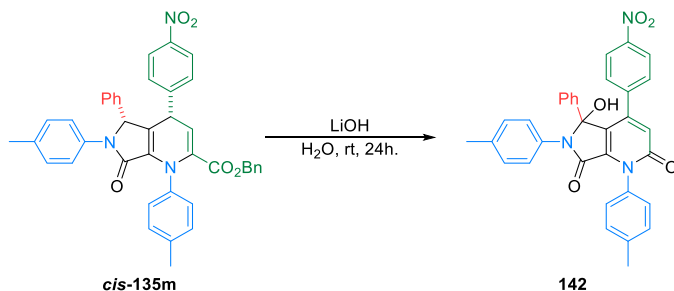
¹H NMR (400 MHz, CDCl₃) δ 7.36 (d, ³J_{HH} = 8.6 Hz, 2H, 2xCH_{Ar}), 7.16 (d, ³J_{HH} = 8.6 Hz, 2H, 2xCH_{Ar}), 7.12 (d, ³J_{HH} = 8.3 Hz, 2H, 2xCH_{Ar}), 6.93 (d, ³J_{HH} = 8.3 Hz, 2H, 2xCH_{Ar}), 6.87 (s, 5H, 5xCH_{Ar}), 6.59 (d, ³J_{HH} = 8.0 Hz, 2H, 2xCH_{Ar}), 6.54 (d, ³J_{HH} = 8.0 Hz, 2H, 2xCH_{Ar}), 5.43 (d, ⁴J_{HH} = 1.2 Hz, 1H, CHN), 4.43 (hept, ³J_{HH} = 6.3 Hz, 1H, CH ⁱPr), 4.26 (t, ³J_{HH} = 5.0 Hz, 1H, CH-CO₂ⁱPr), 3.98 (t, ³J_{HH} = 5.0 Hz, 1H, CH-Ar), 2.57 (dt, ²J_{HH} = 13.5, ³J_{HH} = 4.5 Hz, 1H, CH_ACH_B), 2.46 (dt, ²J_{HH} = 13.5, ³J_{HH} = 5.7 Hz, 1H, CH_ACH_B), 2.32 (s, 3H, CH₃ tolyl), 2.16 (s, 3H, CH₃ tolyl), 2.11 (s, 3H, CH₃ tolyl), 1.03 (d, ³J_{HH} = 6.3 Hz, 3H, CH₃ ⁱPr), 0.64 (d, ³J_{HH} = 6.3 Hz, 3H, CH₃ ⁱPr) ppm.

¹³C {¹H} NMR (101 MHz, CDCl₃) δ 170.7 (C=O), 164.8 (C=O), 143.0 (C_{quat}), 137.6 (C_{quat}), 137.3 (C_{quat}), 135.2 (2xC_{quat}), 134.9 (2xC_{quat}), 133.5 (C_{quat}), 129.3 (2xCH_{Ar}), 129.2 (2xCH_{Ar}), 128.3 (2xCH_{Ar}), 128.2 (2xCH_{Ar}), 128.1 (2xCH_{Ar}), 127.1 (CH_{Ar}), 126.9 (2xCH_{Ar}), 125.8 (2xCH_{Ar}), 125.3 (C_{quat}), 121.4 (2xCH_{Ar}), 68.7 (CH ⁱPr), 65.6 (CHN), 63.1 (CH-CO₂ⁱPr), 38.6 (CH-Ar), 33.7 (CH₂), 21.7 (CH₃), 21.2 (CH₃), 21.0 (CH₃), 20.9 (CH₃), 20.8 (CH₃) ppm.

FTIR ν_{max} 1739 (C=O_{st} ester), 1701 (C=O_{st} amide), 1653 (C=C_{st}) cm⁻¹.

HRMS (ESI-TOF) *m/z* calcd. for C₃₈H₃₈N₂O₃ [M+H]⁺ 571.2960, found 571.2961.

Synthesis of 5-hydroxy-4-(4-nitrophenyl)-5-phenyl-1,6-di-*p*-tolyl-5,6-dihydro-1*H*-pyrrolo[3,4-*b*]pyridine-2,7-dione **142**.



Lithium hydroxide (23.5 mg, 2 mmol) was slowly added to a 3 mL solution of **cis-135m** (323 mg, 0.5 mmol) in THF/H₂O (1:1) at room temperature, and the reaction was stirred for 12 hours. The resulting mixture was washed with a 0.1 M aqueous solution of HCl (2×5 mL) and extracted with AcOEt (3×10mL). The combined organic layers were dried over anhydrous MgSO₄ and concentrated under reduced pressure. The crude residue was purified by flash column chromatography (Hexanes/AcOEt 70:30), affording 195 mg (72%) of **142** as a white-yellow solid.

Mp (Et₂O): 267 - 269 °C (dec.).

¹H NMR (400 MHz, CDCl₃) δ 7.96 (d, ³J_{HH} = 8.7 Hz, 2H, 2xCH_{Ar}), 7.41 - 7.28 (m, 2H, 2xCH_{Ar}), 7.16 (d, ³J_{HH} = 8.7 Hz, 2H, 2xCH_{Ar}), 7.14 - 7.09 (m, 2H, 2xCH_{Ar}), 7.04 (t, ³J_{HH} = 7.5 Hz, 2H, 2xCH_{Ar}), 6.99 - 6.89 (m, 7H, 7xCH_{Ar}), 6.60 (s, 1H, =CH), 4.17 (bs, 1H, OH), 2.40 (s, 3H, CH₃ tolyl), 2.17 (s, 3H, CH₃ tolyl) ppm.

¹³C {¹H} NMR (101 MHz, CDCl₃) δ 162.8 (C=O), 159.9 (C=O), 148.1 (C_{quat}), 147.8 (C_{quat}), 141.4 (C_{quat}), 139.6 (C_{quat}), 137.4 (C_{quat}), 136.4 (C_{quat}), 136.2 (C_{quat}), 132.5 (C_{quat}), 131.5 (C_{quat}), 130.1 (2xCH_{Ar}), 129.7 (2xCH_{Ar}), 129.4 (2xCH_{Ar}), 128.7 (CH_{Ar}), 128.3 (2xCH_{Ar}), 128.1 (C_{quat}), 127.3 (2xCH_{Ar}), 126.4 (2xCH_{Ar}), 126.1 (2xCH_{Ar}), 125.0 (=CH), 122.8 (2xCH_{Ar}), 90.0 (C_{quat}), 21.5 (CH₃ tolyl), 21.1 (CH₃ tolyl) ppm.

³¹P NMR (162 MHz, CDCl₃) δ 39.1 ppm.

FTIR ν_{max} 3347 (O-H_{st}), 1726 (C=O_{st} Ketone), 1710 (C=O_{st} amide), 1663 (C=CH_{st}), 1624 (C=C_{st}), 1517 (NO₂_{st} as), 1346 (NO₂_{st} sym) cm⁻¹.

HRMS (ESI-TOF) *m/z* calcd. for C₃₃H₂₅N₃O₅ [M+H]⁺ 544.1872, found 544.1874.



Experimental Section II

Biological assays

Chapter 7. Evaluation of the antiproliferative activity and the apoptosis induction capability.

Compound purity analysis.

Before any biological assay, the purity of the synthesized compounds was analyzed by HPLC. The analyses were performed on an Agilent 1260 Infinity HPLC system (Agilent, Santa Clara, CA, United States) (C-18 column, Hypersil, BDS, 5 μm , 0.4 mm \times 25 mm) at room temperature. All the tested compounds were dissolved in dichloromethane, and 5 μL of the sample were loaded onto the column. Ethanol and heptane were used as the mobile phase, and the flow rate was set at 1.0 mL/min. The maximal absorbance within the range of 190 - 625 nm was used as the detection wavelength. The purity of all the tested compounds was in all cases over 95%.

Cytotoxicity assays.

I. Cell culture.

Human lung carcinoma epithelial cells (A549) (ATCC[®] CCL-185[™]) were grown in Kaighn's Modification of Ham's F-12 Medium (ATCC[®] 30-2004[™]), supplemented with 10% of fetal bovine serum (FBS) (Gibco[®]) and with 1% of Normocin solution (Thermo Fisher).

Human non-malignant lung fibroblast cells (MRC5) (ATCC[®] CCL-171[™]) were grown in Eagle's Minimum Essential Medium (EMEM) (ATCC[®] 30-2003[™]), supplemented with 10% of fetal bovine serum (FBS) (Gibco[®]) and with 1% of Normocin solution (Thermo Fisher).

Human ovary adenocarcinoma epithelial cells (SKOV3) (ATCC[®] HTB-77[™]) were grown in McCoy's 5A medium (ATCC[®] 30-2007[™]), supplemented with 10% of fetal bovine serum (FBS) (Gibco[®]) and with 1% of NORMOCIN solution (Thermo Fisher).

Human colon carcinoma epithelial cells (RKO) (ATCC[®] CRL-2577[™]) were grown in Eagle's Minimum Essential Medium (EMEM, ATCC[®] 30-2003[™]), supplemented with 10% of fetal bovine serum (FBS) (Gibco[®]) and with 1% of Normocin solution (Thermo Fisher).

Human kidney carcinoma epithelial cells (HEK293) (ATCC® CRL-3249™) were grown in Eagle's Minimum Essential Medium (EMEM, ATCC® 30-2003™), supplemented with 10% of fetal bovine serum (FBS) (Gibco®), 2 mM L-glutamine (Thermo Fisher), 1 mM sodium pyruvate (Thermo Fisher), 1% non-essential amino acids (Thermo Fisher) and with 1% of Normocin solution (Thermo Fisher).

Human breast adenocarcinoma epithelial cells (MCF7) (ATCC® HTB-22™) were grown in Eagle's Minimum Essential Medium (EMEM, ATCC® 30-2003™), supplemented with 10% of fetal bovine serum (FBS) (Gibco®), 0.01 mg/ml human recombinant insulin (Thermo Fisher) and with 1% of Normocin solution (Thermo Fisher).

Human prostate carcinoma epithelial cells (HTB81) (ATCC® HTB-81™) were grown in Eagle's Minimum Essential Medium (EMEM, ATCC® 30-2003™), supplemented with 10% of fetal bovine serum (FBS) (Gibco®) and with 1% of Normocin solution (Thermo Fisher).

Human cervix adenocarcinoma epithelial cells (HeLa) (ATCC® CCL-2™) were grown in Eagle's Minimum Essential Medium (EMEM) (ATCC® 30-2003™), supplemented with 10% of fetal bovine serum (FBS) (Gibco®) and with 1% of Normocin solution (Thermo Fisher).

Cells were plated into a culture flask and incubated at 37 °C, 5% CO₂ atmosphere and 95% humidity. Cells were split every time it was needed (70 - 80 % of confluence) in order to maintain a monolayer coverage.

Subculturing procedure. (Volumes given for a 150 cm² flask).

1. Remove and discard the culture medium.
2. Briefly rinse the cell layer with 5 mL of phosphate-buffered saline 1X (PBS) (Gibco®) twice.
3. Add 1.5 mL of Trypsin-EDTA (0.25%) (Gibco®) solution to the flask and incubate at 37 °C until the cell layer is dispersed (usually 5 minutes).
4. Add 3 mL of complete growth medium and aspirate cells by gently pipetting.
5. Add appropriate aliquots of the cell suspension to new culture vessels with additional new medium.

II. Determination of the IC₅₀ values.

Day 1. For cytotoxicity experiments, cells were seeded in 96-well plates at a density of 2500 - 3000 cells per well in 100 µL of the corresponding medium and incubated overnight at 37 °C, 5% CO₂ atmosphere and 95% humidity in order to achieve 70% of confluence.

1. Follow subculturing procedure until step 4.
2. Take 2 mL of the resuspended cells and homogenize them in a Falcon® with an additional 9 mL of medium. There will be a total of 11 mL in the Falcon®.
3. From this Falcon® take 20 µL of cells and pour them into an Eppendorf with additional 20 µL of Tryptan Blue and homogenize carefully the mixture. Then, introduce 20 µL of the Tryptan Blue colored cell mixture in the Neubauer chamber and count the number of living cells in each quadrant: the average number of living cells (ANLC).
4. Total number of live cells (TNLC) = ANLC × 10⁴ × 11 mL.
5. In each 96-well plate 2 compounds are measured, and each compound is tested at seven different concentrations with one additional well without compound. Each concentration is repeated four times, so, for each plate, 64 wells are filled.
6. Each well needs to be filled with 100 µL of medium with 2500 - 3000 cells:

Required volume for each plate: 100 µL × 64 wells/plate × 1 plate = 6.4 mL/plate.

Required cell number for each plate: 3000 cells/well × 64 wells/plate × 1 plate = 192000 cells/plate.
7. Calculate how many milliliters must be taken from the Falcon® with 11 mL cells. $x_{\text{mL}} = (11 \text{ mL} \times 192000 \text{ cells}) / \text{TNLC}$.
8. Take x_{mL} of cell mixture and add up to 6.4 mL in a new Falcon® and homogenize.
9. With a multichannel pipette add 100 µL of the cell mixture to each well.
10. Incubation overnight at 37 °C, 5% CO₂ atmosphere and 95% humidity.

Day 2. The corresponding substrates were added into the 96 well plate in order to obtain a final concentrations of 50 µM, 30 µM, 20 µM, 10 µM, 5 µM, 2.5 µM, 1 µM and 0 µM (control experiment). All stock solutions of the investigated substrates were prepared by dissolving the powdered materials in appropriate amounts of DMSO. The final concentration of DMSO in the wells never exceeded 5% (v/v). The plate was incubated for 48 hours.

Day 4. 10 µL of CCK8 (Sigma Aldrich) were added into each well in the darkness, and the plate was incubated for additional 1.5 - 2 h at 37 °C under a 5% CO₂ atmosphere with 95% humidity. After the incubation, the absorbance of each well was determined by an Automatic Elisa Reader System (Thermo Scientific Multiskan FC, Thermo Scientific) at a wavelength of 450 nm.

Each compound was tested at least three times, and, if the obtained IC₅₀ value was below 1 μM, the assay was repeated at lower concentrations (10 μM, 5 μM, 2.5 μM, 1 μM, 0.5 μM, 0.2 μM and 0.1 μM).

Flow cytometry assays.

These experiments were conducted using a FACSCalibur system flow cytometer (Becton Dickinson Bioscience, Franklin Lakes, NJ, USA), in order to identify apoptotic cells and differentiate them from necrotic cells. A549 cells were exposed to 5 μM of γ-lactam **72c** and cell apoptosis and necrosis were evaluated at 12, 24, and 48 hours after exposure. In addition, the apoptosis induction capability of γ-lactam **86n** (1 μM) and 1,4-dihydropyridine **cis-135u** (5 μM) 24 hours after exposure was also evaluated.

After the exposure time, treated cells were washed with phosphate-buffered saline 1X (PBS) (Gibco®) and detached with trypsin/EDTA (0.25%) (Gibco®). Then, the collected cells in suspension were centrifuged at 10000 rpm for 5 min, and then the resulting pellet was resuspended in cell growth media and transferred to specific flow cytometer tubes. Propidium iodide (Sigma-Aldrich) at 1:300 dilution was used in each sample to detect necrotic cell and eBioscience™ Annexin V Apoptosis Detection Kit FITC (Thermo Fisher) was used to detect apoptotic cells following the manufacturer's instructions. The fluorescent signals corresponding to necrotic cells and apoptotic cells were measured at 650 nm (FL3) and 525 nm (FL1), respectively.

Non-treated cells, used as negative control samples, were displayed on a forward scatter (FSC) versus side scatter (SSC) dot plot in order to establish a collection gate and exclude cells debris. Cells treated with 1 μM of Camptothecin (Sigma-Aldrich) served as a positive control for an apoptosis-based mechanism and were used to establish cytometer settings and channel compensations. The experiments were carried out in triplicate for each condition. For each sample, 10⁴ events were collected.

Visualization of cell growth and morphology.

Qualitative analysis of A549 cell growth and morphology after exposure to 1.1, 0.11 and 0.02 μM of compound **86n** was conducted using Cytation™ 1 Cell Imaging Multi-Mode Reader (Biotek). Cell images were acquired immediately after the addition of the compound and at the following time points after exposure: 1, 6, 12, 24, and 48 hours.

Chapter 8. Evaluation of the MDM2/MDMX-p53 protein-protein interaction inhibitory capacity.

SDS-PAGE electrophoresis.

Sodium dodecyl sulfate-polyacrylamide gel electrophoresis (SDS-PAGE) gels were used to identify the proteins at the different stages of the purification in order to determine their purity. The composition of the used reagents, gels and buffers to perform the SDS-PAGE is shown in Table 27.

These gels have two different sections. The first third of the gel is the stacking gel, which has a low acrylamide concentration, whereas in the last two-thirds of the gel, the separation gel, has a higher concentration of acrylamide, which forms a mesh-like matrix suitable for the separation of proteins.

Samples were mixed with *Sample Buffer* and incubated for 5 minutes at 95 °C. The samples containing bacterial pellets were resuspended in 10% SDS by vortexing and then centrifuged at room temperature for 15 minutes at 15000 *g* prior to sample buffer addition.

Electrophoresis was run using *Cathode* and *Anode Buffers* at 90 V for the separation gel and 140 V for the stacking gel and the gel was stained in a Coomassie-blue solution for 15 min and decolorized in the destaining solution for 1 hour to enable visualization of bands.

Table 27. Composition of the reagents, gels and buffers used for SDS-PAGE.

Buffer / Reagent / Gel	Composition
Cathode Buffer	100 mM Tris, pH 8.25 100 mM tricine 0.1% SDS
Anode Buffer	3 M Tris pH 8.45 0.3% SDS
Sample Buffer	125 mM Tris-HCl, pH 6.8 20% (v/v) Glycerol 4% (m/v) SDS 0.05% (m/v) Coomassie Brilliant Blue G-250 5% (m/v) DTT
Gel Buffer	3 M Tris pH 8.45 0.3% SDS
Stacking Gel 4% (For 2 gels)	7.6 mL deionized H ₂ O 1 mL acrilamide 40% 1.3 mL gel buffer 10 µL TEMED 100 µL APS
Separation Gel 10 % (For 2 gels)	0.95 mL deionized H ₂ O 8 mL acrilamide 30% (29:1) 3.9 mL gel buffer 2 mL glycerol 80% 12 µL TEMED 150 µL APS
Coomassie-blue solution for protein visualization	0.25% (w/v) Commassie Brilliant Blue G-250 50% (v/v) methanol 10% (v/v) acetic acid
Destaining solution	20%(v/v) methanol 10% (v/v) acetic acid

Protein expression and purification buffers.

In Table 28 the composition of the buffers used for the expression and purification of MDM2 (18 - 125) and MDMX (1 - 134) proteins is described.

Table 28. Composition of the buffers used for protein expression and purification.

Denaturalizing Buffer	Equilibrium Buffer
100 mM Tris, pH 8.25	10 mM Tris-HCl, pH 7.0
6 M guanidine hydrochloride	1 mM EDTA
1 mM EDTA	10 mM β -mercaptoethanol
10 mM β -mercaptoethanol	1.5 M ammonium sulfate
Dialysis Buffer	MDM2 Elution Buffer
4 M guanidine hydrochloride, pH 3.5	100 mM Tris, pH 7.2
10 mM β -mercaptoethanol	10 mM β -mercaptoethanol
Refolding Buffer	MDMX Elution Buffer
10 mM Tris-HCl, pH 7.0	300 mM NaCl, pH 8.0
1 mM EDTA	50 mM NaH_2PO_4
10 mM β -mercaptoethanol	250 mM imidazole
Assay Buffer	Binding Buffer
150 mM NaCl, pH 7.4	300 mM NaCl, pH 8.0
50 mM Na_2HPO_4	50 mM NaH_2PO_4
50 mM KH_2PO_4	10 mM imidazole
5mM DTT	
FP Buffer	
100 mM Tris, pH 7.2	
100 mM NaCl	
1 mM EDTA	

Expression and purification of MDM2 (18 - 125).

The expression and purification of MDM2 (18 - 125) protein was performed following Figure 83.

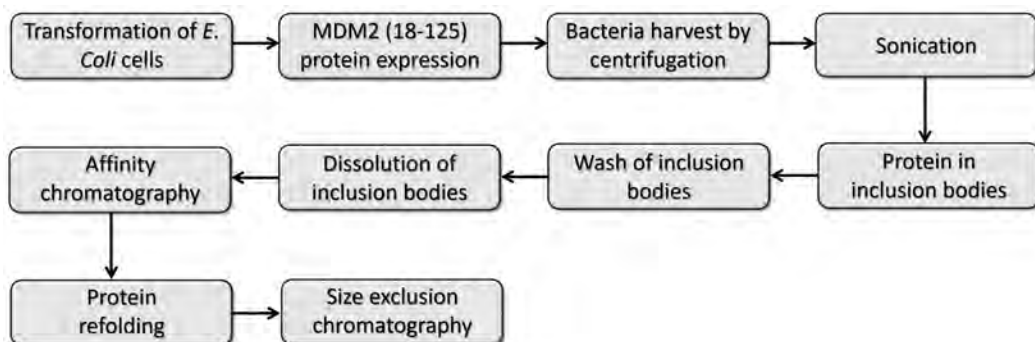


Figure 83. Followed methodology for the expression and purification of MDM2 (18 - 125).

I. Transformation of chemically competent *E. Coli*.

E. Coli BL21-CodonPlus (DE3) RIL strain cells were thawed in ice for 15 min and then mixed with 4 μL of pET20 plasmid (Novagen) (81 $\text{ng}/\mu\text{L}$) encoding MDM2 sequence (18 - 125). The cells were incubated in ice for 30 min. Incubation was followed by a heat shock of 90 seconds at 42 $^{\circ}\text{C}$, 4 min cooling in ice and the addition of 700 μL of LB (Luria-Bertani) medium (BioShop). After 1 hour of incubation at 37 $^{\circ}\text{C}$, 200 μL of the mixture was spread out on LBA (Luria-Bertani 1.5% w/v Agar) Petri plates supplemented with Ampicillin (100 $\mu\text{g}/\text{mL}$) and Chloramphenicol (34 $\mu\text{g}/\text{mL}$) and incubated overnight at 37 $^{\circ}\text{C}$.

II. MDM2 (18 - 125) protein expression.

The next day, the growth of colonies in the Petri plate was observed. A single colony was taken and inoculated in an Erlenmeyer with 200 mL of LB medium supplemented with 200 μL Ampicillin (100 $\mu\text{g}/\text{mL}$) and 200 μL Chloramphenicol (34 $\mu\text{g}/\text{mL}$) and was incubated overnight at 37 $^{\circ}\text{C}$ with 180 rpm shaking.

After 18 - 24 hours, it was observed that the medium became dense due to bacterial growth. The 200 mL of LB medium were separated into four Erlenmeyer flasks (50 mL each) with 1 L of LB medium supplemented with 1 mL Ampicillin (100 $\mu\text{g}/\text{mL}$) and 1 mL of Chloramphenicol (34 $\mu\text{g}/\text{mL}$) and was incubated at 37 $^{\circ}\text{C}$ with 200 rpm shaking until the $\text{OD}_{600\text{nm}}$ (Optical Density at 600 nm) reached a value between 0.6 and 0.8. This was measured with NanoDrop 2000 spectrophotometer (Thermo Scientific).

Next, 1 mL of a 1 M aqueous solution of *iso*-propyl β -D-1-thiogalactopyranoside (IPTG) was added at each Erlenmeyer and the culture was incubated at 37 °C for 4 hours. Finally, the harvesting of cells was achieved by centrifugation (20 min, 5000 *g*, 4 °C). Whenever required, the cell pellets were stored at -20 °C.

III. Sonication.

Sonication is a method where ultrasounds induce the formation of cavitations in solution, which collapse producing sheer stress-inducing rupture of the cells. It is a simple method for the disruption of cells with the advantage of generating a relatively low viscosity lysate due to nucleic acid fragmentation. First, the obtained pellets in the previous step were resuspended in 30 mL of PBS 1X with 20 μ L of Protease Inhibitor Cocktail (PIC) (Sigma-Aldrich) for each liter of culture medium used before.

Sonication was performed in ice in 3 steps of 3 min each, with 5 min intervals between steps. Pulse mode was applied with the output control parameter of sonicator Sonifier 250 (Branson Ultrasonics Corporation) set to power 5 and duty cycle to 50%. Then, the lysate was centrifuged for 20 minutes at 20000 *g* at 4 °C to collect the inclusion bodies (the supernatant is discarded) since MDM2 protein is expressed in a non-soluble form.

IV. Purification of MDM2 (18 - 125) protein.

The following steps were followed to purify MDM2 (18 - 125) construct:

1. The collected inclusion bodies were washed twice with 120 ml PBS 1X containing 0.05% Triton-X100 (BioShop) and once with 120 ml PBS 1X and centrifuged (15 min, 15000 *g*, 4 °C) after each wash.
2. Purified inclusion bodies were solubilized in 20 ml of *Denaturalizing Buffer* and stirred overnight at 4 °C.
3. After 12 - 18 hours the solution was centrifuged for 30 min at 15000 *g* and 4 °C, and the supernatant was collected, since the protein is denaturalized and is soluble, and the residual inclusion bodies were discarded.
4. The protein was dialyzed against 1 L *Dialysis Buffer* for 6 hours at 4 °C using a 6-8 kDa Molecular Weight Cut Off (MWCO) dialysis bag.
5. After 6 hours it was centrifuged (30 min, 20000 *g*, 4 °C) and the supernatant was collected.

6. The protein was refolded by dropwise addition into 1 L of *Refolding Buffer* and slowly mixing overnight at 4 °C.
7. Ammonium sulfate (198.2 g) was added to the final concentration of 1.5 M, mixed for 2 h and centrifuged for 40 min (10000 g, 4 °C).
8. The refolded protein was recovered on Butyl Sepharose 4 Fast Flow (GE Healthcare) previously equilibrated with *Equilibrium Buffer*. The column was washed and the protein was eluted using *MDM2 Elution Buffer*. Fractions were collected and the protein content was evaluated by Bradford assay (Coomassie Brilliant Blue G-250 dye).
9. Fractions containing the protein were pooled, concentrated to <10 ml and further purified by gel filtration with HiLoad 16/600 S75 µg (GE Healthcare) on FPLC ÄKTA Pure (GE Healthcare) with *Assay Buffer*.

The purity of the protein was monitored at each step by SDS-PAGE and the final concentration of pure MDM2 (18 - 125) was determined by measuring the absorption at 280 nm with NanoDrop 2000 spectrophotometer (Thermo Scientific). Then, $A_{280\text{nm}} = E_p \times c_p \times L$ equation was applied, where E_p is the molar extinction coefficient of the protein (0.830), c_p is the protein concentration, and L is the length of the cuvette in cm. E_p was calculated based on the amino acid composition of the protein using ProtParam Tool (ExpASY Bioinformatics Resource Portal, Swiss Institute of Bioinformatics).

Expression and purification of MDMX (1 - 134).

The expression and purification of MDMX (1 - 134) protein was performed following Figure 84.

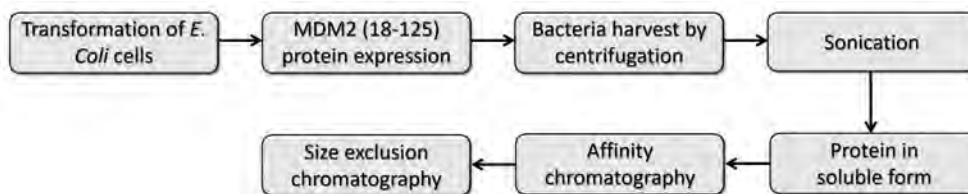


Figure 84. Followed methodology for the expression and purification of MDMX (1 - 134).

I. Transformation of chemically competent *E. Coli*.

E. Coli BL21-CodonPlus (DE3) RIL strain cells were thawed in ice for 15 min and then mixed with 4 μL of pET-46 Ek/LIC plasmid (Novagen) (160 $\text{ng}/\mu\text{L}$) encoding MDMX sequence (1 - 134). The cells were incubated in ice for 30 min. Incubation was followed by a heat shock of 90 seconds at 42 $^{\circ}\text{C}$, 4 min cooling in ice and the addition of 700 μL of LB (Luria-Bertani) medium (BioShop). After 1 h of incubation at 37 $^{\circ}\text{C}$, 200 μL of the mixture was spread out on LBA (Luria-Bertani 1.5% w/v Agar) Petri plates supplemented with Ampicillin (100 $\mu\text{g}/\text{mL}$) and Chloramphenicol (34 $\mu\text{g}/\text{mL}$) and incubated overnight at 37 $^{\circ}\text{C}$.

II. MDMX (1 - 134) protein expression.

The next day, a single colony was taken and inoculated in an Erlenmeyer with 200 mL of LB medium supplemented with 200 μL Ampicillin (100 $\mu\text{g}/\text{mL}$) and 200 μL Chloramphenicol (34 $\mu\text{g}/\text{mL}$) and was incubated overnight at 37 $^{\circ}\text{C}$ with 180 rpm shaking.

After 18 - 24 hours, the 200 mL of LB medium were separated into four Erlenmeyer flasks (50 mL each) with 1 L of LB medium supplemented with 1 mL Ampicillin (100 $\mu\text{g}/\text{mL}$) and 1 mL Chloramphenicol (34 $\mu\text{g}/\text{mL}$) and was incubated at 37 $^{\circ}\text{C}$ with 200 rpm shaking until the $\text{OD}_{600\text{nm}}$ (Optical Density at 600 nm), measured with NanoDrop 2000 spectrophotometer (Thermo Scientific), reaches a value between 0.6 and 0.8.

Next, 0.5 mL of a 1 M aqueous solution of isopropyl β -D-1-thiogalactopyranoside (IPTG) was added to each Erlenmeyer and the culture was incubated at 20 $^{\circ}\text{C}$ for 12 hours. Finally, the harvesting of cells was achieved by centrifugation (20 min, 5000 g , 4 $^{\circ}\text{C}$).

III. Sonication.

The obtained pellets in the previous step were resuspended in 30 mL of PBS 1X with 20 μ L of Protease Inhibitor Cocktail (PIC) (Sigma-Aldrich) for each liter of culture medium used in the previous step.

Sonication was performed in ice in 3 steps of 3 min each, with 5 min intervals between steps. Pulse mode was applied with the output control parameter of sonicator Sonifier 250 (Branson Ultrasonics Corporation) set to power 5 and duty cycle to 50%. Then, the lysate was cleared by centrifugation (30 min, 30000 *g*, 4 °C) and the supernatant was collected (discarding the inclusion bodies) since MDMX protein is expressed in a soluble form.

IV. Purification of MDMX (1 - 134) protein.

The following steps were followed to purify MDMX (1 - 134) construct:

1. The supernatant obtained from the lysate was loaded on Ni-chelating HiPrep™ IMAC FF 16/10 (GE Healthcare) previously equilibrated with *Binding Buffer*. The column with the protein was first washed with *MDMX Binding Buffer* and, then, the protein was eluted with *MDMX Elution Buffer*. Purified inclusion bodies were solubilized in 20 ml of *Denaturilizing Buffer* and stirred with a magnet overnight at 4 °C.
2. Fractions containing the protein were pooled, concentrated to <10 ml and further purified by gel filtration with HiLoad 16/600 S75 pg (GE Healthcare) on FPLC ÄKTA Pure (GE Healthcare) with *Assay Buffer*.

The purity of the protein was monitored at each step by SDS-PAGE and the final concentration of pure MDMX (1 - 134) was determined by measuring the absorption at 280 nm with NanoDrop 2000 spectrophotometer (Thermo Scientific). Then, $A_{280nm} = E_p \times c_p \times L$ equation was applied, where E_p is the molar extinction coefficient of the protein (0.460), c_p is protein concentration, and L is the length of the cuvette in cm.

Differential Scanning Fluorimetry (DSF).

Thermal melting experiments were carried out using CFX96TM Real-Time PCR thermal cycler (BioRad). Protein thermal unfolding was monitored following the increase in the fluorescence of the SYPRO Orange (Invitrogen) dye. To perform DSF experiments the following solutions (in *Assay Buffer*) were added to each well of a 96-well PCR plate: 15 μL of 53.3 μM MDM2 (or 15 μL of 53.3 μM MDMX), 15 μL of 26.7X SYPRO Orange dye and 10 μL of 400 μM of the corresponding compound. Following this procedure, in each well final concentrations of 20 μM of protein, 10X SYPRO Orange dye and 100 μM of the compound were obtained. Subsequently, the samples were heated in a PCR system from 25 $^{\circ}\text{C}$ to 95 $^{\circ}\text{C}$ at a rate of 0.4 $^{\circ}\text{C}/10$ seconds, monitoring the fluorescence intensities at 492 nm excitation and 610 nm emission.

Control wells were used to compare the melting temperature (T_m) without compound (replaced by the same amount of DMSO) as the negative control, and with 100 μM of Nutlin-3a as a positive control. T_m values were obtained from the maximum value of first derivative (dF/dT) plots of the unfolding protein curves and then analyzed in Microsoft Excel. Experiments were performed in triplicate.

Thermal shift values (ΔT_m) were obtained through subtraction of the unfolding temperature of the protein in the presence of DMSO ($T_{m \text{ Prot. + DMSO}}$) from unfolding temperatures of the protein in the presence of the corresponding compound (T_m), according to the following equation:

$$\Delta T_m (^{\circ}\text{C}) = T_m - T_{m \text{ Prot. + DMSO}}$$

Fluorescence Polarization (FP).

Fluorescence Polarization assay was used for the monitoring of the interactions between MDM2 and MDMX proteins and the γ -lactam derivatives.

For each assay, fresh protein stocks of MDM2 (18-125) and MDMX (1-134) were thawed and the protein concentrations were determined using NanoDrop 2000 spectrophotometer (Thermo Scientific).

First, the binding affinity of FAM-P2 peptide (sequence: LTFEHYWAQLTS, labeled with carboxyfluorescein) towards MDMX2 and MDMX was determined. For this purpose, 10 nM of the fluorescent peptide was contacted with serial dilutions (in *FP Buffer*) of tested protein (range from 750 to 0.012 nM for MDM2 and from 3750 to 0.10 nM for MDMX) in a final volume of 100 μ L in a 96-well plate, and fluorescence polarization was determined. K_d was determined by fitting the curve using the below equation to experimental data:

$$FP = \frac{(FP_{max} - FP_{min}) \cdot c}{(K_d + c)} + FP_{min}$$

where FP is the determined value of fluorescence polarization, FP_{min} is the fluorescence polarization value for ligand only, FP_{max} is the fluorescence polarization at protein concentration saturating the ligand, and c protein concentration.

Competition binding assay was performed using 10 nM fluorescent FAM-P2 peptide (in *FP Buffer*) and the optimal concentrations of proteins to perform the FP assays were selected according to Huang and coworkers, choosing the concentration at $FP = 80\%$.²³⁹

$$FP_{F0} = FP_{min} + 0.8 (FP_{max} - FP_{min})$$

$$X = \frac{K_d (FP_{F0} - FP_{min})}{(FP_{max} - FP_{F0})}$$

where FP_{F0} is the Fluorescence Polarization value at 80% of the curve, and X is the concentration of the protein at 80% of the curve, which is the ideal one to carry out the competitive assays. The optimal concentrations for MDM2 and MDMX were 30.58 nM and 56.44 nM respectively.

The assays were performed in Corning black 96-well NBS assay plates, and dilutions were performed using *FP Buffer*. In each well 70 μ L of 43.7 nM MDM2 (or 70 μ L of 80.6 nM MDMX), 25 μ L of 40 nM of FAM-P2 peptide and 5 μ L of compound (in concentrations ranging from 40 mM to 40 μ M) to afford final concentrations of 30.6 nM MDM2 (or 56.4 μ M MDMX), 10 nM of FAM-P2 peptide and compound concentration ranging from 2 mM to 2 μ M.

In this assay, several control experiments were used:

1. Maximum FP: 70 μ L of 1.07 μ M MDM2 (or 70 μ L of 5.36 μ M MDMX), 25 μ L of 40 nM of FAM-P2 peptide and 5 μ L DMSO.
2. Minimum FP: 70 μ L of *FP Buffer*, 25 μ L of 40 nM of FAM-P2 peptide and 5 μ L DMSO.
3. DMSO control: 70 μ L of 43.7 nM MDM2 (or 70 μ L of 80.6 nM MDMX), 25 μ L of 40 nM of FAM-P2 peptide and 5 μ L of DMSO.
4. Positive control: 70 μ L of 43.7 nM MDM2 (or 70 μ L of 80.6 nM MDMX), 25 μ L of 40 nM of FAM-P2 peptide and 5 μ L of 0.5 mM Nutlin-3a.

Fluorescence polarization was determined using Infinite 200 PRO M Multi-Mode Plate Reader (Tecan) with the 485 nm excitation and 535 nm emission filters. The fluorescence intensities, parallel and perpendicular to the plane of excitation, were determined in Corning black 96-well NBS assay plates at room temperature.

All the experiments were prepared in duplicate and plates and were read at 15 min after mixing all the assay components. Inhibition curves were fitted using GraphPad (Binding Competitive, One site) in order to obtain the final K_i values.

Molecular dynamics simulations.

Molecular docking was used to predict the binding mode of γ -lactams **93c** and **93m** to MDM2 and MDMX proteins respectively.

The structure of compounds **93c** and **93m** was generated and optimized with *Vega ZZ* molecular toolkit.²⁴⁹ For the optimization, the following parameters were set: Force Field - AM1BCC, Charges - Gasteiger, Method - Boltzmann jump, Steps - 5000, Temperature - 300K.

Crystal structures of MDM2 (PDB code 1T4E) and MDMX (PDB code 3DAB) were prepared with *AutoDockTools* by removing the ligand, deleting water molecules and adding hydrogen atoms. The center of the GridBox (x, y, z) were 42.935, 10.623 and 26.702 for MDM2 (PDB code 1T4E) and -1.716, -26.552 and 11.523 MDMX (PDB code 3DAB), and, in both cases x, y and z size of the GridBox was set to 20 and the exhaustiveness parameter was set to 8.

Molecular docking was then conducted with *AutoDock Vina*,²⁵⁰ obtaining stable protein-inhibitor complexes, which were visualized in *PyMOL* and *DiscoveryStudio*.

²⁴⁹ Pedretti, A.; Mazzolari, A.; Gervasoni, S.; Fumagalli, L.; Vistoli, G. *Bioinformatics* **2021**, *37*, 1174-1175.

²⁵⁰ Trott, O.; Olson, A. J. *J. Comput. Chem.* **2010**, *31*, 455-461.

THE END ?



FARMAZIA FAKULTATEA
KIMIKA ORGANIKOA I SAILA



γ -Laktama-deribatuen osagai anitzeko sintesia eta aplikazioak minbizi-kontrako agente gisa

XABIER DEL CORTE SOLAGUREN-BEASCOA



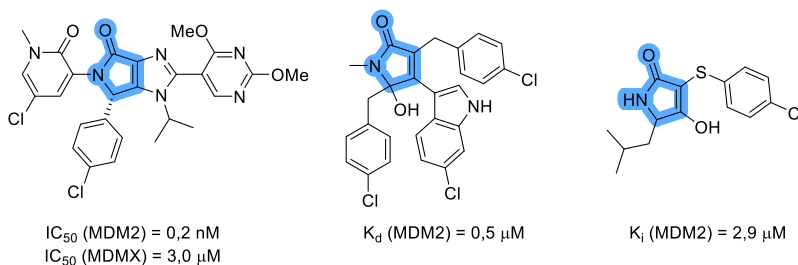
Vitoria-Gasteiz, 2022

Laburpena

Minbizia, gaixotasun neoplasikoen multzo bati emandako izena da eta munduko bigarren heriotza-kausa garrantzitsuen da. Urteetan zehar, gaixotasun horien tratamendua oso prozesu konplexua izan da, eta zenbait tratamendu berritzaile garatu eta klinikian onartu diren arren, gaur egun, lehenetasuna duten terapia, kirurgiaren eta kimioterapia edo erradioterapiaren arteko konbinazioa izaten jarraitzen du.

Arlo honetan orain arte egindako aurrerapenak handiak badira ere, oraindik, maila molekularrean itu selektiboak dituzten agente kimioterapeutiko berriak aurkitzeko premia larria da. Testuinguru honetan, giza minbizien %50-ean mutaturik dagoen edo funtzio galdua duen p53 transkripzio-faktorearen eta MDM2 (Murine Double Minute 2) eta MDMX (Murine Double Minute X) proteinen arteko elkarrekintza da etorkizun handiko helburu biokimikoa.

MDM2/MDMX-p53 proteina-proteina elkarrekintza inhibitzeko gaitasuna duten molekula-familien artean, pirrolidona nukleo bat (γ -laktama) dutenek inhibizio-ahalmena oparoa dute, eta, gainera, orain arte ez dira sakonean aztertu (I. irudia).



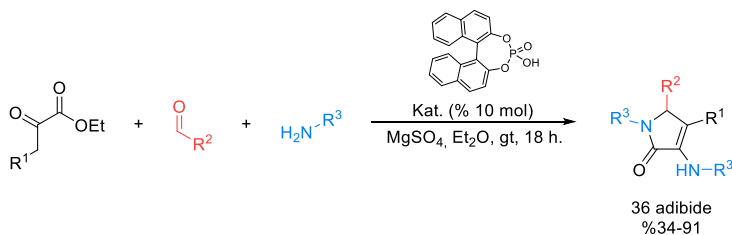
I. irudia. Pirrolidona (urdin kolorea) nukleoa duten MDM2-ren eta MDMX-aren inhibitzaileak.

Farmako berrien garatzeko prozesu luzean, osagai anitzeko erreakzioak (OAE) protokolo sintetiko oso baliagarriak dira, non hiru erreaktibok edo gehiagok ontzi bakarreko (“one pot”) prozedura baten bidez erreakzionatzen dute, oinarriko urrats-segida batzuen bidez. Arestian aipatutakoa kontuan hartuta, tesi honen helburu nagusiak honako hauek dira: batetik, osagai anitzeko prozesu organokatalizatu eraginkorrek garatea, γ -laktama-deribatuen sintesirako, bestetik, substratu horien aplikazio sintetikoak aztertzea, eta azkenik, substratu hauek zenbait minbizi zelula-lerroen aurrean duten aktibitate antiproliferatiboa neurtzea eta, MDM2/MDMX-p53 proteina-proteina elkarrekintzaren ahalmen inhibitzailea aztertzea (II. irudia).



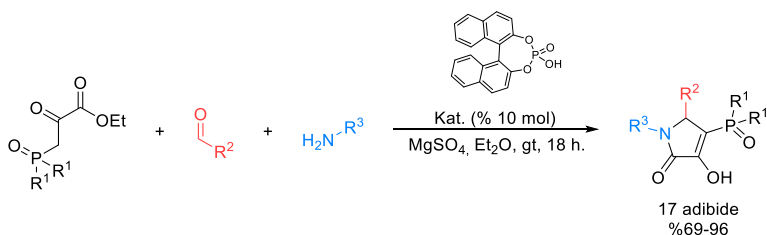
II. irudia. Tesiaren helburu orokorrak.

Doktoretza-tesi honen lehen helburua, azido fosforiko bidez katalizatutako pirubato deribatuen, aldehidoen eta aminen arteko hiru osagairen protokolo bat garatzea da, 3-amino γ -laktamak eskuratzeko (I. eskema).



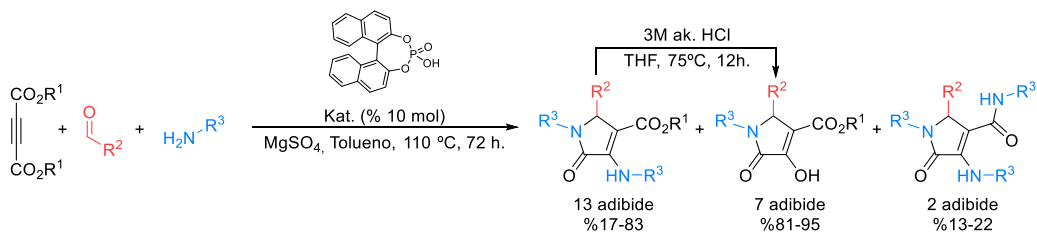
I. eskema. Pirubato-deribatu, aldehido eta aminen arteko hiru osagaiko erreakzioa.

Gainera, fluorodun edo fosforodun talde funtzionalek molekula bioaktiboetan duten garrantzia dela eta, ondoren, osagai anitzeko protokolo hau fosforoa edo fluorra duten γ -laktama-deribatuen sintesira zabaldu da. Azpimarratu beharra dago, fosforodun pirubatoak erabiltzen direnean, enolaren deribatu diren γ -laktamak sortzen direla (II. eskema).



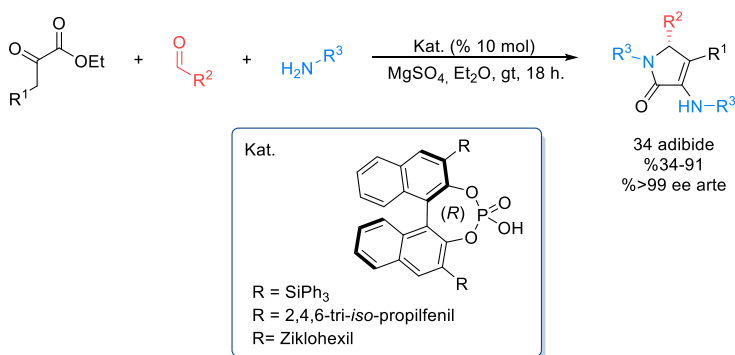
II. eskema. Fosforodun pirubato-deribatu, aldehido eta aminen arteko hiru osagaiko erreakzioa.

Jarraian, Brønsted azidoak katalizatutako osagai anitzeko erreakzioa hedatu egin da, pirubato esterren ordez, dialkil azetilendikarboxilatoak erabiltzera, amina eta aldehidoekin batera. Dakigunez, erreakzio honetarako azido fosforikoa katalizatzaile gisa erabili den lehen adibidea da (III. eskema).



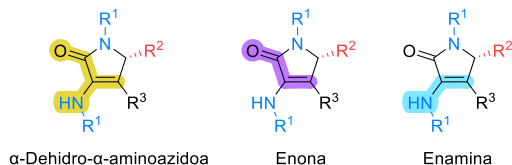
III. eskema. Dialkil azetilendikarboxilatoak, aldehido eta aminen arteko hiru osagaiko erreakzioa.

Gaur egun, medikamentuak arautzen dituzten agentziek, eta industria farmazeutikoak, beren lehentasun sintetikoaren artean molekula enantiomeriko puruen sintesia ezarri dute. Hala, optikoki puruak diren molekula kiralak lortzeko metodologia berriak garatzea interes handiko helburu bilakatu da kimika organikoan. Hau kontuan hartuta, eta, Brønsted azidoek hiru osagaiaren erreakzioa katalizatzen duten gaitasuna frogatu ondoren, erreakzio horren bertsio enantioselektiboa garatu dugu optikoki aberastutako γ -laktama deribatuen prestatzeko, etekin eta soberakin enantiomeriko bikainak lortuz (IV. eskema).



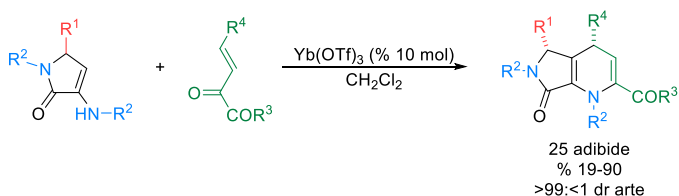
IV. eskema. Hiru osagaiko erreakzio enantioselektiboa.

Osagai anitzeko erreakzioaren bidez lortutako 3-amino-1,5-dihidro-2H-pirrol-2-ona substratuak tresna bikainak dira sintesi kimikoan, bere egituraren baitan α -dehidro- α -aminoazido, enona eta enamina zikliko funtzio taldeka dituztelako (III. irudia).



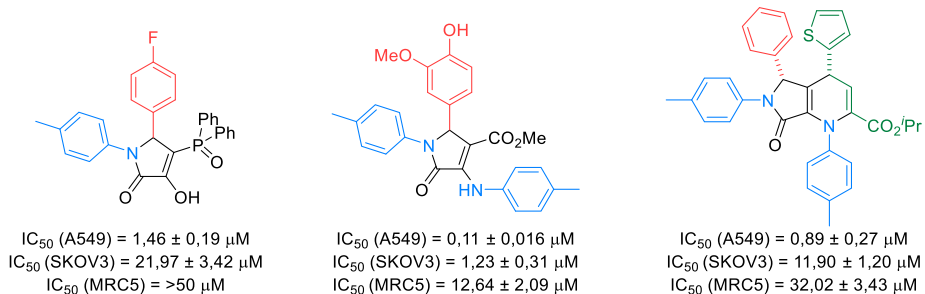
III. irudia. 3-Amino-1,5-dihidro-2H-pirrol-2-onen egituran dauden talde funtzional desberdinak.

Beraz, γ -laktama-deribatuen potentzial sintetikoa zenbait eraldaketaren bidez nabarmendu da, hala nola, hidrogenazio diastereoselektiboak, alkilazio-erreakzioak eta Horner-Wadsworth-Emmons erreakzioak. Zehazki, iterbio bidez katalizatutako γ -laktama deribatu eta α -zetoester β,γ -asegabean arteko [3+3] zikloadizio-erreakzio formalak, 1,4-dihidropiridinak sortzen ditu, erregio eta diastereoselektibitate maila handietan (V. eskema).



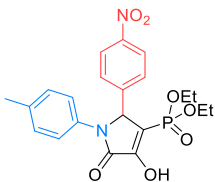
V. eskema. [3+3] Zikloadizio formal diastereoselektiboa.

Doktoretza-tesi honen bigarren atalean, γ -laktama-deribatuen minbiziaren kontrako jarduera aztertu da. Lehenik eta behin, sintetizatutako substratuek zenbait giza-minbizi zelula-lerroren kontra duten *in vitro* aktibitate antiproliferatiboa ebaluatu da. Oro har, γ -laktamek aktibitate handia erakutsi zuten A549 birika-minbizi zelula-lerroan, 0,11 μ M-eko IC_{50} baliorik onena eman baitu. Gainera, ez zuten jarduerarik izan MRC5 birika zelula-lerro ez-gaiztoan. Konposatu aktiboenetako batzuk IV. irudian ageri dira. Halaber, zelularen morfologia aztertu da konposatu aktiboenaren kontzentrazio eta denbora desberdinen eraginpean, eta fluxu-zitometria bidez egindako saiakuntza batzuek zehaztu ahal izan dute konposatu hauek apoptosiaren mekanismoa pizteko gai direla.

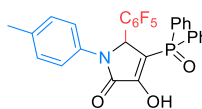


IV. irudia. γ -Laktama aktiboenak entsegu zitotoxikoen arabera.

Azkenik, hirurogeita hamar γ -laktama-deribatuen MDM2/MDMX-p53 proteina-proteina elkarrekintzaren inhibizio-ahalmena ebaluatu zen. Horretarako, bi baheketa-teknika erabili dira, Ekortze-Fluoreszentzia Diferentziala (EKF) eta Fluoreszentzia-Polarizazio (FP) esperimentuak. Proteina bakoitzerako emaitzarik onenak V. irudian ageri dira. Hala ere, ezin da segurtasunez ondorioztatu γ -laktama-deribatuen jardura zitotoxikoa MDM2/MDMX-p53 proteina-proteina elkarrekintzaren inhibizioaren ondorio dela. Dena den, bi γ -laktama-deribaturen interakzio modua MDM2 eta MDMX proteinek modelizazio dinamiko molekularreko simulazioen bidez aurreikusi ahal izan zen.



K_i (MDM2) = $47,69 \pm 1,68 \mu\text{M}$



K_i (MDMX) = $98,58 \pm 1,81 \mu\text{M}$

V. irudia. MDM2/MDMX-p53 proteina-proteina elkarrekintza inhibitzen duten γ -laktama aktiboenak.

Laburdurak eta akronimoak

°C	Celsius graduak
1D	Dimentsio bat
2D	Bi dimentsio
3D	Hiru dimentsio
Å	Ángstrom
ADN	Azido desoxirribonukleikoa
AIBN	Azobisisobutironitriloa
ak.	Urtsua
Alk	Alkiloa
APTS	Azido <i>p</i> -toluensulfonikoa
Ar	Funtzio-talde aromatiko
AU	Arbitrary Units / Unitate Arbitrarioa
bal.	Baliokide
BBBSI	1,1'-Butilenebis(3-sulfo-3 <i>H</i> -imidazol-1-ium)
BINOL	1,1'-Bi-2-naftola
Bn	Bentziloa
Bu	Butiloa
CDK	Cyclin-dependent kinase / Ziklinaren Mendeko Kinasa
cod	1,5-Ziklooktadienoa
COX2	Ziklooxigenasa-2
Cy	Ziklohexiloa
d.g.	Determinatu gabe
Da	Dalton
DABCO	1,4-Diazabiziklo[2.2.2]oktanoa
DCM	Diklorometanoa
DE	Desbiderapen estandarra
Disol.	Disolbatzailea
DMF	<i>N,N</i> -Dimetilformamida
DMSO	Dimetil sulfoxidoa
dr	Proporzio diastereoisomerikoa
E	Elektroizalea
EAE	Egitura-aktibitate erlazioa
EC ₅₀	Kontzentrazio efektibo maximoaren erdia
ee	Soberakin enantiomerikoa

EFD	Ekortze-Fluorimetria Diferentziala
EMN	Erresonantzia Magnetiko Nuklearra
erref.	Erreferentzia
Et	Etiloa
Etek.	Etekina
F	Fluoreszentzia
FL	Fluoreszentzia kanala Fluxuzko Zitometrian
FP	Fluoreszentzia-Polarizazioa
GIB	Giza Immunoeskasiaren Birusa
gt	Giro tenperatura
HDAC	Histonen deazetilasa
HMQC	Heteronuclear Multiple Quantum Coherence Experiment / Kuantu anitzeko koherentzia heteronuklearra
HPLC	High-performance liquid chromatography / Berizmen handiko kromatografia likidoa
HRMS	Erresoluzio handiko masa espektroskopia
IC₅₀	Inhibizio kontzentrazio maximoaren erdia
IMAC	Immobilized Metal Affinity Chromatography / Immobilizatutako metal bidezko afinitate-kromatografia
<i>i</i>Pr	<i>iso</i> -Propiloa
IR	Espektroskopia infragorria
<i>J</i>	Akoplamendu konstantea
Kat.	Katalizatzailea
K_d	Disoziazio-konstantea
K_i	Inhibizio-konstantea
Konb.	Konbertsioa
LDA	Litio di- <i>iso</i> -propilamida
M	Molar
MDM2	Murine Double Minute 2
MDMX	Murine Double Minute X
Me	Metiloa
MTBE	Metil <i>tert</i> -butil eterra
NOE	Nuklear Overhauser Efektua / Overhauser efektu nuklearra
NOESY	Nuklear Overhauser Efektuko Espektroskopia / Overhauser efektu nuklearraren bidezko espektroskopia
Nu	Nukleozalea
ORTEP	Oak Ridge Thermal Ellipsoid Plot
PCR	Polymerase Chain Reaction / Polimerasaren kate-erreakzioa
PDB	Proteinen data-bankua

PG	Talde babeslea
Ph	Feniloa
Piv	Pibaliloa
PMP	<i>p</i> -Metoxifeniloa
PPI	Proteina-Proteina Elkarrekintza
ppm	Parts per million / milioiko parte
Pr	Propiloa
Prod.	Produktua
Prop.	Proporzioa
Py	Piridina
PyBOX	Bis(oxazolin)piridina
rac	Errazemiko
ROS	Oxigeno espezie-erreaktiboak
Sarr.	Sarrera
SDS-PAGE	Sodium Dodecyl Sulphate-Polyacrylamide Gel Electrophoresis
SO	Sypro Orange
SOD	Superoxido Dismutasak
T	Tenperatura
TfO	Triflato a
THF	Tetrahidrofuranoa
T_m	Urtze-tenperatura
TMS	Trimetilsililoa
Tol	Toliloa
TS	Trantsizio-egoera
UV	Argi ultramorea
VEGF-R	Vascular Endothelial Growth Factors and Receptors

Aurkibidea

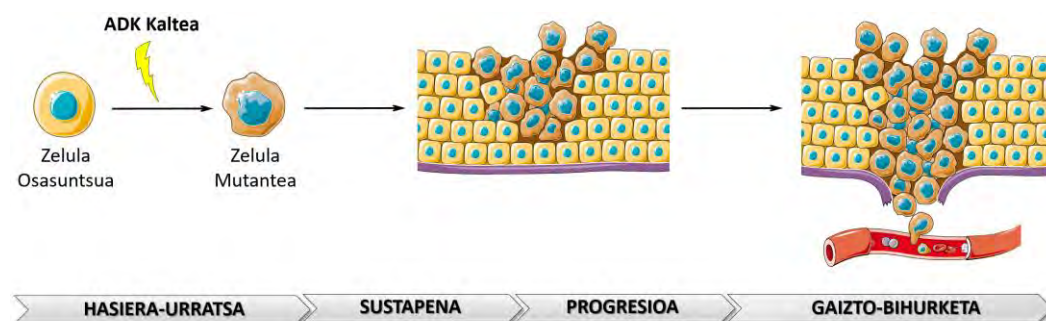
Sarrera	15
Helburuak	55
I. Atala. γ-Laktama-deribatu asegabeen osagai anitzeko sintesia eta aplikazioak	59
1. Kapitulua. γ -Laktama-deribatu asegabeen osagai anitzeko sintesia pirubatoak erabiliz	61
2. Kapitulua. Fluorra eta fosforoa duten γ -laktamen osagai anitzeko sintesia.....	69
3. Kapitulua. Alkino aktibatuen erabilera osagai anitzeko erreakzioan γ -laktama-deribatuen sintesirako	79
4. Kapitulua. γ -Laktamen osagai anitzeko sintesi enantioselektiboa	87
5. Kapitulua. γ -Laktama-deribatuen eraldaketa sintetikoak.....	101
6. Kapitulua. 3-Amino γ -laktama-deribatuen [3+3] erreakzio formal estereoselektiboa	109
II. Atala. γ-Laktama deribatuen minbiziaren kontrako jarduera	125
7. Kapitulua. Aktibitate antiproliferatiboaren eta apoptosi indukzioa indultzeko gaitasunaren ebaluazioa	137
7.1. γ -Laktama α,β -asegabeen aktibitate antiproliferatiboa.	137
7.2. 1,4-Dihidropiridina biziklikoen aktibitate antiproliferatiboa.	153
7.3. Apoptosiaren detekzio-esperimentuak eta zelula morfologiaren behaketa.	158
8. Kapitulua. γ -Laktama-deribatuen ebaluazioa MDM2/MDMX-p53 elkarrekintzaren inhibitzaile gisa	165
8.1. MDM2 eta MDMX proteinen adierazpena eta purifikazioa.....	165
8.2. Ekortze-Fluorimetria Diferentzialaren (EFD) entsegua.	168
8.3. Fluoreszentzia-Polarizazio (FP) entsegua.....	175
8.4. Modelizazio molekularren bidezko simulazioak.	178
Ondorioak	181

Sarrera



Minbizia, gaixotasun neoplasiko talde bati ematen zaion izena da eta heriotzaren bigarren kausa globala da. Patologia honetan zelula-hazkuntza anormal bat gertatzen da, tumore izeneko masa bat eratzera daramana. Prozesu osoa neoplasma deitzen da. Hala ere, tumore guztiak ez dira minbizidunak. Tumore batzuk onberak dira, leku jakin batean mugatuta daudenak, beste leku batzuetara zabaldu gabe, eta ez dira minbizi bihurtzen. Bestalde, minbizi gisa kodetuta dauden tumoreak daude, horietako batzuk gaiztoak, hau da, ehunak inbaditzen dituzten neoplasmak, eta beste batzuk potentzialki gaiztoak direnak, oraindik lokalizatuta daudenak, baina gaizto bihurtzeko bidean daudenak.¹

Kartzinogenesisia zelula normalen eraldaketa da, mekanismo homeostatiko egokia izatetik hazkuntza autonomo eta inbasio ahalmena izatera duten zelulak bihurtuz. Hasiera, sustapena, progresioa eta bihurketa gaiztoa dira prozesu honen lau faseak (1. irudia).



1. irudia. Kartzinogenesi prozesua.

Zelulak minbizi-sortzaile diren eragileekin elkarrekintza sekuentziala izan eta gero, ADNan kalteak sor daitezke. Kalte hau prozesu endogenoa izan daiteke (ADNaren erreplikazioan erroreak, zenbait ADNren baseen ezegonkortasun kimiko intrintsekoa edo metabolismoan zehar sortutako erradikal askeen eraso) edo agente kimiko, fisiko edo biral exogenoekin izandako elkarrekintzaren ondorioz. Konpontzen ez bada, ADNaren kalteak mutazioak eragin ditzake. Eraldaketa hautako gehienek ez dute garrantzirik minbizi-arriskuaren ikuspuntutik eta ez dituzte zelularen funtzio nagusiak aldatzen. Hala ere, zenbait mutaziok zelularen biziraupenerako erabakigarriak diren geneak kaltetu ditzakete, zelula horretarako letal bilakatuz. Noizean behin bakarrik, mutazio hauek abantaila batzuk ematen dizkiote zelulari, hala nola ugaltze-ahalmena areagotu, proto-onkogeneak aktibatu eta gene tumore-

¹ Roy, M.; Datta, A. Cancer: Types and Hallmarks. In *Cancer, Genetics and Therapeutics*; Springer, 2019; pp 1-26.

ezabatzaileak desaktibatu. Une honetan, zelula sartzen da kartzinogenesi prozesuaren hasiera-urratsean. Ondoren, sustapena edo hedapen klonala hasten da eta zelula aurreneoplasikoak eratzen dira. Hemen sustatzaileek hartzen dute parte, hau da, kartzinogenesiaren eraginkortasunean eragina duten substantziak. Sustatzaileak normalean ez-mutagenikoak eta ez-kartzinogenikoak dira eta eragin biologikoa sortzen dute aktibazio metabolikorik gabe. Progresioa tumore gaizto baten sustapenaren eta formazioaren arteko tarteari ematen zaion izena da. Urrats honetan, zelulak zatitu eta beren populazioa handitu egiten dute azken fasera iritsi arte, hots gaizto bihurtu arte.²

Urrats ugari prozesu honetan, zelula-kopuru mugatu batek bakarrik egingo du aurrera etapa batetik hurrengora, azkenean tumore gaizto bat osatzera iritsiz. Honen arrazoia, kartzinogenesi-prozesuaren urrats bakoitzean dauden minbizi kontrako defentsa-mekanismo naturalak dira, minbizi arriskua gutxitzen dutenak.³

Horregatik, une honetan, beharrezkoa da zelula “normalen” eta minbizi-zelulen arteko ezberdintasunen hobeto ezagutzea gaixotasuna bera hobeto ulertu ahal izateko. Hanahan-ek eta Weinberg-ek beharbada minbizi guztien patogenesisian kontuan hartu beharreko hamar ezaugarri definitu zituzten (2. irudia). Ezaugarri hauek gaitasun bereizgarri eta osagarriak dira, tumoreen hazkundera eta barriadura metastasikoa ahalbidetzen dutenak.⁴



2. irudia. Minbiziaren ezaugarriak.

² Bertram, J. S. *Mol. Aspects Med.* **2001**, *21*, 167-223.

³ Jakóbiński, M.; Lasek, W.; Gołęb, J. *Immunol. Lett.* **2003**, *90*, 103-122.

⁴ (a) Hanahan, D.; Weinberg, R. A. *Cell* **2011**, *144*, 646-674. (b) Hanahan, D.; Weinberg, R. A. *Cell* **2000**, *100*, 57-70.

- I. Autosufizientzia hazkuntza-seinalizazioan. Zelula normalek garatzeko eta banatzeko zelula kanpoko hazkuntza-faktoreak edo seinaleak behar dituzten bitartean, minbizi-zelulek ez dute kanpoko seinalerik behar ugaltzeko eta honek kontrolaezinezko ugalketa dakar.¹
- II. Anti hazkuntza-seinaleen aurrean sorgortasuna. Zelula normal batean seinale anitzek funtzionatzen dute homeostasia mantentzeko. Hala ere, minbizi-ehunak erresistenteak dira hazkuntza murrizteko seinaleen aurrean.
- III. Apoptosia saihestea. Apoptosia zelula kaltetuek euren heriotza programatzeko erabiltzen duten mekanismoa da. Seinale ezberdinek abiarazten dute eta hainbat gertakari bultzatzen dute, azkenean mintz zelularren haustura, nukleoaren eta zitoplasmaren eskeletoaren eta haustura, kromosomen degradazioa eta nukleoaren txikizioa. Hala ere, minbizi-zelulek mekanismo hau gainditzeko gaitasuna dute.
- IV. Erreplikazio ahalmen mugagabea. Hayflick-ek 1997an deskribatu zuen bezala, zelulek potentzial erreplikatibo mugatua dute.⁵ Zelulak ugaltze kopuru mugatu batera iritsi ondoren, hazteari uzten diote (seneszentzia). Minbizidun zelulak muga hau gainditzeko gai dira, zatiketa eta hazkunde gaitasun infinituak dituztelarik.
- V. Angiogenesisia laguntzea. Elikagaiak, oxigenoa eta sistema baskularra funtsezkoak dira zelularen funtzio eta biziraupenerako. Angiogenesisia deritzon odol-hodi berrien hazkundera iragankorra eta kontu handiz arautua da. Kartzinogenesisia-prozesuaren uneren batean, tumoreek gaitasun angiogenikoa aktibatu eta handitu egiten dutela dirudi, prozesu honen oreka aldatuz.
- VI. Ehunen inbasioa eta metastasia. Giza minbizi mota gehienek garapenean, tumore-zelula primarioak irteten dira eta ondoko ehunak inbaditzen dituzte, gorputzean zehar kolonia berriak sortuz. Metastasia sortu berri hauek zelula osasuntsu eta minbizien amalgama dira. Kontzeptu hau da ezberdintasun nagusia zelula onbera eta zelula gaiztoaren artean.
- VII. Metabolismo desregulatzea. Minbizidun zelulak beren glukosa-metabolismoa ber programatzeko gai dira zelulen hazkuntza eta zatiketa bultzatzeko.
- VIII. Immunitate-sistema saihestea. Sistema immunologikoa zelulak eta ehunak etengabe behatzen ari da eta gaizto bilakatzen diren zelula normal gehienak ezagutzen eta ezabatzen

⁵ Hayflick, L. *Biochemistry* **1997**, *62*, 1180-1190.

ditu.⁶ Minbizia garatzen bada, minbizi-zelulek immunitate-sistemaren detekzioa ekiditea lortu dutela eta erradikazioa saihestu dutela esan nahi du.

- IX. Genomaren ezegonkortasuna eta mutazioak. Aurretik deskribatutako ezaugarrietako batzuk, neurri handi batean, zelula neoplasikoen ondoz ondoko alterazio genomikoen mende daude. Zenbait genoma-mutazioek abantaila ematen diete subklonatutako zelulei tokiko ehunean hazten eta nagusitasuna lortzen aukera emanez.
- X. Tumoreek eragindako hantura. Patologoek onartzen dutenez, lesio neoplasiko guztiek zelula immunologikoak dituzte infiltratuta, infiltrazio arinetatik hasi eta hantura gordinetara irits daitezkeelarik.⁷ Erantzun inflamatorioak sortzen ari diren neoplasiei ahalmena nabarmena lortzen laguntzen die, molekula bioaktiboak (hazkuntza-faktoreak, biziraupen-faktoreak eta proangiogenikoak) tumorearen mikroingurunera eramanez.⁸

Babes mekanismo ez-immuneak kartzinogenesiaren aurka.

Zelulak berak baditu babes edo defentsa mekanismo natural immune eta ez-immuneak, zelula mutatu berriak zelula gaizto bihurtzeko bidea jarraitzea eragozten dutenak. Ondoren, babesteko mekanismo ez-immuneak aurkeztuko dira.

I. Oxigenodun espezie errektiboen desaktibazioa eta eliminazioa.

Kanpoko zenbait faktorek, konposatu kimikoek, UV eta erradiazio ionizatzaileek edo beste faktore fisiologiko batzuek, hala nola arnasketa zelularrak mitokondrian edo bide metaboliko batzuk, oxigeno espezie errektiboak (ROS) sor ditzakete, adibidez O_2^- , H_2O_2 eta $\cdot OH$. Espezie hauek ADNan kalteak sor ditzakete. Entzima batzuk gai dira konposatu kartzinogeniko horiek kentzeko. Adibidez, superoxido dismutasak (SOD) erradikal superoxidoak (O_2^-) H_2O_2 bihurtzen du, azken hau, ondoren katalasek eta peroxidasek ezabatuko dutena. Glutation S-transferasak molekula elektroizale toxikoak (tabakoan dauden hidrokarburo aromatiko poliziklikoak barne) glutacionarekin konjugatzen ditu eta horrela haien ezabatzea laguntzen ditu. Halaber, P450 entzima produktu kimiko endogeno eta exogenoen metabolismoaren erantzulea da. Bestalde, zelula-mintzan dauden proteina batzuek, hala nola P-glikoproteinak, molekula toxiko edo potentzialki toxiko batzuen eskrezioaz arduratzen dira. Zoritxarrez, garraio-proteina hauek, agente kartzinoginogenikoetatik babestu behar gaituztenak, minbizi batzuetan

⁶ Nakajima, K.; Nangia-Makker, P.; Hogan, V.; Raz, A. *Cancer Res.* **2017**, *77*, 5441-5444.

⁷ Pages, F.; Galon, J.; Dieu-Nosjean, M.C.; Tartour, E.; Sautes-Fridman, C.; Fridman, W.H. *Oncogene* **2010**, *29*, 1093-1102.

⁸ (a) DeNardo, D.G.; Andreu, P.; Coussens, L.M. *Cancer Metastasis Rev.* **2010**, *29*, 309-316. (b) Grivennikov, S.I.; Greten, F.R.; Karin, M. *Cell* **2010**, *140*, 883-899 (c) Qian, B.Z.; Pollard, J.W. *Cell* **2010**, *141*, 39-51.

gainadierazita daude eta tumore-zelulak suntsipenetik babesten dituzte, agente kimioterapeutikoak zelulatik kanporatuz.⁹

II. ADNaren kalteen konponketa.

ADNa molekulak etengabe daude barne eta kanpoko genotoxiko askoren aktibitate kaltegarriaren pean. Zorionez, kalte mota bakoitzeko konponketarako bideak daude, hala nola O6-metilguanine-ADN methyl transferase (MGMT), basea edo nukleotideo-eszisioa konpontzeko bideak, eta homologoak edo ez-hologoak diren bukaera-loturazko birkonbinazio-bideak.¹⁰

III. Gene tumore-ezabatzaileak.³

Garago aipatu bezala, ADNren kalteak eraginkortasunez konpontzen dira kasu gehienetan. Hala ere, alterazio hauek konpontzen ez badira, mutazioak eragin daitezke eta, mutazio hauek gene kritikotetan gertatzen badira, zelula osasuntsuak minbizi-zelula bihurtu daitezke. Gene hauek, kartzinogenesisia sustatzen dutenak, bi kategoriatan banatzen dira: proto-onkogeneak eta tumore-ezabatzaile diren geneak (anti-onkogeneak).

Proto-onkogeneek funtzio askoren erregulatzailerik positibo gisa jarduten dute, hala nola, zelulen proliferazioa, zelulen diferentziazioa eta zelulen heriotza programatua. Proto-onkogene batean mutazio bat gertatzen denean, onkogene bihurtzen da eta etengabe dago aktibo. Beraz, zelula kontrolatik kanpo hazten da, eraldaketa neoplasikoan esku hartuz.

Tumore-ezabatzaile diren geneak identifikatu ohi dira hereditutako mutazioak dituztelako eta mutazio horiek gizaki batzuei minbizi forma batzuk heredatzeko joera eragiten dutelako. Gene hauen inaktibazioak, funtzioak galtzea dakarten mutazioak direla medio, minbizia garatzen laguntzen du. Tumore-ezabatzaile diren gene batzuk eta beraien funtzioak adibide 1. taulan laburbiltzen dira.

Tumore-ezabatzaile diren gene garrantzitsuenetako bat TP53 da, p53 proteina kodetzen duena. Gizaki batzuek gene honen alelo mutante bat dute, Li-Fraumeni sindromea eragiten duena, eta honen ezaugarri nagusia da hainbat minbiziren arrisku handitzen dela.¹¹ Giza-minbizi guztien % 50ean gene hau ezabatuta, mutaturik edo konprometiturik dago, p53 proteinaren bidearen eraginkortasuna mugatuz.

⁹ Jakóbsiak, M.; Lasek, W.; Gołęb, J. *Immunol. Lett.* **2003**, *90*, 103-122.

¹⁰ Kiwerska, K.; Szyfter, K. *J. Appl. Genet.* **2019**, *60*, 329-334.

¹¹ Harris, C.C.; Hollstein, M.; N. *Engl. J. Med.* **1993**, *329*, 1318-1327.

1. taula. Gene tumore-ezabatzaileen adibideak.^{3,12}

Genea	Funtzioa
TP53	Zelula-zikloaren erregulazioa, hazkuntza-gelditzearen eta apoptosiaren indukzioa
RB1	Zelula-zikloaren erregulazioa.
P19ARF	p53 egonkortzailea.
p16(INK4a)	Zelula-zikloaren erregulazioa.
KLF6	Transkripzioaren erregulazioa.
Wt1	Transkripzioaren erregulazioa.
BRCA1/2	Transkripzioaren erregulazioa eta ADNaren konponketa.
MSH2/ 6	ADNaren konponketa.
MLH1	ADNaren konponketa.
TGF R I/II	Hazkuntzaren inhibizioa.
TSC2	Zelula-zikloaren erregulazioa.
PMS1/ 2	ADNaren konponketa.
Maspin	Tumoreen metastasiaren eta tumoreek induzitutako angiogenesiaren inhibizioa.

Beste gene garrantzitsu batzuk dira, adibidez, RB1 genea edo BRCA1/2 geneak. RB1 geneak pRB proteina kodetzen du eta proteina honen funtzio nagusia zelulen kontrolik gabeko zatiketa geldiaraztea da.¹³ BRCA1/1 geneek, berriz, kaltetutako ADN detektatzen eta konpontzen aritzen diren proteinak kodetzen dituzte. Gene hauek obulutegi eta bularreko minbizia goiz detektatzeko proba gisa erabiltzen dira.¹⁴

M. Seneszentzia zelularra.

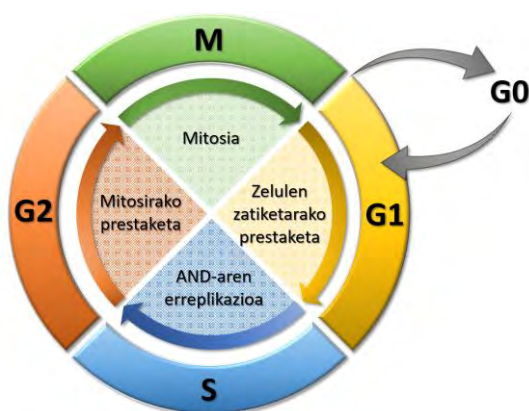
Ziklo zelularra (3. irudia), zelula eukariotoak zatikatu eta erreplikatu egiten direneko lau etapako prozesu bat da. G1 fasean zenbait aldaketa metaboliko gertatzen da, zelula zatiketarako prestatuz. Ondoren, zelula S fasera (sintesi fasea) mugitzen da, non ADNa sintetizatzen den. Gero, zelula mitosirako prestatzen hazten da, ADNa bikoitzen eta elikagaiak metatzen. Urrats honi interfase edo G2 fasea deritzo. Behin zelula prestatuta dagoela, M fasera (Mitosis) mugitzen da, elkarrekin oso lotuta dauden bi prozesutan banatuta dagoena: mitosis bera eta zitokinesia. Mitosi azpiprosuan, zelula bi zelula berdinean zatitzen da kromosomak erreplikatu eta zitokinesian zitoplasma erdibitzen da, bi alaba zelula sortuz amaieran. Azkenik, G0 edo atseden fasea zelulak egoera lasaian edo kieszentzian dauden fasea da, non zatiketa aldi baterako geldituta dago.¹⁵

¹² Wang, L. H.; Wu, C. F.; Rajasekaran, N.; Shin, Y. K. *Cell. Physiol. Biochem.* **2019**, *51*, 2647-2693.

¹³ Dyson, N. J. *Genes Dev.* **2016**, *30*, 1492-1502.

¹⁴ Haffty, B. G.; Euhus, D. M. Pierce, L. J. *Int. J. Clin. Oncol.* **2020**, *38*, 2220-2229.

¹⁵ Malumbres, M.; Barbacid, M. *Nat. Rev. Cancer* **2001**, *1*, 222-231.



3. irudia. Ziklo zelularra.

Zelulen seneszentzia, zelula zikloaren geldialdi egoera iraunkorra da; kieszentzia aldiz, egoera itzulgarria da. Zelularen ondorengoak ez-bideragarriak egingo zituzten ADNaren kalteari edo degradazioari aurre egiteko gertatzen da seneszentzia. Era berean, babes mekanismo gisa tipifikatzen da, zelulen hazkuntza mugatuz eta ugaltzeko ahalmena murriztuz, zatiketa kopuru jakin baten ondoren. Mitosi kopuru zehatz baten ondoren, hazkuntza inhibitzeko mekanismo hori da zelulen hilezintasunaren aurka eta minbizi gaixotasunaren garapenaren kontra egiteko.⁹

V. Apoptosisa.

Apoptosisa zelula-heriotza erregulatuaren mekanismoa da, eta zelulen kalte baten edo kanpoko estresaren ondorioz ez ezik, zelulen garapen normalean ere gertatzen da. Mekanismo hau erregulazio-molekula ezberdinek modulatuzen dute, eta kromatina materialaren kondentsazioa, ADN fragmentazioa, zelulen uzkurdura, mintzaren apurketa eta matrize estrazelularrekiko atxikidura-ahalmena galtzea ditu ezaugarri. Zelulen heriotza mota hau eta nekrosia bereizi behar dira, azken honek kontrakoa adierazten baitu, hau da, trauma larri baten ondorioz gertatzen den desordenatutako zelularen heriotza da.¹⁶

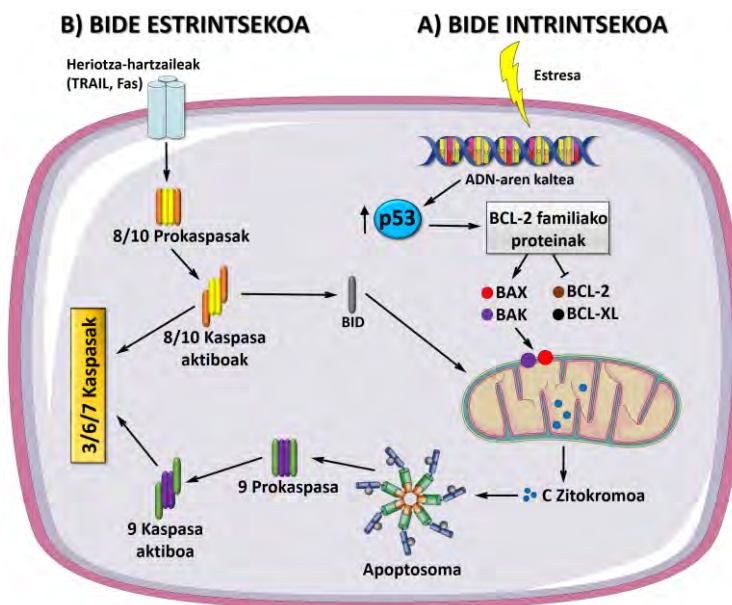
Apoptosi-bideen indukzioan akatsak baldin badaude, zelula neoplasikoak biderkatu daitezke. Minbizi-zeluletan apoptosis eragin daiteke bide intrintsekoen eta estrintsekoen bidez:

Bide intrintsekoa. Bide hau abian jartzeko eskakizun nagusiak honako hauek dira: mitokondriaren kanpoaldeko mintz permeabilizazioa (Mitochondrial Outer Membrane Permeabilization, MOMP) eta ondorengo C zitokromoa zitoplasman askatzea. C zitokromoaren askapena BCL-2 proteina familiako kide pro-apoptotikoek (BIM, BID, PUMA eta NOXA) bultzatzen dute eta familia bereko kide anti-

¹⁶ Jan, R.; Chaudhry, G-S. *Adv Pharm Bull* **2019**, *9*, 205-218.

apoptotikoe (BCL-2 eta BCL-XL) inhibitzen dute. Proteina pro-apoptotikoe apoptosiaren eragile zentralak diren BAX eta BAK1 aktibatzen dituzte, eta hauek mintz mitokondrialean poro bat eratzen dute, MOMPa sortuz. Ondoren, C zitokromoa askatzen da, apoptosomaren eraketara eramanez. Azkenik, kaspasa-proteina batzuen aktibazio sekuentzialaren ondoren, apoptosia gertatzen da (4A irudia).¹⁷

Bide estrintsekoa. Bide hau, Fas eta TRAIL (TNFrekin erlazionatutako apoptosia eragiten duen ligandoa) bezalako heriotza-hartzaileek (mintz proteina zelularrek) abiarazten dute. Hartzaile hauek lotugaiarekin elkartu ondoren trimerizatu eta multzokatu egiten dira. Prozesu honen ondoren, 8 eta 10 kaspasak aktibatzen dira, hauek kaspasa efektoreak aktibatzen dituzte eta apoptosia abiarazten da. Gainera, 8 eta 10 kaspasek BID proteina pro-apoptotikoa ere aktibatzen dute, proteina hau mitokondriara translokatur eta C zitokromoa askatzen lagunduz. BID proteina apoptosiaren bide estrintseko eta intrintsekoen arteko lotura da (4B irudia).¹⁷



4. irudia. Apoptosiaren bideak. (Egokitua: Jan *et al*, 2019).¹⁶

VI. Angiogenesiaren inhibizioa.

Goian deskribatu dugun bezala, tumorea handitzen hazten denean, odol hornidura bat garatu behar du bere eskakizun metabolikoei eusteko gai dena. Odol-hodi berri hauek metastasirako ihesbide gisa ere erabil daitezke. Angiogenesia hainbat angiogenesi-faktorek (fibroblastoen hazkuntza-

¹⁷ Carneiro, B. A.; El-Deiry, W. S. *Nat. Rev. Clin. Oncol.* **2020**, *17*, 395-417.

faktoreak, angiogenina eta endotelio baskularraren hazkuntza-faktoreak) susta dezakete eta molekula angiostatikoek (angiostatina, interleukinak eta α , β eta γ interferonak), aldiz, inhibitu. Molekula angiogeniko eta angiostatikaen arteko oreka hausten denean hasten dira tumorearen angiogenesia eta kontrolik gabeko metastasia.⁹

Minbiziaren kontrako terapia farmakologikoak

Urteetan, minbizi gaixotasunen tratamendua prozesu oso konplexua izan da eta, erabilera klinikorako hainbat hurbilketa berritzaile garatu eta onartu diren arren, hala nola, zelula amen terapia, gene-terapia, farmakoen terapia bideratua¹⁸ eta immunoterapia (adibidez, antigorputz monoklonalak eta farmako-antigorputz konplexuak)¹⁹ gaur egun nagusi diren terapia orokorrak kirurgia eta kimioterapia edo erradiazio terapiaren konbinazioak dira (5. irudia).



5. irudia. Estrategia konbentzionalak eta estrategia aurreratuak eta berritzaileak minbiziaren tratamenduan

Minbiziaren tratamendurako estrategiarik ohikoenetako bat erresekzio kirurgikoa eta gero erradiazio terapia dira. Azken honek, erradiazio ionizagarria baliatzen du minbizi tumorea eta tumorearen mikroinguruaren zelula guztiak jomuga izanik. Erradiazioaren osagarri edo alternatiba gisa, kimioterapiak pisu molekular baxuko molekula natural edo sintetikoak erabiltzen ditu. Molekula hauek gai dira azkar zatitzen diren zelula guztiak hiltzeko eta gorputz osoa tratatzeko erabil daitezke.²⁰

Erradioterapia eta kimioterapia elkarrekin erabilia oso eraginkorrak dira minbiziari eraso egiteko hurbilketa anitzen bidez, eta minbizi-zelulak tratamenduarekiko erresistenteak izan ez daitezen lagundu dezakete. Modu desberdinetan egin daiteke, tratamendu-motaren arabera.²¹

¹⁸ Debela, D. T.; Muzazu, S. G.; Heraro, K. D.; Ndalama, M. T.; Mesele, B. W.; Haile, D. C.; Kitui, S. K.; Manyazewal, T. *SAGE Open Med.* **2021**, *9*, 1-10.

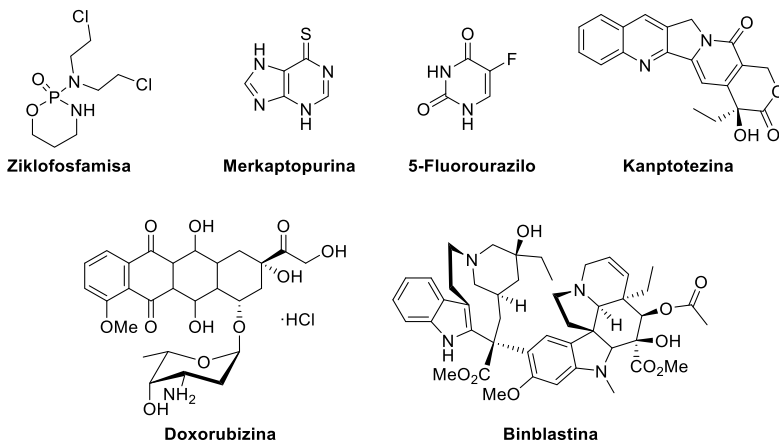
¹⁹ Chau, C. H.; Steeg, P. S.; Figg, W. D. *Lancet* **2019**, *394* (10200), 793–804.

²⁰ Arruebo, M.; Vilaboa, N.; Sáez-Gutierrez, B.; Lambea, J.; Tres, A.; Valladares, M.; González-Fernández, Á. *Cancers*. **2011**, *3*, 3279-3330.

²¹ Baudino, T. *Curr. Drug Discov. Technol.* **2015**, *12*, 3-20.

- **Terapia neoadjubanteak** kimioterapia baliatzen du, eta gero erradiazio bidezko terapia kirurgia baino lehen. Tumorearen tamaina murrizteko eta behar den kirurgiaren bolumena txikiago egiteko erabiltzen da.
- **Terapia adjubantea** kirurgiaren ondoren erabiltzen da, baldin eta oraindik zenbait minbizi zelula gaixoaren gorputzean badaude. Kimioterapia eta erradioterapia ez ezik, hormona bidezko terapia, immunoterapia eta terapia gidatua ere erabil daitezke.
- **Terapia konkomitantea** kimioterapia eta erradiazio terapia erabiltzea da, interbentzio kirurgikorik gabe.

Kimioterapia ekintza mekanismo zein egitura kimiko ezberdinak dituzten farmakoak erabiltzen dira: agente alkilatzaileak (adibidez, ziklofosfamida edo oxaliplatina),²² antimetabolitoak edo azido nukleikoaren analogoak (adibidez, merkaptopurina, 5-fluorourazilo edo metotrexato),²³ topoisomerasaren inhibitzaileak (kanptotezina edo topotekan, kasu),²⁴ antraziklinak (daunorubizina edo doxorubizina, esaterako)²⁵ eta landareen alkaloideak (adibidez, binblastina edo binkristina)²⁶ (6. irudia).



6. irudia. Agente kimioterapeutiko batzuen egiturak.

²² Puyo, S.; Montaudon, D.; Pourquier, P. *Crit. Rev. Oncol. Hematol.* **2014**, *89*, 43-61.

²³ Peters, G. J.; Van Der Wilt, C. L.; Van Moorsel, C. J. A.; Kroep, J. R.; Bergman, A. M.; Ackland, S. P. *Pharmacol. Ther.* **2000**, *87*, 227-253.

²⁴ Liang, X.; Wu, Q.; Luan, S.; Yin, Z.; He, C.; Yin, L.; Zou, Y.; Yuan, Z.; Li, L.; Song, X.; He, M.; Lv, C.; Zhang, W. *Eur. J. Med. Chem.* **2019**, *171*, 129-168.

²⁵ Baka, S.; Califano, R.; Ferraldeschi, R.; Ascroft, L.; Thatcher, N.; Taylor, P.; Faivre-Finn, C.; Blackhall, F.; Lorigan, P. *Br. J. Cancer* **2008**, *99*, 442-447.

²⁶ Mondal, A.; Gandhi, A.; Fimognari, C.; Atanasov, A. G.; Bishayee, A. *Eur. J. Pharmacol.* **2019**, *858*, 172472.

Farmakoen bidezko terapia honek hainbat muga ditu, hala nola, dosifikazioaren aukeraketa zaila, farmakoen metabolismo azkarra eta albo-efektu kaltegarri askoren garapena.²⁷ Gaixoengan kontrako efektu hauek gertatzen dira batez ere zelula gaiztoekiko espezifikotasunik ezaren ondorioz. Agente kimioterapeutikoez azkar zatitzen eta hazten diren zelulak erasotzen dituzte batik bat, eta, minbizi-zelulak gure gorputzean ezaugarri hauek dituzten zelula bakarrak ez direnez, beste zelula mota batzuk ere pairatzen dute tratamendua, besteak beste, hezur-muinean, digestio-hodian eta ile-folikulan dauden zelulak.²⁰ Beste desabantaila nagusietako bat farmakoen aurreko erresistentzia da, minbizi-zelulek minbiziaren tratamendurako farmakoen aurkako erresistentzia garatzen dutenean gertatzen dena.²⁸

Kontsiderazio hauek kontuan hartuta, argi dago oraindik beharrezkoa dela agente kimioterapeutiko berriak aurkitzea, maila molekularrean dauden ituekin modu selektiboan lotu ahal izateko. Adibidez, azken hamarkadan, gure ikerketa-taldeak I Topoisomerasaren inhibitzaile berriak garatu ditu eta minbizi kontrako ahalmena probatu du minbizi mota ezberdinen eta beste gaixotasun infekzioso batzuen aurka.²⁹ Testuinguru horretan, etorkizun oparoko itu biokimikoa p53 transkripzio-faktorearen (TP53 gene tumore-ezabatzailea kodetzen duena) eta MDM2 (MURINE DOUBLE MINUTE 2) eta MDMX (MURINE DOUBLE MINUTE X) proteinen arteko elkarrekintza da.

Izan ere, minbizi-mota askotan ohikoa da mutazioak antzematea p53 proteinan. Halaber, tumoreek ere maiz izaten dute WTP53 (Wild Type p53) proteina, p53 seinalizazio-bide kaltetuekin, mutaturako edo desregulatutako proteina laguntzaileekin.³⁰ MDM2 eta MDMX proteinen aktibitate handitua edo gainadierazitaren ondorioz, tumore askotan p53aren inaktibazioa eta degradazioa faboratzen dira, honela, p53aren minbizi-zelulen ugalketaren aurkako aktibitatea mugatuz.³¹ Izan ere, MDM2 eta MDMX proteinen mutazioak eta gainadierazpena antzeman izan dira giza minbizietan, hala nola,

²⁷ Debela, D. T.; Muzazu, S. G.; Heraro, K. D.; Ndalama, M. T.; Mesele, B. W.; Haile, D. C.; Kitui, S. K.; Manyazewal, T. *SAGE Open Med.* **2021**, *9*, 1-10.

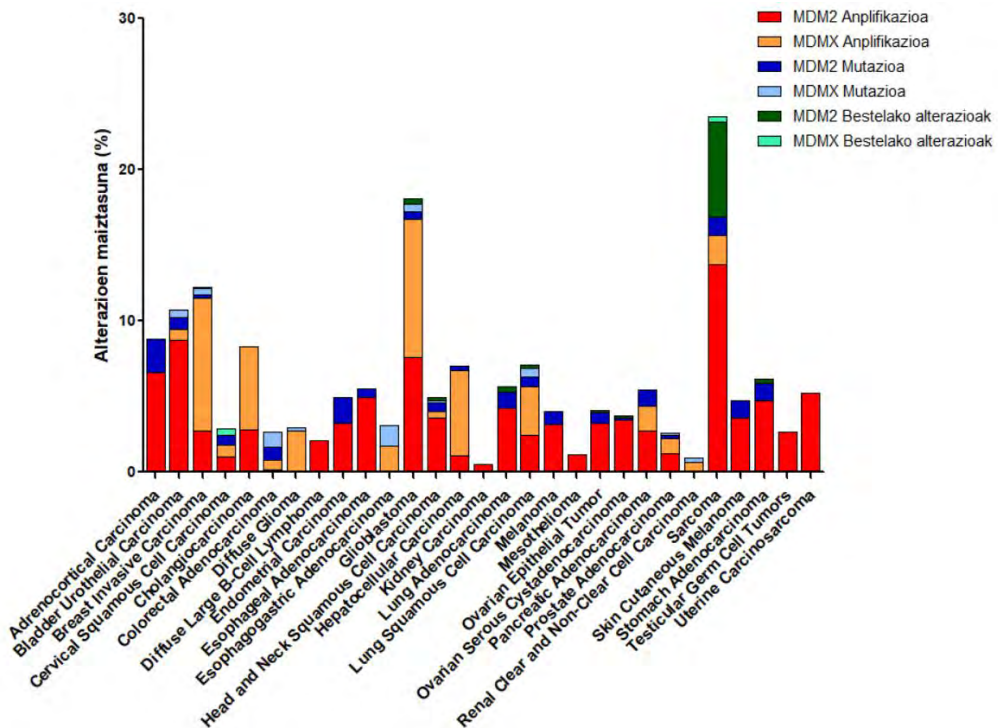
²⁸ Shapira, A.; Livney, Y. D.; Broxterman, H. J.; Assaraf, Y. G. *Drug Resist. Updat.* **2011**, *14*, 150-163.

²⁹ (a) Selas, A.; Fuertes, M.; Melcón-Fernández, E.; Pérez-Pertejo, Y.; Reguera, R. M.; Balaña-Fouce, R.; Knudsen, B. R.; Palacios, F.; Alonso, C. *Pharmaceuticals* **2021**, *14*, 784 (b) Rizo-Liendo, A.; Arberas-Jiménez, I.; Martín-Encinas, E.; Sifaoui, I.; Reyes-Batlle, M.; Chao-Pellicer, J.; Alonso, C.; Palacios, F.; Piñero, J. E.; Lorenzo-Morales, J. *Pharmaceuticals* **2021**, *14*, 1013. (c) Carramiñana, V.; Ochoa de Retana, A. M.; Palacios, F.; de los Santos, J. M. *Molecules* **2021**, *26*, 4265. (d) Tejería, A.; Pérez-Pertejo, Y.; Reguera, R. M.; Carbajo-Andrés, R.; Balaña-Fouce, R.; Alonso, C.; Martín-Encinas, E.; Selas, A.; Rubiales, G.; Palacios, F. *Eur. J. Med. Chem.* **2019**, *162*, 18-31.

³⁰ Miller, J. J.; Gaidon, C.; Storr, T. *Chem. Soc. Rev.* **2020**, *49*, 6995-7014.

³¹ Momand, J.; Jung, D.; Wilczynski, S.; Niland, J. *Nucleic Acids Res.* **1998**, *26*, 3453-3459.

sarkoman,³² neuroblastoman,³³ glioblastoman,³⁴ bularrean,³⁵ prostatan,³⁶ obulutegi,³⁷ kolonean³⁸ eta birikietan.³⁹ Beste adibide batzuk eta eragiten duten aldaketa espezifikoak 7. irudian ageri dira.



7. irudia. MDM2 eta MDMX geneen aberrazio genetiko eskematikoak giza minbiziaren lagin klinikoetan.

Datuak hemendik ekarrita: TCGA PanCancer Atlas (cBioPortal).⁴⁰

³² Flørenes, V. A.; Mælandsmo, G. M.; Forus, A.; Andreassen, Å.; Myklebost, O.; Fodstad, Ø. *J. Natl. Cancer Inst.* **1994**, *86*, 1297-1302.

³³ (a) Zafar, A.; Wang, W.; Liu, G.; Xian, W.; McKeon, F.; Zhou, J.; Zhang, R. *Cancer Lett.* **2021**, *496*, 16-29. (b) Corvi, R.; Savelyeva, L.; Breit, S.; Wenzel, A.; Handgretinger, R.; Barak, J.; Oren, M.; Amler, L.; Schwab, M. *Oncogene* **1995**, *10*, 1081-1086.

³⁴ (a) He, J.; Reifenger, G.; Liu, L.; Collins, V.P.; James, C.D. *Genes Chromosom. Cancer* **1994**, *11*, 91-96. (b) Reifenger, G.; Liu, L.; Ichimura, K.; Schmidt, E.E.; Collins, V.P. *Cancer Res.* **1993**, *53*, 2736-2739.

³⁵ (a) Loo, L. W. M.; Gao, C.; Shvetsov, Y. B.; Okoro, D. R.; Hernandez, B. Y.; Bargonetti, J. *Breast Cancer Res. Treat.* **2019**, *174*, 257-269. (b) Turbin, D. A.; Cheang, M. C. U.; Bajdik, C. D.; Gelmon, K. A.; Yorida, E.; De Luca, A.; Nielsen, T. O.; Huntsman, D. G.; Gilks, C. B. *Mod. Pathol.* **2006**, *19*, 69-74.

³⁶ Wang, H.; Yu, D.; Agrawal, S.; Zhang, R. *Prostate* **2003**, *54*, 194-205.

³⁷ (a) Palazzo, J. P.; Monzon, F.; Burke, M.; Hyslop, T.; Dunton, C.; Barusevicius, A.; Capuzzi, D.; Kovatich, A. *J. Hum. Pathol.* **2000**, *31*, 698-704. (b) Skomedal, H.; Kristensen, G. B.; Abeler, V. M.; Børresen-Dale, A. L.; Tropé, C.; Holm, R. *J. Pathol.* **1997**, *181*, 158-165.

³⁸ (a) Barcherini, V.; Almeida, J.; Lopes, E. A.; Wang, M.; Magalhães e Silva, D.; Mori, M.; Wang, S.; Saraiva, L.; Santos, M. M. *ChemMedChem* **2021**, *16*, 250-258. (b) Zhang, R.; Wang, H.; Agrawal, S. *Curr. Cancer Drug Targets* **2005**, *5*, 43-49.

³⁹ Eymin, B.; Gazzeri, S.; Brambilla, C.; Brambilla, E. *Oncogene* **2002**, *21*, 2750-2761.

⁴⁰ cBioPortal Home Page. <https://www.cbioportal.org/> (accessed 2021-09-12)

Zelula normalek (osasuntsuek edo ez gaiztoek) hiltzeko joera txikiagoa dute p53aren aurrean minbizi-zelulek baino, horregatik p53-MDM2/MDMX konplexuaren inhibitzaile espezifikoko oso tresna interesgarriak dira p53 aktibitate normala berrezartzeko eta zelula gaiztoen gainean selektiboki jokatzeko, beraz, minbizi-terapiarako hurbilketa egiaztatua eta etorkizun handikoa da honako hau.⁴¹

MDM2 eta MDMX proteinekiko afinitate handia duten peptido-motako inhibitzaile asko garatu diren arren,⁴² normalean zelula-permeabilitate baxua jasaten dute eta proteolitikoki ezegonkorrak dira.⁴³ Gaur egungo etorkizun oparoko ikerketa arlo gisa, peptidoen alternatiba molekula txikiak erabiltzea da, p53/MDM2-MDMX konplexua inhibitzeko helburuarekin. Jarraian, familia eta konposatu adierazgarrietako batzuk deskribatuko dira. Atal honetan zehar, inhibizioa hiru modutan adieraziko da. Batetik, IC₅₀-aren balio gisa emango da, neurri kuantitatiboa baita adierazteko zenbat farmako behar den prozesu biologiko bat edo osagai biologiko bat % 50ean inhibitzeko (normalean zelulen bideragarritasun entseguetatik lortua). Bestetik, K_d parametroa, afinitate-konstantea da eta mikroeskalako termoforesia (Microscale Thermophoresis, MST), gainazaleko plasmoien erresonantzia (Surface Plasmon Resonance, SPR) edo erresonantzia magnetiko nuklearra (Nuclear Magnetic Resonance, NMR) izeneko esperimentu eta tekniken bidez eskuratu ahal da. Beste batzuetan, K_i parametroa, hau da, inhibizio-konstantea erabiliko da, fluoreszentiaren polarizazioa (Fluorescence Polarization, FP) eta denbora-errealako fluoreszentzia homogenea (Homogeneous time-resolved fluorescence, HTRF) esperimentuen bitartez neurtua.

p53-MDM2 eta MDMX inhibitzaieak.

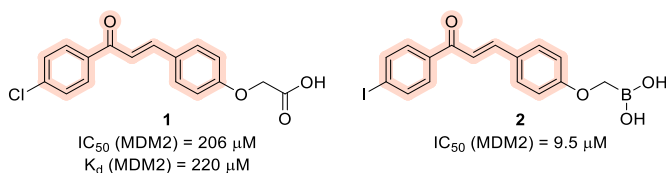
Txalkonen antzeko konposatuak izan ziren p53-MDM2 konplexuaren pisu molekular baxuko lehen inhibitzaile klasea (8. irudia). Holak-ek eta lankideek deskribatu zituzten 2001ean⁴⁴ eta lotura-eredu bat ere proposatu zuten **1** txalkonarako, non π -sistema hedatua, zurruna eta laua izanik, lotura-poltsikoan sartuta dagoen eta *p*-klorofenil taldea Trp23-ren gune aktiboan edo loturagunean. Hala ere, minbizi-zelulekiko selektibitate baxua erakutsi zuen, zelula ez-gaiztoekin konparatuta, eta **1** konposatuarekin tratatu ondoren, askatutako p53ak ezin izan zuen berriro ADNrekin lotu.

⁴¹ Khoury, K.; Popowicz, G. M.; Holak, T. A.; Dömling, A. *Med. Chem. Comm.* **2011**, *2*, 246-260.

⁴² (a) Wang, X.; Ni, D.; Liu, Y.; Lu, S. *Front. Chem.* **2021**, *9*, 682-675. (b) Giustiniano, M.; Daniele, S.; Pelliccia, S.; La Pietra, V.; Pietrobono, D.; Brancaccio, D.; Cosconati, S.; Messere, A.; Giuntini, S.; Cerofolini, L.; Fragai, M.; Luchinat, C.; Taliani, S.; La Regina, G.; Da Settimo, F.; Silvestri, R.; Martini, C.; Novellino, E.; Marinelli, L. *J. Med. Chem.* **2017**, *60*, 8115-8130.

⁴³ Baek, S.; Kutchukian, P. S.; Verdine, G. L.; Huber, R.; Holak, T. A.; Lee, K. W.; Popowicz, G. M. *J. Am. Chem. Soc.* **2012**, *134*, 103-106.

⁴⁴ Stoll, R.; Renner, C.; Hansen, S.; Palme, S.; Klein, C.; Belling, A.; Zeslawski, W.; Kamionka, M.; Rehm, T.; Mühlhahn, P.; Schumacher, R.; Hesse, F.; Kaluza, B.; Voelter, W.; Engh, R. A.; Holak, T. A. *Biochemistry*, **2001**, *40*, 336-344.



8. irudia. Txalkonan (krema kolore gorria) oinarritutako analogoak, deskribatu ziren lehen MDM2-ren inhibitzaileak.

Urte batzuk geroago, Khan-ek eta taldekideek azido boronikoen deribatu den **2** txalkona deskribatu zuten, IC_{50} balioen arabera emaitza hobekak eskaintzen zuenak.⁴⁵ Kontuan hartuta proteinarekiko selektibitate eskasa, txalkonan oinarritutako analogoek duten interesa p53-MDM2 multzoaren inhibitzaile moduan oso mugatua izan da, baina lan hauek atea ireki zion ibilbide luze bati, zenbait inhibitzailearen sintesira eramanez. Jarraian, konposatu-familia adierazgarrienak aurkeztu dira.

I. Nutlin-motako konposatuak.

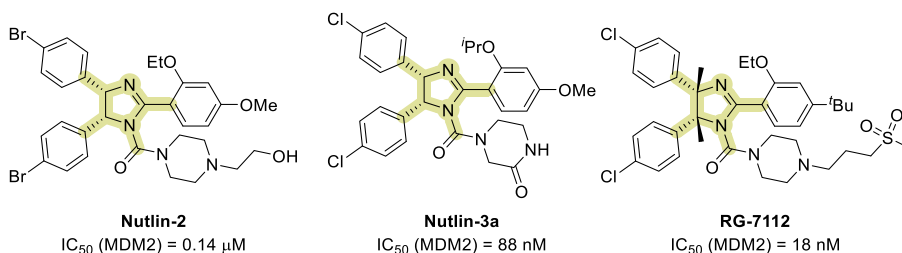
2004ean, Vassilev eta lankideek 1,2,4,5-tetraordezkatutako-4,5-*cis*-imidazolina nukleoa duten Nutlinak identifikatu zituzten MDM2 proteinaren inhibitzaile sendo gisa (9. irudia).⁴⁶ MDM2-rekin lotutako **Nutlin-2**ren ko-kristalaren egiturak erakusten duenez, halogenoz ordezkatutako bi fenil zikloek Trp23 eta Leu26 poltsikoak betetzen dituzte eta, aldi berean, etil taldea Phe19 poltsikoan dago, beraz p53 proteinaren metaketa eta egonkortzea bultzatuz, bai eta p21-aren gora-erregulazioa ere. Honek dakar zelularen zikloaren gelditzea G1 etapan eta apoptosiaren indukzioa zelula lerro eta sagu ereduetan.⁴⁷ Familia honetako kiderik ahaltsuena, **Nutlin-3a**-k MDM2-p53 proteina-proteina elkarrekintza modu eraginkor eta selektiboan blokeatzeko gai da. **Nutlin-3a**ren egitura-eraldaketa optimizatu ondoren, Roche enpresako zientzialariek **RG-7112** konposatu analogoa lortu zuten eta lehen faseko entsegu klinikoak amaitu ziren 2012an. Proba hauetan zelulen aktibitate hobea, ahozko administratzearako propietate farmakozinetiko onak, egonkortasun kimikoa eta potentzia inhibitzaile lau aldiz handiagoa erakutsi zuen konposatu honek.⁴⁸

⁴⁵ Kumar, S. K.; Hager, E.; Pettit, C.; Gurulingappa, H.; Davidson, N. E.; Khan, S. R. *J. Med. Chem.* **2003**, *46*, 2813-2815.

⁴⁶ Vassilev, L. T.; Vu, B. T.; Graves, B.; Carvajal, D.; Podlaski, F.; Filipovic, Z.; Kong, N.; Kammlott, U.; Lukacs, C.; Klein, C.; Fotouhi, N.; Liu, E. A. *Science*, **2004**, *303*, 844-848.

⁴⁷ Tovar, C.; Rosinski, J.; Filipovic, Z.; Higgins, B.; Kolinsky, K.; Hilton, H.; Zhao, X.; Vu, B.T.; Qing, W.; Packman, K.; Myklebost, O.; Heimbrook, D. C.; Vassilev, L. T. *Proc. Natl. Acad. Sci. U.S.A.* **2006**, *103*, 1888-1893.

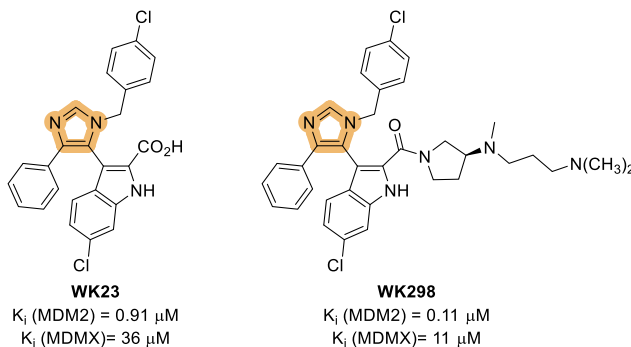
⁴⁸ Vu, B.; Wovkulich, P.; Pizzolato, G.; Lovey, A.; Ding, Q.; Jiang, N.; Liu, J.-J.; Zhao, C.; Glenn, K.; Wen, Y.; Tovar, C.; Packman, K.; Vassilev, L.; Graves, B. *ACS Med. Chem. Lett.* **2013**, *4*, 466-469.



9. irudia. Nutlin (kolore horia) motako MDM2 inhibitzaileak.

II. Imidazolak and Imidazotiazolak.

Beste imidazol deribatu batzuk MDM2ren inhibitzaile gisa ere deskribatu izan dira. Egia esan, konposatu familia hau inhibitzaile dualtzat hartu beharko litzateke, MDM2 ez ezik, MDMX proteina ere inhibitzeko duten gaitasunagatik. Holak-ek eta lankideek garatutako bi molekula txikik, **WK23**k MDM2rekin eta **WK298**k MDMXrekin sortzen dituzten konplexuen kristalizazioak, bi proteinen lotura guneetako aldeak aztertzea ahalbidetu zuen (10. irudia). Bi proteinak inhibitzeko gai izan arren, afinitatea handiagoa da MDM2arekiko, Leu26 inguruko aminoazidoen ondorioz, MDMXren loturarako eskualdea edo gune aktiboa disolbatzaileak errazago okupatzen baitu eta imidazolekiko afinitatea murriztu.⁴⁹



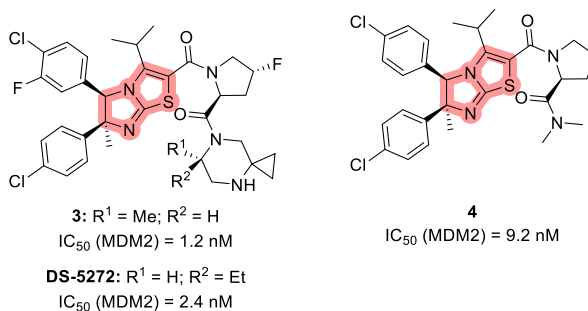
10. irudia. Imidazol (kolore laranja) motako MDM2 eta MDMX inhibitzaile dualak.

Gainera, imidazotiazolen antzeko antagonistak ere deskribatu dira (11. irudia). Adibidez, Uoto et al. **3** dihidroimidazotiazol biziklikoa sintetizatu zuten. Bertan, imidazol eraztuna dihidroimidazotiazol txantilo batek ordezten du, eta MDM2arekiko 1.2 nM den IC₅₀ balioa lortzen da.⁵⁰ 2013an, Miyazakik

⁴⁹ Popowicz, G. M.; Czarna, A.; Wolf, S.; Wang, K.; Wang, W.; Dömling, A.; Holak, T. A. *Cell Cycle* **2010**, *9*, 1104–1111.

⁵⁰ Uoto, K.; Kawato, H.; Sugimoto, Y.; Naito, H.; Miyazaki, M.; Taniguchi, T.; Aonuma, M. Patent Application WO 2009/151069 A1, 2009.

eta lankideek egitura bizikliko hau baren duten inhibitzaile multzoa diseinatu zuten,⁵¹ hala nola, **4** konposatua, **Nutlin-3a** baino 10 aldiz aktiboagoa dena. Urte batzuk geroago, autore hauek **DS-5272** konposatua sintetizatu zuten ere, **3** dihidroimidazotiazolaren deribatua dena eta SJSA-1 tumore xenomentuan tumore kontrako aktibitate ona erakusten duena, segurtasun altuarekin eta propietate farmakozinetiko onekin.⁵²



11. irudia. Imidazotiazolaren antzeko (kolore gorria) MDM2 inhibitzaileak.

III. Bentzodiazepinak.

Beste molekula inhibitzaile mota bat, **5** 1,4-benzodiazepin-2,5-diona, 2005ean jakinarazi zen lehen aldiz (12. irudia).⁵³ Egileek MDM2 eta **5** konposatuaren arteko konplexuaren kristal-egitura isolatu ahal izan zuten, baina, emaitza esperantzagarria izan arren, molekula hau ez zen oso aktiboa minbizi-zelulen aurka, zelulen permeabilitatea hobetzeko beharra agerian utziz.⁵⁴ Optimizazio gehiagoren ondoren, **6** konposatuan piperazina talde bat txertatuz sartzearekin batera, MCF7 bularreko minbizi-zeluletan egindako esperimentuen jarduera handiagoa antzeman zen.⁵⁵ Horrez gain, **7** eta **8** tiobenzodiazepinek

⁵¹ (a) Miyazaki, M.; Naito, H.; Sugimoto, Y.; Yoshida, K.; Kawato, H.; Okayama, T.; Shimizu, H.; Miyazaki, M.; Kitagawa, M.; Seki, T.; Fukutake, S.; Shiose, Y.; Aonuma, M.; Soga, T. *Bioorg. Med. Chem.* **2013**, *21*, 4319-4331. (b) Miyazaki, M.; Naito, H.; Sugimoto, Y.; Kawato, H.; Okayama, T.; Shimizu, H.; Miyazaki, M.; Kitagawa, M.; Seki, T.; Fukutake, S.; Aonuma, M.; Soga, T. *Bioorg. Med. Chem. Lett.* **2013**, *23*, 728-732.

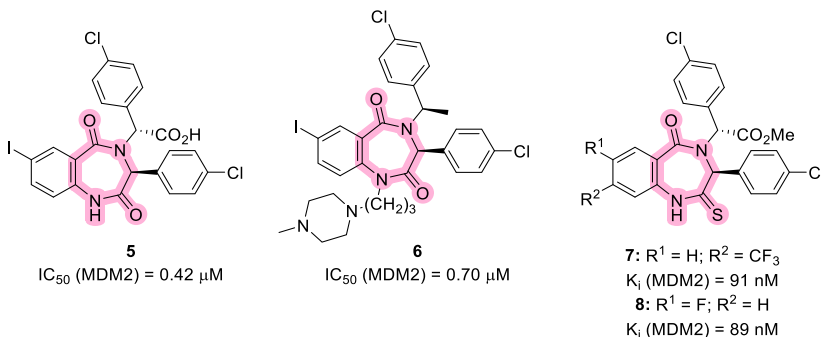
⁵² Miyazaki, M.; Uoto, K.; Sugimoto, Y.; Naito, H.; Yoshida, K.; Okayama, T.; Kawato, H.; Miyazaki, M.; Kitagawa, M.; Seki, T.; Fukutake, S.; Aonuma, M.; Soga, T. *Bioorg. Med. Chem.* **2015**, *23*, 2360-2367.

⁵³ (a) Parks, D. J.; LaFrance, L. V.; Calvo, R. R.; Milkiewicz, K. L.; Gupta, V.; Lattanze, J.; Ramachandren, K.; Carver, T. E.; Petrella, E. C.; Cummings, M. D.; Maguire, D.; Grasberger, B. L.; Lu, T. *Bioorg. Med. Chem. Lett.* **2005**, *15*, 765-770. (b) Raboisson, P.; Marugán, J. J.; Schubert, C.; Koblisch, H. K.; Lu, T.; Zhao, S.; Player, M. R.; Maroney, A. C.; Reed, R. L.; Huebert, N. D.; Lattanze, J.; Parks, D. J.; Cummings, M. D. *Bioorg. Med. Chem. Lett.* **2005**, *15*, 1857-1861.

⁵⁴ (a) Parks, D. J.; LaFrance, L. V.; Calvo, R. R.; Milkiewicz, K. L.; José Marugán, J.; Raboisson, P.; Schubert, C.; Koblisch, H. K.; Zhao, S.; Franks, C. F.; Lattanze, J.; Carver, T. E.; Cummings, M. D.; Maguire, D.; Grasberger, B. L.; Maroney, A. C.; Lu, T. *Bioorg. Med. Chem. Lett.* **2006**, *16*, 3310-3314. (b) Grasberger, B. L.; Lu, T.; Schubert, C.; Parks, D. J.; Carver, T. E.; Koblisch, H. K.; Cummings, M. D.; LaFrance, L. V.; Milkiewicz, K. L.; Calvo, R. R.; Maguire, D.; Lattanze, J.; Franks, C. F.; Zhao, S.; Ramachandren, K.; Bylebyl, G. R.; Zhang, M.; Manthey, C. L.; Petrella, E. C.; Pantoliano, M. W.; Deckman, I. C.; Spurlino, J. C.; Maroney, A. C.; Tomczuk, B. E.; Molloy, C. J.; Bone, R. F. *J. Med. Chem.* **2005**, *48*, 909-912.

⁵⁵ Koblisch, H. K.; Zhao, S.; Franks, C. F.; Donatelli, R. R.; Tomínovich, R. M.; LaFrance, L. V.; Leonard, K. A.; Gushue, J. M.; Parks, D. J.; Calvo, R. R.; Milkiewicz, K. L.; Marugán, J. J.; Raboisson, P.; Cummings, M. D.; Grasberger, B. L.; Johnson, D. L.; Lu, T.; Molloy, C. J.; Maroney, A. C. *Mol. Cancer Ther.* **2006**, *5*, 160-169.

MDM2arekiko afinitate bikainak erakusten dituzte eta osteosarkoma zeluletan **Nutlin-3a** baino jarduera biologiko hobea.⁵⁶



12. irudia. Benzodiazepinak eta tiobenzodiazepinak (kolore arrosa) MDM2 inhibitzaile gisa.

IV. Espirooxindolak, indolak and indoil hidantoinak.

p53-MDM2 konplexuaren egitura kristalinoaren analisi zabal baten ondoren, eta ikusita Trp23-ren indol eratzuna elkarrekin honen gako egitura dela, Wang eta lankideek **9** konposatua sintetizatu zuten, lotura-modu edo ahokadura hau imitatzeko lehen espirooxindol antagonista bezala (13. irudia).⁵⁷ Geroztik, azken hamarkadan zehar, espirooxindoloak MDM2ren antagonista gisa luze aztertu eta eraldatu dira eta entsegu prekliniko eta klinikoetara iritsi diren analogo indartsuen garapena gauzatu da.⁵⁸ Adibidez, analogo boteretsuenetakoen artean bi **SAR405838** eta **APG-115** dira, eta MDM2rekiko nanomolar azpiko lotzeko afinitate izanik, minbizi-zeluletan eta sagu-ereduetan p53 aktibatze gaitasuna frogatu dute bai eta I faseko entsegu klinikoetan emaitza esperantzagarriak erakutsi ere.⁵⁹

Gainera, 3-ordezkatutako indol deribatuak, hala nola **10** konposatua, MDM2ren inhibitzaileak bezala ere deskribatu dituzte Holak-ek eta Dömling-ek.⁶⁰ Konposatu hauek MDM2arekiko p53 proteinaren hiru aminoazido karakteristikoaren lotura modua imitatze gai dira. Gainera, indol egitura

⁵⁶ Guo, Z.; Zhuang, C.; Zhu, L.; Zhang, Y.; Yao, J.; Dong, G.; Wang, S.; Liu, Y.; Chen, H.; Sheng, C.; Miao, Z.; Zhang, W. *Eur. J. Med. Chem.* **2012**, *56*, 10-16.

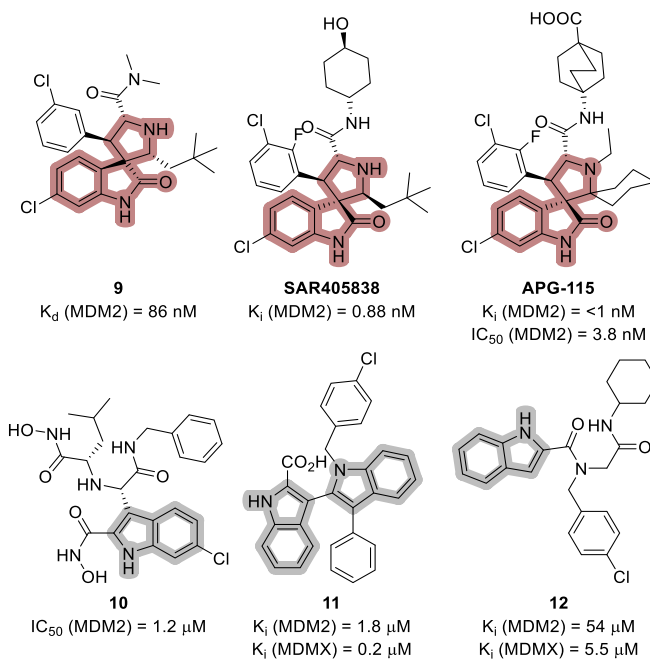
⁵⁷ Ding, K.; Lu, Y.; Nikolovska-Coleska, Z.; Qiu, S.; Ding, Y.; Gao, W.; Stuckey, J.; Krajewski, K.; Roller, P. P.; Tomita, Y.; Parrish, D. A.; Deschamps, J. R.; Wang, S. *J. Am. Chem. Soc.* **2005**, *127*, 10130-10131.

⁵⁸ Gupta, A. K.; Bharadwaj, M.; Kumar, A.; Mehrotra, R. *Top. Curr. Chem.* **2017**, *375*, 1-25.

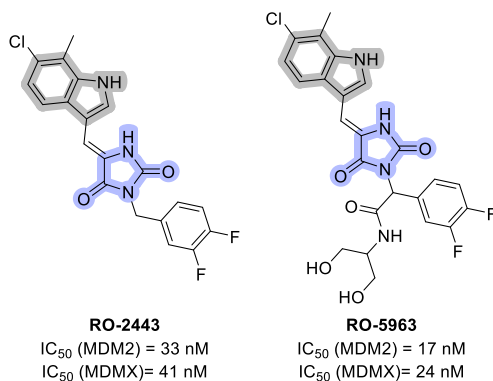
⁵⁹ (a) Aguilar, A.; Lu, J.; Liu, L.; Du, D.; Bernard, D.; McEachern, D.; Przybranowski, S.; Li, X.; Luo, R.; Wen, B.; Sun, D.; Wang, H.; Wen, J.; Wang, G.; Zhai, Y.; Guo, M.; Yang, D.; Wang, S. *J. Med. Chem.* **2017**, *60*, 2819-2839. (b) Wang, S.; Sun, W.; Zhao, Y.; McEachern, D.; Meaux, I.; Barrière, C.; Stuckey, J. A.; Meagher, J. L.; Bai, L.; Liu, L.; Hoffman-Luca, C. G.; Lu, J.; Shangary, S.; Yu, S.; Bernard, D.; Aguilar, A.; Guerif, S.; Pannier, P.; Gorge-Bernat, D.; Debussche, L. *Cancer Res.* **2014**, *74*, 5855-5865.

⁶⁰ (a) Huang, Y.; Wolf, S.; Beck, B.; Köhler, L. M.; Khoury, K.; Popowicz, G. M.; Goda, S. K.; Subklewe, M.; Twarda, A.; Holak, T. A.; Dömling, A. *ACS Chem. Biol.* **2014**, *9*, 802-811. (b) Bista, M.; Wolf, S.; Khoury, K.; Kowalska, K.; Huang, Y.; Wrona, E.; Arciniega, M.; Popowicz, G. M.; Holak, T. A.; Dömling, A. *Structure* **2013**, *21*, 2143-2151.

duten beste inhibitzaile batzuk MDMXarekiko afinitate handiagoa dute, adibidez, **11** bis-indol⁶¹ eta **12** ordezkatutako indolak.⁶²



13. irudia. Espirooxindol (kolore marroia) eta indol (kolore grisa) motako MDM2/X inhibitzaileak.



14. irudia. Indolil (kolore gris)-hidantoina (kolore more argia) konposatuak MDM2 eta MDMX inhibitzaile dual gisa.

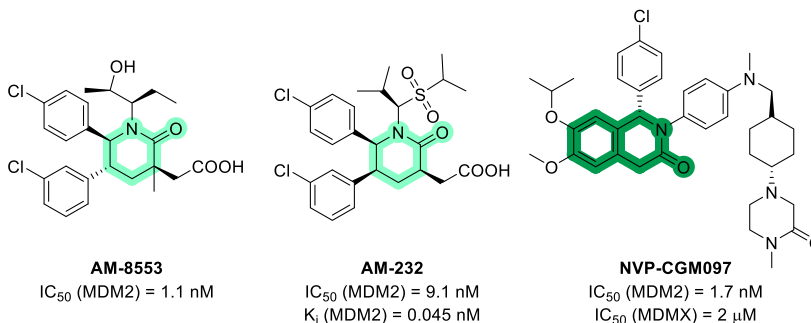
⁶¹ Neochoritis, C. G.; Wang, K.; Estrada-Ortiz, N.; Herdtweck, E.; Kubica, K.; Twarda, A.; Zak, K. M.; Holak, T. A.; Dömling, A. *Bioorg. Med. Chem. Lett.* **2015**, *25*, 5661-5666.

⁶² Boltjes, A.; Huang, Y.; Van De Velde, R.; Rijkee, L.; Wolf, S.; Gaugler, J.; Lesniak, K.; Guzik, K.; Holak, T. A.; Dömling, A. *ACS Comb. Sci.* **2014**, *16*, 393-396.

Klase honetako beste indol deribatu batzuk, hala nola, indolil hidantoinak inhibitzaile dual ahaltso gisa agertu dira (14. irudia). Adibidez, **RO-2443k** aktibitate nanomolarra erakusten badu ere bi proteinen aurrean, bere ur-disolbagarritasun eskasak eragina du zelulen analisisetan, eta horren ondorioz optimizazio kimiko batzuk egin behar izan ziren. Modu honetan afinitate eta disolbagarritasun hobea duen **RO-5963** konposatua aurkitu ahal izan zen.⁶³

V. Piperidinonak and isoquinolinak.

Azken hamarkadan zehar, ahalegin handiak egin dira piperidona nukleoa duten MDM2 inhibitzaileak optimizatzeko eta kasu batzuetan emaitza bikainak lortu dira. Emaitzarik aipagarrienak Sun eta kolaboratzaileek jakinarazi zituzten, zeinek, X izpien bidezko kristalen egituren analisek bultzatutako egituren optimizazio batzuen ondoren, **AM-8553** (15. irudia) konposatua proposatu zuten.⁶⁴ Ondoren, egitura aldaketa gehiagoren ondoren, **AM-232** konposatua garatu zuten.⁶⁵ Honek p53ren gora erregulazioa eragiten du, klinikarako propietate farmakozinetiko egokiak erakusten ditu tumore kontrako *in vivo* jardueran sagu ereduetan, eta gaur egun I faseko entsegu klinikoetan dago.⁶⁶



15. irudia. Piperidona (kolore berde argia) eta isokinolina (kolore berde iluna) motako MDM2/X antagonistak.

⁶³ Graves, B.; Thompson, T.; Xia, M.; Janson, C.; Lukacs, C.; Deo, D.; Di Lello, P.; Fry, D.; Garvie, C.; Huang, K. Sen; Gao, L.; Tovar, C.; Lovey, A.; Wanner, J.; Vassilev, L. T. *Proc. Natl. Acad. Sci. U. S. A.* **2012**, *109*, 11788-11793.

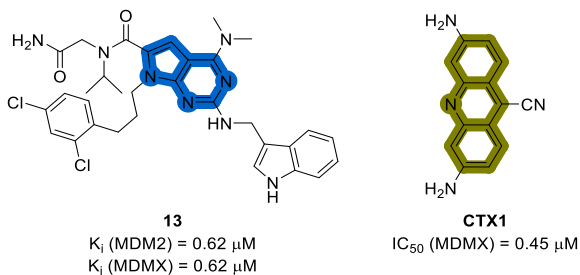
⁶⁴ Rew, Y.; Sun, D.; Gonzalez-Lopez De Turiso, F.; Bartberger, M. D.; Beck, H. P.; Canon, J.; Chen, A.; Chow, D.; Deignan, J.; Fox, B. M.; Gustin, D.; Huang, X.; Jiang, M.; Jiao, X.; Jin, L.; Kayser, F.; Kopecky, D. J.; Li, Y.; Lo, M. C.; Long, A. M.; Michelsen, K.; Oliner, J. D.; Osgood, T.; Ragains, M.; Saiki, A. Y.; Schneider, S.; Toteva, M.; Yakowec, P.; Yan, X.; Ye, Q.; Yu, D.; Zhao, X.; Zhou, J.; Medina, J. C.; Olson, S. H. *J. Med. Chem.* **2012**, *55*, 4936-4954.

⁶⁵ Rew, Y.; Sun, D. *J. Med. Chem.* **2014**, *57*, 6332-6341.

⁶⁶ (a) Her, N. G.; Oh, J. W.; Oh, Y. J.; Han, S.; Cho, H. J.; Lee, Y.; Ryu, G. H.; Nam, D. H. *Cell Death Dis.* **2018**, *9*, 1-12. (b) Canon, J.; Osgood, T.; Olson, S. H.; Saiki, A. Y.; Robertson, R.; Yu, D.; Eksterowicz, J.; Ye, Q.; Jin, L.; Chen, A.; Zhou, J.; Cordover, D.; Kaufman, S.; Kendall, R.; Oliner, J. D.; Coxon, A.; Radinsky, R. *Mol. Cancer Ther.* **2015**, *14*, 649-658.

Antzeko txantilo kimiko batean oinarrituta, Holzer-en taldeak **NVP-CGM097** (17. irudia) garatu zuen, MDM2arekiko lotzeko afinitate nanomolarra duena eta aktibitate txikiagoa MDMXren aurka.⁶⁷ Izan ere, molekula honekin burututako azterketa biologikoen MDM2arekiko selektibitate handia adierazten dute beste proteina batzuekin konparatuta eta aparteko profil toxikologiko eta farmakologikoa. Konposatu honek I faseko entsegu klinikoak amaitu zituen 2020an.⁶⁸

Nitrogenoa duten beste konposatu batzuk ere deskribatu dira, tartean **13** pirrolopirimidina, bi proteinen aurrean ahalmen inhibitzaile berdina erakutsi duenak,⁶⁹ eta **CTX1** akridinaren deribatua, MDMXarekiko afinitate selektiboa duena. Zeluletan egindako esperimentu batzuek baieztatu zuten **CTX1** gai dela p53 maila handitzeko, G2-M fasean zelula zikloaren progresioa gelditzeko, eta apoptosia eramateko jatorrizko p53 duten MCF7, HCT116 eta A549 minbizi-zelula lerroetan (16. irudia).⁷⁰



16. irudia. Pirrolopirimidina (kolore urdin iluna) eta akridina (oliba kolorea) motako inhibitzaileak.

VI. Pirrolidinak and pirrolidonak.

Nutlin deribatua den **RG-7112** konposatuarekin entsegu klinikoetan ondorio kaltegarri larriak antzeman ondoren, eta egitura hau abiapuntutzat hartuz, Graves-ek eta lankideek (Hoffmann-La Roche) **RG-7388** (Idasanutlin bezala ere ezagututa) pirrolidina deribatua aurkitu zutela jakinarazi zuten, MDM2 inhibitzeko potentzia eta selektibitate handia duena (17. irudia).⁷¹ Konposatu horrek modu eraginkorrean aktibatzen du p53 bidea, zelula zikloan geldialdia edo jatorrizko tipoko p53 adierazita duten zelula lerroetan apoptosia eraginez. Gainera, konposatu horrek erakutsi zuen saguetan

⁶⁷ Holzer, P.; Masuya, K.; Furet, P.; Kallen, J.; Valat-Stachyra, T.; Ferretti, S.; Berghausen, J.; Bouisset-Leonard, M.; Buschmann, N.; Pissot-Soldermann, C.; Rynn, C.; Ruetz, S.; Stutz, S.; Chène, P.; Jeay, S.; Gessier, F. *J. Med. Chem.* **2015**, *58*, 6348-6358.

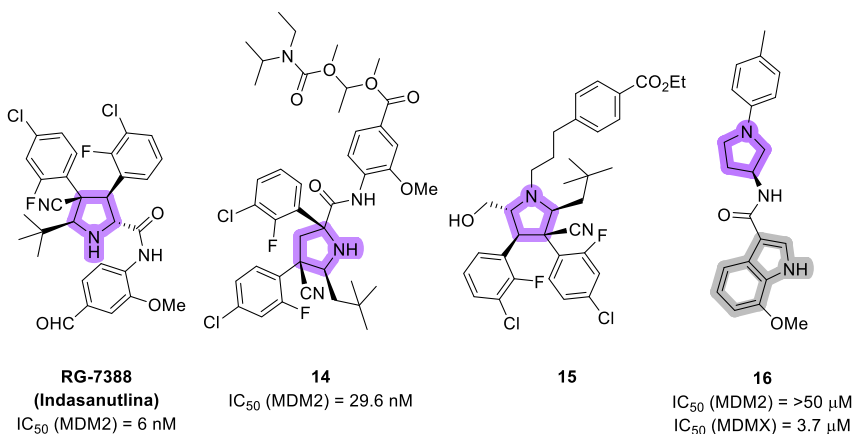
⁶⁸ Weisberg, E.; Halilovic, E.; Cooke, V. G.; Nonami, A.; Ren, T.; Sanda, T.; Simkin, I.; Yuan, J.; Antonakos, B.; Barys, L.; Ito, M.; Stone, R.; Galinsky, I.; Cowens, K.; Nelson, E.; Sattler, M.; Jeay, S.; Wuerthner, J. U.; McDonough, S. M.; Wiesmann, M.; Griffin, J. D. *Mol. Cancer Ther.* **2015**, *14*, 2249-2259.

⁶⁹ Lee, J. H.; Zhang, Q.; Jo, S.; Chai, S. C.; Oh, M.; Im, W.; Lu, H.; Lim, H.-S. *J. Am. Chem. Soc.* **2011**, *133*, 676-679.

⁷⁰ Karan, G.; Wang, H.; Chakrabarti, A.; Karan, S.; Liu, Z.; Xia, Z.; Gundluru, M.; Moreton, S.; Sauntharajah, Y.; Jackson, M. W.; Agarwal, M. K.; Wald, D. N. *Mol. Cancer Ther.* **2016**, *15*, 574-582.

⁷¹ Ding, Q.; Zhang, Z.; Liu, J. J.; Jiang, N.; Zhang, J.; Ross, T. M.; Chu, X. J.; Bartkovitz, D.; Podlaski, F.; Janson, C.; Tovar, C.; Filipovic, Z. M.; Higgins, B.; Glenn, K.; Packman, K.; Vassilev, L. T.; Graves, B. *J. Med. Chem.* **2013**, *56*, 5979-5983.

osteosarkoma tumorearen hedapena inhibitzeko gaitasuna, eta leuzemia mieloide akuturako entsegu klinikoan III fasea amaitu zuen 2020. Pirrolidinaren deribatu diren beste inhibitzaile aktibo batzuk ere deskribatu izan dira, hala nola, ordezkatutako pirrolidin-2-karboxamida **14** eta zianohidroxitimetilfenil pirrolidina **15** (nahiz eta egileek IC₅₀ balioen berri eman ez).⁷² Gainera, Furet-ek eta Kallen-ek indol eta pirrol egitura biak dituen **16** konposatua deskribatu zuten, MDMXarekiko hamahiru aldiz afinitate handiagoa duena MDM2rekiko baino.⁷³



17. irudia. Pirrolidina moduko (kolore more iluna) MDM2 eta MDMX inhibitzaileak.

Pirrolidina ez ezik, karbonilo dute horren deribatuek, hots, pirrolidonak, MDM2 eta MDMX proteinak (18. irudia) inhibitzeko duten gaitasuna ere frogatu dute. Pirrolidona egitura beste sistema heteroaromatikoekin fusionatua duten adibide aktibo ugari dira, esaterako, **17** pirrolo pirrolidona,⁷⁴ **18** pirazol pirrolidona⁷⁵ eta dihidropirro-imidazol deribatua den **HDM201**. Azken honek, adibidez, Novartis Ag enpresak diseinatua, I faseko entsegu klinikoak amaitu zituen 2019an, bera bakarrik eta beste farmako batzuekin konbinazioan (B-Raf inhibitzaileak) ere.⁷⁶ Gainera, MDM2/MDMX inhibitzaile biologiko bi-funtzional gehiago ere badaude, beste egitura ziklokoekin fusionatu gabeko pirrolidona dutenak. Adibidez, 2012an, Zhang-ek eta kolaboratzaileek p53-MDM2 proteina-proteina

⁷² (a) Bartkovitz, D.J.; Chu, X. J.; Vu, B.T.; Zhao, C.; Fishlock, D. Patent Application US 2013/0244958 A1, 2013. (b) Liu, J. J.; Ross, T. M. Patent Application US 2012/0149660 A1, 2012.

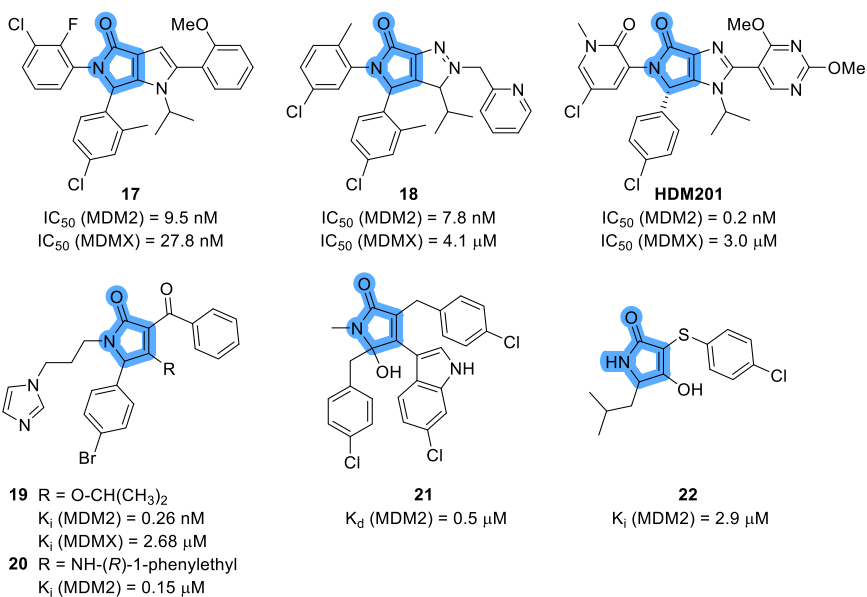
⁷³ Kallen, J.; Izaac, A.; Chau, S.; Wirth, E.; Schoepfer, J.; Mah, R.; Schlapbach, A.; Stutz, S.; Vaupel, A.; Guagnano, V.; Masuya, K.; Stachyra, T. M.; Salem, B.; Chene, P.; Gessier, F.; Holzer, P.; Furet, P. *ChemMedChem* **2019**, *14*, 1305-1314.

⁷⁴ Cotesta, S.; Furet, P.; Guagnano, V.; Holzer, P.; Kallen, J.; Mah, R.; Masuya, K.; Schlapbach, A.; Stutz, S.; Vaupel, A. Patent Application US 2013/317024 A1, 2013.

⁷⁵ (a) Kallen, J.; Izaac, A.; Chau, S.; Wirth, E.; Schoepfer, J.; Mah, R.; Schlapbach, A.; Stutz, S.; Vaupel, A.; Guagnano, V.; Masuya, K.; Stachyra, T. M.; Salem, B.; Chene, P.; Gessier, F.; Holzer, P.; Furet, P. *ChemMedChem* **2019**, *14*, 1305-1314. (b) Furet, P.; Guagnano, V.; Holzer, P.; Mah, R.; Masuya, K.; Schlapbach, A.; Stutz, S.; Vaupel, A. Patent Application WO 2013/080141 A1, 2013

⁷⁶ Skalniak, L.; Surmiak, E.; Holak, T. A. *Expert Opin. Ther. Pat.* **2019**, *29*, 151-170.

elkarrekintzaren inhibitzaile diren pirrolidona berriak aurkeztu zituzten. Zehazki, **20** konposatuak bi proteinekiko afinitatea erakutsi zuen, baina molekula aktiboenetako batek (**19**) MDM2rekiko bakarrik adierazi zuen afinitatea, Nutlin-3a berak baino tumore kontrako *in vitro* potentzia altuagoa eta p53a ezabatua duten minbizi-zelulen kontrako selektibitate ona. Harrigarriro, **19** konposatua administrazio oral bidez aktiboa zela ere aurkitu zuten, A549 sagu eredueta.⁷⁷ Antzeko konposatu batzuk, hala nola 3-pirrolin-2-ona **21**, proteina dimerizatzeko gaitasuna duenak, plazaratu zituzten Holak-ek eta Dubin-ek 2016an.⁷⁸ Urte batzuk geroago, autore hauek entitate molekular analogoen berri eman zuten, esaterako **22** azido tetramikoaren deribatua, nahiz eta kasu honetan MDM2arekiko afinitate baxuagoak agertuz.⁷⁹



18. irudia. Pirrolidona nukleoa (kolore urdina) duten MDM2 eta MDMX inhibitzaileak.

Pirrolidona nukleoa (γ -laktama) bat daramaten konposatu hauek erakusten duten gaitasun inhibitzailea dela eta, hurrengo atalean, konposatu hauen prestakuntzarako eskura dauden osagai anitzeko erreakzioen bidezko metodo sintetikoak aztertuko ditugu.

⁷⁷ Zhuang, C.; Miao, Z.; Zhu, L.; Dong, G.; Guo, Z.; Wang, S.; Zhang, Y.; Wu, Y.; Yao, J.; Sheng, C.; Zhang, W. *J. Med. Chem.* **2012**, *55*, 9630-9642.

⁷⁸ Surmiak, E.; Twarda-Clapa, A.; Zak, K. M.; Musielak, B.; Tomala, M. D.; Kubica, K.; Grudnik, P.; Madej, M.; Jablonski, M.; Potempa, J.; Kalinowska-Tluscik, J.; Dömling, A.; Dubin, G.; Holak, T. A. *ACS Chem. Biol.* **2016**, *11*, 3310-3318.

⁷⁹ Muszak, D.; Łabuzek, B.; Brela, M. Z.; Twarda-Clapa, A.; Czub, M.; Musielak, B.; Surmiak, E.; Holak, T. A. *J. Mol. Struct.* **2019**, *1189*, 161-174.

Osagai anitzeko erreakzioak (OAR) γ -laktama α,β -asegabeak sintetizatzen.

γ -Laktama funtzio-taldea jarduera biologikoen espektro zabala eskaintzen duten konposatu natural eta ez-naturalen kopuru handi baten egituraren funtsezko zatia da. Historikoki, egitura kimiko honekiko interesa bakterioek antibiotiko β -laktamiko tradizionalen aurrean erakusten duten erresistentzia gero eta handiagoarekin hasi zen.⁸⁰ Ondorioz, arreta γ -laktama deribatuetan eta horien analogoetan jartzen hasi zen, eta kimika farmazuetikoaren eremuan interes handiko molekulak bilakatu dira. Familia honen barnean, γ -laktama α,β -asegabeak edo 1,5-dihidropirrol-2-onak konposatu apartak dira eta haren egitura farmazuetiko aktibo diren produktu natural eta sintetiko askotan.⁸¹ γ -Laktama asegabearen nukleoa honako konposatu naturaletan dago: polizetido zitotoxiko diren E, C, eta D Mizelioterminetan,⁸² zitotoxikoa den E Pukeleumidan, *Lyngbya majuscula* algan aurkitzen dena,⁸³ GIB-integrasaren inhibitzailea den Oteromizinan⁸⁴ eta A Pirrozidinan,⁸⁵ biak onddo ezberdinetatik isolatuak, eta 1,2-ditiol taldeko antibiotikoen oinarriko egituretan ere (Holotina, Holomizina, Tiolutina and Aureotrizina)⁸⁶ (19. irudia).

⁸⁰ (a) Allen, N. E.; Boyd, D. B.; Campbell, J. B.; Deeter, J. B.; Elzey, T. K.; Foster, B.J.; Hatfield, L.D.; Hobbs, J.N.; Homback, N.J.; Hunden, D.C.; Jones, N.D.; Kinnick, M.D.; Morin, J.M.; Munroe, J.E.; Swartzendrubber, J.K.; Vogt, D.G. *Tetrahedron*, **1989**, *45*, 1905-1928. (b) Baldwin, J. E.; Lowe, C.; Schofield, C. J.; Lee, E. *Tetrahedron Lett.* **1986**, *27*, 3461-3464. (c) Boyd, D. B.; Elzey, T. K.; Hatfield, L. D.; Kinnick, M. D.; Morin, J. M. *Tetrahedron Lett.* **1986**, *27*, 3453-3456.

⁸¹ Caruano, J.; Muccioli, G. G.; Robiette, R. *Org. Biomol. Chem.* **2016**, *14*, 10134-10156.

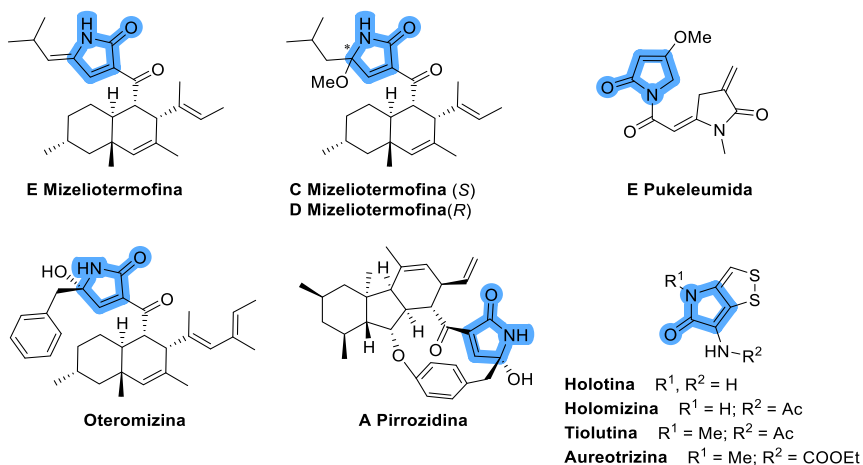
⁸² Yang, Y.; Lu, C.; Chen, M.; Chen, K.; Wu, Y.; Wu, S. *Chem. Eur. J.* **2007**, *13*, 6985-6991.

⁸³ Janecka, A.; Wyre, A.; Gach, K.; Fichna, J.; Janecki, T. *Drug Discov. Today* **2012**, *17*, 561-572.

⁸⁴ (a) Hazuda, D.; Blau, C. U.; Felock, P.; Hastings, J.; Pramanik, B.; Wolfe, A.; Bushman, F.; Farnet, C.; Goetz, M.; Williams, M.; Silverman, K.; Lingham, R.; Singh, S. *Antivir. Chem. Chemother.* **1999**, *10*, 63-70. (b) Singh, S. B.; Goetz, M. A.; Jones, E. T.; Bills, G. F.; Giacobbe, R. A.; Herranz, L.; Stevens-Miles, S.; Williams, D. L. *J. Org. Chem.* **1995**, *60*, 7040-7042.

⁸⁵ He, H.; Yang, H. Y.; Bigelis, R.; Solum, E. H.; Greenstein, M.; Carter, G. T. *Tetrahedron Lett.* **2002**, *43*, 1633-1636.

⁸⁶ Li, B.; Wever, W. J.; Walsh, C. T.; Bowers, A. A. *Nat. Prod. Rep.* **2014**, *31*, 905-923.



19. irudia. Bioaktiboak diren 1,5-dihidro-2H-pirrol-2-ona naturalak.

Bestalde, bibliografian, gizakiak egindako farmako gai ugariren hainbat adibide daude, dihidro-2H-pirrol-2-ona egitura izan eta jarduera farmakologiko anitzak dituztenak. 18. irudian deskribatutako MDM2 eta MDMX proteinen inhibitzaileez gain, γ -laktama asegabeen deribatuek askotariko jarduerak erakusten dituzte, hala nola, GIB integrasaren inhibitzaileak,⁸⁷ malariaren kontrakoak,⁸⁸ anti-biofilm direnak,⁸⁹ P2X3 hartzailaren antagonistak (analegesiko),⁹⁰ minbizi kontrako aktibitatea duten HDAC-ren inhibitzaileak,⁹¹ minbizi kontrako VEGF-R-ren inhibitzaileak⁹² eta Imrekoxib bezalako COX2 inhibitzaileak⁹³ ere (20. irudia).

⁸⁷ Ma, K.; Wang, P.; Fu, W.; Wan, X.; Zhou, L.; Chu, Y.; Ye, D. *Bioorg. Med. Chem. Lett.* **2011**, *21*, 6724-6727.

⁸⁸ (a) Kanishchev, O. S.; Lavoignat, A.; Picot, S.; Médebielle, M.; Bouillon, J. P. *Bioorg. Med. Chem. Lett.* **2013**, *23*, 6167-6171. (b) Cornut, D.; Lemoine, H.; Kanishchev, O.; Okada, E.; Albrieux, F.; Beavogui, A. H.; Bienvenu, A.-L.; Picot, S.; Bouillon, J.-P.; Médebielle, M. *J. Med. Chem.* **2012**, *56*, 73-83.

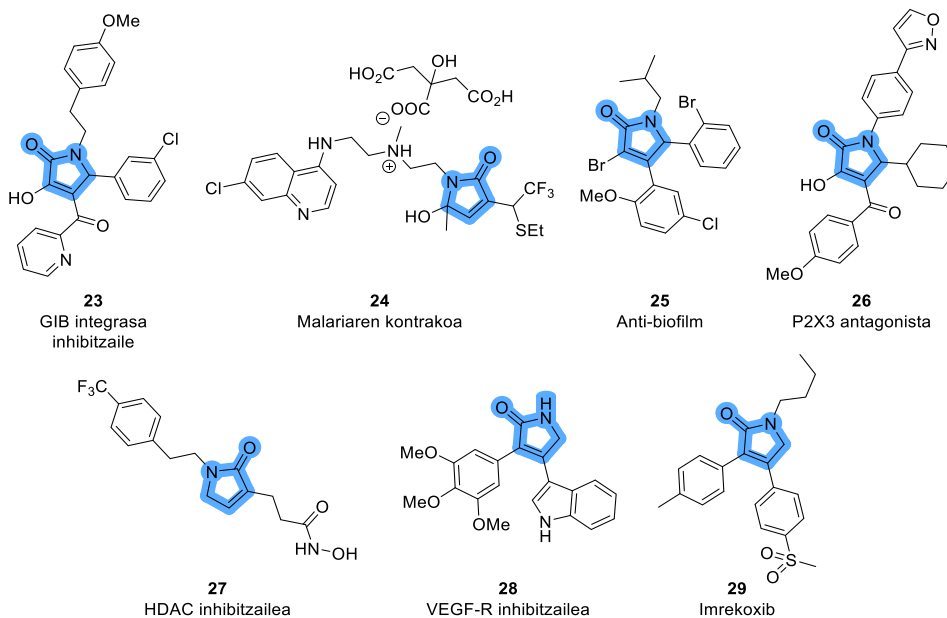
⁸⁹ (a) Sordi, M. B.; Moreira, T. A.; Montero, J. F. D.; Barbosa, L. C.; Benfatti, C. A. M.; Magini, R. de S.; Pimenta, A. de L.; Souza, J. C. M. de. *J. Appl. Oral Sci.* **2018**, *26*, 1-8. (b) Pereira, U. A.; Barbosa, L. C. A.; Maltha, C. R. A.; Demuner, A. J.; Masood, M. A.; Pimenta, A. L. *Eur. J. Med. Chem.* **2014**, *82*, 127-138.

⁹⁰ Tobinaga, H.; Kameyama, T.; Oohara, M.; Kobayashi, N.; Ohdan, M.; Ishizuka, N.; Kume, M.; Tomari, M.; Tanaka, Y.; Takahashi, F.; Kinoshita, H.; Shimada, S.; Shinohara, S.; Kai, H. *Bioorg. Med. Chem. Lett.* **2018**, *28*, 2338-2342.

⁹¹ (a) Lee, C.; Choi, E.; Cho, M.; Lee, B.; Oh, S. J.; Park, S. K.; Lee, K.; Kim, H. M.; Han, G. *Bioorg. Med. Chem. Lett.* **2012**, *22*, 4189-4192. (b) Choi, E.; Lee, C.; Cho, M.; Seo, J. J.; Yang, J. S.; Oh, S. J.; Lee, K.; Park, S. K.; Kim, H. M.; Kwon, H. J.; Han, G. *J. Med. Chem.* **2012**, *55*, 10766-10770.

⁹² Peifer, C.; Selig, R.; Kinkel, K.; Ott, D.; Totzke, F.; Scha, C.; Heidenreich, R.; Schollmeyer, D.; Laufer, S. *J. Med. Chem.* **2008**, *51*, 3814-3824.

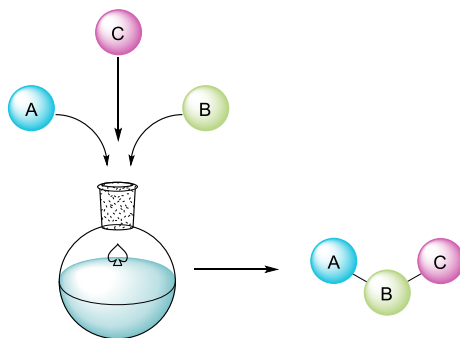
⁹³ (a) Feng, Z.; Chu, F.; Guo, Z.; Sun, P. *Bioorg. Med. Chem. Lett.* **2009**, *19*, 2270-2272. (b) Xu, H.; Zhang, Y.; Sun, Y.; Zhang, P.; Chu, F.; Guo, Z.; Zhang, H.; Zhong, D.; Zhang, Y.; Sun, Y.; Zhang, P.; Chu, F.; Guo, Z.; Zhang, H.; Zhong, D. *Xenobiotica* **2006**, *36*, 441-455.



20. irudia. Interes farmakologikoko 1,5-dihidro-2H-pirrol-2-ona ez-naturalak.

Ikuspuntu sintetikotik, erreakzio protokolo ideal batek helburua den produktua etekin onarekin lortu beharko luke, ahalik eta urrats gutxien baliatuz, bai eta ingurunearekiko erreaktibo eta disolbatzaile ekologikoak ere. Optimizatu behar diren aldagaiak hauek dira: kostua, erraz eskura daitezkeen lehengaiak, denbora, etekin globala, prozeduraren zailtasuna, ingurumenarekiko onargarratasuna, segurtasuna eta, gaur egungo estandarren arabera, erregio-, kimio- eta estereo-selektibitatea. Urrats anitzeko prozesuetan, sintesi denbora eta konplexutasunaren faktoreak gero eta handiagoak dira urrats-kopurua handitzen den neurrian. Alternatiba moduan, molekula konplexuak osagai anitzeko erreakzioen (OAE) bidez ere lor daitezke, non hiru erreaktibo edo gehiagok erreakzionatzen dute 'ontzi bakarrek' prozeduran molekula berri bat eratzeko. Molekula berri honek, erreakzioan parte hartzen duten erreaktibo guztien egituraren zati esanguratsuak ditu (21. irudia). Esan beharrekoa da, protokolo sintetiko hauetan, lehengaiak ez dutela zertan denak batera erreakzionatu behar alde berean urrats bakar batean, baizik eta oinarrizko urratsen sekuentzia moduan (bitarteko erreakzioak), eta, beraz, erreakzio horien arten itzulezin direnak azken produktuen formaziora eramaten dute oreka.⁹⁴

⁹⁴ (a) Török, B.; Schäfer, C.; Kokel, A. Cancer: Multicomponent reactions. In *Heterogeneous Catalysis in Sustainable Synthesis*; ScienceDirect, 2022; pp 443-489. (b) Dömling, A.; Ugi, I. *Angew. Chem. Int. Ed.* **2000**, *39*, 3168-3210.



21. irudia. Osagai anitzeko erreakzio (OAE) baten eskema.

OAEak abantaila batzuk ditu sintesi sekuentzial arruntekin konparatuz, hala nola, efizientzia atomikoaren maila handia, bitarteko produktuen isolamendurako protokolorik beharrezkoak ez izatea, hondakinen ekoizpena optimizatzea eta denboraren kontsumoa murriztea. Horregatik, OAE "sintesi ideal" baten ideiatik oso gertu dago.⁹⁵

XIX. Mendez geroztik, OAE asko garatu dira egitura organiko konplexuak eraikitzeko, hala nola, Strecker erreakzioa, α -aminoazido sintesirako (1850),⁹⁶ Hantzsch erreakzioa, dihidropiridinak sintetizatzen (1882),⁹⁷ Biginelli erreakzioa, dihidropirimidinak prestatzeko (1891),⁹⁸ Mannich erreakzioa (1912)⁹⁹ edo isozianuroan oinarritutako Passerini (1921)¹⁰⁰ eta Ugi (1959)¹⁰¹ erreakzioak (1921). Erreakzio hauek sintesi organikoan potentzial sinestezina dute eta funtsezko tresna bilakatu dira Kimika Farmazeutikoaren alorrean. Izan ere, azken hamarkadetan konposatu polifuntzionalen bilduma handien edo biblioteka kimikoen eskariak areagotu egin dira, farmakoaren aurkikuntza prozesuan baheketa biologikoetarako substratuak behar direlako.¹⁰²

OAEak erabili dira γ -laktama asegabeen prestakuntzarako ere.¹⁰³ Laburbilduz, ziklazio erreakzio batzuk ezagutarazi dira, hala nola, [2+2+1] zikloadizioak alkino, karbono monoxidoa (edo fenil formiatoa) eta iminen artean (1. eskema, a), edo alkino, akrilato eta isozianatoak erabilita (1. eskema, b). Gainera, [3+2] zikloadizio erreakzioak azetilendikarboxilato, aldehido eta isozianuroen artean ere deskribatu dira (1. eskema, c). γ -Laktama substratuak prestatu daitezke isozianuro, konposatu 1,3-

⁹⁵ Orru, R. V. A.; Greef, M. *Synthesis* **2003**, 1471-1499.

⁹⁶ Strecker, A. *Justus Liebigs Ann Chem*, **1850**, 75, 27-45.

⁹⁷ Hantzsch, A. *Justus Liebigs Ann. Chemie*, **1882**, 215, 1-82.

⁹⁸ Biginelli, P. *Ber.* **1891**, 24, 1317-1319.

⁹⁹ Mannich, C.; Krosche, W. *Arch. Pharm.* **1912**, 250, 647-667.

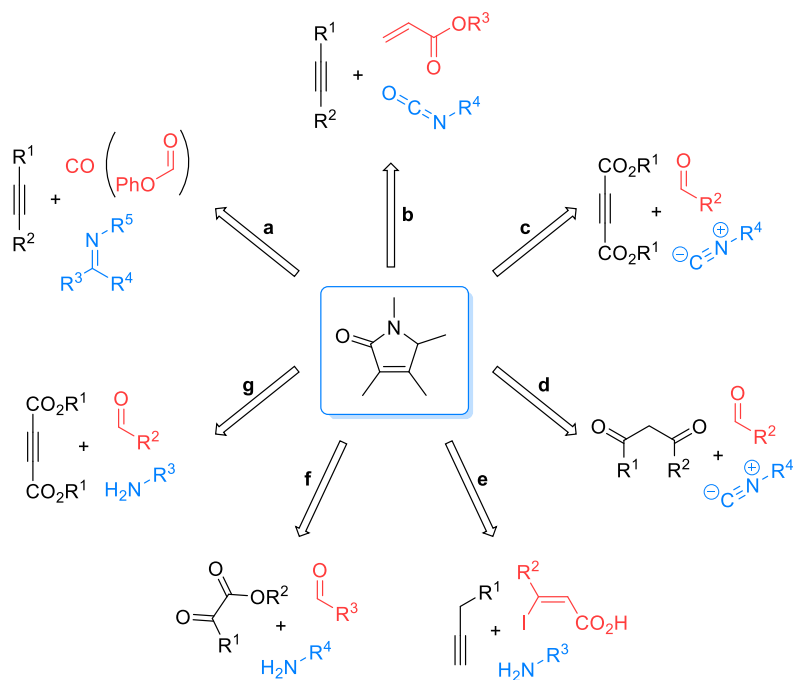
¹⁰⁰ Passerini, M *Gazz. Chim. Ital.*, **1921**, 51, 126-129.

¹⁰¹ Ugi, I. *Angew. Chem., Int. Ed.* **1959**, 71, 386-386.

¹⁰² Zhu, J.; Bienaymé, H. In *Multicomponent Reactions*; Wiley-VCH, Weinheim **2005**, p 1-3.

¹⁰³ (a) Martínez de Marigorta, E.; de Los Santos, J. M.; Ochoa de Retana, A.; Vicario, J.; Palacios, F. *Beilstein J. Org. Chem.* **2019**, 15, 1065-1085. (b) Martínez de Marigorta, E.; de Los Santos, J. M.; Ochoa de Retana, A.; Vicario, J.; Palacios, F. *Synthesis* **2018**, 50, 4539-4554.

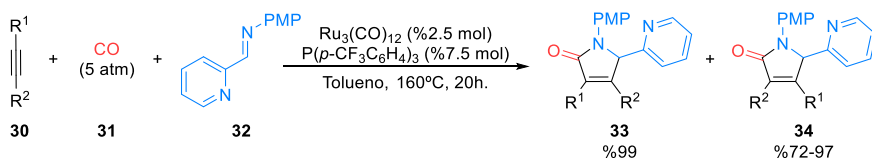
dikarboniliko eta aldehidoak konbinatuta ere (1. eskema, d). Horrez gain, γ -laktama α,β -asegabeak Sonogashira izeneko akoplamendu erreakzioan prestatu ahal dira, muturreko alkino, azido (Z)- β -iodo- α,β -asegabe eta amina alifatikoen artean (1. eskema, e). Azkenik, pirubatoen deribatuak edo pirubatoen ordezkioak erabiltzea ere, hala nola, azetilenozko espezie aktibatuak, aldehido eta aminekin konbinatuta, dihidro-2H-pirrol-2-onen sintesirako posiblea da (1. eskema, f-g).



1. eskema. Osagai anitzeko estrategia sintetikoak γ -laktama α,β -asegabeak sintetizatzen.

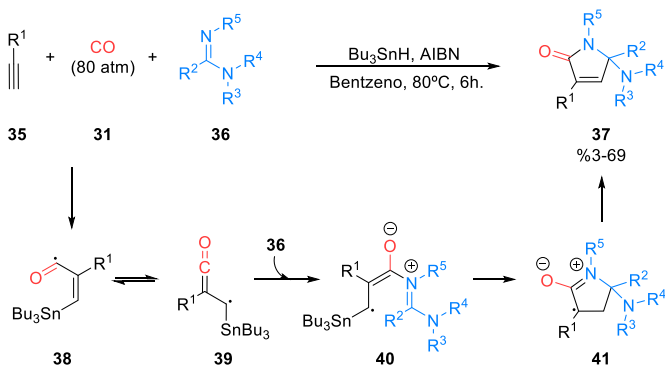
[2+2+1] Zikloadizioa osagai anitzeko hurbilketa zuzenetakoa da γ -laktama heterozikloa prestatzeko (1. eskema, a). Adibidez, 2000n, Murai-k eta lankideek, **33** 1,5-dihidro-2H-pirrol-2-onen sintesia plazaratu zuten, difenilazetilenoa (**30**, $R^1, R^2 = Ph$), bi karbonoko π -sistema gisa, karbono monoxidoa (**31**) eta **32** imina erabiliz, rutenio metalak katalizatutako Pauson-Khand motako erreakzioan (2. irudia).¹⁰⁴. Gainera, erreakzioan **30** azetileno ez-simetrikoak ($R^1 = TMS$; $R^2 = Me, Ph$) erabiltzean eta berezko desililazioaren ondoren, **33** eta **34** γ -laktama deribatuak sortzen ditu etekin ezin hobean, erregioismeroaren nahasketa bezala (15:85-92:8).

¹⁰⁴ Chatani, N.; Tobisu, M.; Asaumi, T.; Murai, S. *Synthesis* **2000**, 7, 925-928.



2. eskema. Ruteniok katalizatutako Pauson-Khand erreakzioa.

Ryu-k eta kolaboratzaileek hedatu zuten erreakzio hau, **35** muturreko alkinoak ($\text{R}^1 = \text{Alk}$) karbono monoxidoaren (**31**) presio handiko atmosferan jarrita eta **36** amidinak ($\text{R}^2, \text{R}^3, \text{R}^4, \text{R}^5 = \text{Alk}$) erabiliz. Modu horretan, **37** γ -laktama deribatuak prestatu zituzten, tributilestannanoak abiarazitako erradikal askeen bidezko [2+2+1] zikloadizioaz (3. eskema).¹⁰⁵ Erreakzioa hasten da **38** azil erradikal α, β -asegabearen formazioarekin, **35** azetileno, tributyltin erradikal eta karbono monoxidoaren (**31**) konbinaziotik. **38** Espezie erradikalarioa orekan dago **39** α -ketenil isomero erradikalarekin, honek **36** amidinarekin erreakzionatu ondoren **40** bitartekariaren formazioa eramaten du. *Endo* motako ziklazioak **41** erradikal ziklikoa sortzen du eta, azkenean, β -fizioak **37** γ -laktama α, β -asegabeak eratuko ditu etekin ertain-onarekin.

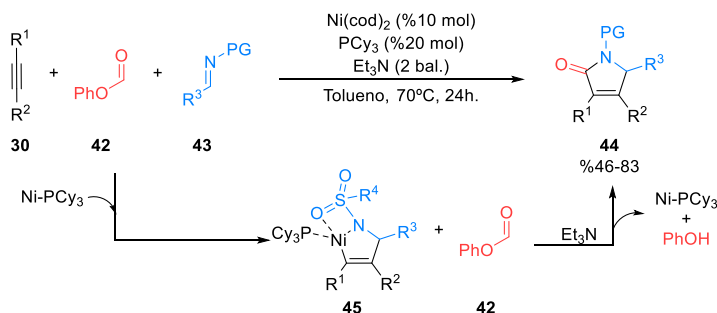


3. eskema. Erradikal askeen bidezko [2+2+1] zikloadizio erreakzioa.

Nikelek katalizatutako antzeko [2+2+1] zikloadizio karbonilatiboa deskribatu zuen Ogoshi-k 2014an, **44** 1,5-dihidro-2*H*-pirrol-2-onak prestatzeko (4. eskema). Kasu honetan, autoreek **30** alkinoak ($\text{R}^1, \text{R}^2 = \text{Ar, Alk, TMS}$), **43** *N*-tosiliminak edo *N*-(difenilfosfinil) iminak (DPP) eta fenil formiatoa (**42**), karbono monoxidoaren ordezkotza gisa, erabili zituzten. Metodo honek emaitza hobek ematen ditu azetileno substratuetan ordezkotzaile aromatikoak daudenean.¹⁰⁶

¹⁰⁵ Fukuyama, T.; Nakashima, N.; Okada, T.; Ryu, I. *J. Am. Chem. Soc.* **2013**, *135*, 1006-1008.

¹⁰⁶ Hoshimoto, Y.; Ohata, T.; Sasaoka, Y.; Ohashi, M.; Ogoshi, S. *J. Am. Chem. Soc.* **2014**, *136*, 15877-15880.



4. eskema. Nikelek katalizatutako [2+2+1] zikloadizio erreakzioa.

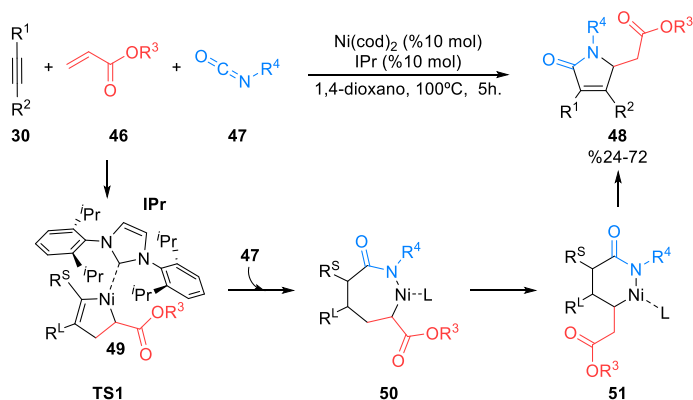
Ikertzaileek erreakzio honen mekanismoa xehetasunez aztertu ez zuten arren, jakina da nikel (0), **30** alkinoak eta **43** sulfonilimina (PG = Ts) kantitate ekimolekularrean nahastean, **45** heteronikelazikloak eratzen direla eta hauek fenil formiatoarekin (**42**) tratatu ondoren, **44** γ -laktamak sortzen dituztela.¹⁰⁷ Beraz, erreakzio honen bertsio katalitikoak modu berean gertatzen dela proposatu da. Interesgarria da antzematea fenil formiatoa (**42**) karbono monoxidoaren iturri gisa erabiltzen denean trietilaminaren presentzian, katalitikoki geldoak diren nikel-karbonil konplexuen formazioa ekiditen dela.

γ -Laktama deribatuak prestatzeko aurrekoarekin erlazionatutako beste osagai anitzeko [2+2+1] erreakzioa, Kurahashi-k eta Matsubara-k jakinarazi zuten 2010ean. Kasu partikular honetarako, **48** asegabeko γ -laktamak lortu dira, lehengaiak **30** alkino diordezkatuak ($R^1, R^2 = \text{Alk}$), **46** akrilatoak ($R^3 = \text{Alk}$) eta **47** isozianatoak ($R^4 = \text{Ar, Alk}$) izanik eta nikel kantitate katalitikoaren presentzian (5. eskema).¹⁰⁸ Erregioselektibitate maila handia hautematen da, azken produktuak **30** alkinoaren ordezkatzaille handiena γ -laktama eratzunaren 4. posizioan baitu.

Erreakzio honen ziklo katalitikoaren hasieran, nikel-IPr konplexuak, **30** alkinoak eta **46** akrilatoak sortutako elkarketaren ziklazio oxidatiboa gertatzen da eta horrela bitarteko **49** nikel konplexua eratzen da. Bertan, nagusiki, ordezkatzaille handiena (R^4) ligandotik urrunen dagoen posizioan kokatzen da, horrela oztopo esterikoa (**TS1**) minimizatuz. Jarraian, **47** isozianatoa txertatzen da, nikel (II) den **50** bitartekari ziklikoa emateko eta, ondoren, hidruoaren β -eliminazioa eta nikel atomoaren beste txertaketa direla medio, **51** espeziea sortzen da. Azkenean, eliminazio erreduktiboak nikel konplexu aktiboa eta **48** 1,5-dihidro-2H-pirrol-2-ones askatzen ditu.

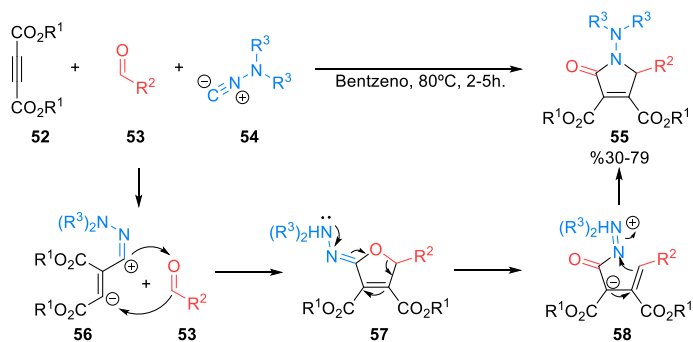
¹⁰⁷ Ogoshi, S.; Ikeda, H.; Kurosawa, H. *Angew. Chem. Int. Ed.* **2007**, *46*, 4930-4932.

¹⁰⁸ Ozawa, T.; Horie, H.; Kurahashi, T.; Matsubara, S. *Chem. Commun.* **2010**, *46*, 8055-8057.



5. eskema Nikelek katalizatutako hiru osagaien [2+2+1] zikloadizio erreakzioa.

OAEetan isozianuroen erabilera ere aztertu da, γ -laktama α,β -asegabek erakitzeko. Bereziki, **52** dimetil azetilendikarboxilatoa ($\text{R}^1 = \text{Me}$), **53** bentzaldehidoak ($\text{R}^2 = \text{Ar}$) eta *iso*-propil isozianuroa (**54**, $\text{R}^2 = \text{iPr}$) bentzenoan birfluxuan berotuz gero, **55** 1-amino-2-oxo-2,5-dihidro-1*H*-pirrol-3,4-dikarboxilatoak eratzen dira etekin ertain-onekin (6. eskema).¹⁰⁹ Balizko erreakzio-mekanismoaren arabera, hasieran, **54** isozianuroaren adizio nukleozalea gerta daiteke aktibatutako **52** azetiledikarboxilatoaren gainean, **56** 1,3-dipoloa emanez. Honek **53** aldehidoekin erreakzionatzen du [3+2] zikloadizio baten bidez **57** bitarteko konposatua sortzeko. Segidan, hidrazonaren Dimroth motako berrantolatetaren ondorioz, egitura irekia duen **58** bitartekari ezegonkorra sortu eta horren ziklazioa **55** γ -laktama eratzen da. Aldehidoen ordeaz azil haluroak erabili dira ere antzeko erreakzio batean.¹¹⁰

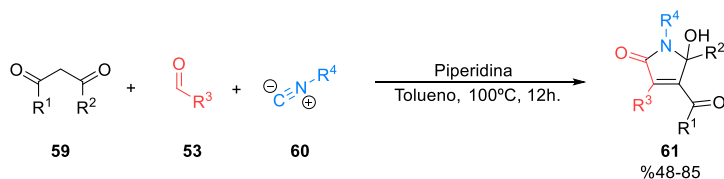


6. eskema. **52** Azetilen dikarboxilatoa, **53** aldehidoak eta **54** isozianuroaren arteko hiru osagaien erreakzioa.

¹⁰⁹ (a) Nair, V.; Mathen, J. S.; Viji, S.; Srinivas, R.; Nandakumar, M. V.; Varma, L. *Tetrahedron* **2002**, *58*, 8113-8118. (b) Nair, V.; Mathen, J. S.; Vinod, A. U.; Varma, R. L. *Chem. Lett.* **2001**, *3*, 738-739.

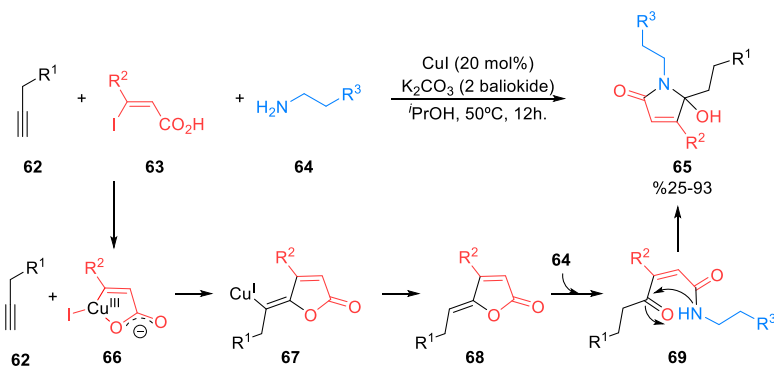
¹¹⁰ Yavari, I.; Mokhtarporiani-Sanandaj, A.; Moradi, L.; Mirzaei, A. *Tetrahedron* **2008**, *64*, 5221-5225.

Horrez gain, Liang-ek eta lankideek **59** 1,3-dikarbonil konposatuak erabili zituzten alkinoen ordez, **53** aldehido ($R^3 = Ar$), ziklohexil isozianuro (**60**, $R^4 = Cy$) eta piperidina katalizatzailearekin batera, honela **61** 5-hidroxi-1,5-dihidro-2H-pirrol-2-onak etekin ertain-onekin lortuz (7. eskema).¹¹¹



Scheme 7. Hiru osagaien erreakzioa **61** 5-hidroxi-1,5-dihidro-2H-pirrol-2-onen sintesirako.

Commeiras-ek eta Parrain-ek kobreak katalizatutako hirugarren osagaien erreakzio baten kasu zehatz baten berri eman zuten, **62** muturreko alkinoak ($R^1 = Ar, Alk$), **63** azido (Z)-β-iodo-α,β-asegabeak ($R^2 = Ar, Alk$) eta **64** amina alifatikoak ($R^3 = Ar, Alk$) erabiliz, **65** 5-hidroxi-1H-pirrol-2(5H)-onak etekin ertain-bikainekin (8. eskema).¹¹² Ikertzaileek Sonogashira motako akoplamendua proposatzen dute, eta hasieran kobreaeren (I) adizio oxidatiboa **63** iodoalkenoaren C-I loturaren gainean gertatzen da, kobre (III) den **66** bitartekaria lortzeko. Ondoren, kobre atomoa **62** alkinoaren lotura hirukoitzarekin koordinatzen da, **67** bitartekaria eta gero, protodemetalazio prozesuaren bitartez, **68** laktona sortzeko. Azkenik, **64** amina alifatikoak **68** laktonearekin erreakzionatzen du **65** γ-laktama α,β-asegabeak eratzeko, **69** bitartekari irekiaren bidez.



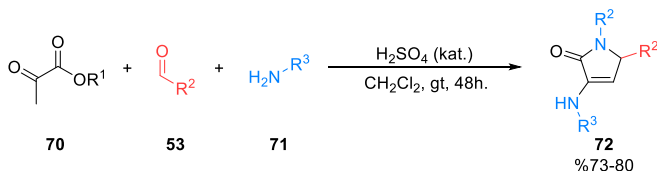
8. Eskema. Kobre bidez katalizatutako **65** γ-hidroxi-butirrolaktamen sintesirako OAE.

γ-Laktama deribatuen osagai anitzeko sintesiaren azterketari jarraituz, γ-laktama nukleoa eraikitzeko metodo sinpleenetako bat Brønsted azidoek katalizatutako pirubato, aldehido eta aminen

¹¹¹ Fan, M. J.; Qian, B.; Zhao, L. B.; Liang, Y. M. *Tetrahedron* **2007**, *63*, 8987-8992.

¹¹² (a) Mardjan, M. I. D.; Mayooufi, A.; Parrain, J. L.; Thibonnet, J.; Commeiras, L. *Org. Process Res. Dev.* **2020**, *24*, 606-614. (b) Mardjan, M. I. D.; Perie, S.; Parrain, J. L.; Commeiras, L. *Org. Biomol. Chem.* **2017**, *15*, 3304-3309. (c) Mardjan, M. I. D.; Parrain, J.; Commeiras, L. *Adv.Synth. Catal* **2016**, *358*, 543-548.

arteko erreazioa da. Erreakzio honetan, 3-hidroxi edo 3-amino taldez ordezkaturako γ -laktama α,β -asegabek lortzen dira. Testuinguru horretan, 2006an gure ikerketa-taldeak deskribatu zuen hiru osagaien erreazio eraginkor bat **72** 3-amino-1,5-dihidro-2H-pirrol-2-onak oso etekin onarekin (9. eskema).¹¹³ Erreakzioan etil pirubatoak (**70**, $R^1 = Et$), **53** aldehidoak ($R^2 = Ar, Alk, CO_2Et$), eta **71** amina aromatikoen hartzen dute parte, azido sulfuriko kopuru katalitikoaren aurrean.



9. eskema. Brønsted azidoak katalizatutako **70** etil pirubato, **53** aldehidoak eta **71** aminen arteko hiru osagaien erreazioa.

Lan honen jarraipen gisa, hurrengo urteetan, Brønsted azido katalizatzaile batzuk erreazio berean eraginkorrak zirela frogatu zuten. Katalizatzaile eta baldintza adierazgarrietako batzuk 2. taulan eta 22. irudian laburbiltzen dira.

2. taula. **72** 1,5-Dihidro-2H-pirrol-2-onen prestakuntzarako metodologia batzuk.

Sarrera	Katalizatzailea	Erreakzio baldintzak	Etekin (%)
1	I edo II (%10 mol)	Tolueno, Na_2SO_4 , giro temperatura.	51-89 ¹¹⁴
2	$[\text{Et}_3\text{NH}][\text{HSO}_4]$ (baliokide 1)	ⁿ Hexano, giro temperatura.	45-93 ¹¹⁵
3	$\text{SiO}_2\text{-FeCl}_3$	Disolbatzailezik ez, giro temperatura /100°C	60-74 ¹¹⁶
4	III (baliokide 1)	Etanol, giro temperatura.	69-93 ¹¹⁷
5	$\text{Yb}(\text{OTf})_3$ (%20 mol)	Disolbatzailezik ez, giro temperatura.	57-84 ¹¹⁸
6	IV (%5 mol)	MeCN, Na_2SO_4 , giro temperatura.	41-93 ¹¹⁹
7	V (%12 mol)	Disolbatzailezik ez, giro temperatura.	78 ¹²⁰
8	VI (%10 mol)	Disolbatzailezik ez, 60°C	78-83 ¹²¹
9	-	ⁿ Hexano, 70°C	60-97 ¹²²
10	-	Disolbatzailezik ez, 80°C	45-95 ¹²³

¹¹³ Palacios, F.; Vicario, J.; Aparicio, D. *Eur. J. Org. Chem.* **2006**, 2843-2850.

¹¹⁴ Li, X.; Deng, H.; Luo, S.; Cheng, J. P. *Eur. J. Org. Chem.* **2008**, 4350-4356.

¹¹⁵ Reza, M.; Shafiee, M.; Najafabadi, B. H.; Ghashang, M. *J. Chem. Res.* **2011**, 35, 634-636.

¹¹⁶ Ghashang, M.; Shaterian, H. R. *Chin. J. Chem.* **2011**, 29, 1851-1855.

¹¹⁷ Ghashang, M. *Res. Chem. Intermed.* **2013**, 39, 2187-2195.

¹¹⁸ Nagarajan, A. S.; Reddy, B. S. R. *Synth. Commun.* **2013**, 43, 1229-1236.

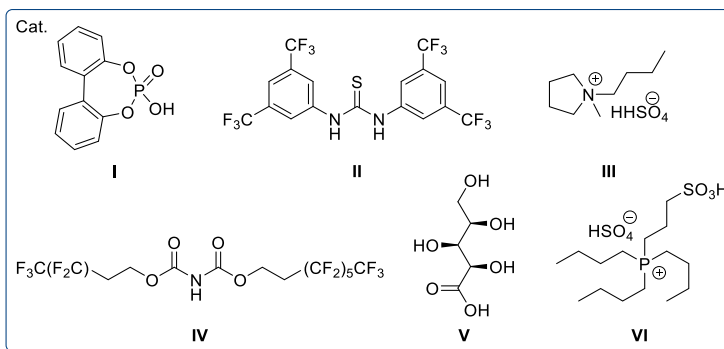
¹¹⁹ Qian, J. L.; Yi, W. Bin; Cai, C. *Tetrahedron Lett.* **2013**, 54, 7100-7102.

¹²⁰ Ma, J.; Zhong, L.; Peng, X.; Sun, R. *Green Chem.* **2016**, 18, 1738-1750.

¹²¹ Yarie, M.; Zolfigol, M. A.; Saeidi-Rad, M. *J. Mol. Liq.* **2018**, 249, 144-152.

¹²² Shaterian, H. R.; Ranjbar, M. *Res. Chem. Intermed.* **2014**, 40, 2059-2074.

¹²³ (a) Bavadi, M.; Niknam, K.; Gharibi, M. *Monatsh. fur Chemie* **2017**, 148, 1025-1034. (b) Niknam, K.; Mojikhalifeh, S. *Mol. Divers.* **2014**, 18, 111-117.



22. irudia. 72 3-Amino-1,5-dihidro-2H-pirrol-2-onen prestakuntzarako katalizatzaile batzuk.

Nabarmenki, erreakzio honen kasu partikular gisa, 2002an Gein eta lankideek 2002an propanodiamina erabili zuten γ -laktama α,β -asegabe dimerikoak ekoizteko, etekin ertain-onak izanik.¹²⁴

Erreakzio honen hedapen bat Kawasuji eta kolaboratzaileek ikertu zuten. Kasu honetan, egileek katalizatzailearik gabeko hiru osagaien erreakzioa deskribatu zuten, talde heteroaromatikoz ordezkaturako **73** azilpirubatoak, formaldehidoa (**53**, $R^3 = H$) eta **71** amina alifatikoak ($R^4 = Alk$) erabiliz, eta C-4n ordezkaturako **74** 3-hidroxi-1,5-dihidroxi-2H-pirrol-2-onak etekin ertain edo onekin lortzeko (10. eskema).¹²⁵ Horrez gain, (*E*)-zinamil taldez ordezkaturako **73** pirubatoaren deribatua ($R^1 = Me$; $R^2 = (E)-CH=CHPh$) birfluxuan dagoen azido azetikoan erabilita, **74** γ -laktamak eman zituen, etekin ertainak izanik (%42-45).¹²⁶ Azido azetikoaren erabilera erabakigarria da, erreakzioaren irismena azilpirubato ezberdinetara hedatu ahal izateko, hala nola, metil benzoil pirubatoa (**73**, $R^1 = Me$; $R^2 = Ph$)¹²⁷ edo talde heteroaromatikoez ordezkaturako **73** pirubatoak ($R^1 = Me$; $R^2 = 2\text{-furiil}, 2\text{-tienil}$).^{126,128} Erreakzio honen beste adibide batzuk Dehaen-ek,¹²⁹ Hamzah-ek¹³⁰ eta Komiotis-ek¹³¹ jakinarazi dituzte.

¹²⁴ (a) Gein, V. L.; Kasimova, N. N.; Aliiev, Z. G.; Vakhrin, M. I. *Russ. J. Org. Chem.* **2010**, *46*, 875-883. (b) Gein, V. L.; Kasimova, N. N.; Potemkin, K. D. *Russ. J. Gen. Chem.* **2002**, *72*, 1229-1230.

¹²⁵ Kawasuji, T.; Fuji, M.; Yoshinaga, T.; Sato, A.; Fujiwara, T.; Kiyama, R. *Bioorg. Med. Chem.* **2007**, *15*, 5487-5492.

¹²⁶ Vydzhak, R. N.; Panchishin, S. Y. *Russ. J. Gen. Chem.* **2008**, *78*, 1641-1642.

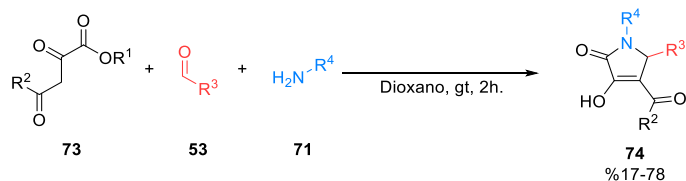
¹²⁷ Gein, V. L.; Tsypliyakova, E. P.; Stashina, G. A.; Bakulev, V. A. *Russ. J. Org. Chem.* **2008**, *44*, 478-480.

¹²⁸ Gein, V. L.; Mar'Yasov, M. A. *Russ. J. Org. Chem.* **2015**, *51*, 110-115.

¹²⁹ Metten, B.; Kostermans, M.; Van Baelen, G.; Smet, M.; Dehaen, W. *Tetrahedron* **2006**, *62*, 6018-6028.

¹³⁰ Mohammat, M. F.; Shaameri, Z.; Hamzah, A. S. *Molecules* **2009**, *14*, 250-256.

¹³¹ Manta, S.; Tzioumaki, N.; Kollatos, N.; Andrea, P.; Margaritoulis, M.; Panagiotopoulou, A.; Papanastasiou, I.; Tsoinisi, A.; Schols, D.; Komiotis, D. *Curr. Microw. Chem.* **2018**, *5*, 23-31.



10. eskema. **73** Azilpirubato, **53** aldehidoak eta **71** aminen arteko hiru osagaien erreakzioa.

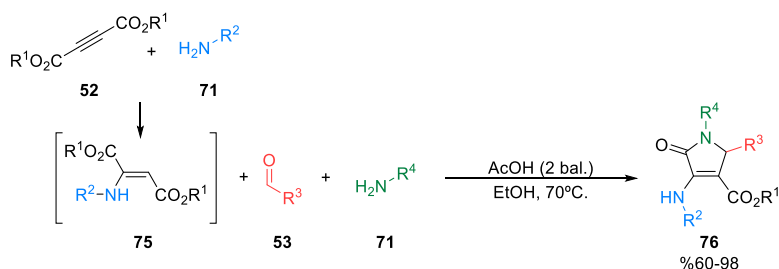
Azken hamarkadetan, Kimika Organikoan eta Kimika Farmazeutikoan protokolo sintetiko honen garrantzia Gein eta lankideek egiaztatu dute. Amina, aldehido eta pirubato deribatuen OA erreakzioa baliatzean hainbat γ -laktama deribatu polifuntzional sintetizatu egin dira eta horien aktibitate biologikoa ebaluatu da, propietate interesgarriak erakutsiz hala nola GIBaren integrasaren inhibitzaileak, kemokina hartzailearen modulatzaileak, hantura kontrakoak, analgesikoak edo antimikrobialak.¹³²

Gainera, **52** azetilendikarboxilatoak berdin erabil daitezke pirubatoen ordez, prozeduran aldakuntza arinekin, γ -laktama deribatuak prestatzeko. Kasu honetan, enamina bitartekaria prestatzen da aldez aurretik **71** amine eta **52** azetilendikarboxilatetik, ondoren, gainontzeko bi erreaktiboak gehituz (**53** aldehidoa eta **71** aminaren bigarren baliokidea). Metodologia hau OAE baten eta “ontzi bakarreko” prozeduraren erdibidean dago. Protokolo honen abantaila nagusia **76** konposatuak lortu ahal direla bi amina ordezkatzaile desberdinak dituztela (11. eskema).

Hurbilketa honen bidez, Jiang eta kolaboratzaileek 5-amino ordezkatutako γ -laktama deribatuak lortu zituzten, **52** azetilenedikarboxilatoak ($R^1 = \text{Me, Et}$), **53** aldehidoak ($R^3 = \text{H, Ph, Me}$), eta **71** amina aromatiko eta alifatikoak ($R^4 = \text{Ar, Alk}$) lehengaitzat hartuz, eta azido azetikoaren presentzian. Modu horretan **76** 3-amino-1,5-dihidro-2*H*-pirrol-2-onak isolatu ahal ziren etekin ertain eta onekin (11. eskema).¹³³

¹³² (a) Gein, V. L.; Odegova, T. F.; Rogachev, S. N.; Bobyleva, A. A.; Gein, L. F. *Pharm. Chem. J.* **2015**, *49*, 175-177. (e) Gein, V. L.; Rubtsova, D. D.; Bobyleva, A. A.; Ryabova, O. V.; Novikova, V. V.; Kasimova, N. N.; Yankin, A. N. *Russ. J. Gen. Chem.* **2020**, *90*, 1222-1228. (b) Ortiz Zacarías, N. V.; Van Veldhoven, J. P. D.; Portner, L.; Van Spronsen, E.; Ullo, S.; Veenhuizen, M.; Van Der Velden, W. J. C.; Zweemer, A. J. M.; Kreekel, R. M.; Oenema, K.; Lenselink, E. B.; Heitman, L. H.; Ijzerman, A. P. *J. Med. Chem.* **2018**, *61*, 9146-9161. (c) Ma, K.; Wang, P.; Fu, W.; Wan, X.; Zhou, L.; Chu, Y.; Ye, D. *Bioorg. Med. Chem. Lett.* **2011**, *21*, 6724-6727. (d) Gein, V. L.; Vychezhnina, V. N.; Levandovskaya, E. B.; Syropyatov, B. Y.; Vakhrin, M. I.; Voronina, E. V.; Danilova, N. V. *Pharm. Chem. J.* **2010**, *44*, 370-373.

¹³³ (a) Zhu, Q.; Gao, L.; Chen, Z.; Zheng, S.; Shu, H.; Li, J.; Jiang, H.; Liu, S. *Eur. J. Med. Chem.* **2012**, *54*, 232-238. (b) Zhu, Q.; Jiang, H.; Li, J.; Liu, S.; Xia, C.; Zhang, M. *J. Comb. Chem.* **2009**, *11*, 685-696.



11. eskema. 52 Dialkil azetilendikarboxilatoak, 53 aldehidoak eta 71 aminen arteko hiru osagaien erreakzioa 76 3-amino-1,5-dihidro-2H-pirrol-2-onak sintetizatzen.

Erreakzio hau luze aztertu dute ikertzaile ezberdinek azken hamarkadetan, eta baldintza esperimental garrantzitsuenak 3. taulan laburbiltzen dira.

3. taula. 76 3-Amino-1,5-dihidro-2H-pirrol-2-onen prestakuntzarako beste prozedura batzuk.

Sarrera	Katalizatzailea	Erreakzio baldintzak	Etekin (%)
1	I ₂ (%10 mol)	Metanol, giro tenperatura.	76-83 ¹³⁴
2	Azido bentzoikoa (%20 mol)	Etanol, giro tenperatura.	47-72 ¹³⁵
3	Katalizatzailerik ez edo DABCO	Etanol	10-72 ¹³⁶
4	(CuOAc)·H ₂ O (%40 mol) + Azido salizilikoa (%30 mol)	Metanol, giro tenperatura.	40-93 ¹³⁷
5	Limoi zukua	110°C	74-86 ¹³⁸

Gainera, bibliografian prozedura ugari aurki daitezke non katalizatzaile heterogeneoak erabiltzen diren goiko sintesia burutzeko. Katalizatzaile hauetako batzuk honako hauek dira: TiO₂ nanohautsa,¹³⁹ BF₃/nano-zerrautsa,¹⁴⁰ bio-oinarria duen nanozelulosa estaldurako Fe₃O₄-a,¹⁴¹ L-arginina estaldurako Fe₃O₄ nanopartikulak¹⁴² eta grafeno oxidoaren nanoxaflak.¹⁴³

Era berean, 77 3-hidroxi-1-5 dihidro-2H-pirrol-2-onak lor daitezke 71 aminaren baliokide bakarra erabiltzen bada. Yan-ek eta lankideek 2011n deskribatu zuten lehen aldiz osagai anitzeko metodo hau, azido *p*-toluenesulfonikoa katalizatzaile gisa erabiliz eta 77 γ-laktamak lortu zituzten etekin ertainekin

¹³⁴ Khan, A. T.; Ghosh, A.; Musawwer Khan, M. *Tetrahedron Lett.* **2012**, *53*, 2622-2626.

¹³⁵ Gao, H.; Sun, J.; Yan, C. G. *Tetrahedron* **2013**, *69*, 589-594.

¹³⁶ Gao, H.; Sun, J.; Yan, C. G. *Beilstein J. Org. Chem.* **2013**, *9*, 2934-2939.

¹³⁷ Lv, L.; Zheng, S.; Cai, X.; Chen, Z.; Zhu, Q.; Liu, S. *ACS Comb. Sci.* **2013**, *15*, 183-192.

¹³⁸ Khan, M. M.; Khan, S.; Saigal; Sahoo, S. C. *ChemistrySelect* **2018**, *3*, 1371-1380.

¹³⁹ Rana, S.; Brown, M.; Dutta, A.; Bhaumik, A.; Mukhopadhyay, C. *Tetrahedron Lett.* **2013**, *54*, 1371-1379.

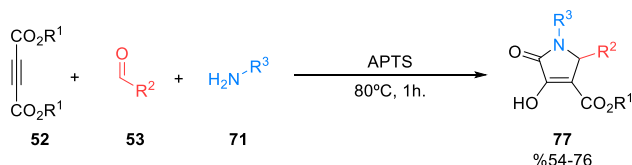
¹⁴⁰ Mirjalili, B. B. F.; Zare Reshquiyea, R. *RSC Adv.* **2015**, *5*, 15566-15571.

¹⁴¹ Salehi, N.; Fatameh Mirjalili, B. B. *RSC Adv.* **2017**, *7*, 30303-30309.

¹⁴² Ghasemzadeh, M. A.; Abdollahi-Basir, M. H.; Elyasi, Z. *Curr. Organocatalysis* **2018**, *6*, 61-68.

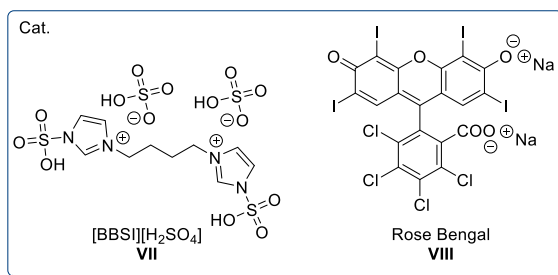
¹⁴³ Saha, M.; Das, A. R. *ChemistrySelect* **2017**, *2*, 10249-10260.

(%54-76) (12. eskema).¹⁴⁴ Gainera, protokoloa azido laktikoa edo azido azetikoa katalizatzaile gisa erabiltzera zabalduta ahal da, eta enol egiturako **77** γ -laktamak ere lortzen dira antzeko etekinekin (%52-83).¹⁴⁵ Era berean, **53** aldehidoen ordez, oxalil kloruroa erabiltzean, γ -laktamak eratzea dakar, etekinak bikainak izanda.¹⁴⁶



12. eskema. **52** Dialkil azetilendikarboxilatoak, **53** aldehidoak eta **71** aminen arteko hiru osagaien erreakzioa **77** 3-hidroxi-1,5-dihidro-2*H*-pirrol-2-onak sintetizatzen.

2019an 1,1'-butilenbis (3-sulfo-3*H*-imidazol-1-ium) hidrogeno sulfatoa ([BBSI][HSO₄]) **VII** (1 mol%) (25. irudia) katalizatzaile gisa erabili zen **76** produktuak lortzeko, disolbatzaile gabeko baldintzetan, eta etekin bikainekin (%82-92).¹⁴⁷ Zenbait urte geroago, 2021ean, Nongkhaw-ek eta kolaboratzaileek metalik gabeko fotorredox katalisia deskribatu zuten, LED urdinarekin (450 nm) irradiatuta eta Bengalako arrosa (Rose Bengal) **VIII** katalizatzaile gisa (15 mol%) erabilia (25. irudia). Modu honetan, γ -laktamen deribatu sorta zabala lortu da, erreakzio denbora laburrean (0,5 ordu) eta etekin ezin hobeak izanik (%77-94).¹⁴⁸



25. irudia. [BBSI][HSO₄] **VII** eta Bengalako arrosa **VIII** katalizatzaileak.

Gainera, adibide ugari daude katalizatzaile heterogeneoak erabiliz, **52** dialkil azetilendikarboxilatoak ($\text{R}^1 = \text{Alk}$), **53** aldehidoekin eta **71** aminen baliokide bakar batekin, **77** 3-hidroxi-1,5-dihidro-2*H*-pirrol-2-onak lortzeko. Interesgarrietako batzuk hauek dira: TiO₂ edo ZrO₂

¹⁴⁴ Sun, J.; Wu, Q.; Xia, E. Y.; Yan, C. G. *Eur. J. Org. Chem.* **2011**, *16*, 2981-2986.

¹⁴⁵ Yang, J.; Tan, J. N.; Gu, Y. *Green Chem.* **2012**, *14*, 3304-3317.

¹⁴⁶ Yavari, I.; Souri, S. *Synlett* **2008**, *8*, 1208-1210.

¹⁴⁷ Khaligh, N. G.; Mihankhah, T.; Johan, M. R. *Synth. Commun.* **2019**, *49*, 1334-1342.

¹⁴⁸ Dutta, A.; Rohman, M. A.; Nongrum, R.; Thongni, A.; Mitra, S.; Nongkhaw, R. *New J. Chem.* **2021**, *45*, 8136-8148.

nanopartikulak,¹⁴⁹ grafeno oxidoaren nanoxaflak¹⁴³ eta CoFe_2O_4 -aren nanopartikula magnetikoak azido zitriko edo azido sulfuriko-silizearekin funtzionalizatuta.¹⁵⁰

¹⁴⁹ (a) Sarkar, R.; Mukhopadhyay, C. *Tetrahedron Lett.* **2013**, *54*, 3706–3711. (b) Saha, A.; Payra, S.; Banerjee, S. *RSC Adv.* **2016**, *6*, 101953-101959.

¹⁵⁰ (a) Ahankar, H.; Ramazani, A.; Ślepokura, K.; Lis, T.; Kinzhybalov, V. *Res. Chem. Intermed.* **2019**, *45*, 5007-5025. (b) Hosseinzadeh, Z.; Ramazani, A.; Ahankar, H.; Ślepokura, K.; Lis, T. *Silicon* **2019**, *11*, 2933-2943.

Helburuak

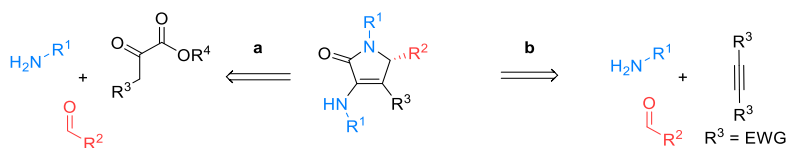


Aurrean aipatu dena kontuan hartuta, tesi honen helburu orokorra osagai anitzeko prozesu organokatalitiko eraginkorra garatzea da γ -laktama-deribatuen sintetizatzeke. Gainera, lortutako produktuen aplikazio sintetikoak aztertu eta haien aktibitate antiproliferatiboa ikertuko da hainbat zelula-lerroetan. Halaber, γ -laktamek MDM2/MDMX-p53 elkarrekintzaren gainean duten inhibizio-ahalmena neurtuko da (26. irudia).



26. irudia. Tesiaren helburu orokorrak.

Ikuspegi sintetikotik, helburu nagusia 1,5-dihidro-2*H*-pirrol-2-onak prestatzeko metodologia sintetiko eraginkorra garatzea da, osagai anitzeko protokoloak erabiliz. Aurretiaz deskribatutako amina, aldehido eta pirubato-deribatuen osagai anitzeko erreakzioan oinarritua,¹¹³ gure lehenengo helburua, protokolo sintetiko hori organokatalizatzaileen erabilerara zabaltzea da, γ -laktama asegabe, kiral eta oso funtzionalizatuen familia zabal bat prestatzeko (13. eskema, a). Ondoren, pirubatoaren ordeztze, beste lehengai batzuk probatuko dira, hala nola, alkino aktibatuen, horrela γ -laktama eratzuneko ordezkatzailen egitura-aniztasuna are gehiago zabaltzeko (13. eskema, b). Fluorra edo fosforoa (V) barne dituzten egitura kimikoen propietate biologiko apartak direla eta, ahalegin berezia egingo da funtzio-talde horiek dituzten substratu γ -laktamikoak prestatzeko, horretarako fluoroz edo/eta fosforoz ordezkaturako aldehido eta pirubatoak erabiliz.



13. irudia. 3-Amino-1,5-dihidro-2*H*-pirrol-2-onen erretrosintesia.

Organokatalizatutako osagai anitzeko protokoloa eraginkortasunez optimizatu ondoren, hurrengo urratsa metodologia enantioselektiboa garatzea izango da, Brønsted azido-katalizatzaile kiralak baliatuz optikoki aberastutako substratuak lortzeko.

Gainera, 3-amino-1,5-dihidro-2*H*-pirrol-2-ona eskeletoaren egitura-ezaugarriak aprobetxatuz, batez ere enamina eta enona egiturak, substratu horiek lehengai gisa erabiliko dira eraldaketa sintetiko batzuk burutzeko. Horri esker, molekula hauen potentzial sintetikoa justifikatzeaz gain, γ -laktama-eraztunaren egitura-aniztasuna are gehiago hedatuko da. Bost kideko eraztunearan karbono kiral bat dagoenez, arreta berezia jarriko da erreakzio diastereoselektiboetan (14. eskema).



14. eskema. 3-Amino-1,5-dihidro-2*H*-pirrol-2-ona egituraren funtzionalizazioa.

Sarreran adierazi den bezala, iturri naturaletatik eta ez-naturaletatik eratorritako γ -laktamak balio handiko egiturak direla frogatu da, kimika farmazeutikoaren arloan, jarduera biologiko interesgarriak eta etorkizun handikoak erakusten baitituzte, minbiziaren kontrako propietateak barne. Eraginkortasun terapeutikoa hobetu eta aldi berean albo-ondorioak murriztu eta minbiziaren aurkako farmakoterapiaren aurreko erresistentzia gainditzeko helmuga orokorraren baitan, tesi honen beste helburu nagusia da sintetizatutako γ -laktama deribatuen *in vitro* aktibitate zitotoxikoa minbizi-lerro zelular ezberdinetan ebaluatzea proposatzen da, etorkizun handieneko molekulak identifikatzeko egitura-aktibitate profilak eginez.

Azkenik, *in vitro* zitotoxikotasunaren mekanismoa aztertuko da, eta, zehazki, γ -laktama deribatuek apoptosia eragiteko duten gaitasuna ikertuko da. Halaber, substratu hauek duten aktibitatearen erantzule izan daitekeen maila molekularreko elkarrekintza espezifikoren bat identifikatzen saiatuko da, hala nola, MDM2/MDMX-p53 proteinen elkarrekintzaren inhibiziorako ahalmena.

I. Atala

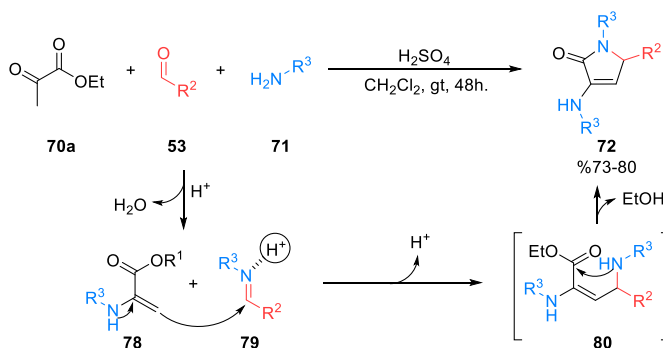
*γ -Laktama-deribatu asegabeen osagai
anitzeko sintesia eta aplikazioak*



1. Kapitulu

γ -Laktama-deribatu asegabeen osagai anitzeko sintesia pirubatoak erabiliz

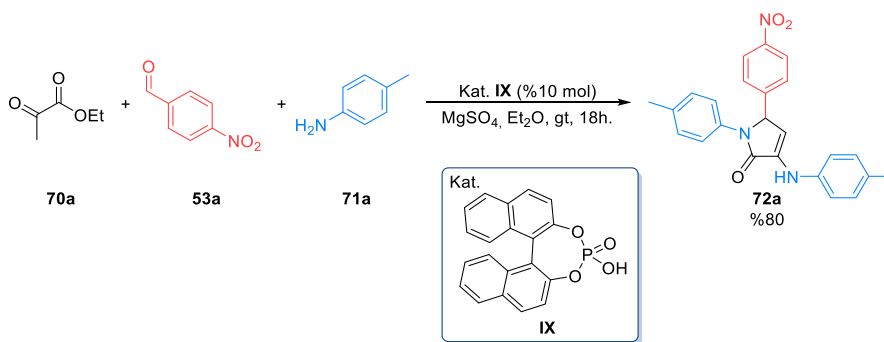
2006-an, gure ikerketa-taldeak, azido bidez katalizatutako etil pirubato (**70a**), **53** aldehidoak eta **71** amina aromatikoen hiru osagaiko erreakzioa deskribatu zuen, **72** 3-amino-1,5-dihydro-2*H*-pirrol-2-onak eskuratzeko (15. eskema).¹¹³ Erreakzio horren mekanismoa honako hau dela jotzen da: etil pirubatoak (**70a**) eta **53** aldehidoek, **71** aminarekin kondentsazio-erreakzio independente bana ematen dituzte, eta horrela **78** enamina eta **79** imina espezieak eratzen dira, hurrenez hurren. Ondoren, Brønsted azidoak **79** aldimina aktibatzen du, **78** enaminarekin Mannich-en erreakzioa sustatuz, eta horri esker, **80** bitartekaria sortzen da. Azkenik, **80** espezieak, ester taldera bideratutako aminaren eraso nukleozalea jasango du, eraztuna itxiz eta **72** α -dehidroaminoazido ziklikoak sortuz.



15. eskema. Brønsted azido bidez katalizatutako etil pirubato (**70a**), **53** aldehido eta **71** amina aromatikoen arteko hiru osagaiko erreakzioa.

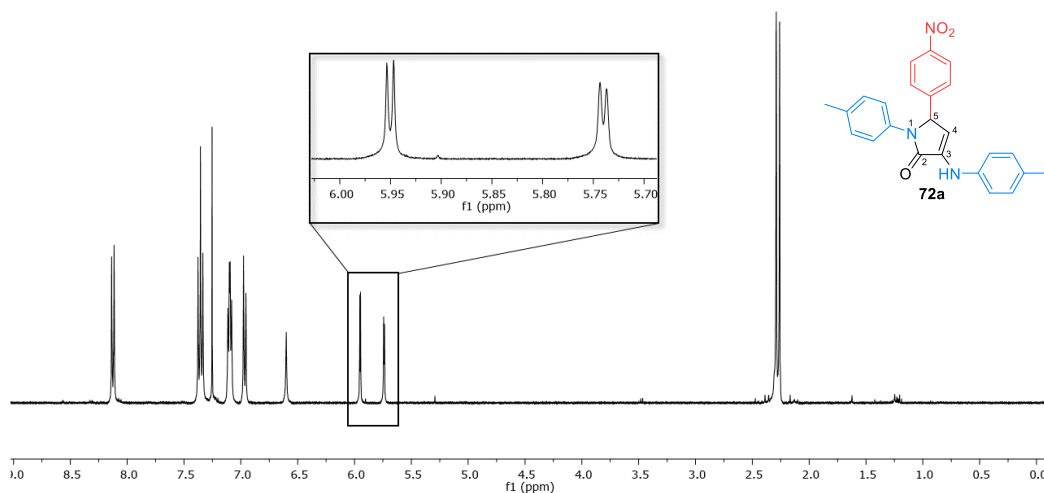
Aurrekari horietan oinarrituta, gure lehen helburu sintetikoa osagai anitzeko erreakzioaren (OAE) protokoloa azido fosforikoak organokatalizatzaile gisa erabiltzera hedatzea izan zen. Hori dela eta, lehenbizi, etil pirubato (**70a**), *p*-nitrobenzaldehido (**53a**) eta *p*-toluidinaren (**71a**) arteko osagai anitzeko erreakzioa aztertu zen, hainbat baldintza ezberdinetan. Erreakzioaren estekiometria 2:1:1

izan bada ere (amina/aldehido/pirubato), pirubato deribatuaren hiru baliokide behar dira etekin onak arrazoizko erreakzio-denboretan lortzeko. Dietil eterra erreakzio-ingurune optimotzat hartu zen; izan ere, disolbatzaile kloratuetan, toluenoan edo azetonitriloan saiaturako erreakzioak γ -laktama-deribatuak eman zituzten etekin txikiagoekin eta erreakzio-denbora luzeagoetan. Gainera, MgSO_4 beharrezkoa da, prozesuan sortutako ura kentzeko. Erreakzioan beste katalizatzaile azido batzuk erabiltzean (H_2SO_4 , H_3PO_4 , $\text{Mg}(\text{HSO}_4)_2$) antzeko eraginkortasuna lortu zen arren, oso komenigarria da BINOL-etik eratorritako **IX** azido fosforikoa katalizatzaile gisa erabiltzea, purifikazio-prozesua errazten baitu eta ez duelako interakziorik sortzen lehorte-agentearekin. Horren ondorioz, etil pirubatoaren (**70a**) hiru baliokide, *p*-nitrobenzaldehidoaren (**53a**) baliokide bat eta *p*-toluidinaren (**71a**) bi baliokide erabili ziren eredu-erreakzioan, BINOL-etik eratorritako **IX** azido fosforiko razemikoaren % 10 mol-en eta MgSO_4 -ren presentzian. Horrela, **72a** γ -laktama lortu zen etekin onarekin 18 ordu eta gero (16. eskema).



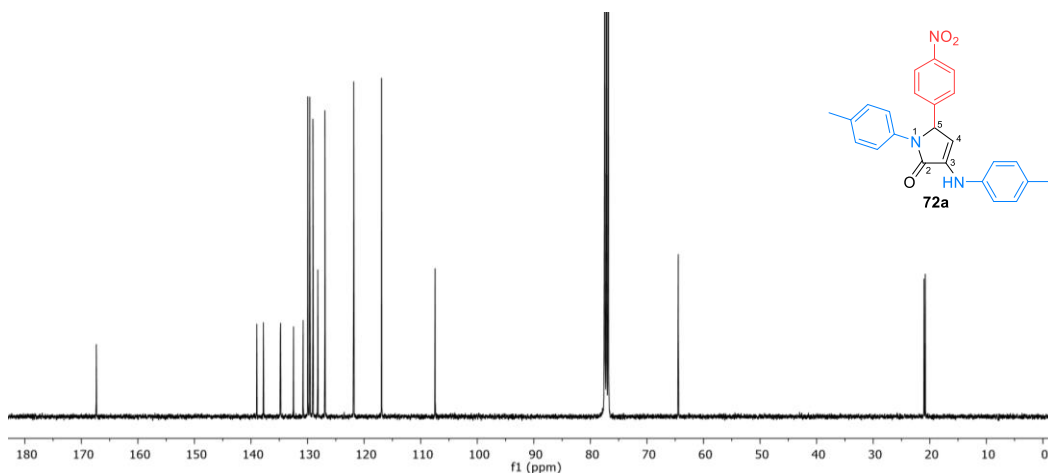
16. eskema. Hiru osagaiko erreakzioa **72a** γ -laktamaren sintesi errazemikoa burutzeko.

72a γ -Laktama deribatua guztiz karakterizatu zen, EMN eta IR eta HRMS espektroetan oinarrituta. γ -Laktama α,β -asegabearen ^1H EMN espektroaren seinale esanguratsuenak eraztuneko bi protoiei eslelitutako bi dobleteak dira, $\delta_{\text{H}} = 5,75$ eta $5,96$ ppm-tan ($^3J_{\text{HH}} = 2,7$ Hz) ageri direnak, hurrenez hurren, zentro estereogenikoaren CH alifatikoari eta olefina =CH-ri dagozkionak (28. irudia). Gainera, $\delta_{\text{H}} = 6,61$ ppm-tan agertzen den eta D_2O -rekin trukutzen den singlete zabala enamina talde funtzionalaren NH-ri dagokio, imina forma tautomerikoa ez dagoela adieraziz. Azkenik, $\delta_{\text{H}} = 2,30$ eta $2,27$ ppm-ko bi singlete handi, eskualde aromatikoko 12 protoien presentziarekin batera, erreakzioan bi *p*-toluidina baliokideek erreakzioan parte hartu dutela ondorioztatzeko informazioa ahalbidetzen du, balizko enol deribatu baten eraketa baztertzeko (28. irudia).



28. irudia. 72a konposatuaren ^1H EMN espektroa CDCl_3 -n.

Gainera, 72a konposatuaren ^{13}C EMN espektroko seinale adierazgarrienak, γ -laktama eraztunaren lau karbonoei dagozkie (29. irudia). Enamina talde funtzionala nabarmena da, $\delta_{\text{C}} = 138,5$ (C-N) eta 105,3 (CH) ppm-tan ageri diren bere bi karbonoen lerrakuntza kimikoak direla eta. Amida konjugatu ziklikoen ohiko eremu barruan ageri da karbonilo taldea, $\delta_{\text{C}} = 167,0$ ppm-tan hain zuzen ere, eta karbono asimetrikoaren seinalea $\delta_{\text{C}} = 63,6$ ppm-tan azaltzen da. ^1H EMN espektroarekin bat etorriz, $\delta_{\text{C}} = 21,0$ eta 20,8 ppm-ko bi seinaleak, *p*-toluidina talde bien ordezkatzailerikoei dagozkie. Bestalde, eremu aromatikoko sei seinale zorrotzak *para* ordezkaturako hiru eraztun aromatikoen 12 CH unitateek sortuak dira (DEPT). Azkenik, eraztun aromatikoen karbono kuarternarioen gainontzeko 6 seinaleak eremu baxuagoan agertzen dira, $\delta_{\text{C}} = 130$ -140 ppm tartean.



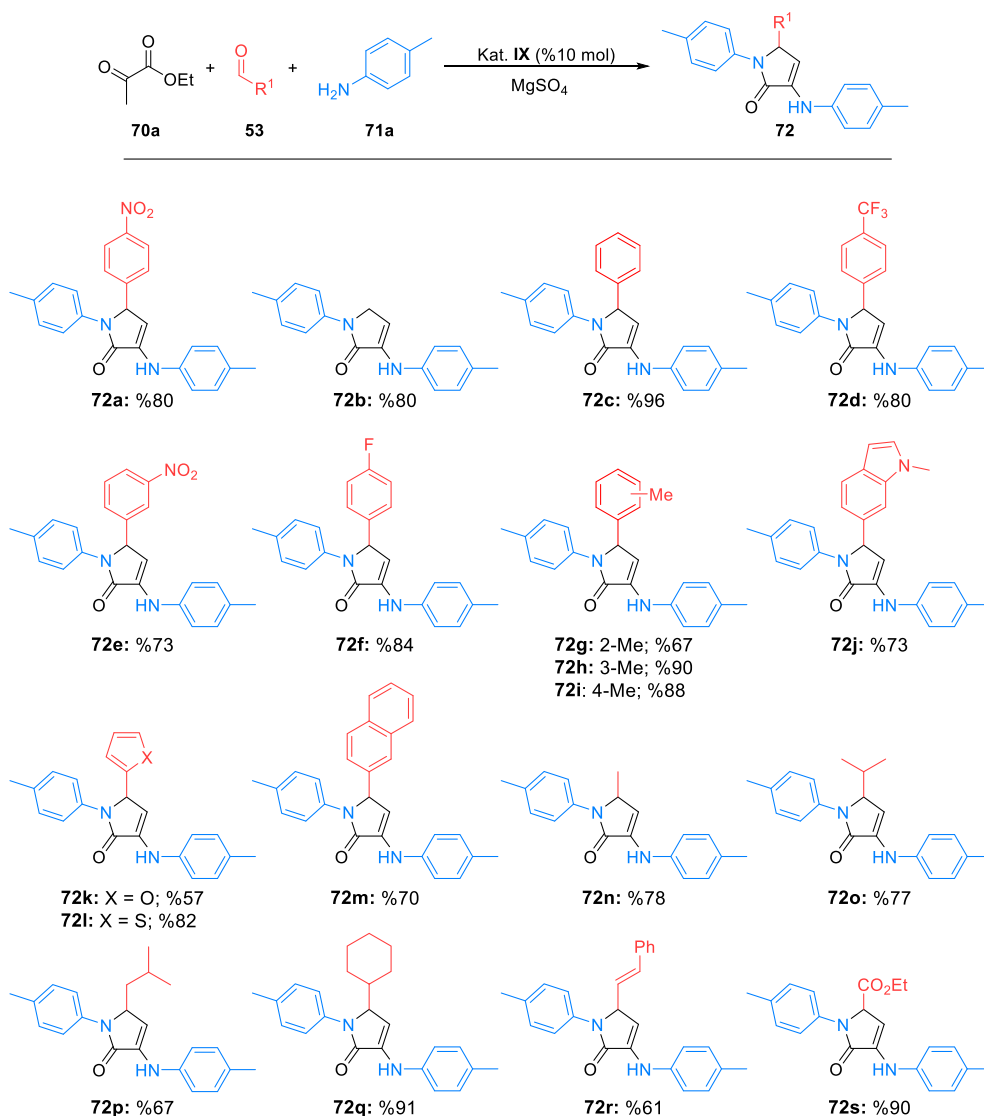
29. irudia. 72a konposatuaren ^{13}C EMN espektroa CDCl_3 -n.

OAE horren izaera modularra kontuan hartuta, errektibo bakoitzaren sorta ezberdinak erabiltzeak aukera emango luke γ -laktama oinarritzko egitura duten molekula desberdin ugari prestatzeko, heterozikloan ordezkatzaille desberdinak txertatuz. Beraz, erreakzioaren potentzial sintetiko frogatzeko helburuarekin, erreakzioaren irismena hainbat γ -laktama funtzionalizatuen sintesira zabaldu zen.

Lehenik eta behin, hainbat **72** γ -laktama sintetizatu ziren aktibatzaile izaera ahula duen *p*-toluidina (**71a**) amina erabiliz, etil pirubato (**70a**) eta aldehido ezberdinekin konbinatuta (1. zerrenda). Formaldehido (**53b**, $R^1 = H$) edo bentzaldehidoa (**53c**, $R^1 = Ph$) erabili zirenean, erreakzioak modu egokian jardun zuen, eta, horri esker, **72b-c** dihidro-2*H*-pirrol-2-onak lortu ziren oso etekin onarekin (1. zerrenda). Gainera, elektroitan urriak diren aldehido aromatikoak (**53d-e**, $R^1 = 4-CF_3C_6H_4$ eta $3-NO_2C_6H_4$) erabili zirenean, erreakzioak modu egokian funtzionatu zuen ere, baina, *p*-trifluorometilbentzaldehidotik eratorritako **72d** deribatua etekin onarekin lortu zen bitartean, *m*-nitrobentzaldehidoaren erabilerak, **72e** γ -laktama eman zuen etekin txikiagoarekin (1. zerrenda). Are gehiago, *p*-fluorobentzaldehidoaren (**53f**, $R^1 = 4-FC_6H_4$) kasuan erreakzio-denbora handitu behar izan zen, baina **72f** γ -laktama oso etekin onean lortu zen (1. zerrenda).

Hala ere, osagai anitzeko erreakzioan ordezkatzaille alifatiko elektro-emaile ahulak dituzten aldehidoak (**53g-i**, $R^1 = 2-MeC_6H_4$, $3-MeC_6H_4$ eta $4-MeC_6H_4$) erabili zirenean, helburu diren γ -laktamak etekin apalagoekin lortu ziren, eta erreakzio-denbora luzeagoak behar izan ziren. Joera hau, erreakzioaren bitartekari den **79** iminaren izaera elektroizale txikiagoaren ondorioz gertatzen da segur aski, eta beraz, irakite-puntu handiagoa duen metil *tert*-butil eterra (MTBE) erabili zen dietil eterraren ordeiz. Erreakzio baldintza horietan, **72g-i** γ -laktamen sintesiaren etekinak onak edo oso onak izan ziren (1. zerrenda), arrazoizko erreakzio denborak erabilita (18-72 ordu).

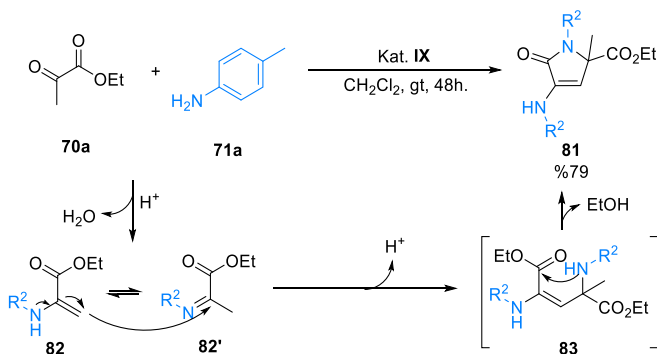
Ondoren, hiru osagaiko erreakzio hau **53j-l** aldehido heteroaromatikoetara ($R^1 = 6-(N-Me-indolil)$, 2-furil and 2-tienil) zabaldu zen, eta **72j-l** γ -laktamak eskuratu ziren etekin moderatu edo onetan (1. zerrenda). Gainera, **72m** substratuan eragozpen esteriko handia espero bazen arren, frogatu ahal izan zen 2-naftaldehidoa (**53m**, $R^1 = 2$ -naftilo) ere errektibo aproposa dela erreakzio honetan erabiltzeko (1. zerrenda). Bestalde, erreakzioaren irismena arrakastaz zabaldu zen **53n-q** aldehido alifatikoak erabiltzera ($R^1 = Me$, iPr , tBu eta Cy), eta **72n-q** γ -laktama deribatuak lortu ziren etekin onak edo bikainak izanda (1. zerrenda). Harrigarria bada ere, erreakzioa beste aldehido polifuntzional batzuekin ere funtzionatzen du; izan ere, zinamaldehido (**53r**, $R^1 = CH=CHPh$) edo etil glioxilatoa (**53s**, $R^1 = CO_2Et$) erabiliz, zinamil eta ester taldeez ordezkaturako **72r-s** konposatuak sortu ziren, etekin onak edo bikainak eskuratuta (1. zerrenda).



1. zerrenda. Sintetizatutako 72a-s 3-p-tolil-1,5-dihidro-2H-pirrol-2-onak.

Aurrekoaz aparte, hainbat ahalegin egin zen osagai anitzeko erreakzioa aldehidoen ordez zetonekin burutu ahal izateko, karbono asimetriko kuarternariodun 3-amino-1,5-dihidro-2H-pirrol-2-onak lortu ahal izango zirelakoan. Zetona ez-simetriko desberdinak erabili arren, hala nola, 2-butanona, azetofenona eta metil 3,3,3-trifluoropirubatoa, ahalegin guztiak alferrekoak izan ziren, eta kasu guztietan **81** substratu dimerikoa bakarrik lortu zen (17. eskema). Dimerizazio hau, pirubatotik eratorritako **82** enamina bitartekariaren erreaktibitate areagotuaren ondorioz gertatzen da, zeinek bere buruarekin erreakzionatzen duen zetona eta amina sortutako imina bitartekariarekin egin ordez.

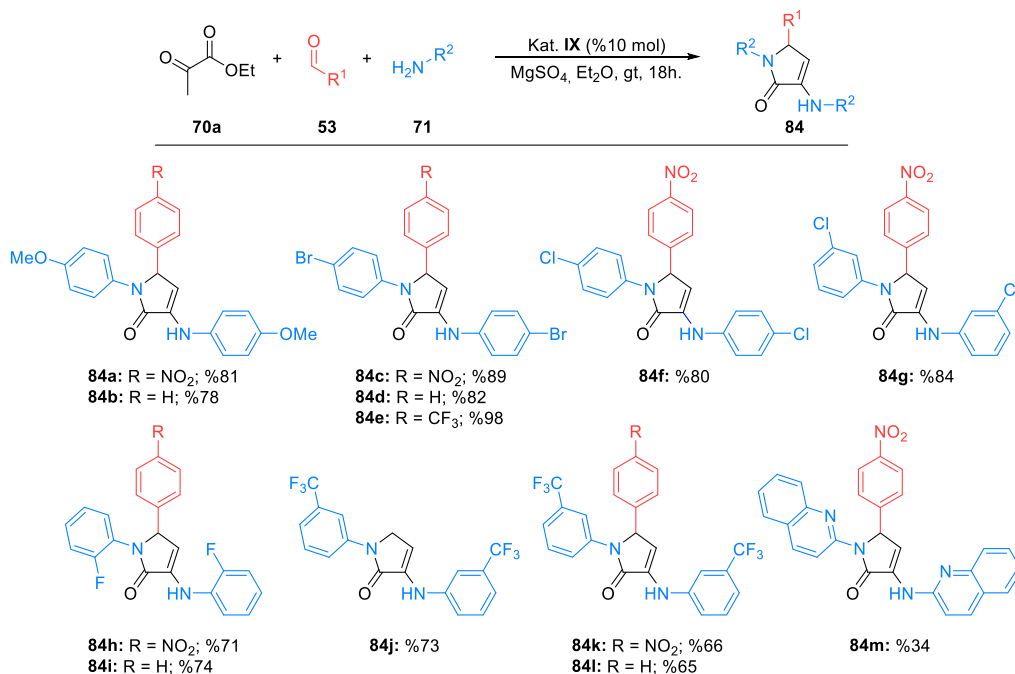
Beraz, erreazio horren mekanismoa *p*-toluidina (**71a**) eta etil pirubatoaren (**70a**) arteko kondentsazio bidez lortutako, eta orekan dauden, **82** eta **82'** enamina eta imina tautomeroen formazioarekin hasten da. Enaminak imina tautomeroa eraso egiten du **83** bitartekaria sortuz, eta jarraian, kondentsazio intramolekular baten ondoren, **81** γ -laktama eratzen da.



17. eskema. **81** γ -Laktama α,β -asegabearen sintesia.

Ikerketaren hurrengo etapan, erreazioaren irismena amino substratu desberdinen erabilera zabaltzen zen (2. zerrenda), etil pirubatoa (**70a**) erabiliz. Adibidez, elektroitan aberatsa den *p*-anisidina (**71b**, $R^2 = 4\text{-MeOC}_6\text{H}_4$) eta *p*-nitrobenzaldehidoa (**53a**) edo benzaldehidoa (**53c**) erabiltzean, osagai anitzeko erreazioak **84a-b** γ -laktama deribatuak eman zituen oso etekin onean (2. zerrenda). Hala ere, **84a** konposatuaren sintesia burutzeko erreazio-denbora handiagoak behar izan ziren, elektroitan aberatsa den aldehido aromatiko bat erabiltzearen ondorioz, **79** imina bitartekari elektroizalearen desaktibazio handiagoa baita, bitarteko **78** enamina nukleozalerako espero den aktibazioaren aldean (15. eskema, *vide supra*). Gainera, zenbait *orto*, *meta* eta *para* halogenoz ordezkaturako **71c-f** anilinak ($R^2 = 4\text{-BrC}_6\text{H}_4$, $4\text{-ClC}_6\text{H}_4$, $3\text{-ClC}_6\text{H}_4$ eta $2\text{-FC}_6\text{H}_4$) *p*-nitrobenzaldehido (**53a**, $R^1 = 4\text{-NO}_2\text{C}_6\text{H}_4$), benzaldehido (**53c**, $R^1 = \text{Ph}$) edo *p*-trifluorometil benzaldehydorekin (**53d**, $R^1 = 4\text{-CF}_3\text{C}_6\text{H}_4$) konbinatuta arrakastaz erabili ziren, kasu guztietan **84c-i** halogenodun γ -laktamak etekin onekin edo bikainekin lortu baitziren (2. zerrenda). Hala ere, *p*-kloroanilina (**71d**, $R^2 = 4\text{-ClC}_6\text{H}_4$) erabiltzeak, erreazioa MTBE-en berotzea ($55\text{ }^\circ\text{C}$) beharrezkoa izan zen, eta *m*-kloroanilina (**71e**, $R^2 = 3\text{-ClC}_6\text{H}_4$) lehengai gisa baliatu zenean, erreazio-denbora luzatu behar izan zen (72 ordu). Nahiz eta desaktibatutako amina aromatikoak erabiltzearen ondorioz bitarteko enamina desaktibazioa espero den, *m*-trifluorometilanilina (**71g**, $R^2 = 3\text{-CF}_3\text{C}_6\text{H}_4$) kasuan, formaldehido (**53b**, $R^1 = \text{H}$), *p*-nitrobenzaldehido (**53a**, $R^1 = 4\text{-NO}_2\text{C}_6\text{H}_4$) edo benzaldehydorekin (**53c**, $R^1 = \text{Ph}$) konbinatuta, **84j-l** produktuak lortu ziren etekin onetan (2. zerrenda). Espero zen moduan, erreaktibotasun txikiagoa hauteman zen kasu hauetan, eta **84j-l** γ -laktamak modu eraginkorrean lortu ziren, erreazio-denborak 72 ordutara luzatuz. Azkenik, kinolinatik eratorritako **71h** amina heteroaromatikoa ($R^2 = 2\text{-kinolinil}$) baliatu zenean, helburu

den **84m** γ -laktama etekin baxuetan isolatu zen, egitura horretan dagoen eragozpen esteriko handiaren ondorioz.

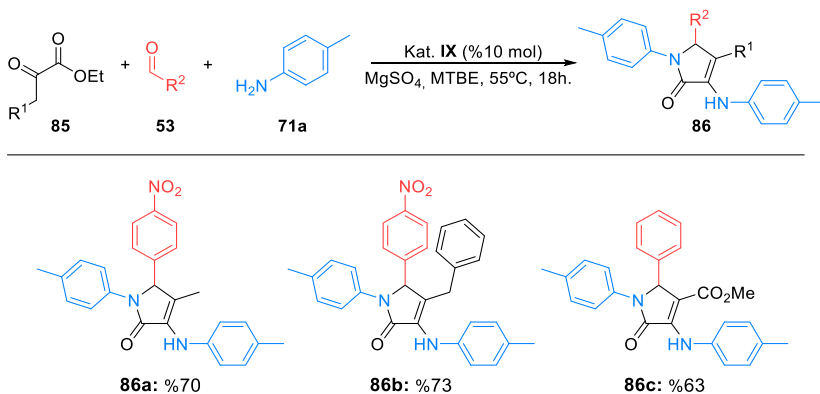


2. zerrenda. Sintetizatutako **84** 3-amino-1,5-dihidro-2H-pirrol-2-onak.

Nahiz eta beste amina alifatiko eta (hetero)aromatiko asko probatu ziren, hala nola bentzilamina, tritilamina, *p*-nitroanilina, *o*- eta *m*-anisidina edo 2, 3 edo 4-aminopiridina, ez zen hauteman γ -laktama substratuen eraketa esanguratsurik, enamina eta imina espezieen erreaktibotasunaren arteko oreka kritikoa dela eta. Amina alifatikoak edo elektroitan aberatsak diren anilinak erabiliz gero, enamina nukleozale oso erreakzionakorra sor daiteke, baina, ordea, imina bitartekariaren izaera elektroizalea gutxitua izango da. Aitzitik, elektroitan urriak diren aminak erabiltzen direnean, erreaktibotasun falta enamina nukleozalearen desaktibazio samarraren ondorio izan daiteke, nahiz eta imina-espezieia oso aktibatua egon. Gainera, *orto* ordezkatutako anilina substratuek eragindako efektu esterikoek erreaktibitatea murrizten dute.

Erreakzioaren irismena ikertzen amaitzeko, pirubatoaren deribatuen ordezkatzaileek duten eragina aztertu zen. Izaera aktibatzaile ahula duen *p*-toluidina (**71a**) erabiliz, **85a-c** ordezkatutako pirubato-deribatuek ($\text{R}^1 = \text{Me}$, Bn eta CO_2Me) *p*-nitrobentzaldehido edo bentzaldehidoarekin erreakzionatu zuten, eta **86** 4-ordezkatutako γ -laktama-deribatuek lortu ziren etekin onekin (3. zerrenda). Kasu hauetan, pirubato-deribatuetan dagoen oztopo esteriko handiagoaren ondorioz,

enamina bitartekariaren errektibitatea murrizten da, beraz, erreakzioak 55 °C-tan berotu behar izan ziren, MTBE-a disolbatzaile gisa erabiliz.



3. zerrenda. Sintetizatutako 86 4-ordezkatutako 3-amino-1,5-dihidro-2H-pirrol-2-onak.

Laburbilduz, kapitulu honetan pirubato-deribatu, amina eta aldehidoen arteko osagai anitzeko erreakzio oso eraginkorra deskribatu da, eta horren ondorioz, 3-amino ordezkatutako γ -laktama α,β -asegabe ugari lortu dira. Protokolo hau, hainbat amina aromatikorik, aldehido aromatiko eta alifatikorik eta ordezkatutako pirubato-deribatu desberdinei aplikatu dakieke funtzionalizazio handiko γ -laktamen sintesi zuzena ahalbidetuz, merke eta eskuragarri diren lehengaiak baliatuz.

2. Kapitulu

Fluorra eta fosforoa duten γ -laktamen osagai anitzeko sintesia

Jakina da, molekula bioaktiboetan fluorra edo fosforoa duten ordezkatzailak sartzeak, askotan jarduera biologiko berriak sortu edo hauen potentzia areagotzen duela. Alde batetik, fosfonato-deribatuek jarduera biologiko ugari dituzte, fosfato-metabolito naturalekin duten antzekotasun kimikoagatik. Hori dela eta, aplikazio ugari dituzte medikuntzan eta agrokimikan.¹⁵¹ Bestalde, nahiz eta konposatu organikoen egituretan fluor atomoak sartzearen eragina auresatea nahiko zaila izan, maiz, molekulen izaera lipofilikoa handitzen da, eta horrek aktibitate biologikoa areagotzen du, zelula-mintzak zeharkatzeko gaitasuna hobetzen baita.¹⁵² Halaber, fluorodun konposatuak kimika biologikoan erakargarri bilakatzen dira, beste propietate batzuei esker, hala nola, erradio atomiko txikia, elektronegatibotasun handia, C-F loturaren polarizazio txikia eta ¹⁹F atomoaren isotopo natural bakarrak $\frac{1}{2}$ ko spin nuklearra duenez, ezin hobea da EMN bidezko monitorizaziorako.

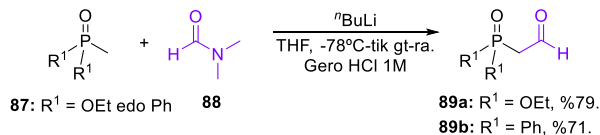
Hau guztia kontuan hartuta, eta ikusirik aurreko kapitulan γ -laktama funtzionalizatuak prestatzeko garatu den metodologia eraginkorra, ondoren, osagai anitzeko erreakzio hau fosforoa eta fluorra duten γ -laktama α,β -asegabean sintesira zabaltzea erabaki genuen, aldehido eta pirubato fluoratuak edo fosforilatuak erabiliz.

Lehenik eta behin, osagai anitzeko erreakzioaren irismena hedatu egin zen fosforoa edo fluorra duten aldehidoak erabiliz. Trifluoroazetaldehidoa eta perfluorobenzaldehidoa iturri komertzialetatik eskuratu ziren bitartean, fosfonato ($R^1 = CH_2P(O)(OEt)_2$) edo fosfina-oxidotik ($R^1 = CH_2P(O)Ph_2$)

¹⁵¹ (a) Horsman, G. P.; Zechel, D. L. *Chem. Rev.* **2017**, *117*, 5704-5783. (b) Mucha, A.; Kafarski, P.; Berlicki, L. *J. Med. Chem.* **2011**, *54*, 5955-5980. (c) Karl, D. M. *Nature* **2000**, *406*, 31-33. (d) Engel, R. Handbook of Organophosphorus Chemistry; M. Dekker Inc.: New York, **1992**. (e) Kafarski, P.; Lejczak, B. *Phosphorus, Sulfur Silicon Relat. Elem.* **1991**, *63*, 193-215.

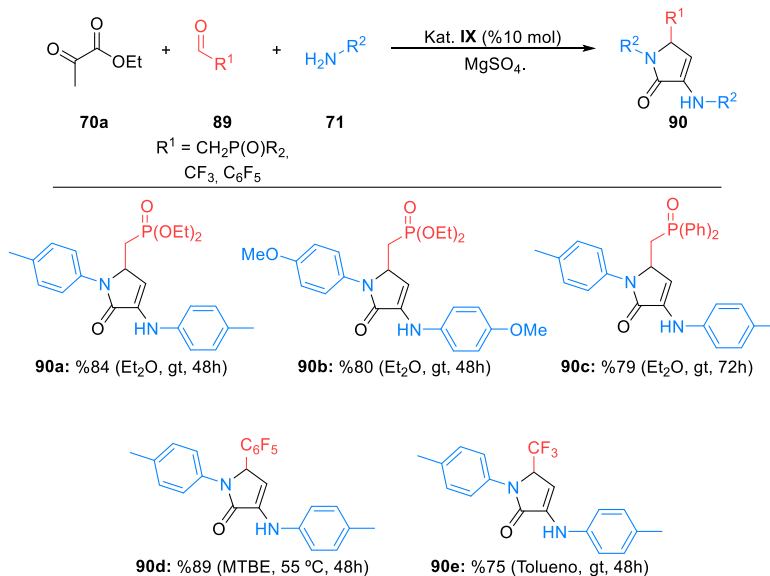
¹⁵² (a) Müller, K.; Faeh, C.; Diederich, F. *Science* **2007**, *317*, 1881-1886. (b) Shah, P.; Westwell, A. D. *J. Enzyme Inhib. Med. Chem.* **2007**, *22*, 527-540. (c) Bégué, J. P.; Bonnet-Delpon, D. In *Bioorganic and Medicinal Chemistry of Fluorine*; Wiley, 2007; pp 1-365

errotorritako **89** aldehido β -fosforatuak, metilfosfonato edo metilfosfina-oxido eta *N,N*-dimetilformamida (DMF) erabiliz prestatu ziren, Savignac-en prozedura jarraituz (18. eskema).¹⁵³



18. eskema. 89a-b Aldehido β -fosforilatuen Savignac-en sintesia.

Hasieran, osagai anitzeko erreakzioa probatzeko, etil pirubato (**70a**), **71** amina aromatikoak eta ordezkatzailu fluoratu edo fosforatuak dituzten **89** aldehidoak erabili ziren, BINOL-etik errotorritako **IX** azido fosforikoaren kantitate katalitikoaren presentzian. Prozedura hau jarraituz, γ -laktama eratzunaren 5. posizioan ordezkatzailu fluoratu edo fosforatuak dituzten **90** deribatuak etekin onarekin sintetizatu ziren (4. zerrenda).



4. zerrenda. Forforoa edo fluorra duten **90** γ -laktamen osagai anitzeko sintesirako.

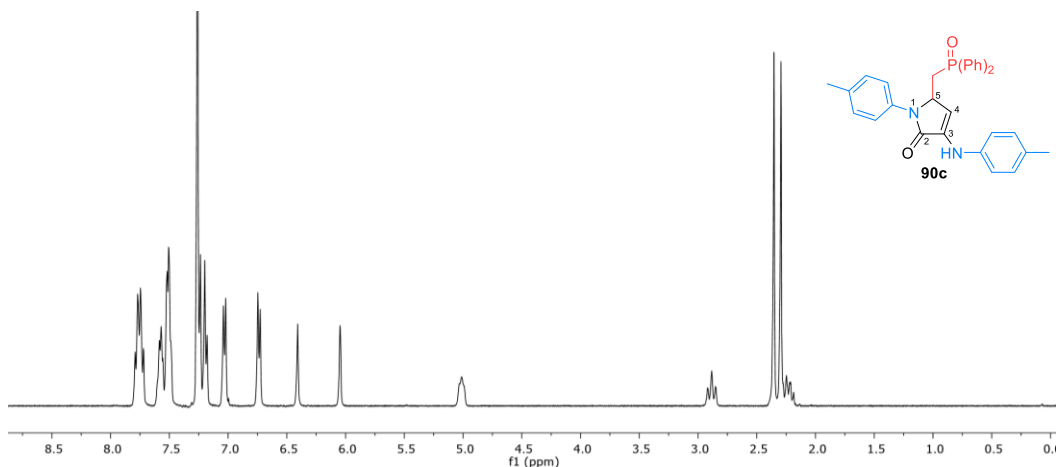
Erreakzioa fosfonatotik errotorritako **89a** aldehidoa ($\text{R}^1 = \text{CH}_2\text{P}(\text{O})(\text{OEt})_2$), etil pirubato (**70a**) eta *p*-toluidina (**71a**, $\text{R}^2 = 4\text{-MeC}_6\text{H}_4$) edo *p*-anisidinarekin (**71b**, $\text{R}^2 = 4\text{-MeOC}_6\text{H}_4$) burutzean, dietil eterrean eta giro tenperaturan, **90a-b** γ -laktama fosforatuak lortu ziren erraz (4. zerrenda). Hala ere, fosfina-oxidotik errotorritako **89b** ($\text{R}^1 = \text{CH}_2\text{P}(\text{O})\text{Ph}_2$) aldehidoa erabiltzean, erreakzioak denbora gehiago behar izan zuen **90c** produktu analogoa lortzeko. Erreaktibotasun desberdin hau difenilfosfinil taldeak

¹⁵³ Aboujaoude, E. E.; Collignon, N.; Savignac, P. *Synthesis* **1983**, 634-636.

dietil fosfonatoarekin alderatuta, duen eragozpen esteriko handiagoari egotz dakiok. Bestalde, baldintza berberetan, komertziala den perfluorobenzaldehidoak (**89c**, $R^1 = C_6F_5$) ez zuen inolako erreaktibotasunik erakutsi. Arazo hau konpontzeko, MTBE erabili zen disolbatzaile gisa birfluxuan, eta perfluorofenil taldez ordezkaturako **90d** γ -laktama lortu zen oso etekin onarekin (4. zerrenda).

Trifluoroazetaldehidoari (**89d**, $R^1 = CF_3$) dagokionez, aldehido-substratu purua zuzenean erabiltzea ezinezkoa da, irakite-puntu txikia baitu ($-20^\circ C$). Hala ere, jakina da aldehido espeziea *in situ* sor daitekeela komertziala den aitzindari hidratatutik abiatuta. Hori dela eta, trifluorometilimina bitartekaria trifluoroazetaldehido hidratoaren ur disoluziotik eta *p*-toluidinatik (**71a**, $R^2 = 4-MeC_6H_4$) abiatuta prestatu zen, toluenon birfluxuan eta Dean-Stark erabiliz ur guztia kentzeko. Ondoren, etil pirubato baliokide bat eta **IX** azido fosforiko katalizatzailea gehitu ziren eta nahastea 72 orduz irabiatu zen. Prozedura eraldatu hau erabiliz, trifluorometil taldez ordezkaturako **90e** γ -laktama etekin onean lortu zen (4. zerrenda).

Fluorodun edo fosforodun **90** γ -laktamak EMN, IR eta HRMS bidez erabat karakterizatu ziren. Hauen artean, **90c** substratua eredu gisa hautatu da eta seinale adierazgarrienak ondoren aurkezten dira (30. irudia).

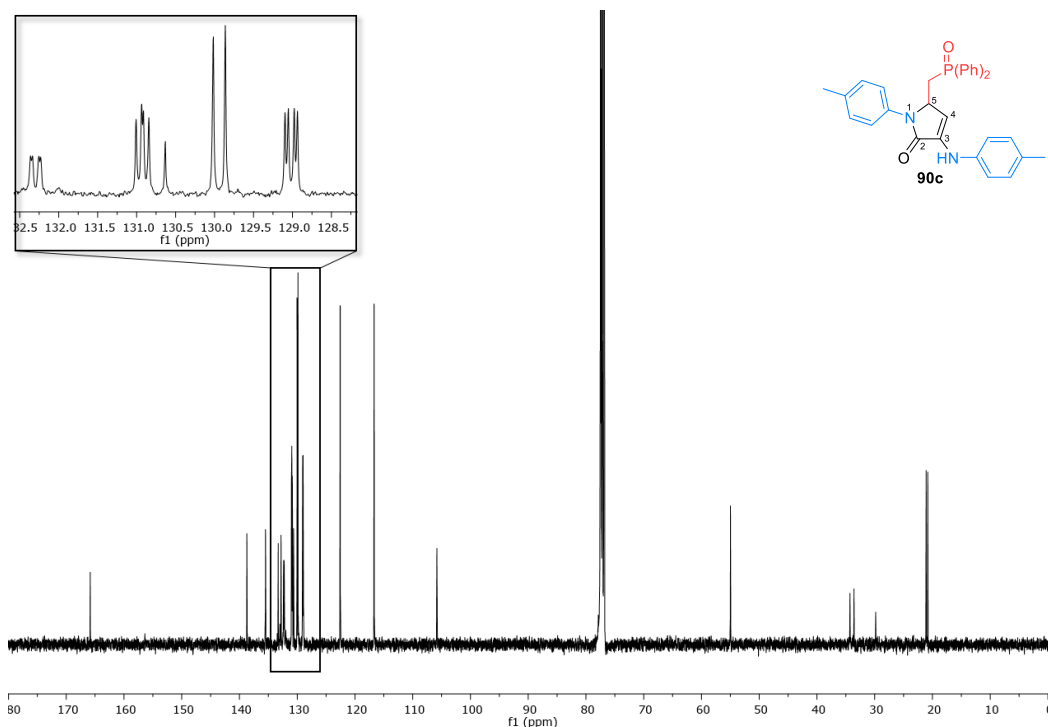


30. irudia. **90c** konposatuaren 1H EMN espektroa $CDCl_3$ -n.

1H EMN espektroan enamina endozikliko taldearen presentzia nabaria da $\delta_H = 6,41$ ppm-tan singlete zabal bat eta $\delta_H = 6,05$ ppm-tan ($^3J_{HH} = 2,6$ Hz) doblete bat behatzen direlako, NH talde funtzionalari eta =CH talde olefinikoari dagozkienak, hurrenez hurren. Karbono kiraleko protoiaren seinalea multiplete bat bezala ageri da, protoi olefinikoarekin, metilen taldearekin eta fosforo atomoarekin akoplatzearen ondorioz. Horrez gain, $\delta_H = 2,89$ and $2,22$ ppm-ko bi multipleteak CH_2 taldearenak dira, non, protoi bakoitza, karbono berean dagoenarekin, CH taldearekin eta fosforo

atomoarekin akoplatuta dagoen. Seinale hauek bi multiplete independente gisa agertzeak, bakar baten ordez, agerian uzten du egitura estereozentro bat dagoela, eta honek egiten ditu protoi hauek diastereotopiko. Azkenik, $\delta_H = 2,35$ and $2,29$ ppm-ko bi seinale sendok eta eskualde aromatikoan 18 protoi egoteak daudela adierazten dute, bi *p*-toluidina talde eta difenilfosfina-oxido taldea daudela molekulean.

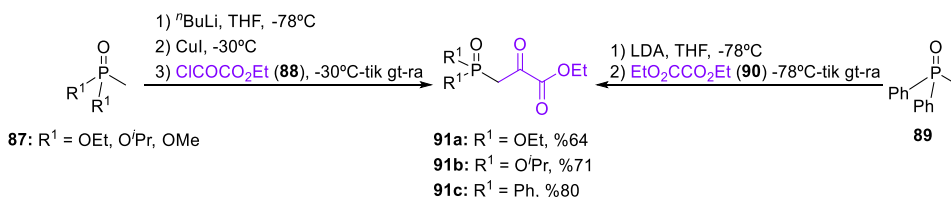
Gainera, **90c** konposatuaren ^{13}C EMN espektroak γ -laktama eraztunaren lau karbonoen seinale bereizgarri erakusten ditu (31. irudia). Enamina talde funtzionalaren bi karbonoak $\delta_C = 130,6$ eta $105,8$ ppm-tan ageri dira, karbonilo taldeko seinalea $\delta_C = 165,9$ ppm-tan nabarmen da, eta $\delta_C = 55,0$ ppm-tako seinalea karbono estereogeniko alifatikoari dagokio. Bestalde, $\delta_C = 33,9$ ppm-ko dobletea metileno taldearena da, eta $^1J_{PC} = 69,8$ Hz-ko akoplamendu konstante bereizgarria erakusten du fosforo atomoarekin. Bi *p*-toluidina egitura daudela argi dago $\delta_C = 21,1$ eta $20,8$ ppm-tan bi seinale eta eremu aromatikoan lau seinale zorrotz ageri direlako. Difenilfosfina taldeko fenilo taldeek akoplamendu gehigarria daukate ^{31}P -ko nukleo dipolarrarekin; eta horri gehitzen badiogu bi *p*-tolil talde daudela, patroi konplexu bat ikusten da ^{13}C EMN espektroaren eremu aromatikoan.



31. irudia. **90c** konposatuaren ^{13}C EMN espektroa CDCl_3 -n.

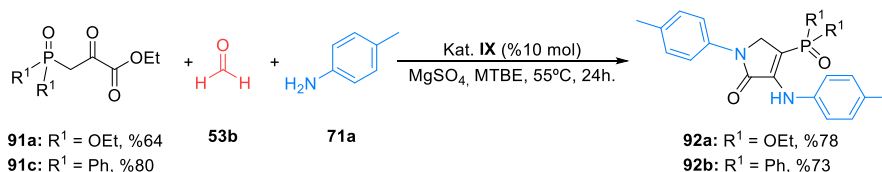
Fosforodun γ -laktama deribatuetan dugun interesari jarraituz, eta OAE-ren irismena are gehiago zabaltzeko, erreakzioan fosforo ordezkatzailak dituzten pirubato-deribatuak erabiltzea aztertu zen.

89 Aldehido β -fosforatuak bezala, fosfonato ($R^1 = O^iPr, OEt, OMe$) edo fosfina-oxido ($R^1 = Ph$) talde funtzionalak dituzten **91a-c** pirubatoak erraz lor daitezke, lehenik eta behin **87** metilfosfonato esterrak edo metildifenilfosfina-oxidoa (**89**) metalatuz, eta ondoren etil oxalil kloruroa (**88**) edo dietil oxalatoa (**90**) gehituz, hurrenez hurren (19. eskema).¹⁵⁴



19. eskema. 91 Pirubato fosforatuen sintesia.

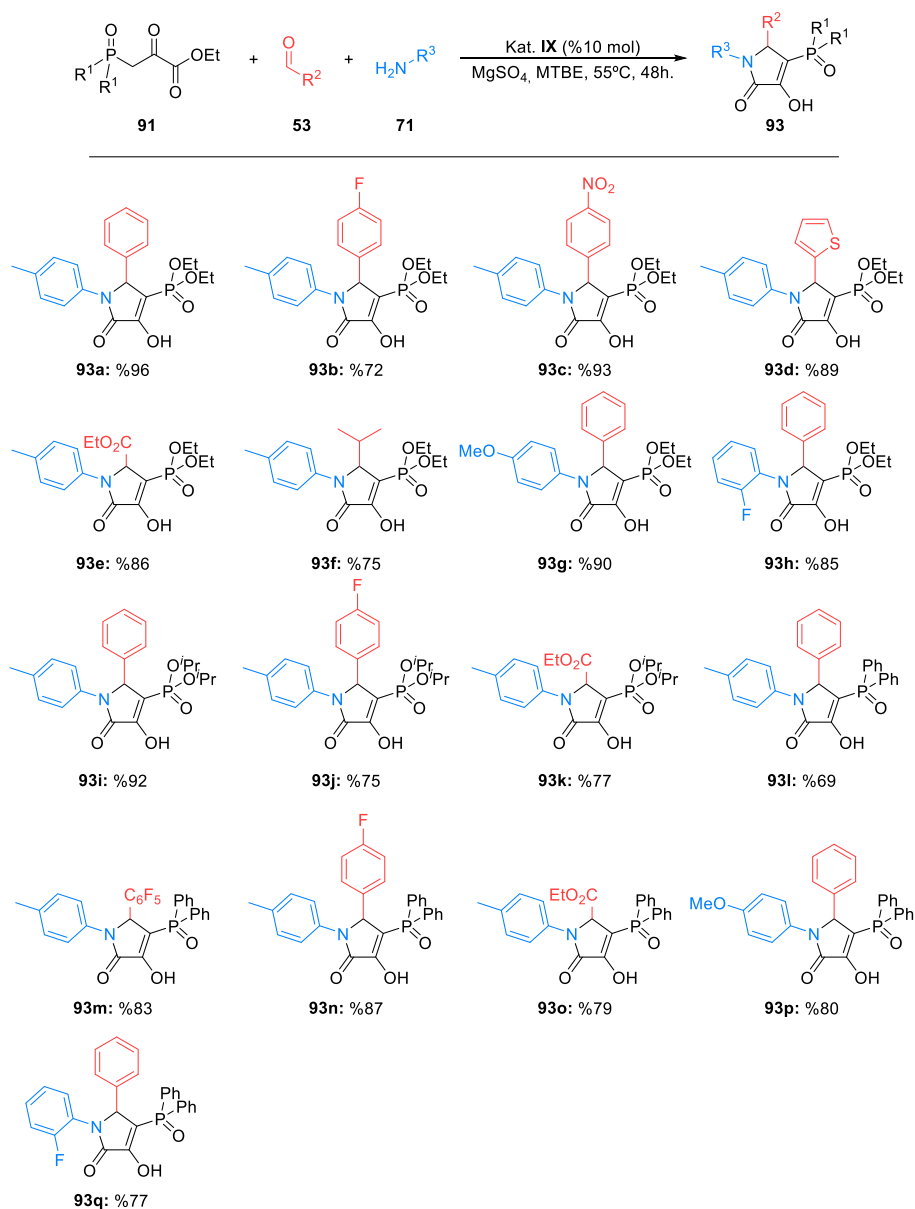
Hasieran, osagai anitzeko erreakzioa fosfonatotik eta fosfina-oxidotik eratorritako **91a,c** pirubatoak ($R^1 = OEt, Ph$) erabiliz burutu zen, formaldehido (**53b**) eta *p*-toluidinarekin (**71a**) konbinatuta. Erreakzioa BINOL-en deribatua den **IX** azido fosforikoaren katalizatzailearen presentzian, $MgSO_4$ gehituta, kanporatutako ura bereganatzeko, eta birfluxuan dagoen MTBE disolbatzailean berotuta burutu zen, **92** 3-amino-1,5-dihydro-2*H*-pirrol-2-onak eskuratzeko etekin onean (20. eskema).



20. eskema. 92 C-5 ordezkatu gabeko 3-amino-1,5-dihydro-2*H*-pirrol-2-onen sintesia.

Bestalde, erreakzio-baldintza berdinetan, formaldehidoaren ordeztaldea erabili zenean, etil fosfonatoa duen **91a** pirubatoarekin ($R^1 = OEt$) eta *p*-toluidinarekin (**71a**) batera, espero zen enamina-deribatua ordez enol talde funtzionala duen **93a** γ -laktama lortu zen, oso etekin onean (5. zerrenda). Erreakzio horretan lortutako produktuaren garrantzia kontuan hartuta, azido *iso*-tetroniko oinarritzko egitura duena, erreakzio berdina beste amina (**71**), pirubato fosforatu (**91**) eta aldehido aromatiko eta alifatikoak (**53**, $R^2 = Ar, Alk$) erabiliz aztertu zen (5. zerrenda).

¹⁵⁴ (a) Palacios, F.; Vicario, J.; Aparicio, D. *J. Org. Chem.* **2006**, *71*, 7690-7696. (b) Varlte, J.-M.; Colliguon, N.; Savignac, P. *Can. J. Chem.* **1979**, *57*, 3216-3220.



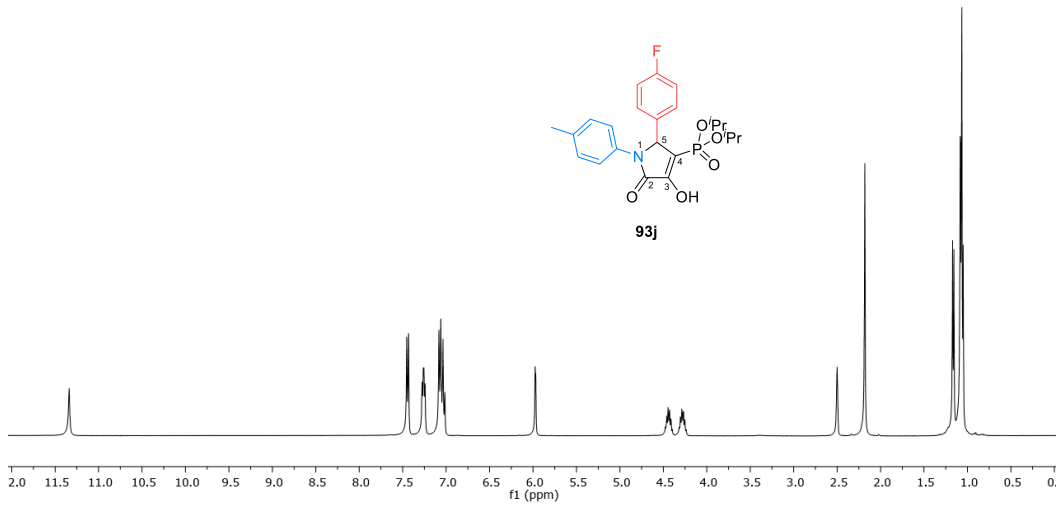
5. zerrenda. **93** 3-hidroxi-1,5-dihidro-2*H*-pirrol-2-ona fosforatuen hiru osagaiko erreakzioaren irismena.

Lehengai bezala erabilitako hiru substratuen osagai antzeko erreakzioaren irismena oso zabala izan zen. Pirubato deribatuei dagokionez, fosfonato edo fosfina-oxido talde desberdinetatik eratorritako **93** γ -laktamak oso etekin onean lor daitezke (5. zerrenda). Talde elektro-emaile ahulak edo sendoak dituzten amina aromatikoak hiru osagaien erreakzioan erabil daitezke, hala nola, *p*-toluidina (**71a**, $R^3 = 4\text{-MeC}_6\text{H}_4$), *p*-anisidina (**71b**, $R^3 = 4\text{-MeOC}_6\text{H}_4$) eta *o*-fluoroanilina (**71f**, $R^3 = 2\text{-FC}_6\text{H}_4$). Zoritxarrez,

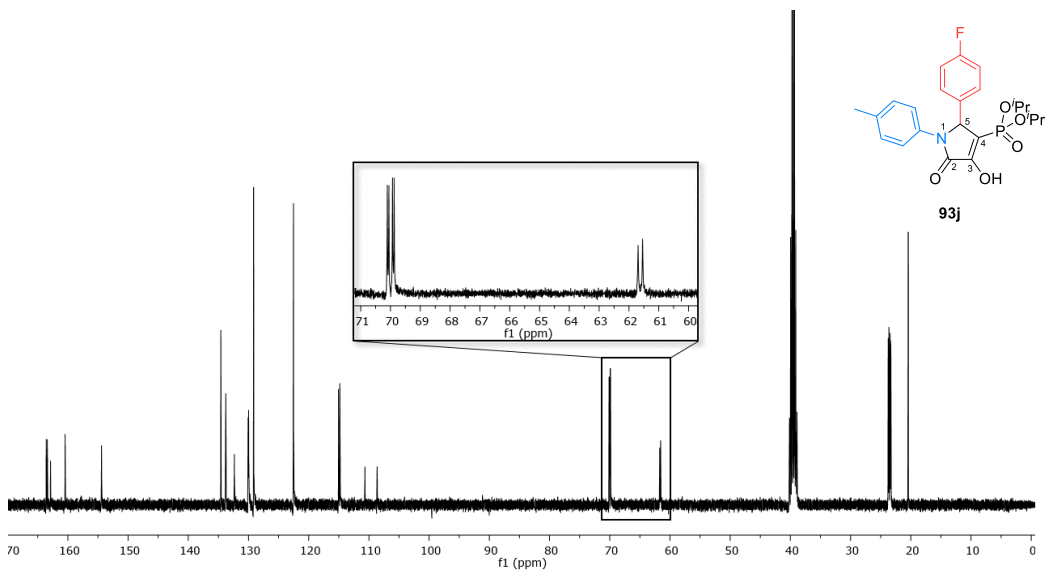
amina alifatikoak edo elektroitan urriak diren anilinak erabiltzea ez zen eraginkorra izan osagai anitzeko erreakzio honetan, eta ez zen hauteman γ -laktama produktuen eraketa.

Osagai anitzeko protokoloan erabilitako **53** aldehido substratuei dagokienez, bentzaldehidoa (**53c**) iminaren aitzindari gisa erabiltzeaz gain, erreakzioa modu eraginkorrean gertatu zen beste aldehido aromatiko batzuekin ere, hala nola, *p*-fluorobenzaldehidoa (**53h**), fluorodun **93b,j,n** γ -laktamen sintesi eraginkorrerako, eta *p*-nitrobenzaldehidoarekin (**53a**), C-5 posizioan elektroierakarle talde bat duen **93c** γ -laktamaren prestakuntzarako. Halaber, erreakzioa eraginkorra da 2-tiofenokarboxaldehido (**53i**) erabilita, eta **93d** 3-hidroxi-1,5-dihidro-2*H*-pirrol-2-ona isolatu da etekin bikainarekin. Gainera, etil glioxalatoa (**53s**) substratu ona da erreakzio honetarako ere, eta horren ondorioz, α -aminoazidoaren deribatuak diren **93e,k,o** γ -laktamak etekin onetan lortu ziren. Azkenik, metodologia hau erabiliz, *iso*-butiraldehido alifatikotik (**53o**) eratorritako **93f** substratua ere etekin egokiarekin prestatu ahal izan zen (5. zerrenda).

Orain arte egin dugun bezala, **92** eta **93** γ -laktamak guztiz karakterizatu ziren RNM, IR eta HRMS tekniken bidez dagoela (32. irudia).. Zehazki, **93j** 3-hidroxi deribatutako γ -laktamak patroia argi eta bereizgarria erakusten du EMN-ean. Konposatu honen ^1H EMN espektroaren seinale adierazgarrienak $\delta_{\text{H}} = 11,34$ ppm-ko singlete zabala, OH enolikoari dagokiona, ziur aski molekularneko hidrogeno zubi baten presentziaren ondorioz eremu oso altuan agertzen dena, eta $\delta_{\text{H}} = 5,97$ ppm-ko dobletea ($^3J_{\text{PH}} = 2.8$ Hz) aldameneko fosforo atomoarekin akoplatuta dagoen karbono kiraleko protoiari dagokiona. Espero den bezala, egituran zentro estereogeniko bat dagoenez, bi talde *iso*-propilikoaren CH protoi diastereotopikoaren seinaleak bi multiplete independente gisa agertzen dira $\delta_{\text{H}} = 4,44$ eta $4,27$ ppm-tan, eta, CH_3 protoiak gainjarrita dauden lau doblete bezala ikusten dira $\delta_{\text{H}} = 1,20$ and $1,00$ ppm artean. Azkenik, metil talde bati dagokion $\delta_{\text{H}} = 2,18$ ppm-ko singlete baten presentziak eta eskualde aromatikoan zortzi protoi egoteak iradokitzen dute egituran *p*-toluidina-unitate bakar bat



32. irudia. 93j konposatuaren ^1H EMN espektroa DMSO- d_6 -n.

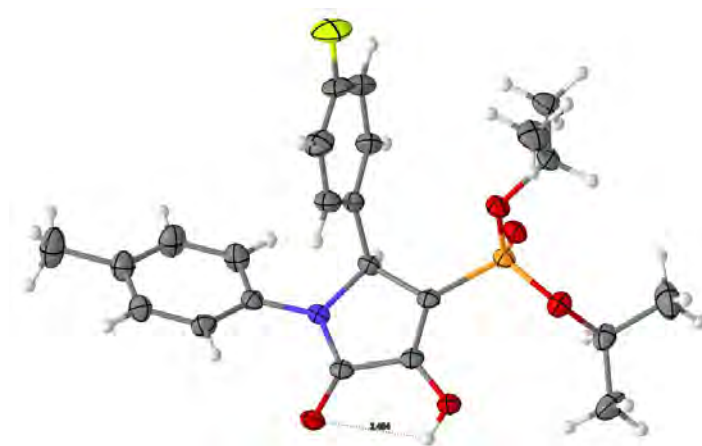


33. irudia. 93j konposatuaren ^{13}C EMN espektroa DMSO- d_6 -n.

Era berean, **93j** konposatuaren ^{13}C EMN espektroak, espero bezala, γ -laktama eraztuneko lau karbonoen seinale bereizgarriak erakusten ditu. Doblete despantailatuena $\delta_{\text{C}} = 154,4$ ppm-tan ($^3J_{\text{PC}} = 4,2$ Hz) ageri da eta karbonilo taldeari dagokio, eta argi dago enol egitura dagoela, $\delta_{\text{C}} = 163,5$ eta $109,6$ ppm-tako bi dobleteen presentziagatik, $^2J_{\text{PC}} = 18,4$ Hz and $^1J_{\text{PC}} = 203,6$ Hz-ko akoplamendu geminal eta *ipso* tipikoak dituztenak, hurrenez hurren. Karbono estereogeniko alifatikoa doblete gisa agertzen da $\delta_{\text{C}} = 61,6$ ppm-tan, fosforo atomoarekin ere akoplatuta ($^2J_{\text{PC}} = 15,3$ Hz). *iso*-propil fosfonato talde funtzionalari dagokionez, CH karbonoak bi doblete gisa ikusten dira, $\delta_{\text{C}} = 70,1$ ($^2J_{\text{PC}} = 5,4$ Hz) eta $69,9$

($^2J_{PC} = 5,7$ Hz) ppm-tan, eta metilo diastereotopikoek lau doblete sortzen dituzte $\delta_C = 23,7 - 23,3$ ($^3J_{PC} \approx 4-5$ Hz) ppm tartean. Azkenik, *p*-toluidina eraztuna $\delta_C = 20.4$ ppm-ko metilo seinale baten bidez eta eremu aromatikoko bi seinale sendoekin batera detektatzen da. Eremu berean, *p*-fluorofenil taldea fluor atomoarekiko akoplamendu-konstante desberdinak dituzten lau doblete agertzen dira CH karbono aromatikotarako (33. irudia).

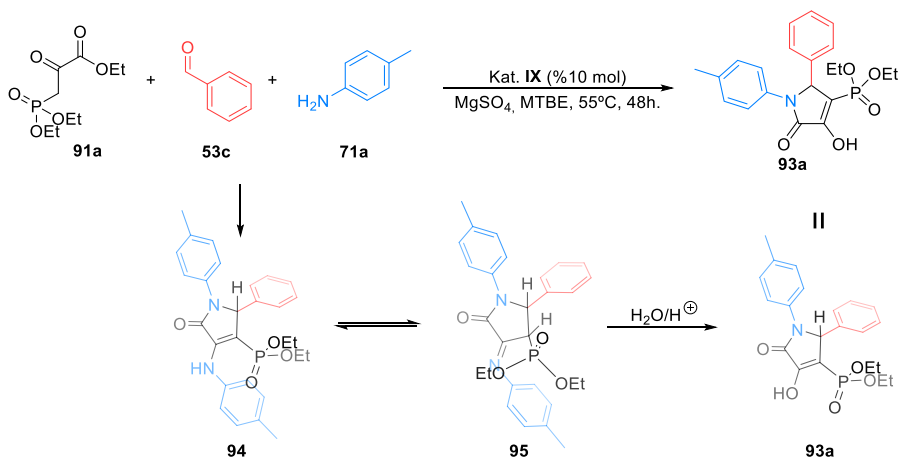
3-Hidroxi γ -laktamaren eta 3-amino γ -laktonaren egituren antzekotasuna eta formula molekular berdina ikusirik, **93j** substratuaren monokristal bat prestatu zen diklorometano/hexanoaren nahasketa batetik abiatuta, eta haren X izpien difrakzioaren bidez, produktuaren egitura zalantzarik gabe argitu ahal izan zen (34. irudia).



34. irudia. 93j konposatuaren elipsoide termalaren/ORTEP irudikapena.

Substratu honen kristal-egituraren ezaugarri nagusiak honako hauek dira: γ -laktama nukleoaren egitura ia laua da, amida zikliko α,β -asegabeak behartua, eta molekularneko hidrogeno-zubi baten presentzia, enolaren hidrogenoaren eta amidaren karbonilo taldearen artekoa, *pseudo* bost kideko eraztun-konfigurazio bat sortuz.

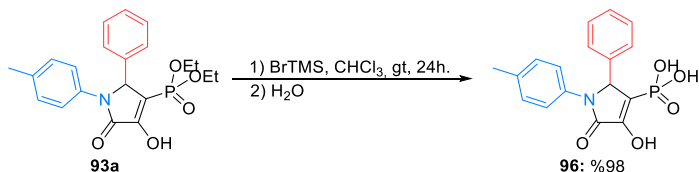
Kasu honetan deribatu enoliken formazio eskusiboa, enamina deribatuen orde, azaldu daiteke C-4 posizioiko bolumen handiko fosforil taldearen presentziagatik, honek bost kideko eraztuneari tentsio nabaria sortzen duelako. Izan ere, egitura heteroziklikoa ia laua da karbonilo taldea eta C=C lotura bikoitz endozikliko konjugatua daudelako, eta horregatik enamina hidrolisi espontaneoan faboratuta dago, **95** imina bitartekaria eratu ondoren. Beraz, enol OH taldearen eraketa bultzatzen da, zeinek fosforo taldearekiko interakzio esteriko txikiagoa erakusten duelako, **94** enamina baino egitura termodinamiko egonkorragoaren formazioa lehenetsiz (21. eskema).



21. eskema. Proposatutako mekanismoa **93a** 3-hidroxi-1,5-dihidro-2*H*-pirrol-2-onaren sintesirako.

Proposatutako mekanismo hau berresteko beste esperimentu batzuk burutu ziren. Adibidez, amina substratuaren baliokide bakar bat erabili zen osagai anitzeko erreakzioan, eta bakarrik enolaren deribatuak diren **93** produktuak lortu ziren, nahiz eta etekin baxuagoekin. Gainera, lehengai gisa alde aurretik prestatutako imina eta enamina espezieak erabiltzen direnean, emaitza berdina lortzen da. Horren arabera, hasieran **94** enamina γ -laktamen sorrera guztiz beharrezkoa da **93** enol deribatuak lortu ahal izateko.

Enol egitura duten **93** γ -laktametatik abiatuta azido fosfonikoaren deribatuak prestatzeko, tratamendu azido edo basikoak erabili ziren, baina huts egin zuten. Berriz, 93a γ -laktama α,β -asegabearen fosfonatoaren hidrolisia trimetilsilil bromuroaz gauzatu zen, eta **96** azido fosfonikoa etekin kuantitaboetan eskuratu zen (22. eskema).



22. eskema. **93a** Fosfonatoaren hidrolisia.

Laburbilduz, kapitulu honetan Brønsted azido bidez katalizatutako osagai anitzeko metodologia bat deskribatzen da fluorra edo/eta fosforoa duten γ -laktama-deribatuen sintesirako. Produktuak 3-hidroxi-1,5-dihidro-2*H*-pirrol-2-ona eran lortzen dira edo haren enamina deribatu moduan, 5 kideko eraztun heterozikloko ordezkatzailen arabera.

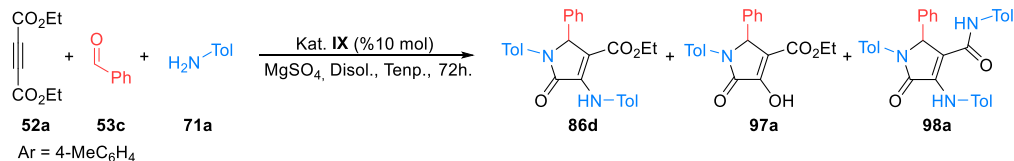
3. Kapitulu

Alkino aktibatuen erabilera osagai anitzeko erreakzioan γ -laktama-deribatuen sintesirako

Arestian aipatu den moduan, literaturan alkino aktibatu, aldehido eta aminen arteko OAE-en hainbat adibide dago γ -laktamen derivatuen sintesirako. Hala ere, guk dakigunez, ez dago azido fosforikoaren organokatalisia erabiltzen duen erreakzio horren adibiderik. Horregatik, **79** iminen gainean pirubatotik eratorritako **78** enaminen adizio nukleozalea sustatzeko **IX** katalizatzaileak duen gaitasuna ongi frogatuta dagoenez (15. eskema, *vide supra*), jarraian Brønsted azido bidez katalizatutako OAE zabaldu egin zen, eta pirubato-esterren ordez dialkil azetilendikarboxilatoak erabiltzea proposatu genuen. Lehenik eta behin, erreakzio-baldintzak optimizatu ziren, eredu gisa dietil azetilendikarboxilato (**52a**), bentzaldehido (**53c**) eta *p*-toluidina (**71a**) erabiliz, BINOL-etik eratorritako **IX** azido fosforikoaren katalizatzailearen presentzian (4. taula).

Hasiera batean, hiru osagaiko erreakzioa BINOL-etik eratorritako **IX** azido fosforikoarekin burutu zen, birfluxuan dagoen diklorometanoa disolbatzaile gisa erabiliz (4. taula, 1. sarrera). Hala ere, erreakzio gordinaren ¹H NMR espektroak iminaren eta enaminaren bitartekarien eraketa baino ez zuen erakutsi. Hauek, **71a** *p*-toluidinak **53c** benzaldehidorekin eta **52a** alkinoarekin erreakzioaren ondorio dira, baina sortutako imina eta enamina bitartekariak beraien artean erreakzionatzeko gaitasunik ez dute. Oso ordezkatuta dauden γ -laktama hauetan eragozpen esteriko handia espero denez, eta gainera, pirubatoaren partez **52a** azetilenodikarboxilatoa erabilita sortzen den enamina bitartekariaren desaktibazio gehigarriarekin batera, erreakzioa tenperatura altuagoetan burutu zen. Antzeko emaitza lortu bazen ere disolbatzaile gisa tetrahidrofuranoa (THF) edo dimetoxietanoa (DME) erabili zirenean (4. taula, 2-3. sarrerak), gure gozamenerako, lehengaien konbertsio osoa hauteman zen metil *tert*-butil etera (MTBE) birfluxuan erabili zenean, eta **86d** enamina derivatutako eta **86d** enola deribaturako γ -laktamak lortu ziren 40:60 proportzioan (4. taula, 4. sarrera).

4. taula. 52a Azetilendikarboxilatoren, bentzaldehidoaren (**53c**) eta *p*-toluidinaren (**71a**) osagai anitzeko erreakzio-baldintzen optimizazioa.



Sarr.	Prop. 52a:53c:71a	Disolbatzailea	T (°C)	Etekin (%) ^a	Prop. 86d:97a:98a ^b
1	1:1:2	CH ₂ Cl ₂	40	0	d.g.
2	1:1:2	THF	65	0	d.g.
3	1:1:2	DME	85	0	d.g.
4	1:1:2	MTBE	55	72	40:60:0
5	3:1:2	MTBE	55	0	d.g.
6	1:1:1	MTBE	55	0	d.g.
7	1:1:2	Dioxano	101	81	80:0:20
8	1:1:2	Tolueno	110	77	95:0:5
9	1:1:4	Tolueno	110	82	92:0:8

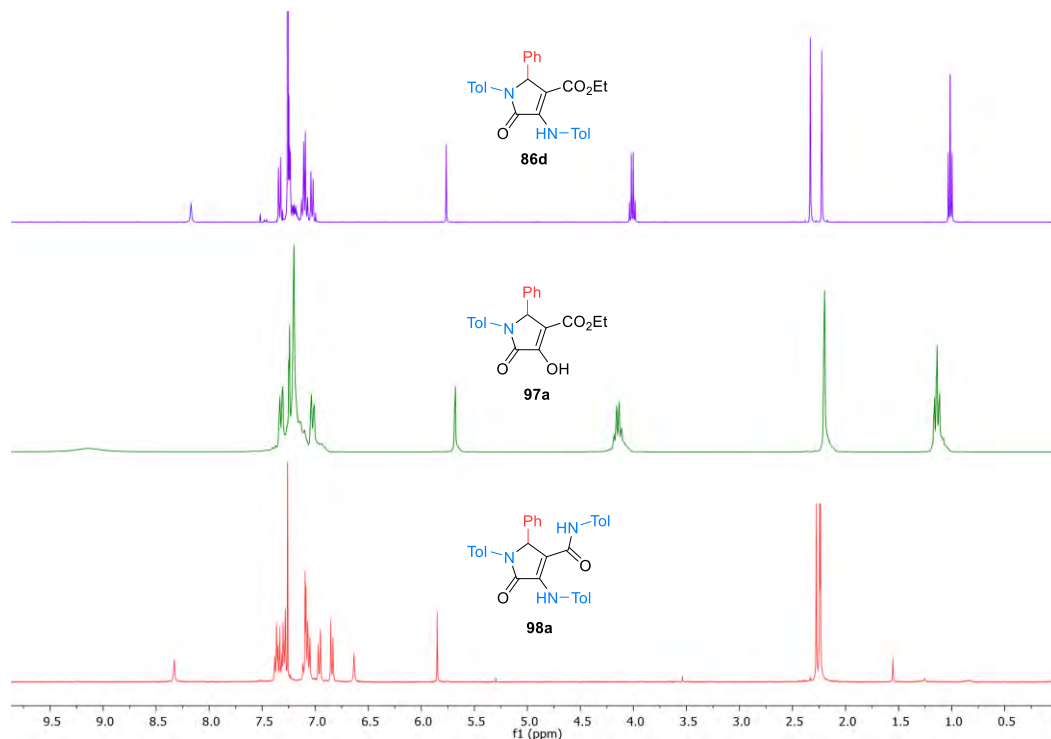
^aIsolatu etekin totala. ^b¹H EMN bidez zehaztuta.

Etil pirubatoarekin egiten de osagai anitzeko erreakzioan, zetoester substratuaren soberakina erabiltzeak, erreakzio-denborak eta tenperaturak murrizteko eraginkorra izan zela frogatu zen. Hala ere, kasu honetan, azetileno dikarboxilatoaren (**52a**) hiru baliokide erabili zirenean, **86d** edo **97a** γ -laktama α,β -asegabe deribatuen arrastorik ez zen detektatu, **71a** aminak agortzeraino erreakzionatu baitzuen dietil dicarboxilatoarekin (**52a**) (4. taula, 5. sarrera). Arrazoi beragatik, *p*-toluidinaren (**71a**) baliokide bakarra baliatu zenean, erreakzioak ez zuen funtzionatu (4. taula, 6. sarrera).

Enamina talde funtzionala duen **86d** γ -laktama eskuratzeko selektibitate handiagotu egin zen erreakzioa dioxanon eta 101 °C-tan burutu zenean, baina kasu honetan, **86d** produktua amida talde funtzionala duen **98a** substratuarekin batera lortu zen (4. taula, 7. sarrera). Hala ere, erreakzioaren selektibitatea are gehiago hobetu zen erreakzio-disolbatzaile gisa tolueno birfluxuan erabili zenean, eta **86d** enamina-deribatutako γ -laktama eskuratu zen, **98a** amida deribatu-kantitate oso txikiarekin (%5) (4. taula, 8. sarrera). Bitxia bada ere, *p*-toluidinaren (**71a**) lau baliokideren erabilerak ez zuen sortu **98a** amida-deribatua produktu nagusi gisa (4. taula, 9. sarrera).

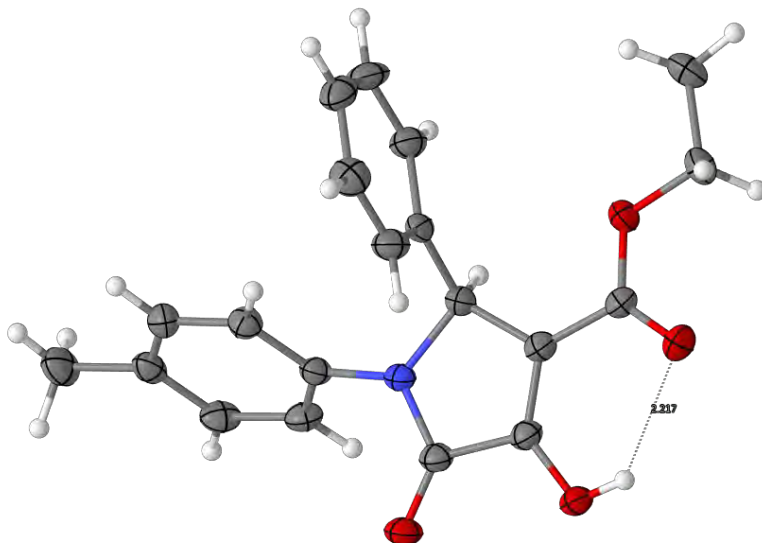
Erreakzioan lortutako hiru substratuak isolatu ondoren, EMN eta IR espektroskopia eta HRMS bidez karakterizatu ziren guztiz. Produktuen ¹H EMN espektroak 35. irudian ageri dira pilatuta, eta, hainbat desberdintasun nabarmen daitezke. Enamina eta etil karboxilatoa dituen **86d** γ -laktamaren seinalerik adierazgarrienak, karbono asimetrikoko protoiari dagokion singletea ($\delta_H = 5,76$ ppm-tan), enamina NH-ren protoiaren singletea, D₂O-rekin trukutzen dena, $\delta_H = 8,17$ ppm-tan, eta bi *p*-tolil taldeei

dagozkien bi singlete zorrotzak ($\delta_H = 2,33$ and $2,22$ ppm). Ordea, enola eta etil karboxilatoa dituen **97a** γ -laktamaren karbono asimetrikoko protoia eremu altuagoan ($\delta_H = 5,69$ ppm) ageri da, **86d** konposatuarekin alderatuz gero. Gainera, $\delta_H = 9,12$ ppm-ko singlete zabala OH taldeari dagokio, eta *p*-tolil taldearen seinale bakarra baino ez dago ($\delta_H = 2,21$ ppm) **97a** konposatuaren espektroan. Bi substratuek, **86d** eta **97a**-k, etoxi talde baten tipikoak diren A_2X_3 seinale-sistema adierazgarria erakusten dute. Enamina eta amida egiturak dituen **98a** deribatuaren espektroari dagokionez, berriz, karbono asimetrikoko protoiaren seinalea singlete gisa ageri da beste bi konposatuetan baino eremu baxuagoan ($\delta_H = 5,85$ ppm). Halaber, bi NH protoiak singlete zabal moduan ikus daitezke $\delta_H = 8,33$ eta $6,63$ ppm-tan, eta biak trukagarriak dira D_2O -rekin. Etoxi frakzioari dagozkion seinalerik ezak, eta $\delta_H = 2,28$, $2,24$ eta $2,23$ ppm-ko hiru seinale sendoek, argi uzten dute egitura hirugarren *p*-toluidina molekula bat txertatu dela (35. irudia).



35. irudia. **86d**, **97a** eta **98a** konposatuen 1H EMN espektroen konparaketa.

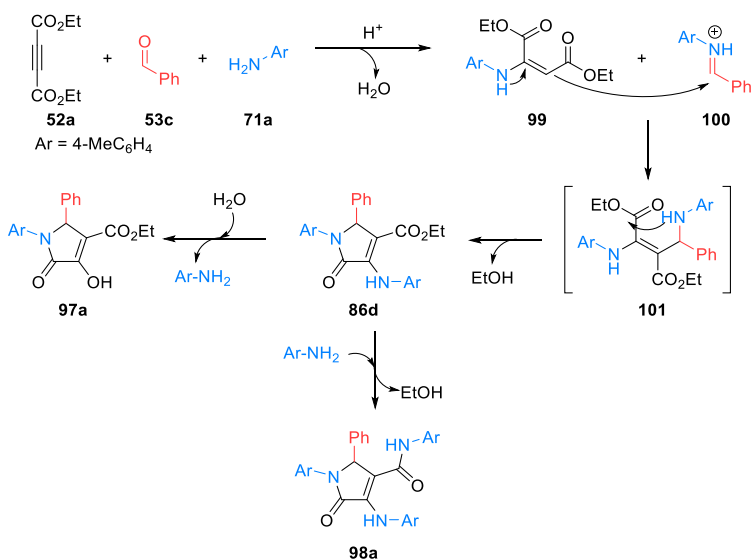
Lortutako γ -laktama-deribatu guzti hauen egitura antzekotasuna dela eta, erreakzioaren produktu minoritarioaren egitura zalantzarik gabe zehazteko, enola duen **97a** substratoaren monokristala prestatu zen, eta haren X-izpien difrakzio-egitura lortu zen (36. irudia).



36. irudia. 97a γ -laktamaren X-izpien bidezko egitura.

Enol deribatua den **97a** γ -laktamaren kristal-egituraren ezaugarri bereizgarrienak honako hauek dira: bost-kideko eraztunaren forma ia laua, eta hidrogeno-zubi baten presentzia (36. Irudia). Aurreko kapituluko **93j** enol γ -laktaman hidrogeno-lotura amidaren karboniloarekin sortzen den bitartean, **97a** konposatu honetan, enolaren hidrogenoaren eta karboxilato taldearen artean gertatzen da, sei kideko pseudo eraztun-konfigurazioa eratuz (34. irudia, *vide supra*).

Pirubatoekin gertatzen den erreakzioaren antzera, erreakzio-mekanismoa *p*-toluidinak (**71a**) egindako aldibereko adizioarekin has daiteke, bai dietil azetilendikarboxilatoari (**52a**) eta bai bentzaldehidoari (**53c**) ere, **99** enamina eta **100** aldimina eratuta, hurrenez hurren (23. eskema). Gero **101** aduktua sortu ahal da Mannich-en erreakzio baten bidez. Ondoren, **101** bitartekariaren amina eta karboxilato funtzioen arteko molekula barneko ziklazioaren ondorioz, **86d** γ -laktama sortzen da. Gainera, erreakzio-ingurunean ura badago, **86d** substratuaren enamina taldearen hidrolisia gerta daiteke, eta enola duen **97a** γ -laktama eratu. Izan ere, proposamen mekanistiko honen sostengu moduan, irakite-puntu altuko disolbatzaileak erabiliz gero, ez da **97a** substratua sortzen, ura lurruntzen delako eta horrek enamina hidrolisia saihesten duelako. Bestalde, erreakzio nahastean soberako amina badago, *p*-toluidinak (**71a**) etanola desplazatuko du eta amida egitura duen **98a** deribatua sortuz.



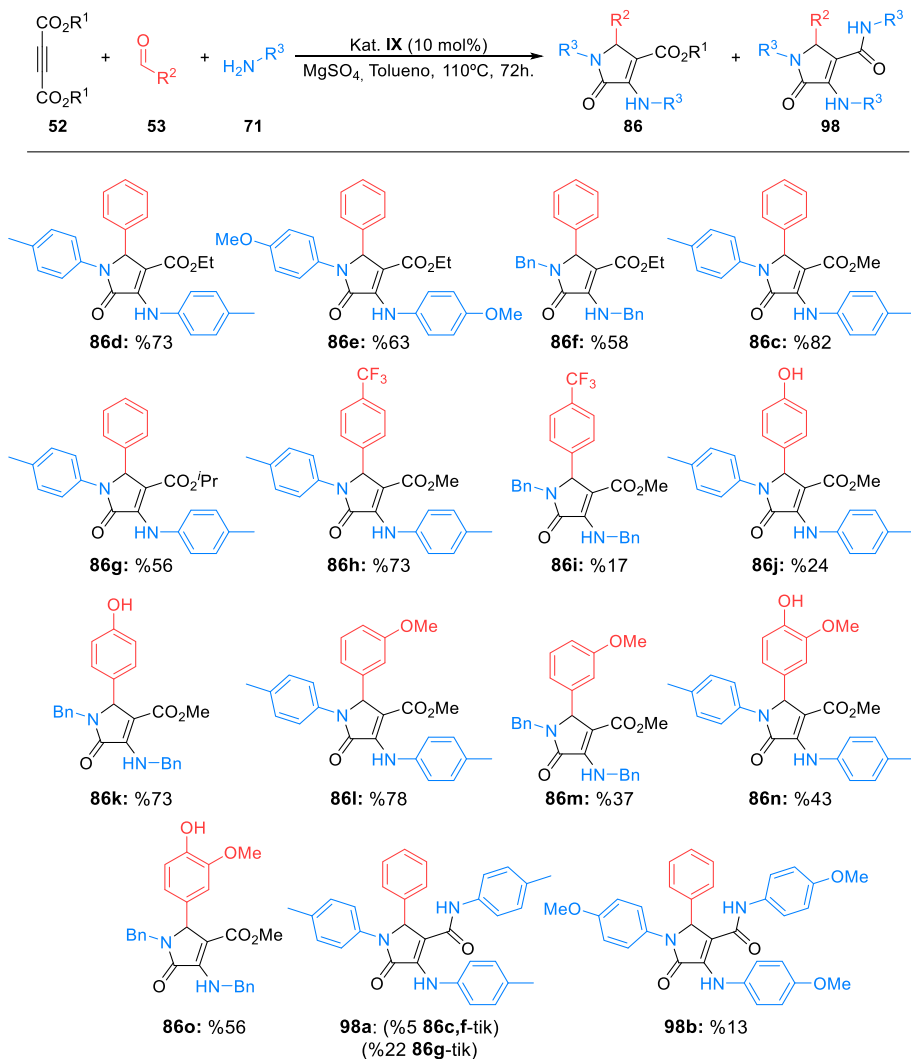
23. eskema. Etil azetilenedikarboxilato (**52a**), bentaldehido (**53c**) eta *p*-toluidinaren (**71a**) osagai anitzeko erreakzioarako proposatutako mekanismoa.

Behin osagai anitzeko protokoloaren baldintzak ezarrita, ondoren, erreakzioa γ -laktama α,β -asegabe ezberdinen sorta bat prestatzera hedatu zen (6. zerrenda).

Lehenik eta behin, hainbat **71** amina desberdin erabili zen, bentaldehido (**53c**, $R^2 = Ph$) eta dietetil azetilendikarboxilatorekin (**52a**, $R^1 = Et$) batera. Elektroitan aberatsak diren anilinak edo amina alifatikoak erabiltzean, hala nola, *p*-anisidina (**71b**, $R^3 = 4-CH_3OC_6H_4$) edo bentzilamina (**71i**, $R^3 = Bn$), **86e** eta **86f** konposatuak lortu ziren, etekin baxuagoarekin, **86d** produktua sortzen duen eredu-erreakzioarekin alderatuta (6. zerrenda). Ordea, elektroitan urriak diren amina aromatikoak lehengai gisa erabili zirenean, hala nola, *p*-nitroanilina edo *p*-trifluorometilanilina, **100** imina eta **99** enamina bitartekarien eraketa EMN bidez hauteman zen arren, erreakzioak ez zuen aurrera egin.

Aipatu behar da, erreakzio horretarako proposatutako mekanismoa ikusita (23. eskema, *vide supra*), substratu aminikoaren izaera elektronikoa funtsezko faktorea izan daitekeela osagai anitzeko prozesuaren gako-urratsaren errektibotasunean. Horren ondorioz, elektroitan aberatsak diren aminak erabilita, **99** enamina espeziearen izaera nukleozaleari mesede egin diezaiokeen bitartean, honek **100** imina espeziearen izaera elektroizalea murriztuko luke. Aldiz, amina desaktibatua erabiliz gero, **100** iminaren izaera elektroizalea hobetuko baten ere, aldi berean **99** enamaren izaera nukleozalea kaltetuko litzateke. Portaera honek azaldu dezake *p*-anisidina (**71b**) erabili zenean lortutako etekina *p*-toluidina (**71a**) erabiltzean baino txikiagoa izatea, eta, gainera, amida talde

funtzionala duen **98b** albo-produktuaren kantitate handiagoak sortzean (proportzioa **86e:98b** 70:30), **86e** deribatuaren etekina ere murriztuko litzateke.



6. zerrenda. **52** Dialkil azetilenodikarboxilato, **53** aldehido eta **71** aminen hiru osagaien erreakzioaren irismena.

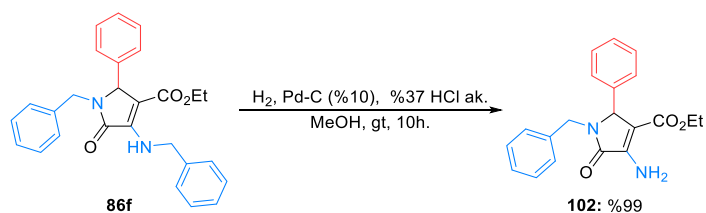
Ondoren, zenbait **52** azetilenodikarboxilato desberdin ikertu ziren osagai anitzeko erreakzioan substrato elektroizale gisa, *p*-toluidina (**71a**) eta bentzaldehidoa (**53a**) erabilia. Dietil azetilenodikarboxilato (**52a**, $\text{R}^1 = \text{Et}$) erabiltzen denean ikusitakoaren antzera, dimetil azetilenodikarboxilatoarekin (**52b**, $\text{R}^1 = \text{Me}$), **86c** γ -laktama eskuratu zen etekin onean, amida-deribatua den **98a** γ -laktamaren kantitate txiki batekin batera (%5) (6. zerrenda). Ordea, bolumen handiagoko di-*iso*-propil azetilenodikarboxilatoa (**52c**, $\text{R}^1 = i\text{Pr}$) lehengaia denean, erreakzio-

denbora luzeagoak behar izan ziren (72 ordu), eta horrek **98a** amida alboko produktuaren eraketa erraztu zuen (**86g:98a** 70:30 proportzioa), *p*-toluidina (**71a**) eta **86g** γ -laktama denbora luzeagoan kontaktuan egotearen ondorioz.

Azkenik, erreakzioaren dibertsitatea aldehido desberdinetara zabaldu zen, dimetil azetilenodikarboxilato (**52b**, $R^1 = \text{Me}$) elektroizale gisa erabiliz, eta *p*-toluidina (**71a**) edo bentzilamina (**71i**) amina erreaktiboekin batera. Osagai anitzeko erreakzioan elektroitan urria den *p*-trifluorometil bentzaldehidoa (**53i**, $R^2 = 4\text{-CF}_3\text{C}_6\text{H}_4$) erabiltzeak, **100** imina bitartekari elektroizaleagoa ematen du, erreaktibotasuna areagotuz Mannich bitarteko urratsean. Izan ere, *p*-toluidina (**71a**) erabiltzean, **86h** γ -laktama etekin onean lortu zen amida albo-produkturik gabe. Hala ere, bentzilaminarekin (**71i**) burututako erreakzioak **99** enamina bitartekari nukleozaleagoa sortzen badu ere, kasu konkretu honetan **86i** γ -laktama etekin apalean baino ez da lortzen, **100** *N*-bentzilimina bitartekariaren izaera elektroizale txikiagoaren ondorioz. Aitzitik, Mannich tarteko erreakzioa defaboratua egotea espero behar da talde elektroizale indartsuak dituzten aldehidoak erabiltzean, izaera elektroizale ahulagoa duten **100** iminak sortzen direlako. Hortaz, osagai anitzeko erreakzioan *p*-hidroxibentzaldehidoa (**53t**, $R^2 = 4\text{-HOC}_6\text{H}_4$) eta *p*-toluidina (**71a**) erabiliz gero, **86j** γ -laktama eratzen da etekin apalean, **100** *N*-arilimina bitartekariaren izaera elektroizale eskasagoaren ondorioz. Hala ere, erreakzioa berdina bentzilaminarekin (**71i**) burutu zenean, **86k** γ -laktama deribatua sortu zen etekin onean, izan ere, **99** enamina bitartekariaren izaera nukleozalea handitzeak Mannich erreakzioa aurrera bideratzen duela dirudi, eta **100** *N*-bentzilimina espezierako aurreikus daitekeen elektroizaletasunaren murrizketa gaindituz.

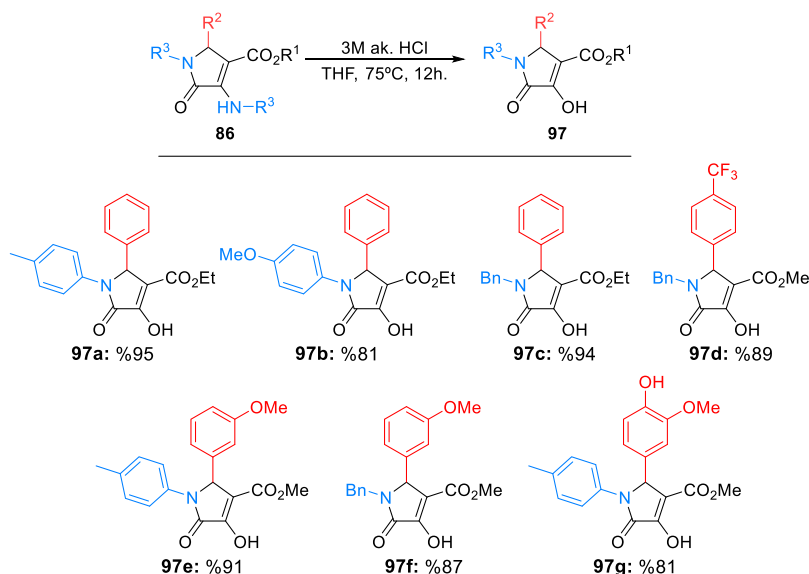
Erreaktibitatearekin behatutako joerekin bat, *m*-anisaldehidoak (**71u**, $R^2 = 3\text{-MeOC}_6\text{H}_4$) bentzaldehidoaren (**53a**) antzeko emaitzak eman zituen, eta *p*-toluidinatik eratorritako **86l** γ -laktama oso etekin onean lortu zen, baina erreaktibotasun txikiagoa antzeman zen bentzilaminatik eratorritako **86m** γ -laktamarako. Azkenik, erreakzioaren irismenaren azterketarekin bukatzeko, bi ordezkatzaila dituen banilina (**53v**, $R^2 = 3\text{-MeO-4-HO-C}_6\text{H}_3$) erabili zen, eta **86n-o** γ -laktamak etekin ertain eta onekin lortu ziren.

Bentzilaminatik eratorritako produktuen transformazio sinple bat, nitrogeno atomoetan dauden talde bentzilikoaren eliminazioa da. Hortaz, **86f** γ -laktamaren enamina talde funtzionalaren bentzilo taldea hidrogenolisi bidez selektiboki kendu zen, 80 psi-ko H_2 atmosferan, metanolean eta %10 mol paladio-karbonoaren presentzian, eta **102** γ -laktama-deribatua isolatu zen etekin kuantitatiboan (24. eskema). Harrigarria bada ere, baldintza horietan, bi talde bentzilikoetako bat baino ez da eliminatzen, eta gainera, bost kideko zikloko lotura bikoitza ez da erreduzitzen.



24. eskema. 86f bentzil-deribatuaren desbabespen-erreakzioa.

γ -Laktama-deribatuaren aniztasun molekularra hedatzeko, beste transformazio simple bat da enamina talde funtzionalaren hidrolisia burutzea, enola eskuratzeko asmoarekin. Hortaz, enolaren deribatu diren **97** γ -laktamak sintetizatu ahal izan ziren etekin bikainetan, **86** substratuen HCl urtsuaren tratamenduaren bidez (7. zerrenda).



7. zerrenda. 86 3-amino-1,5-dihidro-2H-pirrol-2-onen hidrolisia.

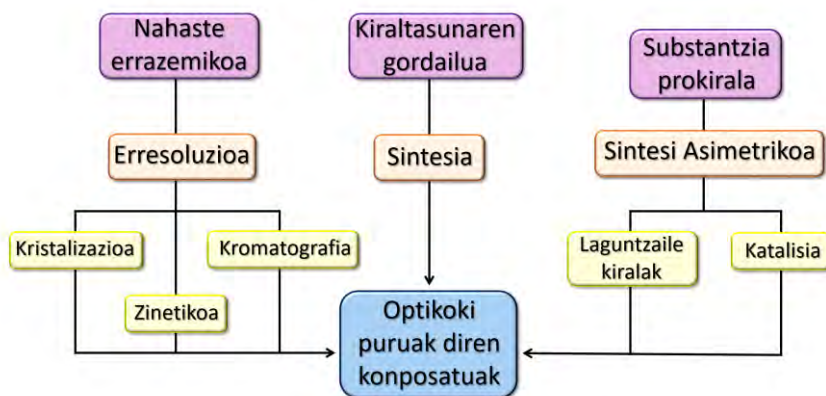
Laburbilduz, kapitulu honetan Brønsted azidoarekin katalizatutako dialkil azetilendikarboxilato, amina eta aldehido aromatikoaren osagai anitzeko prozedura bat deskribatzen da, 3-amino 1,5-dihidro-2H-pirrol-2-onak prestatzeko. Guk dakigunez, hau da erreakzio honetarako azido fosforikoak katalizatzaile gisa erabili den lehen adibidea. Gainera, orain arte ere ez da deskribatu enamina duten **86** substratuen hidrolisia enol deribatuak diren **97** 1,5-dihidro-2H-pirrol-2-onak lortzeko.

4. Kapitulu

γ -Laktamen osagai anitzeko sintesi enantioselektiboa

Talidomidaren ezbeharraren berriro gertatzea saihesteko,¹⁵⁵ farmazia-industriak eta medikamentuen ekoizpena arautzen dituzten agentzia gehienek, enantiomerikoki puruak diren molekulen sintesia ezarri dute haien lehentasun sintetikoaren artean. Horren arabera, optikoki puruak diren molekula kiralak lortzeko metodologia sintetiko berriak garatzea interes handiko helburua da kimika organikoan.

Substratu kiralaren sintesia burutzeko, protokolo konbentzionalak erabiltzean, normalean nahaste errazemikoak lortzen dira. Hala ere, azken hamarkadetan, enantiomerikoki aberastutako konposatuak sintetizatzeko metodologia-eskaera gero eta handiagoa denez, ez bakarrik laborategi-eskalan, industria-mailan ere,¹⁵⁶ interesa areagotu da optikoki puruak diren molekula sortuko dituzten estrategien garapenean (37. irudia).



37. irudia. Optikoki puruak diren molekula sintetizatzeko metodoak.

¹⁵⁵ Therapontos, C.; Erskine, L.; Gardner, E. R.; Figg, W. D.; Vargesson, N. *Proc. Natl. Acad. Sci.* **2009**, *106*, 8573-8578.

¹⁵⁶ (a) Núñez, M. C.; García-Rubiño, M. E.; Conejo-García, A.; Cruz-López, O.; Gallo, M. A.; Espinosa, A.; Campos, J. M. *Curr. Med. Chem.* **2009**, *16*, 2064-2074. (b) Collins, A. N.; Sheldrake, G. N.; Crosby, J. In *Chirality in industry: The commercial manufacture and applications of optically active compounds*. John Wiley & Sons, 1992.

Metodorik klasikoena, eta industrian gehien erabiltzen den metodoetako bat, errazematoen erresoluzioa da, hots, nahasketa errazemiko baten bi enantiomeroak bereiztea. Prozedura nagusienak kristalizazio-bidezko erresoluzioa, kromatografia kiralaren bidezko erresoluzioa, erresoluzio zinetikoa eta erresoluzio zinetiko-dinamikoa dira.¹⁵⁷ Jakina, teknika horiek erabiliz lor daitekeen prozesu globalaren etekin maximoa %50-ekoa da, salbu erresoluzio zinetiko-dinamikoaren bidez.¹⁵⁸ Azken kasu honetan, batzuetan enantiomero bakarra lor daiteke etekin kuantitatiboan.

Kiraltasunaren gordailu edo erreserba (*Chiral pool*) izeneko estrategia, konposatu optikoki puruak lortzeko beste metodologia bat da. Honetan, optikoki puruak eta merkeak diren konposatu naturalak erabiltzen dira abiapuntu gisa, hala nola, aminoazidoak, terpenoak, azukreak edo alkaloideak, helburu den produktu kiralaren enantiomero bakarraren sintesirako. Konposatu bioaktibo sinpleak eskala handian lortzeko oso teknika eraginkorra bada ere, estrategia honek desabantaila batzuk ditu beste teknika batzuekin alderatuta, esaterako, konposatu bakoitzerako sintesi bide bat diseinatu behar da, lehengaien eskuragarritasunarekiko mendekotasuna eta erreazio-baldintza batzuetan karbono estereogenikoaren errazemizazioaren arriskua. Hala ere, oraindik oso estrategia erabilgarria da interes biologikoa duten konposatu batzuen sintesirako, adibidez, Taxol® edo ingenol.¹⁵⁹

Sintesi asimetrikoa enantiomerikoki puruak diren konposatuak lortzeko hirugarren estrategia bat da,¹⁶⁰ non erreazio estereokontrolatuak erabiltzen diren enantiomerikoki aberastutako produktuak zuzenean lortzeko. Bi planteamendu ezberdin har daitezke kontuan:

- **Laguntzaile kiralen erabilera (metodologia diastereoselektiboak):** Nahiz eta teknika honek erreazioaren estereoselektibitatea eraginkortasunez kontrolatzeko aukera ematen duen, beharrezkoa da sintesi bideari beste bi urrats gehitzea, bata laguntzaile kirala lehengaiari txertatzeko, eta bestea, hau kentzeko. Gainera, laguntzaile kiralaren kantitate estekiometrikokoak behar izateaz gain, ideala izango litzateke hau berreskuratzea eta birziklatuko balitz.

¹⁵⁷ Some reviews about racemate resolution: (a) Faigl, F.; Fogassy, E.; Nógrádi, M.; Pálovics, E.; Schindler, J. *Tetrahedron Asymmetry* **2008**, *19*, 519-536. (b) Anderson, N. G.; Solutions, P.; Lane, G.; Jackson, V. *Org. Process Res. Dev.* **2005**, *9*, 800-813. (c) Vedejs, E.; Jure, M. *Angew. Chem. Int. Ed.* **2005**, *44*, 3974-4001.

¹⁵⁸ Pellissier, H. *Tetrahedron* **2008**, *64*, 1563-1601.

¹⁵⁹ Brill, Z. G.; Condakes, M. L.; Ting, C. P.; Maimone, T. J. *Chem. Rev.* **2017**, *117*, 11753-11795.

¹⁶⁰ (a) Hughes, D. L. Introduction to industrial applications of asymmetric synthesis. In *Comprehensive Chirality*; Elsevier Science, 2012, pp 1-26. (b) Farina, V.; Reeves, J. T.; Senanayake, C. H.; Song, J. J. *Chem. Rev.* **2006**, *106*, 2734-2793.

- **Metodo katalitiko asimetrikoak:** Metodologia hauek biokatalisia,¹⁶¹ katalisi metalikoa¹⁶² eta organokatalisia¹⁶³ hartzen dituzte bere baitan. Teknika hauetan, induktore kiral baten kantitate azpiestekimetroko bat katalizatzaile gisa erabiltzen da, enantiomerikoki aberastutako substratuak zuzenean lortzeko. Metodologia hauen erabilerak abantaila batzuk ditu, hala nola fabrikazio-prozesuek ingurumenean duten inpaktua txikiagotu, urrats sintetikoaren kopurua murriztean, beharrezkoak diren erreaktiboen kantitateak gutxitu, eta hondakinen produkzioa murriztu.¹⁶³

Metodologia enantioselektiboek beste batzuen aldean dituzten abantaila nabariak direla eta, ahalegin handiak egin dira azken hamarkadetan protokolo enantioselektibo berriak garatzeko, enantiomerikoki aberastutako γ -laktama-deribatuek prestatzeko. Hala ere, deskribatutako protokolo gehienak zenbitu etapatan egiten diren sintesiak dira, eta osagai anitzeko erreakzio enantioselektibo berruzko bibliografia oraindik urria da.¹⁶⁴

Tesi honetan ikertutako hiru osagairen erreakzioaren bidez, bi kasutan bakarrik prestatu dira, orain arte, γ -laktamak soberakin enantiomerikoekin, eta bietan oso emaitza apalekin. Lehenik eta behin, 2008-an, Cheng eta Luo-k **72** 3-amino-1,5-dihidro-2H-pirrol-2-onen sintesi enantioselektiboa deskribatu zuten, BINOL-etik eratorritako **X** azido fosforiko katalizatzaile kirala erabiliz (%10 mol) (38. irudia). Autore horiek hiru osagairen erreakzioa burutu zuten etil pirubato (**70a**), bentzaldehido (**53c**) eta *p*-anisidina (**71b**) 3:1:2 proportzioan nahastuz giro-tenperaturan, eta toluenoan, **84b** γ -laktama asegabea eskuratuz %77-ko etekinarekin eta %44-ko soberakin enantiomerikoarekin.¹⁶⁵ Beranduago, 2013. urtean, Huang-ek eta Luok beste adibide bat argitaratu zuten, metil pirubato (**70b**), *tert*-butil glioxalato (**53t**) eta *p*-anisidina (**71b**) 1:1:2 erlazioan erabiliz, **XI** katalizatzailearekin (%5 mol) batera, toluenon eta giro tenperaturan, eta **84n** γ -laktama asegabea lortu zuten %90-eko etekinarekin eta %72-ko soberakin enantiomerikoarekin (38. irudia).¹⁶⁶

¹⁶¹ Wells, A. Industrial applications of biocatalysis: An overview. In *Comprehensive Chirality*; Elsevier Science, 2012, pp 253-287.

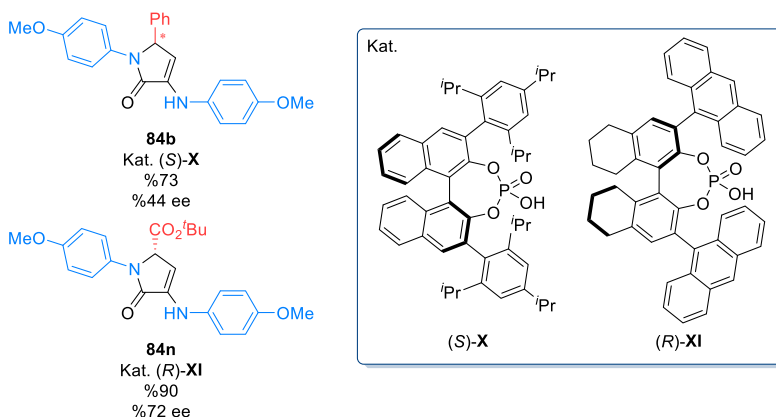
¹⁶² For more information see: (a) Ager, D. J.; de Vries, J. G. Industrial applications of asymmetric reduction of C=C Bonds. In *Comprehensive Chirality*; Elsevier Science, 2012, pp 73-82. (b) Komiyama, S.; Shimizu, H.; Nagasaki, I. Industrial application of the asymmetric reduction of C=O and C=N bonds, including enamides and enamines. In *Comprehensive Chirality*; Elsevier Science, 2012, pp 83-103. (c) Wu, G. G.; Chen, F. X.; Yong, K. Industrial applications of metal-promoted C-C, C-N, and C-O asymmetric bond formations. In *Comprehensive Chirality*; Elsevier Science, 2012, pp 147-208.

¹⁶³ Bulger, P. G. Industrial applications of organocatalysis. In *Comprehensive Chirality*; Elsevier Science, 2012, pp 228-252.

¹⁶⁴ del Corte, X.; Maestro, A.; Martínez de Marigorta, E.; Palacios, F.; Vicario, J. In *Targets in Heterocyclic Systems 22*; Società Chimica Italiana, 2022, pp 22-52.

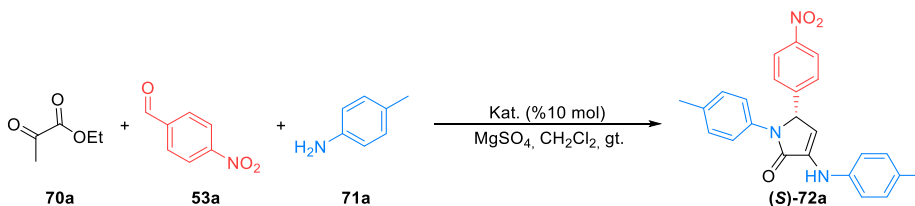
¹⁶⁵ Li, X.; Deng, H.; Luo, S.; Cheng, J. P. *Eur. J. Org. Chem.* **2008**, 25, 4350-4356.

¹⁶⁶ Luo, C.; Huang, Y. *J. Am. Chem. Soc.* **2013**, 135, 8193-8196.



38. iruida. Enantiomerikoki aberastutako **84** 3-amino-1,5-dihidro-2*H*-pirrol-2-ona lortuak.

Aurrekari horietatik abiatuta, eta Brønsted azido katalizatzaileek pirubato, aldehido eta aminen arteko hiru osagaien erreakzioa sustatzeko gaitasuna kontuan hartuta, jarraian, erreakzio horren enantioselektibitate altuko bertsioa garatzeko ahaleginak egin ziren, optikoki puruak diren γ -laktama α,β -asegabeak prestatzeko. Horren ondorioz, osagai anitzeko erreakzioa katalizatzaile kiralen presentzian eta diklorometanoan aztertu zen, etil pirubato (**70a**), bentaldehido (**53c**) eta *p*-toluidinaren (**71a**) arteko erreakzioa eredu gisa erabiliz (25 eskema).



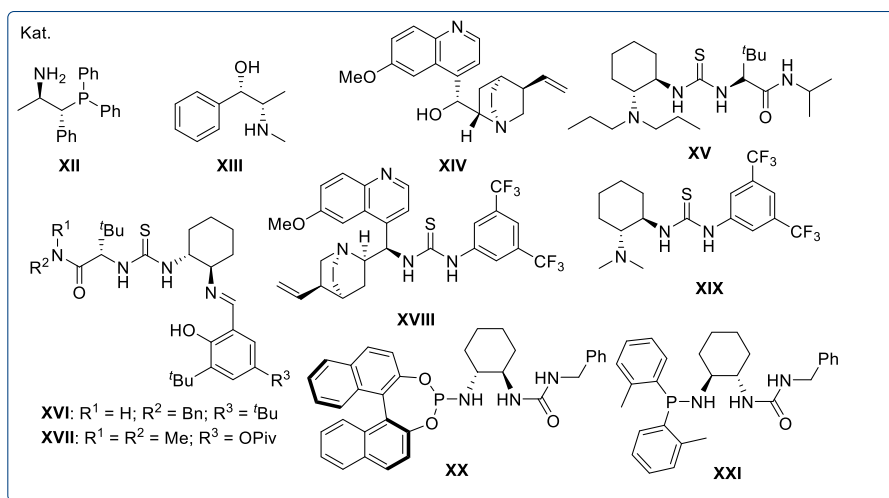
25. eskema. Osagai anitzeko erreakzio enantioselektiboa optimizatzeke eredu-erreakzioa.

Ikerketa honen lehen etapan, zenbait organokatalizatzaile-familia erabili ziren (39. irudia). Lehenik eta behin, erreakzioa katalizatzaile gisa %10 mol aminofosfina **XII**-arekin egin zen, baina enamina eta imina bitartekarien nahasteak soilik eman zuen, eta ez zen hauteman γ -laktamaren formaziorik (5. taula, 1. sarrera). Erreakzioak ere ez zuen arrakastarik izan **XIII** eta **XIV** aminoalkoholak katalizatzaile gisa erabili zirenean (5. taula, 2-3. sarrerak). Ondoren, **XV-XIX** tiourea egitura duten katalizatzailearen erabilera ebaluatu zen (7. taula, 4-8. sarrerak), eta konbertsio moderatua erakutsi zuten arren, **XVIII** eta **XIX** espezieekin soberakin enantiomeriko txikiak neurtu ahal izan ziren (7. taula, 7-8. sarrerak). Gainera, osagai anitzeko erreakzioa oso konbertsio txikian gertatu zen **XX** fosoramidito-urea katalizatzaileak erabili zenean (5. taula, 9. sarrera), eta ez zen inolako erreakziorik hauteman **XXI** fosfinamida-urearekin (5. taula, 10. sarrera).

5. taula. Eredu-erreakzioan erabilitako aminofosfina, aminoalkohol, tiourea, fosforamidito-urea eta fosfinamide-urea egitura duten katalizatzaileak.

Sarr.	Kat.	Konb. (%) ^a	ee (%)	Sarr.	Kat.	Konb. (%) ^a	ee (%)
1	XII	Err. Ez.	-	6	XVII	Err. Ez.	-
2	XIII	Err. Ez.	-	7	XVIII	82	3
3	XIV	Err. Ez.	-	8	XIX	80	14
4	XV	Err. Ez.	-	9	XX	12	1
5	XVI	Err. Ez.	-	10	XXI	Err. Ez.	-

^a ¹H EMN bidez zehaztuta.

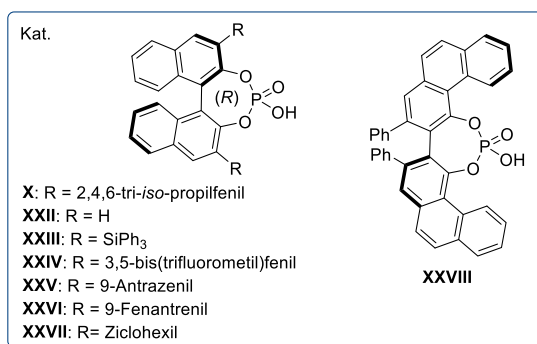


39. irudia. XII-XXI katalizatzaileen egitura.

Behin **XII-XXI** katalizatzaileak baztertuta, BINOL-aren deribatueiko azido fosforikoak aztertu ziren (40. irudia). Ordezkatzaileak ez duen **XXII** BINOL katalizatzailea eraginkorra zen erreakzioa katalizatzen, baina ez zen soberakin enantiomeriko nabarmenik eragin (6. taula, 1. sarrera). Aitzitik, trifenilsilil eta 2,4,6-tri-*iso*-propilfenil ordezkatzailak dituzten **XXIII** eta **X** katalizatzaileek eraginkortasuna frogatu zuten, erreakzioa katalizatuz eta gainera enantioselektibitate onak emanez (%67 eta %61, hurrenez hurren) (6. taula, 2-3. sarrerak). Osagai anitzeko erreakzioa modu eraginkorrean aurrera egin zuen ere 3,5-bis(trifluorometil)fenil, 9-antrazenil eta 9-fenantranil ordezkatzailak dituzten **XXIV-XXVI** azido fosforikoekin, hala ere, enantiokontrola oso eskasa izan zen (%3-11) (6. taula, 4-6. sarrerak). Ziklohexil ordezkatzaila duen BINOL-aren eratorritako **XXVII** katalizatzailearen erabilerak soberakin enantiomeriko moderatua eman bazuen ere, **XXIII** eta **X** katalizatzaileekin lortutakoa oraindik hobea izan da (6. taula, 7. sarrera vs. 2-3. sarrerak). Azkenik, VAPOL-aren deribatutako **XXVIII** katalizatzailearen erabilerak ere konbertsio bikaina erakutsi zuen arren, ez zen enantiokontrol esanguratsurik ikusi (6. taula, 8. sarrera).

6. taula. Eredu-erreakzioan erabilitako BINOL-aren eta VAPOL-aren deribatutako azido fosforikoak.

Sarr.	Kat.	Konb. (%) ^a	ee (%)	Sarr.	Kat.	Konb. (%) ^a	ee (%)
1	XXII	100	1	5	XXV	100	3
2	XXIII	100	67	6	XXVI	100	11
3	X	100	61	7	XXVII	100	45
4	XXIV	100	5	8	XXVIII	100	2

^a ¹H EMN bidez zehaztuta.**40. irudia.** BINOL-aren eta VAPOL-aren deribatutako X, XXII-XXVIII katalizatzaileen egitura.

Osagai anitzeko erreakzio enantioselektiboa burutzeko egokienak diren katalizatzaileak identifikatu ostean, erreakzioaren enantioselektibitatean disolbatzaileak duen eragina aztertu zen ondoren. Hortaz, katalizatzaile eraginkorrena, **XXIII** azido fosforikoa, erabili zen, eta eredu-erreakzioa disolbatzaile ezberdinetan burutu zen. Translazio elektronikoaren energia molar normalizatuak (*Normalized molar electronic translation energies*) (E_T^N)¹⁶⁷ erabili dira disolbatzaileen polarizteraren adierazle gisa. Lortutako soberakin enantiomerikoak 7. taulan daude laburtuta.

7. taula. Disolbatzailearen optimizazioa hiru osagairen eredu-erreakzioan.

Sarr.	Disol.	E_T^N	Konb. (%) ^a	ee (%)	Sarr.	Disol.	E_T^N	Konb. (%) ^a	ee (%)
1	CCl ₄	0.052	90	68	8	CHCl ₃	0.259	100	35
2	Toluene	0.099	100	82	9	CH ₂ Cl ₂	0.309	100	67
3	<i>i</i> Pr ₂ O	0.105	100	78	10	Cl(CH ₂) ₂ Cl	0.327	100	52
4	Et ₂ O	0.117	100	96	11	DMF ^b	0.386	0	-
5	MTBE	0.124	100	85	12	MeCN	0.460	100	89
6	THF	0.207	100	58	13	MeOH ^b	0.762	0	-
7	DME	0.231	100	66	14	CH ₂ Cl ₂ :Et ₂ O (10:1)	-	100	90

^a ¹H EMN bidez zehaztuta. ^b24 orduz irabiatuta.¹⁶⁷ Reichardt, C. *Chem. Rev.* **1994**, *94*, 2319.

Disolbatzaile ez-koordinatzaileei dagokienez, diklorometanon burututako jatorrizko erreakzioaren aldean (7. taula, 9. sarrera), polaritate baxuko disolbatzaileek, hala nola, karbono tetrakloruroak eta toluenoak, hobekuntza txikia erakutsi zuten enantioselektibitatean (9. taula, 1-2. sarrerak), aldiz, erreakzioa polarragoa diren kloroformo eta dikloroetanoan burutu zenean, soberakin enantiomerikoaren murrizketa gertatu zen (7. taula, 8, 10. sarrerak). Harrigarria bada ere, erreakzioa dietil eterren egitean, enantioselektibitatearen hazkuntza dramatikoak neurtzen da (7. taula, 4. sarrera).

Azken emaitza hau ikusita, zenbait eter probatu ziren osagai anitzeko erreakzioan disolbatzaile gisa, emaitza desberdinak behatuz, eta, soberakin enantiomeriko apalagoak lortu ziren di-*iso*-propil eterra, metil *tert*-butil eterra, tetrahidrofuranoa edo dimetoxietanoa erabili zirenean (7. taula, 3, 5-7. sarrerak). Gainera, azetonitriloan egindako erreakzioak ere enantioselektibitate ona erakutsi zuen (7. taula, 12. sarrera). Ordea, erreakzioa ez zen gertatu, inolaz ere, dimetilformamida edo metanola bezalako disolbatzaile polar sendoetan (7. taula, 11. eta 13. sarrerak), agian katalizatzailearen neutralizazioaren ondorioz, disolbatzaile hauek koordinatzeko gaitasun handia dutelako.

Eter disolbatzaileen efektua estereoselektibitatean, normalean, trantsizio-egoera ionikoen aktibazio energia eta disolbatzailearen polaritatearekin lotuta dago, baina gure kasuan, erreakzioaren estereokontrolaren hobekuntza, disolbatzaileak trantsizio-egoeran parte hartzearen ondorioz azaldu daiteke.¹⁶⁸ Ideia honen oinarria zera da, eredu-erreakzioa 10:1 diklorometano:dietil eter nahastean burutzen denean antzeko soberakin enantiomerikoa lortzen dela (7. taula, 14. sarrera). Emaitza horrek adierazten du, eter molekularak trantsizio-egoeran nolabait parte hartzen duela, enaminak imina bitartekariaren gain egiten duen adizio nukleozalea lagunduz, eterraren heteroatomoa organokatalizatzailearekin koordinatuz.

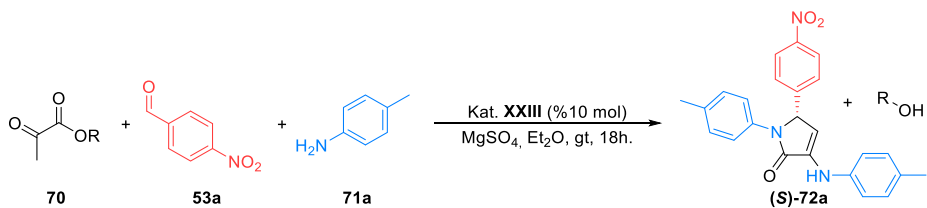
Optimizazio-prozesuaren hurrengo urratsean, pirubato substratuaren ester taldeak enantioselektibitatean duen eragina aztertu zen. Esterraren ordezkatzalea erreakzioaren ziklazio fasean kanporatzen da, γ -laktama egiturari eragin gabe, baina prozesuan lortutako soberakin enantiomerikoan efektua eduki dezake efektu esterikoengatik, beraz, esperimentu hauen bidez, zehaztu nahi da pirubato desberdinen erabilerak erreakzioaren estereokontrollean zein eragin duen (8. taula).

Hortaz, fenil pirubatoa (**70d**) erabiltzen denean, (**S**)-**72a** 1,5-dihidro-2*H*-pirrol-2-ona eskuratzen da soberakin enantiomeriko bikainarekin, baina oso konbertsio txikian (8. taula, 4. sarrera). Bestalde, emaitza are okerragoak lortzen dira, konbertsio eta estereoselektibitateari dagokienez, bolumen handiagoko *iso*-propilodun **70c** deribatuekin. Bolumen txikiagoko substratuak erabiltzean, hala nola,

¹⁶⁸ Some examples: (a) Fukaya, H.; Morokuma, K. *J. Org. Chem.* **2003**, *68*, 8170-8178. (b) Gajewski, J. J. *J. Am. Chem. Soc.* **2001**, *123*, 10877-10883.

metil eta etil pirubatoak (**70a,b**), erabateko konbertsioa behatu zen (8. taula, 1-2. sarrerak), eta soberakin enantiomeriko hobereana etil pirubatorako (**70a**) eskuratu zen.

8. taula. Pirubato ester desberdinen erabilera hiru osagaien eredu-erreakzioan.



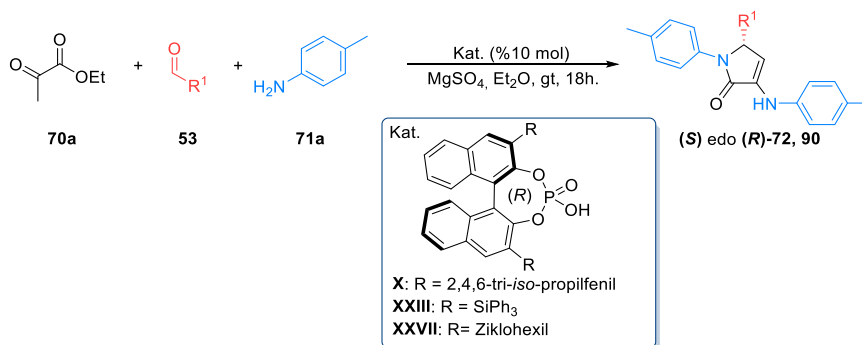
Sarr.	R	Konb. (%) ^a	ee (%)	Sarr.	R	Konb. (%) ^a	ee (%)
1	Me	100	89	3	<i>i</i> Pr	7	43
2	Et	100	96	4	Ph	5	99

^aH EMN bidez zehaztuta.

Osagai anitzeko erreakzioaren optimizazioarekin aurrera egiteko, eta, agente-lehortzailearen Mg²⁺ katioiak erreakzioaren estereokontrolan eraginik izan ote zuen egiaztatzeko, bi esperimendu egin ziren, non Na₂SO₄ eta 4Å-eko bahe molekularra erabili ziren MgSO₄-arenordez. Proba hauen ondorioz, Mg-ak ez du inolako eraginik sistema katalitikoan, ez baitzen aldaketa nabarmenik hauteman ez erreaktibitatean ez eta enantioselektibitatean ere.

Azkenik, erreakzioa katalizatzaile-karga desberdinekin burutu zen. Enantioselektibitate berdina hauteman zen katalizatzailearen karga aldehidoarekiko %20 mol-era igo egin zenean, baina, soberakin enantiomerikoaren jaitiera nabarmena neurtu zen karga %5 mol-era murriztu zenean (%76 ee).

Hiru osagaien erreakzio enantioselektiborako baldintza optimoak ezarri ondoren, protokolo sintetikoa ordezkatzaille desberdinak dituzten lehengaien erabilera zabaldu zen. Lehenik eta behin, **53** aldehido ezberdinen aukera aztertu zen, etil pirubato (**70a**) eta *p*-toluidinarekin (**71a**) batera, BINOL-etik eratorritako **X**, **XXIII** eta **XXVII** azido fosforiko ordezkatu aktiboekin. Aldehido-substratuaren irismenari buruzko emaitzak 9. taulan jaso dira.

9. taula. OAE enantioselektiboa **53** aldehido desberdinak baliatuz.

Sarrera	Prod.	R ¹	Etekinak (%) ^a	ee (%)	ee (%)	ee (%)
				Kat. X	Kat. XXIII	Kat. XXVII
1	(S)-72a	4-NO ₂ C ₆ H ₄	73	95	96	10
2	(S)-72c	Ph	90	83	87	13
3	(S)-72d	4-CF ₃ C ₆ H ₄	86	82	79	9
4	(S)-72e	3-NO ₂ C ₆ H ₄	73	28	80	15
5	(S)-72f ^b	4-FC ₆ H ₄	81	18	52	4
6	(S)-72g ^{c,d}	2-MeC ₆ H ₄	65	d.g.	36	26
7	(S)-72h ^d	3-MeC ₆ H ₄	83	4	42	70
8	(S)-72i ^{c,d}	4-MeC ₆ H ₄	81	9	33	8
9	(S)-72j	6-(<i>N</i> -Me-indolilo)	45	8	0	0
10	(S)-72k	2-Furilo	51	8	16	10
11	(S)-72l ^d	2-Tienilo	86	0	67	d.g.
12	(S)-72m	2-Naftilo	70	0	0	0
13	(R)-72n	Me	54	0	6	36
14	(R)-72o	ⁱ Pr	77	28	82	20
15	(R)-72p	ⁱ Bu	60	7	73	19
16	(R)-72q	Cy	85	72	79	70
17	(R)-72r	CH=CH-Ph	59	32	>99	d.g.
18	(S)-72s	CO ₂ Et	95	41	70	97
20	(S)-90a ^b	CH ₂ P(O)(OEt) ₂	80	d.g.	90	d.g.
21	(S)-90c ^c	CH ₂ P(O)(Ph) ₂	70	d.g.	91	d.g.
22	(S)-90d ^{b,d}	C ₆ F ₅	77	d.g.	60	d.g.
23	(S)-90e ^{b,e}	CF ₃	71	d.g.	5	d.g.

^aEmaitzarik onenerako kalkulaturako produktuaren isolaturako etekina. ^b48 orduko erreazio-denbora. ^c72 orduko erreazio-denbora. ^d Erreakzioa MTBE-en eta 55 °C-tan. ^e Erreakzioa toluenon eta giro tenperaturan.

Erreakzioa baldintza optimizatueta, eta *p*-nitrobenzaldehidoa bezain elektroizalea ez den benzaldehidoa erabil daiteke enantioselektibitate onak lortuta (9. taula, 2. sarrera vs. 1. sarrera). Hala ere, *o*-tolualdehidoa erabili zenean erreakzioa berotu behar izan zen MTBE-en 72 ordutan zehar, eta soberakin enantiomeriko apalak lortu ziren (9. taula, 6. sarrera), segur aski imina bitartekariaren

elektroizetasun txikiago eta eragozpen esteriko handiagoaren ondorioz. Era berean, osagai anitzeko erreakzioa MTBE-en eta tenperatura altuetan burutu behar izan zen *p*-tolualdehidoa erabiltzean, eta neurtutako estereokontrola ere baxua izan zen (9. taula, 8. sarrera). Kasu honetan, eragozpen esteriko berezirik ez dagoenez, erreakzioaren erreaktibotasun baxuaren erantzule bakarra aldehidoaren izaera elektronikoa da. Gainera, *meta* posizioan ordezkatzailak dituzten aldehido aromatikoak erabilia (**S**)-72e,h γ -laktamak lortu ziren etekin onean (9. taula, 4. eta 7. sarrerak). Kasu horietan, lehengaia *m*-nitrobenzaldehidoa denean enantioselektibitate ona hauteman bazen ere (9. taula, 4. sarrera), hain elektroizalea ez den *m*-tolualdehidoarekin erreakzioa berotu behar da eta, ondorioz, soberakin enantiomerikoaren beherapena antzeman da (9. taula, 7. sarrera).

Erreaktibitate eta enantioselektibitate balio onak lortu ziren ere elektroitan urriak diren beste aldehido aromatikoa batzuk erabili zirenean, hala nola, *p*-trifluorometilbenzaldehidoa (9. taula, 3. sarrera). Hala ere, soberakin enantiomerikoa nabarmenki jaisten da, eta erreakzio-denborak handitu behar dira *p*-fluorobenzaldehidoa lehengaiarekin (9. taula, 5. sarrera).

Erreakzioa aldehido heteraromatikoetara zabaldu daiteke, besteak beste 6-(*N*-Me-indolil), 2-furil, 2-tienil eta 2-naftil ordezkatzailak dituzten aldehidoetara. Kasu horietan (**S**)-72j-m γ -laktamak soberakin enantiomeriko txikiarekin lortzen dira (9. taula, 9-12. sarrerak).

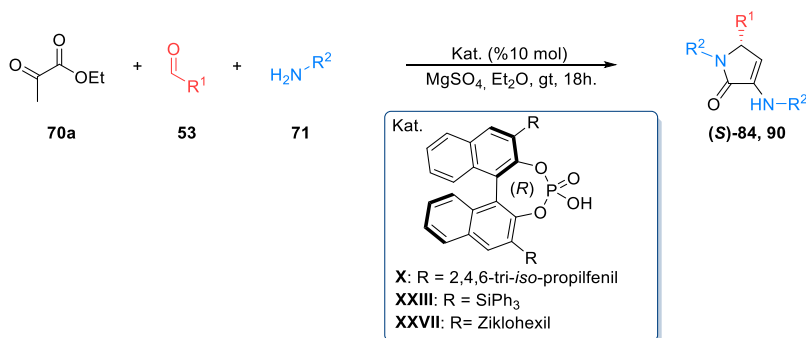
Gainera, aldehido enolizagarri alifatikoak, hala nola, *iso*-butiraldehidoa, *iso*-baleraldehidoa edo ziklohexanokarboxaldehidoa substratu gisa erabili zirenean, enantioselektibitate on samarrak lortu ziren (9. taula, 14-16. sarrerak). Horrez gain, zinamalaldehido edo etil glioxalato bezalako beste aldehido batzuek (**R**)-72r eta (**S**)-72s γ -laktamak eman zituzten enantiokontrol bikainarekin (9. taula, 17-18. sarrerak). Hala ere, azetaldehidoa erabili zenean, estereoselektibitatea jaitsi zen, segur aski aldehidoaren ordezkatzailak duen tamaina txikiaren ondorioz (9. taula, 13. sarrera).

Bestalde, hiru osagaien erreakzio asimetriko organokatalizatua **89** aldehido β -fosfororatu eta perfluoratuen erabilerara zabaldu zen, (**S**)-90 3-amino-1,5-dihidro-2*H*-pirrol-2-onak lortzeko. **89a** Dietil fosfonatodun aldehidoa eta elektroitan aberatsa den *p*-toluidina batera erabiltzean, (**S**)-90a 1,5-dihidro-2*H*-pirrol-2-ona lortu zen etekin onean eta soberakin enantiomeriko handian (9. taula, 20. sarrera). Hortaz gain, nahiz eta disolbatzaile organikoetan difenilfosfina-oxidoek disolbagarritasun txikia izan ohi duten, batez ere eterretan, osagai anitzeko erreakzioa fosfina-oxidotik eratorritako **89b** aldehidoarekin esekiduran burutu zen, erreakzio-denbora luzeagoa behar izanda (**S**)-90c γ -laktama enantioselektibitate onarekin lortzeko (9. taula, 21. sarrera). Aldiz, perfluorobenzaldehidoa substratuarekin erreakzioa MTBE-en berotu behar izan zen birfluxuan (**S**)-90d γ -laktama eskuratzeko etekin onean baina soberakin enantiomeriko moderatuarekin (9. taula, 22. sarrera).

Hala ere, trifluoroazetaldehido hidratoaren ur disoluzioa erabiltzean, **(S)**-**90d** γ -laktamaren nahaste errazemikoa baino ez zuen behatu (9. taula, 23. sarrera). Erreakzio honen enantiokontrolaren faltaren arrazoia trifluorometil ordezkatzailaren tamaina txikia (azetaldehidoaren kasurako proposatzen den bezala) edo errazemizazio-prozesu bat izan daiteke. Errazemizazio hau bitarteko pirrol aromatiko baten bidez gerta daiteke, zentro estereogenikoan talde elektro-erakarle indartsu baten presentziak, posizio horretako hidrogenoa oso azidoa bihurtzen duelako.

Erreakzioaren irismenaren azterketa amina substratu desberdinen erabilerara zabaldu zen ondoren (10. taula). Oso soberakin enantiomeriko onak lortzen dira, *p*-toluidinaren ordezkari, aromatiko oso aktibatua den *p*-anisidina erabiltzen denean (10. taula, 1-3. sarrerak). Hala ere, *p*-nitrobenzaldehidorekin burututako erreakzioa motelago gertatzen da, seguruenik enamina nukleozalearekin alderatuta, imina bitartekari elektroizalearen desaktibazio handiagoaren ondorioz.

10. taula. OAE-ren irismena 71 amina desbernika erabiliz.



Sarr.	Prod.	R ¹	R ²	Etekin (%) ^a	ee (%) Kat. X	ee (%) Kat. XXIII	ee (%) Kat. XXVII
1	(S) - 84a ^b	4-NO ₂ C ₆ H ₄	4-MeOC ₆ H ₄	81	0	90	d.g.
2	(S) - 84b	Ph	4-MeOC ₆ H ₄	74	90	90	5
3	(S) - 90b	CH ₂ P(O)(OEt) ₂	4-MeOC ₆ H ₄	83	d.g.	83	d.g.
4	(S) - 84c	4-NO ₂ C ₆ H ₄	4-BrC ₆ H ₄	89	>99	92	d.g.
5	(S) - 84e	4-CF ₃ C ₆ H ₄	4-BrC ₆ H ₄	89	68	80	d.g.
6	(S) - 84h	4-NO ₂ C ₆ H ₄	2-FC ₆ H ₄	75	86	95	d.g.
7	(S) - 84f ^d	4-NO ₂ C ₆ H ₄	4-ClC ₆ H ₄	74	30	32	42
8	(S) - 84g ^c	4-NO ₂ C ₆ H ₄	3-ClC ₆ H ₄	63	97	85	40
9	(S) - 84k ^{c,d}	4-NO ₂ C ₆ H ₄	3-CF ₃ C ₆ H ₄	63	35	34	62

^aEmaitzarik onenerako kalkulaturako produktuaren isolaturako etekina. ^b48 orduko erreakzio-denbora. ^c72 orduko erreakzio-denbora. ^d Erreakzioa MTBE-en eta 55 °C-tan.

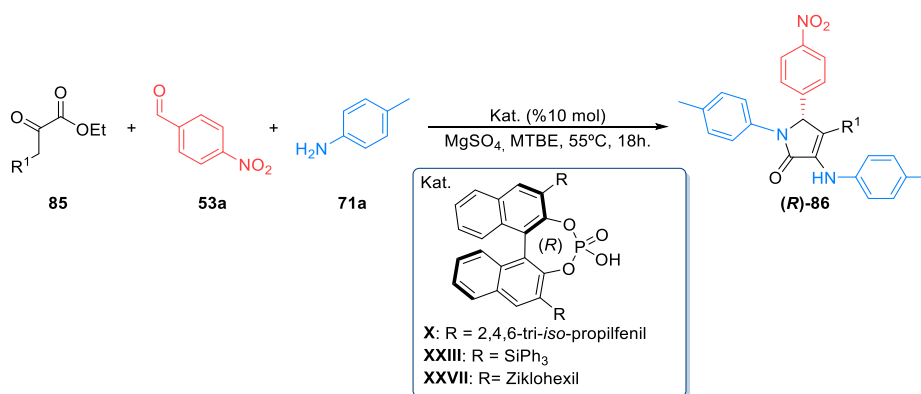
Berriz, izaera desaktibatzaile ahula duten *p*-bromoanilina edo *o*-fluoroanilina erabiltzean, hiru osagaiko erreakzioak aurrera egin zuen, **(S)**-**84c,e** eta **(S)**-**84h** γ -laktamak estereokontrol onarekin lortuz (10. taula, 4-6. sarrerak). *p*-Kloroanilinaren kasuan, temperatura altuagoak behar izan ziren, eta

enantioselektibitate txikia ikusi zen arren (10. taula, 7. sarrera), *m*-kloroanilinarekin (**5**)-**84g** γ -laktama eskuratu zen enantiokontrol bikainarekin erreazio-denbora luzeagoetan (10. taula, 8. sarrera). Azkenik, soberakin enantiomerikoa nabarmen jaitsi zen talde elektro-erakarle sendoak dituzten anilinekin, adibidez, *m*-trifluorometilanilinarekin (10. taula, 9. sarrera).

Kasu gehienetan, enantioselektibitate onenak trifenilsilil ordezkatzaillea duen BINOL-aren deribatutako **XXIII** azido fosforikoa erabiltzean lortu diren arren, hainbat substratu partikularretan emaitza hobekiak lortzen dira tri-*iso*-propilfenil edo ziklohexil taldez ordezkaturako **X** edo **XXVII** katalizatzaile kiralak erabiliz gero. Hala ere, itxuraz, erabilitako katalizatzaileen eta lehengaien egiturak alderatuta ez dago erreazioaren estereoselektibitatea aurreikusteko patroir argirik.

Optikoki aberastutako γ -laktama deribatuen sintesi orokor honekin bukatzeko, bi pirubato ordezkatu erabili ziren protokolo asimetriko organokatalizatu honetan (11. taula).

11. taula. OAE enantioselektiboa ordezkaturako **85** pirubatoak erabiliz.



Sarrera	Prod.	R ¹	Etekin (%) ^a	ee (%)		
				Kat. X	Kat. XXIII	Kat. XXVII
1	(<i>R</i>)- 86a	Me	70	54	43	33
2	(<i>R</i>)- 86b	Bn	71	68	62	10

^aEmaitzarik onenerako kalkulaturako produktuaren isolaturako etekina.

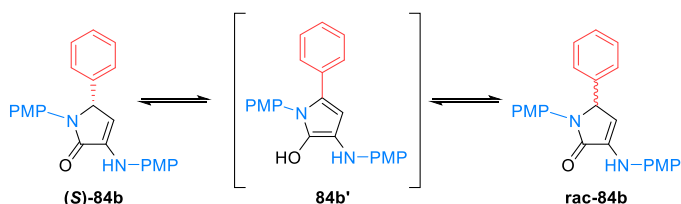
Bi kasuetan, erreazioak birfluxuan zegoen MTBE-en burutu ziren, dagozkion produktuak etekin onean baina entioselektibitate ertainekin lortzeko (11. taula, 1-2. sarrerak). Bentziloz ordezkaturako pirubatoarekin estereokontrol pixka bat hobea behatu zen metiloz ordezkaturako pirubatoarekin alderatuta.

Hurrengo helburua osagai anitzeko metodologia enantioselektiboaren garapenean, fosfonato edo fosfina-oxido talde funtzionalak dituzten **91** pirubatoen erabilerara zabaltzea zen, baina, ahalegin

handiak egin baziren ere, ez genuen arrakastarik izan γ -laktama eraztunaren 4. posizioan fosforoz ordezkaturako **93** produktuen sintesi enantioselektiboa burutzen.

Izan ere, kasu guztietan, γ -laktama substratuen enol egiturak izaera polar handia duenez, oso zaila izan zen bi enantiomeroak HPLC-ren bidez bereiztea. Akenean, banaketa-baldintza onargarriak aurkitu ziren di-*iso*-propil fosfonatoz ordezkaturako **93k** γ -laktamarako (5. zerrenda, *vide supra*). Hala ere, etekin egokiak erreakzioa tenperatura altuan baino ez dira lortzen, eta baldintza hauetan nahaste ia errazemikoa lortu zen **XXIII** azido fosforiko katalizatzaile eraginkorrenarekin. Gainera, polaritate baxuagoa duen enol eterra sortzeko erreakzio gordina TMS-CHN₂-rekin *in situ* tratatzeak, **93a** γ -laktamaren bi enantiomeroak egoki bereiztea ahalbidetu zuen (5. zerrenda 5, *vide supra*). Zoritzarrez, **93k** γ -laktamaren kasuan bezala, neurtutako soberakin enantiomerikoa oso urria izan zen (% 3 ee). Era berean, **52** dialkil azetilenodikarboxilatoak osagai anitzeko erreakziorako erabiltzean ere tenperatura altuak behar direnez, protokolo enantioselektibo hau 4-karboxilatoren deribatu diren **86** γ -laktamak (6. zerrenda, *vide supra*) sintetizatzen hutsala izan zen eta era errazemikoan besterik ez ziren lortu.

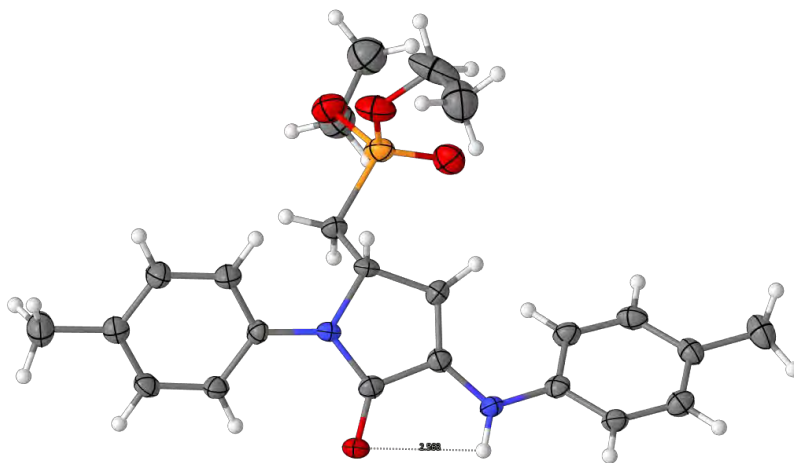
Jarraian, sintetizatutako 3-amino-1,5-dihidro-2*H*-pirrol-2-onen enantiomero nagusiaren karbono estereogenikoaren konfigurazio absolutua zehazteko, (**S**)-**72a** eta (**S**)-**84b** konposatuen monokristal puruak lortzen saiatu ginen, arrakastarik gabe. Izan ere, zenbait kristalizazio-saiakeraren ondoren nahaste errazemikoa baino ez zen eskuratu. Emaitza horiek ikusita, γ -laktama asegabatuaren errazemizazio-prozesu motel baten hipotesia planteatu zen, aromatikoa den bitarteko pirrol-egitura baten bidez (26. eskema).



26. eskema. Proposatutako errazemizazio-prozesua **84b** γ -laktamarako.

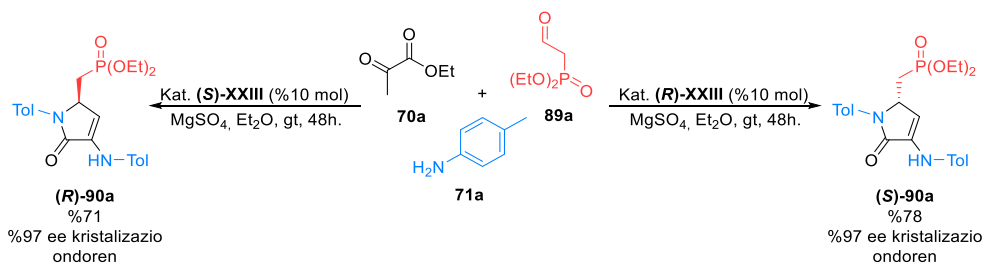
Errazemizazio hori, pirrol espezie bitartekariaren egonkortasunagatik sustatuta egon daiteke, eraztun aromatikoa bat baitago γ -laktama eraztunaren 5. posizioan, sistema oso konjugatua osatuz. Teoria horren arabera, 5-alkil ordeztutako γ -laktamen kasuan errazemizazio prozesua zailagoa izango zen, C-5 posizioan azidotasuna murrizten delako. Izan ere, enantiomerikoki aberastutako alkilfosfonatodun (**S**)-**90a** γ -laktamaren nahastea erabiltzean, optikoki puruak ziren monokristalak lortu ahal izan ziren, eta X-izpien difrakzio-analisiak argi eta garbi erakutsi zuen kristal-egitura bai eta *S* konfigurazio absolutua karbono estereogenikorako zuela (41. irudia).

Arestian agertutako egituretan aipatu den bezala, γ -laktama nukleoaren egitura ia planarra da, karbonilo α,β -asegabearen ondorioz. Gainera, hidrogeno zubi intramolekular bat dago enamina hidrogenoaren eta karbonilo oxigenoaren artean, *pseudo*-bost kideko eraztun bat sortuz.



41. irudia. (S)-90a γ -laktama α,β -asegabearen X-izpien bidezko difrakzio-egitura.

Azkenik, **90a** γ -laktamaren bi enantiomeroak isolatu ziren BINOL-aren eratorritako **XXIII** azido fosforikoaren katalizatzailearen bi isomeroak erabiliz osagai anitzeko erreakzioan (27. eskema). Bi kasuetan, **(R)-90a** edo **(S)-90a** 3-amino-1,5-dihidro-2*H*-pirrol-2-onak %97ko soberakin enantiomeroarekin lortzen dira hainbat kristalizazioen ondoren.



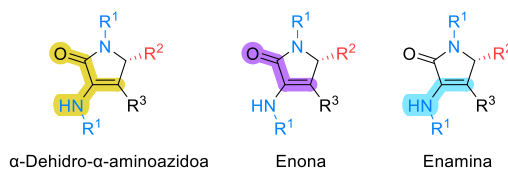
27. eskema. 90a γ -laktamaren bi enantiomeroen sintesia.

Ondorio moduan, kapitulu honetan pirubato, amina eta aldehidoen arteko enantioselektibitate altuko lehen osagai anitzeko erreakzioa deskribatu da, 3-amino-1,5-dihidro-2*H*-pirrol-2-onen sintesireko. Erreakzioa zenbait amina aromatiko, aldehido aromatiko eta alifatiko eta pirubato-deribatu desberdinetara orokortu da, funtzionalizazio handiko γ -laktama deribatuen sintesi asimetrikoa ahalbidetuz.

5. Kapitulu

γ -Laktama-deribatuen eraldaketa sintetikoak

Kimika farmazeutikoan 3-amino-1,5-dihidro-2*H*-pirrol-2-on egitura zeharo interesgarria da, eta gainera, aparteko tresna izan daiteke sintesi kimikoan, haren egituraren baitan α -dehidro α -aminoazido zikliko bat, enona bat eta enamina bat egiturak daudelako (42. irudia).¹⁶⁹ Hau honela izanda, eta γ -laktama α,β -asegabek prestatzeko garatu dugun osagai anitzeko metodologiaren erraztasuna kontuan hartuta, 3-amino-1,5-dihidro-2*H*-pirrol-2-onahuen potentzial sintetikoa agerian jartzeko, kapitulu honetan substratu hauen zenbait eraldaketa sintetiko aztertuko ditugu.

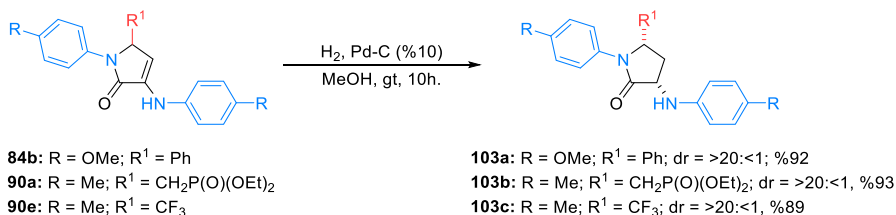


42. irudia. 3-Amino-1,5-dihidropirrol-2-onaren egituran dauden α -dehidro α -aminoazido zikliko (kolore horia), enona konjugatua (kolore morea) eta enamina (kolore urdina) talde funtzionalak.

Lehenik eta behin, 3-amino-1,5-dihydro-2*H*-pirrol-2-onen enamina talde funtzionalaren C=C loturaren erredukzioa proposatu zen, γ -laktama aseak prestatzeko. Hortaz, **84b** γ -laktama asegabea hidrogeno-presiopean (80 psi) eta paladioa katalizatzailearen presentzian, **103a** γ -laktama ase eratu zen, oso etekin onean eta diastereoselektibitate bikainean (28. eskema). Gainera, **(3*S*,5*S*)-103a** produktua ontzi bakarreko prozedura batean bidez lortu daiteke soberakin enantiomeriko onarekin. Lehenik eta behin, **XXIII** katalizatzailearen presentzian hiru osagaiko erreakzio enantioselektibo organokatalizatua, eta gero, tarteko **(*S*)-84b** γ -laktama isolatu gabe, hidrogenazio-erreakzioa burutzen da. Honela, errazemizazioa saihesten da, eta hasierako soberakin enantiomerikoa mantendu egiten da (%95, %90 ee).

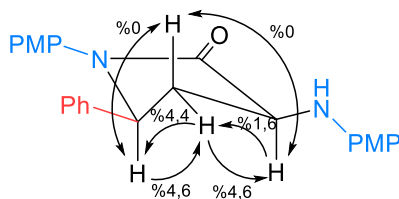
¹⁶⁹ Harmata, M. The Chemistry of Enols and Enamines. *In Organic Mechanisms: Reactions, Stereochemistry and Synthesis*. Springer, 2010, pp 487.-517.

Protokolo hau fosforilatutako **90a** γ -laktamaren eta trifluorometil taldez ordezkatur **90e** γ -laktametaren hidrogenaziorako erabili daiteke, **103 b-c** substratu aseak etekin eta diastereoselektibitate bikainekin lortuz.



28. eskema. 84b, 90a eta 90e γ -laktamen hidrogenazio diastereoselektiboa.

Lortutako **103a** γ -laktamaren estereozentroen konfigurazio absolutua (3*S*, 5*S*), NOE (Nuclear Overhauser Effect) esperimentuaren bidez zehaztu zen. Esperimentu hauek NOE efektuak erakutsi zituzten C3 eta C-5-eko bi zentro kiralen protoien eta CH₂ talde diasteretopikoaren protoi beraren artean, hiru atomo horiek norabide berean orientatuta daudela adieraziz. Horren arabera, hidrogeno molekularren *syn* adizio klasikoa proposatzen da, hots C=C lotura bikoitzera fenil-ordezkatzailearen aurkako aurpegitik hurbiltzen da (43. irudia).



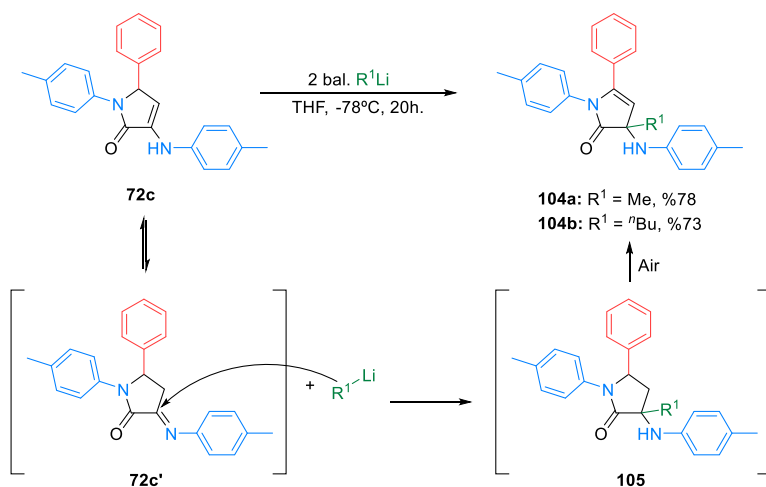
43. irudia. 103a γ -Laktama asearen NOE efektuak.

Bestalde, batetik enonaren egituraren presentzia, eta bestetik, enamina egituraren *in situ* tautomerizazioaren ondorioz imina talde funtzionala sortzeko aukera baliatuz, γ -laktama zikliko asegaberen elektroizaletasuna ebaluatu zen. Horretarako, hasiera batean, **72c** γ -laktama α,β -asegabea erreaktibo organolitikoekin tratatu zen tenperatura baxuan eta THF-n, eta karbono kiral tetra-ordezkatua duten **104a-b** produktuak etekin onekin lortu ziren (35. eskema).

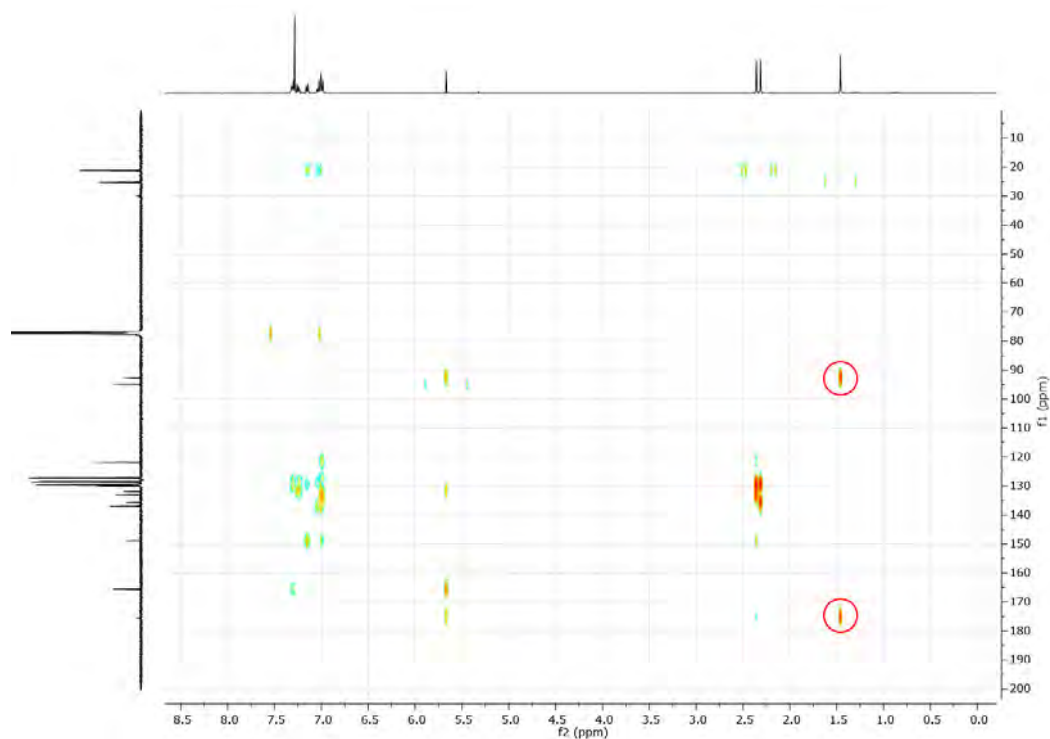
Erreakzio honen mekanismoa, **72c'** imina tautomeroaren gaineko erreaktibo organometalikoaren adizio nukleozalearekin has daiteke, eta jarraian eraztun laktamikoaren berezko oxidazioa atmosferarekin kontaktuan egotearen ondorioz (29. eskema).

Hipotesi hau frogatzea, lotura bikoitzaren hidrogenazio-erreakzioa burutu zen paladio-karbono katalizatzailearen kantitate katalitikoaren presentzian. Erreakzioak aurrera egin zuen, eta azkar iragazi

ondoren, erreakzio-gordinaren ^1H EMN espeketroak **105** bitartekariaren CH_2 taldearen protoi diastereotopikoen seinale bereizgarriak erakutsi zituen. Seinale horiek berehala desagertu ziren, **104a** produktuari dagokion espektra berriz erakutsiz, **105** produktua isolatzea ezinezko izanik.



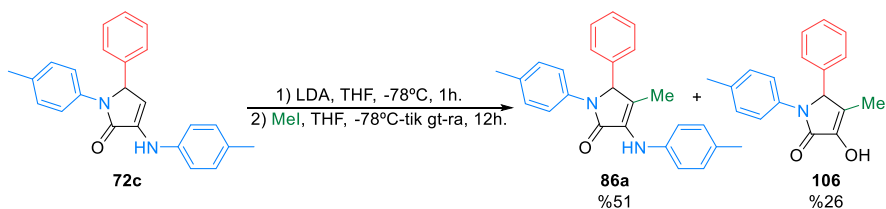
29. eskema. **72a** γ -Laktamaren gaineko erreaktibo organometalikoaren adizio nukleozaleen.



44. irudia. **104a** konposatuaren HMQC espektra.

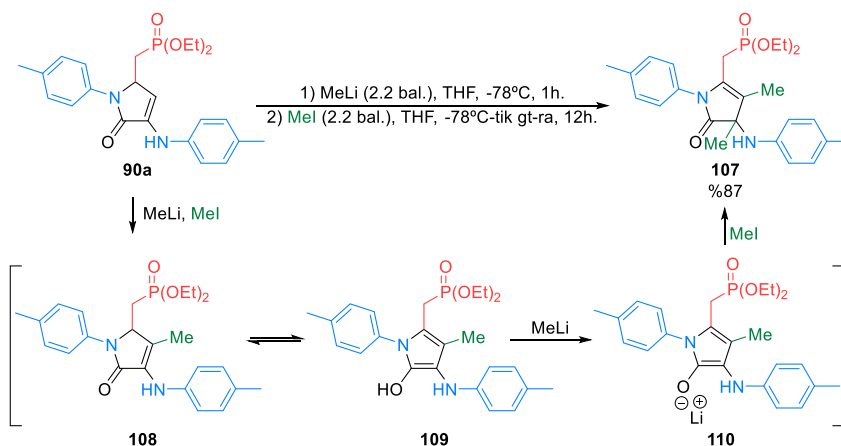
Karbono asimetriko kuarternarioa duen **104a** substratuaren egitura zalantzarik gabe berretsi zen Heteronuclear Multiple Quantum Coherence Experiment (HMQC) bidez. Esperimentu honek, korrelazio bat erakutsi zuen ^1H EMN espektroko metilo taldeari dagokion $\delta_{\text{H}} = 1.45$ ppm-tako singletearen eta ^{13}C EMN espektroko $\delta_{\text{C}} = 94.8$ eta 175.4 ppm-tako seinaleen artean, alkenoaren CH eta amidaren karbonilo taldeei dagozkienak, hurrenez hurren. Are gehiago, ez zen korrelaziorik hauteman metil eta fenil ordezkatzailen karbono edo hidrogenoen artean (44. irudia). Hau guztia kontuan izanda, ondoriozta daiteke γ -laktama eraztunaren C-3 posizioan dagoela ordezkapena.

Gainera, **72** γ -laktama α,β -asegabeetan dagoen enamina taldearen izaera nukleozalea kontuan hartuta, alkilazio-erreakzio simple bat egin zen taldea hau errektibo elektrozaleekin funtzionalizatu daitekeela frogatzeko. Hortaz, LDA-rekin eta tenperatura baxutan tratatutako **72c** γ -laktamari metil ioduroa gehitzean, espero zen **86a** konposatua lortu zen etekin moderatuan (% 51), hidrolizatutako **106** enol-deribatuekin batera (30. eskema).

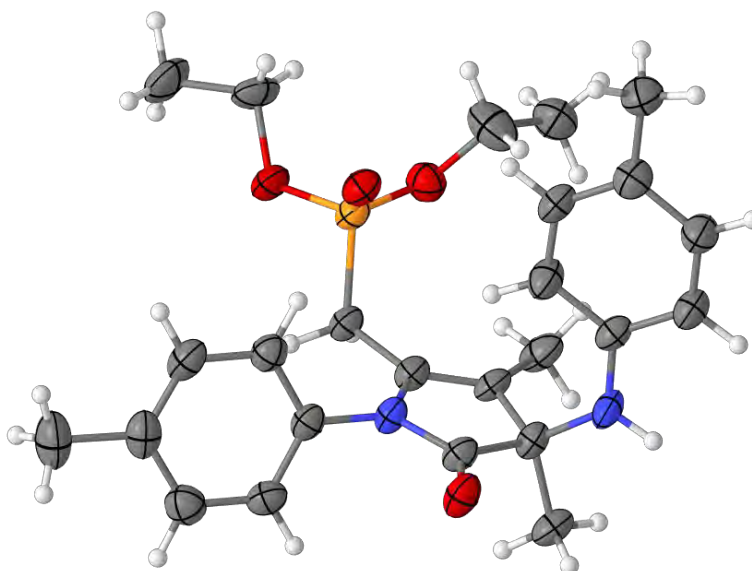


30. eskema. **72c** γ -laktama α,β -asegabearen enaminaaren alkilazioa.

Protokolo hau **90a** γ -laktama fosforilatura zabaltzeko egindako saiakerek ez zuten arrakastarik izan, base konbentzionalak erabilia, hala nola, amina tertziarioak, hidruroak edo alkoxidoak. Gainera, litio di-*iso*-propilamida bezalako base sendo bat baliatuz, lehengaiak aldatu gabe eskuratu ziren. Hala ere, base bezala metil litioa eta metil-ioduro elektroizalea erabilia, **107** γ -laktama dialkilatua eskuratu zen. Substratu difuntzionalizatu honen eraketa, enamina talde funtzionalaren hasierako alkilazio baten bidez azal daiteke, monometilatutako **108** γ -laktama lortzeko, tautomerizazio bidez, **109** hidroxipirrol molekularekin orekan dagoena. Etapa horretan, **109** espezieko enol-funtioa desprotonatu egiten da **110** enolatoa sortuz eta, jarraian, bigarren alkilazio-prozesu bat gertatzen da, **107** deribatu γ -laktamiko dimetilatua eratuz (31. eskema).

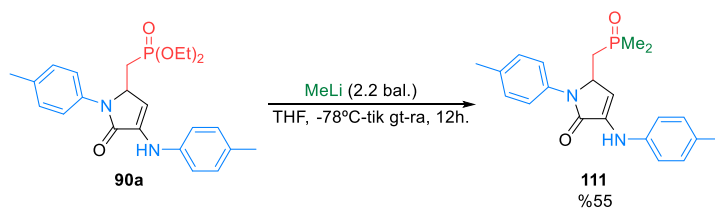
31. eskema. 90a γ -laktamaren dialkilazioa.

Erreakzio horretan lortutako produktuaren ordezkapen-patroia konplexua denez, **107** koposatuaren egitura X-izpien difrakzio bidez zehaztu zen (45. irudia). Dimetilatutako **107** γ -laktama-egituraren ezaugarri aipagarriena, bost kideko eraztunaren ohiko forma ia laua da, C-4 posizioko metilo ordezkatzaila C-5 ordezkatzailaren plano berean egonda, C=C lotura bikoitzaren presentziagatik. Kasu honetan, C-3 posizioko metilo taldeak eragotzi egiten du enaminaren NH-aren eta karbonilo taldearen arteko hidrogeno lotura eratzea, antezko beste substratu batzuen kristal-egituretan ageri dena (41. irudia, *vide supra*).

45. irudia. 107 γ -Laktama α,β -asegabearen X-izpien bidezko difrakzio-egitura.

Nahiz eta zenbait ahalegin egin ziren metil litioaren eta metil ioduroaren proportzioak orekatzeko, mono-metilatutako konposatuak selektiboki lortzeko helburuz, kasu guztietan **107** γ -laktama dimetilatua isolatu zen.

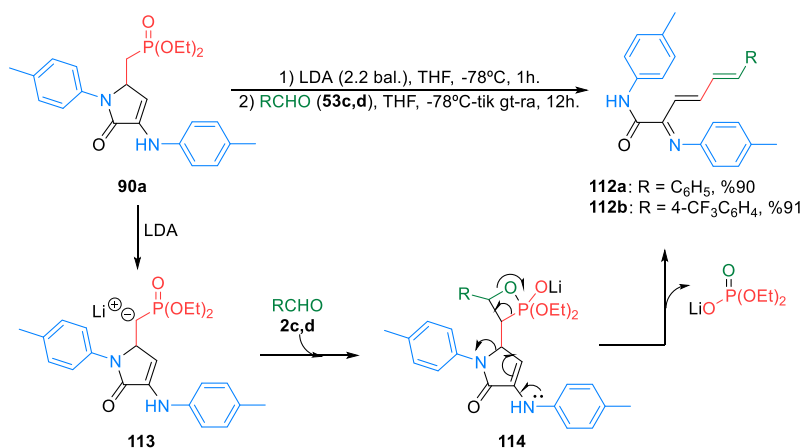
Aurreko esperimentua ikusita, argi dago karbonilo α,β -asegabe egituraren presentziaren ondorioz, 3-amino-1,5-dihidro-2*H*-pirro-2-onek Michael hartzaile gisa ere joka dezaketela. Hala ere, argitu beharra dago ea bi metilo taldeak metil iodurotik datozen, edo horietakoren bat, imina tautomeroaren gaineko adizio nukleozale batetik datorren (29. eskema adierazi bezala) edo lotura bikoi konugatuaren gaineko organometalikoaren Michael adiziotik datorren. Zalantza hau argitzeko, **90a** γ -laktama metil litio soberakinarekin tratatu zen, elektroizalerik erabili gabe. Gure harridurarako, erreakzio nagusia, metil litio nukleozale indartsuak eragindako fosfonato taldeko etoxi taldeen desplazamendua izan zen, **111** substratuan fosfonatoa fosfina-oxido taldea bihurtuz (32. eskema).



32. eskema. Fosfinadun **111** γ -laktamaren sintesia.

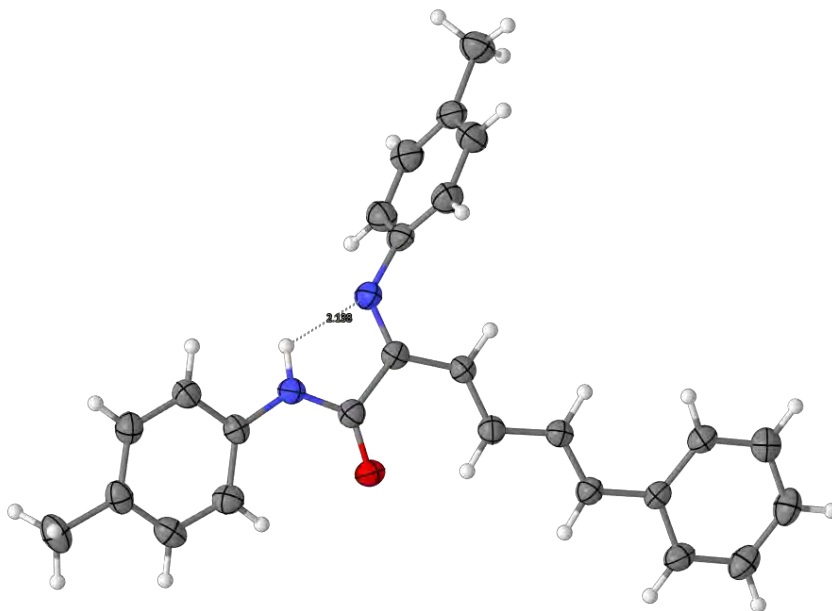
γ -Laktama deribatuen potentzial sintetikoan dugun interesarekin jarraituz, fosforodun substratuetako ordezkatzailerik fosforatuen errektibitatea aztertu zen. Testuinguru horretan, jakina da Horner-Wadsworth-Emmons erreakzioaz baliatuz olefinak eskuratzen direla, fosfonato-karbanioi egonkortuak eta aldehidoak erabiliz.¹⁷⁰ Testuinguru honetan, Etil fosfonatotik eratorritako **90a** γ -laktama LDA-rekin tratatu zenean tenperatura baxuan, eta **53** aldehidoak (R = Ph or 4-CF₃C₆H₄) gehitu zitzaizkionean, **112** aza-trieno konjugauak eratu ziren, ustekabean γ -laktama nukleoaren eraztuna ireki baitzen. Erreakzio horren mekanismoaren azalpen onargarri bat honako hau izan liteke: hasteko base sendo baten (LDA) presentzian **113** espezie anionikoaren eraketa, **53** aldehidoen gaineko eraso nukleozalea eta **114** lau-kideko oxafosfetanoaren formazioa, Horner-Wadsworth-Emmons erreakzioaren bitartekari ezaguna dena. Ondoren, amida talde funtzionalaren nitrogenoa eta fosforo-espezia eliminatu ondoren, **112** aza-trienoa sortuko litzateke (33. eskema).

¹⁷⁰ (a) Wadsworth, W. S.; Emmons, W. D. *J. Am. Chem. Soc.* **1961**, *83*, 1733-1738. (b) Horner, Hoffmann, H.; Wippel, H. *G. Chem. Ber.* **1958**, *91*, 61-63.



33. eskema. 90a γ -laktamaren Horner-Wadsworth-Emmons erreakzioa.

Erreakzio hau beste mekanismo baten bidez gerta daiteke, hain zuzen ere, olefinazioa eta gero eraztunaren irekiera. Hipotesi hau probatzeko **72r** 3-amino-1,5-dihidro-2H-pirrol-2-ona (1. zerrenda 1, *vide supra*) erabili zen, konposatu hau baita **90a** γ -laktama eta bentsaldehidoaren (**53c**) arteko olefinazio-erreakziotik espero den produktua. Beraz, **90a** konposatua baldintza basiko sendoetan edota tenperatura gogorretan jarri zen. Kasu guztietan lehengaia aldaketarik gabe berreskuratu zenez, iradoki daiteke, eraztun-irekidura halabeharrez **114** bitartekaritik datorrela, aurreko mekanismoan proposatu bezala.



46. irudia. 112a Aza-trienoaren X-izpien bidezko difrakzio-egitura.

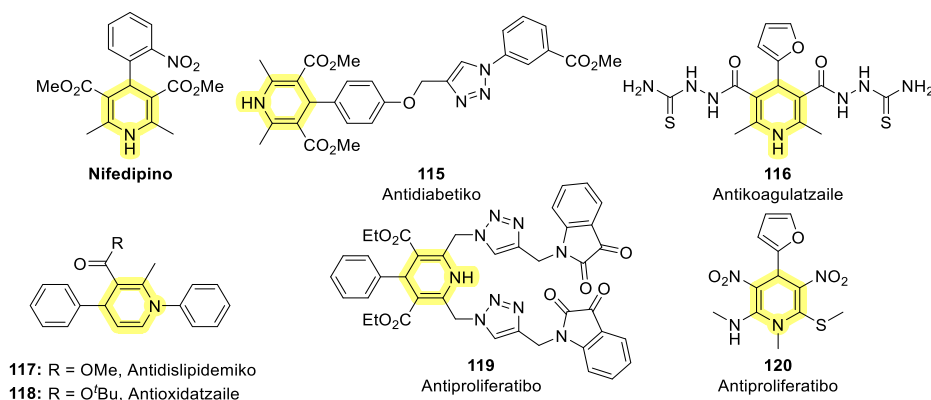
EMN espektroetan behatutako seinale-patroiek konplexutasun handikoak izanik, **112a** aza-trienoaren monokristal bat isolatu zen, eta haren egitura X-izpien difrakzioz zehaztu zen zalantzarik gabe (46. irudia). Substratu honen egituraren ezaugarriak aipagarriena, amidaren karbonilo taldeak, iminak eta bi alkenoek fenil eta *p*-tolil ordezkatzailerik aromatikoekin batera osatutako sistema konjugatu luzea da. Gainera, 46. irudian ageri den bezala, karbonilo eta imina taldeak *anti* konfigurazioan orientatzen dira, amidaren NH eta iminaren nitrogenoen arteko hidrogeno-lotura molekularnekoa dela eta.

Kapitulu honen laburpen gisa, osagai anitzeko erreakziotik lortutako γ -laktama substratuetan amida α,β -asegabe endokikliko eta enamina talde funtzionalen presentziak, oso konposatu interesgarriak bilakatzen dituzte, γ -laktama polifuntzionalen sintesirako lehenengo gisa erabili ahal izateko. Estereozentro kirala aprobeztatuz, diastereoselektibitate altuko hidrogenazio-erreakzioak deskribatu dira. Horrez gain, C-4 posizioako funtzionalizazio selektiboa egin daiteke enaminaren kimikaren bidez. Aldiz, espezie organometalikoak gehituta, C-3 posizioa funtzionalizazioa burutzea posible da. Gainera, fosfonatoa duten substratuak lehenengo gisa erabili daitezke olefinazio-erreakzioetan.

6. Kapitulu

3-Amino γ -laktama-deribatuen [3+3] erreakzio formal estereoselektiboa

1,4-Dihidropiridina eskeletoa egitura pribilegiatua da kimika farmazeutikoan, farmakologikoki aktiboak diren eta jarduera biologiko ugari dituzten substantzia askotan ageri delako,¹⁷¹ hala nola, gaur egun merkaturatutako dihidropiridina familiako kaltzio-kanalen blokeatzaile (i.e. Amlodipino, Nifedipino)¹⁷², antidiabetiko,¹⁷³ antikoagulatzaile,¹⁷⁴ antioxidatzaile,¹⁷⁵ antidislipidemiko,¹⁷⁵ eta agente antiproliferatibo¹⁷⁶ eraginkor ugarietan (47. irudia).



47. irudia. 1,4-Dihidropiridina eskeletoa duten molekula farmakologikoki aktiboak.

¹⁷¹ Reviews: (a) Swarnalatha, G.; Prasanthi, G.; Sirisha, N.; Madhusudhana Chetty, C. *Int. J. ChemTech Res.* **2011**, *3*, 75-89. (b) Edraki, N.; Mehdi pour, A. R.; Khoshneviszadeh, M.; Miri, R. *Drug Discov. Today* **2009**, *14*, 1058-1066.

¹⁷² (a) Siddiq, A.; Mukhtar, I.; Baig, S. G. *World. J. Pharm. Pharm. Sci.* **2019**, *8*, 1674-1687. (b) Elliott, W. J.; Ram, C. V. S. *J. Clin. Hypertens.* **2011**, *13*, 687-689 (c) Elmslie, K. S. *J. Neurosci. Res.* **2004**, *75*, 733-741.

¹⁷³ Praveenkumar, E.; Gurrapu, N.; Kumar Kolluri, P.; Reddy Kunduru, B.; Subhashini, N. J. P. *Bioorg. Chem.* **2019**, *90*, 1-9.

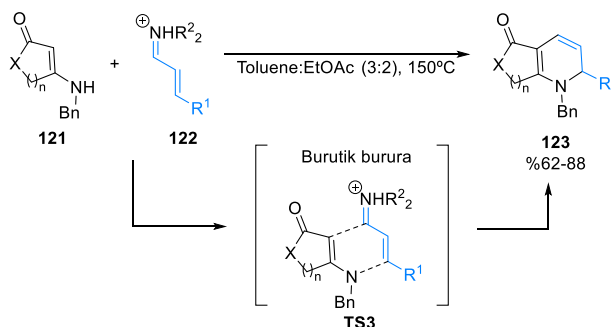
¹⁷⁴ Kumar, R. S.; Idhayadhulla, A.; Abdul Nasser, A. J.; Selvin, J. *Eur. J. Med. Chem.* **2011**, *46*, 804-810.

¹⁷⁵ Kumar, A.; Maurya, R. A.; Sharma, S.; Kumar, M.; Bhatia, G. *Eur. J. Med. Chem.* **2010**, *45*, 501-509.

¹⁷⁶ (a) Deswal, N.; Shrivastava, A.; Summon Hossain, M.; Gahlyan, P.; Bawa, R.; Gupta, R. D.; Kumar, R. *ChemistrySelect* **2021**, *6*, 717-725. (b) Anaikutti, P.; Makam, P. *Bioorg. Chem.* **2020**, *105*, 104379. (c) Abbas, H. A. S.; El Sayed, W. A.; Fathy, N. M. *Eur. J. Med. Chem.* **2010**, *45*, 973-982.

Ikuspegitik sintetikoari dagokionez, frogatu da karbonilo α,β -asegabe eta enaminen arteko ziklazio erreakzioak metodologia ahaltu eta azkarrak direla nitrogenodun heteroziklo prestatzeko.¹⁷⁷ Erreaktibotasun osagarria duten hotz biko bi fragmentuen arteko etapakako prozesu honetan piridina deribatuak sortzen dira, eta mekanismoa ez-kontzertatua denez, “[3+3] zikloadiazio formalak” deitzen zaie.

Testuinguru honetan, 1999. urtean, Hsung-ek **121** enamina ziklikoen eta **122** biniliminio ioien arteko aza-[3+3] ziklazio formala garatu zuen, **123** piperinil heterozikloak eraikitzeko.¹⁷⁸ Erreakzio hau, “burutik burura” motako tandem sekuentzia batean oinarritzen da (**TS2**), **121** enamina eta **122** iminio ioien arteko burututako Knoevenagel erreakzio batekin hasita eta eraztunaren itxiera periziklikoarekin amaituta (34. eskema).



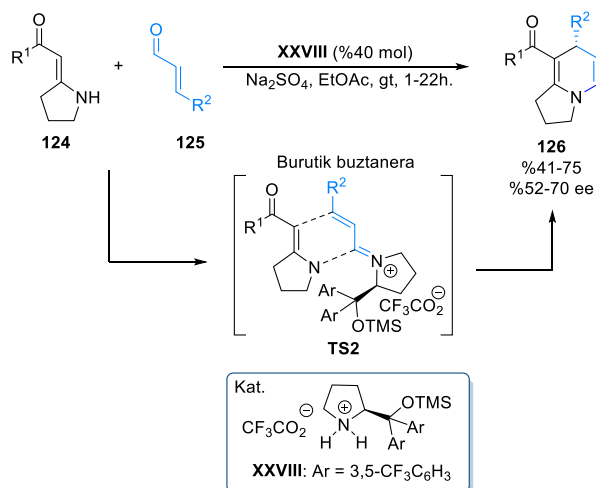
34. eskema. [3+3] Ziklazio-erreakzio formala “burutik burura” motako erregioselektibitatearekin.

Urte batzuk geroago, autore hauek ere, ustekabeko erregiokimikaren inbertsioa deskribatu zuten antzeko erreakzio batean (35. eskema). Izan ere, pirrolidinaren deribatu diren **124** enamina exoziklikoek eta **125** aldehido α,β -asegabeek, **XXVIII** aminaren gatz-kiralaren kantitate azpiestekiometrikoen presentzian, “burutik buztanera” motako [3+3] zikloadiazio-erreakzio formala baten erabera erreakzionatu zuen (**TS3**), **126** 1,4-dihidropiridinak etekin eta enantioselektibitate moderatuekin lortuz. Gainera, erreakzio honetan enamina kiralak erabiltzen direnean, estereokontrol maila handiarekin gertatzen da prozesua. Erreakzioa, **124** enamina adizio konjugatuarekin hasten da **125** olefina konjugatuaren gainean, eta ondoren, eraztunaren itxiera gertatzen da, imonio

¹⁷⁷ Reviews: (a) Xu, X.; Doyle, M. P. *Acc. Chem. Res.* **2014**, *47*, 1396-1405. (b) Buchanan, G. S.; Feltenberger, J. B.; Hsung, R. P. *Curr. Org. Chem.* **2010**, *7*, 363-401. (c) Harrity, J. P. A.; Provoost, O. *Org. Biomol. Chem.* **2005**, *3*, 1349-1358. (d) Hsung, R. P.; Kurdyumov, A. V.; Sydorenko, N. *Eur. J. Org. Chem.* **2005**, 23-44.

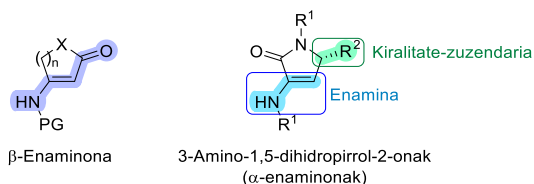
¹⁷⁸ Hsung, R. P.; Wei, L. L.; Sklenicka, H. M.; Douglas, C. J.; McLaughlin, M. J.; Mulder, J. A.; Yao, L. J. *Org. Lett.* **1999**, *1*, 509-512.

funtzioaren gainera enaminaen nitrogenoaren molekula barneko eraso nukleozalearen ondorioz (35. eskema).¹⁷⁹



35. eskema. [3+3] Ziklazio-erreakzio formal "burutik buztanera" motako erregioselektibitatearekin.

[3+3] Zikloadizio-erreakzio formal hauetan ohiko substratuak β -enaminona ziklikoak dira, non enamina taldearen errektibotasuna handituta dagoen β -karbonil taldearen presentziagatik. Ondorioz, 3-amino-1,5-dihidro-2*H*-pirrol-2-onak (**48. irudia**) oso substratu egokiak izan daitezke ziklazio erreakzioetan zenbait arrazoiengatik. Molekula horiek enamina gisa joka dezaketela frogatu dute dagoeneko, eta, gainera, C-5 ordezkaturako substratuak erabiliz gero, bost kideko heteroziklo zurrunean zentro estereogeniko bat egongo da, eta kiralitate-zuzendari bikaina izan daiteke, prozesuan estereoselektibitate-maila handia eraginez.



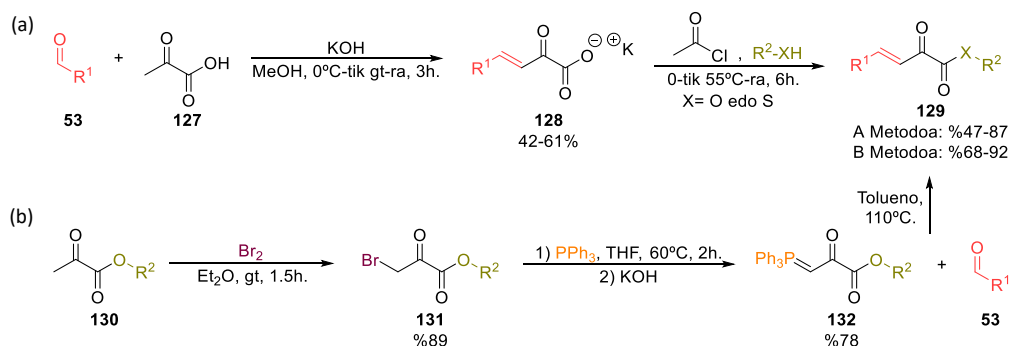
48. irudia. β -Enaminonen and 3-amino-1,5-dihidro-2*H*-pirrol-2-onen egiturak

Arestian aipaturakoa kontuan hartuta, kapitulu honetan, [3+3] zikloadizio-erreakzio formalen bidez piridina deribatuen sintesirako, 3-amino-1,5-dihydro-2*H*-pirrol-2-onak lehengai gisa dituzten

¹⁷⁹ (a) Buchanan, G. S.; Dai, H.; Hsung, R. P.; Gerasyuto, A. I.; Scheinebeck, C. M. *Org. Lett.* **2011**, *13*, 4402-4405. (b) Sklenicka, H. M.; Hsung, R. P.; McLaughlin, M. J.; Wei, L. L.; Gerasyuto, A. I.; Brennessel, W. B. *J. Am. Chem. Soc.* **2002**, *124*, 10435-10442.

aplikazioak aztertuko dira. Erreakzio honetarako kide bezala, α -zetoester β,γ -asegabeak aukeratu dira, sistema konjugatuak karboxilato taldearen eraginez duen aktibazio elektroniko gehigarria dela eta.

Lehengai bezala erabiliko diren α -zetoester β,γ -asegabea hauek deskribatutako prozeduren bidez prestatu ziren. Izan ere, **53** Aldehido eta azido pirubikoaren (**127**) arteko aldol kondentsazio-erreakzioa, potasio hidroxidoaren presentzian, metodo eraginkorra da bitarteko **128** potasio-karboxilatoak etekin moderatuekin lortzeko, eta hauek **129** α -zetoester β,γ -asegabeen sintesirako lehengaiak dira (36. eskema, a).¹⁸⁰ Alternatiba gisa, **130** pirubatoen halogenazioaren bidez, etekin onean lortutako **131** α -bromo pirubatoak lehengai egokiak dira trifenil fosfinaren presentzian, **132** fosforo iluroen sintesirako. Ondoren, **132** iluroen eta **53** aldehidoen arteko Wittig olefinazio-erreakzio klasikoaren bidez **129** zetoesterrak lortzen dira oso etekin onean (36. eskema, b).¹⁸¹



36. eskema. **129** α -Zetoester β,γ -asegabeen sintesirako metodologia osagarriak.

Behin beharrezko lehengaiak lortuta, 5-ordezkatu gabeko **72b** γ -laktama α,β -asegabe eta **129a** α -zetoester β,γ -asegabearen arteko ziklaziorako erreakzio-baldintzak optimizatu ziren, horretarako, zenbait Lewis azidoren kantitate katalitikoak erabilia. Emaitzak 12. taulan laburtu dira.

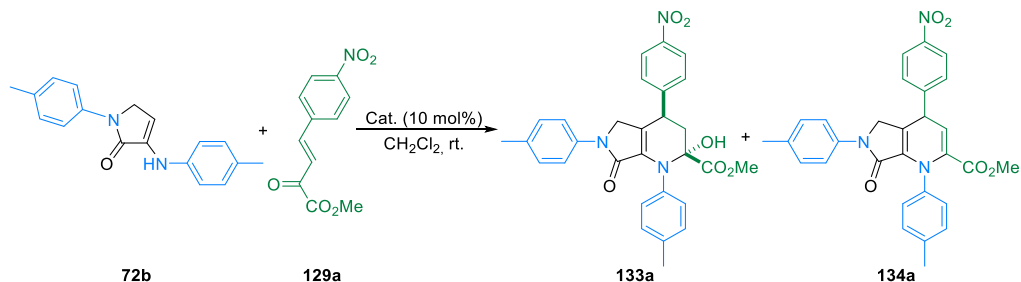
Nahiz eta erreakzioak ez zuen aurrera egin Cu (II) gatz bat erabili zenean (12. taula, 1. sarrera), konbertsio osoa ikusi zen 140 ordutan Cu (I) motako katalizatzailearen aurrean, **133a** tetrahidropiridina selektiboki eta etekin onean lortuz (12. taula, 2. sarrera). **133a** konposatu hau "burutik buztanera" moduko [3+3] zikloadizio-prozesu formal baten bidez gerta daiteke, deskribatu diren beste antzeko erreakzioetan bezala. Prozesu horren hasieran enamina talde funtzionalaren adizio konjugatua gertatzen da **129a** α -zetoester β,γ -asegabearen gainera, eta ondoren, **129a** konposatuaren zetonari enamina nitrogenoak molekularbarko eraso nukleozalea egiten dio. Erreakzioa ZnCl_2 -ren presentzian burutzean, antzeko emaitzak eman zituen, baina konbertsio apalagoetan 140 orduen ondoren (12.

¹⁸⁰ Tang, Q.; Fu, K.; Ruan, P.; Dong, S.; Su, Z.; Liu, X.; Feng, X. *Angew. Chem. Int. Ed.* **2019**, *131*, 11972-11977.

¹⁸¹ Albrecht, Ł.; Dickmeiss, G.; Weise, C. F.; Rodríguez Escrich, C.; Jørgensen, K. A. *Angew. Chem. Int. Ed.* **2012**, *51*, 13109-13113.

taula, 3. sarrera). Gure harridurarako, Ag(OTf) katalizatzaile gisa erabiliz, tetrahidropiridina **133a** eta 1,4-dihidropiridinaren 30:70-ko nahasketa lortzen da (14. taula, 4. sarrera). Aipatu beharra dago, **134a** konposatua, ziurrenik, **133a** tetrahidropiridinaren deshidratazioaren bidez sortzen dela.

12. taula. Katalizatzailearen optimizazioa [3+3] zikloadizio-erreakzio formalerako.

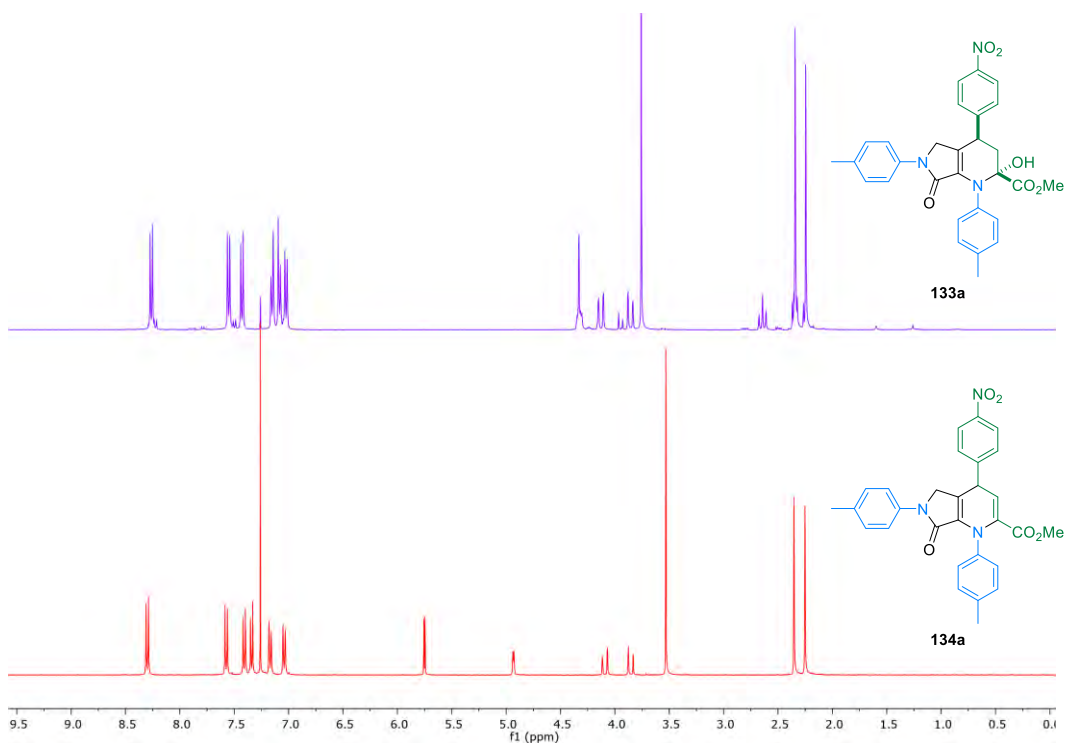


Sarrera	Katalizatzailea	Denb. (h)	Konb. (%)	Prop. 133a:134a ^a	Etek. (%) ^b
1	Cu(OTf) ₂	140	0	-	d.g.
2	Cu(CH ₃ CN) ₄ PF ₆	140	100	>99:<1	88
3	ZnCl ₂	140	40	>99:<1	d.g.
4	Ag(OTf)	120	100	30:70	d.g.
5	NiCl ₂ (PPh ₃) ₂	24	100	<1:>99	d.g.
6	Sml ₂	24	100	<1:>99	d.g.
7	In(OTf) ₃	24	100	<1:>99	d.g.
8	TiCl ₄	24	100	<1:>99	d.g.
9	Sc(OTf) ₃	24	100	<1:>99	d.g.
10	YbCl ₃	24	30	8:92	d.g.
11	Yb(OTf) ₃	1	100	50:50	d.g.
12	Yb(OTf) ₃	7	100	<1:>99	84

^a ¹H EMN bidez zehatua. ^bIsolatutako etekina.

Ziklazio-erreakzio formalaren katalizatzaile eraginkorrenaren bila aurrera eginez, beste Lewis azido batzuk probatu ziren. Gure gozamenerako, [3+3] zikloadizio formalaren **134a** produktuaren eraketa osoa behatu zen 24 ordu igaro ondoren, NiCl₂(PPh₃)₂, Sml₂, In(OTf)₃, TiCl₄ edo Sc(OTf)₃ Lewis azidoak erabili zirenean (12. taula, 5-9. sarrerak). Ordea, YbCl₃-ren presentzian **133a** eta **134a** produktuen 8:92 nahastea lortu zen 24 ordutan, konbertsio baxuarekin (12. taula, 10. sarrera). YbCl₃-aren disolbagarritasun baxua dela eta, ondoren, Yb(OTf)₃ erabili zen ziklazio-erreakzioan katalizatzaile gisa. Kasu honetan, lehengaiak oso azkar desagertu ziren, eta **133a** eta **134a** produktuen 50:50-eko nahasketa eratu zen ordubeteren ondoren (12. taula, 11. sarrera). Hala ere, Yb(OTf)₃ katalizatzaile hobereana zela ondorioztatu zen, erreakzioa diklorometanoan eta giro-tenperaturan 7 ordutan zehar burutzean, **134a** 1,4-dihidropiridina isolatu zelako produktu bakar gisa eta etekin onean (12. taula, 12. sarrera).

Aurreko esperimentuetan prestatutako **133a** and **134a** substratuak isolatuak izan ziren, eta EMR, IR espektroskopia eta HRMS bidez erabat karakterizatu ziren. Erreakzioaren bi produktuen ^1H EMN espektroak pilatuta ageri dira 49. irudian. **133a** Tetrahidropiridina biziklikoaren seinale adierazgarrietako batzuk honako hauek dira: Batetik $\delta_{\text{H}} = 4,33$ ppm-ko singlete zabala (D_2O -rekin trukutzen dena), OH taldeari dagokiona, eta $\delta_{\text{H}} = 4,32$ ppm-ko doblete bikoitzarekin gainjarrita agertzen dena. Seinale hau karbono asimetrikoko CH protoiari dagokio, eta alboko CH_2 talde diastereotopikoarekin akoplatuta dago ($^3J_{\text{HH}} = 1,4$ eta $5,2$ Hz). Gainera, $\delta_{\text{H}} = 4,13$ and $3,86$ ppm-ko bi doblete bikoitzak γ -laktama nukleoko CH_2 -aren bi protoi diastereotopikoen seinaleak dira, eta $^2J_{\text{HH}} = 17,8$ Hz-ko elkarrekiko akoplamendu geminala erakusten dute. Era berean, tetrahidropiridina eraztuneko CH_2 talde funtzionalaren beste bi protoi diastereotopiko bi doblete bikoitz gisa ageri dira, $\delta_{\text{H}} = 2,64$ eta $2,35$ ppm-tan, $^2J_{\text{HH}} = 12,8$ Hz-ko akoplamendu geminal tipikoarekin, eta zentro kiraleko CH taldearekin ere akoplatuta ($^3J_{\text{HH}} = 1,4$ eta $5,2$ Hz hurrenez hurren).



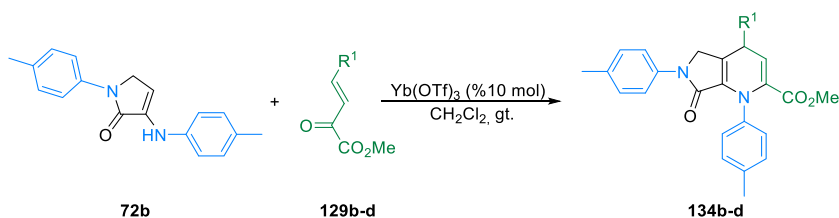
49. irudia. 133a eta 134a konposatuen ^1H EMN espektroen konparaketa.

Bestalde, **134a** 1,4-dihidropiridina ^1H EMN espektroak, bi doblete erakusten ditu **133a** konposatuaren kasuan baino eremu baxuagoan ($\delta_{\text{H}} = 5,75$ and $4,93$ ppm), dihidropiridina-eraztuneko bi CH protoiei esleitua, $^3J_{\text{HH}} = 3,8$ Hz-ko akoplamendu-konstantarekin. Gainera, γ -laktama eraztuneko CH_2 taldeko bi protoi diastereotopikoak bi doblete gisa ageri dira $\delta_{\text{H}} = 4,09$ and $3,85$ ppm-tan, $^2J_{\text{HH}} =$

18,0 Hz-ko akoplamendu geminal indartsua erakutsiz. Halaber, bi konposatuen espektroetan, $\delta_H = 3,50$ - 3,80 ppm-ko tartean, metoxi taldeari dagokion singlete zorrotza agertzeaz gain, $\delta_H = 2,20$ eta 2,40 ppm artean bi singlete zorrotzen presentzia, eta eskualde aromatiko 12 protoiek, egitura bakoitzean bi *p*-toluidina talde eta *p*-nitrofenilo talde bat daudela adierazten dute (49. irudia).

Zikloadizio formalerako erreakzio-baldintza optimoak beste α -zetoester β,γ -asegabe (**129b-d**) batzuen erabilerara zabaldu zen, eta **72b** ordezkatu gabeko γ -laktamarekin aztertu zen erreakzioa (13. taula).

13. taula. Erreakzio-baldintza optimoen aplikazioa C-5 ordezkatu gabeko **72b** γ -laktama eta **129** α -zetoester β,γ -asegabe desberdinekin.



Sarrera	Produktua	R ¹	Denbora (h)	Etekin (%) ^a
1	134b	4-CF ₃ C ₆ H ₄	7	78
2	134c	Ph	14	76
3	134d	4-MeC ₆ H ₄	14	72

^aIsolatutako etekina.

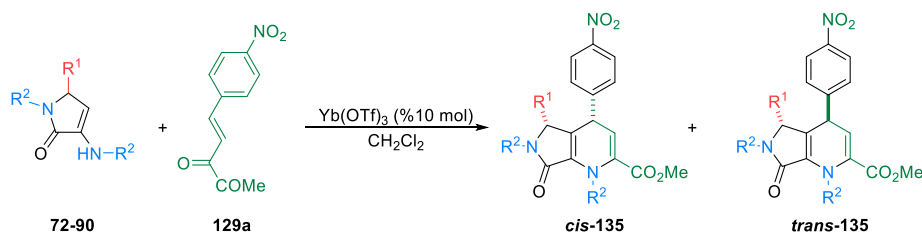
Izaera desaktibatzailea duen trifluorometil taldez ordezkaturako **129b** α -zetoesterrak baldintza berdinetan erreakzionatu zuen **134b** 1,4-dihidropiridina etekin onean sortzeko (13. taula, 1. sarrera). Hala ere, **129c** konposatuan bezala fenil ordezkatzaille sinplea egonda, edo **129d**-ko aktibatutako eraztun aromatiko bat baldin badago erreakzio-denborak handiagoak izan ziren. Edonola ere, **134c,d** 1,4-dihidropiridinak etekin onean lortu ziren gau batez erreakzionatu ondoren (13. taula, 2-3. sarrerak).

Eraitza hauek ikusita, gure hurrengo helburua [3+3] ziklazio formal diastereoselektiboa ikertzea izan zen, kiralak diren lehengaiak baliatuz. Lehenik eta behin, C-5 posizioan karbono asimetrikoa duten **72-90** enamina zikliko desberdinak erabili ziren, eredu-substratu gisa **129a** α -zetoester β,γ -asegabea izanda, eta bi zentro estereogeniko dituzten **135** 1,4-dihidropiridina ziklikoak lortzeko helburuarekin. Eraitzak 14. taulan laburtzen dira.

Fenilo taldez ordezkaturako **72c** enamina ($R^1 = \text{Ph}$, $R^2 = 4\text{-MeC}_6\text{H}_4$) erabat erreakzionatu zuen gau osoan zehar **129a** α -zetoeste β,γ -asegabearekin, eta Yb(OTf)₃ kantitate katalitikoaren aurrean, **135a** 1,4-dihidropiridinaren *cis* isomeroa soilikemateko etekin onean (14. taula, 1. sarrera). Erreakzioa, ordezkatzaille aromatiko desberdinak dituzten hainbat enamina ziklikoen erabilerara hedatu zen, hala

nola, izaera elektroierakarleak (**72d**, $R^1 = 4\text{-CF}_3\text{C}_6\text{H}_4$, $R^2 = 4\text{-MeC}_6\text{H}_4$) edo fluoro ordezkatzailak (**72f**, $R^1 = 4\text{-FC}_6\text{H}_4$, $R^2 = 4\text{-MeC}_6\text{H}_4$) dituztenak. Halaber, ordezkatzaille perfluoratuak (**90d**, $R^1 = \text{C}_6\text{F}_5$, $R^2 = 4\text{-MeC}_6\text{H}_4$) edo heteroaromatikoak (**72i**, $R^1 = 2\text{-tiofeno}$, $R^2 = 4\text{-MeC}_6\text{H}_4$) dituzten γ -laktama deribatuak ere erabili dira, eta kasu guztietan, **135b-e** 1,4-dihidropiridina biziklikoak isolatu ziren etekin onak edo bikainak izanda eta *cis* diastereoisomero bakar gisa (14. taula, 2-5. sarrera).

14. taula. [3+3] Zikoadizio-erreakzio formal diastereoselektiboa. C-5 ordezkatzutako **135** enamina ziklikoen sorta.



Sarr.	Prod.	R^1	R^2	Denb. (h)	Temp. (°C)	<i>Cis/Trans</i> ^a	Etek. (%) ^b
1	135a	Ph	4-MeC ₆ H ₄	14	rt	>99:<1	82
2	135b	4-CF ₃ C ₆ H ₄	4-MeC ₆ H ₄	14	rt	>99:<1	90
3	135c	<i>p</i> -FC ₆ H ₄	4-MeC ₆ H ₄	14	rt	>99:<1	79
4	135d	C ₆ F ₅	4-MeC ₆ H ₄	14	rt	>99:<1	65
5	135e	2-Tiofenilo	4-MeC ₆ H ₄	14	rt	>99:<1	66
6	135f	Cy	4-MeC ₆ H ₄	24	40	<1:>99	19
7	135g	CH ₂ P(O)(OEt) ₂	4-MeC ₆ H ₄	14	rt	<1:>99	87
8	135h	CF ₃	4-MeC ₆ H ₄	14	40	70:30	72 ^c
9	135i	Ph	4-MeOC ₆ H ₄	14	rt	>99:<1	76
10	135j	Ph	2-FC ₆ H ₄	14	rt	>99:<1	84
11	135k	Ph	4-BrC ₆ H ₄	14	40	70:30	91 ^c
12	135l	Ph	3-CF ₃ C ₆ H ₄	56	40	65:35	94 ^c

^a ¹H EMN bidez zehaztua. ^b Isolatutako etekina. ^cEtekin konbinatua bi isomeroentzat.

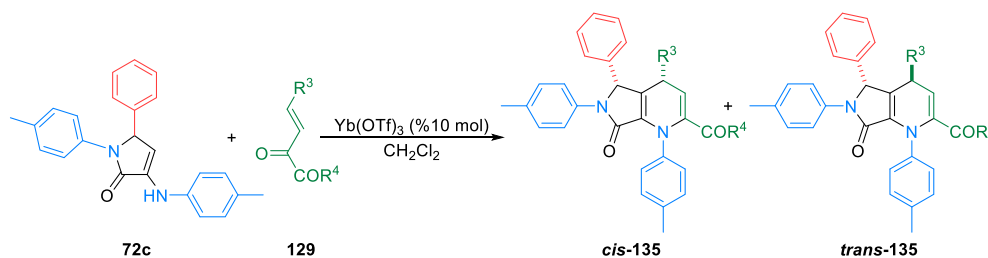
Bitxia bada ere, nukleozale gisa ordezkatzaille alifatikoak dituzten enamina ziklikoak erabili zirenean, hala nola, ziklohexil edo fosforil-metil taldez ordezkatzutako **72q** ($R^1 = \text{Cy}$, $R^2 = 4\text{-MeC}_6\text{H}_4$) eta **90a** ($R^1 = \text{CH}_2\text{P(O)(OEt)}_2$, $R^2 = 4\text{-MeC}_6\text{H}_4$) γ -laktama α,β -asegabek, *trans* isomeroaren eraketa eskusiboa behatu zen (14. taula, 6-7. sarrerak). Hala ere, trifluorometiloz ordezkatzutako **90e** substratuarekin egindako erreakzioan ($R^1 = \text{CF}_3$, $R^2 = 4\text{-MeC}_6\text{H}_4$), *cis* eta *trans* isomeroen 70:30 nahastea sortu zen, etekin onarekin (14. taula, 8. sarrera).

Ordoren, γ -laktama-substratuen bi nitrogenoen ordezkatzailak duten eragina aztertu zen, eta, horretarako, C-5 posizioan feniloz ordezkatzutako enamina zikliko desberdinak erabili ziren eta **129a** α -zetoester β,γ -asegabek erreakzioaren kide elektroizale bezala. Oso erreaktibotasun ona erakutsi zuen

p-anisidinaren eratorritako **84b** enaminak ($R^1 = \text{Ph}$, $R^2 = 4\text{-MeOC}_6\text{H}_4$), eta **135i** 1,4-dihidropiridina oso etekin onean isolatu zen *cis* isomero bakar moduan (14. taula, 9. sarrera). Antzeko emaitza lortu zen *o*-fluoroanilinaren deribatutako **84i** enamina ($R^1 = \text{Ph}$, $R^2 = 2\text{-FC}_6\text{H}_4$) erabili zenean (14. taula, 10. sarrera). Hala ere, *p*-bromoanilina eta *m*-trifluorometilanilinaren deribatutako **84d** ($R^1 = \text{Ph}$, $R^2 = 4\text{-BrC}_6\text{H}_4$) eta **84l** ($R^1 = \text{Ph}$, $R^2 = 3\text{-CF}_3\text{C}_6\text{H}_4$) lehengaiak, erreakzio-tenperatura altuagoak behar izan zituzten, eta ondorioz, *cis* isomero nagusiarekin batera *trans* isomeroaren kantitate esanguratsuak eratu ziren. Etekinak, berriz, bikainak izan ziren (14. taula, 11-12. sarrerak).

Erreakzioaren irismena are gehiago hedatzeko, [3+3] zikloadizio-erreakzio formala erreakziokide elektroizaleak diren **129** α -zeto(tio)ester β,γ -asegabe hotz-biko burutu zen. Emaitzak 15. taulan ikus daitezke.

15. taula. [3+3] Zikloadizio formal diastereoselektiboa. **129** α -Zeto(tio)ester β,γ -asegabeen sorta.



Sarrera	Prod.	R ³	R ⁴	Denb. (h)	Tenp. (°C)	Cis:Trans ^a	Etek. (%) ^b
1	135m	4-NO ₂ C ₆ H ₄	OBn	14	rt	>99:<1	68
2	135n	4-NO ₂ C ₆ H ₄	OEt	14	rt	>99:<1	79
3	135o	4-NO ₂ C ₆ H ₄	O ⁱ Pr	14	rt	>99:<1	76
4	135p	4-NO ₂ C ₆ H ₄	SEt	24	40	88:12	85 ^c
5	135q	4-CF ₃ C ₆ H ₄	O ⁱ Pr	14	rt	>99:<1	89
6	135r	Ph	O ⁱ Pr	14	rt	>99:<1	84
7	135s	4-MeC ₆ H ₄	OMe	14	rt	>99:<1	63
8	135t	4-MeC ₆ H ₄	O ⁱ Pr	14	rt	>99:<1	76
9	135u	2-Tiofenilo	O ⁱ Pr	14	rt	>99:<1	67
10	135v	CO ₂ Et	O ⁱ Pr	14	rt	>99:<1	86
11	135w	CF ₃	O ⁱ Pr	14	rt	>99:<1	84
12	135x	CH ₃	O ⁱ Pr	24	rt	85:15	65 ^c

^a ¹H EMN bidez zehaztua. ^b Isolatutako etekina. ^cEtekin konbinatua bi isomeroentzat.

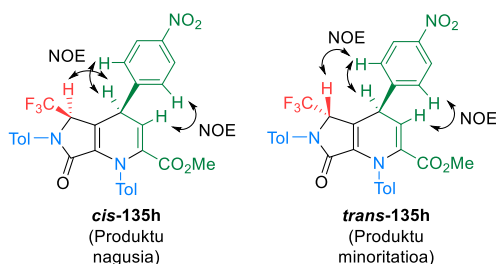
Lehenik eta behin, karboxilato taldeak (R^4) erreakzioaren erreaktivitatean eta diastereoselektibitatean duen eragina aztertu zen. Metil karboxilatoz ordezkaturako **135a** 1,4-dihidropiridinaren kasuan bezala, bentzil, etil edo *iso*-propil karboxilato ordekatzaileak dituzten **135m-o** ($R^3 = 4\text{-NO}_2\text{C}_6\text{H}_4$; $R^4 = \text{OBn, OEt, O}^i\text{Pr}$) substratuak giro-tenperaturan lortu ziren, etekin onean eta *cis* isomero bakar gisa (15. taula, 1-3. sarrerak). Hala eta guztiz ere, ester taldea tioesterraz

ordezkatzerakoan, **129h** α -zetotioester β,γ -asegabearen ($R^3 = 4\text{-NO}_2\text{C}_6\text{H}_4$; $R^4 = \text{SEt}$) kasuan bezala, erreakzioa askoz motelago gertatu zen, eta, 24 orduz berotu behar izan zen birfluxuan zegoen diklorometanoan, **135p** produktu biziklikoa etekin onean lortzeko. (15. taula, 4. sarrera). Kasu honetan, gainera, *cis* eta *trans* isomeroen 88:12 nahastea isolatu zen. Diastereoselektibitate eta erreaktibotasun baxuaren arrazoia, tiokarbonil taldearen eta Lewis azidoaren arteko afinitate txikiagoa izan daiteke, batetik tiokarbonil taldearen basikotasun txikiagoaren ondorioz, eta bestetik ester taldearekin alderatuta, eragozpen esteriko handiagoagatik. Izan ere, sufre atomoaren Van der Waals erradio handiagoa da oxigenoarena baino alderatuta (180 pm vs. 152 pm).

Azkenik, erreakzio honetan aztertu beharreko azken puntua, **129** α -zetoester β,γ -asegabeetako lotura bikoitiz konjugatuko ordezkatzailak duen eragina ebaluatzea da. Espero zitekeen bezala, lehengai elektroizalean, elektroitan urria den beste ordezkatzaille aromatiko bat dagoenean, hala nola *p*-trifluorometilfeniloa, **135q** 1,4-dihidropiridina biziklikoa ($R^3 = 4\text{-CF}_3\text{C}_6\text{H}_4$; $R^4 = \text{O}^i\text{Pr}$) oso etekin eta diastereoselektibitate onaeen isolatu zen (15. taula, 5. sarrera). Halaber, erreakzioak fenilo sinplea ($R^3 = \text{Ph}$), elektroitan aberatsa den eraztun aromatiko ($R^3 = 4\text{-MeC}_6\text{H}_4$) eta ordezkatzaille heteroaromatiko ($R^3 = 2\text{-tiefenilo}$) ere onartzen ditu, eta **135r-u** produktuak etekin onetan eta *cis* isomero bakar gisa lortu ziren (15. taula, 6-9. sarrerak).

Gainera, elektroierakarleak diren beste ordezkatzaille ez-aromatiko batzuen eragina ikertu zen. Etil karboxilato edo trifluorometil taldeak arrakastaz erabili ziren **129m** ($R^3 = \text{CO}_2\text{Me}$; $R^4 = \text{O}^i\text{Pr}$) eta **129n** ($R^3 = \text{CF}_3$; $R^4 = \text{O}^i\text{Pr}$) α -zetoester β,γ -asegabeetan, eta **135v,w** konposatuak eratu ziren *cis* konfigurazioan bakarrik (15. taula, 10-11. sarrerak). Ziklazio-erreakzioaren irismena ikertzen amaitzeko, talde alifatikoa duen **135x** 1,4-dihidropiridina biziklikoa ($R^3 = \text{Me}$; $R^4 = \text{O}^i\text{Pr}$) eskuratu zen etekin moderatuak, baina 85:15-ko *cis:trans* nahaste moduan (15. taula, 12. sarrera).

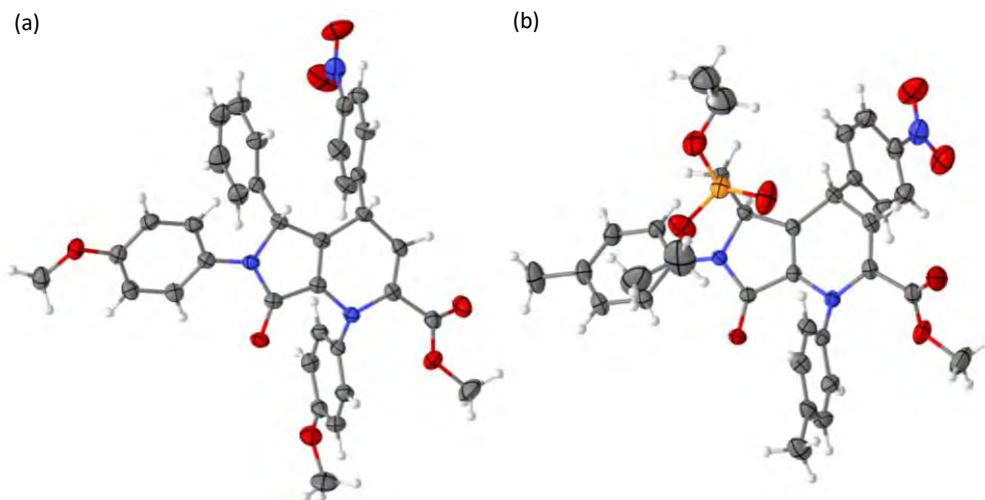
Zikloadizio-erreakzio formalaren bidez lortutako **135h** konposatuaren bi diastereoisomeroak isolatu ziren, eta FTIR, EMN espektroskopia eta HRMS bidez guztiz karakterizatu ziren. Erreakzioaren erregiokimika eta bi estereozentroen konfigurazio erlatiboa zehazteko nuklear Overhauser efektuko espektroskopia (NOESY) esperimentuak egin ziren **135h** 1,4-dihidropiridinaren bi isomeroen gainean. Bi konposatuen eraztun nitro-aromatikoko *ortho* posizioan dauden protoiek %0,9-ko NOE erakutsi zuten C-3 posizioako protoi olefinikoarekin, eta, %5-ekoa dihidropiridina eraztuneko C-4 posizioako protoiarekin. Hala ere, **135h** diastereoisomero nagusiaren eraztun γ -laktamikoko C-H protoiak %1,5-eko NOE-a erakutsi zuen dihidropiridina eraztunaren C-4-ko protoiarekin, eta ez zen NOE-rik ikusi eraztun aromatikoarekin, honek bi protoi hauen *cis* konfigurazio erlatiboa iradokitzen duelarik (50. irudia).



50. irudia. **cis-135h** eta **trans-135h** 1,4-dihidropiridinetan behatutako NOE balioen alderaketa.

Bestalde, **135h** diastereoisomero minoritarioaren bost kideko eraztuneko C-H protoiak, %1,1-eko NOE efektua erakutsi zuen eraztun nitro-aromatikoko *ortho* protoiekin, eta ez zen elkarrekintzarik ikusi dihidropiridina eraztuneko C-4-ko protoiarekin. Ondorioz, bi ordezkatzaileren arteko *trans* konfigurazio erlatiboa dagoela proposatzen da (50. irudia).

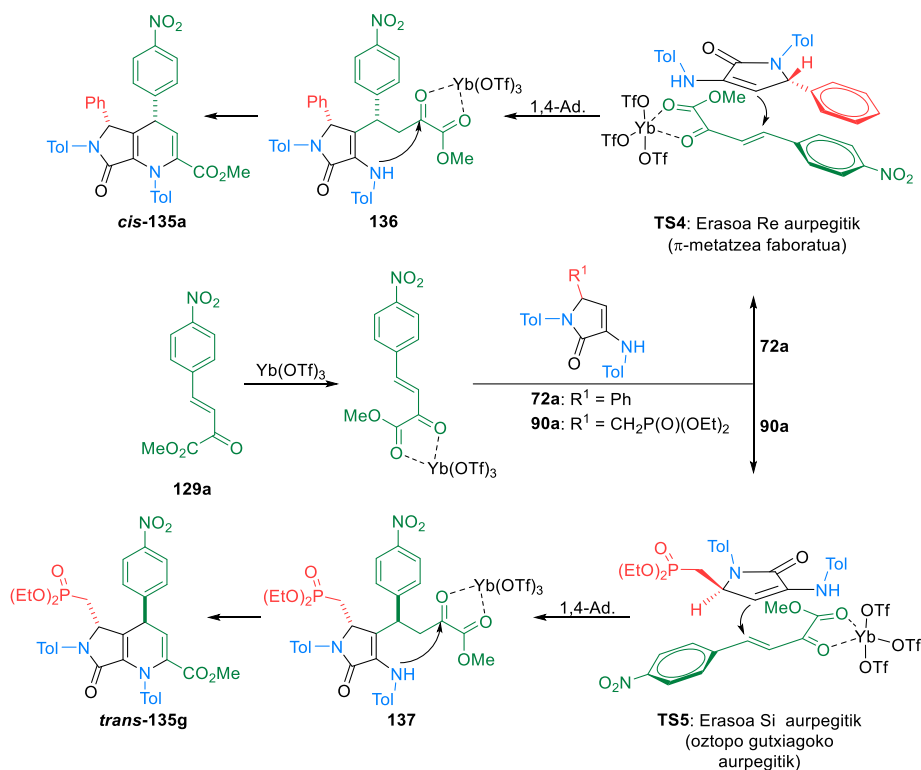
Gainerako **135** 1,4-dihidropiridina biziklikoen konfigurazio erlatiboa, haien NOESY espektroen eta **cis-135h** and **trans-135h** konposatuen espektroen arteko analogiaz ezarri zen (50. irudia). Izan ere, isolatutako **135** konposatuen isomero guztien NOE efektuak **cis-135h**-rekin ala **trans-135h**-rekin aldera zitezkeen kasu guztietan. Hala ere, behatutako NOE efektuak eta **135**-eko bi isomeroen egitura errealak bat ote datozen fidagarrian berresteko, **cis-135i** eta **trans-135g** substratuen konfigurazio absolutua X-izpien difrakzioen bidez determinatu ziren (51. irudia).



51. irudia. **cis-135i** (a) eta **trans-135g** (b) 1,4-dihidropiridinen X-izpien bidezko difrakzioen-egiturak.

Behatutako emaitzetan oinarrituta, ondoren, erreakzio-bide onargarri bat proposatzen da. Mekanismoaren abiapuntua, iterbio triflato katalizatzaileak eragindako **129a** zetoesterraren aktibazioa

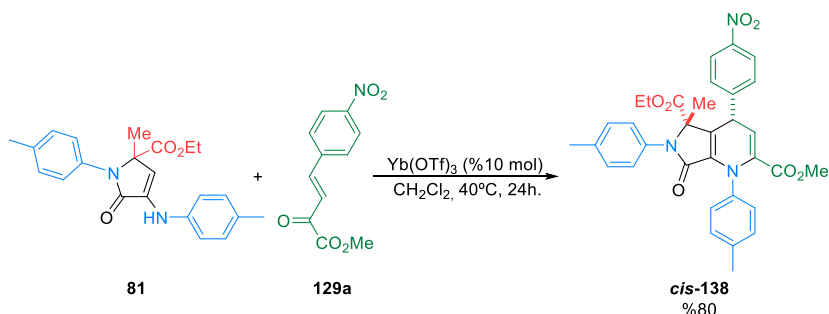
da, eta ondoren, **72** enamina ziklikoak aktibatutako zetoester konjugauaren gainean adizionatzen da (37. eskema). Momentu honetan, *cis* diastereoisomeroaren eraketa selektiboa azaldu ahal izateko, kontuan izan behar da **72c** enamina ziklikoaren estereozentroko eta **129a** α -zetoester β,γ -asegabearren talde aromatikoak, biak π -metatze motako elkarrekin (TS4) ari direla, eta horrek bi ordezkatzailak zonalde berberara bideratuko lituzke. Kontrara, enamina ziklikoaren estereozentroan eraztun aromatikoak egon ezean, diastereoselektibitatea alderapen esterikoaren ondorio da nagusiki, hain zuzen **90a** enamina ziklikoaren talde alifatiko tetrahedrikoaren eta **129a** zetoesterraren ordezkatzailak aromatikoaren artean gertatzen dena, eta horrek ordezkatzailak kontrako norabideetara bidaltzen ditu, *trans* diastereoisomeroa bakarrik eskuratuta (TS5). Erreakzio-mekanismoa eraztunaren itxierarekin amaitzen da, enamina ziklikoaren nitrogenoak zetona taldeari egindako eraso nukleozalearen ondorioz (37. eskema).



37. eskema. 135 1,4-Dihidropiridina biziklikoen bi diastereoisomeroen eraketarako proposatutako mekanismoa.

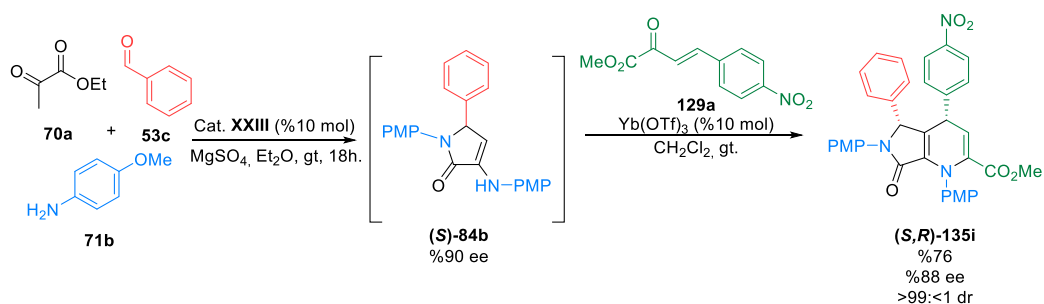
Esan beharra dago bi diastereoisomeroen arteko oreka termodinamikorako aukera baztertu izan dela, izan ere, **135h** substratuaren bi isomero puruak banaka berotu ziren, bakarrik, zein base, azido edo Yb(OTf)₃-ren presentzian, eta kontrako diastereoisomeroaren arrastorik ez zen aurkitu.

Gainera, [3+3] zikloadizio-erreakzio formala, estereozentro kuaternarioa duen **81** enamina ziklikoarekin ere aurrera egin zuen **129a** α -zetoester β,γ -asegabearrekin batera, eta **cis-138** 1,4-dihidropiridina bakarrik sortu zen (38. eskema). Kasu honetan, karboxilato eta eraztun aromatikoaren artean *cis* orientazio erlatiboa azal daiteke ordezkatzailen arteko π -metatze efektua elkarrekintza esterikoari gailentzen zaiolako.



38. eskema. **81** Enamina ziklikoaren [3+3] ziklazio formal estereoselektiboa.

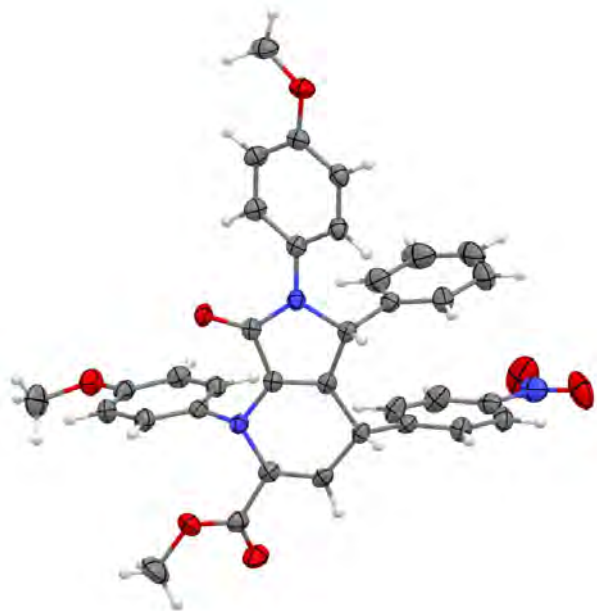
Bestalde, γ -laktama substratuen sintesirako osagai anitzeko protokolo enantioselektiboa eta [3+3] zikloadizio-erreakzio formala konbinatzea proposatu genuen, 1,4-dihidropiridina bizikloen sintesi enantiopurua burutzeko. Hala, 3-amino-1,5-dihidro-2*H*-pirro-2-onetan hautemandako errazemizazio prozesu motela gainditzeko, berriki prestatutako (**S**)-**84b** (%90 ee) γ -laktama eta **129a** α -zetoester β,γ -asegabearre erreakzionatzen jarri ziren Yb(OTf)₃-ren presentzian ontzi bakarreko edo “one pot” prozeduran. Horrela, (**S,R**)-**135i** 1,4-dihidropiridina biziklikoa isolatu zen, etekin oso onean eta %88-ko soberakin enantiomeroarekin, *cis* diastereoisomero bakar moduan (39. eskema).



Scheme 39. Enantiomeroarekin prestatutako (**S,R**)-**135i** 1,4-Dihidropiridinaren sintesia.

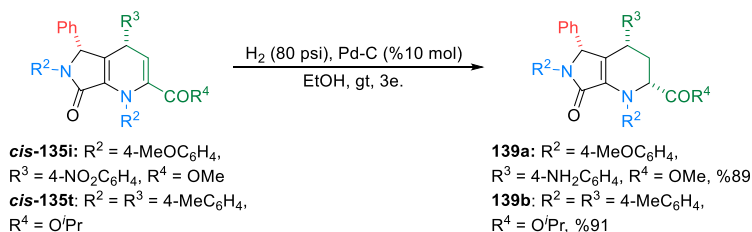
Optikoki aberastutako (**4S,5R**)-**135i** substratua, HPLC kiralaren bidez egiaztatu zen eta, kristalizazioaren ondoren, produktu bizikloaren enantiomero nagusiaren monokristal optikoki puruak lortu ziren. Ondoren, X-izpien difrakzio-espektroaren bidez estereozentroen 4*S* eta 5*R* konfigurazio absolutuak zehaztu ahal izan ziren (52. irudia). Egitura horren funtsezko ezaugarrien artean, batetik

γ -laktama eta 1,4-dihidropiridina nukleoen egitura ia lauak direla, eta bestetik fenil eta *p*-nitrofenil taldeen lerrokadura paraleloa, seguruenik bi talde aromatiko hauen arteko π - π metatze efektuagatik.



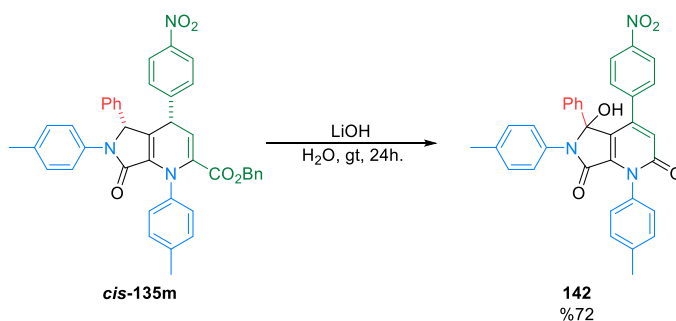
52. irudia. (4*S*, 5*R*)-*cis*-135i 1,4-dihidropiridinaren X-izpien bidezko difrakzio-egitura.

Gainera, **135** 1,4-dihidropiridinen erabilgarritasuna agerian uzteko, substratuen eraldaketa sintetiko batzuk proposatu ziren. Lehenik eta behin, 1,4-dihidropiridina eraztunaren erredukzioa burutu zen, *cis*-135i eta *cis*-135t substratuak presiopeko hidrogenoarekin (80 psi) eta Pd-C kantitate katalitikoekin tratatuz. Horrela, guztiz *cis* konfigurazio erlatiboa duten **139a-b** tetrahidropiridinak isolatu ahal izan ziren. NOESY esperimientuek, estereozentro berria beste bi karbono-kiralekiko *cis* konfigurazio erlatiboan zegoela erakutsi zuten. Datu hau, bat dator hidrogeno molekularren *syn* adizioarekin, hau da, hidrogenoa lotura olefinikora hurbiltzen da bi zentro estereogenikoen ordezkatzailen aurkako aurpegitik. Aipatu beharra dago, erreakzio-baldintza horiek *cis*-135i dihidropiridinari aplikatuta, nitro taldea amino taldera erreduzitzea ere eragin zuela (40 eskema).



40. eskema. 1,4-Dihidropiridina eraztunaren hidrogenazio diastereoselektiboa.

Horrez gain, 1,4-dihidropiridina eraztunean azido karboxiliko talde funtzionala lortze aldera, esterraren hidrolisia burutzeko egindako saiakerek ez zuten arrakastarik izan hidrolisi azidorako edo basikorako ohiko baldintzak erabilita. Ester bentzilikoaren hidrogenolisia ere bideraezina suertatu zen, baina, bitxia bada ere, bentzil esterra duen **cis-135m** substratua litio hidroxidoarekin tratatzean, **142** 2-piridona biziklikoa isolatu ahal izan zen. Konposatu hau, bentzil esterraren hidrolisiaren ondorego deskarboxilazio, oxidazio eta γ -laktama eraztunaren hidroxilazio bidez sor daiteke (41 eskema).



41. eskema. 142 2-Piridona bizikliko deribatuaren sintesia.

Laburbilduz, 1,4-dihidropiridina biziklikoen sintesirako iterbio triflato bidez katalizatutako enamina ziklikoen eta α -zetoester β,γ -asegabeen arteko [3+3] zikloadizio formal oso estereoselektiboa deskribatu da. Erreakzioaren irismena eta orokortasuna agerian geratu da 27 substratu desberdin prestatu baitira. Pausukako prozesu honen azken etapako deshidratazioa baino lehenagoko bitartekariaren detekzioari esker, erreakzio-mekanismoa zehaztu ahal izan zen. Gainera, lortutako emaitzek, iradokitzen dute π - π metatze elkarrekintza eta efektu esterikoak lotuta daudela erreakzioaren estereoselektibitatearekin. Azkenik, eraldaketa sintetiko batzuk ere deskribatu dira, hidrogenazio katalitiko bat barne, hirugarren zentro estereogeniko bat era diastereoselektiboan sortzen duena.

II. Atala

*γ -Laktama deribatuen minbiziaren kontrako
jarduera*



p53 nukleoaren transkripzio-faktorea da, TP53 gene tumore-ezabatzaileak kodetua, “genomaren zaintzaile” gisa ere deitua, giza minbizien %50ean mutaturata edo bere funtzioa galduta baitauka.¹⁸² 1979an zenbait ikerketa-taldeek aurkitu egin zuten, Simian Virus (BS40) T antigeno handiarekin konplexatuta.¹⁸³ Hasiera batean onkogene bezala sailkatu bazen ere, 80ko hamarkadan zenbait ikerketa burutu ondoren ikusi egin zen nola edo hala tumore-zeluletan desaktibatuta zegoela,¹⁸⁴ eta ondorioz, 1989. urtean p53 onkogenea baino kontrakoa zela, hau da tumore-ezabatzaile determinatu zen.¹⁸⁵ Harrezkero, proteina honen funtzioak, erregulazio-mekanismoak eta aplikazio medikoak deskribatu dira, gehien ikertuetako proteinetako bat izanik.¹⁸⁶

p53 proteinak 393 aminoazido ditu, eta, aktibo bihurtzeko homo-tetramero bat eratu behar du. Monomero bakoitzak hainbat eskualde edo domeinu du (53. irudia).¹⁸⁷ Lehenik eta behin, N-muturrean transaktibazio-eremua edo TAD (1-42 aminoazidoak) aurkitzen da, hainbat transkripzio koaktibatzaile edo kosupresoreen lotura gunea. Ondoren, prolina ugaridun eskualdea edo PRR (61-94 aminoazidoak) dago, non PXXP sekuentziaren hainbat kopia dauden, eta oso garrantzitsua dena p53-aren bidezko apoptosiaren indukzioan.¹⁸⁸ Erdiko eremuan edo ADN lotura-eremuan (102-292 hondarrak) ADN elkartzten da, eta eremu honetan Zn²⁺ ioi bat ere lotzen da, proteinaren egiturari egonkortasuna emanez. Azkenik, C-muturreko eremuan (301-393 aminoazidoak), translazio-ondoko zenbait aldaketa gertatzen dira, proteinaren jarduera eta egonkortasunerako garrantzitsuak direnak. Muturreko domeinu honek tetramerizazio domeinua (TD) (324-355 aminoazidoak) dauka, p53-aren tetramero aktiboen eraketa ahalbidetzen duena.¹⁸⁶

¹⁸² (a) Alvi, M. S.; Rizvi, I. F.; Siddiqui, M. H.; Farooqui, A. **2016**, *8*, 112-118. (b) Ozaki, T.; Nakagawara, A. *Cancers (Basel)* **2011**, *3*, 994-1013.

¹⁸³ (a) Lane, D. P.; Crawford, L. V. *Nature* **1979**, *278*, 261-263. (b) Linzer, D. I.; Levine, A. J. *Cell* **1979**, *17*, 43-52. (c) Kress, M.; May, E.; Cassingena, R.; May, P. J. *Virology* **1979**, *31*, 472-483. (d) Melero, J. A.; Stitt, D. T.; Mangel, W. F.; Carroll, R. B. *Virology* **1979**, *93*, 466-480. (e) Smith, A. E.; Smith, R.; Paucha, E. *Cell* **1979**, *18*, 335-346. (f) DeLeo, A. B.; Jay, G.; Apaella, E.; Dubois, G. C.; Law, L. W.; Old, L. J. *Proc. Natl Acad. Sci. USA* **1979**, *76*, 2420-2424.

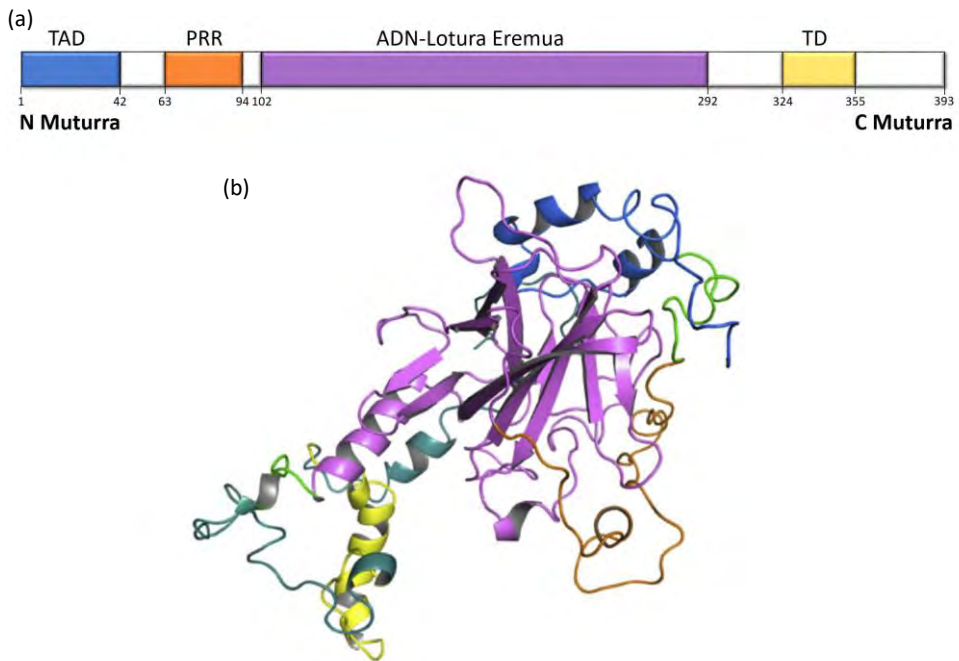
¹⁸⁴ (a) Ben David, Y.; Prideaux, V. R.; Chow, V. *Oncogene* **1988**, *3*, 179-185. (b) Mowat, M.; Cheng, A.; Kimura, N.; Bernstein, A. *Nature* **1985**, *314*, 633-636. (c) Wolf, D.; Rotter, V. *Proc. Natl Acad. Sci. USA* **1985**, *82*, 790-794. (d) Wolf, D.; Rotter, V. *Mol. Cell. Biol.* **1984**, *4*, 1402-1410.

¹⁸⁵ (a) Baker, S. J.; Fearon, E. R.; Nigro, J. M.; Hamilton, A. C.; Preisinger, A. C.; Jessup, J. M.; Van Tuinen, P.; Ledbetter, D. H.; Barker, D. F.; Nakamura, Y.; White, R.; Vogelstein, B. *Science* **1989**, *244*, 217-221. (b) Eliyahu, D.; Michalovitz, D.; Eliyahu, S.; Pinhasi-Kimhi, O.; Oren, M. *Proc. Natl Acad. Sci. USA* **1989**, *86*, 8763-8767. (c) Finlay, C. A.; Hinds, P. W.; Levine, A. J. *Cell* **1989**, *57*, 1083-1093.

¹⁸⁶ Levine, A. J.; Oren, M. *Nat. Rev. Cancer* **2009**, *9*, 749-758.

¹⁸⁷ (a) Saha, T.; Kar, R. K.; Sa, G. *Prog. Biophys. Mol. Biol.* **2015**, *117*, 250-263. (b) Joerger, A. C.; Fersht, A. R. *Annu. Rev. Biochem.* **2008**, *77*, 557-582.

¹⁸⁸ Sakamuro, D.; Sabbatini, P.; White, E.; Prendergast, G. C. *Oncogene* **1997**, *15*, 887-898.



53. irudia. (a) p53ren egitura eskematikoa. (b) Homologia-eredu eta dinamika molekularren simulazioen bidez prestatutako p53ren egitura osoa (Saha *et al.*, 2015).¹⁸⁷

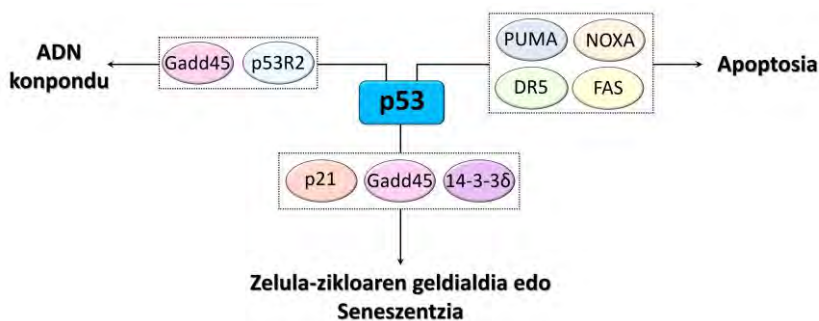
Zelula-estres seinaleen erantzun bezala, hala nola, ADNren kaltea, hipoxia, kalte genotoxikoa, onkogeneen aktibazioa edo zelulen arteko kontaktu normalaren galera, p53-ren aktibazioa sustatzen da *N*-muturreko transaktibazio-eremuaren azetilazio/fosforilazio ugarien eta beste aldaketa post-translazionalen eraginez.¹⁸⁹ Ondorioz, bere traslazioa handitu egiten da, metatu eta beste p53 azpiunitateekin tetrameroak eratu eta gero, transkripzio-faktore funtzioa beteko du. p53 Proteinaren funtzio nagusia zelula-defentsa antolatzea da, eta horretarako seinaleen transdukzio-sarea sinkronizatzen du.¹⁹⁰ p53 Proteinak, zelula-zikloaren gelditzea, seneszentzia edo ADN konpontzea sustatuko du, estres txiki edo konpongarria jasan ez gero, baina, kaltea handia edo konponezina izanez gero, apoptosia aktibatuko du (54. irudia).¹⁹¹ Halaber, ikerketa ugarik erakutsi dute p53 proteina gai dela funtzio gehigarriak betetzeko, hala nola, metabolismo energetikoaren erregulazioa, anti-angiogenesi efektua eta defentsa antioxidatzailea.^{190,192}

¹⁸⁹ (a) Bulavin, D. V.; Saito, S.; Hollander, M. C.; Sakaguchi, K.; Anderson, C. W.; Appella, E.; Fornace, A. J. *EMBO J.* **1999**, *18*, 6845–6854. (b) Canman, C. E.; Lim, D. S.; Cimprich, K. A.; Taya, Y.; Tamai, K.; Sakaguchi, K.; Appella, E.; Kastan, M. B.; Siliciano, J. D. *Science* **1998**, *281*, 1677–1679. (c) Milne, D. M.; Campbell, L. E.; Campbell, D. G.; Meek, D. W. *J. Biol. Chem.* **1995**, *270*, 5511–5518.

¹⁹⁰ Harris, S. L.; Levine, A. J. *Oncogene* **2005**, *24*, 2899–2908.

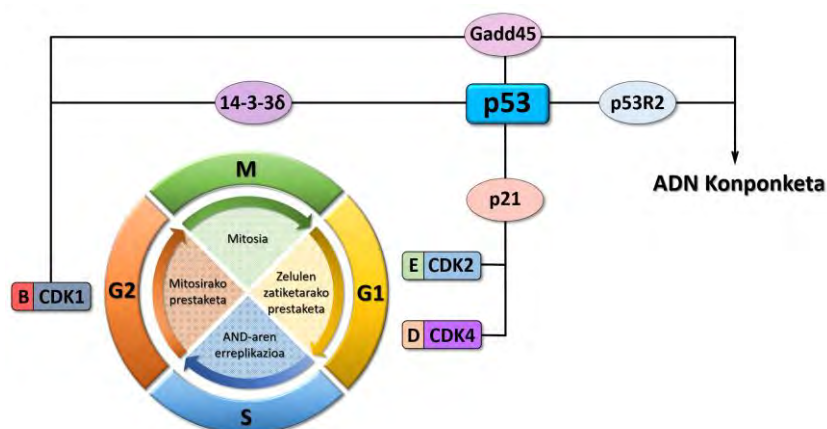
¹⁹¹ Perri, F.; Pisconti, S.; Vittoria Scarpato, G. Della. *Ann. Transl. Med.* **2016**, *4*, 2-5.

¹⁹² Lahalle, A.; Lacroix, M.; De Blasio, C.; Ciss, M. Y.; Linares, L. K.; Le Cam, L. *Cancers* **2021**, *13*, 133-150.



54. irudia. p53 proteinaren tumore-ezabatzaile funtzio nagusiak.

Lehenago azaldu den bezala, badira zenbait etapa zelula-zikloan (G1, S, G2 eta M), eta fase batetik hurrerora pasatu ahal izateko kontrol-puntuak gainditu behar dira, non ziklinek eta ziklinaren mendeko kinasa-komplexuek (CDK) hurrengo etapara igarotzeko baimena emango diote zelulari. p53 Proteinak zelula-zikloan eragindako geldialdia, batez ere, p21ren aktibazio transkripzionalaren bidez gertatzen da. Honek, E/CDK2 eta D/CDK4 ziklina komplexuekin bat egiteko gaitasuna du, zelula-zikloa G1-S fasean gelditzeko, eta, hala, zelula G0 fasean sartzea errazten du (55. irudia). Gainera, p53 proteinaren beste itu-gene batzuek blokea dezakete G2-M trantsizioa, hala nola 14-3-3δ eta Gadd45.¹⁹³ Bestalde, zelularen zikloa geldituta dagoen bitartean, p53 proteinak ADNren konponketa bultzatu dezake, estres txikiko egoeren erantzun bezala, Gadd45 eta p53R2 geneak aktibatuz. Aktibazio horren ondorioz, ADNren kaltea konpon daiteke, mutazioen metaketa eta hauek ondorengo zelulekara transferitzea saihestuz.¹⁹¹



55. irudia. p53 proteinak zelula-zikloan erregulatutako kontrol-puntuak.

¹⁹³ (a) Chen, J. *Cold Spring Harb. Perspect. Biol.* **2016**, 1-16. (b) Chi, S. W. *BMB Rep.* **2014**, *47*, 167-172. (c) Vousden, K. H.; Prives, C. *Cell* **2009**, *137*, 413-431.

Zelulak ADNri kalte itzulezina eragiten dion estres konponezin edo onkogenikoa pairatzen duenean, p53 proteinak apoptosi mekanismo intrintseko eta estrintsekoak aktibatu egiten ditu. Nukleoan, p53 proteina transkripzio-faktore gisa jokatuz hainbat geneen espresioa aktibatuko du, hala nola, BCL-2 familiako proteina pro-apoptotikoak (PUMA, NOXA), apoptosiaren bide intrintsekoa aktibatuz. Bestalde, p53 proteinak FAS eta DR5 bezalako mintz-zeharkako heriotza-hartzaileen espresioa ere eragiten du, apoptosi bide estrintsekoa aktibatuz.¹⁹³

Zelula normaletan eta baldintza fisiologikoetan, p53 proteina maila oso baxu mantentzen da, erregulatuak negatiboak baititu.¹⁹⁴ p53 Proteina tetramerikoa C-muturreko azetilazioaren bidez aktibatzen da, eta horrek esan nahi du, desazetilazioak garrantzi handia izango duela p53 proteina erregulazio negatiboan.¹⁹⁵ Ugaztunen histona-deazetilasi (HDAC) adibide batzuk HDAC1 eta SIRT1 dira, p53 desazetilatu dezaketenak C-muturreko lisinetan, haren funtzioak erreprimatuz.¹⁹⁶ Desazetilazioa aurrera doan heinean ubikuitinazio izeneko prozesua gertatzen da, non ubikuitina proteina bat lotu egiten da p53 proteinan, suntsipenerako markatuz. p53 Proteina ubikuitinazioa ARF-BP1 (ARF lotura-proteina 1), Pirh2 (p53k induzitutako proteina, RING-H2 domeinuarekin), E4F1 (E4F transkripzio-faktore 1) edo MDM2 (Murine Double Minute 2) proteinen menpe dago.¹⁹⁷ Azken hau, MDM2, MDMX (Murine Double Minute X) proteina homologoarekin batera (MDM4 ere deitua), p53 proteina erregulatuak negatibo nagusienak dira.

MDM2 eta MDMX proteinak.

MDM2 genea 1987an identifikatu zen lehen aldiz, Donna George-ren laborategian, MDM1 eta MDM3 geneekin batera, kromosomaz kanpoko elementuetan amplifikatutako ADN-sekuentziak, hots, double-minute (DM) kromosomak, aztertzen ari zirenean.¹⁹⁸ Gainera, gene horiek gainadierazi zituzten saguetan egindako hainbat esperimentuek erakutsi zuten soilik MDM2 gainadierazia zuten saguetan tumoreak garatu zirela.¹⁹⁹ Hau MDM2 genea onkogene gisa deskribatzeko lehen ebidentzia izan zen. MDM2 geneak MDM2 proteina kodetzen du, eta Levin-en taldeak 1992an deskribatu zuen moduan honek p53 proteina erregulatuak negatibo gisa jokatzen du, beraz, proteina hau

¹⁹⁴ Ribeiro, C. J. A.; Rodrigues, C. M. P.; Moreira, R.; Santos, M. M. M. *Pharmaceuticals* **2016**, *9*, 1-33

¹⁹⁵ Reed, S. M.; Quelle, D. E. *Cancers (Basel)* **2014**, *7*, 30-69.

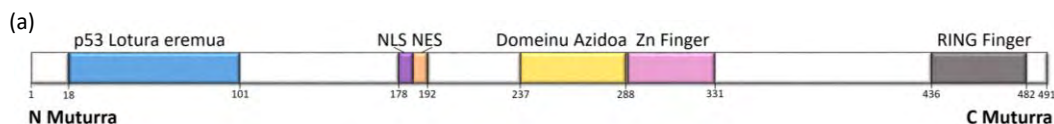
¹⁹⁶ (a) Luo, J. Y.; Nikolaev, A. Y.; Imai, S.; Chen, D. L.; Su, F.; Shiloh, A.; Guarente, L.; Gu, W. *Cell* **2001**, *107*, 137-148. (b) Vaziri, H.; Dessain, S. K.; Eagon, E. N.; Imai, S. I.; Frye, R. A.; Pandita, T. K.; Guarente, L.; Weinberg, R. A. *Cell* **2001**, *107*, 149-159. (c) Luo, J. Y.; Su, F.; Chen, D. L.; Shiloh, A.; Gu, W. *Nature* **2000**, *408*, 377-381.

¹⁹⁷ (a) Lee, S. W.; Seong, M. W.; Jeon, Y. J.; Chung, C. H. *Anim. Cells Syst.* **2012**, *16*, 173-182. (b) Lee, J.T.; Gu, W. *Cell Death Differ.* **2010**, *17*, 86-92.

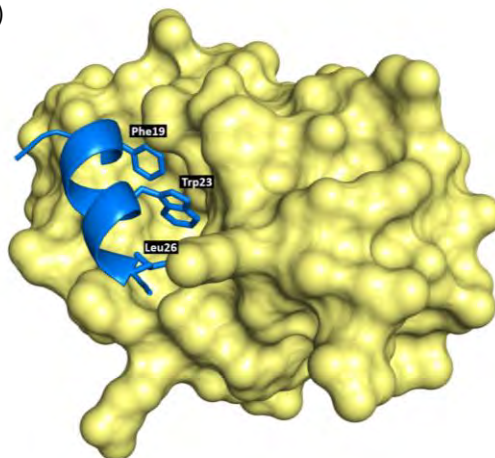
¹⁹⁸ Cahilly-Snyder, L.; Yang-Feng, T.; Francke, U.; George, D. L. *Somat. Cell Mol. Genet.* **1987**, *13*, 235-244.

¹⁹⁹ Fakhrazadeh, S. S.; Trusko, S. P.; George, D. L. *EMBO J.* **1991**, *10*, 1565-1569.

minbiziaren ikerketaren epizentroan kokatu zen.²⁰⁰ Urte berean, Vogelstein-en ikerketa taldeak giza MDM2 genearen klonazioa lortzeaz gain, biak, MDM2 genea zein proteina, 47 giza sarkomen herenean inplikaturik zegoela deskribatu zuen,²⁰¹ agerian utziz MDM2 proteinaren gainadierazpenaren garrantzia minbizien garapenean.



(b)



56. irudia. (a) MDM2 proteinaren egitura eskematikoa (erref.²⁰²). (b) MDM2-p53 peptido konplexuaren egitura kristalinoa (PDB kodea: 4HFZ).

Giza MDM2 proteina funtzio-domeinu desberdinez osaturiko 491 aminoazido-luze den proteina da (56. irudia). *N*-muturra p53 proteinarekiko lotura-eremuarekin hasten da (18-101 aminoazidoak). p53 Proteinaren transaktibazio-eremuko hiru aminoazido (Phe19, Trp23 eta Leu26) MDM2 proteinaren p53-arekiko lotura-eremuko zirrikitu hidrofobiko sakonean sartzen dira, eta horrela p53 proteinaren transkripzio-jarduera inhibitzen da.²⁰³ Eskualde honek, p53 proteinaz gain, beste proteina batzuekin bat egiteko ahalmena dauka. Gainera, MDM2 proteinak nukleo-lokalizazio (NLS) eta nukleo-esportazio (NES) sekuentziak ditu (178-192 aminoazidoak), nukleora sartzeko eta handik irteteko gaitasuna ematen diotenak.²⁰⁴ Erdiguneko domeinu azidoa (237-288 aminoazidoak) MDM2 proteina eta proteina erribosomalen arteko elkarrekintzaren arduraduna izateaz gain, p53 proteinaren degradazioan parte

²⁰⁰ Momand, J.; Zambetti, G. P.; Olson, D. C.; George, D.; Levine, A. J. *Cell* **1992**, *69*, 1237-1245.

²⁰¹ Oliner, J. D.; Kinzler, K. W.; Meltzer, P. S.; George, D. L.; Vogelstein, B. *Nature* **1992**, *358*, 80-83.

²⁰² Wade, M.; Wang, Y. V.; Wahl, G. M. *Trends Cell Biol.* **2010**, *20*, 299-309.

²⁰³ Kussie, P. H.; Gorina, S.; Marechal, V.; Elenbaas, B.; Moreau, J.; Levine, A. J.; Pavletich, N. P. *Science* **1996**, *274*, 948-953.

²⁰⁴ Roth, J.; Dobbstein, M.; Freedman, D. A.; Shenk, T.; Levine, A. J. *EMBO J.* **1998**, *17*, 554-564.

hartzen du. Zink-Finger domeinua 289 eta 331 aminoazidoen arteko eskualde txiki bat da,²⁰⁵ eta azkenik, C-muturrean, RING Finger domeinua dago (436-482 aminoazidoak), MDM2 proteinari E3 ligasa aktibitatea ematen diona, p53 proteina ubikuitinarekin markatuz, ondoren suntsitzeko.²⁰⁶

1996an Jochemsen eta lankideek, enbrioi-fibroblastoen adierazpen-liburutegi bat aztertzen ari zirela p53 proteina erradioaktiboa erabiliz, p53 proteinari lotzen zitzaion eta DM2 proteinaren homologoa zen beste proteina bat deskribatu zuten.²⁰⁷ Hasiera batean MDMX izena eman zitzaion, hala ere, arratoietan *knock-out* ikasketak batzuk burutu ondoren, MDM4 bezala izendatu zen. Bibliografian, bi nomenklaturak onargarriak dira, baina garrantzitsua da azpimarratzea MDMX proteinak ez duela zerikusirik double-minute gene murinoekin, eta horrela izendatu zela bakarrik MDM2 proteinarekin duen homologian oinarrituta.²⁰⁸

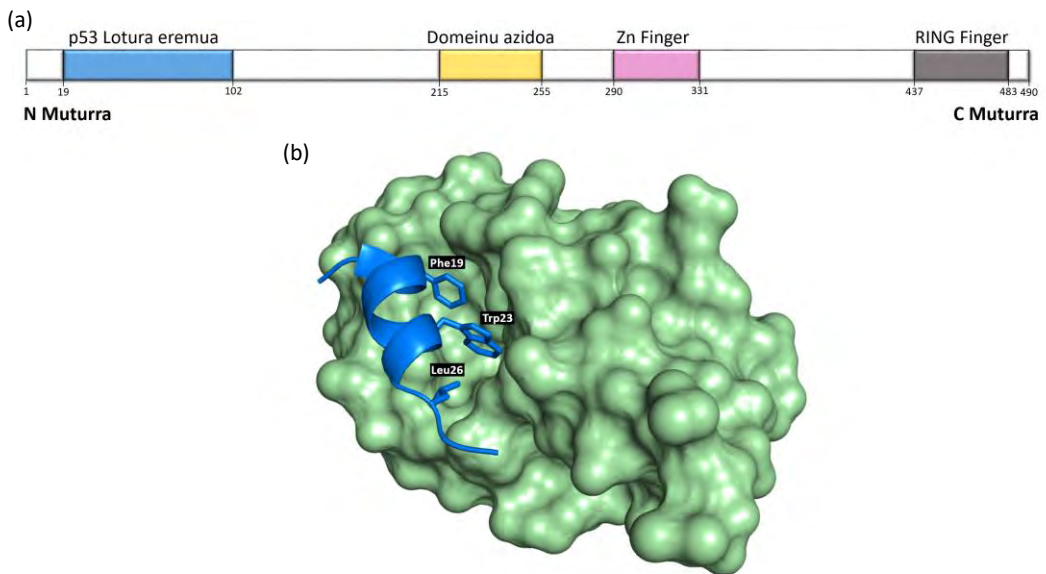


Figure 57. (a) MDMX proteinaren egitura eskematikoa (erref.²⁰²). (b) MDMX-p53 peptido konplexuaren egitura kristalinoa (PDB kodea: 3DAB).

MDMX proteinak, MDM2k bezala, N-muturrean p53-arekiko lotura-eremua (19-102 aminoazidoak), erdiguneko domeinu azidoa (215-255 aminoazidoak), zink-Finger domeinua (290-332

²⁰⁵ Hou, H.; Sun, D.; Zhang, X. *Cancer Cell Int.* **2019**, *19*, 1-8.

²⁰⁶ Lai, Z.; Ferry, K. V.; Diamond, M. A.; Wee, K. E.; Kim, Y. B.; Ma, J.; Yang, T.; Benfield, P. A.; Copeland, R. A.; Auger, K. R. *J. Biol. Chem.* **2001**, *276*, 31357-31367.

²⁰⁷ Shvarts, A.; Steegenga, W. T.; Riteco, N.; Van Laar, T.; Dekker, P.; Bazuine, M.; Van Ham, R. C. A.; Van Der Houven Van Oordt, W.; Hateboer, G.; Van Der Eb, A. J.; Jochemsen, A. G. *EMBO J.* **1996**, *15*, 5349-5357.

²⁰⁸ Berberich, S. J. MDM2 and MDMX involvement in human cancer. In *Mutant p53 and MDM2 in cancer*; Springer, **2014**; pp 263-280

aminoazidoak), eta C-muturreko RING Finger domeinua (437-483 aminoazidoak) baditu.²⁰⁵ Aldiz, MDM2 proteinarekin alderatuta, NLS edo NES sekuentziak ez ditu, eta ondoroz, bere presentzia zitoplasmara mugatzen da (57. irudia).

MDM2 zein MDMXek, homodimeroak eratzeke gaitasuna daukate RING Finger domeinuen bidez elakrtuta, baina soilik MDM2 proteinak dau E3 ligasa aktibitatea bere RING Finger domeinuan, beraz, MDMX proteinak bakarrik ezin du p53 degradatu.²⁰⁹ Gainera, aipatu beharra dago, bi proteinek heterodimeroak sor ditzaketela RING Finger domeinuak elkartuz, eta horrela MDM2 proteinaren E3 ligasa jarduera handituz edo txikiagotuz. Egonkortasunari dagokionez, MDMX proteina oso egonkorra da, 24 ordu baino gehiagoko erdibizitza baitu, berriz, MDM2 proteina ezegonkorragoa da eta 30 minutuko erdibizitza dauka.

MDM2/MDMX-p53 zikloa.

Arestian esan bezala, p53 proteinaren C-muturreko lisinek modu lehiakorrean azetilaziora bideratuta daude eta, horren ondorioz, aktibatu edo ubikitilatu egiten dira, horrela p53 proteina degradaziorako prestatuz.²¹⁰ Ubikuitin-ligasek p53 degradatzeaz gain ubikitilazio bitartez, p53 proteinaren azetilazioa negatiboki erregulatzeko gai dira ere, azetiltransferasa funtzioa duten proteinak ubikitilatu eta hauek proteosoman degradatuz. Ondorioz, p53 azetilazioa murrizten da eta ez da aktibatuko.²¹¹

p53 Proteinaren E3 ubikuitin ligasa eta erregulazaile negatibo nagusia MDM2 proteina da, eta aldi berean p53 proteina beraren transkripzio ituetako bat da. MDM2 proteinaren kontzentrazioa altua denenean, p53ak poliubikitilazioa jasango du, proteosoman gehiago degradatuz. Prozesu horretan, MDMX (edo MDM4) proteinak ere parte hartzen du, p53 proteina lotu eta nukleotik zitoplasmara garraiatuz.²¹² Gainera, MDMX proteinak p53 jarduera inhibi dezake transkripzio-faktore gisa, baina ez du E3 ligasa-jarduerarik MDM2 proteinak duen bezala (58. irudia, gezi beltzak).²¹³

²⁰⁹ Jackson, M. W.; Berberich, S. J.; *Mol Cell Biol.* **2000**, *20*, 1001-1007.

²¹⁰ (a) Ito, A.; Kawaguchi, Y.; Lai, C. H.; Kovacs, J. J.; Higashimoto, Y.; Appella, E.; Yao, T. P. *EMBO J.* **2002**, *21*, 6236-6245. (b) Nakamura, S.; Roth, J.A.; Mukhopadhyay, T. *Mol. Cell. Biol.* **2000**, *20*, 9391-9398. (c) Rodriguez, M.S.; Desterro, J.M.P.; Lain, S.; Lane, D.P.; Hay, R.T. *Mol. Cell. Biol.* **2000**, *20*, 8458-8467. (d) Gu, W.; Roeder, R.G. *Cell* **1997**, *90*, 595-606.

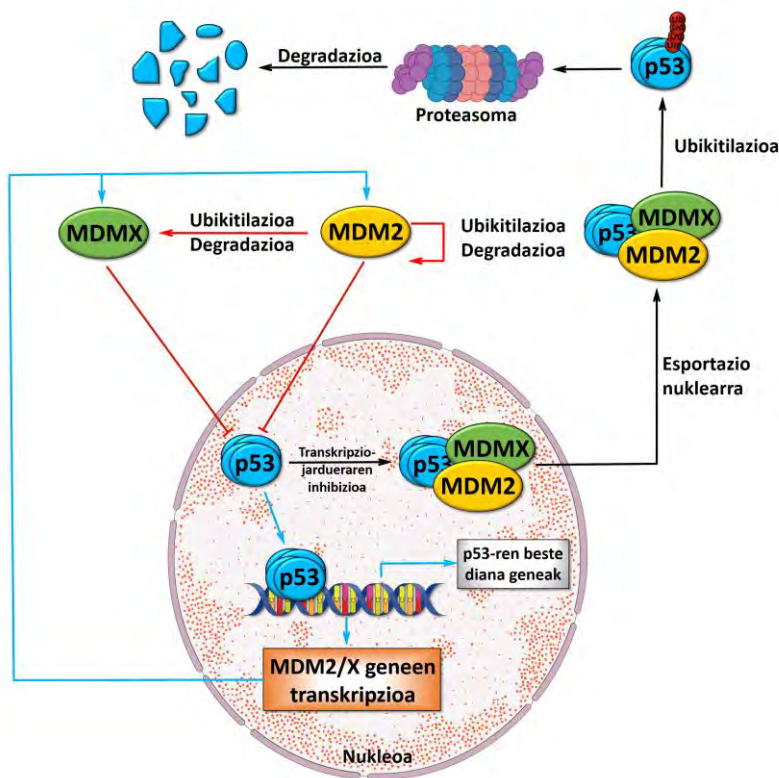
²¹¹ (a) Jin, Y. T.; Zeng, S. X.; Dai, M. S.; Yang, X. J.; Lu, H. J. *Biol. Chem.* **2002**, *277*, 30838-30843. (b) Kobet, E.; Zeng, X. Y.; Zhu, Y.; Keller, D.; Lu, H. *Proc. Natl. Acad. Sci. USA* **2000**, *97*, 12547-12552. (c) Wadgaonkar, R.; Collins, T. J. *Biol. Chem.* **1999**, *274*, 13760-13767. (d) Grossman, S. R.; Perez, M.; Kung, A. L.; Joseph, M.; Mansur, C.; Ziao, Z. X.; Kumar, S.; Howley, P. M.; Livingston, D. M. *Mol. Cell* **1998**, *2*, 405-415.

²¹² (a) Brooks, C. L.; Li, M.; Gu, W. *J. Biol. Chem.* **2007**, *282*, 22804-22815. (b) Li, M. Y.; Brooks, C. L.; Wu-Baer, F.; Chen, D. L.; Baer, R.; Gu, W. *Science* **2003**, *302*, 1972-1975. (c) Lohrum, M. A. E.; Woods, D. B.; Ludwig, R. L.; Balint, E.; Vousden, K. H. *Mol. Cell. Biol.* **2001**, *21*, 8521-8532.

²¹³ Marine, J. C.; Jochemsen, A. G. *Biochem. Biophys. Res. Comm.* **2005**, *331*, 750-760.

Estres-egoeran, MDM2 proteinak bere burua eta MDMX proteina degradatu egiten ditu eta, ondorioz, p53 proteinaren kontzentrazioa handitzen da, p53 tetramerizatuz (58. irudia, gezi gorriak). Nukleoan, aktibatutako p53 tetrameroaren maila handiak honen transkripzioaren xede diren geneak aktibatzen ditu, MDM2/X transkripzio-geneak barne. Ekintza horren ondorioz, MDM2 eta MDMX proteinen kontzentrazio altuak lortzen dira (58. irudia, gezi urdinak). Honek, eragingo du berriro MDM2 proteinak bere burua eta MDMX proteina modo efizienteagoan degradatzea, zikloa berriro errepikatuz eta p53 proteinaren erabateko aktibazioa ahalbidetuz.

Estres egoera gainditu ondoren, MDM2 proteinaren itua ostera ere p53 proteina izango da MDMX proteinaren laguntzarekin, eta p53 inaktibatuko da (58. irudia, gezi beltzak). Azkenik, p53ren kontzentrazioa murriztu denean, MDM2 proteina ere murriztuko da, eta, hala, p53 proteina maila fisiologikoetara handituko da, zikloa osatuz.^{195,214} Aipatu beharra dago, gaur egun, ez dela guztiz ulertzen zergatik estres gabeko zeluletan MDM2 proteinak p53 proteina degradatzen duen, eta aldiz estres egoeran bere burua eta MDMX proteina degradatzen dituen.



58. irudia. p53-MDM2/MDMX zikloaren eskema grafikoa. (Khoury *et al.*, 2011-tik egokitua).²¹⁴

²¹⁴ Khoury, K.; Popowicz, G. M.; Holak, T. A.; Dömling, A. *Med. Chem. Comm.* **2011**, *2*, 246-260.

p53-MDM2/MDMX minbiziaren tratamendurako itua.

p53-aren eta MDM2-aren (edo MDMX) arteko lotura proteina-proteina elkarrekintza (PPI) gisa definitzen da. PPI-en inhibizio egokia burutzeko ahalmena duten molekulen aurkintza erronka konplexua da, bi proteinen arteko interfasearen azaleraren tamaina handiaren ondorioz (600 -1300 Å²), eta proteina bakoitzeko 30 alboko kateren arteko interakzioak egon daitezkeelako.²¹⁵ Hala ere, nahiz eta interakzio-azalera handia izan, aminoazido gutxi batzuek osatutako poltsiko txiki bat egoten da, gunek-aktibo izenekoa, lotura-energia gehiena biltzen duena eta ondorioz pisu molekular baxuko molekulen itu bezala erabil daitekeena.²¹⁶

p53-MDM2/X konplexuaren gunek-aktiboa p53 proteinen Trp23, Leu26 eta Phe19 aminoazidoz osatutako 'hiru atzamarreko farmakofoa' da. Hiru aminoazido hidrofobiko horiek, MDM2 eta MDMX proteinen gunek hidrofobikoan egokitzen dira, forman eta energia elektrostatiakoan osagarri direnak. Gainera, hidrogeno-lotura bat eratzen da p53-ko Trp23 aminoazidoaren indolaren nitrogenoaren eta MDM2-ko Leu54-ren artean (Met53 MDMX-n).²¹³ Beraz, p53-MDM2/X konplexuaren afinitate handiko inhibitzaile batek p53 proteinen gunek aktiboko hiru aminoazidoak (Trp23, Leu26 eta Phe19) imitatzeke gai izan beharko luke.

α,β-Laktama asegabeek frogatu dute MDM2 eta MDMX proteinak inhibitzeke gaitasuna dutela (18. irudia, *vide supra*). Horregatik, hurrengo atalean, lan honen zehar sintetizatutako konposatuak aktibitate zitotoxikoa eta MDM2/MDMX-p53 proteina-proteina interakzioa inhibitzeke gaitasuna ikertuko da.

²¹⁵ Sperandio, O.; Reynes, C. H.; Camproux, A. C.; Villoutreix, B. O. *Drug Discovery Today* **2010**, *15*, 220-229.

²¹⁶ Clackson, T.; Wells, J. A. *Science* **1995**, *267*, 383-386.

7. Kapitulu

Aktibitate antiproliferatiboaren eta apoptosi indukzioa induitzeko gaitasunaren ebaluazioa

Atal honetan, sintetizatutako γ -laktama deribatuen egitura-aktibitate profilak garatuko dira. Horretarako, substratuen *in vitro* jarduera zitotoxikoa hainbat giza minbizi zelula lerroetan ikertu da, beraien aktibitate antiproliferatiboa aztertuz. Zelulen hazkundearen inhibizio-jarduera ebaluatzeko, zelula-zenbaketarako kit kolorimetrikoa (CCK-8) erabili da. Horrez gain, MRC5 birika-fibroblasto ez-gaiztoak analizatu dira toxikotasuna minbizi zelula lerroentzat selektiboa den egiaztatzeko, eta doxorribizina agente kimioterapeutikoa erreferentzia-balio gisa erabili da.

7.1. γ -Laktama α,β -asegabeen aktibitate antiproliferatiboa.

Lehenik eta behin, familia buru bezala **72c** γ -laktama aukeratu eta bere zitotoxikotasuna probatu zen giza-minbizi zazpi zelula-lerroetan: HEK293 (giza-enbrioi giltzurruna), MCF7 (giza-bularreko adenokartzinoma), HTB81 (giza-prostatato kartzinoma), HeLa (giza-zerbixeko epitelioaren kartzinoma), RKO (giza-koloneko epitelioaren kartzinoma), SKOV3 (giza-obulutegiko kartzinoma) eta A549 (giza-albeolo basaleko kartzinoma epiteliala). **72c** γ -Laktamaren zelulen proliferazioaren inhibizio-jarduera, IC_{50} balio bezala adierazi da (59. irudia).

Zelula-lerro	IC_{50} (μM)
HEK293 (Giltzurrun)	>50
MCF7 (Bular)	>50
HTB81 (Prostata)	27.93 \pm 2.73
HeLa (Zerbix)	30.23 \pm 3.75
RKO (Kolon)	22.07 \pm 2.98
SKOV3 (Obulutegi)	9.62 \pm 1.18
A549 (Birika)	2.34 \pm 0.28
MRC5 (Birika)	>50

59. irudia. **72c** γ -Laktamaren aktibitate antiproliferatiboa zelula-lerro ezberdinetan.

HEK293 eta MCF7 zelula-lerroetan aktibitate ez baten hauteman ere, zitotoxikotasun moderatua neurtu zen HTB81, HeLa eta RKO zelula-lerroetan. Nabarmentzekoa da, SKOV3 eta A549 zeluletan aktibitate interesgarria lortu zela, eta, gainera, aipatu beharra dago, MRC5 zeluletan ez zela zitotoxikotasunik neurtu, konposatu honek zelula gaiztoen aurrean selektibitate handia duela agerian utziz (59. irudia).

Emitza horiek ikusita, zelulen aktibitate antiproliferatiboaren ikerkuntza sintetizatutako beste konposatu γ -laktamikoetara zabaldu zen, RKO, SKOV3 eta A549 zelula-lerroak erabiliz. C-5eko (R^1) ordezkatzailak duen eragina ebaluatzeko, *p*-toluidinatik deribatutako **72** eta **90** 3-amino-1,5-dihidro-2*H*-pirrol-2-ona konposatuen IC_{50} balioak 16. taulan aurkitzen dira.

Familia honetako substraturik sinpleena **72b** da, formaldehidotik lortzen da eta eraztunaren 5. posizioan ez du ordezkatzailerik. Konposatu honek ez zuen *in vitro* aktibitate erakutsi SKOV3 zelula-lerroaren aurka, baina toxikotasunean ahula hauteman zen A549 zelula-lerroan, $38,25 \pm 3,35 \mu\text{M}$ -eko IC_{50} balioa lortuz (16. taula, 1. sarrera). **72** γ -Laktama substratuen aktibitatea eraztunaren C-5 posizioko ordezkatzailaren menpekota da, izan ere, fenilo taldez ordezkaturako **72c** laktamak IC_{50} balio hobekak izan zituen, $9,62 \pm 1,18$ eta $2,34 \pm 0,28 \mu\text{M}$ -ekoak SKOV3 eta A549 zelula-lerroetan hurrenez hurren, eta gainera selektibitate onarekin birika fibroblasto ez-gaiztoekin alderatuz (16. taula, 2. sarrera).

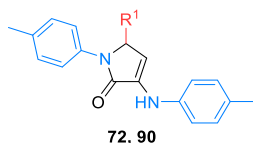
Metil taldeak molekula bioaktibo batean sartzeak bere izaera lipofiloagoa bihurtzen ohi du, zelula-mintzak zeharkatzeko gaitasun hobea duten molekulak sortuz.²¹⁷ Hala ere, gure kasuan, eraztunaren 5. posizioan ordeztutako *ortho*, *meta* edo *para* metilbentzeno taldeek aktibitate zitotoxikoa murriztu zuten A549 zelula-lerroaren kontra, IC_{50} 20-40 μM inguruko balioekin, eta SKOV3 zelula-lerroan aktibitatea erabat galdu zen, 50 μM baino altuagoko IC_{50} balioekin (16. taula, 3-5. sarrerak).

Konposatu organikoen egituretan fluor atomoak gehitzean eragina auresatea nahiko zaila den arren, sarritan aktibitatearen areagotzea dakar.²¹⁸ Hori dela eta, ondoren, fluorodun atomoak dituzten **72d,f** γ -laktamen *in vitro* aktibitate zitotoxikoa determinatu zen SKOV3 eta A549 zelula-lerroetan. Bost kideko eraztunetan *p*-fluorofenil ordezkatzaila sartzeak ez zuen jarduera hobetu, eta $23,52 \pm 0,75$ eta $10,72 \pm 1,21 \mu\text{M}$ -eko IC_{50} balioak lortu ziren SKOV3 eta A549 zeluletan hurrenez hurren, **72f** konposaturako (16. taula, 7. sarrera). Era berean, *para*-trifluorometilfenil ordezkapena duen **72d** γ -laktaman, 50 μM -etik gorako IC_{50} balioak lortu ziren bi minbizi-lerro zelularretan (16. taula, 6. sarrera).

²¹⁷ (a) Schönherr, H.; Cernak, T. *Angew. Chem. Int. Ed.* **2013**, *52*, 12256-12267. (b) Barreiro, E.J.; Kümmerle, A.E.; Fraga, C.A.M. *Chem. Rev.* **2011**, *111*, 5215-5246

²¹⁸ (a) Müller, K.; Faeh, C.; Diederich, F. *Science* **2007**, *317*, 1881-1886. (b) Shah, P.; Westwell, A.D. *J. Enzym. Inhib. Med. Chem.* **2007**, *22*, 527-540.

16. taula. 72 eta 90 3-amino-1,5-dihidro-2H-pirrol-2-onen C-5 posizioko ordezkatzailak jarduera antiproliferatiboan duen eraginaren ebaluazioa.



Sarr.	Prod.	R ¹	IC ₅₀ (μM)			
			A549	SKOV3	RKO	MRC5
1	72b	H	38,25 ± 3,35	>50	d.g.	>50
2	72c	Ph	2,34 ± 0,28	9,62 ± 1,18	22,07 ± 2,98	>50
3	72g	2-MeC ₆ H ₄	41,28 ± 1,29	>50	d.g.	>50
4	72i	3-MeC ₆ H ₄	31,16 ± 1,04	>50	d.g.	>50
5	72h	4-MeC ₆ H ₄	21,02 ± 1,64	>50	d.g.	>50
6	72d	4-CF ₃ C ₆ H ₄	>50	>50	>50	d.g.
7	72f	4-FC ₆ H ₄	10,72 ± 1,21	23,52 ± 0,75	d.g.	>50
8	72a	4-NO ₂ C ₆ H ₄	17,08 ± 1,58	22,87 ± 0,63	23,84 ± 2,53	26,55 ± 2,89
9	72e	3-NO ₂ C ₆ H ₄	7,33 ± 0,57	27,65 ± 1,32	d.g.	27,23 ± 1,24
10	72j	6-(<i>N</i> -Me-indolil)	19,34 ± 0,7	>50	d.g.	>50
11	72k	2-Furil	11,52 ± 0,85	>50	d.g.	>50
12	72l	2-Tienil	12,71 ± 1,07	12,65 ± 1,83	d.g.	>50
13	72m	2-Naftil	12,1 ± 0,74	30,52 ± 1,34	d.g.	21,29 ± 0,74
14	72n	Me	15,68 ± 0,92	29,16 ± 1,00	d.g.	>50
15	72o	ⁱ Pr	11,08 ± 0,71	>50	d.g.	>50
16	72p	^t Bu	20,08 ± 2,00	>50	d.g.	24,05 ± 1,64
17	72q	Cy	10,99 ± 0,90	>50	23,79 ± 1,32	>50
18	72r	CH=CH-Ph	10,26 ± 0,8	9,59 ± 0,82	d.g.	18,24 ± 0,81
19	72s	CO ₂ Et	>50	>50	d.g.	d.g.
20	90d	C ₆ F ₅	33,50 ± 1,68	>50	>50	>50
21	90e	CF ₃	>50	>50	>50	d.g.
22	90a	CH ₂ P(O)(OEt) ₂	11,29 ± 1,80	>50	>50	>50
23	90c	CH ₂ P(O)(Ph) ₂	5,67 ± 0,9	10,76 ± 0,88	28,14 ± 1,47	30,10 ± 0,49
24	Doxorubizina		<0,1	0,13 ± 0,098	<0,1	>50

Gainera, elektroietan urriak diren beste eraztun aromatikoak dituzten γ-laktama substratuek, hala nola, *p*-nitrofenilez ordezkaturako **72a** konposatuak, 22,87 ± 0,63 eta 17,08 1,58 μM-eko IC₅₀ balioak erakutsi zuen, SKOV3 eta A549 zelula-lerroetan, hurrenez hurren (16. taula, 8. sarrera). Bestalde, 27,65 ± 1,32 eta 7,33 ± 0,57 μM-eko IC₅₀ balioak neurtu ziren *m*-nitrofenil taldea duen **72e** γ-laktamarako zelula-lerro berdinetan (16. taula, 9. sarrera). Harrigarria bada ere, **72a** konposatuak zitotoxikotasuna

erakutsi zuen RKO zelula-lerroaren kontra, $23,84 \pm 2,53 \mu\text{M}$ -eko IC_{50} balioekin, baina toxikotasun pixka bat ere hauteman zen MRC5 birika-zelula ez-gaiztoetan (16. taula, 8. sarrera).

Halaber, γ -laktama eraztuneko C-5 posizioako talde aromatikoa ordezkatzaille heteroaromatiko (*N*-metil-indolil, furil, tiofeno) edo naftil talde batekin trukatzek ez zuen eragin positiborik izan aktibitate zitotoxikoan SKOV3 eta A549 zelula-lerroetan. Izan ere, *N*-metil-indolil, furil, tiofeno edo naftil taldez ordezkaturako **72j-m** γ -laktamen deribatuen IC_{50} balio altuagoak izan ziren, fenil taldez ordezkaturako **72c** konposatuarenak baino (16. taula, 10-13. sarrerak).

Jarraian, γ -laktama eraztunaren 5. posizioan ordezkatzaille alifatikoen eragina ikertu zen. Metil taldea duen **72n** substratuak eragin zitotoxiko txikixeagoa izan zuen fenil duen **72c** substratuarekin alderatuta, $29,16 \pm 1,00$ and $15,68 \pm 0,92 \mu\text{M}$ -eko IC_{50} balioak eskuratuz SKOV3 eta A549 zelula-lerroetan, hurrenez hurren (16. taula, 14. sarrera). Posizio honetan talde alifatiko handiagoak kokatuz gero, hala nola *iso*-propil, *iso*-butil edo ziklohexil taldeak, **72o-q** substratuen jarduera zitotoxikoa erabat galdu zen SKOV3 zelula-lerroaren kontra, eta IC_{50} balio ia berdinak, edo pixka bat hobetoagoak, neurtu ziren A549 zelula-lerroan. Hala ere, ziklohexil ordezkatzaillea duen **72q** substratuak $23,79 \pm 1,32 \mu\text{M}$ -ko IC_{50} balioa izan zuen RKO zelula-lerroaren aurka (16. taula, 15-17. sarrerak). Gainera, C-5 posizioan zinamil ordezkatzaillea duen **72r** γ -laktamak, $10 \mu\text{M}$ inguruko IC_{50} balio apalak erakutsi zituen, SKOV3 eta A549 zelula-lerroetan, baina selektibitate handirik ez zelula ez-gaiztoekiko. Azkenik, etil karboxilato taldez ordezkaturako **72s** laktamak ez zuen aktibitate zitotoxikorik azaldu (16. taula, 18-19. sarrerak).

Fluorodun konposatuetara bueltatuz, ondoren, γ -laktam heterozikloko ordezkatzaille perfluoratuek aktibitate antiproliferatiboan duten eragina neurtu egin zen. Hala ere, perfluorofenil eta trifluorometildun **90d,e** γ -laktamek, fluoro-gabeko kideek (**72c** eta **72n**) baino aktibitate zitotoxiko baxuagoa erakutsi zuten (16. taula, 20. eta 21. sarrerak vs. 2. eta 14. sarrerak).

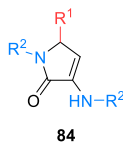
Era berean, molekula bioaktiboetan, fosforodun talde funtzionalen sarreraren ondorioz egindako egitura-aldaketek, askotan, molekularen aktibitatea hobetu edo aldatu dezaketela jakina da.²¹⁹ Hori dela eta, fosfonato eta fosfina-oxido talde funtzionalak dituzten **90a,c** γ -laktamen zelula-proliferazioaren inhibizio jarduerak aztertu ziren. Fosfonatotik eratorria den **90a** substratuak nolabaiteko aktibitate zitotoxikoa azaldu zuen A549 zelula-lerroaren kontra bakarrik, $11,29 \pm 1,80 \mu\text{M}$ -eko IC_{50} neurtuz (16. taula, 22. sarrera). Halaber, fosfina-oxido taldea duen **90c** konposatuak propietate

²¹⁹ (a) Karl, D. M. *Nature* **2000**, *406*, 31-33. (b) Engel, R. *Handbook of Organophosphorus Chemistry*; Dekker M. Inc.: New York, NY, USA, 1992. (c) Kafarski, P.; Lejczak, B. *Phosphorus Sulfur Silicon Relat. Elem.* **1991**, *63*, 193-215.

zitotoxikoak zituen aztertutako hiru minbizi zelula-lerroen kontra, baina toxikoa ere izan zen biriketako fibroblasto ez-gaiztoetan (16. taula, 23. sarrera) .

γ -Laktama-eraztunaren 5. posizioko ordezkatzailleek aktibitate zitotoxikoan duten eragina behin deskribatuta, ondoren egitura-aktibitatearen analisia osatze aldera, heterozikloan dagoen amino ordezkatzailleak duen eragina ikertuko zen (17. taula).

17. taula. 84 3-Amino 1,5-dihidro-2H-pirrol-2-onen aktibitate antiproliferatiboa. Amino ordezkatzaillearen efektua.



Sarr.	Prod.	R ¹	R ²	IC ₅₀ (μM)			
				A549	SKOV3	RKO	MRC5
1	84b	Ph	4-MeOC ₆ H ₄	12,02 ± 1,96	6,84 ± 0,59	d.g.	>50
2	84a	4-NO ₂ C ₆ H ₄	4-MeOC ₆ H ₄	31,48 ± 1,37	>50	>50	>50
3	90b	CH ₂ P(O)(OEt) ₂	4-MeOC ₆ H ₄	6,84 ± 0,22	>50	d.g.	>50
4	84f	4-NO ₂ C ₆ H ₄	4-ClC ₆ H ₄	17,16 ± 2,10	>50	d.g.	>50
5	84g	4-NO ₂ C ₆ H ₄	3-ClC ₆ H ₄	8,37 ± 1,27	16,13 ± 0,81	d.g.	23,81 ± 1,70
6	84c	4-NO ₂ C ₆ H ₄	4-BrC ₆ H ₄	>50	>50	d.g.	d.g.
7	84d	4-CF ₃ C ₆ H ₄	4-BrC ₆ H ₄	>50	>50	>50	d.g.
8	84h	4-NO ₂ C ₆ H ₄	2-FC ₆ H ₄	4,36 ± 0,51	5,55 ± 0,62	d.g.	>50
9	84j	H	3-CF ₃ C ₆ H ₄	22,94 ± 1,13	>50	d.g.	>50
10	84k	4-NO ₂ C ₆ H ₄	3-CF ₃ C ₆ H ₄	2,00 ± 0,78	8,50 ± 0,54	d.g.	44,50 ± 1,16
11	84m	4-NO ₂ C ₆ H ₄	2-Kinolinil	9,25 ± 1,49	>50	d.g.	>50
12	Doxorubizina			<0,1	0,13 ± 0,098	<0.1	>50

Metoxi talde funtzionala ordezkatzaille elektroi-emaile sendoa da eta hainbat farmako eta produktu naturalen egituretan dago talde eraztun aromatikoetan. Askotan, talde funtzional honen presentziak minbizi-aurkako molekulen aktibitatearen eta selektibitatearen hobekuntza ekar dezake, segur aski bere jarduera antimitotiko ahul/ertainaren ondorioz.²²⁰ Hori dela eta, *para*-anisidinatik eratorritako **84a,b** eta **90b** γ -laktamen aktibitate antiproliferatiboa ebaluatu zen. Kasu horietan, **84b** γ -laktamak, C-5 posizioan fenil talde bat duela, zitotoxikotasun hobea erakutsi zuen SKOV3 zelula-lerroan, baina zertxobait okerragoa A549 zelula-lerroan, *p*-toluidina duen **72c** deribatuarekin konparatuta, (IC₅₀ balioa: 6,84 ± 0,59 eta 12,02 ± 1,96 M). Gainera, selektibitatea erakutsi zuen, zelula ez-gaiztoetan

²²⁰ (a) Metwally, K., Khalil, A., Sallam, A.; Pratsinis, H.; Kletas, D.; El Sayed, K. *Med. Chem. Res.* **2013**, *22*, 4481-4491. (b) Patani, G. A.; Lavoie, E. J. *Chem. Rev.* **1996**, *96*, 3147-3176.

aktibitaterik ez zelako antzeman (17. taula, 1. sarrera vs. 16. taula, 2. sarrera). Aldiz, ez zen hobekuntzarik hauteman toxikotasunean C-5 *p*-nitrofeniloz ordezkaturako **84a** substratuaren kasuan, haren analogoa den **72a** deribatuarekin alderatuta (17. taula, 2. sarrera vs. 16. taula, 8. sarrera). Hala ere, **90b** fosfonato-deribatua SKOV3 zelula-lerroan aktibo ez bazen ere, $6,84 \pm 0,22 \mu\text{M}$ -eko IC_{50} balioa neurtu zen A549 zeluletan, bere parekoa den **90a** substratuaren balioak hobetuz (17. taula, 3. sarrera vs. 16. taula, 22. sarrera).

γ -Laktamako amino ordezkatzailak jarduera antiproliferatiboan duen eragina aztertzen jarraitzeko, anilinarene egitura halogeno atomoen presentziak duen efektua ebaluatu zen **84c-g** substratuetan. *p*-Nitrofenil ordezkatzaila duen *p*-kloroanilinarene **84f** deribatuaren kasuan ez zen toxikotasunean aldaketa nabarmenik hauteman, **72a** (*p*-toluidina)edo **84a** (*p*-anisidina) deribatuarekin alderatuta (17. taula, 4. sarrera vs. 17. taula, 2. sarrera vs. 16. taula, 8. sarrera). Zitotoxikotasuna hobetu egin zen A549 eta SKOV3 zelula lerroetan eraztun aromatikoaren kloro atomoa *para* posiziotik *meta* posiziora aldatu zenean, **84g** γ -laktamaren kasurako, baina selektibitatea murriztu zen birika-zelula ez-gaiztoetan toxikotasuna ere neurtu zelako (17. taula, 5. sarrera). Gainera, *p*-bromoanilinarene **84c,d** deribatuak ez zuten inolako inhibizio-jarduerarik sortu zelula-lerroetan (17. taula, 6-7. sarrerak). Hala ere, oso emaitza onak lortu ziren *o*-fluoroanilinarene deribatua den **84h** γ -laktamarekin, zitotoxikotasunari eta selektibitateari dagokienez, $5,55 \pm 0,62$ eta $4,36 \pm 0,51 \mu\text{M}$ -eko IC_{50} balioekin, SKOV3 eta A549 zelula-lerroetan hurrenez hurren. Balio hauek nabarmenki hobeak dira balioidea den **72a** substratu ez-fluoratuaren aldean (17. taula, 8. sarrera vs. 16. taula, 8. sarrera). *m*-Trifluorometil anilinarene erabilerak **84j,k** konposatuetan ahalmen zitotoxikoaren hobekuntza ekarri zuen. Ordezkatu gabeko formaldehidoaren **84j** deribatuak IC_{50} balio hobeak agertu zituen eredu den **72b** deribatuak baino (17. taula, 9. sarrera vs. 16. taula, 1. sarrera), baina **84k** substratuak, C-5 posizioan *p*-nitrofenil ordezkatzaila duena, $8,50 \pm 0,54$ eta $2,00 \pm 0,78 \mu\text{M}$ -eko IC_{50} balio oso onak erakutsi zituen SKOV3 eta A549 zelula lerroetan, hurrenez hurren (17. taula, 10. sarrera vs. 16. taula, 8. sarrera), berriro ere askoz txikiagoak *p*-toluidinarene deribatua den **72a** substratu analogoak baino (17. taula, 10. sarrera vs. 16. taula, 1. sarrera).

γ -Laktamen egitura heteroatomodun aminen efektua ere aztertu egin zen, eta horretarako, lehenik eta behin, amino-kinolina aukeratu zen, farmakoen garapenean garrantzi handiko egitura baita.²²¹ Izan ere, kinolina deribatu askok izugarritzko potentziala erakutsi dute minbizi-contrako agente gisa.²²² Adibidez, A549 zelula-lerroan jarduera zitotoxikoa eta selektibitatea hobetu egin zen

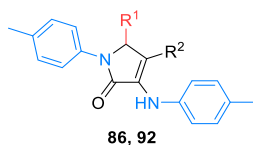
²²¹ (a) Shang, X.-F.; Morris-Natschke, S. L.; Liu, Y.-Q.; Guo, X.; Xu, X.-S.; Goto, M.; Li, J.-C.; Yang, G.-Z.; Lee, K.-H. *Med. Res. Rev.* **2018**, *38*, 775-828. (b) Diaz, G.; Miranda, I. L.; Diaz, M. A. N. Quinolines, Isoquinolines, Angustureine, and Congeneric Alkaloids-Occurrence, Chemistry, and Biological Activity. In *Phytochemicals-Isolation, Characterisation and Role in Human Health*; InTech, 2015; pp 141-162.

²²² Afzal, O.; Kumar, S.; Haider, R.; Ali, R.; Kumar, R.; Jaggi, M.; Bawa, S. *Eur. J. Med. Chem.* **2015**, *97*, 871-910.

2-kinolinilaminaz ordezkatutako **84m** γ -laktamaren kasuan, bere parekoak diren *p*-toluidina, *p*-anisidina, *p*-kloroanilina eta *p*-bromoanilindun **72a**, **84a**, **84f** eta **84c** konposatuen aurrean (17. taula, 11. sarrera vs. 16. taula, 8. sarrera eta 17. taula, 2, 4 eta 6. sarrerak), eta ez zen aktibitatearik detektatu SKOV3 zelula-lerroan.

Aminek eta C-5 posizioako ordezkatzaileek **72**, **84** eta **90** 1,5-dihidro-2*H*-pirro-2-onen aktibitate zitotoxikoan duten eragina ikertu ondoren, hurrengo pausoa C-4 posizioako ordezkatzaileen efektua **86** eta **92** enaminadun γ -laktametan aztertzea izan zen (18. taula).

18. taula. Aktibitate antiproliferatiboan C-4 posizioako ordezkatzaileak duen eragina.

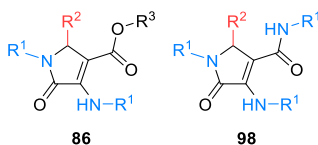


Sarr.	Prod.	R ¹	R ²	IC ₅₀ (μM)			
				A549	SKOV3	RKO	MRC5
1	86a	4-NO ₂ C ₆ H ₄	Me	2,05 ± 0,23	>50	d.g.	>50
2	86b	4-NO ₂ C ₆ H ₄	Bn	9,92 ± 1,15	>50	d.g.	47,56 ± 1,67
3	86c	Ph	CO ₂ Me	1,67 ± 0,49	>50	d.g.	>50
4	92a	H	P(O)(OEt) ₂	>50	>50	>50	>50
5	92b	H	P(O)(Ph) ₂	d.g.	d.g.	d.g.	d.g.
6	Doxorubizina			<0,1	0,13 ± 0,098	<0,1	>50

Substratu horietako bakar batek ere ez zuen SKOV3 zelula-lerroan aktibitatearik erakutsi, baina emaitza interesgarriak lortu ziren A549 zelula-lerroan. 4-Metil eta 4-bentzil taldeak duten **86a,b** γ -laktamek IC₅₀ balio hobetuak erakutsi zituzten, 2,05 ± 0,23 eta 9,92 ± 1,15 μM-ekoak, ordezkatzailearik gabeko **72a** konposatu parekoarekin alderatuta (18. taula, 1, 2. sarrerak vs. 16. taula, 8. sarrera). Halaber, C-4-n metil karboxilato ordezkatzailea duen **86c** γ -laktamak, 1,67 ± 0,49 μM-ko IC₅₀ balio oso ona eman zuen A549 zelula-lerroan, selektibitate esanguratsuekin, SKOV3 edo birika-zelula ez-kartzinogenoekin alderatuta (18. taula, 3. sarrera). Gainera, C-4 posizioan fosfonato-ordezkatzaile baten sarrerak nabarmenki murrizten du aktibitatea zelula-lerro guztietan, **92a** γ -laktamaren kasuan ikusten den bezala, batez ere haren deribatu ez-ordezkatuan (**72b**) hauteman den IC₅₀ balioarekin alderatuta (18. taula, 4. sarrera vs. 16. taula, 1. sarrera). Zoritxarrez, difenil fosfina-oxidodun **92b** konposatuaren jarduera ezin izan zen frogatu, *in vitro* probetan erabiltzen diren disolbatzaileetan disolbagarritasun txikiaren ondorioz (18. taula, 5. sarrera).

Karboxilato ordezkatzaila C-4 posizioan dagoenean (**86c**), jarduera zitotoxikoaren hobekuntza antzeman zenez, xehetasunez aztertu ziren 3-amino-4-karboxilato egitura duten **86** eta **98** 1,5-dihidro-2H-pirrol-2-onen *in vitro* aktibitatea (19. taula).

19. taula. 3-Amino-4-karboxilato ordezkatzailak dituzten **86** eta **98** γ -laktama deribatuen aktibitate antiproliferatiboa.



Sarr.	Prod.	R ¹	R ²	R ³	IC ₅₀ (μM)			
					A549	SKOV3	RKO	MRC5
1	86d	4-MeC ₆ H ₄	Ph	Et	11,70 ± 1,02	>50	>50	>50
2	86e	4-MeOC ₆ H ₄	Ph	Et	14,26 ± 1,80	>50	>50	>50
3	86f	Bn	Ph	Et	2,42 ± 0,15	>50	>50	>50
4	86g	4-MeC ₆ H ₄	Ph	<i>i</i> Pr	3,34 ± 0,29	48,45 ± 2,90	d.g.	>50
5	86c	4-MeC ₆ H ₄	Ph	Me	1,67 ± 0,49	>50	d.g.	>50
6	86h	4-MeC ₆ H ₄	4-CF ₃ C ₆ H ₄	Me	42,58 ± 2,55	30,27 ± 1,03	d.g.	>50
7	86i	Bn	4-CF ₃ C ₆ H ₄	Me	7,64 ± 0,17	>50	d.g.	>50
8	86j	4-MeC ₆ H ₄	4-HOC ₆ H ₄	Me	1,98 ± 0,18	10,37 ± 1,41	d.g.	10,01 ± 1,79
9	86k	Bn	4-HOC ₆ H ₄	Me	10,71 ± 1,35	21,91 ± 1,53	d.g.	17,37 ± 1,68
10	86l	4-MeC ₆ H ₄	3-MeOC ₆ H ₄	Me	13,03 ± 1,48	43,93 ± 1,66	d.g.	30,93 ± 6,16
11	86m	Bn	3-MeOC ₆ H ₄	Me	11,39 ± 1,49	>50	>50	>50
12	86n	4-MeC ₆ H ₄	4-HO,3-MeOC ₆ H ₄	Me	0,11 ± 0,016	1,23 ± 0,31	d.g.	12,64 ± 2,09
13	86o	Bn	4-HO,3-MeOC ₆ H ₄	Me	6,02 ± 1,01	>50	d.g.	>50
14	98a	4-MeC ₆ H ₄	Ph	-	2,97 ± 0,29	6,95 ± 0,59	>50	>50
15	98b	4-MeOC ₆ H ₄	Ph	-	32,38 ± 1,58	16,62 ± 0,19	d.g.	21,42 ± 2,71
16	Doxorubizina				<0,1	0,13 ± 0,098	<0,1	>50

Lehenik eta behin, amino ordezkatzailak duen eragina ebaluatu zen. *p*-Toluidinaren deribatua den **86d** deribatuak IC₅₀ balio apalak erakutsi zituen, 11,70 ± 1,02 μM-ekoak, A549 zelula-lerroan (19. taula, 1. sarrera). Antzeko *p*-anisidina edo bentzilaminadun **86e,f** γ -laktama-deribatuek, 14,26 ± 1,80 eta 2,42 ± 0,15 μM-eko IC₅₀ balioak izan zituzten zelula-lerro berean, hurrenez hurren (19. taula, 2-3. sarrerak). Aipatu beharra dago, **86d-f** substratuek ez zutela zitotoxikotasun esanguratsurik erakutsi SKOV3, RKO eta MRC5 zelulen aurrean (19. taula, 1-3. sarrerak). Horrez gain, *N*-babestu gabeko γ -laktamak, **86f** substratuaren *N*-debentzilazio exoziklotik lortua, jarduera zitotoxiko oso txikia agertu zuen, eta ez zen aintzat hartu izan ikerketan sakontzeko.

Ondoren, ester ordezkatailearen eragina aztertu zen. Etil ester taldea isopropil ester talde batengatik aldatzeak toxikotasun hobekuntza ekarri zuen A549 eta SKOV3 zelula-lerroetan, **86g** substratuan IC_{50} $3,34 \pm 0,29$ eta $48,45 \pm 2,90$ μM -eko balioak neurtuz, hurrenez hurren, eta gainera, ez da aktibitatearik hauteman MRC5 zelula-lerroan (19. taula, 4. sarrera). Metil ester ordezkatailearen presentziak (**86c** konposatua), hobekuntza nabarmena ere ekarri zuen zelula-hazkuntzaren inhibizioan A549 zelula-lerroan, IC_{50} $1,67 \pm 0,49$ μM -eko balio oso onarekin, eta selektibitate oso ona SKOV3 eta MRC 5 zelula-lerroekin alderatuta (19. taula, 5. sarrera).

Kontuan hartuz toxikotasun hoberena metil ester duen **86c** γ -laktamarako neurtu zela, ondoren, metil karboxilato deribatuak erabiliz egitura-aktibitatearen azterketa zabaldu zen γ -laktama eraztuneko zentro kiraleko ordezkataileak duen eragina ebaluatzeko. *Para*-trifluorofenilo ordezkatailea bost kideko eraztunean sartzeak ez zuen jarduera hobetu **86h,i** konposatuentzat, $42,58 \pm 2,55$ eta $7,64 \pm 0,17$ μM -eko IC_{50} balioak lortu baiziren A549 zelula-lerroan, hurrenez hurren. Hala ere, **86h** konposatuak, toxikotasun moderatua erakutsi zuen SKOV3 zelula-lerroaren aurka, eta bi konposatuek oso selektibitate handia erakutsi zuten minbizidun birika-zelulen aurka, MRC5 zelula-lerroan 50 μM -tik gorako IC_{50} balioak neurtu zirelako (19. taula, 6-7. sarrerak).

Jakina da fenolen propietate antioxidatzaileek lotura dutela tumoreen kontrako jardueran, egitura hau barne hartzen duten hainbat konposatutan ikusi den bezala.²²³ Horren arabera, fenola egitura duten **86j,k** konposatuen aktibitate antiproliferatiboa neurtu zen. *p*-Toluidinatik eratorritako **86j** γ -laktama ikertzean $1,98 \pm 0,18$ μM -ko IC_{50} balio bikaina aurkitu zen A549 zelula-lerroan, eta, zelula ez-gaiztoen aurka toxikotasuna erakutsi zuen arren, jarduera bost aldiz txikiagoa izan zen zelula kartzinogenoekin alderatuta. Era berean, obulutegi kartzinomaren zeluletan lortutako toxikotasuna MRC5 zelula-lerroan behatutakoaren antzekoa izan zen (19. taula, 8. sarrera). Gainera, bentzilaminatik eratorritako **86k** γ -laktamak $10,71 \pm 1,35$ eta $21,91 \pm 1,53$ μM -eko IC_{50} balioak eman zituen A549 eta SKOV3 zelula-lerroetan, hurrenez hurren, baina, biriki zelula ez-gaiztoetan antzeko toxikotasuna neurtu zen (19. taula, 9. sarrera). C-5 posizioan *m*-metoxifenil taldez ordezkaturako 3-amino-1,5-dihidro-2*H*-pirrol-2-onen zitotoxikotasunari dagokionez, *p*-toluidinatik eratorritako **86l** γ -laktamak, A549 eta SKOV3 zelula-lerroen aurrean $13,03 \pm 1,48$ eta $43,93 \pm 1,66$ μM -eko zitotoxikotasuna agertu zen, hurrenez hurren (19. taula, 10. sarrera), nahiz eta selektibitate txikia izan zelula ez-gaiztoekin alderatuta. Bentzilaminatik deribatutako **86m** konposatuak antzeko balioak eman zituen A549 zelula-lerroaren aurrean (19. taula, 11. sarrera). Hala ere, **86m** konposatua oso selektiboa izan zen A549 zeluletan, SKOV3, RKO edo MRC5 zelula-lerroekin konparatzerakoan. Bitxia bada ere, hidroxia eta metoxi ordezkatailea aromatikoak konbinatzen direnean, adibidez *p*-toluidina eta bentzilamina duten

²²³ Elford H. L., Van't Riet, B. Phenols and Polyphenols as Antioxidants and Anticancer Agents. In *Eicosanoids and Other Bioactive Lipids in Cancer and Radiation Injury. Developments in Oncology*; Springer, 1991; pp 201-204.

86n,o γ -laktametan, $0,11 \pm 0,016$ eta $6,02 \pm 1,01$ μM -eko IC_{50} balio bikainak lortzen dira A549 zelula-lerroan, hurrenez hurren, eta gainera hautakortasun handiarekin zelula ez-gaiztoekin alderatuz gero. Nabarmendu beharra dago, *p*-toluidinadun **86n** deribatua $1,23 \pm 0,31$ eta $10,92 \pm 1,18$ μM -eko aktibitate oso onak ere eman zituela SKOV3 eta RKO zelulen kontra, hurrenez hurren (19. taula, 12-13. sarrerak).

Hortaz gain, γ -laktama eraztuneko 4. posizioko metil ester taldea amida talde funtzionalarengatik ordezkatzek aktibitate antikantzerigenoan eragindako efektua ikertu egin zen. *p*-Toluidina amidaren deribatua den **98a** konposatuak $2,97 \pm 0,29$ μM -eko IC_{50} balio oso ona agertu zuen A549 zelula-lerroaren aurka, baina, ordea, *p*-anisidinaren deribatua den **98b** substratuaren IC_{50} balioa hamar aldiz handiagoa izan zen. Are gehiago, bi konposatuek toxikotasuna erakutsi zuten SKOV3 zelula-lerroan ere, $6,95 \pm 0,59$ eta $16,62 \pm 0,19$ μM -eko balioekin, hurrenez hurren. Gainera, **98a** konposatua oso selektiboa izan zen birika-zelula gaiztoekiko, MRC5 zelula-lerroarekin alderatuta. **98b** Substratuak, aldiz, toxikotasuna erakutsi zuen birika zelula-lerro ez-gaiztoen aurka ere (19. taula, 14-15. sarrerak).

Tesi honetan aurkeztutako γ -laktama deribatuen egitura-jarduera azterketarekin jarraitzeko, ondoren, **86** enamina produktuen hidrolisi bidez lortutako enol talde funtzionala duten **97** γ -laktamen aktibitate antiproliferatiboa ebaluatu zen (20. taula).

20. taula. **97** 3-Hidroxi-4-karboxilato γ -laktama deribatuen aktibitate antiproliferatiboa.



97

Sarr.	Prod.	R ¹	R ²	R ³	IC ₅₀ (μM)			
					A549	SKOV3	RKO	MRC5
1	97a	4-MeC ₆ H ₄	Ph	Et	$15,73 \pm 1,27$	>50	>50	>50
2	97b	4-MeOC ₆ H ₄	Ph	Et	$13,05 \pm 0,56$	>50	>50	>50
3	97c	Bn	Ph	Et	$4,50 \pm 0,18$	>50	>50	>50
4	97d	Bn	4-CF ₃ C ₆ H ₄	Me	$19,13 \pm 3,00$	>50	d.g.	>50
5	97e	4-MeC ₆ H ₄	3-MeOC ₆ H ₄	Me	$17,64 \pm 3,76$	>50	d.g.	>50
6	97f	Bn	3-MeOC ₆ H ₄	Me	$15,96 \pm 1,97$	>50	d.g.	>50
7	97g	4-MeC ₆ H ₄	4-HO,3-MeOC ₆ H ₄	Me	$13,30 \pm 2,19$	$10,36 \pm 0,35$	d.g.	>50
8	Doxorubizina				<0,1	$0,13 \pm 0,098$	<0,1	>50

Etil esterra duten **86d-f** γ -laktamen enamina talde funtzionala enol batezkin ordezkatzuz gero, antzeko jarduera zitotoxikoa neurtu zen A549 zelula-lerroaren kontra, 5-fenil taldea duten **97a-c**

konposatueta (20. taula, 1-3. sarrerak vs. 19. taula, 1-3. sarrerak). Gainera, konposatu horiek ez zuten toxikotasun handirik erakutsi SKOV3, RKO eta MRC5 zelula-lerroetan. Era berean, metil esterra duen **97d** 3-hidroxi γ -laktamak, karbono kiralean *p*-trifluorometil ordezkatzaila duenak, A549 zelula-lerroaren aldean toxikotasun txikiagoa erakutsi zuen ($19,13 \pm 3,00 \mu\text{M}$) jatorrizko **86i** enaminadun γ -laktamarekin alderatuz gero, eta toxikotasunik ez zuen eman SKOV3 eta MRC5 lerroen aurrean (20. taula, 4. sarrera vs. 19. taula, 7. sarrera). Halaber, A549 zelula-lerroan aktibitate antiproliferatiboaren jardueraren murrizketa bera hauteman zen, *m*-anisil **97e-f** eta banilina **97g** deribatutakoak, jatorrian **86i-n** enaminadun γ -laktametatik sortuak, ikertu zirenean, $17,64 \pm 3,76$, $15,96 \pm 1,97$ eta $13,30 \pm 2,19 \mu\text{M}$ -eko balioak neurtuz, hurrenez hurren (20. taula, 5-7. sarrerak vs. 19. taula, 10-12. sarrerak). **97e-f** Konposatueta batek ere ez zuen toxikotasunik izan SKOV3 edo MRC5 zelula-lerroetan, baina konposatuaren eratzun aromatikoan hidroxil talde bat sartzen denean, **97g** konposatuaren kasu, aktibitatea detektatu zen obulutegi-minbiziaren zelula-lerroan (20. taula, 7. sarrera).

Arestian aipatu dugun moduan, bioisosterismoa asko erabiltzen den kontzeptua da era arrazional batean prototipoa edo serieburua agente terapeutikoak eraldatzeko eta seguruago eta klinikoki eraginkorragoa diren produktu berriak eratzeko.²²⁴ Jakina da, substratu aktibo batean karboxilato talde funtzionala fosfonato batengatik aldatzen denean, jarduera berriak sor daitezkeela edo haren aktibitatea areagotu daitekeela.^{151, 219} Hori dela eta, gure ikerketarekin jarraitzeko, C-4 posizioan fosforodun ordezkatzaila duten **93** γ -laktamen aktibitate antiproliferatiboa neurtu zen (21. taula). Izan ere, fosforoz ordezkaturako **93** γ -laktamen zitotoxikotasuna karboxilatoz ordezkaturako, eta aurretik aztertutako, **97** γ -laktamen jarduerarekin alderatu zen.

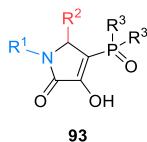
Hain zuzen ere, *p*-toluidinaren eta *p*-anisidinaren deribatutako **97a,b** konposatueta etil karboxilato talde funtzionala dietil fosfonatoarengatik ordezkatzeko denean, aktibitate antiproliferatiboa handitu zen A549 zelula-lerroan **93a,g** γ -laktamentzat, $3,11 \pm 0,31$ eta $4,56 \pm 0,44 \mu\text{M}$ -ko IC_{50} balioak lortuz da, hurrenez hurren. Halaber, selektibitate handia erakutsi zuten konposatu hauek, ez zirelako aktiboak SKOV3 eta MRC5 zelula-lerroetan (20. taula, 1-2. sarrerak vs. 21. taula, 1-2. sarrerak). Hala ere, *o*-fluoroanilinadun **93h** γ -laktama fosforatuak jarduera murriztua agertu zuen A549 biriki minbizi zeluletan, $16,03 \pm 1,49 \mu\text{M}$ -eko balioak lortuz (21. taula, 3. sarrera).

Jarraian, zentro kiraleko ordezkatzailaren eragina ikertu egin zen fosforodun **93b-f** 3-hidroxi dihidropirrol-2-ona konposatueta. Horretarako, *p*-toluidinaren eta dietilo fosfonatoren deribatutako **93a** substratu aktiboena erabili zen eredu gisa. Hala, *p*-fluorofenil ordezkatzaila duen **93b** γ -laktama deribatutako A549 zelula-lerroan $6.6 \pm 0.58 \mu\text{M}$ -eko IC_{50} balio apalagoa eman zuen **93a** oinarriko konposatuarekin alderatuta (21. taula, 4. sarrera vs. 1. sarrera). γ -Laktamaren zentro estereogenikoan

²²⁴ Patani, G. A.; Lavoie, E. J. *Chem. Rev.* **1996**, *96*, 3147–3176.

elektroi erakarle sendoagoa den *p*-nitrobenzaldehido taldea sartzeak eragin oso negatiboa izan zuen zitotoxikotasunean, eta 50 μM -etik gorako IC_{50} balioak aurkitu ziren **93c** konposatuarentzat A549 eta SKOV3 zelula-lerroetan (21. taula, 5. sarrera).

21. taula. Fosforoz ordezkaturako **93** 3-hidroxi γ -laktamen aktibitate antiproliferatiboa.



Sarr.	Prod.	R ¹	R ²	R ³	IC ₅₀ (μM)			
					A549	SKOV3	RKO	MRC5
1	93a	4-MeC ₆ H ₄	Ph	OEt	3,11 ± 0,31	>50	d.g.	>50
2	93g	4-MeOC ₆ H ₄	Ph	OEt	4,56 ± 0,44	>50	>50	>50
3	93h	2-FC ₆ H ₄	Ph	OEt	16,03 ± 1,49	>50	d.g.	>50
4	93b	4-MeC ₆ H ₄	4-FC ₆ H ₄	OEt	6,60 ± 0,58	>50	d.g.	>50
5	93c	4-MeC ₆ H ₄	4-NO ₂ C ₆ H ₄	OEt	>50	>50	>50	d.g.
6	93d	4-MeC ₆ H ₄	2-Thienyl	OEt	23,29 ± 2,40	>50	>50	>50
7	93e	4-MeC ₆ H ₄	CO ₂ Et	OEt	8,27 ± 0,91	>50	d.g.	>50
8	93f	4-MeC ₆ H ₄	<i>i</i> Pr	OEt	24,20 ± 0,81	>50	d.g.	>50
9	93i	4-MeC ₆ H ₄	Ph	O ^t Pr	5,36 ± 0,28	11,56 ± 3,36	33,62 ± 0,41	>50
10	93j	4-MeC ₆ H ₄	4-FC ₆ H ₄	O ^t Pr	5,91 ± 0,69	15,55 ± 1,60	d.g.	>50
11	93k	4-MeC ₆ H ₄	CO ₂ Et	O ^t Pr	>50	>50	d.g.	d.g.
12	93l	4-MeC ₆ H ₄	Ph	Ph	11,86 ± 1,35	>50	>50	>50
13	93p	4-MeOC ₆ H ₄	Ph	Ph	3,72 ± 0,32	>50	>50	>50
14	93q	2-FC ₆ H ₄	Ph	Ph	5,50 ± 1,35	>50	d.g.	>50
15	93n	4-MeC ₆ H ₄	4-FC ₆ H ₄	Ph	1,46 ± 0,19	21,97 ± 3,42	d.g.	>50
16	93m	4-MeC ₆ H ₄	C ₆ F ₅	Ph	20,34 ± 0,79	>50	>50	>50
17	Doxorubizina				<0,1	0,13 ± 0,098	<0.1	>50

Eragin negatiboa ere hauteman zen **93d-f** substratuetan, C-5 posizioan 2-tienil, etoxikarbonil eta *iso*-propil ordezkatzailak dituzten konposatuetan hain zuzen. A549 zelula-lerroan 23,29 ± 2,4, 8,27 ± 0,91 eta 24.20 ± 0.81 μM -eko balioak neurtu bait ziren, hurrenez hurren. Bestalde, SKOV3 eta birika zelula ez-gaiztoen aurkako aktibitate zitotoxiko txikia neurtu zenez, molekula hauek selektiboak direla ondorioztatu daiteke (21. taula, 6-8. sarrerak).

Fosforodun heterozikloen garrantzia kontuan hartuta, ondoren, bolumen handiagoko di-*iso*-propil fosfonatoa duten **93i-k** konposatuen hazkuntza zelularren inhibizio-jarduera neurtu zen. Nahiz eta C-5 posizioan fenil edo *p*-fluorofenil ordezkatzaila duten **93i,j** γ -laktamen IC_{50} balioak (5,36 ± 0,28 eta 5,91 ± 0,69 μM) bere baliokide diren dietilfosfonato **93a,b** deribatuenak baino pixka bat altuagoak izan,

molekula hauek SKOV3 zelula lerroan $11,56 \pm 3,36$ eta $15,55 \pm 1,60$ μM -eko aktibitatea agertu zuten, eta birika zelula ez-gaiztoetan ez zuten zitotoxikotasunik adierazi (21. taula, 9-10. sarrerak vs. 1-4. sarrerak). Gainera, di-iso-propil fosfonatoa duen **93f** γ -laktamaren zentro kiralean, etil karboxilatoaren presentziak aktibitate zitotoxikoaren erabateko galera ekarri zuen zelula-lerro guztietan ikusi zen (21. taula, 11. sarrera).

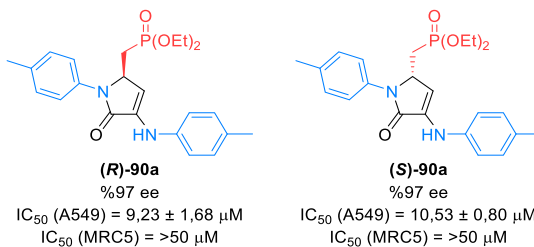
Farmako berrien garapenean fosfina-oxido egitura agertzea arraroa bada ere, bere homologoak diren fosfato, fosfonato edo fosforamidoekin alderatuz, deribatu horietako batzuk minbizi-kontrako sendagai izateko hautagai bikainak direla frogatu da, hala nola, ridaforolimus²²⁵ edo brigatinib.²²⁶ Hori dela eta, fosforodun ordezkatzailen egitura-aktibitate erlazioaren azterketa hedatu zen difenil fosfina-oxidoa duten **93l-q** substratuetara. Lehenik eta behin, laktamaren 5. posizioan feniloa duten difenilfosfinoxido taldea duten molekulen aktibitatea neurtu zen. Horrela, *p*-toluidinaren deribatua den **93l** substratuak $1,86 \pm 1,35$ μM -eko aktibitatea erakutsi zuen A549 zelula lerroan, hain zuzen, bere fosfonato analogoak diren **93a,i** γ -laktamek baino baxuagoa (21. taula, 12. sarrera vs. 1. eta 9. sarrerak). Hala ere, difenil fosfina-oxidoaren presentzia *p*-anisidinaren eta *o*-fluoroanilinaren deribatutako **93p,q** substratuetan zitotoxikotasunaren hobekuntza ekarri zuen, bere homologoak diren **93g,h** dietil fosfonato deribatuekin alderatuta, eta $3,72 \pm 0,32$ eta $5,5 \pm 1,35$ μM -eko IC_{50} balioak neurtu ziren biriki-minbizi zelula-lerroan, hurrenez hurren (21. taula, 13-14. sarrerak vs. 2-3. sarrerak). Era berean, *p*-fluorofeniloaren presentziak **93n** fosfina-oxidozko γ -laktamaren zentro kiralean, oso substratu aktiboa eman zuen $1,46 \pm 0,19$ eta $21,97 \pm 3,42$ μM -eko IC_{50} balioak lortuz A549 eta SKOV3 zeluletan, hurrenez hurren (21. taula, 15. sarrera). Hala ere, parekoa den **93m** perfluorofenilodun substratuak aktibitate okerragoa erakutsi zuen A549 zelula lerroan ($20,34 \pm 0,79$ μM), eta ez zuen toxikotasunik agertu obulutegiko minbizi zeluletan (21. taula, 16. sarrera). Nabarmendu behar da **93** 3-hidroxi γ -laktama fosforatu aktibo guztiek selektibitate bikaina izan zutela zelula kartzinogenoen aurka, zelula ez-gaiztoetan 50 μM baino gorako IC_{50} balioak neurtu zirelako. Azkenik, konposatu hauek ez zuten jarduera nabarmenik izan RKO kolon zelula-lerroan.

Amaitzeko, enantiomero bakoitzaren aktibitatea ikertzeko asmotan, %97-ko purutasun optikoa duten **90a** γ -laktamaren bi enantiomeroen zitotoxikotasuna ebaluatu zen (60. irudia). Hala ere, ez zen desberdintasun nabarmenik hauteman (**R**)-**90a** edo (**S**)-**90a** enantiomeroak modu independentean

²²⁵ (a) Rivera, V. M.; Squillace, R. M.; Miller, D.; Berk, L.; Wardwell, S. D.; Ning, Y.; Pollock, R.; Narasimhan, N. I.; Lulicci, J. D.; Wang, F.; Clackson, T. *Mol. Cancer Ther.* **2011**, *10*, 1059-1071. (b) Ridaforolimus. *Drugs R D* **2010**, *10*, 165-178.

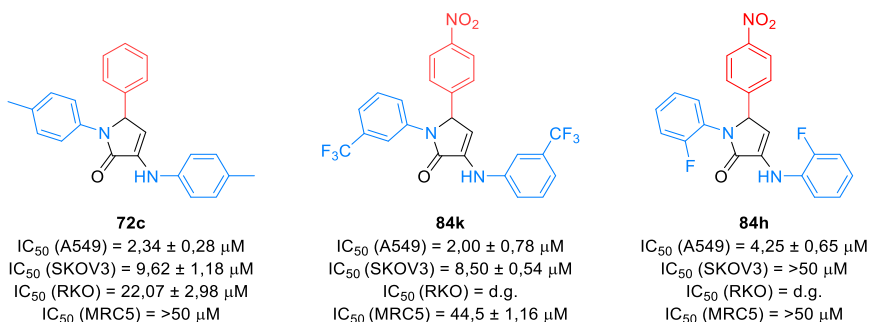
²²⁶ (a) Markham, A. Brigatinib: First Global Approval. *Drugs* **2017**, *77*, 1131-1135. (b) Huang, W. S.; Liu, S.; Zou, D.; Thomas, M.; Wang, Y.; Zhou, T.; Romero, J.; Kohlmann, A.; Li, F.; Qi, J.; Cai, L.; Dwight, T. A.; Xu, Y.; Xu, R.; Dodd, R.; Toms, A.; Parillon, L.; Lu, X.; Anjum, R.; Zhang, S.; Wang, F.; Keats, J.; Wardwell, S. D.; Ning, Y.; Xu, Q.; Moran, L. E.; Mohemmad, Q. K.; Jang, H. G.; Clackson, T.; Rivera, V. M.; Zhu, X.; Dalgarno, D.; Shakespeare, W. C. *J. Med. Chem.* **2016**, *59*, 4948-4964.

ikertzean, lagin errazemikoarekin alderatuta (16. taula, 22. sarrera), eta A549 zelula lerroan $9,23 \pm 1,68$ eta $10,53 \pm 0,80 \mu\text{M}$ -eko IC_{50} balioak eskaini zituen, hurrenez hurren.



60. irudia. 90a γ -Laktamaren enantiomero bakoitzaren aktibitate antiproliferatiboa.

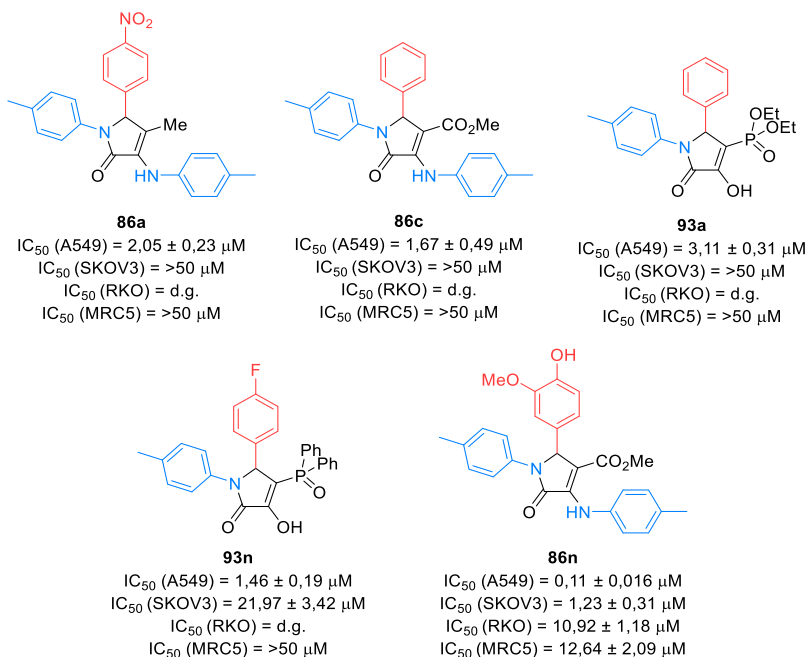
Ondorengo lerroetan, substratu aktiboenen laburpena aurkezten da. C-4 karbonoan ordezkatu gabeko enamina duten substratuen artean, A549 zelula-lerroan, aktibitate hobereana **72c** eta **84k** γ -laktama deribatuek dute, $2,34 \pm 0,28$ eta $2,00 \pm 0,78 \mu\text{M}$ -eko IC_{50} balioekin, hurrenez hurren. Hala ere, **84k** konposatuak lerro zelular ez-gaiztoaren aurka jarduera txikia agertu du. SKOV3 zelula-lerroari dagokionez, jarduera zitotoxiko onena **84h** konposatuarentzat neurtu da, $5,55 \pm 0,62 \mu\text{M}$ -ekoa (61. irudia).



61. irudia. C-4 posizioan ordezkatu gabeko enamina-deribatuak diren γ -laktama aktiboena.

γ -Laktamaren eraztunaren 4. posizioan ordezkatzaille bat sartzeak jarduera zitotoxikoan eragin positiboa zuela probatu zuen. C-4 karbonoan ordezkaturako enamina duten produktuen artean, **86a**-k eta **86c**-k aktibitate bikaina erakutsi zuten A549 zelula-lerroan, $2,05 \pm 0,23$ eta $1,67 \pm 0,49 \mu\text{M}$ -eko IC_{50} balioekin, hurrenez hurren, eta selektibitate ona MRC5 zelula-lerroarekin alderatuta (62. irudia). Gainera, konposatu multzo horretan, ikus daiteke enamina egituren ordezkari enol funtzioa izateak ez duela eraginik jarduera zitotoxikoan. Enol duten γ -laktamaren kasuan, badirudi C-4-an karboxilato taldea baino aukera hobea fosforo-ordezkatzaille bat egotea dela. Fosforo ordezkaturako 3-hidroxi γ -laktama aktiboena **93a** eta **93n** substratuak dira, eta $3,11 \pm 0,31$ eta $1,46 \pm 0,19 \mu\text{M}$ -eko IC_{50} balioekin A549

zelula-lerroan. Gainera, aipatu beharra dago, konposatu hauen kasuan ez zela hobekuntzarik hauteman SKOV3 eta RKO zelula-lerroen aurkako zitotoxikotasun jardueran (62. irudia).



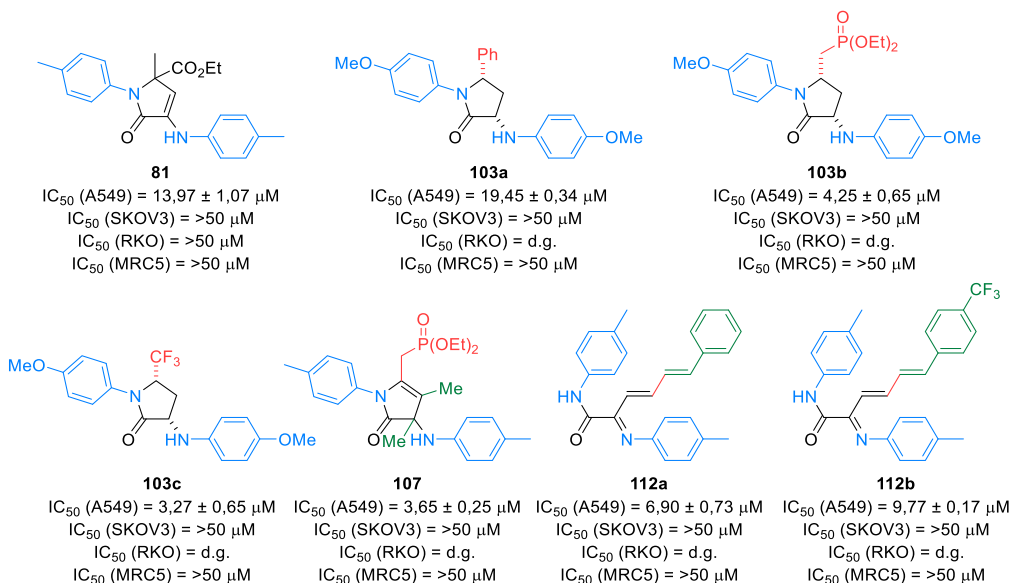
62. irudia. C-4 posizioan ordezkaturako zenbait γ -laktama aktibo.

Azkenik, sintetizatutako γ -laktama deribatu guztien artean konposatu aktiboena **86n** substratua izan zen, $0,11 \pm 0,016$, $1,23 \pm 0,31$ eta $10,92 \pm 1,18 \mu\text{M}$ -eko IC_{50} balioekin A549, SKOV3 eta RKO zelula-lerroetan, hurrenez hurren. Gainera, konposatu honek zelula ez-gaitoen aurrean 115 aldiz handiagoa den IC_{50} balioa erakutsi zuen, zelula kantzerigenoekiko selektibitate handia argi utzita (62. irudia).

EAE azterketa are gehiago zabaltzeko helburuarekin, γ -laktama deribatuetan egindako aldaketetatik lortutako substratuen aktibitate antiproliferatiboa ebaluatu zen. Lehenik eta behin, enamina/imina bitarteko pirubatoen dimerizazio erreakzio bidez lortutako **81** γ -laktamaren zelula proliferazioaren inhibizioa neurtu zen, eta $13,97 \pm 1,05 \mu\text{M}$ -eko balio apala lortu zen A549 zelula-lerroan, baina aktibitaterik ez SKOV3, RKO edo MRC5 zeluletan (63. irudia).

Gainera, *p*-anisidinaren deribatua den enamina endoziklikoaren hidrogenazioz lortutako **103a-c** γ -laktama deribatuen aktibitatea aztertu zen. C-5 posizioan feniloa duen **103a** γ -laktama aseak $19,45 \pm 0,34 \mu\text{M}$ -eko IC_{50} balioa agertu zuen A549 zelula-lerroaren aurrean, bere aitzindaria den **84b** γ -laktama asegabeak baino balio txarragoa izanik (63. irudia vs. 16. taula, 1. sarrera). Hala ere, fosfometiloz eta trifluorometiloz ordezkaturako **103b** eta **103c** substratuek, ordea, A549 zelula-lerroan jarduera zitotoxikoa hobetu egin zuten, haren jatorrizko **90a** eta **90e** γ -laktama asegabeekin alderatuta, $3,27 \pm$

0,65 eta 4,25 ± 0,65 µM balioak lortuz, hurrenez hurren, biriketako minbizi zelula-lerroan (63. irudia vs. 16. taula, 21-22. sarrerak). Aipatu beharra dago, **103** γ-laktama aseetako batek ere ez zuela jarduerarik erakutsi SKOV3 eta MRC5 zelula-lerroetan.



63. irudia. Beste γ-laktama batzuen aktibitate antiproliferatiboa.

Alkanoen izaera lipofilikoa dela eta, molekula bioaktiboak metil taldeekin funtzionalizatzeak, sarritan, aktibitatearen areagotzea dakar.²²⁷ Hori dela eta, lau metil talde dituen **107** γ-laktama deribatuaren zitotoxikotasuna ebaluatu zen. Kasu honetan, 3,65 ± 0,25 µM-eko IC₅₀ balio hobetua lortu zen, jatorrizko **90a** konposatuarekin alderatuta (63. irudia vs. 16. taula, 22. sarrera). Gainera, selektibitate handia erakutsi zuen konposatu honek, ez baitzuen toxikotasunik erakutsi SKOV3, RKO eta MRC5 zelula-lerroen kontra.

Azkenik, **90a** γ-laktamaren eratzunaren irekieraren ondorioz lortutako konjugazio handiko **112a,b** konposatuen aktibitate antiproliferatiboa ikertu zen. Bi konposatuek zitotoxikotasun ona izan zuten A549 zelula-lerroaren aurrean, eta 6,90 ± 0,73 eta 9,77 ± 0,17 µM-eko balioak neurtu ziren, hurrenez hurren, eta ez zuten jarduerarik erakutsi SKOV3 eta MRC5 birika-zelula eta ez-gaiztoen aurrean (63. irudia).

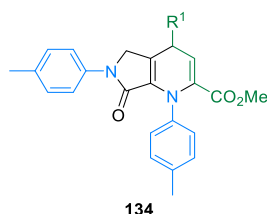
²²⁷ Schönherr, H.; Cernak, T. *Angew. Chem. Int. Ed.* **2013**, *52*, 12256-12267.

7.2. 1,4-Dihidropiridina bizikloen aktibitate antiproliferatiboa.

Lan honetan sintetizatutako substratuen minbizi-aurkako propietateen azterketan aurrera eginez, ondoren, γ -laktama eta α -zetoester β,γ -asegabeen arteko [3+3] ziklazio formalaren bidez lortutako substratu bizikloen aktibitate antiproliferatiboa ikertzeraz bideratu genituen gureahaleginak. 1,4-Dihidropiridinak kaltzio-kanalak modulatzeko dituzten agenteak dira, eta oso egokiak dira hipertentsioa tratatzeko.¹⁷² Harrigarria bada ere, kaltzio-kanalen blokeatzaile askok minbiziaren kontrako agente gisa jokatzeko dutela ere frogatu da, eta 1,4-dihidropiridinak eragile antiproliferatibo eraginkorrak direla jakinarazi da hainbat ikerketetan.¹⁷⁶ Hau kontuan hartuta, eta [3+3] zikloadizio-erreakzio formalekin lortutako substratuek 1,4-dihidropiridina eratzuna izateaz gain γ -laktama egitura fusiostatuta dutela, oso interesgarria izan daiteke substratu hibrido horien hazkunde-inhibizioaren jardura aztertzea.

Azterketa honen lehen zatian, C-5 ordezkapenik gabeko γ -laktametarik abiatuta prestatutako **134** 1,4-dihidropiridina sinpleen jardura zitotoxikoa ebaluatu zen (22. taula). Hala ere, gure harridurarako, 6 kideko eratzunean *p*-nitrofenil ordezkatzaila duen **134a** substratuak bakarrik erakutsi zuen aktibitatea A549 zelula-lerroaren aurka, $44,83 \pm 2,57 \mu\text{M}$ -eko balio apalarekin, eta ez zuen inolako eraginik izan biriketako zelula ez-gaiztoetan (22. taula, 1. sarrera).

22. taula. **134** 1,4-Dihidropiridinen aktibitate antiproliferatiboa.

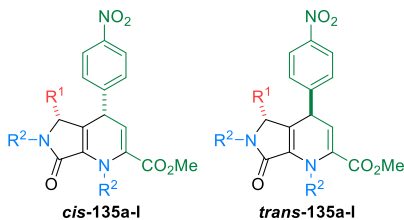


Sarr.	Prod.	R ¹	IC ₅₀ (μM)		
			A549	SKOV3	MRC5
1	134a	4-NO ₂ C ₆ H ₄	44,83 ± 2,57	>50	>50
2	134b	4-CF ₃ C ₆ H ₄	>50	>50	d.g.
3	134c	Ph	>50	>50	d.g.
4	134d	4-MeC ₆ H ₄	>50	>50	d.g.
5	Doxorubizina		<0,1	0,13 ± 0,098	>50

[3+3] Ziklazio-erreakzio formalaren bidez lortutako egitura-aniztasunaren ondorioz, jarraian, aktibitate zitotoxikoan 1,4-dihidropiridinen ordezkatzaila duen eragina ikertu zen. Aurreko azterketan lortutako emaitzak kontuan hartuta, ordezkatu gabeko **134a** produktua erabili zen eredu

gisa, eta γ -laktama nukleoan ordeztaille desberdinak sartzeak duen eragina ebaluatu zen ondoren. Lortutako emaitzak 23. taulan daude laburbilduta.

23. taula. γ -Laktama zikloko ordezkatzailak duen eragina **135a-I** konposatuaren aktibitate antiproliferatiboan.



Sarr.	Prod.	R ¹	R ²	IC ₅₀ (μM)		
				A549	SKOV3	MRC5
1	cis-135a	Ph	4-MeC ₆ H ₄	>50	>50	d.g.
2	cis-135b	4-CF ₃ C ₆ H ₄	4-MeC ₆ H ₄	>50	>50	d.g.
3	cis-135c	4-FC ₆ H ₄	4-MeC ₆ H ₄	>50	>50	d.g.
4	cis-135d	C ₆ F ₅	4-MeC ₆ H ₄	2,04 ± 0,68	9,05 ± 1,39	20,16 ± 0,71
5	cis-135e	2-Tiofenil	4-MeC ₆ H ₄	>50	>50	d.g.
6	trans-135f	Cy	4-MeC ₆ H ₄	>50	>50	d.g.
7	trans-135g	CH ₂ P(O)(OEt) ₂	4-MeC ₆ H ₄	>50	>50	d.g.
8	cis-135h	CF ₃	4-MeC ₆ H ₄	>50	>50	d.g.
9	trans-135h	CF ₃	4-MeC ₆ H ₄	>50	>50	d.g.
10	cis-135i	Ph	4-MeOC ₆ H ₄	>50	>50	d.g.
11	cis-135j	Ph	2-FC ₆ H ₄	>50	>50	d.g.
12	cis-135k	Ph	4-BrC ₆ H ₄	36,51 ± 5,14	>50	>50
13	trans-135k	Ph	4-BrC ₆ H ₄	>50	>50	>50
14	cis-135l	Ph	3-CF ₃ C ₆ H ₄	7,79 ± 1,59	>50	>50
15	trans-135l	Ph	3-CF ₃ C ₆ H ₄	7,33 ± 0,37	>50	>50
16	Doxorubizina			<0.1	0,13 ± 0,098	>50

Proposatutako EAE azterketa honen lehen zatian, γ -laktamaren estereozentroko ordezkatzailak duen eragina balioztatu zen. Beraz, γ -laktama egitura-zatian, eraztun aromatiko desberdinak dituzten **cis-135a-c** 1,4-dihidropiridina biziklikoek 50 μM-tik gorako IC₅₀ balioak agertu zituzten (23. taula, 1-3. sarrerak). Hala ere, γ -laktama eraztuneko C-5 posizioan perfluorofenil talde bat sartzeak (**cis-135d**) aktibitatearen areagotzea ekarri zuen, 2,04 ± 0,68 eta 9,05 ± 1,39 μM-ko IC₅₀ balioak neurtuz A549 eta SKOV3 zelula-lerroetan, hurrenez hurren. Hala ere, MRC5 zelula ez-gaiztoetan nolabaiteko toxikotasuna hauteman zen (23. taula, 4. sarrera). Bestalde, 2-tiofenil heteroatomoz ordezkaturako **cis-135e** substratuak ez zuen toxikotasunik erakutsi bi zelula kantzerigeno lerroen aurrean (23. taula, 5.

sarrera), eta ez zen inolako jarduerarik ere ez neurtu ziklohexil, metil-dietilfosforil edo trifluorometil bezalako ordezkatzaille alifatikoak dituzten **135f-h** 1,4-dihidropiridina biziklikoetan (23. taula, 6-9. sarrerak).

Ordoren, 1,4-dihidropiridina biziklikoen γ -laktama unitateko amina-ordezkatzailleak jarduera antiproliferatiboan duen eragina aztertu zen. Nahiz eta hobekuntzarik ez zen igarri *p*-anisidina edo *o*-fluoroanilina duten **cis-135i,j** deribatueterako (23. taula, 10-11. sarrerak), *p*-bromofenilanilina taldez ordezkaturako **cis-135k** substratuak $36,51 \pm 5,14 \mu\text{M}$ -ko IC_{50} balioa erakutsi zuen A549 zelula-lerroaren aurka, eta ez zen toxikoa izan SKOV3 edo MRC5 zelula-lerroetan (23. taula, 12. sarrera). Bitxia bada ere, kontrako konfigurazioa duen isomeroak, alegia **trans-135k** konposatuak, ez zuen jarduerarik erakutsi (23. taula, 13. sarrera). *m*-Trifluorofenilanilinatik eratorritako **cis-135l** eta **trans-135l** 1,4-dihidropiridina isomeroek zitotoxikotasun eta selektibitate ona erakutsi zuten A549 zelula-lerroan, $7,79 \pm 1,59$ eta $7,33 \pm 0,37 \mu\text{M}$ -eko IC_{50} balioekin, hurrenez hurren (23. taula, 14-15 sarrerak).

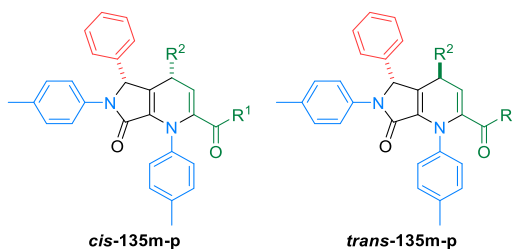
EAE azterketarekin jarraituz, hurrengo helburua 1,4-dihidropiridina unitateko ordezkatzailleak jarduera zitotoxikoan duten eragina ebaluatzea izan zen, eta lehenik eta behin, ester taldearen parte-hartzea aztertu zen (24. taula).

Horretarako, **cis-135a** konposatua erabili zen eredu gisa. Metil esterraren ordeztu bentsil edo etil ester bat jartzeak ez zuen eragin positiborik eduki jarduera antiroliferatiboan, **cis-135m,n** substratuen kasuan (24. taula, 1-2. sarrerak). Hala ere, *iso*-propil esterra duen **cis-135o** 1,4-dihidropiridinak, A549 eta SKOV3 zelula-lerroen aurkako zitotoxikotasuna erakutsi zuen, $10,12 \pm 1,03$ eta $10,71 \pm 0,87 \mu\text{M}$ -eko balioak neurtuz, hurrenez hurren, eta ez zen aktibitaterik igarri biriketako zelula ez-gaiztoen aurka (24. taula, 3. sarrera). Era berean, tioester duten **cis-135p** eta **trans-135p** produktuek ez zuten inolako aktibitaterik agertu (23. irudia, 4-5. sarrerak).

Azkenik, EAE azterketa osatzeko, **135** 1,4-dihidropiridinen eraztuneko karbono kiraleko ordezkatzailleak aktibitate biologikoan duen efektua ebaluatu egin zen. Orain, isopropil esterra duen **cis-135** 1,4-dihidropiridina biziklikoa aukeratu zen patroiz gisa. *p*-Nitrofenil taldea *p*-trifluorometilfenil taldeagatik aldatzeak eragin positiboa izan zuen A549 zelula-lerroan, **cis-135q** konposatuak $8,44 \pm 0,79 \mu\text{M}$ -eko IC_{50} balioa erakutsi baitzuen (24. taula, 6. sarrera). Hala ere, ordezkatzaille horren presentziak SKOV3 zelula-lerroaren aurkako toxikotasunaren erabateko galera ekarri zuen, eta, konposatu honek selektibitate handia erakutsi zuen MRC5 birika zelula gaiztoen aurka, $50 \mu\text{M}$ -retik gorako IC_{50} balioa hauteman baitzen MRC5 zeluletan (24. taula, 6. sarrera). 1,4-Dihidropiridina eraztunaren zentro estereogenikoan beste ordezkatzaille aromatiko batzuen efektua ere ikertu zen, hala nola, fenil (**cis-135r**) edo *p*-tolil (**cis-135t**), eta hauek ez ziren *p*-trifluorometilfenil taldea baino hobetoagoak izan (24. taula, 7-8. sarrerak vs. 6. sarrera). Halaber, tiofeno ordezkatzaillea duen **cis-135u** deribatuak A549

zelula-lerroaren aurka aktibitate bikaina erakutsi zuen, $0,89 \pm 0,27 \mu\text{M}$ -eko IC_{50} balioarekin, eta gainera obulutegi-minbizi zelula-lerroaren aurka $11,90 \pm 1,20 \mu\text{M}$ -eko IC_{50} balio ertaina lortu zen (24. taula, 9. sarrera). Nahiz eta **cis-135u** substratuak MRC5 zelulen aurka toxikotasuna erakutsi zuen ($32,02 \pm 3,43 \mu\text{M}$), lortutako balioa oso urrun dago A549 zeluletan lortutakoarekin alderatuta (24. taula, 9. sarrera). Gainera, 1,4-dihidropiridina zikloko ordezkatzaille aromatikoaren ordezkari karboxilato talde bat txertatzen denean, aktibitate zitotoxikoan eragin negatiboa neurtu zen, eta **cis-135v** konposatuak $50 \mu\text{M}$ -etik gorako IC_{50} balioak izan zituen (24. taula, 10. sarrera). Nahiz eta zitotoxikotasun balio onak neurtu ziren A549 eta SKOV3 zelula-lerroetan trifluorometil taldea duen **cis-135w** 1,4-dihidropiridinarentzat ($5,07$ $0,74$ eta $6,69 \pm 0,13 \mu\text{M}$ hurrenez hurren) aktibitate moderatua antzeman zen MRC5 zelula-lerroan, haren selektibitatea zalantzan jarriz (24. taula, 11. sarrera). Azkenik, 1,4-dihidropiridinaren egitura metil talde simple baten presentziak, zitotoxikotasunaren erabateko galera ekarri zuen **135x** konposatuaren bi isomeroentzat (24. taula, 12-13. sarrerak).

24. taula. 1,4-Dihidropiridina eraztunaren ordezkatzailen eragina aktibitate antiproliferatiboan.

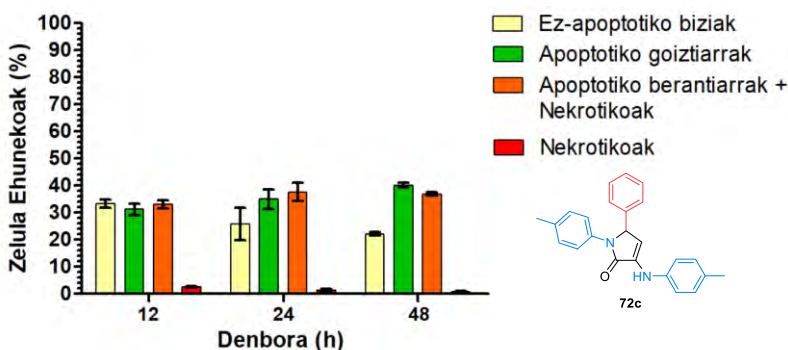


Sarr.	Prod.	R ¹	R ²	IC ₅₀ (μM)		
				A549	SKOV3	MRC5
1	cis-135m	OBn	Ph	>50	>50	d.g.
2	cis-135n	OEt	Ph	>50	>50	d.g.
3	cis-135o	O ⁱ Pr	Ph	10,12 ± 1,03	10,71 ± 0,87	>50
4	cis-135p	SEt	Ph	>50	>50	d.g.
5	trans-135p	SEt	Ph	>50	>50	d.g.
6	cis-135q	O ⁱ Pr	4-CF ₃ C ₆ H ₄	8,44 ± 0,79	>50	>50
7	cis-135r	O ⁱ Pr	Ph	30,69 ± 1,38	>50	>50
8	cis-135t	O ⁱ Pr	4-MeC ₆ H ₄	>50	>50	d.g.
9	cis-135u	O ⁱ Pr	2-Thiophene	0,89 ± 0,27	11,90 ± 1,20	32,02 ± 3,43
10	cis-135v	O ⁱ Pr	CO ₂ Et	>50	>50	d.g.
11	cis-135w	O ⁱ Pr	CF ₃	5,07 ± 0,74	6,69 ± 0,13	15,97 ± 1,11
12	cis-135x	O ⁱ Pr	CH ₃	>50	>50	d.g.
13	trans-135x	O ⁱ Pr	CH ₃	>50	>50	d.g.
14	Doxorubizina			<0,1	0,13 ± 0,098	>50

7.3. Apoptosiaren detekzio-esperimentuak eta zelula morfologiaren behaketa.

Tesi honetarako, gure γ -laktama deribatuek minbizi-zeluletan duten efektu antiproliferatiboaren mekanismoa argitze aldera, substratu aktiboenetako batzuk erabiliz egin ziren esperimentu osagarri batzuetan. Lehenik eta behin, fluxu-zitometria saiakuntzak egin ziren, sintetizatutako γ -laktama deribatuek apoptosi-mekanismoa eragiteko gai diren zehazteko. Annexin V-FITC apoptosia detektatzeko kit komertzialaren bidez, konposatu zitotoxikoarekin tratatutako zelulak lau populaziotan bereiz daitezke: zelula biziak, zelula bizi apoptotiko goiztiarrak, zelula hil apoptotiko berantiarrak, eta zelula hil ez-apoptotikoak (nekrotikoak).

Lehenik eta behin, C-4 posizioan ordezkatzailerik ez duten konposatuaren arteko substratu aktiboenaren (**72c**) apoptosi-indukzio gaitasuna ebaluatu zen A549 zeluletan 5 μ M-eko kontzentrazioan eta 12, 24 eta 48 ordutara (65. irudia).

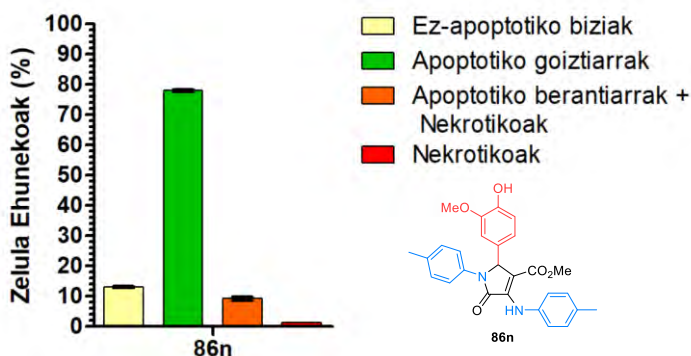


65. irudia. A549 zelula ez-apoptotikoen (barra horiak), apoptotiko goiztiarren (barra berdeak), nekrotiko eta apoptotiko berantiarren (barra laranja), eta nekrotikoen (barra gorriak) ehunekoak, **72c** konposatuaren eraginpean 12, 24 eta 48 orduz egon ondoren. Balio bakoitzak 3 neurriren batezbesteko \pm DE adierazten du.

Zelula apoptotiko goiztiarrak FL-1 positiboak eta FL-3 negatiboak izan ziren. Horrek esan nahi du prozesu apoptotikoa hasi zutela, baina neurketaren unean oraindik bizirik zeudela. Zelula horien ehunekoak, 12, 24 eta 48 ordu igaro ondoren, hauek izan ziren, hurrenez hurren: %31,17 \pm 2,04, %34,97 \pm 3,62 eta %40,13 \pm 0,81. Bestalde, zelula apoptotiko berantiarrak eta nekrotikoak FL-1 eta FL-3 positiboak izan ziren, eta horrek esan nahi du makineria apoptotikoa aktibatzekeo gai direla eta hilda zeudela neurketaren unean. Zelula apoptotiko berantiarren eta nekrotikoen ehunekoak, 12, 24 eta 48 ordu igaro ondoren, hauek izan ziren, hurrenez hurren: %33,03 \pm 1,43, %37,60 \pm 3,37 eta %36,90 \pm 0,70 (65. irudia). Oro har, emaitza hauek iradokitzen dute **72c** konposatuak zitotoxikotasuna eragiten duen

mekanismo nagusietako bat zelula barruan mekanismo apoptotikoen aktibazioan oinarritzen dela. Izan ere, detektatutako hildako zelula guztien artean, FL-1 positiboak zirenak, ia guztiak aldi berean positiboak ziren ere FL-3 kanalarentzat, eta zelula hilen ehuneko txiki bat (%2 edo gutxiago), berriz, FL-1 positibo baino ez ziren. Beraz, azterketa honetan antzemandako hildako zelula gehienak zelula apoptotikoak izan ziren. Horrez gain, zelula apoptotiko goiztiar eta berantiarrek osatutako FL-3 positiboen zelula guztien ehunekoak 60-tik gorakoak izan ziren, eta balio horiek gora egin zuten denborarekin.

Ondoren, C-4 posizioan ordezkatzaila duten laktamen artean, konposatu aktiboenaren (**86n**) apoptosi-indukziorako ahalmena aztertu zen. Hala ere, aurreko esperimentuan esposizio-denbora desberdinen artean ez zenez alde handirik antzeman apoptosiaren ehunekoetan, esperimendu hau egin zen bakarrik 24 orduz kontaktuan egon ondoren eta 1 μM -ko kontzentrazioan (66. irudia).



66. irudia. A549 zelula ez-apoptotikoen (barra horiak), apoptotiko goiztiarren (barra berdeak), nekrotiko eta apoptotiko berantiarren (barra laranja), eta nekrotikoen (barra gorriak) ehunekoak, **86n**-rekin 24 orduz kontaktuan egon ondoren. Balio bakoitzak 3 neurriren batezbesteko \pm DE adierazten du.

Neurketaren unean, **86n** konposatuaren eraginpean zeuden zelulen %80 inguruk FL-1 seinale positiboa eta FL-3 seinale negatiboa erakutsi zuten, zelula-populazio apoptotiko goiztiararen populazioa adieraziz. Une horretan, zelula apoptotiko berantiar eta nekrotikoak positiboak izan ziren bai FL-1 bai FL-3 kanaleetan, eta %10-etik behera zeuden oraindik. Eraitza horiek adierazten dutenez, **86n** konposatuaren eraginpean egon eta 24 ordura, zelulen %90ek mekanismo apoptotikoak aktibatutuztela. Zelula nekrotiko ez-apoptotikoak zelulen populazio osoaren %1 baino gutxiago izan ziren, proba honetan antzemandako zelula hil gehienak zelula apoptotikoak izan zirela adieraziz. Azkenik, zelula bizi ez-apoptotikoak zelula-populazio osoaren %12 inguru izan ziren. Neurketa horiek erakutsi zuten, **86n** γ -laktamak apoptosia eragiteko ahalmen handiagoa du C-4 posizioan ordezkatu gabeko **72c** konposatuarekin alderatuta, baita kontzentrazio txikiagoetan ere.

Azkenik, esperimentu berdina egin zen **cis-135u** 1,4-dihidropiridina bizikliko aktiboena erabiliz, A549 zelula-lerroan, eta 5 μM -ko kontzentrazioaren eraginpean 24 orduz egon ondoren (67. irudia).

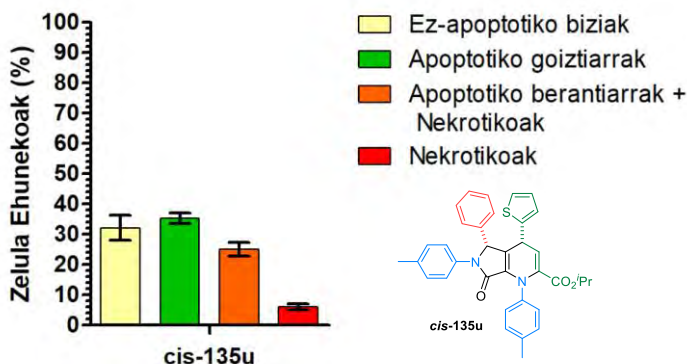


Figure 67. A549 zelula ez-apoptotikoen (barra horiak), apoptotiko goiztiarren (barra berdeak), nekrotiko eta apoptotiko berantiarren (barra laranja), eta nekrotikoen (barra gorriak) ehunekoak, **cis-135u**-rekin 24 orduz kontaktuan egon ondoren. Balio bakoitzak 3 neurriren batezbesteko \pm DE adierazten du.

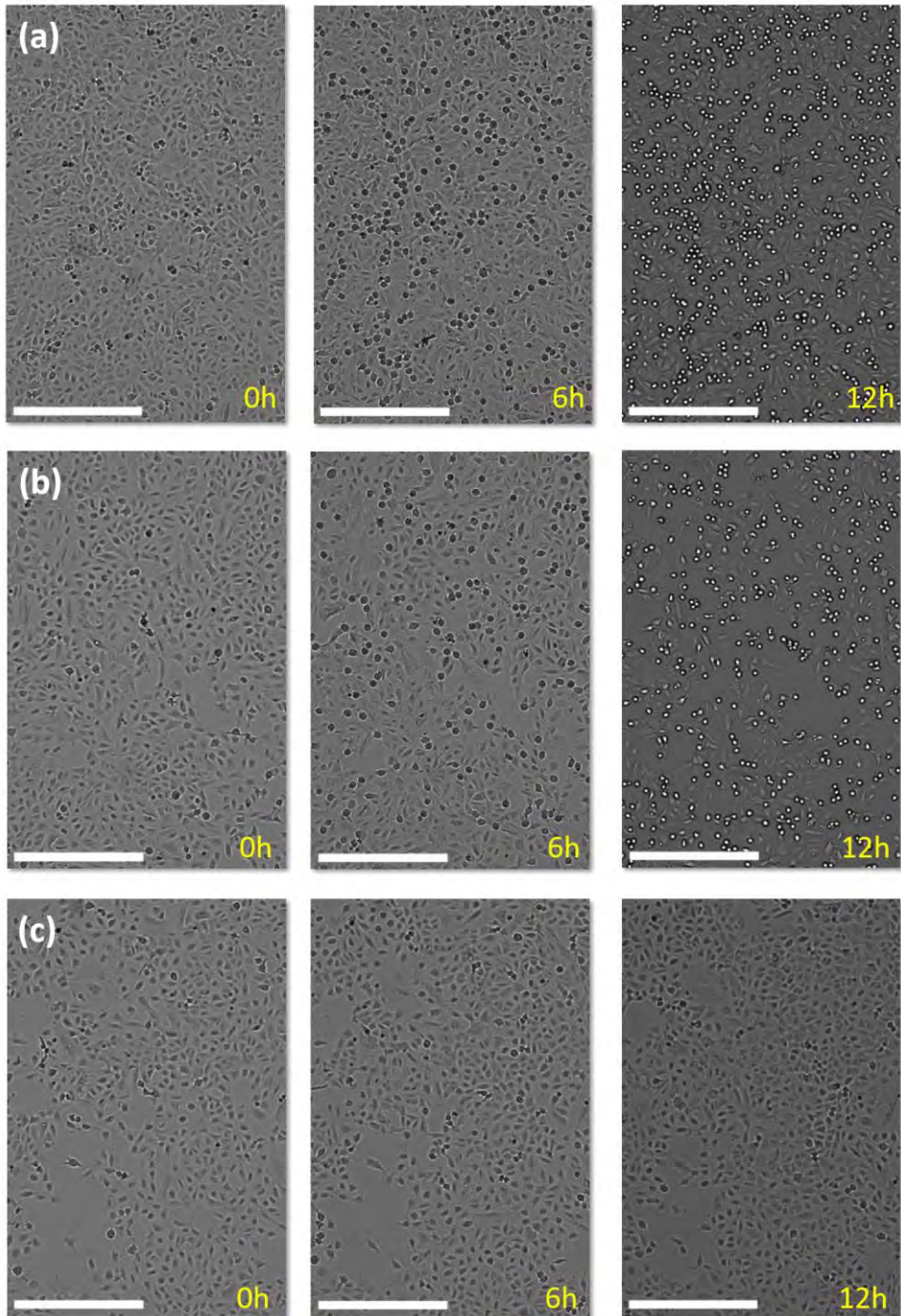
Kasu honetan, **cis-135u** konposatuaren eraginpean, zelula bizien ehunekoa (FL-1 eta FL-3 negatiboa) populazio osoaren %30 baino gehiago izan zen, eta zelulen %35-a baino ez ziren agertu FL-1-en seinale positibo eta FL-3-ren seinale negatibo bezala, zelula-populazio apoptotiko goiztiarra adieraziz. Zelula apoptotiko berantiar eta nekrotikoei dagokienez (FL-1 eta FL-3 positiboak), %26 inguruko ehunekoa lortu zen. Gainera, zelula nekrotiko ez-apoptotikoak (FL-1 negatibo, FL-3 positibo) populazio osoaren ia %6 izan ziren. Lortutako emaitza hauen arabera, **cis-135u** 1,4-dihidropiridinaren 5 μM -eko kontzentraziopean egondako zelulen %60-k mekanismo apoptotikoak aktibatu zituen. Emaitza hau oso urrun dago **86n** konposatuarentzako neurtutako balioetatik (66. irudia), saiakuntza kontzentrazio handiagoetan egiten bada ere. Gainera, **cis-135u** 1,4-dihidropiridinarako lortutako balio hauek, bere lehengai den **72c** γ -laktamarenak bezalakoak dira, kontzentrazio berdinean, nahiz eta **cis-135u** konposatua 2,6 aldiz ahaltuagoa den jarduera zitotoxikoa izan.

Jarraian, A549 zelula-lerroan denboran zehar gertatutako aldaketa morfologikoak aztertu dira zitotoxikotasun handieneko **86n** γ -laktamaren hiru kontzentrazio desberdin gehitu ondoren (68. irudia, 162-163. orrialdeak).

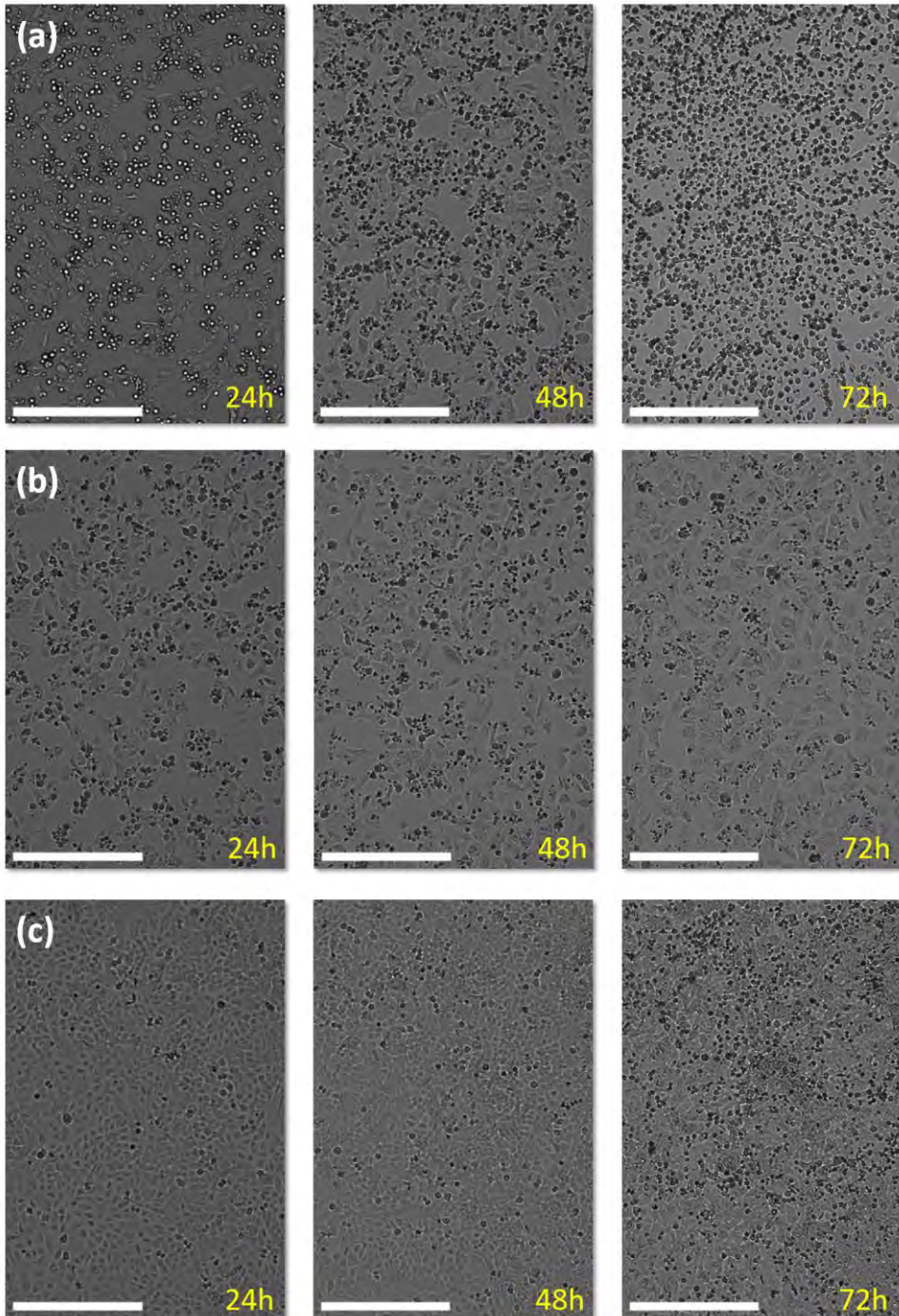
Aztertutako lehen kontzentrazioa 1,1 μM -ekoa izan zen, **86n** γ -laktamaren IC_{50} baino hamar aldiz handiagoa dena. Kontzentrazio altu horretan, zelula-hazkuntzaren etenaldia hauteman zen, batez ere 6 orduko esposizioaren ondoren, eta hau areagotu egin zen denborarekin (68. irudia, a). Ondoren, **86n**-ren IC_{50} kontzentrazioa erabili zen (0,11 μM), eta zelularen heriotzaren maximoa konposatua gehitu

eta 24 edo 48 ordura ikusi zen. Gero, zelulak berriro hazten hasi ziren, eta 72 orduren ondoren konfluentzia zelular nabaria behatu ahal izan zen (68. irudia, b). Berriz, **86n** konposatua 0,02 μM -eko kontzentrazioan gehitzean, hau da, neurtutako IC_{50} baino bost aldiz kontzentrazio txikiagoan, morfologia osasuntsu eta uniformeak duten zelulak behatu ziren, eta zelula-hazkuntza nabaria izan zen denboran zehar, zelulek kontzentrazio hau ondo toleratze dutela adieraziz (68. irudia, c).

Laburbilduz, tesi honetan sintetizatutako konposatuen jarduera zitotoxikoa ebaluatu da zenbait minbizi-lerro zelularren kontra. Oro har, lortutako γ -laktama deribatuek *in vitro* zitotoxikotasuna erakutsi dute, bereziki A549 zelula-lerroaren aurka (zelula epitelial albeolar basal kartzinomikoa), baina SKOV3 (giza-obulutegiko kartzinoma) eta RKO (giza-koloneko kartzinoma epiteliala) zelula-lerroak, berriz, erresistenteagoak izan ziren. Gainera, MRC5 biriketako fibroblasto ez-gaiztoen aurkako jarduera oro har apala izan zen. Azterketa honek erakutsi zuen, halaber, γ -laktama eraztunaren C-5 ordezkatzaila funtsezkoa dela jarduera zitotoxikorako. Gainera, C-4 posizioan ordezkatzailerik ez duten deribatuen arteko konposaturik aktiboena **72c** γ -laktama izan zen. Honek 2,34 μM -eko IC_{50} balioa du A549 zelula-lerroan, eta selektibitate oso handia MRC5 zelula-lerroarekin alderatuz gero. C-4 atomoan ordeztutako γ -laktama-deribatuei dagokienez, jarduera antiproliferatibo hobeak lortzen dira ester taldea heterozikloaren C-4 posizioan dagoenean, fosfonato tetraedrikoarekin edo fosfina-oxido taldearekin alderatuta. Konposatu aktiboena **86n** izan zen, 0,11 eta 1,23 μM -eko IC_{50} balio bikainak ematen baitzituen A549 eta SKOV3 zelula-lerroetan, eta selektibitate handia du zelula ez-gaiztoekin alderatuta. Are gehiago, **90a** γ -laktamaren bi enantiomeroak modo independentean ebaluatu dira, eta ez da desberdintasunik hauteman haien artea ez eta substratu errazemikoaren aktibitate zitotoxikoen artean ere. Horrez gain, **135** 1,4-dihidropiridina biziklikoen jarduera ere ebaluatu zen, eta **cis-135u** konposaturako zitotoxikotasun datu onenak neurtu ziren, 0,89 eta 11,90 μM -eko IC_{50} balioekin A549 eta SKOV3 zelula-lerroetan, hurrenez hurren. Azkenik, agerian geratu da γ -laktama deribatuek minbizi-zeluletan zitotoxikotasuna eragiteko zelula barneko mekanismo apoptotikoak aktibatzen dituztela.



68. irudia. Morfologia zelularren behaketa X4 lentearekin **86n** konposatua gehitu eta 0, 6, 12, 24, 48 eta 72 ordutara. Eskala: 300 μm. (A) **86n** konposatuaren 1.1 μM-eko kontzentrazioz tratatutako A549 zelulak. (B) **86n** konposatuaren 0.11 μM-eko kontzentrazioz tratatutako A549 zelulak (C) **86n** konposatuaren 0.02 μM-eko kontzentrazioz tratatutako A549 zelulak.



8. Kapitulua

γ -Laktama-deribatuen ebaluazioa MDM2/MDMX-p53 elkarrekintzaren inhibitzaile gisa

Tesiaren azken zati honen helburua, sintetizatutako γ -laktama derivatuen ekintza biologikoaren mekanismoa zehaztea da, aktibitate antiproliferatiboaren eta apoptosiaren indukzio-mekanismoen arteko erlazioari buruzko ebidentzia gehiago ezartzeko asmoarekin. Horretarako, γ -laktama horiek MDM2/MDMX-p53 proteina-proteina elkarrekintza inhibitzeko duten gaitasuna aztertu zen, kontuan hartuta bibliografian aktibitate hori burutzen duten antzeko substratuen hainbat adibide daudelako (18. irudia, *vide supra*).

8.1. MDM2 eta MDMX proteinen adierazpena eta purifikazioa.

Giza-proteina errekonbinanteak *Escherichia coli*-n (*E. coli*) adierazi ziren, sistema sinpleena eta erabilieta baita. Izan ere, metodo honek hainbat abantaila eskaintzen ditu, hala nola hazkunde azkarra, kostu txikiak eta errendimendu handiko prozedura sinpleak.²²⁸ Helburu-proteina, modu disolbagarrian adierazi zen MDMX-ren kasuan (1-134 aminoazidoak) aldiz, MDM2-ren kasuan (18-125 aminoazidoak), inklusio-gorputz gisa (forma ez-disolbagarria). Proteinak jatorrizko edo desnaturalizatutako baldintzetan purifikatu ziren, birtolestatzearekin jarraituz. Stoll²²⁹ eta Popowicz-ek²³⁰ deskribatutako prozedura eraldatu bat erabili zen MDM2 eta MDMX proteinen p53 lotura-eremuen adierazpen eta purifikaziorako. Protokoloak xehetasunez deskribatzen dira “Experimental Section II” atalean.

MDM2 eta MDMX proteina-konstruktuen purifikazio-prozesuaren azken urratsa, ÄKTA Pure sistemari konektatutako HiLoad 16/600 S75 pg (120 mL) zutabean egindako gel filtrazioa da, *Assay Buffer-a* erabiliz. Gainera, proteinaren purutasuna SDS-PAGE bidez monitorizatu zuen purifikazio

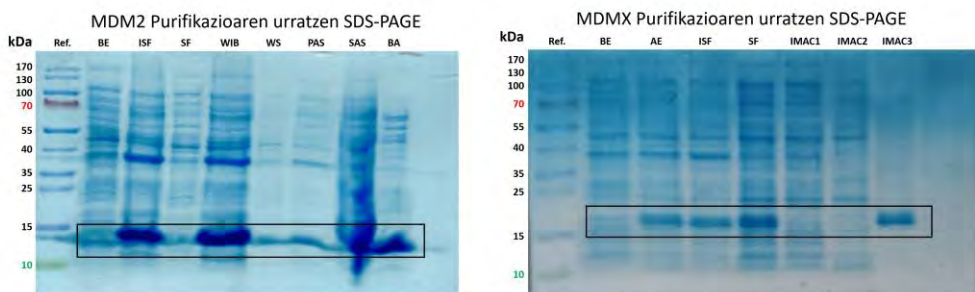
²²⁸ (a) Rosano, G. L.; Morales, E. S.; Ceccarelli, E. A. *Protein Sci.* **2019**, *28*, 1412-1422. (b) Rosano, G. L.; Ceccarelli, E. A. *Front. Microbiol.* **2014**, *5*, 1-17.

²²⁹ Stoll, R.; Renner, C.; Hansen, S.; Palme, S.; Klein, C.; Belling, A.; Zeslawski, W.; Kamionka, M.; Rehm, T.; Mühlhahn, P.; Schumacher, R.; Hesse, F.; Kaluza, B.; Voelter, W.; Engh, R. A.; Holak, T. A. *Biochemistry* **2001**, *40*, 336-344.

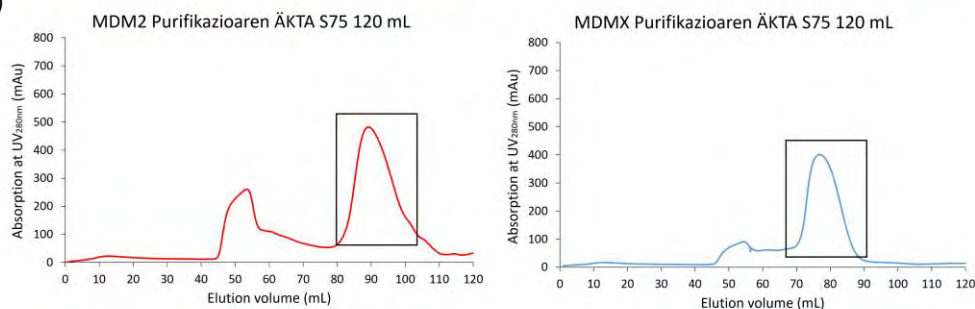
²³⁰ Popowicz, G. M.; Czarna, A.; Rothweiler, U.; Szwagierczak, A.; Krajewski, M.; Weber, L.; Holak, T. A. *Cell Cycle* **2007**, *6*, 2386-2392.

prozesuaren etapa bakoitzean. MDM2 eta MDMX proteinen kromatogramak eta SDS-PAGE-ren emaitzak 69. irudian aurkezten dira.

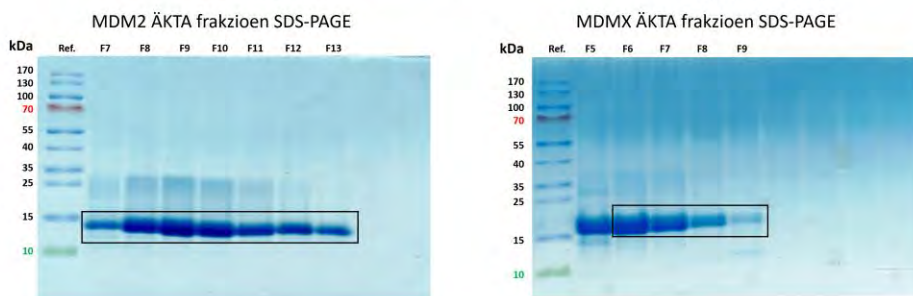
(a)



(b)

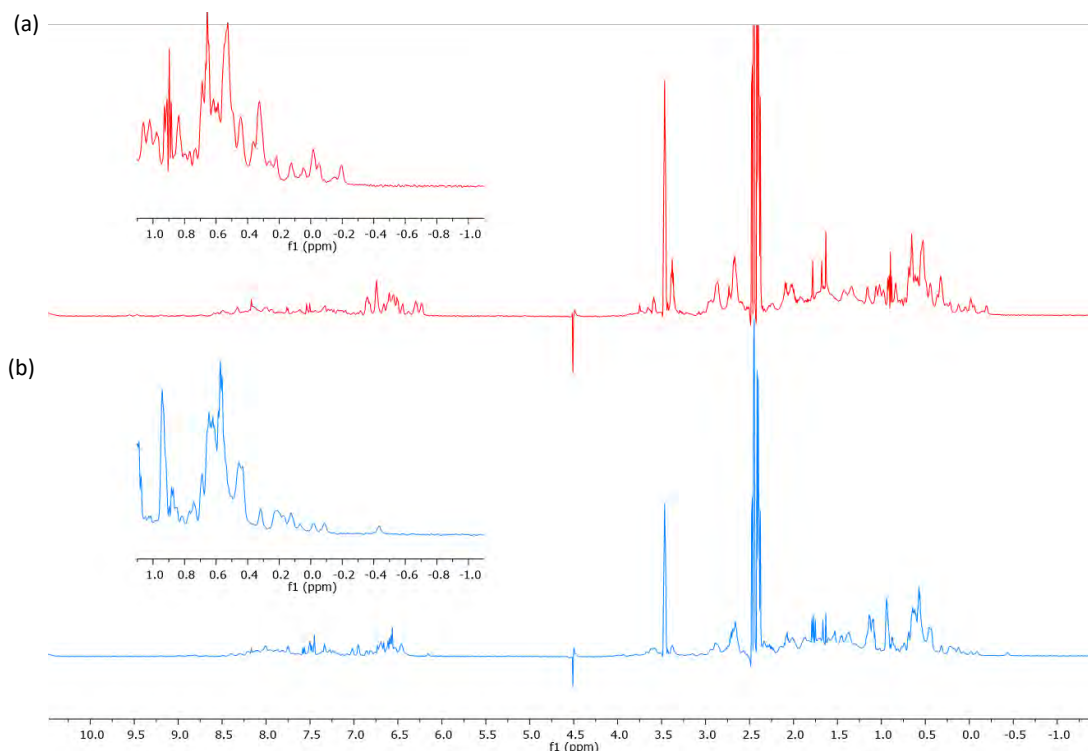


(c)



69. iruida. (a) Purifikazio-etapa desberdinen SDS-PAGE-rako jasotako laginak: Adierazpena baino lehen (BE), Adierazpena eta gero (AE), sonikazio eta gero jasotako Frakzio solugaitza (ISF) eta Frakzio solugarria (SF), Triton X-100 bidez garbitutako Inklusio gorputzak (WIB) eta Gainjalkina (WS), Guanidina Hidrokloruroarekin solubilizatu osteko Pellet-a (PAS) eta Gainjalkina (SAS), eta, birtolestutako eta interakzio hidrofobiko kromatografiaren ondorengo proteina-frakzioak, hau da, ÄKTA baino lehen (BA), IMAC1-3, MDMX proteinaren IMAC ondorengo frakzio desberdinak dira. (b) MDM2 eta MDMX-ren kromatogramak HiLoad 16/600 S75 pg zutabean burututako gel filtrazioaren ondoren (MDM2 tontorra 90 ml inguruan eta MDMX tontorra 77 ml inguruan). (c) ÄKTA-n jasotako frakzioen SDS-PAGE.

Azkenik, bi proteinak modu egokian tolestuta ote dauden jakiteko, dimentsio bakarreko ^1H EMN espektroak erregistratu ziren (70. irudia). Espektroen eremu alifatikoko seinaleen sakabanatze handiak ($\delta_{\text{H}} = 1,0$ eta $-1,0$ ppm), proteinak egitura egokia hartu duela esan nahi du. Ordea, tontor nagusi eta zorrotz bakar baten presentzia $\delta_{\text{H}} = 1,0$ ppm inguruan, proteina desordenatuta dagoela adierazten du.²³¹ Izan ere, seinaleak ingurune kimiko desberdinen ondorioz sakabanatzen dira, eta, proteina modu egokian tolestuta dagoenean, protoien desplazamendu kimikoak frekuentzia-tarte zabalago batean zehar hedatzeko joera izaten dute.



70. irudia. (a) MDM2-ren (18-125) 1D ^1H EMN espektroa. (b) MDM2-ren (1-134) 1D ^1H EMN espektroa.

Hau guztia kontuan hartuta, eta MDM2 eta MDMX proteinen ^1H NMR espektroei erreparatuta (70. irudia), ondorioztatu daiteke disoluzioan proteinak behar bezala tolestuta daudela.

γ -Laktama-deribatuen MDM2/MDMX-p53 proteina-proteina elkarrekintzaren inhibizio-ahalmenaren ebidentzia sendoa lortzeko, pausukako metodologia bat erabili zen, lehenengo ekortze-fluorimetria diferentzialarekin (EFD) eta gero, fluoreszentzia-polarizazioko (FP) saiakuntzarekin.

²³¹ Rehm, T.; Huber, R.; Holak, T. A. *Structure* **2002**, *10*, 1613-1618.

8.2. Ekortze-Fluorimetria Diferentzialaren (EFD) entsegua.

EFD esperimentuan, proteina puruak egonkortzen (edo ezegonkortzen) dituzten pisu molekular txikiko ligandoak identifikatzeko aukera ematen duen metodoa azkar eta merkea da. Proba hau, denbora-errealeko PCR termozikladore konbentzional bat erabiliz burutzen da, eta, proteina eta koloratzaile fluoreszentea duten PCR plaka baten putzuetan gehitzen dira ligando disoluzioak. Temperatura poliki igotzen da eta horrela zehazten da proteinaren destoleste-termikoa.²³² Metodologia hau proteina sorta zabal bati aplikatu dakioke,²³³ MDM2 eta MDMX barne.²³⁴

Erabilitako koloratzaileak, hala nola *SYPRO orange* (SO), oso fluoreszenteak dira ingurune ez-polarretan, ur-disoluzioekin alderatuta, non fluoreszentsia indargabetuta dagoen. Proteina destolesten den temperatura (fusio-tenperatura, T_m), koloratzailearen fluoreszentsiaren igoerarekin neurtzen da. Izan ere, koloratzaileak proteinaren zati hidrofobikoekin afinitate handia dauka, eta hauek agerian geratzen dira tenperaturaren eraginez proteina destolesten denean (71. irudia, a). Behin proteina guztiz destolestu denean, fluoreszentsia intentsitatea maximora ailegatzen da, eta ondoren, fluoreszentsiaren gutxitzea hautematen da, proteina, prezipitazio eta agregazio bidez disoluziotik baztertzen delako. Hala, EFD esperimentuan, fluoreszentsiaren intentsitatea tenperaturaren arabera irudikatzen da, kurba sigmoideo baten arabera.

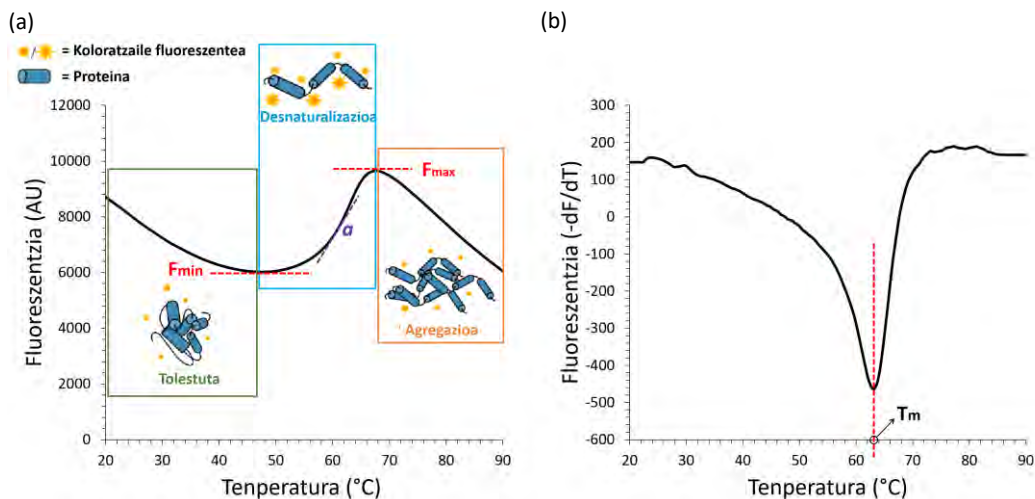
Trantsizio-kurbaren inflexio-puntua (T_m), Boltzmann-en ekuazioaren bidez kalkulatzen da (71. irudia, b), non F_{min} eta F_{max} intentsitate minimo eta maximoren balioak diren, hurrenez hurren. Hala ere, T_m balioa kalkulatzeko metodarik sinpleena fluoreszentsiaren kurbak tenperaturarekiko duen lehenengo deribatuaren maximoa zehaztea da (71. irudia, c).

Hainbat faktoreek eragin dezakete proteinaren egonkortasunean, hala nola, elkarrekintza ez-espezifikoa osagai generikoekin (tanpoiak, gatzak eta detergenteak), edo proteinaren gune jakin batean lotzen diren ligandoak. Ligando eta proteinaren arteko elkarrekintzek, proteinaren destoleste tenperaturan (T_m) eragin dezakete, beraz, esperimendu hau balio handikoa izan daiteke efektore alosterikoak identifikatzeko, horixe baita farmako berriak garatzeko prozesuaren abiapuntua.

²³² (a) Gao, K.; Oerlemans, R.; Groves, M. R. *Biophys. Rev.* **2020**, *12*, 85-104. (b) Niesen, F. H.; Berglund, H.; Vedadi, M. *Nat. Protoc.* **2007**, *2*, 2212-2221.

²³³ Ericsson, U. B.; Hallberg, B. M.; DeTitta, G. T.; Dekker, N.; Nordlund, P. *Anal. Biochem.* **2006**, *357*, 289-298.

²³⁴ (a) Anil, B.; Riedinger, C.; Endicott, J. A.; Noble, M. E. M. *Acta Crystallogr. Sect. D Biol. Crystallogr.* **2013**, *69*, 1358-1366. (b) Kallen, J.; Goepfert, A.; Blechschmidt, A.; Izaac, A.; Geiser, M.; Tavares, G.; Ramage, P.; Furet, P.; Masuya, K.; Lisztwan, J. J. *Biol. Chem.* **2009**, *284*, 8812-8821.



$$(c) \quad F = \frac{F_{min} - F_{max}}{1 + e^{\left(\frac{T - T_m}{a}\right)}} + F_{max}$$

71. irudia. (a) Proteinaren destolesteko prozesuaren temperatura vs fluoreszentzia intentsitatearen erregistro tipikoa *SYPRO orange* erabiliz. (b) Boltzmann-en ekuazioa. (c) Fluoreszentziaren lehenengo deribatua vs temperaturaren kurba.

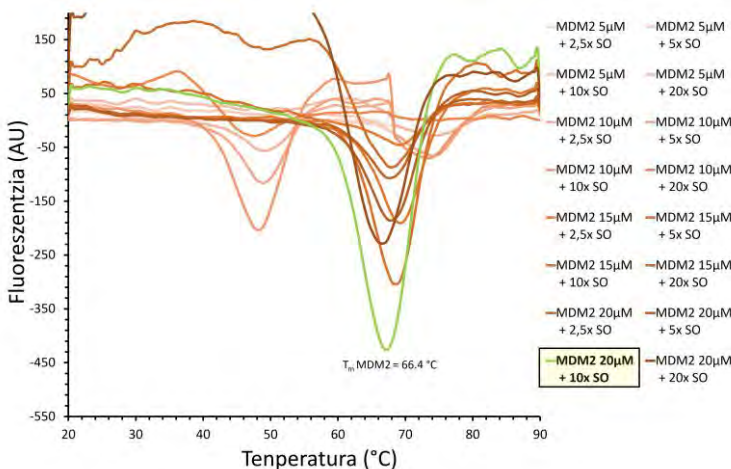
Proteina baten egonkortasuna, haren destolestean Gibbs energia askearekin erlazionatuta dago (ΔG_u), eta hau temperaturaren menpekoa da. Temperatura handitzen denean, ΔG_u murrizten da, eta zero bihurtuko da orekara ailegatzean, hau da, tolestutako eta destolestutako proteina-kontzentrazioak berdinak direnean. Temperatura hori fusio-tenperaturatzat (T_m) hartzen da.²³⁵ Ligando bat proteina batekin elkartzean, molekularren lotze-energia askearen ekarpenak ΔG_u balioari eragiten dio. Interakzio honen ondorioz proteina egonkortzen bada, T_m handituko da, ordea, konposatuak proteina ezegonkortzen badu, urtze-temperaturaren balioa txikiagoa izango da.

Egonkortze-efektua, ligandoak proteinarekiko duen afinitatearekiko proportzionala dela deskribatu da. Hala ere, termodinamikarekin zerikusia duten interpretazioak kontuz egin behar dira eta beste metodo batzuen bidez berretsi behar dira.²³²

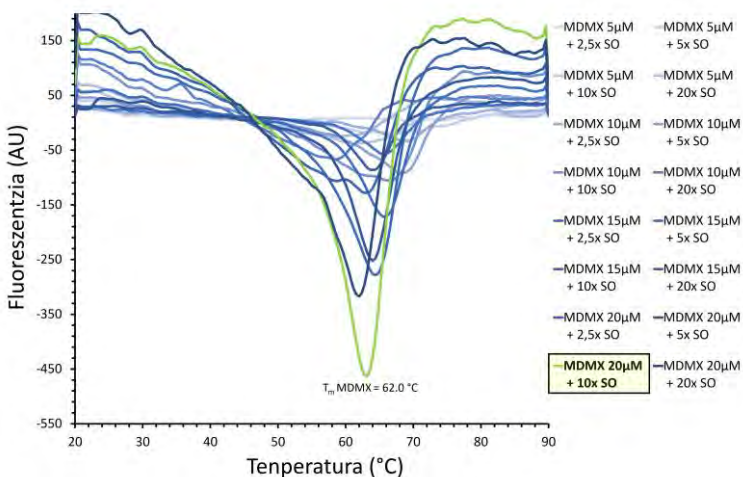
Tesi honetan deskribatutako γ -laktama-deribatuek MDM2 eta MDMX proteinen T_m aldatzeko gai diren aztertzeko, lehenik eta behin, proteinaren eta *SYPRO Orange*-ren kontzentrazio idealak identifikatu behar dira, fluoreszentziaren seinale fluoreszente onena lortzeko eta konposaturik gabeko proteinaren T_m balioa identifikatzeko. Hori dela eta, EFD esperimentuak hamasei konbinazio

²³⁵ Schellman, J. A. *Biophys. J.* **1997**, *73*, 2960-2964.

desberdinetan burutu ziren, proteina-kontzentrazio (MDM2 edo MDMX) eta *SYPRO Orange* kontzentrazio desberdinak erabiliz (72. eta 73. irudiak).



72. irudia. Proteina eta SO-ren kontzentrazio-konbinazio desberdinekin lortutako MDM2 proteinaren urtze-kurbak.

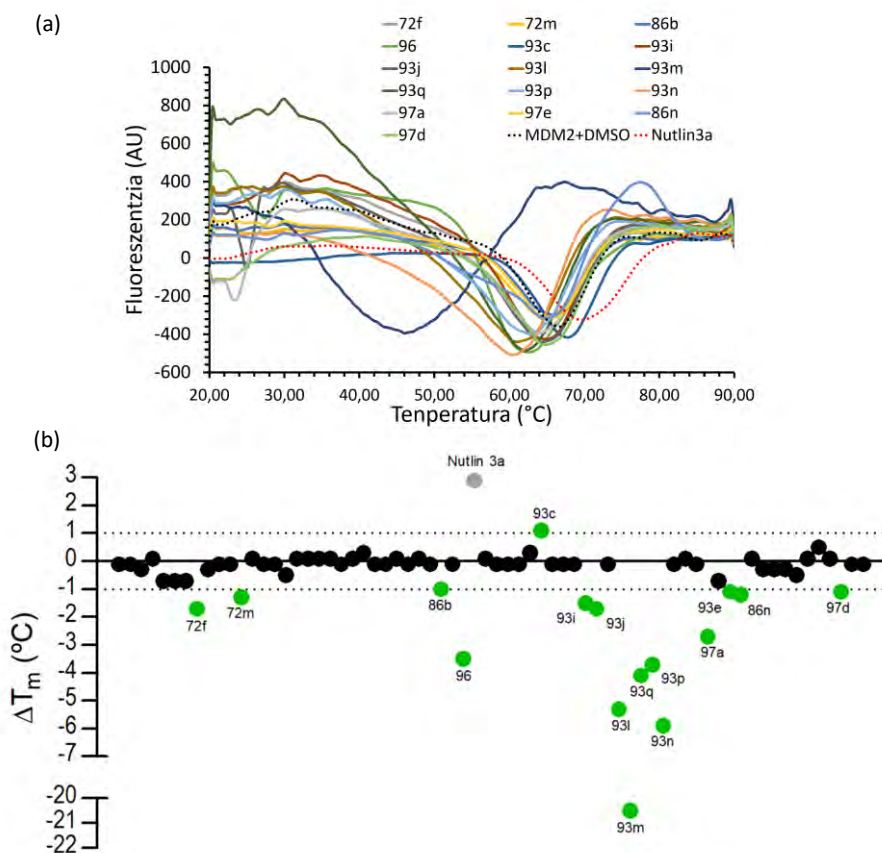


73. irudia. Proteina eta SO-ren kontzentrazio-konbinazio desberdinekin lortutako MDMX proteinaren urtze-kurbak.

Aurreko irudietan (72. eta 73. irudiak) ikus daitekeenez, fluoreszentzia balio onena lortzeko behar diren proteinaren eta koloratzaile fluoreszentearen kontzentrazio optimoak berdinak dira, hau da, dagokion proteinaren 20 µM eta *SYPRO Orange*-ren 10x. Gainera, MDM2-rako ($T_m \text{ MDM2}$) neurtutako fusio-temperatura 66,4 °C-koa izan zen, eta 62,0 °C-koa MDMX ($T_m \text{ MDMX}$) proteinarako.

Behin baldintza optimoak finkatu zirenean, guztira 70 γ -laktama-deribatu bahetu ziren esperimentu honen bidez. Konposatuak singletoi gisa probatu ziren 100 μ M-ko amaierako kontzentrazioan eta, konposatuak DMSO-n disolbatzen direnez, DMSO-aren kontzentrazio berdina (% 0,2 v/v) duen proteina erabili zen kontrol gisa. MDM2 proteinaren fusio-puntua zertxobait aldatu zen DMSO-ren presentzian ($T_{m \text{ MDM2+DMSO}} = 66.2 \text{ }^\circ\text{C}$), ordea, MDMX proteinarena ez zen aldatu ($T_{m \text{ MDMX+DMSO}} = 62,0 \text{ }^\circ\text{C}$).

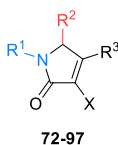
EFD-ren emaitza positibotzat, MDM2 edo MDMX proteinen fusio-tenperatura gutxienez 1°C -tan handitzeko edo murrizteko gaitasuna duten substratuak hartu ziren. Konposatu bakoitzaren ΔT_m balioa, konposatu horren T_m eta proteinaren balioen kenketaren bidez determinatu zen ($\Delta T_m = T_m - T_{m \text{ Prot. +DMSO}}$). Esperimentu horretarako, Nutlin-3a erabili zen kontrol positibo gisa, MDM2 proteina egonkortzen duena. Emaitzak 74. eta 75. irudietan laburbiltzen dira.



74. irudia. EFD-ren emaitzak MDM2 proteinarako. (a) MDM2 proteinaren fusio-kurbak. Bakarrik emaitza positiboak ($\Delta T_m = \pm 1 \text{ }^\circ\text{C}$) erakusten dira. (b) Emaitza positiboaren identifikazioa. MDM2 proteinan probatutako koposatuaren ΔT_m balioen adierazpen eskematikoa.

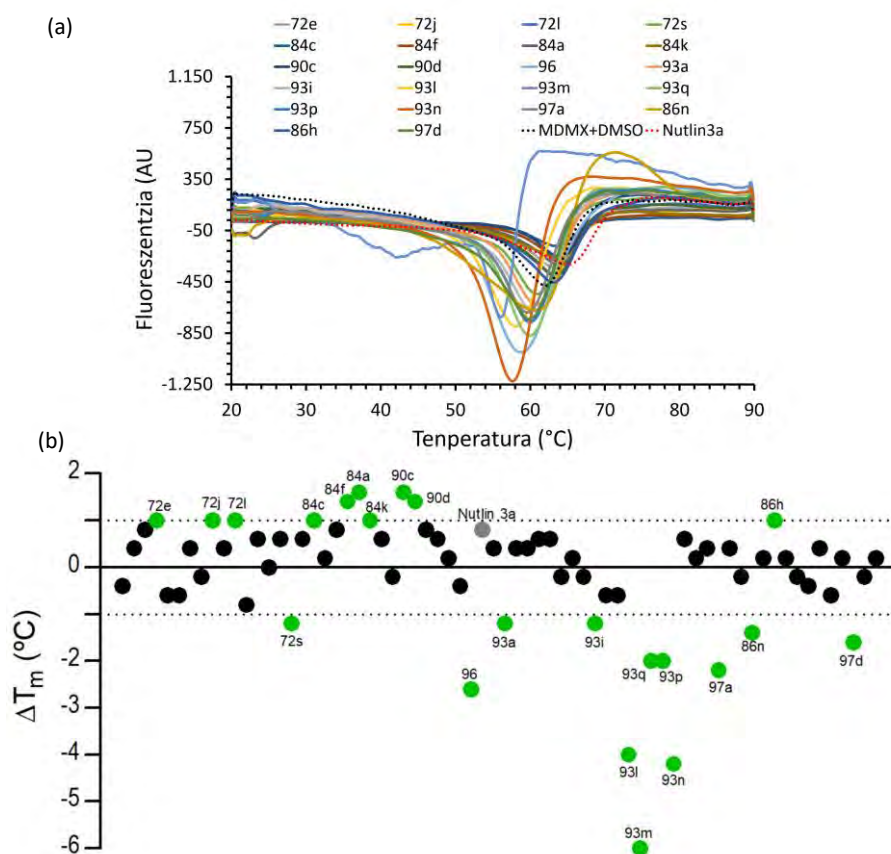
74. irudian eta 25. taulan ikus daitekeen bezala, hamasei γ -laktama-deribatu positibo moduan identifikatu ziren MDM2 proteinaren aurka. C-4 posizioan ordezkatu gabeko **72**, **84**, **86** eta **90** 3-amino-1,5-dihydro-2H-pirrol-2-onen artean, **72f** eta **72m** substratuak baino ez ziren positibo bezala izan, $-1,7 \pm 0,3$ eta $-1,3 \pm 0,1$ °C-ko ΔT_m balioak neurtuz, hurrenez hurren, eta gainera biek proteina desegonkortu zuten (25. taula, 1-2. sarrerak). Posizio horretan bentzil edo metil karboxilato ordezkatzailak dituzten **86b** eta **86n** enamina desegonkortzaileak ere izan ziren, ΔT_m -1.0 ± 0.0 eta $-1.2 \pm 0,2$ °C balioekin (25. taula, 3-4. sarrerak). Hala ere, emaitza positibo gehienak, hamabi hain zuzen ere, enolaren deribatu diren **93**, **96** eta **97** konposatuen artean lortu ziren (25. taula, 5-16. sarrerak). Konposatu-multzo honen barruan, **93m** γ -laktama substratu ezegonkortzaileena izan zen, $-20,5 \pm 1,5$ °C-ko ΔT_m -ko balioa neurtuz (25. taula, 9. sarrera). Zoritxarrez, MDM2 proteina egonkortzen zuen konposatu bakarra aurkitu genuen, **93c** γ -laktama, $1.1 \pm 0,1$ °C-ko ΔT_m positiboarekin (25. taula, 5. sarrera).

25. taula. MDM2 proteinan EFD esperimenduaren bidez lortutako emaitza positiboaren ΔT_m balioak.



Sarr.	Prod.	X	R ¹	R ²	R ³	ΔT_m (°C)
1	72f	NH-4-MeC ₆ H ₄	4-MeC ₆ H ₄	4-FC ₆ H ₄	H	$-1,7 \pm 0,3$
2	72m	NH-4-MeC ₆ H ₄	4-MeC ₆ H ₄	2-Naftil	H	$-1,3 \pm 0,1$
3	86b	NH-4-MeC ₆ H ₄	4-MeC ₆ H ₄	4-NO ₂ C ₆ H ₄	Bn	$-1,0 \pm 0,0$
4	86n	NH-4-MeC ₆ H ₄	4-MeC ₆ H ₄	4-OH-3-MeOC ₆ H ₄	CO ₂ Me	$-1,2 \pm 0,2$
5	93c	OH	4-MeC ₆ H ₄	4-NO ₂ C ₆ H ₄	P(O)(OEt) ₂	$+1,1 \pm 0,1$
6	93i	OH	4-MeC ₆ H ₄	Ph	P(O)(<i>i</i> Pr) ₂	$-1,5 \pm 0,3$
7	93j	OH	4-MeC ₆ H ₄	4-FC ₆ H ₄	P(O)(<i>i</i> Pr) ₂	$-1,7 \pm 0,1$
8	93l	OH	4-MeC ₆ H ₄	Ph	P(O)(Ph) ₂	$-5,3 \pm 0,1$
9	93m	OH	4-MeC ₆ H ₄	C ₆ F ₅	P(O)(Ph) ₂	$-20,5 \pm 1,5$
10	93n	OH	4-MeC ₆ H ₄	4-FC ₆ H ₄	P(O)(Ph) ₂	$-5,9 \pm 0,7$
11	93p	OH	4-MeOC ₆ H ₄	Ph	P(O)(Ph) ₂	$-3,7 \pm 0,7$
12	93q	OH	4-MeC ₆ H ₄	Ph	P(O)(Ph) ₂	$-4,1 \pm 0,5$
13	96	OH	4-MeC ₆ H ₄	Ph	P(O)(OH) ₂	$-3,5 \pm 0,1$
14	97a	OH	4-MeC ₆ H ₄	Ph	CO ₂ Me	$-2,7 \pm 0,3$
15	97d	OH	Bn	4-CF ₃ C ₆ H ₄	CO ₂ Me	$-1,1 \pm 0,1$
16	97e	OH	4-MeC ₆ H ₄	3-MeOC ₆ H ₄	CO ₂ Me	$-1,1 \pm 0,1$

MDMX proteinaren kasuan (75. irudia eta 26. taula), hogeita bi emaitza positibo identifikatu ziren. Emaitza horietako ia erdiak C-4 ordezkatu gabeko **72**, **84**, **86** eta **90** 3-amino-1,5-dihydro-2H-pirro-2-onetan lortu ziren (26. taula, 1-10 sarrerak). Konposatu horiek guztiek, $-1,2 \pm 0,2$ °C-ko ΔT_m balioa eman zuten **72s** γ -laktama izan ezik (26. taula, 4. sarrera), MDMX proteina egonkortu zuten, eta horien artean, **84a** eta **90c** substratuak ligando egonkortzaileenak izan ziren, $1,6 \pm 0,0$ eta $1,6 \pm 0,2$ °C-ko ΔT_m balioekin, hurrenez hurren (26. taula, 5. eta 9. sarrerak). C-4 posizioan ordezkaturako enamina ziklikoen artean, **86n** eta **86h** γ -laktamak emaitza positibo gisa detektatu ziren, -1.4 ± 0.2 eta $+1.0 \pm 0.0$ °C-ko ΔT_m balioekin, hurrenez hurren (26. taula, 11-12 sarrerak). Gainera, enolaren deribatu diren **93**, **96** eta **97** γ -laktamen artean konposatu aktibo ugari identifikatu ziren. Hala ere, konposatu horietako gehienak MDMX proteinaren ezegonkortzaileak zirela erakutsi zuten (26. taula, 13-22. sarrerak). Hauen artean, aktiboena **93m** substratua izan zen, $-6,0 \pm 0,4$ °C-ko ΔT_m balioarekin (26. taula, 16. sarrera).



75. irudia. EFD-ren emaitzak MDMX proteinarako. (a) MDMX proteinaren fusio-kurbak. Bakarrik emaitza positiboak ($\Delta T_m = \pm 1$ °C) erakusten dira. (b) Emaitza positiboaren identifikazioa. MDMX proteinaren probatutako konposatuen ΔT_m balioen adierazpen eskematikoa.

Table 26. MDMX proteinan EFD esperimenduaren bidez lortutako emaitza positiboaren ΔT_m balioak.

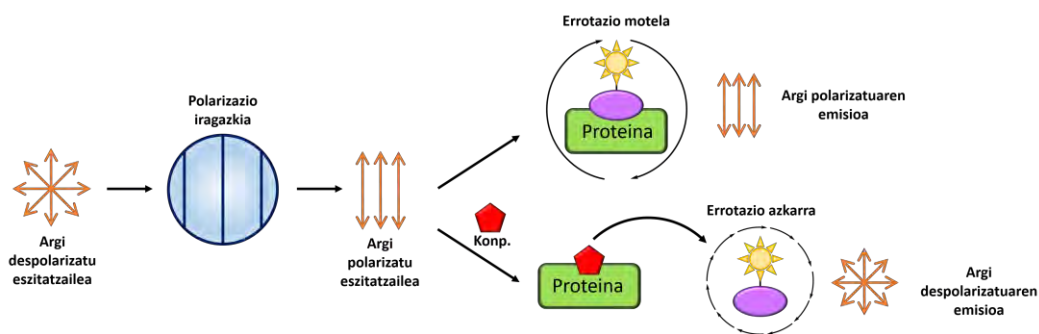
Sarr.	Prod.	X	R ¹	R ²	R ³	ΔT_m (°C)
1	72e	NH-4-MeC ₆ H ₄	4-MeC ₆ H ₄	3-NO ₂ C ₆ H ₄	H	+1,0 ± 0,2
2	72j	NH-4-MeC ₆ H ₄	4-MeC ₆ H ₄	6-(N-Me-indolil)	H	+1,0 ± 0,2
3	72l	NH-4-MeC ₆ H ₄	4-MeC ₆ H ₄	2-Tienil	H	+1,0 ± 0,0
4	72s	NH-4-MeC ₆ H ₄	4-MeC ₆ H ₄	CO ₂ Et	H	-1,2 ± 0,2
5	84a	NH-4-MeOC ₆ H ₄	4-MeOC ₆ H ₄	4-NO ₂ C ₆ H ₄	H	+1,6 ± 0,0
6	84c	NH-4-BrC ₆ H ₄	4-BrC ₆ H ₄	4-NO ₂ C ₆ H ₄	H	+1,0 ± 0,4
7	84f	NH-4-ClC ₆ H ₄	4-ClC ₆ H ₄	4-NO ₂ C ₆ H ₄	H	+1,4 ± 0,2
8	84k	NH-3-CF ₃ C ₆ H ₄	3-CF ₃ C ₆ H ₄	4-NO ₂ C ₆ H ₄	H	+1,0 ± 0,2
9	90c	NH-4-MeC ₆ H ₄	4-MeC ₆ H ₄	CH ₂ P(O)(Ph) ₂	H	+1,6 ± 0,2
10	90d	NH-4-MeC ₆ H ₄	4-MeC ₆ H ₄	C ₆ F ₅	H	+1,4 ± 0,4
11	86n	NH-4-MeC ₆ H ₄	4-MeC ₆ H ₄	4-OH-3-MeOC ₆ H ₄	CO ₂ Me	-1,4 ± 0,2
12	86h	NH-4-MeC ₆ H ₄	4-MeC ₆ H ₄	4-CF ₃ C ₆ H ₄	CO ₂ Me	+1,0 ± 0,0
13	93a	OH	4-MeC ₆ H ₄	Ph	P(O)(Et) ₂	-1,2 ± 0,4
14	93i	OH	4-MeC ₆ H ₄	Ph	P(O)(<i>i</i> Pr) ₂	-1,2 ± 0,2
15	93l	OH	4-MeC ₆ H ₄	Ph	P(O)(Ph) ₂	-4,0 ± 0,6
16	93m	OH	4-MeC ₆ H ₄	C ₆ F ₅	P(O)(Ph) ₂	-6,0 ± 0,4
17	93n	OH	4-MeC ₆ H ₄	4-FC ₆ H ₄	P(O)(Ph) ₂	-4,2 ± 0,4
18	93p	OH	4-MeOC ₆ H ₄	Ph	P(O)(Ph) ₂	-2,0 ± 0,2
19	93q	OH	2-FC ₆ H ₄	Ph	P(O)(Ph) ₂	-2,0 ± 0,4
20	96	OH	4-MeC ₆ H ₄	Ph	P(O)(OH) ₂	-2,6 ± 0,4
21	97a	OH	4-MeC ₆ H ₄	Ph	CO ₂ Me	-2,2 ± 0,2
22	97d	OH	Bn	4-CF ₃ C ₆ H ₄	CO ₂ Me	-1,6 ± 0,0

Laburbilduz, emaitza gehiago lortu dira MDMX proteinarako MDM2 proteinarako baino (25. taula vs. 26. taula). Halaber, konposatu idealak proteina egonkortzeko gai direnak direla kontuan hartuta, MDMX proteinarako ere konposatu egonkortzaile gehiago dago MDM2-rakot baino. Biek, enolaren zein enamaren deribaturiko γ -laktamek, bi proteinen T_m aldatzeko gai zirela erakutsi zuten. Hala ere, esan beharra dago, oro har, emaitza gehiago lortu direla γ -laktama eraztunaren C-4 posizioan fosforil ordezkatzaila duten substratuen artean, posizio horretan karboxilato taldea duten produktuekin alderatuta. Ordezkatzaile fosforatuari dagokionez, fosfina-oxidoa, fosfonatoa baino aukera hobea dela dirudi. Azkenik, **86n**, **93i**, **93l**, **93m**, **93n**, **93p**, **93q**, **96**, **97a**, eta **97d** konposatuak positiboak izan ziren MDM2 zein MDMX proteinen aurrean.

EFD entsegua burututa eta MDM2 eta MDMX proteinen ΔT_m balioan eraginik ez duten konposatuak baztertuta, emaitza positibo ema zuten konposatuekin Fluoreszentziaren-Polarizazio (FP) entsegua egin zen, MDM2 eta MDMX proteinekiko inhibizio-konstantea (K_i) zehazteko helburuz.

8.3. Fluoreszentzia-Polarizazio (FP) entsegua.

Teknika honen arabera, fluoreszentziaz markatutako molekula bat argi polarizatuaren bidez eszitatzen denean, errotazio-molekularraren abiadurarekiko alderantziz proportzionala den polarizazio-maila duen argia igortzen du. Ondorioz, teknika hau oso baliagarria da pisu molekular baxua duen markatutako ligando eta proteina baten arteko elkarrekintza neurtzeko, modu zuzenenean edo beste substratu batzuekin lehian, eta hau, bereziki baliotsua da proteina-proteina interakzioen inhibitzailak hautemateko.²³⁶ Fluoreszentzia-Polarizazio teknikaren printzipioa 76. irudian modu grafikoan azaltzen da.



76. irudia. Fluoreszentzia-Polarizazio entseguaeren printzipio teorikoa.

Fluoroforo bat erantsita duen pisu molekular baxuko ligando bat, peptido bat adibidez, argi polarizatuaren bidez eszitatzen denean, igorriko duen argia nabarmen despolarizatuta egongo da, markatutako espeziearen errotazio molekular azkarraren ondorioz. Ordea, markatutako ligandoa, pisu molekular handiko (>10 kDa) proteina bati lotuta badago, igorritako argia, maila esanguratsu batean, polarizatuta jarraituko du, konplexuaren errotazio-abiadura nabarmen txikiagoa delako. Ondorioz, teknika hau ligando potentzialen lotura-ahalmena neurtzeko erabiltzen da, izan ere, ligando markatu eta hartzailearen nahaste batean neurtutako argi polarizatu lotuta dagoen ligandoaren frakzioarekiko proportzionala da. Beraz, erraza da lotura-lehiakorraren entsegu ezartzea, non argi polarizatuaren

²³⁶ Moerke, N. J. *Curr. Protoc. Chem. Biol.* **2009**, *1*, 1-15.

seinalean intentsitatearen jaitiera hautematen da, markatutako ligandoaren nahasteari inhibitzaile bat eranstean bazaio eta hartzailearekin lotzen bada.²³⁷

Lehenik eta behin, p53-tik eratorritako eta karboxifluoreszeinaz markatutako FAM-P2 (LTFEHYWAQLTS sekuentzia) afinitate handiko peptidoaren K_d balioak zehaztu ziren, MDM2 eta MDMX proteinekiko, %5 DMSO-ren presentzian. Horretarako, FAM-P2 peptidoaren 10 nM-eko soluzioak proteina bakoitzaren diluzio-serie batekin tratatu ziren (750 eta 0,012 nM artean MDM2-rako eta 3750 eta 0,10 nM artean MDMX-rako). Fluoreszentzia-polarizazioa lotura-ekuazioaren bidez ezarri zen 1:1 konplexuaren eraketarako (77. irudia, a). Ekuazio horretan, FP_{min} , fluoreszentzia-polarizazioaren balio ligandoarentzat soilik, FP_{max} , fluoreszentzia-polarizazioaren balioaproteinaren kontzentrazioa ligandoa asetzen duenean, eta c proteinaren kontzentrazioa da 1:1 konplexuaren eraketarako. MDM2 proteinareako kalkulaturako K_d balioa $5,47 \pm 0,67$ nM-ekoa izan zen (77. irudia, b), ordea, MDMX proteinarako $13,89 \pm 1,59$ nM-eko balioa neurtu zen (77. irudia, c). Lortutako emaitzak bat etorri ziren bibliografiako datuekin.²³⁸

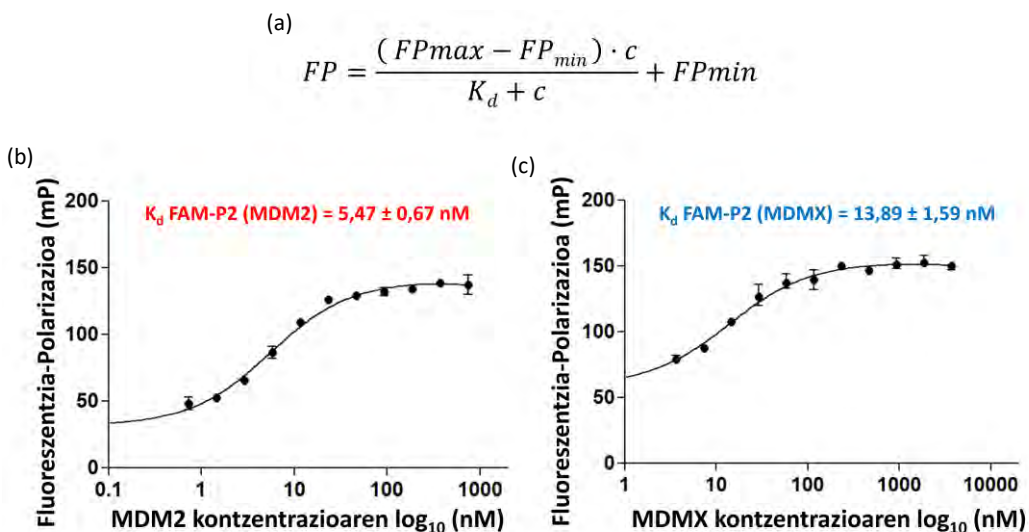


Figure 77. (a) Fluoreszentziaren polarizazioa zehazteko lotura-ekuazioa. (b) FAM-P2 peptidoaren FP lotura-kurba MDM2 proteinarako. (c) FAM-P2 peptidoaren FP lotura-kurba MDMX proteinarako.

²³⁷ (a) Jameson, D.; Croney, J. *Comb. Chem. High Throughput Screen.* **2003**, *6*, 167-176. (b) Jameson, D. M.; Seifried, S. E. *Methods A Companion to Methods Enzymol.* **1999**, *19*, 222-233.

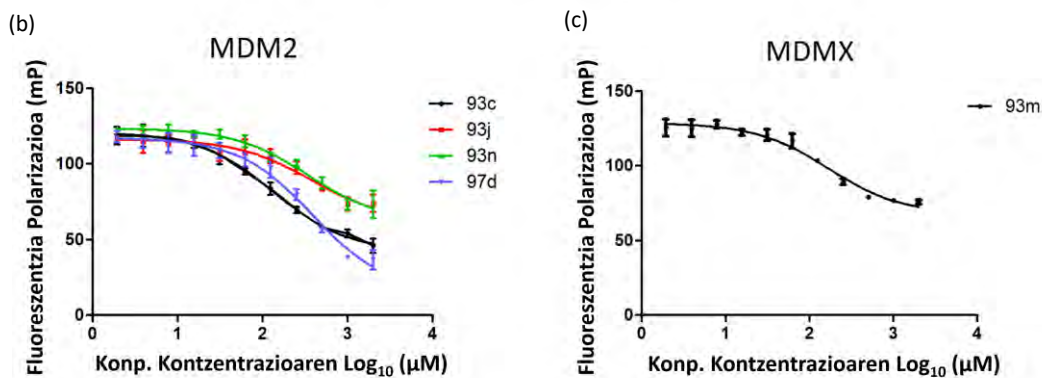
²³⁸ Czarna, A.; Popowicz, G. M.; Pecak, A.; Wolf, S.; Dubin, G.; Holak, T. A. *Cell Cycle* **2009**, *8*, 1176-1184.

Ondoren, γ -laktamekin FP saiakuntzak burutzeko, proteinaren kontzentrazio optimoak zehaztu ziren, eta, Huang eta kolaboratzaileek deskribatu zutenaren arabera, FP %80 lortzeko behar den proteina-kontzentrazioa ideala da ligandoekin lotura lehiakorren-esperimentuak burutzeko.²³⁹

MDM2 eta MDMX proteinekiko peptido fluoreszentearen K_d eta proteinaren kontzentrazio balio optimoak zehaztu ondoren, EFD esperimentuan lortutako emaitza positiboekin, hau da, hamasei konposatu MDM2 proteinarako eta hogeita bi molekula MDMX proteinarako, lotura lehiakorren entseguak burutu ziren. Saiakuntza hauetan γ -laktama-deribatuek 2 mM-etik 2 μ M arteko kontzentrazioetan erabili ziren, eta Nutlin-3a kontrol positibo gisa baliatu zen. γ -Laktama-substratuen inhibizio-konstantearen balioak (K_i) 78a irudian adierazitako ekuazioen bidez kalkulatu ziren. Ekuazio hauetan, x eta y ardatz bakoitzaren balioak dira loturaren %50 dagoenean, FP_{max} eta FP_{min} , goiko eta beheko mesetaren balioei dagozkie, c erabilitako afinitate-peptidoaren kontzentrazioa da (10 nM), eta azkenik, K_d aurretik kalkulaturako FAM-P2 peptidoaren proteina bakoitzarekiko duen lotura-afinitatea da (5.5 nM MDM2-n eta 13.9 nM MDMX-en).

$$(a) \log EC_{50} = \log \left(10^{\log K_i \cdot \left(\frac{1+c}{K_d} \right)} \right)$$

$$y = FP_{min} + \frac{FP_{max} - FP_{min}}{1 + 10^{(x - \log EC_{50})}}$$



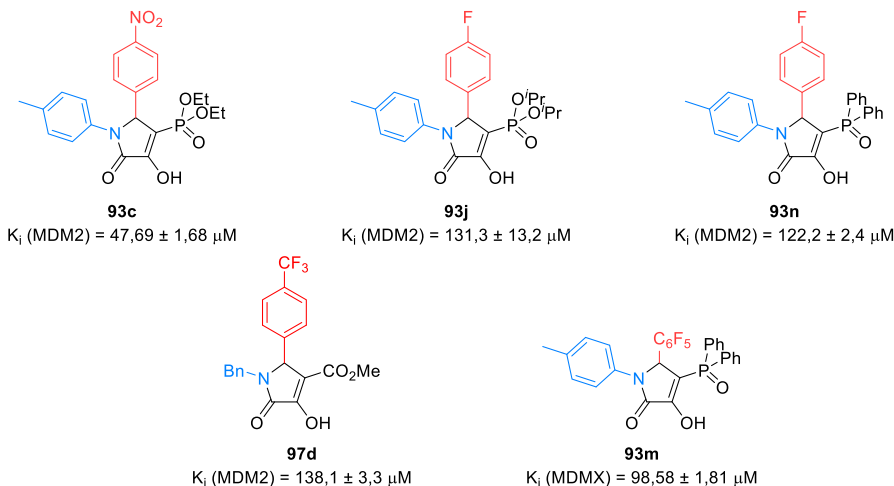
78. irudia. (a) K_i kalkulatzeko ekuazioak. (b) MDM2 proteina γ -laktama desberdinekin baloratzean eskuratutako FP lotura-kurbak. (c) MDMX proteina **93m** γ -laktamarekin baloratzean eskuratutako FP lotura-kurba.

Zoritxarrez, MDM2-ren kasuan, lau konposatuk bakarrik eman zituzten emaitza neurgarriak (78. irudia, b); izan ere, neurtutako kontzentrazioetan beste γ -laktama-deribatuek ez zuten proteinarekiko afinitaterik erakutsi. Hortaz, C-4 posizioan fosforodun ordezkatzailak dituzten **93c**, **93j** eta **93n**

²³⁹ Huang, X. J. *Biomol. Screen.* **2003**, *8*, 34-38.

3-hidroxi-1,5-dihidro-2*H*-pirrol-2-onak $47,69 \pm 1,68$, $131,30 \pm 13,2$ eta $122,2 \pm 2,4$ μM -ko inhibizio-konstantearen balioak (K_i) erakutsi zituen, hurrenez hurren. Halaber, C-4 posizioan metilkarboxilato talde funtzionala duen enolaren deribatuetan **97d** γ -laktamak K_i balio ahulagoa izan zuen, $138,1 \pm 3,3$ μM -ekoa (79. irudia).

MDMX proteinaren kasuan, neurtzeko moduko emaitza bakarra lortu zen (78. irudia, c). Bitxia bada ere, konposatu aktiboa **93m** enol deribatua da, ere, oraingoan, difenil fosfina-oxido eta perfluorofenil talde funtzionalekin C-4 eta C-5 posizioetan, hurrenez hurren (79. irudia).



79. irudia. γ -Laktama-deribatuen inhibizio konstanteak MDM2 eta MDMX proteinen aurrean.

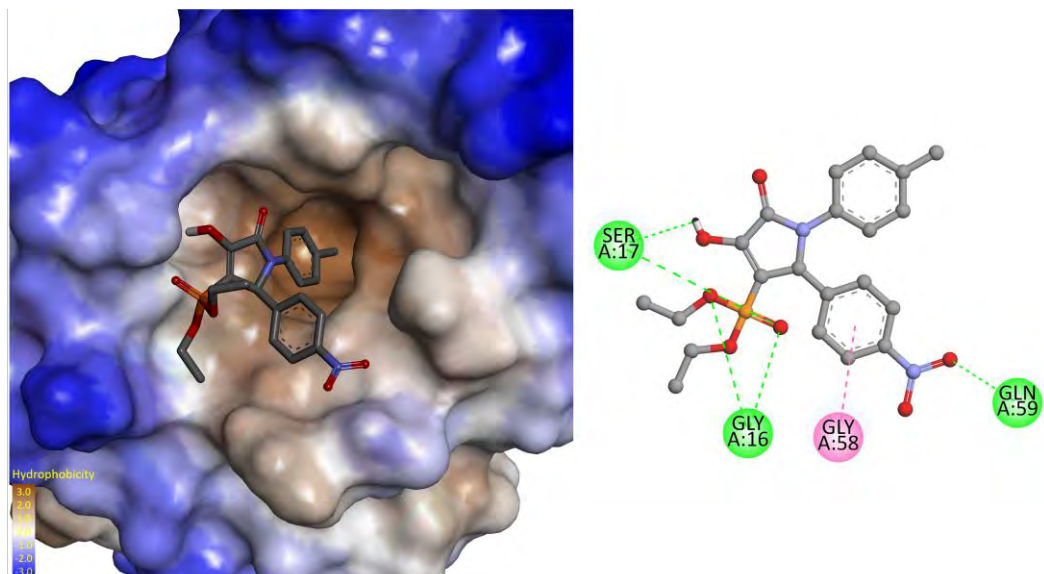
Laburbilduz, MDM2 proteinaren inhibitzaile indartsuena **93c** konposatua izan zen, $47,69$ μM -ko K_i balioarekin. Bestalde, MDMX proteinaren inhibizio-konstantearen baliorik onena **93m** konposatuarekin lortu zen ($K_i = 98,58$ μM).

8.4. Modelizazio molekularren bidezko simulazioak.

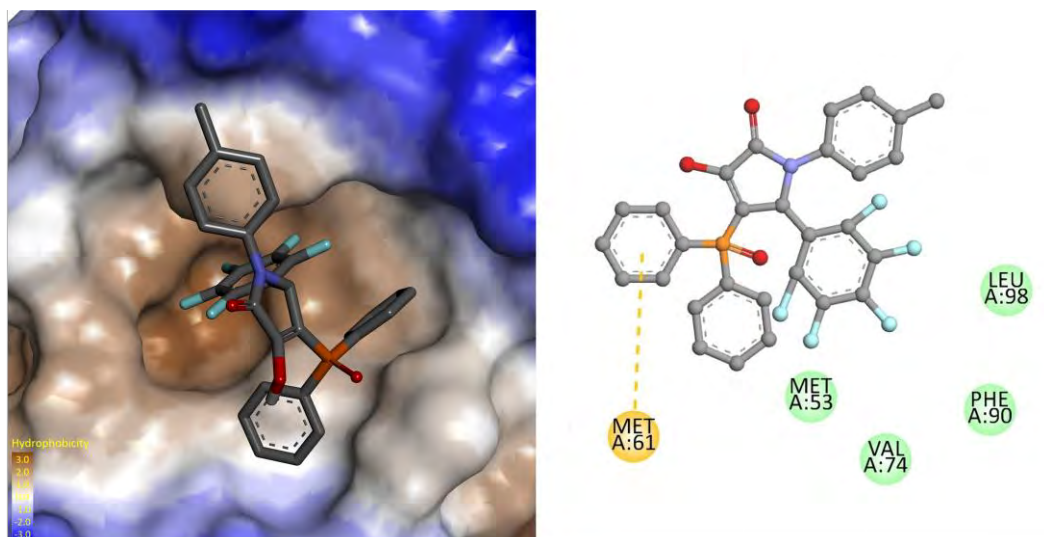
Afinitate txikiak neurtu diren arren, konposatu horien lotura-modua aurreikusi ahal izateko, proteina bakoitzerako aktiboena den γ -laktama-substratuen *docking* edo uztartze-molekularren simulazioak egin ziren.

Autodock VINA programarekin egindako **93c** substratuaren eta MDM2 proteinaren arteko lotura-moduaren iragarpenak adierazten du, *p*-toluidina taldeak p53-ko Trp23 lotura hidrofobikoaren gunea betetzen duela, eta OH eta P=O taldeek, H-lotura eratzten dutela MDM2-ko Ser17 aminoazidoarekin. Gainera, etil fosfonato talde funtzionalaren fosforil eta etoxi taldeek interakzio polarra sor dezakete Gly16-ren alboko katearekin. γ -Laktama eratzunaren 5. posizioko ordezkatzailari dagokionez, eraztun

aromatikoko nitro taldeak Gln59-rekin elkarrekintzan jarduten du, eta π -amida pilatze-elkarrekintza eratzen da Gly58-rekin (80. irudia).



80. irudia. 93c substratuaren eta MDM2 proteinaren arteko duen 3D eta 2D lotura-moduaren proposamena (PDB kodea: 1T4E).



81. irudia. 93m substratuaren eta MDMX proteinaren arteko 3D eta 2D lotura-moduaren proposamena (PDB kodea: 3DAB).

Bestalde, **93m** γ -laktamaren eta MDMX proteinaren arteko elkarrekintzarako proposatutako lotura-modua ikusita (81. irudia), aurreko atalean neurtutako K_i -ren balio txikiagoa azal daiteke elkarrekintza-ereduan H-loturarik ez dagoelako. Kasu honetan, heterozikloaren C-5 posizioan perfluorofenil taldea p53-ko Trp23 lotura-lekuan txertatzen da, Met53, Val74, Phe90 eta Leu98 aminoazidoen alboko kateekin sortutako Van der Waals elkarrekintzen bidez. Hala ere, MDM2-rekin alderatuta, MDMX proteinaren gune aktiboaren itxura estuagoaren ondorioz, *p*-tolil eta fosfina-oxido taldeak perfluorofenilo-eraztuna sakonago joatea saihesteko moduan kokatuta daude. Gainera, π -sufre elkarrekintza hautematen da MDMX-ren Met61 aminoazidoaren eta γ -laktamaren difenil fosfina-oxido taldeko eraztun aromatikoetako baten artean.

Laburbilduz, γ -laktama-deribatuek MDM2/MDMX-p53 proteina-proteina interakzioa inhibitzeko duten ahalmena bi baheketa-teknika desberdinen bidez ebaluatu da. Lehenik eta behin, Ekortze-Fluorimetria Diferentzial (EFD) saiakuntzaren bidez, konposatu ugari probatu ziren, metodo horren sinpletasuna aprobetxatuz. Ondoren, emaitza positiboak eman zituzten γ -laktamen inhibizio-konstanteak zehaztu ziren Fluoreszentzia-Polarizazio (FP) saiakuntzen bidez. Lortutako balio apalak kontuan hartuta, pentsa daiteke, MDM2/MDMX-p53 proteina-proteina interakzioaren inhibizioa γ -laktama-deribatuen jarduera zitotoxikoaren erantzule dela bina soilik modu partzial batean. Izan ere, konposatu hauen ekintza-mekanismo nagusiak gehiago ikertu behar dira.

Ondorioak



Brønsted azido bidez katalizatutako pirubatoaren, aminen eta aldehidoen deribatuen hiru osagaiko erreakzio eraginkorra baliatuz 3-amino- γ -laktama α,β -insaturatu anitz prestatu daitezke. Erreakzio hau hainbat amina aromatikori, aldehido aromatikoki eta alifatikoei eta ordezkaturako pirubato-deribatu desberdinei aplikatu dakieke, eta, hala, oso funtzionalizatuta dauden γ -laktama-deribatuen sintesia burutu daiteke. Gainera, osagai anitzeko metodologia hau fluor eta/edo fosforo duten γ -laktama-deribatuen sintesirako erabil daiteke, eta 3-hidroxi-1,5-dihidro-2*H*-pirrol-2-onak edo hauen enamina eratorriak lortu daitezke, bost kideko heterozikloko eratzunaren ordezkatzailen arabera.

Dialkil azetilendikarboxilatoak ere erabilgarriak dira 3-amino 1,5-dihidro-2*H*-pirrol-2-onen osagai anitzeko sintesirako pirubatoen ordezeko bezala. Gainera, erreakzio honen lehen adibidea deskribatu da, non azido fosforikoak katalizatzaile gisa erabiltzen diren. Halaber, orain arte deskribatu ez dena 1,5-dihidro-2*H*-pirrol-2-onen enamina talde funtzionalaren hidrolisia egin da enola lortuz.

Azido fosforikoek osagai anitzeko prozesua katalizatzeke duten gaitasuna aprobetxatuz, enantioselektibitate handiko hiru osagaiko erreakzioaren bertsio organokatalitiko bat garatu da, pirubato, amina eta aldehidotik abiatuta, optikoki puruak diren 3-amino-1,5-dihidro-2*H*-pirrol-2-onak prestatzeko aukera ematen duena.

Osagai anitzeko erreakzioaren bidez lortutako γ -laktama substratuen potentzial sintetikoa ebaluatu da, eta produktu horiek lehengai gisa erabili dira deribatu γ -laktamiko polifuntzionalen sintesirako. Zentro estereogenikoa aprobetxatuz, oso diastereoselektiboak diren hidrogenazio-erreakzioak deskribatu dira. Horrez gain, C-4 posizioan funtzionalizazio selektiboa egin daiteke enamina kimikaz baliatuz, eta espezie organometalikoak gehituta, berriz, C-3-n funtzionalizatu ahal da. Gainera, fosfonatotik eratorritako substratuak lehengai gisa erabil daitezke olefinazio-erreakzioetan.

Iterbio bidez katalizatutako [3+3] zikloadizio formal oso estereoselektibo bat deskribatu da, non enamina zikliko eta α -zetoester asegabeak erabiliz 1,4-dihidropiridina ziklikoak lortzen diren, eta gainera, erreakzioaren orokortasuna agerian jarri da hogeita zazpi substratuko multzo zabala lortuz. Erreakzio-bitartekariaren detekzioari esker, erreakzio-mekanismoa zehaztu ahal izan zen. Lortutako emaitzen arabera, badirudi erlazioa dagoela erreakzioaren estereoselektibitatearen eta efektu esteriko eta π -metatze efektuaren artean. Gainera, konposatu bizikliko horien eraldaketa sintetiko batzuk ere burutu dira, hala nola, tartean hirugarren zentro estereogeniko bat era diastereoselektiboan sortzen duen hidrogenazio katalitikoak.

Sintetizatutako konposatuen jarduera antiproliferatiboa neurtu da hainbat minbizi-lerro zelularren aurka. Oro har, lortutako γ -laktama-deribatuek *in vitro* zitotoxikotasuna erakutsi zuten, bereziki A549 zeluletan (zelula epitelial albeolar basal kartzinomikoa). Ordea, SKOV3 (giza-obulutegiko kartzinoma) eta RKO (giza-koloneko kartzinoma epiteliala) zelula-lerroak erresistenteagoak izan ziren, eta zitotoxikotasun balio apalagoak lortu ziren. Gainera, normalean, lortutako konposatuek aktibitate ahula eduki dute biriketako MRC5 fibroblasto ez-gaiztoen aurka. Konposatu aktiboanek 0,11 eta 1,23 μM -eko IC_{50} balio bikainak ematen dituzte A549 eta SKOV3 zelula-lerroetan, selektibitate handiarekin MRC5 birika zelula ez-gaiztoen aurka. Era berean, agerian geratu da γ -laktama-deribatuek zitotoxikotasuna indultzeko zelula barneko mekanismo apoptotikoen aktibazioa eragiten dutela.

γ -Laktama-deribatuen MDM2/MDMX-p53 proteina-proteina elkarrekintzaren inhibizio-ahalmena ere ebaluatu da, bi teknika desberdin erabiliz. Lehenik, Ekortze-Fluorimetria Diferentzia (EFD) esperimentuaren bidez, eta gero, lortutako emaitza positiboetarako Fluoreszentzia-Polarizazio saiakuntza egin zitzaion, γ -laktamen inhibizio-konstanteen balioak zehazteko. Hala ere, lortutako balioak txikiak izan zirela kontuan hartuta, ezin da segurtasun osoz ondorioztatu γ -laktama-deribatuen jarduera zitotoxikoa MDM2/MDMX-p53 proteina-elkarrekintzaren inhibizioaren ondorio denik.